VOLUME 108 PART C NUMBER 13 MARCH 1961

The Proceedings

OF

THE INSTITUTION OF ELECTRICAL ENGINEERS

FOUNDED 1871: INCORPORATED BY ROYAL CHARTER 1921

PART C

MONOGRAPHS Nos. 387–421

Price Fifteen Shillings

The Institution of Electrical Engineers

FOUNDED 1871
INCORPORATED BY ROYAL CHARTER 1921

PATRON: HER MAJESTY THE QUEEN

COUNCIL 1960–1961

President

SIR HAMISH D. MACLAREN, K.B.E., C.B., D.F.C.*, LL.D., B.Sc.

Past-Presidents

W. H. ECCLES, D.Sc., F.R.S.
THE RT. HON. THE EARL OF MOUNT EDGCUMBE, T.D.
J. M. DONALDSON, M.C.
PROF. E. W. MARCHANT, D.Sc.
H. T. YOUNG.
SIR GEORGE LEE, O.B.E., M.C.
J. R. BEARD, C.B.E., M.Sc.
SIR NOEL ASHBRIDGE, B.Sc.(Eng.).
SIR HARRY RAILING, D.Eng.
P. DUNSHEATH, C.B.E., M.A., D.Sc. (Eng.), LL.D.
SIR VINCENT Z. DE FERRANTI, M.C.
T. G. N. HALDANE, M.A.
PROF. E. B. MOULLIN, M.A., Sc.D., LL.D.
SIR ARCHIBALD J. GILL, B.Sc.(Eng.).
SIR JOHN HACKING.
COL. B. H. LEESON, C.B.E., T.D.
SIR HAROLD BISHOP, C.B.E., B.Sc.(Eng.), F.C.G.I.
SIR JOSIAH ECCLES, C.B.E., D.Sc.
THE RT. HON. THE LORD NELSON OF STAFFORD.
SIR W. GORDON RADLEY, K.C.B., C.B.E., Ph.D.(Eng.).
S. E. GOODALL, M.Sc.(Eng.), F.Q.M.C.
SIR WILLIS JACKSON, D.Sc., D.Eng., LL.D., F.R.S.

Vice-Presidents

B. DONKIN, B.A.
O. W. HUMPHREYS, C.B.E., B.Sc.
G. S. C. LUCAS, O.B.E., F.C.G.I.
C. T. MELLING, C.B.E., M.Sc.Tech.
A. H. MUMFORD, O.B.E., B.Sc.(Eng.).

Honorary Treasurer

C. E. STRONG, O.B.E., B.A., B.A.I.

Ordinary Members of Council

J. C. ARKLESS, B.Sc.
PROF. H. E. M. BARLOW, Ph.D., B.Sc.(Eng.).
D. A. BARRON, M.Sc.
C. O. BOYSE, B.Sc.(Eng.).
F. H. S. BROWN, C.B.E., B.Sc.
PROF. M. W. HUMPHREY DAVIES, M.Sc.
SIR JOHN DEAN, B.Sc.
L. DRUCQUER.
J. M. FERGUSON, B.Sc.(Eng.).
D. C. FLACK, B.Sc.(Eng.), Ph.D.
R. J. HALSEY, C.M.G., B.Sc.(Eng.), F.C.G.I.
R. A. Hore, M.A., B.Sc.
J. S. MCCULLOCH.
PROF. J. M. MEEK, D.ENG.
THE HON. H. G. NELSON, M.A.
H. V. PUGH.
J. R. RYLANDS, M.Sc., J.P.
R. L. SMITH-ROSE, C.B.E., D.Sc., Ph.D., F.C.G.I.
G. A. V. SOWTER, Ph.D., B.Sc.(Eng.).
H. G. TAYLOR, D.Sc.(Eng.).
D. H. TOMPSETT, B.Sc.(Eng.).

Chairmen and Past-Chairmen of Sections

Electronics and Communications:
T. B. D. TERRONI, B.Sc.
†M. J. L. PULLING, C.B.E., M.A.

Measurement and Control:
C. G. GARTON.
†PROF. A. TUSTIN, M.Sc.

Supply:
E. L. ROBINSON, M.Sc.
†J. R. MORTLOCK, Ph.D., B.Sc.(Eng.).

Utilization:
J. M. FERGUSON, B.Sc.(Eng.).
†T. E. HOUGHTON, M.Eng.

Chairmen and Past-Chairmen of Local Centres

East Midland Centre:
LT.-COL. W. E. GILL, T.D.
†D. H. PARRY, B.Sc.

North-Western Centre:
F. LINLEY.
†F. J. HUTCHINSON, M.Eng.

Mersey and North Wales Centre:
D. A. PICKEN.
†T. A. P. COLLEDGE, B.Sc.(Eng.).

Northern Ireland Centre:
J. MCA. IRONS.
†T. S. WYLIE.

Southern Centre:
R. GOFORD.
†W. D. MALLINSON, B.Sc.(Eng.).

North-Eastern Centre:
D. H. THOMAS, M.Sc.Tech., B.Sc.(Eng.).
†H. WATSON-JONES, M.Eng.

Scottish Centre:
R. B. ANDERSON.
†J. A. AKED, M.B.E.

Western Centre:
A. C. THIRTLE.
†H. JACKSON, B.Sc.(Eng.).

North Midland Centre:
F. W. FLETCHER.
†PROF. G. W. CARTER, M.A.

South Midland Centre:
BRIGADIER F. JONES, C.B.E., M.Sc.
†G. F. PEIRSON.

† Past Chairman.

Secretary

W. K. BRASHER, C.B.E., M.A., M.I.E.E.

Deputy Secretary

F. JERVIS SMITH, M.I.E.E.

Principal Assistant Secretary

F. C. HARRIS.

Editor-in-Chief

G. E. WILLIAMS, B.Sc.(Eng.), M.I.E.E.

THE PROCEEDINGS OF
THE INSTITUTION OF ELECTRICAL ENGINEERS

EDITED UNDER THE SUPERINTENDENCE OF W. K. BRASHER, C.B.E., M.A., M.I.E.E., SECRETARY

VOL. 108. PART C. NO. 13. MARCH 1961

DISCUSSION ON 'EXTENSION OF THE DUAL-INPUT DESCRIBING-FUNCTION TECHNIQUE TO SYSTEMS CONTAINING REACTIVE NON-LINEARITY'*

Dr. E. A. Freeman (*communicated*): In their introduction the authors state that one of the principal limitations of the describing-function method of analysis is that the amplitude-dependent characteristics of the system must be completely separable from the frequency-dependent characteristics. This, of course, is not so, and would, if true, present a severe limitation to the method because of the frequent occurrence of frequency-dependent non-linear elements in practice. For example, backlash and friction[A] in a mechanical system introduce such a non-linearity. Again, if both coulomb and viscous[B] friction are present, the non-linear element is of the inseparable frequency-dependent type. Other examples occur when backlash and resilience,[C] velocity limiting [D] and pneumatic controllers of the flapper-nozzle variety[E] are present in the closed sequence of an automatic control system. In view of its practical importance, therefore, this problem certainly merits attention.

However, the method presented by the authors for analysing reactive non-linearities would appear to have only limited application, for it depends on the existence of an amplitude-dependent frequency-independent relationship. In many examples of practical importance no such relation exists and the describing functions are transcendental functions of both amplitude and frequency.

To solve such practical problems one may derive a family of describing functions, each member of the family being plotted for a range of amplitudes and a fixed frequency. Intersections of this family by the open-loop frequency-response vector $\psi(j\omega)$ indicate possible sustained oscillations. The existence of these may be verified by determining whether $\psi(j\omega)$ at a point of intersection, $\psi(j\omega_k)$, intersects the describing function plotted for the frequency ω_k. In a recent paper[A] this method has been used to analyse a system employing a motor driving a load through gearing having backlash, for the case when both motor and load are opposed by speed-dependent friction. The family of frequency-dependent describing functions for combined coulomb and viscous friction may also be derived and used in a similar way.[B]

Messrs. R. M. Huey, O. Pawloff and **T. Glucharoff** (*in reply*): At the time when our paper was passed for press, Dr. Freeman's paper[A] had not come to our notice. One cannot help feeling that his first and major criticism is simply a matter of a difference in definition of the term 'describing function'. To quote, for example, from a recent text by Bower and Schultheiss,[F] 'It should be pointed out that not all non-linearities lend themselves to the elementary form of the describing function analysis presented here. Most frequently violated is the requirement that the amplitude-dependent gain function be independent of frequency.'

The use of frequency-dependent describing functions can become quite cumbersome, and in this connection it is of interest to note O. J. M. Smith's[G] opinion that, where the amplitude- and frequency-dependence of a non-linearity cannot readily be separated by other simple means, it is worth while to attempt a linear transformation from the variables a and ω into a new pair of variables, say b and u, chosen so that the system and non-linear element response may be written as separable functions in these new variables. In general, $b = f_b(j\omega, a)$ and $ju = f_u(\omega, a)$, together with some recombinations of the block diagram, could result in separable response functions, say $N(b)$ and $H(ju)$, which may be treated graphically in a similar way to the functions $N(a)$ and $KG(j\omega)$ in simple describing-function analysis.

We have considered the possibility of a frequency-dependent dual-input describing-function; although this is no doubt of interest as an alternative attack, it would involve considerable complication.

Our paper is concerned with the dual-input describing-function, where the greater generality with which the input to the non-linear element is defined allows one to search for a wider class of instabilities including sub-harmonic or harmonic instabilities as well as jumps.

Dr. Freeman's technique seems to offer some advantages when the problem is a specific servo-mechanism synthesis, particularly when one of the major design constraints is availability of components. Our paper was intended as a contribution in the wider context of non-linear circuit theory.

* HUEY, R. M., PAWLOFF, O., and GLUCHAROFF, T.: Monograph No. 383 M, June, 1960 (107 C, p. 334).

REFERENCES

(A) FREEMAN, E. A.: 'The Effect of Speed-Dependent Friction and Backlash on the Stability of Automatic Control Systems', *Transactions of the American I.E.E.*, 1958, **77**, Part II, p. 680.
(B) FREEMAN, E. A.: 'The Effect of Some Nonlinearities on the Performance of Automatic Control Systems', Ph.D. Thesis, King's College, University of Durham, November, 1958.
(C) LIVERSEDGE, J. H.: 'Backlash and Resilience within the Closed Loop of Automatic Control Systems', in 'Automatic and Manual Control' (Butterworth, 1952).
(D) TRUXALL, J. G.: 'Automatic Feedback Control System Synthesis' (McGraw-Hill, 1955), pp. 585–592.
(E) JACKSON, R.: 'Nonlinear Theory of the Dynamical Behaviour of Pneumatic Devices', *Transactions of the Society of Instrument Technology*, 1958, **10**, p. 161.
(F) BOWER, J. L., and SCHULTHEISS, P. M.: 'Introduction to the Design of Servomechanisms' (Wiley, 1958), p. 443.
(G) SMITH, O. J. M.: 'Feedback Control Systems' (McGraw-Hill, 1958) pp. 493–495.

621.316.923.2

The Institution of Electrical Engineers
Monograph No. 387 S
June 1960

AN ANALYTICAL METHOD FOR PREDICTING THE PERFORMANCE OF SEMI-ENCLOSED FUSES

By COLIN ADAMSON, M.Sc.(Eng.), Associate Member, and M. VISESHAKUL, M.Sc.Tech.

(*The paper was first received* 23rd *April*, 1959, *and in revised form* 9th *March*, 1960. *It was published as an* INSTITUTION MONOGRAPH *in June*, 1960.)

SUMMARY

An analysis has been made and a design procedure established for fuses other than those using round wire and with, or without, a restricted cross-section for part of the fuse length. Fuses of restricted section are, however, the major interest since they may be used to give different current/time characteristics by varying their dimensions. These different characteristics may be predicted accurately by the method indicated in the paper. In all the cases of semi-enclosed tin-strip fuses investigated in this way very close agreement between predicted and experimental results has been obtained.

LIST OF PRINCIPAL SYMBOLS

t = Time, sec.
x = Axial distance measured along the fuse from one end, cm.
$\theta - \theta_0$ = Temperature rise, deg C.
θ_0 = Initial ambient temperature, deg C.
T = Temperature of fuse at distance x along the fuse axis independent of time.
ψ = Transient temperature, a function of x and t.
A_1, A_2 = Fuse cross-sectional areas, cm^2.
p = Perimeter of fuse, cm.
l = Length of fuse, cm.
H = Coefficient of heat transfer between the fuse surface and the medium surrounding the fuse.
k = Mean thermal conductivity.
c = Specific heat, cal/g.
J = Joule's equivalent.
ρ = Density, g/cm^3.
σ = Mean electrical conductivity between room temperature and the melting temperature of the fuse, mhos/cm.

(1) INTRODUCTION

Over-current time-limit fuses associated with direct-acting-trip circuit-breakers are in widespread use on medium-voltage systems. Tin-wire fuses are usually employed and are connected in shunt across the circuit-breaker trip coils, which are supplied directly from current transformers. The fuses are in varying working lengths and their current/time characteristics vary with different manufacturers and, to some extent, among samples from any one manufacturer. The required characteristics have never been laid down as closely, say, as 415-volt high-breaking-capacity fuses, but their ratings have been specified in B.S. 116: 1952.

These fuses are of interest from the point of view of protective-gear co-ordination, and thus the question arises of the extent to which different current/time characteristics can be obtained. Hitherto, fuses manufactured from flat strip or round wire have been used; round wires are, however, the only fuses to have received systematic mathematical consideration. The possibility has now been investigated of designing fuses of restricted section in such a way as to predict the resulting characteristic. This has involved the formulation and solution of a thermal equation involving discontinuity and the establishment of a design procedure based on this solution.

Correspondence on Monographs is invited for consideration with a view to publication.
Mr. Adamson and Mr. Viseshakul are in the Power Systems Laboratory, Department of Electrical Engineering, Manchester College of Science and Technology.

(2) THERMAL EQUATION OF A FUSE

When a constant current flows in a round wire, heat is generated; either the temperature rises and reaches equilibrium or the wire fuses and interrupts the current.

The equation for the temperature rise, $\theta - \theta_0$, in a thin wire heated by electric current was given by Verdet in 1872:

$$\frac{\partial\theta}{\partial t} = K\frac{\partial^2\theta}{\partial x^2} - \lambda(\theta - \theta_0) + a \quad . \quad . \quad . \quad (1)$$

where $K = \dfrac{kA}{Ac\rho}$ $\lambda = \dfrac{Hp}{Ac\rho}$ $a = \dfrac{I^2}{JA^2c\rho\sigma}$

Eqn. (1) was applied to fuse problems by Schubert[1] and Carne,[2] both of whom neglected the radial heat loss. Guile[3] included radial heat loss for round wires by the application of Grunberg's[4] analysis for cable heating.

(2.1) Strip Fuses

The basic equations are applicable to fuses enclosed in any medium, but the solutions are very difficult to obtain in most cases, e.g. oil-immersed fuses, because of the uncertainty in assigning values to H and hence to λ. The solution obtained in the present paper is applicable to either strip- or round-fuse elements, in free air or semi-enclosed, taking into account surface heat losses. The analysis is based on Straneo's[5] work for determining thermal constants.

Suppose the temperature conditions of the surrounding medium are

$$\theta = 0 \text{ when } t = 0 (0 < x < l)$$
$$\theta = 0 \text{ at } x = l \text{ and } x = 0$$

The problem is divided into one of steady temperature and one of variable temperature, i.e.

$$\theta = T + \psi \quad . \quad . \quad . \quad . \quad . \quad . \quad . \quad (2)$$

where T represents temperature which is independent of time and has a finite value for particular values of x. T satisfies eqn. (1):

$$0 = K\frac{\partial^2 T}{\partial x^2} - \lambda T + a \quad . \quad . \quad . \quad . \quad . \quad (2a)$$

where $T = 0$ at $x = 0$ and l.

ψ is a function of x and t and, for the case of axial heat transfer from both directions, satisfies eqn. (1):

$$2\frac{\partial\psi}{\partial t} = K\frac{\partial^2\psi}{\partial x^2} - \lambda\psi \quad . \quad . \quad . \quad . \quad . \quad (2b)$$

where $\psi = 0$ at $x = 0$ and $x = l$
$\psi = T$ at $t = 0$ $\psi_n = -T_n \exp -\beta_n t$

and the coefficient 2 originates from the axial heat transfer from both ends of the fuse towards the centre.

From eqns. (2), (2*a*) and (2*b*) the temperature rise for a strip fuse becomes

$$\theta_x = \frac{4b}{\pi} \sum_{n=1}^{\infty} \frac{\mu^2 l^2 \sin \dfrac{(2n-1)\pi x}{l}}{(2n-1)[(2n-1)^2\pi^2 + \mu^2 l^2}$$

$$\left\{1 - \exp\left[-\frac{\lambda t}{2} - \frac{Kt}{2}(2n-1)^2\frac{\pi^2}{l^2}\right]\right\} \quad . \quad (3)$$

where $\mu = \sqrt{(\lambda/K)}$ and $b = a/\lambda$

From this equation, if the melting-point of the fuse element is known, the time/current characteristic of the fuse element can be obtained.

(2.2) Fuse Element with Single Discontinuity

(2.2.1) Assumptions regarding Fuse Parameters and Associated Equipment.

For the purpose of the analysis to follow, mean values of electrical and thermal resistivity have been assumed. As shown by the final results, this involves very little inaccuracy in determining the time/current characteristic of the fuse. It is possible that mean values are not accurate for analytical determination of the instantaneous distribution of temperature over the whole of the length of the fuse. This is considered further in Section 4. It is also necessary to consider the physical termination of the fuse and the influence of its associated equipment. Fuse links are normally terminated in what are known as 'fixed-ends', each of which invariably consists of a substantial mass of material to which a satisfactory and highly conductive cable joint has to be made. For practical purposes, this situation can be simulated by terminating the experimental fuses in solid-copper blocks which behave as thermal sinks. The main electrical factor affecting the fuse, in so far as protective-gear co-ordination is concerned, is the impedance of the circuit-breaker trip coil in shunt. Although the impedance chosen for such a coil may vary over wide limits, correct operation is clearly impossible unless its impedance is high compared with that of the fuse, so ensuring that there is little current through the coil unless the fuse breaks: for this reason, no impedance in shunt with the fuse appears in the calculations to follow. The case of an impedance in parallel with a non-linear resistance, in our opinion, constitutes a separate analytical and practical problem from the one discussed below and cannot, in any event, be attempted until a solution has been found for the non-linear behaviour of the fuse in the first instance.

(2.2.2) Solution for Fuse with Single Discontinuity.

For a fuse with a restricted section for part of its length as shown in Fig. 1, the ends being terminated in solid-copper blocks, eqn. (2*a*) becomes

$$0 = K\frac{\partial^2 T_1}{\partial x_1^2} - \lambda_1 T_1 + a_1 \quad . \quad . \quad . \quad . \quad (4)$$

where $T_1 = 0$ at $x_1 = 0$ and $T_1 = T_s$ at $x_1 = l_1$.

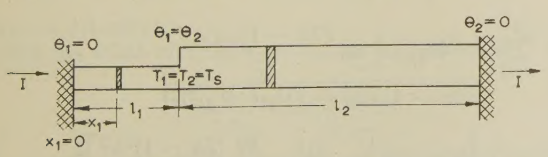

Fig. 1.—Fuse element with single discontinuity.

A solution of eqn. (4), for steady-state conditions independent of time, may be found such that

$$T_{x1} = b_1\left[1 - \frac{Q_1 \sinh \mu_1 x_1 + \sinh \mu_1(l_1 - x_1)}{\sinh \mu_1 l_1}\right] \quad . \quad (4a)$$

where $\mu_1 = \sqrt{(\lambda_1/K_1)}$, $b_1 = a_1/\lambda_1$ and $Q_1 = 1 - T_s/b_1$.

A similar expression can be written for T_{x2}.

T_x denotes the melting-point temperature at the point where the fuse breaks and T_s is the steady-state temperature ultimately attained at the point when the change in cross-section occurs on the fuse. These quantities are needed to find the minimum fusing current. T_s may now be found; at the point where the cross-sectional area changes,[5]

$$A_1\frac{dT_1}{dx_1} = -A_2\frac{dT_2}{dx_2}$$

where $x_1 = l_1$ and $x_2 = l_2$, the directional distances x_1 and x_2 both being considered as positive when measured towards the centre of the fuse. Differentiating eqn. (4*a*) with respect to x and introducing the relationship immediately above,

$$T_s = \frac{\tanh \mu_1 l_1 \tanh \mu_2 l_2}{\mu_1 \tanh \mu_2 l_2 + \mu_2 \dfrac{A_2}{A_1} \tanh \mu_1 l_1}$$

$$\left[\frac{b_2\mu_2\dfrac{A_2}{A_1}}{\sinh \mu_2 l_2}(\cosh \mu_2 l_2 - 1) + \frac{b_1\mu_1}{\sinh \mu_1 l_1}(\cosh \mu_1 l_1 - 1)\right] \quad . \quad (5)$$

The point where the fuse breaks, for the case of minimum fusing current, may now be found; at this point

$$\frac{dT}{dx} = \frac{b\mu}{\sinh \mu l}[\cosh \mu(l - x) - Q \cosh \mu x] = 0$$

which is the condition for maximum temperature.

Differentiating eqn. (4*a*) and using this last condition,

$$x = \frac{y}{2\mu}$$

where $\exp y = \dfrac{\exp \mu l - Q}{Q - \exp(-\mu l)}$ and $Q = 1 - T_s/b$.

To find the instantaneous temperature rise, eqn. (4*a*) may be expressed in terms of a sine series as follows:

$$T_{x1} = \sum_{n=1}^{\infty} \frac{4b_1\mu_1^2 l_1^2 \sin \dfrac{(2n-1)\pi x_1}{l_1}}{\pi(2n-1)[(2n-1)^2\pi^2 + \mu_1^2 l_1^2]} + \frac{8}{\pi^2}\sum_{n=1}^{\infty}\frac{T_s(-1)^{n+1}}{(2n-1)^2}\sin\frac{(2n-1)\pi x_1}{2l_1} \quad . \quad (6)$$

Eqn. (6) is a solution to eqn. (2*a*). When the conditions defined in eqn. (2*b*) are applied and substitution is made into eqn. (2), a solution for θ_{x1t} is obtained.

$$\theta_{x1t} = + \sum_{n=1}^{\infty} \frac{4b_1\mu_1^2 l_1^2 \sin \dfrac{(2n-1)\pi x_1}{l_1}}{\pi(2n-1)[(2n-1)^2\pi^2 + \mu_1^2 l_1^2]} \left\{1 - \exp\left[-\frac{\lambda_1 t}{2} - \frac{Kt}{2}\frac{(2n-1)^2\pi^2}{l_1^2}\right]\right\}$$

$$+ \sum_{n=1}^{\infty}\frac{8}{\pi^2}\frac{(-1)^{n+1}T_s}{(2n-1)^2}\sin\frac{(2n-1)\pi x_1}{2l_1} \left\{1 - \exp\left[-\frac{\lambda_1 t}{2} - \frac{Kt}{2}\frac{(2n-1)^2\pi^2}{4l_1^2}\right]\right\} \quad . \quad . \quad . \quad (7)$$

A similar expression may be written for θ_{x2t}. Eqn. (7) is derived by application of the method introduced by Straneo,[5] and it should follow that the temperature at the point of change of cross-section ($x_1 = l_1$; $x_2 = l_2$) should have the same value from whichever cross-section and direction it was obtained. This is not the result obtained from the equations above, however, and it thus follows that the function θ is more complex than hitherto assumed. Eqn. (7) has therefore been modified by the introduction of a term $\pm\theta_t = f(x, t)$, which is a function of heat transfer and distance for a particular value of time, and which represents the additional factor to be introduced to achieve heat balance between the two sections at any particular time and distance.

Referring again to eqn. (7), consider the point at which the cross-sectional area changes, i.e. $x_1 = l_1$ and $x_2 = l_2$ at time t. Inserting these values, the first term falls to zero, giving

$$\theta_{1t} = \sum_{n=1}^{\infty} \frac{8}{\pi^2} \frac{(-1)^{n+1}T_s}{(2n-1)^2} \sin\frac{(2n-1)\pi x_1}{2l_1} \left\{1 - \exp\left[-\frac{\lambda_1 t}{2} - \frac{Kt}{2}\frac{(2n-1)^2\pi^2}{4l_1^2}\right]\right\} \quad . \quad (7a)$$

$$\theta_{2t} = \sum_{n=1}^{\infty} \frac{8}{\pi^2} \frac{(-1)^{n+1}T_s}{(2n-1)^2} \sin\frac{(2n-1)\pi x_2}{2l_2} \left\{1 - \exp\left[-\frac{\lambda_2 t}{2} - \frac{Kt}{2}\frac{(2n-1)^2\pi^2}{4l_2^2}\right]\right\} \quad . \quad (7b)$$

These expressions represent the temperature at the same point and must clearly be equal. Suppose the value of θ at this point is θ_l' ($=\theta_{1t} = \theta_{2t}$): it follows that the heat to produce heat balance must have been transferred from one section to the other in order that the temperature θ_{1t} should have been reduced to θ_l' and the temperature θ_{2t} should have been increased to θ_l'. The situation may be represented graphically as in Fig. 2; since the mass and specific-heat terms are constant, integration of eqn. (7) can be carried out to give the heat transferred from one section to the other. The shaded areas of Fig. 2 are equal. The heat lost in section (1) is

$$A_1c\rho l_1\left(\frac{8}{\pi^2}\int_0^{l_1}\sum_{n=1}^{\infty}\frac{(-1)^{n+1}T_s}{(2n-1)^2}\sin\frac{(2n-1)\pi x_1}{2l_1}\left\{1-\exp\left[-\frac{\lambda_1 t}{2}-\frac{Kt}{2}\frac{(2n-1)^2\pi^2}{4l_1^2}\right]\right\} - \frac{8}{\pi^2}\int_0^{l_1}\sum_{n=1}^{\infty}\frac{(-1)^{n+1}T_s}{(2n-1)^2}\sin\frac{(2n-1)\pi x_1}{2l_1}\left\{1-\exp\left[-\frac{\lambda_1 t'}{2}-\frac{Kt'}{2}\frac{(2n-1)^2\pi^2}{4l_1^2}\right]\right\}\right) \quad . \quad (7c)$$

The heat gained in section (2) is

$$A_2c\rho l_2\left(\frac{8}{\pi^2}\int_0^{l_2}\sum_{n=1}^{\infty}\frac{(-1)^{n+1}T_s}{(2n-1)^2}\sin\frac{(2n-1)\pi x_2}{2l_2}\left\{1-\exp\left[-\frac{\lambda_2 t}{2}-\frac{Kt}{2}\frac{(2n-1)^2\pi^2}{4l_2^2}\right]\right\} - \frac{8}{\pi^2}\int_0^{l_2}\sum_{n=1}^{\infty}\frac{(-1)^{n+1}T_s}{(2n-1)^2}\sin\frac{(2n-1)\pi x_2}{2l_2}\left\{1-\exp\left[-\frac{\lambda_2 t''}{2}-\frac{Kt''}{2}\frac{(2n-1)^2\pi^2}{4l_2^2}\right]\right\}\right) \quad . \quad (7d)$$

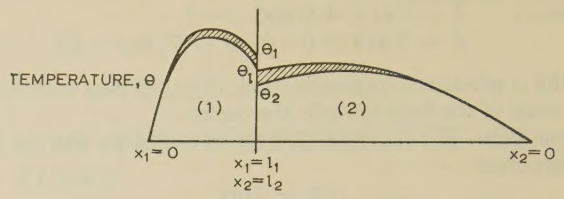

Fig. 2.—Determination of temperature at point of discontinuity.

Particular values of time, t' and t'', must be assigned to the correction factor in order to establish the correct heat balance; these may be obtained from eqns. (7*c*) and (7*d*).

However, for times greater than 0·5 sec, an approximate value can be obtained on the assumption that

$$\frac{8}{\pi^2}\sum_{n=1}^{\infty}\frac{(-1)^{n+1}T_s}{(2n-1)^2}\sin\frac{(2n-1)\pi x}{2l}\left\{1-\exp\left[-\frac{\lambda t}{2}-\frac{Kt}{2}\frac{(2n-1)^2\pi^2}{4l^2}\right]\right\}$$

is approximately a straight-line function. θ_l', at any particular time t, will be given by

$$\int_0^{l_1} A_1c\rho(\theta_{1t} - \theta_l')\frac{x_1}{l_1}dx = \int_0^{l_2} A_2c\rho(\theta_l' - \theta_{2t})\frac{x_2}{l_2}dx$$

θ_{1t} and θ_{2t} may be obtained from eqns. (7*a*) and (7*b*), and

$$\theta_l' = \frac{A_1l_1\theta_{1t} + A_2l_2\theta_{2t}}{A_1l_1 + A_2l_2} \quad . \quad . \quad . \quad . \quad . \quad (7e)$$

whence

$$\theta_l' = \sum_{n=1}^{\infty}\frac{8}{\pi^2}\frac{(-1)^{n+1}T_s}{(2n-1)^2}\sin\frac{(2n-1)\pi}{2}\left\{1-\exp\left[-\frac{\lambda_1 t'}{2}-\frac{Kt'}{2}\frac{(2n-1)^2\pi^2}{4l_1^2}\right]\right\}$$

or

$$\theta_l' = \sum_{n=1}^{\infty}\frac{8}{\pi^2}\frac{(-1)^{n+1}T_s}{(2n-1)^2}\sin\frac{(2n-1)\pi}{2}\left\{1-\exp\left[-\frac{\lambda_2 t''}{2}-\frac{Kt''}{2}\frac{(2n-1)^2\pi^2}{4l_2^2}\right]\right\} \quad . \quad (7f)$$

Thus t' and t'' may be evaluated.

The final value of the instantaneous temperature, θ_{xt}, will be

$$\theta_{x1t} = \sum_{n=1}^{\infty}\frac{4b_1l_1^2\mu_1^2\sin\frac{(2n-1)\pi x_1}{l_1}}{\pi(2n-1)[(2n-1)^2\pi^2 + \mu_1^2l_1^2]}\left\{1-\exp\left[-\frac{\lambda_1 t}{2}-\frac{Kt}{2}\frac{(2n-1)^2\pi^2}{l_1^2}\right]\right\} + \sum_{n=1}^{\infty}\frac{8}{\pi^2}\frac{(-1)^{n+1}T_s}{(2n-1)^2}\sin\frac{(2n-1)\pi x_1}{2l_1}\left\{1-\exp\left[-\frac{\lambda_1 t'}{2}-\frac{Kt'}{2}\frac{(2n-1)^2\pi^2}{4l_1^2}\right]\right\} \quad . \quad . \quad (8a)$$

and

$$\theta_{x2t} = \sum_{n=1}^{\infty}\frac{4b_2l_2^2\mu_2^2\sin\frac{(2n-1)\pi x_2}{l_2}}{\pi(2n-1)[(2n-1)^2\pi^2 + \mu_2^2l_2^2]}\left\{1-\exp\left[-\frac{\lambda_2 t}{2}-\frac{Kt}{2}\frac{(2n-1)^2\pi^2}{l_2^2}\right]\right\}$$

$$+ \sum_{n=1}^{\infty} \frac{8}{\pi^2} \frac{(-1)^{n+1} T_s}{(2n-1)^2} \sin \frac{(2n-1)\pi x_2}{2l_2}$$

$$\left\{1 - \exp\left[-\frac{\lambda_2 t''}{2} - \frac{Kt''}{2} \frac{(2n-1)^2\pi^2}{4l_2^2}\right]\right\} \quad . \quad (8b)$$

(2.3) Expulsion Fuse Element with Restricted Section and Double Discontinuity

The argument above may be extended to the more complex case of a fuse having a cross-section as shown in Fig. 3(*b*). This section, cut from tin strip, is closely analogous to a fuse element in widespread use shown in Fig. 3(*c*). It should be noted, however, that the wire element in Fig. 3(*c*) appears in normal manufactured form as an h.r.c. fuse enclosed in a silica-type filler, and not normally in free air or semi-enclosed.

The general equations are again given by eqns. (1) and (2*a*). At the point of discontinuity, $T_1 = T_2 = T_s$.

$$\left.\begin{aligned} T_1 &= T_s \text{ at } x_1 = 0 \\ T_1 &= T_s \text{ at } x_1 = l_1 \end{aligned}\right\} \quad . \quad . \quad . \quad . \quad . \quad (9a)$$

$$\left.\begin{aligned} T_2 &= 0 \text{ at } x_2 = 0 \\ T_2 &= T_s \text{ at } x_2 = l_2 \end{aligned}\right\} \quad . \quad . \quad . \quad . \quad . \quad (9b)$$

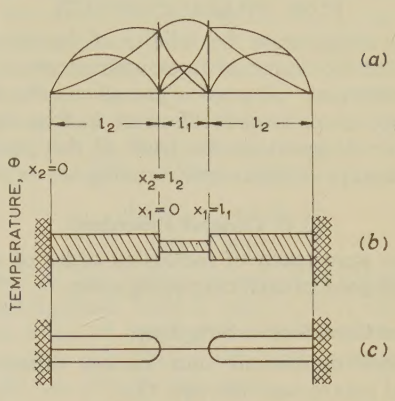

Fig. 3.—Fuse element with double discontinuity.

(*a*) Pattern of temperature distribution along the fuse.
(*b*) Strip element.
(*c*) Element composed of three wires.

Applying this condition after differentiating eqns. (10) and (11),

$$T_s = \frac{b_1\mu_1(1 - \cosh \mu_1 l_1) \operatorname{cosech} \mu_1 l_1 + b_2\mu_2 \frac{A_2}{A_1}(1 - \cosh \mu_2 l_2) \operatorname{cosech} \mu_2 l_2}{\mu_1 \operatorname{cosech} \mu_1 l_1 - \mu_1 \coth \mu_1 l_1 - \frac{A_2}{A_1}\mu_2 \coth \mu_2 l_2} \quad . \quad . \quad . \quad . \quad . \quad . \quad . \quad (12)$$

From eqns. (2*a*) and (9*b*),

$$T_{x2} = b_2\left[1 - \frac{\sinh \mu_2 x_2 + \sinh \mu_2(l_2 - x_2)}{\sinh \mu_2 l_2}\right] + T_s \frac{\sinh \mu_2 x_2}{\sinh \mu_2 l_2} \quad . \quad . \quad . \quad . \quad (10)$$

Eqn. (10) may be expressed in terms of a sine series:

$$T_{x2} = \sum_{n=1}^{\infty} \frac{4b_2\mu_2^2 l_2^2}{(2n-1)\pi[(2n-1)^2\pi^2 + \mu_2^2 l_2^2]} \sin \frac{(2n-1)\pi x_2}{2l_2}$$

$$+ \sum_{n=1}^{\infty} \frac{(-1)^{n+1} 8 T_s c_2 \mu_2 l_2}{(2n-1)^2\pi^2 + 4\mu_2^2 l_2^2} \sin \frac{(2n-1)\pi x_2}{2l_2} \quad . \quad (10a)$$

where $c_2 = 1/\tanh \mu_2 l_2$.

From eqns. (2*a*) and (9*a*),

$$T_{x1} = b_1\left[1 - \frac{\sinh \mu_1 x_1 + \sinh \mu_1(l_1 - x_1)}{\sinh \mu_1 l_1}\right]$$

$$+ T_s \frac{\sinh \mu_1 x_1 + \sinh \mu_1(l_1 - x_1)}{\sinh \mu_1 l_1} \quad . \quad (11)$$

Eqn. (11) may be expressed in terms of a sine series:

$$T_{x1} = \sum_{n=1}^{\infty} \frac{4b_1\mu_1^2 l_1^2}{(2n-1)\pi[(2n-1)^2\pi^2 + \mu_1^2 l_1^2]} \sin \frac{(2n-1)\pi x_1}{l_1}$$

$$+ \sum_{n=1}^{\infty} \frac{(-1)^{n+1} 8 T_s c_1 \mu_1 l_1}{(2n-1)^2\pi^2 + 4\mu_1^2 l_1^2}$$

$$\left[\sin \frac{(2n-1)\pi x_1}{2l_1} + \sin \frac{(2n-1)\pi(l_1 - x_1)}{2l_1}\right] \quad . \quad (11a)$$

where $c_1 = 1/\tanh \mu_1 l_1$.

To find the value of T_s at $x_2 = l_2$, $x_1 = 0$, as before,[5]

$$A_2 \frac{dT_2}{dx_2} = A_1 \frac{dT_1}{dx_1}$$

where x_1 and x_2 are both measured in the same direction, as shown in Fig. 3.

From eqns. (10*a*) and (11*a*), in the same manner as described in Section 2.2, the instantaneous temperature becomes

$$\theta_{x1t} = \sum_{n=1}^{\infty} \frac{4b_1\mu_1^2 l_1^2 \sin \frac{(2n-1)\pi x_1}{l_1}}{\pi(2n-1)[(2n-1)^2\pi^2 + \mu_1^2 l_1^2]}$$

$$\left\{1 - \exp\left[-\frac{\lambda_1 t}{2} - \frac{Kt}{2} \frac{(2n-1)^2\pi^2}{l_1^2}\right]\right\}$$

$$+ \sum_{n=1}^{\infty} \frac{(-1)^{n+1} 8 T_s c_1 \mu_1 l_1}{(2n-1)^2\pi^2 + 4\mu_1^2 l_1^2} \sin \frac{(2n-1)\pi(l_1 - x_1)}{2l_1}$$

$$\left\{1 - \exp\left[-\frac{\lambda_1 t'}{2} - \frac{Kt'}{2} \frac{(2n-1)^2\pi^2}{4l_1^2}\right]\right\}$$

$$+ \sum_{n=1}^{\infty} \frac{(-1)^{n+1} 8 T_s c_1 \mu_1 l_1}{(2n-1)^2\pi^2 + 4\mu_1^2 l_1^2} \sin \frac{(2n-1)\pi x_1}{2l_1}$$

$$\left\{1 - \exp\left[-\frac{\lambda_1 t'}{2} - \frac{Kt'}{2} \frac{(2n-1)^2\pi^2}{4l_1^2}\right]\right\} \quad . \quad . \quad (13)$$

and

$$\theta_{x2t} = \sum_{n=1}^{\infty} \frac{4b_2\mu_2^2 l_2^2 \sin \frac{(2n-1)\pi x_2}{l_2}}{\pi(2n-1)[(2n-1)^2\pi^2 + \mu_2^2 l_2^2]}$$

$$\left\{1 - \exp\left[-\frac{\lambda_2 t}{2} - \frac{Kt}{2} \frac{(2n-1)\pi^2}{l_2^2}\right]\right\}$$

$$+ \sum_{n=1}^{\infty} \frac{(-1)^{n+1} 8 T_s c_2 \mu_2 l_2}{(2n-1)^2\pi^2 + 4\mu_2^2 l_2^2} \sin \frac{(2n-1)\pi x_2}{2l_2}$$

$$\left\{1 - \exp\left[-\frac{\lambda_2 t''}{2} - \frac{Kt''}{2} \frac{(2n-1)^2\pi^2}{4l_2^2}\right]\right\} \quad . \quad (14)$$

(3) PROCEDURE FOR NUMERICAL DERIVATION OF FUSE CHARACTERISTICS

In order to demonstrate the validity of the equations above, a procedure for the design of fuses with chosen characteristics has been established. Examples are given, the fuse material being tin strip, either semi-enclosed or in free air. After the fuses had been designed on the basis of this procedure, their characteristics were verified experimentally.

(3.1) General Procedure

Three cases were taken of increasing order of difficulty, the procedures adopted in each case being given.

(3.1.1) Uniform-Cross-Section Strip Fuse.

(*a*) Substitute dimensions and known values of material constants and parameters into eqn. (3).

(*b*) Equate eqn. (3) to the melting temperature of the material employed as the fuse element.

(*c*) Substitute various values of time from $t = 0{\cdot}05$ to 20 sec into eqn. (3) and thence evaluate the corresponding values of current, I.

(*d*) A plot of I against corresponding values of t will give the current/time characteristic of the fuse.

(3.1.2) Fuse of Restricted Cross-Section with a Single Discontinuity.

(*a*) Substitute the dimensions and known values of the material constants and parameters to evaluate a_1, a_2, λ_1, λ_2, b_1, b_2, μ_1 and μ_2.

(*b*) Substitute the values from (*a*) into eqn. (5) in order to obtain the steady-state temperature at the point of change of cross-section.

(*c*) Determine, from eqn. (6), the point where the minimum fusing current breaks the fuse.

(*d*) The minimum fusing current can be found from eqn. (4*a*) after substituting the values obtained [from (*a*)] and the distance x [from (*c*)] to the point where the minimum fusing current breaks the fuse; now, by equating eqn. (4*a*) to the melting temperature of the material used for the fuse element, the minimum fusing current can be found.

(*e*) From eqns. (8*a*) and (8*b*), the currents corresponding the various pre-arcing times can be found; the simplest way of doing this is to solve graphically by considering, say, the points $(\frac{1}{2}l_1, \frac{3}{4}l_1, l_1)$ and $(\frac{1}{2}l_2, \frac{3}{4}l_2, l_2)$.

(*f*) After dividing eqns. (8*a*) and (8*b*) each into two parts, substitute values of t from 0·02 to 20 sec. Evaluate the temperatures (due to each part of the divided equations) for different distances, as in (*e*).

(*g*) Find an approximate value, from eqn. (7*e*), of θ_l', the instantaneous temperature at the point of discontinuity.

(*h*) Find an accurate value of θ_l', from the first parts of eqns. (7*c*) and (7*d*).

(*i*) The rises of temperature at points $(\frac{1}{2}l_1, \frac{3}{4}l_1, l_1)$ and $(l_2, \frac{3}{4}l_2, \frac{1}{2}l_2)$, corresponding to the second parts of eqns. (8*a*) and (8*b*), may now be tabulated or plotted.

(*j*) The rises in temperature from (*i*), when added to the temperature rises for the first parts of eqns. (8*a*) and (8*b*), give a final accurate value of the temperature rise.

(*k*) For any given time t find graphically the product of the maximum temperature times I^2, and equate this to the melting temperature; then determine the correspondence between I and t, and plot the I/t characteristic; as a check this characteristic may be compared experimentally by testing a fuse of the material and geometry assumed above.

(3.1.3) Fuse of Restricted Cross-Section with Double Discontinuity

(*a*) Evaluate a_1, a_2, λ_1, λ_2, b_1, b_2, μ_1 and μ_2 as before.

(*b*) Substitute from (*a*) into eqn. (12) to obtain the steady-state temperature at the change of cross-section.

(*c*) From eqn. (11) find the minimum fusing current for this type of fuse; the breaking point will be at $\frac{1}{2}l$. Equate eqn. (11) to the melting temperature and find the corresponding current which will be the minimum fusing current.

(*d*) From eqn. (13) evaluate θ_{1t} for the distances $x_1 = 0$ and $x_1 = \frac{1}{2}l_1$ along the fuse; evaluate also θ_{2t} for the distance $x_2 = l_2$.

(*e*) Determine the value of θ_l' as indicated in Section 3.1.2 (*g*) and (*h*).

(*f*) Plot the relationship between $\theta_{1t}(x_1 = 0)$, $\theta_{1t}(x_1 = \frac{1}{2}l_1)$, $\theta_{2t}(x_2 = l_2)$ and θ_l', and evaluate the second and third parts of eqn. (13).

(*g*) Evaluate θ_{1t} for the point $x_1 = \frac{1}{2}l_1$ in the first part of eqn. (13).

(*h*) Add the first part of eqn. (13) to the second and third parts of eqn. (13) and equate the sum to the melting temperature.

(*i*) As in Section 3.1.2 (*k*) determine the correspondence between current and time, plot the I/t characteristic, and check.

(3.2) Data for the Material used in the Fuse Experiments and Analysis

The material used throughout the experiments and analysis was pure solid white tin[4] of 0·013 cm thickness. From the Smithsonian physical Tables, the numerical values of the various quantities used in the calculations were: $k = 0{\cdot}142$, $c = 0{\cdot}055$, $\rho = 7{\cdot}18$, $H_{air} = 5{\cdot}25 \times 10^{-5}$, $\sigma = 1/18{\cdot}2 \times 10^{-6}$, $J = 1/0{\cdot}239$, melting-point of tin = 232° C and $K = k/c\rho = 0{\cdot}359$.

(3.3) Derivation of the Characteristic of a Strip Fuse

The length and width of the specimen strip fuses were 2·032 and 0·343 cm, respectively. Following the general procedure of Section 3.1.1, and taking the ambient temperature as 10° C, substitution in eqn. (3) gives

$$222 = 8{\cdot}49I^2 \sum_{n=1}^{\infty} \frac{\sin \dfrac{(2n-1)\pi}{2}}{(2n-1)[(2n-1)^2\pi^2 + 0{\cdot}249]} \{1 - \exp[-0{\cdot}011t - (2n-1)^2 0{\cdot}428t]\}$$

By substituting various values of t from 0·05 to 20 sec into this equation, evaluating the corresponding currents and checking experimentally, the results of Table 1 are obtained.

Table 1

From calculation		From test	
Time	Current	Pre-arcing time	Current
sec	amp	sec	amp
0·05	129·2	0·062	110·0
0·1	87·0	0·164	73·0
0·2	64·2	0·49	40·5
0·5	39·25	1·30	28·0
1·0	28·75	5·0	19·8
2·0	21·8	20·0	17·0
5·0	17·5	—	16·5
10·0	16·6		(m.f.c.)
20·0	16·55		

Comparison between these results is illustrated in Fig. 4.

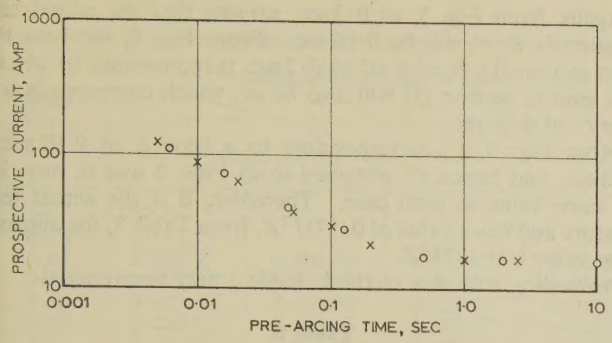

Fig. 4.—Comparison of characteristics of a single strip fuse obtained by numerical derivation and by experiment.

○ Test results.
× Calculation.

Thence from Section 3.1.2(*e*) and (*f*), by dividing eqns. (8*a*) and (8*b*) each into two parts, taking ($\frac{1}{2}l_1$, $\frac{3}{4}l_1$, l_1) and ($\frac{1}{2}l_2$, $\frac{3}{4}l_2$, l_2) as the parameters of x_1 and x_2, respectively, and putting $Z = 8T_s/\pi^2$, the temperatures at various times can be found for each end of the fuse. It should be noted that, with this type of fuse, the breaking point varies for different currents.

From Section 3.1.2(*g*), an approximation to the instantaneous temperature θ_l' at the point of discontinuity is given by

$$\theta_l' = \frac{A_1 l_1 \theta_{1t} + A_2 l_2 \theta_{2t}}{A_1 l_1 + A_2 l_2}$$

Table 3 gives θ_l', for various values of t, obtained by substituting θ_{1t} and θ_{2t} from Table 2, when $x_1 = l_1$ and $x_2 = l_2$.

An accurate value of θ_l' may now be found from the first parts of eqns. (7*c*) and (7*d*) which each represent the heat generated in the fuse without any losses.

Table 2

Time	Temperature θ_{1t}						Temperature θ_{2t}					
	1st part of eqn. (8*a*)			2nd part of eqn. (8*b*)			1st part of eqn. (8*a*)			2nd part of eqn. (8*b*)		
	$\frac{1}{2}l_1$	$\frac{3}{4}l_1$	l_1	$\frac{1}{2}l_1$	$\frac{3}{4}l_1$	l_1	$\frac{1}{2}l_2$	$\frac{3}{4}l_2$	l_2	$\frac{1}{2}l_2$	$\frac{3}{4}l_2$	l_2
sec												
0·02	$0·022I^2$	—	0	$0·007I^2Z$	$0·019I^2Z$	$0·164I^2Z$	—	—	—	—	—	—
0·05	$0·052I^2$	$0·045I^2$	0	$0·014I^2Z$	$0·067I^2Z$	$0·260I^2Z$	$0·013I^2$	$0·013I^2$	0	$0·003I^2Z$	—	$0·057I^2Z$
0·10	$0·093I^2$	$0·074I^2$	0	$0·046I^2Z$	$0·146I^2Z$	$0·368I^2Z$	$0·029I^2$	$0·029I^2$	0	$0·005I^2Z$	—	$0·093I^2Z$
0·20	$0·143I^2$	$0·109I^2$	0	$0·126I^2Z$	$0·276I^2Z$	$0·520I^2Z$	$0·054I^2$	$0·054I^2$	0	$0·007I^2Z$	$0·011I^2Z$	$0·132I^2Z$
0·50	$0·187I^2$	$0·140I^2$	0	$0·326I^2Z$	$0·544I^2Z$	$0·812I^2Z$	$0·144I^2$	$0·131I^2$	0	$0·012I^2Z$	$0·041I^2Z$	$0·211I^2Z$
1	$0·193I^2$	$0·145I^2$	0	$0·497I^2Z$	$0·768I^2Z$	$1·060I^2Z$	$0·267I^2$	$0·224I^2$	0	$0·027I^2Z$	$0·096I^2Z$	$0·301I^2Z$
2	$0·193I^2$	$0·145I^2$	0	$0·600I^2Z$	$0·903I^2Z$	$1·201I^2Z$	$0·465I^2$	$0·364I^2$	0	$0·076I^2Z$	$0·196I^2Z$	$0·427I^2Z$
5	$0·193I^2$	$0·145I^2$	0	$0·623I^2Z$	$0·903I^2Z$	$1·230I^2Z$	$0·720I^2$	$0·544I^2$	0	$0·232I^2Z$	$0·419I^2Z$	$0·678I^2Z$
10	$0·193I^2$	$0·145I^2$	0	$0·623I^2Z$	$0·933I^2Z$	$1·233I^2Z$	$0·803I^2$	$0·603I^2$	0	$0·407I^2Z$	$0·691I^2Z$	$0·926I^2Z$
20	—	—	—	—	—	—	$0·813I^2$	$0·611I^2$	0	$0·556I^2Z$	$0·844I^2Z$	$1·140I^2Z$
50	—	—	—	—	—	—	$0·813I^2$	$0·611I^2$	0	$0·620I^2Z$	$0·929I^2Z$	$1·230I^2Z$

(3.4) Characteristic of a Fuse of Restricted Cross-Section with a Single Discontinuity

Referring to Fig. 1, the data and derived values for this case are:

$l_1 = 0·508$ cm
$l_2 = 2·032$ cm
$p_1 = 0·381$ cm
$p_2 = 0·711$ cm
$K = K_1 = K_2 = k/c\rho = 0·359$
$c = 0·055$
$\rho = 7·18$
$J = 1/0·239$
$k = 0·142$
$H = 5·25 \times 10^{-5}$

$\sigma = 1/18·2 \times 10^{-6}$
$a_1 = I^2/JA_1^2\rho c\sigma = 2·16I^2$
$a_2 = 0·58I^2$
$\lambda_1 = Hp_1/A_1\rho c = 2·24 \times 10^{-2}$
$\lambda_2 = 2·17 \times 10^{-2}$
$\mu_1 = \sqrt{(\lambda_1/K)} = 0·249$
$\mu_2 = 0·246$
$b_1 = a_1/\lambda_1 = 96·33I^2$
$b_2 = 26·75I^2$

Substituting into eqn. (5), to obtain the steady-state temperature at the point of change of cross-section, $T_s = 1·53I^2$. From eqn. (6) to find the point where the minimum fusing current breaks the fuse,

$$x_1 = \frac{y_1}{2\mu_1} \text{ and } \exp y_1 = \frac{\exp(\mu_1 l_1) - Q_1}{Q_1 - \exp(-\mu_1 l_1)}$$

where $Q_1 = 1 - T_s/b_1$, $x_2 = y_2/2\mu_2$, etc.

These relationships give $x_1 = 0·56$ cm and $x_2 = 1·51$ cm.

Following the procedure of Section 3.1.2(*d*), substitution of $x_2 = 1·51$ cm into eqn. (4*a*) gives

$$232 - 10 = 26·75I^2 \times 0·06$$

i.e. $I = 11·8$ amp minimum fusing current.

Table 3

Time	Approximate instantaneous temperature, θ_t
sec	
0·2	$0·177I^2Z$
0·5	$0·280I^2Z$
1	$0·387I^2Z$
2	$0·516I^2Z$
5	$0·741I^2Z$
10	$0·961I^2Z$
20	$1·149I^2Z$
50	$1·230I^2Z$

Thus

$$\text{Heat}_1 = \frac{8}{\pi^2}\int_0^{l_1} \sum_{n=1}^{\infty} \frac{(-1)^{n+1}T_s}{(2n-1)^2} \sin\frac{(2n-1)\pi x_1}{2l_1} \left\{1 - \exp\left[-\frac{\lambda_1 t}{2} - \frac{Kt}{2}\frac{(2n-1)^2\pi^2}{4l_1^2}\right]\right\}$$

$$\text{Heat}_2 = \frac{A_2 l_2}{A_1 l_1}\frac{8}{\pi^2}\int_0^{2} \sum_{n=1}^{\infty} \frac{(-1)^{n+1}T_s}{(2n-1)^2} \sin\frac{(2n-1)\pi x_2}{2l_2} \left\{1 - \exp\left[-\frac{t\lambda_2}{2} - \frac{Kt}{2}\frac{(2n-1)^2\pi^2}{4l_2^2}\right]\right\}$$

Substituting $T_s = 1·53I^2$ and $A_2 l_2/A_1 l_1 = 7·86$, the results of Table 4 are obtained.

As an illustration, θ_l' corresponding to 0·2 sec will be found using the second parts of eqns. (8*a*) and (8*b*) from Table 2. The values from Table 2 are plotted in Figs. 5 and 7; those from Table 4 are plotted in Fig. 6. From Fig. 5, at 0·2 sec,

Table 4

Time	Heat$_1$	Heat$_2$
sec		
0·02	$0·009I^2Z$	—
0·05	$0·024I^2Z$	$0·051I^2Z$
0·1	$0·044I^2Z$	$0·099I^2Z$
0·2	$0·085I^2Z$	$0·198I^2Z$
0·5	$0·177I^2Z$	$0·491I^2Z$
1·0	$0·256I^2Z$	$0·964I^2Z$
2·0	$0·303I^2Z$	$1·840I^2Z$
5·0	$0·313I^2Z$	$4·210I^2Z$
10·0	$0·314I^2Z$	$4·220I^2Z$

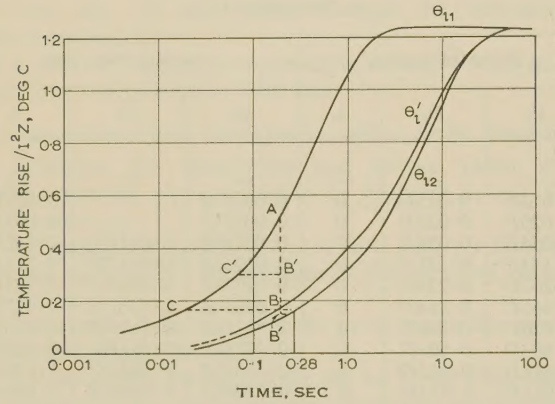

Fig. 5.—Graphical determination of temperature rise at the discontinuity.

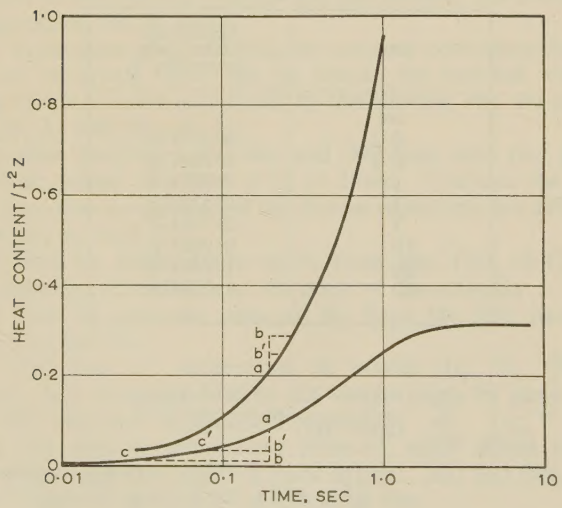

Fig. 6.—Heat content.

assume the actual temperature to be B′; t' will be 0·07 sec. From Fig. 6, the heat loss from section (1), from 0·07 to 0·2 sec, will be represented by ab'; the heat gain in section (2) will also be ab' which corresponds to a time t'' of 0·24 sec.

From Fig. 5, t'', corresponding to a time t' of 0·07 sec, is 0·92 sec. The time t'' obtained from Figs. 5 and 6 is not the same in each case; hence B' is not the correct actual temperature.

Again, from Fig. 5, at 0·2 sec, assume that the actual temperature is B; t' will be 0·02 sec. From Fig. 6, the heat loss from section (1), from 0·02 to 0·2 sec, is represented by ab; the heat gain in section (2) will also be ab, which corresponds to a time t'' of 0·28 sec.

From Fig. 5, t'' corresponding to a time t' of 0·02 sec is 0·28 sec, and hence t'', obtained from Figs. 5 and 6, now has the same value in each case. Therefore, B is the actual temperature and has a value of $0·173I^2Z$; from Table 3, the approximate value is $0·177I^2Z$.

Proceeding with this method, Table 5 may be prepared.

Table 5

Time	θ_l'
sec	
0·2	$0·173I^2Z$
0·1	$0·105I^2Z$
0·05	$0·065I^2Z$

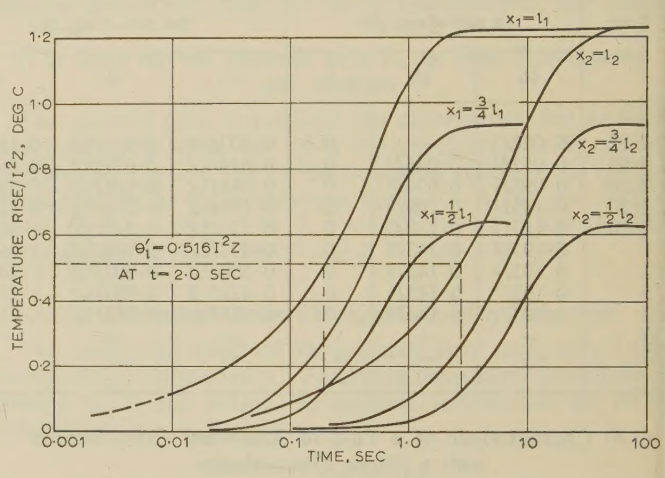

Fig. 7.—Temperature rises at intermediate distances along the fuse with single discontinuity.

From Tables 3 and 5, plotted in Fig. 7, the temperature rise at the points ($\frac{1}{2}l_1$, $\frac{3}{4}l_1$, l_1) and ($\frac{1}{2}l_2$, $\frac{3}{4}l_2$, l_2) corresponding to the second part of eqns. (8*a*) and (8*b*) will now be known.

The method of obtaining Table 6 is illustrated by Fig. 7 at 2 sec, θ_t from Table 3 is $0·516I^2Z$, the corresponding temperature at $\frac{3}{4}l_1$ (from Fig. 7) will be $0·28I^2Z$, and $0·12I^2Z$ at $\frac{1}{2}l_1$, etc.

The following Table of temperature rise, for the second part of eqns. (8*a*) and (8*b*) when added to the temperature rise for

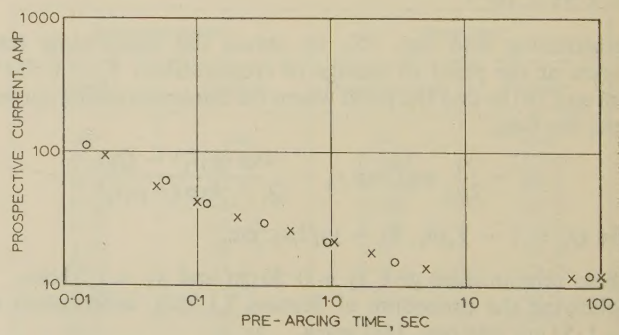

Fig. 8.—Comparison of characteristics of a fuse with single discontinuity obtained by numerical derivation and by experiment.

○ Test results.
× Calculation.

Table 6

Actual time	Temperature θ'_t from 2nd part of eqns. (8*a*) and (8*b*)					$\theta_{t\,max} = XI^2$	Corresponding current, $\sqrt{\frac{222}{X}}$	Current	Time
	at l_1 and l_2	at $\frac{1}{2}l_1$	at $\frac{3}{4}l_1$	at $\frac{1}{2}l_2$	at $\frac{3}{4}l_2$	By combination with the first part of eqns. (8*a*) and (8*b*)		By test	
sec							amp	amp	sec
0·02	—	—	—	—	—	$0{\cdot}025I^2$	95·0		
0·05	$0{\cdot}06I^2Z$	$0{\cdot}005I^2Z$	$0{\cdot}01I^2Z$	$0{\cdot}003I^2Z$	$0{\cdot}005I^2Z$	$0{\cdot}075I^2$	54·5	110·0	0·0149
0·10	$0{\cdot}105I^2Z$	$0{\cdot}007I^2Z$	$0{\cdot}015I^2Z$	$0{\cdot}005I^2Z$	$0{\cdot}01I^2Z$	$0{\cdot}131I^2$	41·0	60·0	0·059
0·20	$0{\cdot}172I^2Z$	$0{\cdot}009I^2Z$	$0{\cdot}02I^2Z$	$0{\cdot}015I^2Z$	$0{\cdot}02I^2Z$	$0{\cdot}216I^2$	32·0	41·0	0·120
0·50	$0{\cdot}280I^2Z$	$0{\cdot}02I^2Z$	$0{\cdot}09I^2Z$	$0{\cdot}02I^2Z$	$0{\cdot}09I^2Z$	$0{\cdot}350I^2$	25·2	29·0	0·320
1	$0{\cdot}387I^2Z$	$0{\cdot}06I^2Z$	$0{\cdot}075I^2Z$	$0{\cdot}06I^2Z$	$0{\cdot}16I^2Z$	$0{\cdot}500I^2$	21·0	20·5	0·96
2	$0{\cdot}516I^2Z$	$0{\cdot}12I^2Z$	$0{\cdot}28I^2Z$	$0{\cdot}12I^2Z$	$0{\cdot}27I^2Z$	$0{\cdot}670I^2$	18·0	15·0	3·0
5	$0{\cdot}741I^2Z$	$0{\cdot}275I^2Z$	$0{\cdot}475I^2Z$	$0{\cdot}281I^2Z$	$0{\cdot}48I^2Z$	$1{\cdot}150I^2$	13·8	12·1	80·0
10	$0{\cdot}96I^2Z$	$0{\cdot}43I^2Z$	$0{\cdot}7I^2Z$	$0{\cdot}44I^2Z$	$0{\cdot}68I^2Z$	—	—		
20	$1{\cdot}149I^2Z$	$0{\cdot}565I^2Z$	$0{\cdot}86I^2Z$	$0{\cdot}57I^2Z$	$0{\cdot}865I^2Z$	—	—		
50	$1{\cdot}233I^2Z$	$0{\cdot}62I^2Z$	$0{\cdot}93I^2Z$	$0{\cdot}62I^2Z$	$0{\cdot}93I^2Z$	$1{\cdot}60I^2$	11·8		
time for m.f.c.	—	—	—	—	—	$1{\cdot}60I^2$	11·8	12 (m.f.c.)	time for m.f.c.

$Z = 8T_s/\pi^2 = 1{\cdot}25$. Melting temperature = 222° C.
M.F.C. Minimum fusing current.

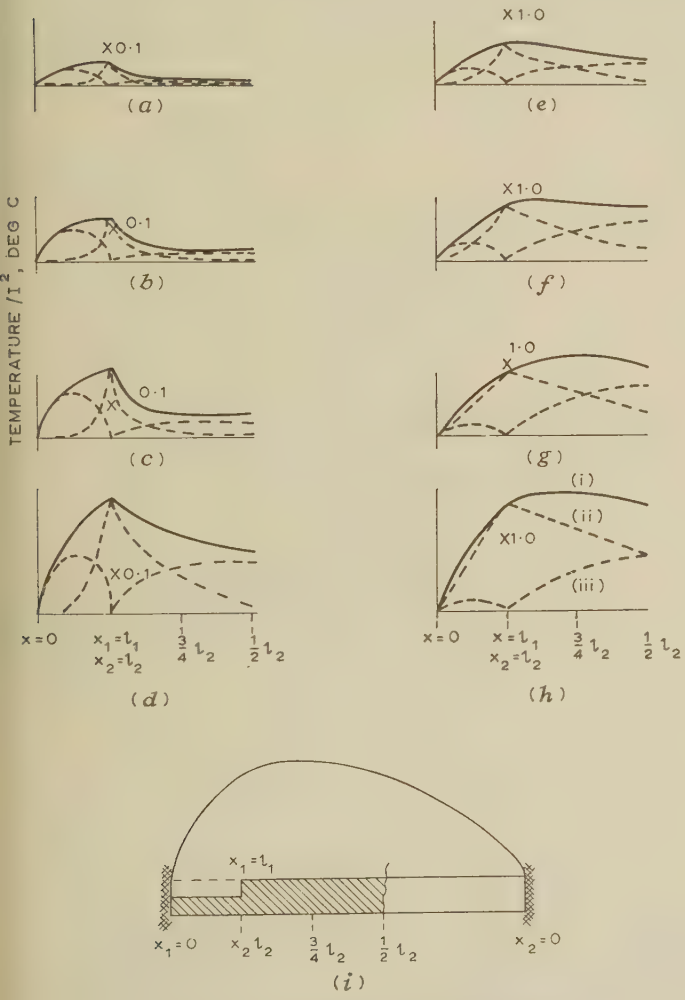

Fig. 9.—Approximate instantaneous temperature distribution along a strip fuse with a single discontinuity.

(*a*) $t = 0{\cdot}05$ sec.
(*b*) $t = 0{\cdot}1$ sec.
(*c*) $t = 0{\cdot}2$ sec.
(*d*) $t = 0{\cdot}5$ sec.
(*e*) $t = 1$ sec.
(*f*) $t = 2$ sec.
(*g*) $t = 5$ sec.
(*h*) $t = 0{\cdot}5$ sec.
(i) Combined temperature.
(ii) From Table 6.
(iii) From Table 2.
(*i*) Steady-state temperature distribution with minimum fusing current.

the first part of eqns. (8*a*) and (8*b*) (Table 2) will give the final temperature rise.

Fig. 8 illustrates graphically the correlation between the predicted and experimentally determined fuse characteristic, both from Table 6. An approximate instantaneous temperature distribution along the fuse is shown in Fig. 9.

(3.5) Characteristic of a Fuse of Restricted Cross-Section with a Double Discontinuity

As a further example, the characteristic of an expulsion fuse with a restricted section in its middle and hence a double discontinuity will be found numerically. The fuse-element shape is shown in Fig. 10, and the dimensions chosen were as follows:

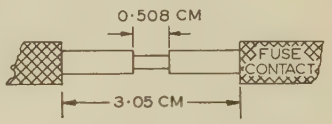

Fig. 10.—Fuse element with double discontinuity.

Length = 3·05 cm
Width = 0·381 cm
Neck width (width of restricted section) = 0·127 cm
Neck length = 0·508 cm

The dimensions, data and derived values, where different from the case considered in Section 3.4, are as follows:

$l_1 = 0{\cdot}508$ cm
$l_2 = 1{\cdot}27$ cm
$p_1 = 0{\cdot}279$ cm
$p_2 = 0{\cdot}787$ cm
$a_1 = I^2/JA_1^2\rho c\sigma = 4{\cdot}234I^2$
$a_2 = 0{\cdot}470I^2$
$\lambda_1 = Hp_1/A_1c\rho = 0{\cdot}0230$
$\lambda_2 = 0{\cdot}0216$
$b_1 = a_1/\lambda_1 = 183{\cdot}85I^2$
$b_2 = 21{\cdot}75I^2$
$\mu_1^2 = \lambda_1/K = 0{\cdot}064$
$\mu_1 = 0{\cdot}253$
$\mu_2^2 = 0{\cdot}060$
$\mu_2 = 0{\cdot}245$

From eqn. (12)

$$T_s = \frac{[b_1\mu_1(1 - \cosh \mu_1 l_1) \operatorname{cosech} \mu_1 l_1 + b_2\mu_2\frac{A_2}{A_1}(1 - \cosh \mu_2 l_2) \operatorname{cosech} \mu_2 l_2]}{\mu_1 \operatorname{cosech} \mu_1 l_1 - \mu_1 \coth \mu_1 l_1 - \frac{A_2}{A_1}\mu_2 \coth \mu_2 l_2}$$

Substituting the values above, $T_s = 2{\cdot}226I^2$.

To find the minimum fusing current, substituting in eqn. (11),

$$222 = 183{\cdot}85I^2(1 - \operatorname{sech} \tfrac{1}{2}\mu_1 l_1) + 2{\cdot}226I^2 \operatorname{sech} \tfrac{1}{2}\mu_1 l_1$$
$$= 2{\cdot}599I^2$$

whence $I = 9{\cdot}25$ amp

From eqns. (13) and (14) at $x_1 = 0$ and $x_2 = l_2$ and time t, θ_l can now be found (see Section 3.4).

$$\theta_{1t} = 17{\cdot}91I^2 \sum_{\mu=1}^{\infty} \frac{1}{(2n-1)^2 9{\cdot}868 + 0{\cdot}0662} \left\{1 - \exp - t[0{\cdot}012 + 1{\cdot}719(2n-1)^2]\right\}$$

$$\theta_{2t} = 18{\cdot}38I^2 \sum_{n=1}^{\infty} \frac{1}{(2n-1)^2 9{\cdot}868 + 0{\cdot}389} \left\{1 - \exp - t[0{\cdot}011 + 0{\cdot}275(2n-1)^2]\right\}$$

These results are given in Table 7.

Table 7

Time	θ_{1t} $x_1 = 0$	θ_{1t} $x_1 = \frac{1}{2}l_1$	θ_{2t} $x_2 = l_2$	θ_l'
sec				
0·02	$0{\cdot}297I^2$	$0{\cdot}012\,5I^2$	$0{\cdot}123I^2$	$0{\cdot}141I^2$
0·05	$0{\cdot}469I^2$	$0{\cdot}024I^2$	$0{\cdot}193I^2$	$0{\cdot}226I^2$
0·10	$0{\cdot}663I^2$	$0{\cdot}082I^2$	$0{\cdot}273I^2$	$0{\cdot}319I^2$
0·20	$0{\cdot}938I^2$	$0{\cdot}227I^2$	$0{\cdot}387I^2$	$0{\cdot}452I^2$
0·50	$1{\cdot}466I^2$	$0{\cdot}588I^2$	$0{\cdot}610I^2$	$0{\cdot}711I^2$
1	$1{\cdot}904I^2$	$0{\cdot}897I^2$	$0{\cdot}862I^2$	$0{\cdot}985I^2$
2	$2{\cdot}169I^2$	$1{\cdot}085I^2$	$1{\cdot}213I^2$	$1{\cdot}33I^2$
5	$2{\cdot}225I^2$	$1{\cdot}124I^2$	$1{\cdot}8I^2$	$1{\cdot}85I^2$
10	$2{\cdot}226I^2$	$1{\cdot}125I^2$	$2{\cdot}123I^2$	$2{\cdot}135I^2$
time for m.f.c.	$2{\cdot}226I^2$	$1{\cdot}125I^2$	$2{\cdot}23I^2$	$2{\cdot}23I^2$

Taking the first part of eqn. (13),

$$\theta_{xt} = \sum_{n=1}^{\infty} \frac{4b_1\mu_1^2 l_1^2 \sin \dfrac{(2n-1)\pi x_1}{l_1}}{(2n-1)\pi[(2n-1)^2\pi^2 + \mu_1^2 l_1^2]} \left\{1 - \exp - \frac{t}{2}\left[\frac{\lambda_1 + K(2n-1)^2\pi^2}{l_1^2}\right]\right\}$$

and substituting the value for $x_1 = \frac{1}{2}l_1$, the relationship shown in Table 8 between θ_{1t} and time is obtained.

Table 8

Time	θ_{1t} $x_1 = \frac{1}{2}l_1$
sec	
0·02	$0{\cdot}043I^2$
0·05	$0{\cdot}103I^2$
0·1	$0{\cdot}182I^2$
0·2	$0{\cdot}28I^2$
0·5	$0{\cdot}366I^2$
1	$0{\cdot}37I^2$
2	$0{\cdot}378I^2$
5	$0{\cdot}38I^2$

In accordance with the procedure of Section 3.1.3(*h*), the results (Table 9) for the first part of eqn. (13) are combined with the second and third parts of the same equation using Table 7 and Fig. 11, for the point $x_1 = \frac{1}{2}l_1$ where the fuse breaks.

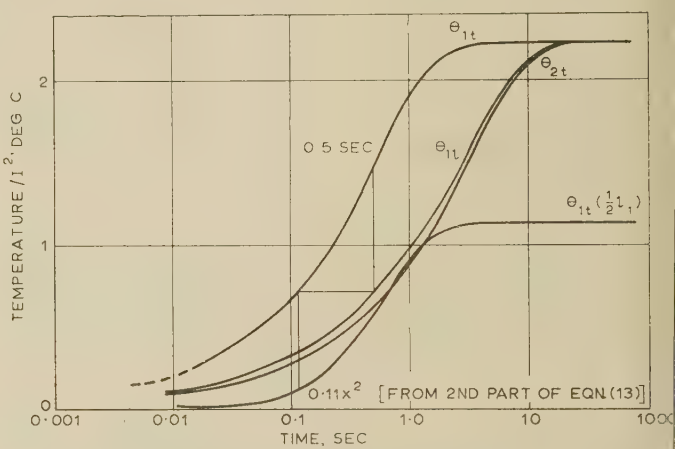

Fig. 11.—Graphical determination of temperature rise at a distance $\frac{1}{2}l$, for fuse with double discontinuity.

The comparison between the test results and the predicted results from numerical derivation are shown in Fig. 12.

(4) ALLOWANCE FOR VARIABLE ELECTRICAL AND THERMAL CONDUCTIVITIES

The electrical and thermal conductivities applied in the calculations and derivations above are average values betwee

Table 9

Time	θ_{1t} From eqn. (13) (1st part) and Table 8	θ_{1t} From eqn. (13) (2nd, 3rd part) Table 7, Fig. 11	Total temperature $= XI^2$	$I = \sqrt{\frac{222}{X}}$	Test results: Current	Test results: Time
sec				amp	amp	sec
0·01	$0{\cdot}022I^2$		$0{\cdot}022I^2$	100·1	165·0	0·005
0·02	$0{\cdot}042\,5I^2$	$0{\cdot}005I^2$	$0{\cdot}047\,5I^2$	68·5	81·0	0·016
0·05	$0{\cdot}103I^2$	$0{\cdot}01I^2$	$0{\cdot}113I^2$	44·5	51·0	0·045
0·10	$0{\cdot}182I^2$	$0{\cdot}027I^2$	$0{\cdot}209I^2$	32·6	35·0	0·090
0·20	$0{\cdot}279I^2$	$0{\cdot}044I^2$	$0{\cdot}323I^2$	26·2	23·6	0·250
0·50	$0{\cdot}366\,3I^2$	$0{\cdot}22I^2$	$0{\cdot}586I^2$	19·5	15·0	0·90
1	$0{\cdot}378I^2$	$0{\cdot}49I^2$	$0{\cdot}868I^2$	15·8	11·5	3·00
2	$0{\cdot}378I^2$	$0{\cdot}96I^2$	$1{\cdot}338I^2$	12·85		
5	$0{\cdot}38I^2$	$1{\cdot}68I^2$	$2{\cdot}06I^2$	10·38		
10	$0{\cdot}38I^2$	$2{\cdot}14I^2$	$2{\cdot}52I^2$	9·4		
time for m.f.c.	$0{\cdot}38I^2$	$2{\cdot}226I^2$	$2{\cdot}60I^2$	9·25	9·3	Time for m.f.c.

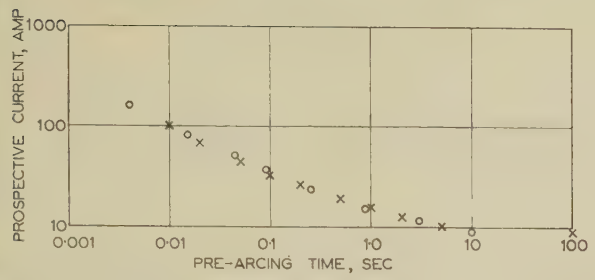

Fig. 12.—Comparison of characteristics of a fuse with double discontinuity obtained by numerical derivation and by experiment.

○ Test results
× Calculated.

room temperature and melting temperature. Eqns. (3), (8*a*) and (8*b*) give the transient temperature corresponding to various positions along the length of the fuse at various times; it should be noted that these equations are accurate only in respect of final derivations of the current/time characteristics and not for precise prediction of temperature distribution. It may readily be demonstrated that the use of average conductivities gives very similar results to the use of the appropriate temperature coefficients so far as these characteristics are concerned. Thus, from eqn. (1),

$$\frac{\partial\theta}{\partial t} = K\frac{\partial^2\theta}{\partial x^2} - \lambda\theta' + a_r(1 + \alpha\theta') \quad . \quad . \quad . \quad (15)$$

where $\theta' = \theta - \theta_0$.

α = Temperature coefficient of conductivity.

Solving eqn. (15), the transient temperature is

$$\theta = \frac{4M}{\pi}\sum_{n=1}^{\infty}\frac{Q^2l^2\sin\dfrac{(2n-1)\pi x}{l}}{(2n-1)[(2n-1)^2\pi^2 + l^2Q^2]}\left\{1 - \exp -\frac{t}{2}\left[\frac{K(2n-1)^2\pi^2}{2} + \lambda - \alpha a_r\right]\right\} \quad . \quad (16)$$

where

$$M = a_r/(\lambda - \alpha a_r)$$
$$Q^2 = (\lambda - \alpha a_r)/K$$
$$\alpha_{tin} = 0{\cdot}027\,75$$
$$1/\sigma_{tin/(10°C)} = 13{\cdot}36 \times 10^{-6}$$

Considering the example of Section 3.3, the results obtained from three methods of solution are shown in Table 10.

Table 10

Method of solution	Minimum fusing current
	amp
From eqn. (3), i.e. using average conductivity	16·55
From eqn. (16), i.e. using temperature coefficient of conductivity	16·58
Experimental	16·5

(5) CONCLUSIONS

It has been shown that semi-enclosed fuses can be given particular chosen characteristics by controlling their physical dimensions. Any particular characteristic may be predicted accurately by a method based on Straneo's work for determining thermal constants. The outline shapes of the fuses used were simple in that each fuse was of restricted cross-section for part of its length; suitable choice of the dimensions for the length and cross-section of each part of a particular fuse provided the means of controlling and predicting the characteristic.

The analytical approach to the prediction of the current/time fuse characteristics is supported by numerical solution of the equations. These solutions have been shown to be in accord with experimental tests to destruction of fuses manufactured in the laboratory workshop. The method of analysis which has been used is an improvement on those hitherto employed in that account has been taken of radial heat loss in addition to that conducted axially along the fuse; furthermore, restricted sections have been considered in addition to uniform-section fuses. It has not so far been found possible to determine experimentally the instantaneous distribution of temperature along a fuse element, and thereby to check the analytically derived results in this respect. Notwithstanding this deficiency, the temperature-distribution results are not likely to be greatly inaccurate, since very close correlation has been obtained between the analytically and experimentally derived current/time characteristics for the three main cases which have been considered.

An interesting supplementary point arises in connection with the values assigned to the resistivity of the fuse element. With tin—the material used in the paper—the resistance increases approximately twice from working to melting temperature: the investigation shows that the difference between the analytical result obtained by taking an assumed average value on the one hand and an initial value with temperature coefficient on the other is less than 1%. It is hoped to apply this theoretical analysis more generally in the future to embrace material with wider variations in resistivity, e.g. copper, and more complex ambient conditions. There does not appear to be any reason for thinking, in view of the results obtained by Guile[3] and Jaeger,[6] that either of these methods for dealing with the variable resistivity will be subject to appreciable error.

(6) ACKNOWLEDGMENTS

The authors wish to acknowledge the assistance of their colleague Mr. B. Horsley, and to express their gratitude for the facilities provided by the Electrical Engineering Department (Professor E. Bradshaw) of the Manchester College of Science and Technology for carrying out the work described in the paper.

(7) REFERENCES

(1) Schubert, G. U.: 'Heat Conduction Equation for Fuses', *Zeitschrift für angewandte Physik*, 1950, **2**, p. 174.
(2) Guile, A. E., and Carne, E. B.: 'An Analysis of an Analogue Solution applied to the Heat Conduction Problem in a Cartridge Fuse', *Transactions of the American I.E.E.*, 1954, **72**, Part I, p. 861.
(3) Guile, A. E.: 'The Calculation of the Complete Time/Current Characteristic of a Fuse', *ibid.*, 1955, **74**, p. 1108.
(4) 'Smithsonian Physical Tables', Smithsonian Society Collection, **63**, No. 6.
(5) Carslaw, H. S., and Jaeger, J. C.: 'Conduction of Heat in Solids' (Clarendon Press, 1947).
(6) Jaeger, J. C., and Newstead, G. H.: 'Transient Heating of Buried Cables', *Proceedings I.E.E.*, Monograph No. 253 S, August, 1957 (**105** C, p. 57).

621.372.6: 621.375.4

The Institution of Electrical Engineers
Monograph No. 388 E
July 1960

SIGNAL FLOW-GRAPH ANALYSIS AND FEEDBACK THEORY

By R. F. HOSKINS, M.Sc.

(*The paper was first received 8th September, 1959, and in revised form 13th January, 1960. It was published as an* INSTITUTION MONOGRAPH *in July, 1960.*)

SUMMARY

The solution of a system of simultaneous linear equations may be obtained by inspection of an associated system of nodes and connecting branches called a 'signal flow-graph'. This provides an alternative to conventional algebraic methods which is of particular interest in the case of network analysis, since the flow graph can be set up directly by inspection of the network without having to formulate the associated equations. In the paper the formal theory of flow-graph analysis is developed and applied to certain aspects of feedback theory, and it is shown that the classical results of Bode can be obtained and generalized relatively simply by this approach.

LIST OF SYMBOLS

Δ = General determinant of order n.
Δ' = Modified determinant occurring in the numerator of the general gain formula.
Δ_k = Residue of kth node.
Δ_{jk} = Residue of the branch going from the jth node to the kth node.
Δ_r^k = Graph determinant when the loop G_r^k is removed.
A_p = General open path.
A_{rm} = Open path from the rth node to the mth node.
D_k = Loop difference of the kth node.
D_{jk} = Loop difference of the branch from the jth node to the kth node.
D_W = Loop difference of the parameter W.
G = Graph gain.
G_r^k = Loop gain of the rth loop which passes through the kth node.
L_k = Loop gain of the kth node.
L_{jk} = Loop gain of the branch going from the jth node to the kth node.
S = Sensitivity.
S' = Relative sensitivity.
T_p = General loop of a determinant.
T_r^p = Loop which does not touch the open path A_p.
W = General parameter associated with a network.
W_0 = Value of W for which the graph gain is zero.
W' = $W - W_0$.
e^θ = Normal value of gain.
e^{θ_0} = Gain when $W = W_0$.
e^{θ_F} = Fractionated gain.

(1) INTRODUCTION

The analysis of a linear network reduces ultimately to the solution of a system of simultaneous linear equations. As an alternative to conventional algebraic methods it is possible to obtain a solution by considering the properties of a certain linear graph associated with the system which is called a 'flow graph'. The unknowns of the equations correspond to the nodes or vertices of the graph, while the linear relations between them appear in the form of directed branches connecting the nodes. Algebraic operations on the equations then correspond to simple alterations of the graph, while the solution of the system can be expressed in terms of the graph structure. The method is of particular interest in the field of network analysis, since the flow graph can be set up directly by inspection of the network without the necessity of first formulating the associated equations.

Detailed accounts of the topological and algebraic properties of flow graphs are to be found in the papers by Mason,[1,2] Lorens[3] and Boisvert.[4] The main purpose of this paper is to show that certain network functions introduced by Bode in his classical text[5] on feedback theory can be defined quite simply in flow-graph terms. Recent work by Blecher[6] has indicated the desirability of using a concept of a slightly different nature to Bode's return difference in the case of transistorized amplifiers, and it is shown that the flow-graph definition of return difference can be generalized to include Blecher's concept. In addition, a number of Bode's network theorems are derived using flow-graph techniques and thereby avoiding the use of the relatively complicated apparatus of the theory of determinants.

The paper starts with a brief account of the fundamental theory of flow graphs which is designed to show the relationships between the determinants of conventional algebra and certain analogous expressions derived from the flow graph.

(2) FUNDAMENTAL THEORY OF FLOW GRAPHS

(2.1) Expansion of a Determinant in Terms of Loops

We begin by establishing some results concerning the expansion of a determinant. While these are of little intrinsic interest so far as the evaluation of a determinant is concerned, they lead naturally to a formal definition of a flow graph in terms of the associated system of linear equations. Further, it then becomes possible to prove Mason's general gain formula immediately and thus to write down the solution of the equations by inspection of the flow graph.*

For convenience we write the general determinant of order n in a form which differs from the conventional notation in that the rows and columns are interchanged:

$$\Delta = \begin{vmatrix} a_{11} & a_{21} & \dots & a_{n1} \\ a_{12} & a_{22} & \dots & a_{n2} \\ \cdot & \cdot & \cdot & \\ a_{1n} & a_{2n} & \dots & a_{nn} \end{vmatrix}$$

One term in the expansion of Δ will be the product of the diagonal elements $a_{11}a_{22} \dots a_{nn}$. Every other term can be obtained from this one by carrying out one or more interchanges of the row suffixes, the sign of a particular term being positive or negative according as the number of such interchanges is even or odd. We shall use the following notation: every product of the form $a_{kj}a_{jk}$ will be called a '2-loop', similarly every product of the form $a_{kj}a_{jp}a_{pk}$ will be called a '3-loop', and so on. The

Correspondence on Monographs is invited for consideration with a view to publication.
Mr. Hoskins is at the Research Laboratory of A.E.I. (Woolwich), Ltd.

* Mason[2] gives a proof of this formula which is more topological in character. Other algebraic proofs will be found in Lorens[3] and Boisvert.[4]

order of a loop is defined as the number of elements which it contains.

It is clear that interchanges of the row suffixes in the diagonal term $a_{11}a_{22}\ldots a_{nn}$ will always result in expressions which take the form of a product of a certain number of loops and a residual set of diagonal elements. Further, if a term in the expansion of Δ contains some non-diagonal element, a_{jk}, first, this element belongs to some loop occurring in the term, and secondly, the term can contain no other element with column suffix j or with row suffix k. This last condition may be described by saying that the loops occurring in any one term must be 'non-touching'. Finally, the sign of a term is determined by the number of loops it contains. To see this, note that if we start with the diagonal term, $a_{11}a_{22}\ldots a_{nn}$, to obtain a term containing one loop, of order p, we need to carry out $p-1$ interchanges of the row suffixes, i.e. the term has $n-p$ diagonal elements, contains one loop, and its sign is $(-1)^{p-1}$. A term containing two loops, of orders p and q respectively, can be obtained by carrying out a total of $(p-1)+(q-1)$ interchanges of the row suffixes. Such a term has $n-(p+q)$ diagonal elements, contains two loops and its sign is $(-1)^{p+q-2}=(-1)^{p+q}$. Similarly, a term containing three loops, of order p, q and r respectively, will have $n-(p+q+r)$ diagonal elements and its sign will be $(-1)^{p+q+r-1}$. In general, we have the rule that if a term has $n-k$ diagonal coefficients, its sign will be $(-1)^k$ or $(-1)^{k-1}$, according as the number of loops formed by the remaining k elements is even or odd.

(2.2) The Solution of Simultaneous Linear Equations

Consider the set of linear equations

$$\left.\begin{aligned} a_0x_0 &= (a_{11}-1)x_1 + a_{21}x_2 + \ldots + a_{n1}x_n \\ 0 &= a_{12}x_1 + (a_{22}-1)x_2 + \ldots + a_{n2}x_n \\ &\cdots\cdots\cdots\cdots \\ 0 &= a_{1n}x_1 + a_{2n}x_2 + \ldots + (a_{nn}-1)x_n \end{aligned}\right\} \quad . \quad . \quad (1)$$

We can solve for any of the x_m in terms of x_0 by Cramer's rule, to get $x_m/x_0=\Delta'/\Delta$, where Δ denotes the determinant of the coefficients on the right-hand side of eqns. (1) and Δ' is the determinant obtained by substituting $a_0, 0, \ldots, 0$ for the mth column of Δ. In this case the diagonal elements of Δ all have the form $a_{kk}-1$ and the general term in the loop expansion of Δ will be the product of a certain number of loops and the expression

$$\prod_{}^{n-p}(a_{kk}-1)=(-1)^{n-p}\prod(1-a_{kk})$$
$$=(-1)^{n-p}(1-\Sigma a_{kk}+\Sigma a_{kk}a_{jj}-\Sigma a_{kk}a_{jj}a_{rr}+\ldots)$$

If the number of loops formed by the p non-diagonal elements is even, the sign of the term will be given by $(-1)^{n-p}(-1)^p=(-1)^n$; otherwise the sign is given by $(-1)^{n-1}$. By analogy with the notation already in use we shall refer to the elements a_{kk} as '1-loops'. With this notation, on multiplying out the bracket and rearranging terms, it is clear that the expansion of Δ can be written in the form

$$\Delta=(-1)^n\Big(1-\sum_p T_p+\sum_{p,q}T_pT_q-\sum_{p,q,r}T_pT_qT_r+\ldots\Big) \quad (2)$$

Here the T_p terms denote the loops of the determinant $\det(a_{ij})$, including the 1-loops defined above, and, in forming the products of loops, the proviso is observed that the loops occurring in any one product are mutually non-touching. Conversely, every possible product of this kind appears in the expansion.

In Δ' we replace every a_{mj} $(j\neq 1)$ by zero. In particular, the diagonal element $a_{mm}-1$ vanishes when $m\neq 1$. As a result, the terms of Δ' will be those terms of Δ which involve a loop containing the element a_{m1}, and in each case this element is to be replaced by a_0. Now any loop of Δ which contains a_{m1} must also contain some element with column suffix 1 and, in general, another with row suffix m. Removal of a_{m1} leaves a product of elements a_{jk} which can be arranged to have the form in which the first element has column suffix 1, the last has row suffix m, and the row suffix of each coefficient is equal to the column suffix of its right-hand neighbour. Such an expression will be called an 'open path' from 1 to m. For example, the loop $a_{12}a_{24}a_{4m}a_{m1}$ in Δ becomes the product $a_0(a_{12}a_{24}a_{4m})$ in Δ'. It follows that we can write the expansion of Δ' as

$$\Delta'=(-1)^n a_0\Big(-\sum_p A_p+\sum_{p,r}A_pT_r^p-\sum_{p,r,s}A_pT_r^pT_s^p+\ldots\Big) \quad (3)$$

In this, A_p denotes an open path from 1 to m; the T_r^p terms denote those loops which do not touch the open path A_p. In forming the products it should be noted that the loops occurring in any one product are not only mutually non-touching, but also do not touch the corresponding A_p. Rearranging terms gives the alternative expansion

$$\Delta'=-a_0(-1)^n\sum_p A_p\Big(1-\sum_r T_r^p+\sum_{r,s}T_r^pT_s^p-\ldots\Big) \quad (4)$$

The result holds also for the case $m=1$, since in this case there is only one term, A_p, equal to unity, and $\Delta'=a_0\Delta_{11}$, where Δ_{11}, the co-factor of $a_{11}-1$ in Δ, is given by eqn. (2) with $n-1$ for n and T_p^r (loops not touching the 1-loop a_{11}) for T_p.

In particular, if $a_0=-1$ the complete solution becomes

$$\frac{x_m}{x_0}=\frac{\Delta'}{\Delta}=\frac{\sum_p A_p\Big(1-\sum_r T_r^p+\sum_{r,s}T_r^pT_s^p-\ldots\Big)}{1-\sum_p T_p+\sum_{p,q}T_pT_q-\sum_{p,q,r}T_pT_qT_r+\ldots} \quad (5)$$

(2.3) Flow-Graph Formulation of the Problem

With $a_0=-1$, rewrite eqns. (1) in the form

$$\left.\begin{aligned} x_1 &= x_0 + a_{11}x_1 + a_{21}x_2 + \ldots + a_{n1}x_n \\ x_2 &= \quad a_{12}x_1 + a_{22}x_2 + \ldots + a_{n2}x_n \\ &\cdots\cdots\cdots\cdots \\ x_n &= \quad a_{1n}x_1 + a_{2n}x_2 + \ldots + a_{nn}x_n \end{aligned}\right\} \quad . \quad . \quad (6)$$

The flow graph corresponding to eqns. (6) is a network of nodes 0, 1, 2, ... n, linked by directed branches, jk, the direction from j to k being indicated by an arrowhead on the branch. The variable x_k in the equations corresponds to the node k in the graph and the coefficient a_{kj} is termed the 'gain' of the branch kj which originates from node k and terminates on node j. The products of coefficients referred to above as loops are now seen to correspond to actual closed paths or loops in the graph. In particular, the coefficients a_{kk} are represented by self-loops at the appropriate nodes and a_{kk} is called the 'loop gain' of the self-loop at node k. An example in the case $n=3$ is shown in Fig. 1.

The algebra of such a graph is defined by that of the associated equations in the sense that $x_j=\sum_{k=1}^{n}a_{kj}x_k$ evidently implies that the output signal from node j is the sum of all incoming signals, $a_{kj}x_k$, from the nodes of the graph. From this point of view eqn. (5), which gives the ratio of x_m to x_0, can be regarded as expressing the output from node m in terms of the input to node 1. In accordance with this, the ratio Δ'/Δ will be called the 'graph gain' from node 1 to node m.

In practice the external source, node 0, is often omitted from

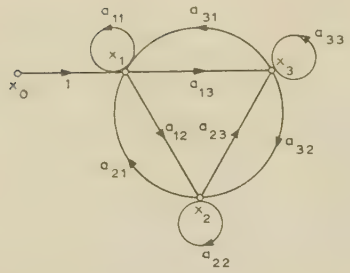

Fig. 1.—General flow graph of order $n = 3$.

the graph, and, in speaking of the gain from node 1 to node m, it is implied that a known input signal is applied to node 1. (Strictly, with no external source node, Fig. 1 would represent a homogeneous system of three equations in three unknowns.) Similarly, we speak loosely of a node x_k rather than of the node k associated with the unknown x_k.

Finally, the preceding analysis allows us to write down the general expression for the graph gain from, say, x_r to x_m in terms of the graph structure:

(*a*) Compute all open-path gains, A_{rm}, from node x_r to node x_m. This amounts to tracing a path on the graph which originates at x_r, terminates at x_m and passes through any intermediate node once only, and multiplying the gains of the individual branches traversed to give the appropriate A_{rm}.

(*b*) Given any A_{rm}, we select those loops T_r in the graph which do not touch the open path A_{rm} and form the product

$$A_{rm}\Big(1 - \sum_r T_r + \sum_{r,s} T_r T_s - \dots\Big) \quad . \quad . \quad . \quad . \quad (7)$$

The products are to be formed of non-touching loops, and this is now seen to mean that the loops are to have neither nodes nor branches in common. The sum of all such products (7) is the numerator of the required gain expression.

(*c*) The denominator of the gain expression is formed by taking all the loops occurring in the graph and combining them in the same manner. The resulting quantity, which, as has been seen, differs from the determinant of the associated equations by at most a change of sign, will be called the 'graph determinant'. In view of this, the symbol Δ will be used throughout the rest of the paper to denote the graph determinant as defined here.

(2.4) Construction and Transformation of Flow Graphs

In the case of a network of fairly simple structure it is often possible to construct a flow graph by inspection without first having to form the associated linear equations. In general, it is necessary to carry out either a nodal or a mesh analysis of the network in order to obtain a set of equations from which the required flow graph can be found. However, Boisvert[4] has developed a method of short-circuiting this procedure which allows the flow graph corresponding to a nodal analysis to be constructed directly from the given network. The essence of the method lies in a one-to-one correspondence between the nodes of the network and the nodes of the flow graph. A similar situation is encountered in the case of a mesh analysis, the correspondence now being between the meshes of the network and the nodes of the flow graph. Full details are given in the paper by Boisvert.

Once a flow graph has been constructed it is possible to write down a solution for the graph gain from, say, x_1 to x_m immediately. However, it is usually an advantage to carry out some simplification of the graph before applying the general gain formula derived above. There are a number of techniques available for this, each of which has its analogue in the field of conventional algebraic operations on systems of linear equations. For comprehensive accounts of such transformations of flow graphs, reference should be made to Mason[1] and Lorens.[3] For our purposes it is enough to note that any given node, say x_1, can be eliminated from the graph without affecting the gain between any other two nodes, provided that certain simple modifications are made to the branch gains. In effect we have

$$x_1 = \sum_{r=2}^{n} \frac{a_{r1}}{1 - a_{11}} x_r$$

By substituting for x_1 in the remaining equations it is seen that the elimination of node x_1 from the graph amounts to altering the gain of the branch joining x_k to x_j from a_{kj} to $a_{kj} + \dfrac{a_{1j}a_{k1}}{1 - a_{11}}$.

(3) THE FLOW-GRAPH FORMULATION OF BODE'S NETWORK FUNCTIONS

(3.1) Loop Gain and Loop Difference

The simplest form of feedback amplifier may be regarded as a combination of a linear amplifier (μ-circuit) and a passive network (β-circuit) by means of which part of the output of the μ-circuit is fed back to its input. When we come to consider more complicated feedback networks it is, in general, no longer possible to separate a given network into two isolated transmission paths corresponding to the μ- and β-circuits of the simple case. It is also no longer clear what is meant by the phrase 'gain without feedback'. It is necessary, therefore, to determine what quantities in the general case correspond to the feedback factor, $1 - \mu\beta$, and the sensitivity, S, of the simple feedback amplifier. Bode's classical treatment of these problems involves considerable manipulation of determinantal identities. If, however, we treat the required functions as parameters of the associated flow graph the derivation of many of Bode's results is greatly simplified. We begin by developing the concepts of 'loop gain' and 'loop difference' of a node of a flow graph originally introduced by Mason.[1]

Given a general flow graph of n nodes, $x_1, x_2, \dots x_n$, consider the new graph obtained if we divide some particular node, x_k, into two new nodes x_{k1}, x_{k2}, in the following manner: every branch in the original graph which originated from x_k now becomes a branch which originates from x_{k1} in the new graph; similarly, every branch which terminated on x_k in the original graph becomes a branch terminating on x_{k2} in the new graph. An example of this process of node-splitting is shown in Fig. 2.

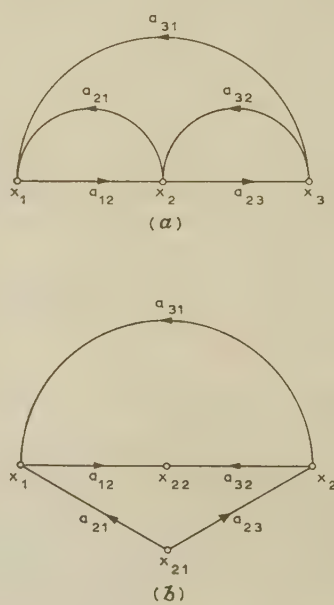

Fig. 2.—Example of node splitting.

The effect of splitting x_k is to create a pure source, x_{k1}, and a sink, x_{k2}. In the degenerate case in which the only feedback loop which passes through x_k is a self-loop of loop gain a_{kk}, it is readily seen that splitting x_k leaves one open branch, of gain a_{kk}, which goes from x_{k1} to x_{k2}. In this case the graph gain from x_{k1} to x_{k2} in the split graph is a_{kk}. By analogy, the graph gain in the general case from x_{k1} to x_{k2} will be called the loop gain of node x_k and will be denoted by L_k. The quantity $D_k = 1 - L_k$ will be called the loop difference of node x_k. In the example of Fig. 2 we have

$$L_2 = a_{21}a_{12} + a_{23}a_{32} + a_{23}a_{31}a_{12}$$

$$D_2 = 1 - (a_{21}a_{12} + a_{23}a_{32} + a_{23}a_{31}a_{12})$$

In the general case we can compute L_k by using the general gain formula derived in Section 2. We recall that a quantity Δ, called the graph determinant, was defined as a sum of products of non-touching loops of the graph. In addition, we now adopt the following notation. Δ_k denotes the determinant of the graph obtained when node x_k is split. Since this operation interrupts all loops which pass through x_k, Δ_k could also be defined as the determinant of the graph obtained when x_k is removed from the original graph together with all its connecting branches. It will be referred to as the 'residue' of x_k.

G_r^k denotes the loop gain of the rth feedback loop which passes through node x_k, and Δ_r^k denotes the determinant of the graph obtained when the whole loop G_r^k is removed, i.e. when every node through which G_r^k passes is removed, together with all its connecting branches.

We have $\Delta = \Delta_k - \sum_r G_r^k \Delta_r^k$, the minus sign arising from the sign rule relating to loop products occurring in the graph determinant. (If, for example, a term of Δ_r^k has an even number of loops it will be positive in the expansion of Δ_r^k; the term $G_r^k \Delta_r^k$ is a term of Δ with an odd number of loops and so will be negative.)

However, when x_k is split, each G_r^k becomes an open path from x_{k1} to x_{k2}. Applying the general gain formula it follows immediately that

$$L_k = \frac{\sum_r G_r^k \Delta_r^k}{\Delta_k}$$

Hence,
$$D_k = 1 - L_k = \frac{\Delta_k - \sum_r G_r^k \Delta_r^k}{\Delta_k} = \frac{\Delta}{\Delta_k} \quad . \quad . \quad (8)$$

Thus we can define the loop difference of a node x_k as the ratio of the graph determinant to the residue of x_k.

The concepts of loop gain, loop difference and residue can easily be extended to apply to a branch of a flow graph as well as to a node. In Fig. 3(*a*) a particular branch, a_{jk}, of a graph is shown, while in Fig. 3(*b*) the graph is modified by the introduction of a new node, x'. This new node has no effect on the graph so far as the calculation of graph gains is concerned. The loop gain, L_{jk}, of the branch a_{jk} of the original graph is now defined to be the loop gain of the inserted node x' in the new graph. As before we can define the loop difference, D_{jk}, of a_{jk} by the equation $D_{jk} = 1 - L_{jk}$. The residue, Δ_{jk}, of a_{jk} will be the determinant of the graph obtained when x' is removed together with all its connecting branches or, equivalently, when the branch gain a_{jk} reduces to zero. As before we can deduce the result

$$D_{jk} = \frac{\Delta}{\Delta_{jk}} \quad . \quad . \quad . \quad . \quad . \quad . \quad . \quad (9)$$

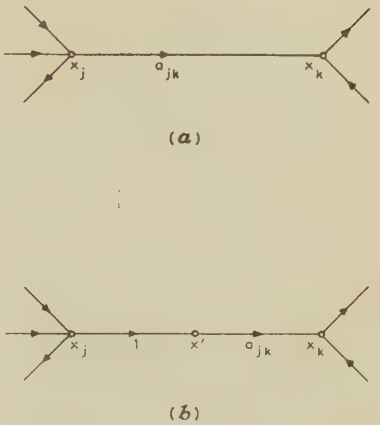

Fig. 3.—Insertion of an extra node.

(3.2) Generalizations of the Loop Difference

The graph determinant, Δ, is clearly a linear function of the gain of any one of the branches of the graph. This fact suggests an immediate generalization of the loop difference: if Δ is linear in some parameter W, then we define the loop difference of W to be the quantity $D_W = \Delta/\Delta_W$, where Δ_W denotes the value of the graph determinant when $W = 0$. If W is simply the gain of one particular branch of the graph, this generalized loop difference reduces to the ordinary loop difference of an inserted node in the graph, as described in the last Section. We now consider one or two other cases in which the loop difference of a parameter can be expressed in terms of the flow-graph functions defined above.

If the gain of some branch of the graph is a linear function of a parameter W, then Δ is certainly linear in W. The loop difference of W can be considered as the loop difference of an inserted node, as shown in Figs. 4(*a*) and (*b*).

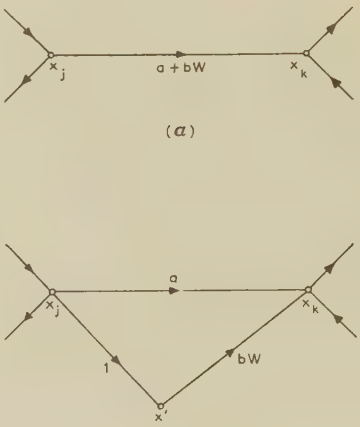

Fig. 4.—Branch gain linear in a parameter W.

This transformation makes it clear that, without loss of generality, we need only consider branch gains which are multiples of W.

If several branches which all leave (or all converge on) the same node x have gains which are linear multiples of W, then Δ is again linear in W. As before, the loop difference of W can be defined in terms of an inserted node x', as shown in Figs. 5(*a*) and (*b*).

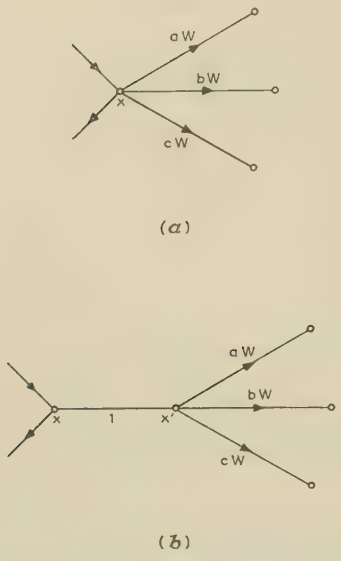

Fig. 5.—Confluent branches whose gains are multiples of W.

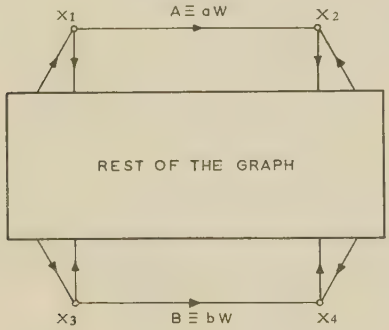

Fig. 6.—Disjoint branches whose gains are multiples of W.

Suppose now that the gains of two distinct branches of the graph, which need have no common nodes, are each multiples of W. The situation is illustrated in Fig. 6. In general, Δ will not be a linear function of W in this case. Linearity is of particular importance in considering the relationships between loop difference and sensitivity, as discussed below. Accordingly, we assume here that the branches A and B do not form part of the same feedback loop; also we suppose that there exist no two disjoint loops such that A forms part of the one and B forms part of the other. Under these hypotheses Δ will certainly be linear in W. The loop difference of branch A is simply $D_A = \Delta/\Delta_{A=0}$. This means that we allow the gain of the branch going from x_1 to x_2 to become zero but suppose that the gain of the branch going from x_3 to x_4 retains its original value. If W itself is allowed to take the value zero everywhere, both these branches will have zero gains and the determinant of the resulting graph will be Δ_W, the residue of W. Now suppose that we compute the loop difference of the branch linking x_3 to x_4, after the gain, aW, of the branch A has been reduced to zero. To avoid confusion we denote this quantity by the symbol D'_B. The determinant of the graph obtained when branch A has zero gain is $\Delta_{A=0}$. The residue of branch B in this graph is seen to be Δ_W, i.e. $D'_B = \Delta_{A=0}/\Delta_W$. Hence we obtain the result

$$D_W = \frac{\Delta}{\Delta_W} = \frac{\Delta}{\Delta_A}\frac{\Delta_A}{\Delta_W} = D_A D'_B \quad . \quad . \quad . \quad (10)$$

Using this last result we can consider a case which has particular importance in the analysis of certain transistorized networks. If the gain of some branch is of the form $(a + bW)/(1 - cW)$, we can carry out the transformation shown in Figs. 7(*a*) and (*b*). The introduction of the two new nodes x

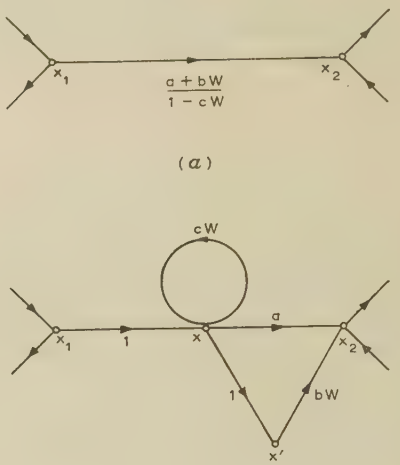

Fig. 7.—Construction for a partial loop difference.

and x' will have no effect as regards the calculation of graph gains between any pair of nodes of the original graph. However, the graph determinant, Δ, does change; in particular, the determinant of the graph of Fig. 7(*b*) is clearly linear in W. As a result we can discuss the loop difference of the parameter W in terms of loop differences of the inserted nodes x and x' as has been indicated in the preceding paragraph. For the moment we merely note that the loop difference of node x' is the ratio Δ/Δ^0, where Δ^0 is the graph determinant obtained when the gain of the branch bW reduces to zero, although the loop of gain cW is allowed to retain its original value. In terms of the original graph this cannot be interpreted as a loop difference in any of the senses used hitherto. It could be described as a sort of 'partial' loop difference of the parameter W in that we compute Δ^0 by allowing the parameter W to vanish where it occurs in the numerator of the branch gain concerned but we retain its original value in the denominator. The significance of this point will become apparent when we come to discuss Blecher's concept of the return difference for a common-emitter amplifier stage.

Finally, we can introduce Bode's concept of the loop difference for a general reference. Take first a flow graph in which just one branch has gain W and consider the new graph obtained if we replace this branch by one of gain K. The residue, Δ_W, of the branch will be the same in each graph. In the original graph the loop difference of the branch is given by $D_W = \Delta/\Delta_{W=0}$; in the new graph, the graph determinant becomes $\Delta_{W=K}$ so that the loop difference is now $D_K = \Delta_{W=K}/\Delta_{K=0} = \Delta_{W=K}/\Delta_W$. We define the loop difference of W for the reference value K to be

$$D_W(K) = D_W/D_K = \Delta/\Delta_{W=K} \quad . \quad . \quad . \quad (11)$$

The ordinary loop difference of W is then seen to be a special case of this, namely the loop difference of W for the reference value zero.

Evidently we can extend this definition to generalized loop differences. If Δ is linear in W, the loop difference of W for

the reference value K is defined to be the ratio $\Delta/\Delta_{W=K}$, where $\Delta_{W=K}$ is the graph determinant obtained when we replace W by K wherever it occurs in Δ.

(3.3) Loop Difference and Return Difference

At this stage we present an illustration of the use of the flow-graph functions defined in the preceding Section. Recall that the stability of a feedback amplifier depends on its possible transient responses and that these are determined by the zeros of the network determinant Δ. For stability we require that these zeros are confined to the left half of the complex frequency plane. Hence, if F is some analytic function of complex frequency which is directly proportional to Δ, the problem of stability can be reduced to the study of the behaviour of F over a suitable contour in the complex frequency plane. In the case of valve amplifiers Bode's return difference is such a function and also fulfils the practical requirement of being a readily measurable physical quantity. Recently, Blecher has suggested definitions of such a return difference for transistors in the common-base and common-emitter connections. For the common-emitter, in particular, the resultant quantity cannot be interpreted as a return difference in the sense used by Bode. It is the purpose of this Section to discuss the concepts of Bode and Blecher in flow-graph terms and to show their relations to our loop difference.

For Bode, the return difference of a circuit-element W is the ratio Δ/Δ^0, where Δ is the circuit determinant and Δ^0 is obtained from Δ by allowing W to vanish wherever it occurs. This is, of course, identical with our definition of the loop difference for the parameter W. If the circuit-element is a valve, the corresponding flow graph contains a node e representing the voltage appearing between the grid and cathode. If we split this node, assuming all external connections to the grid are effectively unilateral, the loop gain T_e is easily seen to be the voltage which would be returned to the grid circuit if a unit voltage were applied to the grid and the circuit opened just behind it. The loop difference, $D_e = 1 - L_e$, is therefore the difference between a unit voltage applied to the grid and the voltage returned to the grid circuit by various feedback paths. It is clear that $D_e = \Delta/\Delta_{\mu=0}$, where μ is the amplification factor, so that Bode's return difference in this case is identical with the loop difference of a node. Now consider the simplified equivalent circuit for a common-emitter stage, as shown in Fig. 8.

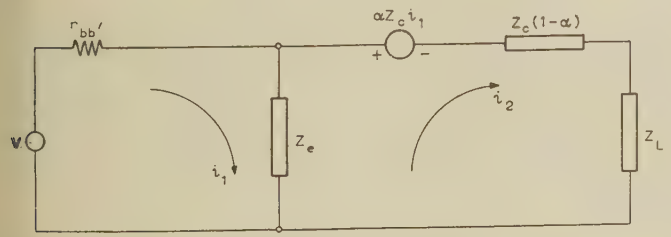

Fig. 8.—Equivalent circuit for a common-emitter stage.

Blecher[6] suggests that the return difference of the stage be defined as the quantity measured in the following manner. All external feedback paths returning to the input of the stage are connected to earth through an impedance $Z_e + r_{bb'}$ and a voltage $Z_e i_2$. If a unit-current generator is applied to the input of the stage, the return difference is defined to be the algebraic difference between the unit input current and the current which is returned to earth via the feedback paths.

The flow graph corresponding to the circuit of Fig. 8 is shown in Fig. 9. For simplicity we write $K = Z_e + Z_L + Z_c$. It is

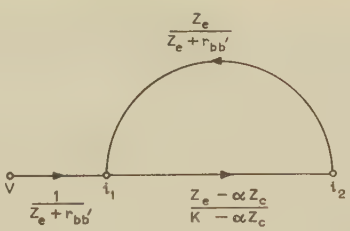

Fig. 9.—Flow graph for a common-emitter stage.

clear that the loop gain of the branch going from i_1 to i_2 is precisely the current which would flow to earth through the external feedback paths if these were terminated as in Blecher's measurement circuit, i.e. Blecher's return difference is simply the loop difference of this branch. We now transform the flow graph to the equivalent one shown in Fig. 10.

In this graph, branch A corresponds to the active part of the stage while the term αZ_c in the loop B is due to the impedance $Z_c(1 - \alpha)$. Now the loop difference of the branch linking i_1 to i_2 in Fig. 9 is the ratio Δ/Δ^0, where, to obtain Δ^0, we set $(Z_e - \alpha Z_c)/(K - \alpha Z_c) = 0$. Referring to Fig. 10, this is clearly

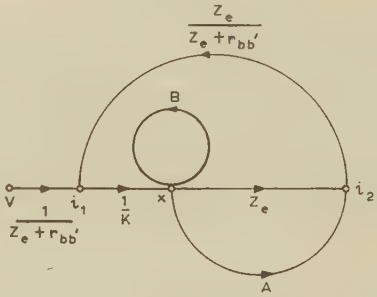

Fig. 10.—Modified flow graph for a common-emitter stage.
$A = -\alpha Z_c$
$B = \alpha Z_c/K$

the loop difference of the branch A for the reference value Z_e. In fact this is a case of a partial loop difference of the parameter αZ_c as it occurs in the original graph of Fig. 9 and as has been discussed above. The return difference of the stage in Bode's sense, however, would be the loop difference of the parameter αZ_c for the reference value Z_e.

(3.4) Sensitivity

In conclusion, we prove, by way of illustration of flow-graph techniques, some of the network theorems established by Bode by conventional algebraic methods. To begin with we define sensitivity.

The graph gain, G (or in Bode's terminology, e^θ), from x_1 to x_n can be put in the form $e^\theta = \Delta'/\Delta$. This can be written $\theta = \log \Delta' - \log \Delta$. If Δ is linear in W we have

$$\frac{\partial\theta}{\partial \log W} \equiv W\frac{\partial\theta}{\partial W} = \frac{W}{\Delta'}\frac{\partial\Delta'}{\partial W} - \frac{W}{\Delta}\frac{\partial\Delta}{\partial W} \quad . \quad . \quad (12)$$

If Δ_W is the residue of W, we can write $\Delta = \Delta - \Delta_W + \Delta_W$, where $\Delta - \Delta_W$ is the sum of those terms of Δ which contain W. Hence, $\partial\Delta/\partial W = (\Delta - \Delta_W)/W$. A similar argument applied to Δ' shows that $\partial\Delta'/\partial W = (\Delta' - \Delta'_W)/W$. Therefore, if we define the sensitivity, S, by the equation $1/S = \partial\theta/\partial \log W$, we have

$$\frac{1}{S} = \frac{\Delta' - \Delta'_W}{\Delta'} - \frac{\Delta - \Delta_W}{\Delta} = \frac{\Delta_W}{\Delta} - \frac{\Delta'_W}{\Delta'} \quad . \quad (13)$$

If we compute the graph gain from x_1 to x_n using the graph obtained by setting $W = 0$ everywhere in the original graph, we obtain $e^{\theta_0} = \Delta'_{W=0}/\Delta_{W=0}$.

This gives a new expression for S:

$$\frac{1}{S} = \frac{\Delta_W}{\Delta}\left(1 - \frac{\Delta'_W}{\Delta'}\frac{\Delta}{\Delta_W}\right) = \frac{\Delta_W}{\Delta}\left(1 - \frac{\Delta'_W}{\Delta_W}\frac{\Delta}{\Delta'}\right)$$

$$= \frac{1}{D_W}(1 - e^{\theta_0}/e^{\theta})$$

or
$$e^{\theta} - e^{\theta_0} = \frac{D_W}{S}e^{\theta} \quad . \quad . \quad . \quad . \quad . \quad (14)$$

Bode's relative sensitivity, S', can similarly be defined in terms of flow-graph parameters. If W_0 is that value of W for which $e^{\theta} = 0$, i.e. such that all transmission from source to sink is interrupted, write $W' = W - W_0$. Then the relative sensitivity, S', for the parameter W is defined to be the sensitivity with respect to the parameter W':

$$\frac{1}{S'} \equiv \frac{\partial\theta}{\partial \log W'} = W'\frac{\partial\theta}{\partial W} = \frac{W'}{W}\left(\frac{\Delta_W}{\Delta} - \frac{\Delta'_W}{\Delta'}\right) = \frac{1 - W_0/W}{S}$$

Hence,
$$S/S' = 1 - W_0/W \quad . \quad . \quad . \quad . \quad . \quad (15)$$

Now, from eqn. (14) we have $(e^{\theta} - e^{\theta_0})/e^{\theta} = D_W/S$, where e^{θ_0} is the gain when $W = 0$. If $e^{\theta_0} = 0$, i.e. if setting $W = 0$ interrupts all transmission from source to sink, then clearly $S = D_W$. By definition, setting $W = W_0$ interrupts all transmission from source to sink, so that the sensitivity with respect to W' is equal to the loop difference of W'. Hence, $S' = D_{W'} = \Delta/\Delta_{W'}$. Now $\Delta_{W'} = \Delta_{W=W_0}$ so that $D_{W'}$ is the loop difference of W for the reference value W_0. As a result we can write

$$S' = D_W/D_{W_0} \quad . \quad . \quad . \quad . \quad . \quad (16)$$

Next, we derive a result of Bode's which enables a precise meaning to be given to the phrase 'gain without feedback'. If $W = 0$, the gain reduces to e^{θ_0}; the effect of allowing W to assume its normal value should be to introduce a term due to the transmission through those branches of the graph whose gains involve W, and this term will be modified by the overall feedback due to loops which contain such branches. Thus, heuristically, we should expect to be able to derive an equation of the form

$$e^{\theta} = e^{\theta_0} + \frac{1}{D_W}e^{\theta_F} \quad . \quad . \quad . \quad . \quad . \quad (17)$$

In this, e^{θ_F} denotes the gain due to transmission through the branches of the graph whose gains involve W, it being supposed that all the feedback loops which involve these branches have been interrupted; i.e. e^{θ_F} (Bode's 'fractionated gain') denotes the gain without feedback associated with the element W.

In the first place we consider a general flow graph originally involving n nodes, $x_1, x_2, \ldots x_n$, which has been reduced by elimination of other nodes to a form containing only x_1, x_n and some other specified node, x_k. The configuration in the most general case is shown in Fig. 11(*a*). In Fig. 11(*b*) the graph is shown with node x_k split.

We require to find the effect on the graph gain from x_1 to x_n of transmission through node x_k. If G denotes the graph gain from x_1 to x_n, D_k the loop difference of node x_k, and Δ_k the residue of x_k, then

$$G = \frac{a(1 - k) + ef}{D_k\Delta_k} \text{ (since } \Delta = D_k\Delta_k)$$

$$\Delta_k = 1 - ad - g - h + gh$$

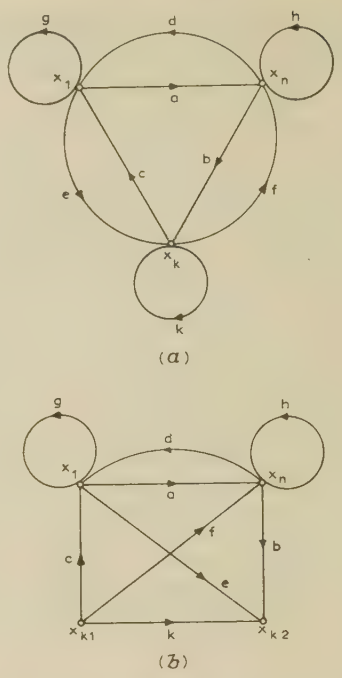

Fig. 11.—Determination of gain without feedback.

and $D_k = 1 - \left[\frac{ce(1 - h) + bf(1 - g) + abc + def}{\Delta_k} + k\right]$

$$= 1 - \frac{A}{\Delta_k} - k$$

Hence,

$$G = \frac{aD_k + a\frac{A}{\Delta_k} + ef}{D_k\Delta_k} = \frac{a}{\Delta_k} + \frac{1}{D_k}\frac{aA + ef\Delta_k}{\Delta_k\Delta_k}$$

$$= \frac{a}{\Delta_k} + \frac{1}{D_k}\frac{e(1 - h) + ab}{\Delta_k}\frac{f(1 - g) + ac}{\Delta_k} \quad . \quad (18$$

Inspection of Fig. 11(*b*) shows that a/Δ_k is simply the graph gain from x_1 to x_n when x_k is removed from the graph or split, so that there is no transmission from x_1 to x_n via x_k. The quantity $[e(1 - h) + ab]/\Delta_k$ is the gain from x_1 to x_{k2}, while $[f(1 - g) + ac]/\Delta_k$ is the gain from x_{k1} to x_n. The product of these two terms would be the contribution to the total graph gain from x_1 to x_n due to transmission through x_k, supposing that all feedback loops passing through x_k had been interrupted.

If we let e^{θ_F} denote the product of the gain from x_1 to the split node x_{k2} and the gain from the split node x_{k1} to x_n, we can write

$$e^{\theta} - e^{\theta_0} = \frac{1}{D_k}e^{\theta_F} \quad . \quad . \quad . \quad . \quad . \quad (19$$

Finally, if W is a parameter whose loop gain can be computed by splitting some specific node we can use this last result and that of eqn. (14) to obtain another well-known result of Bode's:

$$e^{\theta} = \frac{S}{D_W^2}e^{\theta_F} \quad . \quad . \quad . \quad . \quad . \quad . \quad (20$$

(4) CONCLUSIONS

It has been shown that the general theory of flow-graph analysis can be applied to any linear network and that it affords a straigh

forward technique for the solution of many circuit problems. The principal advantage over conventional algebraic methods is that it leads to a relatively simple development of many of the network theorems which arise in connection with feedback theory. In particular, the use of complicated determinantal identities is avoided.

(5) ACKNOWLEDGMENTS

Acknowledgment is made to the Director, A.E.I. (Woolwich), Ltd., Research Laboratory, for permission to publish the paper. The author would also like to express his appreciation of the advice and helpful suggestions of Mr. G. H. Parks and Mr. K. Lamont in the preparation of this work.

(6) REFERENCES

(1) MASON, S. J.: 'Feedback Theory—Some Properties of Signal Flow Graphs', *Proceedings of the Institute of Radio Engineers*, 1953, **41**, p. 1144.

(2) MASON, S. J.: 'Feedback Theory—Further Properties of Signal Flow Graphs', *ibid.*, 1956, **44**, p. 920.

(3) LORENS, C. S.: 'Theory and Application of Flow Graphs', Thesis submitted for the degree of Doctor of Science, Massachusetts Institute of Technology, July, 1956.

(4) BOISVERT, M.: 'Les diagrammes de fluence de signal', *Annales des Télécommunications*, 1958, **13**, p. 50.

(5) BODE, H. W.: 'Network Analysis and Feedback Amplifier Design' (D. van Nostrand, 1945).

(6) BLECHER, F. H.: 'Design Principles for Single Loop Transistor Feedback Amplifiers', *Transactions of the Institute of Radio Engineers*, 1957, **CT-4**, p. 145.

621.391.812.63

The Institution of Electrical Engineers
Monograph No. 389 E
July 1960

THE RECEIVED-AMPLITUDE DISTRIBUTION PRODUCED BY RADIO SOURCES OF RANDOM OCCURRENCE AND PHASE

By W. C. BAIN, M.A., B.Sc., Ph.D., Associate Member.

(*The paper was first received 7th January, and in revised form 6th April*, 1960. *It was published as an* INSTITUTION MONOGRAPH *in July*, 1960.)

SUMMARY

A theoretical calculation is given of the amplitude probability distribution to be expected on an ionospheric v.h.f. forward-scatter circuit due to reflections from meteor trails alone. The analysis is based on the addition of a large number of signals with a frequency of occurrence inversely proportional to the square of their amplitude, and will therefore apply to other problems in which this relation holds. The calculated distribution is compared with a small number of practical results, and a method is outlined for deriving the relative proportion of meteoric and turbulent-scattering components in the signal.

(1) INTRODUCTION

The forward-scattering process which enables v.h.f. signals to be propagated to a distant point via the ionosphere is due to the existence of certain irregularities in electron density at heights in the ionosphere of about 100 km. Some doubt, however, exists as to whether these irregularities are produced by turbulence in and below the E region or by meteors continually causing local concentrations of ionization.[1–3] It may be, of course, that both contribute a significant number of scattering sources. Whichever is the true explanation, it is useful to know as much as possible about the characteristics of the received signal which would be given by meteors alone, so that these can be compared with observed results. The paper is concerned with the signal amplitude distribution to be expected from meteor reflections. Although the formulation of the problem here is in terms of meteors, the mathematical treatment is general and may apply to other problems, such as the amplitude distribution of atmospherics.[4]

(2) GENERAL CONSIDERATIONS

It is well known in meteor astronomy[5] that the number of sporadic meteors of mass greater than m incident on a given area is inversely proportional to m. This implies that the number of meteors with masses between m and $m + dm$ must be proportional to dm/m^2. The electron line density, q, in the trail is proportional to m, and for an under-dense trail the amplitude of the received signal, E, is proportional to q. Under-dense and over-dense trails are those in which the electron line density is less than and greater than $10^{14}/m^3$, respectively; this numerical value corresponds to a change-over in the reflection properties of the trail. (See, for instance, Villard *et al.*[3]) The amplitude also depends on a great many other factors such as frequency, transmitter power and co-ordinates specifying the position and direction of the trail. This does not, however, alter the result that the number of received signals, $f(E)dE$, say, whose maximum amplitude lies in the range $(E, E + dE)$ is given by

$$f(E)dE = \frac{k}{E^2}dE$$

where k is a constant whose value will depend upon these other factors. This result will be valid as long as the factors are not correlated with q, as seems reasonable to assume.

To proceed from this relation to the amplitude distribution resulting from the simultaneous reception of many meteor reflections, we require to know the variation with time of the signal from a single meteor. This has been given by various workers as a rapid increase to a maximum followed by small oscillations about a particular level. The oscillations die out quickly, and the level itself falls exponentially to zero at a comparatively slow rate.[6] The time-constant of the decay depends on the diffusion coefficient of the atmosphere at the height of reflection. However, on long transmission paths the percentage of reflections at small heights contributing to the total signal will be much reduced, thus concentrating the reflection heights to values near and somewhat above 100 km. Hence the time-constant will be taken here to be the same for each reflection.

It is now necessary to simplify somewhat the function representing the envelope of the received signal from each meteor trail to one which can be dealt with analytically. The results of two different approximations are described below.

(3) RECTANGULAR-PULSE APPROXIMATION

The received signal from each meteor is assumed to rise instantaneously to E and to fall instantaneously from this amplitude to zero after a fixed time. The exact time is not important except that it must be very much less than any period of observation. Suppose now that the probability of a meteor having an amplitude in the range $(E, E + dE)$ is $h(E)dE$. From the considerations given previously, $h(E)$ should be given by

$$h(E) = k_1/E^2 \quad . \quad . \quad . \quad . \quad . \quad . \quad (1)$$

However, this means that $\int_0^\infty h(E)dE$ is infinite. To overcome this difficulty the definition in eqn. (1) is therefore replaced by

$$h(E) = \frac{k_1}{E^2 + b^2} \quad . \quad . \quad . \quad . \quad . \quad (2)$$

where b is taken to be small and will eventually be made to tend to zero, thus making eqn. (2) identical with eqn. (1). The value of k_1 can now be found by equating the total probability to unity, and $h(E)$ can be written as

$$h(E) = \frac{2b}{\pi}\frac{1}{E^2 + b^2} \quad . \quad . \quad . \quad . \quad . \quad (3)$$

At any instant a number, n, of meteor signals, each with this amplitude probability distribution, will be taken to exist, and the amplitude distribution of their resultant will be calculated under the condition that n tends to infinity. In the actual physical situation n cannot be truly infinite but it will be very large, and the assumption that it is infinite should affect the results very little. To keep the mean amplitude level finite it will be supposed

Correspondence on Monographs is invited for consideration with a view to publication.

The paper is an official communication from the Radio Research Station, Department of Scientific and Industrial Research.

that the level which is exceeded by only one signal on the average has the fixed value p. The average number of signals above a certain level E is defined by

$$\lim_{T\to\infty} \frac{1}{T}\int_0^T N(E, t)dt$$

where $N(E, t)$ is the number of signals above that level at time t.

The expected number of signals in the range $(E, E + dE)$ must be $nh(E)dE$. The expected number above the level p will be $\int_p^\infty nh(E)dE$. Thus the condition we have imposed requires that

$$\int_p^\infty nh(E)dE = 1 \quad . \quad . \quad . \quad . \quad . \quad (4)$$

Substituting from eqn. (3) gives the result:

$$\text{arc tan}\frac{b}{p} = \frac{\pi}{2n}$$

As b is small and n large, the tangent can replace the angle, giving

$$b = \frac{\pi p}{2n} \quad . \quad . \quad . \quad . \quad . \quad . \quad . \quad (5)$$

The problem of finding the resultant of n signals of random phases and different amplitudes must now be considered. This is a 'random walk' problem, and the answer has been given by Rayleigh.[7] If the signals have amplitudes $E_1, E_2, \ldots E_n$, and their resultant has amplitude r, the final amplitude distribution for r is

$$Q(r, E_1, E_2, \ldots E_n) = r\int_0^\infty xJ_0(rx)J_0(E_1x)J_0(E_2x)\ldots J_0(E_nx)dx \quad . \quad . \quad . \quad . \quad (6)$$

The distribution of each E_k is given as in eqn. (3), so that the distribution $P(r)$ of the resultant amplitude is given by

$$P(r) = \int_0^\infty \frac{2b}{\pi}\frac{1}{E_1^2 + b^2}dE_1 \int_0^\infty \frac{2b}{\pi}\frac{1}{E_2^2 + b^2}dE_2 \ldots \int_0^\infty \frac{2b}{\pi}\frac{1}{E_n^2 + b^2}Q(r, E_1, E_2, \ldots E_n)dE_n$$

Substituting for Q from eqn. (6) and changing the order of integration,

$$P(r) = r\int_0^\infty xJ_0(rx)dx\left[\int_0^\infty \frac{2b}{\pi}\frac{J_0(Ex)}{E^2 + b^2}dE\right]^n \quad . \quad (7)$$

Now

$$\int_0^\infty \frac{2b}{\pi}\frac{J_0(Ex)}{E^2 + b^2}dE = I_0(bx) - L_0(bx) \quad . \quad . \quad (8)$$

as is given by Watson;[8] the functions involved are the modified Bessel's function of the first kind and the modified Struve's function, respectively. The first three terms of the power-series expansion of eqn. (8) are

$$I_0(bx) - L_0(bx) = 1 - \frac{2}{\pi}bx + \tfrac{1}{4}(bx)^2 + \ldots$$

$$= 1 - \frac{p}{n}x + \tfrac{1}{4}\left(\frac{\pi p}{2n}x\right)^2 + \ldots$$

using eqn. (5). All subsequent terms will contain powers of $1/n$ higher than the second. Hence

$$\lim_{n\to\infty}[I_0(bx) - L_0(bx)]^n = \lim_{n\to\infty}\left(1 - \frac{px}{n}\right)^n = \varepsilon^{-px} \quad . \quad . \quad . \quad . \quad . \quad . \quad (9)$$

Eqn. (7) now becomes

$$P(r) = r\int_0^\infty xJ_0(rx)\varepsilon^{-px}dx = \frac{rp}{(r^2 + p^2)^{3/2}} \quad . \quad . \quad . \quad . \quad . \quad (10)$$

This is the required distribution. The probability $P_1(r)$ of the amplitude exceeding a given value r is expressed by

$$P_1(r) = \frac{p}{\sqrt{(r^2 + p^2)}} \quad . \quad . \quad . \quad . \quad . \quad (11)$$

A plot of eqn. (10) is shown in Fig. 1. It agrees with the Rayleigh distribution only at low amplitude levels.

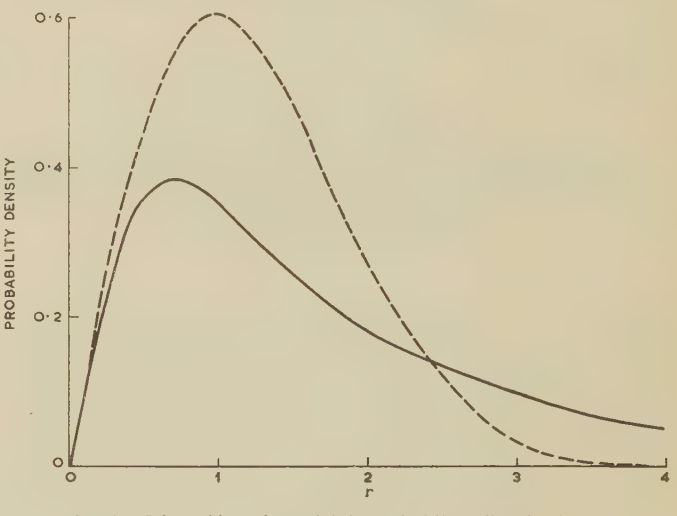

Fig. 1.—The $P(r)$ and Rayleigh probability distributions.

----- Rayleigh $[(r/\sigma)\exp(-r^2/2\sigma^2)]$
—— $P(r)$
$p = 1 \quad \sigma = 1$

(4) EXPONENTIAL APPROXIMATION

There will now be considered a different, and probably better, approximation to the envelope of a meteor signal. It is assumed to rise instantaneously to a level E_0, and t seconds later its amplitude E is given by

$$E = E_0\varepsilon^{-t/\tau} \quad . \quad . \quad . \quad . \quad . \quad . \quad . \quad (12)$$

It would be desirable to give E_0 a probability distribution proportional to $1/E_0^2$, but again this leads to infinite integrals. The difficulty can be overcome as before in eqn. (3), although the analysis is simplified if, instead of the expression used previously, we take

$$h_1(E_0) = \frac{b}{(E_0 + b)^2} \quad . \quad . \quad . \quad . \quad . \quad (13)$$

as the probability distribution for E_0; b will ultimately be made to tend to zero.

Before we can find the distribution of E we must assign some probability to the different values of t in eqn. (12). Let us consider only a meteor trail created at some time in the $s\tau$

seconds before a particular instant of time, where s is a large but finite number. Trails created before that time make a negligible contribution to the total signal amplitude. The probability $h_2(t)dt$ that t lies in the interval $(t, t + dt)$ in eqn. (12) is given by

$$h_2(t) = \frac{1}{s\tau} \quad . \quad . \quad . \quad . \quad . \quad . \quad . \quad (14)$$

The combined probability that E_0 lies in $(E_0, E_0 + dE_0)$ and t lies in $(t, t + dt)$ is given by

$$h_1(E_0)h_2(t)dE_0dt = \frac{b}{(E_0 + b)^2}\frac{1}{s\tau}dE_0dt$$

If the variables are changed from E_0, t to E, E_0, the corresponding probability $h_3(E, E_0)dEdE_0$ that E lies in $(E, E + dE)$ and E_0 in $(E_0, E_0 + dE_0)$ is found to be

$$h_3(E, E_0)dEdE_0 = \frac{1}{sE}\frac{b}{(E_0 + b)^2}dEdE_0$$

The required amplitude distribution $h(E)$ is then given by

$$h(E) = \int_E^{E\varepsilon^s} h_3(E, E_0)dE_0$$

$$= \frac{1}{s}\left(\frac{1}{E + b\varepsilon^{-s}} - \frac{1}{E + b}\right) \quad . \quad . \quad . \quad (15)$$

The argument can now be followed through as in the last Section, with eqn. (15) replacing eqn. (3). We consider n meteors and require that

$$\int_p^\infty nh(E)dE = 1$$

i.e.
$$\frac{n}{s}\log\frac{p + b}{p + b\varepsilon^{-s}} = 1$$

Since s is large, we may therefore approximate, obtaining

$$\frac{n}{s}\log\left(1 + \frac{b}{p}\right) = 1$$

i.e.
$$\frac{nb}{sp} = 1 \quad . \quad . \quad . \quad . \quad . \quad . \quad (16)$$

as b is very small.

We require eventually that $n \to \infty$, $b \to 0$ and $s \to \infty$. These requirements can be met and eqn. (16) satisfied by choosing

$$b = cp/\sqrt{n} \quad s = c\sqrt{n} \quad . \quad . \quad . \quad . \quad . \quad (17)$$

where c is a finite constant.

The distribution of the resultant signal from n meteors is obtained as in the previous Section:

$$P(r) = r\int_0^\infty dx x\mathrm{J}_0(rx)\left[\int_0^\infty \frac{\mathrm{J}_0(Ex)}{s}\left(\frac{1}{E + b\varepsilon^{-s}} - \frac{1}{E + b}\right)dE\right]^n$$

$$. \quad . \quad . \quad . \quad . \quad (18)$$

Now
$$\int_0^\infty \frac{\mathrm{J}_0(Ex)}{s}\left(\frac{1}{E + b\varepsilon^{-s}} - \frac{1}{E + b}\right)dE$$

$$= \frac{\pi}{2s}[\mathrm{H}_0(bx\varepsilon^{-s}) - \mathrm{Y}_0(bx\varepsilon^{-s}) - \mathrm{H}_0(bx) + \mathrm{Y}_0(bx)] \quad (19)$$

as given by Watson;[8] the functions involved are Struve's function and Weber's function of the second kind.

Now $\mathrm{Y}_0(z) = \frac{2}{\pi}\sum_{m=0}^{\infty}\frac{(-1)^m(\frac{1}{2}z)^{2m}}{(m!)^2}[\log(\frac{1}{2}z) - \psi(n + 1)]$

Hence

$$\frac{\pi}{2s}[\mathrm{Y}_0(bx) - \mathrm{Y}_0(bx\varepsilon^{-s})] = \Sigma\varepsilon^{-2ms}\frac{(-1)^m(\frac{1}{2}bx)^{2m}}{(m!)^2}$$

$$+ \frac{1}{s}\Sigma(1 - \varepsilon^{-2ms})\frac{(-1)^m(\frac{1}{2}bx)^{2m}}{(m!)^2}[\log(\tfrac{1}{2}bx) - \psi(m + 1)]$$

$$= 1 - \varepsilon^{-2s}(\tfrac{1}{2}bx)^2 + \ldots + \frac{1}{s}[0 + \text{terms in } (bx)^2 \text{ and higher powers}]$$

$$= 1 - \varepsilon^{-2c\sqrt{n}}\frac{c^2p^2}{4n}x^2 + \ldots + \frac{1}{c\sqrt{n}}\left[0 + \text{terms in } \frac{c^2p^2}{n}x^2 \text{ and higher powers}\right] \quad (20)$$

As n increases all the terms of the first series in eqn. (20) after the first vanish more rapidly than $1/n$. In the second series all terms vanish to an order greater than $1/n$, taking into account the $1/\sqrt{n}$ multiplying factor.

Also
$$\mathrm{H}_0(z) = \sum_{m=0}^{\infty}\frac{(-1)^m(\frac{1}{2}z)^{2m+1}}{[\Gamma(m + \frac{3}{2})]^2}$$

Hence the other part of eqn. (19) may be written:

$$\frac{\pi}{2s}[\mathrm{H}_0(bx\varepsilon^{-s}) - \mathrm{H}_0(bx)] = \frac{\pi}{2s}\sum_{m=0}^{\infty}\frac{(-1)^m(\frac{1}{2}bx)^{2m+1}[\varepsilon^{-(2m+1)s} - 1]}{[\Gamma(m + \frac{3}{2})]^2}$$

$$= \frac{\pi}{2s}\left[-\frac{2}{\pi}bx(1 - \varepsilon^{-s}) + \text{terms in } (bx)^3 \text{ and higher powers}\right]$$

$$= \frac{\pi}{2c\sqrt{n}}\left[-\frac{2}{\pi}\frac{cp}{\sqrt{n}}x(1 - \varepsilon^{-c\sqrt{n}}) + \text{terms in } \frac{c^3p^3}{n^{3/2}}x^3 \text{ and higher powers}\right]$$

Of these terms, all but the first vanish more rapidly than $1/n$ as n increases; $\varepsilon^{-c\sqrt{n}}$ also vanishes.

Thus

$$\frac{\pi}{2s}[\mathrm{H}_0(bx\varepsilon^{-s}) - \mathrm{H}_0(bx)] = -\frac{px}{n} + \text{terms in higher powers of } \frac{1}{n} \quad (21)$$

So that, if we take the relevant terms from eqns. (20) and (21),

$$\lim_{n\to\infty}\left\{\frac{\pi}{2s}[\mathrm{H}_0(bx\varepsilon^{-s}) - \mathrm{Y}_0(bx\varepsilon^{-s}) - \mathrm{H}_0(bx) + \mathrm{Y}_0(bx)]\right\}^n$$

$$= \lim_{n\to\infty}\left(1 - \frac{px}{n}\right)^n$$

$$= \varepsilon^{-px}$$

This result is the same as that deduced from the rectangular pulse approximation [see eqn. (9)]. Hence the amplitude probability distribution for the resultant signal will be the same in this case as that given in eqns. (10) and (11). It would appear that the final result is not sensitive to quite considerable changes in the shape of the amplitude/time curve assumed for individual meteors.

(5) DISCUSSION

Certain properties of the distribution given by eqn. (10) can be readily calculated. For example, the median amplitude is given by $r = \sqrt{3}p$ and the mode by $r = p/\sqrt{2}$.

The mean and mean-square values of the distribution are infinitely large. However this is only to be expected from the initial statement of the problem, in which the probability of large signal amplitudes, r, was taken to be inversely proportional to r^2. In any case, these quantities will frequently not be required.

If mean and mean-square values have to be obtained in a particular case, a change must be made in the initial distribution to make the probability tend to zero more rapidly with increase of amplitude. The values must exist in practice: in the meteor reflection problem, for instance, the relevant change in the probability dependence occurs when the meteor mass is so large that the trail of ionization produced by it becomes over-dense. The received signal then becomes proportional to the fourth root of the electron line density in the trail instead of a linear function of it, and this, of course, reduces the probability of a large signal occurring. No calculations have been made of the amplitude distribution with this condition included; however, in forward-scatter circuits the change-over may take place at a level of about 40 dB above the median, so that the change in the distribution will be appreciable only at very high signal levels.

It is of interest to compare this theoretical distribution with distributions obtained in practice, although a good fit cannot be expected if turbulent scattering plays an appreciable part in the process. In certain of the published results large meteor signals have been excluded, which, of course, spoils the results for this purpose, and in others the period of observations is too long—about 30 min would probably be best, as stable conditions on a scatter link do not often last longer than this. The data given by Williams[9] for the path from Gibraltar to Christchurch on 70 Mc/s (reception on four Yagi aerials) appear to be the most suitable, and a plot of his values for a September evening is shown in Fig. 2. The co-ordinates are such that a Rayleigh

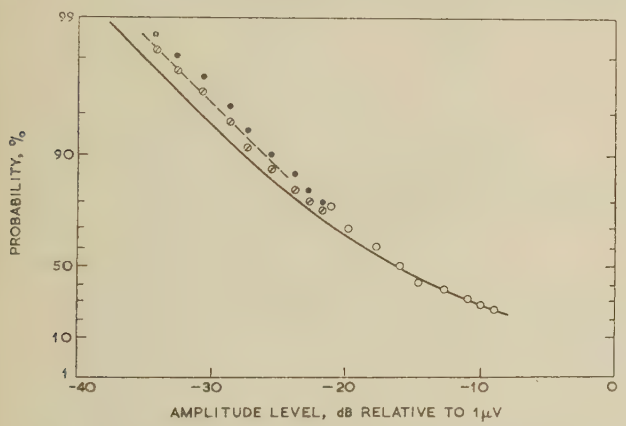

Fig. 2.—Comparison of the theoretical distribution with the experimental results of Williams[9] on 70 Mc/s.

The cumulative amplitude probability distribution is shown.
---- Rayleigh distribution.
—— Distribution $P_1(r)$ [eqn. (11)].
● ⊖ Range of values obtained.
◡ Values when range was too small to be shown. } Williams's results.

distribution would appear as a straight line inclined at an angle of 45° to the axes. The solid line is the cumulative theoretical distribution fitted as well as possible to the curved portion of the results which occurs at the right of the diagram, where the signal is most likely to be due to meteors alone. Taking the broken line to represent the best fit of a Rayleigh distribution to the weak-signal points, it can be seen that there is an increase in signal of about 1 dB in this region over that which would be expected from meteors alone. This difference can be attributed to the presence of some other source of signal with a Rayleigh distribution of amplitude, e.g. turbulent scattering; if the actual amplitude distribution continued to be Rayleigh up to high levels it could then be said that 21% of the power in the actual distribution was due to turbulent scattering, and 79% to meteors. As it is, it can only be said that in this case turbulent scattering appears to contribute 21% of the power which would be contained in a Rayleigh distribution fitted to the weak-signal points of the actual distribution.

A number of signal amplitude distributions taken over a long period exist, and two of these taken from Reference 10 are shown in Fig. 3 compared with the theoretical distribution. The

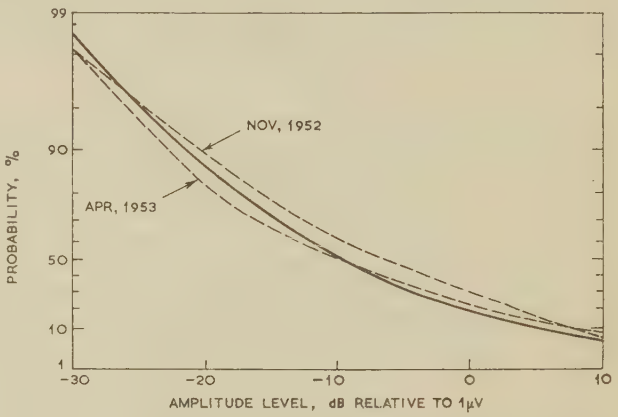

Fig. 3.—Comparison of the theoretical distribution with the experimental results of Bray *et al.*[10]

The cumulative amplitude probability distribution is shown.
---- Experimental results on 41 Mc/s.
—— Distribution $P_1(r)$ [eqn. (11)].

observations were made on a path from Lerwick to Jersey at 41 Mc/s, a rhombic aerial being used for reception; it will be seen that there is some similarity in the general shape of the curves. Each experimental curve represents the result of several days' observations, during which time considerable changes in propagation conditions would have taken place. However, a much more detailed study of amplitude distributions from this standpoint is required than can be given here on the basis of available data.

(6) CONCLUSIONS

The amplitude distribution given by meteor signals alone on an ionospheric forward-scatter link has been calculated with the aid of two different approximations to the variation with time of a meteor signal; both gave the same result. The derived distribution illustrates the point that the addition of an infinite number of signals need not necessarily yield a Rayleigh distribution of amplitude. A method has been given for calculating the relative proportion of meteoric and turbulent-scattering components in the signal in a forward scatter link. Only a limited application of this method could be given here; it would appear desirable to use it to examine the signal at all times of the day and of the year.

(7) ACKNOWLEDGMENT

The work was carried out as part of the programme of the Radio Research Board. This paper is published by permission of the Director of Radio Research of the Department of Scientific and Industrial Research.

(8) REFERENCES

(1) Bailey, D. K., Bateman, R., and Kirby, R. C.: 'Radio Transmission at V.H.F. by Scattering and other Processes

in the Lower Ionosphere', *Proceedings of the Institute o Radio Engineers*, 1955, **43**, p. 1181.

(2) SAXTON, J. A.: 'La physique de la diffusion ionosphérique sur ondes métriques', *Onde Electrique*, 1957, **37**, p. 450.

(3) VILLARD, O. G., ESHLEMAN, V. R., MANNING, L. A., and PETERSON, A. M.: 'The Role of Meteors in Extended-Range V.H.F. Propagation', *Proceedings of the Institute of Radio Engineers*, 1955, **43**, p. 1473.

(4) HORNER, F., and HARWOOD, J.: 'An Investigation of Atmospheric Radio Noise at Very Low Frequencies', *Proceedings I.E.E.*, Paper No. 2147 R, November, 1956 (**103** B, p. 743).

(5) LOVELL, A. C. B.: 'Meteor Astronomy' (Oxford University Press, 1954).

(6) KAISER, T. R.: 'Radio Echo Studies of Meteor Ionization', *Philosophical Magazine*, 1953, **2**, Supplement, p. 495.

(7) LORD RAYLEIGH: 'On the Problem of Random Vibrations and of Random Flights in 1, 2 and 3 Dimensions', Scientific Papers VI, p. 604.

(8) WATSON, G. N.: 'The Theory of Bessel Functions' (Cambridge University Press, 1944), 2nd Edition.

(9) WILLIAMS, D.: 'The Structure of High-Frequency Ionospheric Scatter Signals', *Proceedings I.E.E.*, Paper No. 2529 R, January, 1958 (**105** B, Suppl. 8, p. 19).

(10) BRAY, W. J., SAXTON, J. A., WHITE, R. W., and LUSCOMBE, G. W.: 'V.H.F. Propagation by Ionospheric Scattering and its Application to Long-Distance Communication', *ibid.*, Paper No. 1920 R, October, 1955 (**103** B, p. 236).

621.315.212.1

The Institution of Electrical Engineers
Monograph No. 390 S
July 1960

A BRIEF REVIEW OF THE THEORY OF PAPER LAPPING OF A SINGLE-CORE HIGH-VOLTAGE CABLE

By P. GAZZANA-PRIAROGGIA, Dr.Ing., Associate Member, E. OCCHINI, Dr.Ing., and N. PALMIERI, Dr.Ing.

(*The paper was first received 9th November, 1959, and in revised form 22nd March, 1960. It was published as an* INSTITUTION MONOGRAPH *in July, 1960.*)

SUMMARY

A brief outline of the theory of the lapping operation for high-voltage single-core paper-lapped cable is given, showing the stability conditions which the insulation thickness must satisfy in order that bending of the cable on the reel or capstan does not cause any damage to the insulation itself.

An example of the design of a high-voltage cable is considered, showing the application of the theory outlined and its practical use.

LIST OF SYMBOLS

E_1, E_2 = Normal elastic moduli of the paper in the machine direction and in the cross direction, kg/cm^2.
E_θ, E_z = Equivalent moduli of the paper in the direction of co-ordinates θ and z, kg/cm^2.
$E_3 = E_r$ = Normal modulus in the direction at right angles to the paper surface, kg/cm^2.
f = Static friction coefficient.
G = Shear elastic modulus of the paper, kg/cm^2.
h = Width of the butt-space between two contiguous turns of a helically-wound paper tape, cm.
$K = r/r_0$.
$K_1 = r_1/r_0$.
L = Width of paper tape, cm.
l = Free flexural length of paper ring, cm.
N_{1z} = Axial internal stress in paper ring, kg/cm.
$n = E_\theta/E_r$.
P_0 = Critical load of paper ring, kg/cm.
R_0 = Bending radius of the cable, cm.
r_0 = Radius of the conductor, cm.
r_1 = Outer radius, cm.
r_x = Radius of the tensioned paper tape, cm.
r = Actual radius on which the pressure is determined, cm.
s = Thickness of paper sheet, cm.
T = Lapping tension, kg.
α = Winding angle of paper tape.
$\nu = E_\theta/E_z$.
$\mu_z = G/E_z$.
$\mu_\theta = G/E_\theta$.
ϕ_r, ϕ_θ = Partial radial and transverse pressure due to lapping of a paper tape on the underlying ones, kg/cm^2.
Φ_{0r}, $\Phi_{0\theta}$ = Radial and transverse pressure due to lapping, kg/cm^2.
Φ_{1r}, Φ_{1z} = Radial and axial pressure due to bending, kg/cm^2.
Φ_∞ = Plateau pressure, kg/cm^2.
$\Phi_{u,r}$ = Allowable upper value of the radial pressure, kg/cm^2.
$\Phi_{l,r}$ = Allowable lower value of the radial pressure, kg/cm^2.

Correspondence on Monographs is invited for consideration with a view to publication.
The authors are at the Pirelli Cable Research Laboratories, Milan, Italy.

(1) INTRODUCTION

(1.1) General

The object of the paper is to give a brief survey of the theory of the lapping operation with insulating paper tapes for high-voltage cables from a mechanical point of view; for a complete treatment of this theory reference is made to a more extensive work by the authors to be published shortly.[1]

As is well known, the paper tapes which constitute the insulation of high-voltage cables are, in general, lapped as open helices (i.e. discontinuously) with one start only for each layer and with a lapping sense which is either constant or reversed periodically. The gaps in the single helices lapped in the same sense are always staggered between one layer and the next by a certain interval which varies from 50 to 25% of the lay.

As one of the fundamental characteristics required in a cable is its ability to bend during manufacture and laying without damaging the insulation, it would, of course, be ideal if the diameter of the reel or capstan on which the cable is wound were large enough to ensure that the deformation of the insulation during bending could be maintained within the elastic limits of the paper. An attempt could then be made to obtain such compact lapping that there would be no movement of the tapes during bending, the friction stresses being larger than the elastic stresses.

But in this manner a winding diameter would be necessary which could not be realized in practice, and therefore it has to be accepted that the papers must slide with respect to one another during bending. It is also obvious that the movement of the papers can only be assured if lapping is carried out with open helices, up to the point at which the edges of the tapes constituting the helix come into contact with one another.

(1.2) Forces Acting During Bending

It is easy to understand that, owing to the radial pressure caused by the lapping operation and bending, friction forces are created which, on bending the cable, stress the paper tapes in the slipping direction. In the compressed part of the cable these forces exert an end-thrust on each single paper turn, and in this manner they can set up critical conditions which generally cause some damage to the insulation: the damage can be described as wrinkles or creases according to whether the edges are rounded off or at a sharp angle.

(1.3) Damage to the Insulation as a Result of Bending

In Figs. 1(*a*), (*b*) and (*c*) some types of damage to the insulation as a result of bending are represented.

Fig. 1(*a*) shows the butt-space creases which occur in the compressed part of the insulation where the friction forces necessary for the sliding of the paper tapes are such as to cause the collapse of the paper owing to end-thrust in correspondence with the butt-spaces (see Section 5).

Collapse creases [Fig. 1(*b*)] occur in the compressed zone when the paper tapes also collapse outside the butt-spaces (see

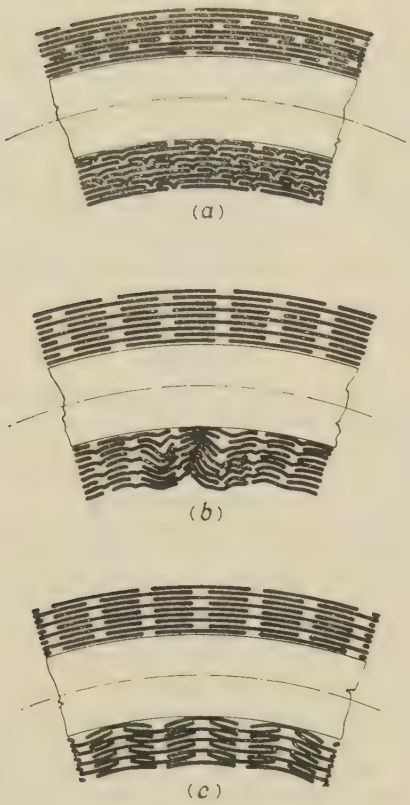

Fig. 1.—Creases and wrinkles.
(*a*) Butt-space creases (paper tapes staggered by 30%).
(*b*) Collapse creases (tapes staggered by 50%).
(*c*) Collapse wrinkles (tapes staggered by 50%).

Section 5). They are characterized by the total collapse of a considerable thickness of insulation and appear in the form of deep buckling with rather sharp edges.

Collapse wrinkles [Fig. 1(*c*)] occur in the compressed zone of the insulation owing to defective compactness and are the result of the collapse of the single paper turns due to the axial and radial forces acting on the paper tape during bending (see Sections 3 and 5).

(1.4) Influence of Wrinkles and Creases on the Dielectric Strength of Cables

It is easy to see that every crease or wrinkle of the insulating paper modifies locally the electric field distribution, causing an increase in the electric stress; also, stress components acting along the paper stratification are originated and it is known that the electric strength of paper layers is lower along the stratification than perpendicularly to it. Moreover, every wrinkle or crease can produce between adjacent layers a separation larger than the thickness of the paper itself.

Experimental results on cable models,* in which creases are purposely introduced, show a decrease of the impulse electric strength as large as 25% depending on the depth, sharpness and extent of the creases. These laboratory results find very good practical confirmation in incorrectly lapped cables.

It therefore appears that the cable insulation must be designed in such a way that creases or wrinkles cannot be produced. To this end it is necessary to have as much knowledge as possible of the radial compression conditions existing in the cable in order to determine whether the paper can withstand the friction forces set up during bending.

* The physical characteristics of these models are described in Reference 2.

In Sections 2 and 3 the pressures due to the lapping operation and bending are considered, while in Section 4 the critical conditions due to bending are examined.

(2) MECHANICAL STRESSES IN THE PAPER INSULATION CAUSED BY THE LAPPING OPERATION

(2.1) General

During the lapping operation the cable assumes the configuration of a circular infinite cylinder on which paper tapes of thickness s and width L are helically wound with such a lay that the turns are separated from one another by a distance h, which is very small compared with L.

Assuming a system of cylindrical co-ordinates as shown in Fig. 2(*a*) with the z-axis in the direction of the axis of the

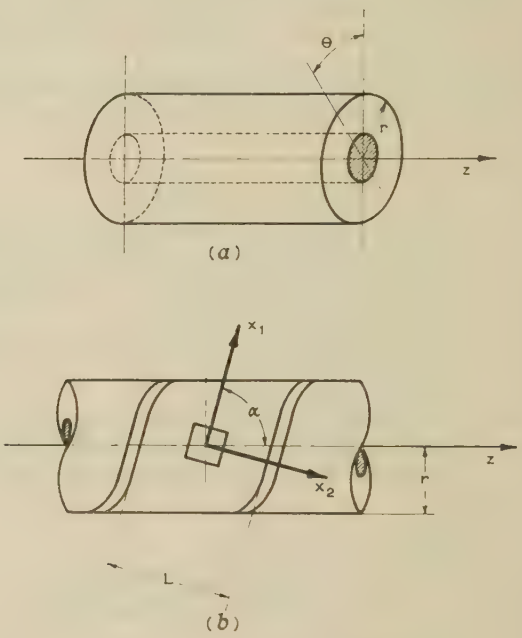

Fig. 2.—Cylindrical co-ordinates.
(*a*) Reference frame for the cable during lapping.
(*b*) Definition of angle α.

cylinder, the angle α between the machine direction* of the paper tapes and the z-axis is given by

$$\cos\alpha = \frac{L+h}{2\pi r} \simeq \frac{L}{2\pi r}$$

r being the radius of the layer under consideration, Fig. 2(*b*).

In many practical cases $\alpha \simeq \pi/2$ (since $L \ll 2\pi r$), and therefore, in order to simplify the problem, throughout the following analysis it will be assumed that each layer at radius r, actually consisting of helically lapped paper tapes, may be considered to be a series of contiguous rings, all of radius r, separated from one another by a distance h which is negligible compared with L; this assumption is also justified if the preceding relation is not strictly true.[1]

It has been experimentally verified that the paper is strongly anisotropic with respect to its mechanical properties. If E_1 is the normal modulus in the machine direction, E_2 the normal modulus in the cross direction, and G the shear modulus, then according to the simplifying assumptions made in this Section,

$$\left.\begin{aligned} E_1 &= E_\theta \\ E_2 &= E_z \end{aligned}\right\} \quad \ldots\ldots\ldots \quad (1)$$

* Throughout the paper 'machine direction' is the direction of travel of the paper-making machine and 'cross direction' is at right angles to it.

E_θ and E_z being the equivalent normal moduli in directions θ and z which, in our hypothesis, coincide with the machine and the cross directions. If the actual helically lapped layer is considered, eqns. (1) no longer hold and a more accurate analysis is necessary.

Let $E_3 = E_r$ represent the normal compression modulus of several paper layers in the direction at right angles to their surface and hence in the radial direction for the actual cable. Experiments show that, while E_1, E_2 and G are constant throughout a wide range of the applied stresses, this does not hold for E_3. In fact, generally speaking, the strain in the direction normal to the paper plane is not a single-valued function of the stress, as the paper layers show considerable hysteresis in this direction. On the other hand, it has been shown that the theory developed assuming E_3 to have a suitable constant value is in good agreement with practice.[1] Therefore E_3 will be assumed to be constant and Section 2.2 gives a suitable method for its determination.

As a result of many experiments the following ranges of values of the above moduli have been obtained:

$$\left.\begin{aligned} E_1 &= 50000 \text{ to } 70000\,\text{kg/cm}^2 \\ E_2 &= 20000 \text{ to } 30000\,\text{kg/cm}^2 \\ E_3 &= 20 \text{ to } 100\,\text{kg/cm}^2 \\ G &= 14000 \text{ to } 16000\,\text{kg/cm}^2 \end{aligned}\right\} \quad . \quad . \quad . \quad . \quad (2)$$

Experiments have also proved that Poisson's ratios for the paper are negligible, and therefore the elastic equations may be written

$$\left.\begin{aligned} \Phi_1 &= E_1\eta_1 \qquad \Phi_2 = E_2\eta_2 \\ \Phi_{12} &= G\eta_{12} \qquad \Phi_3 = E_3\eta_3 \end{aligned}\right\} \quad . \quad . \quad . \quad . \quad (3)$$

where Φ_1 is the normal stress in the machine direction, Φ_2 is the normal stress in the cross direction, Φ_{12} is the tangential stress in the paper plane, Φ_3 is the normal stress in the direction normal to the paper plane and η_1, η_2, η_{12}, η_3 are the relative strains.

Finally, it will be assumed that the compression values of E_1 and E_2 are practically coincident with the tensile ones, this assumption being sufficiently confirmed by experiments in the practical range of the stress values. Obviously it is necessary for Φ_3 to be a compression stress for the stability of the insulation and also $\eta_{13} = \eta_{23} = 0$.

(2.2) Equilibrium and Compatibility Equations

In order to calculate the stresses in the insulation thickness caused by the lapping operation we first consider the elementary effect of a paper tape wound with tension T on the underlying tapes, which are assumed to be applied with no tension and are considered as a compact body; i.e. it is assumed that there are no sliding movements between the layers but only compression effects. By successively summing up the effects of the single tapes the total stresses on a certain layer due to all the overlying tapes will be calculated. If $\phi_r(r, r_x)$ and $\phi_\theta(r, r_x)$ are the elementary stresses due to the effect of a paper tape wound at radius r_x on an insulating element of cable at radius r (see Fig. 3), and $\Phi_r(r)$, $\Phi_\theta(r)$ are the total stresses on the same element due to all the tapes overlying it, it can be shown that[1]

$$\left.\begin{aligned} \Phi_r(r) &= \int_r^{r_1} \phi_r(r, r_x)\frac{dr_x}{s} \\ \Phi_\theta(r) &= \int_r^{r_1} \phi_\theta(r, r_x)\frac{dr_x}{s} - \left(\frac{T\sin^2\alpha}{Ls}\right)_{r_x=r} \end{aligned}\right\} \quad . \quad . \quad (4)$$

where r_1 is the outer radius of the lapped cable and s is the paper thickness.

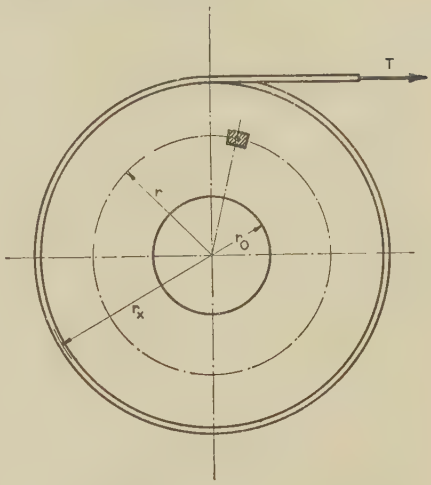

Fig. 3.—Effect at radius r due to the tape wound at radius r_x.

The elementary stresses ϕ_r and ϕ_θ and the corresponding strains ε_r and ε_θ satisfy the classic equations for the symmetrical equilibrium problem in cylindrical co-ordinates, i.e.

$$\left.\begin{aligned} \frac{\partial\phi_r(r, r_x)}{\partial r} + \frac{1}{r}[\phi_r(r, r_x) - \phi_\theta(r, r_x)] &= 0 \\ \frac{\partial\varepsilon_\theta(r, r_x)}{\partial r} + \frac{1}{r}[\varepsilon_\theta(r, r_x) - \varepsilon_r(r, r_x)] &= 0 \end{aligned}\right\} \quad . \quad . \quad (5)$$

for $r < r_x$, where

$$\phi_r = E_r\varepsilon_r \qquad \phi_\theta = E_\theta\varepsilon_\theta \quad . \quad . \quad . \quad . \quad . \quad (6)$$

The boundary conditions are

$$\left.\begin{aligned} [\phi_r(r, r_x)]_{r=r_x} &= \frac{T\sin^2\alpha}{Lr_x} \\ [\varepsilon_\theta(r, r_x)]_{r=r_0} &= 0 \end{aligned}\right\} \quad . \quad . \quad . \quad . \quad (7)$$

where r_0 is the radius of the conductor and the compressive stresses are assumed to be positive.

From eqns. (5) and (6),

$$r^2\frac{\partial^2\phi_r(r, r_x)}{\partial r^2} + 3r\frac{\partial\phi_r(r, r_x)}{\partial r} - (n-1)\phi_r(r, r_x) = 0 \quad . \quad (8)$$

where

$$n = \frac{E_\theta}{E_r} > 1 \qquad r_0 \leqslant r < r_x \quad . \quad . \quad . \quad . \quad (9)$$

Performing the calculation for the case in which T, L, s and $\sin\alpha$ can be considered constant, the radial pressure is

$$\Phi_r(r) = \frac{T\sin^2\alpha}{sL}\left[\left(\frac{K}{x}\right)^{\sqrt{n}-1}\frac{1+K^{-2\sqrt{n}}}{\sqrt{n}-1}\right.$$
$$\left.\left(1 - \frac{\sqrt{n}-1}{3\sqrt{n}-1}x^{-2\sqrt{n}} + \frac{\sqrt{n}-1}{5\sqrt{n}-1}x^{-4\sqrt{n}}\ldots\right)\right]_{K_1}^{K} \quad . \quad (10)$$

where $K = r/r_0 > 1$, $K_1 = r_1/r_0$ and $x = r_x/r$

Similarly, the transverse pressure becomes

$$\Phi_\theta(r) = \frac{T\sin^2\alpha}{sL}\left[\sqrt{n}\left(\frac{K}{x}\right)^{\sqrt{n}-1}\frac{1-K^{-2\sqrt{n}}}{\sqrt{n}-1}\right.$$
$$\left.\left(1 - \frac{\sqrt{n}-1}{3\sqrt{n}-1}x^{-2\sqrt{n}} + \frac{\sqrt{n}-1}{5\sqrt{n}-1}x^{-4\sqrt{n}}\ldots\right)\right]_{K_1} - \frac{T\sin^2\alpha}{sL}$$
$$\quad . \quad . \quad . \quad . \quad (11)$$

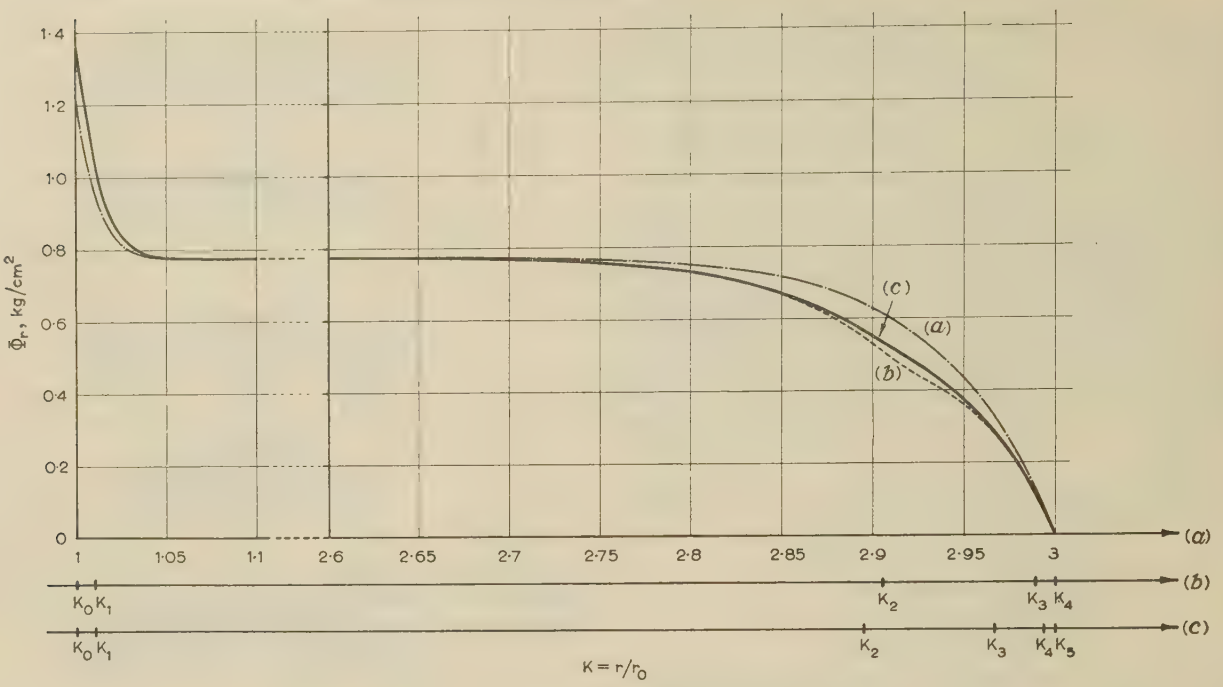

Fig. 4.—Theoretical distribution of Φ_r in the insulation thickness.

———— Results obtained by assuming for E_r the constant value corresponding to $\Phi\infty$ throughout the insulation thickness.
– – – – – Intermediate stage obtained by subdividing the insulation thickness into four layers as indicated at (*b*).
———— Final results obtained by subdividing the insulation thickness into five layers as indicated at (*c*).

For actual values of n (from 500 to 1 500) it is easy to see that, if $r/r_0 \geqslant 1{\cdot}05 - 1{\cdot}1$, it may be assumed that $K^{-2\sqrt{n}} \ll 1$ and eqns. (10) and (11) simplify to

$$\Phi_r(r) = \frac{T\sin^2\alpha}{sL}\,\frac{1}{\sqrt{n}-1}\left[1-\left(\frac{r}{r_1}\right)^{\sqrt{n}-1}\right] \quad . \quad (10a)$$

$$\Phi_\theta(r) = \frac{T\sin^2\alpha}{sL}\,\frac{1}{\sqrt{n}-1}\left[1-\sqrt{n}\left(\frac{r}{r_1}\right)^{\sqrt{n}-1}\right] \quad . \quad (11a)$$

Moreover, for $r/r_1 \leqslant 0{\cdot}9$ both Φ_r and Φ_θ tend to a constant value Φ_∞, which is usually called the plateau pressure, given by

$$\Phi_\infty = \frac{T\sin^2\alpha}{sL}\,\frac{1}{\sqrt{n}-1} \quad . \quad . \quad . \quad . \quad (12)$$

Then, if the insulation thickness is such that $r_1/r_0 \geqslant 1{\cdot}5$ (as happens for high-voltage cables), a great internal part of the insulation thickness is subjected to the isotropic inward pressure Φ_∞, which is independent of r.

It is worth noting that the extension of the zone of the plateau pressure is a consequence of the values of n. Actually, the larger $\sqrt{n}$ the larger is the part of the insulation thickness subjected to pressure Φ_∞; this suggests that the calculations should be made with the value of E_r, obtained from the stress/strain diagram, corresponding to the value of Φ_∞.

In Fig. 4 the result of the calculations of radial pressure in a cable with homogeneous insulation is shown assuming the constancy of E_r against Φ_r.

The same Figure also shows the calculated distribution of Φ_r taking into account the variability of E_r against Φ_r (see Fig. 5), and it can be seen that the variations so obtained are negligible for practical purposes.

These calculations are made by subdividing the insulation thickness into a suitable number of layers for which E_r has a variation so small that the linear theory can be adopted, as shown in Section 2.3.

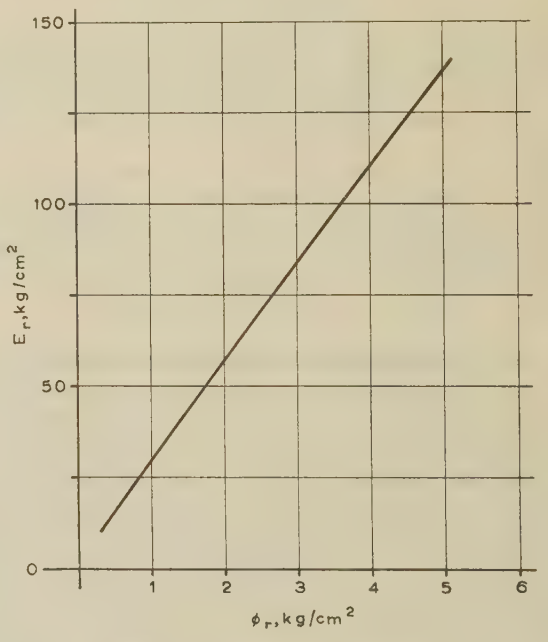

Fig. 5.—Variation of E_r with Φ_r.

(2.3) Extension of the Theory to an Inhomogeneous Insulation Thickness

The considerations developed in the preceding Sections may be extended to the case of inhomogeneous lapping; this occurs when the paper tapes show different mechanical properties, or are applied with different tension or different lay, or if one or more of the parameters T, α, s, L, n, E_r, E_θ assume different values when passing from one layer to a successive one. In this way it is possible[1] to overcome practically the limitations

ntroduced by assuming α to be constant and also to take into ıccount the variability of E_r against Φ_r.

In fact, if these parameters vary continuously or discontinuously from layer to layer, it is always possible to group together some adjacent layers so that in these groups there is a relatively small variation of the parameters; then for each group of layers one can introduce the average values of the corresponding parameters in the equations in this Section.

In the present Section the expression 'elementary layer' will be used to indicate a single paper tape, while 'layer' will be used to indicate a group of elementary layers which can be assumed to be homogeneous in accordance with the preceding considerations.

For the sake of simplicity the general formulae are given without the corresponding deductions.

If the insulation thickness consists of N different layers, the total radial stress in the layer p ($p = 1, 2, \ldots, N$) due to the

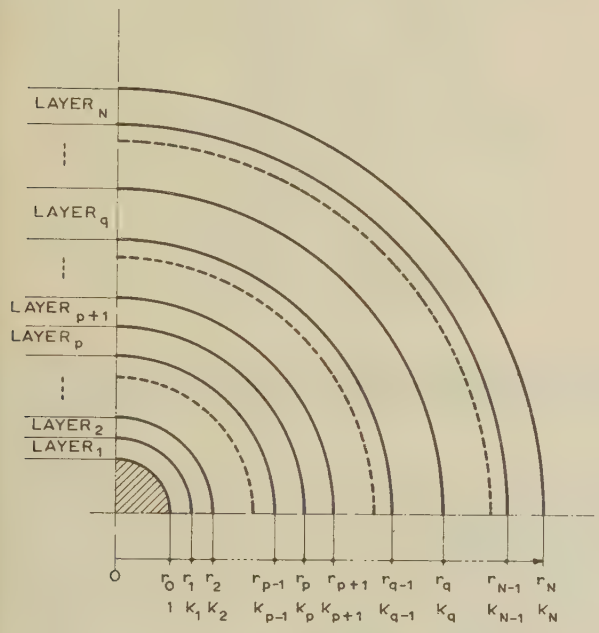

Fig. 6.—Example of insulation thickness made up of N inhomogeneous paper layers.

elementary tapes wound successively on the layers $p+1$, $p+2, \ldots q, \ldots, N$ (see Fig. 6), is given by

$$\Phi_r(r) = S_p K^{\sqrt{n_p}-1}\left(1 + \frac{R_p}{S_p}K^{-2\sqrt{n_p}}\right) \times \left\{\frac{T_p \sin^2\alpha_p}{s_p L_p}\left[\Omega_p\right]_{Kp}^{K} + \sum_{p+1}^{N} 2^{q-p}\frac{T_q \sin^2\alpha_q}{s_q L_q}\left(\prod_{p}^{q-1}\gamma_m\sqrt{n_{m-1}}\right)\left[\Omega_q\right]_{Kq}^{K_{q-1}}\right\} \quad . \quad (13)$$

for $K_{p-1} < K < K_p$ and $p = 1, 2, \ldots N-1$

and by

$$\Phi_r(r) = S_N K^{\sqrt{n_N}-1}\left(1 + \frac{R_N}{S_N}K^{-2\sqrt{n_N}}\right)\frac{T_N \sin^2\alpha_N}{s_N L_N}\left[\Omega_N\right]_{K_N}^{K} \quad . \quad (13a)$$

for $K_{N-1} < K < K_N$ and $p = N$.

In a similar way the total transverse stress is given by

$$\Phi_\theta(r) = \sqrt{(n_p)}S_p K^{\sqrt{n_p}-1}\left(1 - \frac{R_p}{S_p}K^{-2\sqrt{n_p}}\right) \left\{\frac{T_p \sin^2\alpha_p}{s_p L_p}\left[\Omega_p\right]_{K_p}^{K} + \sum_{p+1}^{N} 2^{q-p}\frac{T_q \sin^2\alpha_q}{s_q L_q}\left(\prod_{p}^{q-1}\gamma_m\sqrt{n_{m-1}}\right)\left[\Omega_q\right]_{K_q}^{K_{q-1}}\right\} - \frac{T_p \sin^2\alpha_p}{s_p L_p} \quad . \quad (14)$$

for $K_{p-1} < K < K_p$ and $p = 1, 2, \ldots N-1$

and by

$$\Phi_\theta(r) = \sqrt{n_N}S_N K^{\sqrt{n_N}-1}\left(1 - \frac{R_N}{S_N}K^{-2\sqrt{n_N}}\right) \left\{\frac{T_N \sin^2\alpha_N}{s_N L_N}\left[\Omega_N\right]_{K_N}^{K}\right\} - \frac{T_N \sin^2\alpha_N}{s_N L_N} \quad . \quad (14a)$$

for $K_{N-1} < K < K_N$ and $p = N$.

In eqns. (13), (13a), (14) and (14a),

$$\Omega_p(x) = \frac{1}{S_p}\frac{x^{1-\sqrt{n_p}}}{\sqrt{n_p}-1}\sum_{0}^{\infty}{}^{l}\frac{\sqrt{n_p}-1}{(2l+1)\sqrt{n_p}-1}\left(\frac{R_p}{S_p}x^{-2\sqrt{n_p}}\right)^l$$

$$R_p = K_{p-1}^{\sqrt{n_p}+\sqrt{n_{p-1}}}\left[S_{p-1}(\gamma_{p-1}\sqrt{n_p} - \sqrt{n_{p-1}}) + R_{p-1}K_{p-1}^{-2\sqrt{n_{p-1}}}(\gamma_{p-1}\sqrt{n_p} + \sqrt{n_{p-1}})\right]$$

$$R_1 = 1$$

$$S_p = K_{p-1}^{-\sqrt{n_p}+\sqrt{n_{p-1}}}\left[S_{p-1}(\gamma_{p-1}\sqrt{n_p} + \sqrt{n_{p-1}}) + R_{p-1}K_{p-1}^{-2\sqrt{n_{p-1}}}(\gamma_{p-1}\sqrt{n_p} - \sqrt{n_{p-1}})\right]$$

$$S_1 = 1$$

$$\gamma_p = \frac{E_{p,\theta}}{E_{p+1,\theta}}$$

A complete example of the numerical calculations regarding the insulation of a cable lapped with several paper layers is outlined in Section 6.

(3) MECHANICAL STRESSES IN THE PAPER INSULATION CAUSED BY BENDING OF THE CABLE

(3.1) General

The study of the stresses in the insulation during the lapping operation provides a basis for the calculation of stresses during bending of the cable.

It can be shown that wrinkles or creases generally form during the first bending of the cable, before drying. In fact, as the latter operation greatly reduces the radial pressure in the main part of the insulation thickness[1] and the subsequent oil impregnation reduces the friction coefficient between the paper tapes, the collapse phenomena due to axial pressures do not occur during subsequent bendings if they have not occurred at the first one.

Therefore the main purpose of the following considerations is the mathematical analysis of the cable bending on the take-up drum of the lapping machine.

Let us consider a paper-lapped cable with an insulation thickness made of tapes staggered by 50% and wound with tension T. In a straight cable this tension produces a radial pressure Φ_{0r} and a transverse pressure $\Phi_{0\theta}$ on the tape wound at radius r. This tape may be considered as a series of contiguous rings, all

of radius r (see Section 2.1). Φ_{0r} and $\Phi_{0\theta}$ can be considered to be known functions of r according to the preceding analysis.*

If the cable is straight, Φ_{0r} and $\Phi_{0\theta}$ do not depend on θ and z; Φ_{0r} gives an equilibrated system, S_0, of distributed external forces applied to both faces of the ring under consideration. When the cable axis is bent with a radius of curvature R_0, another equilibrated system, S_1, of distributed external forces is superimposed on the ring: system S_1, which depends on θ and z, tends to deform the ring in order to make it congruent with the toroidal surface assumed after bending by the elementary layer to which the ring itself belongs. System S_1 also depends on system S_0 owing to the friction effects.

The analysis of system S_1 is somewhat intricate.[1] The starting points are the equilibrium and compatibility equations of a thin cylindrical shell of radius r and the conditions of congruence of the deformed ring surface with the toroidal surface to which the elementary layer of the ring considered belongs after bending; this toroidal surface is generated by a circle of radius r rotating around an axis in the same plane at distance R_0 from the centre of the circumference.

(3.2) Stresses and Forces in a Paper Ring During Bending

The analysis gives the values of the radial and tangential components Φ_{1r} and Φ_{1z} of the distributed external force of system S_1, while component $\Phi_{1\theta}$ is everywhere zero.

If f is the static friction coefficient, L the width of the ring, s its thickness, and Φ_{0r} the radial force of system S_0 due to the lapping operation, we get

$$\Phi_{1z}(\theta) = 2f\Phi_{0r}\cos\theta \quad . \quad . \quad . \quad . \quad (15)$$

$$\Phi_{1r}(z,\theta) = \left[\frac{sE_\theta}{R_0}g_1\left(\frac{z}{r}\right) - 2f\Phi_{0r}g_2\left(\frac{z}{r}\right)\right]\cos\theta \quad . \quad (16)$$

where

$$g_1\left(\frac{z}{r}\right) = -a_1\cosh p_1\frac{z}{r} + a_2\cosh p_2\frac{z}{r}$$

$$g_2\left(\frac{z}{r}\right) = \frac{\nu}{p_1^2 - p_2^2}\left(-b_1\cosh p_1\frac{z}{r} - \frac{1}{p_1}\varepsilon^{-p_1\frac{z}{r}} + b_2\cosh p_2\frac{z}{r} + \frac{1}{p_2}\varepsilon^{-p_2\frac{z}{r}}\right)$$

$$a_1 = \frac{1}{p_2 D}\sinh p_2\frac{L}{2r} \qquad a_2 = \frac{1}{p_1 D}\sinh p_1\frac{L}{2r}$$

$$b_1 = \frac{B}{D}\cosh p_2\frac{L}{2r} - \frac{C}{D}\sinh p_2\frac{L}{2r}$$

$$b_2 = \frac{B}{D}\left(\frac{p_2}{p_1}\right)^2\cosh p_1\frac{L}{2r} - \frac{C}{D}\frac{p_2}{p_1}\sinh p_1\frac{L}{2r}$$

$$B = \left(\frac{p_1}{p_2}\right)^2(1 - \varepsilon^{-p_2\frac{L}{2r}}) - (1 - \varepsilon^{-p_1\frac{L}{2r}})$$

$$C = \left(\frac{p_1}{p_2}\right)^2\varepsilon^{-p_2\frac{L}{2r}} - \frac{p_2}{p_1}\varepsilon^{-p_1\frac{L}{2r}}$$

$$D = p_1\cosh p_2\frac{L}{2r}\sinh p_1\frac{L}{2r} - p_2\cosh p_1\frac{L}{2r}\sinh p_2\frac{L}{2r}$$

* Subscript 0 in Φ_{0r} and $\Phi_{0\theta}$ is introduced here to distinguish these pressures from pressures Φ_{1r} and $\Phi_{1\theta}$ due to cable bending.

$$p_1 = \frac{1}{\sqrt{2}}\left[\frac{1}{\mu_\theta} + \left(\frac{1}{\mu_\theta^2} - 4\nu\right)^{1/2}\right]^{1/2},$$

$$p_2 = \frac{1}{\sqrt{2}}\left[\frac{1}{\mu_\theta} - \left(\frac{1}{\mu_\theta^2} - 4\nu\right)^{1/2}\right]^{1/2}$$

$$\nu = \frac{E_\theta}{E_z}, \quad \mu_z = \frac{G}{E_z}, \quad \mu_\theta = \frac{G}{E_\theta}$$

The paper ring referred to the usual cylindrical co-ordinates r, θ, z is represented in Fig. 7. As regards the sign conventions

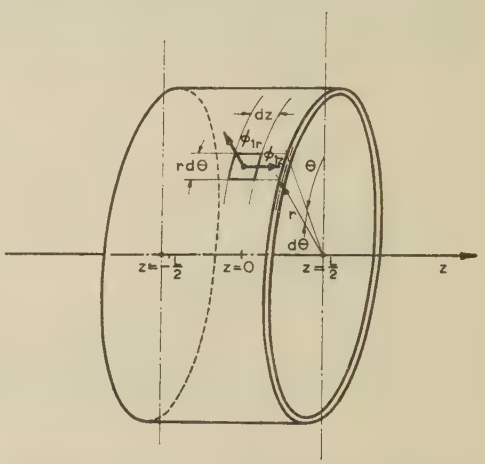

Fig. 7.—Cylindrical co-ordinates used as reference frame for a paper ring, and the sign convention for the components of the external force.

used in eqns. (15) and (16), Φ_{1z} is positive when it is a tensile force, and Φ_{1r} is positive when it is directed outwards, i.e. in the direction of increasing values of r.

In the preceding equations, g_1 and g_2 depend only on the two non-dimensional ratios z/r, $L/2r$ and on the non-dimensional physical coefficients $\nu = E_\theta/E_z$, $\mu_z = G/E_z$ and $\mu_\theta = G/E_\theta$, which may be assumed constant for a number of different paper qualities, while Φ_{1z} does not depend on z.

The compressive internal axial stress N_{1z} caused by system S_1 is obtained in a similar way; it is a significative parameter for the analysis of the collapse, as will be seen later:

$$N_{1z}(z,\theta) = r\left[\frac{sE_\theta}{R_0}m_1\left(\frac{z}{r}\right) - 2f\Phi_{0r}m_2\left(\frac{z}{r}\right)\right]\cos\theta \quad . \quad (17$$

where

$$m_1\left(\frac{z}{r}\right) = \frac{1}{\nu}\left(1 + p_2^2a_1\cosh p_1\frac{z}{r} - p_1^2a_2\cosh p_2\frac{z}{r}\right)$$

$$m_2\left(\frac{z}{r}\right) = \frac{\nu}{p_1^2 - p_2^2}\left[\frac{1}{p_1^2}\left(b_1\cosh p_1\frac{z}{r} + \frac{1}{p_1}\varepsilon^{-p_1\frac{z}{r}}\right) - \frac{1}{p_2^2}\left(b_2\cosh p_2\frac{z}{r} + \frac{1}{p_2}\varepsilon^{-p_2\frac{z}{r}}\right)\right.$$

Extensive diagrams of g_1, g_2, m_1 and m_2 are not plotted here, but the following considerations are sufficient in most practical cases.

The maximum absolute values of Φ_{1r} are, in general, reached for $z = \pm L/2$ and $\theta = 0, \pi$, i.e. at the ends of the ring in the bending plane; therefore in Fig. 8, $g_1(L/2r)$ and $g_2(L/2r)$ are plotted against $L/2r$ so that one can easily calculate by means of eqn. (16) the maximum radial stress of the ring for given values of R_0 and Φ_{0r}.

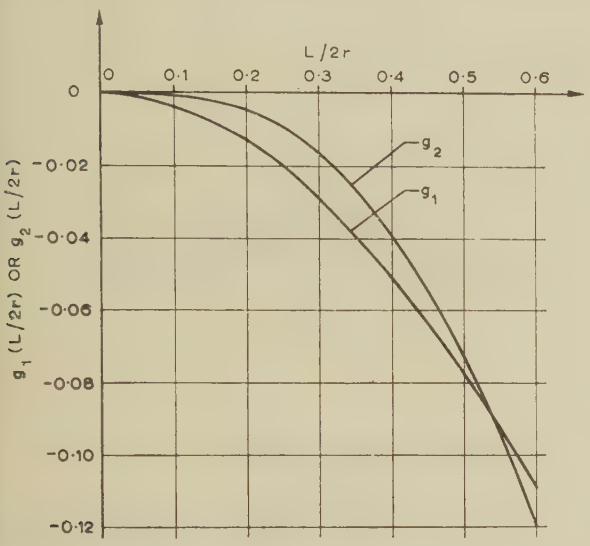

Fig. 8.—Distribution of g_1 and g_2 against $L/2r$.
$\nu = 3$; $\mu_\theta = 0{\cdot}25$; $\mu_z = 0{\cdot}75$.

The maximum absolute values of N_{1z} are reached, on the other hand, for $z = 0$ and $\theta = 0, \pi$, i.e. at the middle of the ring in the bending plane; N_{1z} is a tensile stress for $\theta = 0$ and compressive for $\theta = \pi$.

Calculations show that in the range of practical cases, for R_0 between 100 and 200cm, the first term of N_{1z} in eqn. (17) is absolutely negligible compared with the second one, and it is also possible to verify that a very good approximation for $m_2(0)$ is given by $m_2(0) = L/2r$. Therefore $N_{1z}(z, \theta)$ does not in practice depend on R_0 and

$$|N_{1z}(0, 0)| = |N_{1z}(0, \pi)| = N_{z\,max} = fL\Phi_{0r} \quad . \quad . \quad (18)$$

In Section 5 it will be seen that the stress $N_{z\,max}$ is responsible for the occurrence of the critical conditions in the paper ring.

It is worth noting that the preceding values of external forces and internal stresses are calculated on the assumption that no detachment has occurred between contiguous rings during bending: it can be proved[1] that this is so if the following relation between the forces Φ_{0r} and Φ_{1r} of systems S_0 and S_1 holds for all values of z and θ:

$$\Phi_{0r} \geqslant |\Phi_{1r}(z, \theta)| \quad . \quad . \quad . \quad . \quad . \quad (19)$$

From the preceding considerations it follows that eqn. (19) may be also written

$$\Phi_{0r} \geqslant |\Phi_{1r}(L/2, 0)| \quad . \quad . \quad . \quad . \quad . \quad (20)$$

where $\Phi_{1r}(L/2, 0)$ may be obtained from Fig. 8 and eqn. (16). This relation is the first mechanical stability condition for the cable during bending (see Section 4).

These considerations deduced for the case in which the tapes are staggered by 50% may be extended to other values of stagger.[1] For example, it is found that in the case of 30% staggering, the maximum value of N_{1z} is given by $N_{z\,max} = \frac{2}{3} fL\Phi_{0r}$.

(4) ANALYSIS OF THE POSSIBLE CRITICAL CONDITIONS OF THE INSULATION DURING BENDING

(4.1) General

On the basis of the preceding results it is possible to analyse the conditions causing wrinkle formations in the paper ring subjected to systems S_0 and S_1 during bending of the cable on the take-up drum of the lapping machine.

It is assumed as usual that each layer consists of contiguous rings of thickness s and width L, separated by a butt-space h (see Fig. 9), and the assumption is made that the maximum axial

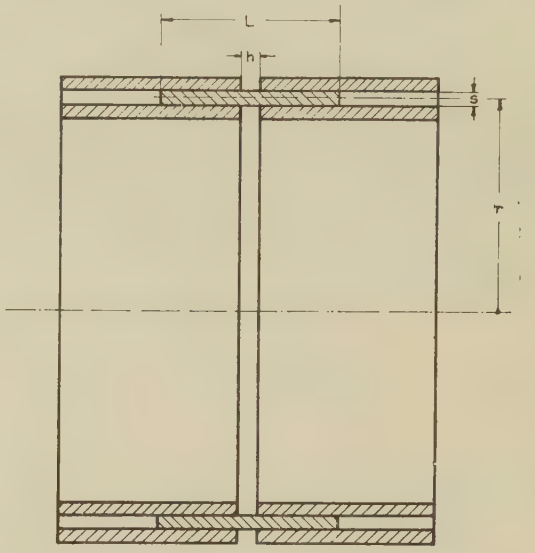

Fig. 9.—Contiguous paper rings in the case of paper tapes staggered by 50%.

deformation due to the cable bending is larger than the elastic limit of the paper (about 0·5%) but less than the limit corresponding to the disappearance of the butt-spaces in the most compressed zone (about 5–10%).

It follows that bending will produce no damage to the insulation only if the axial compressive stress on each tape, partially due to the friction forces between adjacent layers, does not exceed a certain critical load which can produce paper collapse with wrinkle formation.

As will be shown in Section 5, the collapse problem is quite different in the case of tight lapping $[\Phi_{0r} \geqslant |\Phi_{1r}(L/2, 0)|]$ and in the case of loose lapping $[\Phi_{0r} < |\Phi_{1r}(L/2, 0)|]$.

(4.2) Critical Load of a Compressed Ring

The analysis of the critical conditions of a ring can be carried out[1] by transforming the problem, which is essentially asymmetrical, into a simpler symmetrical one, namely the study of the collapse conditions of a thin cylindrical shell having a free flexural length, l, subjected to an axial compression load, P, uniformly distributed over the cylinder periphery. In effect it can be shown[1] that the deformation consists of a great number of waves along the cylinder periphery (under practical conditions 7 to 20 transverse waves are verified), except for very small values of l for which the deformation itself may be considered to be axially symmetrical. This fact shows how the collapse is a very localized phenomenon along the periphery of the cylinder, and leads to acceptance of the hypothesis that this phenomenon is controlled by the local distribution of the axial load in correspondence with the arc of circumference where a single wave takes place. It appears then that we can accept the

results obtained on the assumption of a uniformly loaded ring, substituting for P the largest value of the compressive axial stress, $N_{1z}(z, \theta)$, calculated from eqn. (17) for $z = 0$, $\theta = \pi$. The calculations give the following critical values of the compressive stress, assuming that during buckling the cylinder collapses in a number of sinusoidal waves:[1]

$$P_0 = \frac{1}{\sqrt{3}} \frac{s^2}{r} \sqrt[4]{(4G^2 E_\theta E_z)} \quad . \quad . \quad . \quad . \quad (21)$$

or, in non-dimensional terms, introducing the parameters of the preceding Section,

$$p_0 = \frac{1}{\sqrt{3}} \frac{s}{r} \sqrt[4]{\left(\frac{4\mu_\theta \mu_z}{\nu^2}\right)} \quad . \quad . \quad . \quad . \quad (21a)$$

where $p_0 = P_0/(sE_\theta)$.

It is worth noting that these formulae are independent of the flexural length l. This fact, strictly speaking, holds if l does not assume very small values, as in this last case the value of P_0 is larger than the value given by eqn. (21); on the other hand, eqn. (21) itself may be eventually used for the whole practical range of values of l, since it gives a value of the critical load which is not larger than the true one.

In Fig. 10 only a qualitative diagram of p_0 against l/r is

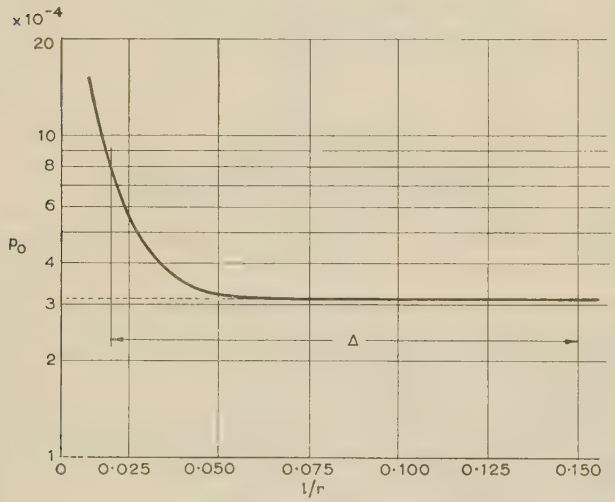

Fig. 10.—Qualitative diagram of p_0 against l/r.

Δ is the range of the values assumed in practice by l/r.

traced, since the values of p_0 given by eqn. (21a) are sufficient in most practical cases.

It can also be shown[1] that, if the values of G, E_θ and E_z referred to in Section 2.1 are introduced in eqn. (21) or in its generalization, the values calculated for the critical load show a good agreement with the experimental measurements of buckling in paper rings.

(5) STABILITY CONDITIONS OF THE INSULATION THICKNESS

(5.1) Stability Condition for Collapse Wrinkles not to Occur

The results of Sections 3 and 4 can be easily applied in order to verify the stability of the cable insulation during bending.

If the lapping is too loose or if the tapes are too large and too thick compared with the diameter on which they are wound, eqn. (20) does not hold everywhere and separation between contiguous rings may occur. In this case there is no mutual interaction between adjacent rings, as the flexural length l may be of the order of L and also each ring with its edges facilitates the collapse of the inner adjacent ones at the point $z = 0$, $\theta = \pi$ (see Fig. 11). Then the collapse wrinkles described in Section 1.3

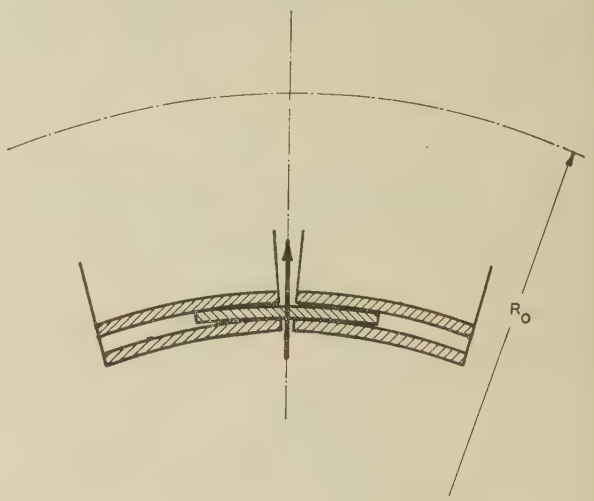

Fig. 11.—Simplified representation of the effects transmitted by overlying rings for $\theta = \pi$.

[Fig. 1(c)] may occur, and in order to avoid them it appears necessary to assume as the first stability criterion that the cable is lapped in such a way that, during bending with a radius of curvature R_0, eqn. (20) holds everywhere.*

(5.2) Stability Conditions for Collapse Creases or Butt-Space Creases not to Occur

The results of Section 4.2 show as a further criterion that the axial stresses due to the bending and lapping pressures [see eqn. (17)] must satisfy the condition

$$N_{z\,max} \leqslant cP_0(s, r; l) \quad . \quad . \quad . \quad . \quad . \quad (22$$

where P_0 is the critical value obtained for given values of s, r and l, while c is a suitable safety coefficient less than unity ($c \leqslant 0{\cdot}6$ to $0{\cdot}8$).

Recalling eqn. (18), the preceding equation may be written for the case of 50% staggering as

$$fL\Phi_{0r} \leqslant cP_0(s, r; l) \quad . \quad . \quad . \quad . \quad . \quad (23$$

i.e.

$$\Phi_{0r} \leqslant \frac{c}{fL} P_0(s, r; l) \quad . \quad . \quad . \quad . \quad . \quad (24$$

With regard to the suitable flexural length to be used in eqn. (23) or (24), it is worth observing that the rings belonging to neighbouring elementary layers have an almost identical critical load and therefore they must collapse almost simultaneously; thus, it is not *a priori* correct to assume that the considered ring is supported by the adjacent ones and that collapse occurs only in the butt-space. Actually some support effects can only take place between those layers for which the critical conditions are quite different; obviously this support is more effective for small values of r/s, for which the variation of P_0 versus r/s is very large.

Strictly speaking, the stability of a ring with a flexural length $l = L$, loaded with the distributed system S_1 should be considered. The complete solution of this problem is quite cumbersome but following the simplifications introduced in Section 4.1, we will consider the stability of the ring assumed to be loaded with

* In order to obtain this result it may be necessary to use tapes with a width which decreases as r decreases, so that the ratio $L/2r$ determining the bending pressure (Fig. 8) remains practically constant for the whole insulation thickness.

compressive distributed force $N_{z\,max}$ and having an equivalent exural length, l, which is unknown but in general is larger than h. Then two different cases may arise:

(a) If h/r is small ($h/r < 0{\cdot}1$), since the critical load P_0 greatly decreases when l/r increases in the range of small values (see Fig. 10), it follows that $P_0(s, r; l) \ll P_0(s, r; h)$.

If, moreover, r/s is large (e.g. $r/s > 300$), given that the above-mentioned support effect is in this case negligible, then buckling occurs in the whole length l, and, since a large number of rings is loaded in a similar way, the collapse creases described in Section 1.3 [Fig. 1(b)] eventually occur.

(b) If h/r is not small ($h/r > 0{\cdot}1$) then $P_0(s, r; h)$ is quite close to the value given by eqn. (21), which does not depend on l, and therefore $P_0(s, r; l) \simeq P_0(s, r; h)$ also if $l \gg h$.

If, furthermore, r/s is not large (e.g. $r/s < 300$), some support effect does take place between neighbouring layers, and then buckling occurs in the butt-space only and the butt-space creases described in Section 1.3 are produced [Fig. 1(a)].

In practical cases, if h/r is small but r/s is not large (or vice ersa) it has also been found that both occurrences hold at the ame time.

As experiments show that collapse creases may occur in a length $l \simeq L/2$, the preceding analysis proves that it is, in general, advisable to introduce in eqn. (23) either the value of the critical load corresponding to $l = L/2$ or its minimum value given by eqn. (21), which does not depend on l. In practice these two values are the same.

(6) FINAL REMARKS AND NUMERICAL EXAMPLE

Many important questions other than those considered in this paper are met in the mechanical design of paper-lapped cables. For example, lapping with paper tapes staggered in a general way is not fully considered in the preceding Sections although it is a very important topic. It has already been shown in Section 3 that the maximum compressive stress $N_{z\,max}$ in the case of lapping with 30% staggering is

$$N_{z\,max} = \frac{2}{3} f L \Phi_{0r} \quad . \quad . \quad . \quad . \quad . \quad (25)$$

Consequently, the upper limit of the allowable radial pressure in this case becomes

$$\Phi_{0r} \leqslant \frac{3}{2} \frac{c}{fL} P_0(s, r; l) . \quad . \quad . \quad . \quad . \quad (26)$$

Also, for the sake of brevity, the drying operation is not treated here, although it has some important consequences, but reference is made to the more extensive work in course of publication.[1]

However, the topics outlined are sufficient to provide a quantitative basis on which to state the problem, giving methods for studying the questions which may arise.

In order to show the application of the theory, an example of the design of the insulation of a very-high-voltage cable is now given.

As the calculations of Φ_{0r} and $\Phi_{0\theta}$ are very cumbersome, it is convenient to assume a known distribution of the lapping tension T and of the paper tapes; the corresponding distribution of Φ_{0r} will be calculated and its consistency with eqns. (24) and (20) will be checked.

Experience of similar cases is useful in assuming a good starting distribution. The insulation is assumed to be by paper tapes of different thickness in order to satisfy electrical requirements, and the distribution of T is correspondingly assumed to vary for the different layers.

In Table 1 the values of the physical and geometrical parameters characterizing the different layers are given; it is worth observing that the distribution of the radial and transverse pressures is independent of the actual value of r_0 but depends only on the non-dimensional ratio, K_p; therefore the distributions calculated are valid for all cables having geometrical and physical similarity in lapping.

Table 1

LAYER PARAMETERS

Layer number	E_θ	$\sqrt{n}$	s	r	K	T	T/L	Υ
	kg/cm² ×10³		cm ×10⁻²	cm		kg		
1	68	41	1·5	1·94	1·023	1·08	36	0·907
2	75	55	1·1	2·08	1·095	0·79	36	1·103
3	68	45	1·3	2·28	1·198	0·75	29	1·06
4	64	34	2·0	2·52	1·327	1·40	35	1·00
5	64	29	2·0	2·89	1·520	2·00	50	1·00
6	64	30	2·0	3·82	2·010	1·84	46	1·00

$r_0 = 1{\cdot}9$ cm. $L = 2$ cm.

Fig. 12 shows Φ_{0r} and $\Phi_{0\theta}$ plotted against the non-dimensional ratio K. It also shows the values of the allowable upper pressure given by

$$\Phi_{u,r} = \frac{1}{fL} P_0 \quad . \quad . \quad . \quad . \quad . \quad . \quad (27)$$

and the values of the allowable lower pressure given by

$$\Phi_{l,r} = \left| \Phi_{1r}\left(\frac{L}{2}, 0\right) \right| \quad . \quad . \quad . \quad . \quad . \quad (28)$$

Therefore eqns. (24) and (20) easily hold.

It is interesting to observe that, if the conductor radius is increased from 1·9cm to 2·6cm, the distribution of $\Phi_{u,r}$ and $\Phi_{l,r}$ changes as shown in Fig. 12; both $\Phi_{u,r}$ and $\Phi_{l,r}$ decrease, and for eqn. (24) to hold, lower values of T are necessary. The actual distribution of T may be kept unaltered if lapping is carried out with paper tapes staggered in a different way (for example by 30%).

Lastly, observing that the distribution of Φ_{0r} depends only on $T_p/(L_p s_p)$, n_p and γ_p, the following considerations are useful in designing the insulation.

If the pressure $\Phi_{l,r}$ is too large for some values of radius, it may be decreased, without at the same time changing the distribution of Φ_{0r}, by reducing width or thickness of the paper

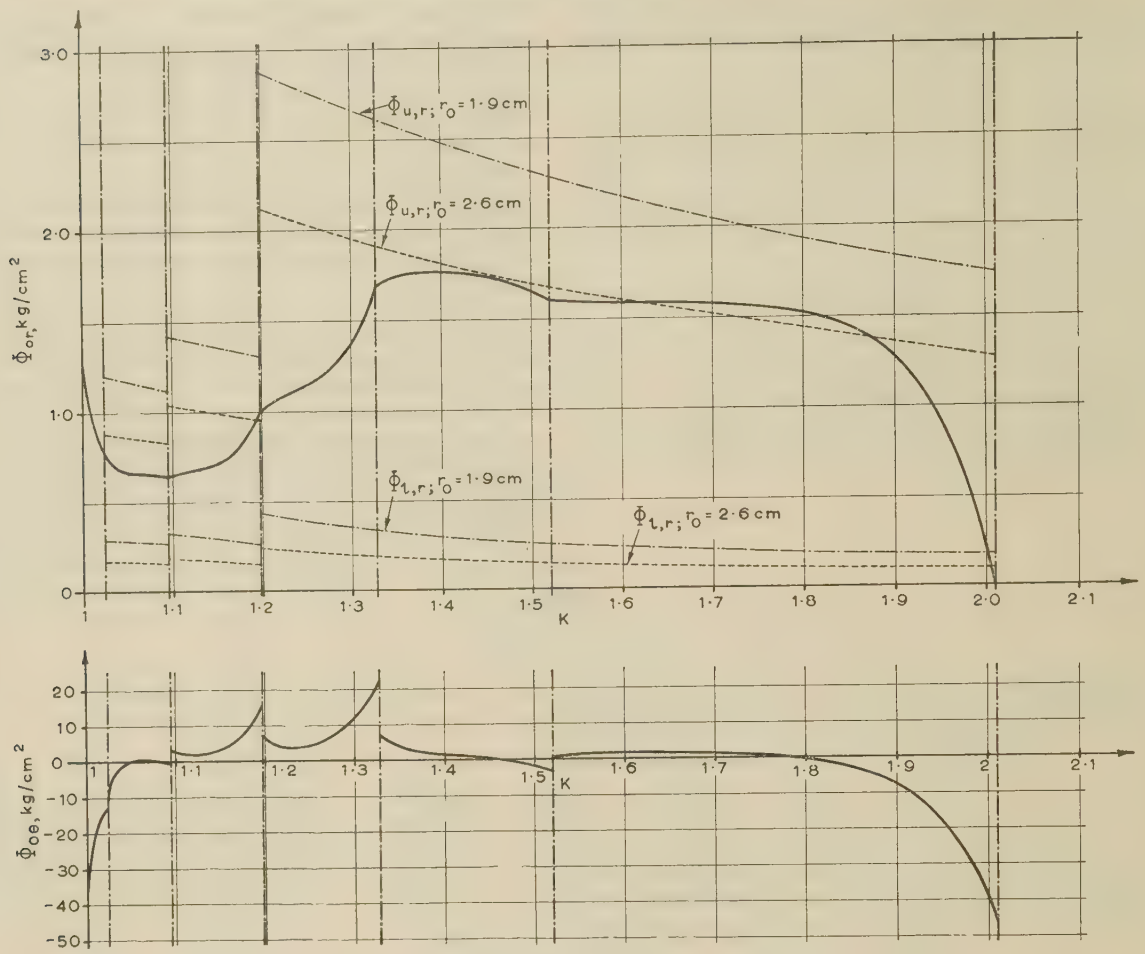

Fig. 12.—Distribution of Φ_{0r} and $\Phi_{c\theta}$ in a cable with six layers of insulation.

—·—·— Upper and lower allowable pressure for $r_0 = 1{\cdot}9$ cm.
– – – – Upper and lower allowable pressure for $r_0 = 2{\cdot}6$ cm.

As the first layer is made with carbon-paper tapes, the stability conditions do not apply to it, being outside the cable dielectric.

tapes and by varying T in such a way that T/Ls does not change.

In a similar way, if the upper pressure $\Phi_{u,r}$ is too small, it is possible to increase it by increasing the thickness of the paper tapes, taking into account that the electric strength of the paper generally decreases as s increases. On the other hand, it is not correct to rely upon a decrease of h in order to increase P_0, because the flexural length of the paper ring is not rigidly defined (see Section 5).

The paper has been prepared to illustrate the basis on which cable lapping can be established from the mechanical point of view, thus attempting to set on a scientific basis an operation which is normally carried out almost empirically.

The theory has made possible the lapping of high-voltage cables which could be reeled on extremely small drums and which showed a very high electric strength particularly to impulse voltages. The theory has therefore had very good practical confirmation.

(7) ACKNOWLEDGMENT

The development of the theory has been sponsored ar constantly encouraged by Dr. Luigi Emanueli, to whose memo the authors dedicate their most grateful thanks.

In addition to the authors, many members of the Pirelli Cab Research Laboratories have contributed to this development.

The authors are grateful to the Management of Pirelli S.p.A for permission to publish the paper.

(8) REFERENCES

(1) Gazzana Priaroggia, P., Occhini, E., and Palmieri, N 'Fundamentals of the Theory of Paper Lapping of Single-Core High-Voltage Cable' (Pirelli—General Cab Works Ltd., 1961).

(2) Gazzana Priaroggia, P., and Palandri, G.: 'Research the Electric Breakdown of Fully Impregnated Pap Insulation for High-Voltage Cables', *Transactions of t American I.E.E.*, 1955, **74**, Part III, p. 1343.

621.372.412

The Institution of Electrical Engineers
Monograph No. 391 E
July 1960

A NEW TYPE OF PIEZO-ELECTRIC FLEXURAL VIBRATOR IN THE FORM OF BALANCED CANTILEVERS

By SHEILA AYERS.

(*The paper was first received 5th November*, 1959, *and in revised form 17th March*, 1960. *It was published as an* INSTITUTION MONOGRAPH *in July*, 1960.)

SUMMARY

The flexural vibrator, designed to vibrate at about 1 kc/s, basically consists of identical cantilever arms extending from a common area to form a symmetrical element. Two distinct shapes have been considered—the H and the 'zigzag'. Some of the H elements have uniform cross-section while others are arranged to have most of their mass at the free ends in order to reduce the frequency for a specimen of given length. The 'zigzags' have folded arms of any number of sections (increasing the number of sections reduces the frequency).

The theory of the various forms and their frequency equations are derived. Conditions for perfect balance of the reactions at the supports are discussed.

Measurements have been made on H and 'zigzag' forms made from quartz slices ZYbΦ($\Phi = 0 - 10°$) and on 'zigzag' form from r.d.t.XY*ltl* Φ, 90°, 90°. Frequency, temperature behaviour, Q-factor and displacement patterns of the elements are compared with theory. Since some of the conventional driving methods proved unsatisfactory a short Section is included on circuits.

LIST OF SYMBOLS

f = Frequency, c/s.
l = Length, cm.
b = Breadth, cm.
t = Thickness, cm.
a = Cross-sectional area, cm^2.
(of one arm of H form, of one section of 'zigzag'.)
m = Mass per unit length of section, g/cm.
E = Young's modulus.
ρ = Density.
k = Radius of gyration.
y = Lateral deflection.
W_k = Kinetic energy.
W_p = Potential energy.
U = Unbalance factor of 'zigzag' arm.

(1) INTRODUCTION

There is always a demand for piezo-electric crystals which will vibrate at frequencies of 1 kc/s or less for oscillators and filters. Ideally the frequencies of these crystals should be unaffected by small changes in their ambient temperature. At present, specimens[1–3] designed to vibrate at these frequencies are large and uneconomical in material, and the best existing quartz elements have their minimum change of frequency with temperature at inconveniently low temperatures (below 15° C). With these factors in mind, a new type of piezo-electric element[4] has been developed which has the added advantage of a large nodal area at which supports can be fixed.

This new element can take various forms but basically consists of identical cantilever arms extending from a common area to form a symmetrical element. If the mountings are attached to the common area, all the reactions due to the vibrations of the arms can be substantially balanced out by choice of the number, arrangement and shape of the arms.

In one of these forms, a quartz element with overall dimensions 26 × 9 × 2 mm can vibrate at 800 c/s, and an ethylene diamine tartrate element with dimensions 30 × 15 × 1·5 mm, at 250 c/s.

Part 1 is devoted to the theory of these vibrators, while Part 2 covers the experimental work and includes tables comparing measured frequencies with those calculated according to theory.

PART 1.—THEORETICAL

(2) H FORM

The crystal element takes the form of an H with four identical cantilever arms extending from a central bar (see Fig. 1). Con-

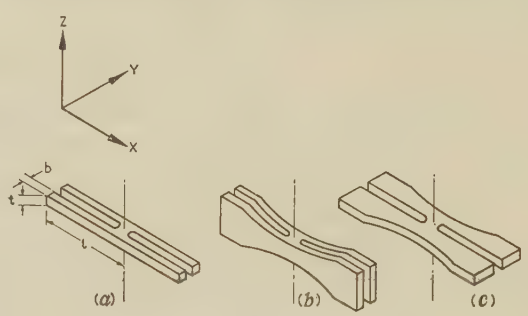

Fig. 1.—Balanced cantilevers of H form.
(*a*) Uniform. (*b*) Variable thickness. (*c*) Variable breadth.

nection is normally made at the centre of gravity, but it can be made anywhere on this central bar. The element is excited in such a way that each arm vibrates in flexure as a mirror image of its adjacent arms. Thus all the reaction forces at the centre of the specimen are substantially balanced. Provided that the four arms are identical, the element vibrates as a whole at the same frequency as a single cantilever with the dimensions of one arm. The frequency, f, for an H form of uniform cross-section is given by

$$f = \frac{\kappa^2}{4\pi\sqrt{3}} \frac{b}{l^2} \sqrt{\frac{E}{\rho}} \quad . \quad . \quad . \quad . \quad . \quad (1)$$

where b and l = Breadth and length of one arm, respectively.
ρ = Density.
E = Young's modulus for the element.
κ = A root of the equation

$$\cosh \kappa \cos \kappa = -1 \quad . \quad . \quad . \quad . \quad . \quad . \quad (2)$$

The first three roots are $\kappa = 1{\cdot}8751,\ 4{\cdot}6941,\ 7{\cdot}855$. The fundamental mode gives

$$f = 0{\cdot}161\,54 \frac{b}{l^2} \sqrt{\frac{E}{\rho}} \quad . \quad . \quad . \quad . \quad . \quad (3)$$

Correspondence on Monographs is invited for consideration with a view to publication.

Mrs. Ayers is in the Post Office Engineering Department.

(2.1) Arms of Non-Uniform Cross-Section

The natural frequency of an H form of given length can be lowered by concentrating the mass towards the free ends, e.g. by increasing the area of the cross-section as in Figs. 1(*b*) and (*c*). The frequency of such a specimen can be calculated approximately using Rayleigh's method[5] on a single cantilever shaped like one of the arms. A deflection curve is assumed which satisfies the end conditions, and the maximum kinetic and potential energies are then derived and equated. For any straight cantilever of non-uniform cross-section, satisfactory results can be obtained by expressing the lateral deflection y as

$$y = \tfrac{1}{2}l^2x^2 - \tfrac{1}{3}lx^3 + \tfrac{1}{12}x^4 \quad . \quad . \quad . \quad . \quad (4)$$

where x is measured along the length from the fixed end.

The maximum kinetic energy, W_k, and potential energy, W_p, are given by

$$W_k = \int_0^l \tfrac{1}{2}\rho\omega^2 a(x)y^2dx \quad . \quad . \quad . \quad . \quad . \quad (5)$$

$$W_p = \int_0^l \tfrac{1}{2}Ea(x)k^2(x)\left(\frac{d^2y}{dx^2}\right)^2 dx \quad . \quad . \quad . \quad (6)$$

where ω is the angular frequency. The cross-sectional area, $a(x)$, and the radius of gyration, $k(x)$, are expressed as functions of x.

where the thickness, $t(x)$, and breadth, $b(x)$, are expressed as functions of x. The angular frequency, ω, is then given by

$$\omega^2 = \frac{E\int_0^l t(x)b^3(x)\left(\frac{d^2y}{dx^2}\right)^2 dx}{12\rho\int_0^l t(x)b(x)y^2dx} \quad . \quad . \quad . \quad . \quad (9)$$

which, when evaluated, can be expressed as

$$\omega^2 = \frac{C^2b_0^2E}{\rho l^4} \quad . \quad . \quad . \quad . \quad . \quad . \quad (10)$$

where C^2 is a shape constant and b_0 is the breadth at the clamped end of the cantilever. C^2 for a uniform arm is 1·038 5.

Expressions for C^2 for different shapes with constant breadth and variable thickness [see Fig. 1(*b*)] are given in Table 1. In each example, the thickness, $t(x)$, increases from t_0 at the clamped end of an arm to a point γl along the bar and then remains constant at t_1 to the end of the arm at l. C^2 decreases parabolically with increasing γ, and its minimum value for each shape (giving the lowest frequency) and the corresponding values of γ are given in cols. 5 and 6.

Although it is equally simple to calculate C^2 for various shapes of an arm of constant thickness and variable breadth, only one

Table 1

C^2 FOR ARMS OF VARIABLE THICKNESS

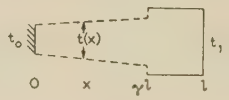

Shape	t_1	$t(x)$	C^2	C^2_{min}	γ for C^2_{min}
1 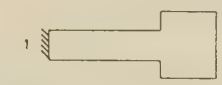	$2t_0$	t_0	$\frac{108(2 - 5\gamma + 10\gamma^2 - 10\gamma^3 + 5\gamma^4 - \gamma^5)}{208 - 324\gamma^5 + 360\gamma^6 - 180\gamma^7 + 45\gamma^8 - 5\gamma^9}$	0·550 7	0·5
2 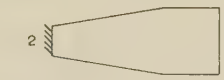	$2t_0$	$t_0\left(1 + \frac{x}{\gamma l}\right)$	$\frac{252(12 - 15\gamma + 20\gamma^2 - 15\gamma^3 + 6\gamma^4 - \gamma^5)}{2912 - 756\gamma^5 + 720\gamma^6 - 315\gamma^7 + 70\gamma^8 - 7\gamma^9}$	0·653 0	0·8
3 	$2t_0$	$t_0\left(1 + \frac{x^2}{\gamma^2 l^2}\right)$	$\frac{396(42 - 70\gamma + 105\gamma^2 - 84\gamma^3 + 35\gamma^4 - 6\gamma^5)}{16016 - 7128\gamma^5 + 6930\gamma^6 - 3080\gamma^7 + 693\gamma^8 - 70\gamma^9}$	0·591 6	0·7
	$3t_0$	$t_0\left(1 + \frac{2x^2}{\gamma^2 l^2}\right)$	$\frac{396(31{\cdot}5 - 70\gamma + 105\gamma^2 - 84\gamma^3 + 35\gamma^4 - 6\gamma^5)}{12012 - 7128\gamma^5 + 6930\gamma^6 - 3080\gamma^7 + 693\gamma^8 - 70\gamma^9}$	0·433 8	0·75
	$4t_0$	$t_0\left(1 + \frac{3x^2}{\gamma^2 l^2}\right)$	$\frac{396(28 - 70\gamma + 105\gamma^2 - 84\gamma^3 + 35\gamma^4 - 6\gamma^5)}{10677{\cdot}33 - 7128\gamma^5 + 6930\gamma^6 - 3080\gamma^7 + 693\gamma^8 - 70\gamma^9}$	0·352 0	0·75

The above equations will now be applied to specific examples.

For arms of rectangular cross-section the maximum energy equations can be written as

$$W_k = \tfrac{1}{2}\rho\omega^2\int_0^l t(x)b(x)y^2dx \quad . \quad . \quad . \quad . \quad . \quad (7)$$

$$W_p = \tfrac{1}{24}E\int_0^l t(x)b^3(x)\left(\frac{d^2y}{dx^2}\right)^2 dx \quad . \quad . \quad . \quad (8)$$

shape has been considered. In this the breadth increases parabolically from the clamped to the free end of the arm,

i.e. $b(x) = \left(1 + \frac{\beta x^2}{l^2}\right)b_0$, and C^2 is given by

$$C^2 = \frac{18(462 + 66\beta + 11\beta^2 + \beta^3)}{8008 + 5353\beta} \quad . \quad . \quad . \quad (1$$

C^2 decreases quite rapidly until $\beta = 2$ ($C^2 = 0{\cdot}621$) and the

flattens to a minimum of 0·585 at $\beta = 3{\cdot}45$. Thus the major reduction in frequency occurs by the time $\beta = 2$, and little further is achieved by increasing β beyond this point.

C^2 for other shapes can be easily derived in the same manner.

(3) 'ZIGZAG' FORM

The element has only two arms which are folded any desired number of times in zigzag formation (Fig. 2). The central

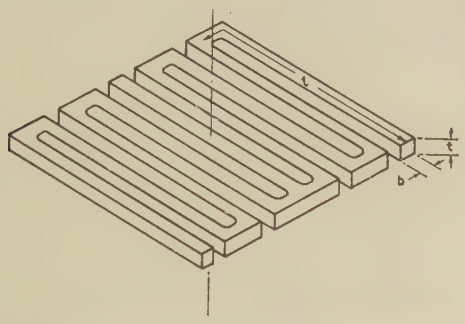

Fig. 2.—Balanced cantilevers of 'zigzag' form (four sections).

tongue extending from the common area does not affect the frequency of vibration of the specimen and is included merely so that the element can be mounted at its centre of gravity. The individual sections of an arm do not need to be the same size or length provided that one arm is an exact mirror image of the other. The frequency and balance of the reactions at the centre can be varied by adjusting the number, size and length of the sections.

(3.1) Frequency of Vibration of a 'Zigzag' with Arms of any Number of Sections

If the two arms of a 'zigzag' are mirror images of each other, the specimen will vibrate as a whole at the same frequency as one of the arms clamped at the junction with the central tongue. The frequency equation is therefore derived by considering such an arm. Each section of the arm is considered as a vibrating beam and the boundary conditions at the ends and junctions are taken into account; the influence of the bridges between the sections is neglected. The simple differential equation for lateral vibration of a beam, neglecting shear and rotary inertia, is given by

$$\frac{\partial^4 y}{\partial x^4} + \frac{\rho}{Ek^2}\frac{\partial^2 y}{\partial t^2} = 0 \quad . \quad . \quad . \quad . \quad . \quad (12)$$

Since only natural modes of vibrations are considered, the deflection at any point varies harmonically with time and can be represented by $y = Y\varepsilon^{j\omega t}$. The differential equation can then be written as

$$\frac{\partial^4 Y}{\partial x^4} - \frac{\rho\omega^2}{Ek^2}Y = 0 \quad . \quad . \quad . \quad . \quad . \quad (13)$$

Let the displacement amplitudes $Y_n(x)$, $(n = 1 \ldots N)$ for the N sections be

$$Y_n = A_n\varepsilon^{\alpha x} + B_n\varepsilon^{-\alpha x} + C_n\varepsilon^{j\alpha x} + D_n\varepsilon^{-j\alpha x} \quad . \quad (14)$$

where

$$\alpha^4 = \frac{\rho\omega^2}{Ek^2} \quad . \quad . \quad . \quad . \quad . \quad . \quad (15)$$

and the frequency is

$$f = \frac{\alpha^2 k}{2\pi}\sqrt{\frac{E}{\rho}} \quad . \quad . \quad . \quad . \quad . \quad . \quad (16)$$

The value of α can be derived by equating to zero the determinant formed from the equations for the boundary conditions. The boundary conditions are:

Fixed end	Displacement and slope are zero.
Junction of adjacent sections	Displacement and slopes of sections are equal and of same sign; bending moments and shearing forces are equal and of opposite sign.
Free end	Bending moment and shearing force are zero.

For an arm of two sections and uniform cross-section the boundary equations are:

At the fixed end, $x = x_1$.

Displacement $Y_1 = 0$:

$$A_1\varepsilon^{\alpha x_1} + B_1\varepsilon^{-\alpha x_1} + C_1\varepsilon^{j\alpha x_1} + D_1\varepsilon^{-j\alpha x_1} = 0 \quad . \quad (17)$$

Slope $\frac{\partial Y_1}{dx} = 0$:

$$\alpha[A_1\varepsilon^{\alpha x_1} - B_1\varepsilon^{-\alpha x_1} + jC_1\varepsilon^{j\alpha x_1} - jD_1\varepsilon^{-j\alpha x_1}] = 0 \quad . \quad (18)$$

At the junction, $x = x_2$.

Displacement $Y_1 = Y_2$:

$$A_1\varepsilon^{\alpha x_2} + B_1\varepsilon^{-\alpha x_2} + C_1\varepsilon^{j\alpha x_2} + D_1\varepsilon^{-j\alpha x_2} = A_2\varepsilon^{\alpha x_2} + B_2\varepsilon^{-\alpha x_2} + C_2\varepsilon^{j\alpha x_2} + D_2\varepsilon^{-j\alpha x_2} \quad . \quad (19)$$

Slope $\frac{\partial Y_1}{\partial x} = \frac{\partial Y_2}{\partial x}$:

$$\alpha[A_1\varepsilon^{\alpha x_2} - B_1\varepsilon^{-\alpha x_2} + jC_1\varepsilon^{j\alpha x_2} - jD_1\varepsilon^{-j\alpha x_2}] = \alpha[A_2\varepsilon^{\alpha x_2} - B_2\varepsilon^{-\alpha x_2} + jC_2\varepsilon^{j\alpha x_2} - jD_2\varepsilon^{-j\alpha x_2}] \quad . \quad (20)$$

Bending moment $EI\frac{\partial^2 Y_1}{\partial x^2} = -EI\frac{\partial^2 Y_2}{\partial x^2}$:

$$EI\alpha^2[A_1\varepsilon^{\alpha x_2} + B_1\varepsilon^{-\alpha x_2} - C_1\varepsilon^{j\alpha x_2} - D_1\varepsilon^{-j\alpha x_2}] = -EI\alpha^2[A_2\varepsilon^{\alpha x_2} + B_2\varepsilon^{-\alpha x_2} - C_2\varepsilon^{j\alpha x_2} - D_2\varepsilon^{-j\alpha x_2}] \quad . \quad (21)$$

Shearing force $\frac{\partial}{\partial x}\left(EI\frac{\partial^2 Y_1}{\partial x^2}\right) = -\frac{\partial}{\partial x}\left(EI\frac{\partial^2 Y_2}{\partial x^2}\right)$:

$$EI\alpha^3[A_1\varepsilon^{\alpha x_2} - B_1\varepsilon^{-\alpha x_2} - jC_1\varepsilon^{j\alpha x_2} + jD_1\varepsilon^{-j\alpha x_2}] = -EI\alpha^3[A_2\varepsilon^{\alpha x_2} - B_2\varepsilon^{-\alpha x_2} - jC_2\varepsilon^{j\alpha x_2} + jD_2\varepsilon^{-j\alpha x_2}] \quad . \quad . \quad . \quad . \quad (22)$$

At the free end, $x = x_3$.

Bending moment $EI\frac{\partial^2 Y_2}{\partial x^2} = 0$:

$$EI\alpha^2[A_2\varepsilon^{\alpha x_3} + B_2\varepsilon^{-\alpha x_3} - C_2\varepsilon^{j\alpha x_3} - D_2\varepsilon^{-j\alpha x_3}] = 0 \quad . \quad (23)$$

Shearing force $\frac{\partial}{\partial x}\left(EI\frac{\partial^2 Y_2}{\partial x^2}\right) = 0$:

$$EI\alpha^3[A_2\varepsilon^{\alpha x_3} - B_2\varepsilon^{-\alpha x_3} - jC_2\varepsilon^{j\alpha x_3} + jD_2\varepsilon^{-j\alpha x_3}] = 0 \quad . \quad (24)$$

The boundary conditions for any number of sections can be expressed in a similar manner, and the determinant for up to four sections is given below. This determinant can be generalized to cover any number of sections, as shown in Appendix 10.1.

(3.1.1) Arms of two Sections.

The determinantal equation for an arm of two sections with lengths l_1 and l_2 is

$$1 + \cosh\alpha l_1 \cosh\alpha l_2 \cos\alpha(l_1 + l_2) + \sinh\alpha l_1 \sinh\alpha l_2 \cos\alpha(l_1 - l_2) = 0 \quad . \quad (25)$$

1 Section	$\varepsilon^{\alpha x_1}$	$\varepsilon^{-\alpha x_1}$	$\varepsilon^{\alpha x_1}$	$\varepsilon^{-j\alpha x_1}$	0	0	0	0	0	0	0	0	0	0	0	0
	$\varepsilon^{\alpha x_1}$	$-\varepsilon^{-\alpha x_1}$	$j\varepsilon^{j\alpha x_1}$	$-j\varepsilon^{-j\alpha x_1}$	0	0	0	0	0	0	0	0	0	0	0	0
	$\varepsilon^{\alpha x_2}$	$\varepsilon^{-\alpha x_2}$	$-\varepsilon^{j\alpha x_2}$	$-\varepsilon^{-j\alpha x_2}$	$-\varepsilon^{\alpha x_2}$	$-\varepsilon^{-\alpha x_2}$	$\varepsilon^{j\alpha x_2}$	$\varepsilon^{-j\alpha x_2}$	0	0	0	0	0	0	0	0
	$\varepsilon^{\alpha x_2}$	$-\varepsilon^{-\alpha x_2}$	$-j\varepsilon^{j\alpha x_2}$	$j\varepsilon^{-j\alpha x_2}$	$-\varepsilon^{\alpha x_2}$	$\varepsilon^{-\alpha x_2}$	$j\varepsilon^{j\alpha x_2}$	$-j\varepsilon^{-j\alpha x_2}$	0	0	0	0	0	0	0	0
2 Sections	$\varepsilon^{\alpha x_2}$	$\varepsilon^{-\alpha x_2}$	$\varepsilon^{j\alpha x_2}$	$\varepsilon^{-j\alpha x_2}$	$\varepsilon^{\alpha x_2}$	$\varepsilon^{-\alpha x_2}$	$\varepsilon^{j\alpha x_2}$	$\varepsilon^{-j\alpha x_2}$	0	0	0	0	0	0	0	0
	$\varepsilon^{\alpha x_2}$	$-\varepsilon^{-\alpha x_2}$	$j\varepsilon^{j\alpha x_2}$	$-j\varepsilon^{-j\alpha x_2}$	$\varepsilon^{\alpha x_2}$	$-\varepsilon^{-\alpha x_2}$	$j\varepsilon^{j\alpha x_2}$	$-j\varepsilon^{-j\alpha x_2}$	0	0	0	0	0	0	0	0
	0	0	0	0	$\varepsilon^{\alpha x_3}$	$\varepsilon^{-\alpha x_3}$	$\varepsilon^{j\alpha x_3}$	$\varepsilon^{-j\alpha x_3}$	$-\varepsilon^{\alpha x_3}$	$-\varepsilon^{-\alpha x_3}$	$\varepsilon^{j\alpha x_3}$	$\varepsilon^{-j\alpha x_3}$	0	0	0	0
	0	0	0	0	$\varepsilon^{\alpha x_3}$	$-\varepsilon^{-\alpha x_3}$	$-j\varepsilon^{j\alpha x_3}$	$j\varepsilon^{-j\alpha x_3}$	$-\varepsilon^{\alpha x_3}$	$\varepsilon^{-\alpha x_3}$	$j\varepsilon^{j\alpha x_3}$	$-j\varepsilon^{-j\alpha x_3}$	0	0	0	0
3 Sections	0	0	0	0	$\varepsilon^{\alpha x_3}$	$\varepsilon^{-\alpha x_3}$	$\varepsilon^{j\alpha x_3}$	$\varepsilon^{-j\alpha x_3}$	$\varepsilon^{\alpha x_3}$	$\varepsilon^{-\alpha x_3}$	$\varepsilon^{j\alpha x_3}$	$\varepsilon^{-j\alpha x_3}$	0	0	0	0
	0	0	0	0	$\varepsilon^{\alpha x_3}$	$-\varepsilon^{-\alpha x_3}$	$j\varepsilon^{j\alpha x_3}$	$-j\varepsilon^{-j\alpha x_3}$	$\varepsilon^{\alpha x_3}$	$-\varepsilon^{-\alpha x_3}$	$j\varepsilon^{j\alpha x_3}$	$-j\varepsilon^{-j\alpha x_3}$	0	0	0	0
	0	0	0	0	0	0	0	0	$\varepsilon^{\alpha x_4}$	$\varepsilon^{-\alpha x_4}$	$\varepsilon^{j\alpha x_4}$	$\varepsilon^{-j\alpha x_4}$	$-\varepsilon^{\alpha x_4}$	$-\varepsilon^{-\alpha x_4}$	$\varepsilon^{j\alpha x_4}$	$\varepsilon^{-j\alpha}$
	0	0	0	0	0	0	0	0	$\varepsilon^{\alpha x_4}$	$-\varepsilon^{-\alpha x_4}$	$j\varepsilon^{j\alpha x_4}$	$-j\varepsilon^{-j\alpha x_4}$	$-\varepsilon^{\alpha x_4}$	$\varepsilon^{-\alpha x_4}$	$j\varepsilon^{j\alpha x_4}$	$-j\varepsilon^{-j\alpha}$
4 Sections	0	0	0	0	0	0	0	0	$\varepsilon^{\alpha x_4}$	$\varepsilon^{-\alpha x_4}$	$\varepsilon^{j\alpha x_4}$	$\varepsilon^{-j\alpha x_4}$	$\varepsilon^{\alpha x_4}$	$\varepsilon^{-\alpha x_4}$	$\varepsilon^{j\alpha x_4}$	$\varepsilon^{-j\alpha}$
	0	0	0	0	0	0	0	0	$\varepsilon^{\alpha x_4}$	$-\varepsilon^{-\alpha x_4}$	$j\varepsilon^{j\alpha x_4}$	$-j\varepsilon^{-j\alpha x_4}$	$\varepsilon^{\alpha x_4}$	$-\varepsilon^{-\alpha x_4}$	$j\varepsilon^{j\alpha x_4}$	$-j\varepsilon^{-j\alpha}$
	0	0	0	0	0	0	0	0	0	0	0	0	$\varepsilon^{\alpha x_5}$	$\varepsilon^{-\alpha x_5}$	$\varepsilon^{j\alpha x_5}$	$\varepsilon^{-j\alpha}$
	0	0	0	0	0	0	0	0	0	0	0	0	$\varepsilon^{\alpha x_5}$	$-\varepsilon^{-\alpha x_5}$	$j\varepsilon^{j\alpha x_5}$	$-j\varepsilon^{-j\alpha}$

Determinant for 'zigzag' of up to four sections.

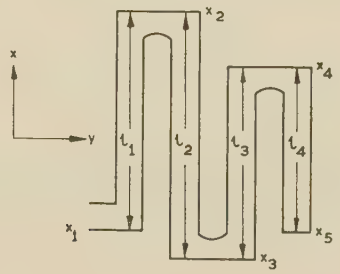

Fig. 3.—'Zigzag' arm of four sections.

This equation is unaltered by interchanging l_1 and l_2, and so the sections can be interchanged without affecting the natural flexural frequencies of the arm. For given values of l_1 and l_2, the solutions $|\alpha|$ fall into two distinct sets which give displacement patterns of different character and different fundamental frequencies. Examples of the displacement patterns for one arm (the other being a mirror image) are given in Fig. 4. The finite cross-section and the bridges have been neglected so that the sections appear superposed. Curves of αl_1 are plotted as a function of l_2/l_1 in Fig. 5.

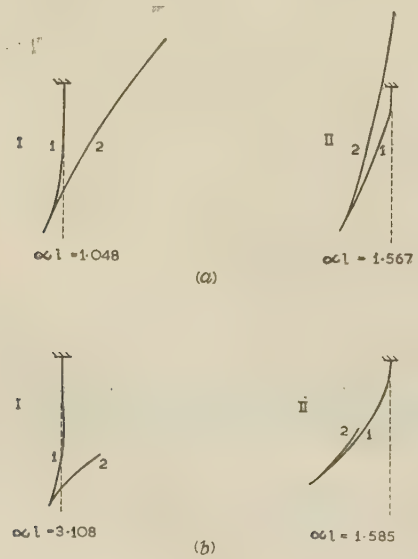

Fig. 4.—Calculated displacement patterns for the two fundamental flexural modes of 'zigzags' with arms of two unequal sections.
(a) $l_2 = 1{\cdot}5l_1$ (b) $l_2 = 0{\cdot}5l_1$

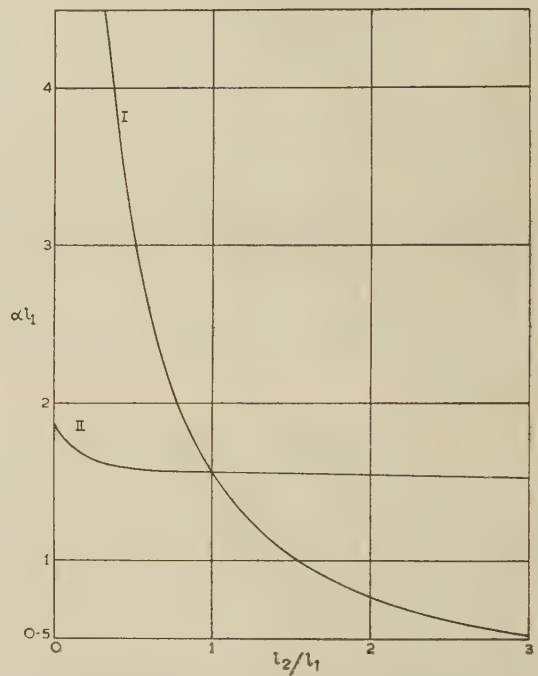

Fig. 5.—Values of αl_1 for the fundamental flexural modes of a 2-section 'zigzag' plotted as a function of l_2/l_1.

When $l_2 = l_1$, eqn. (25) becomes

$$\cosh^2 \alpha l_1 \cos^2 \alpha l_1 = 0 \quad . \quad . \quad . \quad . \quad . \quad (26)$$

and the two sets of solutions coincide: $\alpha l_1 = \pm \dfrac{(2n-1)\pi}{2}$ (n integral).

When $l_2 = 0$, the equation reduces to that for a single cantilever:

$$\cosh \alpha l_1 \cos \alpha l_1 = -1 \quad . \quad . \quad . \quad . \quad . \quad (27)$$

The first root is $\alpha l_1 = \pm 1{\cdot}875\,1$.

(3.1.2) Arms of any Number of Sections.

The determinantal equation for an arm of three sections is

$$\begin{aligned} 1 &+ \cosh \alpha l_1 \cosh \alpha l_2 \cosh \alpha l_3 \cos \alpha(l_1 + l_2 + l_3) \\ &+ \cosh \alpha l_1 \sinh \alpha l_2 \sinh \alpha l_3 \cos \alpha(l_1 + l_2 - l_3) \\ &+ \sinh \alpha l_1 \cosh \alpha l_2 \sinh \alpha l_3 \cos \alpha(l_1 - l_2 + l_3) \\ &+ \sinh \alpha l_1 \sinh \alpha l_2 \cosh \alpha l_3 \cos \alpha(l_1 - l_2 - l_3) = 0 \quad . \quad (28) \end{aligned}$$

Increasing the number of sections considerably lengthens this equation as can be seen from the expression for four sections given in Appendix 10.1, which also describes a quick method of solving the determinant and derives an empirical rule for writing the equation for an arm of any number of sections.

The determinantal equations are considerably simplified for arms with sections of equal length, so that even the page-long equation for six sections reduces to three terms. For any number of sections, each of length l, the equation contains only terms of the form $(\cosh \alpha l \cos \alpha l)^n$. Expressing $\cosh \alpha l \cos \alpha l$ as G, the general equation for n sections can be expressed by

$$1 + Tn(G) = 0$$

where $Tn(G)$ is a Chebÿshev polynomial defined by

$$Tn(G) = \cos n\phi \quad \text{where} \quad G = \cos \phi$$

whence $$\cos n\phi = -1 \quad \text{and} \quad \phi = \frac{2m+1}{n}\pi$$

so $$\cosh \alpha l \cos \alpha l = \cos \frac{2m+1}{n}\pi \quad \text{for} \quad m = 0, 1, 2 \ldots \leqslant \frac{n-1}{2}$$

The expressions for up to six sections are given in Table 2. Though a 'zigzag' with arms of n unequal sections has, in general, n sets of modes, when the sections are of equal length some of these sets coincide, as shown by the repeated roots of G. The case discussed in Section 3.1.1 is an example.

For a 'zigzag' whose arms are of rectangular cross-section the frequency is given by

$$f = \frac{(\alpha l)^2}{4\pi\sqrt{3}} \frac{b}{l^2}\sqrt{\frac{E}{\rho}} \quad . \quad . \quad . \quad . \quad . \quad (29)$$

The first roots of αl and values of $(\alpha l)^2/4\pi\sqrt{3}$ for the fundamental modes are also given in Table 2.

Calculated displacement patterns for the two fundamental modes of an arm of three equal sections are plotted in Fig. 6. For the mode which has $\alpha l = 1{\cdot}8751$, the displacement of the second section is the same as that for the first, while the displacement of the third section is equal and opposite to that of the first. The displacement patterns for the two fundamental modes of an arm of four equal sections are shown in Fig. 7.

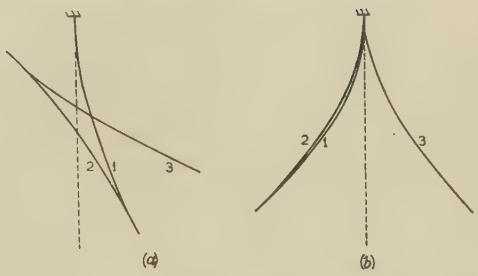

Fig. 6.—Calculated displacement patterns for the two fundamental flexural modes of a 'zigzag' with arms of three equal sections.
(a) $\alpha l = 1{\cdot}3184$ (b) $\alpha l = 1{\cdot}8751$

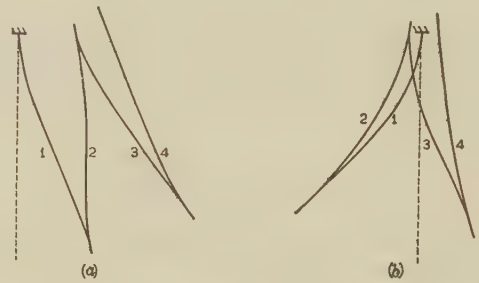

Fig. 7.—Calculated displacement patterns for the two fundamental flexural modes of a 'zigzag' with arms of four equal sections.
(a) $\alpha l = 1{\cdot}1524$ (b) $\alpha l = 1{\cdot}8003$

(3.2) Balancing Reactions on the Supports

For an arm in flexural vibration, the primary reactions on the supports are lateral, but there are also secondary reactions due to the longitudinal components of the acceleration. In tuning forks, for example, the lateral reactions but not the longitudinal ones are balanced. For minimum damping by the supports both reactions should be balanced. This is achieved in the H elements by having four symmetrical arms. The 'zigzag' elements have only two arms which, by virtue of their symmetry, balance the lateral reactions, while the longitudinal reactions of the folded arms are smaller than for a simple tuning fork and can be made to vanish by choice of the dimensions or the number of sections.

The longitudinal reaction for a single vibrating cantilever can be calculated as follows. Consider an element dx (Fig. 8) at a distance x from the support, where the lateral displacement is $y(x, t)$ and the slope is dy/dx. Acting over the length dx, this slope contributes an amount

$$d\xi = -\tfrac{1}{2}dx\left(\frac{dy}{dx}\right)^2 \quad . \quad . \quad . \quad . \quad . \quad (30)$$

Table 2

SOLUTION FOR THE DETERMINANT IN α FOR 'ZIGZAGS' WITH ARMS OF EQUAL SECTIONS

Number of sections	Determinantal equation (G = cosh αl cos αl)	Values of G to satisfy equation	First root of αl	$(\alpha l)^2/4\pi\sqrt{3}$ for the fundamental modes for rectangular arms
1	$1 + G = 0$	-1	$\pm 1{\cdot}8751$	0·16154
2	$G^2 = 0$	0, 0	$\pm 1{\cdot}5708$	0·11336
3	$1 - 3G + 4G^3 = 0$	$\frac{1}{2}, \frac{1}{2}$	$\pm 1{\cdot}3184$	0·07986
		-1	$\pm 1{\cdot}8751$	0·16154
4	$1 - 4G^2 + 4G^4 = 0$	$+\sqrt{\frac{1}{2}}, +\sqrt{\frac{1}{2}}$	$\pm 1{\cdot}1524$	0·06101
		$-\sqrt{\frac{1}{2}}, -\sqrt{\frac{1}{2}}$	$\pm 1{\cdot}8003$	0·14891
5	$1 + 5G - 20G^3 + 16G^5 = 0$	0·809, 0·809	$\pm 1{\cdot}0353$	0·04925
		−0·309, −0·309	$\pm 1{\cdot}6821$	0·13000
		-1	$\pm 1{\cdot}8751$	0·16154
6	$9G^2 - 24G^4 + 16G^6 = 0$	$+\sqrt{\frac{3}{4}}, +\sqrt{\frac{3}{4}}$	$\pm 0{\cdot}9743$	0·04123
		0, 0	$\pm 1{\cdot}5708$	0·11336
		$-\sqrt{\frac{3}{4}}, -\sqrt{\frac{3}{4}}$	$\pm 1{\cdot}8419$	0·15587

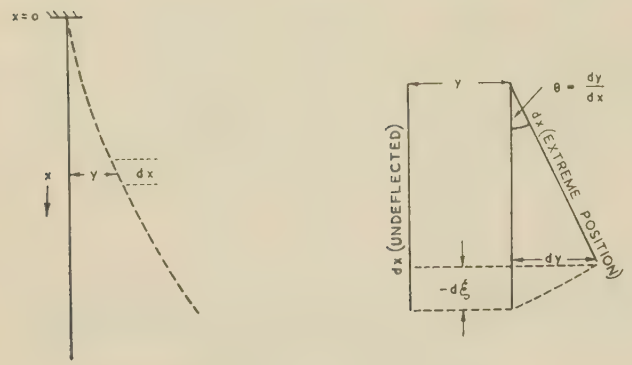

Fig. 8.—Element, dx, of single cantilever.

to the longitudinal displacement of all subsequent regions of the cantilever. All other elements dx make similar contributions, so that at a distance x from the support the net longitudinal displacement is

$$\xi(x, t) = -\tfrac{1}{2}\int_0^x \left(\frac{dy}{dx}\right)^2 dx \quad . \quad . \quad . \quad . \quad (31)$$

The longitudinal acceleration $\ddot{\xi}$ of the element dx at this point creates a reaction at the support

$$dF = m dx \ddot{\xi} \quad . \quad . \quad . \quad . \quad . \quad . \quad (32)$$

where m is the mass per unit length. The total reaction on the support is therefore

$$F(t) = m\int_0^l \ddot{\xi} dx \quad . \quad . \quad . \quad . \quad . \quad (33)$$

This analysis is extended in Appendix 10.2 to cover a folded cantilever arm of several sections. It is shown that some sections can make negative contributions to the total reaction.

To compare the degree of balance of the longitudinal forces for the different elements, an unbalance factor U has been formulated:

$$U = \frac{\Sigma F_+ - \Sigma F_-}{\Sigma F_+ + \Sigma F_-} \quad . \quad . \quad . \quad . \quad . \quad (34)$$

where ΣF_+ and ΣF_- are, respectively, the sums of the positive and negative contributions of all the sections to the longitudinal force at the support. This factor U is unity for a single cantilever arm (e.g. tuning fork) in the fundamental mode as there are no negative contributions, and it is zero for perfect balance.

Values of U have been calculated for 'zigzags' with arms of uniform cross-section, neglecting the bridges between the sections, to give a rough guide to the possibility of achieving longitudinal balance. Fig. 9 shows the results for the two modes of a 2-section element. For mode I a low natural frequency requires $l_2 > l_1$, but good balance is only obtained when $l_2 \simeq 0{\cdot}2l_1$ and the natural frequency is then much higher. In mode II the frequency is almost independent of l_2, and intermediate between the extremes of mode I, but for good balance l_2 needs to be approximately equal to $3l_1$, making an uneconomic shape.

The only other case investigated is a 'zigzag' with four sections of equal length. The first mode, which has a very low natural frequency, also has the low unbalance factor of only 0·17. The calculations are approximate and tedious, and so no attempt has been made to seek a closer balance theoretically. A more favourable 2-section 'zigzag' could undoubtedly be realized by varying the cross-section of the arm along its length.

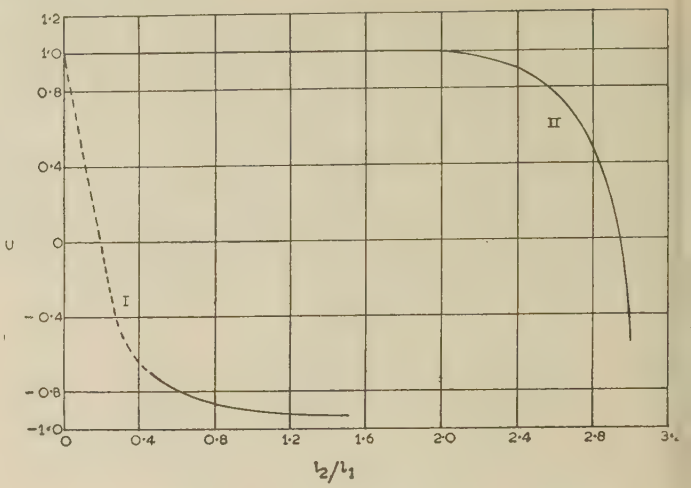

Fig. 9.—Unbalance factor U for modes I and II of 'zigzag' with arms of two unequal-length sections.

PART 2—EXPERIMENTAL

(4) BALANCED CANTILEVER ELEMENTS OF QUARTZ

H-elements with both uniform and variable cross-section and 'zigzag' elements with arms of up to four sections were made from quartz slices ZY$b\Phi(\Phi = 0 - 10°)$[6] by making 1 mm saw cuts parallel to the Y′-axis, as shown in the examples in Fig. 10. The H elements with non-uniform cross-section [Figs. 1(*b*) and (*c*)] were made by hollowing out the appropriate direction with the edge of a lapping wheel. The electrode arrangements

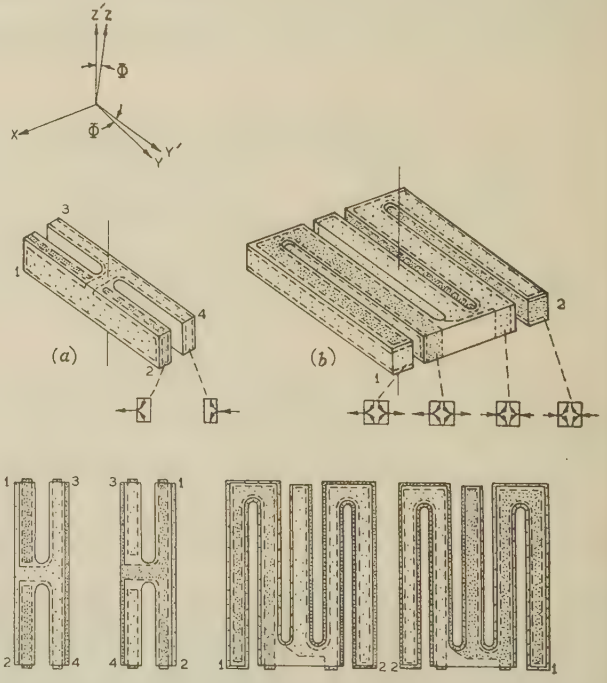

Fig. 10.—Electrode arrangement for quartz ZY $b\Phi$ balanced cantilevers.
(*a*) H form. (*b*) 'Zigzag' form.

illustrated in Fig. 10 hold for all quartz elements used. The sides of the saw cuts of the H-elements carried no electrodes, but those of the 'zigzag' were silvered by rotating the specimens during evaporation. The directions of the electric field are

shown in the cross-sections under the Figures (components in the Z′-direction excite no piezo-electric effect). The arms are caused to flex in the H bars by the outer halves being excited to expand and contract along their length while the inner halves are not excited directly, and in the 'zigzags' by the two halves of each section being excited in opposition.

As the elements were only experimental, no special jigs were made for cutting them and no attempts at lapping for balance were made, with the result that some of the possible advantages of this type of vibrator were not achieved. Errors in locating saw cuts gave deviations in the breadth of individual elements up to $\pm 5\%$, which in turn affected the natural frequencies and spoiled the balance and thus the Q-factors of the elements. In spite of this, measurements of frequency, temperature behaviour and Q-factor on 50 specimens satisfactorily confirmed the theory. Sample results are given in Tables 3–6.

(4.1) Frequency Measurements

The measured frequencies have been compared in the Tables with those calculated using the derived equations and Mason's values[7] for the elastic constants. With these elements, as with tuning forks, it is difficult to decide the effective length of the cantilever. For the H arm, the length has been taken as the distance from the free end to the head of the saw cut plus half the breadth. The length of a 'zigzag' section was measured as shown in Fig. 2.

The theory of the non-uniform H elements was checked satisfactorily by measuring specimens with various values of γ, t_1/t_0 and β (see Section 2.1). The predicted reduction in frequency of these elements over those of uniform H bars was confirmed.

The existence of the distinct sets of modes for 'zigzags' of up

Table 3

QUARTZ *ZYb* 5° UNIFORM H ELEMENTS

Average dimensions of arm			Frequency at 50° C			Temperature behaviour						Q	
						Envelope open to air			Envelope evacuated				
l	b	t	Measured	Calculated	% difference	T_M	a	$Tf_{50°C}$	T_M	a	$Tf_{50°C}$	in air	in vacuum
mm	mm	mm	kc/s	kc/s		°C	$\times 10^{-6}$	$\times 10^{-6}$	°C	$\times 10^{-6}$	$\times 10^{-6}$		
30·86	0·97	2·01	0·933	0·927	−0·6	20		−3·1	<-20		−7·1		14 000
18·65	1·03	2·01	2·678	2·694	0·6	45	−0·060	−2·0	12	−0·033	−2·1	7000	19 000
14·06	0·97	2·00	4·475	4·465	−2·2	53	−0·185	0	−7	−0·039	−3·6	5000	21 000

T_M = Temperature at peak of parabola.
a = Parabolic constant.
$Tf_{50°C}$ = First-order temperature coefficient at 50° C.

Table 4

QUARTZ *ZYb* 5° H ELEMENTS WITH VARIABLE THICKNESS

Average dimension of arm							Frequency at 50° C			Temperature behaviour						Q in vacuum
										Envelope open to air			Envelope evacuated			
l	γl	γ	b	t_0	t_1	t_1/t_0	Measured	Calculated	% difference	T_M	a	$Tf_{50°C}$	T_M	a	$Tf_{50°C}$	
mm	mm		mm	mm	mm		kc/s	kc/s		°C	$\times 10^{-6}$	$\times 10^{-6}$	°C	$\times 10^{-6}$	$\times 10^{-6}$	
26·61	21·37	0·80	0·97	2·00	6·02	3·0	0·802	0·811	1·1	60	−0·058	0·6	<-20		−8·0	
18·64	18·64	1·0	1·09	2·06	6·07	3·0	1·931	1·962	1·6	60	−0·069	2·4	15	−0·034	−2·5	32 000
11·52	8·75	0·76	0·97	1·85	5·94	3·2	4·252	4·220	−0·7	60	−0·056	0·3	−2	−0·039	−3·9	17 000

Table 5

QUARTZ *ZYb* 5° H ELEMENTS WITH VARIABLE BREADTH FOR $\gamma = 1$

Average dimensions of arm					Frequency at 50° C			Temperature behaviour						Q in vacuum
								Envelope open to air			Envelope evacuated			
l	b_0	b_1	$(1+\beta)$	t	Measured	Calculated	% difference	T_M	a	$Tf_{50°C}$	T_M	a	$Tf_{50°C}$	
mm	mm	mm		mm	kc/s	kc/s		°C	$\times 10^{-6}$	$\times 10^{-6}$	°C	$\times 10^{-6}$	$\times 10^{-6}$	
30·00	2·10	5·87	2·8	2·00	1·533	1·667	8·7	29	−0·031	−1·2	5	−0·028	−2·2	19 000
20·07	1·14	2·96	2·6	2·00	2·099	2·045	−2·0	53	−0·175	0·6	13	−0·038	−2·7	27 000
19·95	1·94	5·95	3·1	2·00	3·484	3·428	−1·6	43	−0·095	−1·4	20	−0·033	−1·7	34 000

Table 6

QUARTZ *ZYb* 5° UNIFORM 'ZIGZAGS'

Average dimensions of each section			Frequency at 50° C			Temperature behaviour						Q in vacuum
						Envelope open to air			Envelope evacuated			
l	b	t	Measured	Calculated	% difference	T_M	a	$Tf_{50°C}$	T_M	a	$Tf_{50°C}$	
mm	mm	mm	kc/s	kc/s		°C	$\times 10^{-6}$	$\times 10^{-6}$	°C	$\times 10^{-6}$	$\times 10^{-6}$	
2 *Sections*												
26·00	0·91	2·04	0·827	0·859	3·9	<20		−11·9	−15	−0·075	−10·8	11 000
37·14	1·96	2·02	0·871	0·907	4·1	32	−0·072	−2·1	5	−0·039	−3·2	19 000
21·15	2·04	2·09	2·881	2·912	1·1	26	−0·049		<−20		−3·8	13 000
3 *Sections*												
21·04	1·96	2·04	1·850(W)	1·992	7·1	29		−5·6	<−20		−6·4	7 000
			2·082		−4·3	20		−5·4	−9	−0·066	−6·9	12 000
			4·085(W)	4·029	−1·4							
			4·119		−2·2							
4 *Sections*												
21·14	1·94	2·01	1·650	1·492	−9·6	20		−2·0	10	−0·037	−3·2	32 000
			3·544	3·641	2·7							

to four sections was confirmed and the frequencies agreed well with theory. Slight departures from the assumed condition of equal arms were, however, observed in some cases, in that when single modes were expected, two modes very close together were found, one much weaker than the other (marked W in the Tables). The two modes had distinct vibration patterns illustrated in Figs. 11 and 12 by the two components of the

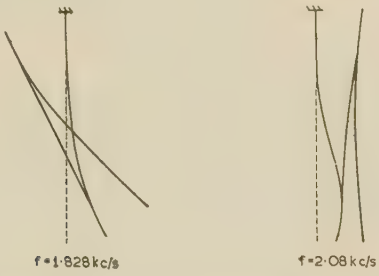

Fig. 11.—Measured displacement patterns for two frequencies for the lower fundamental mode of an arm of three sections.

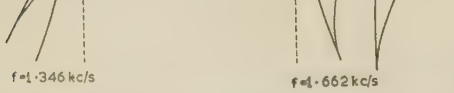

Fig. 12.—Measured displacement patterns for the two frequencies for the lower fundamental mode of an arm of four sections.

lower fundamental mode of a 3- and 4-section 'zigzag'. The patterns resemble those calculated for two unequal-length sections in Fig. 4. The pattern for the stronger frequency is also similar to that calculated for a single mode (Figs. 6 and 7).

Two frequencies close together would be undesirable in practical use and therefore, for production, either the accuracy of manufacture must be improved or the sections made of such different dimensions that adjacent frequencies are well separated.

(4.2) Frequency/Temperature Behaviour

The frequency/temperature behaviour of all the elements is parabolic. The large difference in turn-over temperature, T_M, in air and *in vacuo* would appear to be due to air loading. T_M, although not greatly affected by small changes of angle Φ, is highest for elements *in vacuo* when $\Phi = 5°$. For a given frequency, the highest value of T_M can be obtained by using a 4-section 'zigzag' *in vacuo*. Using H elements *in vacuo*, the highest value of T_M for a given frequency is achieved when the breadth increases towards the free end.

(4.3) Q-Factor Measurements

As previously mentioned, the Q-factors, measured by decay time, were lower than was expected, owing to inaccuracies in dimensions spoiling the balance.

In badly balanced H elements, each end acted independently as a tuning fork vibrating at its own natural frequency, resulting in two frequencies and a moderate Q-factor. In slightly better elements, each end again vibrated strongly at its natural frequency but also drove the other end weakly (verified with a stroboscope), causing a low Q-factor. A perfectly balanced specimen would have only one natural frequency and a very high Q-factor, but in order to attain this it would be necessary to lap the element for perfect balance during manufacture.

The Q-factors of the 4-section 'zigzag' are higher than those of the 2-section one, confirming the better longitudinal balance (see Section 3.2).

(5) 'ZIGZAG' ELEMENTS OF ETHYLENE DIAMINE TARTRATE (E.D.T.)

Unlike quartz, e.d.t. offers a large series of orientations with zero temperature coefficients of frequency above room temperature (see Fig. 13). Although the curve has been plotted for $\Psi = 90°$, it holds approximately for any value of Ψ since the temperature behaviour is only slightly affected by this angle. From such a large choice of orientations, it is possible to find cuts which have additional desirable properties such as low frequency for a given size of element and a large piezo-electric reaction. The orientation XY*ltl* 4°, 90°, 90° meets these requirements and is also simple to cut. To raise the turn-over temperature above 20° C, specimens were cut at angles of Φ slightly larger than 4°.

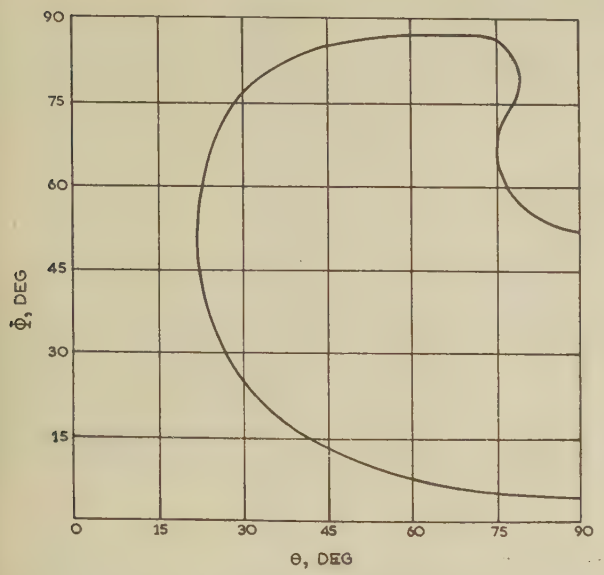

Fig. 13.—Orientations of e.d.t. bars XY*ltl*, Φ, Θ, 90° with zero temperature coefficient of frequency for the flexural mode.

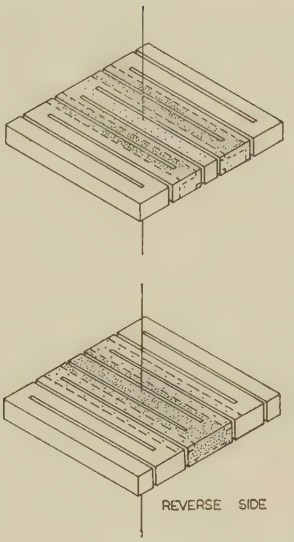

Fig. 14.—Electrode arrangement for ethylene-diamine-tartrate 'zigzags'.

An e.d.t. 'zigzag' can be cut from a parallel slice with a wet-string saw in a single set of operations since the saw can travel up or down. The finish is quite smooth and free from strains. Since the width of the cut is only 0·15 mm very compact specimens can be made. The electrodes used on these 'zigzags' are illustrated in Fig. 14. The cuts were left free and the silver on the main faces was divided along the length of the central sections by gently applying the wet-string saw. The outer sections are disconnected since a field on them has little influence on the drive (deduced from displacement patterns). The electrodes are the same for a 2-section 'zigzag.' The e.d.t. 'zigzags' were held between spring contacts at their nodal areas during measurements. The breadths of the sections differed by as much as ±3%. One cause was drift of the wet string due to different rates of solution in different directions.

Agreement between measured and calculated frequencies is quite fair (see examples in Tables 7 and 8). The second sections of some of the 2-section 'zigzags' were made shorter than the first to confirm the two fundamental frequencies predicted by theory. As shown by the results on the few experimental elements, it is possible to design a cut with a turn-over point at any desired temperature. The frequency/temperature para-

Table 7

E.D.T. *XYltl*, Φ°, 90°, 90° 'Zigzags' (Two Sections)

Φ	Average dimensions of each section					Frequency at 50° C			Temperature behaviour					
									In air			In vacuum		
	l_1	l_2	l_2/l_1	b	t	Measured	Calculated	% difference	T_M	a	$Tf_{50°C}$	T_M	a	$Tf_{50°C}$
	mm	mm		mm	mm	kc/s	kc/s		°C	×10⁻⁶	×10⁻⁶	°C	×10⁻⁶	×10⁻⁶
5°	20·21	20·21	1	1·51	2·16	1·122	1·099	−2·0	31	−1·086	−41·3	28	−0·344	
7° 16′	16·29	12·03	0·738	1·53		1·913	1·750	−8·5	40	−0·956	−17·4	41	−0·533	−11·7
						3·392	3·188	−6·0						
10°	17·07	12·89	0·755	1·53		1·695	1·630	−4·5	48	−1·000	−49·9	45	−1·085	−8·9
						3·025	2·889	−3·8						
14° 30′	20·44	20·44	1	1·48	2·01	1·377	1·153	−16·3	77	−1·275	+51·1	80	−0·541	+25·7

Table 8

E.D.T. *XYltl*, Φ°, 90°, 90° 'Zigzags' (4 Sections)

Φ	Average dimensions of section			Frequency at 50° C			Temperature behaviour in air		
	l	b	t	Measured	Calculated	% difference	T_M	a	$Tf_{50°C}$
	mm	mm	mm	kc/s	kc/s		°C	×10⁻⁶	×10⁻⁶
4° 53′	24·50	1·50	1·86	0·374	0·400	+7·0	35	−1·039	−18·0
6° 30′	31·21	1·52	1·86	0·240	0·252	+5·0	50	−1·045	0
10° 50′	20·11	1·52	1·47	0·560	0·632	+12·9	70	−1·068	+30·5

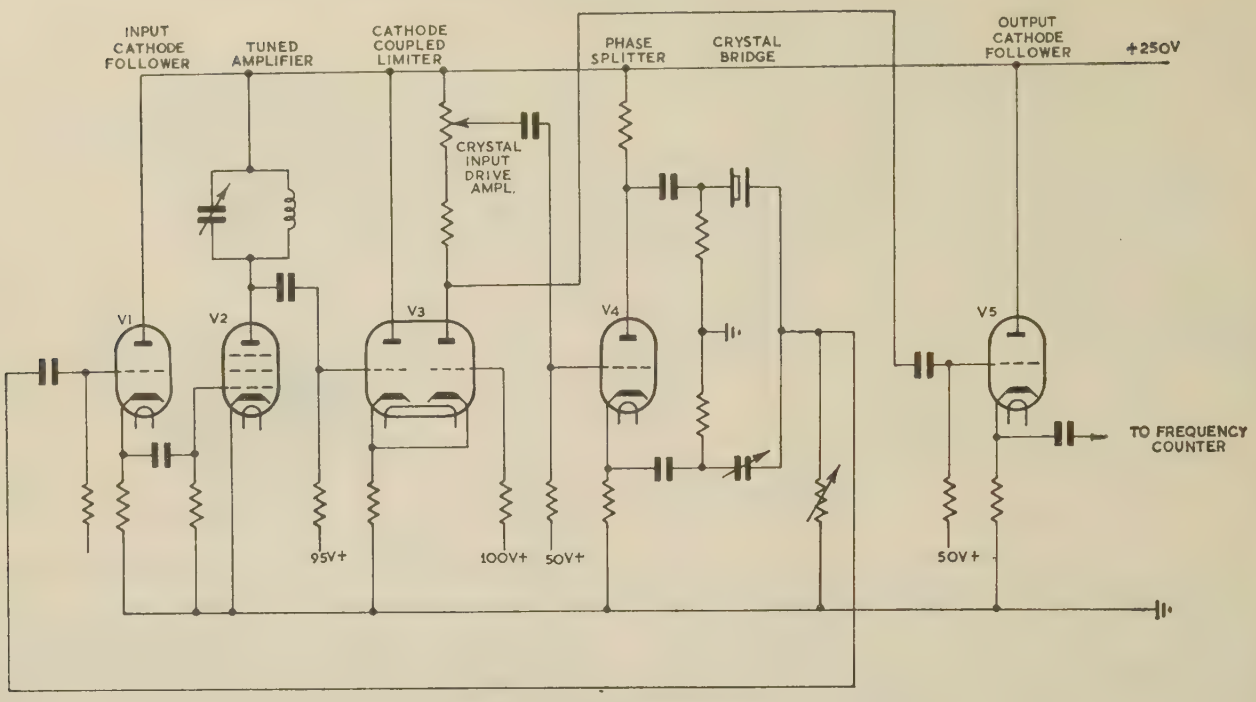

Fig. 15.—Crystal-maintaining circuit.

bolas of the cuts tried were, unfortunately, steep compared with those of quartz, but from the large choice of cuts with zero temperature coefficients it should be possible to find one with a low parabola constant.

From the dimensions given in the Tables it is clear that these crystals are very compact for low frequencies; for example, a 4-section 'zigzag' with overall dimensions of 30 × 15 × 1·5 mm vibrates at approximately 250 c/s, and a 2-section 'zigzag' with overall dimensions of only 20 × 8 × 2 mm vibrates at approximately 1 kc/s.

(6) CRYSTAL-MAINTAINING CIRCUIT

The essentials of the crystal-maintaining circuit, omitting bias and decoupling components, are shown in Fig. 15. The circuit was designed to facilitate control of the crystal amplitude and investigation of minor frequency changes. A simpler version would suffice for normal use. The bridge incorporating the phase splitter, V_4, is balanced at frequencies remote from the series resonance of the crystal. Near resonance, the bridge is unbalanced so that the output of V_4 is coupled to the input of V_1. A complete loop is thus formed and oscillation takes place at the frequency at which the net phase shift is zero. V_2 is tuned to favour the wanted mode, and V_3 acts as a cathode-coupled limiter absorbing the excess loop gain and at the same time defining the amplitude of the drive to the crystal. The square-wave output from V_3 is fed via the buffer valve V_5 to a frequency counter.

(7) CONCLUSIONS

Unfortunately the high Q-factors which should result from using these designs have not been attained owing to inaccuracies in dimensions and the unlapped surfaces of the experimental elements. However, it should be possible to remedy this if a suitable manufacturing process were developed. It is intended to investigate the possibilities of ultrasonic cutting.

The final restriction on the size of a flexural element and thus on the minimum frequency is fixed by the size of the oriented slice of the natural crystal. Since balanced cantilevers are smaller than the usual form of flexural vibrator for a given frequency, it is practicable to make these elements at lower frequencies than those usually reached. Of the balanced cantilevers, the 'zigzag' shape is the most economical of material. In particular the e.d.t. 'zigzags' are very compact so that they can easily be made for frequencies down to 100 c/s or even lower before the size becomes impracticable.

Although for low-frequency balanced cantilevers of quartz the peak of the frequency/temperature parabola occurs at a high temperature in air, it drops below room temperature *in vacuo*. With e.d.t. balanced cantilevers there is such a wide choice of cuts that the peak can be designed to occur at any desired temperature—this was illustrated by the few cuts chosen. However, the parabola constants of these few cuts were large compared with quartz, and for constant frequency over a wide range of temperature it would be necessary to investigate some of the other zero-coefficient cuts.

The e.d.t. 'zigzags' would make very compact elements for filters or resonators operating at about 200 c/s.

(8) ACKNOWLEDGMENTS

Acknowledgment is made to the Engineer-in-Chief of the Post Office and to the Controller of H.M. Stationery Office for permission to publish the paper.

(9) REFERENCES

(1) HEISING, R. A., *et al.*: 'Quartz Crystals for Electrical Circuits' (Van Nostrand, 1946), p. 537.
(2) BECKERATH, H. VON: 'Piezoelektrisch erregte Tonfrequente Biegungschwingungen von Quartzstäben mit sehr kleiner Temperaturabhängigkeit', *Verhandlungen der Deutschen Physikalischen Gesellschaft*, 1942, **23**, p. 92.
(3) DAVIES, A. O.: British Patent No. 701432.
(4) AYERS, S.: British Patent No. 814123.

5) RAYLEIGH, LORD: 'Theory of Sound' 2nd ed. (Macmillan, 1894), pp. 111 and 287.
6) 'Standards on Piezoelectric Crystals, 1949', *Proceedings of the Institute of Radio Engineers*, 1949, **37**, p. 1378.
7) MASON, W. P.: 'Zero Temperature Coefficient Quartz Crystals for very High Temperatures', *Bell System Technical Journal*, 1951, pp. 366–380.

(10) APPENDICES

(10.1) Method of Solving the Determinant in α for a 'Zigzag' Arm of any Number of Sections

The full determinant for four sections set out earlier can be reduced by manipulation to the form shown in Table 9 which can be extended for any number of sections.

The 2 × 2 sub-matrices at the beginning and end of the main diagonal, called the 'initial' and 'terminal' arrays, cover the effects of the first section and the free end, respectively. The influence of each of the other sections is expressed by two 2 × 2 sub-matrices flanking the main diagonal as shown by the boxes. The determinant for an arm of two sections, in which x_3 is the co-ordinate of the free end, is given by the array of elements in the top left-hand corner enclosed by the dotted line *a* when the sub-matrix of 0's in the right corner is replaced by the terminal array in x_3. Similarly the determinant for three sections (x_4 at free end) is given by the array to the left of the dotted line *b* when the sub-matrix of 0's in the extreme right-hand corner is replaced by the terminal array in x_4. The determinant can be built up in the same manner for any number of sections.

This determinant for any number of sections, *n*, can be expanded by the Laplace method, by partitioning the matrix into pairs of adjacent columns, denoted by $m = 1, 2, \ldots$ numbered from the left-hand side, and by operating with minors of the order 2. With the exception of the first and *n*th pairs of columns, each pair yields six minors of the following form:

$$ {}^1A_m = \begin{vmatrix} \varepsilon^{j\alpha x_m} & 0 \\ 0 & -\varepsilon^{-j\alpha x_m} \end{vmatrix} = -1 $$

$$ {}^2A_m = \begin{vmatrix} \varepsilon^{j\alpha x_m} & 0 \\ -\varepsilon^{j\alpha x_{m+1}} \cosh \alpha(x_{m+2} - x_{m+1}) & -\varepsilon^{-j\alpha x_{m+1}} \sinh \alpha(x_{m+2} - x_{m+1}) \end{vmatrix} = -\varepsilon^{-j\alpha(x_{m+1} - x_m)} \sinh \alpha(x_{m+2} - x_{m+1}) $$

$$ {}^3A_m = \begin{vmatrix} \varepsilon^{j\alpha x_m} & 0 \\ \varepsilon^{j\alpha x_{m+1}} \sinh \alpha(x_{m+2} - x_{m+1}) & \varepsilon^{-j\alpha x_{m+1}} \cosh \alpha(x_{m+2} - x_{m+1}) \end{vmatrix} = \varepsilon^{-j\alpha(x_{m+1} - x_m)} \cosh \alpha(x_{m+2} - x_{m+1}) $$

$$ {}^4A_m = \begin{vmatrix} 0 & -\varepsilon^{-j\alpha x_m} \\ -\varepsilon^{j\alpha x_{m+1}} \cosh \alpha(x_{m+2} - x_{m+1}) & -\varepsilon^{-j\alpha x_{m+1}} \sinh \alpha(x_{m+2} - x_{m+1}) \end{vmatrix} = -\varepsilon^{j\alpha(x_{m+1} - x_m)} \cosh \alpha(x_{m+2} - x_{m+1}) $$

$$ {}^5A_m = \begin{vmatrix} 0 & -\varepsilon^{-j\alpha x_m} \\ \varepsilon^{j\alpha x_{m+1}} \sinh \alpha(x_{m+2} - x_{m+1}) & \varepsilon^{-j\alpha x_{m+1}} \cosh \alpha(x_{m+2} - x_{m+1}) \end{vmatrix} = \varepsilon^{j\alpha(x_{m+1} - x_m)} \sinh \alpha(x_{m+2} - x_{m-1}) $$

$$ {}^6A_m = \begin{vmatrix} -\varepsilon^{j\alpha x_{m+1}} \cosh \alpha(x_{m+2} - x_{m+1}) & -\varepsilon^{-j\alpha x_{m+1}} \sinh \alpha(x_{m+2} - x_{m+1}) \\ \varepsilon^{j\alpha x_{m+1}} \sinh \alpha(x_{m+2} - x_{m+1}) & \varepsilon^{-j\alpha x_{m+1}} \cosh \alpha(x_{m+2} - x_{m+1}) \end{vmatrix} = -1 $$

The minors for the first pair of columns are

$$ {}^1A_1 = \begin{vmatrix} -\varepsilon^{j\alpha x_1} \cosh \alpha(x_2 - x_1) & -\varepsilon^{-j\alpha x_1} \sinh \alpha(x_2 - x_1) \\ \varepsilon^{j\alpha x_1} \sinh \alpha(x_2 - x_1) & \varepsilon^{-j\alpha x_1} \cosh \alpha(x_2 - x_1) \end{vmatrix} = -1 $$

$$ {}^2A_1 = \begin{vmatrix} -\varepsilon^{j\alpha x_1} \cosh \alpha(x_2 - x_1) & -\varepsilon^{-j\alpha x_1} \sinh \alpha(x_2 - x_1) \\ -\varepsilon^{j\alpha x_2} \cosh \alpha(x_3 - x_2) & -\varepsilon^{-j\alpha x_2} \sinh \alpha(x_3 - x_2) \end{vmatrix} = \varepsilon^{-j\alpha(x_2 - x_1)} \cosh \alpha(x_2 - x_1) \sinh \alpha(x_3 - x_2) - \varepsilon^{j\alpha(x_2 - x_1)} \sinh \alpha(x_2 - x_1) \cosh \alpha(x_3 - x_2) $$

$$ {}^3A_1 = \begin{vmatrix} -\varepsilon^{j\alpha x_1} \cosh \alpha(x_2 - x_1) & -\varepsilon^{j\alpha x_1} \sinh \alpha(x_2 - x_1) \\ \varepsilon^{j\alpha x_2} \sinh \alpha(x_3 - x_2) & \varepsilon^{-j\alpha x_2} \cosh \alpha(x_3 - x_2) \end{vmatrix} = -\varepsilon^{-j\alpha(x_2 - x_1)} \cosh \alpha(x_2 - x_1) \cosh \alpha(x_3 - x_2) + \varepsilon^{j\alpha(x_2 - x_1)} \sinh \alpha(x_2 - x_1) \sinh \alpha(x_3 - x_2) $$

$$ {}^4A_1 = \begin{vmatrix} \varepsilon^{j\alpha x_1} \sinh \alpha(x_2 - x_1) & \varepsilon^{-j\alpha x_1} \cosh \alpha(x_2 - x_1) \\ -\varepsilon^{j\alpha x_2} \cosh \alpha(x_3 - x_2) & -\varepsilon^{-j\alpha x_2} \sinh \alpha(x_3 - x_2) \end{vmatrix} = -\varepsilon^{-j\alpha(x_2 - x_1)} \sinh \alpha(x_2 - x_1) \sinh \alpha(x_3 - x_2) + \varepsilon^{j\alpha(x_2 - x_1)} \cosh \alpha(x_2 - x_1) \cosh \alpha(x_3 - x_2) $$

$$ {}^5A_1 = \begin{vmatrix} \varepsilon^{j\alpha x_1} \sinh \alpha(x_2 - x_1) & \varepsilon^{-j\alpha x_1} \cosh \alpha(x_2 - x_1) \\ \varepsilon^{j\alpha x_2} \sinh \alpha(x_3 - x_2) & \varepsilon^{-j\alpha x_2} \cosh \alpha(x_3 - x_2) \end{vmatrix} = \varepsilon^{-j\alpha(x_2 - x_1)} \sinh \alpha(x_2 - x_1) \cosh \alpha(x_3 - x_2) - \varepsilon^{j\alpha(x_2 - x_1)} \cosh \alpha(x_2 - x_1) \sinh \alpha(x_3 - x_2) $$

$$ {}^6A_1 = \begin{vmatrix} -\varepsilon^{j\alpha x_2} \cosh \alpha(x_3 - x_2) & -\varepsilon^{-j\alpha x_2} \sinh \alpha(x_3 - x_2) \\ \varepsilon^{j\alpha x_2} \sinh \alpha(x_3 - x_2) & \varepsilon^{-j\alpha x_2} \cosh \alpha(x_3 - x_2) \end{vmatrix} = -1 $$

Table 9

REDUCED DETERMINANT FOR 'ZIGZAG' OF UP TO FOUR SECTIONS

$$
\begin{array}{c|cccccccccc}
 & -\varepsilon^{j\alpha x_1}\cosh\alpha(x_2-x_1) & -\varepsilon^{-j\alpha x_1}\sinh\alpha(x_2-x_1) & \varepsilon^{j\alpha x_2} & 0 & 0 & 0 & 0 & 0 & 0 & 0 \\
a & \varepsilon^{j\alpha x_1}\sinh\alpha(x_2-x_1) & \varepsilon^{-j\alpha x_1}\cosh\alpha(x_2-x_1) & 0 & -\varepsilon^{-j\alpha x_2} & 0 & 0 & 0 & 0 & 0 & 0 \\
 & -\varepsilon^{j\alpha x_2}\cosh\alpha(x_3-x_2) & -\varepsilon^{-j\alpha x_2}\sinh\alpha(x_3-x_2) & 0 & 0 & \varepsilon^{j\alpha x_3} & 0 & 0 & 0 & 0 & 0 \\
 & \varepsilon^{j\alpha x_2}\sinh\alpha(x_3-x_2) & \varepsilon^{-j\alpha x_2}\cosh\alpha(x_3-x_2) & 0 & 0 & 0 & -\varepsilon^{-j\alpha x_3} & 0 & 0 & 0 & 0 \\
 & 0 & 0 & -\varepsilon^{j\alpha x_3}\cosh\alpha(x_4-x_3) & -\varepsilon^{-j\alpha x_3}\sinh\alpha(x_4-x_3) & 0 & 0 & \varepsilon^{j\alpha x_4} & 0 & 0 & 0 \\
 & 0 & 0 & \varepsilon^{j\alpha x_3}\sinh\alpha(x_4-x_3) & \varepsilon^{-j\alpha x_3}\cosh\alpha(x_4-x_3) & 0 & 0 & 0 & \varepsilon^{-j\alpha x_4} & 0 & 0 \\
b & 0 & 0 & 0 & 0 & -\varepsilon^{j\alpha x_4}\cosh\alpha(x_5-x_4) & -\varepsilon^{-j\alpha x_4}\sinh\alpha(x_5-x_4) & 0 & 0 & -\varepsilon^{j\alpha x_5} & 0 \\
 & 0 & 0 & 0 & 0 & \varepsilon^{j\alpha x_4}\sinh\alpha(x_5-x_4) & \varepsilon^{-j\alpha x_4}\cosh\alpha(x_5-x_4) & 0 & 0 & 0 & \varepsilon^{-j\alpha x_5}
\end{array}
$$

The minors for the nth pair of columns are

$$
{}^1A_n = \begin{vmatrix} \varepsilon^{j\alpha x_n} & 0 \\ 0 & -\varepsilon^{-j\alpha x_n} \end{vmatrix} = -1
$$

$$
{}^2A_n = \begin{vmatrix} \varepsilon^{j\alpha x_n} & 0 \\ -\varepsilon^{j\alpha x_{n+1}} & 0 \end{vmatrix} = 0
$$

$$
{}^3A_n = \begin{vmatrix} \varepsilon^{j\alpha x_n} & 0 \\ 0 & \varepsilon^{-j\alpha x_{n+1}} \end{vmatrix} = \varepsilon^{-j\alpha(x_{n+1}-x_n)}
$$

$$
{}^4A_n = \begin{vmatrix} 0 & -\varepsilon^{-j\alpha x_n} \\ -\varepsilon^{j\alpha x_{n+1}} & 0 \end{vmatrix} = -\varepsilon^{j\alpha(x_{n+1}-x_n)}
$$

$$
{}^5A_n = \begin{vmatrix} 0 & -\varepsilon^{j\alpha x_n} \\ 0 & \varepsilon^{-j\alpha x_{n+1}} \end{vmatrix} = 0
$$

$$
{}^6A_n = \begin{vmatrix} -\varepsilon^{j\alpha x_{n+1}} & 0 \\ 0 & \varepsilon^{-j\alpha x_{n+1}} \end{vmatrix} = -1
$$

The method of expansion is as follows: Take one minor from each pair of columns in such a way that each row of the determinant enters once and once only, and form the product of these. The value of the determinant is the sum of all such products which are possible.

The rules for selecting the minors for the products can be found by inspecting the determinant. It can be seen that a minor in any pair of columns can only influence the selection of minors from the following two pairs of columns. In the lists given below, the different types of minors are set out, together with all the possible minors by which they can be multiplied. The same rules hold for all the pairs of columns with the exception of the first and $(n-1)$th pairs; the rules for these are listed separately. The signs of the products must be found by inspecting the determinant.

Rules for selecting the minors for the products.

Minor in pair 1	can be multiplied by minor in pair 2	and by minor in pair 3
${}^1A_1$	${}^6A_2$	${}^1A_3 \to {}^6A_3$
${}^2A_1$	${}^4A_2, {}^5A_2, {}^6A_2$	${}^4A_3, {}^5A_3, {}^6A_3$
${}^3A_1$	${}^4A_2, {}^5A_2, {}^6A_2$	${}^2A_3, {}^3A_3, {}^6A_3$
${}^4A_1$	${}^2A_2, {}^3A_2, {}^6A_2$	${}^4A_3, {}^5A_3, {}^6A_3$
${}^5A_1$	${}^2A_2, {}^3A_2, {}^6A_2$	${}^2A_3, {}^3A_3, {}^6A_3$
${}^6A_1$	${}^1A_2 \to {}^6A_2$	${}^6A_3$

Minor in pair m	can be multiplied by minor in pair $m+1$	and by minor in pair $m+2$
${}^1A_m$, ${}^2A_m$, ${}^3A_m$, ${}^4A_m$, ${}^5A_m$, ${}^6A_m$	${}^1A_{m+1} \to {}^6A_{m+1}$	${}^1A_{m+2} \to {}^6A_{m+2}$ ${}^4A_{m+2}, {}^5A_{m+2}, {}^6A_{m+2}$ ${}^2A_{m+2}, {}^3A_{m+2}, {}^6A_{m+2}$ ${}^4A_{m+2}, {}^5A_{m+2}, {}^6A_{m+2}$ ${}^2A_{m+2}, {}^3A_{m+2}, {}^6A_{m+2}$ ${}^6A_{m+2}$

Minor in pair $(n-1)$	can be multiplied by minor in pair n
${}^1A_{n-1}$	${}^1A_n, {}^3A_n, {}^4A_n, {}^6A_n$ (${}^2A_n$, ${}^5A_n$ are zero)
${}^2A_{n-1}$	${}^1A_n, {}^3A_n$
${}^3A_{n-1}$	${}^1A_n, {}^4A_n$
${}^4A_{n-1}$	${}^1A_n, {}^3A_n$
${}^5A_{n-1}$	${}^1A_n, {}^4A_n$
${}^6A_{n-1}$	${}^1A_n$

As an example, the solution of the determinant for an arm of four sections is given below. It is expressed in terms of the lengths l_m of the sections. When replacing the x co-ordinates by l_m, the positive direction of x must be taken into account (see Fig. 3), e.g. $x_2 - x_1 = l_1$, $x_2 - x_3 = l_2$, $x_4 - x_3 = l_3$, $x_4 - x_5 = l_4$.

Solution of the determinant in α for an arm of four sections.

$$A_1^6A_2^1A_3^6A_4 + {}^2A_1^4A_2^5A_3^4A_4 + {}^2A_1^5A_2^4A_3^3A_4 - {}^3A_1^4A_2^3A_3^4A_4 - {}^3A_1^5A_2^2A_3^3A_4 - {}^4A_1^2A_2^5A_3^4A_4 - {}^4A_1^3A_2^4A_3^3A_4 + {}^5A_1^2A_2^3A_3^4A_4 + {}^5A_1^3A_2^2A_3^3A_4 + {}^6A_1^1A_2^6A_3^1A_4 = 0 \quad . \; . \; . \quad (35)$$

giving

$$\begin{aligned} &1 + \cosh \alpha l_1 \cosh \alpha l_2 \cosh \alpha l_3 \cosh \alpha l_4 \cos \alpha(l_1 + l_2 + l_3 + l_4) \\ &+ \cosh \alpha l_1 \cosh \alpha l_2 \sinh \alpha l_3 \sinh \alpha l_4 \cos \alpha(l_1 + l_2 + l_3 - l_4) \\ &+ \cosh \alpha l_1 \sinh \alpha l_2 \cosh \alpha l_3 \sinh \alpha l_4 \cos \alpha(l_1 + l_2 - l_3 + l_4) \\ &+ \sinh \alpha l_1 \cosh \alpha l_2 \sinh \alpha l_3 \cosh \alpha l_4 \cos \alpha(l_1 - l_2 + l_3 + l_4) \\ &+ \cosh \alpha l_1 \sinh \alpha l_2 \sinh \alpha l_3 \cosh \alpha l_4 \cos \alpha(l_1 + l_2 - l_3 - l_4) \\ &+ \sinh \alpha l_1 \cosh \alpha l_2 \cosh \alpha l_3 \sinh \alpha l_4 \cos \alpha(l_1 - l_2 + l_3 - l_4) \\ &+ \sinh \alpha l_1 \sinh \alpha l_2 \sinh \alpha l_3 \sinh \alpha l_4 \cos \alpha(l_1 - l_2 - l_3 + l_4) \\ &+ \sinh \alpha l_1 \sinh \alpha l_2 \cosh \alpha l_3 \cosh \alpha l_4 \cos \alpha(l_1 - l_2 - l_3 - l_4) \\ &= 0 \quad . \; . \; . \quad (36) \end{aligned}$$

Empirical rule for writing directly the equation for α for an arm of any number of sections.

From inspection of the equations for α for arms of up to five sections, the following rule has been deduced:

Starting from

$$1 + \cosh \alpha l_1 \cosh \alpha l_2 \ldots \cosh \alpha l_m \ldots \cosh \alpha l_n \cos \alpha(l_1 + l_2 + \ldots + l_m \ldots + l_n)$$

add all the similar terms derived from all the possible sign combinations of the l's in $\cos \alpha(l_1 + l_2 \ldots + l_m \ldots + l_n)$ multiplied by their appropriate hyperbolic functions [the total possible number of combinations is halved since $\cos(-x) = \cos x$]. Whenever l_m in the cosine term is negative, $\cosh \alpha l_{m-1} \cosh \alpha l_{m+1}$ is replaced by $\sinh \alpha l_{m-1} \sinh \alpha l_{m+1}$, and when l_n is negative, $\cosh \alpha l_{n-1} \cosh \alpha l_n$ is replaced by $\sinh \alpha l_{n-1} \sinh \alpha l_n$. If there are an even number of changes affecting any one cosh term it will remain unchanged.

This rule was found to give the correct solution for an arm of six sections.

(10.2) Step-Wise Computation of Longitudinal Forces on the Sections of an Arm of a 'Zigzag' when Vibrating Flexurally

Consider an arm of a 'zigzag' with any number of sections whose lengths are parallel to the X-axis vibrating laterally in the Y-direction.

First Section.

Divide the length l_1 of the first section into N subsections, each of length $L_1 = l_1/N$, labelling the sections $1, 2 \ldots n \ldots N$ and calculate the x co-ordinates of the centre points of the subsections, e.g. if the first subsection starts at $x = 0$ and the nth ends at $x = l_1$,

$$x_n = \frac{2n-1}{2}L_1 = (2n-1)\frac{l_1}{2N} \quad . \; . \; . \quad (37)$$

Consider the First Subsection.

The centre-point Q moves to Q″ (Fig. 16), but the horizontal distance QQ′ is known and is the calculated lateral displacement

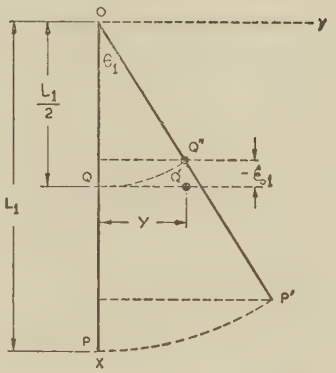

Fig. 16.—First sub-section.

$y(x, t)$ at this point, i.e. $y_1(t)$. The longitudinal displacement $Q'Q'' = -\xi_1$, say, is given by

$$-\xi_1(t) = \frac{L_1}{2}(1 - \cos\theta_1) = L_1 \sin^2\frac{\theta_1}{2} \simeq L_1\frac{\theta_1^2}{4} \quad . \quad (38)$$

where $\theta_1 = \theta_1(t)$.

But
$$\theta_1(t) \simeq \frac{2y_1(t)}{L_1} \quad . \; . \; . \; . \; . \; . \; . \quad (39)$$

and so
$$-\xi_1(t) \simeq \frac{L_1}{4}\frac{4}{L_1^2}y_1^2(t) = \frac{y_1^2(t)}{L_1} \quad . \; . \; . \quad (40)$$

Now
$$y_1(t) = \hat{y}_1\varepsilon^{j\omega t}$$

Thus
$$-\xi_1(t) = \frac{1}{L_1}\hat{y}_1^2\varepsilon^{2j\omega t} \quad . \; . \; . \; . \; . \; . \; . \quad (41)$$

$$\dot{\xi}_1(t) = \frac{-2j\omega}{L_1}\hat{y}_1^2\varepsilon^{2j\omega t} \quad . \; . \; . \; . \; . \; . \quad (42)$$

$$\ddot{\xi}_1(t) = \frac{4\omega^2}{L_1}\hat{y}_1^2\varepsilon^{2j\omega t} \quad . \; . \; . \; . \; . \; . \; . \quad (43)$$

This has a maximum value

$$\hat{\ddot{\xi}}_1 = \frac{4\omega^2}{L_1}\hat{y}_1^2 \quad . \; . \; . \; . \; . \; . \; . \quad (44)$$

The longitudinal force required to give this first subsection this acceleration is

$$F_1(t) = mL_1\frac{4\omega^2}{L_1}\hat{y}_1^2\varepsilon^{2j\omega t} = 4\omega^2 m\hat{y}_1^2\varepsilon^{2j\omega t} \quad . \; . \; . \; . \; . \; . \; . \quad (45)$$

(positive value in $-X$ direction)

where m is the mass per unit length.

This has a maximum value $\hat{F}_1 = 4\omega^2 m\hat{y}_1^2$.

Second Subsection.

The centre-point S of the second sub-section PR (Fig. 17) may be regarded as moving laterally by y_2; and longitudinally by $2\xi_1$, to position S′, in addition to the longitudinal movement of ξ_2 due to its own rotation through θ_2.

As the lateral movement of P is $2y_1$,

$$\theta_2(t) \simeq \frac{2}{L_1}[y_2(t) - 2y_1(t)] \quad . \; . \; . \; . \quad (46)$$

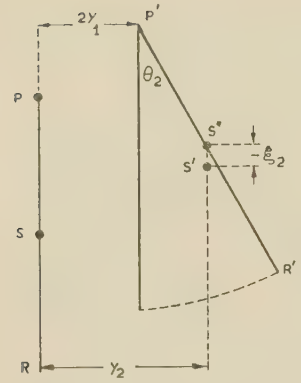

Fig. 17.—Second sub-section.

Now $$-\xi_2(t) = \frac{L_1}{2}(1 - \cos\theta_2) \simeq L_1\frac{\theta_2^2}{4} \qquad [\theta_2 = \theta_2(t)]$$

$$= \frac{L_1}{4}\frac{4}{L_1^2}[y_2(t) - 2y_1(t)]^2$$

$$= \frac{1}{L_1}[y_2(t) - 2y_1(t)]^2 \quad . \quad . \quad . \quad . \quad . \quad . \quad (47)$$

Now $y_2(t) = \hat{y}_2\varepsilon^{j\omega t}$ and $y_1(t) = \hat{y}_1\varepsilon^{j\omega t}$

So $$-\xi_2(t) = \frac{1}{L_1}(\hat{y}_2 - 2\hat{y}_1)^2\varepsilon^{2j\omega t} \quad . \quad . \quad . \quad . \quad . \quad . \quad (48)$$

and $$\ddot{\xi}_2(t) = \frac{4\omega^2}{L_1}(\hat{y}_2 - 2\hat{y}_1)^2\varepsilon^{2j\omega t} \quad . \quad . \quad . \quad . \quad . \quad . \quad (49)$$

Remembering that

$$\ddot{\xi}_1(t) = \frac{4\omega^2}{L_1}\hat{y}_1^2\varepsilon^{2j\omega t} \quad . \quad . \quad . \quad . \quad . \quad . \quad . \quad . \quad (50)$$

$$F_2(t) = 4\omega^2 m[2\hat{y}_1^2 + (\hat{y}_2 - 2\hat{y}_1)^2]\varepsilon^{2j\omega t} \quad . \quad . \quad . \quad (51)$$

nth Subsection.

Note: The lateral displacement at end of subsection 1 is $2y_1$. At the end of subsection 2 it is

$$2y_1 + 2(y_2 - 2y_1) = 2(y_2 - y_1)$$

At the end of subsection 3 it is

$$2(y_2 - y_1) + 2[y_3 - 2(y_2 - y_1)] = 2(y_3 - y_2 + y_1)$$

At the end of subsection n it is

$$2[y_n - y_{n-1} + y_{n-2} \ldots] = 2(-1)^n\sum_{r=1}^{n}(-1)^r y_r$$

So

$$\theta_n = \frac{2}{L_1}\left[y_n - 2(-1)^{n-1}\sum_{r=1}^{n-1}(-1)^r y_r\right] \quad . \quad . \quad . \quad . \quad . \quad (52)$$

where $\theta, y = \theta(t), y(t)$

$$-\xi_n(t) = \frac{1}{L_1}\left[y_n - 2(-1)^{n-1}\sum_{r=1}^{n-1}(-1)^r y_r\right]^2$$

$$= \frac{1}{L_1}\left[\hat{y}_n - 2(-1)^{n-1}\sum_{r=1}^{n-1}(-1)^r\hat{y}_r\right]^2\varepsilon^{2j\omega t} \quad . \quad . \quad (53)$$

$$\ddot{\xi}_n(t) = \frac{4\omega^2}{L_1}\left[\hat{y}_n - 2(-1)^{n-1}\sum_{r=1}^{n-1}(-1)^r\hat{y}_r\right]^2\varepsilon^{2j\omega t} \quad . \quad . \quad (54)$$

and

$$F_n(t) = mL_1\left[\ddot{\xi}_n(t) + 2\sum_{r=1}^{n-1}\ddot{\xi}_r(t)\right] \quad . \quad . \quad . \quad . \quad . \quad . \quad (55)$$

('Local' contribution plus accrued contribution to acceleration)

The total longitudinal force on support due to section is

$$F(t) = \sum_{n=1}^{N} F_n(t) \quad . \quad . \quad . \quad . \quad . \quad . \quad (56)$$

At the end of the first section, i.e. the end of the Nth subsection, the lateral displacement is

$$2(-1)^N\sum_{r=1}^{N}(-1)^r y_r \quad \text{where } y_r = y_r(t) = \hat{y}_r\varepsilon^{j\omega t}.$$

Second Section.

Consider now the second section, length l_2, folded back. Divide it into M subsections each of length $L_2 = l_2/M$ and number the subsections from $N + 1$ to $N + M$, starting from

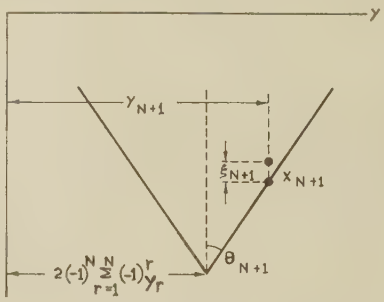

Fig. 18.—Junction of first and second sections.

the subsection nearest the junction with the first section (Fig. 18). If the beginning of the first section is fixed at $x = 0$,

$$x_p = l_1 - \frac{2(p - N) - 1}{2}L_2 \quad . \quad . \quad . \quad . \quad . \quad (57)$$

where $$N + 1 \leqslant p \leqslant N + M$$

and the values for y_p can be calculated.

$$\theta_{N+1} \simeq \frac{2}{L_2}\left[y_{N+1} - 2(-1)^N\sum_{r=1}^{N}(-1)^r y_r\right] \quad . \quad . \quad . \quad (58)$$

$$+\xi_{N+1}(t) = \frac{1}{L_2}\left[\hat{y}_{N+1} - 2(-1)^N\sum_{r=1}^{N}(-1)^r\hat{y}_r\right]^2\varepsilon^{2j\omega t} \quad . \quad (59)$$

$$\ddot{\xi}_{N+1}(t) = -\frac{4\omega^2}{L_2}\left[\hat{y}_{N+1} - 2(-1)^N\sum_{r=1}^{N}(-1)^r\hat{y}_r\right]^2\varepsilon^{2j\omega t} \quad . \quad (60)$$

$$F_{N+1}(t) = mL_2\left[\ddot{\xi}_{N+1}(t) + 2\sum_{r=1}^{N}\ddot{\xi}_r(t)\right] \quad . \quad . \quad . \quad . \quad (61)$$

At the end of the $(N + 1)$th subsection the lateral displacement is

$$2(-1)^N\sum_{r=1}^{N}(-1)^r y_r + 2\left[y_{N+1} - 2(-1)^N\sum_{r=1}^{N}(-1)^r y_r\right]$$

$$= 2(-1)^{N+1}\sum_{r=1}^{N+1}(-1)^{N+1}\sum_{r=1}^{N+1}(-1)^r y_r$$

and at the end of the pth subsection the lateral displacement is

$$2(-1)^p \sum_{r=1}^{p} (-1)^r y_r$$

And $$\theta_p = \frac{2}{L_2}\left[y_p - 2(-1)^{p-1} \sum_{r=1}^{p-1} (-1)^r y_r \right] \quad . \quad . \quad . \quad . \quad (62)$$

$$\ddot{\xi}_p(t) = -\frac{4\omega^2}{L_2}\left[\hat{y}_p - 2(-1)^{p-1} \sum_{r=1}^{p-1} (-1)^r \hat{y}_r \right]^2 \varepsilon^{2j\omega t} \quad . \quad (63)$$

$$F_p(t) = mL_2\left[\ddot{\xi}_p(t) + 2 \sum_{r=1}^{p-1} \ddot{\xi}_r(t) \right] \quad . \quad . \quad . \quad . \quad . \quad . \quad (64)$$

and $$F(t) = \sum_{p=1}^{M} F_p(t) \quad . \quad . \quad . \quad . \quad . \quad . \quad . \quad . \quad . \quad . \quad (65)$$

In a similar manner the calculation can be continued to cover any number of sections.

21.391 : 621.374.32 : 681.142

The Institution of Electrical Engineers,
Monograph No. 392 M
July 1960

CHAIN CODES AND THEIR ELECTRONIC APPLICATIONS

By F. G. HEATH, B.Sc., Associate Member, and M. W. GRIBBLE, B.Sc.

(*The paper was first received* 15*th October*, 1959, *and in revised form* 22*nd April*, 1960. *It was published as an* INSTITUTION MONOGRAPH *in July*, 1960.)

SUMMARY

A type of binary digital code is described which is easily generated by computer circuits. The important properties of these codes are described, and various electronic applications enumerated.

DEFINITIONS

The operation '*a* and *b*' is written *ab*.

The operation '*a* or *b*' is written $a \vee b$.

The operation 'not *a*' is written a'.

The operation '*a* not equivalent to *b*' is written $a \oplus b$, and the corresponding Boolean function is $ab' \vee a'b$.

The symbols for the 'and' gate, 'or' gate and 'not' circuit, together with those used for the flip-flop circuit and its counter-connected version, are shown in Fig. 1.

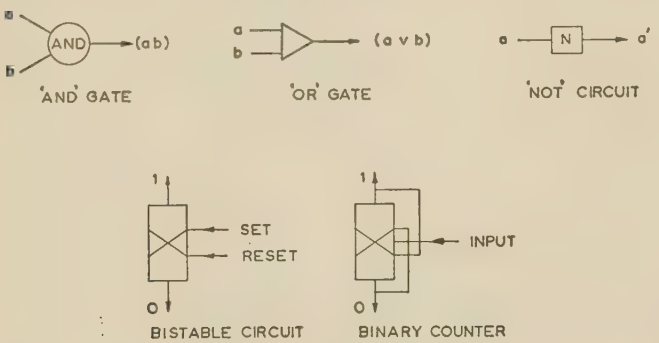

Fig. 1.—Graphical symbols.

When dealing with chain codes as a succession of digits it is most convenient to write them as *a*, *b*, *c*, *d*, etc., making *a* the oldest digit. When working on shift registers and code generators it is much better to make *A* the most recent digit, and this convention is adopted wherever suitable in the paper.

(1) INTRODUCTION

Digital methods are now being exploited in a wide range of applications. Apart from the most obvious example—digital computation—there are digital servo-mechanisms, data-processing equipments and data links, both line and radio.

In many of these applications it is found that the basic binary number system of counting, where decimal digits 0, 1, 2, 3, 4, 5, etc., are represented as 0, 1, 10, 11, 100, 101, etc., is frequently not as appropriate as some other arrangement of digit patterns.

Chain codes are one alternative to the normal binary code and have application in high-speed counters, error-correcting equipment and digital pick-offs. Their basic mathematical property is perhaps best illustrated by drawing a typical code round the periphery of a circle, as shown in Fig. 2. The following facts will be observed: there are 16 binary digits in all; and if adjacent digits are taken four at a time all possible patterns are present (and, therefore, no pattern is duplicated), as shown in Table 1.

Fig. 2.—Complete chain code, $n = 4$ (16 4-digit patterns).

Table 1

COMPLETE 4-DIGIT CHAIN-CODE PATTERNS

Step	Pattern
0	1111
1	1110
2	1101
3	1010
4	0101
5	1011
6	0110
7	1100
8	1001
9	0010
10	0100
11	1000
12	0000
13	0001
14	0011
15	0111

It follows that the sequence shown in Fig. 2 may be used for counting from 0 to 15, exactly as with binary numbers.[1, 2] Most of the special properties of chain codes arise from the fact that the change of pattern is accomplished by a shift to the left and the generation of one new digit. As the number of digits in the pattern is increased, so the number of different codes obtainable increases enormously. It can be shown by elimination that there are two complete chains for $n = 3$ and sixteen for $n = 4$ (a complete chain has 2^n patterns). It has been proved[3] that there are 2 to the power $(2^{n-1} - n)$ complete chains for any n: many more incomplete chains exist which are useful in electronic applications.

Although chain codes have many fascinating mathematical properties, they would be of little use if it were not for the fact that the sequential patterns can be easily generated using computer-type circuits. Section 7.1 shows that all possible chain codes can be classified and generated by using the ideas and elements of Boolean algebra.

A simple example of a rule which generates a chain code is as follows.

Fig. 3(*a*) represents some form of binary store, with four elements each capable of assuming two states corresponding to '0' and '1'. The initial state is defined as *abcd*. The next

Correspondence on Monographs is invited for consideration with a view to publication.

Mr. Heath is in the Department of Electrical Engineering, Manchester College of Science and Technology, University of Manchester, and Mr. Gribble is with Ferranti Ltd.

Fig. 3.—Typical step in a chain code.
(*a*) Initial state.
(*b*) First pattern.

pattern is generated by moving *b*, *c* and *d* one place to the eft and introducing a new digit in the right-hand space, which in his case is constrained to be the opposite of *d* if $a = 1$ and the ame as *d* if $a = 0$. This has the logical form $ad' \vee a'd$, the peration of half-adding or not-equivalence, i.e. $a \oplus d$. Fig. 3(*b*) hows the next pattern.

Applying this rule repeatedly to the pattern 1111 we obtain 1110, 1101, 1010, 0101, 1011, 0110, 1100, 1001, 0010, 0100, 1000, 0001, 0011, 0111, which is drawn as a chain in Fig. 4, pattern 0000 being absent.

A useful property of chain codes, which can be seen from this example, is that fifteen different 4-digit patterns can be defined in order using only fifteen binary symbols. If the normal binary code were used, sixty binary symbols would be necessary. This property was used by Baudot for his telegraph decoding disc, presumably to ease the manufacturing problem.

Fig. 4.—15-digit chain code generated by $a \oplus d$, $n = 4$.

It can be seen from Fig. 4 that a chain code need not be complete, i.e. have 2^n patterns: in fact, all lengths can be generated by suitable techniques as described in Sections 2 and 3.

The digits adjacent to a pattern bear a fixed relationship to that pattern, a property which makes it possible to use chain codes directly in error-detecting or -correcting equipment. The virtue of chain codes compared with other binary codes in this type of application lies in the small amount of apparatus which is needed to generate the complete code sequence.

Quite apart from any technical merits, chain codes are very good for teaching the elements of Boolean algebra and thoroughly testing high-speed computing elements. These rather unexpected benefits stem from the self-contained nature of the code generation and the easily recognized output waveform.

(2) ELECTRONIC GENERATION OF CHAIN CODES

It can be seen from Fig. 3 that a shift register is the obvious device for moving the digits one place to the left when a new pattern is generated. Any form of shift register may be used, but here only shift registers composed of a series of bistable elements will be discussed. A 4-stage shift register is required to generate the chain shown in Fig. 4, since only a circuit which provides the new input digit is needed.

It would be possible to generate the next digit, *n*, by a logic circuit which satisfied the relationship $n = ad' \vee a'd$. In this particular case, however, it is more convenient to generate a 'change' signal for the first stage (the *X* method of Section 7.1), since the first stage already has *d* stored in it. The 'change' signal is merely *a*, so that the code can be generated by making stage A a counter and applying a signal derived from stage D to its input. The block diagram is shown in Fig. 5. The

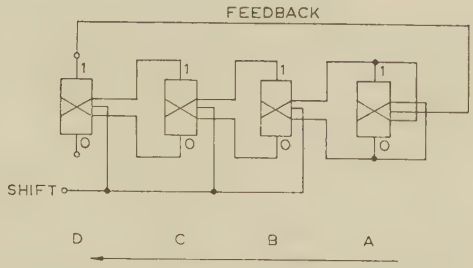

Fig. 5.—Chain-code generator for 15-digit code.

normal convention of signal input at the left has been reversed so that the new digit appears at the right in the circuit as well as in the written code.

Any other 4-digit code progression may be generated by using a 4-stage shift register and adding appropriate logic to generate the new digit. Longer codes are obtained by adding stages to the shift register.

(3) GENERATION OF SHORT CHAIN CODES

The method described above is adequate for complete chain codes and for arrangements where the starting pattern is injected into the shift-register stages initially: in other cases additional precautions are necessary for the following reason.

It frequently happens that a particular Boolean function for *n* digits gives a sequence which has less than 2^n digits. This means that certain patterns of digits are missing in the code, and if one of these is impressed upon the register before starting code generation, then a second sequence of digits will be produced having no common patterns with the first. If the total number of digits in both sequences is less than 2^n, this process can be repeated by impressing on the register a starting pattern which is not present in either sequence. The total number of digits in all sequences produced by a given Boolean function of order *n* is always 2^n.

For example, the arrangement shown in Fig. 3 normally generates the chain shown in Fig. 4, but if the starting pattern happens to be 0000, then 0's will be generated indefinitely, since $0 \oplus 0 = 0$. A less trivial example is provided by this same rule for $n = 5$. Four chains are generated, with 21, 7, 3 and 1 patterns, totalling 2^5. This effect is a nuisance in equipment where short codes are being used, since it is necessary either to control the starting pattern or use extra logic to suppress the unwanted chains.

It was partly this effect and partly the difficulty of finding chain codes with a stated number of patterns which led to the development of a method for shortening a chain code by jumping over some of the patterns.

If it is desired to shorten the code of Fig. 4 to ten patterns,

Fig. 6.—15-digit code shortened to ten patterns.

for example, the pattern 1101 is replaced by 1100. This gives the sequence 1111, 1110, 1100, 1001, 0010, 0100, 1000, 0001, 0011, 0111, shown as a chain in Fig. 6.

The merit of this method can be seen by imagining that an equipment using the code of Fig. 6 is switched on and for-

tuitously assumes one of the forbidden patterns, say 1010. Then the rule 'next = first ⊕ last' will take the pattern successively through 0101, 1011, 0110, 1100, at which point normal operation occurs. The effect is shown pictorially in Fig. 7.

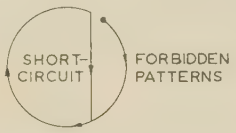

Fig. 7.—Method of chain code-shortening.

Section 7.2 gives codes and shortening methods for generating all code lengths from 128 to 3.

This technique does not lessen the risk of the all 0's pattern starting and continuing. Any method which injects a '1' at switch-on will overcome this effect. A transient signal from one supply line to a '1' input is the simplest solution, while at the other extreme an n-way 'and' gate connected to the '0' outputs and injecting a '1' is a certain remedy. Many useful chain codes have the all 0's (or all 1's) pattern missing, so that this precaution is frequently needed.

Taking the example already quoted—the generation of the ten-pattern code shown in Fig. 6—the shortening circuit must recognize the pattern 1110 (as preceding 1101) and modify the basic generator by causing 1100 to appear next. The circuit is shown in Fig. 8, the extra components being mainly crystal diodes.

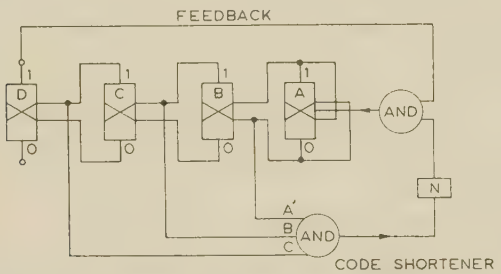

Fig. 8.—Schematic of 10-pattern-code generator.

If some simple device cannot be used to insure against the all 0's condition, the logical diagram of the correction circuit shown in Fig. 9 must be used, again composed mainly of diodes. Since four 0's does not appear in the code only three inputs to the 'and' gate are needed, arranged so that when B, C and D are all '0' the first stage is constrained to be '1'.

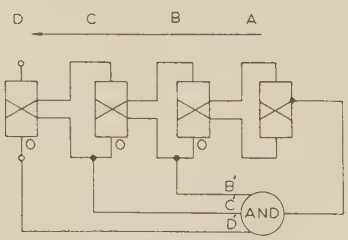

Fig. 9.—All-0's inhibitor.

(4) TYPICAL APPLICATIONS OF CHAIN CODES

(4.1) Counting and Frequency Division

There are many counting applications, both in computing and general electronics, where the use of the binary number sequence gives no direct advantage. For instance, a counter which is being used for selecting certain counts and providing output signals from them can use any progression of binary digits which is unique, since the coincidence detectors can be connected to recognize the appropriate patterns.

If the chain code of Fig. 2 is used, the application of shift pulses to the generator will provide the sequences of Table 1, and if 1111 is taken as the start, 1010 is the third pattern and 0010 is the ninth. Suitable diode coincidence detectors can recognize these patterns, and the whole arrangement divides the input pulses by 16, giving output pulses at the third and ninth count.

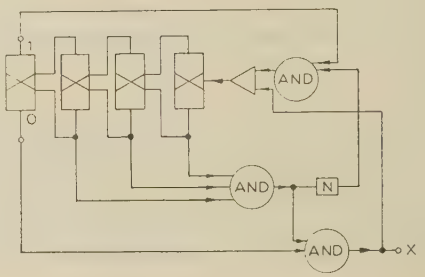

Fig. 10.—16-pattern generator (i.e. divide-by-16 counter or selector).

Fig. 10 shows the equipment, which generates the code of Fig. 4, having only 15 digits. An additional circuit detects 1000 and adds an extra '0', giving 0000. 0000 is then detected and a '1' inserted giving 0001, after which the simple rule $n = A \oplus D$ is adequate.

The advantage of this kind of counter is that the count operation is completed in the shift time of one element. The equipment is therefore comparable in performance with a gated counter (which is prodigal in components), rather than the simpler form of binary counter where each stage triggers the next, giving rise to 'propagated carry'. A chain-code counter realizes, with economy of components, the maximum counting speed of the basic valve or transistor circuits used.

A general electronic application of this arrangement is the frequency division of variable-frequency input pulses. Here again it is immaterial in what order the binary digit patterns are generated, and chain-code methods are useful. The circuit of Fig. 10 can be directly used as a divide-by-16 device, since the pulse at X will occur only once per 16 shift pulses. Whenever the shortening method is used, the appropriate divided output is automatically present in the circuit which gives the shortening effect. An n-stage chain-code generator giving a ratio of less than $(2^n - 1)$ can therefore be immediately used as a frequency divider.

We have used chain codes in many applications along the lines described, always with complete success. The list includes selection counters in a digital computer, digital data-link equipment, frequency dividers and a random-number generator.

(4.2) Error Detection and Correction

The normal method of error detection and correction for messages composed of binary digits is to add extra digits which are related in special ways to the message digits.[4] In a chain code the digits in the chain which follow any particular pattern are generated in precisely this way, and so chain codes can be applied directly to error detection and correction.[5]

For example, if the simple code of Fig. 4 is written vertically with each digit written in terms of the first four, a, b, c and d, Table 2 is obtained.

Table 2

CODE OF FIG. 4 RELATED TO STARTING DIGITS

Code	Derivation
1	a
1	b
1	c
1	d
0	$a \oplus d$
1*	$a \oplus b \oplus d$
0	$a \oplus b \oplus c \oplus d$
1	$a \oplus b \oplus c$
1*	$b \oplus c \oplus d$
0	$a \oplus c$
0	$b \oplus d$
1*	$a \oplus c \oplus d$
0	$a \oplus b$
0	$b \oplus c$
0	$c \oplus d$

* In form of error-correcting digits proposed by Hamming.[4]

The modulo 2 expressions for the various digits are true whatever phase of the code is written in the left-hand column.

It is normally economic to use the immediately adjacent digits when chain codes are employed for this purpose, and an example is to add four extra digits to each pattern of Fig. 4. This gives a series of fifteen 8-digit patterns, as shown in Table 3.

Table 3

CHAIN OF FIG. 4 LENGTHENED FOR ERROR CORRECTION OR DETECTION

Step	Pattern
0	11110101
1	11101011
2	11010110
3	10101100
4	01011001
5	10110010
6	01100100
7	11001000
8	10010001
9	00100011
10	01000111
11	10001111
12	00011110
13	00111101
14	01111010
15 (≡0)	11110101

An exhaustive check of error in these patterns shows that one error can always be corrected, two can sometimes be corrected but always detected, while three errors, unfortunately distributed, can pass undetected.

It is not possible to give general encoding and decoding circuits for chain-code error-detecting and -correcting equipment unless other characteristics of the data link are specified, e.g. whether the link is binary or ternary, etc. In general, however, the appropriate number of digits would be added at the transmitter. At the receiver the received pattern would be compared with every possible lengthened pattern in the code using a coincidence detector which counts the number of digits by which coincidence was missed. (This process, which can be carried out very rapidly with electronic devices, corresponds in essence to the complete rotation of a telegraph printing wheel for every received character.) According to the design of the system it is known how many digits may be ignored, while still preserving a unique decoded signal.

(4.3) Special Applications

There are applications for binary digital methods where a chain code may be used because of its unique property that the last $(n-1)$ digits of one pattern become the first $(n-1)$ digits of the next. Baudot's telegraph decoder[10] has already been mentioned, where the use of a chain code enabled the code wheel to have one-fifth of the contacts which would be needed for any other binary-code system.

A chain-code device does not, in general, possess the freedom from commutation errors of a cyclic permuted code, and one of the reading methods developed for normal binary code must be used.[6] Many digital decoding methods (mechanical and electronic) use a high-speed rotating decoder, in which case commutation errors cause only transient effects which are shorter than the resolving time of the detecting circuit. In such cases chain codes can be used as simply as any other binary code.

If the magnetic drum of a digital computer were to be coded for angle (instead of using an incremental counting method) and 1024 positions were to be identified on each track, a chain-code method would need only one track for satisfactory identification, whereas simple binary-counting or cyclic-permitted-code methods would need ten tracks.

Also, a complete chain code of order n contains every combination of n 0's and 1's, and can be used for testing purposes on magnetic drums and tape stores.

(5) ACKNOWLEDGMENTS

The authors are grateful to Ferranti, Ltd., for permission to publish the paper, much of which was included in an internal memorandum dated November, 1955. Thanks are also due to their colleagues in the Wythenshawe branch of Ferranti, Ltd., for many stimulating discussions.

(6) REFERENCES

(1) JOHNSON, E. A.: 'A Chain Code of Binary Symbols', R.R.E. Technical Note 539.

(2) ELDERT, C., GRAY, H. J., JR., GURK, H. M., and RUBINOFF, M.: 'Shifting Counters', *Transactions of the American I.E.E.*, 1958, **35**, Part I, p. 70.

(3) DE BRUIJN, N. G.: 'A Combinatorial Problem', *Indigationes Mathematicae*, 1946, **8**, p. 461.

(4) HAMMING, R. W.: 'Error Detecting and Error Correcting Codes', *Bell System Technical Journal*, 1950, **29**, p. 147.

(5) GREEN, J. H., JR., and SAN SOUCI, R. L.: 'An Error-Correcting Encoder and Decoder of High Efficiency', *Proceedings of the Institute of Radio Engineers*, 1958, **46**, p. 1741.

(6) ELLIOTT, W. S., ROBBINS, R. C., and EVANS, D. S.: 'Remote Position Control and Indication by Digital Means', *Proceedings I.E.E.*, Paper No. 1897 M, November, 1955 (**103** B, Suppl. 3, p. 437).

(7) CHERRY, C., Editor: 'Information Theory' (Butterworth, 1956): HUFFMAN, D. A.: 'The Synthesis of Linear Sequential Coding Networks', p. 77.

(8) ELSPAS, B.: 'The Theory of Autonomous Linear Sequential Networks', *Transactions of the Institute of Radio Engineers*, 1959, **CT-6**, p. 45.

(9) BAUDOT, E.: 'Des appareils télégraphiques à signaux independants', *Annales Télégraphiques*, 1877, **4**, p. 20.

(10) BAUDOT, E.: 'La télégraphie multiple', *ibid.*, 1895, **22**, p. 172.

(7) APPENDICES

(7.1) Mathematical Properties

(7.1.1) Application of Boolean Algebra.

Each place in a chain of 2^n digits can be occupied in two ways;

either by an '0' or by a '1', so that there are 2^{2^n} ways in which a sequence of 2^n 0's and 1's may be written. Only some of these arrangements will have the properties of chain codes, however.

There are 2^{2^n} Boolean functions of n variables, so that each of the code sequences can be specified in terms of a Boolean function of n variables.

In general, any digit in the chain may be specified as a Boolean function of n other digits anywhere in the chain but whose position relative to the specified digit is fixed. However, this fact does not enable a chain code to be generated unless two further conditions are met, namely: the pattern of n digits must occur somewhere in the chain it is required to generate; and sufficient information must be available to generate the next digit in the sequence. These requirements are automatically met if the $(n + 1)$th digit is specified as a Boolean function of the n previous consecutive digits.

It is possible, if part of a chain code of, say, $n + p$ digits is known to specify the $(n + p + 1)$th digit as another Boolean function of any n of the $n + p$ digits. However, such rules are ambiguous, since they may generate chains which are characteristic of either n or $n + p$ digits.

It is of interest to consider what types of Boolean function generate chain codes, for only relatively few of the 2^{2^n} Boolean functions of n variables do so.

If we start with n consecutive digits $a, b, c, d, \ldots n$, where n is the nth digit, and let the $(n + 1)$th digit be s, then s must be some Boolean function of $a, b, c, \ldots n$. Moreover it must be a function involving the first digit, a, since otherwise the chain code produced would be characteristic not of n digits but of some number of digits less than n.

If s is a Boolean function of a and is never independent of a, we can write

$$s = a\psi \vee a'\phi$$

where ϕ and ψ are functions of the other $n - 1$ variables $b, c, \ldots n$. For s never to be independent of a, we can never have

$$s = a'\psi$$

or

$$s = a\phi$$

i.e. a particular pattern of $b, c, d, \ldots n$ which gives s with a must give s' with a', and vice versa. Let ψ be the Boolean function of $b, c, d, \ldots n$ which represents all the patterns of $b, c, d, \ldots n$ for which $s = 1$ when $a = 1$.

Then $a'\psi = 0$

and if $s = a\psi \vee a'\phi$

then $s' = a'\psi \vee a\phi$

but $s' = (a\psi \vee a'\phi)'$

$= (a' \vee \psi')(a \vee \phi')$

$= a\psi' \vee a'\phi'$

Therefore $a\psi' \vee a'\phi' = a\phi \vee a'\psi$

or, simplifying, $\psi = \phi'$

so that $s = a\phi' \vee a'\phi$

This is a function of the remaining $n - 1$ variables, so that there are $2^{2^{n-1}}$ such functions. However, half of these will be the inverse function ϕ', so that the number of different functions is $2^{2^{n-1}-1}$. This, then, is the number of rules which can give rise to chain codes characteristic of n.

Since the number of complete chains has been shown by de Bruijn[3] to be $2^{2^{n-1}-n}$, only 1 in 2^{n-1} of the rules generate complete chains. The characteristics of the functions ϕ which generate complete chains are not fully known. However, it seems that ϕ must be a Boolean function of all the other $n - 1$ digits, although s must be at some time independent of each of the $n - 1$ digits.

The simplest function of the form $s = a\phi' \vee a'\phi$ which is not ambiguous is

$$s = an' \vee a'n$$

This rule gives chains $2^n - 1$ digits long for $n = 2, 3, 4, 6, 7$. The n 0's pattern is missing, since this generates an infinite string of 0's.

Any chain of $2^n - 1$ digits must have only one group missing, and this must be either the group of n 0's or the group of n 1's. For, if $abcd \ldots n$ is the group which is to be missing, where a, b, c, etc., can each be '0' or '1', the group $abcd \ldots n'$ must be written instead, since only the last digit can be altered, the first $n - 1$ digits being already determined.

The next group would ordinarily be $bcd \ldots ns$, so that if only one group is to be missing $abc \ldots (n - 1)n' = bcd \ldots ns$. Thus $a = b, b = c, c = d, \ldots n - 1 = n, n' = s$

i.e. $$a = b = c = d = \ldots = (n - 1) = n$$

Thus the missing group must be either the group of n 1's or the group of n 0's.

There are, in addition, certain types of rule which will generate chains of $2^n - 2$ digits and have two missing groups. The missing groups can either be separate, when they must be the group of n 0's and the group of n 1's, as already proved, or else they must be adjacent groups.

In the latter case, let the missing groups be

$$abc \ldots (n - 1)n \text{ and } bcd \ldots ns$$

and let the group be written $abc \ldots n'$ instead of $abc \ldots n$.

Then

$$abc \ldots (n - 2)(n - 1)n' = cde \ldots nst$$

Thus $a = c, b = d, \ldots n - 2 = n, n - 1 = s, n' = t$

i.e. $$a = c = e = g \ldots$$

and $$b = d = f = h \ldots$$

This is true whether or not $a = b$.

Therefore the missing groups are either n 1's or n 0's or the adjacent groups 10101010 . . . and 01010101 . . . The missing groups form a minor chain

$$1010101010101010 \ldots$$

Let the rule which generates this be

$$s = \mathrm{f}(a, b, c, \ldots n)$$

where f is some Boolean function of $abc \ldots n$. Then, from the nature of the minor chain, we also have

$$s' = \mathrm{f}(a', b', c', \ldots n')$$

Now $s = \mathrm{f}(a, b, c, \ldots n)$ must be of the form

$$s = a\phi'(b, c, \ldots n) \vee a'\phi(b, c, \ldots n)$$

where ϕ is a Boolean function of $b, c, d, \ldots n$. It follows that

$$s' = a\phi(b, c, \ldots n) \vee a'\phi'(b, c, \ldots n)$$

$$s' = \mathrm{f}(a', b', c', \ldots n')$$

$$= a'\phi'(b', c', \ldots n') \vee a\phi(b', c', \ldots n')$$

so that, equating coefficients of a,

$$\phi(b, c, \ldots n) = \phi(b', c', \ldots n')$$

The simplest function of this form is a function of two variables, say b and c.

If we put $\phi(b, c) = (bc \vee b'c')$

en clearly $\phi(b', c') = (b'c' \vee bc)$

$= \phi'(b, c)$

hain codes generated from rules of the above form have com-ementary symmetry, for, since $s = f(a, b, c, \ldots n)$ and $= f(a', b', c', \ldots n')$, for every group of n for which $s = 1$, s inverse has $s = 0$. Starting with the group of n 1's, the roup of n 0's occurs half-way through the chain, the second alf of which is the inverse of the first half.

.1.2) **Transformation of Rules to generate Inverted or Reversed Chain Codes.**

Every basic chain code can be inverted (i.e. 0's and 1's inter-hanged) or reversed to form three others, so that, unless these perations leave the sequence unchanged, or are equivalent, as n the complete chains for $n = 2$ and $n = 3$ respectively, the roup of all possible chain codes is split into subgroups of four, hich are interrelated by the operations of inversion and reversal. he group of chains exhibiting complementary symmetry is split nto subgroups of two only, since the operation of inversion eaves the sequence unchanged. There are also completely ymmetrical chain codes which remain the same whether reversed r inverted.

7.1.2.1) *Inversion of Chain Codes.*

If the generating rule for the chain code is

$$s = a\phi' \vee a'\phi$$

where $\phi = \phi(b, c, \ldots n)$, the inverted series is generated by the ule

$$s' = a'\psi \vee a\psi$$

where $\psi'(b, c, \ldots n) = \phi(b', c', \ldots n')$

Therefore $s = a\psi \vee a'\psi'$

i.e. to invert the chain code we replace every term in ϕ by its inverse.

If, as before, the generating rule is

$$s = a\phi' \vee a'\phi$$

then $s' = a\phi \vee a'\phi'$

It follows that $s\phi' = a\phi'$

and $s'\phi = a\phi$

so that $a = s\phi' \vee s'\phi$

Thus, to reverse the chain code, a is written as the same function of s as s was of a. However, because the sequence is written in the reverse order, in the function ϕ, b becomes n, c becomes $(n - 1)$, etc.

(7.1.3) **Other Transformations of Rules.**

Instead of expressing s, the next digit in the sequence, directly as a Boolean function, it may be represented as a change of one of the digits in the group. The 'change operator' X will be a different Boolean function of the digits.

Let X signify 'change'; then X' will mean 'not change'. Further, a suffix will indicate which digit is changed to give s. For instance, X_n means that the last digit is changed, whilst X_a means that the first digit is changed to give s. Thus, $X_n = 1$ means s and n are not equivalent, i.e.

$$s \oplus n \quad X_n = 1$$

$$s \equiv n \quad X_n = 0$$

i.e. $X_n = sn' \vee s'n$

In general $X_j = sj' \vee s'j$

where s is one of the n digits in a group. All rules which generate chain codes must be of the form

$$s = a\phi' \vee a'\phi$$

Now $X_n = sa' \vee s'a$

$= \phi$

For rules of the type

$$s = an' \vee a'n$$

$$X_a = sn' \vee s'n$$

$$= an' \vee an$$

$$= n$$

X_n is of practical interest, since when a rule is put into this form it enables the last stage of a shift register to be a counter, which often results in some simplification of the logic.

(7.2) **Design Data for Chain Codes of Length 128 and Less**

This Section gives the information which makes it possible to design chain-code frequency dividing or counting equipment to give division ratios between 3 and 128. The method to be employed is described in Section 3. Tables may be prepared for numbers greater than 128, but it is usually best to work out each particular case for long chains. Typical ratios that have been found are 1000, 625 and 405: in no case did the code take longer than two hours to discover.

(7.2.1) **Ratios 128 Downwards.**

Ratios of 128 and less can be realized by using the simple 7-digit rule, $n = a'g \vee ag'$ (or $X_a = g$), which generates the code shown in Table 4. The code is divided into groups of 10 merely for convenience of reading.

Table 4

SIMPLE CHAIN CODE, $n = 7$

Pattern number 1 2 3 4 5 6 7 8 9 . . . 11 1 1 1 1 1 1 1 0 1 0	21 1 0 1 0 0 1 1 0 0 1	1 1 0 1 1 1 0 1 0 0
31 . . . 1 0 1 1 0 0 0 1 1 0	41 1 1 1 1 0 1 1 0 1 0	51 1 1 0 1 1 0 0 1 0 0
61 . . . 1 0 0 0 1 1 1 0 0 0	71 0 1 0 1 1 1 1 1 0 0	81 1 0 1 0 1 1 1 0 0 1
91 . . . 1 0 1 0 0 0 1 0 0 1	101 1 1 1 0 0 0 1 0 1 0	111 0 0 0 1 1 0 0 0 0 0
121 . . . 1 0 0 0 0 0 0 and repeats		

Table 5.—Chain Codes for Ratios 126–64

To produce a chain code of pattern length	jump from	Pattern number	to	Pattern number
126	0111111	127	1111110	2
125	1101010	6	1010100	9
124	1100100	54	1001000	58
123	0011101	18	0111010	23
122	1101101	43	1011011	49
121	1100000	114	1000000	121
120	1000001	115	0000011	123
119	1110110	42	1101100	51
118	1111001	75	1110011	85
117	0100010	92	1000101	103
116	0010111	70	0101110	82
115	1010000	107	0100000	120
114	0011011	36	0110110	50
113	1000011	109	0000111	124
112	0101001	10	1010010	26
111	1101000	90	1010000	107
110	1110111	20	1101111	38
109	0010110	29	0101101	48
108	1111010	4	1110100	24
107	0011100	63	0111001	84
106	0101100	30	1011001	52
105	0111011	19	1110110	42
104	0110010	53	1100101	77
103	1000100	93	0001000	118
102	1111100	74	1111000	100
101	1001010	78	0010100	105
100	1100011	33	1000111	61
99	1001111	97	0011111	126
98	0001100	111	0011001	14
97	1010010	26	0100100	57
96	0010100	105	0101001	10
95	0010001	59	0100010	92
94	1101111	38	1011111	72
93	1101011	46	1010111	81
92	0000101	68	0001010	104
91	0111000	64	1110001	101
90	1111101	3	1111011	41
89	0011001	14	0110010	53
88	1001001	55	0010011	95
87	1110101	5	1101011	46
86	1001011	28	0010111	70
85	1100001	66	1000011	109
84	0010011	95	0100110	12
83	1011010	44	0110100	89
82	1001110	17	0011100	63
81	0011000	112	0110001	32
80	0100111	96	1001110	17
79	1110000	65	1100000	114
78	1000010	67	0000100	117
77	0100101	27	1001010	78
76	0000110	110	0001101	35
75	0001101	35	0011010	88
74	1100110	86	1001100	13
73	1011111	72	0111111	127
72	0010101	79	0101010	8
71	0111110	73	1111101	3
70	1110011	85	1100111	16
69	1110001	101	1100011	33
68	1011110	39	0111100	99
67	1001000	58	0010000	119
66	1101110	21	1011100	83
65	0110100	89	1101001	25
64	1000111	61	0001111	125

Table 5 shows how to realize any number between 128 an 64 by a suitable jump from one pattern to another. Numbe below 64 will normally be obtained from a shorter chain cod but can be obtained by reversing the direction of the jump, i which case the two code lengths obtained total 128, i.e. the co jump which gives 100 patterns will, if reversed, give 28.

A code of length 128 can be derived by adding an extra 0 t the 000000 pattern, as described in Section 4.1, while 127 pattern are given by the unmodified code.

(7.2.2) **Ratios 63 downwards.**

Ratios of 63 and less can be realized by using the simp 6-digit rule, $n = a'f \vee af'$ (or $\chi_a = f$), which generates the co shown in Table 6.

Table 7

Chain Codes for Ratios 63–32

To produce a chain code of pattern length	jump from	Pattern number	to	Pattern number
63	—	—	—	—
62	011111	63	111110	2
61	110101	5	101011	8
60	101001	24	010011	28
59	011011	15	110110	20
58	110000	52	100000	58
57	100001	53	000011	60
56	001101	14	011010	22
55	000101	35	001010	44
54	011100	31	111001	41
53	101000	46	010000	57
52	010110	9	101101	21
51	100011	48	000111	61
50	101110	17	011100	31
49	110001	33	100011	48
48	111101	3	111011	19
47	110011	12	100111	29
46	010010	25	100101	43
45	110101	4	110100	23
44	111000	32	110000	52
43	100010	34	000100	55
42	110111	16	101111	38
41	110100	23	101000	46
40	001100	50	011001	11
39	101111	38	011111	63
38	001010	44	010101	7
37	011110	39	111101	3
36	000110	49	001101	14
35	101011	8	010111	37
34	100100	26	001000	56
33	011001	11	110010	42
32	000111	61	001110	30

Table 7 shows how to realize any number between 63 and by a suitable jump from one pattern to another. Chains of le than 32 patterns can be generated by reversing the direction jump.

(7.2.3) **Ratios 31 Downwards.**

Ratios of 31 and less can be realized using the 5-digit ru $n = c'e \vee ce'$, which generates the code shown in Table 8.

Table 6.—Simple Chain Code, $n = 6$

Pattern number																					
1	2	3	4	5	6	7	8	9	10	11										21	
1	1	1	1	1	1	0	1	0	1	0	1	1	0	0	1	1	0	1	1	1	0
1	0	1	1	0	1	0	0	1	0												
31 . . .										41										51	
0	1	1	1	0	0	0	1	0	1	1	1	1	0	0	1	0	1	0	0	0	1
0	1	1	0	0	0	0	1	0	0												
61 . . .																					
0	0	0	and repeats																		

Table 8

SIMPLE CHAIN CODE, $n = 5$

Pattern number	1	2	3	4	5	6	7	8	9	10	11	. . .	21	. . .	31	
	1	1	1	1	1	0	0	0	1	1	0	1	1	0	1	0 and repeats

Table 9 shows how to realize ratios between 31 and 16. (Ratios less than 16 are given by the reversed jump.)

Table 9

CHAIN CODES FOR RATIOS 31–16

To produce a chain code of pattern length	jump from	Pattern number	to	Pattern number
31	—	—	—	—
30	01111	31	11110	2
29	11010	13	10100	16
28	00010	20	00101	28
27	01101	8	11010	13
26	10100	16	01001	22
25	01001	22	10011	29
24	01100	27	11000	4
23	10011	29	00110	7
22	11110	2	11101	12
21	10101	14	01011	25
20	00111	30	01110	11
19	10110	26	01101	8
18	11000	4	10000	18
17	10001	5	00010	20
16	01011	25	10111	10

(7.2.4) **Ratios 15 Downwards.**

Ratios of 15 and less can be realized by using the 4-digit rule, $n = a'd \vee ad'$ (or $X_a = d$), which generates the code shown in Table 10.

Table 10

SIMPLE CHAIN CODE, $n = 4$

Pattern number	1	2	3	4	5	6	7	8	9	10	11	12	13	14	15	
	1	1	1	1	0	1	0	1	1	0	0	1	0	0	0	and repeats

Table 11 shows how to realize ratios between 15 and 8.

Table 11

CHAIN CODES FOR RATIOS 15–8

To produce a chain code of pattern length	jump from	Pattern number	to	Pattern number
15	—	—	—	—
14	0111	15	1110	2
13	1101	3	1011	6
12	1100	8	1000	12
11	1001	9	0011	14
10	1110	2	1100	8
9	1010	4	0100	11
8	0011	14	0110	7

(7.2.5) **Ratios 7 Downwards.**

Ratios of 7 and less can be realized using the 3-digit rule, $n = a'c \vee ac'$ ($X_a = c$), which generates the code shown in Table 12.

Table 12

SIMPLE CHAIN CODE, $n = 3$

Pattern number	1	2	3	4	5	6	7	
Code	1	1	1	0	1	0	0	and repeats

Table 13 shows how to realize ratios between 7 and 4.

Table 13

CHAIN CODES FOR RATIOS 7–4

To produce a chain code of length	jump from	Pattern number	to	Pattern number
7	—	—	—	—
6	011	7	110	2
5	110	2	100	5
4	101	3	011	7

(7.2.6) **Ratio of 3.**

The ratio of 3 is given by the simple 2-digit rule, $n = a'b \vee ab'$.

(7.3) The Baudot Telegraph System

Emil Baudot organized the French alphabetic telegraph system in the last century. Although this work involved much more than the telegraph code he employed, his published articles were always mainly concerned with codes and associated apparatus.

In 1877 his first paper was published[9] which gives a general survey of binary and ternary telegraph codes but no mention of chain codes. In 1895 he published a survey paper[10] in which he stated that the chain code employed was discovered by systematic trial and error, in order to reduce the decoding wheel complexity. The original code is shown below, and is thought to be the first engineering application of a chain code.

Table 14

THE ORIGINAL BAUDOT CHAIN CODE

Letters	Figures, etc.	Letter / figure } code	Chain code
A	1	1 0 0 0 0	1
E	2	0 1 0 0 0	0
Y	3	0 0 1 0 0	0
J	6	1 0 0 1 0	1
X	,	0 1 0 0 1	0
U	4	1 0 1 0 0	1
G	7	0 1 0 1 0	0
T	!	1 0 1 0 1	1
H	–	1 1 0 1 0	1
W	?	0 1 1 0 1	0
C	9	1 0 1 1 0	1
M	)	0 1 0 1 1	0
S	;	0 0 1 0 1	0
Figure space		0 0 0 1 0	0
t	.	1 0 0 0 1	1
E′	&	1 1 0 0 0	1
I	0	0 1 1 0 0	0
B	8	0 0 1 1 0	0
K	(	1 0 0 1 1	1
Z	:	1 1 0 0 1	1
O	5	1 1 1 0 0	1
D	0	1 1 1 1 0	1
P	%	1 1 1 1 1	1
N	No.	0 1 1 1 1	0
Q	/	1 0 1 1 1	1
L	=	1 1 0 1 1	1
V	′	1 1 1 0 1	1
F	F	0 1 1 1 0	0
R	–	0 0 1 1 1	0
ϒ	ϒ	0 0 0 1 1	0
Letter space		0 0 0 0 1	0

621.313.32.072.9

The Institution of Electrical Engineer
Monograph No. 393
July 196

FREQUENCY RESPONSE ANALYSIS OF THE STABILIZING EFFECT OF A SYNCHRONOUS MACHINE DAMPER

By A. S. ALDRED, M.Sc., Ph.D., Associate Member, and G. SHACKSHAFT, B.Eng., Ph.D., Graduate

(*The paper was first received* 11*th December*, 1959, *and in revised form* 19*th April*, 1960. *It was published as an* INSTITUTION MONOGRAPH *in July*, 1960.)

SUMMARY

The paper describes the application of frequency-response concepts to the analysis of a synchronous machine damper in so far as it affects the stability of the machine. The analysis of damper effects is based on Park's equations. Small-displacement theory is introduced to organize the equations into the correct form for frequency-response computation.

Nyquist diagrams are used to show the stabilizing effect of a damper and to illustrate the method of optimizing damper parameters.

LIST OF SYMBOLS

δ = Rotor angle.
f, ω = Frequency.
H = Inertia constant.
$M = H/180f$.
T_i = Torque input.
T_u = Torque output.
$p\theta$ = Speed.
v_{fd} = Field voltage.
R_{fd} = Field resistance.
i_{fd} = Field current.
X_{ffd} = Field reactance.
X_{afd} = Mutual reactance between generator field and direct-axis armature winding.
X_{a1d} = Mutual reactance between direct-axis armature winding and direct-axis damper.
X_{11d} = Direct-axis damper reactance.
$V_{fd} = \frac{v_{fd}}{R_{fd}} X_{afd}$ = Open-circuit terminal voltage at normal speed.
ψ_{fd} = Field flux linkage.
ψ_d = Direct-axis armature flux linkage.
ψ_q = Quadrature-axis armature flux linkage.
v = Busbar voltage.
v_d = Direct-axis terminal voltage.
v_q = Quadrature-axis terminal voltage.
i_d = Direct-axis armature current.
i_q = Quadrature-axis armature current.
i_{1d} = Direct-axis damper current.
i_{1q} = Quadrature-axis damper current.
X_d = Direct-axis synchronous reactance.
X_q = Quadrature-axis synchronous reactance.
X_{11q} = Quadrature-axis damper reactance.
X_{a1q} = Mutual reactance between quadrature-axis armature and quadrature-axis damper.
$\tau_{d0} = \frac{X_{ffd}}{R_{fd}}$ = Field time-constant.
$\tau_{1d} = \frac{X_{11d}}{R_{1d}}$ = Direct-axis damper time-constant.
$\tau_{1q} = \frac{X_{11q}}{R_{1q}}$ = Quadrature-axis damper time-constant.
ψ_{1d} = Direct-axis damper flux linkage.
ψ_{1q} = Quadrature-axis damper flux linkage.
R = Armature resistance.
R_{1d} = Direct-axis damper resistance.
R_{1q} = Quadrature-axis damper resistance.

Correspondence on Monographs is invited for consideration with a view to publication.
Dr. Aldred and Dr. Shackshaft are in the Department of Electrical Engineering, University of Liverpool.

(1) INTRODUCTION

The primary function of a synchronous-machine damper is t assist in suppressing rotor oscillations and to aid in synchr nizing the machine by generating positive damping and synchr nizing torques,[1] both of which influence the stability of th machine. In a recent paper[2] the authors developed a frequen response method for assessing the stability of synchrono machines. In the concluding remarks of that paper refere was made to the possibility of using frequency-response conce to determine the influence of a damper on stability; this co panion paper is concerned with this problem.

The frequency-response method is based on a rigorous analys of synchronous-machine dynamics, both electrical and me anical. By the application of small-displacement theory to th dynamical equations it is possible to construct the small-displac ment equation of motion of the machine. The form of th equation, combined with the visualization of the synchrono machine as a closed-loop system, suggests a basic single-loc configuration. The final step is the derivation of the Nyqui diagram, which is a frequency-response plot in polar form the open-loop transfer function of this basic single-loop co figuration. The Nyquist[3] criterion of stability is concerned wit the location of the Nyquist diagram relative to the critical poi (−1, 0). Consequently the effect of a damper on stability ma be deduced by observing how the position of the Nyqui diagram, in the vicinity of the critical point, changes as a resu of introducing a damper. Optimum values of damper par meters may be determined by observing the movement of th Nyquist diagram throughout a range of parameters. In th manner the frequency-response method goes some way towar solving the problem of a rigorous design of damper windings.

(2) ANALYSIS OF A SYNCHRONOUS MACHINE WITH A DAMPER

Modern analysis of synchronous machines is based almo entirely on Park's[4] equations, which are obtained by analysi the machine in a reference frame fixed to the field structu The direct and quadrature axes of this reference frame are alo and at right angles to the pole axis respectively, and in th frame the synchronous-machine equations apply equally well the d.c. machine shown in Fig. 1. This analogy[9] is well know and is reproduced here as a convenient illustration of the quan ties used in the following analysis. The object of this analy is to develop an equation of motion of the machine in which t only dependent variable is a small displacement of rotor ang

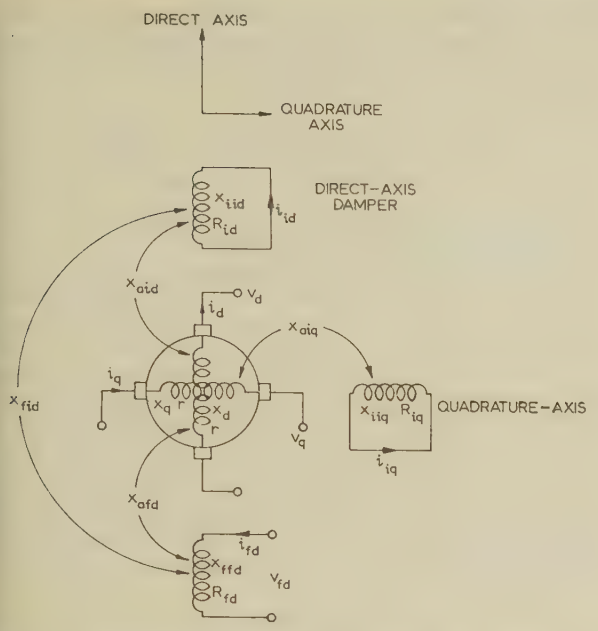

Fig. 1.—An interpretation of Park's equations for a synchronous machine with damper windings.

(2.1) Analysis of Synchronous-Machine Dynamics

The sole assumption made at this stage is that the machine is ideal as defined by Park.[5] The synchronous machine is directly connected to an infinite system and has constant excitation. The equations, in per-unit notation, are

Armature.
$$v_d = p\psi_d - \psi_q p\theta - Ri_d = v \sin \delta \quad . \quad . \quad . \quad . \quad (1)$$
$$v_q = p\psi_q + \psi_d p\theta - Ri_q = v \cos \delta \quad . \quad . \quad . \quad . \quad (2)$$

in which
$$\psi_d = -X_d i_d + X_{afd} i_{fd} + X_{a1d} i_{1d} \quad . \quad . \quad . \quad . \quad (3)$$

and
$$\psi_q = -X_q i_q + X_{a1q} i_{1q} \quad . \quad . \quad . \quad . \quad . \quad . \quad . \quad (4)$$

Field.
$$v_{fd} = p\psi_{fd} + R_{fd} i_{fd} \quad . \quad . \quad . \quad . \quad . \quad . \quad . \quad . \quad (5)$$
$$\psi_{fd} = -X_{afd} i_d + X_{ffd} i_{fd} + X_{f1d} i_{1d} \quad . \quad . \quad . \quad . \quad (6)$$

Damper.
$$0 = p\psi_{1d} + R_{1d} i_{1d} \quad . \quad . \quad . \quad . \quad . \quad . \quad . \quad . \quad (7)$$
$$0 = p\psi_{1q} + R_{1q} i_{1q} \quad . \quad . \quad . \quad . \quad . \quad . \quad . \quad . \quad (8)$$

in which
$$\psi_{1d} = -X_{a1d} i_d + X_{f1d} i_{fd} + X_{11d} i_{1d} \quad . \quad . \quad . \quad (9)$$

and
$$\psi_{1q} = -X_{a1q} i_q + X_{11q} i_{1q} \quad . \quad . \quad . \quad . \quad . \quad . \quad . \quad (10)$$

If the field current, i_{fd}, and the damper currents, i_{1d} and i_{1q}, are eliminated from the above equations, the expressions for ψ_d and ψ_q become

$$\psi_d = G(p) v_{fd} - X_d(p) i_d \quad . \quad . \quad . \quad . \quad . \quad (11)$$
$$\psi_q = -X_q(p) i_q \quad . \quad . \quad . \quad . \quad . \quad . \quad . \quad (12)$$

The quantities $X_d(p)$ and $X_q(p)$ are the operational reactances and $G(p)$ is an operational transfer function given by

$$X_d(p) = X_d - \frac{(X_{11d}X_{afd}^2 - 2X_{f1d}X_{a1d}X_{afd} + X_{ffd}X_{a1d}^2)p^2 + (X_{afd}^2 R_{1d} + X_{a1d}^2 R_{fd})p}{(X_{11d}X_{ffd} - X_{f1d}^2)p^2 + (X_{11d}R_{fd} + X_{ffd}R_{1d})p + R_{fd}R_{1d}} \quad . \quad . \quad . \quad . \quad . \quad . \quad (13)$$

$$X_q(p) = X_q - \frac{X_{a1q}^2 p}{X_{11q}p + R_{1q}} \quad . \quad . \quad . \quad . \quad (14)$$

$$G(p) = \frac{(X_{11d}X_{afd} - X_{f1d}X_{a1d})p + X_{afd}R_{1d}}{(X_{11d}X_{ffd} - X_{f1d}^2)p^2 + (X_{11d}R_{fd} + X_{ffd}R_{1d})p + R_{1d}R_{fd}} \quad . \quad . \quad . \quad . \quad (15)$$

Eqns. (1) and (2) become

$$v_d = -\psi_q p\theta - Z_d(p) i_d = v \sin \delta \quad . \quad . \quad (16)$$
$$v_q = \psi_d p\theta - Z_q(p) i_q = v \cos \delta \quad . \quad . \quad . \quad (17)$$

in which
$$Z_d(p) = X_d(p)p + R \quad . \quad . \quad . \quad . \quad (18)$$

and
$$Z_q(p) = X_q(p)p + R \quad . \quad . \quad . \quad . \quad (19)$$

The quantities $Z_d(p)$ and $Z_q(p)$ are the operational impedances[7] and eqns. (11)–(19) are the operational equations for a synchronous machine.

For dynamical studies it is necessary to derive the equation of motion; this is

$$T_i = M\frac{d^2\delta}{dt^2} + T_u \quad . \quad . \quad . \quad . \quad . \quad (20)$$

in which the machine electrical torque is

$$T_u = \psi_d i_q - \psi_q i_d \quad . \quad . \quad . \quad . \quad . \quad (21)$$

(2.2) Small-Displacement Theory

Frequency-response analysis is based on the linearization of the machine equations using the technique of small displacements. Consequently small-displacement equations describe the behaviour of the machine for small changes about some initial condition state. Initial conditions of the variables are denoted by the suffix zero.

From eqns. (20) and (21) the equation of motion for small displacements is

$$\Delta T_i = M\frac{d^2\Delta\delta}{dt^2} + i_{q0}\Delta\psi_d + \psi_{d0}\Delta i_q - i_{d0}\Delta\psi_q - \psi_{q0}\Delta i_d \quad . \quad (22)$$

In eqn. (22) the initial condition values of i_{d0} and i_{q0} are obtained by solving eqns. (16) and (17) for known values of v, δ_0, $p\theta_0$, v_{fd} and the machine parameters. The expressions for i_{d0} and i_{q0} are

$$i_{d0} = \frac{V_{fd}X_q(p\theta_0)^2 - v\cos\delta_0 X_q p\theta_0 - Rv\sin\delta_0}{R^2 + X_d X_q (p\theta_0)^2} \quad . \quad (23)$$

$$i_{q0} = \frac{V_{fd}Rp\theta_0 - Rv\cos\delta_0 + X_d v\sin\delta_0 p\theta_0}{R^2 + X_d X_q (p\theta_0)^2} \quad . \quad . \quad (24)$$

in which V_{fd} is given by

$$V_{fd} = \frac{v_{fd}}{R_{fd}} X_{afd} \quad . \quad . \quad . \quad . \quad . \quad (25)$$

and is the generated voltage on open-circuit at normal speed. The initial condition values ψ_{d0} and ψ_{q0} may now be determined from

$$\psi_{d0} = V_{fd} - X_d i_{d0} \quad . \quad . \quad . \quad . \quad . \quad (26)$$
$$\psi_{q0} = -X_q i_{q0} \quad . \quad . \quad . \quad . \quad . \quad . \quad (27)$$

It remains to determine Δi_d, Δi_q, $\Delta\psi_d$ and $\Delta\psi_q$; but since, from eqns. (11) and (12),

$$\Delta\psi_d = -X_d(p)\Delta i_d \quad . \quad . \quad . \quad . \quad (28)$$

and
$$\Delta\psi_q = -X_q(p)\Delta i_q \quad . \quad . \quad . \quad . \quad (29)$$

it will suffice to obtain expressions for Δi_d and Δi_q. These quantities are derived as follows:

From eqns. (16) and (17).

$$\Delta v_d = -\Delta\psi_q p\theta_0 - Z_d(p)\Delta i_d - \psi_{q0}p\Delta\theta = v\cos\delta_0\Delta\delta \quad . \quad (30)$$

$$\Delta v_q = \Delta\psi_d p\theta_0 - Z_q(p)\Delta i_q + \psi_{d0}p\Delta\theta = -v\sin\delta_0\Delta\delta \quad . \quad (31)$$

But since $\delta = \theta - (p\theta_0)t$, $p\Delta\theta = p\Delta\delta$.

Therefore

$$\Delta v_d = -\Delta\psi_q p\theta_0 - Z_d(p)\Delta i_d = (v\cos\delta_0 + \psi_{q0}p)\Delta\delta \quad . \quad (32)$$

$$\Delta v_q = \Delta\psi_d p\theta_0 - Z_q(p)\Delta i_q = -(v\sin\delta_0 + \psi_{d0}p)\Delta\delta \quad . \quad (33)$$

Substituting from eqns. (28) and (29) into eqns. (32) and (33) and solving the resulting equations gives

$$\Delta i_d = \frac{[p\theta_0 X_q(p)(v\sin\delta_0 + \psi_{d0}p) - Z_q(p)(v\cos\delta_0 + \psi_{q0}p)]\Delta\delta}{X_d(p)X_q(p)(p\theta_0)^2 + Z_d(p)Z_q(p)} \quad . \quad . \quad . \quad . \quad (34)$$

$$\Delta i_q = \frac{[p\theta_0 X_d(p)(v\cos\delta_0 + \psi_{q0}p) + Z_d(p)(v\sin\delta_0 + \psi_{d0}p)]\Delta\delta}{X_d(p)X_q(p)(p\theta_0)^2 + Z_d(p)Z_q(p)} \quad . \quad . \quad . \quad . \quad (35)$$

Hence eqn. (22) becomes

$$\Delta T_i = Mp^2\Delta\delta - i_{q0}X_d(p)\frac{[p\theta_0 X_q(p)(v\sin\delta_0 + \psi_{d0}p) - Z_q(p)(v\cos\delta_0 + \psi_{q0}p)]\Delta\delta}{X_d(p)X_q(p)(p\theta_0)^2 + Z_d(p)Z_q(p)} + \psi_{d0}\frac{[p\theta_0 X_d(p)(v\cos\delta_0 + \psi_{q0}p) + Z_d(p)(v\sin\delta_0 + \psi_{d0}p)]\Delta\delta}{X_d(p)X_q(p)(p\theta_0)^2 + Z_d(p)Z_q(p)} + i_{d0}X_q(p)\frac{[p\theta_0 X_d(p)(v\cos\delta_0 + \psi_{q0}p) + Z_d(p)(v\sin\delta_0 + \psi_{d0}p)]\Delta\delta}{X_d(p)X_q(p)(p\theta_0)^2 + Z_d(p)Z_q(p)} - \psi_{q0}\frac{[p\theta_0 X_q(p)(v\sin\delta_0 + \psi_{d0}p) - Z_q(p)(v\cos\delta_0 + \psi_{q0}p)]\Delta\delta}{X_d(p)X_q(p)(p\theta_0)^2 + Z_d(p)Z_q(p)} \quad . \quad . \quad . \quad . \quad (36)$$

Thus the equation of motion is of the form

$$\Delta T_i = Mp^2\Delta\delta + f(p)\Delta\delta \quad . \quad . \quad . \quad . \quad (37)$$

(2.3) Approximating to the Function $f(p)$

It is apparent that, when the function $f(p)$ in eqn. (37) is obtained by the procedure outlined in Section 2.2, the computation of this function is a formidable task, particularly when the expressions for $X_d(p)$ and $X_q(p)$ are included. The function $f(p)$ may be simplified considerably if it is assumed that armature resistance can be neglected. For the majority of synchronous machines this assumption is valid and is in doubt only in the case of small machines in which the magnitude of armature resistance may be comparable with the synchronous reactance. However, the analysis up to this point is rigorous for the reasons that before intelligent approximations are made we must know what we are omitting and also that the exact form of $f(p)$ is available if required.

Neglecting armature resistance and considering the initial condition of speed to be rated speed (i.e. $p\theta_0 = 1$), the expression for $f(p)$ reduces to

$$f(p) = \left[\frac{V_{fd}v\cos\delta_0}{X_d} + v^2\frac{(X_d - X_q)}{X_d X_q}\cos 2\delta_0\right] + \left[v^2\sin^2\delta_0\left(\frac{1}{X_d(p)} - \frac{1}{X_d}\right)\right] + \left[v^2\cos^2\delta_0\left(\frac{1}{X_q(p)} - \frac{1}{X_q}\right)\right] \quad . \quad (38)$$

It is interesting to note that when armature resistance is neglected the same expression for $f(p)$ is obtained irrespective of the inclusion or exclusion of the $p\psi_d$ and $p\psi_q$ terms and speed variation in the original equations.

(3) FREQUENCY-RESPONSE ANALYSIS

(3.1) The Synchronous Machine as a Closed-Loop System

The dynamical equation of motion of a synchronous generator for small displacements has been shown to be

$$\Delta T_i = Mp^2\Delta\delta + \Delta T_u = Mp^2\Delta\delta + f(p)\Delta\delta \quad . \quad (39)$$

For a synchronous machine to exhibit instability it must be capable of representation in a closed-loop manner, since feedback, in some form, is an inherent part of any unstable system. Examination of eqn. (39) shows that the machine tends to accelerate as a result of a small difference between the torque input and the electro-mechanical generated torque, namely $\Delta T_i - \Delta T_u$. The small change in rotor angle, $\Delta\delta$, arises as a result of a double integration of this acceleration. This argument suggests that the correct closed-loop interpretation of eqn. (39) is that shown in Fig. 2. The Nyquist diagram may now

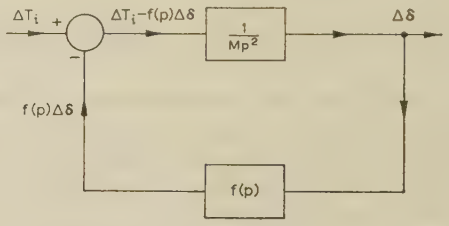

Fig. 2.—A basic closed-loop representation of a synchronous machine for small displacements.

be constructed by plotting the open-loop transfer function of Fig. 2, i.e. $f(p)/Mp^2$, for $p = j\omega$ over a range of ω. Plotting for values of p between $-j\infty$ and $+j\infty$ results in a diagram of the form shown in Fig. 3. Since there are no poles of $f(p)/Mp^2$ in the right-hand half of the p-plane, the Nyquist criterion reduces to the statement that for stability the closed curve of Fig. 3 must not encircle the point (−1, 0), which it clearly does

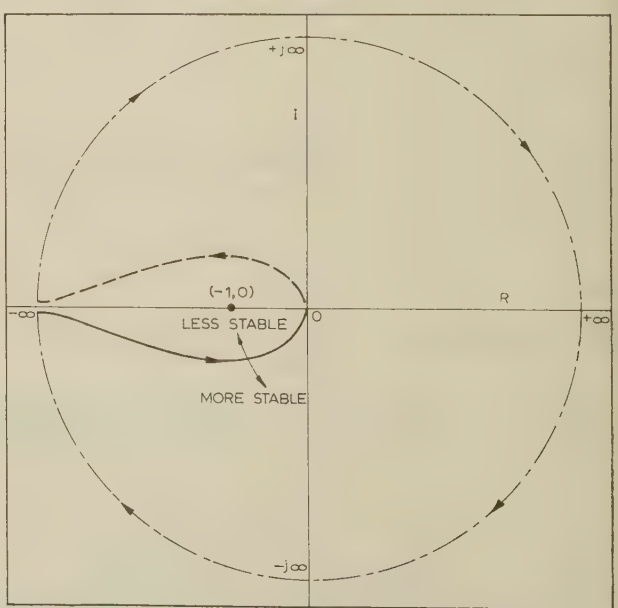

Fig. 3.—Typical open-loop frequency-response characteristic of circuit shown in Fig. 2.

t. The nearer the curve approaches the point (−1, 0), the s stable the machine becomes, and vice versa. Hunting will cur when the curve just passes through the critical point. It therefore necessary to examine only the position of that part the curve for $p = +j\omega$ in the neighbourhood of the critical int. The effect of a damper can be determined by observing e change in the position of the curve in this vicinity.

(3.2) Frequency-Response Characteristics

To illustrate the frequency-response method a salient-pole ernator whose parameters have the values shown in Table 1

Table 1

$X_d = 1{\cdot}2$	$R_{fd} = 0{\cdot}0011$
$X_q = 0{\cdot}8$	$R_{1d} = 0{\cdot}02$
$X_{ffd} = 1{\cdot}1$	$R_{1q} = 0{\cdot}04$
$X_{11q} = 0{\cdot}8$	$R = 0$
$X_{11d} = 1{\cdot}1$	$H = 5$ kWs/kVA
$X_{afd} = 1$	$v = 1$
$X_{a1d} = 1$	Power factor $= 1$
$X_{f1d} = 1$	$\delta_0 = 45°$
	$X_{a1q} = 0{\cdot}6$
	$V_{fd} = 1{\cdot}75$

considered. These values are expressed in per-unit notation, r direct substitution into the per-unit equations, and are taken om Reference 6.

For purposes of computation it is convenient to develop pressions for $\frac{1}{X_d(p)} - \frac{1}{X_d}$ and $\frac{1}{X_q(p)} - \frac{1}{X_q}$ in time-constant rm, as shown in the Appendix. These expressions are

$$\frac{1}{X_d(p)} - \frac{1}{X_d} = \frac{[K_1 + K_2 - 2\sqrt{(K_1K_2K_3)}]\tau_{d0}\tau_{1d}p^2 + (K_2\tau_{1d} + K_1\tau_{d0})p}{X_d\{[1 - K_1 - K_2 - K_3 + 2\sqrt{(K_1K_2K_3)}]\tau_{d0}\tau_{1d}p^2 + [(\tau_{1d} - K_2\tau_{1d} + \tau_{d0} - K_1\tau_{d0})p + 1]\}} \quad . \quad . \quad (40)$$

$$\frac{1}{X_q(p)} - \frac{1}{X_q} = \frac{K_4\tau_{1q}p}{X_q[1 + (1 - K_4)\tau_{1q}p]} \quad . \quad . \quad (41)$$

Using the parameters of Table 1, the values of K_1, K_2, K_3 and K_4 are

$$K_1 = K_2 = \frac{1}{1{\cdot}32}, \quad K_3 = \frac{1}{1{\cdot}21}, \quad K_4 = 0{\cdot}563$$

From examination of eqn. (38) it is seen that its second and hird bracketed terms are the only terms which can make a contribution to the imaginary component of the open-loop ransfer function, i.e. $f(j\omega)/M(j\omega)^2$. The second term contains only direct-axis parameters and the third term only quadrature-axis parameters, so that the contribution from each axis to the damping and synchronizing torques may be considered separately. The second term, of course, contains the contributions from both the field winding and the direct-axis damper.

Curve (*a*) of Fig. 4 shows the open-loop transfer function for a machine having the parameters given in Table 1 with the exception that no damper is present. The effect of the addition of the direct-axis damper is shown by curve (*b*) and the effect of the quadrature-axis damper by curve (*c*). Clearly curves (*b*) and (*c*) indicate that the quadrature-axis damper has the greater effect on stability, since curve (*c*) is further from the critical point than curve (*b*). However, it is seen that the total contribution from the direct-axis windings to the damping torque is greater than that of the quadrature axis windings.

The method used for selecting optimum values for the direct- and quadrature-axis damper time-constants is also shown in Fig. 4. Point A ($\omega = 10$ rad/sec) on curve (*a*) is selected as being a convenient one to consider since it is near the critical

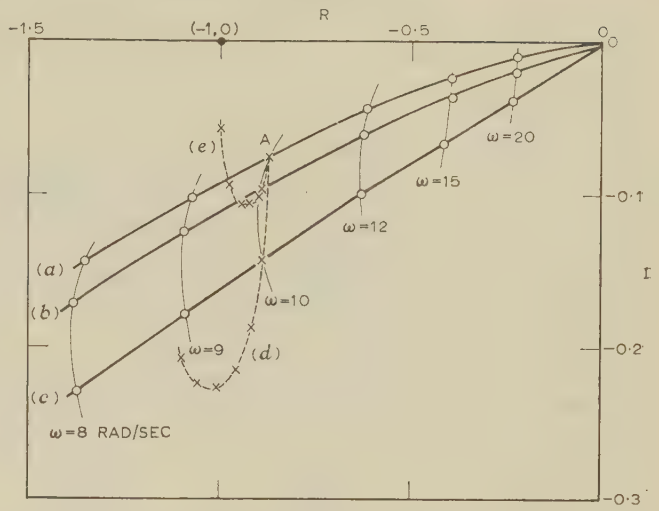

Fig. 4.—Nyquist diagrams for a synchronous machine, showing the effect of the damper on stability.

(*a*) No damper.
(*b*) Direct-axis damper.
(*c*) Quadrature-axis damper.
(*d*) Locus of point A as τ_{1q} is varied.
(*e*) Locus of point A as τ_{1d} is varied.

point. The locus of this point as either τ_{1d} or τ_{1q} is varied demonstrates the effect of these two parameters on the position of the open-loop transfer function. The quadrature-axis damper time-constant is given the following range of values, commencing with $\tau_{1q} = 0$ at point A: $\tau_{1q} = 0$, 0·053, 0·1, 0·15, 0·2, 0·3, 0·4 sec and $\tau_{1d} = 0$. As τ_{1q} is varied between 0 and 0·4 sec the locus of point A is shown by curve (*d*). The optimum value of τ_{1q} may be estimated by mentally drawing a series of curves, similar in shape to curves (*a*)–(*c*), through points on curve (*d*); the curve which is furthest away from the critical point corresponds to the optimum value of τ_{1q}. In the example this value is $\tau_{1q} = 0{\cdot}15$ sec.

In a similar way the direct-axis damper time-constant is given

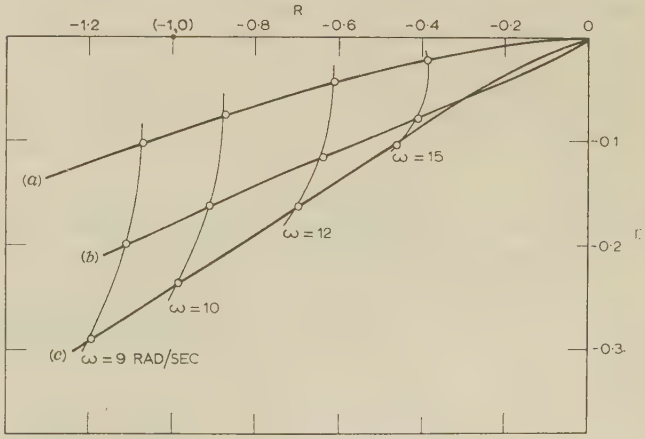

Fig. 5.—Comparison of Nyquist diagrams showing effect of optimized time-constants.

(*a*) No damper.
(*b*) Damper with Table 1 time-constants.
(*c*) Damper with optimized time-constants.

the following values, commencing with $\tau_{1d} = 0$ at point A: $\tau_{1d} = 0$, 0·15, 0·2, 0·3, 0·5, 1·0, 2·0 sec and $\tau_{1q} = 0$. The locus of point A is now curve (*e*). Again an optimum of τ_{1d} for maximum stabilizing effect is selected in a similar manner to that described for τ_{1q}; this value is $\tau_{1d} = 0{\cdot}15$ sec.

From examination of the loci of point A as τ_{1d} and τ_{1q} are varied it is seen that, when the optimum values of these two parameters are used, the contributions to the damping torque from both the direct- and quadrature-axis windings are approximately equal. Eqn. (38) therefore reveals that the choice of operating point will not significantly affect the optimum values of τ_{1d} and τ_{1q} and that the damping torque will remain very nearly constant as the operating point is changed.

Finally, in Fig. 5 a comparison is made of the frequency-response characteristics for the conditions: (*a*) no damper; (*b*) a damper with the values of time-constants of Table 1; and (*c*) a damper with the optimized values of time-constants obtained from Figs. 4(*d*) and (*e*).

(4) CONCLUSIONS

The frequency-response method illustrates the influence of a damper on the stability of a synchronous machine. It allows a comparison of different damper windings to be made in a convenient manner, and indicates that optimum values for the quadrature- and direct-axis damper time-constants can be deduced.

It enables synchronizing and damping-torque coefficients to be considered simultaneously and not separately as hitherto. Furthermore it goes some way towards providing a rigorous basis for the design of dampers, but the problem of constructing dampers to have the necessary parameters for optimum stability still remains. The solution of this problem is outside the scope of the paper.

Because the frequency-response method is essentially graphical in application, it is ideally suited to the analysis of machines for which data concerning the operational reactances are available in the form of frequency-response loci.[8] A particular example of this occurs in the analysis of permanent-magnet alternators.

(5) ACKNOWLEDGMENTS

The authors are grateful to Professor J. M. Meek for his interest in the work and for facilities provided in the Electrical Engineering Department of Liverpool University. They are indebted to Sir David Brunt, Chairman of the Electricity Supply Research Council, and to the Central Electricity Generating Board for financial support. They also wish to thank Charles Concordia for his advice concerning synchronous-machine parameters.

(6) REFERENCES

(1) CONCORDIA, C.: 'Synchronous Machine Damping and Synchronizing Torques', *Transactions of the American I.E.E.*, 1951, **70**, p. 731.

(2) ALDRED, A. S., and SHACKSHAFT, G.: 'A Frequency-Response Method for the Predetermination of Synchronous-Machine Stability', *Proceedings I.E.E.*, Monograph No. 340 S, August, 1959 (**107** C, p. 2).

(3) NYQUIST, H.: 'Regeneration Theory', *Bell System Technical Journal*, 1932, **2**, p. 126.

(4) PARK, R. H.: 'Two-Reaction Theory of Synchronous Machines, Generalized Method of Analysis—Part I', *Transactions of the American I.E.E.*, 1929, **48**, p. 716.

(5) PARK, R. H.: 'Definition of an Ideal Synchronous Machine and Formula for the Armature Flux Linkages', *General Electric Review*, 1928, **31**, p. 332.

(6) CONCORDIA, C.: 'Synchronous Machines' (Wiley, New York, 1951), p. 63.

(7) WARING, M. L., and CRARY, S. B.: 'The Operational Impedances of a Synchronous Machine', *General Electric Review*, 1932, **35**, p. 578.

(8) SEN, S. K., and ADKINS, B.: 'The Application of the Frequency-Reponse Method to Electrical Machines', *Proceedings I.E.E.*, Monograph No. 178 S, May, 1956 (**103** C, p. 378).

(9) KRON, G.: 'Non-Riemannian Dynamics of Rotating Electric Machinery', *Journal of Mathematics and Physics*, 1934, **13**, p. 103.

(7) APPENDIX

Derivation of $X_d(p)$ and $X_q(p)$ in a Form Suitable for Frequency-Response Analysis

In order to compute the $f(p)$ function derived in Section 2.3 it is necessary to obtain convenient expressions for $X_d(p)$ and $X_q(p)$. Since the paper is concerned with damper windings, a convenient form would be one in which only the damper time-constants appear as variables in $f(p)$ itself. This condition is realized by developing expressions for $X_d(p)$ and $X_q(p)$ in the following manner. The conventional expressions for $X_d(p)$ and $X_q(p)$ have been developed elsewhere,[7] and are

$$X_d(p) = X_d - \frac{(X_{11d}X_{afa}^2 - 2X_{f1d}X_{a1d}X_{afd} + X_{ffd}X_{a1d}^2)p^2 + (X_{afd}^2R_{1d} + X_{a1d}^2R_{fd})p}{(X_{11d}X_{ffd} - X_{f1d}^2)p^2 + (X_{11d}R_{fd} + X_{ffd}R_{1d})p + R_{fd}R_{1d}} \quad \ldots\ldots \quad (42$$

$$X_q(p) = X_q - \frac{X_{a1q}^2 p}{X_{11q}p + \quad} \quad \ldots\ldots \quad (43$$

Introduce the following relationships between self and mutual reactance:

$$X_{afd}^2 = K_1X_dX_{ffd} \quad \ldots\ldots \quad (44$$

$$X_{a1d}^2 = K_2X_dX_{11d} \quad \ldots\ldots \quad (45$$

$$X_{f1d}^2 = K_3X_{ffd}X_{11d} \quad \ldots\ldots \quad (46$$

$$X_{a1q}^2 = K_4X_qX_{11q} \quad \ldots\ldots \quad (47$$

where K_1, K_2, K_3 and K_4 are constants.

Substitution from eqns. (44)–(46) in eqn. (42) gives

$$X_d(p) = X_d - \frac{[X_{11d}X_dX_{ffd}K_1 + X_{ffd}X_dX_{11d}K_2 - 2X_dX_{11d}X_{ffd}\sqrt{(K_1K_2K_3)}]p^2 + (X_dX_{ffd}K_1R_{1d} + X_dX_{11d}K_2R_{fd})p}{(X_{11d}X_{ffd} - X_{ffd}X_{11d}K_3)p^2 + (X_{11d}R_{fd} + X_{ffd}R_{1d})p + R_{1d}R_{fd}} \quad (48$$

dividing by $X_{11d}X_{ffd}$ gives

$$X_d(p) = X_d - \frac{X_d\left\{[K_1 + K_2 - 2\sqrt{(K_1K_2K_3)}]p^2 + \left(K_1\frac{R_{1d}}{X_{11d}} + K_2\frac{R_{fd}}{X_{ffd}}\right)p\right\}}{\left[(1 - K_3)p^2 + \left(\frac{R_{fd}}{X_{ffd}} + \frac{R_{1d}}{X_{11d}}\right)p + \frac{R_{1d}R_{fd}}{X_{11d}X_{ffd}}\right]} \quad \ldots\ldots \quad (49$$

Now $\frac{X_{ffd}}{R_{fd}} = \tau_{d0}$, the field time-constant, and $\frac{X_{11d}}{R_{1d}} = \tau_{1d}$, the direct-axis damper time-constant.

Eqn. (49) becomes

$$X_d(p) = X_d - \frac{X_d\{[K_1 + K_2 - 2\sqrt{(K_1K_2K_3)}]p^2\tau_{d0}\tau_{1d} + (K_2\tau_{1d} + K_1\tau_{d0})p\}}{(1 - K_3)\tau_{d0}\tau_{1d}p^2 + (\tau_{1d} + \tau_{d0})p + 1} \quad . \quad . \quad (50)$$

Also for convenience in subsequent equations,

$$\frac{1}{X_d(p)} - \frac{1}{X_d} = \frac{[K_1 + K_2 - 2\sqrt{(K_1K_2K_3)}]\tau_{d0}\tau_{1d}p^2 + (K_2\tau_{1d} + K_1\tau_{d0})p}{X_d\{[1 - K_1 - K_2 - K_3 + 2\sqrt{(K_1K_2K_3)}]\tau_{d0}\tau_{1d}p^2 + (\tau_{1d} - K_2\tau_{1d} + \tau_{d0} - K_1\tau_{d0})p + 1\}} \quad . \quad . \quad (51)$$

Similarly, for the quadrature axis, combining eqns. (43) and (47) yields

$$X_q(p) = X_q - \frac{K_4X_qX_{11q}p}{R_{1q} + X_{11q}p} \quad . \quad . \quad . \quad (52)$$

$$= X_q - \frac{K_4X_q\tau_{1q}p}{1 + \tau_{1q}p} \quad . \quad . \quad . \quad (53)$$

in which $\tau_{1q} = X_{11q}/R_{1q}$ is the quadrature-axis damper time-constant.
Furthermore

$$\frac{1}{X_q(p)} - \frac{1}{X_q} = \frac{K_4\tau_{1q}p}{X_q[1 + (1 - K_4)\tau_{1q}p]} \quad . \quad . \quad (54)$$

621.313.1

The Institution of Electrical Engineers
Monograph No. 394 U
Aug. 1960

THE MAGNETIC FIELD AND CENTRING FORCE OF DISPLACED VENTILATING DUCTS IN MACHINE CORES

By K. J. BINNS, B.Sc., Graduate.

(*The paper was first received* 17*th February, and in revised form* 10*th May*, 1960. *It was published as an* INSTITUTION MONOGRAPH *in August*, 1960.)

SUMMARY

This paper examines analytically the field between equal stator and rotor ducts when displaced from each other and evaluates, for any relative position, the total flux crossing the air-gap and the amount entering the sides of each duct. The flux entering the sides of the stator ducts in a.c. machines varies at supply frequency and produces eddy currents the path of which is not restricted by the direction of the laminations and which consequently give rise to considerable loss. With relative displacement of the ducts the fluxes entering the two sides of a duct become unequal and produce an axial magnetic force of engineering importance.

Numerical values are given for the variation of gap permeance and magnetic centring force, and are plotted in curves directly applicable to design calculation for ratios of duct to gap width varying from $\frac{1}{2}$ to 5 and for any relative displacement.

LIST OF SYMBOLS

w = Complex magnetic potential function.
ϕ = Magnetic flux function.
ψ = Scalar magnetic potential function.
t, z = Complex variables of position.
k_0, c_0, c_1, c_2, c_3, c_4, k_1 = Constants.
μ_0 = Permeability of free space.
B = Flux density.
H = Field strength.
g = Air-gap width.
p = Peripheral length of core.
s = Slot width.
$\mathrm{F}(x, k)$ = Elliptic integral of the first kind.
$\mathrm{E}(\alpha, k)$ = Elliptic integral of the second kind.
$\Pi(x, k_1, k)$ = Legendre's third elliptic integral.
$\Pi_J(u, \alpha)$ = Jacobi's third elliptic integral.
$\mathrm{K}(k)$ = First complete elliptic integral.
$\mathrm{E}(k)$ = Second complete elliptic integral.
$\mathrm{K}'(k)$ = First complete elliptic integral to the complementary modulus.
$\Theta(\alpha)$ = Principal Jacobian theta function.
$\mathrm{Z}(\alpha)$ = Jacobian zeta function.

(1) INTRODUCTION

Radial ventilating ducts are nearly always of equal width on the two sides of the air-gap and that condition is assumed in the paper; the case of unequal displaced ducts presents greater analytical and computational complexity. Since ventilating ducts are widely spaced, a pair of them can be considered in isolation and unaffected by the ends of the core.

There are two limiting relative positions of ducts: they can be exactly opposite to each other, and they can be entirely remote. In the remote position the field of each duct is the same as that of an isolated deep slot opposite to a plane surface—the subject of Carter's original paper[1] of 1901. In the opposite position there is a plane of symmetry midway between the two sides of the gap and, again, the case is that of an isolated deep slot opposite to a plane (the plane of symmetry) for each pair of ducts. In both the opposite and the remote positions the flux is divided equally between the two sides of each duct and there is no resultant axial magnetic force. The general case is with the ducts displaced by a finite amount, and it is this case which has not previously been calculated accurately.

As the ducts are displaced from each other the total flux between the surfaces decreases; the flux entering each side of a duct becomes different and a centring force occurs, tending to align them. The permeance variation with displacement is very small compared with the permeance of a typical machine air-gap and it is difficult to find with accuracy the resulting centring force.

The problem is treated as a 2-dimensional one, i.e. the variation of the field in a peripheral direction is assumed to be very small over distances comparable with the duct and gap widths. The analysis of the field is achieved by conformal transformation, assuming the iron to be infinitely permeable; this involves negligible error if the relative permeability of the iron is greater than 25, a condition normally realized in practice. Carter[2] also examined this problem by conformal transformation, but, because of the limitations of calculation at that time, he represented the core surfaces by pairs of thin plates, each pair separated by a distance equal to the slot width.

This approximation gives an estimate of the general shape of the centring-force curves, but clearly underestimates the quantity of flux entering the sides of ducts and consequently the gap permeance. Moreover, the centring force in this approximate model would occur entirely at the tips of the plates, a condition very different from the practical case.

Using a resistance-network analogue Liebmann[3] determined the shape of the permeance curve, and earlier, Blake in unpublished work used an electrolytic tank for the same end but with no great accuracy. These experimental methods involve deducing the centring force from the slope of the permeance curve, a method which is not accurate and which is discussed later.

(2) ANALYSIS BY THE SCHWARZ–CHRISTOFFEL EQUATION

Consider first a plane extending to infinity with the real axis as a boundary below which there is iron of infinite permeability. This plane will be designated the t-plane (Fig. 1). Let w denote the complex magnetic 'potential' at any point t, where t is the complex variable of position; i.e. if ϕ is the flux function and ψ is the scalar potential function,

$$w = \phi + j\psi \quad . \quad . \quad . \quad . \quad . \quad . \quad (1)$$

Let a line current at $t = 0$ be perpendicular to this plane; its magnetic field may be expressed as

$$w = \frac{1}{\pi} \log_\varepsilon t \quad . \quad . \quad . \quad . \quad . \quad . \quad (2)$$

Correspondence on Monographs is invited for consideration with a view to publication.

Mr. Binns is with Associated Electrical Industries (Manchester), Ltd.

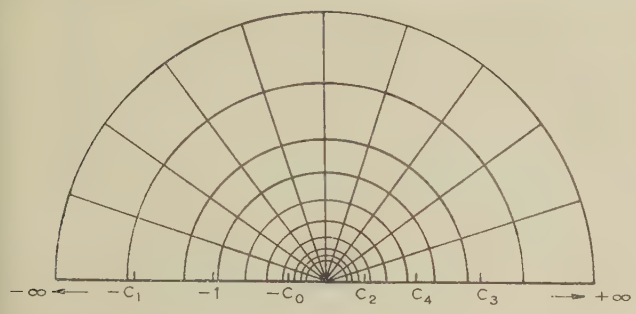

Fig. 1.—The field in the t-plane.

On the iron boundary, where $t > 0$, $\log t$ is real and so $\psi = 0$; where $t < 0$, $\log t = \log |t| + j\pi$ and so $\psi = 1$. Hence, a magnetic potential difference equal to unity exists between the two parts of the iron boundary on either side of the conductor and is maintained by the line current of unit magnitude.* The flux lines, given by ϕ = constant, are semicircles with centre at $t = 0$, and the equipotential lines, given by ψ = constant, are radial lines passing through $t = 0$.

Consider now a pair of displaced ducts in iron boundaries (Fig. 2). These boundaries and the region between them will be

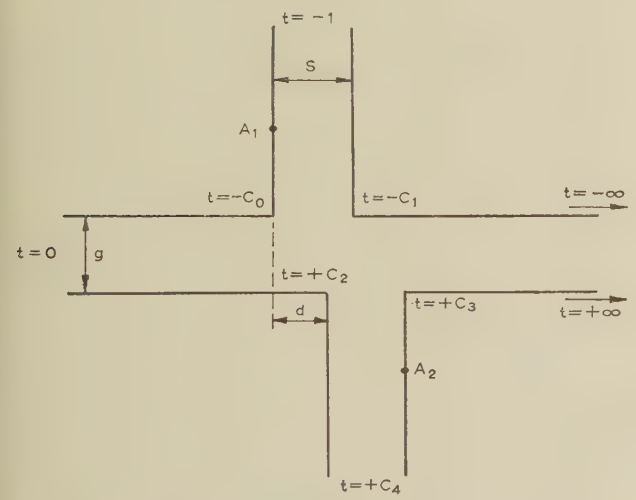

Fig. 2.—The z-plane boundary.

designated the z-plane. By means of the Schwarz–Christoffel equation,[4] the real axis in the t-plane is transformed into the boundary shape in the z-plane in such a way that the point $t = 0$, where the current is, corresponds to a point infinitely far down the air-gap from the ducts, and points $t = -c_0$, $-c_1$, c_2 and c_3 correspond to the right-angled corners in the z-plane. The field in the t-plane is then transformed into the field between the iron surfaces containing the ducts.

The relation between z and t to meet the above conditions is given by

$$\frac{dz}{dt} = \frac{k_0\sqrt{[(t + c_0)(t + c_1)(t - c_2)(t - c_3)]}}{t(t + 1)(t - c_4)} \quad . \quad . \quad (3)$$

This equation connects the complex co-ordinates of corresponding points, i.e. points of identical complex potential. Before the transformation can be usefully employed it is necessary to express the constants k_0, c_0, c_1, c_2, c_3 and c_4 in terms of the boundary dimensions in the z-plane.

To set the scale in the z-plane, the gap width is made equal to unity. Then, by evaluating the residues at the poles of dz/dt, it can be shown that

$$k_0 = 1/\pi \quad . \quad . \quad . \quad . \quad . \quad . \quad . \quad . \quad (4)$$

and that

$$s(c_4 + 1) = \sqrt{[(1 - c_0)(c_1 - 1)(1 + c_2)(1 + c_3)]} \quad . \quad (5)$$

where s is the width of the ducts.

The boundary has skew-symmetry, i.e. at points A_1 and A_2 in Fig. 2, equidistant from their respective corners, the field is the same. From this it can be shown that

$$c_2 = c_4/c_1 \quad . \quad . \quad . \quad . \quad . \quad . \quad . \quad . \quad (6)$$

and

$$c_3 = c_4/c_0 \quad . \quad . \quad . \quad . \quad . \quad . \quad . \quad . \quad (7)$$

It is this feature which makes this case more simple to calculate than the case of unequal ducts, which contains an additional variable. It remains to find a relationship between the t-plane constants which makes the iron surfaces on either side of the ducts co-linear. This necessitates evaluating the integral derived from eqn. (3), namely

$$z = \int \frac{\sqrt{[(t + c_0)(t + c_1)(t - c_2)(t - c_3)]}dt}{\pi t(t + 1)(t - c_4)} \quad . \quad (8)$$

It is important to realize that, while z can be found for a given value of t, t cannot be found for a given value of z except by iteration or interpolation. The integral is elliptic and difficult to handle; its analytical treatment is described in Section 7.1, where it is shown how the integral may be expressed in Jacobian form.

For practical purposes, however, it is more convenient to evaluate the integral numerically using Simpson's quadratic and cubic rules, and this was done with high accuracy on a digital computer. This procedure of numerical integration, described in Section 7.2, was used to determine accurately the t-plane constants for a wide range of values of duct width and displacement.

(3) DETERMINATION OF FLUX DISTRIBUTION

The constants having been found, the field in the z-plane configuration can now be calculated from eqns. (2) and (8).

(*a*) *Total Flux.*—The flux crosses the gap in straight lines when remote from the ducts and these are represented by concentric semicircles in the t-plane. Since flux is conserved in the transformation its quantity between two corresponding flux lines can be calculated readily in the simple t-plane field. Comparing the air-gap flux thus calculated with its value between two smooth boundaries shows the effect of the ducts on the total flux; this is shown diagrammatically in Fig. 3 for the two limiting positions and one intermediate position. For unit flux density in the gap,* the variation, with displacement, of the change in permeance due to the presence of the ducts, divided by the duct width is shown in Fig. 4 for a range of duct widths.

It can also be shown that, for unit gap density, the total flux entering the sides of each duct is given by $-(1/\pi)\log_\varepsilon c_0$ and $(1/\pi)\log_\varepsilon c_1$. This flux is of importance, since it alternates on the stator at supply frequency and produces considerable loss there, the eddy currents being produced in the plane of the laminations. The variation of this flux with duct displacement is shown in Fig. 5.

(*b*) *Flux Density.*—The flux density in the air-gap is repre-

* In the rationalized M.K.S. system of units a current of 1amp gives rise to unit potential difference between the two parts of the iron boundary on either side of the conductor.

* In the rationalized M.K.S. system of units a gap current of $1/\mu_0$ amperes gives rise to unit flux density in the air-gap remote from the ducts.

sented as unity at all points remote from the ducts; its value anywhere is given by $\left|\frac{dw}{dz}\right|$ and its direction is the argument of $\frac{dw}{dz}$. Now

$$\frac{dw}{dz} = \frac{dw}{dt} \times \frac{dt}{dz} = \frac{1}{\pi t(dz/dt)}$$

and, since dz/dt is given by eqn. (3) and z by eqn. (8), the density distribution can be evaluated. The distribution down the sides of the duct is shown in Fig. (6) and along part of the gap in Fig. (7) for particular examples of duct width and displacement.

(*c*) *Field Map.*—It has been shown that the complex potential function in the t-plane is logarithmic, and for given values of ϕ and ψ is easily found. By a process of numerical integration of complex numbers, described in Section 7.3, the point in the z-plane corresponding to any particular point in the t-plane is found, and hence the points of intersection of a system of flux and equipotential lines are found. The author is not aware of any published work involving the numerical integration of a function of a complex variable, but the method is very useful. Using Simpson's rule with complex step size to integrate between two values of t, the complex ordinates of dz/dt are evaluated and then the real and imaginary parts of the integral are calculated separately. While the physical interpretation as the area under a single curve does not exist, the method is none the less valid. Two field maps for $s/g = 1$ and 2 are shown in Figs. 8 and 9 respectively.

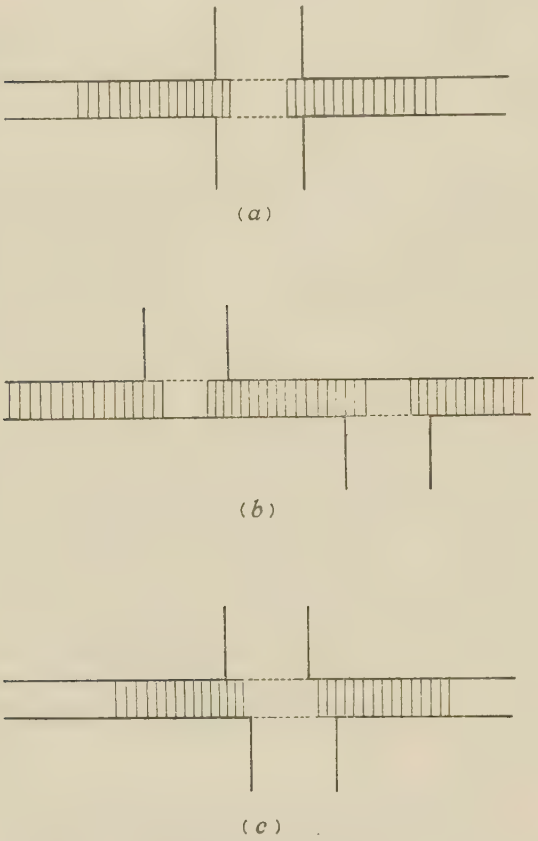

Fig. 3.—Diagrammatic representation of flux.
(*a*) Ducts opposite.
(*b*) Ducts remote.
(*c*) Ducts slightly displaced.

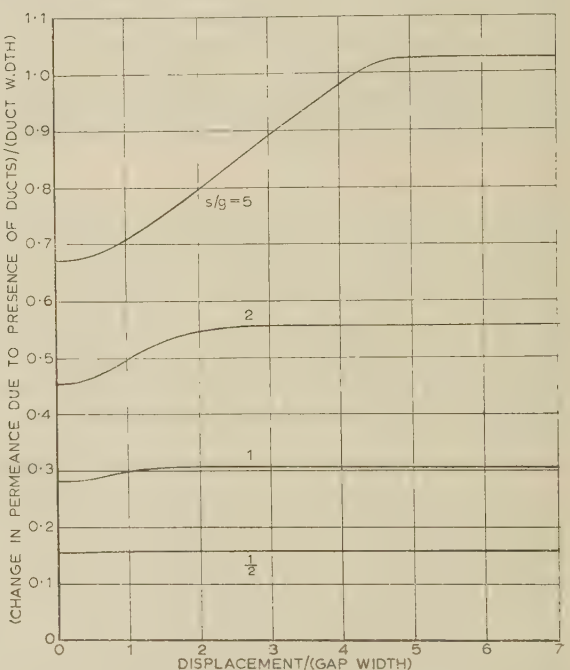

Fig. 4.—Change in permeance due to presence of ducts.

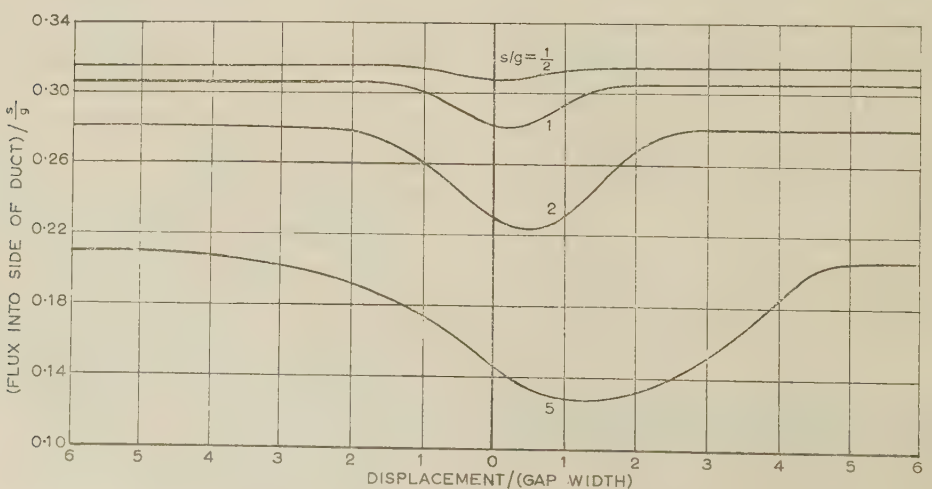

Fig. 5.—The flux entering the sides of a duct.

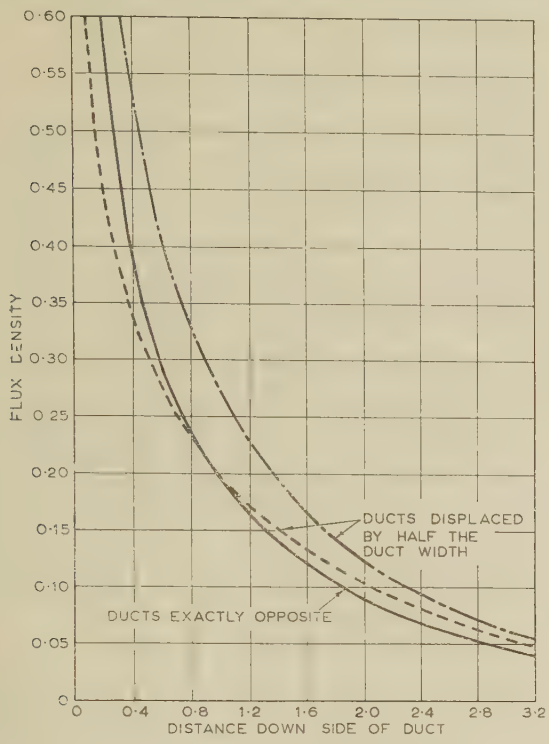

Fig. 6.—Flux density variation down the side of a duct, $s/g = 5$.

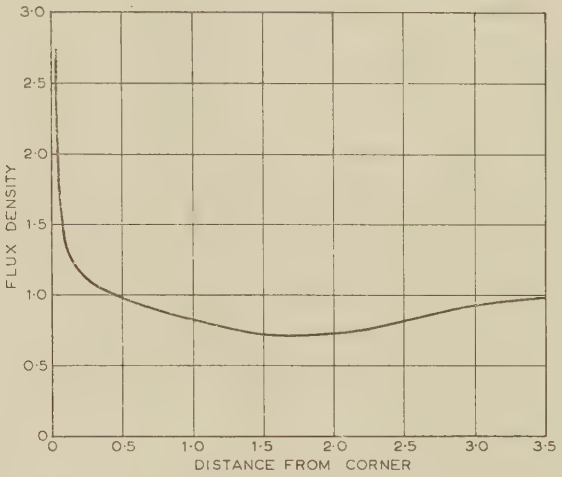

Fig. 7.—Flux density variation along the gap surface.
$s/g = 2$. Duct displacement = 2·5 × (duct width).

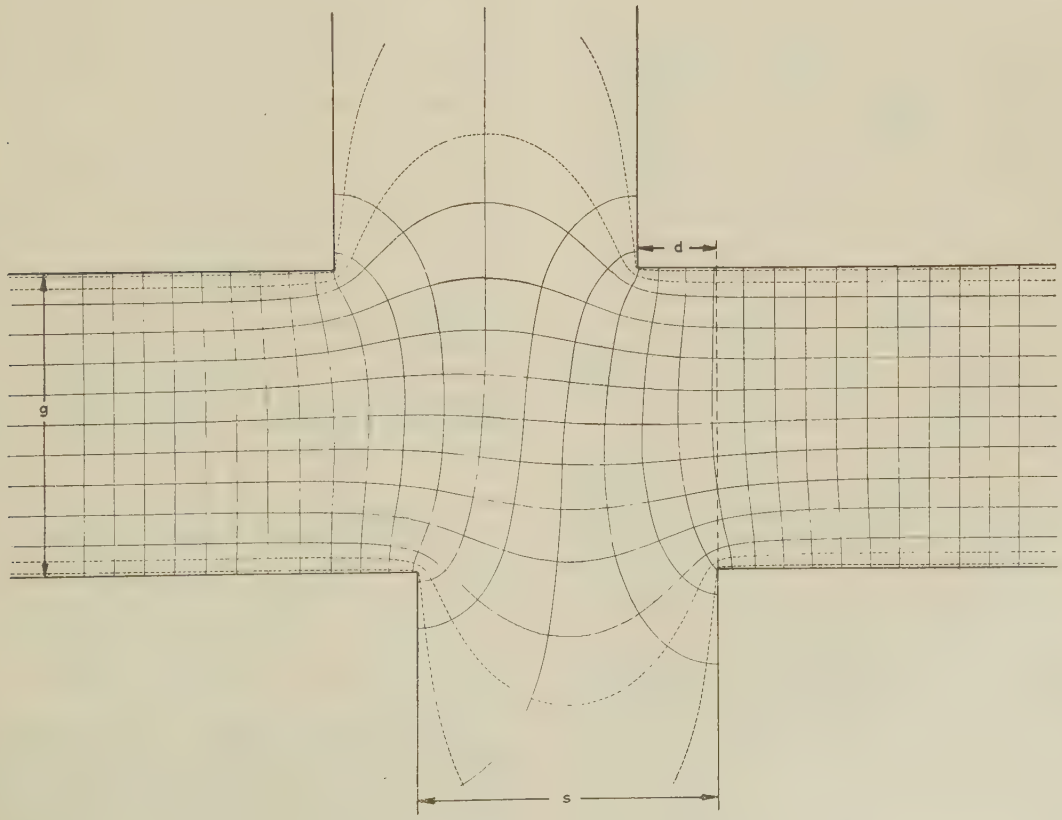

Fig. 8.—Field map, $g = 1$, $s = 1$, $d = 0{\cdot}25$.

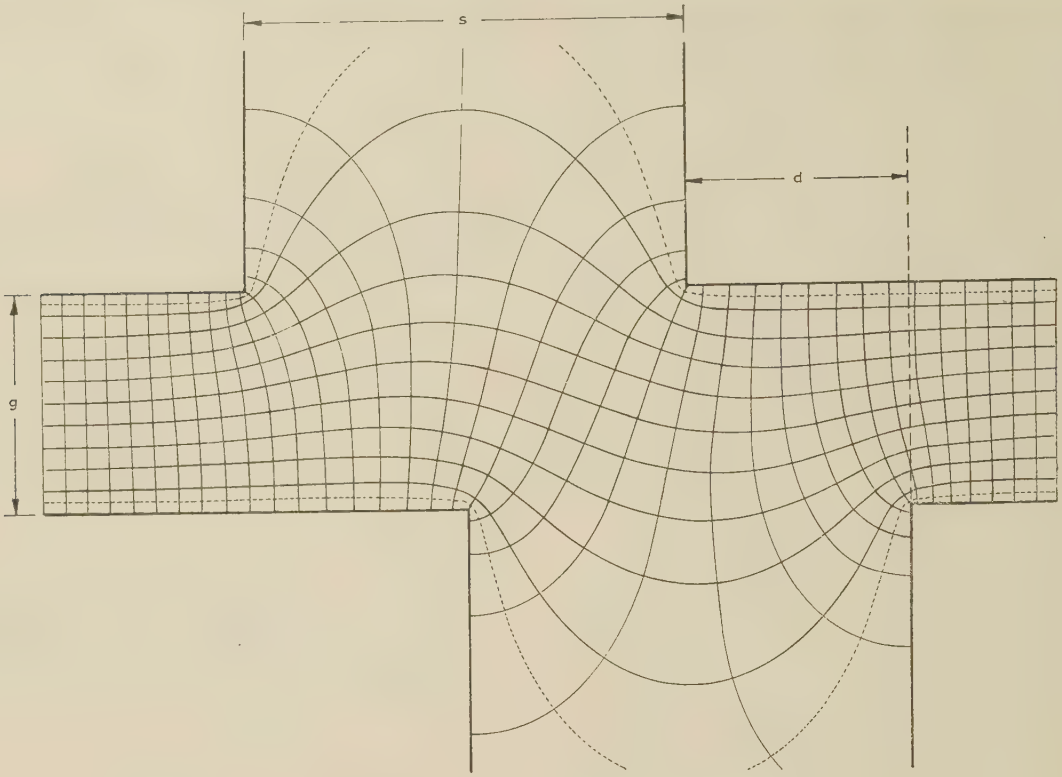

Fig. 9.—Field map, $g = 1$, $s = 2$, $d = 1$.

(4) DETERMINATION OF AXIAL CENTRING FORCE

(4.1) General Expression

The axial restoring force in any position is equal to the rate of diminution of the total stored energy of the magnetic field with further axial displacement of the ducts. Since the iron is assumed to be infinitely permeable, the field strength in it is zero and all the energy is stored in the air space. The centring force is calculated per unit peripheral length and this quantity can be calculated in two ways. In the first method, the force is given by half the product of the magnetic potential difference and the rate of change of total flux with displacement, and this is the one which has been employed by Carter and Liebmann. The change in total flux is a very small quantity and it is very difficult to find with accuracy, and its variation with displacement having been obtained approximately, the numerical differentiation of this curve greatly increases the inaccuracy. The second method calculates the force directly by integrating $B^2dz/2\mu_0$ down the sides of a duct. The method is based on the fact that the restoring force is the rate of change of the stored energy in the gap, which is $\frac{1}{2}\int\int BHdxdy$. But for an infinitely small change in the duct displacement there will be no change in the field, except in the volume element swept out by the sides of the displaced duct. The change in stored energy in this element becomes $\frac{1}{2\mu_0}\int B^2dz$ per unit displacement per unit periphery and the resultant force is the difference between these two integrals over the two sides of the duct. This integral can be solved more simply as a function of t rather than of z, and since, for unit gap density, $B = dw/dz$,

$$\frac{1}{2\mu_0}B^2dz = \frac{1}{2\mu_0}\left(\frac{dw}{dz}\right)^2 dz$$

$$= \frac{1}{2\mu_0}\left(\frac{dw}{dt}\right)^2 \frac{dt}{dz}dt$$

From eqn. (2), $dw/dt = 1/\pi t$, and dz/dt is given in terms of t by eqn. (3). Hence, by numerical integration of this function of t, performed in the same way as the integration of the Schwarz–Christoffel equation, the force on each side of the duct is evaluated accurately and the centring force is given by the difference of the two quantities.

(4.2) Numerical Values

A calculation is made of the centring force for unit gap, unit gap density, per unit periphery and per duct pair. A graph is plotted dividing the centring force by the ratio s/g to fit all the curves on one sheet, and the displacement is given in units of gap width. It is interesting to note that the product of gap width and peripheral length is the cross-sectional area of the gap, and that the reading from the graph, K_1, is for a gap density of $1\,\mathrm{Wb/m^2}$ for $1\,\mathrm{m^2}$ gap cross-section for one duct pair and divided by s/g. Thus, for practical purposes, if the gap density is $B\,\mathrm{Wb/m^2}$, the periphery is p in and the gap width is g in, the centring force per duct pair is

$$1{\cdot}45 \times 10^{-4}K_1(s/g)B^2gp \text{ pounds}$$

For values of s/g of $\frac{1}{2}$, 1, 2 and 5, curves are plotted for K_1 in Fig. 10. Considering a typical induction motor for which

$$B = 1\,\mathrm{Wb/m^2} \quad g = 0{\cdot}175\,\mathrm{in}$$
$$p = 107\,\mathrm{in} \quad s/g = 2{\cdot}14$$

and for 14 ducts per side, the force is 2280 lb for a displacement of 0·175 in.

Comparison of the present results with those published by Liebmann show differences of force up to 30%; the difference is believed to be due to the inaccuracy of his measurement of the slope of a curve, on which the points have been obtained by measurement with an analogue. The method of numerical integration used in this paper was, however, applied on a digital

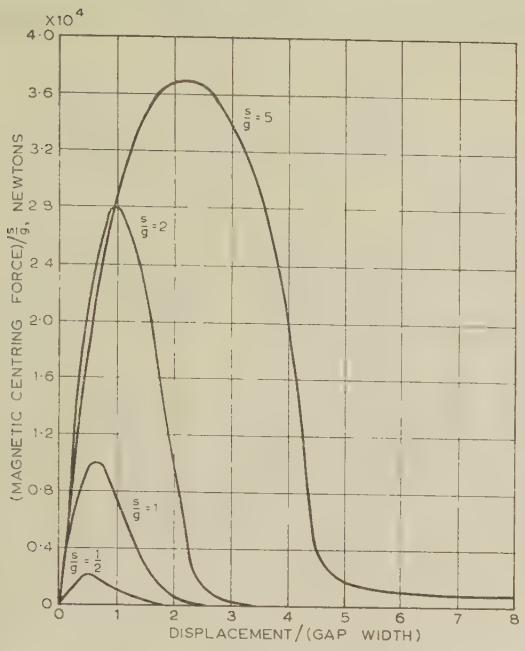

Fig. 10.—Magnetic centring force.

computer and employed a very small step size which was further decreased when the gradient became appreciable. Further, by halving the step size and by testing for any change in the result, the accuracy of the method was continually checked and, indeed, the error was shown to be never greater than 0·5% and mostly less than 0·1%. It is interesting to note that Carter's estimate of the general shape of these curves agrees quite well with those of Fig. 10.

(5) ACKNOWLEDGMENTS

The paper was prepared in the Electrical Machines Laboratory of Associated Electrical Industries (Manchester), Ltd., and the author wishes to thank Sir Willis Jackson, Director of Research and Education, for permission to publish it. The author is indebted to Mr. S. Neville and Dr. W. J. Gibbs for helpful suggestions in the presentation of the paper, and to Mrs. H. M. Battersby for assistance with calculations and the preparation of graphs.

(6) REFERENCES

(1) CARTER, F. W.: 'Air Gap Induction', *Electrical World and Engineer*, 1901, **38**, p. 884.

(2) CARTER, F. W.: 'The Magnetic Field of the Dynamo-Electric Machine', *Journal I.E.E.*, 1926, **64**, p. 1115.

(3) LIEBMANN, G.: 'The Change of Air-Gap Flux in Electrical Machines due to the Displacement of Opposed Slots', *Proceedings I.E.E.*, Monograph No. 208 M, November, 1956 (**104** C, p. 204).

(4) SCHWARZ, H. A.: 'Uber einige Abbildungsaufgaben', *Journal für die reine und angewandte Mathematik*, 1869, **70**, p. 105. Also
CHRISTOFFEL, E. B.: 'Sul Problema delle Temperature Stazionarie e la Rappresentazione di una Data Superficie', *Annali di Matematica Pura ed Applicata*, 1867, **1**, p. 95.

(7) APPENDICES

(7.1) Expression in Jacobian Form

The integral can be expressed in the form

$$\int \frac{(t+c_0)(t+c_1)(t-c_2)(t-c_3)}{\pi t(t+1)(t-c_4)} \frac{dt}{\sqrt{Q}}$$

where $Q = (t+c_0)(t+c_1)(t-c_2)(t-c_3)$, and Q may be expressed in terms of even powers only of the variable by using the transformation $t = (p+qt')/(1+t')$. Then $dt/\sqrt{Q}$ becomes of the form

$$\frac{c'dt'}{\sqrt{[(t'^2-g^2)(t'^2-h^2)]}}$$

and the rational part of the integral can be expressed in partial fractions of the form

$$c''\left(1+\Sigma\frac{At'}{t'^2-u^2}+\Sigma\frac{B}{t'^2-u^2}\right)$$

Hence, the whole integral becomes of the form

$$\int \frac{A'dx}{\sqrt{[(1-x^2)(1-k^2x^2)]}} + \Sigma\int \frac{B'dx}{(1-k_1^2x^2)\sqrt{[(1-x^2)(1-k^2x^2)]}} + \Sigma\int \frac{c'xdx}{(x^2-w_0^2)\sqrt{[(1-x^2)(1-k^2x^2)]}}$$

The first term is an elliptic integral of the first kind to modulus k and equals $A'\mathrm{F}(x, k)$.

The second term is an elliptic integral of the third kind to modulus k and equals $\Sigma B'\Pi(x, k_1, k)$.

The third term can be integrated in terms of elementary functions by substituting $y = x^2$, which makes the term under the root sign a quadratic, and then $y - (\text{a constant}) = 1/v$, which turns the integral into the form

$$\int \frac{dv}{\sqrt{[(v-s)^2+l^2]}} = \text{arc sinh}\frac{v-s}{l}$$

Hence, the integral reduces to standard elliptic integrals together with an elementary function.

The numerical evaluation of the third elliptic integral is most easily performed in Jacobian notation, by putting $x = \mathrm{sn}\,u$ and $k_1 = k\,\mathrm{sn}\,\alpha$.

The Jacobian form of the third elliptic integral, Π_J, is given by

$$\Pi(x, k_1, k) = u + \frac{\mathrm{sn}\alpha}{\mathrm{cn}\alpha\mathrm{dn}\alpha}\Pi_J(u, \alpha)$$

and it can be shown that

$$\Pi_J(u, \alpha) = \tfrac{1}{2}\log\frac{\Theta(u-\alpha)}{\Theta(u+\alpha)} + u\mathrm{Z}(\alpha)$$

The theta function can be evaluated from a Fourier series

$$\Theta(\alpha) = 1 + 2\sum_{n=1}^{\infty}(-1)^n q^{n^2}\cos\frac{n\pi\alpha}{K}$$

in which $q = \varepsilon^{-\pi K'/K}$.

Also, $\mathrm{Z}(\alpha)$ is defined as $\mathrm{E}(\alpha) - \mathrm{F}(\alpha)E/K$.

In this way, the integral as a whole can be expressed in terms of elliptic integrals of the first and second kind which have been tabulated or which can be evaluated from well-known series.

(7.2) Determination of Constants

In order to find a relationship between the t-plane constants which will make the iron surfaces on either side of the ducts co-linear, it is necessary to consider points on either side of $t = -1$ and very close to it, remembering that when $t = -1$, $z = \infty$. Let $t = -1+\delta$ and $t = -1-\delta$ be points on either side of $t = -1$, where δ is very small but not zero. dz/dt is the same in magnitude though not in sign at these

points, i.e. when t is very close to -1, z approaches infinity at the same rate, whichever way t approaches -1.

For the iron surface to be co-linear,

$$\int_{t=-c_0}^{t=-1+\delta} \left(\frac{dz}{dt}\right) dt = -\int_{-1-\delta}^{-c_1} \left(\frac{dz}{dt}\right) dt$$

This expresses the remaining relationship between the constants, and these integrals are evaluated numerically on a digital computer.

The value of c_1 is chosen bearing in mind that duct displacement is approximately proportional to $\log c_4$. Next, a value of c_1 is taken from an estimate of the total flux entering the duct side. Eqns. (4)–(7) are solved and the two integrals are evaluated. Depending on which is the larger and by what amount, c_1 is modified and the process is repeated until the two integrals differ by less than 0·001. The whole of this process is programmed to occur automatically in the computer and takes about 2 minutes.

Fitting either a cubic or a quadratic equation to groups of points on the curve and using a small step size, reducing it where the gradient is steep, the integrals are evaluated with high accuracy. The accuracy was determined by comparison with values for the limiting cases (evaluated correct to 1 part in 10^5) and by repeated reduction of step size to see if any appreciable change resulted, this method being used to determine the most desirable step size.

The actual duct displacement is found by subtracting the two integrals

$$\int_{-\delta}^{-c_0} \left(\frac{dz}{dt}\right) dt \text{ and } \int_{+\delta}^{c_2} \left(\frac{dz}{dt}\right) dt$$

and suitable values for δ were found to lie between 0·001 and 0·005.

(7.3) Numerical Integration of a Function of a Complex Variable to Obtain a Field Map

Since $\phi + j\psi = (1/\pi) \log_\varepsilon t$, the positions in the t-plane of points of intersection of flux and equipotential lines are given by

$$t = \varepsilon^{\pi(\phi+j\psi)} = \varepsilon^{\pi\phi} (\cos \pi\psi + j \sin \pi\psi) \quad . \quad . \quad (9)$$

Hence, in order to follow an equipotential line and locate the points of intersection of flux lines on it, it is required to select a potential, ψ, and to calculate from eqn. (9) the values of t for any chosen step in flux function, ϕ. If two such points in the t-plane are t_1 and t_2, it is necessary to calculate the change in z by numerically integrating eqn. (8). Then, if n steps are taken in Simpson's rule, the complex step size is $h = (t_2 - t_1)/n$, where n is an even number. The complex ordinates are evaluated from eqn. (3), and taking the ordinates f_m in groups of three in the usual way, Simpson's rule is applied. Taking an arbitrary origin in the z-plane at the point of intersection of a flux line and an equipotential line, the other points of intersection can be plotted and a field map constructed.

621.311.161:621.316.728

The Institution of Electrical Engineers
Monograph No. 395 S
Sept. 1960

AN ANALYTICAL REVIEW OF POWER-SYSTEM FREQUENCY, TIME AND TIE-LINE CONTROL

By D. BROADBENT, B.Sc., M.Eng.Sc., Ph.D., Associate Member,
and K. N. STANTON, B.E., Student.

(*The paper was first received* 19*th November*, 1959, *in revised form* 28*th January, and in final form* 18*th May*, 1960. *It was published as an* INSTITUTION MONOGRAPH *in September*, 1960.)

SUMMARY

Over the past decade and a half there have been proposed three schemes of control for electricity supply systems interconnected through tie lines. In chronological order they are the speed-governed system with frequency biasing, the time-governed system and the load-phase energy control.

The paper describes computer studies which compare the three systems using a performance index of the integral square error. Certain conclusions are drawn by applying this criterion both to the frequency error of the isolated system and to the tie power-flow error of the interconnected system.

LIST OF SYMBOLS

D = Damping coefficient, p.u./rad/time-rad.
K = Gain of time-error loop, p.u./rad.
K_b = Stabilizing feedback gain.
K_c = Integral of time-error gain, p.u./time-rad/rad.
K_t = Tie-line controller gain, p.u./time-rad/p.u. error.
M_l = Load torque, p.u.*
M_p = Prime-mover torque, p.u.
M_t = Tie-line torque, p.u.
ΔM_t = Deviation from scheduled value, M_t.
$p = \frac{d}{dt}$.†
δ = P.U. regulation of speed controller.‡
τ' = Steam-header time-constant, time-rad.
τ'' = Servo-motor time-constant, time-rad.
T_a = Acceleration time of machine or area, time-rad.
τ_b, τ_1, τ_2 = Stabilizing feedback time-constants.
T_{s12} = Tie-line synchronizing coefficient, p.u./rad.
Ω = Machine or area speed, rad/time-rad.
ω = Speed signals within controller, rad/time-rad.
$\Delta\omega$ = Deviation from scheduled value, Ω.
ϕ = Machine or area angle, rad.
$\boldsymbol{\phi}$ = Standard time, rad.
θ = Angle signals within controller, rad.
$\Delta\theta$ = Deviation of θ from scheduled value, $\boldsymbol{\theta}$.

Per-unit values are used throughout.

(1) INTRODUCTION

The analysis and control of power flow in interconnected electricity supply systems is somewhat complex. It might be said that, traditionally, power flow has been separated into two conceptions with a possible mode of oscillation associated with each. First, electrical power flow takes place between points in the system and the term stability, when used in relation to a synchronous power network, refers to the property of the system which allows it to develop restoring forces greater than the disturbing forces affecting synchronism between two parts of the system. After a disturbance in which the stability limit is not exceeded, i.e. synchronism is not lost, the two parts will oscillate with respect to each other in a manner which is determined by the system parameters, inertia, damping and synchronizing coefficients. This oscillatory system may be modified by feedback controls such as voltage regulators and tie-line controllers. Secondly, power flow is controlled at the turbine throttle by the governor feedback signal, and mechanical power oscillations due to governor action have been investigated; the term stability has been used in its mathematical or servo-mechanism sense in connection with these oscillations. This second mode of oscillation is influenced by the same factors that affect electrical synchronism, together with others associated with the governor, to an extent depending upon the nature of the system. For example, in a simple system which is closely coupled electrically, the natural frequency of possible governor oscillations is remote from that of the natural frequency of the synchronous system and the analyses are quite separate. On the other hand, in a loosely coupled system with tie-line power controllers acting through the turbine governors, the two analyses can no longer be separated; the change in electrical angle across a tie line, measured as a function of time, becomes comparable in magnitude and frequency to the integral of the change in speed of the turbine. It is with this latter problem that the paper is concerned.

To make the system more amenable to analysis, certain approximations are made. First, the synchronous generators and their associated transformers are considered to be electrically stiff compared with the tie line and the controllers, i.e. the electrical angle between rotor and output voltage is neglected in comparison with tie-line angle and time-error angle. Secondly, the damping coefficients associated with the turbines, electrical apparatus and loads are made constants by considering small departures only from normal working conditions. This treatment also allows the tie-line synchronizing coefficients, which are sinusoidal functions, to be linearized.

The four schemes of control dealt with in this paper are:

(*a*) The speed governor (with integral of speed error and tie power control); this method of control is referred to[1,3] as 'speed governing with frequency-biased tie-line control'.

(*b*) Integral of speed governing (with tie-line control), referred to elsewhere as 'load-phase tie-line energy control'.[4]

(*c*) Time-error governing (with integral of time-error and tie-line power control)[2,5,6]; a time-error governor has also been referred to as a synchronous governor.[8] Mathematically, the integral of speed governor as described in Reference 4 performs the same function as a time-error governor; however, they differ physically in that deviations in speed are measured and integrated to provide a feedback signal in the former, while actual angle or time error is measured in the latter. In addition, the gains of described time-error governors are greater by a factor of approximately 100 than the gains of

* The system is synchronous and therefore p.u. power = p.u. torque.
† Time measured in radians swept by the rotor of a 4-pole 50 c/s machine: Time in radians = 157 × time in seconds.
‡ The p.u. gain of the speed controller = $1/\delta$; e.g. a speed governor having 5% regulation has a gain of 1/0·05 p.u.

Correspondence on Monographs is invited for consideration with a view to publication.
Prof. Broadbent is Associate Professor of Electrical Engineering, and Mr. Stanton is at the University of New South Wales, Australia.

described 'load-phase' controllers which appear to be the normal supplementary system time controllers.

(*d*) Integral of time-error (with tie-line control); this method of control has not been suggested previously and is included in the paper for the sake of completeness.

It is proposed first to describe these schemes, and the signal flow diagram (see Section 8.1) has been chosen as the medium to do this; by having the controlling signals specifically represented, the similarities and differences will be apparent. Similar control loops may be identified in the diagrams of the various schemes.

Secondly a quantitative comparison is drawn between these schemes as they could be applied to an actual power system, the basis of comparison being the integral square error of certain variables within the system. These variables are the tie-line power transfer, the speed or frequency of the system and the electrical time of the system. The errors in these quantities are the amounts by which they depart from the scheduled or correct values. The integral square error is frequently used to describe the quality of a servo mechanism and is obtained by squaring the error and integrating with respect to time over a long period. For example, the integral square error of the power flow through a tie-line is

$$\text{I.S.E.} = \int_{-\infty}^{+\infty} (\Delta M_t)^2 dt,$$

where ΔM_t is the instantaneous error in tie-line flow from the scheduled value, M_t.

There are a few properties of the integral square error which are worthy of note and which have a bearing on the results of Section 4:

(i) The error itself, $\Delta M_t(t)$, a function of time, must eventually go to zero, otherwise the integral square error is infinite.

(ii) The value of the integral depends on the length of time the error is not zero.

(iii) Because of the squared term the value of the integral is sensitive to large errors.

(iv) Minimization of the integral square error as a design criterion does tend to give a somewhat oscillatory response; in consequence, the degree of stability of the system must be checked when applying this criterion.

The signal flow diagram is drawn from the system equations; for example, eqn. (1) is the p.u. torque equation of a machine coupled to others by tie-lines (Section 8.2):

$$T_a p^2\phi + Dp\phi + M_t + M_p + M_l = 0 \quad . \quad . \quad (1)$$

This equation could equally well represent a closely coupled area, in which case the coefficients would be composite ones describing the area as viewed from the outside. The tie-line and load contributions, M_t and M_l respectively, are considered to be frequency-invariant, and damping torques from these sources are included in the general damping coefficient, D.

The prime-mover contribution, M_p, may itself consist of several components; a speed-error governor will provide a component $\Delta\omega/\delta$; a time-error governor gives $K\Delta\theta$; tie-line and integral of time error controllers have their effect on M_p when fitted. These are introduced at the input node A (Fig. 1), which has the units of equivalent p.u. torque. In addition to these signals from outside sources, the prime-mover torque is influenced dynamically by any energy-storage elements in its tributaries; the steam-header lag and the servo-motor lag are represented by the transmittance $1/[(\tau' p + 1)(\tau'' p + 1)]$; in addition, there may be feedback signals inserted for stabilizing purposes.

It will be seen that Fig. 1 represents the area torque signals for any configuration of governor and controller; it is the basic diagram to which will be added the feedback-signal flow paths depending on the controlling system used.

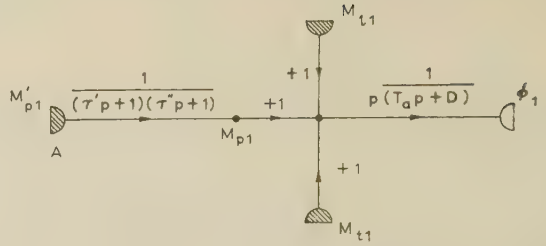

Fig. 1.—Basic signal flow diagram of a machine set or compact area showing the various torques acting.

(2) SCHEMES OF CONTROL FOR THE SYSTEM

(2.1) Speed Governor (with Integral of Speed Error and Tie Power Control)[1,3]

This is the conventional frequency-biased tie-line control; eqn. (2) gives the component parts of an increment in M_{p1} [see eqn. (1)] for one of two speed-governed areas connected by a tie-line (small departures from normal load conditions are taken):

$$\Delta M_{p1} = \frac{1}{(\tau' p + 1)(\tau'' p + 1)}\left(\frac{1}{\delta_1}\Delta\omega_1 + \frac{K_1}{p}\Delta\omega_1 + \frac{K_{t1}}{p}\Delta M_t\right) \quad . \quad (2)$$

where

$$\Delta M_t = \frac{T_{s12}}{p}(\Delta\Omega_1 - \Delta\Omega_2) \quad . \quad . \quad . \quad . \quad (3)$$

Fig. 2 is the signal flow diagram of area 1 when controlled according to eqns. (1), (2) and (3). It includes the reference levels of frequency, Ω, scheduled load setting, M_l, and scheduled tie-line power setting, M_t, the first and the last being common to the two areas considered.

A negative-feedback path results in the speed error of area 1 being identified at the node ω_1. This is used by the speed-governor transmittance, $1/\delta_1$, and the integral of speed transmittance, K_1/p, to produce a contribution to the throttle command at node A. The integral loop will ensure that there is no frequency error of the area in the steady state, but there will be a time error depending on the area load and the value of K_1. This time error could become excessive owing either to inaccuracies in the controller or to a low value of K_1, or for both reasons, in which case a supplementary integral of time-error loop is required, manual or automatic, not shown in Fig. 2.

The tie-line controller detects the error in M_t from its scheduled value, M_t, and applies integral-type correction through the transmittance K_{t1}/p so that there is no steady-state error in tie-line power flow. It is assumed there are no essential time lags in these control paths comparable to the header and servo motor lags τ' and τ''.

(2.2) Integral of Speed Governor (with Tie-Line Control)[4]

Eqn. (4) gives the component parts of an increment in M_{p1} of eqn. (1) for this scheme of control. Again the equation refers to small departures in order that the coefficients may be considered constants, and the subscript 1 denotes parameters and variables associated with the first of two areas connected by a tie-line.

$$\Delta M_{p1} = \frac{1}{(\tau' p + 1)(\tau'' p + 1)}\left(\frac{K_1}{p}\Delta\omega_1 + \frac{K_{t1}}{p}\Delta M_t\right) \quad . \quad (4)$$

Fig. 3 is the signal flow diagram of one area which as shown does not correct for an error between electrical and standard time.

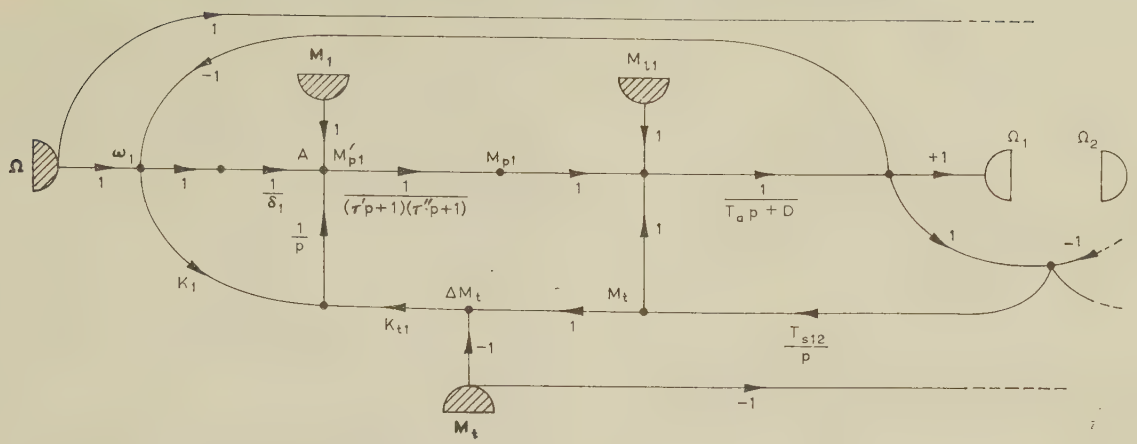

Fig. 2.—Flow diagram of a speed-governed set or area with integral of speed and tie-line controllers.

(2.3) Time-Error Governor (with Integral of Time Error and Tie Power Control)[2, 5, 6]

This is a complete scheme of control for an interconnected system, and while, when designed for a particular situation, certain simplifications and approximations can be made, as will be seen later, it is felt that the correct starting-point should be the complete control. Eqn. (5) is the expression for an increment in the prime-mover torque of eqn. (1).

$$\Delta M_{p1} = \frac{1}{(\tau' p + 1)(\tau'' p + 1)}\left(K_1 \Delta\theta_1 + \frac{K_{c1}}{p}\Delta\theta_1 + \frac{K_{t1}}{p}\Delta M_t\right) \quad . \quad (5)$$

where

$$\Delta M_t = T_{s12}(\Delta\phi_1 - \Delta\phi_2) = T_{s12}\Delta\theta_{12} \quad . \quad . \quad . \quad . \quad . \quad . \quad (6)$$

The signal flow diagram is shown in Fig. 4 where it will be seen that there are four reference quantities in each area; standard time, ϕ, and the tie-line setting, M_t, are common to both areas; the area setting, M_1; the area time-angle reference, θ_1, is related to the other area time-angle reference by the scheduled tie power and the effective tie-line constant at that level, T'_{s12}. The significance of these reference levels is seen in Fig. 5, which is a diagram of equivalent time angles traced out as the machine rotates. OB, OA, OC and OC′ rotate anti-

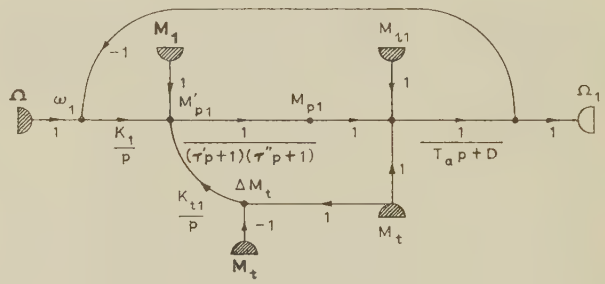

Fig. 3.—Flow diagram of a set with integral of speed and tie-line controllers.

clockwise and indicate the angles at the various nodes of Fig. 4. OA is standard time and traces out ϕ from the datum. OC′ indicates the actual rotors' position of the tightly coupled area while θ_1 is the time error. OC is the scheduled rotor position and could coincide with OA for one tightly coupled area of the system. OB represents the correction exerted by the controller in that signal, θ'_1 radians, appears at node B of Fig. 4 such that

$$\theta'_1 = \theta_1 + \frac{K_{c1}}{K_1}\frac{\Delta\theta_1}{p}$$

In the steady state, because of the integrating term, $\theta'_1 \rightarrow \theta_1 \rightarrow \boldsymbol{\theta_1}$ and OB coincides with OA.

Referring to Fig. 4, the path involving K_{c1}/p ensures that there is no steady-state error, $\Delta\theta_1$, i.e. no supplementary time control is necessary. The tie power deviation is zero in the steady state owing to the path K_{t1}/p, while the operation is stabilized under transient conditions by the feedback with transmittance $K_b p^2/(\tau_b p + 1)$.

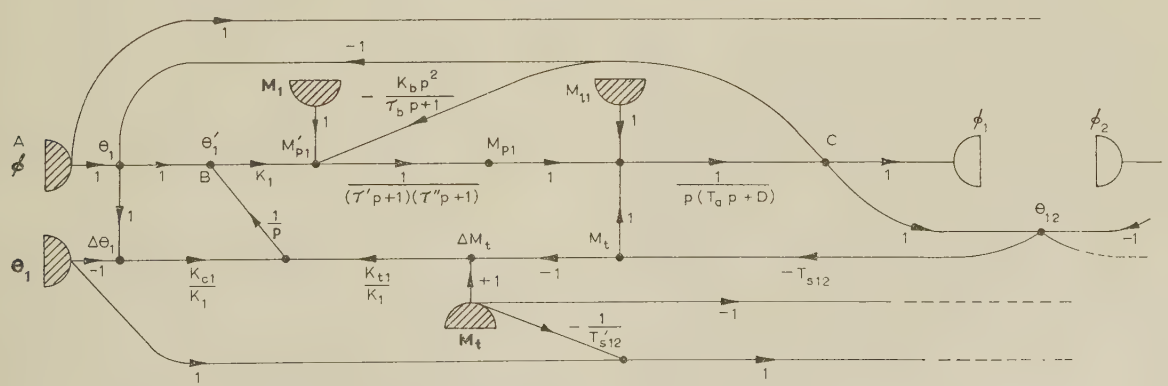

Fig. 4.—Flow diagram of a time-governed set or area with integral of time-error and tie-line controllers.

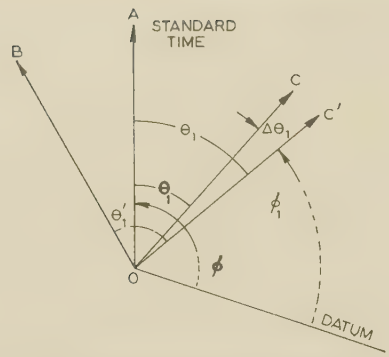

Fig. 5.—Angle or electrical time diagram indicating node values of Fig. 4.

(2.4) Integral of Time-Error Governor (with Tie-Line Control)

This configuration of control (Fig. 6) gives the correct steady-state conditions for the interconnected system; it remains to discover if they are ever reached owing to the dynamic errors

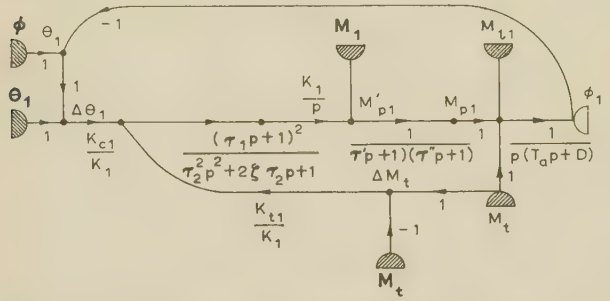

Fig. 6.—Flow diagram of a set with integral of time-error and tie-line controllers.

being considerable in magnitude and duration for normal power-system parameters.

The optimum form of stabilizing for this system is a series transmittance of $(\tau_1 p + 1)^2/(\tau_2^2 p^2 + 2\zeta\tau_2 p + 1)$ where $\tau_1 \simeq T_a/D$.

(3) COMPARISON OF CONTROLLERS

It was mentioned earlier that this analysis is mainly directed at optimizing the control of tie-line power transfer, which must be done consistently with satisfactory operation of the areas as individual units. This involves, first, choosing the type of system (proportional, integral, etc.) controlling the variables which affect the tie-line power transfer in any way, and secondly, obtaining the correct values of the parameters of these controlling systems to give optimum control on the criterion of minimum integral square error of tie-line power transfer, frequency and system angle with respect to the time standard.

It is clear that, as a steady-state value of zero is required for the tie-line power deviation from its scheduled value, an integral type of controller is necessary. This is common to all modern systems[3,4,5] and can be identified as the feedback loop including K_t/p from M_t to M_p in Figs. 2, 3, 4 and 6.

Depending on the parameters, a control of this nature, in the absence of any other feedback control, can produce incorrect operation in a system consisting of areas coupled by tie-lines. Consider the two-area case; a load increase in area 1 involves a contribution by the machines in both areas, the contribution from area 2 causing a tie-power deviation in the direction towards area 1. Suppose the tie controller, as a result of the signal received, throttles-up the prime movers in area 1; it must, by the same token, throttle-down those in area 2. This last action is incorrect as the load has not changed in area 2. The tie controller's action is identical in the case of a load decrease in area 2 except that now the act of throttling-up area 1 is incorrect. The final result could be hunting between the areas through the tie-line.

The feedback loops involving frequency-biasing (the K/p path of Fig. 2), load-phase control (the K/p path of Fig. 3) or time-error governing (the K path of Fig. 4), assist correct operation. The action of each of these paths is identical in that they detect the increment in time error consequent upon a load increase and generate a signal tending to throttle-up the machines of both areas.

For the above example of a load increase in area 1, this controller (or time-error governor) produces, in the steady state, a signal directing throttling-up action in area 2 in opposition to the signal directing throttling-down action received from the tie-line controller. Thus the tie-line deviation is allowed to decrease to zero in a relatively short time.

It is commonly held that, for a speed-governed system, optimum values of K, K_t and δ are given by

$$\frac{1}{\delta} = \frac{K}{K_t} \quad . \quad . \quad . \quad . \quad . \quad . \quad . \quad . \quad (7)$$

This is a steady-state relationship relating to a possible state of affairs at the node A of Fig. 2; for the system parameters investigated here, the dynamic equivalence of signals from speed governor and tie-line controller is not given by the above relationship. The same remarks apply to the postulation that K should be equal numerically to the ratio K_c/K_t of Fig. 4.

In comparing the systems of Figs. 2, 3 and 4 it can be seen that they have certain similarities. First, although for practical accuracy reasons the angle is measured in the time-error system while the frequency is integrated in the other two systems, mathematically the results are identical. Secondly, the speed-governor signal of Fig. 2 which can be considered as a feedback stabilizing signal, is replaced in Fig. 4 by more efficient stabilizing feedback, $K_b p^2/(\tau_b p + 1)$, while the system of Fig. 3 operates without stabilizing but at a reduced gain. Thirdly, all three systems basically require time correction in the nature of a contribution to M_p of the form $K_c\Delta\omega/p^2$ or $K_c\Delta\theta/p$. However, if K can be kept reasonably high, the time error will be tolerable enough for most purposes, particularly if a drift-free type of pick-off for time error is used, as in the case of Fig. 4. Alternatively, if a low value of K_c is used in Fig. 4 (and there does not seem much point practically in making it high) then the reference θ_1 can be the same as standard time, an arrangement which makes the practical circuits much simpler.

(4) RESULTS OF QUANTITATIVE STUDY

In this Section the effectiveness of the various control schemes for interconnected systems will be compared by considering the integral square errors of the controlled variables following a step load impact of 0·1 p.u. in one area. These errors have been evaluated by analogue computer, the system being linearized by taking small departures about full load. The extent of interconnection has been limited to two areas, and to simplify the problem further, these have been chosen as identical since this represents the most critical case.

(4.1) Operation of One Area in Isolation

The operation of one area in isolation is not presented in detail but the results are summarized in Table 1. The parameters for

Table 1

OPTIMUM ISOLATED SYSTEMS

Type of control	(1) Speed governor with integral of frequency loop operative	(2) Integral of speed control	(3) Time-error governor	(4) Integral of time-error control
Variable parameters	$\delta = 0{\cdot}043$ $K = 0{\cdot}05$ p.u./rad	$K = 0{\cdot}01$ p.u./rad	$K = 0{\cdot}1$ p.u./rad $K_b = 7\,400$ p.u./rad/time-rad^2 $\tau_b = 314$ time-rad $= 2$ sec	$K_c = 0{\cdot}000\,04$ p.u./rad $\times$ time-rad $\tau_1 = T_a/D$ time-rad $\tau_2 = 15{\cdot}7$ time-rad $= 0{\cdot}1$ sec $\zeta = 0{\cdot}1$
I.S.E. of speed for 0·1 p.u. step load	0·011 5 rad^2/time-rad	0·259	0·010 7	0·108
Invariable parameters	$T_a = 1\,050$ time-rad $= 6{\cdot}7$ sec $\tau' = \tau'' = 65$ time-rad $= 0{\cdot}42$ sec		$D = 3$ p.u./rad/time-rad	

each area have been optimized by using as a criterion the degree of stability of the governor response to a step load disturbance combined with low integral square errors of speed for the area when isolated. These values form a basis for setting up the interconnected study.

(4.2) Interconnected Operation

Curves 1(*a*), 2(*a*) and 3(*a*) of Fig. 7 are for interconnected operation of systems 1, 2 and 3 of Table 1 and show integral

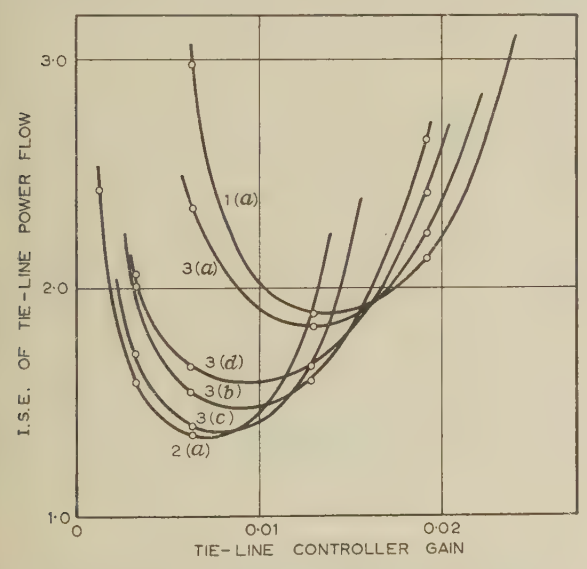

Fig. 7.—Effect of governors on tie-line power flow.

$T_a = 6{\cdot}7$ sec, D $= 3$ p.u./rad/time-rad
$\tau' = \tau'' = 0{\cdot}42$ sec, $T_{s12} = 0{\cdot}5$ p.u./rad

Curve 1(*a*).—Speed governor. $K = 0{\cdot}05$ p.u./rad $\delta = 0{\cdot}043$
Curve 2(*a*).—Integral of speed governor. $K = 0{\cdot}01$ p.u./rad
Curve 3(*a*).—Time-error governor. $K = 0{\cdot}1$ p.u./rad, $K_b = 7\,400$ p.u./rad/time-rad^2, $\tau_b = 2$ sec
Curve 3(*b*).—$K = 0{\cdot}06$ p.u./rad, $K_b = 8\,600$, $\tau_b = 4$ sec
Curve 3(*c*).—$K = 0{\cdot}02$, $K_b = 8\,600$, $\tau_b = 8$ sec
Curve 3(*d*).—$K = 0{\cdot}1$, $K_b = 8\,600$, $\tau_b = 4$ sec

square error of the tie-line power flow plotted against tie-line controller gain, K_t, for a tie-line synchronizing torque coefficient of 0·5 p.u./rad. The interesting result is that system 2, integral of speed control, allows the lowest integral square error for the tie power despite the large frequency and time errors due to low governor gain. Curves 1(*a*) and 3(*a*) show that high-gain speed and time-error governors behave very similarly as regards tie power errors, and the minimum integral square error obtainable from each system is almost the same and about 50% greater than for system 2. It would appear that increasing governor gain adversely affects tie power errors. This view is further confirmed by considering curves 3(*a*), 3(*b*) and 3(*c*) which show that reducing the time-error governor gain does reduce the tie power errors. However, it should be noted that for each value of governor gain the feedback stabilizing has been adjusted to give suitably stable governor responses.

In order to separate the effect of governor and stabilizing loops on tie power, curve 3(*d*) was obtained for a system having the same governor gain as 3(*a*), but with feedback stabilizing identical to that used for curve 3(*b*). The minimum error for 3(*d*) is greater than for 3(*b*), indicating that increasing the gain of the time-error loop does increase tie power errors, but less than for 3(*a*) which indicates that a reduced time-constant in the feedback stabilizing loop also adversely affects control of tie power. The important point is that both time-error and stabilizing loops affect the integral square error for tie-line power flow. By making either of these loops more responsive the tie power errors are increased.

Curves 1(*a*) and 3(*b*) enable speed and time-error governors of approximately equal gains ($K = 0{\cdot}05$ and 0·06 respectively) to be compared and they show that the latter system is superior in controlling tie power errors. The conclusion here is that the $K_b p^2/(\tau_b p + 1)$ loop of the time-error governor does not adversely affect the tie-line power swings as much as does the speed feedback loop of the speed governor.

Comparison of curves 3(*a*), 3(*c*) and 3(*b*) shows that, by introducing stabilizing feedback, $K_b p^2/(\tau_b p + 1)$, into system 2 (thereby obtaining a time-error system) the governor gain can be increased by a factor of 2 or 3 with very little adverse effect on tie power errors and considerable improvement in frequency and time control.

To compare speed and time-error systems further and to study the effect of strength of tie between areas the results shown in Fig. 8 were obtained. The similarity between the two systems already observed for $T_{s12} = 0{\cdot}5$ is equally apparent for $T_{s12} = 1$ and 0·1 p.u./rad.

More important is the variation of the integral square errors of tie power with T_{s12}. For T_{s12} equal to 0·5 p.u./rad these errors have a maximum, which means that interaction between area control loops and power transfer between areas is most critical in this range. Therefore its choice for the results of Fig. 7 emphasized the characteristics dependent on interaction between governor and tie power loops which were observed in this Figure.

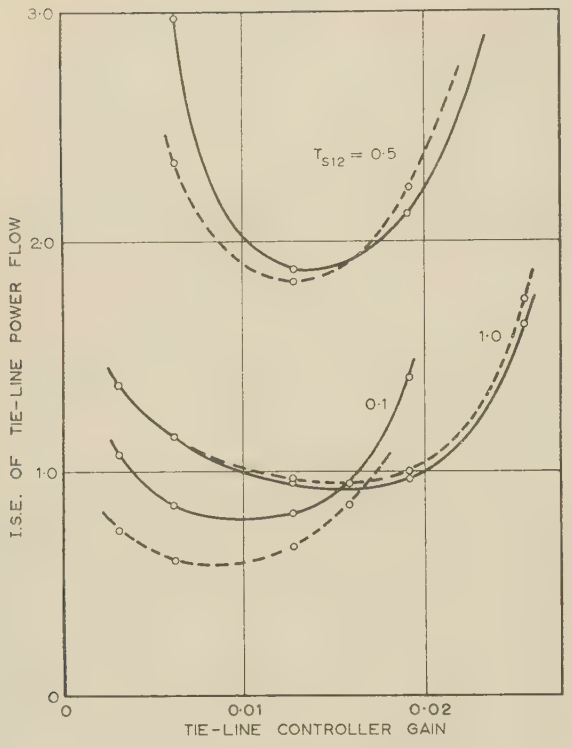

Fig. 8.—Effect of T_{s12} on tie-line power flow.
—— Speed governor.
---- Time-error governor.
Parameters as listed for respective governors in Table 1.

Table 2

EFFECT OF K_c ON INTEGRAL SQUARE ERROR OF TIE-LINE POWER FLOW

K_t	I.S.E. for $K_c = 0$	I.S.E. for $K_c = 0·000\,13$
0·0064	2·36	2·04
0·0127	1·82	1·80
0·0191	2·23	2·23

$T_{s12} = 0·5$ p.u./rad. Other parameters as listed in Table 1, column 3.

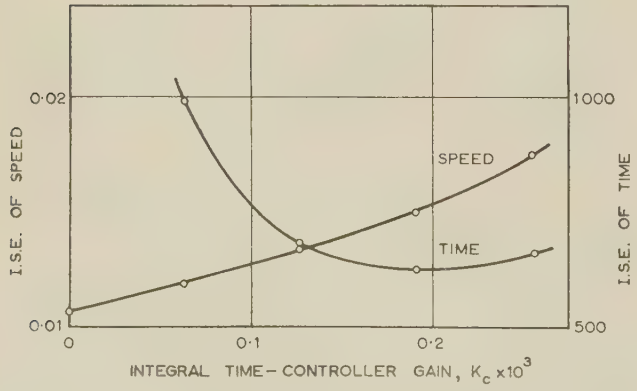

Fig. 9.—Effect of integral of time controller on time-error governor of an isolated system.
Parameters as listed for time-error governor in Table 1.
$T_{s12} = 0$, $K_t = 0$

It has been pointed out that a continuously acting integral-of-time controller can be added to the time-error governor, and tests indicate that a comparatively high gain is feasible. Table 2 shows that a value of K_c equal to 0·000 13 p.u./rad time-rad does not seriously affect the integral square errors of tie power flow. Fig. 9 shows first, that K_c does increase integral square errors of speed in an isolated area but not very rapidly; secondly, that K_c can be chosen so as to minimize integral square errors of time. These two results are also true in an interconnected system.

(5) CONCLUSIONS

In an interconnected system there are three controlled variables to be considered—frequency, time, and tie-line power flow—and results show that only one of these can be optimized by suitably adjusting whatever control system is chosen. The choice of system determines the minimum errors obtainable, one system being best suited for small tie-line errors, another giving the lowest frequency errors.

To keep accurate frequency and time, high-gain governors such as system 1 or 3 are required, and these systems give tie-line errors greater than those obtained when using system 2.

Comparing systems 1 and 3, the time-error governor can be designed with the higher gain and has the lower integral square errors for frequency and time. When each system is designed for maximum gain ($K = 0·05$ and $0·1$ p.u./rad, respectively), they each have approximately equal integral square errors for tie-line power flow. If the gain of the time-error system is reduced to equal that of the speed governor ($K = 0·05$ p.u./rad) it gives similar frequency and time errors, but the integral square errors of tie power are now about 75% of those for the speed system.

System 2, integral of speed control, gives the lowest integral square error for tie-line power but has the disadvantage of large frequency errors. A low-gain time-error governor having much lower frequency and time error can be designed to give tie-line power errors almost as low as those for system 2.

A time-error system with a gain of 0·06 p.u./rad gives a minimum integral square error for tie-line power which is only about 10% greater than that for system 2 and has frequency and time errors as low as those obtainable with the best possible speed governor. Such a system appears to offer the best compromise for frequency and tie-line control. If desirable, a low-gain integral of time-error loop can be added to this system causing a small increase in frequency error (about 10%) but without any serious increase in tie-line power error.

(6) ACKNOWLEDGMENTS

The authors are indebted to Mr. C. P. Gilbert, Officer in Charge of Utac, the analogue computer at the School of Electrical Engineering, University of New South Wales, for his assistance in this study.

(7) REFERENCES

(1) KELLER, R.: 'Operating Results with New Method of Frequency—Biased Tie-Line Control', *Brown Boveri Review*, 1945, **32**, p. 223.
(2) BROADBENT, D.: 'Integral Governing of Turbo-Alternators', *Electrical Engineer* (Melbourne), 1953, **29**, p. 354.
(3) CONCORDIA, C., and KIRCHMAYER, L. K.: 'Tie-Line Power and Frequency Control of Electric Power Systems', *Transactions of the American I.E.E.*, 1953, **72**, Part II, p. 562.

(4) CAHEN, F., and CHEVALLIER, A.: 'Le réglage puissance-phase. Nouvelle méthode pour le réglage automatique de la fréquence d'un réseau comportant de multiples usines génératrices', *Bulletin de la Société Française des Électriciens*, 1953, **3** (VII), No. 34.
(5) BROADBENT, D.: 'Governing in Power Systems by Time-Error', *Proceedings I.E.E.*, Monograph No. 200, September, 1956 (**104** C, p. 130).
(6) BROADBENT, D.: 'Time-Error Control for Interconnected Synchronous Electric Power Systems', *Transactions of the American I.E.E.*, 1958, **77**, Part III, p. 1554.
(7) TRUXAL, J. G.: 'Automatic Feedback Control System Synthesis' (McGraw-Hill, 1955).
(8) BROADBENT, D.: Discussion contribution, *Proceedings I.E.E.*, 1960, **107** A, p. 399.

(8) APPENDICES

(8.1) Signal Flow Diagram

The signal flow diagram is an alternative to the block diagram in the representation of an interconnected system and its reduction in a systematic form. The values of system variables are indicated by the values of the nodes connected to each other by transmittances, the independent variables being the input nodes, shown as hatched semicircles. The diagram has a particular advantage when considering complex interconnected systems, in that the variables are immediately available for inspection and the factors influencing their values are clearly discernible if the incoming paths to the respective nodes are inspected.

The signal flow diagram is drawn from the n simultaneous equations of the system; these are written in terms of the n dependent variables and their coefficients which contain the system parameters and the operator p. The compilation of the diagram involves simply multiplying a node value by the outgoing transmittance to obtain the contribution to the adjacent node; naturally the dimensions of the nodes and transmittance must be correct.

For example, if the per-unit torque equations of two machines coupled by a tie are written for small departures from the steady state we get

$$\Delta M_{l1} + \Delta M_t + T_{a1}p\Delta\omega_1 + D_1\Delta\omega_1 + \Delta M_{p1} = 0 \quad . \quad (8)$$

$$\Delta M_t + T_{a2}p\Delta\omega_2 + D_2\Delta\omega_2 + \Delta M_{p2} = 0 \quad . \quad . \quad (9)$$

We may rewrite eqn. (8) for the dependent variable, $\Delta\omega_1$, and choosing its sign for convenience,

$$\Delta\omega_1 = \frac{1}{T_ap + D}(\Delta M_{l1} + \Delta M_t + \Delta M_{p1})$$

or

$$\Delta\theta_1 = \frac{1}{p(T_ap + D)}(\Delta M_{l1} + \Delta M_t + \Delta M_{p1}) \quad . \quad (10)$$

The torque from the prime mover, ΔM_{p1}, can only be controlled through the throttle servo motor and the steam header, each of which can be considered to have a time-constant. Let the torque deviation in the absence of these two elements be $\Delta M'_{p1}$. Then eqn. (10) becomes

$$\Delta\theta_1 = \frac{1}{p(T_ap + D)}\left[\Delta M_{l1} + \Delta M_t + \frac{\Delta M'_{p1}}{(\tau'p + 1)(\tau''p + 1)}\right] \quad . \quad (11)$$

This is the equation representing small departures from the node values given in Fig. 1.

A similar diagram may be obtained for the second machine through eqn. (9), and the two diagrams may be connected by using eqn. (12):

$$\Delta M_t = \frac{T_{s12}}{p}\Delta\omega_1 - \frac{T_{s12}}{p}\Delta\omega_2 \quad . \quad . \quad . \quad (12)$$

This leads to the interconnection shown in Figs. 2 and 4 and implied in Figs. 3 and 6. It will be seen from Fig. 2 that the signal flow diagram allows the steady-state quantities, e.g. M_t, and the scheduled quantities, e.g. M_t, to be explicitly shown, as well as the incremental quantities or errors.

(8.2) Derivation of the Per-Unit Torque Equation of a Closely Coupled Area

Let ω_b be the base speed of rotation of the machine, from which time may be measured in time radians, the angle swept out by a vector rotating at ω_b for the period concerned. Then 1 sec equals ω_b time-rad. If

D = p.u. damping torque/p.u. slip
= p.u. damping torque/p.u. departure from ω_b
= p.u. damping torque/rad angular displacement/time-rad,

then DT_b = damping in torque units/rad/time-rad
where T_b = base torque in torque units.

For a change in speed of $p\Delta\phi$ rad/sec the damping torque equals $DT_bp\Delta\phi/\omega_b$ torque units, where the units of p are sec^{-1}. The torque equation is then

$$Jp^2\Delta\phi + DT_p\frac{p\Delta\phi}{\omega_b} + \Delta T_b + \Delta T_l = 0 \quad . \quad . \quad (13)$$

where J is the moment of inertia of the rotating parts, ΔT_p is the prime-mover torque change and ΔT_l is the load torque change. If we define the starting time as $J\omega_b/T_b$ sec, then $T_a = J\omega_b^2/T_b$ time-rad.

Substituting for J in eqn. (13),

$$T_a\frac{p^2}{\omega_b^2}\Delta\phi T_b + DT_b\frac{p\Delta\phi}{\omega_b} + \Delta T_p + \Delta T_l = 0$$

or

$$T_a\frac{p^2\Delta\phi}{\omega_b^2} + D\frac{p\Delta\phi}{\omega_b} + \Delta M_p + \Delta M_l = 0$$

Changing the units of p from sec^{-1} to rad^{-1}, we get

$$T_ap^2\Delta\phi + Dp\Delta\phi + \Delta M_p + \Delta M_l = 0 \quad . \quad . \quad (14)$$

(8.3) Derivation of Controller Equations

This Section is concerned with the way in which the feedback paths of the several controllers and governors influence the value of M'_{p1} in Figs. 1, 2, 3, 4 and 6. The node M'_{p1} has the units of per-unit torque, whence gain constants will be contained in the incoming transmittances.

Between M'_{p1}, the torque at the turbine if there were no throttle servo-motor time lag, τ'', or steam-header time lag, τ', and M_{p1}, the actual torque at the turbine, is the transmittance $1/(\tau''p + 1)(\tau'p + 1)$. This may be explained physically if we say that M'_{p1} is the torque equivalent of the input movement of the servo motor (the flyball collar movement of a speed governor) and M''_{p1} is the torque equivalent of the actual movement of the throttle. The transmittance between M'_{p1} and M''_{p1} is then $1/(\tau''p + 1)$. The torque equivalent of the actual steam available is M_{p1}, and hence the transmittance between M''_{p1} and M_{p1} is

$1/(\tau' p + 1)$. It will be seen that this is an approximation and only justified if small departures are taken.

(8.3.1) **Speed Governor.**

The per-unit regulation of a speed governor is defined as the per-unit change in speed for 1·0p.u. change in torque. The incremental value, δ, has the same basis, and hence the incremental gain of the governor is $1/\delta$ p.u. change in torque/p.u. change in speed. For a simple speed governor, therefore,

$$M_p' = \frac{1}{\delta}\Delta\omega \quad . \quad . \quad . \quad . \quad . \quad . \quad . \quad (15)$$

(8.3.2) **Integral-of-Speed Governor.**[4]

The mechanism of the integral-of-speed governor integrates the speed change over a period measured from a certain point in time. It therefore produces a signal depending on the angle associated with this speed change. For small increments the mathematical treatment is the same as that of the time-error governor. For a simple integral-of-speed governor,

$$M_p' = K\frac{\Delta\omega}{p} \quad . \quad . \quad . \quad . \quad . \quad . \quad . \quad (16)$$

(8.3.3) **Time-Error Governor.**[5]

The time-error governor measures the actual angle between the machine rotor and standard time, the torque of the prime mover being made proportional to this angle:

$$M_p' = K\Delta\theta \quad . \quad . \quad . \quad . \quad . \quad . \quad . \quad (17)$$

There is no steady-state speed error with this system.

(8.3.4) **Integral-of-Time-Error Controller.**

The integral-of-time-error controller integrates the angle by which the machine rotor lags on standard time, and applies a corrective torque at the turbine proportional to the integral. In a miniature system on which References 5 and 6 were based, this function was performed by an electrical circuit involving operational amplifiers. In conventional power systems, it is often done by a throttle inching control on the speed-setting screw operated from a time clock. This component to turbine torque is

$$K_c\frac{\Delta\theta}{p}\,\frac{1}{(\tau' p + 1)(\tau'' p + 1)}$$

(8.3.5) **Integral-of-Tie-Power-Error Controller.**

The tie-power-error controller measures the deviation in tie power from its scheduled value and provides a correcting torque at the prime mover proportional to the time integral of this deviation, i.e.

$$K_t\frac{\Delta M_t}{p}\,\frac{1}{(\tau' p + 1)(\tau'' p + 1)}$$

It can work in conjunction with the controller of Section 8.3.4 and can, with advantage, employ the same control circuits.

621.318.132:621.374.32

The Institution of Electrical Engineers
Monograph No. 396 M
Sept. 1960

THE MAGNETIC EXCITATION INSIDE A CYLINDRICAL THIN-FILM FERROMAGNET

By T. H. O'DELL, B.Sc., Graduate.

(*The paper was first received* 11*th February, and in revised form* 9*th June*, 1960. *It was published as an* INSTITUTION MONOGRAPH *in September* 1960.)

SUMMARY

An expression for the magnetic excitation inside a cylindrical thin-film ferromagnet is derived, and a Table of computed values is given. The results are considered to be relevant to work on thin ferromagnetic films for digital-storage applications.

LIST OF PRINCIPAL SYMBOLS

$\boldsymbol{B}$ = Magnetic field strength, Wb/m^2.
$\boldsymbol{H}$ = Magnetic excitation, A/m.
$\boldsymbol{M}$ = Magnetization, A/m.
ψ = Magnetostatic potential, A.
$\mu_0 = 4\pi \times 10^{-7}$ henry/m.
b = Mean radius of the cylindrical thin film, m.
a = Half length of the cylindrical thin film, m.
δ = Thickness of the cylindrical thin film, m.

(1) INTRODUCTION

When the direction of magnetization in a very thin film of ferromagnetic material is reversed, by the application of a strong reversing field, the formation and movement of domain walls in the film should be prohibited by energy considerations,[1] and the magnetic reversal should take place as a uniform procession of magnetization throughout the entire volume of the film.

This effect, which should occur in films about $0{\cdot}2\,\mu$ thick, has been discussed by several authors and has been demonstrated experimentally.[2,3] Because the magnetic reversal should take place very rapidly under these conditions, the use of a thin film as the element of a high-speed digital store has been proposed.

Fig. 1 shows one of the forms that a thin-film storage element

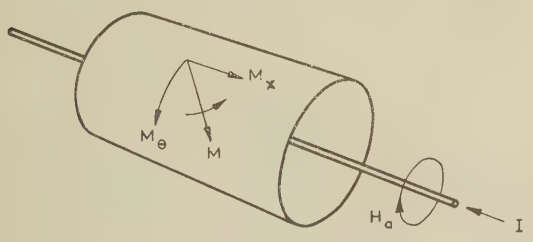

Fig. 1.—A thin-film storage element.

could have. The film is deposited round a cylindrical substrate, and the store is built up from several of these elements, used in a similar way to the familiar ferrite toroids. As the direction of M_θ is reversed in an element, the vector $\boldsymbol{M}$ will rotate. Energy considerations, however, will prevent any considerable component of magnetization being produced in the radial direction during this rotation, so that a component M_z must be produced that rises to a maximum value, nearly equal to the saturation magnetization, and falls to near zero again as the reversal is completed. Unless the film is infinitely long this will mean that a component of excitation H_z, in opposition to M_z, will be produced inside the film during reversal. This so-called 'demagnetizing excitation' will have a considerable effect on the magnetic reversal[5] unless it is negligible in comparison with the applied excitation H_a.

An alternative arrangement for a cylindrical storage element has been proposed,[4] where the cylindrical elements are normally magnetized in the axial direction and the reversing field is produced by solenoidal windings around the film. In this case the demagnetizing excitation affects both the static and dynamic behaviour of the film.

In this paper a general expression is obtained for the magnetic excitation inside a thin cylindrical film, and a Table of computed values is given for a range of length/diameter ratios. The calculation is a magnetostatic one, so that any application to the dynamic problem of magnetic reversal must be under quasi-static conditions.

(2) THEORETICAL CONSIDERATIONS

The equations of the magnetostatic field are[6]

$$\text{curl}\,\boldsymbol{H} = 0 \quad . \quad . \quad . \quad . \quad . \quad . \quad . \quad . \quad (1)$$

$$\text{div}\,\boldsymbol{B} = 0 \quad . \quad . \quad . \quad . \quad . \quad . \quad . \quad . \quad (2)$$

$$\boldsymbol{B} = \mu_0(\boldsymbol{H} + \boldsymbol{M}) \quad . \quad . \quad . \quad . \quad . \quad (3)$$

so that, from eqns. (2) and (3),

$$\text{div}\,\boldsymbol{H} = -\,\text{div}\,\boldsymbol{M} \quad . \quad . \quad . \quad . \quad . \quad (4)$$

In view of eqn. (1), $\boldsymbol{H}$ may be described by

$$\boldsymbol{H} = -\,\text{grad}\,\psi \quad . \quad . \quad . \quad . \quad . \quad . \quad (5)$$

so that, from eqns. (4) and (5),

$$\nabla^2\psi = \text{div}\,\boldsymbol{M} \quad . \quad . \quad . \quad . \quad . \quad . \quad (6)$$

is obtained as the equation of the magnetostatic field. Given a complete description of $\boldsymbol{M}$ within a ferromagnetic body, eqn. (6) may be integrated as follows.

Consider a ferromagnetic body in any state of magnetization. Let $\boldsymbol{n}$ and $\boldsymbol{n}'$ be unit vectors normal to the surface of the body, $\boldsymbol{n}$ pointing out of the body and $\boldsymbol{n}'$ into it. In view of eqn. (2) the normal component of $\boldsymbol{B}$ must be continuous across the surface of the ferromagnet, so that eqn. (3) gives

$$\frac{\partial\psi}{\partial n} + \frac{\partial\psi}{\partial n'} = \boldsymbol{M}\,.\,\boldsymbol{n}' \quad . \quad . \quad . \quad . \quad . \quad (7)$$

Eqn. (6) can now be integrated using the boundary condition (7) and the condition that ψ vanishes sufficiently strongly at infinity, by the usual application of Green's theorem.[7] The result is

$$\psi = \frac{-1}{4\pi}\int_v \frac{\text{div}\,\boldsymbol{M}}{r_{ik}}\,dv - \frac{1}{4\pi}\int_s \frac{\boldsymbol{M}\,.\,\boldsymbol{n}'}{r_{ik}}\,ds \quad . \quad . \quad . \quad (8)$$

Correspondence on Monographs is invited for consideration with a view to publication.

Mr. O'Dell is at the U.K.A.E.A. Atomic Energy Research Establishment.

where the volume integral is taken throughout the entire volume of the ferromagnet, the surface integral over its entire inside surface, and r_{ik} is the distance from the point of integration, i, to the point k at which ψ is to be evaluated. The point k can be either inside or outside the ferromagnet.

Having determined ψ at any point, the excitation $\boldsymbol{H}$ is found by using eqn. (5).

(3) THE INTERNAL EXCITATION OF A THIN CYLINDRICAL FILM

Consider the cylindrical thin film shown in Fig. 2, set in cylindrical co-ordinates (r, θ, z).

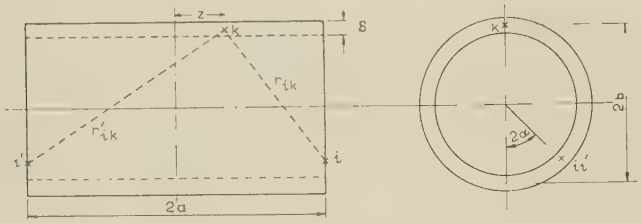

Fig. 2.—A cylindrical thin film.

It will be assumed that the film is uniformly magnetized, so that

$$\operatorname{div} \boldsymbol{M} = 0 \quad . \quad . \quad . \quad . \quad . \quad . \quad . \quad (9)$$

which implies that the film is a single ferromagnetic domain.

It will also be assumed that the film is extremely thin, so that

$$\left.\begin{aligned} \delta &\ll b \\ \delta &\ll a \end{aligned}\right\} \quad . \quad . \quad . \quad . \quad . \quad . \quad . \quad (10)$$

and that ψ is to be evaluated only at points where $r = b$ and z is such that

$$(a - |z|) \gg \delta \quad . \quad . \quad . \quad . \quad . \quad . \quad . \quad (11)$$

Under these conditions, if

$$\alpha = \left(\frac{\pi - \theta}{2}\right) \quad . \quad . \quad . \quad . \quad . \quad . \quad . \quad (12)$$

r_{ik} and r'_{ik} (Fig. 2), occurring in eqn. (8), can be written approximately as

$$\left.\begin{aligned} (r_{ik})^2 &= (a - z)^2 + 4b^2(1 - \sin^2 \alpha) \\ (r'_{ik})^2 &= (a + z)^2 + 4b^2(1 - \sin^2 \alpha) \end{aligned}\right\} \quad . \quad . \quad (13)$$

because, provided condition (11) is satisfied, the variation in r_{ik} with r can be neglected. Similarly ds is simply

$$ds = 2b\delta d\alpha \quad . \quad . \quad . \quad . \quad . \quad . \quad . \quad (14)$$

Now if

$$(k_1)^2 = \frac{(2b/a)^2}{(2b/a)^2 + (1 - z/a)^2} \quad . \quad . \quad . \quad (15)$$

and

$$(k_2)^2 = \frac{(2b/a)^2}{(2b/a)^2 + (1 + z/a)^2} \quad . \quad . \quad . \quad . \quad (16)$$

substitution of eqns. (9), (13), (14), (15) and (16) into eqn. (8) gives

$$\psi = \frac{M_z\delta}{2\pi} \int_0^{\pi/2} \left\{ \frac{k_1}{[1 - (k_1)^2 \sin^2 \alpha]^{1/2}} - \frac{k_2}{[1 - (k_2)^2 \sin^2 \alpha]^{1/2}} \right\} d\alpha \quad . \quad . \quad . \quad . \quad (17)$$

so that

$$\psi = \frac{M_z\delta}{2\pi}[k_1 K(k_1) - k_2 K(k_2)] \quad . \quad . \quad . \quad (18)$$

where $K(k)$ is the complete elliptic integral of the first kind.

Eqn. (18) is the required solution for ψ, subject to the condition (11) that restricts the permissible range of z. Eqn. (5) is now used to find H_z:

$$H_z = -\frac{M_z\delta}{2\pi} \left[\frac{dk_1}{dz} K(k_1) + k_1 \frac{dK(k_1)}{d(k_1)^2} \frac{d(k_1)^2}{dz} - \frac{dk_2}{dz} K(k_2) - k_2 \frac{dK(k_2)}{d(k_2)^2} \frac{d(k_2)^2}{dz} \right] \quad . \quad (19)$$

The identity[8]

$$\frac{dK(k)}{d(k)^2} \equiv \frac{E(k) - (1 - k^2)K(k)}{2k^2(1 - k^2)^{1/2}} \quad . \quad . \quad . \quad (20)$$

where

$$E(k) = \int_0^{\pi/2} (1 - k^2 \sin^2 \alpha)^{1/2} d\alpha. \quad . \quad . \quad . \quad (21)$$

and the derivatives of eqns. (15) and (16),

$$\frac{d(k_1)^2}{dz} = \frac{(k_1)^3[1 - (k_1)^2]^{1/2}}{b} \quad . \quad . \quad . \quad (22)$$

$$\frac{d(k_2)^2}{dz} = \frac{-(k_2)^3[1 - (k_2)^2]^{1/2}}{b} \quad . \quad . \quad . \quad (23)$$

can all be used to simplify eqn. (19) to

$$H_z = \frac{-M_z\delta}{4\pi b} \left\{ \frac{(k_1)^2 E(k_1)}{[1 - (k_1)^2]^{1/2}} + \frac{(k_2)^2 E(k_2)}{[1 - (k_2)^2]^{1/2}} \right\} . \quad (24)$$

Eqn. (24) is the required result for the internal excitation as a function of z/a, b/a and δ/b. The result depends upon condition (11) being satisfied, however, so that eqn. (24) cannot be used to calculate H_z at the very ends of the cylinder, where $z = \pm a$, because the integrand of eqn. (17) has a singularity at $z = \pm a$ due to the use of eqn. (13) as an approximation for r_{ik}.

In order to calculate H_z when

$$0 \leqslant (a - |z|) \sim \delta \quad . \quad . \quad . \quad . \quad . \quad (25)$$

it is assumed, in view of eqns. (10) and (25), that one end of the cylinder can be approximately represented by the flat infinite half-film shown in Fig. 3. The effect of the other end of the film is therefore neglected, and ψ is evaluated at points on the line $x = 0$, $y = 0$.

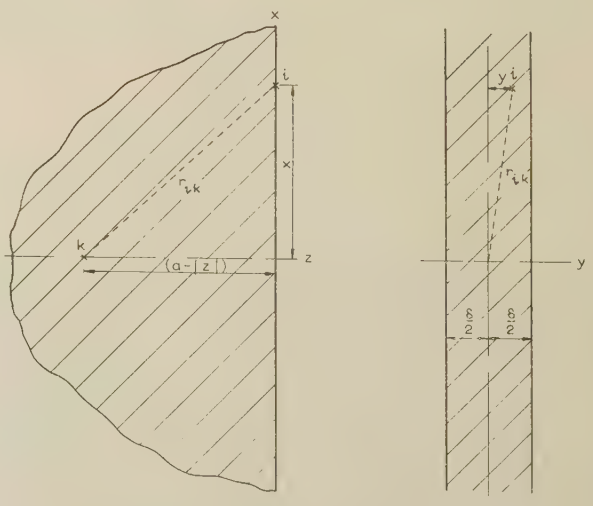

Fig. 3.—The flat infinite half-film representing one end of the cylinder.

Table 1

VALUES OF $D(z/a, b/a)$

z/a \ b/a	3·0	2·0	1·5	1·0	0·75	0·5	0·4	0·3	0·2	0·15	0·10	0·08	0·06	0·05
	×1	×1	×1	×1	×1	×1	×1	×10⁻¹	×10⁻¹	×10⁻¹	×10⁻²	×10⁻²	×10⁻²	×10⁻²
0·00	0·9765	0·6602	0·5004	0·3355	0·2476	0·1520	0·1117	0·7178	0·3582	0·2110	0·9711	0·6280	0·3562	0·2481
0·05	0·9789	0·6617	0·5016	0·3363	0·2482	0·1525	0·1121	0·7211	0·3603	0·2124	0·9779	0·6325	0·3588	0·2500
0·10	0·9861	0·6665	0·5051	0·3386	0·2500	0·1539	0·1133	0·7312	0·3667	0·2165	0·9987	0·6463	0·3668	0·2556
0·15	0·9983	0·6746	0·5111	0·3426	0·2530	0·1563	0·1154	0·7483	0·3776	0·2237	1·035	0·6700	0·3805	0·2652
0·20	1·016	0·6862	0·5198	0·3483	0·2575	0·1597	0·1184	0·7728	0·3934	0·2341	1·087	0·7049	0·4007	0·2794
0·25	1·040	0·7019	0·5314	0·3560	0·2634	0·1642	0·1224	0·8054	0·4146	0·2482	1·158	0·7526	0·4284	0·2989
0·30	1·070	0·7221	0·5464	0·3659	0·2710	0·1699	0·1275	0·8470	0·4421	0·2666	1·253	0·8159	0·4653	0·3249
0·35	1·109	0·7476	0·5654	0·3785	0·2807	0·1771	0·1338	0·8989	0·4769	0·2903	1·376	0·8986	0·5137	0·3590
0·40	1·157	0·7796	0·5891	0·3942	0·2926	0·1860	0·1415	0·9626	0·5206	0·3205	1·535	1·006	0·5769	0·4037
0·45	1·217	0·8194	0·6189	0·4138	0·3076	0·1968	0·1509	1·041	0·5750	0·3587	1·742	1·147	0·6599	0·4625
0·50	1·293	0·8694	0·6568	0·4384	0·3262	0·2102	0·1624	1·136	0·6428	0·4075	2·011	1·331	0·7701	0·5409
0·55	1·388	0·9327	0·7031	0·4696	0·3498	0·2268	0·1765	1·252	0·7277	0·4699	2·366	1·578	0·9190	0·6473
0·60	1·511	1·014	0·7637	0·5097	0·3800	0·2479	0·1943	1·397	0·8347	0·5506	2·843	1·915	1·125	0·7953
0·65	1·672	1·121	0·8435	0·5625	0·4196	0·2752	0·2170	1·581	0·9714	0·6566	3·496	2·386	1·419	1·008
0·70	1·890	1·266	0·9518	0·6343	0·4734	0·3117	0·2471	1·820	1·150	0·7981	4·415	3·066	1·853	1·327
0·75	2·200	1·472	1·106	0·7363	0·5499	0·3632	0·2890	2·148	1·391	0·9924	5·745	4·084	2·529	1·832
0·80	2·669	1·784	1·339	0·8914	0·6659	0·4409	0·3517	2·631	1·737	1·272	7·753	5·682	3·644	2·688
0·85	3·456	2·308	1·732	1·152	0·8613	0·5711	0·4562	3·423	2·288	1·710	10·98	8·355	5·636	4·280
0·90	5·040	3·363	2·523	1·679	1·255	0·8333	0·6659	4·999	3·354	2·533	16·91	13·37	9·614	7·635
0·95	9·807	6·541	4·905	3·265	2·444	1·625	1·299	9·738	6·513	4·912	33·14	26·71	20·18	16·81

Here
$$(r_{ik})^2 = (a - |z|)^2 + x^2 + y^2 \quad . \quad . \quad . \quad (26)$$

and
$$ds = dxdy \quad . \quad . \quad . \quad . \quad . \quad . \quad . \quad (27)$$

so that, from eqns. (9), (26) and (27), eqn. (8) becomes

$$\psi = \frac{M_z}{4\pi} \int_{-\infty}^{+\infty} \int_{-\delta/2}^{+\delta/2} \frac{dydx}{[(a - |z|)^2 + x^2 + y^2]^{1/2}} \quad . \quad (28)$$

From eqn. (5),

$$H_z = \frac{-M_z}{4\pi} \int_{-\infty}^{+\infty} \int_{-\delta/2}^{+\delta/2} \frac{(a - |z|)dydx}{[(a - |z|)^2 + x^2 + y^2]^{3/2}} \quad . \quad (29)$$

Hence
$$H_z = \frac{-M_z}{\pi} \text{ arc cot } \left[\frac{2(a - |z|)}{\delta}\right] \quad . \quad . \quad . \quad (30)$$

Eqn. (30) gives the value of H_z at the ends of the cylinder, where $z = \pm a$, and at distances of the order of δ away from the ends. Combined with eqn. (30), eqn. (24) now gives an almost complete description of the excitation inside the film.

At $z = \pm a$, eqn. (30) gives $H_z = -M_z/2$, which is a typical result for any uniformly magnetized body that has plane end faces.[6] In a real film, however, small reverse domains, of volume of the order of δ^3, would be formed round the edges of the cylinder to relieve this high value of excitation. The formation of these domains would have a negligible effect on the values of H_z well inside the cylinder, that had been calculated using eqn. (24), subject to eqn. (11), because the initial assumption of uniform magnetization is still valid over almost the entire film, div $\boldsymbol{M}$ being non-zero within a volume of the order of $2\pi b\delta^2$ at either end. In addition, the real edge of any evaporated or electrodeposited film is unlikely to be perfectly plane; a ragged edge will also reduce the value of H_z from the high value given by eqn. (30) at $z = \pm a$ because the term $\boldsymbol{M} \cdot \boldsymbol{n}'$, that occurs in eqn. (8), will be reduced.

(4) COMPUTED VALUES OF EXCITATION

In practice, δ will usually be less than one micron, while a and b will be not less than one millimetre. Condition (11) should therefore be well satisfied within the range $0 \leqslant |z| \leqslant 0{\cdot}95a$.

The ratio H_z/M_z is of primary interest, corresponding as it does to the demagnetizing factor often attributed to ellipsoidal bodies. Eqn. (24) is rewritten as

$$H_z/M_z = \frac{-\delta}{b}[D(z/a, b/a)] \quad . \quad . \quad . \quad . \quad (31)$$

where
$$D(z/a, b/a) = \frac{1}{4\pi}\left\{\frac{(k_1)^2 E(k_1)}{[(1 - (k_1)^2]^{1/2}} + \frac{(k_2)^2 E(k_2)}{[1 - (k_2)^2]^{1/2}}\right\} \quad . \quad (32)$$

Table 1 gives the computed values for $D(z/a, b/a)$ over the range, $0 \leqslant z/a \leqslant 0{\cdot}95$ and $0{\cdot}05 \leqslant b/a \leqslant 3{\cdot}0$.

As an example of using the Table, consider a film of 80/20 nickel-iron alloy for which $\delta = 0{\cdot}2\mu$, $a = 1{\cdot}0$ mm and $b = 1{\cdot}0$ mm. Using eqn. (31) and the tabulated values of $D(z/a, b/a)$, it follows that the values of H_z/M_z are

$-0{\cdot}671 \times 10^{-4}$, at $z = 0$
$-1{\cdot}783 \times 10^{-4}$, at $z = 0{\cdot}80$ mm
$-6{\cdot}530 \times 10^{-4}$, at $z = 0{\cdot}95$ mm

If the film were magnetized to saturation in the z-direction, M_z would be of the order of 8×10^5 A/m for this particular alloy so that the actual values of H_z would be

-55 A/m, at $z = 0$
-140 A/m, at $z = 0{\cdot}80$ mm
-520 A/m, at $z = 0{\cdot}95$ mm

(5) CONCLUSIONS

The above calculations show that the magnetic excitation inside a uniformly magnetized cylindrical thin film depends very strongly upon position. When there is a component of magnetization, M_z, in the axial direction the excitation can rise to such a high value, as the edge of the film is approached, that the initial assumption of uniform magnetization, i.e. that the film is a single ferromagnetic domain, can no longer be justified.

The effect of this axial demagnetizing excitation will have to be considered in any theoretical discussions of magnetic reversal in thin ferromagnetic films.

(6) ACKNOWLEDGMENTS

The author wishes to thank Dr. E. Franklin, of A.E.R.E., for suggesting the problem to him.

The computing facilities were provided by the United Kingdom Atomic Energy Authority, whose permission to publish the paper is gratefully acknowledged.

(7) REFERENCES

(1) KITTEL, C.: 'Theory and Structure of Ferromagnetic Domains in Films and Small Particles', *Physical Review*, 1946, **70**, p. 965.
(2) OLSON, C. D., and POHM, R. V.: 'Flux Reversal in Ni–Fe Films', *Journal of Applied Physics*, 1958, **29**, p. 274.
(3) HUMPHREY, F. B.: 'Transverse Flux Change in Soft Ferromagnetics', *ibid.*, 1958, **29**, p. 284.
(4) MEIER, D. A.: 'Millimicrosecond Magnetic Switching and Storage Elements', *ibid.*, 1959, Supplement to **30**, p. 355.
(5) CALLEN, H. B.: 'A Ferromagnetic Dynamical Equation', *Journal of Physics and Chemistry of Solids*, 1958, **4**, p. 256.
(6) SOMMERFELD, A.: 'Electrodynamics' (Academic Press, 1952), p. 78.
(7) SOMMERFELD, A.: 'Mechanics of Deformable Bodies' (Academic Press, 1950), p. 147.
(8) JAHNKE, E., and EMDE, F.: 'Tables of Functions' (Dover, 1945).

DISCUSSION ON 'FLUX DISTRIBUTION IN A PERMEABLE SHEET WITH A HOLE NEAR AN EDGE'*

Mr. W. E. Thomson (*communicated*): The author says that the flux on the circumference of the hole may also be approximately calculated as

$$\psi_c = \sqrt{(b^2 - R^2)} \quad . \quad . \quad . \quad . \quad . \quad (3)$$

This equation is in fact exact, which may be shown as follows.

Transform from the z-plane to the ζ-plane ($\zeta = \xi + j\eta$) by the transformation $z = a \tanh \zeta$, where $a = \sqrt{(b^2 - R^2)}$. This transforms the first quadrant of the z-plane, excluding the hole, into the rectangle in the ζ-plane bounded by the lines $\xi = 0$, $\xi = \xi_c$ (where $\operatorname{sech} 2\xi_c = R/b$), $\eta = 0$, $\eta = \pi/2$. The line from (0, 0) to (ξ_c, 0) corresponds to the x-axis from the origin to the edge of the hole; the line from (ξ_c, 0) to (ξ_c, $\pi/2$) corresponds to the upper semi-perimeter of the hole; the line from (ξ_c, $\pi/2$) to (0, $\pi/2$), to the remainder of the x-axis; and the line from (0, 0) to (0, $\pi/2$), to the y-axis.

In the ζ-plane, the required complex potential function is readily determined as

$$w = \phi + j\psi = \sum_{n=-\infty}^{\infty} ja \tanh (\zeta - 2n\xi_c)$$

which is obtained by the multiple-image technique; its application is easier in the ζ-plane because the curves with respect to which images are required are the two parallel straight lines $\xi = 0$, $\xi = \xi_c$.

The flux at the edge of the hole is now determined as

$$\psi_c = \mathscr{R}\left[\sum_{n=-\infty}^{\infty} a \tanh (\xi_c + j\eta - 2n\xi_c)\right]$$

$$= \sum_{n=-\infty}^{\infty} \frac{a \tanh [(1 - 2n)\xi_c](1 + \tan^2 \eta)}{1 + \tanh^2 [(1 - 2n)\xi_c] \tan^2 \eta}$$

This is best considered as

$$\psi_c = \lim_{N\to\infty} \sum_{n=-N}^{N} (\text{same summand as previously})$$

$$= \lim_{N\to\infty} \frac{a \tanh [(1 + 2N)\xi_c](1 + \tan^2 \eta)}{1 + \tanh^2 [(1 + 2N)\xi_c] \tan^2 \eta}$$

since the term for $n = 0$ cancels that for $n = 1$, that for $n = -1$ cancels that for $n = 2$, and so on, leaving only the term for $n = -N$. Hence

$$\psi_c = a = \sqrt{(b^2 - R^2)}$$

as required.

Dr. B. V. Jayawant (*in reply*): I am most indebted to Mr Thomson for providing the proof that the value of the stream function as calculated by eqn. (3) of my paper is in fact exact. It was by a coincidence that I noticed the relationship of ψ_c in some of the cases, as computed to the square roots of natural numbers. I was, however, unable to prove this result from the imaginary part of eqn. (1). There was just a slight divergence of the computed value of ψ_c from the square roots of natural numbers in mathematical tables, no doubt due to taking account of the first five terms only of eqn. (1), to prevent me from drawing any definite conclusions. Incidentally, Mr. Thomson's proof means that eqn. (4) also is exact.

* JAYAWANT, B. V.: *Proceedings I.E.E.*, Monograph No. 368 M, March, 1960 (see 107 C, p. 238).

!.385.032.213.13

The Institution of Electrical Engineers
Monograph No. 397 E
Sept. 1960

THE CONDUCTIVITY OF OXIDE CATHODES

Part 9.—Thermo-Electric Power

By G. H. METSON, M.C., D.Sc., Ph.D., M.Sc., B.Sc.(Eng.), Member, and M. F. HOLMES, B.Sc.

(*The paper was first received* 10*th March, and in revised form* 17*th May*, 1960. *It was published as an* INSTITUTION MONOGRAPH *in September*, 1960.)

SUMMARY

The thermo-electric power of an oxide cathode has been examined ·ently by J. R. Young, who finds it to be a complex function of nperature, dependent on the dual nature of oxide-cathode con- ctivity. By an experimental artifice the present authors show that apparently complex form of behaviour is, in fact, the result of the perposition of two quite simple phenomena. Two parallel-acting ermo-electric power functions are involved, and each of these is variant with temperature and temperature gradient. The two nctions are physically separated and each is measured over an propriate temperature range. The larger function, of magnitude 0 — 3·0mV/degC, is associated with the vacuum movement of ctrons through the hollow pores of the oxide matrix; the smaller ıe, of magnitude 0·5mV/degC, occurs in the chains of contiguous lid particles of the matrix. Owing to the parallel connection and equality of these functions, it is concluded that a temperature adient through an oxide matrix leads to a continuous circulation of rrent, vacuum-wise in one direction and solid-wise in the other. nce the larger function is essentially one involving thermionic emis- on of electrons in a vacuum, it can be satisfactorily explained in terms Richardson's law.

(1) INTRODUCTION

Relatively little attention has so far been given to the thermo-lectric properties of oxide cathodes. Measurements of thermo-lectric power (t.e.p.) have been made by Becker and Sears,[1] lewett[2] and Lovett,[3] who find a value of about 2mV/deg C ver a restricted range of temperature. A much more detailed xperimental study was made in 1952 by Young,[4] who measured .e.p. over a wide temperature range and attempted to relate its omplex variation to the pore model of the oxide cathode ntroduced by Loosjes and Vink.[5]

In Young's experiment a flat circular disc of barium strontium xide of the usual density was pressed between two flat electrodes f active nickel. The electrodes were provided with individual hermocouples and insulated heaters. After high-vacuum pro- essing and activation, the thermo-electric power, $V/\Delta T$ milli- olts per degree, was measured between 300 and 1 100° K. A esult taken from Young's paper is set out in Fig. 1.

The object of the present Part is to confirm and considerably xtend the work of Young, to develop a more adequate theoretical xplanation of the experimental observations, and to see whether he overall thermo-electric picture has any significant bearing on he operation of common receiving valves.

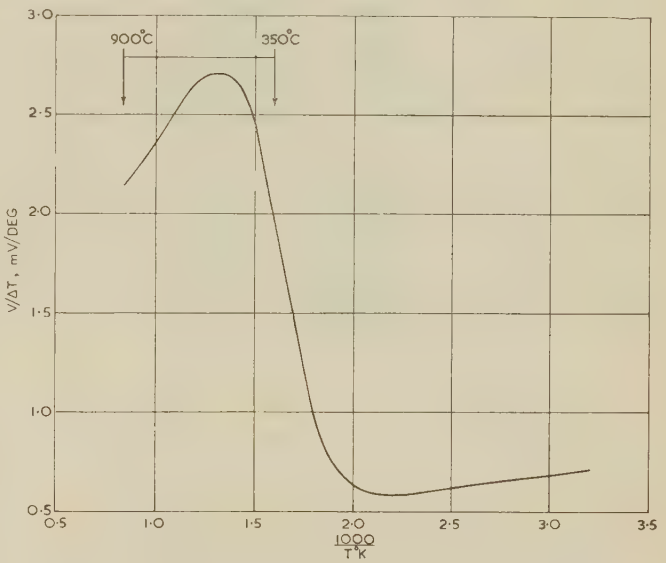

Fig. 1.—Typical characteristic of $V/\Delta T$, from Young.

(2) EXPERIMENTAL OBSERVATIONS

(2.1) Description of Experimental Valves

The several forms of valve used in the experimental work are all based on the standard S-type assembly* and are shown diagrammatically in Fig. 2. Case (*a*) shows the standard S-type assembly with its flat plate of activated barium strontium oxide of density 1·0 sandwiched between the two rectangular box cores of active nickel. It is seen to be provided with insulated heaters H_1 and H_2 which are brought out of the evacuated envelope separately, and with individual thermocouples of platinum and platinum-rhodium. The system between the working core faces is thus a barium strontium oxide matrix only and the device is symmetrical. Case (*b*) is identical to case (*a*), except that it is provided with a vacuum gap separating the matrix into two halves. Case (*c*) has core 1 coated with barium strontium oxide matrix while core 2 has only a thin film of alkaline earth oxide which is deposited on it by evaporation during the activation of core 1. Case (*c*) is therefore asymmetrical and can be tested in the two possible directions of temperature gradient, i.e. $T_1 > T_2$ or $T_2 > T_1$. It can moreover be examined with the film in an activated or passive state.

The valves differ slightly in respect of mechanical construction. Case (*a*) is self-supporting, with its light tungsten springs pressing

* Specification of the standard S-type assembly:

Cores:	Active nickel or pure platinum.
Matrix:	Co-precipitated equimolar barium strontium oxide.
Matrix density:	About 1·0.
Matrix thickness:	150 μ.
Matrix area:	0·25 cm².

The assemblies are vacuum-processed to the standard schedule detailed in Table 1 of Part 1.

The paper is a continuation of Monographs Nos. 221 R and 243 R, published in February and June, 1957 (see **104** C, pp. 316 and 496), Nos. 268 R, 269 R and 289 R, published in December, 1957, and February, 1958 (see **105** C, pp. 183, 189 and 374), No. 317 R, published in November, 1958 (see **106** C, p. 55), No. 347 E, published in October, 1959 (see **107** C, p. 91), and No. 357 E, published in February, 1960 (see 107 C).

Correspondence on Monographs is invited for consideration with a view to publication.

Dr. Metson and Mr. Holmes are at the Post Office Research Station.

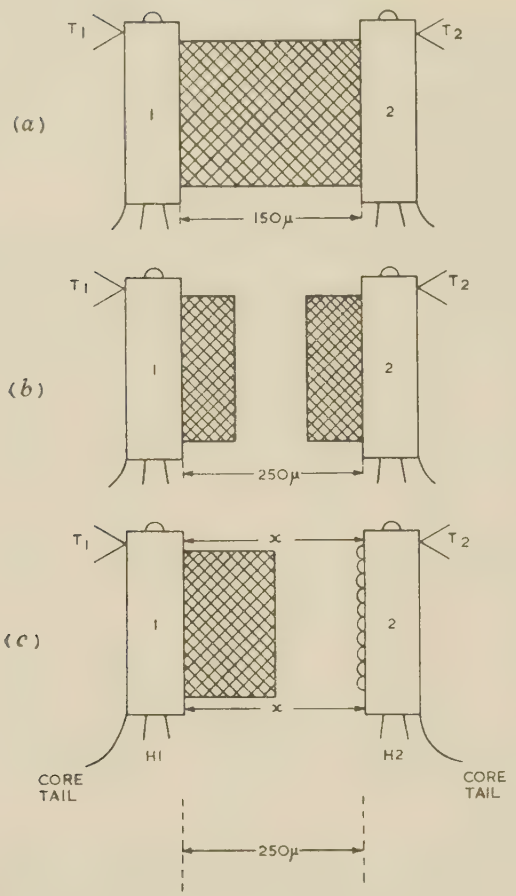

Fig. 2.—Schematic representation of experimental valves.
(*a*) Solid matrix.
(*b*) Matrix-gap-matrix.
(*c*) Matrix-gap-film.

on the outer surfaces of box cores. The vacuum-gapped cases (*b*) and (*c*) require mechanical separators, and these take the form of thin slips of sapphire ground to a standard thickness of 250μ. These slips are inserted between the uncoated ends of the core pieces as shown at *xx* in case (*c*).

The dimensions of the sections of matrix in cases (*b*) and (*c*) are largely unimportant and considerable variations have little effect on measurements of $V/\Delta T$.

(2.2) Measurement of Thermo-Electric Power by Integral and Differential Methods

The actual measurement of t.e.p. is a very simple procedure. The two core heaters are supplied individually with power from separate d.c. stabilized power packs which are adjusted to give the two required core temperatures T_1 and T_2. These temperatures are measured with sufficient accuracy on a wide-scale moving-coil instrument which is switched at will between the two core thermocouples. The thermo-electric voltage, V, is measured between the two cores by means of a vibrating-reed electrometer of effectively infinite impedance. The instrument has switched ranges with full-scale deflections of 10, 30, 100, 300 and 1 000 mV, which give a suitable accuracy of reading over an adequate voltage range.

There are two conventional ways of measuring a t.e.p. characteristic of $V/\Delta T$ versus T and both will be used. In the integral method the two cores are, for example, set initially at $T_1 = T_2 = 700°$ C, where V should have some value approximating to zero. Core 1 is now maintained at 700° C, while

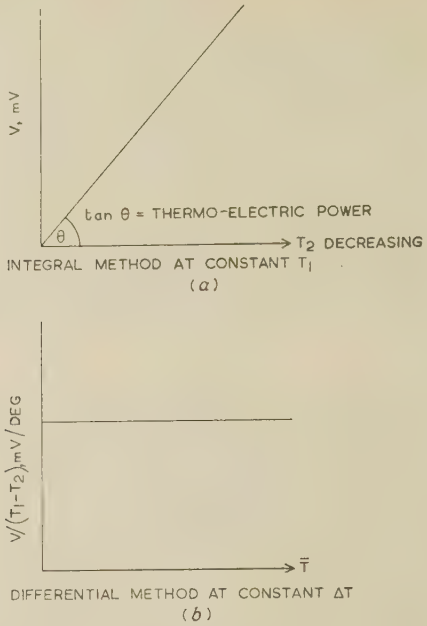

Fig. 3.—Integral (*a*) and differential (*b*) methods of measuring therm electric power.
In (*a*), tan θ = thermo-electric power.

core 2 is steadily reduced in temperature to give a characteris of V/T_2 at constant T_1. The integral method, shown in Fig. 3(is particularly useful and accurate if the t.e.p. happens to constant over a wide temperature range.

The second technique, known as the differential metho involves the direct measurement of t.e.p. at small temperatu gaps ($T_1 - T_2$) of about 30° over a wide range of mean te perature $\bar{T} = \frac{1}{2}(T_1 + T_2)$. The characteristic is then drawn $V/(T_1 - T_2)$ against $\bar{T}$.

Each method has its own advantages and both will be used the present work.

(2.3) Matrix-Gap-Matrix System

It is proposed to start with case (*b*) of Fig. 2, since it prov from experience to be the least complicated of the three pos bilities. In this symmetrical matrix-gap-matrix system the el trons can pass freely in either direction across the vacuum g and the complications introduced by a solid electronic se conduction path between the electrodes, present in case (are avoided.

The principal evidence results from measurements using t integral method. In a typical test a valve is set up w $T_1 = T_2 = 850°$ C and the electrometer reading of V is observ to be less than ± 5 mV. With T_1 maintained at exactly 850 the temperature T_2 is reduced to 825° C and the voltage V again observed. This procedure is repeated until a characteris of V/T_2 at constant T_1 has been obtained over an adequ range of T_2. The whole experiment is then restarted w $T_1 = T_2 = 800°$ C, and so on to assemble such a typical fam of characteristics as are set out in Fig. 4. If the image fam of V/T_1 at constant T_2 is next measured, it is found to be sensi identical.

The lines drawn through the experimental points are strai and the slope of a line is the t.e.p.; it will be obvious from Fig that not only is this constant over the temperature range o single characteristic but it is very nearly constant over the wh family of characteristics. The mean value is 2·23 mV/deg C; the observed variation between individual characteristics

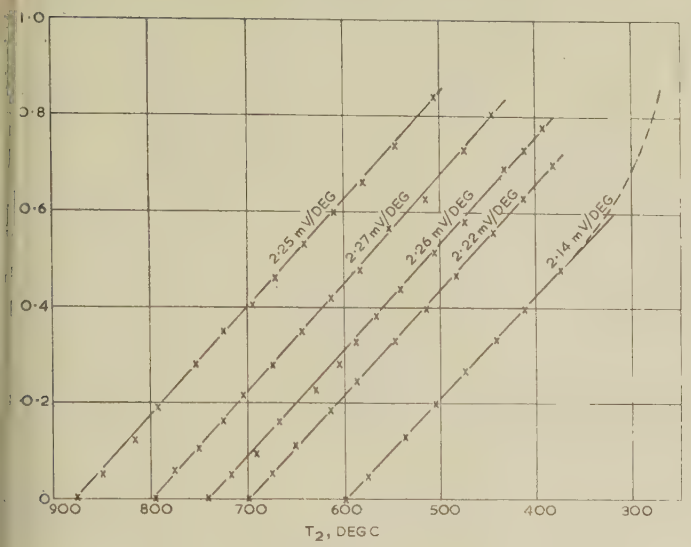

Fig. 4.—Characteristics of V/T_2 at constant T_1.

probably random—it shows no systematic trend amongst different valve samples.

Conclusions drawn at this stage for case (*b*) can thus be written:

(*a*) $V \propto (T_1 - T_2)$ at constant T_1.
(*b*) $V/(T_1 - T_2)$ at constant T_1 is independent of T_1.
(*c*) By symmetry, the image relationships hold.

This constancy of t.e.p. over the wide temperature range of 900–350° C is in remarkable contrast to the result of Young set out in Fig. 1 for the same temperature range. It must be remembered, however, that Young obtained his result on a system similar to case (*a*) in Fig. 2.

With the same sample valve, the t.e.p. is now measured using the differential method. T_1 and T_2 are initially adjusted so that a difference of about 30° is obtained and V is measured. Both temperatures are now dropped by the same small amount and V is remeasured. The sequence is continued until a characteristic of t.e.p. or $V/(T_1 - T_2)$ against mean temperature, $\frac{1}{2}(T_1 + T_2)$, is completed over an adequate temperature range. Results by two individual operators are set out in Fig. 5. No obvious temperature trend is discernible and the differential method is clearly of much lower repetition precision than the integral method. Allowing for the obvious experimental errors involved, it would seem that the t.e.p. has a mean value of about

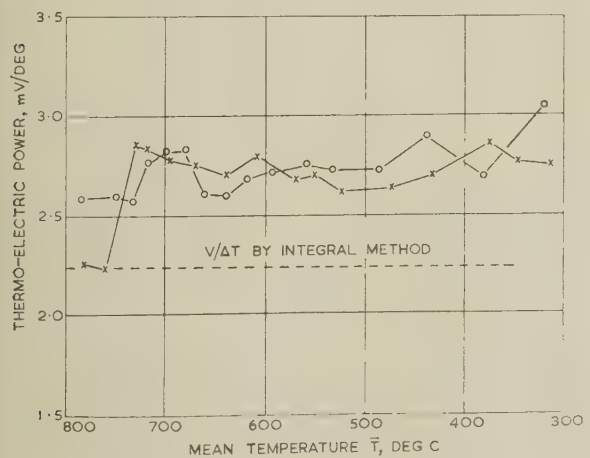

Fig. 5.—Characteristics of $V/\Delta T$ versus $\bar{T}$ by differential method.

2·7 mV/deg C compared with the previous value of 2·2 mV/deg C by the integral method. No significance is seen in this deviation, which is probably due to the common difficulty in accurately measuring the small difference, ΔT, of two large quantities, T_1 and T_2. Between 900 and 400° C it is therefore concluded that the matrix-gap-matrix system [case (*b*)] has a t.e.p. which is constant at about 2·2 mV/deg.

It may have been noticed that no attempt has been made so far to explore the t.e.p. in the region below 400° C. This omission has been a deliberate one designed to keep the pattern of behaviour as simple as possible at the outset of the work. In the range 900–400° C the matrix-gap-matrix system is able to pass electrons with relative ease in either direction; below 350° C the thermionic emission becomes negligibly small in one direction and new circumstances arise. In the integral characteristics shown in Fig. 4 the effect takes the form of a progressive increase in slope of each line as it passes the 400° C ordinate, i.e. the hitherto straight lines of slope 2·2 mV/deg C start bending upwards. The effect will, of course, be first seen in the characteristic at the right-hand side of Fig. 4 and will take the trend indicated by the broken line. As an overall consequence of the effect the t.e.p. will lose its constant value below about 350° C and start to increase in magnitude. This low-temperature increase is brought out more clearly in the differential method of measurement and is shown in Fig. 6, which extends one of

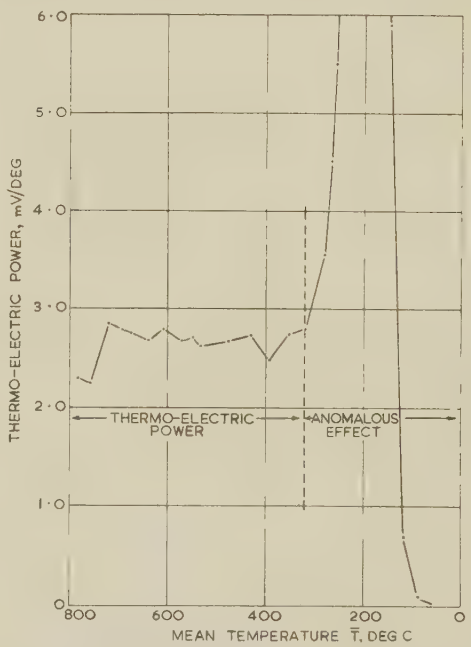

Fig. 6.—Characteristic of $V/\Delta T$ by differential method extended to low values of $\bar{T}$.

the measurements set out in Fig. 5. Between 350 and 300° C a sudden and relatively great increase is observed and this falls to zero as the temperature is lowered to 90° C. These anomalous low-temperature effects will, except for brief consideration in Section 2·7, be largely ignored in the rest of the paper, which is mainly concerned with the wide temperature range wherein the t.e.p. is virtually constant.

(2.4) Matrix-Gap-Film Systems

The next system to be examined is that of case (*c*) in Fig. 2. Both cores are of active nickel, but only core 1 is sprayed with the usual barium strontium carbonate matrix to a nominal

thickness of 70 μ; core 2 is assembled clean and free from spray. After the usual vacuum processing, core 1 is activated to give a stable current/voltage characteristic in the direction of electron flow $1 \rightarrow 2$. The characteristic in the reverse direction $2 \rightarrow 1$ is negligibly small. At this stage core 1 is set at 727° C and core 2 at 927° C, with the cores connected through a 5-volt battery and a milliameter. The potential direction is such as to draw electrons from core 2 to core 1. The result of this arrangement is to evaporate alkaline earth oxide from the matrix of core 1 on to the bare surface of core 2, where a film builds up and is thermally activated. As the film materializes, the electron flow $2 \rightarrow 1$ increases and the process is allowed to continue until the current has reached a steady space-charge-limited value. The whole operation may take from one to two hours to complete, and the deposited film is probably less than 0·1 μ thick. Both cores are now set at 794° C, and if the operation has been satisfactorily completed, the current/voltage relationships in the two directions of operation are effectively identical. Furthermore, the work functions of the two core surfaces, measured by the Richardson line method, should both have the value $1{\cdot}3 \pm 0{\cdot}1$ eV.

The valve is next arranged for measurement of the two characteristics V/T_{film} at constant T_{matrix}, V/T_{matrix} at constant T_{film}, and families of such results in integral form are set out in Figs. 7 and 8 respectively. The slope of the straight-line part

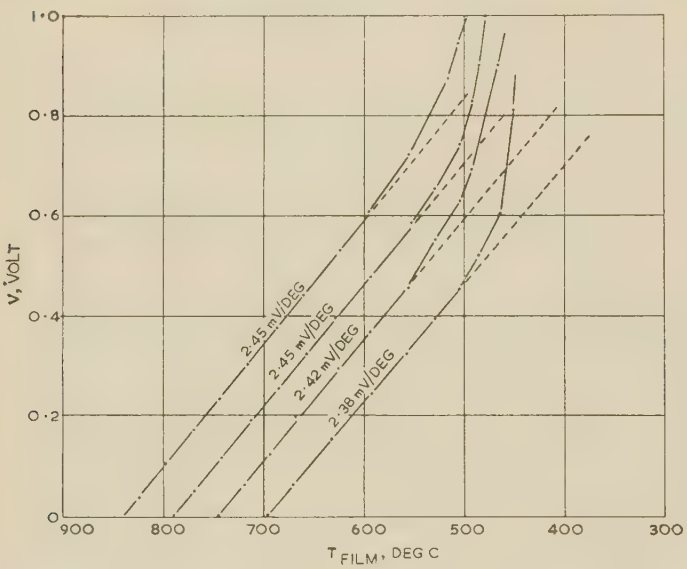

Fig. 7.—Characteristics of V/T_{film} at constant matrix temperature.

of each characteristic is seen to be effectively constant at 2·3–2·4 mV/deg C irrespective of the direction of thermal gradient or the maximum test temperature. In short, there is no electrical difference in any way so far explored between case (*b*) and case (*c*) of Fig. 2, provided that the film in the latter case is fully activated with a work function of about 1·3 eV.

The next step in the experimental sequence will be to repeat the measurements on a case (*c*) type of valve which has a thermionically inert film on core 2. A suitable valve is one in which the bare core 2 is made of pure platinum. After activation of the matrix-coated core 1, the bare-platinum core 2 is run at 1 000° C for ten hours to clear it of evaporated alkaline earth oxide. Such treatment leaves core 2 with a high work function of 2·4 eV* and the valve with a negligible conductance

* This value of 2·4 eV corresponds to the work function of barium metal dissolved in platinum and is probably the highest value which can be expected from a platinum electrode working in the vicinity of an oxide cathode.

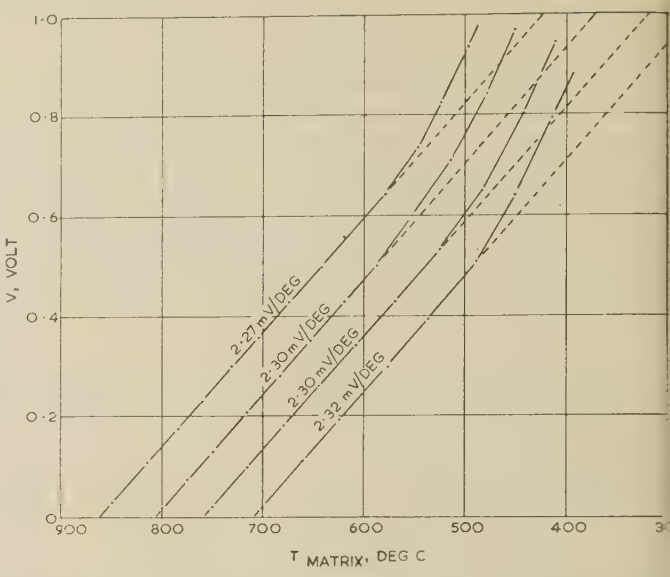

Fig. 8.—Characteristics of V/T_{matrix} at constant film temperature.

in the electron flow direction $2 \rightarrow 1$. The valve, unlike th active film version, is electrically asymmetrical.

Measurements of t.e.p. in both directions of temperatur gradient are now carried out using the integral method. Result are set out in Figs. 9 and 10, and are essentially the same i

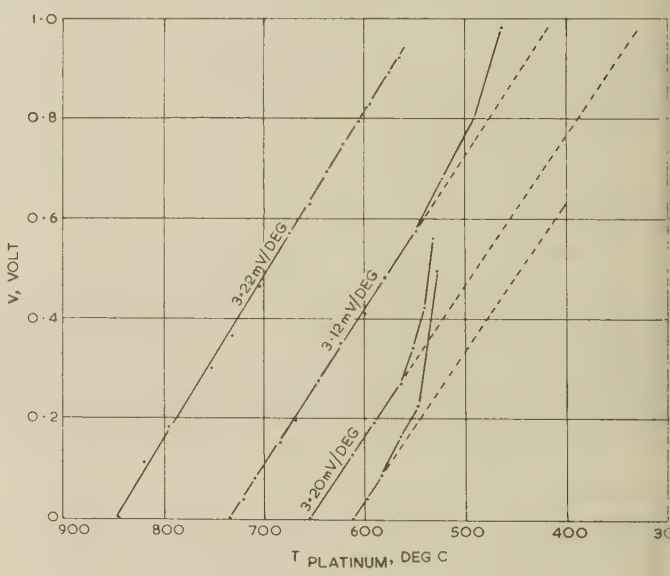

Fig. 9.—Characteristics of $V/T_{platinum}$ at constant matrix temperature.

kind as those of Figs. 7 and 8. The t.e.p. values of 3·2 an 2·7 mV/deg C for the passive film case are higher than th corresponding values of 2·4 and 2·3 mV/deg C for the activ film case. This difference may have significance, since a repea experiment using a passive film on a nickel core likewise gav high figures of 2·9 and 2·7 mV/deg C. The result in Fig. for the case of the cooler platinum electrode brings out clearl the departure from linearity of the $V/T_{platinum}$ characteristic since the platinum surface ceases to deliver electrons at a adequate rate to the system, i.e. the electron-exchange mechanism has ceased to operate.

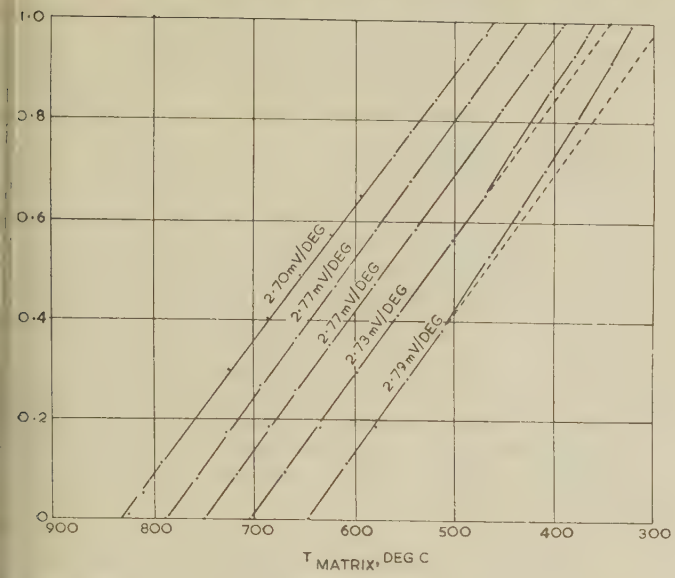

Fig. 10.—Characteristics of V/T_{matrix} at constant value of $T_{platinum}$.

(2.5) Discussion of Cases (*b*) and (*c*)

For temperatures above 600° C all systems so far examined have in near identical fashion and can be generalized in the llowing form:

(*a*) $V \propto (T_1 - T_2)$.
(*b*) $V/(T_1 - T_2)$ is independent of T_1.
(*c*) $V/(T_1 - T_2) = V/(T_2 - T_1)$.
(*d*) The constant $V/(T_2 - T_1)$ may have any value in the range 1·9–2·4 mV/deg C for wholly active systems, and 2·7–3·2 mV/deg C for a system with one passive electrode.

ver the tested temperature range 1 000–600° C it is generally bserved that the slope $V/(T_1 - T_2)$ does not vary by more an $\pm 2\%$ of its mean value. In other words, the t.e.p. of the veral systems and their image arrangements is almost exactly nstant over a wide range of temperature. This conclusion is ased on the integral method of measurement—the differential ethod appears much less reliable, possibly owing to its depenence on the accuracy of measurement of a small difference of wo large temperature readings.

For temperatures below 600° C for the cooler electrode the haracteristic V/T_2 at constant T_1 loses its linearity and the slope ncreases rapidly. This effect seems to be due to a failure of the wo-way mechanism of electron exchange between the two elecrodes, i.e. the cooler electrode ceases to emit thermionically at n adequate rate. If, for example, the two electrodes are perectly insulated and the cooler one develops no thermionic mission whatever, then a continuous increase in potential must e expected as a result of the Maxwellian distribution of energies f electrons emitted from the hotter electrode. In the presence f a leakage resistance between the electrodes the potential will evel off at a value appropriate to the resistance. If the temerature of the system is now lowered still further, as in the ifferential method, until the hotter electrode also ceases to mit, the potential will leak away to zero. This explanation is hought to cover the low-temperature range of Fig. 6. The ctual temperature at which the potential rise sets in depends, f course, on the thermionic activity of the cooler electrode nd the temperature of potential fall on that of the hotter lectrode. The temperature of rise is always below 600° C and n the case of very well activated electrodes may be as low s 350° C.

The apparently abrupt increase of thermo-electric power indicated in Fig. 6 must therefore be regarded as an anomalous effect and outside the context of the present part.

(2.6) Matrix System [Case (*a*)]

The work of Young and others was carried out on matrix systems similar to case (*a*) in Fig. 2. Structurally this arrangement is the most simple of the three cases, but, in fact, it involves electrical complications which are best avoided in a preliminary approach to the thermo-electric phenomenon. In cases (*b*) and (*c*), for instance, the only possible method of electron transfer between electrodes is by vacuum flight across the gap. In case (*a*), however, the situation is different, for electrons can travel in either direction by vacuum flight through the hollow pores of the matrix or by a solid semiconduction process through the contiguous chains of activated matrix particles. The different circumstances are indicated in Fig. 11 where the shunt

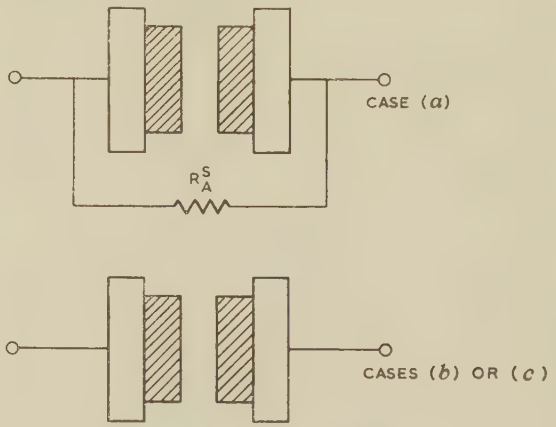

Fig. 11.—Models for the three cases.

resistance, R_A^S, is the reciprocal of the solid semiconductance of the standard S-type assembly.

Suppose now that the matrix-gap-matrix system of case (*b*) is provided with a wire-wound variable resistance of magnitude R_A^S. If the resistance is high enough, the differential characteristic in Fig. 6 will be largely unaffected over the higher temperature range 800–400° C, but there will be no build-up of potential below 350° C, since the electrons will leak away through the shunt resistance. As the cooler electrode ceases to emit thermionically, the t.e.p. will start falling, and this trend will continue until the hotter electrode likewise ceases to emit, when the t.e.p. will be effectively zero.

The behaviour of the matrix in case (*a*) can now be predicted to follow the course shown in Fig. 12. During the higher-temperature vacuum phase, AB, the t.e.p. should be constant until at B the electron emission from the cooler electrode begins

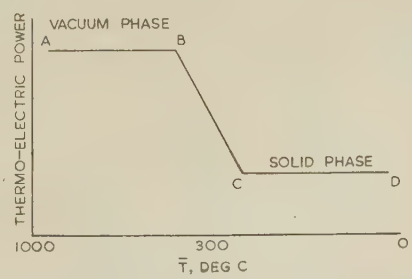

Fig. 12.—Predicted behaviour of matrix system.

to fail. The characteristic then falls to C when emission likewise ceases from the hotter electrode. In the solid phase, CD, the t.e.p. will be roughly constant and at a level appropriate to a continuous chain of solid barium strontium oxide particles.

Fig. 13 shows the differential characteristics of two typical

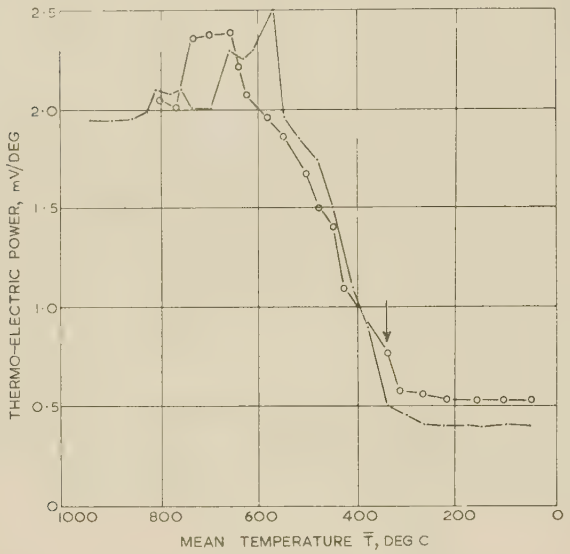

Fig. 13.—Characteristic of $V/\Delta T$ versus $\bar{T}$ for standard S-type assemblies.

The arrow indicates the temperature of the knee of the log-conductivity against $1/T$ characteristic.

case (*a*) samples of the standard S-type assembly. Comparison of these results with that of Young in Fig. 1 shows their basic similarity, both qualitatively and quantitatively. The main difference lies in the appearance of a low-valued activation energy in the solid phase in Young's work which is persistently absent in our measurements.

In Fig. 14 an attempt is made to synthesize the complex

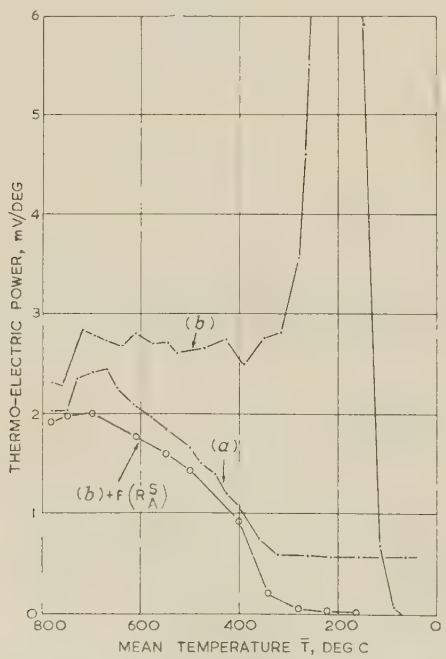

Fig. 14.—Structural synthesis of case (*a*).

case (*a*) from a matrix-gap-matrix sample provided with an appropriate external shunt resistance. The synthesis is completed in the following four stages:

(i) Plot the differential characteristic of the matrix-gap-matrix system as curve (*b*).

(ii) Plot the differential characteristic of a standard S-type assembly as curve (*a*).

(iii) From the familiar characteristic of log σ/(reciprocal of temperature) derive the resistance R_A^S of the S-type assembly as a function of temperature over the range 800–50° C.

(iv) Place a variable wire-wound resistance box in parallel with the matrix-gap-matrix system, setting the resistance to a value appropriate to temperature as indicated by (iii). Measure the differential characteristic of the combination.

The result of operation (iv) is drawn as curve $[(b) + f(R_A^S)]$ in Fig. 14, and it transforms curve (*b*) to something closely approximating to curve (*a*) in the temperature range 800–400° C. Below 400° C the composite arrangement falls to zero, since no thermo-electric voltage is developed across the metallic shunt resistance R_A^S.

(2.7) Current Circulation in the Matrix of Case (*a*)

It will be clear now that case (*a*) consists of two separate and physically distinct channels of electron flow, with each of which is associated a thermo-electric power. The two channels are connected in parallel with the junctions resting on the hot and cold terminals of the device, which is itself on open-circuit as shown in Fig. 15. Since the two thermal e.m.f.'s act in the

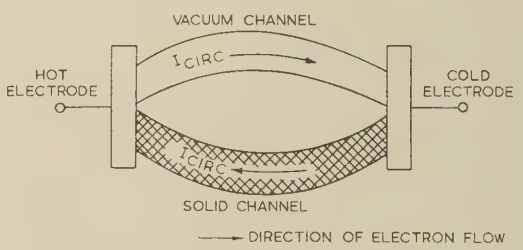

Fig. 15.—Circulating current in the matrix system.

sense of urging electrons from hot to cold junction, they will oppose each other around the channel-loop. There will therefore exist a resultant e.m.f. of magnitude $(2{\cdot}0–0{\cdot}5)\,\Delta T$ millivolts around the loop which will give rise to a circulating current I_{circ}, of magnitude

$$I_{circ} = \frac{(2{\cdot}0–0{\cdot}5) \times 100 \times 10^{-3}}{14 + 250} \text{ amperes}$$
$$= 0{\cdot}6 \text{ milliamperes}$$

Under the stated conditions there will therefore be a continuous circulating current in the S-type assembly with a net electron flow through the vacuum pores from hot to cold electrode, and an equal flow in the solid semiconducting particles from cold to hot electrode.

In cases (*b*) and (*c*) there is no solid-state conductance between the electrodes and no circulation is possible; the steady-state net flow of electrons is therefore zero.

(2.8) Integral Characteristics of the Matrix System

Measurements of t.e.p. on the matrix system [case (*a*)] using the integral method are set out in Fig. 16, and two points of interest arise. In the first place the characteristics do not show the increase in slope of $V/\Delta T$ as the temperature of the cooler electrode decreases. This difference from cases (*b*) and (*c*)

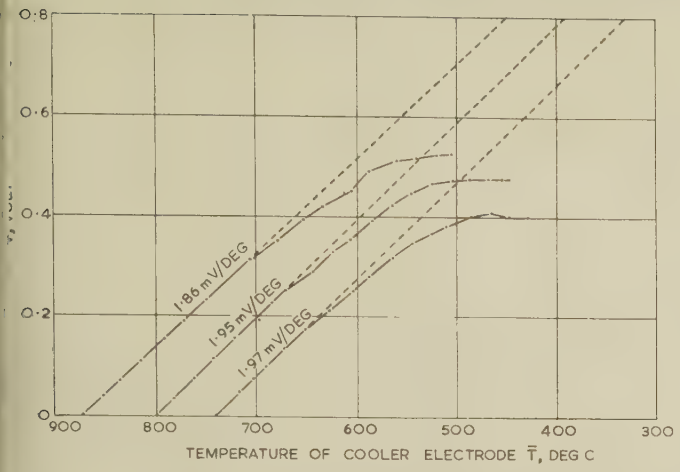

Fig. 16.—Integral characteristics for matrix system, case (*a*).

lue, of course, to the internal shunting action of the solid-state conductance path. The second point of interest is in the constancy of the t.e.p. in marked contrast to its rather random irregularity when measured by the differential method. The integral method of measurement, in which reliance is placed on the accuracy of slope of a straight line drawn through a number of experimental points, seems to be inherently more accurate than the differential method. For this reason the authors hold to the view that, in the higher-temperature region AB of Fig. 12, the t.e.p. is substantially constant.

(3) THEORETICAL CONSIDERATIONS

A simple pattern of thermo-electric behaviour has now been established experimentally. The pattern involves the superposition of two parallel-acting thermo-electric powers which are apparently invariant with temperature, are widely different in magnitude and can be physically separated for independent measurement. The larger function, of magnitude 2·0–3·2 mV/deg C, is associated with the vacuum movement of electrons through the hollow pores of the oxide matrix; the smaller one, of magnitude 0·5 mV/deg, occurs in the chains of contiguous solid particles of the matrix. Since the larger element is essentially a vacuum phenomenon, it must be related in some way to Richardson's law and an attempt will next be made to demonstrate such a link.

(3.1) Derivation of Thermo-Electric Power

The thermo-electric power developed in a pore of an oxide cathode matrix at a temperature $T°$K has been obtained by Hensley[6] as

$$\frac{dV}{dT} = \frac{1}{e}\left[2k + e\frac{(\phi + V_m)}{T}\right] \quad . \quad . \quad . \quad . \quad (1)$$

where e = Electronic charge, coulomb.
k = Boltzmann's constant, watt-sec/deg C.
ϕ = Work function, volts.
V_m = Magnitude of potential minimum, volts.

The factor $2k$ arises from the T^2 term in Richardson's equation, which is used in the derivation.

It is proposed to derive a similar formula for a symmetrical diode with an active film on each electrode and with a vacuum spacing much larger than the pore dimensions. The potential diagram which applies in such a case is shown in Fig. 17(*a*). The temperatures of the electrodes, T_1 and T_2, are assumed to be separated by only a few degrees, and the potential minimum is located at the mid-point. The emission constants of each electrode are assumed identical. Under these conditions, with $T_1 > T_2$, the higher emission from electrode 1 will cause negative charge to collect on electrode 2 to just such an extent that the equilibrium illustrated in Fig. 17(*a*) is reached.

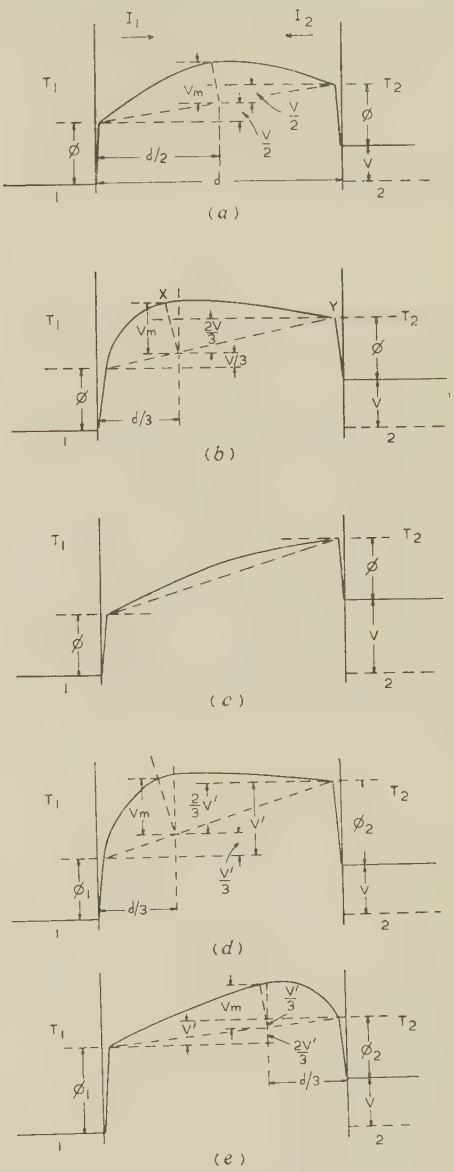

Fig. 17.—Potential diagrams for the theoretical calculation.

At equilibrium $I_1 = I_2$, and as an approximation, since $T_2 \to T_1$, V_m is increased by $V/2$ for I_1 and diminished by $V/2$ for I_2. Thus

$$\left.\begin{aligned} I_1 &= I_{S1} \exp\left[-\frac{e}{kT_1}(V_m + V/2)\right] \\ I_2 &= I_{S2} \exp\left[-\frac{e}{kT_2}(V_m - V/2)\right] \end{aligned}\right\} \quad . \quad . \quad (2a)$$

where

$$\left.\begin{aligned} I_{S1} &= A \exp - e\phi/kT_1 \\ I_{S2} &= A \exp - e\phi/kT_2 \end{aligned}\right\} \quad . \quad . \quad . \quad . \quad (2b)$$

The de Boer form of emission equation is used for convenience. Eqns. (2) reduce to the following expression:

$$V = 2(\phi + V_m)\frac{(T_1 - T_2)}{(T_1 + T_2)} \quad . \quad . \quad . \quad . \quad (3)$$

and this, in the limit as $T_2 \rightarrow T_1$, gives

$$\frac{dV}{dT} = \frac{\phi + V_m}{T} \quad . \quad . \quad . \quad . \quad . \quad . \quad (4)$$

Eqn. (4) differs from eqn. (1) only because the de Boer form of emission equation is used in place of the Richardson form.

(3.2) Theoretical Approach to the Experimental Results

The expression for the t.e.p. of a pore has been shown to be identical with the comparable expression for a diode. The general conclusion (*a*) of Section 2.5 shows, however, that the integral characteristics are linear over a large temperature range. This means that the t.e.p. is constant with temperature, and neither eqn. (1) nor eqn. (4) predicts this result. Both these equations are nevertheless approximations, and so it is necessary to look more closely at the theoretical background of the integral characteristic. The symmetrical film-gap-film diode will be used as an approximation to case (*b*) for this purpose.

Using the integral curve of Fig. 3(*a*) we have

$$\text{t.e.p.} = \tan\theta = \frac{V}{T_1 - T_2} \quad . \quad . \quad . \quad . \quad (5)$$

and from eqn. (3), where $T_2 \rightarrow T_1$,

$$\frac{V}{T_1 - T_2} = \frac{2(\phi + V_m)}{(T_1 + T_2)}$$

yielding, at the foot of the integral characteristic,

$$\text{t.e.p.} = \frac{\phi + V_m}{T_1} \quad . \quad . \quad . \quad . \quad . \quad . \quad (6)$$

For this condition it is possible to use the method suggested by Loosjes and Vink[5] to calculate V_m. If both electrodes are assumed to have emissions of 1 amp/cm^2 at 1 000° K and work functions of 1·3 eV, then, for a spacing of 100 μ, V_m is 0·43 volt at 1 000° K. This gives a t.e.p. of 1·73 mV/deg C according to eqn. (6).

As soon as T_2 is reduced below T_1, Loosjes and Vink's calculation of V_m cannot be used in eqn. (6). Hensley reports that the attempt to obtain a simple expression for V_m in the presence of a field failed owing to the approximations and numerical integrations involved. In this case we have a field and, in addition, the fact that the electrodes are at different temperatures. Consequently, any simple general formula is still more difficult to obtain.

In order to examine the trend of the integral curve at least at one point other than $T_2 \rightarrow T_1$, without attempting the lengthy calculations involved in a rigorous solution, the following argument is suggested. For $T_2 = 700°$ K, I_{S2} can be calculated from eqn. (2*b*) to be 1·49 mA/cm^2. This emission is so low that the diode approximates to the normal thermionic diode with a standard anode. Under these circumstances V_m and d_m can be calculated from normal diode theory to be 0·35 volt and 31 μ respectively in the absence of a field. If it is also assumed that the thermo-electric voltage is so low that the basic shape of the potential diagram remains unaltered, the voltage configuration is approximately that illustrated in Fig. 17(*b*). Eqn. (2) can then be restated as

$$\left.\begin{aligned} I_1 &= I_{S1}\exp\left[-\frac{e}{kT_1}(V_m + V/3)\right] \\ I_2 &= I_{S2}\exp\left[-\frac{e}{kT_2}(V_m - 2V/3)\right] \end{aligned}\right\} \quad . \quad .$$

which yields $$V = 3(\phi + V_m)\frac{T_1 - T_2}{2T_1 + T_2} \quad . \quad . \quad . \quad .$$

and a t.e.p. of 1·8 mV/deg C at $T_2 = 700°$ K.

For $T_2 = 700°$ K, however, eqn. (8) is marginally inapplicab Eqns. (7) can be constructed only if the point X in Fig. 17(is at a higher potential than point Y. From eqn. (8) the potent of X is $\phi + V_m + V/3$ or $\phi + 0{\cdot}51$, whereas that of Y is $\phi +$ or $\phi + 0{\cdot}54$. It is possible to recast eqn. (7) to fit a potent diagram such as Fig. 17(*c*), and then

$$\left.\begin{aligned} I_1 &= I_{S1}\exp(-eV/kT_1) \\ I_2 &= I_{S2} \end{aligned}\right\} \quad . \quad . \quad . \quad .$$

leading to $$V = \phi\frac{(T_1 - T_2)}{T_2} \quad . \quad . \quad . \quad . \quad . \quad (1$$

This gives a t.e.p. of 1·63 mV/deg C. Both eqn. (8) and eqn. (1 therefore give a t.e.p. for $T_1 = 1\,000°$ K and $T_2 = 700°$ K wh is in close agreement with 1·73 mV/deg C derived for $T_2 \rightarrow$ at 1 000° K. These calculations support the experiment linearity of the integral curve over a range of some 300°.

The second conclusion, (*b*) of Section 2.5, indicates that t t.e.p. is independent of T_1. This can be verified by consider the slopes of the integral characteristics where $T_2 \rightarrow T_1$. He eqn. (6) applies and, using the same emission constants as befo the values of the t.e.p. are given in Table 1.

Table 1

VALUES OF T.E.P.

T_1	V_m	T.E.P.
deg K	volt	mV/deg C
1 000	0·43	1·73
900	0·28	1·75
800	0·14	1·80

The next conclusion, (*c*), states that the t.e.p.'s of all the syste examined are substantially independent of the direction of t temperature gradient. This requires no theoretical support cases (*a*) and (*b*), which are, in fact, physically symmetric Case (*c*), with an inactive film, is asymmetrical both in physi dimensions and in activity and yet gives t.e.p.'s which are v similar (2·7 and 3·2 mV/deg C) on reversal of the temperat gradient. This case will be considered in a little more detail.

The reversal of the temperature gradient in case (*c*) is illustra by the potential diagrams of Figs. 17(*d*) and (*e*). An acti film-gap-inactive-film diode is used as a theoretical mo (The approximation of an active film for an active matri discussed later.) The inactivity is expressed by a change work function from ϕ_1 to ϕ_2. In Fig. 17(*d*) the active film maintained at T_1 and in Fig. 17(*e*) the reverse applies. equilibrium equations for Fig. 17(*d*) are a development eqns. (7), i.e.

$$\left.\begin{aligned} I_1 &= I_{S1}\exp\left[-\frac{e}{kT_1}(V_m + V'/3)\right] \\ I_2 &= I_{S2}\exp\left[-\frac{e}{kT_2}(V_m - 2V'/3)\right] \\ I_{S1} &= A\exp - e\phi_1/kT_1 \\ I_{S2} &= A\exp - e\phi_2/kT_2 \\ V' &= \phi_2 + V - \phi_1 \end{aligned}\right\} \quad . \quad . \quad (11)$$

ading to $$V = 3(T_1 - T_2)\frac{\frac{\phi_2}{3} + V_m + \frac{2\phi_1}{3}}{2T_1 + T_2} \quad . \quad . \quad . \quad (12)$$

or Fig. 17(*e*) the equations are

$$\left.\begin{aligned} I_1 &= I_{S1}\exp\left[-\frac{e}{kT_1}(V_m + 2/3V')\right] \\ I_2 &= I_{S2}\exp\left[-\frac{e}{kT_2}(V_m - V'/3)\right] \\ I_{S1} &= A\exp - e\phi_1/kT_1 \\ I_{S2} &= A\exp - e\phi_2/kT_2 \\ V' &= \phi_2 - \phi_1 + V \end{aligned}\right\} \quad . \quad . \quad (13)$$

eading to $$V = 3(T_1 - T_2)\frac{2/3\phi_2 + V_m + \phi_1/3}{2T_2 + T_1} \quad . \quad . \quad (14)$$

n the limit $T_2 \to T_1$, eqn. (12) is exactly equivalent to eqn. (14), ince ϕ_2 in eqn. (12) equals ϕ_1 in eqn. (14) and vice versa. Thus, even in an asymmetrical system, the simple theory predicts hermo-electric symmetry for small reversals of temperature radient.

So far only the theoretical aspects of cases (*b*) and (*c*) have been considered and little attention has been directed to case (*a*), he S-type assembly. For a single pore of this assembly with dimension of 10 μ and with the same emission constants that were assumed earlier for the symmetrical diode, the value of V_m can be calculated for $T_2 \to T_1$ to be 0·103 volt. This gives t.e.p. of 1·4 mV/deg C from eqn. (6). In order to construct he integral characteristic of the whole S-type assembly, it is necessary to know how V_m varies with T and to sum the t.e.p.'s obtained for a series of pores between the two electrodes. Since $T_2 \to T_1$ for each pore, corresponding values of V_m can be calculated on the assumption of a smooth temperature gradient. Table 2 gives V_m for a pore dimension of 10 μ and for $J_S = 1$ amp/cm^2 at 1 000° K.

Table 2

VARIATION OF V_m WITH T FOR A 10 μ PORE

T	V_m
deg K	volt
1 000	0·103
950	0·067
900	0·040
850	0·022
800	0·010

If the summation is carried out for various T_2 values for the whole assembly, an integral characteristic results which has a similar degree of linearity as the theory suggests for the symmetrical diode.

Finally, the numerical values of t.e.p. obtained from theory and experiment will be compared. It is argued that the film-gap-film diode is a close approximation to cases (*b*) and (*c*) despite the intrusion of the cathode matrix in the latter instances. The approximation is close, because, first, there is no potential drop across the matrix as no current flows and, secondly, the temperature gradient across the matrix is small compared with that across the gap. Table 3 sets out the comparison of t.e.p. from theory and experiment.

Table 3

T.E.P. FROM THEORY AND EXPERIMENT

System	Case	T.E.P.	
		Experiment	Theory
		mV/deg C	mV/deg C
S-type assembly	(*a*)	1·86–1·97	1·40
Diode	(*b*)	2·14–2·27	1·73
Diode with active film ..	(*c*)	2·27–2·45	1·73
Diode with inactive film ..	(*c*)	2·70–3·22	2·03*

* Using an inactive work function of 2·4 eV and $V_m = 0{\cdot}33$ volt in eqn. (12).

The theoretical predictions are in fair agreement with experiment and are in the same ascending order. Nearer agreement may result from an examination of work function measurements in symmetrical diodes.

(4) THERMO-ELECTRIC EFFECTS IN NORMAL RECEIVING VALVES

The structure used in case (*c*) with an inactive film approximates closely to the cathode/control-grid section of a normal receiving valve, and thermo-electric voltages have, in fact, been measured between these two electrodes considered in isolation. Despite these results the thermo-electric effects do not intrude generally into normal valve operation, since cathode and control grid are not usually isolated. They are connected via a grid leak resistor, R_G, and an auto-bias resistor, R_K. The relevant potential

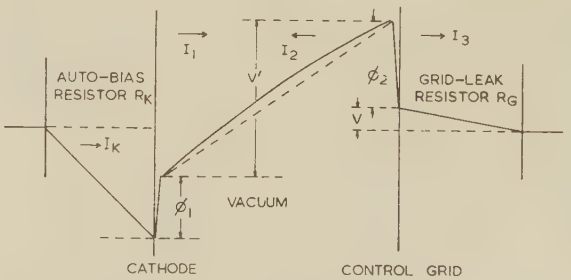

Fig. 18.—Potential diagram for the cathode/control-grid section of a pentode.

diagram is shown in Fig. 18. Under equilibrium, and assuming zero reverse grid current,

$$I_1 = I_2 + I_3 \quad . \quad . \quad . \quad . \quad . \quad . \quad (15)$$

where I_2 = Grid emission to cathode.
I_3 = Grid-leak current.

The voltage V', the effective bias, is not, however, determined by a thermo-electric balance between I_1 and I_2 as hitherto. It is,

on the contrary, determined chiefly by the auto-bias voltage $I_K R_K$ and the contact potential V_{CP}, i.e.

$$V' = \phi_2 - \phi_1 + V + I_K R_K$$
$$= V_{CP} + V + I_K R_K \quad . \quad . \quad . \quad . \quad . \quad (16)$$

The factor V is the only part of the effective bias which is attributable to a combined thermo-electric and leakage-current balance and which is additional to the normally accepted components of the effective bias. The fact that V is very small arises from the following argument:

$$I_1 = I_{S1} \exp -eV'/kT_1$$
$$= \varepsilon^{-11 \cdot 6 V_1} \text{ for } I_{S1} = 1 \text{ amp/cm}^2 \text{ and } T = 1\,000^\circ \text{K}$$

Now

$V' > V_{CP} + I_K R_K$ [cf. eqn. (16)]
$> 0 \cdot 7 + 2 \cdot 0$ for $V_{CP} = 0 \cdot 7$ volt and a bias of -2 volts
$> 2 \cdot 7$ volts, and therefore
$I_1 < \varepsilon^{-32 \cdot 5}$
$< 7 \cdot 7 \times 10^{-15}$ amp
$I_3 < 7 \cdot 7 \times 10^{-15}$ amp [cf. eqn. (15)]

but $V = R_G I_3$, and therefore
$V < 7 \cdot 7 \times 10^{-9}$ volt for a grid-leak resistance of 1 megohm

Since V is so small, it can be stated that the effective bias is independent of thermo-electric voltages under normal operating conditions.

(5) ACKNOWLEDGMENT

Acknowledgment is made to the Engineer-in-Chief of the Post Office for permission to make use of the information contained in the paper.

(6) REFERENCES

(1) BECKER, J. A.: 'Phenomena in Oxide-Coated Filaments', *Physical Review*, 1929, **34**, p. 1323.
(2) BLEWETT, J. P.: 'Oxide-Coated Cathodes, Part 1', *Journal of Applied Physics*, 1939, **10**, p. 668.
(3) LOVETT, C. M.: 'Some Measurements of the Electrical Conductivity, Thermo-Electric Power, and other Properties of the Coating in the Oxide-Coated Cathode', *Proceedings of the Physical Society*, 1954, **B67**, p. 387.
(4) YOUNG, J. R.: 'Electrical Conductivity and Thermo-Electric Power of (BaSr)O and BaO', *Journal of Applied Physics*, 1952, **23**, p. 1129.
(5) LOOSJES, R., and VINK, H. J.: 'The Conduction Mechanism in Oxide-Coated Cathodes', *Philips Research Reports*, 1949, **4**, p. 449.
(6) HENSLEY, E. B.: 'On the Electrical Properties of Porous Semi-Conductors', *Journal of Applied Physics*, 1952, 23, p. 1122.

.373.431.4

The Institution of Electrical Engineers
Monograph No. 398 E
Sept. 1960

FORCED OSCILLATION IN AN OSCILLATOR WITH TWO DEGREES OF FREEDOM

By B. R. NAG, M.Sc.(Tech.).

(*The paper was first received 20th April, and in revised form 29th December*, 1959. *It was published as an* INSTITUTION MONOGRAPH *in September*, 1960.)

SUMMARY

Resonance curves of an oscillator with two degrees of freedom and e criteria of stability of the synchronized state are determined eoretically by van der Pol's method of approximation and verified perimentally by an electronic differential analyser. An experimental ethod for obtaining the phase trajectories is described. Charac- ristics of oscillations outside the zone of synchronization are also scribed.

(1) INTRODUCTION

Characteristics of the van der Pol oscillator subjected to a rcing signal have engaged the attention of several workers[1–3] ecause of its wide applications and also because their features e hardly predictable from linear circuit theory. In some pplications, the oscillator tuned circuit is coupled to a tuned econdary circuit. The oscillator has then two degrees of eedom and its behaviour differs in many ways from the van der ol oscillator. Free oscillations in an oscillator of this type have een studied by van der Pol,[4] Fontana[5] and Schaffner.[6] It is he purpose of the paper to study the characteristics of forced scillation in an oscillator with two degrees of freedom. A uned-anode oscillator is considered, the anode coil of which is nductively coupled to a tuned secondary circuit with a finite esistance, the forcing signal being applied in series with the rimary. Non-linearity in the oscillator is assumed to be of he cubic type.

Theoretical analysis of the differential equation describing the ehaviour of the oscillator is made by van der Pol's method of pproximation, and the resonance characteristics and the zone of ynchronization are deduced. Experimental results obtained rom an oscillator set on an electronic differential analyser are resented with a view to checking the calculated results and to larifying the nature of oscillations on the border of synchro- nization. A method for obtaining the phase trajectories, which re helpful in this connection, is described. Some experimental rajectories are also presented.

(2) FIRST-ORDER APPROXIMATE SOLUTION FOR THE SYNCHRONIZED OSCILLATION

The equivalent circuit of a tuned-anode oscillator coupled to a tuned load is shown in Fig. 1. To simplify the describing differential equations, the effect of the anode resistance is neglected and the external signal is assumed to be applied in series with the anode coil. From this equivalent circuit the following mesh equations may be written:

$$g_m M_{12}\frac{dI_1}{dt} = I_1 + I_c \quad . \quad . \quad . \quad . \quad . \quad (1)$$

$$L_1\frac{d^2I_1}{dt^2} + R_1\frac{dI_1}{dt} - M\frac{d^2I_2}{dt^2} - \omega V \sin \omega t = \frac{I_c}{c_1} \quad . \quad (2)$$

$$L_2\frac{d^2I_2}{dt^2} + R_2\frac{dI_2}{dt} + \frac{I_2}{c_2} - M\frac{d^2I_1}{dt^2} = 0 \quad . \quad . \quad . \quad . \quad (3)$$

Symbols used in the above equations have the meanings as detailed in Fig. 1.

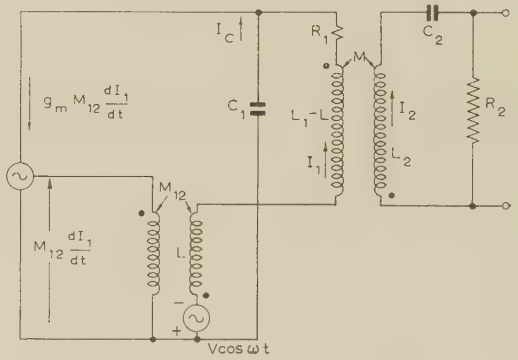

Fig. 1.—Equivalent circuit of the oscillator.

On combining eqns. (1) and (2) and rearranging,

$$\frac{d^2I_1}{dt^2} + \left(\frac{R_1}{L_1} - g_m\frac{M_{12}}{L_1C_1}\right)\frac{dI_1}{dt} + \frac{I_1}{L_1C_1} - \frac{M}{L_1}\frac{d^2I_2}{dt^2} = \frac{\omega V}{L_1}\sin \omega t \quad . \quad . \quad . \quad . \quad (4)$$

$$\frac{d^2I_2}{dt^2} + \frac{R_2}{L_2}\frac{dI_2}{dt} + \frac{I_2}{L_2C_2} - \frac{M}{L_2}\frac{d^2I_1}{dt^2} = 0 \quad . \quad . \quad . \quad . \quad . \quad (5)$$

The non-linearity is introduced in the oscillator owing to the non-linear character of g_m. For the sake of simplicity it is assumed that g_m is dependent only on the grid voltage and may be written as

$$g_m = g_{m0} - g_{m2}\left(\frac{dI_1}{dt}\right)^2$$

On putting $\frac{R_1}{L_1} - g_{m0}\frac{M_{12}}{L_1C_1} = -a_1$, $\frac{g_{m2}M_{12}}{L_1C_1} = a_3$, $\frac{1}{L_1C_1} = \omega_1^2$,

$\frac{1}{L_2C_2} = \omega_2^2$, $\frac{M}{L_1} = \frac{M}{L_2} = k_1$, $\frac{R_2}{L_2} = a_2$, $I_1 = x_1$, $I_2 = x_2\frac{\omega V}{L_1} = H$

eqns. (4) and (5) reduce to

$$\frac{d^2x_1}{dt^2} - a_1\frac{dx_1}{dt} + a_3\left(\frac{dx_1}{dt}\right)^3 + \omega_1^2x_1 - k_1\frac{d^2x_2}{dt^2} = H\sin \omega t \quad (6)$$

$$\frac{d^2x_2}{dt^2} + a_2\frac{dx_2}{dt} + \omega_2^2x_2 - k_1\frac{d^2x_1}{dt^2} = 0 \quad . \quad . \quad . \quad . \quad . \quad (7)$$

On combining the two equations,

$$(1 - k_1^2)\frac{d^4x_1}{dt^4} + (\omega_1^2 + \omega_2^2)\frac{d^2x_1}{dt^2} + \omega_1^2\omega_2^2x_1$$

Correspondence on Monographs is invited for consideration with a view to publication.

Mr. Nag is at the Institute of Radio Physics and Electronics, University of Calcutta.

$$= (\omega_2^2 - \omega^2)H \sin \omega t + a_2 \omega H \cos \omega t$$
$$+ a_1\left(\frac{d^3x_1}{dt^3} + \omega_2^2 \frac{dx_1}{dt}\right) - a_3\left[\frac{d^2}{dt^2}\left(\frac{dx_1}{dt}\right)^3 + \omega_2^2\left(\frac{dx_1}{dt}\right)^3\right]$$
$$- a_2\left(\frac{d^3x_1}{dt^3} + \omega_1^2 \frac{dx_1}{dt}\right) + a_1 a_2 \frac{d^2x_1}{dt^2} - a_3 a_2 \frac{d}{dt}\left(\frac{dx_1}{dt}\right)^3 \quad (8)$$

It should be noted that the second-order terms like a_1a_2, a_3a_2 cannot be neglected, since, as ω is very close to ω_1 and ω_2, other terms in the equation may be of the same order.

In general, the solution to eqn. (8) should contain terms to represent oscillations at the forcing frequency, free oscillations, their harmonics and the combination oscillations. Since the forcing oscillation must always be present, effect of the various other oscillations when ω is close to ω_1 and ω_2 may be considered to cause variations in the amplitude and phase of the forced oscillation. Hence the general solution to eqn. (8) may be written as

$$x_1 = A \sin(\omega t + \phi) \quad . \quad . \quad . \quad . \quad . \quad (9)$$

where A and ϕ are time-varying functions.

On substituting for x_1, retaining up to the second-order terms and equating the coefficients of sine and cosine terms on the two sides of eqn. (8), one obtains

$$[(\omega_1^2 + \omega_2^2) - 2(1 - k_1^2)\omega^2]2\omega \frac{dA}{dt} = -(\omega_2^2 - \omega^2)H \sin \phi$$
$$+ a_2 \omega H \cos \phi + a_1(\omega_2^2 - \omega^2)\omega A - a_2(\omega_1^2 - \omega^2)\omega A$$
$$+ (\omega_2^2 - 3\omega^2)a_1 A \frac{d\phi}{dt} - (\omega_1^2 - 3\omega^2)a_2 A \frac{d\phi}{dt}$$
$$- \tfrac{3}{4}a_3(\omega A)^2(\omega_2^2 - \omega^2)\omega A - \tfrac{3}{4}a_3(\omega A)^2(3\omega_2^2 - 5\omega^2)A \frac{d\phi}{dt} \quad (10)$$

$$-[(\omega_1^2 + \omega_2^2) - 2(1 - k_1^2)\omega^2]2\omega A \frac{d\phi}{dt} = (\omega_2^2 - \omega^2)H \cos \phi$$
$$+ a_2 \omega H \sin \phi + a_1(\omega_2^2 - 3\omega^2)\frac{dA}{dt} - a_2(\omega_1^2 - 3\omega^2)\frac{dA}{dt}$$
$$- a_1 a_2 \omega^2 A + \tfrac{3}{4}a_3 a_2(\omega A)^3 \omega - \tfrac{3}{4}a_3(\omega_2^2 - 7\omega^2)(\omega A)^2 \frac{dA}{dt}$$
$$- [(\omega_1^2 - \omega^2)(\omega_2^2 - \omega^2) - k_1^2\omega^4]A \quad . \quad . \quad . \quad . \quad . \quad (11)$$

On putting $a_2/a_1 = a$, $k_1/a_1 = k$, $4a_1/3a_3 = \rho_0^2$, $\omega A/\rho_0 = \rho$, $H/a_1\rho_0 = F$ and $(\omega_2^2 - \omega^2)/a_1\omega = \delta$ and introducing the restriction that $\omega_1^2 = \omega_2^2 = \omega_0^2$ (it should be noted that though $\omega_1 = \omega_2$, for finite values of k the frequencies of free oscillation are different and the oscillator has two degrees of freedom),

$$4\left(k^2\omega + \frac{\delta}{a_1}\right)\frac{d\rho}{dt} - \left[\left(\frac{\delta}{\omega} - \frac{2}{a_1}\right)(1 - a) - \left(\frac{3\delta}{\omega} - \frac{2}{a_1}\right)\rho^2\right]\rho \frac{d\phi}{dt}$$
$$= -\delta F \sin \phi + aF \cos \phi + \delta\rho(1 - a - \rho^2) \quad (12)$$

$$\left[\left(\frac{\delta}{\omega} - \frac{2}{a_1}\right)(1 - a) - \left(\frac{\delta}{\omega} - \frac{6}{a_1}\right)\rho^2\right]\frac{d\rho}{dt} + 4\left(k^2\omega + \frac{\delta}{a_1}\right)\rho \frac{d\phi}{dt}$$
$$= -\delta F \cos \phi - aF \sin \phi + \rho[a(1 - \rho^2) + \delta^2 - k^2\omega^2] \quad (13)$$

Hence

$$\frac{d\rho}{dt} = \left\{4\left(k^2\omega + \frac{\delta}{a_1}\right)[-\delta F \sin \phi + aF \cos \phi + \delta\rho(1 - a - \rho^2)]\right.$$
$$+ \left[\left(\frac{\delta}{\omega} - \frac{2}{a_1}\right)(1 - a) - \left(\frac{3\delta}{\omega} - \frac{2}{a_1}\right)\rho^2\right][-\delta F \cos \phi$$
$$\left. - aF \sin \phi + \rho(a - a\rho^2 + \delta^2 - k^2\omega^2)]\right\}$$
$$\times \left\{16\left(k^2\omega + \frac{\delta}{a_1}\right)^2 + \left[\left(\frac{\delta}{\omega} - \frac{2}{a_1}\right)(1 - a)\right.\right.$$
$$\left.\left. - \left(\frac{3\delta}{\omega} - \frac{2}{a_1}\right)\rho^2\right]\left[\left(\frac{\delta}{\omega} - \frac{2}{a_1}\right)(1 - a) - \left(\frac{\delta}{\omega} - \frac{6}{a_1}\right)\rho^2\right]\right\}^{-1} \quad (14)$$

$$\rho \frac{d\phi}{dt} = \left\{4\left(k^2\omega + \frac{\delta}{a_1}\right)[-\delta F \cos \phi - aF \sin \phi\right.$$
$$\left. + \rho(a - a\rho^2 + \delta^2 - k^2\omega^2]\right.$$
$$- \left[\left(\frac{\delta}{\omega} - \frac{2}{a_1}\right)(1 - a) - \left(\frac{\delta}{\omega} - \frac{6}{a_1}\right)\rho^2\right]$$
$$\left.[-\delta F \sin \phi + aF \cos \phi + \delta\rho(1 - a - \rho^2)]\right\}$$
$$\times \left\{16\left(k^2\omega + \frac{\delta}{a_1}\right)^2 + \left[\left(\frac{\delta}{\omega} - \frac{2}{a_1}\right)(1 - a)\right.\right.$$
$$\left.\left. - \left(\frac{3\delta}{\omega} - \frac{2}{a_1}\right)\rho^2\right]\left[\left(\frac{\delta}{\omega} - \frac{2}{a_1}\right)(1 - a) - \left(\frac{\delta}{\omega} - \frac{6}{a_1}\right)\rho^2\right]\right\}^{-1} \quad (15)$$

If the oscillator is synchronized, it executes only the forced oscillation and hence in the synchronized state $d\rho/dt = d\phi/dt = 0$. Amplitude of oscillations in the synchronized state are therefore obtained from

$$\delta F \cos \phi + aF \sin \phi = \rho[a(1 - \rho^2) + \delta^2 - k^2\omega^2] \quad (16)$$
$$\delta F \sin \phi - aF \cos \phi = \delta\rho(1 - a - \rho^2) \quad . \quad . \quad . \quad (17)$$

Thus the amplitude and phase of oscillation in the synchronized state are given by

$$\frac{F^2}{\rho^2} = \delta^2 + (1 - \rho^2)^2 + \frac{k^2\omega^2\{k^2\omega^2 + 2[\delta^2 + a(1 - \rho^2)]\}}{\delta^2 + a^2} \quad (18)$$

$$\tan \phi = \frac{\delta^2(1 - \rho^2) + a[a(1 - \rho^2) - k^2\omega^2]}{\delta(\delta^2 + a^2 - k^2\omega^2)} \quad . \quad (19)$$

(3) CHARACTERISTICS OF THE RESONANCE CURVES

Plots of ρ^2 against δ with F^2 as a parameter are referred to as the resonance curves. A family of resonance curves for $a = 0{\cdot}5$, $k = 1$, $\omega = 1$, $a_1 = 0{\cdot}1$ and negative values of δ are shown in Fig. 2.

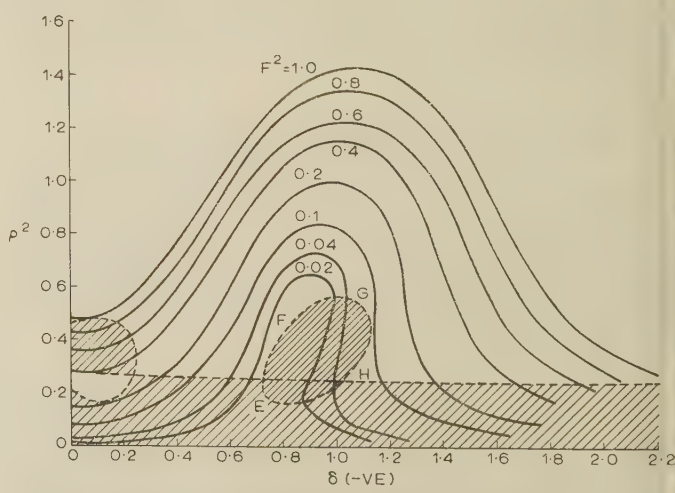

Fig. 2.—Resonance curves of the oscillator obtained theoretically.
$a_1 = 0{\cdot}1$, $a = 0{\cdot}5$, $k = 1$.

For low values of F^2, with increase in δ, ρ^2 at first increases, attains a maximum and then falls to zero. For very low values of F^2 the falling region has triple values for some δ. As F^2 increases the nature of the curves does not change much but the triple-valued region vanishes.

Evidently, all the equilibrium states represented by these resonance curves may not be stable. Stability conditions of the equilibrium states may be obtained by expanding $d\rho/dt$ and $d\phi/dt$ about the equilibrium points, retaining only the first-order terms and considering the first-order equation thus obtained. Accordingly, the equilibrium is stable if[7]

$$\left[\frac{\partial}{\partial\rho}\left(\frac{d\rho}{dt}\right)\right]_0+\left[\frac{\partial}{\partial\phi}\left(\frac{d\phi}{dt}\right)\right]_0<0 \quad . \quad . \quad . \quad (20)$$

and

$$\left[\frac{\partial}{\partial\rho}\left(\frac{d\rho}{dt}\right)\right]_0\left[\frac{\partial}{\partial\phi}\left(\frac{d\phi}{dt}\right)\right]_0 - \left[\frac{\partial}{\partial\rho}\left(\frac{d\phi}{dt}\right)\right]_0\left[\frac{\partial}{\partial\phi}\left(\frac{d\rho}{dt}\right)\right]_0<0 \quad (21)$$

The zero subscripts indicate the values of the coefficients for $d\rho/dt = d\phi/dt = 0$.

On evaluating the coefficients the above inequalities reduce to

$$\begin{aligned}&\{8(1+10\delta)(0{\cdot}5-2\rho^2)\delta+2[0{\cdot}5(1-\rho^2)+\delta^2-1]\\&\quad\times[(\delta-20)0{\cdot}5-2(\delta-20)\rho^2]\\&\qquad-\rho^2[(\delta-20)0{\cdot}5-(3\delta-20)\rho^2]\}\\&\quad\times\{16(1+10\delta)^2+[(\delta-20)0{\cdot}5-(3\delta-20)\rho^2]\\&\qquad+[(\delta-20)0{\cdot}5-(\delta-60)\rho^2]\}^{-1}<0 \quad (22)\end{aligned}$$

and

$$\begin{aligned}&(\delta^2+0{\cdot}25)[\delta^2+(1-\rho^2)(1-3\rho^2)]\\&\qquad+\{1-2[\delta^2+0{\cdot}5(1-2\rho^2)]\}>0 \quad (23)\end{aligned}$$

For large δ, inequality (22) reduces to

$$2\rho^2>0{\cdot}5 \quad . \quad . \quad . \quad . \quad . \quad . \quad . \quad (24)$$

Conditions imposed by the two inequalities are shown in Fig. 2 by shading the unstable region of the $\rho^2\delta$-plane.

For very low F^2, the oscillator has two separate zones of synchronization on the two sides of the ρ^2-axis. It is not synchronized at $\delta = 0$, but as δ is increased it becomes synchronized at a value of δ for which $\rho^2 \simeq 0{\cdot}25$. With further increase in δ it remains synchronized until the resonance curve meets the inequality curve EFGH on which the synchronized state becomes critical. As F^2 is increased, the lower value of δ for synchronization shifts towards zero. Also, on the border of synchronization for $0{\cdot}05 < F^2 < 0{\cdot}09$ there are two stable equilibrium states. Hence jump effect and the associated hysteresis phenomena as observed in the van der Pol oscillator[2] may be exhibited.

The oscillator becomes synchronized at $\delta = 0$ for values of F^2, for which, at this point, $\rho^2 > 0{\cdot}46$, and the two zones of synchronization are then linked together. The limit of δ up to which the synchronized state is stable is determined in this range by inequality (24).

It may be noted that the oscillator may also be synchronized at $\delta = 0$ for values of ρ for which $0{\cdot}21 < \rho^2 < 0{\cdot}29$.

The above discussion indicates that in practical applications of such an oscillator, if F^2 is low, the oscillator circuits have to be so tuned that the forcing signal frequency is approximately equal to one of the free-oscillation frequencies. If, however, F^2 is so large that the two zones of synchronization are linked together, the oscillator tuned circuits may be individually tuned to the forcing frequency.

(4) OSCILLATIONS OUTSIDE THE ZONE OF SYNCHRONIZATION

When the state of synchronization becomes unstable, the oscillator executes not only the forced oscillation but also free oscillations. If the detuning is not large, excitation of free oscillations results in the production of combination frequencies, amplitudes of which may not be much reduced by the selectivity characteristic of the oscillator circuits. For large detunings, however, amplitudes of the combination frequencies will be small and the solution may be assumed to be given by

$$\begin{aligned}x_1 = {}&A\sin(\omega t+\phi)+A_1\sin(\omega_{10}t+\phi_1)\\&+A_2\sin(\omega_{20}t+\phi_2) \quad (25)\end{aligned}$$

Both the free oscillations having the frequencies ω_{10} and ω_{20} are assumed to be present. The assumption that the solution would be of the above form, though strictly valid for large values of detuning, is expected to be approximately valid also for smaller values and may give a qualitative idea of the nature of oscillations on the border of the zone of synchronization.

Reduced equations relating the derivatives of ρ, ϕ, A_1, ϕ_1, A_2 and ϕ_2 with respect to t with the oscillator parameters may be obtained by substituting for x_1 from eqn. (25) in eqn. (8). Considerations become involved if the second-order terms are all retained. If, however, a_1 is assumed to be such that effects of the second-order terms are negligible, when ω_{10}, ω_{20}, ω and the combination frequencies are non-integrally related, the reduced equations are:

$$\frac{d\rho}{dt}=\frac{-\delta F\sin\phi+aF\cos\phi+\delta\rho(1-a-\rho^2-2\rho_1^2-2\rho_2^2)}{4\left(k^2\omega+\dfrac{\delta}{a_1}\right)} \quad . \quad . \quad . \quad . \quad (26)$$

$$\rho\frac{d\phi}{dt}=\frac{-\delta F\cos\phi-aF\sin\phi+\rho(\delta^2-k^2\omega^2)}{4\left(k^2\omega+\dfrac{\delta}{a_1}\right)} \quad . \quad . \quad . \quad (27)$$

$$\frac{d\rho_1}{dt}=\frac{(\omega_0^2-\omega_{10}^2)a_1(1-a-\rho_1^2-2\rho^2-2\rho_2^2)\rho_1}{2(1-k_1^2)(\omega_{20}^2-\omega_{10}^2)} \quad . \quad . \quad . \quad (28)$$

$$\frac{d\rho_2}{dt}=\frac{(\omega_{20}^2-\omega_0^2)a_1(1-a-\rho_2^2-2\rho^2-2\rho_1^2)\rho_2}{2(1-k_1^2)(\omega_{20}^2-\omega_{10}^2)} \quad . \quad . \quad (29)$$

$$\frac{d\phi_1}{dt}=\frac{d\phi_2}{dt}=0 \quad . \quad . \quad . \quad . \quad . \quad . \quad . \quad . \quad . \quad . \quad . \quad (30)$$

where $\rho_1 = \omega_{10}A_1/\rho_0$ and $\rho_2 = \omega_{20}A_2/\rho_0$.

For large values of δ, ρ is approximately given by

$$\rho^2\simeq\frac{F^2}{\delta^2+k^2\omega^2(k^2\omega^2-2\delta^2)/\delta^2} \quad . \quad . \quad . \quad (31)$$

and $d\rho/dt$, $d\phi/dt$ may be taken to be zero for all time.

Thus for large values of δ, the equilibrium conditions reduce to

$$\rho_1(1-a-2\rho^2-\rho_1^2-2\rho_2^2)=0 \quad . \quad . \quad . \quad (32)$$

$$\rho_2(1-a-2\rho^2-\rho_2^2-2\rho_1^2)=0 \quad . \quad . \quad . \quad (33)$$

These equations have three combinations of solutions, namely

$$\rho_1=0 \quad \rho_2^2=1-a-2\rho^2 \quad . \quad . \quad . \quad . \quad . \quad (34)$$

$$\rho_2=0 \quad \rho_1^2=1-a-2\rho^2 \quad . \quad . \quad . \quad . \quad . \quad (35)$$

$$\rho_1^2=\frac{1-a-2\rho^2}{3} \quad \rho_2^2=\frac{1-a-2\rho^2}{3} \quad . \quad (36)$$

On applying the stability criteria it is readily shown that only the first two combinations may be stable. It may therefore be

concluded that far away from the zone of synchronization free oscillations at both the frequencies cannot be simultaneously excited if the frequencies of free oscillation and their combinations are non-integrally related.

Equations giving the derivatives of ρ_1, ϕ_1, ρ_2 and ϕ_2 with respect to t are, however, modified if ω, ω_{10}, ω_{20} and their combination frequencies have an integral relation. If it is considered that $\omega > \omega_{20} > \omega_{10}$, then for the cubic non-linearity we have to consider only the combination $2\omega_{20} - \omega$, and if it is equal to ω_{10}, the expressions are modified to

$$\frac{d\rho_1}{dt} = \frac{(\omega_0^2 - \omega_{10}^2)a_1\rho_1\left(1 - a - 2\rho^2 - \rho_1^2 - 2\rho_2^2 - \frac{\rho\rho_2^2}{\rho_1}\cos\Phi\right)}{2(1 - k_1^2)(\omega_{20}^2 - \omega_{10}^2)} \quad . \quad . \quad . \quad . \quad (37)$$

$$\frac{d\phi_1}{dt} = \frac{-(\omega_0^2 - \omega_{10}^2)a_1\rho\frac{\rho_2^2}{\rho_1}\sin\Phi}{2(1 - k_1^2)(\omega_{20}^2 - \omega_{10}^2)} \quad . \quad . \quad . \quad . \quad . \quad . \quad . \quad (38)$$

$$\frac{d\rho_2}{dt} = \frac{(\omega_{20}^2 - \omega_0^2)a_1\rho_2(1 - a - 2\rho^2 - \rho_2^2 - 2\rho_1^2 - 2\rho\rho_1\cos\Phi)}{2(1 - k_1^2)(\omega_{20}^2 - \omega_{10}^2)} \quad . \quad . \quad . \quad . \quad (39)$$

$$\frac{d\phi_2}{dt} = \frac{(\omega_{20}^2 - \omega_0^2)a_1 2\rho\rho_1\sin\Phi}{2(1 - k_1^2)(\omega_{20}^2 - \omega_{10}^2)} \quad . \quad . \quad . \quad . \quad . \quad . \quad . \quad (40)$$

where $\Phi = 2\phi_2 - \phi - \phi_1$ . . . . . (41)

Equilibrium conditions in this case are given by $d\rho_1/dt = d\rho_2/dt = d\phi/dt = 0$. On applying these conditions and considering the resultant equations, it is observed that in this case simultaneous free oscillations at both the frequencies may occur if the equality $2\omega_{20} - \omega = \omega_{10}$ is satisfied only approximately. Simultaneous oscillations at both the frequencies will be exhibited by the appearance of a steady double periodicity in the amplitude variation. It should be noted that similar simultaneous oscillations at the two frequencies of free oscillation may also be obtained for other combinations in other ranges, such as for $\omega_{10} < \omega < \omega_{20}$; the combination $2\omega - \omega_{10} = \omega_{20}$ gives stable simultaneous oscillation.

(5) EXPERIMENTAL STUDY OF THE OSCILLATIONS

An experimental oscillator was set on an electrode differential analyser, the describing differential equations of which are the same as eqns. (6) and (7). The experimental resonance curves shown in Fig. 3 were obtained from measurements on this oscillator. The magnitude of the variable representing x_1 i eqns. (6) and (7) was measured by a thermocouple and a d.c millivoltmeter. δ was varied by varying ω_1^2 and ω_2^2 simul taneously, keeping ω^2 constant. On comparing the experimenta curves with those calculated from eqn. (18) it may be noted tha in most of the regions the agreement is better than 1%.

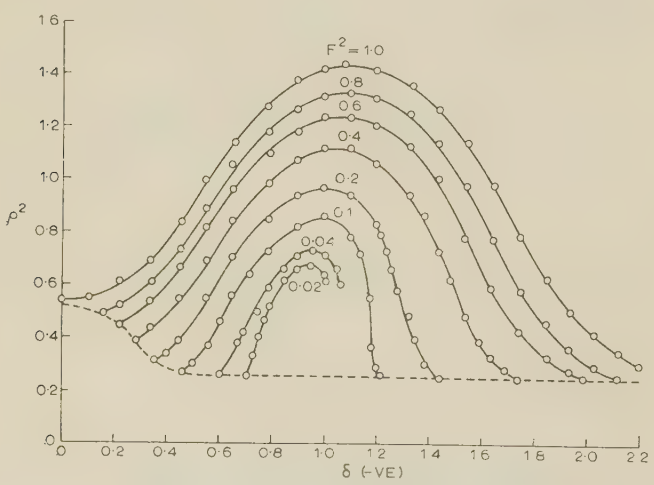

Fig. 3.—Experimental resonance curves.

The limiting values of δ up to which the oscillator remain synchronized are given by the end-points of the resonance curve shown in Fig. 3. These values also agree very closely with thos given by the inequalities (22) and (23) shown by the dotted lin in Fig. 2. However, the lower range of ρ^2 in which the oscillato may be synchronized at $\delta = 0$ could not be obtained. It i believed that, since this range is surrounded by unstable regions the close adjustment of parameters required for synchronizatio could not be practically attained.

A visual representation of the transformation of the synchro nized oscillation to the asynchronous condition for differen values of δ and fixed F^2 may be obtained by the phase trajectorie in the $(A\cos\phi - A\sin\phi)$-plane. Voltages proportional t $A\cos\phi$ may be obtained as follows: (*a*) add the output of th oscillator to the forcing signal and obtain the square of th resultant amplitude; (*b*) subtract the oscillator output from th forcing signal and obtain the square of the resultant amplitude and subtract (*b*) from (*a*). $A\sin\phi$ may be obtained by com bining the oscillator output with a signal in phase quadratur with the forcing signal. The square of the amplitude may b obtained by a thermocouple, with the heater time-constant larg compared with the frequencies of oscillations but small compare with the difference frequency. In Fig. 4 are shown some of th

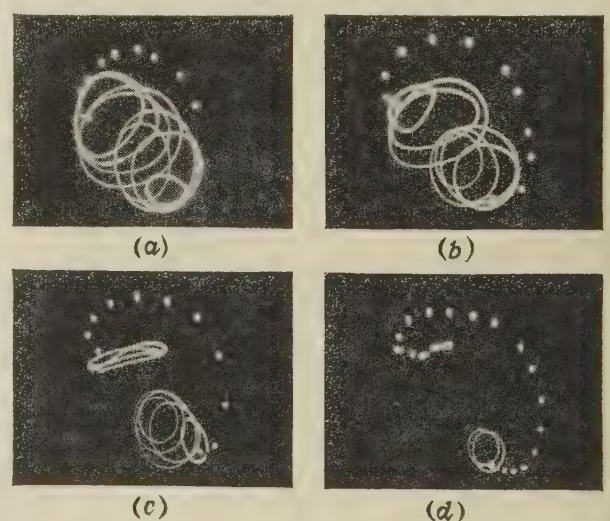

Fig. 4.—Experimental phase trajectories.
(*a*) $F^2 = 0·2$. (*c*) $F^2 = 0·6$.
(*b*) $F^2 = 0·4$. (*d*) $F^2 = 0·8$.

plots of voltages proportional to $A\cos\phi$ against voltages propo tional to $A\sin\phi$ obtained in this way. The dots in the Figur correspond to values of δ for which the oscillator is synchronize and the closed curves correspond to values of δ for which t oscillator is in the asynchronous state. δ in each case increas from left to right. It may be noted that they show clearly t transformation of the limit cycles corresponding to the asynchr nous states to stable singularities corresponding to the synchr nous states for low values of δ and also the reverse transformati for higher values of δ. Also, the gradual disappearance of t limit cycles with increase in F^2 for low values of δ is clea indicated.

It has been deduced theoretically and confirmed experimentally hat far away from the zone of synchronization only one of the ree oscillations may be excited, whereas on the border zones, if $2\omega_{20} - \omega_{10} = \omega$ or $2\omega - \omega_{20} = \omega_{10}$, oscillations at both the requencies of free oscillation may be excited. In Fig. 5 are hown some oscillograms for $F^2 = 0{\cdot}4$ in which x_1 is plotted gainst time. Figs. 5(*a*)–(*c*) correspond to adjustments of

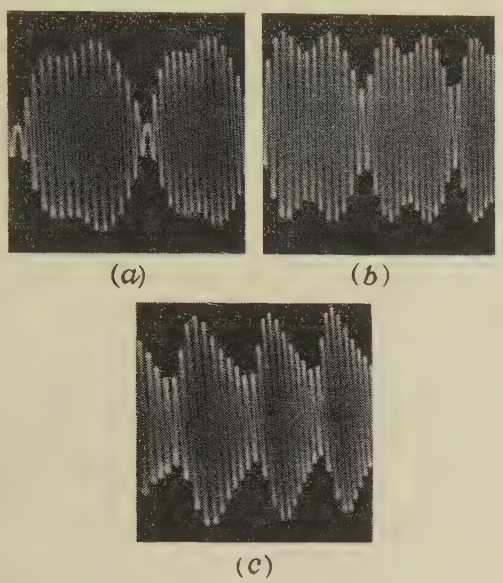

Fig. 5.—Oscillograms of asynchronous oscillations.

(*a*) $\omega_{10} = 0{\cdot}842$, $\omega_{20} = 0{\cdot}931$.
(*b*) $\omega_{10} = 0{\cdot}823$, $\omega_{20} = 0{\cdot}912$.
(*c*) $\omega_{10} = 0{\cdot}810$, $\omega_{20} = 0{\cdot}895$.

frequencies such that the equality $2\omega_{20} - \omega_{10} = \omega$ or the equality $2\omega - \omega_{20} = \omega_{10}$ is approximately satisfied. The existence of double periodicity, in each case, in the amplitude variation indicates oscillation at both the frequencies of free oscillation. It may be noted that oscillation at the lower of the two frequencies of free oscillation gradually develops as the equality is approached. It, however, dies out as the tuning is moved away from equality.

(6) CONCLUSIONS

Resonance characteristics of an oscillator with two degrees of freedom have been obtained theoretically and have been found to agree with those obtained with the help of a differential analyser to within 1% for most of the ranges.

It has also been shown that outside the zone of synchronization, when the frequencies of free oscillation and their combination frequencies are non-integrally related with the forcing frequency, in addition to the forced oscillation, oscillation at one of the frequencies of free oscillation is excited. However, if they are approximately integrally related oscillations, at both the frequencies of free oscillation may be excited.

(7) ACKNOWLEDGMENTS

The author is deeply indebted to Professor J. N. Bhar for his constant help and guidance. Thanks are also due to Dr. A. K. Choudhury for his help in a part of the experimental work.

(8) REFERENCES

(1) VAN DER POL, B.: 'Forced Oscillation in a Circuit with Non-linear Resistance', *Philosophical Magazine*, 1927, **3**, p. 65.
(2) CARTWRIGHT, M. L.: 'Forced Oscillation in Nearly Sinusoidal Systems', *Journal I.E.E.*, March, 1948, **95**, Pt. III, p. 88.
(3) TUCKER, D. G.: 'Forced Oscillations in Oscillator Circuits, and the Synchronization of Oscillators', *Journal I.E.E.*, September, 1945, **92**, Pt. III, p. 226.
(4) VAN DER POL, B.: 'On Oscillation Hysteresis in a Triode Generator with Two Degrees of Freedom', *Philosophical Magazine*, 1922, **43**, p. 700.
(5) FONTANA, R. E.: 'Internal Resonance in Circuits Containing Nonlinear Resistance', *Proceedings of the Institute of Radio Engineers*, 1951, **39**, p. 945.
(6) SCHAFFNER, J. S.: 'Simultaneous Oscillation in Oscillators', *Transactions of the Institution of Radio Engineers*, 1954, p. 2.
(7) MINORSKY, N.: 'Introduction to Non-linear Mechanics' (Edward Brothers, 1947), pp. 51 and 344.

621.372.6

The Institution of Electrical Engineers
Monograph No. 399 E
Sept. 1960

MATRIX ANALYSIS OF CONSTRAINED NETWORKS

By A. NATHAN, M.S., D.Sc. (Eng.), Associate Member.

(*The paper was first received* 2nd *December*, 1958, *in revised form* 31st *March*, 1959, *and* 26th *January*, 1960, *and in final form* 21st *May*, 1960. *It was published as an* INSTITUTION MONOGRAPH *in September*, 1960).

SUMMARY

Following a review of nodal analysis of unconstrained lumped linear time-invariant networks it is shown how networks with imposed unilateral constraints, i.e. transmittances and voltage sources, can conveniently be analysed by matrix methods. Their admittance matrix is equal to the product of a submatrix of the admittance matrix before the application of the constraints and a transmittance matrix which describes the constraints. Constraints lower the rank of the original admittance matrix, thus making the method quite attractive in practice. Applications included are a computing network, difference amplifiers, a d.c. amplifier and signal-flow graphs.

LIST OF PRINCIPAL SYMBOLS

Network N contains n nodes, of which n_d are driven, n_e eliminated, n_f free, and n_{ne} not eliminated.

$\boldsymbol{m}$ = Matrix associated with N.

$\boldsymbol{m}_{[\alpha}$ = Submatrix of $\boldsymbol{m}$ consisting of its rows which are associated with α, where $\alpha = d$, e, f or ne (driven, eliminated, free, or not eliminated).

$\boldsymbol{m}'$ = The transpose of $\boldsymbol{m}$.

$\boldsymbol{t}$ = Transmittance matrix.

$\boldsymbol{y}$ = Admittance matrix.

$\boldsymbol{I}$ = Unit matrix.

(1) INTRODUCTION

It is rather unusual to analyse networks containing transmittances by matrix methods. The reason is that an ideal transmittance corresponds to a unilateral device of zero output impedance and infinite transconductance. The common methods of matrix analysis of networks would therefore become quite circuitous, requiring a limiting process for the derivation of the final result. A proper method should avoid this roundabout path and tackle directly the real nature of a transmittance as a constraint which controls (i.e. drives) the voltage of a node, thereby lowering by one the number of independent variables which describe the state of the network. Such a method will be developed; it should make the analysis of these networks as amenable to matrix methods as that of the unconstrained species.

Nodal analysis will be used throughout although an analogous loop analysis could readily be established. For the majority of active circuits encountered in practice nodal analysis is more convenient. The method consists essentially of simple operations with and upon the admittance matrix of the network without the constraints and a transmittance matrix which defines the constraints; it is an extension of the familiar methods of network analysis.

(2) REVIEW OF NODAL ANALYSIS OF NETWORKS

A short review of conventional nodal analysis of lumped linear time-invariant networks will be given.

Considering first passive networks,[1] let $Y_{\alpha\beta} = Y_{\beta\alpha}$ denote the admittance of the branch connecting nodes α and β, let v_α denote the voltage of node α with respect to an arbitrary reference, and let $i_{(s)\alpha}$ denote the source current flowing into node α. All quantities such as v_α, $i_{(s)\alpha}$ and $Y_{\alpha\beta}$ are to be understood as complex in steady-state analysis, or, in the transient case, as Laplace transforms of the corresponding time-dependent quantities or differential operators.

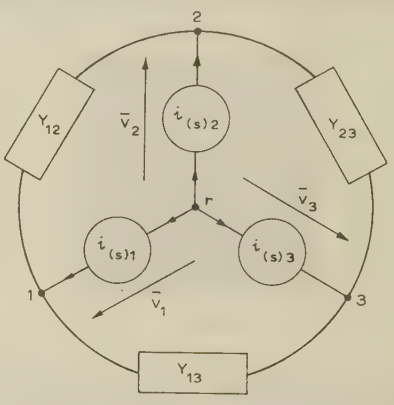

Fig. 1.—3-node indefinite network.

Fig. 1 shows a network containing the three nodes 1, 2 and 3 and an isolated reference node r. By Kirchhoff's second law the source current into node 1 is

$$i_{(s)1} = (v_1 - v_2)Y_{12} + (v_1 - v_3)Y_{13} = v_1(Y_{12} + Y_{13}) - v_2Y_{12} - v_3Y_{13} \quad (1)$$

and similarly for nodes 2 and 3, so that in matrix notation

$$\begin{bmatrix} i_{(s)1} \\ i_{(s)2} \\ i_{(s)3} \end{bmatrix} = \begin{bmatrix} Y_{12} + Y_{13} & -Y_{12} & -Y_{13} \\ -Y_{12} & Y_{12} + Y_{23} & -Y_{23} \\ -Y_{13} & -Y_{23} & Y_{13} + Y_{23} \end{bmatrix} \begin{bmatrix} v_1 \\ v_2 \\ v_3 \end{bmatrix} \quad (2)$$

The square matrix is called the indefinite admittance matrix of the network and will be denoted $\bar{y}$. Writing $\bar{i}_{(s)}$ for the source current vector and $\bar{v}$ for the node voltage vector,

$$\bar{i}_{(s)} = \bar{y}\bar{v} \quad . \quad . \quad . \quad . \quad . \quad . \quad . \quad . \quad (3)$$

or, equivalently

$$i_{(s)\alpha} = \sum_{\beta} \bar{y}_{\alpha\beta}v_\beta \quad . \quad . \quad . \quad . \quad . \quad . \quad (4)$$

where the summation extends over all the nodes of the network. In general we have n nodes and an isolated reference node. For convenience we define $Y_{\alpha\alpha}$ by

$$\sum_{\beta=1}^{n} Y_{\alpha\beta} = 0 \quad . \quad . \quad . \quad . \quad . \quad . \quad . \quad . \quad (5)$$

i.e.

$$-Y_{\alpha\alpha} = \sum_{\substack{\beta=1 \\ \beta\neq\alpha}}^{n} Y_{\alpha\beta} \quad . \quad . \quad . \quad . \quad . \quad . \quad (6)$$

In eqn. (2), for example, $-Y_{11} = Y_{12} + Y_{13}$.

Correspondence on Monographs is invited for consideration with a view to publication.

Dr. Nathan is Senior Lecturer in the Department of Electrical Engineering, Technion, Israel Institute of Technology, Haifa.

Kirchhoff's second law, applied to node α, then states that

$$i_{(s)\alpha} = \sum_{\beta=1}^{n} - Y_{\alpha\beta} v_\beta; \quad \alpha = 1, 2, \ldots n \quad . \quad . \quad (7)$$

which is the generalization of eqn. (2). Comparing eqn. (7) with the equivalent equation (4) [eqns. (3) and (4) hold in general] we find for the $\alpha\beta$ element $\bar{y}_{\alpha\beta}$ of the indefinite admittance matrix $\bar{y}$

$$\bar{y}_{\alpha\beta} = - Y_{\alpha\beta} \quad . \quad . \quad . \quad . \quad . \quad . \quad (8)$$

$Y_{\alpha\beta}$ is thus seen to enter $\bar{y}$ as follows:

$$\bar{y} = \begin{array}{c} \begin{matrix} \quad & \alpha & \quad & \beta & \quad \end{matrix} \\ \begin{bmatrix} \cdots & \cdots & \cdots & \cdots & \cdots \\ \cdots & Y_{\alpha\beta} & \cdots & -Y_{\alpha\beta} & \cdots \\ \cdots & \cdots & \cdots & \cdots & \cdots \\ \cdots & \cdots & \cdots & \cdots & \cdots \\ \cdots & -Y_{\alpha\beta} & \cdots & Y_{\alpha\beta} & \cdots \\ \cdots & \cdots & \cdots & \cdots & \cdots \end{bmatrix} \end{array} \begin{matrix} \\ \alpha \\ \\ \\ \beta \\ \\ \end{matrix} \quad . \quad . \quad . \quad (9)$$

$\bar{y}$ can therefore be written down by inspection of the network diagram to which it corresponds, considering the contributions of one admittance at a time. [Compare the correspondence between Fig. 1 and eqn. (2).] Note that $\bar{y}$ is symmetric and that any row or column sums to zero.

To solve eqn. (3), i.e. to solve the network, we must first fix the reference voltage. Taking as reference the voltage of node i,

$$v_i = 0 \quad . \quad . \quad . \quad . \quad . \quad . \quad . \quad . \quad (10)$$

we pass from the indefinite admittance matrix $\bar{y}$ to the admittance matrix y of the network by deleting the ith row and column in $\bar{y}$, and from $\bar{v}$, $\bar{i}_{(s)}$ to v, $i_{(s)}$ by omitting their ith components.

For example, in Fig. 1 let us take node 3 as reference node; thus nodes r and 3 coincide and Fig. 2 results. All node

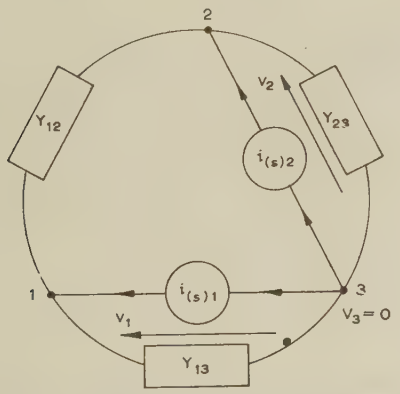

Fig. 2.—The network of Fig. 1 with node 3 as reference node.

voltages are now measured with respect to node 3. Eqn. (2) becomes

$$\begin{bmatrix} i_{(s)1} \\ i_{(s)2} \end{bmatrix} = \begin{bmatrix} Y_{12} + Y_{13} & -Y_{12} \\ -Y_{12} & Y_{12} + Y_{23} \end{bmatrix} \begin{bmatrix} v_1 \\ v_2 \end{bmatrix} \quad . \quad (11)$$

In general,

$$yv = i_{(s)} \quad . \quad . \quad . \quad . \quad . \quad . \quad . \quad (12)$$

with the solution

$$v = y^{-1} i_{(s)} \quad . \quad . \quad . \quad . \quad . \quad . \quad . \quad (13)$$

where y^{-1} is the inverse of y. y can be shown to be non-singular, so that y^{-1} exists and eqn. (12) can be solved. $\bar{y}$ is of course a singular matrix, because of the linear dependence of its rows (and columns), and eqn. (3) has no unique solution.

We now apply a non-vanishing source, $i_{(s)\alpha}$, to node α of the network only. The (through-) transmittance from α to β is then defined as

$$H_{\alpha\beta} = v_\beta / v_\alpha \quad . \quad . \quad . \quad . \quad . \quad . \quad (14)$$

From eqn. (13), bearing in mind that $i_{(s)\alpha}$ is now the only component of $i_{(s)}$ which does not vanish, we have

$$H_{\alpha\beta} = y_{\beta\alpha}^{-1} i_{(s)\alpha} / y_{\alpha\alpha}^{-1} i_{(s)\alpha} = y^{\alpha\beta} / y^{\alpha\alpha} \quad . \quad . \quad (15)$$

where superscripts denote cofactors.

Similarly, the input impedance at terminal α is equal to

$$Z_{(in)\alpha} = y^{\alpha\alpha} / |y| \quad . \quad . \quad . \quad . \quad . \quad (16)$$

where $|y|$ denotes the determinant of y.

For an n-terminal linear time-invariant device[2-4] which is not necessarily passive (an n-port), eqns. (3) and (4) still apply. y is now not necessarily symmetric. We proceed to show that the sum of the components of any row or column in $\bar{y}$ is zero under simple assumptions even in this more general case.

For eqn. (4) to be a consistent set of equations any one equation must be a linear combination of the others. Moreover no current may flow into the reference node in the indefinite case, because it is an isolated node. Therefore, from Kirchhoff's second law,

$$\sum_{\alpha=1}^{n} \bar{i}_{(s)\alpha} = 0$$

Summing eqn. (4) over all α we obtain the identity

$$\sum_{\alpha} \sum_{\beta} \bar{y}_{\alpha\beta} v_\beta \equiv 0$$

from which follows $\sum_{\alpha} y_{\alpha\beta} = 0$, i.e. the columns sum to zero.

We further demand that the addition of equal voltages to all n terminals leaves $\bar{i}_{(s)}$ unchanged.

Whence

$$\sum_{\beta} \bar{y}_{\alpha\beta} (v_0 + v_\beta) = \bar{i}_{(s)\alpha}$$

must be independent of v_0, which implies the vanishing of the coefficient of v_0,

i.e. $$\sum_{\beta} \bar{y}_{\alpha\beta} = 0$$

and the sum of the components of any row of y is zero.

For triodes with cathode k as reference node we have, neglecting grid current,

$$y = \begin{array}{c} \begin{matrix} g & p \end{matrix} \\ \begin{bmatrix} 0 & 0 \\ g_m & g_p \end{bmatrix} \end{array} \begin{matrix} g \\ p \end{matrix} \quad . \quad . \quad . \quad . \quad . \quad (17)$$

where g, p denote grid and anode, and g_m and $r_p = 1/g_p$ are the transconductance and anode resistance, respectively.

Fig. 3 shows the series connection of a transmittance A and

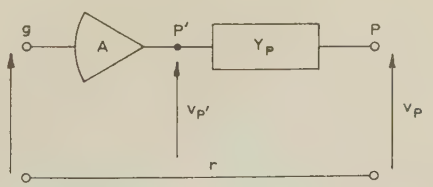

Fig. 3.—Series-connected transmittance and admittance.

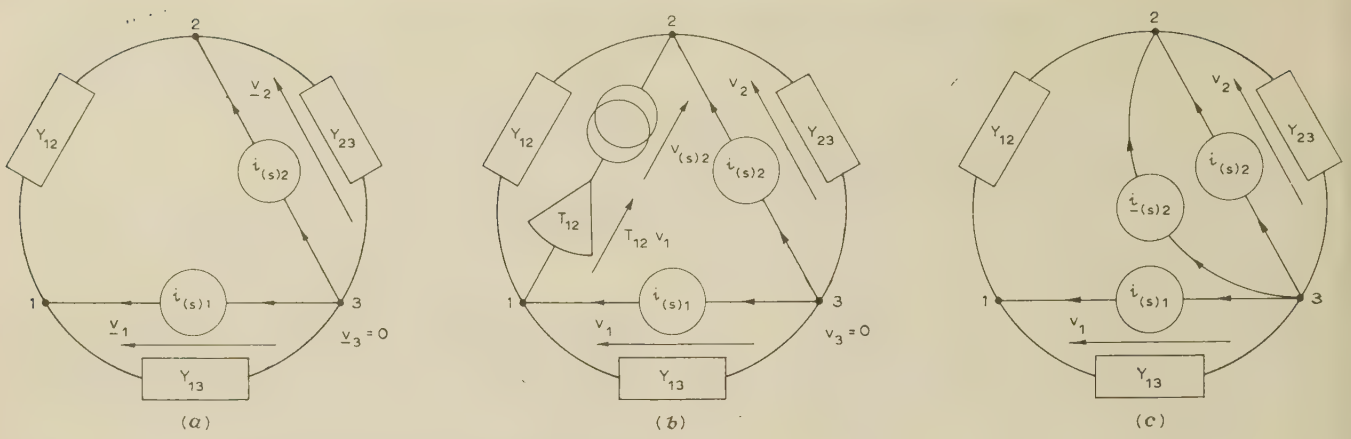

Fig. 4.—Network analysed in the introductory example.

(*a*) 'Parent' network $\underline{N}$.
(*b*) Network N, derived from $\underline{N}$ by introduction of a constraint.
(*c*) Network $\underline{N}$ equivalent to N.

an output admittance Y_p. If node p' is constrained by g without loading g, so that $v_{p'} = Av_g$ and $i_{(s)g} = 0$, we have

$$0v_g + 0v_p = 0$$
$$-AY_pv_g + Y_pv_p = i_{(s)p}$$

so that

$$y = \begin{matrix} \\ g \\ p \end{matrix}\begin{matrix} \begin{matrix} g & p \end{matrix} \\ \begin{bmatrix} 0 & 0 \\ -AY_p & Y_p \end{bmatrix} \end{matrix} \quad . \quad . \quad . \quad . \quad . \quad (18)$$

which corresponds, as it should, to the previous example of a triode, eqn. (17), with $g_m = -AY_p$ and $g_p = Y_p$.

p' does not appear in the network equations and we say that it is eliminated. Note that this procedure is not readily applicable if a pure constraint operates between g and p, i.e. if $Z_p = 1/Y_p = 0$. In the sequel we shall be concerned with networks including such pure constraints.

The indefinite admittance matrix $\bar{y}$ corresponding to eqn. (17) is formed by augmentation of y to yield zero sums in rows and columns, i.e.

$$\bar{y} = \begin{matrix} \\ g \\ p \\ k \end{matrix}\begin{matrix} \begin{matrix} g & p & k \end{matrix} \\ \begin{bmatrix} 0 & 0 & 0 \\ g_m & g_p & -g_m - g_p \\ -g_m & -g_p & g_m + g_p \end{bmatrix} \end{matrix} \quad . \quad . \quad . \quad (19)$$

For transistors (or any other 3-terminal network) in terms of h parameters,[5] for example,

$$y = \begin{bmatrix} 1/h_{11} & -h_{12}/h_{11} \\ h_{21}/h_{11} & |\boldsymbol{h}|/h_{11} \end{bmatrix} \quad . \quad . \quad . \quad . \quad (20)$$

Eqns. (15) and (16) are valid for active as well as for passive networks.

(3) CONSTRAINED NETWORKS

(3.1) Analysis of an Example

Let us take a network $\underline{N}$ as in Section 2. This network will be described by its admittance matrix $\underline{y}$, which, in conjunction with the source current vector $\underline{i}_{(s)}$, then determines its node voltage vector $\underline{v}$ through eqn. (12), which now reads $\underline{i}_{(s)} = \underline{y}\underline{v}$. We introduce one or more unilateral voltage constraints in $\underline{N}$ and denote the resulting network by N. The constraints will in general change the values of the node voltages and we denote the new node voltage vector by $\boldsymbol{v}$. It is our object to determine $\boldsymbol{v}$.

As an example we take for $\underline{N}$ the network of Fig. 2, as redrawn in Fig. 4(*a*), in which the node voltages are redesignated as $\underline{v}_1$ and $\underline{v}_2$. Network N which is to be analysed is shown in Fig. 4(*b*). It consists of $\underline{N}$ with an additional transmittance T_{12} and a voltage source $v_{(s)2}$ between nodes 1 and 2, such that

$$v_2 = T_{12}v_1 + v_{(s)2} \quad . \quad . \quad . \quad . \quad . \quad (21)$$

where the new node voltages are v_1 and v_2. T_{12} must not load node 1, i.e. no current flows into the device implementing T_{12}.

The general and more formal considerations which will be described later are closely parallel to the following analysis which may not appear to be handled in a particularly straightforward way. The advantage of our method is that, once it has been developed, its application is extremely simple, so that the solution of the example could be written down by inspection of Fig. 4(*b*).

The constraining branch injects a current into node 2. This current is withdrawn from the reference node. The network of Fig. 4(*c*), in which the constraint has been replaced by the current source $\underline{i}_{(s)2}$, is therefore equivalent to N, provided that the node voltages obey the constraining equation (21). This equivalence is in the sense that corresponding nodes are at equal voltages. The network of Fig. 4(*c*) is identical with $\underline{N}$ Fig. 4(*a*); only its sources are different. We can therefore use eqn. (12), replacing $\underline{i}_{(s)2}$ by $i_{(s)2} + \underline{i}_{(s)2}$, i.e.

$$\begin{bmatrix} i_{(s)1} \\ i_{(s)2} + \underline{i}_{(s)2} \end{bmatrix} = \begin{bmatrix} Y_{12} + Y_{13} & -Y_{12} \\ -Y_{12} & Y_{12} + Y_{23} \end{bmatrix} \begin{bmatrix} v_1 \\ v_2 \end{bmatrix} \quad (22)$$

$\underline{i}_{(s)2}$ is an additional unknown; we have now, however, three equations, namely eqn. (21) and eqns. (22), from which v_1, v_2 and $\underline{i}_{(s)2}$ can be found. To do so, we supplement eqn. (21) by the identity $v_1 = v_1$ and have, in matrix form,

$$\begin{bmatrix} v_1 \\ v_2 \end{bmatrix} = \begin{bmatrix} 1 \\ T_{12} \end{bmatrix} v_1 + \begin{bmatrix} 0 \\ v_{(s)2} \end{bmatrix} \quad . \quad . \quad . \quad (23)$$

Note that the right-hand side does not contain v_2. Substituting eqn. (23) into eqn. (22) we obtain

$$\begin{bmatrix} i_{(s)1} \\ i_{(s)2} + \underline{i}_{(s)2} \end{bmatrix} = \begin{bmatrix} Y_{12} + Y_{13} & -Y_{12} \\ -Y_{12} & Y_{12} + Y_{23} \end{bmatrix} \begin{bmatrix} 1 \\ T_{12} \end{bmatrix} v_1 + \begin{bmatrix} Y_{12} + Y_{13} & -Y_{12} \\ -Y_{12} & Y_{12} + Y_{23} \end{bmatrix} \begin{bmatrix} 0 \\ v_{(s)2} \end{bmatrix} \quad (24)$$

The first of eqns. (24) can be solved for v_1; v_2 is obtained from eqn. (21). If $\underline{i}_{(s)2}$ is required, we use the second of eqns. (24). v_1 and v_2 could be found without the second of eqns. (24); i.e. it would have been sufficient to write

$$i_{(s)1} = [Y_{12} + Y_{13} - Y_{12}]\begin{bmatrix} 1 \\ T_{12} \end{bmatrix} v_1 + [Y_{12} + Y_{13} - Y_{12}] \begin{bmatrix} 0 \\ v_{(s)2} \end{bmatrix} = (Y_{12} + Y_{13} - T_{12}Y_{12})v_1 - Y_{12}v_{(s)2} \quad (25)$$

which results from eqns. (24) by omission of the second rows of the source-current vector and of the square admittance matrix.

It is now an easy matter to generalize these considerations.

(3.2) Separable Problems

Let $\underline{N}$ be a lumped linear time-invariant network, described by its (definite) admittance matrix $\underline{y}$. Let $\underline{\boldsymbol{v}}$ be the voltage vector whose αth component, $\underline{v}_\alpha$, denotes the voltage of node α with respect to a reference node, and let $\boldsymbol{i}_{(s)}$ be the source-current vector, $i_{(s)\beta}$ denoting the source current withdrawn from the reference node and flowing into node β. Then, for network $\underline{N}$,

$$\underline{\boldsymbol{y}}\,\underline{\boldsymbol{v}} = \boldsymbol{i}_{(s)} \quad . \quad . \quad . \quad . \quad . \quad . \quad (26)$$

Now consider network N which results from the imposition of unilateral transmittances $T_{\alpha\beta}$ on $\underline{N}$ and the inclusion of source voltages $v_{(s)\beta}$ (Fig. 5). No current is to be withdrawn from any

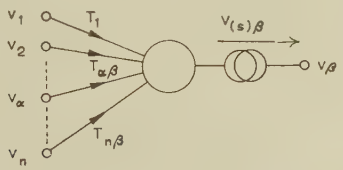

Fig. 5.—Relating to the definition of a constraint.

node α by $T_{\alpha\beta}$. Moreover we shall, at present, exclude all cases in which any $T_{\alpha\beta}$ emanates from a node that is itself driven. In other words, all driving nodes must be free.

We now have the constraining equations:

$$v_\beta = \sum_\alpha T_{\alpha\beta}v_\alpha + v_{(s)\beta} \quad . \quad . \quad . \quad . \quad (27)$$

where $T_{\beta\beta} = 1$ for all free nodes, which is equivalent to supplementing the relations by the identities $v_\beta = v_\beta$. This is in order to have one relation (27) for each node of N. The summation over α scans all n_f free nodes, whereas $\beta = 1, 2, \ldots n$.

$T_{\alpha\beta}$ is the matrix element of the transmittance matrix $\boldsymbol{t}$ which is of order $n_f \times n$. Eqn. (27) is equivalent to

$$\boldsymbol{v} = \boldsymbol{t}'\boldsymbol{v}_{[f} + \boldsymbol{v}_{(s)} \quad . \quad . \quad . \quad . \quad . \quad (28)$$

where $\boldsymbol{t}'$ denotes the transpose of $\boldsymbol{t}$, i.e.

$$(t')_{\alpha\beta} = (t)_{\beta\alpha} = T_{\beta\alpha}$$

Wherever two or more transmittances control the same node we stipulate the provision of a mixing-point, as in Fig. 5. Note that the introduction of a transmittance pointing into a mixing-point of a given network is not a constraint; only the simultaneous imposition of all transmittances that converge upon a mixing-point constitutes a constraint. In passing from $\underline{N}$ to N we shall exclude the introduction of transmittances that do not impose constraints.

As an example of the formation of $\boldsymbol{t}$ consider Fig. 6(*a*).

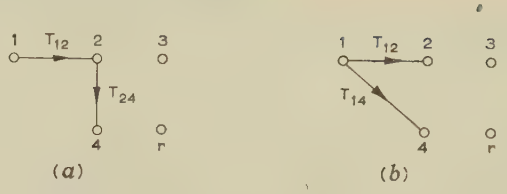

Fig. 6.—Example of constraints imposed on a network of 4 nodes and a reference node.

(*a*) Original constraints.
(*b*) Constraints equivalent to (*a*) provided that $T_{14} = T_{12}T_{24}$.

Node 2 is both driving and driven, which seems to exclude such a situation from the present considerations. Fig. 6(*b*), with $T_{14} = T_{12}T_{24}$ is, however, clearly equivalent to it, and accordingly

$$t = \begin{matrix} \\ 1 \\ 3 \end{matrix}\begin{matrix} \begin{matrix} 1 & 2 & 3 & 4 \end{matrix} \\ \begin{bmatrix} 1 & T_{12} & 0 & T_{14} \\ 0 & 0 & 1 & 0 \end{bmatrix} \end{matrix}$$

Any situation which does not contain one or more loops consisting of a cascade of transmittances, i.e. a transmittance loop as, for example, in Fig. 7, in which 232 forms such a loop, can be dealt with similarly.

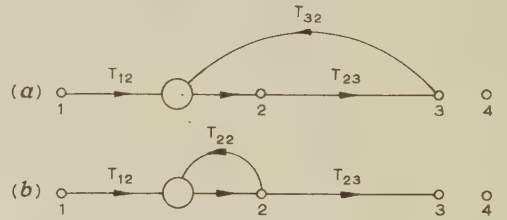

Fig. 7.—Example of constraints embodying a transmittance loop.

(*a*) Original constraints.
(*b*) Constraints equivalent to (*a*) provided that $T_{22} = T_{23}T_{32}$.

As far as $\boldsymbol{v}$ is concerned the constraints in N and their associated voltage sources can be replaced by suitable source currents, $\underline{\boldsymbol{i}}_{(s)}$ say, flowing into the constrained nodes.

Having carried out the replacement we have now returned to the original network $\underline{N}$ for which $\boldsymbol{i}_{(s)} = \underline{\boldsymbol{y}}\,\underline{\boldsymbol{v}}$, except that $\boldsymbol{i}_{(s)}$ must be replaced by $\boldsymbol{i}_{(s)} + \underline{\boldsymbol{i}}_{(s)}$ and $\underline{\boldsymbol{v}}$ by $\boldsymbol{v}$; thus

$$\underline{\boldsymbol{y}}\,\boldsymbol{v} = \boldsymbol{i}_{(s)} + \underline{\boldsymbol{i}}_{(s)} \quad . \quad . \quad . \quad . \quad . \quad (29)$$

Eqns. (28) and (29) can be solved for $\boldsymbol{v}$. To do so, note that

$$\underline{\boldsymbol{i}}_{(s)[f} = 0 \quad . \quad . \quad . \quad . \quad . \quad . \quad (30)$$

Taking the subset of eqn. (29) corresponding to the free nodes we thus have

$$\underline{y}_{[f}\boldsymbol{v} = \boldsymbol{i}_{(s)[f} \quad . \quad . \quad . \quad . \quad . \quad . \quad (31)$$

into which we substitute $\boldsymbol{v}$ from eqn. (28), obtaining

$$\underline{y}_{[f}\boldsymbol{t}'\boldsymbol{v}_{[f} + \underline{y}_{[f}\boldsymbol{v}_{(s)} = \boldsymbol{i}_{(s)[f} \quad . \quad . \quad . \quad . \quad (32)$$

and finally the n_f equations

$$y\boldsymbol{v}_{[f} = \boldsymbol{i}_{(s)[f} - \underline{y}_{[f}\boldsymbol{v}_{(s)} \quad . \quad . \quad . \quad . \quad . \quad (33)$$

where

$$y = \underline{y}_{[f}\boldsymbol{t}' \quad . \quad . \quad . \quad . \quad . \quad . \quad (34)$$

is the admittance matrix of N and the right-hand side of eqn. (33) is its source vector. $\underline{y}$ and $\boldsymbol{t}$ are of order $n \times n$ and $n_f \times n$, respectively; therefore $\underline{y}_{[f}$ is of order $n_f \times n$; $\boldsymbol{t}'$ is $n \times n_f$; and y is a square matrix of order n_f. In Section 7 it is shown that y is non-singular, i.e. its rank is also n_f.

The solution of eqn. (33) yields $\boldsymbol{v}_{[f}$. $\boldsymbol{v}_{[d}$ can then be determined from eqn. (28), or from its subset of n_d equations

$$\boldsymbol{v}_{[d} = \boldsymbol{t}'_{[d}\boldsymbol{v}_{[f} + \boldsymbol{v}_{(s)[d} \quad . \quad . \quad . \quad . \quad . \quad (35)$$

the other n_f equations of (28) being simply identities. In practice it is usually more convenient to write down the components of $\boldsymbol{v}_{[d}$ directly by inspection of the circuit diagram once $\boldsymbol{v}_{[f}$ has been determined.

This problem is termed separable, because eqn. (33) can be solved independently of eqn. (35).

Since $\boldsymbol{y}$ is of rank $n_f = n - n_d$, each constraint has lowered the order (and rank) of the admittance matrix by one. Note, moreover, that the current sources associated with the driven nodes do not affect $\boldsymbol{v}$. This is owing to the definition of a transmittance as a rigid constraint, having zero output impedance, and thus overriding all impedances and sources at the node which it controls.

(3.3) The General Case

We now waive the restriction of Section 3.2; a constrained node may now be a driving node, and the network is allowed to contain transmittance loops. In the previous case we succeeded in eliminating all driven nodes from the network equations (33). This is now no longer possible and only some of the driven nodes can be eliminated; all other nodes of N are not eliminated (n.e.). The choice of eliminated nodes is not unique. In each transmittance loop we arbitrarily regard at least one node as a controlling node. Having done so we can state that all driven nodes that are not controlling can be eliminated. The transmittance matrix $\boldsymbol{t}$ is defined as in eqns. (27) and (28), with the only difference that α now assumes all values associated with the n_{ne} n.e. nodes. $\boldsymbol{t}$ is now of order $n_{ne} \times n$.

As an example consider the transmittance diagram of Fig. 7(*a*). Regard 2 as a controlling node and thus eliminate node 3. Nodes 1, 2 and 4 are the n.e. nodes. Fig. 7(*b*) is equivalent to Fig. 7(*a*), with $T_{22} = T_{23}T_{32}$, and

$$\boldsymbol{t} = \begin{array}{c} \begin{matrix} 1 & 2 & 3 & 4 \end{matrix} \\ \begin{bmatrix} 1 & T_{12} & 0 & 0 \\ 0 & T_{22} & T_{23} & 0 \\ 0 & 0 & 0 & 1 \end{bmatrix} \end{array} \begin{matrix} 1 \\ 2 \\ 4 \end{matrix}$$

which could have been written down without first drawing Fig. 7(*b*).

In lieu of the equation of constraints (28) we now have

$$\boldsymbol{v} = \boldsymbol{t}'\boldsymbol{v}_{[ne} + \boldsymbol{v}_{(s)} \quad . \quad . \quad . \quad . \quad . \quad (36)$$

We replace all constraints by current sources feeding the driven nodes, and thus eqn. (30) survives and eqns. (29) and (36) must be solved. Substituting eqn. (36) into eqn. (29),

$$\underline{\boldsymbol{y}}[\boldsymbol{t}'\boldsymbol{v}_{[ne} + \boldsymbol{v}_{(s)}] = \boldsymbol{i}_{(s)} + \underline{\boldsymbol{i}}_{(s)} \quad . \quad . \quad . \quad (37)$$

of which we take the subset of rows corresponding to the free nodes, use eqn. (30), rearrange and obtain the n_f equations

$$\boldsymbol{y}\boldsymbol{v}_{[ne} = \boldsymbol{i}_{(s)[f} - \underline{\boldsymbol{y}}_{[f}\boldsymbol{v}_{(s)} \quad . \quad . \quad . \quad . \quad (38)$$

where

$$\boldsymbol{y} = \underline{\boldsymbol{y}}_{[f}\boldsymbol{t}' \quad . \quad . \quad . \quad . \quad . \quad . \quad (34)$$

as before. $\underline{\boldsymbol{y}}$ and $\boldsymbol{t}$ are of order $n \times n$ and $n_{ne} \times n$, respectively; therefore $\underline{\boldsymbol{y}}_{[f}$ is $n_f \times n$, $\boldsymbol{t}'$ is $n \times n_{ne}$ and $\boldsymbol{y}$ is $n_f \times n_{ne}$.

In a network that contains transmittance loops, $n_f < n_{ne}$, and its equations are therefore not separable, i.e. eqn. (38) alone has no unique solution.

To complete the solution we need, in addition to eqn. (38), eqn. (36) or its subset of n_d equations

$$\boldsymbol{v}_{[d} = \boldsymbol{t}'_{[d}\boldsymbol{v}_{[ne} + \boldsymbol{v}_{(s)[d} \quad . \quad . \quad . \quad . \quad (39)$$

the other n_f equations of (36) being merely identities.

Although our formulation has been in terms of voltage, current and admittance, the procedure holds for any situation that is represented by lumped linear time-invariant networks, in particular for linear control systems which may include mechanical and hydraulic as well as electrical transducers.

(3.4) Summary of Procedure

(*a*) A network of admittance matrix $\underline{\boldsymbol{y}}$ and current-source vector $\boldsymbol{i}_{(s)}$ is given, as are a set of constraints $T_{\alpha\beta}$ and voltage sources $v_{(s)\beta}$.

(*b*) Choose a sufficient number of driven nodes so as to have at least one in each transmittance loop. These nodes and the free nodes constitute the n.e. nodes of the network.

(*c*) Form the constraints into the $n_{ne} \times n$ matrix $\boldsymbol{t}$, putting for free nodes $T_{\alpha\alpha} = 1$.

(*d*) Form $\underline{\boldsymbol{y}}_{[f}$ and $\boldsymbol{i}_{(s)[f}$ by striking out those rows of $\underline{\boldsymbol{y}}$ and components of $\boldsymbol{i}_{(s)}$ that correspond to driven nodes.

(*e*) $\boldsymbol{y} = \underline{\boldsymbol{y}}_{[f}\boldsymbol{t}'$ is then the admittance matrix, and $\boldsymbol{i}_{(s)[f} - \underline{\boldsymbol{y}}_{[f}\boldsymbol{v}_{(s)}$ is the source vector of the constrained network which is solved by eqns. (38) and (39).

For separable networks (no transmittance loops), substitute f for ne in the above, omit step (*b*), and solve first eqn. (33) and then eqn. (35).

(4) APPLICATIONS

(4.1) Single Transmittances

(4.1.1) General Theory.

Consider first the case of a single constraint. Let v_1 be controlled by v_2 through

$$V_1 = T_{21}v_2 + v_{(s)1} \quad . \quad . \quad . \quad . \quad . \quad (40)$$

all other nodes being free. Following rule (*c*) and denoting the unit matrix by $\boldsymbol{I}$, we have, using the notation of partitioned matrices,

$$\boldsymbol{t} = \begin{array}{c} \begin{matrix} 1 & 2\,3\ldots \end{matrix} \\ \left[\begin{array}{c|c} T_{21} & \\ 0 & \\ 0 & \boldsymbol{I} \\ \cdot & \\ \cdot & \\ \cdot & \end{array}\right] \end{array} \begin{matrix} 2 \\ 3 \\ \cdot \\ \cdot \\ \cdot \\ \cdot \end{matrix}$$

and therefore

$$\boldsymbol{t}' = \left[\begin{array}{c} T_{21}\,0\ldots \\ \hline \boldsymbol{I} \end{array}\right]$$

Moreover,

$$\boldsymbol{v}_{(s)} = \begin{bmatrix} v_{(s)1} \\ 0 \\ 0 \\ \cdot \\ \cdot \\ \cdot \end{bmatrix}$$

$\underline{y}_{[f}$ is simply $\underline{y} = [\underline{y}_{\alpha\beta}]$ without its first row. Explicitly,

$$\underline{y}_{[f} = \begin{array}{c} \begin{matrix} 1 & 2 & \dots \end{matrix} \\ \begin{bmatrix} \underline{y}_{21} & \underline{y}_{22} & \dots \\ \underline{y}_{31} & \underline{y}_{32} & \dots \\ \cdot & \cdot & \\ \cdot & \cdot & \\ \cdot & \cdot & \end{bmatrix} \end{array} \begin{matrix} 2 \\ 3 \\ \cdot \\ \cdot \\ \cdot \end{matrix}$$

Multiplying these matrices to obtain y according to rule (*e*),

$$y = \begin{array}{c} \begin{matrix} 2 & 3 & \dots \end{matrix} \\ \begin{bmatrix} T_{21}\underline{y}_{21} + \underline{y}_{22} & \underline{y}_{23} & \dots \\ T_{21}\underline{y}_{31} + \underline{y}_{32} & \underline{y}_{33} & \dots \\ \cdot & \cdot & \\ \cdot & \cdot & \\ \cdot & \cdot & \end{bmatrix} \end{array} \begin{matrix} 2 \\ 3 \\ \cdot \\ \cdot \\ \cdot \end{matrix} \quad \dots \quad (41)$$

and the important rule results:

If β is driven by α through $T_{\alpha\beta}$, y is derived from $\underline{y}$ by the addition of $T_{\alpha\beta}$ times column β to column α and subsequent deletion of row β and column β.

$$v_{(s)} = \begin{bmatrix} 0 \\ \cdot \\ \cdot \\ \cdot \\ 0 \\ v_{(s)\beta} \\ 0 \\ \cdot \\ \cdot \\ \cdot \\ 0 \end{bmatrix}$$

and therefore

$$i_{(s)[f} - \underline{y}_{[f} v_{(s)} = i_{(s)[f} - \begin{bmatrix} \underline{y}_{\beta 1} \\ \underline{y}_{\beta 2} \\ \cdot \\ \cdot \\ \cdot \end{bmatrix}_{[f} v_{(s)\beta} \quad \dots \quad (42)$$

where the subscript $_{[f}$ indicates that $\underline{y}_{\beta\beta}$ is omitted in the column vector.

(4.1.2) A Simple Example.

Let us apply these results to the network of Fig. 4(*b*). There are just two nodes, not counting the reference node. Of these node 1 is free and node 2 is driven. To find y by the above rule we add T_{12} times the second column in $\underline{y}$ to the first and subsequently delete the second row and column. $\underline{y}$ is the square matrix in eqn. (11), and thus

$$y = Y_{12} + Y_{13} - T_{12}Y_{12}$$

The source-current vector is, by eqn. (42) with $\alpha = 1$, $\beta = 2$,

$$i_{(s)1} - \underline{y}_{21} v_{(s)2}$$

Eqn. (39) therefore reads

$$(Y_{12} + Y_{13} - T_{12}Y_{12})v_1 = i_{(s)1} + Y_{12}v_{(s)2}$$

in accord with eqn. (25). v_2 is then written down by inspection of Fig. 4(*b*).

(4.1.3) A Computing Network.

Now consider the network of Fig. 8, which is used as a network performing a mathematical operation on a voltage applied at terminal 4. The output voltage is provided by terminal 2. The admittance matrix $\underline{y}$ of the parent network (without A) is, by eqn. (9),

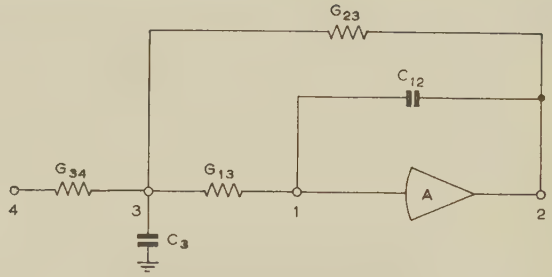

Fig. 8.—A computing network.

$$\underline{y} = \begin{array}{c} \begin{matrix} 1 & 2 & 3 & 4 \end{matrix} \\ \begin{bmatrix} G_{13}+pC_{12} & -pC_{12} & -G_{13} & 0 \\ -pC_{12} & G_{23}+pC_{12} & -G_{23} & 0 \\ -G_{13} & -G_{23} & G_{13}+G_{23}+G_{34}+pC_3 & -G_{34} \\ 0 & 0 & -G_{34} & G_{34} \end{bmatrix} \end{array} \begin{matrix} 1 \\ 2 \\ 3 \\ 4 \end{matrix}$$

Note that pC_3 appears in $\underline{y}_{33}$, only because it is connected to the reference node. All other admittances appear with four entries each.

There is one constraint, $T_{12} = A$; hence we eliminate node 2, and

$$y = \begin{array}{c} \begin{matrix} 1 & 3 & 4 \end{matrix} \\ \begin{bmatrix} G_{13}+pC_{12}-ApC_{12} & -G_{13} & 0 \\ -G_{13}-AG_{23} & G_{13}+G_{23}+G_{34}+pC_3 & -G_{34} \\ 0 & -G_{34} & G_{34} \end{bmatrix} \end{array} \begin{matrix} 1 \\ 3 \\ 4 \end{matrix}$$

With a little practice y could have been written down directly without first writing $\underline{y}$.

The through transmittance from node 4 to node 2 is of interest in this example. Using eqn. (15) we have

$$H_{42} = AH_{41} = A\frac{y^{41}}{y^{44}} = \frac{AG_{13}G_{34}}{\begin{vmatrix} G_{13}+pC_{12}-ApC_{12} & -G_{13} \\ -G_{13}-AG_{23} & G_{13}+G_{23}+G_{34}+pC_3 \end{vmatrix}}$$

Let us also determine the impedance level at node 1. By definition this is the impedance looking into 1 with all voltage sources short-circuited and all current sources opened. In our case we must short-circuit 4 to earth, which corresponds to the deletion of row 4 and column 4 in y. Hence, by eqn. (16),

$$Z_{(in)1} = \frac{\tilde{y}^{11}}{|\tilde{y}|} = \frac{G_{13}+G_{23}+G_{34}+pC_3}{\begin{vmatrix} G_{13}+pC_{12}-ApC_{12} & -G_{13} \\ -G_{13}-AG_{23} & G_{13}+G_{23}+G_{34}+pC_3 \end{vmatrix}}$$

where $\tilde{y}$ is y without row 4 and column 4.

(4.2) Dual Controls

This case obtains if a node is controlled by two other nodes, i.e.

$$v_1 = T_{21}v_2 + T_{31}v_3$$

which describes a difference amplifier if $T_{21} = -T_{31}$. (We assume in this example that $v_{(s)} = 0$.) Thus

$$t' = \left[\begin{array}{ccc} T_{21} & T_{31} & 0 \dots \\ \hline & I & \end{array}\right].$$

and therefore

$$y = \underline{y}_{[f}t' = \begin{array}{c} \begin{matrix} 2 & 3 & 4 \end{matrix} \\ \begin{bmatrix} T_{21}\underline{y}_{21} + \underline{y}_{22} & T_{31}\underline{y}_{21} + \underline{y}_{23} & \underline{y}_{24} \cdots \\ T_{21}\underline{y}_{31} + \underline{y}_{32} & T_{31}\underline{y}_{31} + \underline{y}_{33} & \underline{y}_{34} \cdots \\ \cdot & \cdot & \cdot \\ \cdot & \cdot & \cdot \\ \cdot & \cdot & \cdot \end{bmatrix} \end{array} \begin{matrix} 2 \\ 3 \\ \cdot \\ \cdot \\ \cdot \end{matrix} \quad (43)$$

(4.3) Voltage Sources as Constraints

The connection of a voltage source between two free nodes of $\underline{N}$ is a bilateral constraint, yet in one important instance it may be regarded as unilateral, namely when one terminal of the voltage source is connected to the reference node. The latter case is evidently equivalent to the series connection of a transmittance of zero strength and the given voltage source; it can therefore be treated by our methods.

For the driven nodes we now have

$$v_{[d} = v_{(s)}$$

so that

$$\underline{y}_{[f}v = i_{(s)[f} \quad . \quad . \quad . \quad . \quad . \quad . \quad (31)$$

is a suitable set of equations for the solution in this case. Eqn. (31) looks deceptively simple. n_d components of v are the given voltage sources and the other $n - n_d = n_f$ components must be solved in terms of these.

The same result follows from the general formulae (33) and (34), noting that

$$t = \begin{array}{c} \begin{matrix} 1 \ldots l & l+1 \ldots n \end{matrix} \\ \left[\begin{array}{c|c} \multicolumn{1}{c}{\mathbf{0}} & \multicolumn{1}{c}{\boldsymbol{I}} \end{array}\right] \end{array} \begin{matrix} l+1 \\ \cdot \\ \cdot \\ \cdot \\ n \end{matrix}$$

where $1, 2, \ldots l$ are the driven nodes and $l + 1, \ldots n$ are free. The details of such a derivation are left to the reader.

In the case of a branch network (i.e. a network consisting of a plurality of branches) eqn. (31) is trivial. It is simply the statement of Kirchhoff's second law for the free nodes.

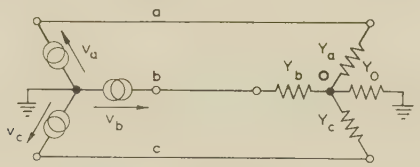

Fig. 9.—A 3-phase network.

(4.3.1) An Example.

Consider the somewhat trivial example of Fig. 9. There is just one free node, 0, and eqn. (31) reads

$$y_{[f}v = [\Sigma Y - Y_a - Y_b - Y_c]\begin{bmatrix} v_0 \\ v_a \\ v_b \\ v_c \end{bmatrix} = 0$$

or

$$v_0 = (Y_a v_a + Y_b v_b + Y_c v_c)/\Sigma Y$$

(4.4) An Example for Sections 4.2 and 4.3: A Valve Network

The Miller d.c. amplifier[7, 8] of Fig. 10 consists of a direct-coupled difference amplifier stage in which node 1 is the input

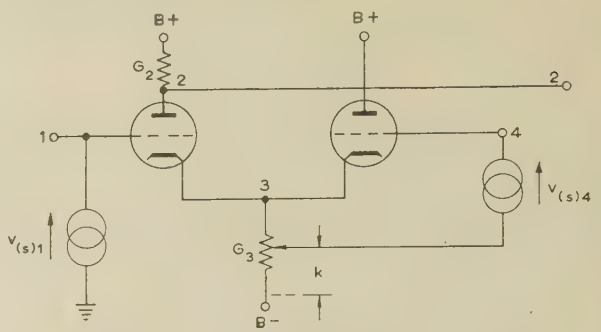

Fig. 10.—Miller compensated d.c. amplifier.

grid and the other grid, at node 4, is returned to a suitable tap on the common cathode resistor, for compensation of drift due to changes in heater current. Such drift is equivalent to voltages $v_{(s)1}$ and $v_{(s)4}$ in series with the respective grids. Assuming equal drifts, $v_{(s)1} = v_{(s)4}$, the tap must be so chosen that the output voltage, v_2, is zero for simultaneous operation of the two equal source voltages. We assume valves of equal μ, g_m, and g_p and consider node 1 controlled through a transmittance of zero strength and source voltage $v_{(s)1}$, and node 4 driven from node 3 with transmittance k and source voltage $v_{(s)4}$. Consequently we eliminate nodes 1 and 4, and y will be a 2×2 matrix.

Let us start with the derivation of $\underline{y}_{[f}$, which has rows 2 and 3 and columns 1, 2, 3 and 4. Nodes B_+ and B_- are regarded as short-circuited to the reference node in an a.c. (small-signal) analysis. Of the four entries of G_2, for example, only that at 22 remains. The contributions to $\underline{y}_{[f}$ of the left-hand valve are found by assigning to g, p and k the values 1, 2 and 3, respectively. The contributions are

$$\begin{array}{c} \begin{matrix} 1 & 2 & 3 \end{matrix} \\ \begin{bmatrix} g_m & g_p & -g_m - g_p \\ -g_m & -g_p & g_m + g_p \end{bmatrix} \end{array} \begin{matrix} 2 \\ 3 \end{matrix}$$

To find the contributions of the right-hand valve we write 4 for g and 3 for k and delete the row and column p in eqn. (19), leaving

$$\begin{array}{c} \begin{matrix} 4 & 3 \end{matrix} \\ \begin{bmatrix} 0 & 0 \\ -g_m & g_m + g_p \end{bmatrix} \end{array} \begin{matrix} 4 \\ 3 \end{matrix}$$

or equivalently

$$\begin{array}{c} \begin{matrix} 3 & 4 \end{matrix} \\ \begin{bmatrix} g_m + g_p & -g_m \\ 0 & 0 \end{bmatrix} \end{array} \begin{matrix} 3 \\ 4 \end{matrix}$$

Hence

$$\underline{y}_{[f} = \begin{array}{c} \begin{matrix} 1 & 2 & 3 & 4 \end{matrix} \\ \begin{bmatrix} g_m & G_2 + g_p & -g_m - g_p & 0 \\ -g_m & -g_p & G_3 + 2(g_m + g_p) & -g_m \end{bmatrix} \end{array} \begin{matrix} 2 \\ 3 \end{matrix}$$

The transmittances are $T_{r1} = 0$ and $T_{34} = k$. Accordingly we add k times column 4 to column 3 and subsequently delete columns 1 and 4, obtaining

$$y = \begin{array}{c} \begin{matrix} 2 & 3 \end{matrix} \\ \begin{bmatrix} G_2 + g_p & -g_m - g_p \\ -g_p & G_3 + 2(g_m + g_p) - kg_m \end{bmatrix} \end{array} \begin{matrix} 2 \\ 3 \end{matrix}$$

Now $v'_{(s)} = [v_{(s)1}, 0, 0, v_{(s)4}]$ and consequently

$$-\underline{y}_{[f}v_{(s)} = -g_m \begin{bmatrix} v_{(s)1} \\ -v_{(s)1} - v_{(s)4} \end{bmatrix}$$

which becomes, for $v_{(s)1} = v_{(s)4}$,

$$g_m v_{(s)1} \begin{bmatrix} -1 \\ 2 \end{bmatrix}$$

The set of network equations (33) therefore reads

$$\begin{bmatrix} G_2 + g_p & -g_m - g_p \\ -g_p & G_3 + 2(g_m + g_p) - kg_m \end{bmatrix} \begin{bmatrix} v_2 \\ v_3 \end{bmatrix} = g_m v_{(s)1} \begin{bmatrix} -1 \\ 2 \end{bmatrix}$$

and $v_2 = 0$ implies and is implied by

$$\begin{vmatrix} -1 & -g_m - g_p \\ 2 & G_3 + 2(g_m + g_p) - kg_m \end{vmatrix} = 0$$

which reduces on expansion to $k = G_3/g_m$ or $kR_3 = 1/g_m$, which is the familiar result for drift compensation.

A solution of this problem using nodal analysis without the methods of the paper would require an admittance matrix of order 4; the tap on G_3 would have to be taken as an additional node and v_4 would not be eliminated. Moreover, it would not be readily possible to deal with both sources $v_{(s)1}$ and $v_{(s)4}$ simultaneously. The present method shares the advantages of nodal analysis, e.g. it does not require equivalent schematics, and effects a considerable simplification of the analysis.

For an additional application to multiple constraints, using the method of the paper but not its notation, see Reference 9.

(4.5) Transmittance Networks (Signal-Flow Graphs)

(4.5.1) General Theory.

Transmittance networks present the opposite extreme to a network without constraints. They consist exclusively of transmittances (and mixing-points). According to rule (*b*) of Section 3.4 a sufficient number of nodes must be left uneliminated so as to break all loops. Eqn. (36) only is required for the solution. Let us take the subset of eqn. (36) that corresponds to the n.e. nodes and set $\boldsymbol{v}_{(s)} = 0$; thus

$$[\boldsymbol{t}'_{[ne} - \boldsymbol{I}]\boldsymbol{v}_{[ne} = 0 \quad . \quad . \quad . \quad . \quad . \quad (44)$$

$\boldsymbol{t}'$ is an $\kappa \times n_{ne}$ matrix; $\boldsymbol{t}'_{[ne}$ and $[\boldsymbol{t}'_{[ne} - \boldsymbol{I}]$ are therefore square matrices of order n_{ne}. Note that

$$[\boldsymbol{t}'_{[ne} - \boldsymbol{I}]$$

is singular; any of its columns that corresponds to a free node consists wholly of zeros. The set of homogeneous equations (44) therefore possesses non-trivial solutions. If there is only one input node in the network, $n_f = 1$, and the matrix is of rank $n_{ne} - 1$. The node voltages are proportional to its cofactors. If there is more than one input node it is usually best to consider one input at a time and derive the actual node voltages by superposition.

In treating transmittance networks we may omit the subscript *ne*.

For a network with the single input node α we obtain the transmittance from α to β from eqn. (44):

$$H_{\alpha\beta} = \frac{v_\beta}{v_\alpha} = \frac{(\boldsymbol{t}' - \boldsymbol{I})^{\alpha\beta}}{(\boldsymbol{t}' - \boldsymbol{I})^{\alpha\alpha}} = \frac{(\boldsymbol{t} - \boldsymbol{I})^{\beta\alpha}}{(\boldsymbol{t} - \boldsymbol{I})^{\alpha\alpha}} \quad . \quad . \quad (45)$$

Topological rules for the solution of transmittance networks have been developed.[10, 11] Eqn. (45) would form a convenient starting-point for the derivation of these rules. It is felt, however, that only a few networks specialists would really benefit from a study of the topological methods; the rules of the paper are considerably easier to learn and apply.

Note, finally, that eqn. (44) is readily established directly[12] without the considerations of Section 4.1. From the definition of $\boldsymbol{t}$ it follows at once for transmittance networks that

$$[\boldsymbol{t}']_{[ne}\boldsymbol{v}_{[ne} = \boldsymbol{v}_{[ne}$$

which is clearly equivalent to eqn. (44).

Fig. 11.—Transmittance network (signal-flow graph).

(4.5.2) An Example.

Fig. 11 presents an example. It is sufficient to retain nodes 1 (input node) and 4. Introducing the notation

$$T_{\alpha\beta}T_{\beta\gamma}T_{\gamma\delta} = T_{\alpha\beta\gamma}T_{\gamma\delta} = T_{\alpha\beta\gamma\delta} \quad . \quad . \quad . \quad (46)$$

and similarly for other products of transmittances, and noting that

$$T_{\alpha\beta\gamma\ldots\alpha} = T_{\beta\gamma\ldots\alpha\beta} = T_{\gamma\ldots\alpha\beta\gamma}, \text{ etc.} \quad . \quad . \quad (47)$$

we have

$$\boldsymbol{t} = \begin{matrix} \\ 1 \\ 4 \end{matrix} \begin{matrix} \begin{matrix} 1 & \qquad\qquad 4 \end{matrix} \\ \begin{bmatrix} 1 & T_{1234} \\ 0 & T_{4234} + T_{4534} + T_{4564} \end{bmatrix} \end{matrix} \begin{matrix} \\ 1 \\ 4 \end{matrix}$$

from which follows, for example, the through-transmittance H_{16}:

$$H_{16} = v_6/v_1 = H_{14}T_{456} = \frac{(\boldsymbol{t} - \boldsymbol{I})^{41}}{(\boldsymbol{t} - \boldsymbol{I})^{11}} T_{456}$$

$$= \frac{T_{123456}}{1 - (T_{2342} + T_{3453} + T_{4564})}$$

(5) CONCLUSIONS

The introduction of the transmittance matrix provides a natural extension of prior techniques to the analysis of unilaterally constrained networks.

The field of application ranges from valve circuits to signal-flow graphs. The proposed method is straightforward and leads in many cases to simplifications in the analysis of networks.

(6) REFERENCES

(1) MAXWELL, J. C.: 'A Treatise on Electricity and Magnetism', 3rd edition, 1891.
(Reprinted by Dover Publications, 1954), Section 280.

(2) SHEKEL, J.: 'Matrix Representation of Transistor Circuits', *Proceedings of the Institute of Radio Engineers*, 1952, **40**, p. 1493.

(3) SHEKEL, J.: 'Voltage Reference Node. Its Transformation in Nodal Analysis', *Wireless Engineer*, 1954, **31**, p. 6.

(4) ZADEH, L. A.: 'A Note on the Analysis of Vacuum Tube and Transistor Circuits', *Proceedings of the Institute of Radio Engineers*, 1953, **41**, p. 989.

(5) 'Reference Data for Radio Engineers', 4th edition (International Telephone and Telegraph Corporation, New York, 1956).

(6) AITKEN, A. C.: 'Determinants and Matrices', 3rd edition (Oliver and Boyd, 1944), Section 39.

(7) MILLER, S. E.: 'Sensitive D.C. Amplifier with A.C. Operation', *Electronics*, November, 1941.

(8) KORN, G. A., and KORN, T. S.: 'Electronic Analog Computers', 2nd edition (McGraw-Hill, 1956), p. 211.

(9) NATHAN, A.: 'Computing and Error Matrices in Linear Differential Analysers', *Transactions of the Institute of Radio Engineers*, 1958, *EC–7*, p. 32.

(10) MASON, S. J.: 'Feedback Theory—Some Properties of Signal Flow Graphs', *Proceedings of the Institute of Radio Engineers*, 1953, **41**, p. 1144.

(11) MASON, S. J.: 'Feedback Theory—Further Properties of Signal Flow Graphs', *ibid.*, 1956, **44**, p. 920.

(12) NATHAN, A.: 'Algebraic Approach to Signal Flow Graphs', *ibid.*, 1958, **46**, p. 1955.

(7) APPENDIX

(7.1) Proof of the Non-Singularity of the Admittance Matrix in the Separable Case

If $\underline{y}$ is a non-singular square matrix of order n, and n_d nodes are driven, y will be a square matrix of order $n_f = n - n_d$.

Now t is of order $n_f \times n$; its structure ensures that it is always possible, subject at most to a renumbering of nodes, to single out a triangular submatrix of order n_f with non-vanishing diagonal elements. Thus t is of rank n_f. $y_{[f}$ is of order $n_f \times n$, and, since $\underline{y}$ is non-singular by assumption, of rank n_f. It follows from the Binet–Cauchy theorem[6] that the $n_f \times n_f$ matrix $y = y_{[f}t'$ is of rank n_f; i.e. y is indeed non-singular.

621.375.121

The Institution of Electrical Engineers
Monograph No. 400 E
Sept. 1960

LIMITATIONS ON REALIZABLE RESPONSE SHAPES FOR CERTAIN WIDE-BAND BANDPASS AMPLIFIER CIRCUITS

By R. A. WOODROW, B.Sc., Associate Member.

(*The paper was first received* 21*st October*, 1959, *in revised form* 26*th April, and in final form* 18*th June*, 1960. *It was published as an* INSTITUTION MONOGRAPH *in September*, 1960.)

SUMMARY

A procedure is described for the design of wide-band bandpass amplifiers using either stagger-tuned stages or a chain of feedback pairs to realize Chebȳshev or Butterworth response shapes.

A graphical test has been developed by which it is possible to verify, at the outset, that a given design specification is a realizable one. Certain fundamental limitations which are imposed upon the response shapes by the choice of these circuit configurations are revealed by this test. Thus it is shown that any response shape which may be realized by a chain of feedback pairs can also be realized with stagger-tuned stages, while the converse is not true.

An example demonstrating the application of the procedure to a design problem has been included to demonstrate that the procedure for a Chebȳshev response is no more complicated than for a Butterworth response, neither is any additional complication introduced by increasing the number of singularities in the desired response shape beyond the first pair, since each pair of singularities is separately realized.

LIST OF SYMBOLS

f = Frequency variable.
f_u, f_l = Upper and lower 3 dB frequency limits of the specified passband.
B = Specified bandwith $= f_u - f_l$.
f_m = Geometric mid-band frequency $= \sqrt{(f_u f_l)}$.
f_1, f_2 = Resonant frequency of a stagger-tuned pair ($f_1 f_2 = f_u f_l = f_m^2$).
$\omega, \omega_u, \omega_l, \omega_m, \omega_1, \omega_2$ = Angular frequencies corresponding to the above.
$\lambda = j\omega$.
z = Bandpass frequency variable $= \lambda/\omega_m + \omega_m/\lambda$.
$z_1, z_2 = \lambda/\omega_1 + \omega_1/\lambda$ and $\lambda/\omega_2 + \omega_2/\lambda$ respectively.
$\mu_1 = \omega_1/\omega_m + \omega_m/\omega_1$.
g_m = Mutual conductance of valve.
g = Conductance term of the load admittance of a feedback pair.
g_{min} = Minimum realizable value of g.
g_f = Feeback conductance of a feedback pair.
g_1, g_2 = Conductance of the load admittance of the first and second stage of a stagger-tuned pair.
C = Capacitance shunting load admittance.
$z_{p1}, z_{p2}, z_{p1}^*, z_{p2}^*$ = Conjugate pairs of poles of the transfer function.
x_p = Real part of z_p.
y_p = Imaginary part of z_p.
G = Complex voltage gain.
G_m = Value of G at $\omega = \omega_m$.
$d_1 = g_1/\omega_1 C = g_2/\omega_2 C$ = damping factor of stagger-tuned pair.
d_{min} = Minimum realizable value of d_1.
$d = B/f_m$ = overall damping factor.
s = Specified gain tolerance, dB.
$\epsilon = 0{\cdot}115s$.

$$\kappa = \frac{1}{\cosh\left(\frac{1}{2n}\operatorname{arc\,cosh}\frac{1}{\epsilon}\right)}.$$

$$\theta = \operatorname{Arc\,cosh}\left[\frac{1+(-1)^{n+1}\epsilon}{\epsilon}\right].$$

n = Number of poles in gain function = number of valve stages in the amplifier.
r = Integers 1, 2, . . . etc.

(1) INTRODUCTION

Two amplifier circuit configurations that have been recommended in the literature[7] for use when wide-band bandpass properties are required are stagger-tuned amplifiers and chains of inverse-feedback pairs. The investigation from which this paper results attempted to unify and simplify the design procedures proposed[7] for these circuits by developing simple graphical constructions to replace, as far as possible, procedures requiring algebraic manipulative ability and by devising a simple test which can be applied at the beginning of a design problem to verify that the specification may be realized with a given circuit.

It was not the primary object of this study to compare the relative merits of the two circuits for the experimental realization of a given specification, as this has been done elsewhere.[7] Therefore no experimental results are offered. However, it so happens that, in the development of the test mentioned above, certain fundamental limitations of the circuits are disclosed. There thus emerges a criterion by which the merits of different circuit configurations could be compared.

(2) THE DESIGN PROCEDURE

The designer of a wide-band bandpass amplifier normally seeks to realize a design specification which requires that the amplifier shall

(*a*) Amplify a given band of frequencies defined by $f_l \leqslant f \leqslant f_u$.
(*b*) Provide a certain specified passband gain with a permitted tolerance of s dB.

When proceeding from such a specification to a physical realization, two distinct problems occur, which may be called the 'approximation problem' and the 'realization problem'.

The solution of the approximation problem provides a suitable analytic approximation to the design specification, thereby defining the desired response shape. The approximation usually employed [1,2,3,4] is either a Chebȳshev or a Butterworth (maximally flat) polynomial. By an artifice developed here, it can be shown that the latter is a limiting case of the former, so that one solution of the approximation problem can be made to serve both types of approximation in common use.

Initially, the realization problem requires the development of a simple test to establish that the response shape given by the solution of the approximation problem can be obtained with a

Correspondence on Monographs is invited for consideration with a view to publication.
Mr. Woodrow is in the Electrical Engineering Department, Battersea College of Technology.

certain circuit configuration; if it cannot, alternative circuits must be considered; if it can, the solution of the realization problem yields the required circuit.

The test of realizability has been reduced to a simple graphical construction defining the region(s) in a complex plane within which singularities of the desired response shape may be realized. A comparison with the positions of the singularities of the desired response shape in the same plane immediately reveals any unrealizable desired responses. The essential simplicity of this test is the result of a careful choice of the basic amplifier circuit (see Figs. 1 and 3). In each case this is chosen in such a way that it can be made to realize a complex conjugate pair of singularities. By cascading the appropriate number of basic units, the desired overall response shape is realized. In this way, the design of an n-stage amplifier can be reduced to repeated applications of the design procedure of the basic circuit.

(3) THE INVERSE-FEEDBACK PAIR

(3.1) The Gain Expression

As a first example of the application of this general procedure, suppose the amplifier of Fig. 1 is chosen as the basic amplifier circuit.

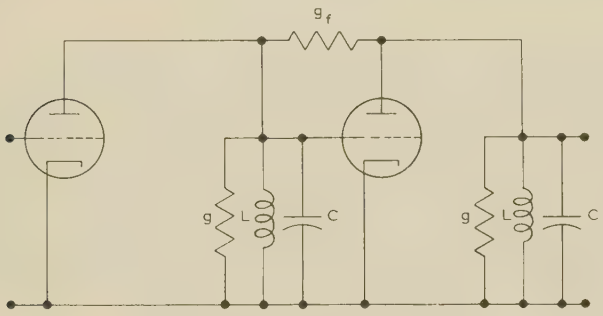

Fig. 1.—The inverse-feedback pair.

The voltage gain of this arrangement is given by

$$G = \frac{\dfrac{g_m(g_m - g_f)}{(\omega_m C)^2}}{z^2 + 2z\left(\dfrac{g + g_f}{\omega_m C}\right) + \dfrac{g^2 + 2gg_f + g_f g_m}{(\omega_m C)^2}} \quad . \quad (1)$$

where $\omega_m^2 = \omega_u \omega_l = 1/LC$.

Factorizing the denominator of eqn. (1) gives

$$G = \frac{\dfrac{g_m(g_m - g_f)}{(\omega_m C)^2}}{(z - z_{p1})(z - z_{p2})} \quad . \quad . \quad . \quad . \quad . \quad (2)$$

Provided that $g_m > g_f$, the poles z_{p1} and z_{p2} of the gain function G in eqn. (2) are complex conjugates. If $g_m \leqslant g_f$, both z_{p1} and z_{p2} are real and negative. This last situation is of little interest in the realization of Chebȳshev approximations, and is not pursued.

Taking $g_m > g_f$, so that

$$\left.\begin{aligned} z_{p1} &= x_p + jy_p \\ z_{p2} &= x_p - jy_p \end{aligned}\right\} \quad . \quad . \quad . \quad . \quad . \quad . \quad (3)$$

it follows from eqns. (1), (2) and (3) that

$$\omega_m C x_p = -(g + g_f) \quad . \quad . \quad . \quad . \quad . \quad (4)$$

and

$$(\omega_m C y_p)^2 = g_f(g_m - g_f) \quad . \quad . \quad . \quad . \quad . \quad (5)$$

(3.2) Regions of Realizable Singularities

It is essential, for a successful solution of the realization problem, that g and g_f be physically realizable conductances; i.e. they must be real, positive constants. This places certain restrictions on permitted values of z_{p1} and z_{p2}.

From eqn. (5) it follows that

$$g_f = \tfrac{1}{2}\left\{g_m \pm \sqrt{[g_m^2 - (2\omega_m C y_p)^2]}\right\} \quad . \quad . \quad . \quad (6)$$

which shows that g_f is real provided that

$$-\frac{g_m}{2\omega_m C} \leqslant y_p \leqslant +\frac{g_m}{2\omega_m C} \quad . \quad . \quad . \quad . \quad . \quad (7)$$

and that g_f is positive for all values of y_p for which it is real, whichever sign is associated with the square root.

From eqns. (4) and (6) it follows that

$$g = -\tfrac{1}{2}\left\{2\omega_m C x_p + g_m \pm \sqrt{[g_m^2 - (2\omega_m C y_p)^2]}\right\} \quad . \quad (8)$$

which shows that g is real if eqn. (7) is satisfied and is positive if

$$2\omega_m C x_p + g_m \pm \sqrt{[g_m^2 - (2\omega_m C y_p)^2]} \leqslant 0 \quad . \quad (9)$$

In the region where $-g_m/2\omega_m C \leqslant x_p \leqslant 0$, the quantity $2\omega_m C x_p + g_m$ is positive. In this region eqn. (9) can only be satisfied if the negative root sign is adopted, and then only if

$$\sqrt{[g_m^2 - (2\omega_m C y_p)^2]} \geqslant 2\omega_m C x_p + g_m \quad . \quad . \quad (10)$$

which is the interior of the semicircle with centre $(-g_m/2\omega_m C, 0)$ and radius $g_m/2\omega_m C$ in Fig. 2.

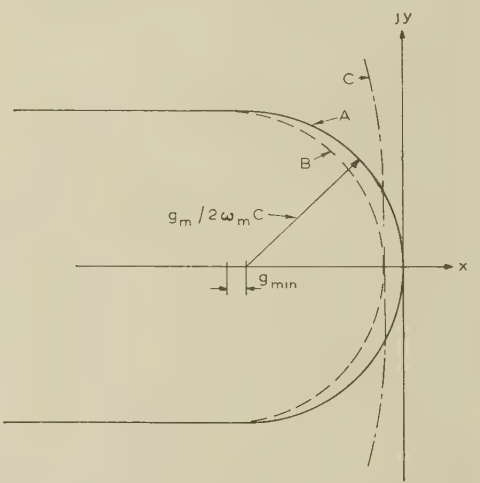

Fig. 2.—Regions of physically realizable singularities.

In the region where $-\infty \leqslant x_p \leqslant -g_m/2\omega_m C$, the quantity $2\omega_m C x_p + g_m$ is negative, and eqn. (9) is satisfied in the whole of this region if the negative root sign is adopted.

In part of this region the choice of the positive root sign is also permitted, but the numerator of eqn. (2) suggests that the negative root sign is preferred where a choice is possible. Hence

$$\left.\begin{aligned} g_f &= \tfrac{1}{2}\left\{g_m - \sqrt{[g_m^2 - (2\omega_m C y_p)^2]}\right\} \\ \text{and} \quad g &= -(\omega_m C x_p + g_f) \end{aligned}\right\} \quad . \quad . \quad (11)$$

define positive real values of g and g_f only if the singularities $x_p \pm jy_p$ lie within or on the boundary line A shown in Fig. 2.

If a desired response shape requires the realization of a pair of singularities in any part of the z-plane outside this boundary

that response shape cannot be realized with a chain of inverse-feedback pairs.*

(3.3) The Constraint $g \geqslant g_{min}$

In practice, finite damping must be associated with the tuned load admittances caused by coil losses, valve damping, etc. This prevents the circuit designer from realizing values of g less than some specified minimum value, g_{min}.

The effect of this practical limitation on the position of realizable singularities can be assessed by requiring that g in eqn. (8) shall satisfy the condition

$$g \geqslant g_{min} \quad . \quad . \quad . \quad . \quad . \quad . \quad (12)$$

This constraint modifies eqn. (9) to

$$2\omega_m C x_p + g_m + 2g_{min} \pm \sqrt{[g_m^2 - (2\omega_m C y_p)^2]} \leqslant 0 \quad (13)$$

Curve B of Fig. 2 shows the reduction in the region of realizable singularities necessary to satisfy eqns. (12) and (13).

(4) THE STAGGER-TUNED AMPLIFIER

(4.1) The Gain Expression

As an alternative, the stagger-tuned pair of Fig. 3 may be chosen as the basic amplifier element.

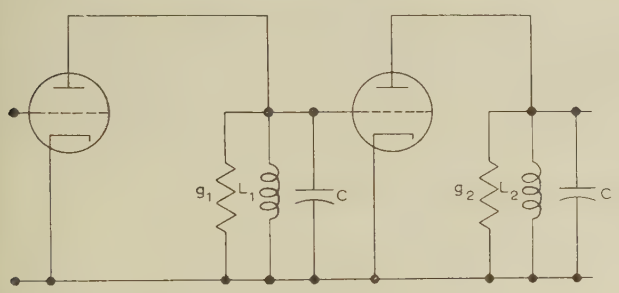

Fig. 3.—The stagger-tuned pair.

The voltage gain of this circuit is given by

$$G = \frac{\dfrac{g_m^2}{\omega_1\omega_2 C^2}}{\left(\dfrac{g_1}{\omega_1 C} + z_1\right)\left(\dfrac{g_2}{\omega_2 C} - z_2\right)} \quad . \quad . \quad . \quad (14)$$

where $\omega_1^2 = 1/L_1C$ and $\omega_2^2 = 1/L_2C$.

If ω_1, ω_2, g_1 and g_2 are chosen to satisfy the conditions

$$\omega_1\omega_2 = \omega_l\omega_u = \omega_m^2 \quad . \quad . \quad . \quad . \quad . \quad (15)$$

and

$$g_1/\omega_1 C = g_2/\omega_2 C = d_1 \quad . \quad . \quad . \quad . \quad (16)$$

then eqn. (14) can be manipulated to give

$$G = \frac{\left(\dfrac{g_m}{\omega_m C}\right)^2}{z^2 + d_1\mu_1 z + (d_1^2 + \mu_1^2 - 4)} \quad . \quad . \quad . \quad (17)$$

where $\mu_1 = \omega_1/\omega_m + \omega_m/\omega_1 = \omega_2/\omega_m + \omega_m/\omega_2$. From eqn. (17),

$$G = \frac{\left(\dfrac{g_m}{\omega_m C}\right)^2}{(z - z_{p1})(z - z_{p2})} \quad . \quad . \quad . \quad . \quad (18)$$

* The case of unequal load damping conductances, g_1 and g_2, in place of the equal conductances, g, has not been considered. This case can be treated as above, when it is found that a reduction in the area of physically realizable singularities results if $g_1 \neq g_2$.

and provided that $(d_1\mu_1)^2 < 4(d_1^2 + \mu_1^2 - 4)$, the poles z_{p1} and z_{p2} occur in complex conjugate pairs, as before.

For this circuit arrangement,

$$z_{p1}z_{p2} = x_p^2 + y_p^2 = d_1^2 + \mu_1^2 - 4 \quad . \quad . \quad (19)$$

$$-(z_{p1} + z_{p2}) = -2x_p = d_1\mu_1 \quad . \quad . \quad . \quad . \quad . \quad (20)$$

Eqns. (19) and (20) for the stagger-tuned amplifier correspond to eqns. (4) and (5) for the inverse-feedback pair.

(4.2) Regions of Realizable Singularities

The constraints imposed upon the positions of realizable singularities must again be considered. Since ω_1, ω_2, g_1 and g_2 must be positive real constants, it follows that d_1 is positive real, and μ_1 is real and within the range $2 \leqslant \mu_1 \leqslant +\infty$. In practice, the constraint that g_1 shall be a real positive constant is not sufficiently strong, because load circuits of infinite Q-factor are unattainable. This is allowed for by imposing a more severe constraint on d_1 than above, namely that d_1 is real and within the range $d_{min} \leqslant d_1 \leqslant +\infty$, where d_{min} is the minimum damping factor (=1/maximum Q-factor) attainable.

Eliminating d_1 from eqns. (19) and (20) and solving the resulting quadratic for μ_1 gives

$$\mu_1 = \left[\tfrac{1}{2}\left\{(x_p^2 + y_p^2 + 4) \pm \sqrt{[(x_p^2 + y_p^2 + 4)^2 - 16x_p^2]}\right\}\right]^{1/2} \quad (21)$$

But $(x_p^2 + y_p^2 + 4)^2 - 16x_p^2 \equiv (x_p^2 + y_p^2 - 4)^2 + 16y_p^2$, which is positive for all values of x_p and y_p. This shows that μ_1 is real for all values of x_p and y_p.

To satisfy the condition $2 \leqslant \mu_1 \leqslant \infty$ requires that

$$0 \leqslant (x_p^2 + y_p^2 - 4) \pm \sqrt{[(x_p^2 + y_p^2 - 4)^2 + 16y_p^2]} \quad (22)$$

Eqn. (22) can only be satisfied if the positive root is adopted and is always satisfied when this root is taken. Hence

$$\mu_1 = \left[\tfrac{1}{2}\left\{(x_p^2 + y_p^2 + 4) + \sqrt{[(x_p^2 + y_p^2 + 4)^2 - 16x_p^2]}\right\}\right]^{1/2} \quad (23)$$

From eqns. (19) and (23), it follows that

$$d_1 = \left[\tfrac{1}{2}\left\{(x_p^2 + y_p^2 + 4) - \sqrt{[(x_p^2 + y_p^2 + 4)^2 - 16x_p^2]}\right\}\right]^{1/2} \quad (24)$$

while from eqn. (20) it follows that only negative values of x_p are realizable, since both μ_1 and d_1 are positive and real.

From eqn. (24) and the condition $d_{min} \leqslant d_1 \leqslant \infty$ it follows finally that

$$1 \leqslant \frac{x_p^2}{d_{min}^2} - \frac{y_p^2}{4 - d_{min}^2} \quad . \quad . \quad . \quad . \quad . \quad (25)$$

which, for points in the left-half z-plane, defines a region bounded by a hyperbola such as is indicated in part by curve C of Fig. 2.*

The regions in the z-plane within which complex conjugate pairs of singularities are permitted for both an amplifier of inverse-feedback pairs and a stagger-tuned amplifier having been determined, it is necessary to turn to the approximation problem and to determine the position of the singularities in the z-plane corresponding to desired response shapes.

(5) THE APPROXIMATION PROBLEM

(5.1) General Remarks

The response shapes usually required are the Chebyshev or equal ripple response, and the Butterworth or maximally flat response. However, by a suitable choice of parameters, the

* The possibility of pairs of real roots situated on the negative axis of this region has not been investigated. It should not be assumed that arbitrary selections of pairs of negative real singularities in this region are admitted.

latter can be treated as a limiting case of the former, so that one analysis can be applied to both. This will be done here.

(5.2) The Chebyshev Response

A theorem due to Chebyshev,[5] and a subsequent discussion of the theorem by Bernstein,[6] shows that, if a polynomial of degree n in a real variable, x, satisfies the condition that $-1 \leqslant f(x) \leqslant +1$ for $-1 \leqslant x \leqslant +1$, then, for any value of x in the range $|x| > 1$, there is a maximum value which $f(x)$ cannot exceed, and this maximum value is achieved if $f(x)$ is a Chebyshev polynomial of the first kind and of order n. Chebyshev polynomials therefore exhibit just the property required of a bandpass amplifier, namely the maximum attainable rate of cut-off outside the passband, and a maximum range within the passband having a gain which does not differ from the mid-band gain by more than s dB, the gain tolerance. For this reason, the Chebyshev polynomial is considered the most suitable polynomial with which to approximate the design specification in situations in which the phase response is unimportant.

Since eqns. (11), (23) and (24) express the circuit parameters in terms of the positions of the singularities in the z-plane of the voltage transfer function, and since the constraints imposed upon the positions of these singularities are known, it is convenient to specify the desired response shape in terms of the positions of desired singularities in the plane of z.

Define $\omega_m^2 = \omega_l\omega_u$, $2\pi B = \omega_u - \omega_l$ and $d = B/f_m$.

When $\omega = \omega_l$,

$$z = x + jy = j(\omega_l/\omega_m - \omega_m/\omega_l) = -jd$$

When $\omega = \omega_m$,

$$z = x + jy = 0$$

When $\omega = \omega_u$,

$$z = x + jy = j(\omega_u/\omega_m - \omega_m/\omega_u) = +jd$$

Consider next the expression

$$\left|\frac{G}{G_{in}}\right| = \left[\delta + \epsilon T_{2n}\left(\frac{y}{\kappa d}\right)\right]^{-1/2} \quad . \quad . \quad . \quad (26)$$

where $|G_m|$ is the mid-band gain modulus,

$$T_{2n}(y/\kappa d) = \cos\,[2n \arccos\,(y/\kappa d)]$$

is the Chebyshev polynomial of the first kind and of order $2n$ and δ, ϵ and κ are constants to be specified.

These constants can be chosen to relate eqn. (26) to the design specification through the following conditions:

When $\omega = \omega_m$ and hence $y = 0$,

$$|G| = |G_m| \text{ by definition of } |G_m|$$

When $T_{2n}(y/\kappa d) = +1$ and n is odd,

$$20 \log_{10} |G/G_m| = -s$$

(see Section 10.1).

When $T_{2n}(y/\kappa d) = -1$ and n is even,

$$20 \log_{10} |G/G_m| = +s$$

(see Section 10.1).

When $\omega = \omega_l$ or ω_u and hence $y = \pm d$,

$$|G/G_m| = 1/\sqrt{2}$$

from the specification of ω_u and ω_l as the upper and lower 3 dB frequencies.

Choosing δ, ϵ and κ in eqn. (26) to satisfy these conditions gives:

If n is odd,

$$\left.\begin{aligned} |G/G_m| &= [(1+\epsilon) + \epsilon T_{2n}(y/\kappa d)]^{-1/2} \\ \text{where} \quad \epsilon &= \tfrac{1}{2}(10^{S/10} - 1) \simeq 0{\cdot}115s, \text{ if } s \ll 8{\cdot}7 \\ \text{and} \quad 1/\kappa &= \cosh\left(\frac{1}{2n} \operatorname{arc\,cosh} \frac{1-\epsilon}{\epsilon}\right) \end{aligned}\right\} \quad . \quad (27)$$

If n is even,

$$\left.\begin{aligned} |G/G_m| &= [(1-\epsilon) + \epsilon T_{2n}(y/\kappa d)]^{-1/2} \\ \text{where} \quad \epsilon &= \tfrac{1}{2}(1 - 10^{-s/10}) \simeq 0{\cdot}115s, \text{ if } s \ll 8{\cdot}7 \\ \text{and} \quad 1/\kappa &= \cosh\left(\frac{1}{2n} \operatorname{arc\,cosh} \frac{1+\epsilon}{\epsilon}\right) \end{aligned}\right\} \quad . \quad (28)$$

From eqns. (27) and (28), it follows that the appropriate form of eqn. (26) for both odd and even values of n is

$$\left.\begin{aligned} |G/G_m| &= \left\{[1 + (-1)^{n+1}\epsilon] + \epsilon T_{2n}(y/\kappa d)\right\}^{-1/2} \\ \text{where} \quad \epsilon &\simeq 0{\cdot}115s \\ 1/\kappa &\simeq \cosh\left(\frac{1}{2n} \operatorname{arc\,cosh} \frac{8{\cdot}686}{s}\right) \end{aligned}\right\} \quad . \quad (29)$$

The singularities z_p of the minimum phase gain function G/G_m having a modulus $|G/G_m|$ defined by eqn. (29) are given by the zeros in the left half z-plane of the function[8]

$$H(z) = 1 + (-1)^{n+1}\epsilon + \epsilon T_{2n}\left(\frac{z}{j\kappa d}\right)$$

which reduces to the condition

$$T_{2n}\left(\frac{z_p}{j\kappa d}\right) = \cos 2n \arccos\left(\frac{z_p}{j\kappa d}\right) = -\frac{1 + (-1)^{n+1}\epsilon}{\epsilon} = -\cosh\theta \quad (30)$$

where $$\theta = \operatorname{arc\,cosh} \frac{1 + (-1)^{n+1}\epsilon}{\epsilon} \quad . \quad . \quad . \quad . \quad (31)$$

From eqn. (30),

$$\cos\left[2n \arccos\left(\frac{z_p}{j\kappa d}\right)\right] = -\cosh\theta = \cos\,[j\theta - (2r-1)\pi]$$

$$\left.\begin{aligned} \text{or} \quad z_p &= j\kappa d \cos\left\{\frac{1}{2n}[j\theta - (2r-1)\pi]\right\} \\ \text{where} \quad r &= 1, 2, \ldots n \end{aligned}\right\} \quad . \quad . \quad (32)$$

Equating the real and imaginary parts of eqn. (32) yields

$$\left.\begin{aligned} x_p &= -\kappa d \sinh\theta/2n \sin\frac{(2r-1)\pi}{2n} \\ y_p &= \kappa d \cosh\theta/2n \cos\frac{(2r-1)\pi}{2n} \end{aligned}\right\} \quad . \quad . \quad (33)$$

Eqns. (33) are the parametric equations of the ellipse

$$\frac{x_p^2}{(\kappa d \sinh\theta/2n)^2} + \frac{y_p^2}{(\kappa d \cosh\theta/2n)^2} = 1 \quad . \quad . \quad (34)$$

which shows that the required poles lie on an ellipse having a semi-major axis $\kappa d \cosh\theta/2n \simeq d$ along the imaginary axis and a semi-minor axis $\kappa d \sinh\theta/2n \simeq d\sqrt{(1-\kappa^2)}$ along the real axis.

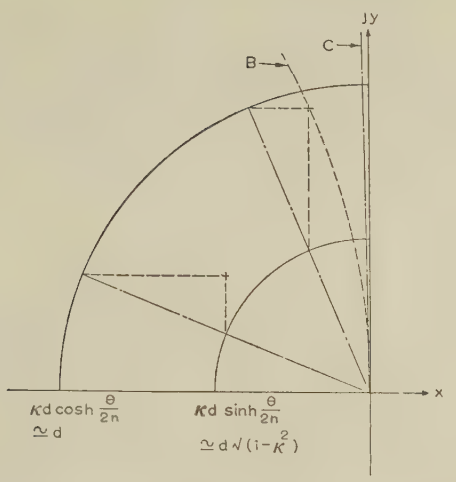

Fig. 4.—Locating the singularities of a desired response shape.

Assuming for the moment that a value of n has been established, the required pole positions may be rapidly plotted (see Fig. 4) as follows:

(*a*) Draw circles of radii d and $d\sqrt{(1-\kappa^2)}$ for the given specification, with centres at $x = y = 0$.

(*b*) Draw, in the second quadrant of the z-plane, radial lines making angles $(2r-1)\pi/2n$ with the $+jy$ axis.

(*c*) Read off the x-co-ordinate of the points of intersection of the smaller circle and each radial line, and the jy-co-ordinate of the points of intersection of the larger circle and each radial line. These co-ordinates are

$$x_p = -\kappa d \sinh\frac{\theta}{2n}\sin\frac{(2r-1)\pi}{2n}$$

$$y_p = \kappa d \cosh\frac{\theta}{2n}\cos\frac{(2r-1)\pi}{2n}$$

which define the required poles.

It only remains to superimpose curves B and C of Fig. 2 on Fig. 4, to test a particular specification for physical realizability.

(5.3) The Butterworth Response

The Chebýshev response having been defined in terms of a 3 dB bandwidth specification, the Butterworth (maximally flat) response follows by making the passband gain tolerance, s, tend to zero.

As s tends to zero, $\kappa\cosh\theta/2n \to \kappa\sinh\theta/2n \to 1$ so that a Butterworth response requires poles z_p defined by

$$\left.\begin{aligned} x_p &= -d\sin\frac{(2r-1)\pi}{2n} \\ y_p &= d\cos\frac{(2r-1)\pi}{2n} \end{aligned}\right\} \quad . \quad . \quad . \quad . \quad (35)$$

which is the parametric equation of a circle centred on the origin and of radius d.

(6) CHOOSING THE VALUE OF n

The only requirement in the original specification yet to be considered is the specified mid-band gain. It is to realize this that the value of n must be chosen.

Consider first the case of an n-stage amplifier consisting of either $n/2$ inverse-feedback pairs if n is even, or $(n-1)/2$ feedback pairs together with a single stage without feedback if n is odd. It follows from eqn. (2) and the equation

$$G = \frac{\dfrac{g_m}{\omega_m C}}{z + g_1/\omega_m C}$$

for the gain of a single stage, that

$$|G| = \left(\frac{\text{Geometric mean } g_m'}{\omega_m C}\right)^n \times (y^{2n} + a_{2n-2}y^{2n-2} + \ldots a_2y^2 + a_0)^{-1/2} \quad (36)$$

for such amplifiers. In eqn. (36) $a_{2n-2}, \ldots a_2, a_0$ are constants, and

$$(\text{Geometric mean } g_m')^n = g_m^{n/2}\prod_{r=1}^{n/2}(g_m - g_{f,2r}) \text{ if } n \text{ is even,}$$

$$= g_m^{(n+1)/2}\prod_{r=1}^{(n-1)/2}(g_m - g_{f,2r}) \text{ if } n \text{ is odd,}$$

where $g_{f,2r}$ is the feedback conductance of the rth pair in the chain.

The gain of an n-stage stagger-tuned amplifier may be developed from eqn. (17), and is of the form

$$|G| = [g_m/\omega_m C]^n[y^{2n} + a_{2n-2}y^{2n-2} + \ldots + a_2y^2 + a_0]^{-1/2} \quad (37)$$

The desired response shape is found from eqn. (29) by expressing $T_{2n}(y/\kappa d)$ in polynomial form (Section 10.2), when the desired $|G|$ becomes

$$|G| = |G_m|\epsilon^{-1/2}2^{-(2n-1)/2}(\kappa d)^n \times (y^{2n} + a_{2n-2}y^{2n-2} + \ldots + a_2y^2 + a_0)^{-1/2} \quad (38)$$

Locating the singularities of the gain functions, eqns. (36) and (37), in the same positions as those of the desired response shape eqn. (38) ensures the identity of the polynomials in these three expressions. Hence

$$|G_m| = \epsilon^{1/2}2^{(2n-1)/2}\left(\frac{g_m}{2\pi\kappa BC}\right)^n \quad . \quad . \quad . \quad (39)$$

for an n-stage stagger-tuned amplifier with a Chebýshev response, and

$$|G_m| = \epsilon^{1/2}2^{(2n-1)/2}\left(\frac{\text{Geometric mean } g_m'}{2\pi\kappa BC}\right)^n \quad . \quad (40)$$

for an n-stage amplifier of feedback pairs with a Chebýshev response.

It can be shown (Section 10.3) that

$$(\text{Geometric mean } g_m')^n = g_m^n \prod_{r=1}^{n/2 \text{ or } (n-1)/2}\frac{1}{2}\left\{1 + \left[1 - \left(\frac{4\pi CB}{g_m}\right)^2\cos^2\frac{(2r-1)\pi}{2n}\right]^{1/2}\right\} \quad (41)$$

when eqn. (40) becomes

$$|G_m| = \epsilon^{1/2}2^{(2n-1)/2}\left(\frac{g_m}{2\pi\kappa BC}\right)^n \times \prod_{r=1}^{n/2 \text{ or } (n-1)/2}\frac{1}{2}\left\{1 + \left[1 - \left(\frac{4\pi CB}{g_m}\right)^2\cos^2\frac{(2r-1)\pi}{2n}\right]^{1/2}\right\} \quad (42)$$

Expressions for the mid-band gain of a Butterworth approximation follow from eqns. (39) and (42) by setting the gain tolerance, s, to zero. This gives

$$|G_m| = \left(\frac{g_m}{2\pi BC}\right)^n \quad . \quad . \quad . \quad . \quad . \quad (43)$$

for an n-stage stagger-tuned amplifier with a Butterworth response, and

$$|G_m| = \left(\frac{g_m}{2\pi BC}\right)^n \times \prod_{r=1}^{n/2 \text{ or } (n-1)/2} \frac{1}{2}\left\{1 + \left[1 - \left(\frac{4\pi CB}{g_m}\right)^2 \cos^2 \frac{(2r-1)\pi}{2n}\right]^{1/2}\right\} \quad (44)$$

for an n-stage amplifier of feedback pairs with a Butterworth response.

Eqns. (39), (42), (43) and (44) contain n as the only unknown parameter on the right-hand side. The smallest integral value of n which makes $|G_m| \geqslant$ (specified mid-band gain) defines the appropriate number of stages.

The value of n required by eqn. (43) for a given mid-band gain modulus is easily deduced, and suggests values of n to explore when seeking a solution of any of eqns. (39), (42) and (44).

(7) A DESIGN EXAMPLE

(7.1) The Design Specification

The above procedures will now be applied to a particular design problem to illustrate the simplicity of the method.

It is required to design an amplifier with a passband gain of at least 66 dB and a passband defined by the 3 dB frequencies f_l and f_u, where $f_l = 7{\cdot}5$ Mc/s and $f_u = 20$ Mc/s. It is further required that the passband gain shall not vary by more than $\frac{1}{4}$ dB over as great a part of the passband as possible.

Initial experiments suggest that, for the available components,

$$g_m = 7{\cdot}6\,\text{mA/volt} \qquad C = 17\,\text{pF}$$
$$g_{min} = 10^{-5}\ \text{mho}$$

for the inverse feedback case, and $d_{min} = 8 \times 10^{-3}$ for the stagger-tuned amplifier.

(7.2) Choosing n

The first step in the design is to decide upon a suitable number of stages. Eqn. (43) suggests trying

$$n = 20 \log_{10} |G_m| \Big/ 20 \log_{10}\left(\frac{g_m}{2\pi BC}\right) = \frac{66}{15{\cdot}1} \simeq 4$$

With a gain tolerance $s = \frac{1}{4}$ dB specified, a Chebȳshev approximation can be used.

Since $\epsilon = 0{\cdot}115s \simeq 0{\cdot}029$

$$B = 20 \times 10^6 - 7{\cdot}5 \times 10^6 = 12{\cdot}5 \times 10^6\,\text{c/s}$$
$$\omega_m = 2\pi \times 10^6\sqrt{(20 \times 7{\cdot}5)} = 2\pi \times 12{\cdot}25 \times 10^6\,\text{rad/s}$$
$$1/\kappa = \cosh\left(\frac{1}{2n} \operatorname{arc\,cosh} \frac{8{\cdot}686}{s}\right) = \cosh(2{\cdot}12/n)$$
$$C = 17 \times 10^{-12}\,\text{F}$$
$$g_m = 7{\cdot}6 \times 10^{-3}\ \text{mho}$$

it follows from eqns. (39) and (42) that, for a Chebȳshev approximation, using stagger-tuned amplifier stages [eqn. (39)],

$$|G_m| \simeq 70\,\text{dB for } n = 4$$
$$|G_m| \simeq 47\,\text{dB for } n = 3$$

and using a chain of feedback pairs [eqn. (42)]

$$|G_m| \simeq 70\,\text{dB for } n = 4$$
$$|G_m| \simeq 47\,\text{dB for } n = 3$$

Hence, whichever circuit configuration is used, four stages are required to achieve the desired mid-band gain.

(7.3) The Desired Response

With $n = 4$, the pole positions of the desired response shape may be determined by the method already described (see Fig. 4). The radii appropriate to this problem are $d = B/f_m = 12{\cdot}5/12{\cdot}25 = 1{\cdot}02$, and $d\sqrt{(1-\kappa^2)} = 1{\cdot}02\sqrt{[1 - (1/\cosh 0{\cdot}53)^2]} = 0{\cdot}5$, while the radial lines make angles $\pi/8$ and $3\pi/8$ with the $+jy$ axis.

Carrying out this construction and reading off the appropriate co-ordinates gives

$$z_{p1},\ z_{p1}^* = -0{\cdot}188 \pm j0{\cdot}950 \quad . \quad . \quad . \quad (45)$$
$$z_{p2},\ z_{p2}^* = -0{\cdot}455 \pm j0{\cdot}395 \quad . \quad . \quad . \quad (46)$$

Plotting the boundaries of the regions of realizable singularities in Fig. 4 immediately shows that the specification can be realized with both stagger-tuned and feedback amplifier circuits.

(7.4) The Stagger-Tuned Realization

The first pair are designed to realize z_{p1} and z_{p1}^*, and the second pair subsequently designed to realize z_{p2} and z_{p2}^*.

Substituting $x_p = -0{\cdot}188$, $y_p = \pm 0{\cdot}950$ in eqn. (23) yields the appropriate value of μ_1 for the first pair. Thus

$$\mu_1 = \left[\tfrac{1}{2}\left\{0{\cdot}188^2 + 0{\cdot}95^2 + 4 + \sqrt{[(0{\cdot}188^2 + 0{\cdot}95^2 + 4)^2 - 16 \times 0{\cdot}188^2]}\right\}\right]^{1/2}$$
$$= 2{\cdot}23 = \omega_1/\omega_m + \omega_m/\omega_1$$

Therefore $(\omega_1/\omega_m)^2 - 2{\cdot}23(\omega_1/\omega_m) + 1 = 0 \quad . \quad . \quad . \quad (47)$

and $\omega_1 = 1{\cdot}62\omega_m$ or $0{\cdot}62\omega_m$ and hence† $\omega_2 = \omega_m^2/\omega_1 = 0{\cdot}62\omega_m$ or $1{\cdot}62\omega_m$.

We next determine d_1. From eqn. (20), $d_1 = -2x_p/\mu_1 = 0{\cdot}376/2{\cdot}23 = 0{\cdot}168$. Hence the load circuit of one stage of the first pair is tuned to $0{\cdot}62\omega_m$ (=7·6 Mc/s), and has $Q = 1/d_1 = 5{\cdot}9$, while the other stage is tuned to $1{\cdot}62\omega_m$ (=19·75 Mc/s) and has the same Q-factor.

The calculations of this Section can now be repeated for the next pair of singularities, eqn. (46), giving $\omega_1 = 0{\cdot}635\omega_m$, $\omega_2 = 1{\cdot}575\omega_m$ and $d_1 = 0{\cdot}41$ as the appropriate values for the second pair of stages of the 4-stage amplifier. One stage of the second pair is thus tuned to 7·7 Mc/s and has a Q-factor of 2·45, while the second stage is tuned to 19·5 Mc/s, also with a Q-factor of 2·45.

Although it is convenient in the design process to consider the stages in pairs in this way, thereby realizing each pair of complex conjugate singularities by a separate circuit, the stages, once designed, may be cascaded in any order.

(7.5) Realization with Inverse-Feedback Pairs

Eqns. (11) are appropriate for the solution of the realization problem with this circuit configuration. Substituting $x_p = -0{\cdot}188$, $y_p = \pm 0{\cdot}95$ in eqn. (11) yields

$$g_f = \tfrac{1}{2}\left\{7{\cdot}6 \times 10^{-3} - \sqrt{[(7{\cdot}6)^2 \times 10^{-6} - (4\pi \times 12{\cdot}25 \times 10^6 \times 17 \times 10^{-12} \times 0{\cdot}950)^2}\right\}$$
$$= 0{\cdot}22 \times 10^{-3}\ \text{mho}$$

and

$$g = 2\pi \times 12{\cdot}25 \times 10^6 \times 17 \times 10^{-12} \times 0{\cdot}188 - 0{\cdot}22 \times 10^{-3}$$
$$= 0{\cdot}024 \times 10^{-3}\ \text{mho}$$

Hence both load circuits of the first feedback pair have a Q-factor (=$\omega_m C/g$) of 53, and are tuned to 12·25 Mc/s. The feedback resistance (=$1/g_f$) is 4·5 kilohms.

† It is a general property of eqn. (47) that the product of the roots of this quadratic is unity, so that the two values of ω_1 have ω_m as their geometric mean. Thus either root may be selected as the appropriate ω_1, when the other root automatically becomes the corresponding ω_2.

Repeating this procedure for the pair of singularities z_{p2}, z_{p2}^* of eqn. (46) gives $g_f = 0{\cdot}035 \times 10^{-3}$ mho and $g = 0{\cdot}556 \times 10^{-3}$ mho. The second pair of the 4-stage feedback chain require identical load circuits, also tuned to 12·25 Mc/s, having Q-factors of 2·3. The required feedback resistance for this pair ($=1/g_f$) is 28·6 kilohms. Connecting these two feedback pairs in cascade provides the desired overall response.

(8) CONCLUSIONS

The above examples demonstrate the simplicity of this design procedure. This simplicity results from designing stages in pairs, each pair realizing a pair of conjugate singularities. In this way the complete network is broken down into a number of basic elements from which the whole circuit is developed. These basic elements, though designed separately, have only to be connected in cascade to produce the required overall response.

No matter how large the value of n required to satisfy a given design specification, no extra complication is introduced, because the basic element remains unchanged throughout. It is this fact which makes this method of design particularly useful when n is large.

Determination of the regions of the z-plane within which conjugate singularities are realizable enables the designer to test the realizability of any Chebȳshev or Butterworth response which he may require.

The specification of regions of realizable singularities also serves to compare different circuit configurations. The circuit configuration which permits the greatest freedom of choice of positions of singularities is to be preferred. Fig. 2 clearly shows that any response shape which can be realized by the use of cascaded feedback pairs can also be realized by the use of stagger-tuned stages, while the converse is not true.

(9) REFERENCES

(1) BAUM, R. H.: 'Design of Broad Band I.F. Amplifiers', *Journal of Applied Physics*, 1946, **17**, p. 519.

(2) DISHAL, M.: 'Design of Dissipative Band-Pass Filters Producing Desired Exact Amplitude-Frequency Characteristics', *Proceedings of the Institute of Radio Engineers*, 1949, **37**, p. 1050.

(3) GREEN, E.: 'Exact Amplitude Frequency Characteristics of Ladder Networks', *Marconi Review*, 1953, **16**, p. 25.

(4) LANDON, V. D.: 'Cascade Amplifiers with Maximal Flatness', *RCA Review*, 1941, **5**, p. 347.

(5) CHEBȲSHEV, S.: 'Sur les fonctions qui s'écartent peu de zero', Oeuvres, 1899, **1**.

(6) BERNSTEIN, S.: 'Leçons sur les propriétés extrémales et la meilleure approximation des fonctions analytiques d'une variable réelle', Borel Monograph, 1926.

(7) VALLEY, G. E., and WALLMAN, H.: 'Vacuum Tube Amplifiers', M.I.T. Radiation Laboratory Series, Vol. 18 (McGraw-Hill, 1948), Chaps. 4 and 6.

(8) BODE, H.: 'Network Analysis and Feedback Amplifiers' (Van Nostrand, 1945), Chap. 14.

(10) APPENDICES

(10.1) The Chebȳshev Polynomial

The Chebȳshev polynomial $T_n(x)$ of the first kind and of order n is defined by

$$T_n(x) = \cos(n \arccos x) \quad . \quad . \quad . \quad . \quad (48)$$

It follows that

$$T_n(-x) = \cos n\pi \cos(n \arccos x) = (-1)^n T_n(x)$$

Hence $T_n(x)$ is an odd function of x if n is odd, and is an even function of x if n is even.

Since the desired amplitude response function is an even function, only even-order Chebȳshev polynomials are of interest here, and hence it is only necessary to study

$$T_{2n}(x) = \cos(2n \arccos x) \quad . \quad . \quad . \quad . \quad (49)$$

where n is a positive integer. From eqn. (49),

$$\frac{d}{dx}T_{2n}(x) = 2n \sin(2n \arccos x)/\sqrt{(1-x^2)} = 0$$

if $$x = \cos r\pi/2n,\ r = 1, 2, \ldots (2n-1) \quad . \quad (50)$$

Hence, $T_{2n}(x)$ has $2n-1$ stationary values in the range $|x| < 1$. Substituting eqn. (50) into eqn. (49) shows that

$$T_{2n}(x) = \cos[2n \arccos(\cos r\pi/2n)] = \cos r\pi = \pm 1 \text{ at the stationary points.}$$

Again, from eqn. (49) $T_{2n}(x) = 0$ when $2n \arccos x = (2r-1)\pi/2$, i.e. when

$$x = \cos\frac{(2r-1)\pi}{4n};\ r = 1, 2, \ldots (2n-1) \quad . \quad . \quad (51)$$

Finally, from eqn. (49),

$$T_{2n}(0) = \cos[2n \arccos(0)] = \cos 2n(2r-1)\pi/2$$

$$= -1 \text{ for } n \text{ odd, and } +1 \text{ for } n \text{ even} \quad . \quad . \quad . \quad (52)$$

Using the results of eqns. (50)–(52), the shape of the functions $T_{2n}(x)$ may be sketched by the method illustrated in Fig. 5 for $n = 3$ and $n = 4$ respectively.

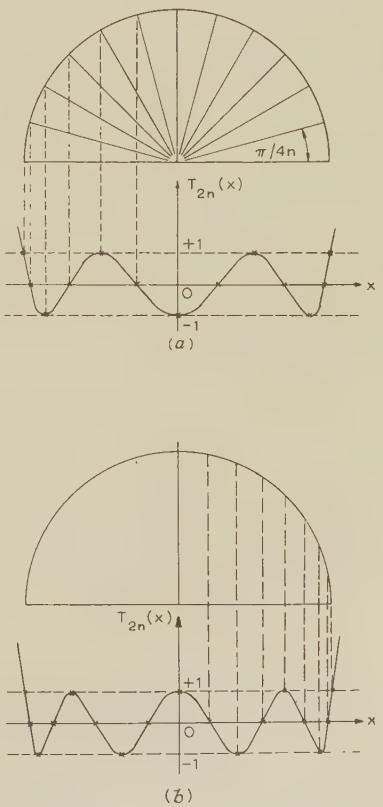

Fig. 5.—Chebȳshev responses $T_{2n}(x)$.
(*a*) n odd (=3).
(*b*) n even (=4).

(10.2) The Expansion of Chebyshev Polynomials

From the trigonometric identity

$$\cos 2n\Phi = 2\cos(2n-2)\Phi\cos 2\Phi - \cos(2n-4)\Phi$$

by setting $\Phi = \arccos x$ it follows that

$$T_{2n}(x) = 2T_2(x)T_{2n-2}(x) - T_{2n-4}(x) \quad . \quad . \quad (53)$$

From eqn. (49),

$$\begin{aligned} T_2(x) &= \cos(2\arccos x) = \cos^2(\arccos x) - \sin^2(\arccos x) \\ &= x^2 - (1-x^2) \\ &= 2x^2 - 1 \quad . \quad . \quad . \quad . \quad . \quad . \quad . \quad . \quad . \quad . \quad . \quad . \quad (54) \end{aligned}$$

and

$$T_0(x) = \cos(0\arccos x) = 1 \quad . \quad . \quad . \quad . \quad . \quad . \quad . \quad . \quad . \quad (55)$$

From eqns. (53) and (54),

$$T_{2n}(x) = 2(2x^2-1)T_{2n-2}(x) - T_{2n-4}(x) \quad . \quad . \quad (56)$$

Putting $n = 2$ in eqn. (56)

$$\begin{aligned} T_4(x) &= 2(2x^2-1)T_2(x) - T_0(x) \\ &= 2(2x^2-1)^2 - 1 \\ &= 2^3x^4 - 8x^2 + 1 \quad . \quad . \quad . \quad . \quad . \quad . \quad . \quad (57) \end{aligned}$$

Putting $n = 3, 4, \ldots$ in succession in eqn. (56) gives the higher-order Chebyshev polynomial expansions of $T_{2n}(x)$.

The following observations follow from inspection of eqn. (56) (or may be proved by mathematical induction if required):

(*a*) $T_{2n}(x)$ is an even polynomial of order $2n$ in x.
(*b*) The coefficient of x^{2n} in $T_{2n}(x)$ is $2^{(2n-1)}$.

Thus,

$$T_{2n}(x) = 2^{(2n-1)}x^{2n} + \alpha_{2n-2}x^{2n-2} + \ldots + \alpha_2x^2 + \alpha_0 \quad (58)$$

The coefficients $\alpha_{2(n-r)}$ for $r = 1, 2, \ldots n$ may be determined, if required, through the recurrence relation (56).

Eqn. (38) follows immediately from eqns. (29) and (58).

(10.3) The Value of [Geometric Mean g'_m]^n

From the definition,

$$\left.\begin{aligned} &[\text{Geometric mean } g'_m]^n \\ &\quad = g_m^{n/2}\prod_{r=1}^{n/2}(g_m - g_{f,2r}) \qquad \text{if } n \text{ is even} \\ &\quad = g_m^{(n+1)/2}\prod_{r=1}^{(n-1)/2}(g_m - g_{f,2r}) \quad \text{if } n \text{ is odd} \end{aligned}\right\} \quad (59)$$

From eqn. (11),

$$\begin{aligned} g_{f,2r} &= g_m\frac{1}{2}\left\{1 - \left[1 - \left(\frac{2\omega_m C}{g_m}\right)^2 y_{p,2r}^2\right]^{1/2}\right\} \\ &= g_m\frac{1}{2}\left\{1 - \left[1 - \left(\frac{2\omega_m C}{g_m}\right)^2 \kappa^2 d^2 \cosh^2\frac{\theta}{2n}\cos^2\frac{(2r-1)\pi}{2n}\right]^{1/2}\right\} \end{aligned}$$

from eqn. (33).

But $\kappa\cosh\theta/2n \simeq 1$ and hence

$$g_{f,2r} = g_m\frac{1}{2}\left\{1 - \left[1 - \left(\frac{4\pi BC}{g_m}\right)^2\cos^2\frac{(2r-1)\pi}{2n}\right]^{1/2}\right\} \quad (60)$$

since $d = B/f_m$.

Eqn. (41) follows immediately from eqns. (59) and (60).

621.372.6:621—52

The Institution of Electrical Engineers
Monograph No. 401 M
Sept. 1960

APPLICATION OF THE THEORY OF ORTHOGONAL POLYNOMIALS IN TWO VARIABLES TO A MULTI-GAIN EQUIVALENT LINEARIZATION PROBLEM

By J. L. BROWN, Ph.D.

(*The paper was first received* 22*nd March, and in revised form* 14*th June*, 1960. *It was published as an* INSTITUTION MONOGRAPH *in September*, 1960.)

SUMMARY

It is shown that the multi-gain representation for a single-valued non-linearity with multiple inputs as developed by Somerville and Atherton may be regarded as an approximation problem involving orthogonal polynomials in two variables.

Consider two stationary random processes, $x(t)$ and $y(t)$, possibly correlated, with a given second-order (zero-delay) joint probability density, $p(x, y)$. If the input to a specified zero-memory non-linear device having the input/output characteristic $v_0(t) = f[v_i(t)]$ is $x(t) + y(t)$, the relevant polynomials satisfy orthonormality conditions over the xy-plane with respect to $p(x, y)$ as weighting function. An inherent minimum property of these polynomials then allows the equivalent gains to be determined directly in terms of the expansion coefficients of $f(x + y)$ with respect to the polynomials. When x and y are uncorrelated, the gains reduce to the values previously obtained by Somerville and Atherton.

A further property of the polynomials is sufficient to prove that the zero-delay cross-correlation between the input and the error involved in the approximation is zero, and that this result remains true as the order of the approximation is increased.

(1) INTRODUCTION

The basic idea of representing the output of a zero-memory non-linear device subjected to a random input, $x(t)$, by the simple linear approximant, $kx(t)$, where k (the equivalent gain) depends on the input statistics and the particular device in question, was evolved independently and almost simultaneously by Booton,[1] and Kazakov.[2] Since these original papers, the technique of equivalent gains has attracted much attention from engineers, partially because there is no alternative in many applications, but also because the results obtained with the linearization yield surprisingly good results in a useful selection of closed-loop systems having Gaussian inputs.

While the method of equivalent gains may be thought of as a generalization of describing-function techniques to handle random inputs, other recent work[3] has dealt with generalizations of equivalent-gain theory to take care of composite random inputs, e.g. $x(t) + y(t)$, where each function represents a random time disturbance. Additional references to such generalizations are given by Somerville and Atherton.[3]

Oddly enough, orthogonal polynomials have not been invoked *per se* in this problem, although the approximant in the single-input case, kx, and that in the case of two additive inputs, $k_1x + k_2y$, are clearly polynomials in one and two variables, respectively. A connection between equivalent gain and polynomials generated by the first-order probability density of the input process has been noted,[4] but the use of polynomial theory to derive the equivalent gain has apparently been overlooked in the literature.

In the paper, the results obtained by Somerville and Atherton[3] are generalized to the case of correlated inputs, using the theory of orthogonal polynomials in two variables.

(2) THE PROBLEM

To facilitate comparison, the notation of Reference 3 will be adopted.

The non-linearity is characterized by the relationship

$$v_0(t) = f[v_i(t)] \quad . \quad . \quad . \quad . \quad . \quad . \quad (1)$$

where $v_0(t)$ is the instantaneous output value corresponding to the instantaneous input value, $v_i(t)$, and f is a single-valued function of its argument. Furthermore, the input to the non-linearity is assumed to be of the form

$$v_i(t) = \beta + x(t) + y(t) \quad . \quad . \quad . \quad . \quad . \quad (2)$$

where $x(t)$ and $y(t)$ are correlated zero-mean, stationary random processes and β is a constant specifying the d.c. input level. Let $p_2(x, y; \tau)$ represent the second-order joint probability density[5] of the two processes and define

$$p_2(x, y; 0) = p(x, y) \quad . \quad . \quad . \quad . \quad . \quad (3)$$

Thus $p(x, y)$ is essentially the zero-delay joint probability density for the two processes.

The problem consists of finding the 'best' linear approximation, having the form $k_1x(t) + k_2y(t)$, to the output, $f[\beta + x(t) + y(t)]$, of the non-linearity by choice of the constants k_1 and k_2. The criterion of optimization adopted here is that of minimum mean squared error, i.e. the quantity

$$M = \int_{-\infty}^{\infty}\int_{-\infty}^{\infty}[e(x, y)]^2 p(x, y)dxdy \quad . \quad . \quad . \quad (4)$$

is to be minimized, where $e(x, y)$ is the approximation error defined by

$$e(x, y) = f(\beta + x + y) - (k_1x + k_2y) \quad . \quad . \quad (5)$$

If, in addition to stationarity, it is assumed that both $x(t)$ and $y(t)$ are ergodic, M has the equivalent expression

$$M = \lim_{T\to\infty}\frac{1}{T}\int_0^T \{e[x(t), y(t)]\}^2 dt \quad . \quad . \quad . \quad (6)$$

which is perhaps a more familiar expression of mean square error. For non-stationary processes, M as given by eqn. (4) will depend on t_1, and the pertinent quantity for minimization would be

$$\lim_{T\to\infty}\frac{1}{T}\int_0^T M(k_1, k_2, t_1)dt_1 . \quad . \quad . \quad . \quad . \quad (7)$$

It might be noted at this point that taking an approximation of the form $k_1x + k_2y + k_3$ does not add anything essential to the analysis. If $e_1(x, y)$ is defined as

$$e_1(x, y) = f(\beta + x + y) - (k_1x + k_2y + k_3) \quad . \quad (8)$$

and

$$M_1 = \int_{-\infty}^{\infty}\int_{-\infty}^{\infty} e_1^2(x, y)p(x, y)dxdy \quad . \quad . \quad . \quad (9)$$

Correspondence on Monographs is invited for consideration with a view to publication.

Dr. Brown is in the Ordnance Research Laboratory, Pennsylvania State University, University Park, Pa., U.S.A.

it is easily verified that

$$M_1 = M + k_3^2 \quad . \quad . \quad . \quad . \quad . \quad (10)$$

i.e. the same values of k_1 and k_2 which minimize M will minimize M_1 and conversely. Consequently, k_3 may be interpreted as a constant bias equal to the average value of the output, $f(\beta + x + y)$, and the shortened form $k_1x + k_2y$ may be used without loss of generality.

The pertinent facts concerning orthogonal polynomials in two variables are summarized in the Appendix.

(3) APPLICATION

The problem, as posed in Section 2, is now easily resolved using the minimum property proved in the Appendix. In the theory given in the Appendix, identify the non-negative weighting function $\rho(x, y)$ with the second-order joint density, $p(x, y)$, of the input processes $x(t)$ and $y(t)$ and let R be the entire xy-plane. Then, by the minimum theorem, the best mean-square approximation to $f(\beta + x + y)$ limited to linear terms (i.e. to terms of first degree in x and y) is given by the partial sum

$$\begin{aligned} S_1(x, y) &= \sum_{k=0}^{1} \sum_{i=0}^{k} c_{ki} q_{ki}(x, y) \\ &= c_{00}q_{00}(x, y) + c_{10}q_{10}(x, y) + c_{11}q_{11}(x, y) \quad . \quad (11) \end{aligned}$$

where the c_{ki} are given by

$$c_{ki} = \int_{-\infty}^{\infty}\int_{-\infty}^{\infty} p(x, y) f(\beta + x + y) q_{ki}(x, y) dxdy \quad . \quad (12)$$

for $i = 0$, k and $k = 0$, 1. The problem is thereby reduced to finding the three polynomials, $q_{00}(x, y)$, $q_{10}(x, y)$ and $q_{11}(x, y)$, and then determining the coefficients c_{00}, c_{10} and c_{11}.

By definition, the unknown polynomials must be of the form

$$\left.\begin{aligned} q_{00} &= c_1 \\ q_{10} &= c_2 + c_3x \\ q_{11} &= c_4 + c_5x + c_6y \end{aligned}\right\} \quad . \quad . \quad . \quad . \quad (13)$$

with $c_1 \neq 0$, $c_3 \neq 0$ and $c_6 \neq 0$.

By application of the orthonormality conditions it is readily deduced that

$$\begin{aligned} c_1 &= 1 \\ c_2 &= 0 \\ c_3 &= 1/\sigma_x \\ c_4 &= 0 \\ c_5 &= \frac{-\phi_{xy}}{\sigma_x}[\sigma_x^2\sigma_y^2 - \phi_{xy}^2]^{-1/2} \\ c_6 &= \sigma_x[\sigma_x^2\sigma_y^2 - \phi_{xy}^2]^{-1/2} \end{aligned}$$

where

$$\left.\begin{aligned} \sigma_x^2 &= \int_{-\infty}^{\infty} x^2 p(x) dx \\ \sigma_y^2 &= \int_{-\infty}^{\infty} y^2 q(y) dy \\ \phi_{xy} &= \int_{-\infty}^{\infty}\int_{-\infty}^{\infty} xy p(x, y) dxdy \end{aligned}\right\} \quad . \quad . \quad . \quad (14)$$

and $p(x)$ and $q(y)$ denote the first-order probability densities of x and y, respectively. Thus the three polynomials in eqn. (13) are determined entirely by the input statistical parameters and can be written down immediately once these parameters are known.

With $c_{00} = \alpha$, $c_{10} = \gamma$ and $c_{11} = \delta$ these quantities are determined by eqn. (12) as

$$\left.\begin{aligned} \alpha &= \int_{-\infty}^{\infty}\int_{-\infty}^{\infty} f(\beta + x + y) p(x, y) dxdy \\ \gamma &= \int_{-\infty}^{\infty}\int_{-\infty}^{\infty} f(\beta + x + y) p(x, y) \left(\frac{x}{\sigma_x}\right) dxdy \\ \delta &= \int_{-\infty}^{\infty}\int_{-\infty}^{\infty} f(\beta + x + y) p(x, y)(c_5x + c_6y) dxdy \end{aligned}\right\} \quad (15)$$

The linear approximant $k_1x + k_2y$ containing the unknown equivalent gains k_1 and k_2 can be expressed in terms of the polynomials

$$\left.\begin{aligned} k_1x + k_2y &= k_1\frac{q_{10}}{c_3} + \frac{k_2}{c_6}q_{11} - \frac{c_5}{c_3}q_{10} \\ &= \frac{k_1}{c_3} - \frac{k_2}{c_3}\frac{c_5}{c_6}q_{10} + \frac{k_2}{c_6}q_{11} \end{aligned}\right\} \quad . \quad . \quad (16)$$

According to the minimum theorem given in the Appendix the best mean-square fit will be obtained when k_1 and k_2 are chosen so that

$$\left.\begin{aligned} \frac{k_1}{c_3} - \frac{k_2}{c_3}\frac{c_5}{c_6} &= \gamma \\ \frac{k_2}{c_6} &= \delta \end{aligned}\right\} \quad . \quad . \quad . \quad . \quad . \quad (17)$$

Thus,

$$k_1 = \frac{\gamma}{\sigma_x} - \frac{\delta\phi_{xy}}{\sigma_x[\sigma_x^2\sigma_y^2 - \phi_{xy}^2]^{1/2}} \quad . \quad . \quad . \quad (18)$$

and

$$k_2 = \frac{\delta\sigma_x}{[\sigma_x^2\sigma_y^2 - \phi_{xy}^2]^{1/2}} \quad . \quad . \quad . \quad . \quad . \quad . \quad (19)$$

where the values of c_3, c_5 and c_6 have been substituted. Eqns. (18) and (19) then express the equivalent gains in the general case of two additive inputs having a zero-delay cross correlation value, ϕ_{xy}.

In the special case where $x(t)$ and $y(t)$ are uncorrelated, the second-order density, $p(x, y)$, is given by

$$p(x, y) = p(x)q(y) \quad . \quad . \quad . \quad . \quad . \quad (20)$$

where $p(x)$ and $q(y)$ are the first-order probability densities of x and y, respectively. Since $\phi_{xy} = 0$ in this case, $c_2 = c_4 = c_5 = 0$, $c_1 = 1$, $c_3 = 1/\sigma_x$ and $c_6 = 1/\sigma_y$. The three polynomials reduce to the simple forms

$$\left.\begin{aligned} q_{00} &= 1 \\ q_{10} &= x/\sigma_x \\ q_{11} &= y/\sigma_y \end{aligned}\right\} \quad . \quad . \quad . \quad . \quad . \quad (21)$$

and

$$\left.\begin{aligned} \gamma &= \frac{1}{\sigma_x}\int_{-\infty}^{\infty}\int_{-\infty}^{\infty} f(\beta + x + y) p(x) q(y) dxdy \\ \delta &= \frac{1}{\sigma_y}\int_{-\infty}^{\infty}\int_{-\infty}^{\infty} f(\beta + x + y) p(x) q(y) dxdy \end{aligned}\right\} \quad . \quad (22)$$

With these expressions, eqns. (18) and (19) become

$$\left.\begin{aligned} k_1 &= \frac{1}{\sigma_x^2}\int_{-\infty}^{\infty}\int_{-\infty}^{\infty} xf(\beta + x + y) p(x) q(y) dxdy \\ \text{and} \quad k_2 &= \frac{1}{\sigma_y}\int_{-\infty}^{\infty}\int_{-\infty}^{\infty} yf(\beta + x + y) p(x) q(y) dxdy \end{aligned}\right\} \quad . \quad (23)$$

which coincide with the determinations given by Somerville and Atherton[3] for this case. The method of Somerville and Atherton can also be used when x and y are correlated to obtain

$$k_1 = \frac{\sigma_y^2 \int_{-\infty}^{\infty}\int_{-\infty}^{\infty} xf(\beta + x + y)p(x, y)dxdy - \phi_{xy}\int_{-\infty}^{\infty}\int_{-\infty}^{\infty} yf(\beta + x + y)p(x, y)dxdy}{\sigma_x^2\sigma_y^2 - \phi_{xy}^2} \quad . \quad . \quad . \quad . \quad . \quad (24)$$

nd

$$k_2 = \frac{\sigma_x^2 \int_{-\infty}^{\infty}\int_{-\infty}^{\infty} yf(\beta + x + y)p(x, y)dxdy - \phi_{xy}\int_{-\infty}^{\infty}\int_{-\infty}^{\infty} xf(\beta + x + y)p(x, y)dxdy}{\sigma_x^2\sigma_y^2 - \phi_{xy}^2} \quad . \quad . \quad . \quad . \quad . \quad (25)$$

Eqns. (24) and (25) result from eqns. (18) and (19) when the ntegral forms of γ and δ are substituted; the two forms are nerefore equivalent.

(4) ERROR UNCORRELATED WITH INPUT

For the single-input case it has been noted[4] that the error etween the actual output and the approximated output is ncorrelated (for zero delay) with the input. The purpose of his Section is to show that the same result holds true for the omposite input $\beta + x(t) + y(t)$.

Theorem.—Let the input to the non-linearity be $\beta + x(t) + y(t)$ s before and consider the approximant $k_1x(t) + k_2y(t) + k_3$, vhere k_1 and k_2 are the equivalent gains as determined in qns. (18) and (19) and k_3 is the average value of $f[\beta + x(t) + y(t)]$. Then the error, $f(\beta + x + y) - (k_1x + k_2y + k_3)$, is ncorrelated (zero delay) with the input, $\beta + x + y$.

Proof.—The theorem states that

$$\int_{-\infty}^{\infty}\int_{-\infty}^{\infty}[f(\beta + x + y) - (k_1x + k_2y + k_3)](\beta + x + y)p(x, y)dxdy = 0 \quad (26)$$

Since the formal expansion of $f(\beta + x + y)$ is

$$f(\beta + x + y) \simeq \sum_{k=0}^{\infty}\sum_{i=0}^{k} c_{ki}q_{ki}(x, y) \quad . \quad . \quad (27)$$

and k_1, k_2 and k_3 have been chosen to satisfy

$$k_1x + k_2y + k_3 = c_{00}q_{00} + c_{10}q_{10} + c_{11}q_{11} \quad . \quad (28)$$

it follows that

$$f(\beta + x + y) - (k_1x + k_2y + k_3) \simeq \sum_{k=2}^{\infty}\sum_{i=0}^{k} c_{ki}q_{ki}(x, y) \quad (29)$$

and it is clear that the right-hand side of eqn. (29) contains only terms of degree $\geqslant 2$ in x and y. But it is noted in the Appendix that $q_{nk}(x, y)$ is orthogonal to every polynomial of degree $< n$ in x and y. Therefore $f(\beta + x + y) - (k_1x + k_2y + k_3)$ is orthogonal to the first-degree polynomial $\beta + x + y$, as asserted.

Of course, this result could have been proved directly using expressions (24) and (25), but the algebra becomes somewhat tedious.

It should also be noted that the theory of orthonormal polynomials in one variable and the corresponding minimum property for such polynomials[7] afford a completely parallel development of equivalent-gain theory for a non-linearity subjected to a single random input. In this simpler case the polynomials are constructed to be orthonormal on the interval $(-\infty, \infty)$ with respect to the first-order probability density, $p(x)$, of the input process. The best mean-square approximation, having the form kx, to the output, $f(x)$, of the device is then obtained by choosing k equal to the coefficient of the first-degree polynomial in the generalized Fourier expansion of $f(x)$ with respect to the orthonormal polynomials. The resulting value of k is identical with Booton's determination[1] of equivalent gain for this case.

(5) CONCLUSIONS

An exposition has been given of the application of orthogonal polynomials in two variables to the determination of the multiple equivalent gains which arise in the linearization of an instantaneous non-linear device subjected to a composite random input. While such results may also be obtained by conventional methods for determining extrema, it is felt that the polynomial setting best exhibits the essential nature of the problem and provides a more uniform approach. Furthermore, the extension to higher-order approximants (e.g. the best mean-square approximation in terms of a second-degree polynomial in x and y) is immediately apparent, whereas conventional techniques become clumsy as the order of the approximation increases.

An immediate consequence of the theory is that the zero-delay cross-correlation between the error and the input is zero. This property remains valid for any finite order of approximation as well as for the first-order approximation. The underlying polynomial theory provides this general result without any additional computation and validates the usefulness of the polynomial approach.

(6) REFERENCES

(1) BOOTON, R. C.: 'The Analysis of Nonlinear Control Systems with Random Inputs', Proceedings of the Symposium on Nonlinear Circuit Analysis, Polytechnic Institute of Brooklyn, N.Y., 1953, p. 369.

(2) KAZAKOV, I. E.: 'Approximate Probability Analysis of the Operational Precision of Essentially Nonlinear Feedback Control Systems', *Automation and Remote Control* (English Translation published by Consultants Bureau, Inc.), 1956, **17**, p. 423.

(3) SOMERVILLE, M. J., and ATHERTON, D. P.: 'Multi-Gain Representation for a Single-Valued Non-Linearity with Several Inputs and the Evaluation of their Equivalent Gains by a Cursor Method', *Proceedings I.E.E.*, Monograph 309 M, July, 1958 (**105** C, p. 537).

(4) BROWN, J. L.: 'On a Cross-Correlation Property for Stationary Random Processes', *Transactions of the Institute of Radio Engineers*, 1957, **IT-3**, p. 28.

(5) LANING, J. H., and BATTIN, R. H.: 'Random Processes in Automatic Control' (McGraw-Hill, 1956), p. 101.

(6) JACKSON, D.: 'Formal Properties of Orthogonal Polynomials in Two Variables', *Duke Mathematical Journal*, 1936, **2**, p. 423.

(7) SZEGÖ, G.: 'Orthogonal Polynomials' (American Mathematical Society Colloquium Publication, 1959), Vol. 23, Revised Edition, p. 38.

(7) APPENDIX

Orthogonal Polynomials in Two Variables

Given an arbitrary, non-negative, integrable function, $\rho(x, y)$, of two real variables which has a positive integral over some specified region R, the usual Schmidt orthonormalization procedure[6] applied to the linearly independent functions

$$\rho^{1/2}, \rho^{1/2}x, \rho^{1/2}y, \rho^{1/2}x^2, \rho^{1/2}xy, \rho^{1/2}y^2, \ldots$$

in the order shown yields a sequence of polynomials $q_{nm}(x, y)$, where $n = 0, 1, 2, \ldots$ and $m = 0, 1, \ldots n$, such that q_{nk} is of exactly nth degree in x and y and of exactly kth degree in y; furthermore, these polynomials satisfy an orthonormality condition of the form

$$\iint_R \rho(x, y) q_{kp}(x, y) q_{nm}(x, y) dx dy = \delta_{mp}\delta_{nk} \quad . \quad (30)$$

where δ_{mn} is the Kronecker delta defined by $\delta_{mn} = \begin{cases} 1 \text{ if } m = n \\ 0 \text{ if } m \neq n \end{cases}$

If the required integrals exist, an arbitrary integrable function $f(x, y)$ defined on R can be expanded in a formal series

$$f(x, y) \simeq \sum_{k=0}^{\infty} \sum_{i=0}^{k} c_{ki} q_{ki}(x, y) \quad . \quad . \quad . \quad (31)$$

where $$c_{ki} = \iint_R \rho(x, y) f(x, y) q_{ki}(x, y) dx dy \quad . \quad . \quad (32)$$

Let $$S_n(x, y) = \sum_{k=0}^{n} \sum_{i=0}^{k} c_{ki} q_{ki}(x, y) \quad . \quad . \quad . \quad (33)$$

denote the partial sum of this series through terms of nth degree in x and y and consider the problem of approximating $f(x, y)$ in the mean-square sense with respect to the weighting function $\rho(x, y)$ by a polynomial in two variables of maximum degree, n, in x and y. First, it is clear that any such approximating polynomial, $\pi_n(x, y)$, may be expressed in terms of the $q_{ki}(x, y)$, where $i = 0, 1, \ldots k$ and $k = 0, 1, \ldots n$; i.e. there exist coefficients, d_{ki}, such that

$$\pi_n(x, y) = \sum_{k=0}^{n} \sum_{i=0}^{k} d_{ki} q_{ki}(x, y) \quad . \quad . \quad . \quad (34)$$

Conversely, any double sum of the form shown in eqn. (34) is a polynomial in x and y of maximum degree n. The minimum property of interest here is as follows.

Minimum Property.—Of all possible polynomials, $\pi_n(x, y)$, having the form of eqn. (34), the one providing the least mean square error on R with respect to weighting function $\rho(x, y)$ in approximating a given function $f(x, y)$ is obtained by choosing $d_{ki} = c_{ki}$, where the c_{ki} are given by eqn. (32).

Proof.—With

$$I = \iint_R \rho(x, y)[f(x, y) - \pi_n(x, y)]^2 dx dy \quad . \quad (35$$

it is easily shown that

$$I = \iint_R \rho(x, y) f^2(x, y) dx dy + \sum_{k=0}^{n} \sum_{i=0}^{k} (d_{ki} - c_{ki})^2 - \sum_{k=0}^{n} \sum_{i=0}^{k} c_{ki}^2$$

$$. \quad . \quad . \quad . \quad . \quad (36$$

from which the theorem is immediately obtained. Furthermore the minimum value of I is given by

$$I_{min} = \iint_R \rho(x, y) f^2(x, y) dx dy - \sum_{k=0}^{n} \sum_{i=0}^{k} c_{ki}^2 . \quad . \quad (37$$

Lastly, since $q_{nk}(x, y)$ is of exactly nth degree in x and y, any polynomial $p_m(x, y)$ of exact degree m, where $m < n$, will be orthogonal* to $q_{nk}(x, y)$. This follows from the orthonormality relation for the $q_{ki}(x, y)$, since $p_m(x, y)$ may be expressed as a linear combination of $q_{jk}(x, y)$ with $k = 0, 1, \ldots j$ and $j = 0, 1, \ldots m$.

* Throughout the paper 'orthogonal' will mean with respect to weighting function $\rho(x, y)$ and over some given region R.

1.385.2

The Institution of Electrical Engineers
Monograph No. 402E
Oct. 1960

UNSTABLE ELECTRON FLOW IN A DIODE

By R. J. LOMAX, M.A., Ph.D.

(*The paper was first received 4th May, and in revised form 2nd July,* 1960. *It was published as an* INSTITUTION MONOGRAPH *in October,* 1960.)

SUMMARY

A perturbation analysis is used to demonstrate the instability of a pe of electron flow in a plane diode known as C-overlap flow, which predicted to be a possible flow in the approximation in which ectrons are emitted from the cathode with a uniform velocity.

LIST OF PRINCIPAL SYMBOLS

E = Electric field.
H = Magnetic field.
J_0, J_1 = Current density divided by ϵ_0, unperturbed and perturbed value, respectively.
t = Time.
t_p, t_q = Transit times.
t_1 = Perturbation of transit time.
T = Time at which an electron is emitted.
v, v_0, v_a = Electron velocity at general position, cathode and anode, respectively.
V_a = Anode-cathode potential difference.
x = Space variable.
x_a = Anode-cathode distance.
ρ = Charge density.
ω = Angular frequency.

(1) INTRODUCTION

Recent interest in stability problems of plasmas, together with he results of some numerical calculations of electron trajectories n a diode under non-steady conditions,* have led the author o a re-examination of a problem which concerns the stability of ı certain type of electron flow in a plane diode.

An exhaustive discussion of the types of steady flow in a plane liode under the assumption that the electrons are all emitted vith the same velocity has been given by Fay, Samuel and Shockley.† They give all possible solutions of their equations or all the various possible combinations of injection velocity, njection current density and cathode-anode potential. They show that for certain values of these parameters, a potential minimum is formed between the cathode and anode at a potential which is sufficiently high to allow a complete transmission of the injected current to the anode. This they called type C flow. It is found that over part of the range of parameters for which type C flow occurs, there is a further possible solution, which they call C-overlap flow, also having the type C characteristics but with a longer transit time, and a potential distribution which is everywhere lower than that of the corresponding type C flow. It is not possible by changing the various parameters slowly to obtain the C-overlap flow from any normal type of flow, although the corresponding normal type C flow can be set up. Mainly for this reason it was postulated that the C-overlap flow was unstable.

During the course of some numerical calculations on the non-steady behaviour of the plane diode,* the author set up the C-overlap solution as the initial state of the diode in order to follow its subsequent behaviour. If the state was stable, no change should have taken place when the injection velocity, injection current density and cathode-anode potential were kept fixed. However, it was found that there was a rapid change-over to the corresponding normal type C flow, which was established completely in 6 to 7 transit times.

It will now be demonstrated that the C-overlap flow is indeed unstable by carrying out an analysis of the flow when it is subjected to a small perturbation. In order that the perturbation analysis will be valid, the discussion is restricted to single-stream unidirectional flow, and so the possibility of electrons overtaking each other is excluded. These limitations are satisfied in both the C-overlap and the normal type C flow.

(2) THE PERTURBATION ANALYSIS

The result of taking the divergence of Maxwell's equation, curl $\boldsymbol{H} = \rho\boldsymbol{v} + \epsilon_0 \partial \boldsymbol{E}/\partial t$, is:

$$\text{div}\,(\rho\boldsymbol{v} + \epsilon_0 \partial \boldsymbol{E}/\partial t) = 0$$

which, in the one-dimensional case appertaining to the plane diode, becomes

$$\frac{\partial}{\partial x}\left(\rho v + \epsilon_0 \frac{\partial E}{\partial t}\right) = 0 \quad . \quad . \quad . \quad . \quad . \quad (1)$$

The equation div $\epsilon_0 \boldsymbol{E} = \rho$ becomes

$$\epsilon_0 \frac{\partial E}{\partial x} = \rho \quad . \quad . \quad . \quad . \quad . \quad . \quad . \quad (2)$$

Combining eqns. (1) and (2),

$$\frac{\partial}{\partial x}\left(\frac{\partial E}{\partial t} + v\frac{\partial E}{\partial x}\right) = 0$$

i.e.

$$\frac{\partial}{\partial x}\left(\frac{dE}{dt}\right) = 0 \quad . \quad . \quad . \quad . \quad . \quad . \quad (3)$$

and so dE/dt must be a function of t only. In the steady state $\partial E/\partial t = 0$, and so dE/dt is a constant, J_0, which is $1/\epsilon_0$ times the current density.

A periodic perturbation of the current density is introduced so that the first integral of eqn. (3) becomes

$$\frac{dE}{dt} = J_0 + J_1 \varepsilon^{j\omega t} \quad . \quad . \quad . \quad . \quad . \quad . \quad (4)$$

J_1 is a constant which is taken to be small compared with J_0, so that $(J_1/J_0)^2$ can be ignored.

In order to integrate eqn. (4), a change is made from the Eulerian variables (x, t) to new Lagrangian variables (t, T), where T is the time at which a particular electron is emitted from the

* LOMAX, R. J.: 'Transient and Steady-State Space-Charge Flow', Ph.D. Thesis, University of Cambridge, 1959.
† FAY, C. E., SAMUEL, A. L., and SHOCKLEY, W.: 'On the Theory of Space-Charge between Parallel Plane Electrodes', *Bell System Technical Journal,* 1938, 17, p. 49.

Correspondence on Monographs is invited for consideration with a view to publication.
Dr. Lomax is at Peterhouse, Cambridge.

cathode. The following relations exist between the new and old variables:

$$\left(\frac{\partial}{\partial T}\right)_t = \left(\frac{\partial x}{\partial T}\right)_t \frac{\partial}{\partial x} \quad . \quad . \quad . \quad . \quad . \quad (5)$$

$$\left(\frac{\partial}{\partial t}\right)_T = \left(\frac{\partial x}{\partial t}\right)_T \frac{\partial}{\partial x} + \left(\frac{\partial}{\partial t}\right)_x = \frac{d}{dt} \quad . \quad . \quad . \quad (6)$$

where the suffix denotes the variable which is held constant during the differentiation. Eqn. (6) implies that eqn. (4) can be written:

$$\left(\frac{\partial E}{\partial t}\right)_T = J_0 + J_1 \varepsilon^{j\omega t}$$

Defining the unit of mass so that the charge/mass ratio is unity, the equation of motion of an electron is

$$\frac{dv}{dt} = \left(\frac{\partial v}{\partial t}\right)_T = E$$

and so, since $v = (\partial x/\partial t)_T$, the equation for x is

$$\left(\frac{\partial^3 x}{\partial t^3}\right)_T = J_0 + J_1 \varepsilon^{j\omega t} \quad . \quad . \quad . \quad . \quad . \quad (7)$$

Integrating eqn. (7) three times with respect to t, and imposing the boundary condition that $v = v_0$ and $x = 0$ at the cathode, which is given by $t = T$,

$$x = \tfrac{1}{6}J_0(t-T)^3 + a_0(t-T)^2 + v_0(t-T) + a_1(t-T)^2 + J_1\omega^{-3}\varepsilon^{j\omega T}\{j[\varepsilon^{j\omega(t-T)} - 1] + \omega(t-T)\} \quad . \quad . \quad . \quad . \quad (8)$$

$a_0 + a_1$ is an arbitrary function of T, a_1 being the departure from the steady-state value, a_0, due to the perturbation. In the steady state, x must be a function of $t - T$ only, and so a_0 is in reality a constant, leaving only the first-order term a_1 dependent upon T.

The perturbation is made subject to keeping constant the injection velocity v_0, the injection current density J_0 and the cathode-anode potential; thus at the cathode it is required that

$$\rho v = \epsilon_0 v \frac{\partial E}{\partial x} = \epsilon_0 J_0 \quad . \quad . \quad . \quad . \quad . \quad (9)$$

From eqn. (5),

$$\frac{\partial E}{\partial x} = \frac{\partial E/\partial T}{\partial x/\partial T} = \frac{J_0 - 2(da_1/dT)}{v_0}$$

at $t = T$. In order to satisfy eqn. (9), it is necessary that $da_1/dT = 0$, and so a_1 is at most a constant.

If the anode potential with respect to the cathode is V_a and the velocity of the electrons on reaching the anode is v_a, in the steady state the energy equation requires that

$$v_a^2 = v_0^2 + 2V_a$$

and so if the steady-state electron transit time is denoted by t_0 and the cathode-anode spacing by x_a, it follows from eqn. (8), and its derivative with respect to t, that

$$x_a = \tfrac{1}{6}J_0 t_0^3 + a_0 t_0^2 + v_0 t_0 \quad . \quad . \quad . \quad . \quad (10)$$

$$(v_0^2 + 2V_a)^{1/2} = \tfrac{1}{2}J_0 t_0^2 + 2a_0 t_0 + v_0 \quad . \quad . \quad . \quad (11)$$

Eliminating a_0,

$$J_0 t_0^3 - 6[v_0 + (v_0^2 + 2V_a)^{1/2}]t_0 + 12x_a = 0 \quad . \quad (12)$$

Having found t_0 from eqn. (12), back-substitution into eqn. (10) or (11) will determine a_0.

The condition that the cathode-anode potential should be V_a in the perturbed state also must now be imposed. This is done by integrating the electric field from the cathode to the anode:

$$V_a \equiv \int_0^{x_a} E(t, T)dx$$

Since it has been postulated that the electrons do not overtake each other and that there is only a single stream, this integral may be written:

$$V_a \equiv \int_{x=0}^{x=x_a} E(t, T)\frac{\partial x}{\partial T}dT \equiv E_a x_a - \int_t^{t-t_0-t_1} x\frac{\partial E}{\partial T}dT \quad . \quad . \quad . \quad . \quad (13)$$

on integrating by parts. E_a is the value of E at the anode, and t_1, which is a function of t, is the modification to the transit time in the perturbed state. Substituting for x and $\partial E/\partial T$ in eqn. (13) and integrating,

$$V_a \equiv (J_0 x_a t_0 + 2x_a a_0 - \tfrac{1}{24}J_0^2 t_0^4 - \tfrac{1}{3}J_0 a_0 t_0^3 - \tfrac{1}{2}J_0 v_0 t_0^2) + t_1 J_0(x_a - \tfrac{1}{6}J_0 t_0^3 - a_0 t_0^2 - v_0 t_0) + a_1(2x_a - \tfrac{1}{3}J_0 t_0^3) + J_1\varepsilon^{j\omega t}[-j\omega^{-1}x_a - j\omega^{-3}t_0 J_0(1 + \varepsilon^{-j\omega t_0}) + 2\omega^{-4}J_0(1 - \varepsilon^{-j\omega t_0})] + \text{terms of higher order} \quad . \quad (14)$$

Examination of the zero-order term on the right-hand side of eqn. (14) with the use of eqns. (10) and (11) shows that it is identically equal to V_a on account of the use of the energy equation in deriving eqn. (11). If the energy equation had not been used, eqn. (11) could have been derived from the zero-order term of eqn. (14).

It will be seen from eqn. (10) that the coefficient of t_1 in eqn. (14) is zero: the two remaining first-order terms in a_1 and J_1 must vanish independently since the latter is a function of t whilst the former is not. Thus, provided that $x_a/J_0 t_0^3 \neq \tfrac{1}{3}$, then $a_1 = 0$ and

$$-j\omega^{-1}x_a - j\omega^{-3}t_0 J_0(1 + \varepsilon^{-j\omega t_0}) + 2\omega^{-4}J_0(1 - \varepsilon^{-j\omega t_0}) = 0 \quad . \quad . \quad . \quad . \quad (15)$$

By writing $j\omega t_0 = \beta$ and $x_a/J_0 t_0^3 = A$, eqn. (15) can be put in the simpler form:

$$(2 + \beta)\varepsilon^{-\beta} = 2 - \beta + A\beta^3 \quad . \quad . \quad . \quad (16)$$

This is the dispersion relation required to investigate the stability of the perturbation.

(3) INSTABILITY OF C-OVERLAP FLOW

The regime is unstable if the dispersion relation, eqn. (16), has a solution with $\mathscr{R}\beta > 0$, because such a value of β will lead to exponential growth of the perturbation.

Consider the functions $y = \varepsilon^{-x}(2 + x)$ and $y = 2 - x + Ax^3$. Near $x = 0$, the exponential function can be written

$$y = 2 - x + \tfrac{1}{6}x^3 + \mathrm{O}(x^4)$$

Thus, if $A < \frac{1}{6}$, the cubic is less than the exponential function in the region of small positive x, but eventually it must become greater than the exponential again, since it becomes infinite as x becomes infinite whilst the other function remains finite. There-

ıre the functions are equal for some positive value of x, and so ın. (16) possesses a real positive root.

Consider now eqn. (12) determining the transit time t_0. Since ıe sum of the roots of the equation is zero and their product negative, there must always be two positive roots when all ıe roots are real. It follows from the analysis of Fay, Samuel nd Shockley that the larger of these two positive roots repre- ents the C-overlap flow, and the smaller the normal type C ow. Let the roots of eqn. (12) be t_p, t_q and $-(t_p + t_q)$, with $> t_q > 0$. The product of the roots is

$$-12x_a/J_0 = -t_p t_q(t_p + t_q)$$

and since $t_p > t_q > 0$,

$$t_p t_q(t_p + t_q) < 2t_p^3$$

But t_p is the C-overlap transit time t_0, and so

$$x_a/J_0 t_0^3 = A < \tfrac{1}{6}$$

This is precisely the condition for eqn. (16) to have a real positive root and for the flow to be unstable.

Thus it has been shown that C-overlap flow is unstable to a small perturbation in which the values of the injection current, injection velocity and the cathode-anode potential are maintained constant.

621.372.6.012.8

The Institution of Electrical Engineers
Monograph No. 403
Oct. 19

A NEW APPROACH TO KRON'S METHOD OF ANALYSING LARGE SYSTEMS

By R. ONODERA.

(*The paper was first received* 15*th December* 1959, *and in revised form* 13*th June*, 1960. *It was published as an* INSTITUTION MONOGRAPH *in October*, 1960.)

SUMMARY

Generally an electrical network is used as a model circuit for a physical field. This circuit is most complicated and the analysis of it is frequently difficult. 'Diakoptics', introduced by Kron, is very effective for analysis of the network. The method entails the operation of 'cutting', which is generally classified into open-circuiting and short-circuiting. The latter operation is the dual of the former, but, as far as the author is aware, has not yet been reported in any of the literature. A method is described, based on Kron's diakoptics, which uses the operation of open-circuiting, and is further extended to dual diakoptics treated by the operation of short-circuiting. Here a simplification of Kron's diakoptics is attempted and a dual method is introduced. It seems that this attempt goes backwards in tensor geometry, but forward in combinatorial topology. The first intention of the paper is to show the duality between diakoptics and codiakoptics.

LIST OF SYMBOLS

$\boldsymbol{D}$ = Node-branch incidence matrix.
$\boldsymbol{R}$ = Mesh-branch incidence matrix.
$\boldsymbol{I}$ = Branch currents.
$\boldsymbol{U}$ = Voltage drops in passive elements.
$\boldsymbol{S}$ = Branch current sources.
$\boldsymbol{E}$ = Branch voltage sources (branch e.m.f.'s).
$\tilde{\boldsymbol{S}} = \boldsymbol{DS}$ = Node current sources.*
$\tilde{\boldsymbol{E}} = \boldsymbol{RE}$ = Mesh voltage sources (mesh e.m.f.'s).
$\boldsymbol{V}$ = Node potentials.
$\boldsymbol{J}$ = Mesh currents.
$\tilde{\boldsymbol{I}} = \boldsymbol{I} - \boldsymbol{S} = \boldsymbol{R'J}$ = Rotational currents (current difference).
$\tilde{\boldsymbol{U}} = \boldsymbol{U} - \boldsymbol{E} = \boldsymbol{D'V}$ = Terminal voltage drops (branch potential differences, branch p.d.'s).
$\boldsymbol{Y}$ = Branch admittances.
$\boldsymbol{Z}$ = Branch impedances.
$\tilde{\boldsymbol{Y}}$ = Node admittances.
$\tilde{\boldsymbol{Z}}$ = Mesh impedance.

(1) INTRODUCTION

'Diakoptics', introduced by Kron[1–4], is very effective for the analysis of large and complicated systems. Quite recently, simplified diakoptics for electrical networks of special connection has been introduced by Wengert[5] and Heyda.[12] Their methods generally are reducible to the following four steps:

(*a*) To split the given network into sub-networks.
(*b*) To solve the problems of the above sub-networks and make sub-networks equivalent to them.
(*c*) To make a network equivalent to the given network by joining the above equivalent sub-networks.
(*d*) To analyse the given problem by analysis of the equivalent network.

* A node current source is positive if it flows into the node and negative if it flows from it.

Correspondence on Monographs is invited for consideration with a view to publication.
Mr. Onodera is at Yamagata University, Yonezawa, Japan.

Step (*a*) entails the operation of 'cutting', and the cutting is generally classified into open-circuiting and short-circuiting. The latter operation has not yet been used in any of the literature. In step (*b*), several equivalent sub-networks are also introduced which are classified into the node type and the mesh type. Step (*c*) entails the operation of interconnecting which is classified into connecting and joining, these being the inverse operations of open-circuiting and short-circuiting in step (*a*). Lastly, in step (*a*), node potentials or mesh currents are treated as unknown quantities with regard to the equivalent networks. A method which is a simplification of Kron's diakoptics, will be treated in the following Sections, and it will be further extended to the branch of codiakoptics, namely 'dual diakoptics', studied by the above considerations. The first intention of the paper is to show the duality between diakoptics and codiakoptics.

(2) PRELIMINARIES

(2.1) Notations[10]

(*a*) Names of elements of a network are shown as follows:

Branches (1-cells, 1-simplex): 1, 2, . . . n.
Independent nodes (0-cells, 0-simplex): 1′, 2′ . . . m'.
Independent meshes (1-cycle): 1″, 2″, . . . k''.

Where it is necessary to distinguish between the elements of the equivalent network and those of the given network, the notation $\underline{1}$, $\underline{\underline{1}}$, etc., will be used.

(*b*) The node-branch incidence matrix* (1-incidence matrix) is denoted by $\boldsymbol{D}$, where rows dependent on the other are omitted. The mesh-branch incidence matrix (cycle incidence matrix and frequently 2-incidence matrix) is denoted by $\boldsymbol{R}$. The symbols $\boldsymbol{D}$ and $\boldsymbol{R}$ correspond to divergence and rotation in a vector field. For example, in the network of Fig. 1,

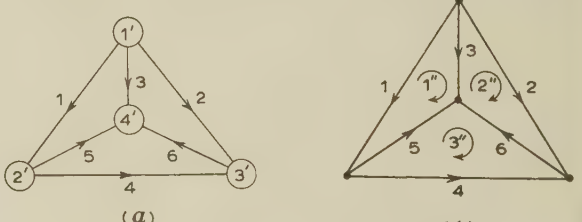

Fig. 1.—Node-branch (*a*) and mesh-branch (*b*) incidence relations

$$\boldsymbol{D} = \begin{array}{c} \\ 1' \\ 2' \\ 3' \end{array} \begin{array}{c} \begin{array}{cccccc} 1 & 2 & 3 & 4 & 5 & 6 \end{array} \\ \begin{bmatrix} 1 & 1 & 1 & 0 & 0 & 0 \\ -1 & 0 & 0 & 1 & 1 & 0 \\ 0 & -1 & 0 & -1 & 0 & 1 \end{bmatrix} \end{array}$$

$$\boldsymbol{R} = \begin{array}{c} \\ 1'' \\ 2'' \\ 3'' \end{array} \begin{array}{c} \begin{array}{cccccc} 1 & 2 & 3 & 4 & 5 & 6 \end{array} \\ \begin{bmatrix} -1 & 0 & 1 & 0 & -1 & 0 \\ 0 & 1 & -1 & 0 & 0 & 1 \\ 0 & 0 & 0 & -1 & 1 & -1 \end{bmatrix} \end{array}$$

* The element is +1 for the outer-oriented branch from a point, and is −1 for the inner oriented one from a point.

he well-known topological relation

$$DR' = 0 \text{ or } RD' = 0$$

rves as a useful check when D and R are written down by spection.

(*c*) Denoting the branch-admittance matrix and the branch-ipedance matrix by Y and Z respectively, the node-admittance atrix $\tilde{Y}$ and the mesh-impedance matrix $\tilde{Z}$ are [see eqns. (13*a*) id (13*b*)]

$$\tilde{Y} = DYD' \text{ and } \tilde{Z} = RZR'$$

(*d*) The fundamental equations of an electrical network are enoted by

1st Kirchhoff law:	$DI = \tilde{S}$	. . . .	(1*a*)
2nd Kirchhoff law:	$RU = \tilde{E}$	. . . .	(1*b*)
Ohm's law:	$I = YU$	. . . .	(2*a*)
or	$U = ZI$	. . . .	(2*b*)
here	$\tilde{S} = DS$	. . . .	(3*a*)
	$\tilde{E} = RE$	. . . .	(3*b*)

ee Figs. 2 and 3.)

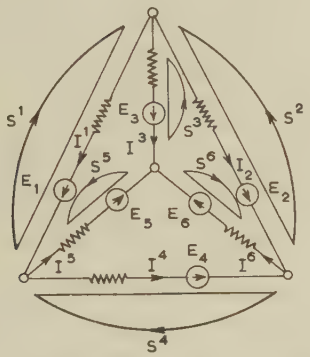

Fig. 2.—Branch current and voltage sources.

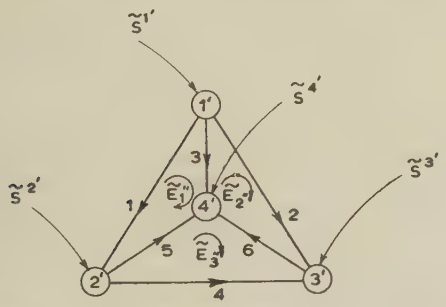

Fig. 3.—Node current and mesh voltage sources.

(*e*) Defining rotational branch currents (current differences) as

$$\tilde{I} = I - S \quad . . . . . \quad (4a)$$

nd terminal voltage-drops (voltage differences, potential dif-erences) as

$$\tilde{U} = U - E \quad . . . . . \quad (4b)$$

uch as in Fig. 4, we have the following relations from eqns. (1), 3) and (4):

$$D\tilde{I} = 0 \quad . . . . . \quad (5a)$$
$$R\tilde{U} = 0 \quad . . . . . \quad (5b)$$
$$\tilde{I} = R'J \quad . . . . . \quad (6a)$$
$$\tilde{U} = D'V \quad . . . . . \quad (6b)$$

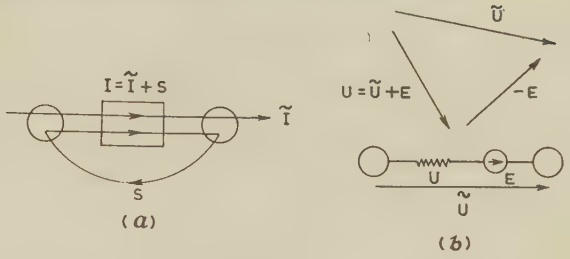

Fig. 4.—Current (*a*) and voltage (*b*) components.

(2.2) Ordinary Methods of Solving[6,10]

The method taking node potentials as the unknown quantities is shown as follows:

$$\tilde{S} = DI = DYU = DY(\tilde{U} + E) \text{ from eqns. (1}a\text{), (2}a\text{) and 4}b\text{)}$$
$$= DY(D'V + E) = DYD'V + DYE \text{ from eqn. (6}b\text{)}$$

namely $$DYD'V = \tilde{S} - DYE$$

Therefore $$V = (DYD')^{-1}(\tilde{S} - DYE) \quad . . . . . \quad (7a)$$

If we determine V by eqn. (7*a*), we can determine the other quantities by eqns. (6*b*), (4*b*) and (2*a*), etc.

If mesh currents are taken as unknown quantities, the dual method is given by

$$\tilde{E} = RU = RZI = RZ(\tilde{I} + S) \text{ from eqns. (1}b\text{), (2}b\text{) and (4}b\text{)}$$
$$= RZ(R'J + S) = RZR'J + RZS \text{ from eqn. (6}a\text{)}$$

Therefore $$RZR'J = \tilde{E} - RZS$$

and $$J = (RZR')^{-1}(\tilde{E} - RZS) \quad . . . . \quad (7b)$$

If we determine J by eqn. (7*b*), we can determine the other quantities by eqns. (6*a*), (4*a*) and (2*b*), etc.

(3) CUTTING THEORY OF NETWORKS

(3.1) Cycles and Co-cycles[7,10,11]

Postulating that the given network is connected, 'the zeroth Betti[7] number' (i.e. the number of unconnected parts of the network[11]) p^0 is equal to one. This network is ordinarily a 1-complex, but if need be, it may be regarded as a 2-complex connected to the given 1-complex, the surface boundaries of which are meshes in the given network. ∂ and δ are symbols for 'boundary' and 'co-boundary' of the complex, respectively. Addition operator[7] is used as mod. 2. 0 denotes the zero set. $\cap$ and $\cup$ denote the 'meet' and 'join' of sets, respectively.

In Fig. 5(*a*), taking boundaries of branches,

$$\partial 1 = 1' + 2'$$
$$\partial(1 + 2) = 2' + 3'$$

and $$\partial(2 + 3 + 6) = 0$$

A '1-cycle' is a set of branches the boundary of which is zero. For example, a closed line such as a set of branches (2 + 3 + 6) is a 1-cycle. Taking co-boundaries of sets of nodes in Fig. 5(*b*),

$$\delta 1' = 1 + 2 + 3 + 19$$
$$\delta(1' + 2') = 2 + 3 + 4 + 5 + 19 + 21$$

and $$\delta(1' + 2' + \ldots + 12') = 0$$

A set of nodes the co-boundary of which is zero is called a '0-cycle', such as the above set of nodes $(1' + 2' + \ldots + 12')$. A 0-cycle is a set of nodes which has no branch connected to nodes of other sets.

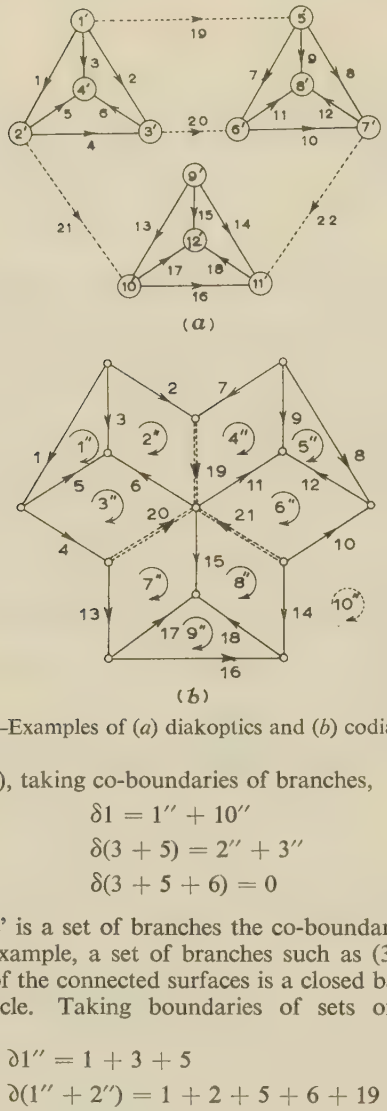

Fig. 5.—Examples of (*a*) diakoptics and (*b*) codiakoptics.

In Fig. 5(*b*), taking co-boundaries of branches,

$$\delta 1 = 1'' + 10''$$

$$\delta(3 + 5) = 2'' + 3''$$

and $$\delta(3 + 5 + 6) = 0$$

A '1-co-cycle' is a set of branches the co-boundary of which is zero. For example, a set of branches such as $(3 + 5 + 6)$ of which a set of the connected surfaces is a closed band or a cone is a 1-co-cycle. Taking boundaries of sets of surfaces in Fig. 5(*b*),

$$\partial 1'' = 1 + 3 + 5$$

$$\partial(1'' + 2'') = 1 + 2 + 5 + 6 + 19$$

find $$\partial(1'' + 2'' + \ldots + 9'' + 10'') = 0$$

A set of surfaces the boundary of which is zero is called a '2-cycle', such as the above set of surfaces $(1'' + 2'' + \ldots + 10'')$. A closed surface is a 2-cycle.

(3.2) Cut Set[8, 9]

The co-boundary of a subset of nodes is a set of branches connected to the other subsets of nodes, and if we open-circuit all the branches in this co-boundary, this subset becomes disconnected from the other subsets. Therefore in Fig. 5(*a*), in order to cut the given network into three subnetworks, namely $(1' + 2' + 3' + 4')$, $(5' + 6' + 7' + 8')$ and $(9' + 10' + 11' + 12')$, we may cut the following branches by the operation of open-circuit:

$$\delta(1' + 2' + 3' + 4') \cup \delta(5' + 6' + 7' + 8') \cup \delta(9' + 10' + 11' + 12')$$
$$= (19 + 20 + 21) \cup (19 + 20 + 22) \cup (21 + 22)$$
$$= 19 + 20 + 21 + 22 \quad . \quad . \quad . \quad . \quad . \quad . \quad . \quad . \quad . \quad . \quad . \quad (8a)$$

The branches of a set cutting the given network into several subnetworks by open-circuit operations are called 'tie branches', and these disconnected subnetworks are called 'subnetworks of node type'. $(19 + 20 + 21 + 22)$ in Fig. 5(*a*) are tie branches.

A set of branches which is a set of all the branches in th co-boundary of a subset of nodes is called a 'cut set'. F example, $(19 + 20 + 21)$, $(19 + 20 + 22)$ and $(21 + 22)$ are c sets, respectively.

The boundary of a subset of surfaces may be a set of all th branches connected to the other sets with regard to a plan network. But generally it is not. For example, in the plan network, the meshes can be chosen so that the arbitrary branc is connected to two meshes, in which case the sum of th boundaries of the meshes, being a set of the arbitrary ones, is set of branches connected to the other sets. In Fig. 5(*b*), if w wish to cut the given network into $1'' + 2'' + 3''$, $4'' +$ $+ 6''$ and $7'' + 8'' + 9''$, we may short-circuit the following s of branches, where the surface $10''$ may be removed as it depen on the others:

$$[(\partial 1'' \cup \partial 2'' \cup \partial 3'') \cap (\partial 4'' \cup \partial 5'' \cup \partial 6'')]$$
$$\cup [(\partial 4'' \cup \partial 5'' \cup \partial 6'') \cap (\partial 7'' \cup \partial 8'' \cup \partial 9'')]$$
$$\cup [(\partial 7'' \cup \partial 8'' \cup \partial 9'') \cap (\partial 1'' \cup \partial 2'' \cup \partial 3'')]$$
$$= 19 \cup 21 \cup 20$$
$$= 19 + 20 + 21 \quad . \quad . \quad . \quad . \quad . \quad . \quad . \quad . \quad . \quad . \quad . \quad . \quad (8$$

The branches of a set cutting the given network into several s networks by short-circuit operations are called 'co-tie branche and these separated subnetworks are called 'subnetworks mesh type'. $(19 + 20 + 21)$ in Fig. 5(*b*) are co-tie branch If the given network is planar, a set of all the branches in t boundary of a subset of meshes is called a 'co-cut set'. F example, $(1 + 2 + 4 + 19 + 20)$, $(7 + 8 + 10 + 19 + 21)$ a $(13 + 14 + 16 + 20 + 21)$ are co-cut sets. When all t branches in a bounding 1-cycle are short-circuited, a new 2-cyc are made and a maximal set of independent meshes is reduced number, but in this case the number of surfaces is invariant.

(4) DIAKOPTICS AND CODIAKOPTICS

(4.1) Diakoptics

First, as an example, we shall consider the network of Fig. 5 and show a simplified version of Kron's method.

(*a*) The open-circuiting branches $(19 + 20 + 21 + 22)$ ha subnetworks I, II and III such as in Fig. 6(*a*). Here we c these 'tie branches', and the subnetworks 'subnetworks of no type'.

(*b*) We make star connections equivalent to the origi subnetworks. For example, I, II and III in Fig. 7(*a*) are equiv lent to I, II and III in Fig. 6(*a*). The former are 'subnetwor of node type structurally equivalent' to the latter. If nc admittances in structurally equivalent subnetworks are equal those in the original subnetworks, the former are called 'el trically equivalent subnetworks of node type'. These relatic are shown as matrix expression as follows:

$$\underline{\tilde{Y}_\alpha} = \tilde{Y}_\alpha \quad . \quad . \quad . \quad . \quad . \quad . \quad . \quad (9$$

To satisfy the above relation, we put the branch-admittan matrix $\underline{Y_\alpha}$ of the equivalent subnetwork α equal to the no admittance matrix of the original subnetwork α, because node-branch incidence matrix of each equivalent subnetwork a unit matrix and hence its node-admittance matrix equals branch-admittance matrix, i.e.

$$\underline{Y_\alpha} = \underline{\tilde{Y}_\alpha} \quad . \quad . \quad . \quad . \quad . \quad . \quad . \quad (10$$

and then by eqn. (9*a*)

$$\underline{Y_\alpha} = \tilde{Y}_\alpha \quad . \quad . \quad . \quad . \quad . \quad . \quad . \quad (11$$

where, if we denote the node-branch incidence matrix of original α by $\boldsymbol{D}_\alpha$, and its branch-admittance matrix by $\boldsymbol{Y}_\alpha$,

$$\tilde{Y}_\alpha = \boldsymbol{D}_\alpha \boldsymbol{Y}_\alpha \boldsymbol{D}_\alpha' \quad . \quad . \quad . \quad . \quad . \quad (11$$

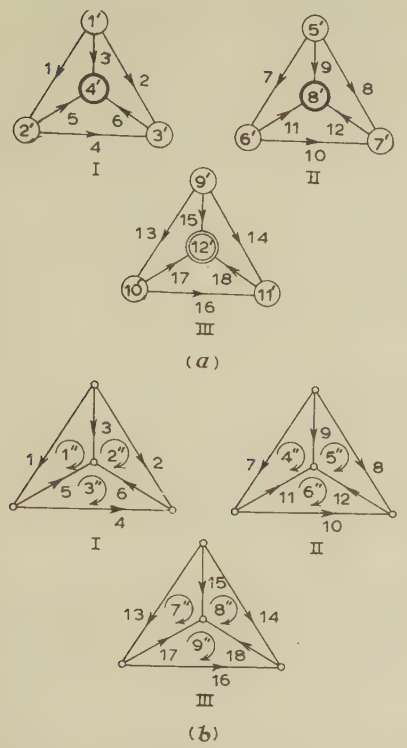

Fig. 6.—Subnetworks of (*a*) node type and (*b*) mesh type.

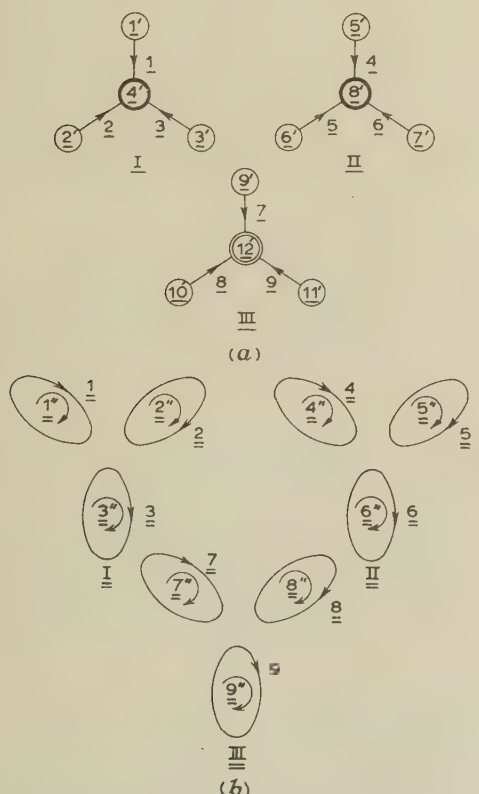

Fig. 7.—Equivalent subnetworks of (*a*) node type and (*b*) mesh type.

For example, if the admittance of each branch element equals 1 mho in the subnetwork $\alpha = 1$ in Fig. 6(*a*), the node-admittance matrix $\tilde{Y}_1$ is given by

$$\tilde{Y}_1 = \begin{array}{c} \\ 1' \\ 2' \\ 3' \end{array} \begin{bmatrix} 1 & 1 & 1 & 0 & 0 & 0 \\ -1 & 0 & 0 & 1 & 1 & 0 \\ 0 & -1 & 0 & -1 & 0 & 1 \end{bmatrix} \begin{array}{c} \\ 1 \\ 2 \\ 3 \\ 4 \\ 5 \\ 6 \end{array} \begin{bmatrix} 1 & 0 & 0 & 0 & 0 & 0 \\ 0 & 1 & 0 & 0 & 0 & 0 \\ 0 & 0 & 1 & 0 & 0 & 0 \\ 0 & 0 & 0 & 1 & 0 & 0 \\ 0 & 0 & 0 & 0 & 1 & 0 \\ 0 & 0 & 0 & 0 & 0 & 1 \end{bmatrix} \begin{array}{c} 1' \quad 2' \quad 3' \\ \\ \\ \\ \\ \\ \end{array} \begin{bmatrix} 1 & -1 & 0 \\ 1 & 0 & -1 \\ 1 & 0 & 0 \\ 0 & 1 & -1 \\ 0 & 1 & 0 \\ 0 & 0 & 1 \end{bmatrix}$$

$$= \begin{array}{c} \\ 1' \\ 2' \\ 3' \end{array} \begin{array}{c} 1' \quad 2' \quad 3' \\ \begin{bmatrix} 3 & -1 & -1 \\ -1 & 3 & -1 \\ -1 & -1 & 3 \end{bmatrix} \end{array} \quad . \quad . \quad . \quad . \quad . \quad . \quad . \quad . \quad . \quad . \quad . \quad (13a)$$

$$\text{Therefore} \qquad \underline{Y}_1 = \begin{array}{c} \\ \underline{1} \\ \underline{2} \\ \underline{3} \end{array} \begin{array}{c} \underline{1} \quad \underline{2} \quad \underline{3} \\ \begin{bmatrix} 3 & -1 & -1 \\ -1 & 3 & -1 \\ -1 & -1 & 3 \end{bmatrix} \end{array} \quad . \quad . \quad . \quad . \quad . \quad . \quad (14a)$$

(*c*) Connecting equivalent subnetworks together by tie branches, we have the equivalent network shown in Fig. 8(*a*). Next, since $\underline{Y}_{II} = \underline{Y}_{III} = \underline{Y}_I$, we have

$$\underline{Y}_I = \underline{Y}_{II} = \underline{Y}_{III} = \begin{bmatrix} 3 & -1 & -1 \\ -1 & 3 & -1 \\ -1 & -1 & 3 \end{bmatrix} \quad . \quad . \quad (15a)$$

and then

$$\underline{Z}_I = \underline{Z}_{II} = \underline{Z}_{III} = \begin{bmatrix} 3 & -1 & -1 \\ -1 & 3 & -1 \\ -1 & -1 & 3 \end{bmatrix}^{-1} = \frac{1}{4}\begin{bmatrix} 2 & 1 & 1 \\ 1 & 2 & 1 \\ 1 & 1 & 2 \end{bmatrix} \quad . \quad (16a)$$

Hence the branch-impedance matrix of the equivalent network is

$$\underline{Z} = \frac{1}{4} \begin{array}{c} \\ \underline{1} \\ \underline{2} \\ . \\ . \\ . \\ . \\ . \\ . \\ . \\ . \\ . \\ \underline{13} \end{array} \begin{array}{c} \underline{1}\ \underline{2}\ . . . . . \underline{13} \\ \begin{bmatrix} 2 & 1 & 1 & 0 & . & . & . & . & . & . & . & . & 0 \\ 1 & 2 & 1 & 0 & . & . & . & . & . & . & . & . & 0 \\ 1 & 1 & 2 & 0 & . & . & . & . & . & . & . & . & 0 \\ 0 & 0 & 0 & 2 & 1 & 1 & 0 & . & . & . & . & . & 0 \\ 0 & 0 & 0 & 1 & 2 & 1 & 0 & . & . & . & . & . & 0 \\ 0 & 0 & 0 & 1 & 1 & 2 & 0 & . & . & . & . & . & 0 \\ 0 & . & . & . & . & 0 & 2 & 1 & 1 & 0 & . & . & 0 \\ 0 & . & . & . & . & 0 & 1 & 2 & 1 & 0 & . & . & 0 \\ 0 & . & . & . & . & 0 & 1 & 1 & 2 & 0 & . & . & 0 \\ 0 & . & . & . & . & . & . & . & 0 & 4 & 0 & 0 & 0 \\ 0 & . & . & . & . & . & . & . & 0 & 4 & 0 & 0 & 0 \\ 0 & . & . & . & . & . & . & . & . & 0 & 4 & 0 & 0 \\ 0 & . & . & . & . & . & . & . & . & . & 0 & 4 & 0 \\ 0 & . & . & . & . & . & . & . & . & . & . & 0 & 4 \end{bmatrix} \end{array} \quad . \quad (17a)$$

In the equivalent network, it is postulated that there are only equivalent node current sources $\underline{\tilde{S}}$ and no branch voltage sources $\underline{E}$. Therefore, denoting node current sources by $\tilde{S}$ and branch voltage sources by E in the given network, it must hold that

$$\underline{\tilde{S}} = \tilde{S} - DYE \quad . \quad . \quad . \quad . \quad . \quad (18a)$$

and

$$\underline{E} = 0 \quad . \quad . \quad . \quad . \quad . \quad . \quad . \quad . \quad . \quad (19a)$$

Since, from Section 2.2,

$\tilde{Y}V = \tilde{S} - DYE$ in the given network

$\underline{\tilde{Y}}\,\underline{V} = \underline{\tilde{S}}$ in the equivalent network

and from eqn. (9*a*) $\tilde{Y} = \underline{\tilde{Y}}$

by the definition of equivalence $V = \underline{V}$

For example, if each of the self-conductances is equal to 1 mho and if

$$\tilde{S} = [1\ 1\ -1\ 1\ -1\ 0\ 1\ 0\ 1\ -1\ 0\ -2]' \text{ amperes} \quad (20a)$$

$$E = [1\ 1\ 0\ 0\ 1\ 0 \ldots 10 \ldots 1\ 0 \ldots 0]' \text{ volts} \quad (21a)$$

[see Fig. 9(*a*)] then, since [See col. 2]

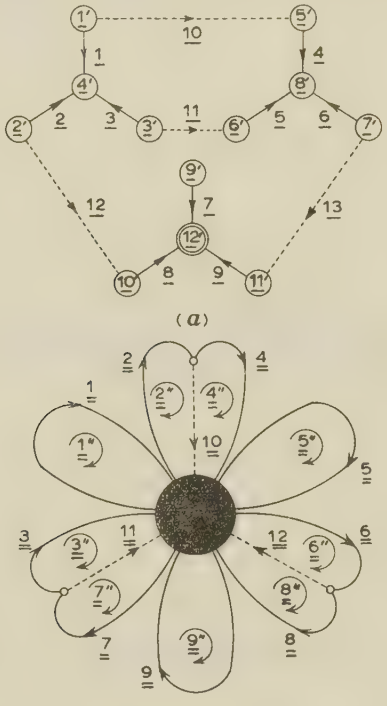

Fig. 8.—Equivalent networks of (*a*) node type and (*b*) mesh type.

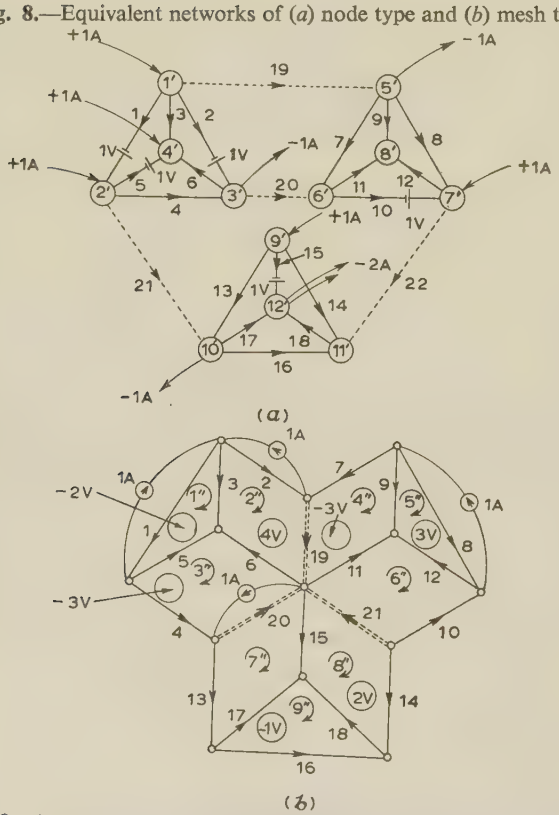

Fig. 9.—Equivalent sources in the equivalent networks of (*a*) node type and (*b*) mesh type.

$$-DYE = \begin{bmatrix} 1' \\ 2' \\ \vdots \\ 11' \end{bmatrix} \begin{bmatrix} 1 & 2 & \cdots & 22 \\ 1 & 1 & \cdots & 0 \\ -1 & 0 & \cdots & 0 \\ 0 & -1 & \cdots & 0 \\ 0 & 0 & \cdots & 0 \\ 1 & -1 & \cdots & 0 \\ 0 & 1 & \cdots & 0 \\ 0 & 0 & \cdots & 0 \\ 1 & 0 & \cdots & 0 \\ -1 & 0 & \cdots & 0 \\ 0 & 0 & \cdots & 0 \end{bmatrix} \begin{bmatrix} 1 & 2 & \cdots & 22 \\ 1 & 0 & \cdots & 0 \\ 0 & 1 & \cdots & 0 \end{bmatrix} \begin{bmatrix} 1 \\ 2 \\ \vdots \\ 22 \end{bmatrix} \begin{bmatrix} 1 & 2 & \cdots & 22 \\ 1 & 0 & \cdots & 0 \\ 0 & 1 & \cdots & 0 \\ 0 & 0 & \cdots & 0 \\ 1 & 0 & \cdots & 0 \\ 0 & 1 & \cdots & 0 \\ 0 & 0 & \cdots & 0 \\ 1 & 0 & \cdots & 0 \\ 0 & 1 & \cdots & 0 \\ 0 & 0 & \cdots & 0 \\ 0 & 0 & \cdots & 1 \end{bmatrix} \begin{bmatrix} 1 \\ 2 \\ \vdots \\ 22 \end{bmatrix}$$

$$= \begin{bmatrix} 1' & 2' & \cdots & 11'' \\ 2 & 0 & \cdots & 0 \\ -1 & -1 & \cdots & 0 \\ -1 & 0 & \cdots & 1 \\ 0 & 1 & \cdots & 0 \\ 0 & 0 & \cdots & 0 \end{bmatrix}' \quad (22a)$$

$$\underline{\tilde{S}} = \tilde{S} - DYE = \begin{bmatrix} 1 \\ 1 \\ -1 \\ 1 \\ -1 \\ 0 \\ 1 \\ 0 \\ 1 \\ -1 \\ 0 \end{bmatrix} - \begin{bmatrix} 2 \\ 0 \\ -1 \\ -1 \\ 0 \\ 1 \\ -1 \\ 0 \\ 1 \\ 0 \\ 0 \end{bmatrix} = \begin{bmatrix} -1 \\ 1 \\ 0 \\ 2 \\ -1 \\ -1 \\ 2 \\ 0 \\ 0 \\ -1 \\ 0 \end{bmatrix} \begin{matrix} 1' \\ 2' \\ . \\ . \\ . \\ . \\ . \\ . \\ . \\ . \\ 11' \end{matrix} \quad . \quad . \quad (23a)$$

and then, by eqn. (9*b*),

$$\underline{\underline{Z_\beta}} = \underline{\underline{\tilde{Z}_\beta}} \quad . \quad . \quad . \quad . \quad . \quad . \quad . \quad (11b)$$

where, if we denote the mesh-branch incidence matrix of the original β by R_β, and its branch-impedance matrix by Z_β,

$$\tilde{Z}_\beta = R_\beta Z_\beta R'_\beta \quad . \quad . \quad . \quad . \quad . \quad . \quad (12b)$$

For example, if the impedance of each branch element equals 1 ohm in the subnetwork $\beta = 1$ in Fig. 6(*b*), the mesh-impedance matrix $\tilde{Z}_I$ is determined as

$$\tilde{Z}_1 = \begin{matrix} 1'' \\ 2'' \\ 3'' \end{matrix} \begin{bmatrix} -1 & 0 & 1 & 0 & -1 & 0 \\ 0 & 1 & -1 & 0 & 0 & 1 \\ 0 & 0 & 0 & -1 & 1 & -1 \end{bmatrix} \begin{matrix} 1 \\ 2 \\ 3 \\ 3 \\ 5 \\ 6 \end{matrix} \begin{bmatrix} 1 & 2 & 3 & 4 & 5 & 6 \\ 1 & 0 & 0 & 0 & 0 & 0 \\ 0 & 1 & 0 & 0 & 0 & 0 \\ 0 & 0 & 1 & 0 & 0 & 0 \\ 0 & 0 & 0 & 1 & 0 & 0 \\ 0 & 0 & 0 & 0 & 1 & 0 \\ 0 & 0 & 0 & 0 & 0 & 1 \end{bmatrix} \begin{bmatrix} 1'' & 2'' & 3'' \\ -1 & 0 & 0 \\ 0 & 1 & 0 \\ 1 & -1 & 0 \\ 1 & 0 & -1 \\ -1 & 0 & 1 \\ 0 & 1 & -1 \end{bmatrix} = \begin{matrix} 1'' \\ 2'' \\ 3'' \end{matrix} \begin{bmatrix} 1'' & 2'' & 3'' \\ 3 & -1 & -1 \\ -1 & 3 & -1 \\ -1 & -1 & 3 \end{bmatrix} \quad . \quad . \quad . \quad (13b)$$

(*d*) Finally we may analyse the given networks by examining the equivalent networks of Fig. 8(*a*). This equivalent network of node type has the same number of nodes as, but less meshes than the given network. Therefore it is convenient to put the mesh currents $\underline{J}$ as unknown quantities. This method of solution has been shown in eqn. (7*b*), i.e.

$$\underline{J} = (\underline{R}\underline{Z}\underline{R})^{-1}(-\underline{R}\underline{Z}\underline{S})$$

since $\underline{\tilde{E}} = \underline{R}\underline{E} = 0$) where $\underline{S}$ is any set of branch current sources satisfying $\underline{D}\underline{S} = \underline{\tilde{S}}$, and where $\underline{R}$ and $\underline{D}$ are found by inspection from Fig. 8(*a*). After the mesh currents $\underline{J}$ have been determined, the node potentials $\underline{V}$ can be found, and these are equal to V in the given network. If V is known, the other quantities such as $\tilde{U}$, U and I can easily be determined.

Therefore

$$\underline{\underline{Z_1}} = \begin{matrix} 1 \\ 2 \\ 3 \end{matrix} \begin{bmatrix} 1 & 2 & 3 \\ 3 & -1 & -1 \\ -1 & 3 & -1 \\ -1 & -1 & 3 \end{bmatrix} \quad . \quad . \quad . \quad . \quad (14b)$$

(*c*) Joining equivalent subnetworks together by co-tie branches, we have the equivalent network shown in Fig. 8. Next, since $\underline{\underline{Z_{II}}} = \underline{\underline{Z_{III}}} = \underline{\underline{Z_I}}$ we have

$$\underline{\underline{Z_I}} = \underline{\underline{Z_{II}}} = \underline{\underline{Z_{III}}} = \begin{bmatrix} 3 & -1 & -1 \\ -1 & 3 & -1 \\ -1 & -1 & 3 \end{bmatrix} \quad . \quad . \quad (15b)$$

and then

$$\underline{\underline{Y_I}} = \underline{\underline{Y_{II}}} = \underline{\underline{Y_{III}}} = \tfrac{1}{4}\begin{bmatrix} 2 & 1 & 1 \\ 1 & 2 & 1 \\ 1 & 1 & 2 \end{bmatrix} \quad . \quad . \quad . \quad . \quad (16b)$$

Hence the branch-admittance matrix of the equivalent network is

$$\underline{\underline{Y}} = \tfrac{1}{4} \begin{matrix} 1 \\ 2 \\ . \\ . \\ . \\ . \\ . \\ . \\ . \\ . \\ . \\ 12 \end{matrix} \begin{bmatrix} 1 & 2 & . & . & . & . & . & . & . & . & . & 12 \\ 2 & 1 & 1 & 0 & . & . & . & . & . & . & . & 0 \\ 1 & 2 & 1 & 0 & . & . & . & . & . & . & . & 0 \\ 1 & 1 & 2 & 0 & . & . & . & . & . & . & . & 0 \\ 0 & 0 & 0 & 2 & 1 & 1 & 0 & . & . & . & . & 0 \\ 0 & 0 & 0 & 1 & 2 & 1 & 0 & . & . & . & . & 0 \\ 0 & 0 & 0 & 1 & 1 & 2 & 0 & . & . & . & . & 0 \\ 0 & . & . & . & . & 0 & 2 & 1 & 1 & 0 & 0 & 0 \\ 0 & . & . & . & . & 0 & 1 & 2 & 1 & 0 & 0 & 0 \\ 0 & . & . & . & . & 0 & 1 & 1 & 2 & 0 & 0 & 0 \\ 0 & . & . & . & . & . & . & . & 0 & 4 & 0 & 0 \\ 0 & . & . & . & . & . & . & . & . & 0 & 4 & 0 \\ 0 & . & . & . & . & . & . & . & . & . & 0 & 4 \end{bmatrix} \quad (17b)$$

In the equivalent network, it is postulated that there are only equivalent mesh voltage sources $\underline{\underline{\tilde{E}}}$ and no branch current sources $\underline{\underline{E}}$. Therefore, denoting mesh voltage sources by $\tilde{E}$ and branch current sources by S in the given network, it must hold that

$$\underline{\underline{\tilde{E}}} = \tilde{E} - RZS \quad . \quad . \quad . \quad . \quad . \quad (18b)$$

and

$$\underline{\underline{S}} = 0 \quad . \quad . \quad . \quad . \quad . \quad . \quad . \quad . \quad (19b)$$

(4.2) Codiakoptics

Fig. 5(*b*) shows the dual method of Kron's diakoptics. This is termed 'dual diakoptics' or 'codiakoptics'.

(*a*) The short-circuiting branches (19 + 20 + 21) have subnetworks I, II and III as in Fig. 6(*b*). Here we call these 'co-tie branches', and these subnetworks 'subnetworks of node type'.

(*b*) We make sets of meshes equivalent to those in the above subnetworks. For example, $\underline{\underline{\text{I}}}$, $\underline{\underline{\text{II}}}$ and $\underline{\underline{\text{III}}}$ in Fig. 7(*b*) are equivalent to I, II and III in Fig. 6(*b*). The former are 'subnetworks of mesh type structurally equivalent' to the latter. If mesh impedances in structurally equivalent subnetworks are equal to those in the original subnetworks, the former are called 'electrically equivalent subnetworks of mesh type'. These relations are shown as matrix expression as follows:

$$\underline{\underline{\tilde{Z}_\beta}} = \underline{\underline{\tilde{Z}_\beta}} \quad . \quad . \quad . \quad . \quad . \quad . \quad . \quad (9b)$$

To satisfy the above relation, we put the branch-impedance matrix $\underline{\underline{Z_\beta}}$ of the equivalent subnetwork $\underline{\underline{\beta}}$ equal to the mesh-impedance matrix of the original β, because the mesh-branch incidence matrix of each equivalent subnetwork is a unit matrix and hence its mesh-impedance matrix equals its branch-impedance matrix, i.e.

$$\underline{\underline{Z_\beta}} = \underline{\underline{\tilde{Z}_\beta}} \quad . \quad . \quad . \quad . \quad . \quad . \quad . \quad (10b)$$

Since, from Section 2.2,

$$\tilde{Z}J = \tilde{E} - RZE \quad \text{in the given network}$$

$$\underset{=}{\tilde{Z}}\underset{=}{J} = \underset{=}{\tilde{E}} \quad \text{in the equivalent network}$$

and, from eqn. (9*a*), $\tilde{Z} = \underset{=}{\tilde{Z}}$

by the definition of equivalence

$$J = \underset{=}{J}$$

For example, if each of the self-resistances is equal to 1 ohm and if

$$\tilde{E} = [-2 \quad 4 \quad -3 \quad -3 \quad 3 \quad 0 \quad 0 \quad 2 \quad -1]' \qquad \begin{matrix} 1'' & 2'' & . & . & . & . & . & . & 9'' \end{matrix} \quad (20b)$$

$$S = [1 \quad 1 \quad 0 \quad . \quad . \quad 1 \quad 0 \quad . \quad . \quad 1 \quad 0]' \qquad \begin{matrix} 1 & 2 & & & 8 & & & 21 & \end{matrix} \quad (21b)$$

[see Fig. 9(*b*)], then, since

eqn. (22*b*) is in col. 2

$$\underset{=}{\tilde{E}} = \tilde{E} - RZS = \begin{bmatrix} -2 \\ 4 \\ -3 \\ -3 \\ 3 \\ 0 \\ 0 \\ 2 \\ -1 \end{bmatrix} - \begin{bmatrix} -1 \\ 1 \\ -1 \\ 0 \\ 1 \\ 0 \\ 1 \\ 0 \\ 0 \end{bmatrix} = \begin{bmatrix} -1 \\ 3 \\ -2 \\ -3 \\ 2 \\ 0 \\ -1 \\ 2 \\ -1 \end{bmatrix} \begin{matrix} 1'' \\ \underset{=}{2''} \\ . \\ . \\ . \\ . \\ . \\ . \\ 9 \end{matrix} \quad (23b)$$

(*d*) Finally we may analyse the given networks by examining the equivalent networks of Fig. 8(*b*). This equivalent network of mesh type has the same number of meshes as, but has less nodes than, the given network. Therefore it is convenient to put node potentials $\underset{=}{V}$ as unknown quantities. This method of solution has been shown in eqn. (7*a*), i.e.

$$\underset{=}{V} = (\underset{===}{DYD'})^{-1}(-\underset{===}{DYE})$$

(since $\underset{=}{\tilde{S}} = \underset{==}{DS} = 0$), where $\underset{=}{E}$ is any set of branch voltage sources satisfying $\underset{==}{RE} = \underset{=}{\tilde{E}}$, and where $\underset{=}{D}$ and $\underset{=}{R}$ are found by inspection from Fig. 8(*b*). After node potentials $\underset{=}{V}$ have been determined the mesh-currents $\underset{=}{J}$ can be found, and these are equal to J in the given network. If J is known, the other quantities such as $\tilde{I}$, I and U in the given network can easily be determined.

(5) CONCLUSIONS

In diakoptics and codiakoptics, mutual coupling may not exist between subnetworks, but may exist between a tie branch (co-tie branch) and the others. The electrical sources may be voltage and current sources, and further exist in all the elements. The choice between diakoptics or codiakoptics must be decided by the type of the given network.

Generally, with regard to a complicated network, it is convenient to analyse it by repeating diakoptics and codiakoptics one after the other. We call this method 'multiplex diakoptics'. The series of the first diakoptics and the second codiakoptics is most useful and called 'double diakoptics'.

$$-RZS = -\begin{matrix} 1'' \\ 2'' \\ 3'' \\ 4'' \\ 5'' \\ 6'' \\ 7'' \\ 8'' \\ 9'' \end{matrix} \begin{bmatrix} -1 & 0 & 1 & 0 & 0 & \cdot & \cdot & \cdot & \cdot \\ 0 & 1 & -1 & 0 & 1 & \cdot & \cdot & \cdot & \cdot \\ 0 & 0 & 0 & -1 & 1 & \cdot & \cdot & \cdot & \cdot \\ 0 & 0 & 0 & -1 & 0 & \cdot & \cdot & \cdot & \cdot \\ 0 & 0 & 0 & 0 & 0 & \cdot & \cdot & \cdot & \cdot \\ 0 & 0 & 0 & 0 & 0 & \cdot & \cdot & \cdot & \cdot \\ 0 & 0 & 0 & 1 & -1 & \cdot & \cdot & \cdot & \cdot \\ 0 & 0 & 0 & -1 & 1 & \cdot & \cdot & \cdot & \cdot \\ 0 & 0 & 0 & 0 & 0 & \cdot & \cdot & \cdot & \cdot \end{bmatrix} \begin{matrix} 1 & 2 & \cdot & \cdot & \cdot & \cdot & \cdot & \cdot & 21 \\ \cdot & \cdot & \cdot & \cdot & \cdot & \cdot & \cdot & \cdot & \cdot \end{matrix}$$

$$= \begin{matrix} 1'' \\ 2'' \\ 3'' \\ 4'' \\ 5'' \\ 6'' \\ 7'' \\ 8'' \\ 9'' \end{matrix} \begin{bmatrix} 0 & 0 & 0 & 0 & 0 & 0 & 0 & 0 & 0 \\ 0 & 0 & 1 & 0 & 0 & 0 & 0 & 1 & 0 \\ 0 & 0 & 0 & -1 & 0 & 0 & 0 & 0 & -1 \\ 0 & 0 & 0 & -1 & 0 & 0 & 0 & 0 & 0 \\ 0 & 0 & 0 & 0 & 0 & 0 & 0 & 1 & 0 \\ 0 & 0 & 0 & 0 & 0 & 0 & 0 & 0 & 1 \\ 0 & 0 & 0 & 1 & -1 & 0 & 0 & 0 & -1 \\ 0 & 0 & 0 & -1 & 1 & 0 & 0 & 0 & 0 \\ 0 & 0 & 0 & 0 & 0 & 0 & 0 & 0 & 0 \end{bmatrix} \begin{matrix} 1 & 2 & \cdot & \cdot & \cdot & \cdot & \cdot & \cdot & 21 \\ \cdot & \cdot & \cdot & \cdot & \cdot & \cdot & \cdot & \cdot & \cdot \end{matrix}$$

$$= \begin{matrix} 1'' \\ 2'' \\ \cdot \\ \cdot \\ \cdot \\ \cdot \\ \cdot \\ \cdot \\ 9'' \end{matrix} \begin{bmatrix} 1 & 0 & \cdot & \cdot & \cdot & \cdot & \cdot & \cdot & 0 \\ 0 & 1 & \cdot & \cdot & \cdot & \cdot & \cdot & \cdot & 0 \end{bmatrix} \begin{matrix} 1 & 2 & \cdot & \cdot & \cdot & \cdot & \cdot & \cdot & 21 \\ \cdot & \cdot & \cdot & \cdot & \cdot & \cdot & \cdot & \cdot & \cdot \end{matrix}$$

$$- \begin{matrix} 1'' \\ 2'' \\ \cdot \\ \cdot \\ \cdot \\ \cdot \\ \cdot \\ \cdot \\ 9'' \end{matrix} \begin{bmatrix} 1 & 1 & 0 & \cdot & \cdot & \cdot & \cdot & \cdot & 1 \\ 1 & 2 & 0 & \cdot & \cdot & \cdot & 1 & \infty & 20 \\ 0 & \cdot & \cdot & \cdot & \cdot & \cdot & \cdot & \cdot & 1 \\ 1 & \cdot & \cdot & \cdot & \cdot & \cdot & \cdot & \cdot & 0 \end{bmatrix} \begin{matrix} 1 & 2 & \cdot & \cdot & \cdot & \cdot & \cdot & \cdot & 21 \\ \cdot & \cdot & \cdot & \cdot & \cdot & \cdot & \cdot & \cdot & \cdot \end{matrix}$$

$$= \begin{matrix} 1'' \\ 2'' \\ \cdot \\ \cdot \\ \cdot \\ \cdot \\ \cdot \\ \cdot \\ 9'' \end{matrix} \begin{bmatrix} 1 & 0 & \cdot & \cdot & \cdot & \cdot & \cdot & \cdot & 0 \\ 0 & 1 & \cdot & \cdot & \cdot & \cdot & \cdot & \cdot & 0 \end{bmatrix} \begin{matrix} 1 & 2 & \cdot & \cdot & \cdot & \cdot & \cdot & \cdot & 21 \\ \cdot & \cdot & \cdot & \cdot & \cdot & \cdot & \cdot & \cdot & \cdot \end{matrix}$$

$$- \begin{matrix} 1'' \\ 2'' \\ \cdot \\ \cdot \\ \cdot \\ \cdot \\ \cdot \\ \cdot \\ 9'' \end{matrix} \begin{bmatrix} -1 & 1 & -1 & 0 & 1 & 0 & 0 & 1 & 0 \\ 1 & -1 & 1 & 0 & 0 & 1 & 0 & 0 & 0 \end{bmatrix} \begin{matrix} 1'' & 2'' & \cdot & \cdot & \cdot & \cdot & \cdot & \cdot & 9'' \\ \cdot & \cdot & \cdot & \cdot & \cdot & \cdot & \cdot & \cdot & \cdot \end{matrix} \quad (22b)$$

(6) REFERENCES

(1) KRON, G.: 'The Analytical Solution of Complex Physical Structures by Diakoptic Methods', *Matrix and Tensor Quarterly*, 1955, **5**, p. 115.

(2) KRON, G.: 'Inverting a 256 × 256 Matrix: Solution of an Engineering System by Method of Sections Using a Card Programme Calculator', *Engineering*, 1955, **178**, p. 309.

(3) KRON, G.: 'A Method of Solving Very Large Physical Systems in Easy Stages', *Proceedings of the Institute of Radio Engineers*, 1954, **42**, p. 680.

(4) KRON, G.: 'A Set of Principles Interconnecting the Solutions of Physical Systems', *Journal of Applied Physics*, August, 1953, **24**, p. 965.

(5) WENGERT, R. E.: 'Simple Diakoptics', *Matrix and Tensor Quarterly*, 1955, **5**, p. 129.

(6) STIGANT, S. A.: 'Modern Electrical Engineering Mathematics' (Hutchinson, 1946).

(7) LEFSCHETZ, S.: 'Topology', American Mathematical Society Colloquium Publications, 1930, **12**.

(8) 'Definitions of Terms in Network Topology, 1950', *Proceeding of the Institute of Radio Engineers*, 1951, **39**, p. 27.

(9) FOSTER, R. M.: 'Topologic and Algebraic Considerations in Network Synthesis', Proceedings of the Symposium on Modern Network Synthesis, April, 1952, p. 8.

(10) OKADA, S., and ONODERA, R.: 'A Unified Treatise on the Topology of Networks and Algebraic Electromagnetism', Memoirs of the Unifying Study of the Basic Problems in Engineering Science by Means of Geometry, December, 1955, **1**, p. 68.

(11) PERCIVAL, W. S.: 'The Solution of Passive Electrical Networks by Means of Mathematical Trees', *Proceedings I.E.E.*, Paper No. 1492 R, May, 1953 (**100**, Part III, p. 143).

(12) HEYDA, P. G.: 'A Simple Numerical Example for the Beginner of Kron's Method of Tearing and Interconnecting', *Matrix and Tensor Quarterly*, 1956, **6**, p. 142.

(13) ONODERA, R.: 'Dualistic Sketch of Kron's Diakoptics', *ibid.*, 1959, **9**, p. 78.

621.313.3.017.31

The Institution of Electrical Engineer
Monograph No. 404 S
Oct. 196(

POLE-FACE LOSSES IN ALTERNATORS

An Investigation of Eddy-Current Losses in Laminated Pole Shoes

By Prof. J. GREIG, M.Sc.(Eng.), Ph.D., Member, and K. SATHIRAKUL, B.Sc.(Eng.), Ph.D., Graduate.

(*The paper was first received* 14*th April, and in revised form* 8*th June*, 1960. *It was published as an* INSTITUTION MONOGRAPH *in October*, 1960.)

SUMMARY

A recent re-examination of the phenomenon of tooth-ripple flux pulsations at laminated pole-faces in alternators resulted in a new theoretical analysis by means of which the pole-face eddy-current loss can be calculated. The primary purpose of the present investigation has been to make measurements of tooth-ripple losses which could be compared with values calculated from the new formulae. In order to make these measurements an experimental homopolar machine was built and values of eddy-current losses were determined over a fairly wide range of flux density and frequency for four different thicknesses of lamination. It is found that there is moderately good agreement between calculation and experiment for the thicker laminations and in general the agreement is markedly better with the new formulae than with those previously developed.

LIST OF PRINCIPAL SYMBOLS

The M.K.S. system of units is used unless otherwise indicated.

B_m = Average air-gap flux density, Wb/m^2.
B_t = Fundamental-frequency tooth-ripple flux density at the pole-face, Wb/m^2.
d = Characteristic depth of penetration, m.
f_r = Tooth-ripple frequency, c/s.
g = Length of air-gap, m.
h = Lamination thickness, m.
m = Odd integer in a Fourier expansion.
n = Any integer in a Fourier expansion.
P_e = Eddy-current loss per unit pole-face area, watts/m^2.
P_h = Hysteresis loss per unit pole-face area, watts/m^2.
s = Width of the armature slot opening, m.
β_1 = Flux-oscillation factor.
λ = Armature slot pitch, m.
μ = Absolute permeability, henrys/m.
μ_r = Relative permeability.
ρ = Resistivity, ohm-m.
$\omega = 2\pi f_r$ = Angular tooth-ripple frequency, rad/sec.

(1) INTRODUCTION

In the air-gap of a salient-pole alternator, the flux density, instead of being uniform over the main part of the pole arc, has superimposed upon it a 'ripple' resulting from the permeance variation along the air-gap produced by the armature teeth and slots. The pole-face is thus subjected to a pulsating flux density which gives rise to eddy-current and hysteresis losses in the pole shoes. At the normal frequency of the flux ripple, however, only the eddy-current-loss component has practical importance in relation to the design of pole shoes. Attention is here concentrated on the eddy-current loss in a smooth laminated pole shoe.

The mathematical analysis of the problem, recently made by Bondi and Mukherji,[1] has shown that there exist in a laminated pole shoe two different modes of flux penetration, one in accordance with the characteristic depth of penetration, and the other of a much greater depth of the order of the slot pitch. The phenomenon of the deeply penetrating flux has been verified in detail by experiment by Greig and Mukherji.[2]

It has been predicted that under normal conditions the major part of the eddy-current losses in laminated pole shoes is to be attributed to the deeply penetrating component of flux ripples. Previous theoretical formulae for eddy-current loss take no account of this phenomenon, and in consequence are subject to quite large errors.

Reference was made by Gibbs[3] to the scarcity of reliable measurements of pole-face losses which may be applied to check theoretical solutions. The earliest experimental measurement of tooth-ripple losses was made with an ordinary salient-pole alternator by the method of air-gap variation.[4] This method is, however, inherently inaccurate, for it involves taking the difference between two nearly equal large quantities, the main loss in the armature core being inevitably measured along with the pole-face loss. It has long been realized, however, that the core loss due to rotation in the main flux is theoretically absent in the homopolar machine, and this fact was first turned to account in the measurement of pole-face losses by Aston and Rao.[5,6] In the homopolar machine, cylindrical symmetry will eliminate the main core loss in the rotating member, and the only major loss present is then that due to hysteresis and eddy currents in the pole shoe. It is therefore possible to measure the pole-face loss directly, utilizing the normal method for separating the effect of friction and windage.

The principle of the homopolar machine has been utilized for this purpose in the present work. In the experimental machine to be described, great care was taken in the design to ensure magnetic symmetry and to minimize magnetic leakage. Losses were measured by the retardation method, and the separation of eddy-current loss from hysteresis loss was made by the conventional graphical method.

(2) CALCULATION OF EDDY-CURRENT LOSS

A mathematical analysis of the phenomenon of tooth-ripple eddy currents in smooth laminated pole shoes is given in a recent paper by Bondi and Mukherji.[1] This analysis involves a simplifying assumption regarding boundary conditions which appears to be thoroughly justified, but whose validity it would be valuable to confirm. The assumption is that the eddy-current distribution in the pole, resulting from the application of a given flux distribution at the pole-face, is unaffected by the proximity of the armature teeth and slots. In other words, viewed from the pole-face, the effective air-gap is infinite.

We have re-examined[7] the problem and have found it practicable to develop a modified solution in which an infinite air-gap is not assumed. The new idealization involves a perfectly smooth air-gap of the correct length and the same applied flux distribution at the pole-face. The concept is in fact that of a smooth rotor magnetized with the requisite number of consequent poles but retaining a sufficiently high permeability for the induced magnetic field due to the pole-face currents to enter its surface normally. The modified solutions have been evaluated for certain values of parameters in the range $g/h > 0{\cdot}1$ and

Correspondence on Monographs is invited for consideration with a view to publication.

Prof. Greig is William Siemens Professor of Electrical Engineering, and Dr. Sathirakul was formerly in the Department of Electrical Engineering, King's College, University of London.

$\mu_r > 100$, and compared with values calculated from the earlier formula. It is found that in this range the modified boundary conditions produce no significant difference.

The new formula for tooth-ripple eddy-current loss per unit pole-face area (watts/m^2) has been derived elsewhere.[7] It comprises nine components as given below.

$$P_e = \hat{B}_t^2[(A)+(B)+(C)+(D)+(E)+(F)+(G)+(H)+(I)] \quad . \quad . \quad . \quad . \quad . \quad (1)$$

The complete expressions for the loss components (A) to (I) in eqn. (1) are given in Section 8. In terms of the average air-gap flux density, B_m, eqn. (1) can be rewritten as

$$P_e = \tfrac{1}{4}\beta_1^2 B_m^2[(A)+(B)+\ldots+(I)] \quad . \quad . \quad (2)$$

where β_1 is the flux-oscillation factor, determining $\hat{B}_t$ as a ratio with B_m for given values of s, λ and g. A family of curves showing the variation of β_1 over a wide range of the ratios s/g and s/λ has been given by Gibbs,[3] and is reproduced in Fig. 1.

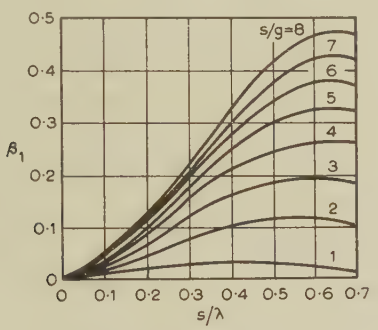

Fig. 1.—Gibbs's β_1 curves.

Numerical examination of eqn. (1) shows that a close approximation may be obtained by considering only the two major loss components (A) and (E). The approximate loss formula is given below.

$$P_e \simeq \beta_1^2 B_m^2 \left\{ \left[\frac{\pi\lambda h\omega^{3/2}}{64\sqrt{2}\sqrt{(\rho\mu)}\hat{\sigma}^2} \right] \left[\frac{\sinh(h/\sqrt{2d}) - \sin(h/\sqrt{2d})}{\sinh^2(h/2\sqrt{2d}) + \sin^2(h/2\sqrt{2d})} \right] + \left[\frac{h^2\omega^{3/2}}{4\sqrt{(\rho\mu)}} \frac{\hat{\gamma}^2}{\hat{\sigma}^2} \right] \left[\mathscr{R} \sum_{m\ \mathrm{odd}}^{\infty} \frac{1}{(m^2\theta_m\bar{\theta}_m'^2)} \right] \right\} \quad . \quad . \quad (3)$$

where

$$\gamma = \left[\cot \frac{(1-j)h}{2\sqrt{2d}} \right] \left(1 + \frac{jh}{\lambda\alpha_1} \right)$$

$$\alpha_n = \frac{2n\pi d}{h}\theta_n + \frac{k_n\theta_n'^2}{2n\pi\mu_r \tanh \frac{gk_n}{h}}$$

$$\sigma = 1 + \sum_{m\ \mathrm{odd}}^{\infty} \frac{4\sqrt{2}(1+j)h}{\pi\lambda} \frac{\gamma}{m^2\theta_m\theta_m'^2}$$

$$\theta_m = \left(\frac{4\pi^2 d^2}{\lambda^2} + \frac{m^2\pi^2 d^2}{h^2} + j \right)^{1/2}$$

$$\theta_m' = \left(\frac{m^2\pi^2 d^2}{h^2} + j \right)^{1/2}$$

$$\theta_n = \left(\frac{4\pi^2 d^2}{\lambda^2} + \frac{4n^2\pi^2 d^2}{h^2} + j \right)^{1/2}$$

$$\theta_n' = \left(\frac{4n^2\pi^2 d^2}{h^2} + j \right)^{1/2}$$

$$k_n = 2\pi\left(n^2 + \frac{h^2}{\lambda^2} \right)^{1/2}$$

$\hat{\gamma}$ and $\hat{\sigma}$ denote the moduli of γ and σ, and $\bar{\theta}_m'$ is the complex conjugate of θ_m'.

For $h/d < 4$, the second term on the right-hand side of eqn. (3) becomes negligible, and the formula is further reduced.

The approximate formula [eqn. (3)] is found to give results accurate to within about 10%. Fig. 6 shows a comparison of the losses as calculated by the approximate formula and the complete formula [i.e. eqn. (1) and Section 8].

(3) EXPERIMENTAL INVESTIGATION

(3.1) The Experimental Machine

As has been stated, an experimental homopolar machine was specially constructed for the purpose of investigating tooth-ripple losses in laminated materials. The machine (see Fig. 2) had two active portions symmetrically disposed about its transverse mid-plane. These each comprised a stack of ring stampings, forming part of the magnetic circuit of the stator and representing the active part of the alternator pole. Separated by the air-gaps from the inner cylindrical faces of these stacks of stampings were the corresponding active portions of the rotor, formed by two mild-steel sleeves slotted to represent the slots and teeth of an unwound armature.

The rotating member consisted of the shaft, mild-steel rotor body and the two identical slotted sleeves. In order to minimize the magnetic end-leakage, the shaft was made of stainless steel, the rotor body being keyed to it and held in place by two brass locking rings. The slotted sleeves, made detachable to permit substitution, had a close clearance fit to the rotor body and were keyed to it, each being held in position by a brass locking ring. The rotor sleeves with which the present series of experiments were made had each 24 parallel-sided open slots milled in them. The dimensions of these rotor sleeves were as follows:

Outer diameter of the sleeves	= 7·9 in
Air-gap	= 0·05 in
Slot width	= 0·375 in
Slot pitch	= 1·034 in
Slot depth	= 0·75 in
Axial length of the slots	= 1·5 in

It should perhaps be mentioned in passing, in relation to the design of the machine, that for a given rotor diameter and average air-gap flux density there is a limitation on the practical axial length of the active part of the machine. This limitation results from the fact that the total flux, which enters the rotor radially, has to be carried longitudinally in the rotor body at an acceptable flux density.

The stator frame of the machine was of cast iron. The end brackets carrying the bearings were made of aluminium in order to reduce magnetic leakage, and the machine was bolted to wooden bearers by brass bolts. The two field coils, wound in brass formers, were mounted symmetrically about the mid-plane of the machine, and separated by an air duct. For convenience in assembly, in relation to the insertion of search coils behind the pole-face, the stacks of pole stampings under test were assembled in cylindrical mild-steel shells which had a close clearance fit in the stator housing. Each stack was held between two aluminium stiffening rings; these were in turn tightened by a system of a clamp and bolts.

The rotor was designed to run at speeds up to about 9 000 r.p.m.

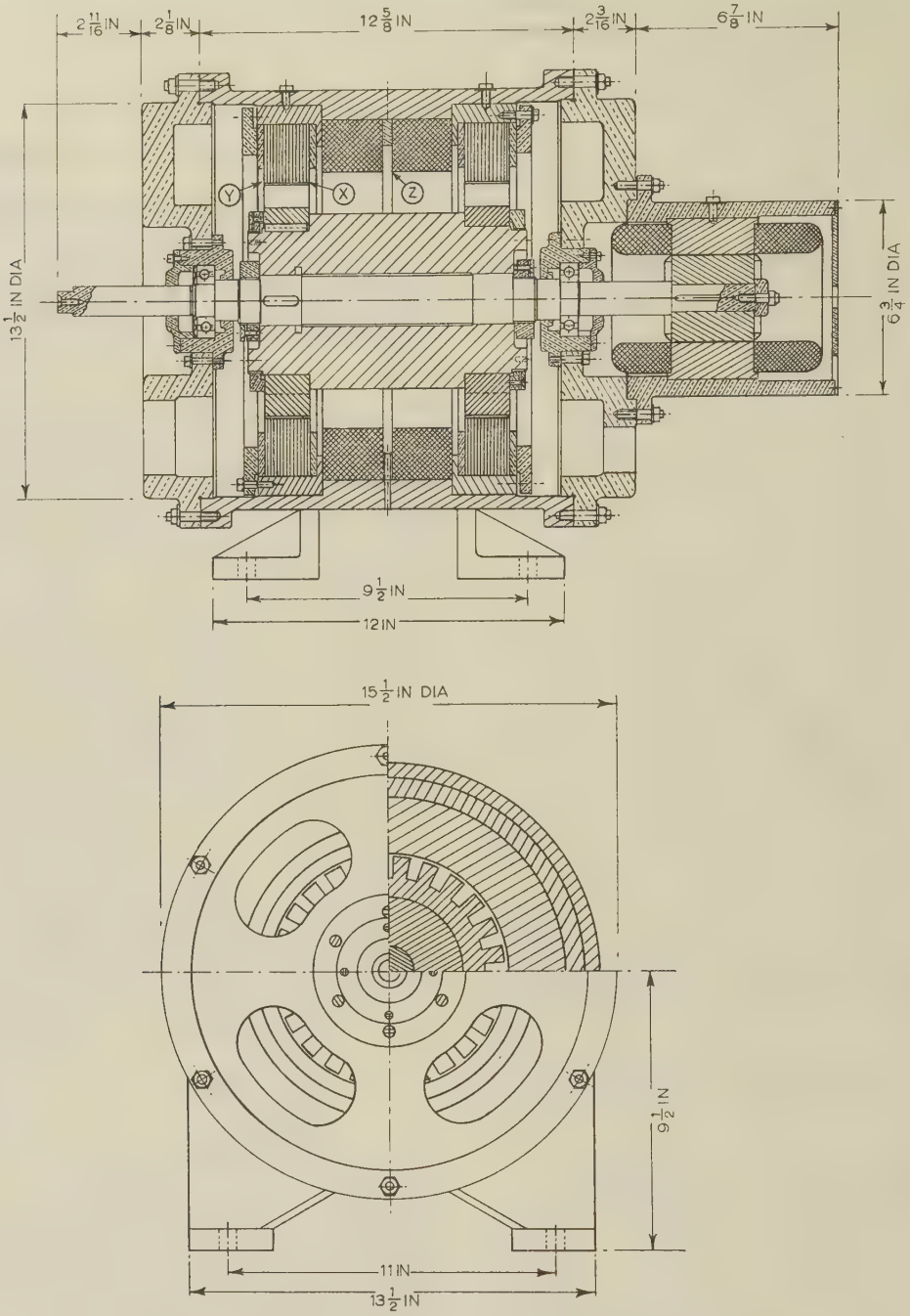

Fig. 2.—Sectional drawing of the experimental homopolar machine.

It was directly driven by a 3 h.p. 2-pole high-speed squirrel-cage induction motor having a rated speed of 8570 r.p.m. at a supply frequency of 150 c/s; this supply was obtained from an alternator. The cage rotor of the induction motor was mounted directly on the extension of the main shaft, and the stator was housed in an aluminium frame bolted to the end bracket of the homopolar machine. It may be mentioned here that the rotor body of the homopolar machine was balanced dynamically, and to facilitate this a number of threaded holes for balance weights were provided on the end surfaces of the rotor. At the maximum speed of the machine, the tooth-ripple frequency for the 24-slot rotor was approximately 3 400 c/s.

The field excitation for the homopolar machine was supplied by a storage battery through a variable resistor, an ammete and a reversing switch. For demagnetizing purposes, a discharg resistance was also arranged in the field circuit. To determin the average flux density in the air-gap for a given field curren two circular single-turn coils having the inner diameter of th ring stampings were mounted in the positions marked X and in Fig. 2. The difference between the total flux linking th search coil X and that linking the coil Y (i.e. the end-leakag flux) measured the radial flux entering the stack of stamping In making a measurement, the two coils in opposition and Grassot fluxmeter were connected in series. The measurement were carried out for the two air-gaps of the machine, the tw results being found to be almost identical. The average flu

density was then obtained by dividing the total useful flux by the air-gap surface area. In the measurements of losses to be described, the required flux density in the air-gap was established by applying the appropriate field current, the direction of the current being first reversed a number of times.

In order to ascertain the amount of leakage flux, fluxmeter readings were taken for the circular single-turn coil Z located roughly at the mid-point of the stator and having the inner diameter of the field coil (see Fig. 2). The difference between the reading for the coil Z and that for the pole search coils (X and Y in opposition), for the same field current, thus indicated the total leakage flux. At an air-gap induction of 1 Wb/m^2, the total leakage was found to be about 7% of the total useful flux in the air-gap.

(3.2) Materials of Pole Stampings

The ring stampings for the two pole-pieces of the homopolar machine were punched from sheet steel, and had outer diameters of 12 in and inner diameters of 8 in. These built up each pole-piece to the same axial length as that of the rotor sleeve, no added insulation being applied between the laminations. The total active area of the pole-faces was approximately 75·4 in^2 (486·4 cm^2). The pole-faces were not tampered with mechanically after the stampings had been assembled.

Four sets of stampings of different lamination thicknesses were used for the pole-pieces in the present investigation; two sets of thin stampings (h = 0·406 mm and 0·635 mm) were of 0·4% silicon sheet steel, and the other two of thicker stampings (h = 1·625 mm and 3·18 mm) of cold-rolled close-annealed (c.r.c.a.) sheet steel. A rectangular strip was cut out of each set for the measurement of the electrical resistivity of the material. For the magnetic measurement, ballistic tests were performed on ring specimens made up of the actual ring stampings which were used for the experimental pole-pieces. Measurements of incremental permeability were carried out on these specimens, employing the normal ballistic method.[8] Average values of the resistivity and incremental permeability to be used for the loss calculation are given in Table 1, the latter being obtained with a polarization of approximately 0·8 Wb/m^2 and a modulation of H of about 50%.

Table 1

ELECTRICAL AND MAGNETIC PROPERTIES OF POLE STAMPINGS

Material	Lamination thickness	Resistivity	Incremental permeability
	mm	ohm-m $\times 10^{-8}$	H/m $\times 10^{-7}$
0·4% silicon sheet steel	0·406 0·635	19	$4\pi \times 275$
Cold-rolled close-annealed sheet steel (c.r.c.a.)	1·625 3·18	15	$4\pi \times 210$

(3.3) Method of Measurement

The retardation method was adopted as a convenient means of measuring losses in the homopolar machine. This requires the determination of the instantaneous angular retardation from the speed/time relation as the machine runs down, the retarding torque being calculated from the relation:

Torque = (moment of inertia) × (angular retardation)

Hence, the loss can be evaluated for any given speed.

The moment of inertia of the rotor was determined by the bifilar suspension method. The speed/time relation was obtained by the 'point-to-point' method, using a stroboscopic disc and a flash tube as a means of measuring the rotor speeds. The repetition frequency of the flash tube (100 c/s) was determined by a quartz-crystal frequency standard, and 1 sec interval pulse signals were obtained from a crystal-controlled clock. A recorder was employed as a chronograph, one of the pens marking the time by second impulses from the clock, and the other receiving signals from a manually operated key to record the instants at which known speeds were observed stroboscopically.

Before commencing the retardation test, the machine was kept running at its rated speed for some time for the bearings to settle down to a steady condition. During this run, demagnetization of the machine was carried out by the normal method of reversing progressively smaller field currents. Complete demagnetization was indicated by the absence of the tooth-ripple e.m.f. in a search wire on the pole-face. In carrying out the retardation test, the machine ran down from its rated speed, the run-down speeds being recorded at intervals of 200, 100 and 50 r.p.m. for high, intermediate and low speeds, respectively. The tests were then repeated with various values of field current, thereby varying the air-gap induction. In the present series of measurements, the test results covered a range of air-gap induction from 0·2 — 1 Wb/m^2.

The pole-face loss was obtained by taking the difference between the loss under a given condition of excitation and that under a demagnetized condition at the same speed. The loss with the machine demagnetized represented the effect of bearing friction and windage. It may be mentioned that the experimental results in the present investigation were found to be repeatable with an accuracy of about ±5%.

Tests were carried out on the four sets of pole stampings (see Table 1). The stampings were used as received, but check tests with added paper insulation between the laminations showed that the differences in losses were negligibly small. Finally, in order to ascertain the degree of freedom of the homopolar machine from other stray losses, retardation tests were made with an unslotted rotor having the same dimensions as the slotted rotor. At an air-gap induction of 1 Wb/m^2 and speed of 4000 r.p.m., the stray loss was found to amount to only about 0·5% of the pole-face loss in the 0·406 mm stampings, and less than 0·07% in the 3·18 mm stampings. These experiments served to confirm that a satisfactorily high degree of symmetry had been achieved in the field distribution of the machine.

(3.4) Experimental Results

Typical torque/speed curves are shown in Fig. 3. These curves, when extrapolated to zero speed, make positive intersections with the torque axis. These intercepts represent the bearing-friction torque in the demagnetized case [see Fig. 3(*a*)], and the sum of the friction and hysteretic torque when magnetized. The presence of other stray losses, such as extra bearing drag,[3] or of mechanical losses due to unbalanced magnetic pull, would make a combined appearance in the intercept on the torque axis together with the hysteretic torque. The experiments with the plain rotor, already described in Section 3.3, indicated, however, that these stray losses were negligible compared with the tooth-ripple loss. The difference between the intercepts in the magnetized and demagnetized cases was therefore taken to be due entirely to hysteresis.

In evaluating the hysteresis component of the tooth-ripple loss, the hysteretic torque for a given air-gap induction was assumed to be independent of speed. No account was therefore taken of the modification in hysteresis loss produced by skin effect at higher frequencies. In fairly thick stampings

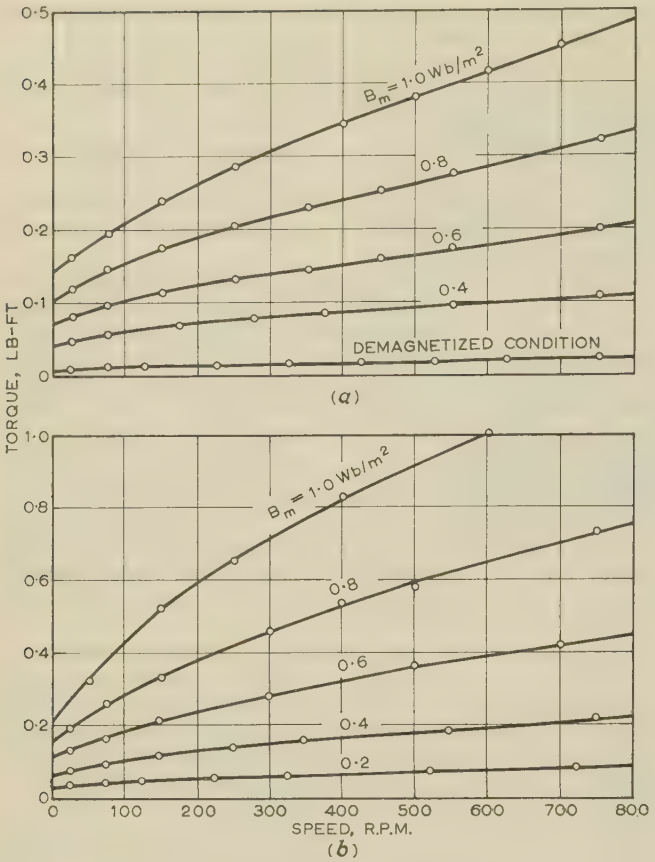

Fig. 3.—Torque/speed curves.
(*a*) 0·4% silicon sheet steel. $h = 0{\cdot}635$ mm.
(*b*) C.R.C.A. sheet steel. $h = 1{\cdot}625$ mm.

the skin effect will be very pronounced, but as in this instance the hysteresis loss calculated on the assumption of negligible eddy-current shielding is less than 10% of the total core loss, it is reasonable to assume that the resultant uncertainty in the magnitude of the eddy-current loss will be small. After deducting the hysteresis loss from the total tooth-ripple loss measured at a corresponding speed and condition of magnetization, the remainder was taken to be that due to eddy currents. Table 2

Table 2

EXPERIMENTAL RESULTS OF LOSS MEASUREMENTS

Material	Lamination thickness	Loss		
		Friction and windage	Hysteresis	Eddy current
	mm	watts	watts	watts
0·4% silicon sheet steel	0·406	105·5	39·4	121
	0·635	105·5	39·4	204
C.R.C.A. sheet steel	1·625	105·5	57	575
	3·18	105·5	57	1,274

$B_m = 0{\cdot}6$ Wb/m²; speed = 4000 r.p.m.; $f_r = 1\,600$ c/s.

gives some examples showing the relative magnitudes of the eddy-current loss and the hysteresis loss for $B_m = 0{\cdot}6\,Wb/m^2$ and $f_r = 1\,600$ c/s, together with the corresponding friction and windage loss for the present set of slotted rotor sleeves employed.

Experimental curves of eddy-current loss per unit pole-face area (watts/m²) against speed are shown in Figs. 4 and 5 for the four sets of pole stampings. The results covered ranges of average air-gap flux densities from 0·2–1 Wb/m², and of speeds up to 8 000 r.p.m. corresponding to tooth-ripple frequencies up to 3 200 c/s. It was therefore possible to study from the test results the effects on the eddy-current loss of the flux density, frequency and lamination thickness. The effects of these variables were conveniently investigated by plotting on a double logarithmic basis the eddy-current loss against each variable individually, keeping the rest constant, the mean slope of these curves thus represented the index of that variable in relation to the loss. In double logarithmic plots of loss and lamination thickness, the two sets of thin laminations ($h = 0{\cdot}406$ and $0{\cdot}635$ mm) were considered separately from the other two sets of thicker laminations ($h = 1{\cdot}625$ and $3{\cdot}18$ mm), the former sets being of silicon sheet steel, while the latter were of c.r.c.a. material. From the analysed results, the measured eddy-current loss per unit pole face area may be expressed as follows:

$$P_e = k_{ea} B_m^{2{\cdot}1} f_r^{1{\cdot}7} h^{1{\cdot}2} \text{ watts per square metre}$$

for 0·4% silicon sheet steel with lamination thickness from 0·406 to 0·635 mm,

$$P_e = k_{eb} B_m^{2{\cdot}1} f_r^{1{\cdot}7} h \text{ watts per square metre}$$

for c.r.c.a. sheet steel with lamination thickness from 1·625 to 3·18 mm, where $k_{ea} \simeq 298$ and $k_{eb} \simeq 80$ for the present 2 open-slot rotor.

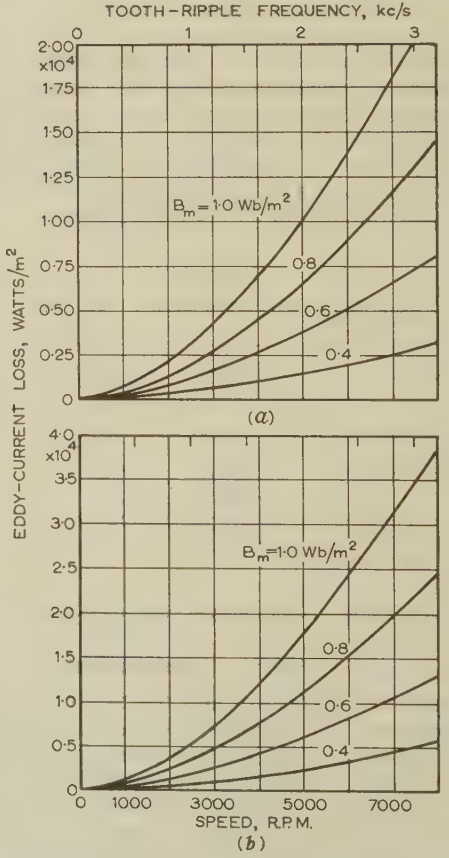

Fig. 4.—Experimental results for 0·4% silicon sheet steel.
(*a*) Lamination thickness = 0·406 mm.
(*b*) Lamination thickness = 0·635 mm.

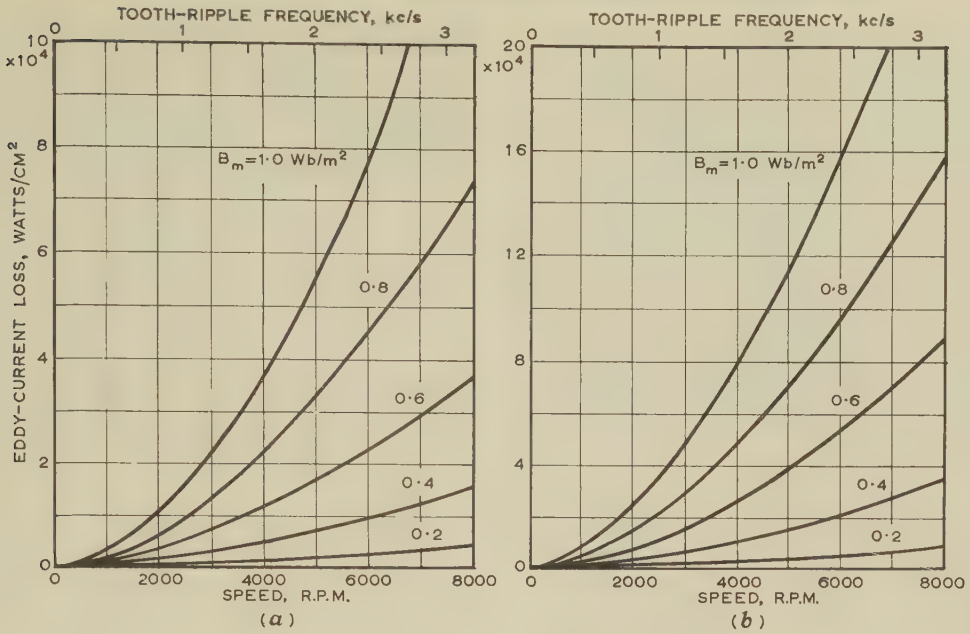

Fig. 5.—Experimental results for c.r.c.a. sheet steel.

(*a*) Lamination thickness = 1·625 mm.
(*b*) Lamination thickness = 3·18 mm.

Hysteresis losses in the pole stampings, determined on the assumption already explained, could be analysed in a similar way. The hysteretic torques at a given air-gap induction were found to be practically the same for pole stampings of the same material, irrespective of the lamination thickness. The index of the average air-gap flux density in relation to the hysteretic torque was found to be approximately 1·4 for the silicon sheet steel and 1·5 for the c.r.c.a. sheet steel. Assuming the hysteresis loss to vary in proportion to the tooth-ripple frequency, the hysteresis loss per unit pole-face area may be expressed as follows:

$P_h = k_{ha} B_m^{1\cdot4} f_r$ watts per square metre for 0·4% silicon sheet steel

$P_h = k_{hb} B_m^{1\cdot5} f_r$ watts per square metre for c.r.c.a. sheet steel

where $k_{ha} \simeq 1\cdot04$ and $k_{hb} \simeq 1\cdot48$ for the present 24 slot rotor.

(4) COMPARISON OF THEORY AND TEST

The formula for tooth-ripple eddy-current loss given in Section 2 involves summations of a number of infinite series which are functions of h, g, λ, d and μ_r. For common values of these variables encountered in practice, however, each of these series is found to converge fairly rapidly, and the evaluation of loss from the formula is in fact not as tedious and difficult as might perhaps appear.* A number of calculations of losses has been made by means of the formula for comparison with the measured values. The dependence of eddy-current loss on the factors B_m, f_r and h as established from the theoretical analysis has been examined and compared with experiment. For the most part these comparisons have been made between the tooth-ripple loss as determined from experimental results and the calculated loss at fundamental frequency, it being assumed that, to a first approximation, the losses at harmonic frequencies could be neglected.

* Numerical calculations covering a practical range of these variables are being made with the aid of an electronic computer. It may be possible to present at a later date the formula in a form more convenient for direct use.

(4.1) Variation of Loss with Certain Factors

The loss formula given in eqn. (1) shows that the eddy-current loss per unit area of a laminated pole-face is proportional to $\hat{B}_t^2$, $\hat{B}_t$ being the amplitude of a sinusoidal flux density at the pole-face and proportional to the average air-gap flux density B_m. This characteristic variation of loss with flux density is in agreement with all previous theoretical and experimental work on tooth-ripple losses, and is also substantially confirmed in the analysis of the present test results for all four sets of pole stampings.

The effects on the eddy-current loss of variations of the lamination thickness and of the tooth-ripple frequency in the loss formula are not obvious. The manner in which the loss varies individually with these two factors cannot be determined without a major analytical work on transformation of the formula. It is, however, possible to study the variation of loss with these factors from numerical results calculated for the formula.

In Fig. 6 is shown on a double logarithmic scale the variation of the calculated eddy-current loss, $P_e/\hat{B}_t^2$, with the lamination thickness for a fixed frequency of 1 kc/s. The calculations were made for pole shoes with six different lamination thicknesses of 0·203, 0·406, 0·635, 0·812, 1·625 and 3·18 mm, the values of resistivity and permeability being assumed to be as those of the c.r.c.a. sheet steel (see Table 1); other parameters were taken to coincide with those of the homopolar machine. It can be seen in Fig. 6 that there is a change in the index of the lamination thickness in relation to the eddy-current loss, represented by the change in the slope of the curve, as the thickness exceeds a certain limit. This limit is found to depend practically solely on the ratio of two parameters, the lamination thickness and the characteristic depth of penetration, i.e. h/d. For the case under consideration, in which $d = 0\cdot301$ mm, the loss is shown to be proportional approximately to the square of the thickness in the range 0·203–1·2 mm (corresponding to $h/d = 0\cdot68$–4), while in the thicker laminations with thickness from 1·2 to 3·18 mm (corresponding to $h/d = 4$–10·57) it varies practically linearly with the thickness.

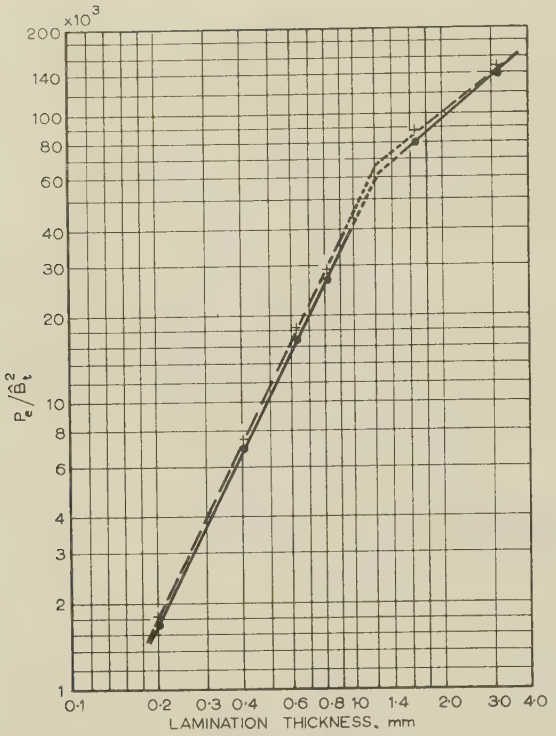

Fig. 6.—Calculated results of $P_e/\hat{B}_t^2$ for different lamination thicknesses.

—·——·— Full formula.
× —— × — Approximate formula.

$\rho = 15 \times 10^{-8}$ ohm-m
$\omega = 2\pi \times 10^3$ rad/sec
$\lambda = 2{\cdot}627 \times 10^{-2}$ m
$\mu = 4\pi \times 210 \times 10^{-7}$ henry/m
$d = 0{\cdot}301 \times 10^{-3}$ m
$g = 0{\cdot}127 \times 10^{-2}$ m

The linear variation of loss with lamination thickness for pole stampings in the 1·2–3·18 mm range is verified by the present series of measurements in the 1·625 and 3·18 mm laminations, and is also in agreement with Aston and Rao's experimental results.[5, 6] For thinner laminations, however, the variation of loss as the square of the lamination thickness is not satisfactorily corroborated by the present measurements. The analysis of the test results in fact shows that the eddy-current loss varies more nearly linearly with the thickness rather than as the square of the thickness. Previous experimental data on tooth-ripple losses in thin laminations with which a comparison may be made are those of Spooner and Kinnard,[9] but their results were presented without separating them into the eddy-current and hysteresis components. However, it has been pointed out elsewhere[5] that after deducting the appropriate hysteresis losses from their results of total tooth-ripple losses, the remaining eddy-current loss is shown to be proportional approximately to the first power of the lamination thickness.

To study the effect of the tooth-ripple frequency on the eddy-current loss, the theoretical formula was used to evaluate the losses in a pole shoe of a given lamination thickness for three different frequencies of 500 c/s, 1 kc/s and 2 kc/s. The calculations were made for the four different lamination thicknesses employed in the experimental work. The variation of loss with frequency was conveniently determined by plotting the calculated results for each set of laminations against frequency on a double logarithmic scale. The index of the frequency in relation to the loss was thus given by the slope of a straight line in each case. It was found that this index varied from about 1·5 to 2, depending on the lamination thickness. For the two sets of thin laminations the indices were approximately 2 and 1·9 respectively, and for the other two sets of thicker laminations the indices were found to reduce to about 1·6 and 1·5 respectively.

This change in the index of the frequency with respect to the lamination thickness was not demonstrated in the present experimental results. It was found in fact that for the same range of frequency (500 c/s–2 kc/s) the measured loss tended to vary very closely as (frequency)$^{1\cdot7}$ in all four sets of

Table 3

VARIATION OF EDDY-CURRENT LOSS WITH CERTAIN FACTORS

Lamination thickness	Indices of					
	B_m		f_r		h	
	Experiment	Theory	Experiment	Theory	Experiment	Theory
mm						
0·406	2·1	2	1·7	2·0	1·2	2
0·635	2·1	2	1·7	1·9	1·2	2
1·625	2·1	2	1·7	1·6	1·0	1
3·18	2·1	2	1·7	1·5	1·0	1

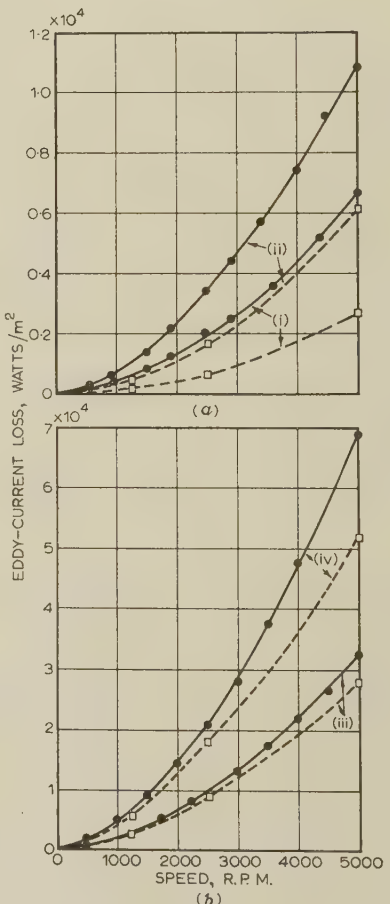

Fig. 7.—Comparison of calculated and measured eddy-current losses.

(*a*) 0·4% silicon sheet steel.
(*b*) C.R.C.A. sheet steel.

(i) $h = 0{\cdot}406$ mm. (iii) $h = 1{\cdot}625$ mm.
(ii) $h = 0{\cdot}635$ mm. (iv) $h = 3{\cdot}18$ mm.

———— Measured.
— — — Calculated.
$B_m = 0{\cdot}8$ Wb/m².

laminations. However, so far as the two sets of thick laminations are concerned, the observed index of about 1·7 agrees fairly well with the corresponding calculated value. In the case of the thinner laminations, the calculated value of the index differs appreciably from the observed value, but this is not unexpected in view of a similar discrepancy in the variation of loss with lamination thickness in this range.

Table 3 shows a comparison of the indices of the flux density, the lamination thickness and the tooth-ripple frequency in relation to the eddy-current loss, as derived from experiment and from theory.

(4.2) Calculated and Measured Eddy-Current Losses

Fig. 7 shows a comparison of the calculated (fundamental frequency) and measured eddy-current losses for $B_m = 0{\cdot}8$ Wb/m^2 at speeds up to 5000 r.p.m. corresponding to tooth-ripple frequencies up to 2 kc/s for the four sets of pole stampings investigated. This comparison is also shown in Table 4 for the frequency of 1 kc/s, and here the calculated values taking account of 2nd, 3rd and 4th harmonics are also given. Corresponding values calculated from Gibbs's and from Carter's[10] formulae are included.

It will be noted that both Gibbs's* and Carter's formulae give results which differ considerably from the measured losses, the former predicting somewhat higher losses and the latter only fractions of the measured values. Moderate agreement is obtained between the measured results and the values calculated from the present formulae for the two sets of thick stampings ($h = 1{\cdot}625$ and $3{\cdot}18$ mm). For the other two sets of thinner stampings ($h = 0{\cdot}406$ and $0{\cdot}635$ mm), however, the measured losses are shown to be substantially higher than the calculated losses.

Referring to the estimation of harmonic losses, it should be mentioned that the harmonic flux amplitudes from which these have been calculated were experimentally determined. The fundamental and harmonic frequency component e.m.f.'s induced in a single search wire on the pole-face were measured by an electronic wave analyser. The 2nd, 3rd and 4th harmonic flux densities as percentages of the fundamental were 40·5%, 5·8% and 10%, respectively.

It has long been realized that the eddy-current loss in thin laminations is invariably found to be considerably higher than that predicted from classical formulae. A loss anomaly factor of about 2 or 3 has been commonly observed in experiments on low-silicon sheet steels with approximately the same thickness as the two sets of thin laminations employed in the present investigation. This problem has been discussed by a number of authors,[11–13] but general theory concerning its cause is still incomplete.

Table 4

COMPARISON OF CALCULATED AND MEASURED EDDY-CURRENT LOSSES

Method of determination	Eddy-current loss per unit pole-face area			
	0·4% silicon sheet steel		C.R.C.A. sheet steel	
	$h = 0{\cdot}406$ mm	$h = 0{\cdot}635$ mm	$h = 1{\cdot}625$ mm	$h = 3{\cdot}18$ mm
	$h/d = 1{\cdot}37$	$h/d = 2{\cdot}14$	$h/d = 5{\cdot}40$	$h/d = 10{\cdot}57$
	kW/m^2	kW/m^2	kW/m^2	kW/m^2
Measured value	2·00	3·44	10·08	21·00
Present formula:				
Fundamental only	0·68	1·64	9·95	17·90
Fundamental, 2nd, 3rd, 4th harmonics	1·01	2·52	13·4	20·0
Gibbs's formula	—	—	24·00	46·95
Carter's formula	0·01	0·04	0·50	2·06

$s = 0{\cdot}954 \times 10^{-2}$ m $g = 0{\cdot}127 \times 10^{-2}$ m $\lambda = 2{\cdot}627 \times 10^{-2}$ m
$\omega = 2\pi \times 1000$ rad/sec $B_m = 0{\cdot}8$ Wb/m^2 $\beta_1 = 0{\cdot}28$ Speed = 2500 r.p.m.

(5) CONCLUSION

In the comparison between theory and test, moderate agreement has been obtained in the case of coarsely laminated pole shoes, both in the magnitude of the eddy-current loss and in the characteristic variation of loss with flux density, frequency and lamination thickness. Marked discrepancies, however, have been found to exist between theoretical and experimental results in the case of finely laminated pole shoes, the experimental loss being found to exceed the theoretical loss by a factor of about 2 for the thinnest laminations. It is believed that the experimental results are reliable, and that the assumptions in the theoretical solutions are justified. Although it would not be justifiable on the evidence available to suggest reasons for this deviation with thin laminations, it is worth noting that this phenomenon is not inconsistent with that normally described as anomalous losses in magnetic sheet materials.

Tooth-ripple eddy-current losses are normally small fractions of the total losses in alternators, even in the coarsely laminated pole shoes commonly employed. The present work cannot therefore be regarded as contributing towards any appreciable improvement in the efficiency of electrical machines. The results do, however, suggest that prediction of losses may become practicable on a valid theoretical basis rather than the empirical or semi-empirical basis which has been customary in the past.

* Gibbs's formula is applicable only when $h \geqslant 0{\cdot}8$ mm. In the present units and notation, Gibbs's general formula for eddy-current loss per unit area of laminated pole-face can be written

$$P_e = \frac{2{\cdot}23(\beta_1 B_m)^2 f_r^{3/2} \lambda h}{(\rho\mu)^{1/2}} \text{ watts per square metre.}$$

It should be noted that Gibbs's flux-oscillation factor, β_2, in which the effect of harmonic losses is incorporated, is invalid for the calculation of eddy-current loss in laminated pole shoes. This results from the fact that flux penetration in laminated pole shoes is not confined within the characteristic depth, as has been assumed by Gibbs.

(6) ACKNOWLEDGMENTS

The authors would like to thank the British Electrical and Allied Industries Research Association for their interest and support for the work. Dr. Sathirakul gratefully acknowledges the receipt of a scholarship from the Government of Thailand, which enabled him to undertake this work. Thanks are also due to Associated Electrical Industries (Rugby), Ltd., for providing the pole stampings used in the experimental work, and to Mr. K. F. Raby of that company for his suggestions and interest.

(7) LIST OF REFERENCES

(1) BONDI, H., and MUKHERJI, K. C.: 'An Analysis of Tooth-Ripple Phenomena in Smooth Laminated Pole-Shoes', *Proceedings I.E.E.*, Monograph No. 225 S, February, 1957 (**104** C, p. 349).

(2) GREIG, J., and MUKHERJI, K. C.: 'An Experimental Investigation of Tooth-Ripple Flux Pulsations in Smooth Laminated Pole-Shoes', *ibid.*, Monograph No. 223 S, February, 1957 (**104** C, p. 332).

(3) GIBBS, W. J.: 'Tooth-Ripple Losses in Unwound Pole-Shoes', *Journal I.E.E.*, February, 1947, **94**, Part II, p. 2.

(4) ADAMS, C. A., *et al.*: 'Pole-Face Losses', *Transactions of the American I.E.E.*, 1909, **28**, p. 1133.

(5) ASTON, K., and RAO, M. V. K.: 'Pole-Face Losses due to Open Slots', *Journal I.E.E.*, June, 1941, **88**, Part II, p. 223.

(6) ASTON, K., and RAO, M. V. K.: 'Pole-Face Losses due to Open Slots on Grooved and Ungrooved Faces', *Proceedings I.E.E.*, Monograph No. 66 U, June, 1953 (**100**, Part IV, p. 104).

(7) GREIG, J., and SATHIRAKUL, K.: 'Pole-Face Losses in Alternators. An Investigation of Eddy-Current Losses in Laminated Pole Shoes', E.R.A. Report Ref. Z/T 121, 1960.

(8) 'Magnetic Materials for Use under Combined D.C. and A.C. Magnetization', B.S. 933: 1941.

(9) SPOONER, T., and KINNARD, I. F.: 'Surface Iron Losses with reference to Laminated Materials', *Transactions of the American I.E.E.*, 1924, **43**, p. 262.

(10) CARTER, G. W.: 'A Note on the Surface Loss in a Laminated Pole-Face', *Proceedings I.E.E.*, Monograph No. 123, March, 1955 (**102** C, p. 217).

(11) BRAILSFORD, F.: 'Investigation of the Eddy-Current Anomaly in Electrical Sheet Steels', *Journal I.E.E.*, February, 1948, **95**, Part II, p. 38.

(12) STEWART, K. H.: 'Losses in Electrical Sheet Steel', *Proceedings I.E.E.*, Paper No. 785 M, April, 1950 (**97**, Part II, p. 121).

(13) ASPDEN, H.: 'An Investigation of the Eddy-Current Anomaly in a Low-Silicon Sheet Steel', *ibid.*, Monograph No. 187 M, July, 1956 (**104** C, p. 2).

(8) APPENDIX

Complete Results of Eddy-Current Loss Equation

In eqns. (1) and (2), the complete results of the loss components are as follows:

$$(A) = \frac{h\lambda\omega^{3/2}}{16\sqrt{2}\sqrt{(\rho\mu)}\hat{\sigma}^2}\left[\frac{\sinh(h/\sqrt{2d}) - \sin(h/\sqrt{2d})}{\sinh^2(h/2\sqrt{2d}) + \sin^2(h/2\sqrt{2d})}\right]$$

$$(B) = -\frac{\sqrt{(\rho\omega)}}{\mu^{3/2}\hat{\sigma}^2}\mathscr{R}\left[\gamma\coth\frac{(1-j)h}{2\sqrt{2d}}\sum_{m\,\mathrm{odd}}^{\infty}\frac{1}{(\theta_m\theta_m'^2)}\right]$$

$$(C) = -\frac{2\pi\rho}{h\mu^2\hat{\sigma}^2}\mathscr{R}\left[\sum_{n=1}^{\infty}\frac{n}{(\bar{\alpha}_n\bar{\theta}_n'^2)}\right]$$

$$(D) = \frac{8\sqrt{2}\pi^2\rho^2}{h^2\lambda\omega\mu^3\hat{\sigma}^2}\mathscr{R}\left\{(1-j)\gamma\left[\sum_{m\,\mathrm{odd}}^{\infty}\frac{1}{(\theta_m\theta_m'^2)}\right]\left[\sum_{n=1}^{\infty}\frac{n}{(\bar{\alpha}_n\bar{\theta}_n'^2)}\right]\right\}$$

$$(E) = \frac{h^2\omega^{3/2}\hat{\gamma}^2}{\pi^2\sqrt{(\rho\mu)}\hat{\sigma}^2}\mathscr{R}\left[\sum_{m\,\mathrm{odd}}^{\infty}\frac{1}{(m^2\theta_m\bar{\theta}_m'^2)}\right]$$

$$(F) = \frac{\sqrt{(\rho\omega)}}{\mu^{3/2}\hat{\sigma}^2}\mathscr{R}\left[\gamma\coth\frac{(1-j)h}{2\sqrt{2d}}\sum_{m\,\mathrm{odd}}^{\infty}\frac{1}{(\theta_m\bar{\theta}_m'^2)}\right]$$

$$(G) = \frac{\sqrt{(\rho\omega)}}{\mu^{3/2}\hat{\sigma}^2}\mathscr{R}\left[j\sum_{n=1}^{\infty}\frac{\theta_n}{(\hat{\alpha}_n^2\theta_n'^2)}\right]$$

$$(H) = \frac{2\pi\rho}{h\mu^2\hat{\sigma}^2}\mathscr{R}\left[\sum_{n=1}^{\infty}\frac{n}{(\bar{\alpha}_n\theta_n'^2)}\right]$$

$$(I) = \frac{8\sqrt{2}\rho}{\lambda\mu^2\hat{\sigma}^2}\mathscr{R}\left[(1-j)\gamma\sum_{m\,\mathrm{odd}}^{\infty}\sum_{n=1}^{\infty}\frac{n(\bar{\theta}_n'^2 - \theta_m'^2)}{(m^2-4n^2)(\theta_m\theta_{mi}'^2\bar{\theta}_n'^2\bar{\alpha}_n)}\right]$$

$\bar{\alpha}_n$, $\bar{\theta}_n'$ and $\bar{\theta}_m'$ are the complex conjugates of α_n, θ_n' and θ respectively; $\hat{\alpha}_n$ is the modulus of α_n; other symbols are already explained in the text.

621.391:621.376.4

The Institution of Electrical Engineers
Monograph No. 405 E
Oct. 1960

AUDIO COMMUNICATION WITH ORTHOGONAL TIME FUNCTIONS

By HENNING F. HARMUTH, Dipl.Ing., Dr.Tech.

The paper was first received 1st January, and in revised form 7th May, 1960. It was published as an INSTITUTION MONOGRAPH *in October, 1960.)*

SUMMARY

An audio signal may be decomposed into components having certain frequency and phase. Half the information of the signal is contained in the phase of the frequency components. Since the human ear is almost insensitive to phase, one may eliminate the phase information without causing a noticeable reduction in the signal quality. The elimination of the phase information implies a permissible reduction of the bandwidth required for the transmission of the signal to one-half and a reduction of the signal power by 3 dB without increase of distortions due to additive white normal noise. A method for the elimination of the phase information is based on the decomposition of the audio signal by correlation with a set of orthogonal functions. These correlations yield for each orthogonal function one coefficient which is represented by a voltage. One may process these coefficients in analogue or digital computers to reduce further the bandwidth required for the transmission of audio signals with certain spectral distribution, e.g. voice signals.

(1) INTRODUCTION

Audio signals may be decomposed into components having certain frequency and phase. One-half of their information is contained in the phase of the frequency components, since any oscillation may occur in two phases that are orthogonal to each other, e.g. as $\sin \omega t$ or $\cos \omega t$. The human ear is insensitive to the phase according to Helmholtz's theory of hearing, although a slight phase sensitivity is observed. Elimination of the phase information thus hardly reduces the quality of an audio signal: on the other hand, it permits the reduction of bandwidth and signal power in a communication channel to one-half or a doubling of the playing time of a gramophone record.

In order to analyse signals of such variety as audio signals it is convenient to represent them by a superposition of orthogonal functions. In this way the time variation of the signals is replaced by that of the orthogonal functions, which is the same for all signals, while the signals are characterized by the amplitude coefficients of the orthogonal functions. The analysis of the transmission of all possible audio signals through a linear system is thus equivalent to the much simpler analysis of the transmission of the orthogonal functions.

The experimental decomposition of audio signals by sets of orthogonal functions is in general rather difficult, since multipliers are required which work over the whole frequency range and which have in addition a sufficiently large dynamic range. These two requirements can be met economically by using silicon diodes in a ring modulator circuit as multiplier. Certain coefficients, represented by voltages, result from the decomposition and these equal the correlation between the orthogonal functions and the signal. This representation of the signals by a set of voltages permits complicated mathematical operations on the signal to be performed in a simple way. For instance, a variable voltage-divider replaces a filter with variable attenuation. More generally, one may feed these sets of voltages into a computer and obtain a flexibility for scientific investigations that cannot be equalled by filtering of the original signal.

The following analysis discusses the decomposition and recomposition of audio signals by orthogonal time functions and the application of this technique to the elimination of the phase information from the signals.

(2) GENERAL THEORY

Consider a time function $f(t)$ in the interval $-\frac{1}{2}\tau \leqslant t \leqslant \frac{1}{2}\tau$. In general, such a function can be represented by an expansion into a set of functions $F_n(t)$ which are orthogonal in this interval:

$$f(t) = \sum_{n=-\infty}^{\infty} a_n F_n(t) \quad . \quad . \quad . \quad . \quad . \quad (1)$$

$$a_n = \frac{1}{\tau}\int_{-\tau/2}^{\tau/2} f(t)F_n(t)dt \quad . \quad . \quad . \quad . \quad . \quad (2)$$

$$W^{-1}\int_{-\tau/2}^{\tau/2} F_n(t)F_k(t)dt = \delta_{nk} = \begin{cases} 1 \text{ for } n = k \\ 0 \text{ for } n \neq k \end{cases} \quad . \quad . \quad (3)$$

The decomposition of the time function $f(t)$ into coefficients a_n is called time sampling if the functions $F_n(t)$ are the delta functions[1,2] $\delta(t - t_n)$, i.e.

$$a_n = \int_{-\infty}^{\infty} f(t)\delta(t - t_n)dt = f(t_n)$$

Let $f(t)$ stand for an audio message represented, for instance, by the output voltage of a microphone. τ may then equal the duration of this message and be arbitrarily large.

For a certain set of orthogonal functions, $F_n(t)$, the time function $f(t)$ is specified by the values of the coefficients a_n and only these coefficients have to be transmitted in a communication system. To perform this transmission one may multiply the function $G_n(t')$ of a set which is orthogonal in the interval $-\frac{1}{2}\tau \leqslant t \leqslant \frac{1}{2}\tau$ with the coefficients a_n and transmit the sum $\phi(t')$:

$$\phi(t') = \sum_{n=-\infty}^{\infty} a_n G_n(t') \quad . \quad . \quad . \quad . \quad . \quad (4)$$

At the receiver the coefficients a_n are recovered from eqn. (4) by correlation:

$$W^{-1}\int_{-\tau/2}^{\tau/2} G_m(t') \sum_{n=-\infty}^{\infty} a_n G_n(t')dt' = a_n\delta_{nm} \quad . \quad . \quad (5)$$

The original time function, delayed by a certain time, is obtained by multiplying the coefficients a_n by the functions $F_n(t'')$ and taking the sum [eqn. (1)]. The functions $F_n(t'')$ are delayed by at least 2τ compared with the functions $F_n(t)$, since two correlations over an interval of duration τ are performed in eqns. (2) and (5). To simplify the notation no primes will be written for the delayed functions $G_n(t')$ and $F_n(t'')$.

Fig. 1 shows the block diagram of an audio communication system using orthogonal functions.

Since the functions $G_n(t)$ are orthogonal there is no redundancy in the transmitted signal $\phi(t)$. Redundancy may be introduced

Correspondence on Monographs is invited for consideration with a view to publication.

Dr. Harmuth is in the Research Division, Stromberg-Carlson Co., a subsidiary of the General Dynamics Corporation, Rochester, N.Y.

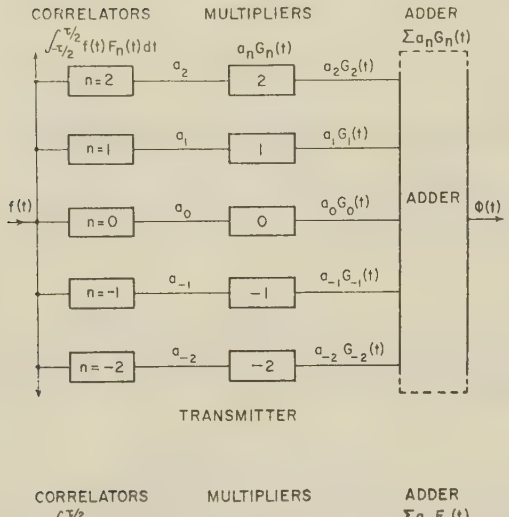

Fig. 1.—Block diagram of an audio communication system.

in two ways. First, a_n may be multiplied by several orthogonal functions, $a_n \Sigma G_i(t)$, $i = 1, 2, \ldots$ This process is equivalent to the repetition of a message. The second way is to decompose a_n in some fashion and to multiply each member of the decomposition by an orthogonal function $G_i(t)$. The best-known example of this process is the decomposition of a_n into binary digits and their transmission as a sequence of pulses.

In the special case $F_n(t) = G_n(t)$ one obtains from eqns. (4) and (1) $\phi(t) = f(t)$. In this case the transmitter of Fig. 1 is eliminated and the receiver performs the function of an ideal low-pass filter.

Consider the set of orthogonal functions $F_n(t)$ in the interval $-\infty < t < +\infty$ which are defined by the frequency spectra $A(n, \nu)$ discussed in Section 8. The first eight spectra are shown in Fig. 2. $A(n, \nu)$ is symmetric for $n = 2i$ and skew symmetric for $n = 2i + 1$. The time functions are obtained in an explicit form by applying a Fourier transformation to $A(n, \nu)$:

$$\left.\begin{aligned} F_{2i}(t) &= \frac{1}{\nu_m}\int_{-\infty}^{\infty} A(2i, \nu)\cos 2\pi\nu\theta\, d\nu \\ F_{2i+1}(t) &= \frac{1}{\nu_m}\int_{-\infty}^{\infty} A(2i+1, \nu)\sin 2\pi\nu\theta\, d\nu \\ F_0(t) &= \frac{\sin \pi\nu_m\theta}{\pi\nu_m\theta} \\ F_1(t) &= \sin \tfrac{1}{2}\pi\nu_m\theta\,\frac{\sin \pi\nu_m\theta/2}{\pi\nu_m\theta/2} \end{aligned}\right\} \quad . \quad . \quad (6)$$

where $\theta = t/\tau$, $\nu = f\tau$

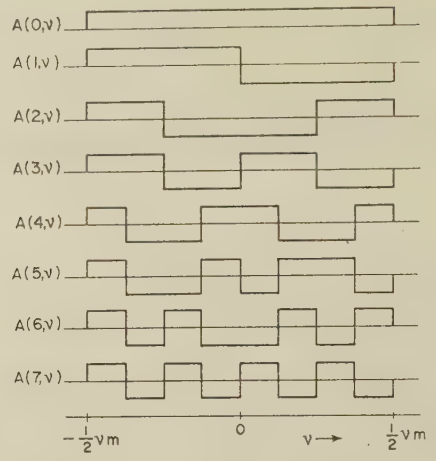

Fig. 2.—Frequency-limited orthogonal functions $A(n, \nu)$.

From the symmetry of the frequency spectra $A(2i, \nu)$ follow the symmetry of the time functions $F_{2i}(t)$; an equivalent statement holds for the spectra $A(2i + 1, \nu)$. Furthermore, the orthogonality of the frequency spectra $A(n, \nu)$ implies the orthogonality of the functions $F_n(t)$. Two frequency spectra $A(2i, \nu)$ and $A(2i + 1, \nu)$ consist of frequency components with the same amplitude but a phase difference of $\frac{1}{2}\pi$.

A time function $f(t)$ is represented by coefficients a_n which are obtained by substituting $F_n(t)$ from eqn. (6) into eqn. (2):

$$f(t) = \frac{1}{\nu_m}\sum_{i=0}^{\infty}\int_{-\infty}^{\infty}[a_{2i}A(2i, \nu)\cos 2\pi\nu\theta + a_{2i+1}A(2i+1, \nu)\sin 2\pi\nu\theta]d\nu$$

$$= \frac{2}{\nu_m}\sum_{i=0}^{\infty}\int_{0}^{\infty} A(2i, \nu)(a_{2i}\cos 2\pi\nu\theta - a_{2i+1}\sin 2\pi\nu\theta)d\nu$$

$$= \frac{2}{\nu_m}\sum_{i=0}^{\infty}\int_{0}^{\infty}(a_{2i}^2 + a_{2i+1}^2)^{1/2}A(2i, \nu)\cos(2\pi\nu\theta - \eta)d\nu \quad . \quad (7)$$

where $$\tan \eta = -a_{2i+1}/a_{2i}$$

A phase-insensitive receiver like the human ear does not make use of the information contained in η and there is no need to transmit this information. Elimination of the phase information distorts $f(t)$ into $f_\eta(t)$:

$$f_\eta(t) = \frac{2}{\nu_m}\sum_{i=0}^{\infty}\int_{0}^{\infty}(a_{2i}^2 + a_{2i+1}^2)^{1/2}A(2i, \nu)\cos 2\pi\nu\theta\, d\nu$$

$$= \sum_{i=0}^{\infty}(a_{2i}^2 + a_{2i+1}^2)^{1/2}F_{2i}(t) \quad . \quad . \quad . \quad . \quad . \quad . \quad . \quad . \quad (8)$$

The functions $F_n(t)$ of eqns. (6) permit the phase information of $f(t)$ to be separated. Instead of transmitting the coefficients a_n individually one may thus transmit them in pairs $(a_{2i}^2 + a_{2i+1}^2)^{1/2}$, with a resulting reduction of the information rate to one-half. At the receiver the function $f_\eta(t)$ is constructed from $F_n(t)$ with either even index only—as in eqn. (8)—or odd index only. Since it would be very difficult to produce the functions defined by eqn. (6) it is necessary to find more practical ways of eliminating the phase information from $f(t)$.

(3) PHASE ELIMINATION BY TRIGONOMETRIC FUNCTIONS

Consider the functions $F_n(t)$:

$$\left.\begin{aligned} F_0(t) &= 1 \\ F_{2i-1}(t) &= \sqrt{2}\sin 2i\pi\theta \\ F_{2i}(t) &= \sqrt{2}\cos 2i\pi\theta \end{aligned}\right\} \quad . \quad . \quad . \quad .$$

$$-\tfrac{1}{2} \leqslant \theta \leqslant \tfrac{1}{2}, \qquad i = 1, 2, \ldots \qquad \theta = t/\tau$$

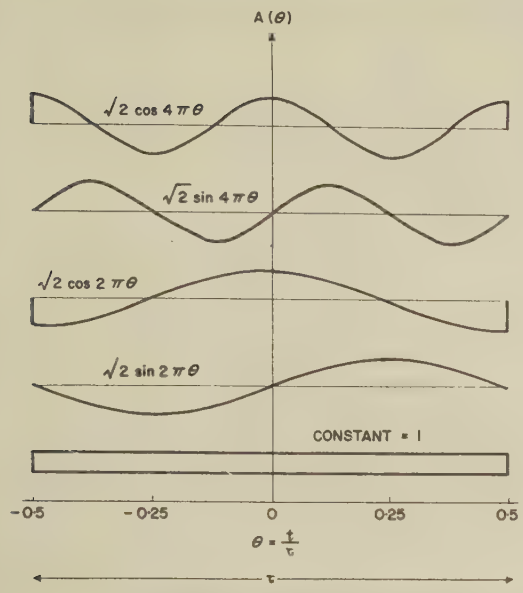

Fig. 3.—Time-limited trigonometric functions.

which are shown for $n = 0, 1, 2, 3, 4$ in Fig. 3; their frequency spectra are plotted in Fig. 4.

$$\left.\begin{aligned} \mathrm{a}(c, 0, \nu) &= \frac{\sin \pi\nu}{\pi\nu} \\ \mathrm{a}(s, i, \nu) &= \tfrac{1}{2}\sqrt{2}\left[\frac{\sin \pi(\nu - i)}{\pi(\nu - i)} - \frac{\sin \pi(\nu + i)}{\pi(\nu + i)}\right] \\ \mathrm{a}(c, i, \nu) &= \tfrac{1}{2}\sqrt{2}\left[\frac{\sin \pi(\nu - i)}{\pi(\nu - i)} + \frac{\sin \pi(\nu + i)}{\pi(\nu + i)}\right] \\ \nu &= f\tau \end{aligned}\right\} \quad . \quad (10)$$

The frequency spectra $\mathrm{a}(s, i, \nu)$ and $\mathrm{a}(c, i, \nu)$ are closely similar, but one is skew symmetric and the other symmetric. This means that these functions consist of frequency components with equal amplitudes but with phase differences of $\frac{1}{2}\pi$. Let the functions of eqn. (9) be used to decompose a voice signal $\mathrm{f}(t)$ with frequency components between 0·3 and 3 kc/s. The period may be chosen as 3·3 millisec. The number of functions required to represent $\mathrm{f}(t)$ can be inferred from Fig. 4. $\mathrm{F}_0(t)$ has practically all its energy below $f = \nu/\tau = 1/\tau = 0{\cdot}3$ kc/s, which is below the required band. $\mathrm{F}_1(t)$ and $\mathrm{F}_2(t)$ have their maximum at about $\nu/\tau = 0{\cdot}3$ kc/s, $\mathrm{F}_{19}(t)$ and $\mathrm{F}_{20}(t)$ at $\nu/\tau = 3$ kc/s. $\mathrm{f}(t)$ will thus be represented with great accuracy by the expansion:

$$\mathrm{f}(t) = \sum_{i=1}^{10} [a_{2i}\mathrm{F}_{2i}(t) + a_{2i-1}\mathrm{F}_{2i-1}(t)] \quad . \quad . \quad (11)$$

$$\left.\begin{aligned} a_{2i} &= \sqrt{2}\int_{-1/2}^{1/2} \mathrm{f}(t) \cos 2i\pi\theta d\theta \\ a_{2i-1} &= \sqrt{2}\int_{-1/2}^{1/2} \mathrm{f}(t) \sin 2i\pi\theta d\theta \end{aligned}\right\} \quad . \quad . \quad . \quad (12)$$

The Fourier integrals of eqn. (12) yield the correlations between the signal $\mathrm{f}(t)$ and the functions $\cos 2i\pi\theta$ and $\sin 2i\pi\theta$. The resulting twenty coefficients a_{2i}, a_{2i-1} are reduced to ten coefficients $(a_{2i}^2 + a_{2i-1}^2)^{1/2}$ as shown in Fig. 5, where the notation $\omega = 2\pi/\tau$ is used.

At the receiver the ten functions $\mathrm{F}_{2i}(t) = \sqrt{2} \cos i\omega t$, $i = 1, \ldots 10$, are multiplied by the coefficients $(a_{2i}^2 + a_{2i-1}^2)^{1/2}$; the sum of the resulting products is the wanted time function $\mathrm{f}_r(t)$:

$$\mathrm{f}_r(t) = \sum_{i=1}^{10} (a_{2i}^2 + a_{2i-1}^2)^{1/2}\mathrm{F}_{2i}(t)$$

The coefficients are present at the points 1a–10a in analogue form, e.g. as voltages. They may be transformed into digital form and transmitted like telegraph signals. This mode of transmission has been discussed in previous papers.[6] For the transmission in analogue form reference may be made to Fig. 6.

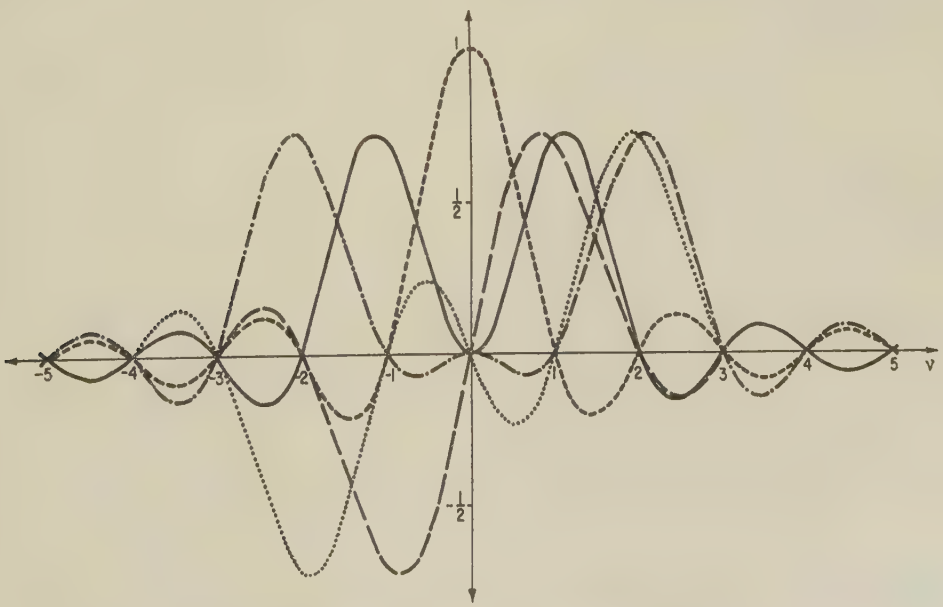

Fig. 4.—Frequency spectra of the functions of Fig. 3.

— — — — a(c, 0, ν).
—— —— a(s, 1, ν).
———— a(c, 1, ν).
..... a(s, 2, ν).
—— · —— a(c, 2, ν).

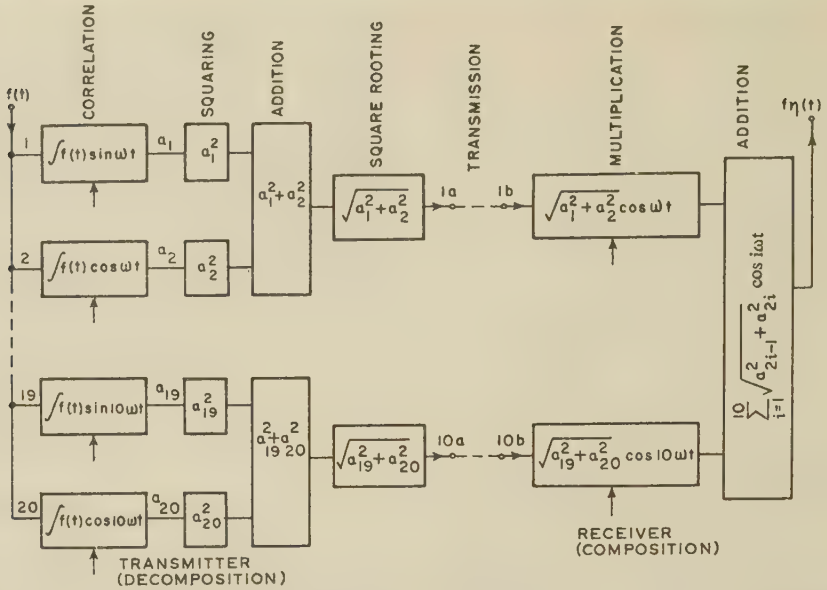

Fig. 5.—Decomposition and composition of an audio signal by time-limited trigonometric functions.

The functions $G_n(t)$ of an orthogonal set, e.g. those defined by eqn. (9), are multiplied by $(a_{2i}^2 + a_{2i-1}^2)^{1/2}$ and the sum

$$\phi(t) = \sum_{\substack{n=1 \\ i = i(n)}}^{10} (a_{2i}^2 + a_{2i-1}^2) F_n(t) \quad . \quad . \quad . \quad (13)$$

is transmitted. The coefficients are recovered at the receiver by correlation:

$$(a_{2i}^2 + a_{2i-1}^2)^{1/2} = K \int_{-1/2}^{1/2} \phi(t) F_n(t) d\theta$$

A saving in equipment is obtained if the functions of eqn. (9) are used for the transmission in the sequence shown by Fig. 6, since in this case one may omit the first five correlators in the receiver of Fig. 6 and the first five multipliers in the receiver of Fig. 5. The function $i = i(n)$ then has the following form:

n	1	2	3	4	5	6	7	8	9	10
i	6	1	7	2	8	3	9	4	10	5

The correlation of a sample, g(t), of white normal noise with a function $G_n(t)$ of duration τ equals the integral over the noise sample after it has passed an ideal low-pass filter of bandwidth $\frac{1}{2}\tau$. Since $F_n(t)$ are orthogonal the noise contributions to f(t) at the receiver of Fig. 1 add arithmetically. If twenty functions $G_n(t)$ are used to transmit f(t) with phase information and a frequency band from 0·3 to 3 kc/s, the contribution of noise to the receiver output is the same as if the noise had passed a filter of bandwidth $20/2\tau = 3$ kc/s. If no phase information is transmitted, only ten functions $G_n(t)$ are required and the contribution of noise to the receiver output is reduced to one-half. Hence, 3 dB signal power can be saved with no resulting increase of distortion due to noise by not transmitting phase information.

(4) SINGLE-SIDEBAND MODULATION

Among the radiocommunication systems in use at present, those with single-sideband modulation require the least bandwidth. The single-sideband modulation will be investigated by means of orthogonal functions in order to compare the transmission of audio signals with and without phase information.

Consider the carrier $\sqrt{2} \cos 2\pi\nu_0\theta$ modulated by the function

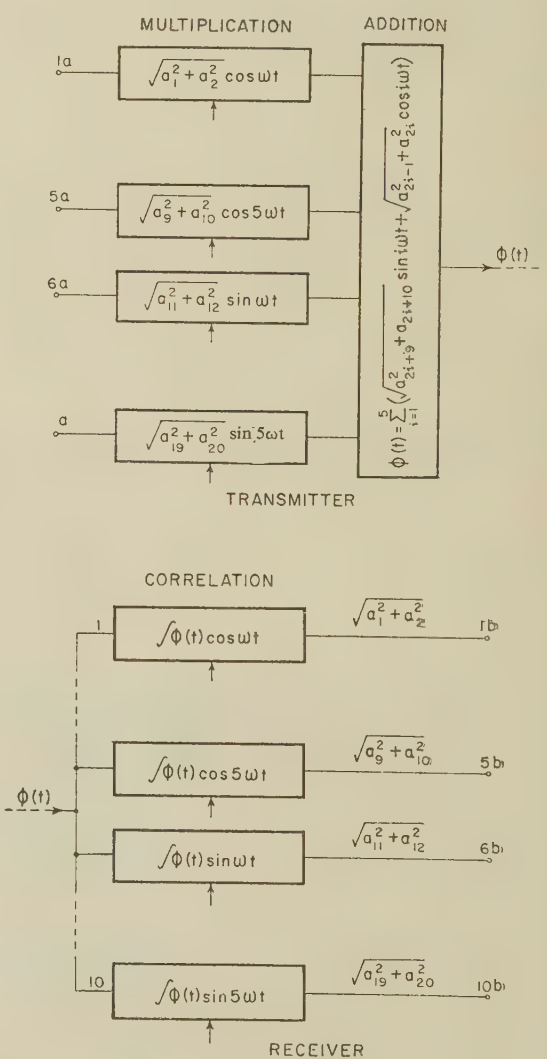

Fig. 6.—Transmission of analogue signals by time-limited trigonometric functions.

(t). Let $f(t)$ be represented by an expansion of orthogonal unctions $F_n(t)$ defined by eqn. (6):

$$\sqrt{2}f(t)\cos 2\pi\nu_0\theta = \sqrt{2}\sum_{i=0}^{\infty}[a_{2i}F_{2i}(t) + a_{2i+1}F_{2i+1}(t)]\cos 2\pi\nu_0\theta \quad . \quad (14)$$

where $\theta = t/\tau, \quad \nu_0 = f_0\tau$

The frequency spectrum $A(\nu_0, \nu)$ of eqn. (14) is obtained with the elp of eqn. (23):

$$A(\nu_0, \nu) = \tfrac{1}{2}\sqrt{2}\sum_{i=0}^{\infty}\{a_{2i}[A(2i, \nu - \nu_0) + A(2i, \nu + \nu_0)] + a_{2i+1}[A(2i+1, \nu - \nu_0) + A(2i+1, \nu + \nu_0)]\} \quad . \quad (15)$$

The spectra $A(2i, \nu \pm \nu_0)$ and $A(2i+1, \nu \pm \nu_0)$ are obtained by shifting the centres of the spectra $A(2i, \nu)$ and $A(2i+1, \nu)$ of Fig. 2 from $\nu = 0$ to $\nu = \pm \nu_0$.

Let the lower sideband of $A(\nu_0, \nu)$ be eliminated by a filter. The resulting frequency spectra $A^*(2i, \nu \pm \nu_0)$ and $A^*(2i+1, \nu \pm \nu_0)$ may be represented as follows:

$$\left.\begin{aligned} A^*(2i, \nu - \nu_0) &= \tfrac{1}{2}[A(2i, \nu - \nu_0) - A(2i+1, \nu - \nu_0)] \\ A^*(2i+1, \nu - \nu_0) &= -\tfrac{1}{2}[A(2i, \nu - \nu_0) - A(2i+1, \nu - \nu_0)] \\ A^*(2i, \nu + \nu_0) &= \tfrac{1}{2}[A(2i, \nu + \nu_0) + A(2i+1, \nu + \nu_0)] \\ A^*(2i+1, \nu + \nu_0) &= \tfrac{1}{2}[A(2i, \nu + \nu_0) + A(2i+1, \nu + \nu_0)] \end{aligned}\right\} (16)$$

The suppression of the lower sideband transforms $A(\nu_0, \nu)$ nto $A^*(\nu_0, \nu)$ which is obtained by substitution of $A^*(n, \nu \pm \nu_0)$ or $A(n, \nu \pm \nu_0)$ in eqn. (15):

$$A^*(\nu_0, \nu) = \tfrac{1}{4}\sqrt{2}\sum_{i=0}^{\infty}\{a_{2i}[A(2i, \nu + \nu_0) + A(2i+1, \nu + \nu_0) + A(2i, \nu - \nu_0) - A(2i+1, \nu - \nu_0)] + a_{2i+1}[A(2i, \nu + \nu_0) + A(2i+1, \nu + \nu_0) - A(2i, \nu - \nu_0) + A(2i+1, \nu - \nu_0)]\} \quad . \quad . \quad . \quad (17)$$

The time function belonging to the spectrum $A^*(\nu_0, \nu)$ is obtained by inserting the time functions represented by the spectra $A(n, \nu \pm \nu_0) \pm A(n, \nu \pm \nu_0)$ as given by eqn. (23):

$$[\sqrt{2}f(t)\cos 2\pi\nu_0\theta]^* = \tfrac{1}{2}\sqrt{2}\sum_{i=0}^{\infty}\{a_{2i}[F_{2i}(t)\cos 2\pi\nu_0\theta + F_{2i+1}(t)\sin 2\pi\nu_0\theta] + a_{2i+1}[F_{2i}(t)\sin 2\pi\nu_0\theta - F_{2i+1}\cos 2\pi\nu_0\theta]\} \quad . \quad (18)$$

Demodulation of eqn. (18) by $\sqrt{2}\cos(2\pi\nu_0\theta + \phi)$ yields, after filtering out the high-frequency components,

$$\{[\sqrt{2}f(t)\cos 2\pi\nu_0\theta]^*\sqrt{2}\cos(2\pi\nu_0\theta + \phi)\}_F = f^*(t)$$

$$f^*(t) = \tfrac{1}{2}\sum_{i=0}^{\infty}\{a_{2i}[F_{2i}(t)\cos\phi - F_{2i+1}(t)\sin\phi] - a_{2i+1}[F_{2i}(t)\sin\phi + F_{2i+1}(t)\cos\phi]\}$$

The spectral composition of $f^*(t)$ is obtained by inserting $F_n(t)$ from eqn. (6):

$$f^*(t) = \frac{1}{2\nu_m}\sum_{i=0}^{\infty}[(a_{2i}\cos\phi - a_{2i+1}\sin\phi)\int_{-\infty}^{\infty}A(2i, \nu)\cos 2\pi\nu\theta d\nu - (a_{2i+1}\cos\phi - a_{2i}\sin\phi)\int_{-\infty}^{\infty}A(2i+1, \nu)\sin 2\pi\nu\theta d\nu]$$

$$= \frac{1}{\nu_m}\sum_{i=0}^{\infty}\int_0^{\infty}(a_{2i}^2 + a_{2i+1}^2)^{1/2}A(2i, \nu)\cos(2\pi\nu\theta - \eta)d\nu \quad . \quad (19)$$

where $\tan\eta = -\dfrac{a_{2i+1}\cos\phi + a_{2i}\sin\phi}{a_{2i}\cos\phi - a_{2i+1}\sin\phi}$

Comparison of eqn. (19) with eqn. (7) shows that single-sideband modulation transmits the phase information contained in η. The carrier phase does not affect the amplitude $(a_{2i}^2 + a_{2i+1}^2)^{1/2}$. For a phase-insensitive receiver the carrier $\sqrt{2}\cos 2\pi\nu_0\theta$ produced at the transmitter and the carrier $\sqrt{2}\cos(2\pi\nu_0\theta + \phi)$ produced at the receiver may have a phase difference ϕ without loss of information. This does not hold for phase-sensitive receivers, since η depends on ϕ. The bandwidth required for voice communication with single-sideband modulation may thus be reduced to one-half by modulating the carrier with $\phi(t)$ of eqn. (13) rather than with $f(t)$. As was pointed out before, this would also permit a reduction of 3 dB in the signal power without increase of distortion caused by white normal noise. The price paid for this improvement is the requirement for the phase difference ϕ to equal zero.

(5) CONCLUSIONS

The decomposition of audio signals by orthogonal functions yields a presentation of the signal by a set of quasi-constant voltages. Simple mathematical operations on these constant voltages, such as voltage division or amplification, are equivalent to filtering of the original signal, but much more complicated operations can be performed. In particular, it is possible to eliminate the phase information from the audio signals, which contains half the information of the signal but is practically of no use to the human ear. It is shown that the phase-free information can be transmitted by single-sideband modulation, but that a phase lock between the carriers produced at the transmitter and the receiver is necessary.

(6) ACKNOWLEDGMENT

The author wishes to express his appreciation to Mr. G. Lachs of the Research Division of the Stromberg–Carlson Co., Rochester, N.Y., for several helpful discussions, and to Mr. B. Gray of the same company for the development of diode multipliers. Furthermore, he wants to direct attention to the work of Mr. G. Franco, also of Stromberg–Carlson Co., on the experimental decomposition of audio signals by orthogonal functions.

(7) REFERENCES

(1) GOODALL, W. M.: 'Telephony by Pulse Code Modulation', *Bell System Technical Journal*, 1947, **26**, p. 395.

(2) OLIVER, B. M., PIERCE, J. R., and SHANNON, C. E.: 'The Philosophy of P.C.M.', *Proceedings of the Institute of Radio Engineers*, 1948, **36**, p. 1324.

(3) GABOR, D.: 'New Possibilities in Speech Transmission', *Journal I.E.E.*, 1947, **94**, Part III, p. 369; Discussion, see 1948, **95**, Part III, p. 39.

(4) DUDLEY, H.: 'Remaking Speech', *Journal of the Acoustical Society of America*, 1939, **11**, p. 165.

(5) HALSEY, R. J., and SWAFFIELD, J. S.: 'Analysis-Synthesis Telephony, with special reference to the Vocoder', *Journal I.E.E.*, 1948, **95**, Part III, p. 391.

(6) HARMUTH, H. F.: 'Orthogonal Codes', *Proceedings I.E.E.*, Monograph No. 369 E, March, 1960 (**107** C, p. 242).

(8) APPENDIX

(8.1) The Functions A(n, ν)

The function A(0, $k\nu$) is defined by

$$\mathrm{A}(0, k\nu) = \left\{ \begin{array}{l} 0 \text{ for } -\nu_m/2k > \nu \\ 1 \text{ for } -\nu_m/2k \leqslant \nu \leqslant \nu_m/2k \\ 0 \text{ for } \quad \nu_m/2k < \nu \end{array} \right\} . \quad . \quad (20)$$

$$\mathrm{A}(0, k\nu) = \mathrm{A}(0, -k\nu)$$

The notation A(0, $\nu - \nu_1$) is used to represent the function A(0, ν) with its centre shifted from $\nu = 0$ to $\nu = \nu_1$. One may write the functions A(n, ν) as follows (Fig. 2):

$$\left.\begin{array}{l} \mathrm{A}(0, \nu) = \mathrm{A}[0, 2(\nu + \nu_m/4)] + \mathrm{A}[0, 2(\nu - \nu_m/4)] \\ \mathrm{A}(1, \nu) = \mathrm{A}[0, 2(\nu + \nu_m/4)] - \mathrm{A}[0, 2(\nu - \nu_m/4)] \\ \mathrm{A}(2, \nu) = \mathrm{A}[1, 2(\nu + \nu_m/4)] - \mathrm{A}[1, 2(\nu - \nu_m/4)] \\ \mathrm{A}(3, \nu) = \mathrm{A}[1, 2(\nu + \nu_m/4)] + \mathrm{A}[1, 2(\nu - \nu_m/4)] \\ \quad \vdots \\ \mathrm{A}(2i, \nu) = \mathrm{A}[i, 2(\nu + \nu_m/4)] + (-1)^i \mathrm{A}[i, 2(\nu - \nu_m/4)] \\ \mathrm{A}(2i+1, \nu) = \mathrm{A}[i, 2(\nu + \nu_m/4)] - (-1)^i \mathrm{A}[i, 2(\nu - \nu_m/4)] \end{array}\right\} . \quad (21)$$

A($2i$, ν) is an even function of ν and A($2i + 1$, ν) an odd function. The orthogonality of A($2i$, ν) and A($2i + 1$, ν),

$$\int_{-\infty}^{\infty} \mathrm{A}(2i, \nu)\mathrm{A}(2i + 1, \nu)d\nu = 0$$

is a consequence of the symmetry of A($2i$, ν) and the skew-symmetry of A($2i + 1$, ν). To show the orthogonality of A($2i$, ν), A($2i + 1$, ν) and A($2k$, ν), A($2k + 1$, ν) it suffices to show the orthogonality of A$[i, 2(\nu - \frac{1}{4}\nu_m)]$ and A$[k, 2(\nu - \frac{1}{4}\nu_m)]$, since A$[n, 2(\nu + \frac{1}{4}\nu_m)]$ and A$[n, 2(\nu - \frac{1}{4}\nu_m)]$ are identical except for the shift $\nu \pm \frac{1}{4}\nu_m$.

$$\int_{-\infty}^{\infty} \mathrm{A}[i, 2(\nu - \nu_m/4)]\mathrm{A}[k, 2(\nu - \nu_m/4)]d\nu$$

$$= \int_{-\infty}^{\infty} \mathrm{A}(i, 2\nu)\mathrm{A}(k, 2\nu)d\nu = \tfrac{1}{2}\int_{-\infty}^{\infty} \mathrm{A}(i, \nu)\mathrm{A}(k, \nu)d\nu \quad . \quad (22)$$

The last integral is zero if i is odd and k even or vice versa, owing to the symmetry or skew symmetry of A(n, ν) for even or odd numbers n. If i and k are even one may repeat the transition [eqn. (22)] for $i/2$, $k/2$. If i and k are odd one may do the same for $(i - 1)/2$, $(k - 1)/2$. After the transition has been repeated sufficiently often one will arrive either at i (k) even and k (i) odd or at i (k) zero. The proof of orthogonality is thus completed if the integral

$$\int_{-\infty}^{\infty} \mathrm{A}(0, \nu)\mathrm{A}(n, \nu)d\nu = \int_{-\infty}^{\infty} \mathrm{A}(n, \nu)d\nu = 0 \quad n \neq 1$$

is shown to hold. This integral is zero since all functions A(n, ν) are obtained by contracting, shifting and multiplying by ± 1 the function A(1, ν), and $\int_{-\infty}^{\infty} \mathrm{A}(1, \nu)d\nu = 0$ is seen to hold from Fig. 2.

The orthogonal set of functions A(n, ν) is related to an orthogonal set of time functions $\mathrm{F}_n(t)$ by the Fourier integrals

$$\int_{-1/2}^{1/2} \mathrm{F}_{2i}(t) \cos 2\pi\nu\theta d\theta = \mathrm{A}(2i, \nu)$$

$$\int_{-1/2}^{1/2} \mathrm{F}_{2i+1}(t) \sin 2\pi\nu\theta d\theta = \mathrm{A}(2i + 1, \nu)$$

Multiplication of the functions $\mathrm{F}_n(t)$ by $\sqrt{2} \cos 2\pi\nu_0\theta$ or $\sqrt{2} \sin 2\pi\nu_0\theta$ produces the following frequency spectra:

$$\left.\begin{array}{l} \sqrt{2}\int_{-1/2}^{1/2} \mathrm{F}_{2i}(t) \cos 2\pi\nu_0\theta \cos 2\pi\nu\theta d\theta \\ \qquad = \frac{1}{2}\sqrt{2}[\mathrm{A}(2i, \nu - \nu_0) + \mathrm{A}(2i, \nu + \nu_0)] \\ \sqrt{2}\int_{-1/2}^{1/2} \mathrm{F}_{2i}(t) \sin 2\pi\nu_0\theta \sin 2\pi\nu\theta d\theta \\ \qquad = \frac{1}{2}\sqrt{2}[\mathrm{A}(2i, \nu - \nu_0) - \mathrm{A}(2i, \nu + \nu_0)] \\ \sqrt{2}\int_{-1/2}^{1/2} \mathrm{F}_{2i+1}(t) \cos 2\pi\nu_0\theta \sin 2\pi\nu\theta d\theta \\ \qquad = \frac{1}{2}\sqrt{2}[\mathrm{A}(2i + 1, \nu - \nu_0) + \mathrm{A}(2i + 1, \nu + \nu_0)] \\ \sqrt{2}\int_{-1/2}^{1/2} \mathrm{F}_{2i+1}(t) \sin 2\pi\nu_0\theta \cos 2\pi\nu\theta d\theta \\ \qquad = -\frac{1}{2}\sqrt{2}[\mathrm{A}(2i + 1, \nu - \nu_0) - \mathrm{A}(2i + 1, \nu + \nu_0)] \end{array}\right\} (23$$

621.313.333.012.8

The Institution of Electrical Engineers
Monograph No. 406 U
Oct. 1960

THE PHYSICAL REALIZATION OF INDUCTION-MOTOR EQUIVALENT CIRCUITS

By N. N. HANCOCK, B.Sc.(Eng.), M.Sc.Tech., Associate Member, and B. H. KARAKARADDI, B.Sc., M.Sc.Tech.

(*The paper was first received* 19*th April, and in revised form* 13*th July*, 1960. *It was published as an* INSTITUTION MONOGRAPH *in October*, 1960.)

SUMMARY

The paper reviews the practicability of setting up physically, in the form of specialized networks, several of the equivalent circuits representing an unbalanced 2-phase induction motor. This motor is sufficiently general to include, as special cases, most induction machines with balanced secondary windings.

LIST OF SYMBOLS

I_A = Auxiliary stator-winding current.
I_B = Backward sequence component of stator-winding currents.
I_F = Forward sequence component of stator-winding currents.
I_M = Main stator-winding current.
I_a = Rotor current of Chang circuit due to auxiliary winding current.
I_b = Backward sequence component of rotor current referred to main winding.
I_f = Forward sequence component of rotor current referred to main winding.
I_m = Rotor current of Chang circuit due to main winding current.
M_B = Mutual inductance for measurement of I_B.
M_F = Mutual inductance for measurement of I_F.
R_A = Resistance of auxiliary winding.
R_M = Resistance of main winding.
R_R = Resistance of rotor winding referred to main winding.
S_A = Shunt for measurement of I_A.
V_A = Voltage applied to auxiliary winding circuit.
V'_A = Voltage produced in auxiliary winding of Morrill circuit by main winding current.
V_M = Voltage applied to main winding.
V'_M = Voltage produced in main winding of Morrill circuit by auxiliary winding current.
V_{Ab} = Voltage across backward sequence magnetizing reactance of auxiliary winding of Morrill circuit.
V_{Af} = Voltage across forward sequence magnetizing reactance of auxiliary winding of Morrill circuit.
V_{Mb} = Voltage across backward sequence magnetizing reactance of main winding of Morrill circuit.
V_{Mf} = Voltage across forward sequence magnetizing reactance of main winding of Morrill circuit.
X_A = Leakage reactance of auxiliary winding.
X_M = Leakage reactance of main winding.
X_R = Leakage reactance of rotor winding referred to main winding.
X_m = Magnetizing reactance referred to main winding.
Z_A = External impedance connected in series with auxiliary winding.
a = Turns ratio, auxiliary winding to main winding.
f = Supply frequency.
s = Fractional slip.

Correspondence on Monographs is invited for consideration with a view to publication.
Mr. Hancock is and Mr. Karakaraddi was formerly at the Manchester College of Science and Technology. Mr. Karakaraddi is now Professor of Electrical Engineering at the B.V. Bhoomraddi College of Engineering and Technology, Hubli, Mysore State, India.

(1) INTRODUCTION

Equivalent circuits of machines have long been widely used as mnemonics for the voltage equations which have been solved manually with nothing more elaborate than a slide-rule. The detailed knowledge of the performance now required in the design stage has however rendered this method inadequate. There are three devices which enable predetermination of performance to be effected more speedily: digital computers, Blackburn analysers and network analysers. It is indisputable that, apart from cost, the digital computer is the most satisfactory of the three in that, in addition to the actual performance calculation, it is capable of determining the machine parameters from the dimensions according to whatever formulae the designers favour. With both transformer and network analysers this operation has to be performed manually with slide-rule or desk calculating machine. Economics may, however, preclude the installation of a digital computer for motor design alone, and if there is no such computer otherwise available, consideration of other types is justified. Both network[1,2] and Blackburn[3–5] analysers have been applied to the determination of induction-motor performance. The purpose of the paper is to consider the practical requirements of a specialized network analyser designed to treat this one problem only.

Consideration is initially restricted to the unbalanced 2-phase motor, since this includes, as particular cases, most single- and polyphase machines. Some special cases are considered in Section 6.5.

The circuits shown relate only to machines with a single balanced polyphase secondary winding. Double-cage motors can be represented if additional circuit-elements are provided similar to those representing the secondary winding of a machine with only one such winding.

(2) REQUIREMENTS OF ANALYSER

The data for the performance calculation, whether by network or transformer analogue, comprise the machine resistances and reactances, the external impedance, if any, connected in series with the auxiliary winding, and the applied voltages. The desirability of attempting to include core loss in the equivalent circuit is controversial, and it will be assumed here that allowance will be made for it subsequently.

From this information it is required to compute, for any given values of slip, (*a*) the magnitude of the current in the main winding, (*b*) the magnitude of the current in the auxiliary winding, (*c*) the magnitude of the total current, (*d*) the phase angle of the total current (and possibly of other currents), and (*e*) the torque. It is desirable that all these can be read directly from indicating meters for each value of slip without any further calculation. It may also be desirable to read the rotor current, or, at least, its components in whatever reference system is used.

The immediate purpose is, of course, to compare the performance with that specified and thereafter to make any changes indicated to the design. For capacitor motors, the main-winding design is, in practice, more or less standardized, and the problem

consists mainly of adjusting the turns ratio of the auxiliary winding, the value of the capacitor and the rotor-winding resistance. In general the transient electrical solution is not required, the steady-state solution being sufficiently accurate for acceleration calculations since, as usual with electrical machinery, the electrical time-constants are small compared with the mechanical one.

For capacitor-start motors it is necessary to have at least part of the torque/speed curves of both capacitor and single-phase operation in order to determine the optimum speed or main-winding current at which to cut out the starting winding. This applies also to motors having different values of capacitance for starting and running, and to split-phase motors.

Some calculation of the circuit-elements from the machine constants is not particularly disadvantageous if only a little of this calculation has to be repeated when a change is made to one of the constants. For the calculation of torque/speed curves it is therefore desirable although not essential that the rotor resistance, R_R, and the slip, s, which is associated with R_R in the equations, can be varied independently. There is a high probability that a change to R_R may be required and this will involve appreciable recalculation of R_R/s, etc., if these terms have to be set directly in the analyser.

(3) EQUIVALENT CIRCUITS

The unbalanced 2-phase motor is, in its most general practical form, the capacitor motor, and much has been written on its performance determination. Morrill's[6] equivalent circuit is widely used as a basis for calculation. Kron[7] published a circuit more suitable for network analysers. Veinott[1] produced a specialized network analyser of the type considered in this paper, using an equivalent circuit of his own devising. All three circuits are based on the so-called 'revolving-field' theory. Chang[8] developed an equivalent circuit based on the 'cross-field' theory. These two theories were derived from different physical interpretations of the mode of operation of the motor. Kron[7] showed that fundamentally both theories are identical and the voltage equations of each can be derived from those of the other by a simple linear transformation. The most important differences between the two circuits lie in their ability to include departures of the actual machine from the ideal. The cross-field theory makes it possible to take differing magnetizing reactances on the two stator-winding axes, thereby allowing for any difference between the degree of saturation on these axes.

On the other hand, the revolving-field circuits make it possible to allow for the difference in resistance of the rotor winding to the two components of its current arising from the different eddy-current effects at the two frequencies, namely, sf and $(2 - s)f$.

The inclusion of core loss in the circuit is probably more justified in the cross-field case than in the revolving-field circuits.

Although it has been stated[5] that the Morrill and cross-field circuits are unsuitable for network analyser, being unsymmetrical, both can in fact be set up as networks. The Morrill circuit requires two active elements, but the cross-field circuit in the form devised by Chang[8] (given also by Kron[9]) requires only passive elements. It has been further stated[5] that the Kron circuit requires 'a good deal of auxiliary calculation' to convert from the actual to the transformed variables and vice versa, whereas the additional calculation required is merely the determination of half the difference of two complex numbers and the division of two real numbers and one complex number by the turns ratio. These divisions are necessary for a network analyser, irrespective of the circuit used, being the reference of the auxiliary winding quantities to the main winding.

(4) PRACTICAL CIRCUIT CONSIDERATIONS

(4.1) Conjugate Representation

The construction of decade inductances is difficult, an inductors of sufficiently high Q-factor are costly. It is necessary therefore, to use resistance and capacitance in place of resistanc and inductance as this will lead to circuits containing only on inductance. This change could be made in three ways:

(*a*) Using a conjugate network[10] in which inductive reactanc is replaced by capacitive reactance and vice versa. This reverse the sign of all phase angles.

(*b*) Using a network in which capacitance replaces resistanc and resistance replaces inductance. This is impractical her since a negative resistance would be required to represent th capacitor.

(*c*) Using a dual network in which the relation $v = Zi$ i replaced by the analogous $i = Yv$. This would require curren sources and hence complicates the supply problem unduly.

The conjugate network is, therefore, preferable. It neces sarily restricts the solution to the steady state but as alread noted this is acceptable for the present purpose. The use of conjugate network necessitates the conversion of three value of reactance to the equivalent capacitances. This is a sma labour compared with the calculation of the reactances them selves from the motor dimensions. Inverse-capacitance decad units are available up to $1\,\mu$F, but the use of these would undul restrict the impedance level and, to be of any advantage, woul require the frequency to be a multiple of $1/\pi$.

(4.2) Impedance Level

The circuit will obviously have to be designed with an impe dance several or even many times that of the actual machines The use of a per unit system does not appear to be necessar and would require more calculation prior to setting up th analyser. A simple scale factor is adequate, but it must b chosen sufficiently low for voltage dividers to be used in th torque measurement without appreciable loading of the networ and for the smallest significant capacitance to be well abov stray-capacitance level; and sufficiently high for the regulatio of the supply and switch-contact resistances (of which there ar many) to be negligible, and for the physical size of the capacitor required not to be an embarrassment.

(4.3) Current and Voltage Level

If the impedance level is fixed, the voltage and current level are interdependent. The voltage level must be high enough t give voltages across shunts sufficiently high for noise not to b a source of error without the shunt resistance becoming a inconveniently high proportion of the circuit resistance. O the other hand, the currents must be low enough not to caus difficulties by overloading the supply units, by causing appre ciable regulation or by overheating the network resistors.

A further practical consideration is that it is necessary t represent voltages $V_A/\sqrt{2}a$ or V_A/a. Since a may be as low a $0{\cdot}5$, it is important to choose a voltage scale which will no make the voltage corresponding to this inconveniently large.

(4.4) Choice of Frequency

All circuits considered require a 2-phase supply, which, t avoid phase shifts on load, must have a low source impedance Operation at standard supply frequency enables this requiremen to be met by Scott- and Leblanc-connected transformers followe by variable-ratio auto-transformers to permit voltage adjustment However, operation at standard frequency increases the poten tiality of stray pick-up to cause errors in the amplifier meters

ius making a higher power level necessary. The alternative of peration at other than standard frequency complicates the ower supply equipment.

(4.5) Auxiliary Winding

There appears to be no reasonable alternative but to refer all auxiliary-winding quantities to the main winding by calculation. his applies, irrespective of the circuit used, to the winding npedance, its applied voltage, and the shunt used for measuring s current. By varying the resistance of the shunt in this manner ne meter gives the actual current directly. This technique is ssential for the measurement of the total current, which is the ector sum of the actual currents of both windings.

(4.6) Rotor Winding

The rotor winding is conventionally referred to the main vinding in all cases.

(4.7) Resistances

The only resistances requiring special consideration are those epresenting the rotor branches of the circuit. These are of the orm R_R/s and either $R_R/(2-s)$ or $R_R/(1-s)$, according to he circuit used. It is considered to be one of the requirements hat, to avoid the necessity for calculating these, it should be ossible to set R_R and s separately into the network. This can e done by using several decade units for R_R which are set imultaneously by one set of 'R_R' dials. These are then selected nd connected in parallel by 's' dials. For example, let the 'R_R' dials set the eight resistances $100R_R$, $50R_R$, $50R_R$, $20R_R$, $10R_R$, $5R_R$, $5R_R$ and $2R_R$. By suitable paralleling by two decade 's' switches, all values of R_R/s from $s=1$ to $s=0$ can be obtained in 0·01 steps.

An exactly similar set switched in the opposite sequence will set $R_R/(1-s)$ from $s=1$ to $s=0$.

To set $R_R/(2-s)$ one extra resistance unit, R_R, is required to cover the range $s=1$ to $s=0$. This unit is not required for $R_R/(2-s)$ between $s=2$ and $s=1$ and it may therefore be used for R_R/s over this range of slip, so that normal motoring and plugging can be covered. However, since negative resistance is excluded, it is not possible to represent super-synchronous speeds, either in the same or in the opposite direction to the field, by revolving-field circuits since they involve both R_R/s and $R_R/(2-s)$. With the cross-field circuit which involves R_R/s and $R_R/(1-s)$ the range is restricted to the motoring condition.

This scheme of setting the rotor resistances is admittedly extravagant in switches and resistors, and its value has to be assessed by considering the saving of time which results from removing the necessity of calculating these resistances.

(4.8) Inductance

The use of the conjugate network reduces the number of inductances required to one—that corresponding to the capacitor. The inductors must be arranged with decade tappings and their design is necessarily a compromise between linearity with current, high Q-factor and reasonable physical size.

(5) MEASUREMENT TECHNIQUES

(5.1) Currents

(5.1.1) Magnitude.

Current magnitudes are most conveniently measured by shunts, the voltages across which are amplified by a feedback amplifier connected to a voltmeter. The resistance of the shunt may be adjusted to allow for the turns ratio for those currents which are 'referred' in the network. However, irrespective of the circuit employed, to measure the magnitude and phase of the total current it is necessary to measure the sum of two currents, one, and only one, of which is, in the network, in quadrature with the corresponding current in the actual machine. Its signal voltage, therefore, has to be phase shifted by 90° before the summation. This can be accomplished by using a mutual inductance in place of a shunt for this part of the network. This method has the further advantage that the secondary winding of the mutual inductance is not connected electrically to the part of the circuit of which it is measuring the current, and it may therefore be connected in series with a shunt in another part of the network to effect the summation.

(5.1.2) Phase.

Many electronic devices for measuring the phase angle between two sinusoidal voltages have been described. The only particular requirement here is that the meter must accept the signal corresponding to a current which varies over a wide range of magnitude. It is not acceptable to have to make manual adjustments of amplifier gain to compensate for this, and hence this signal voltage must be chopped and amplified sufficiently to give a square wave with an adequately steep side over a sufficiently wide range of input-voltage amplitude. Stray pick-up is very important when the motor current is small, having more effect on the phase than on the magnitude of the signal in some operating conditions.

(5.1.3) Effect of Harmonics.

The circuit in conjugate form is an RC network and therefore results in a higher harmonic content in the currents than in the supply voltage. In addition, the mutual inductance used for current measurement is a differentiating element which increases the magnitude of the harmonics relative to that of the fundamental in proportion to their order. Any high harmonic, such as a tooth-ripple, present in the supply voltage therefore appears at the amplifier terminals with an amplitude considerably increased relative to that of the fundamental. Whilst the fundamental component is reasonably large, as in split-phase and capacitor-start motors, such a harmonic causes very little error in the measurement of the fundamental currents if a rectifier meter is used. However, when the fundamental is small, as in capacitor-run motors at low slips, the error may be very great and it is essential to suppress the harmonic. This may be done either at the supply to the network or in the input to the meter amplifier. Such a harmonic can also cause considerable trouble in the measurement of the phase angle even when the fundamental current is not small, if the phase meter depends for its operation on detecting when the instantaneous current passes through zero. The suppression of the harmonics is therefore very desirable.

(5.2) Voltage

The only voltages required to be measured are the input voltages to the network. It is convenient to use the same amplifier-voltmeter combination as is used for current measurement. It is not always possible to supply it from a voltage divider since it may be that neither terminal is at earth potential. A small voltage transformer avoids this difficulty.

(5.3) Torque

Excluding that of Morrill, all circuits considered lead to the torque in synchronous watts in the form of the sum or difference of two scalar products of voltage and current vectors. The most direct method is, therefore, to employ a 2-element dynamometer instrument, each of the four windings of which is supplied from a feedback amplifier using shunts and voltage dividers to provide the input signals.

(6) COMPARISON OF EQUIVALENT CIRCUITS

The circuits will be compared first for suitability for capacitor-motor performance determination and secondly for convenience in representing other types of motor.

(6.1) Morrill Circuit

The Morrill circuit, Fig. 1, appears to be favoured as a basis for the manual solution of equations. This probably arises, at least in part, from its priority, although some[11] hold that it involves slightly less labour. It is possible to set up this circuit but it is not attractive for a network analyser since it requires many more circuit-elements than the other circuits, it requires two active voltage sources in addition to the applied voltages, and it is not possible to obtain simply a direct indication of the torque from the measurable voltages and currents of the network.

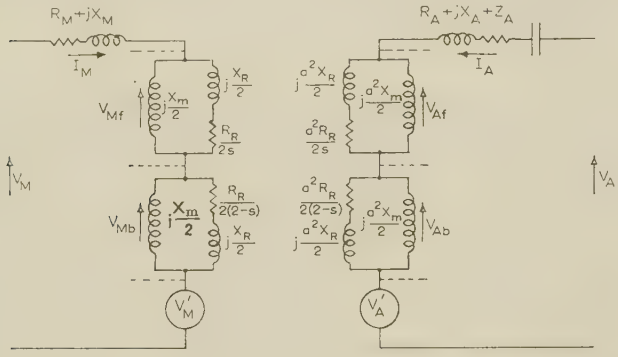

Fig. 1.—Morrill circuit.

$$V'_M = -j(V_{Af} - V_{Ab})/a \qquad V'_A = j(V_{Mf} - V_{Mb})a$$

$$\text{Torque} = \tfrac{1}{2}[(I_M^2 + a^2 I_A^2)(R_f - R_b) + 2aI_M I_A(R_f + R_b)\sin\phi]$$

where I_A leads I_M by an angle ϕ,

$$R_f = X_m^2 \frac{R_R}{s}\Big/\left[\left(\frac{R_R}{s}\right)^2 + (X_m + X_R)^2\right] \text{ and } R_b = X_m^2 \frac{R_R}{2-s}\Big/\left[\left(\frac{R_R}{2-s}\right)^2 + (X_m + X_R)^2\right]$$

(6.2) Kron Circuit

The Kron circuit, Fig. 2, raises no insoluble problems and has a number of advantages, e.g. all signal voltages required for torque and current measurement have one side at earth potential. The supplies required are two equal voltages of $jV_M/\sqrt{2}$ and one of $V_A/\sqrt{2}a$. There are four separate values of impedance to be set, three of which are duplicated but can be set without additional labour by ganging:

(*a*) Two of $R_M + jX_M$.

(*b*) Two of jX_M.

(*c*) Two of R_R and jX_R.

(*d*) One of $\frac{1}{2}\left[\dfrac{R_A + jX_A + Z_A}{a^2} - (R_M + jX_M)\right]$.

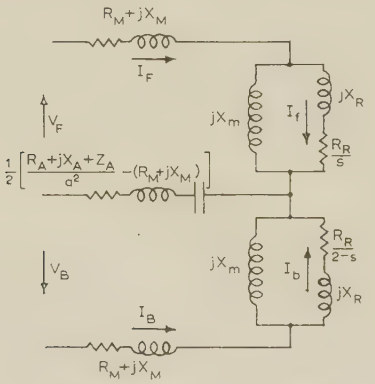

Fig. 2.—Kron circuit.

$$V_F = (V_A/a + jV_M)/\sqrt{2} \qquad V_B = (V_A/a - jV_M)/\sqrt{2}$$

$$I_M = -j(I_F - I_B)/\sqrt{2} \qquad I_A = (I_F + I_B)/\sqrt{2}a$$

$$\text{Torque} = I_f^2 R_R/s - I_b^2 R_R/(2-s)$$

As shown in Fig. 6, two mutual inductances M_F and M_B are required, having a combined secondary voltage proportional to $I_M = -j(I_F - I_B)/\sqrt{2}$, and also a shunt S_A having a voltage drop proportional to $I_A = (I_F + I_B)/\sqrt{2}a$. By connecting the secondary windings of the mutual inductances in series with the shunt S_A a signal proportional to and in phase with the total current is obtained. The shunts S_f and S_b give signals proportional to the rotor current components I_f and I_b, both for the measurements of the magnitudes of these currents and also for supplying the current signals to the amplifiers of the torque meter. The torque is given by the difference of the powers dissipated in the resistances R_R/s and $R_R/(2-s)$.

The denominator $\sqrt{2}$ which occurs in this circuit arises from the concepts of tensor analysis. It has no practical significance here beyond being a part of the voltage and current scaling factors, but is retained to conform with the analysis given by Kron.[7]

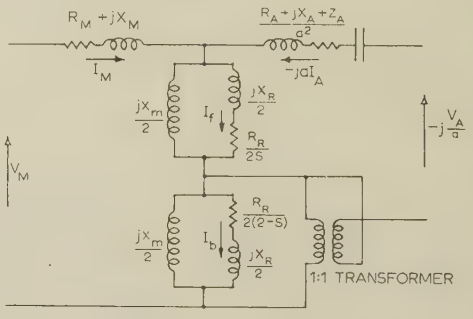

Fig. 3.—Veinott circuit.

$$\text{Torque} = I_f^2 R_R/s - I_b^2 R_R/(2-s)$$

(6.3) Veinott Circuit

The Veinott circuit, Fig. 3, requires two supplies with voltages in quadrature, V_M and $-jV_A/a$.

There are four impedance values to be set some of which are duplicated:

(*a*) One of $R_M + jX_M$.

(*b*) Two of $jX_{m/2}$.

(*c*) One of $\dfrac{R_A + jX_A + Z_A}{a^2}$.

(*d*) Two of $R_{R/2}$ and $jX_{R/2}$.

This circuit requires one impedance branch less than the Kron circuit in which $(R_M + jX_M)$ is duplicated, but it requires in addition a unity-ratio current transformer.

Although the actual winding currents exist in this circuit, that of the auxiliary winding is advanced in phase by 90° compared with the actual motor current and is also referred to the main winding. Current measurements must therefore be made in a similar manner to those described for the Kron circuit, but only one mutual inductance will be required.

The torque can be measured directly as in the Kron circuit

ne currents in the magnetizing and rotor branches being exactly ne same in the two cases.

(6.4) Chang Circuit

The cross-field circuit is not wholly suitable for the present purose in the form given by Chang, Fig. 4, since it is impracticable o set R_R and s independently to provide $(1 - s)R_R/s(2 - s)$.

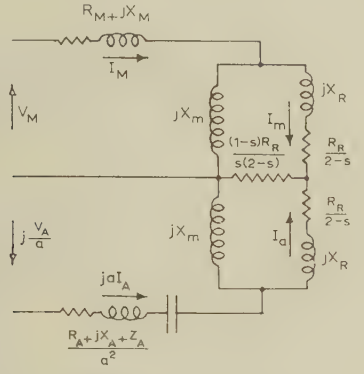

Fig. 4.—Chang circuit.

$$\text{Torque} = [I_m R_R/(2 - s) + (I_m + I_a)(1 - s)R_R/s(2 - s)]I_a^* + [I_a R_R/(2 - s) + (I_m + I_a)(1 - s)R_R/s(2 - s)]I_m^*$$

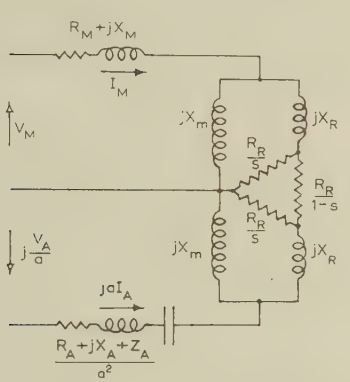

Fig. 5.—Modified Chang circuit.

However, if the star network of resistances is replaced by the equivalent delta, Fig. 5, the values required are R_R/s and $R_R/(1 - s)$, which can be obtained in the manner already described in Section 4.7. Although this circuit contains the same total number of circuit-elements as the Kron and Veinott circuits it includes an additional element dependent on s, which is a distinct disadvantage.

The voltage supply and current measurement are the same as in the Veinott circuit.

The measurement of torque, although similar in practice, is fundamentally different in theory from the previous cases. It is given by the sum of the powers represented by the voltage across each of the R_R/s branches and the current entering the opposite terminal of the delta, Fig. 5. This adds to the practical difficulty of the amplifiers since there can be no common point at earth potential. On the other hand, it inherently gives a more accurate measure of the torque than methods depending upon the difference of the two inputs to the dynamometer instrument.

(6.5) Representation of Motors other than Capacitor Motors

All references to capacitance and inductance here refer to the conjugate network.

(6.5.1) Split-Phase Motors.

The Kron circuit will require no change. The inductance required will be small and could be negative. To represent this a relatively large capacitance would be required and it could probably be neglected. For both Veinott and Chang circuits the inductance would have to be replaced by a capacitance of the same order as X_M; this constitutes an additional circuit-element.

(6.5.2) Single-Phase Motors (including Capacitor-Start under 'Run' Conditions).

In all circuits this corresponds to $Z_A = \infty$ and implies an open-circuit. It might be desirable also to open-circuit both windings of the current transformer of the Veinott circuit.

(6.5.3) Balanced Polyphase Motors.

The following is equally applicable to balanced or unbalanced supply voltages (assuming that zero-sequence currents are excluded in 3-phase machines).

Since the machine is balanced, $a = 1$, $R_A + jX_A = R_M + jX_M$ and $Z_A = 0$.

For the Kron circuit the impedance common to both meshes becomes zero and the applied voltages have to be adjusted according to the unbalance of the motor supply. For a balanced supply only the $jV_M/\sqrt{2}$ supply would be used. Some adjustment of scaling factors is necessary.

For both Veinott and Chang circuits the impedance $(R_A + jX_A + Z_A)/a^2$ becomes equal to $R_M + jX_M$. The adjustment of the voltage is such as to require an additional supply, since $-jV_A/a$ has to be made more nearly equal to V_M in phase as the unbalance decreases, in addition to being changed in magnitude.

(7) CHOICE OF CIRCUIT

The choice of circuit will depend in the first instance on the user's preference for cross-field or revolving-field theory. If he wishes to allow for the different degrees of saturation on the main and auxiliary winding axes, the cross-field circuit must be used. If he wishes to use different rotor-winding resistances for the two rotor current frequencies, one of the revolving-field circuits must be used. If neither of these refinements are required, any circuit can be used irrespective of the user's preference for manual-calculation purposes. All circuits will give the same solutions, and externally there need be no way of telling which circuit is in fact employed. Under these conditions the simpler rotor-resistance arrangement and the wider range of slip of the revolving-field circuits is considered to be sufficient to outweigh the theoretically greater accuracy of torque measurement associated with the cross-field circuit.

Between the revolving-field circuits of Kron and Veinott there is little to choose. Although the Veinott circuit appears to have a slightly smaller number of elements when representing the capacitor motor, additional elements are required to represent the split-phase and balanced machines, so that the advantage is lost. Although for exact representation of a split-phase motor in which X_A/a^2 is greater than X_M the Kron circuit would require large capacitances in place of the inductance, such difference would always be small and most probably negligible. Similarly, the Kron circuit could not represent a motor in which R_A/a^2 was less than R_M. If this were the case it would suggest a curious design and would require an interchange of the main and auxiliary winding representation and possibly an extra inductance unit. Since the inductance occurs in the Kron circuit in a branch whose impedance is only half the difference between the impedances of the main and auxiliary windings its ohmic value is less than half that required in the Veinott circuit.

Taking all factors into account the Kron circuit seems preferable, unless the special characteristics of the cross-field circuit in respect of magnetizing reactances and core loss are desired.

(8) PRACTICAL EXPERIENCE

Three of the circuits discussed were set up and examined. The Veinott circuit was excluded since experience of operating an analyser using this circuit has already been recorded[1] and the problems it poses also arise either in the Kron circuit or the Chang circuit.

(8.1) Kron Circuit

The conjugate Kron circuit, Fig. 6, was set up with full instrumentation arranged for the rapid determination of the currents

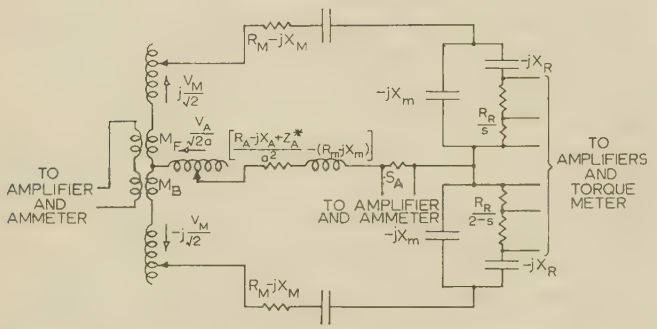

Fig. 6.—Conjugate form of Kron circuit showing supply and measurement arrangements.

and torques at various slips, with the exception that the separate setting of R_R and s was not employed since this analyser was not intended for use in the economic conditions of a manufacturing industry.

The three components of the applied voltage were provided by Leblanc-connected 3-phase transformers, the magnitude being adjusted by three variable-ratio auto-transformers, each supplied from a separate transformer secondary winding. These voltages were measured by the same amplifier-voltmeter combination as was used for the current measurements. The input to the amplifier was obtained from a voltage transformer so that the amplifier might operate with one terminal earthed.

The decade resistors and capacitors used have errors of 1% or less. The decade inductance unit was specially constructed using C-cores and pancake coils to permit adjustment of the numbers of turns of the various tappings after the air-gap had been adjusted. Owing to the non-linearity, the error at the extremes of current is of the order of 2%. The resistance of the inductors and the effect of the core loss was taken into account in setting the resistance in series with it. It was found convenient to bring the effective resistance of the inductors up to the same value on each tap by adding external resistors.

The mutual inductances used for the measurement of I_M have Mumetal cores and a very large number of secondary turns. The primary consequently has few turns and a negligible impedance. A very high degree of linearity with current was obtained by using a relatively large air-gap.

Linearity of the amplifiers used in the measurement of voltage, current and torque was achieved by using considerable feedback.

(8.1.1) Impedance Level.

The parameters of a number of motors between 1/20 and 3/4 h.p. were examined and it was found that an impedance scale of 100 : 1 was convenient for most, although for some 1 000 : 1 would permit a smaller number of decades in some of the elements. This also confirmed, in an indirect manner, th choice of 50 c/s as the operating frequency. The range capacitors required to set the highest magnetizing reactance ar the lowest leakage reactance to within 1% was found to occup the whole of the available range between the limits imposed b physical size on the one hand and stray capacitance on the othe Choice of impedance level thus also fixes the frequency, an 50 c/s was suitable.

(8.1.2) Voltage Level.

To enable an adequate range of voltage to be availab to provide $V_A/\sqrt{2}a$ from a standard variable-ratio auto transformer, V_A as actually applied to the circuit must no exceed 180 volts. A scale of 3 : 4 is, therefore, practicable fo 240-volt motors, but for simplicity a scale of 1 : 2 was preferre

(8.1.3) Current Level.

The resulting current level is 1/200 (or occasionally 1/2000 of the current in the actual motor, and individual currents ar unlikely to exceed 100 mA. This in turn is sufficiently small fo the regulation of the supply transformers to be negligible.

(8.2) Chang Circuit

The Chang circuit was set up in conjugate form with the sam impedance and voltage levels and a few cases were examine In view of the authors' preference for the revolving-field circuit however, full instrumentation was not provided and measure ments were restricted to the magnitudes of the separate windin currents, using resistive shunts in both cases. Full instrumenta tion would require the use of a mutual inductance for one curren to permit summing the two currents.

(8.3) Morrill Circuit

Although it has no practical advantage and several importa disadvantages, the Morrill circuit was set up as an exercis using voltage sources of variable magnitude and phase for th generator elements and adjusting them manually in succession using a null detector as in the balancing of a bridge. Th required reference voltages, which are both the differences o the voltages of two elements in series, can be obtained by th well-known bridge method. In the form published by Morri these generator voltages are in quadrature with their respectiv reference voltages. It was found more convenient to shift a voltages and currents in the auxiliary winding, including th applied voltage, by 90°, thus bringing the generator voltages int phase with their references. This complicates the supply an also the measurement of the total current in a manner similar t the other circuits considered. Adjustment of these voltag sources, which is an iterative process, was found to take a tim of the order of one minute. This process could be eliminate by the use of amplifiers, but the difficulty of measuring th torque directly makes development work on this circu unjustified.

(8.4) Accuracy

The aim was to provide for 1% accuracy in the setting of th circuit-elements, the supply voltage and the current measuremen ensuring a reading better than ±3%. Since more accurat components increase the cost disproportionately, a smalle tolerance was not considered economically justified in view o the possible inaccuracies in the calculated values of the moto parameters. It was appreciated that all elements of the circu are not of the same significance in respect of the accuracy of th results, but, in view of the wide range of both parameters an operating conditions, a detailed investigation of the relativ importance of the accuracy of the various elements was no justified. It is apparent, however, that the accuracy of th

unts and mutual inductances used for measuring the currents of particular importance. Some of the components were utside the desired tolerance; in particular, the variation of the inductance of the decade inductors with saturation, although small, was sufficient for the tolerance to be exceeded at small currents.

Some results are shown in Tables 1, 2 and 3, in which (*a*) gives the calculated values, (*b*) the values obtained from the Chang circuit, (*c*) the values obtained from the Kron circuit without filtering out the harmonics, and (*d*) the values obtained from the Kron circuit with the harmonics removed from the amplifier input. It will be noted that the Chang results seem better than the Kron results, but this apparent superiority arises from the use of resistive shunts for both currents in the Chang case.

This could not be done if the total current were also measured, as it would then be necessary to use a mutual inductance as in the Kron circuit.

The supply contained fifth and twenty-fifth harmonics of 1% and 0·2%, respectively. The necessity for filtering these out is apparent in the case of the capacitor-run motor, Table 3. The accuracy of the results for low slips with this motor, using the filter, was reduced, however, by the attenuation of the filter, which results in relatively small meter deflections and enhances the effect of stray pick-up. A filter causing less attenuation at 50 c/s would therefore improve the accuracy of measurement of such small currents.

The accuracy of the torque indication is almost entirely dependent upon the accuracy of the dynamometer instrument available. Since the elements are in opposition the accuracy is inevitably reduced and may not be better than 2% full-scale deflection, leading to appreciable errors at low torques as at

Table 1

CURRENTS OF A SPLIT-PHASE MOTOR

s		I_M	% Error	I_A	% Error	I	% Error
		amp		amp.		amp	
1·00	(*a*)	7·341 7		8·536 7		15·470	
	(*b*)	7·34	−0·02	8·45	−1·02		
	(*c*)	7·50	+2·16	8·40	−1·6	15·4	−0·45
0·50	(*a*)	6·971 5		7·729 3		14·681	
	(*b*)	7·00	+0·41	7·67	−0·76		
	(*c*)	7·10	+1·84	7·63	−1·28	14·6	−0·55
0·20	(*a*)	5·713		7·362 9		12·732 5	
	(*b*)	5·675	−0·67	7·35	−0·18		
	(*c*)	5·70	−0·23	7·30	−0·85	12·7	−0·26
0·10	(*a*)	4·846 4		7·666 0		11·526	
	(*b*)	4·80	−0·96	7·65	−0·21		
	(*c*)	4·75	−1·98	7·60	−0·86	11·5	−0·23
0·05	(*a*)	4·280 6		8·031		10·794	
	(*b*)	4·22	−1·41	8·00	−0·39		
	(*c*)	4·20	−1·88	8·00	−0·39	10·8	−0·06
0·02	(*a*)	3·898 6		8·344 2		10·332	
	(*b*)	3·86	−1·00	8·30	−0·53		
	(*c*)	3·85	−1·24	8·30	−0·53	10·4	+0·66
0·00	(*a*)	3·63		8·597 5		10·024	
	(*b*)	3·58	−1·38	8·55	−0·56		
	(*c*)	3·60	−0·82	8·5	−1·14	10·05	+0·26

Table 2

CURRENTS OF A CAPACITOR-START MOTOR

s		I_M	% Error	I_A	% Error	I	% Error
		amp		amp		amp	
1·00	(*a*)	7·341 5		3·033 5		8·85	
	(*b*)	7·35	+0·12	3·10	+2·20		
	(*c*)	7·45	+1·46	3·00	−1·11	8·9	+0·57
0·50	(*a*)	6·401		2·655 8		8·525	
	(*b*)	6·45	+0·77	2·71	+2·04		
	(*c*)	6·52	+1·88	2·60	−2·09	8·6	+0·88
0·20	(*a*)	4·734 5		2·887 7		7·621	
	(*b*)	4·78	+0·96	2·95	+2·16		
	(*c*)	4·75	+0·33	2·85	−1·30	7·6	−0·28
0·10	(*a*)	3·805 3		3·406 4		6·932	
	(*b*)	3·85	+1·17	3·46	+1·57		
	(*c*)	3·75	−1·46	3·40	−0·19	6·9	−0·46
0·05	(*a*)	3·336 5		3·849 5		6·425	
	(*b*)	3·40	+1·90	3·88	+0·79		
	(*c*)	3·30	+1·10	3·82	−0·77	6·35	−1·17
0·02	(*a*)	3·132 2		4·194 2		6·043 1	
	(*b*)	3·19	+1·85	4·22	+0·61		
	(*c*)	3·10	−1·03	4·15	−1·06	5·93	−1·87
0·00	(*a*)	3·061 1		4·450 4		5·732 9	
	(*b*)	3·10	+1·27	4·48	+0·67		
	(*c*)	3·00	−2·04	4·42	−0·68	5·6	−2·32

Table 3

CURRENTS OF A CAPACITOR-RUN MOTOR

s		I_M	% Error	I_A	% Error	I	% Error
		amp		amp		amp	
1·00	(*a*)	7·431 5		0·398 3		7·160 5	
	(*b*)	7·35	+0·12	0·39	−2·08		
	(*c*)	7·40	+0·80	0·39	−2·08	7·25	+1·26
	(*d*)	7·38	+0·53	0·404	+1·43	7·27	+1·53
0·50	(*a*)	6·491		0·349 9		6·478 0	
	(*b*)	6·51	+0·29	0·345	−1·40		
	(*c*)	6·55	+0·91	0·34	−2·83	6·55	+1·11
	(*d*)	6·56	+1·06	0·355	+1·46	6·57	+1·42
0·20	(*a*)	4·229		0·436 1		4·460 1	
	(*b*)	4·23	+0·02	0·43	−1·39		
	(*c*)	4·30	+1·68	0·43	−1·39	4·55	+2·01
	(*d*)	4·22	+0·21	0·444	+1·82	4·46	0·00
0·10	(*a*)	2·528 6		0·548 0		2·891 5	
	(*b*)	2·525	−0·14	0·535	−2·37		
	(*c*)	2·63	+4·00	0·54	−1·46	3·00	+3·75
	(*d*)	2·53	+0·06	0·525	−4·2	2·89	−0·05
0·05	(*a*)	1·383		0·631 3		1·770 7	
	(*b*)	1·40	+1·23	0·62	−1·78		
	(*c*)	1·54	+11·4	0·62	−1·78	1·9	+7·3
	(*d*)	1·395	+0·87	0·605	−4·15	1·78	+0·53
0·02	(*a*)	0·790 1		0·690 3		0·989 6	
	(*b*)	0·80	+1·25	0·675	−2·22		
	(*c*)	1·06	+34·2	0·67	−2·94	1·22	+23·3
	(*d*)	0·83	+5·05	0·647	−6·22	0·99	+0·04
0·00	(*a*)	0·855 5		0·733		0·527 3	
	(*b*)	0·865	+1·11	0·715	−2·45		
	(*c*)	1·14	+33·3	0·72	−1·78	0·92	+74·5
	(*d*)	0·89	+4·03	0·709	−3·28	0·565	+7·15

starting with capacitor-run motors with a single low-value capacitor. However, if desired, any torque can be checked quickly by calculation from the measured rotor current components I_f and I_b.

(9) CONCLUSIONS

It seems that the two revolving-field circuits of Kron and Veinott and the cross-field circuit of Chang are all suitable for motor performance calculations and, with attention to the appropriate details, will give results of sufficient accuracy for most design purposes. The choice is determined largely by the considerations which have already been discussed.

(10) ACKNOWLEDGMENTS

The authors wish to acknowledge the benefit derived from discussion with Professor E. Bradshaw and other members of the Staff of the Electrical Engineering Department, Manchester College of Science and Technology, and also the assistance of Crompton Parkinson (Doncaster) Ltd., especially in the provision of the details of a considerable number of motors.

(11) REFERENCES

(1) VEINOTT, C. G.: 'Moneca—A New Network Calculator for Motor Performance Calculations', *Transactions of the American I.E.E.*, 1952, **71**, Part II, p. 231.

(2) 'An Analogue Computer for Induction Motor Design', *Electrical Energy*, September, 1958, p. 362.

(3) HUMPHREY DAVIES, M. W., and SLEMON, G. R.: 'Transformer-Analogue Network Analysers', *Proceedings I.E.E.*, Paper No. 1479 S, October, 1953 (**100**, Part II, p. 469).

(4) LEVY, J. F.: 'Transformer Analogue Computer for Electric Motor Calculations', *BTH Activities*, 1955, **26**, p. 163.

(5) ISMAIL, M. K. E., and ADKINS, B.: 'Performance Calculations of the Capacitor Motor using the Transformer Analogue Analyser', *Proceedings I.E.E.*, Paper No. 2851 U, April, 1959 (**106** A, p. 175).

(6) MORRILL, W. J.: 'The Revolving Field Theory of the Capacitor Motor', *Transactions of the American I.E.E.*, 1929, **48**, p. 614.

(7) KRON, G.: 'Equivalent Circuit of the Capacitor Motor', *General Electric Review*, 1941, **44**, p. 511.

(8) CHANG, S.: 'The Equivalent Circuit of the Capacitor Motor', *Transactions of the American I.E.E.*, 1947, **66**, p. 631.

(9) KRON, G.: 'Equivalent Circuits of Electric Machinery' (Chapman and Hall, 1951), p. 83.

(10) CASSON, W., and HALES, A. W.: 'A Conjugate-Impedance Network Analyser Operating at 50 c/s', *Proceedings I.E.E.*, Paper No. 2607 S, June, 1958 (**105** A, p. 295).

(11) VEINOTT, C. G.: 'Theory and Design of Small Induction Motors' (McGraw-Hill, 1959), p. 226.

621.376.5:621.372.54

The Institution of Electrical Engineers
Monograph No. 407 E
Oct. 1960

OPTIMUM COMBINATION OF PULSE SHAPE AND FILTER TO PRODUCE A SIGNAL PEAK UPON A NOISE BACKGROUND

By H. S. HEAPS, B.Sc., M.A.

(*The paper was first received* 21*st January, and in revised form* 19*th July*, 1960. *It was published as an* INSTITUTION MONOGRAPH *in October*, 1960.)

SUMMARY

The paper concerns the generation of a signal pulse for transmission through a propagating medium and its subsequent detection as a single peak after it is received upon a noise background. It is supposed that the propagating medium behaves as a linear filter and that the noise background is independent of the signal. The pulse is conveniently described as consisting of a central portion attached to a leading edge and a trailing edge. It is found that for a given length of central portion there is an optimum combination of transmitted pulse shape and predetection filter. The results are compared with those arising from the use of certain non-optimum systems, and it is found that the optimum system leads to a significantly high signal/noise ratio.

The results of the paper imply that for the range of parameters considered it is advantageous to transmit a succession of short pulses of a determined form rather than a single smooth pulse.

LIST OF SYMBOLS

$d = n\tau$ = Duration of central portion of transmitted signal.
$F(\omega)$ = Fourier transform of $V_i(t)$.
$H(\omega)$ = Transfer function of filter.
P_N = Root-mean-square noise output.
P_S = Peak output signal.
$T(\omega)$ = Transfer function of propagating medium.
T_0 = Time at which peak output signal occurs.
W_g = Energy of generated signal.
$V_i(t)$ = Transmitted signal at time t.
$V_o(t)$ = Signal at output of filter.
W = Energy of transmitted signal.
$W(T)/n\tau$ = Mean square of n samples of transmitted signal.
α = Parameter of Butterworth filter.
λ = Maximum value of $\dfrac{P_S^2/P_N^2}{W(T)}$.
$|\sigma(\omega)|^2$ = Power spectrum of noise input to filter.
τ = Time interval between samples of transmitted pulse.

(1) INTRODUCTION

A problem which frequently arises in connection with the propagation of acoustic or radio waves is the design of a suitable means of transmission and reception of a pulsed signal which travels through a propagating medium and is received in the presence of a noise background. If the travel time of the pulse between the transmitter and the receiver is sufficiently large, the shape of the pulse at the receiver may differ significantly from its shape at the transmitter. For example, a change of shape results if the propagating medium contains inhomogeneities or reflecting surfaces so that the pulse which reaches the receiver is the sum of a number of pulses which travel by different paths and with different travel times.

Since the received signal pulse is most easily detected when it produces the greatest change in the noise background, it is often desirable to include in the input to the detector a filter whose function is to increase the signal/noise ratio.

Dwork[1] obtained an expression for the transfer function of the filter which, for a given input signal, would produce at its output the greatest possible value of instantaneous peak signal voltage consistent with a fixed value of mean output noise power. Further consideration of the problem was made by Zadeh and Ragazzini.[2] Heaps and McKay[3] obtained the transfer function of the filter required to produce at its output a signal voltage whose value averaged over a given finite time is as large as possible in comparison with the mean-square noise. If the detector responds to the square of the voltage input, the filter should be chosen to maximize the ratio of the mean-square signal voltage to the mean-square noise. The transfer function of such a filter was found in a previous paper.[4]

The papers referred to above concern the optimum transfer function of a filter whose input is a given shape of signal upon a given noise background. The noise background is, of course, given statistically and not as a specific function of time. In general the optimum signal/noise ratio is a function of the shape of the input signal. The problem of determining the best shape of the transmitted pulse was discussed by Chalk,[5] whose criterion for determining the form of the input pulse was based upon the minimization of adjacent-channel interference or upon the maximization of signal energy at the output of a given filter. The influence of the particular form of the noise background was not considered.

In many instances both the shape of the generated pulse and the transfer function of the filter are open to choice. Accordingly, there arises the problem of determining the optimum combination of transmitted pulse and filter transfer function so as to produce at the detector the highest possible signal/noise ratio. The present paper determines the best combination of generated pulse shape and filter function required to produce at the output the greatest possible instantaneous peak signal in relation to the r.m.s. noise. The effect of distortion of the signal during its passage through the propagating medium is allowed for, subject to the assumption that the propagating medium behaves as a known linear filter. In order to ensure that the resulting opti-

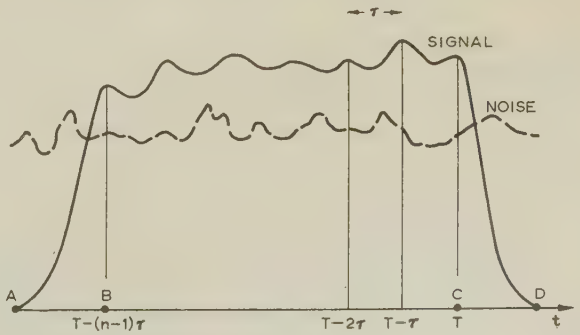

Fig. 1.—The transmitted pulse.

Correspondence on Monographs is invited for consideration with a view to publication.
Mr. Heaps is Associate Professor of Engineering Mathematics, Nova Scotia Technical College, Halifax, N.S.

mum signal shape conforms to the description of a pulse rather than a continuous wave, it will be supposed that there is a finite time interval over which n successive samples of the signal have a given average value. This time interval is the portion BC of the signal shown in Fig. 1.

(2) FORMULATION OF THE PROBLEM

The generated signal may be represented in the form

$$V_i(t) = \frac{1}{2\pi}\int_{-\infty}^{\infty} F(\omega)\varepsilon^{j\omega t}d\omega \quad . \quad . \quad . \quad . \quad (1)$$

where

$$F(\omega) = \int_{-\infty}^{\infty} V_i(t)\varepsilon^{-j\omega t}dt \quad . \quad . \quad . \quad . \quad . \quad (2)$$

Suppose the signal is transmitted through a propagating medium that is equivalent to a linear filter of transfer function $T(\omega)$. After passage through a further filter of transfer function $H(\omega)$ the signal becomes

$$V_o(t) = \frac{1}{2\pi}\int_{-\infty}^{\infty} F(\omega)T(\omega)H(\omega)\varepsilon^{j\omega t}d\omega \quad . \quad . \quad (3)$$

It is supposed that the function $T(\omega)$ includes the effect of whatever transducers or aerials are included in the propagating path between the generated signal, $V_i(t)$, and the input to the filter of transfer function $H(\omega)$.

Let the power spectrum of the noise input to the filter be $|\sigma(\omega)|^2$. The mean-square noise output is then

$$P_N^2 = \frac{1}{2\pi}\int_{-\infty}^{\infty} |\sigma(\omega)|^2|H(\omega)|^2 d\omega \quad . \quad . \quad . \quad (4)$$

According to the method of Dwork, for a fixed value of mean-square noise power the greatest possible instantaneous peak signal output is obtained at time T_0, when the transfer function $H(\omega)$ is chosen to be

$$H(\omega) = \frac{F^*(\omega)T^*(\omega)}{\lambda|\sigma(\omega)|^2}\exp(-j\omega T_0) \quad . \quad . \quad . \quad (5)$$

The asterisk denotes complex conjugation and λ is a constant whose value does not affect the signal/noise ratio. The resulting optimum ratio of peak signal to r.m.s. noise is

$$\frac{P_S^2}{P_N^2} = \frac{1}{2\pi}\int_{-\infty}^{\infty} \frac{|F(\omega)|^2|T(\omega)|^2}{|\sigma(\omega)|^2}d\omega \quad . \quad . \quad . \quad (6)$$

The total signal energy is

$$W = \int_{-\infty}^{\infty} |V_i(t)|^2 dt = \frac{1}{2\pi}\int_{-\infty}^{\infty} |F(\omega)|^2 d\omega \quad . \quad . \quad (7)$$

Before proceeding to determine the form of $F(\omega)$ required to maximize P_S^2/P_N^2, the significance of the expression (6) will be discussed in reference to some specific instances.

If the transmitted pulse is unaffected by its passage through the medium and if the noise is white, $|T(\omega)|^2 = |\sigma(\omega)|^2 = 1$. Eqns. (6) and (7) then indicate that for a given input signal energy the optimum signal/noise ratio is independent of the shape of the signal. If the noise is not white, let ω_0 be the value of ω at which $|\sigma(\omega)|^2$ least. For a given value of W the optimum ratio P_S^2/P_N^2 is clearly a maximum when the signal has infinitesimal bandwidth centred upon $\omega = \omega_0$. P_S^2/P_N^2 is then $W/|\sigma(\omega_0)|^2$. However, the energy in the generated signal is then distributed over an infinite time and any finite sample of the generated signal contains an infinitesimal amount of energy. Thus the generated signal does not have the form of a pulse.

If $|\sigma(\omega)|^2/|T(\omega)|^2 = \exp(-k^2\omega^2)$ and $V_i(t) = (\sin\Omega t)/\Omega^{1/2}t$, then $F(\omega) = \pi\Omega^{-1/2}$ when $|\omega| < \Omega$ and $F(\omega) = 0$ when $|\omega| > \Omega$. Thus $W = \pi$ and

$$\frac{P_S^2}{P_N^2} = \frac{\pi}{\Omega}\int_0^{\Omega}\exp(k^2\omega^2)d\omega = \frac{W}{\Omega}\int_0^{\Omega}\exp(k^2\omega^2)d\omega$$

For a given value of W the optimum ratio P_S^2/P_N^2 may be made as large as required by the use of a pulse $(\sin\Omega t)/\Omega^{1/2}t$ in which Ω is sufficiently large. As Ω tends to infinity $(P_S^2/P_N^2)/W$ tends to infinity. However, the limit of $(\sin\Omega t)/\Omega^{1/2}t$ cannot be regarded as an optimum pulse shape, since for any constant ω_1 a pulse for which $F(\omega) = \pi/\Omega^{1/2}$ if $|\omega - \omega_1| < \frac{1}{2}\Omega$ and $F(\omega) = 0$ if $|\omega - \omega_1| > \frac{1}{2}\Omega$ leads to a larger value of $(P_S^2/P_N^2)/W$. It is clear that the maximum value of $(P_S^2/P_N^2)/W$ results when the generated signal is a continuous wave of infinite frequency, but that $(P_S^2/P_N^2)/W$ may be made as large as is required by the use of a pulse of form $(\sin\Omega t)/\Omega^{1/2}t$ of sufficiently narrow bandwidth.

If $|\sigma(\omega)|^2/|T(\omega)|^2 = \exp(-k^2\omega^2)$, an infinite value of P_S^2/P_N^2 is obtained for any transmitted pulse whose frequency spectrum tends to zero less rapidly than $|\sigma(\omega)|^2/|T(\omega)|^2$ as ω tends to infinity. An example of such a pulse is the rectangular pulse of unit amplitude and duration extending from time $t = -a$ to $t = a$; in this instance $F(\omega) = 2(\sin\omega a)/\omega$.

Since in practical transmission systems $|T(\omega)|^2$ is finite and $|\sigma(\omega)|^2$ is never zero, it appears reasonable to exclude the case in which P_S^2/P_N^2 becomes infinite and to base the analysis upon the assumption that the right-hand side of eqn. (6) remains finite.

The generated signal may be described as having the character of a pulse if it contains a finite amount of energy and if there exists a finite time interval, d, which contains a finite, and non-infinitesimal, amount of energy.

The mean square value of the generated signal sampled at times T, $T - \tau$, $T - 2\tau$, . . ., $T - (n-1)\tau$ is

$$(1/n)\,\Sigma\,|V_i(T - r\tau)|^2$$

where the summation in r is from 0 to $n - 1$. If $W(T)$ denotes the expression

$$W(T) = \tau\,\Sigma\,|V_i(T - r\tau)|^2 \quad . \quad . \quad . \quad . \quad (8)$$

then as $\tau \to 0$ for a fixed value of $d = n\tau$ the expression for $W(T)$ tends to the energy in a continuous sample of the generated signal over a time extending from $T - d$ to T. For finite τ the mean square value of the n samples is $(1/n\tau)W(T)$. Substitution of $V_i(t)$ from eqn. (1) enables expression (8) to be written as

$$W(T) = (1/2\pi)^2\tau\,\Sigma\int F(\omega)\exp[j\omega(T - r\tau)]d\omega \times \int F^*(\omega_1)\exp[-j\omega_1(T - r\tau)]d\omega_1 \quad . \quad (9)$$

The problem considered in Section 3 is the determination of the pulse shape, $V_i(t)$, which for a fixed value of $W(T)$ makes P_S^2/P_N^2 of eqn. (6) have a maximum, but finite, value. The term 'maximum' is here used to signify a stationary value of P_S^2/P_N^2 which is reduced by all infinitesimal variations of $V_i(t)$ from the determined form.

(3) DETERMINATION OF THE OPTIMUM SYSTEM

For a given value of $W(T)$ the stationary values of P_S^2/P_N^2 are obtained when $F(\omega)$ is chosen to satisfy the condition $\partial Q/\partial F = 0$ where

$$Q = \frac{1}{2\pi}\frac{|F(\omega)|^2|T(\omega)|^2}{|\sigma(\omega)|^2} - \frac{\lambda\tau}{(2\pi)^2}\Sigma F(\omega)\exp\left[j\omega(T-r\tau)\right]\times \int F^*(\omega_1)\exp\left[-j\omega_1(T-r\tau)\right]d\omega_1 \quad . \quad (10)$$

and λ is a Lagrangian multiplier.[6] The condition $\partial Q/\partial F = 0$ is satisfied when

$$0 = \frac{1}{2\pi}\frac{F^*(\omega)|T(\omega)|^2}{|\sigma(\omega)|^2} - \frac{\lambda\tau}{(2\pi)^2}\Sigma\exp\left[j\omega(T-r\tau)\right]\times \int F^*(\omega_1)\exp\left[-j\omega_1(T-r\tau)\right]d\omega_1$$

$$= \frac{1}{2\pi}\frac{F^*(\omega)|T(\omega)|^2}{|\sigma(\omega)|^2} - \frac{1}{2\pi}\lambda\tau\Sigma V_i^*(T-r\tau)\exp\left[j\omega(T-r\tau)\right] \quad . \quad (11)$$

Since the procedure used to obtain eqns. (10) and (11) forms the basis of the theory of the present paper, a more detailed derivation is included in the Appendix.

It follows from eqn. (11) that

$$F(\omega) = \lambda\tau\frac{|\sigma(\omega)|^2}{|T(\omega)|^2}\Sigma V_i(T-r\tau)\exp\left[j\omega(r\tau-T)\right] \quad . \quad (12)$$

Substitution of $F(\omega)$ from eqn. (12) into eqn. (1) shows that

$$V_i(t) = \lambda\tau\sum_r \phi(t-T+r\tau)V_i(T-r\tau) \quad . \quad . \quad (13)$$

where

$$\phi(t) = \frac{1}{2\pi}\int_{-\infty}^{\infty}\frac{|\sigma(\omega)|^2}{|T(\omega)|^2}\exp(j\omega t)d\omega \quad . \quad . \quad (14)$$

In particular, for each integer s between 0 and $n-1$,

$$V_i(T-s\tau) = \lambda\tau\sum_r \phi(r\tau-s\tau)V_i(T-r\tau) \quad . \quad . \quad (15)$$

The maximum value of λ for which the n equations (15) have a solution in the n quantities $V_i(T-r\tau)$ is the greatest possible value of $(P_S^2/P_N^2)/W(T)$. The corresponding solutions $V_i(T-r\tau)$ may be substituted into eqn. (13) to determine the optimum pulse shape. From eqns. (6), (12) and (14) it follows that

$$P_S^2/P_N^2 = \lambda^2\tau^2\Sigma\Sigma V_i(T-r\tau)V_i^*(T-s\tau)\phi(r\tau-s\tau) \quad . \quad (16)$$

Although the value of $W(T)$ depends only upon the portion of the generated signal between times $T-(n-1)\tau$ and T, the value of P_S^2/P_N^2 in eqn. (6) is dependent upon the entire pulse. Minimization of $(P_S^2/P_N^2)/W(T)$ thus determines the whole pulse, which may be envisaged as consisting of a 'build-up' portion prior to the time $T-(n-1)\tau$, a central portion extending from time $T-(n-1)\tau$ to T, and a 'fall-off' portion subsequent to the time T. The three portions of the signal are indicated in Fig. 1 as AB, BC, and CD respectively.

Since $\phi(\tau)$ as defined by eqn. (14) has a maximum at $\tau = 0$ and tends to zero as $\tau \to \infty$, if τ is sufficiently large the function $V_i(t)$ of eqn. (13) will exhibit a ripple of period τ as drawn in Fig. 1.

It may be noted that if $T-s\tau$ and $T-r\tau$ are denoted respectively by t and t_1, then as $\tau \to 0$ for a fixed value of $d = n\tau$, eqns. (15) reduce to the Fredholm integral equation

$$V_i(t) = \lambda\int_{T-d}^{T}\phi(t-t_1)V_i(t_1)dt_1 \quad . \quad . \quad . \quad (17)$$

It should also be noted that, for fixed $d = n\tau$, $W(T)$ does not necessarily represent the total energy in the generated pulse, but only the energy between the times $T-d$ and T. The total energy is given by

$$W_g = \int_{-\infty}^{\infty}|V_i(t)|^2dt = \lambda^2\tau^2\Sigma\Sigma V_i(T-r\tau)V_i^*(T-s\tau)\times \int_{-\infty}^{\infty}\phi(t-T+r\tau)\phi^*(t-T+s\tau)dt \quad . \quad (18)$$

regardless of whether τ is finite or tends to zero.

Eqn. (18) represents the least amount of energy required to generate a pulse of the optimum shape for a fixed value of $W(T)$. Thus the maximum possible value of $(P_S^2/P_N^2)/W_g$ is equal to $\lambda_{max}W(T)/W_g$, and $V_i(t)$ according to eqn. (13) represents the most efficient pulse shape to utilize the energy W_g for given values of τ and n.

For a given input noise background the maximum value of λ is the greatest possible value of P_S^2/P_N^2 in comparison with the signal energy $W(T)$ between the times $t = T-d$ and T. An increase in the noise background will clearly decrease λ. The mean-square input noise energy in the time $d = n\tau$ is

$$\frac{n\tau}{2\pi}\int_{-\infty}^{\infty}|\sigma(\omega)|^2d\omega$$

but $|\sigma(\omega)|^2$ affects the maximum λ only through $|\sigma(\omega)|^2/|T(\omega)|^2$. In Section 5 it will be found convenient to introduce λ_0 defined as the magnitude of the maximum λ multiplied by the factor

$$\frac{n\tau}{2\pi}\int_{-\infty}^{\infty}\frac{|\sigma(\omega)|^2}{|T(\omega)|^2}d\omega = d\phi(0)$$

When $|T(\omega)| = 1$, i.e. the component frequencies of the signal suffer phase change but no change in amplitude during passage through the propagating medium, λ_0 denotes the maximum value of

$$\frac{\text{(Output peak signal)}^2/\text{(Mean output noise power)}}{W(T)/\text{(Unit energy of noise input during the signal duration } d)}$$

When $\phi(t) = 0$ for $|t| \geqslant \tau$, eqn. (15) reduces to an identity subject to the condition $\lambda = [\tau\phi(0)]^{-1} = (n/d)/\phi(0)$ and hence $\lambda_0 = n$. Eqn. (13) then shows that the transmitted pulse must consist of a sequence of pulses each of shape $\phi(t)$, and arbitrary heights, centred at the times $T, T-\tau, T-2\tau, \ldots, T-(n-1)\tau$. Then

$$\frac{P_S^2}{P_N^2} = \left[\frac{1}{\phi(0)}\right]^2\Sigma|V_i(T-r\tau)|^2$$

The value of n obtained for λ_0 indicates that the optimum filter combines the individual members of the received pulses to produce their sum at the output.

(4) PHYSICAL REALIZABILITY OF THE OPTIMUM FILTER

According to eqns. (5) and (12) the optimum filter has the transfer function

$$H(\omega) = \frac{\tau}{T(\omega)}\Sigma V_i^*(T-r\tau)\exp\left[j\omega(T-r\tau-T_0)\right] \quad . \quad (19)$$

and hence is a filter of transfer function $1/T(\omega)$ followed by a certain linear combination of time delays.

For the transfer function (19) to be realizable by a physical network, it is necessary that the filter have a positive memory in the sense that the response to a unit impulse applied at time

$t = 0$ should be zero for $t < 0$. Now the response to the unit impulse is

$$h(t) = (1/2\pi)\int_{-\infty}^{\infty} H(\omega)\exp(j\omega t)d\omega$$

$$= \tau \Sigma\, V_i^*(T - r\tau)\psi(t + T - r\tau - T_0) \quad . \quad (20)$$

where $$\psi(t) = (1/2\pi)\int_{-\infty}^{\infty} \frac{1}{T(\omega)}\exp(j\omega t)d\omega \quad . \quad . \quad (21)$$

The condition that $h(t) = 0$ for $t < 0$ is fulfilled if

$$\psi(t) = 0 \quad \text{for } t < T - T_0 \quad . \quad . \quad . \quad . \quad (22)$$

It follows from eqns. (21) and (22) that the condition for physical realizability of the optimum filter depends only upon the form of $T(\omega)$ and is independent of the form of the input noise. This result is in contrast to the results of earlier papers,[3, 4] in which for a given form of input signal the condition for physical realizability of the filter was found to depend upon the form of $|F(\omega)|/|\sigma(\omega)|^2$.

The remainder of the present Section is concerned with illustrations of the significance of condition (22) for particular choices of the function $T(\omega)$. The condition includes, of course, the requirement that the right-hand side of eqn. (21) exists.

Suppose that the pulse suffers no distortion during its passage through the propagating medium but acquires a time delay t_0. Then $T(\omega) = \exp(-j\omega t_0)$ and

$$\psi(t) = (1/2\pi)\int_{-\infty}^{\infty} \exp[j\omega(t + t_0)]d\omega = \delta(t + t_0)$$

where $\delta(t)$ denotes a unit impulse at time $t = 0$. Condition (22) is then satisfied if $T_0 > T + t_0$. Thus the entire central portion of the pulse as shown in Fig. 1 must have entered the filter prior to the instant at which the output peak is formed. However, the trailing edge does not need to have entered the filter and hence does not contribute to the signal peak. Accordingly, it is clear that the sole function of the trailing edge is to terminate the pulse conveniently.

Suppose that the propagating medium contains two possible paths by which the pulse may travel from the transmitter to the receiver. Such a case would arise if the propagating medium were homogeneous and bounded by a perfectly reflecting plane boundary, so that the Lloyd mirror effect would be produced. Let the travel times along these paths be t_1 and t_2. If there is no distortion of the pulse along either path,

$$T(\omega) = \exp(-j\omega t_1) + \exp(-j\omega t_2)$$

and $$\frac{1}{T(\omega)} = \tfrac{1}{2}\exp[\tfrac{1}{2}j\omega(t_1 + t_2)]\sec[\tfrac{1}{2}\omega(t_2 - t_1)].$$

The function $\psi(t)$ of eqn. (21) does not exist in view of the infinite behaviour of $\sec\frac{1}{2}\omega(t_2 - t_1)$ when $\omega = \pi/(t_2 - t_1)$. This result is in agreement with the intuitively obvious statement that a linear filter cannot recombine two identical signals so as to eliminate the time delay between them.

Suppose that the propagating medium contains two possible propagating paths of travel times t_1 and t_2 and that the pulse is unchanged during its passage along the first path but is multiplied by the factor c during its passage along the second path. Then $T(\omega) = \exp(-j\omega t_1) + c\exp(-j\omega t_2)$. If $|c| < 1$, then $1/T(\omega)$ may be expressed as a convergent series of the form

$$\frac{1}{T(\omega)} = \exp(j\omega t_1)\Sigma(-1)^m c^m \exp[jm\omega(t_1 - t_2)] \quad . \quad (23)$$

with summation in m from zero to infinity. Then

$$\psi(t) = \frac{1}{2\pi}\Sigma(-1)^m c^m \int_{-\infty}^{\infty}\exp[j\omega(t + mt_1 + t_1 - mt_2)]d\omega$$

$$= \Sigma(-1)^m c^m \delta(t + mt_1 + t_1 - mt_2) \quad . \quad . \quad . \quad . \quad (24)$$

Hence condition (22) is true if, for each m,

$$T_0 > T + t_1 + m(t_1 - t_2) \quad . \quad . \quad . \quad . \quad (25)$$

Now if $t_2 > t_1$ condition (25) implies that the peak output must occur at a time T_0 chosen so that $T_0 > T + t_1$. Thus the second pulse is not required and the peak is formed from the first, and greatest, pulse only.

If $T(\omega) = \exp(-j\omega t_1) + c\exp(-j\omega t_2)$, where $t_1 > t_2$ and $|c| < 1$, condition (25) implies that $T_0 = \infty$ and the optimum value of $(P_S^2/P_N^2)/W(T)$ cannot be obtained for an observation at a finite time. However, if only the first M terms in eqn. (23) are used to approximate $1/T(\omega)$, condition (25) becomes $T_0 > T + t_1 + M(t_1 - t_2)$ and the resulting values of $(P_S^2/P_N^2)/W(T)$ may be made as close as desired to the true optimum by sufficiently large choice of M. The transfer function $H(\omega)$ has the form

$$H(\omega) = \tau\exp[j\omega(t_1 + T - T_0)]\sum_r V_i^*(T - rt)\exp(-j\omega rt)$$

$$\sum_m (-1)^m c^m \exp[j\omega m(t_1 - t_2)]$$

in which the effect of the factor

$$\Sigma(-1)^m c^m \exp[j\omega m(t_1 - t_2)]$$

is eventually to eliminate most of the first pulse so that detection is of the second, and greatest, pulse only.

(5) COMPARISON WITH TWO SIMPLE NON-OPTIMUM FILTERS WHEN $n = 3$

In this Section the result of using the optimum system of pulse shape and filter described in Section 3 is compared with the result of using two simple non-optimum filters. It will be supposed that $n = 3$ and that

$$|\sigma(\omega)|^2/|T(\omega)|^2 = \exp(-k^2\omega^2) \quad . \quad . \quad . \quad (26)$$

Although the form (26) is assumed for mathematical simplicity, it is believed to be of some practical interest in the case of a noise background in which the low frequencies predominate.

From eqn. (26) it follows from eqn. (14) that

$$\phi(r\tau - s\tau) = \frac{1}{(2\pi)^{1/2}k}\exp\left[-(r - s)^2\frac{\tau^2}{4k^2}\right] \quad . \quad . \quad (27)$$

If $n = 3$, then $d = 3\tau$ and the condition for eqn. (15) to possess a non-zero solution in $V_i(T)$, $V_i(T - \tau)$ and $V_i(T - 2\tau)$ is that

$$(\lambda\tau)^{-1} = \phi(0) - \phi(2\tau)$$

or $$= \phi(0) + \tfrac{1}{2}\phi(2\tau) \pm \tfrac{1}{2}[\phi^2(2\tau) + 8\phi^2(\tau)]^{1/2}$$

The maximum value of $\lambda d\phi(0)$ introduced at the end of Section 3 is thus

$$\lambda_0 = \frac{n\phi(0)}{\phi(0) + \tfrac{1}{2}\phi(2\tau) - \tfrac{1}{2}[\phi^2(2\tau) + 8\phi^2(\tau)]^{1/2}} \quad . \quad (28)$$

and the solution of eqn. (15) is

$$\left.\begin{aligned} V_i(T - 2\tau) &= V_i(T) \\ V_i(T - \tau) &= \frac{-2\phi(\tau)/\phi(0)}{1 - n/\lambda_0}V_i(T)\end{aligned}\right\} \quad . \quad . \quad . \quad (29)$$

Substitution of $V_i(T)$, $V_i(T-\tau)$ and $V_i(T-2\tau)$ into eqn. (12) determines the appropriate transfer function $F(\omega)$.

For $\tau/2k = 1/3$, $2/3$, 1, $4/3$, $5/3$, and 2 it follows from eqns. (26) and (27) that the respective values of λ_0 are 199, 17·3, 6·14, 3·94, 3·29 and 3·08. The corresponding values of $V_i(T-\tau)/V_i(T)$ are −1·82, −1·55, −1·44, −1·42, −1·414, and −1·414. The case of white noise is included by putting $k = 0$, when $\lambda_0 = 3$. It is clear that a large value of λ_0 may be obtained by choosing τ, and hence the duration, d, of the transmitted pulse, sufficiently small in comparison with $2k$, which is proportional to the time required for a significant decay of the function $\phi(t)$.

For comparison with the result of using a non-optimum system it may be noted that, when $\tau/2k = 1$, the optimum λ_0 is 6·14 and is obtained when $V_i(T-\tau) = -1{\cdot}44V_i(T)$. The shape of $V_i(t)$ is as shown in Fig. 2.

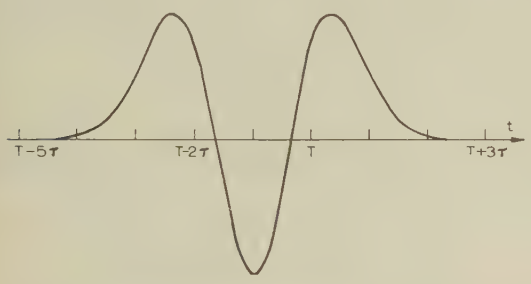

Fig. 2.—Shape of the optimum pulse $V_i(t)$ when $n = 3$, $|\sigma(\omega)|^2/|T(\omega)|^2 = \exp(-k^2\omega^2)$ and $\tau/2k = 1$.

For any parameters V_0, V_1 and V_2 eqn. (12) with $V_i(T)$, $V_i(T-\tau)$ and $V_i(T-2\tau)$ replaced respectively by V_0, V_1 and V_2 gives a transfer function, $F(\omega)$, for which P_S^2/P_N^2 is according to eqn. (16) but is not, in general, an optimum. For the chosen values of V_0, V_1 and V_2 the right-hand side of eqn. (15) may be evaluated to give the quantities $V_i(T)$, $V_i(T-\tau)$ and $V_i(T-2\tau)$. Substitution of these latter quantities into eqn. (8) leads to the appropriate value of $W(T)$. If V_0 and V_2 are chosen to be unity, and V_1 is chosen as $-\infty$, −40, −1·44, 0, 1·40 and ∞, the respective values of λ_0 are 2·36, 3·84, 6·14, 2·34, 3·57, and 2·36. The optimum of 6·14 is thus significantly higher than the other values.

The result of using the optimum combination of transmitted pulse and filter may also be compared with the result of using a rectangular pulse of duration 3τ and a 2-pole Butterworth filter

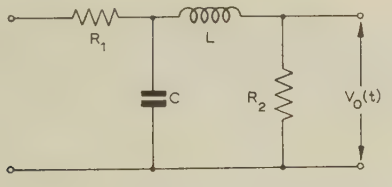

Fig. 3.—The 2-pole low-pass Butterworth filter.

of circuit as shown in Fig. 3. The transfer function of the filter is

$$H(\omega) = \frac{R_2}{R_1+R_2}\,\frac{1}{1+\alpha j\omega-\beta\omega^2} \quad . \quad . \quad . \quad (30)$$

where $\alpha = (L + R_1R_2C)/(R_1 + R_2)$ and $\beta = R_1LC/(R_1 + R_2)$. The filter is said to have Butterworth response if $\beta = \frac{1}{2}\alpha^2$, so that

$$|H(\omega)|^2 = \left(\frac{R_2}{R_1+R_2}\right)^2 \frac{1}{1+\alpha^4\omega^4/4} \quad . \quad . \quad (31)$$

For a rectangular pulse input of unit height over the time from $t = 0$ to $t = 3\tau = d$, $W(T) = 3\tau$ and

$$F(\omega) = \frac{j}{\omega}\left[\exp(-3j\omega\tau) - 1\right] . \quad . \quad . \quad . \quad (32)$$

When $T(\omega) = 1$ and $|\sigma(\omega)|^2 = \exp(-k^2\omega^2)$, eqn. (3) leads to $V_o(t) = \dfrac{R_2}{(R_1+R_2)}\left[1 - \left(\exp-\frac{t}{\alpha}\right)\left(\cos\frac{t}{\alpha} + \sin\frac{t}{\alpha}\right)\right]$ if $t<d$, and

$$V_o(t) = \frac{R_2}{(R_1+R_2)}\left[\left(\exp-\frac{t-3\tau}{\alpha}\right)\left(\cos\frac{t-3\tau}{\alpha} + \sin\frac{t-3\tau}{\alpha}\right) - \left(\exp-\frac{t}{\alpha}\right)\left(\cos\frac{t}{\alpha} + \sin\frac{t}{\alpha}\right)\right] \quad . \quad (33)$$

if $t > d$. Eqn. (4) gives

$$P_N^2 = \left(\frac{R_2}{R_1+R_2}\right)^2 \frac{1}{\pi}\int_0^\infty \frac{\exp(-k^2\omega^2)}{1+\alpha^4\omega^4/4}d\omega$$

For various values of the filter parameter α the corresponding values of λ_0 may be calculated. For example, if α is chosen equal to τ it follows from eqn. (33) that $V_o(t)_{max} = 1{\cdot}042R_2/(R_1+R_2)$, which occurs when $t = 3\tau$. Also, when $\tau/2k = 1$, $P_N^2 = [R_2/(R_1 + R_2)]^2\,(1/\tau)(0{\cdot}385)$ and hence $\lambda_0 = 2{\cdot}25$. For values of the filter parameter α between $0{\cdot}5\tau$ and 3τ the corresponding values of λ_0 are plotted in Fig. 4. The maximum value

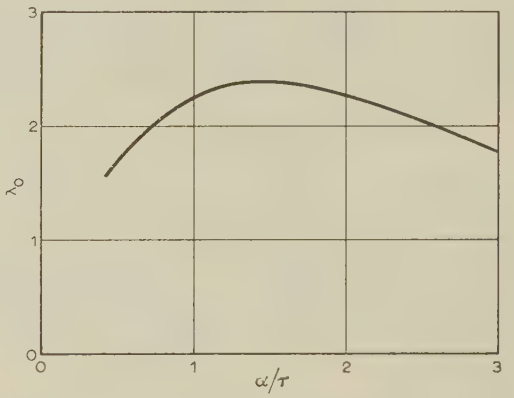

Fig. 4.—Values of λ_0 for the 2-pole low-pass Butterworth filter of parameter α and a rectangular pulse input of duration 3τ.

of λ_0 is approximately 2·5. Thus the maximum value of λ_0 which may be obtained by use of a rectangular pulse and a 2-pole Butterworth filter is significantly less than the value of 6·4 obtained by use of the optimum system.

(6) CONCLUDING REMARKS

In Section 5, in order to permit relatively rapid calculation of results for comparison with non-optimum systems, it was supposed that $n = 3$. Some calculations have also been undertaken for other values of n with $|\sigma(\omega)|^2/|T(\omega)|^2$ as given in eqn. (26).

When $n = 10$ and $d/2k = 6$, 9 and 15, the respective values of λ_0 are 250, 35 and 12, in contrast to the values of 3·08, 3 and 3 which result for the same values of $d/2\tau$ when $n = 3$. It turns out, in fact, that for a fixed pulse length d the optimum value of λ_0 increases very rapidly as n increases.

It was found in Section 5 that when $n = 3$ the optimum pulse

consists of two positive portions separated by a negative portion, and hence the optimum pulse may be described as a sequence of three separate pulses. When $n = 10$ and $d/2k$ varies between 4 and 12, the optimum pulse contains nine distinct portions which are alternatively positive and negative; when $d/2k = 3$ the pulse contains seven distinct parts. In general, the number of separate parts of the optimum pulse increases as n increases.

An application of the results stated in the previous two paragraphs is that, in order to produce a maximum value of output peak signal in relation to the mean noise background, it is advantageous to divide the transmitted pulse into a number of distinct short pulses. Such a result is not surprising in view of the fact that the peak signal is required at a single instant only and hence could well be formed from a superposition of short impulses.

When $n = 1$ this analysis becomes trivial and leads to the result that $\lambda_0 = 1$. Thus the optimum system using a single transmitted pulse in the form of a short impulse does not produce as large a peak signal as does that in which the transmitted pulse is divided into a sequence of separate short pulses of shape given by eqn. (13). As shown in Section 5, the value of λ_0 is affected significantly by changes in the relative amplitudes of the separate pulses.

The formulation in the present paper has led to the conclusion that, if the noise is not white, for a fixed value of the mean of n successive samples of the squared signal there is an optimum signal shape and filter. The optimum signal shape is given by eqn. (13) in which the values of $V_i(T - r\tau)$ are chosen to satisfy eqn. (15).

(7) ACKNOWLEDGMENT

The author wishes to express his appreciation to the Defence Research Board of Canada for permission to publish the paper, which has arisen as part of an investigation under N.R.E. Project D12-38-50-07.

(8) REFERENCES

(1) DWORK, B. M.: 'Detection of a Pulse Superposed on Fluctuation Noise', *Proceedings of the Institute of Radio Engineers*, 1950, **38**, p. 771.

(2) ZADEH, L. A., and RAGAZZINI, J. R.: 'Optimum Filters for the Detection of Signals in Noise', *ibid.*, 1952, **40**, p. 1223.

(3) HEAPS, H. S., and MCKAY, M. R.: 'Optimum Network Functions for the Sampling of Signals in Noise', *Proceedings I.E.E.*, Monograph No. 297 R, March, 1958 (**105** C, p. 438).

(4) HEAPS, H. S.: 'Optimum Filter Functions for the Detection of Pulsed Signals in Noise', *Canadian Journal of Physics*, 1958, **36**, p. 692.

(5) CHALK, J. H. H.: 'The Optimum Pulse-Shape for Pulse Communication', *Proceedings I.E.E.*, Paper No. 904, 1950 (**97**, Part III, p. 88).

(6) WEINSTOCK, R.: 'Calculus of Variations' (McGraw-Hill New York, 1952), pp. 48 and 44.

(9) APPENDIX

The procedure used to obtain eqns. (10) and (11) may b explained as follows.

With arbitrary small error, eqn. (6) may be written in th form

$$\frac{P_S^2}{P_N^2} = \frac{1}{2\pi}\Delta\omega \sum_s \frac{|F_s|^2|T(\omega_s)|^2}{|\sigma(\omega_s)|^2} \quad . \quad . \quad . \quad (34$$

where F_s denotes $F(\omega_s)$ and values of ω_s are chosen at interval $\Delta\omega$ apart along the range of $-\infty$ to ∞. Similarly, eqn. (9 may be written in the form

$$W(T) = (1/2\pi)^2\tau B\Delta\omega \sum_r \sum_s F_s \exp\left[j\omega_s(T - r\tau)\right] \quad . \quad (35$$

where B denotes an integral with respect to ω_1.

Now P_S^2/P_N^2 and $W(T)$ may be regarded as functions o independent complex parameters F_s or as functions of inde pendent real parameters R_s and I_s, where $F_s = R_s + jI_s$. A stationary value of $(P_S^2/P_N^2)/W(T)$ results when, for each valu of s,

$$\frac{\partial}{\partial R_s}\left[\frac{P_S^2/P_N^2}{W(T)}\right] = \frac{\partial}{\partial I_s}\left[\frac{P_S^2/P_N^2}{W(T)}\right] = 0 \quad . \quad . \quad . \quad (36$$

Since $(P_S^2/P_N^2)/W(T)$ is real, eqn. (36) is equivalent to

$$\frac{\partial}{\partial F_s}\left[\frac{P_S^2/P_N^2}{W(T)}\right] = 0 \quad . \quad . \quad . \quad . \quad . \quad (37$$

in which F_s^* is regarded as a constant during the differentiatio with respect to F_s.

If λ is the value of $(P_S^2/P_N^2)/W(T)$ when F_s is chosen to satisf eqn. (37), then eqn. (37) may also be written in the form

$$\frac{1}{W(T)}\frac{\partial(P_S^2/P_N^2)}{\partial F_s} - \frac{\lambda\partial W(T)}{\partial F_s} = 0 \quad . \quad . \quad . \quad (38$$

and so, for each value of s,

$$\frac{\partial}{\partial F_s}\left\{\frac{1}{2\pi}\frac{|F_s|^2|T(\omega_s)|^2}{|\sigma(\omega_s)|^2} - \lambda\left(\frac{1}{2\pi}\right)^2\tau B\sum_r F_s \exp\left[j\omega_s(T - r\tau)\right]\right\}$$

$$. \quad . \quad . \quad . \quad (39$$

However, if eqn. (39) is true, it follows by letting $\Delta\omega$ tend t zero that the equation is also true when ω_s is replaced by ω which is allowed to take any value. Hence eqn. (10) is true fo each value of ω.

521.385.032.213.13

The Institution of Electrical Engineers
Monograph No. 408 E
Oct. 1960

THE POTENTIAL DISTRIBUTION AND THERMIONIC CURRENT BETWEEN PARALLEL PLANE EMITTERS

By F. H. REYNOLDS, B.Sc.(Eng.), Associate Member.

(*The paper was first received* 21*st March, and in revised form* 20*th July*, 1960. *It was published as an* INSTITUTION MONOGRAPH *in October*, 1960.)

SUMMARY

A thermionic system formed of two parallel plane emitters facing each other is analysed. By means of Tables, the distribution of potential between the emitters and the net space-charge-limited current which flows between them can be obtained for any emitter potential, temperature and saturation current density. The results are applied to practical problems including the thermo-electric and conductivity characteristics of oxide cathodes.

LIST OF SYMBOLS

T, T' = Temperatures of facing parallel plane emitters K and K′.
J_s, J_s' = Saturated electron current densities of K and K′.
J = Space-charge-limited current density of electrons passing from K to K′.
J' = Space-charge-limited current density of electrons passing from K′ to K.
$J_{KK'}, J_{K'K}$ = Net current density of electrons passing from K to K′ or from K′ to K.
x = Co-ordinate of point between emitters referred to origin at K.
x' = Co-ordinate of K′.
x_m = Co-ordinate of potential minimum.
V = Potential at point x referred to potential origin at K.
V' = Potential of K′.
V_m = Potential at potential minimum.
v = x-directed velocity of electron at position x.
v_x = x-directed emitted-electron velocity (from K).
$n(v_x)$ = Emitted-electron velocity distribution function.
$\rho(x)$ = Space-charge density at position x.
ϕ = Emitter work-function.
A = Constant in emission equation.
e = Magnitude of the charge on an electron.
m = Electron mass.
k = Boltzmann's constant.
ϵ_0 = Permittivity of free space.
$P(z)$ = Probability function defined by eqn. (8).
$h(z), h'(z)$ = Functions defined by eqns. (22) and (23).
u = Parameter defined by eqn. (4).
l = Parameter defined by eqn. (28).
ξ, η = Generalized Langmuir parameters related by eqns. (30) and (32).

(1) INTRODUCTION

The flow of space-charge-limited current between two infinite parallel plane electrodes, when one is a thermionic emitter, was determined by Langmuir[1] in his classic paper of 1923. His solution has proved to be of great practical importance, because the plane diode forms the basis of many thermionic devices. Subsequent papers on the subject have presented Langmuir's solution in more convenient or more detailed form,[2–4] but his basic mathematical approach has not been superseded, although its validity has recently been questioned by Meltzer[5] and defended by Winwood.[6] The present paper is an extension of Langmuir's treatment to the more general problem of determining the space current when both the electrodes are thermionic emitters.

The results of the analysis can be applied to at least three distinct problems associated with thermionic systems, of which the calculation of the characteristics of the plane diode is one. The second is the determination of the thermo-electric power of either the pore of an oxide cathode as measured by Young[7] or of the symmetrical diode system used by Metson and Holmes.[10] The third problem is the evaluation of the electrical conductivity of the matrix of an oxide-coated cathode, as has been discussed by Loosjes and Vink.[11] All the experimental work referred to in this paragraph has been supported by analyses which are essentially approximations to the solution now presented.

In the application of the results of the analysis it will be found that the potential minimum, characteristic of the space-charge regime, frequently disappears into one or other of the emitters. The analysis is then no longer valid and must be replaced by simple formulae appropriate to conditions described as the retarding/saturation regime.

Except where clear indication is given to the contrary, rationalized M.K.S. units are employed.

(2) THE SPACE-CHARGE REGIME

(2.1) Density of Space Charge

Consider two plane parallel emitters K and K′ facing each other as shown in Fig. 1. Let the emitters have temperatures

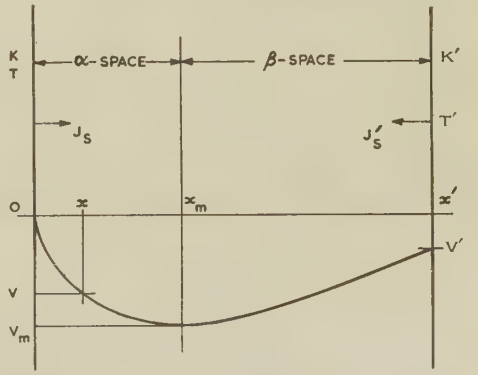

Fig. 1.—System of facing parallel plane emitters.

T and T' and saturated electron current densities J_s and J_s'. Let the location of any point between the emitters be defined by x such that the origin of x is the emitter K and let x' define the position of the emitter K′. Let the potential at any point between the emitters be defined by V, where the potential of the emitter K is taken as zero, and let V' be the potential of the emitter K′.

Correspondence on Monographs is invited for consideration with a view to publication.
Mr. Reynolds is at the Post Office Research Station.

Assume that, at a point x_m between the emitters, a potential minimum forms, of value V_m. The region between the emitter K and the plane through x_m will be called the α-space and the region from this plane up to the emitter K′ will be known as the β-space.

(2.1.1) **Space-Charge Density due to the Emitter K.**

Suppose that an electron leaving the emitter K with an x-directed velocity v_x reaches the point x with a velocity v. Also, let $n(v_x)dv_x$ be the number of electrons leaving the emitter K with a velocity in the range from v_x to $v_x + dv_x$ crossing unit area of the emitter per unit time. If, then, $\rho(x)$ is the space-charge density at x due to the emitter K,

$$\rho(x) = -e\int \frac{n(v_x)dv_x}{v} \quad . \quad . \quad . \quad . \quad (1)$$

where the integration is carried out over all the electrons crossing the plane containing x.

If the velocity distribution of the emitted electrons is Maxwellian,

$$n(v_x) = \frac{J_s m v_x}{ekT}\exp\left(-\frac{mv_x^2}{2kT}\right) \quad . \quad . \quad . \quad . \quad (2)$$

which yields

$$\rho(x) = -J_s\left(\frac{2m}{kT}\right)^{1/2}\exp\left(\frac{eV}{kT}\right)\int \exp(-u^2)du \quad . \quad (3)$$

where

$$u = \left(\frac{m}{2kT}\right)^{1/2} v \quad . \quad . \quad . \quad . \quad . \quad (4)$$

In order to evaluate the above integral, separate consideration must be given to the α- and β-spaces.

α-space.—In the α-space the electrons emitted from the emitter K contribute to the space charge at the point x in two ways. Thus, contributions are made to $\rho(x)$

(*a*) By those electrons with sufficient energy to surmount the barrier presented by V_m.

(*b*) By those electrons with sufficient energy to reach x but not enough to reach x_m; such electrons will pass x twice and make a double contribution to the space charge at x.

Thus

$$\rho(x) = -J_s\left(\frac{2m}{kT}\right)^{1/2}\exp\frac{eV}{kT}\left[\int_{v_x=a}^{\infty}\exp(-u^2)du + 2\int_{v_x=b}^{v_x=a}\exp(-u^2)du\right] \quad (5)$$

where

$$a = \left(-\frac{2eV_m}{m}\right)^{1/2} \text{ and } b = \left(-\frac{2eV}{m}\right)^{1/2}$$

If now J denotes the current density of electrons which surmount the barrier presented by V_m, then, by the retarding-field equation,

$$J = J_s \exp\frac{eV_m}{kT} \quad . \quad . \quad . \quad . \quad . \quad (6)$$

so that eqn. (5) becomes

$$\rho(x) = -J\left(\frac{\pi m}{2kT}\right)^{1/2}\varepsilon^{\eta}[1 + P(\eta^{1/2})] \quad . \quad . \quad (7)$$

where P is the probability integral or error function and η is a measure of potential defined, respectively, by

$$P(z) = \frac{2}{\pi^{1/2}}\int_0^z \exp(-u^2)du \quad . \quad . \quad . \quad . \quad (8)$$

and

$$\eta = \frac{e}{kT}(V - V_m) \quad . \quad . \quad . \quad . \quad . \quad (9)$$

β-space.—In the β-space the electrons leaving the emitter K contribute to the space charge at x in one way only—from those electrons with sufficient energy to surmount the barrier presented by V_m.

Accordingly,

$$\rho(x) = -J_s\left(\frac{2m}{kT}\right)^{1/2}\exp\frac{eV}{kT}\int_{v_x=a}^{\infty}\exp(-u^2)du \quad . \quad (10)$$

which leads to

$$\rho(x) = -J\left(\frac{\pi m}{2kT}\right)^{1/2}\varepsilon^{\eta}[1 - P(\eta^{\frac{1}{2}})] \quad . \quad . \quad (11)$$

(2.1.2) **Space-Charge Density due to the Emitter K′.**

In a manner similar to that of the previous Section, expressions can be obtained for the space-charge density $\rho'(x)$ in the α- and β-spaces due to the electrons leaving the emitter K′. If J' denotes the current density of electrons from the emitter K′ which surmount the barrier presented by V_m,

$$J' = J_s' \exp\frac{e}{kT'}(V_m - V') \quad . \quad . \quad . \quad . \quad (12)$$

and the expressions for $\rho'(x)$ are as follows:

For the α-space:

$$\rho'(x) = -J'\left(\frac{\pi m}{2kT'}\right)^{1/2}\varepsilon^{\eta'}[1 - P(\eta'^{1/2})] \quad . \quad (13)$$

For the β-space:

$$\rho'(x) = -J'\left(\frac{\pi m}{2kT'}\right)^{1/2}\varepsilon^{\eta'}[1 + P(\eta'^{1/2})] \quad . \quad (14)$$

where

$$\eta' = \frac{e}{kT'}(V - V_m) \quad . \quad . \quad . \quad . \quad (15)$$

(2.1.3) **Total Space Charge at Any Point x.**

The total space charge at any point x, either $\rho_\alpha(x)$ or $\rho_\beta(x)$ according to the space concerned, can be expressed by the sum of eqns. (7) and (13) (α-space) and eqns. (11) and (14) (β-space) to give

$$\rho_\beta^\alpha(x) = -J\left(\frac{\pi m}{2kT}\right)^{1/2}\varepsilon^{\eta}[1 \pm P(\eta^{1/2})] - J'\left(\frac{\pi m}{2kT'}\right)^{1/2}\varepsilon^{\eta'}[1 \mp P(\eta'^{1/2})] \quad (16)$$

(2.2) **Potential Gradient**

For a space-charge density of $\rho(x)$, Poisson's equation is

$$\frac{d^2V}{dx^2} = -\frac{\rho(x)}{\epsilon_0} \quad . \quad . \quad . \quad . \quad . \quad (17)$$

from which it readily follows that

$$d\left(\frac{dV}{dx}\right)^2 = -\frac{2\rho(x)}{\epsilon_0}dV \quad . \quad . \quad . \quad . \quad (18)$$

Integrating both sides of this equation from x_m to x yields

$$\left(\frac{dV}{dx}\right)^2 = -\frac{2}{\epsilon_0}\int_{V_m}^{V}\rho(x)dV \quad . \quad . \quad . \quad . \quad (19)$$

Substituting the value of eqn. (16) for $\rho(x)$ then gives, for the α-space,

$$\left(\frac{dV}{dx}\right)_\alpha^2 = \frac{J}{\epsilon_0 e}(2\pi mkT)^{1/2}h(\eta) + \frac{J'}{\epsilon_0 e}(2\pi mkT')^{1/2}h'(\eta') \quad (20)$$

and for the β-space,

$$\left(\frac{dV}{dx}\right)_\beta^2 = \frac{J}{\epsilon_0 e}(2\pi mkT)^{1/2}h'(\eta) + \frac{J'}{\epsilon_0 e}(2\pi mkT')^{1/2}h(\eta') \quad (21)$$

where h and h' are functions given by

$$h(z) = \varepsilon^z - 1 + \varepsilon^z P(z^{1/2}) - 2\left(\frac{z}{\pi}\right)^{1/2} \quad . \quad . \quad (22)$$

and $$h'(z) = \varepsilon^z - 1 - \varepsilon^z P(z^{1/2}) + 2\left(\frac{z}{\pi}\right)^{1/2} \quad . \quad . \quad (23)$$

Now from eqn. (9),

$$d\eta - \frac{e}{kT}dV$$

and with eqn. (15),

$$\eta/\eta' = T'/T \quad . \quad . \quad . \quad . \quad . \quad . \quad (25)$$

so that, for the α-space, eqn. (20) becomes

$$\left(\frac{d\eta}{dx}\right)_\alpha = \pm\frac{1}{l}\left[h(\eta) + \frac{J'}{J}\left(\frac{T'}{T}\right)^{1/2}h'\left(\frac{\eta T}{T'}\right)\right]^{1/2} \quad . \quad (26)$$

and for the β-space eqn. (21) becomes

$$\left(\frac{d\eta}{dx}\right)_\beta = \pm\frac{1}{l}\left[h'(\eta) + \frac{J'}{J}\left(\frac{T'}{T}\right)^{1/2}h\left(\frac{\eta T}{T'}\right)\right]^{1/2} \quad . \quad (27)$$

where $$\frac{1}{l} = \left(\frac{Je}{\epsilon_0}\right)^{1/2}(2\pi m)^{1/4}(kT)^{-3/4} \quad . \quad . \quad . \quad (28)$$

(2.3) Potential Distribution

In order to generalize the integration of eqns. (26) and (27) it will be convenient to eliminate l by the introduction of a new measure of distance, ξ, which for the α-space is defined by

$$\xi_\alpha = \frac{x_m - x}{l} \quad . \quad . \quad . \quad . \quad . \quad . \quad (29)$$

By differentiating eqn. (29) and invoking eqn. (26), it follows that

$$\xi_\alpha = \int_0^\eta \left[h(\eta) + \frac{J'}{J}\left(\frac{T'}{T}\right)^{1/2}h'\left(\frac{\eta T}{T'}\right)\right]^{-1/2} d\eta \quad . \quad (30)$$

Similarly, by defining ξ for the β-space by

$$\xi_\beta = \frac{x - x_m}{l} \quad . \quad . \quad . \quad . \quad . \quad . \quad (31)$$

it follows that

$$\xi_\beta = \int_0^\eta \left[h'(\eta) + \frac{J'}{J}\left(\frac{T'}{T}\right)^{1/2}h\left(\frac{\eta T}{T'}\right)\right]^{-1/2} d\eta \quad . \quad (32)$$

It should be noted that ξ_α and ξ_β are always positive.

From eqns. (30) and (32) it follows that ξ_α and ξ_β can be tabulated in terms of η, but the task is obviously formidable, particularly since there exists a different set of Tables for each pair of values of J'/J and T'/T. A selection of ξ/η Tables is given in Section 9.

(2.4) Calculation of the Space Current

Let η_K and $\eta_{K'}$ be the values of η at K and K', and let $\xi_{\alpha K}(\equiv \xi_K)$ and $\xi_{\beta K'}(\equiv \xi_{K'})$ be the values of ξ_α at K and ξ_β at K', respectively. It then follows that, from eqn. (9),

$$V' = \frac{T}{11\,606}(\eta_{K'} - \eta_K) \quad . \quad . \quad . \quad . \quad (33)$$

and, with eqn. (6),

$$\eta_K = \log_\varepsilon J_s/J \quad . \quad . \quad . \quad . \quad . \quad (34)$$

With the additional aid of eqn. (12),

$$\frac{J'}{J} = \frac{J_s'}{J_s}\exp\left(\eta_K - \frac{T}{T'}\eta_{K'}\right) \quad . \quad . \quad . \quad (35)$$

and from eqns. (29) and (31),

$$\xi_{K'} + \xi_K = \frac{x'}{l} \quad . \quad . \quad . \quad . \quad . \quad (36)$$

Substituting values for the physical constants of eqn. (28) yields

$$J^{1/2} = 1{\cdot}090 \times 10^{-6}\frac{T^{3/4}}{x'}\left(\frac{x'}{l}\right) \quad . \quad . \quad (37)$$

If $J_{KK'}$ is the net electron current density passing from K to K',

$$J_{KK'} = J\left(1 - \frac{J'}{J}\right) \quad . \quad . \quad . \quad . \quad (38)$$

If now, in a system of parallel plane emitters, x', T, T', J_s and J_s' are known, eqns. (34)–(37) together with the appropriate set of ξ/η Tables define a particular potential distribution for every value of J'/J. It is therefore necessary to choose an arbitrary value of J'/J and then find the values of J, η_K and $\eta_{K'}$ (see Section 9) which satisfy all the eqns. (34)–(37). Substituting these values in eqns. (33) and (38) then yields the voltage, V', between the emitters and the corresponding space current $J_{KK'}$.

(3) THE RETARDING/SATURATION REGIME

In the limiting conditions of the space-charge regime the potential minimum forms on either K or K'—a condition easily recognized in the course of any current/voltage determinations based on Section 2.4 by the descent of either η_K or $\eta_{K'}$, respectively, to zero. Beyond these limits the space current is simply compounded of the retarding field current from one emitter and the saturation current of the other.

When the minimum has disappeared into the emitter K,

$$J_{KK'} = J_s - J_s'\exp\left(-\frac{eV'}{kT'}\right) \quad . \quad . \quad . \quad (39)$$

V' having a positive value.

When the minimum has disappeared into the emitter K',

$$J_{KK'} = J_s\exp\left(\frac{eV'}{kT}\right) - J_s' \quad . \quad . \quad . \quad (40)$$

V' having a negative value.

(4) RESULTS

Before applying the methods of Section 2 to new problems, two checks were made. First the ξ/η Tables for $J'/J = 0$, $T'/T = 0$ were checked against Kleynen's version of Langmuir's Tables and everywhere found to agree. Secondly, two values of the potential minimum taken from Loosjes and Vink's Table were checked using the tables $J'/J = 1$ and $T'/T = 1$, and agreement was obtained to within one unit in the last decimal place shown by them.

All the curves of the following Sections are based on the assumption that the saturated current density is 1 amp/cm^2 at 1 000° K. Of the various forms of the emission equation, as, for example, summarized by Herrmann and Wagener,[12] none is

significantly superior to the others in experimental terms; the equation of de Boer

$$J_s = A \exp\left(-\frac{e\phi}{kT}\right) \quad . \quad . \quad . \quad . \quad . \quad (41)$$

has been used on the score of simplicity.

(4.1) Potential Distribution Between Parallel Plane Emitters

The most general problem to which the analysis can be applied is that of two facing emitters differing in temperature and saturation current density, having different potentials and having a net flow of space-charge-limited current (in either direction) between them.

As an example of the general solution, consider a system of parallel emitters spaced 100 μ apart, one emitter operating at 1 000° K and a saturation current density of 1 amp/cm^2 and the other operating at 900° K, the saturated emission being determined from the assumptions of Section 4 with the work function set at $\phi = 1{\cdot}0$ eV. Values of ξ_α and ξ_β have then been abstracted from the Tables for $J'/J = 10$, $T'/T = 0{\cdot}9$ and $J'/J = 0{\cdot}1$, $T'/T = 0{\cdot}9$. With the aid of eqns. (9), (29) and (31) the potential at any point in the system can be obtained and so yield the distributions shown in Fig. 2. The transmitted currents shown in Fig. 2 are readily determined from eqns. (37) and (38).

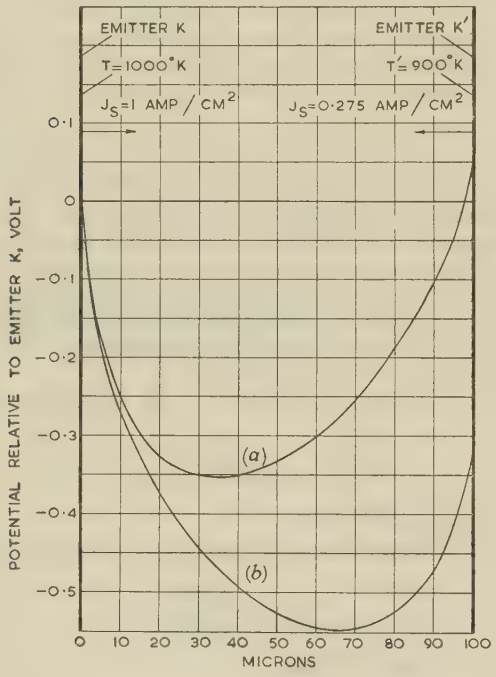

Fig. 2.—Typical potential distributions between parallel plane emitters of dissimilar potential, temperature and saturation current density.

(*a*) $J_{KK'} = 14{\cdot}8$ mA/cm^2.
(*b*) $J_{K'K} = 15{\cdot}6$ mA/cm^2.

(4.2) Thermo-Electric Properties of the Symmetrical Diode

The symmetrical diode comprises two plane parallel emitters facing each other. If no external circuit links the emitters, then, in general, a potential difference will exist between them which can be regarded as a thermo-electric voltage. The magnitude of this voltage can be investigated using the present analysis with the restriction that the transmitted current is always zero. For all thermo-electric calculations, therefore, $J'/J = 1$.

The curves in Fig. 3 show the variation of the thermo-electric

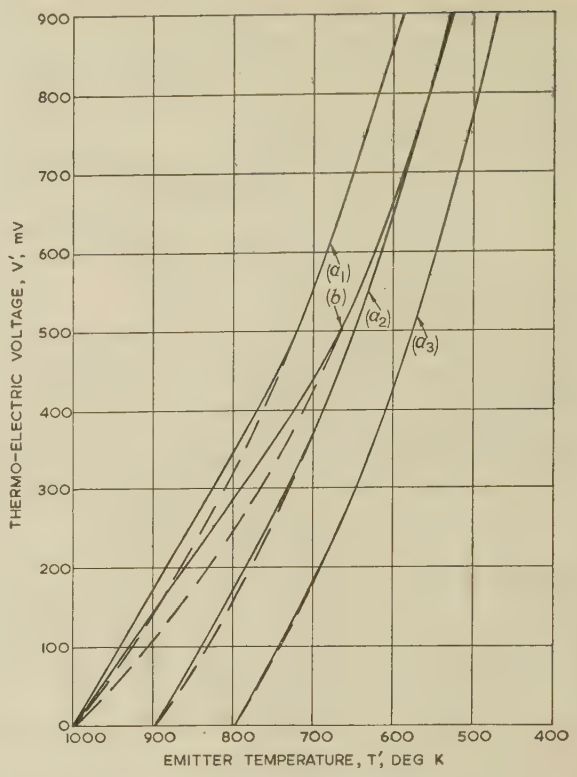

Fig. 3.—Thermo-electric voltage of symmetrical diode system.

Emitter temperatures: T constant and T' variable.
Emitter spacing: $x' = 100\,\mu$.
(a_1) $T = 1\,000°$ K
(a_2) $T = 900°$ K
(a_3) $T = 800°$ K
} $\phi = 1{\cdot}3$ eV.
(b) $T = 1\,000°$ K; $\phi = 1{\cdot}0$ eV.

voltage when one emitter (the 'fixed' emitter) is held at a fixed temperature T and the temperature of the other emitter (the 'variable' emitter), T', is varied down to values below T. The polarity of the thermo-electric voltage is then such that the fixed emitter is positive.

The striking feature of the curves in Fig. 3 is the linearity of the dependence of the thermo-electric voltage on the temperature of the variable emitter, provided, however, that the disparity in the temperatures of the emitters is not too great. The extent of the linear region of the curves increases with the temperature of the fixed emitter. In the course of the calculations for these curves it is readily apparent that the departure from linearity corresponds to the approach of $\eta_{K'}$ to zero, indicating that the potential minimum is nearing the emitter K'. If the temperature of the variable emitter is lowered still further, the potential minimum disappears into the emitter K' and the thermo-electric voltage is given by the simple relationship.

$$V' = -\phi\left(\frac{T}{T'} - 1\right) \quad . \quad . \quad . \quad . \quad (42)$$

derived from eqn. (40). The thermo-electric voltage then depends on the reciprocal of the temperature of the variable emitter.

The broken lines in Fig. 3 show how the thermo-electric voltage would have behaved if eqn. (42) were applicable at all values of T'. It is then clear that the existence of a potential minimum causes a straightening of a limited region of the smooth curve which would otherwise be obtained.

Over the linear region of the curves their slope expresses the thermo-electric power of the system, actual values being

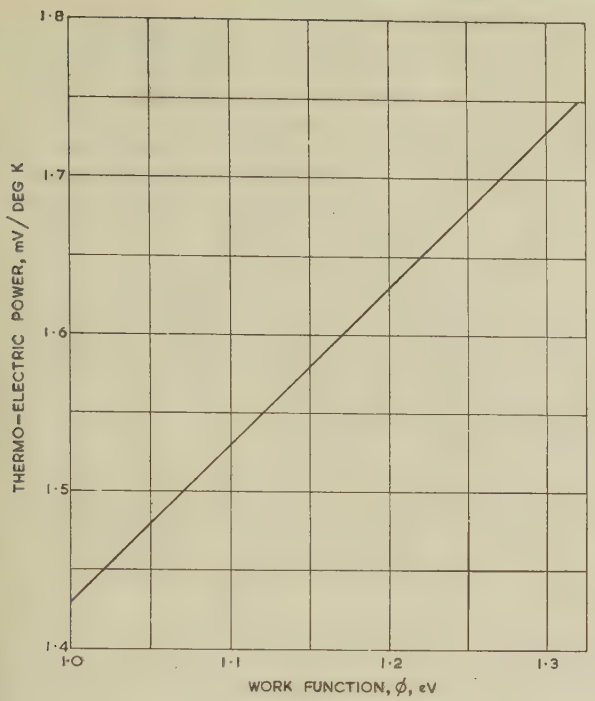

Fig. 4.—Influence of work function on the thermo-electric power of symmetrical diode system.
Emitter temperatures: $T = T' = 1\,000°\,K$.
Emitter spacing: $x' = 100\,\mu$.

$1{\cdot}73\,mV/deg\,K$ at $T = 1\,000°\,K$, $1{\cdot}76\,mV/deg\,K$ at $T = 900°\,K$ and $1{\cdot}81\,mV/deg\,K$ at $T = 800°\,K$, showing that the thermo-electric power increases, albeit slowly, with a decreasing temperature of the fixed emitter. If T is reduced sufficiently, however, the region of linear relationship between the thermo-electric voltage and the variable emitter temperature will become vanishingly small. It will still be possible to define the thermo-electric power as $T' \to T$, the value approximating ever more closely to

$$dV'/dT' = \phi/T \quad . \quad . \quad . \quad . \quad . \quad (43)$$

from eqn. (42).

Further attention to the factors influencing thermo-electric power will be given in Section 4.3, but the effect of work function can be conveniently studied from Fig. 3, which shows the effect of a change in ϕ from 1·3 to 1·0 eV. The dependence of thermo-electric power has also been calculated for a range of work functions reasonably compatible with a saturated emission of $1\,amp/cm^2$, and is shown in Fig. 4. The thermo-electric power is seen to be linearly dependent on the work function of the variable emitter.

In some practical measurements by Metson and Holmes[10] on a symmetrical diode closely approximating to that for which the calculations of this Section apply, the results presented in Fig. 3 are amply supported. They do, however, conclude that the thermo-electric power is independent of the temperature of the fixed emitter, but this is evidently not so, although the variations quoted above are small enough to be easily lost in experimental error. The value of the thermo-electric power quoted by Metson and Holmes is $2{\cdot}23\,mV/deg\,K$, which is certainly higher than the value of $1{\cdot}73\,mV/deg\,K$ (at $1\,000°\,K$) quoted here. It will, however, emerge from Section 4.3 that thermo-electric power increases with the spacing between the emitters. The discrepancy could therefore be due to the spacing being in excess of $100\,\mu$ on account of coating shrinkage during decomposition of the carbonates. Experimental support for the dependence of thermo-electric power on temperature is provided by Young[7] who, with a symmetrical diode of about $300\,\mu$ spacing, measured values ranging from about $2{\cdot}2\,mV/deg\,K$ at $1\,100°\,K$ to $3{\cdot}2\,mV/deg\,K$ at $700°\,K$.

(4.3) Thermo-Electric Properties of the Pore of an Oxide Cathode

In order to explain observed conduction properties of oxide-coated cathodes, Loosjes and Vink[11] proposed that the oxide matrix be regarded as a porous aggregate of crystals, all the crystal surfaces having uniform thermionic properties. They then postulated that, if the cathode temperature were high enough, the transport of current through the matrix was due to the successive emission and absorption of electrons from and by the walls of the pores. It is easy to show that, if the temperature distribution along a chain of pores can be assumed to be linear, the thermo-electric power of the matrix is equal to that of its constituent pores. In order to study the thermo-electric power of an oxide matrix, therefore, it is necessary to examine only a single pore, which—being merely a miniature symmetrical diode—permits a qualitative application of the results given in the previous Section.

In order to appreciate more fully the factors which influence thermo-electric power, Fig. 5 has been prepared to show its dependence, as $T' \to T$, on the reciprocal of the pore temperature. The curves illustrate particularly the effect of pore size and work function. The broken lines are given by eqn. (43); their slope and position depends only on work function, so that the curves for any given size of pore will approximate to the line of appropriate work function as the pore temperature is reduced, the approximation at any given temperature being the closer the smaller the pore.

The curves show at once that the thermo-electric power increases with increasing spacing between the emitters, as suggested in Section 4.2. They also show that it is unsafe to

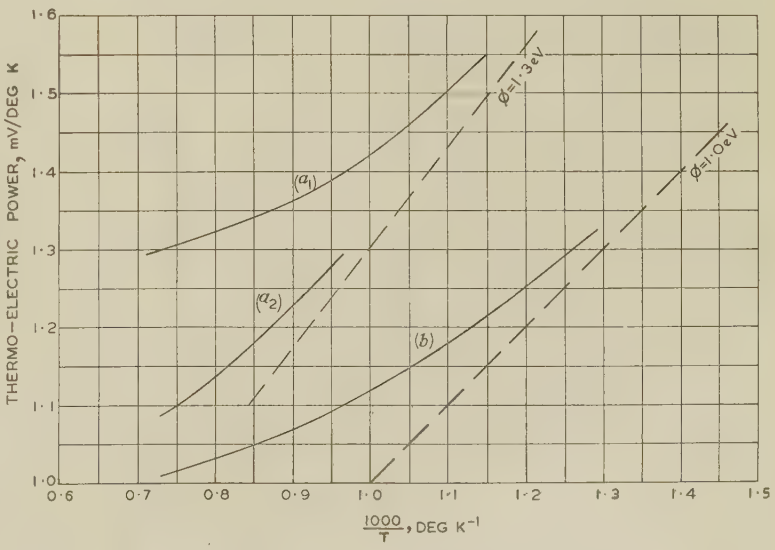

Fig. 5.—Thermo-electric power of the pore of an oxide cathode.
Oxide temperature $= T°\,K$; pore size $= x'$ microns.
(a_1) $x' = 10\,\mu$ } $\phi = 1{\cdot}3\,eV$.
(a_2) $x' = 2\,\mu$ }
(b) $x' = 10\,\mu$; $\phi = 1{\cdot}0\,eV$.

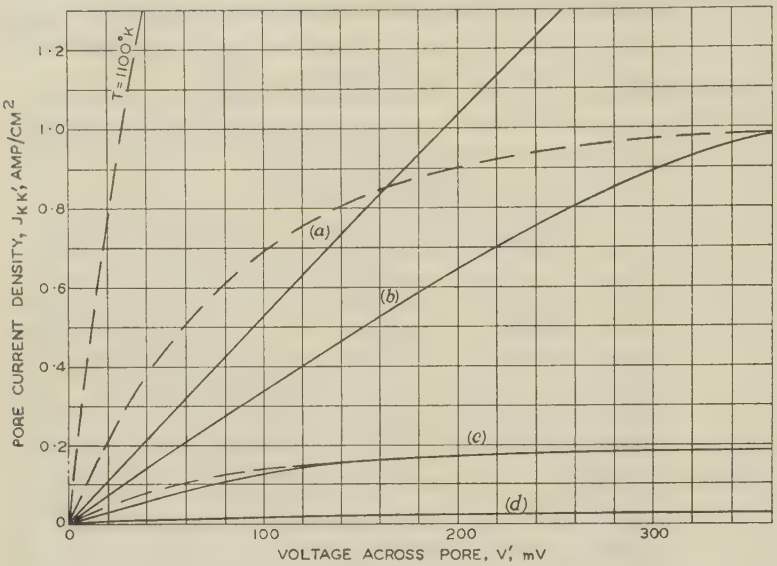

Fig. 6.—Resistive characteristics of the pore of an oxide cathode.
Oxide temperature = $T°$K; $\phi = 1{\cdot}3$eV; pore size $x' = 10\,\mu$.
(*a*) $T = 1\,100°$K.
(*b*) $T = 1\,000°$K.
(*c*) $T = 900°$K.
(*d*) $T = 800°$K.

use the slope of any experimentally plotted curve to estimate the work function, as Young[7] has done. The curves in Fig. 5 are not even linear, although they might well be mistaken for straight lines when obtained from practical measurements over a restricted range of temperature. It should be clearly understood that such curves are never truly linear, no matter how small the pore, because a potential minimum always forms between the walls of two identical emitters at the same temperature and potential. If the position of the appropriate curve for the symmetrical diode system of Section 4.2 is imagined plotted in Fig. 5 (it will lie off the top of the grid tending to the line for $\phi = 1{\cdot}3$), it is easy to see why some authors (Metson and Holmes) have concluded, from measurements, that thermoelectric power is independent of temperature while others (Young), using an oxide matrix, have reported a linear dependence on the reciprocal of the temperature.

(4.4) Electrical Conductivity of the Coating of an Oxide Cathode

Provided that the cathode temperature is sufficiently high, the electrical conductivity of the matrix of an oxide-coated cathode can be calculated from the results of the present analysis by again adopting Loosjes and Vink's concept of pore conduction. Each pore is a pair of facing parallel plane emitters of equal temperature. Current/voltage relationships for the pore can then be obtained by setting $T'/T = 1$ and varying J'/J.

Typical resistive characteristics for a $10\,\mu$ pore are shown in Fig. 6. The curves show that, as the voltage across the pore is increased, the transmitted current increases in an almost linear manner at first, subsequently becoming distinctly non-linear until the current density approaches a constant value. Over the substantially linear portion of these curves the potential minimum is moving from the centre of the pore towards the wall of lower potential. Before the potential minimum reaches the wall, the marked curvature of the current/voltage characteristic has set in. When the minimum reaches and passes into the wall the conditions of the retarding/saturation regime prevail and eqn. (39) applies. The broken lines in Fig. 6 show what the current/voltage relationship would have been if eqn. (39) were valid at all voltages. Once again, therefore, the action of the potential minimum is one of straightening out an otherwise non-linear curve. The constant values to which the curves are asymptotic are, of course, the saturation current densities of the walls of the pore.

The effect of the pore size on the resistive characteristics is illustrated by Fig. 7 at two different matrix temperatures. All the curves of one temperature are seen to merge into the same retarding field/saturation line, the extent of the linear portion of each curve being greater the larger the pore.

It is clear that curves such as those of Figs. 6 and 7 can be used to determine the specific conductivity of an oxide matrix, although the non-linear character of the resistive curves demands care in the definition of conductivity. In the results which follow the specific conductivity has been determined from the slope of the current/voltage curves at the origin. The dependence of specific conductivity on the reciprocal of temperature is then shown by Fig. 8, arranged in a way which illustrates the influence of work function and pore size. The broken lines on the Figure represent the slopes of the retarding/saturation characteristics at the origin.

The importance of Fig. 8 is believed to be twofold. First, it illustrates the hazards in interpreting the slope of any seemingly linear curve obtained from an experimental plot of the logarithm of the conductivity against $1\,000/T$; the effect of the potential minimum in pores of $2\,\mu$ width is not negligible, but by the time the size has reached $10\,\mu$ the curvature is very marked.

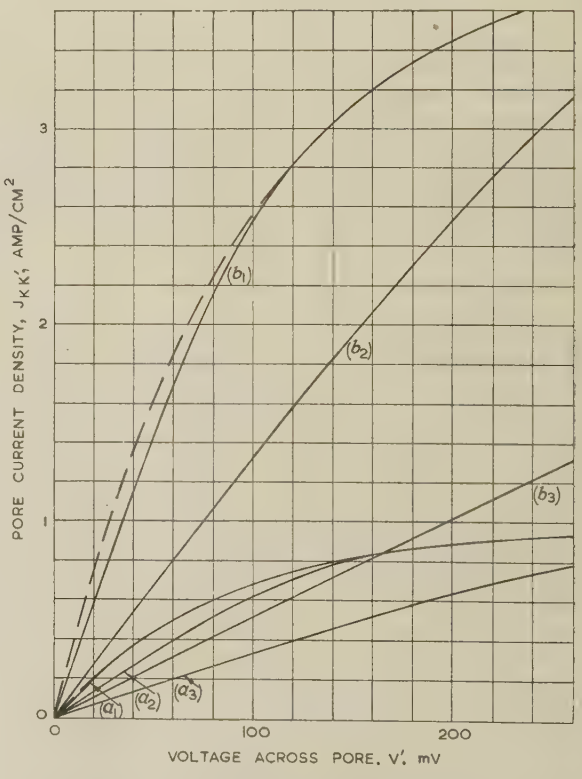

Fig. 7.—Influence of pore size on the resistive characteristics of the pore of an oxide cathode.
Oxide temperature = $T°$K; $\phi = 1{\cdot}3$eV; pore size = x' microns.
(a_1) $x' = 2\,\mu$
(a_2) $x' = 5\,\mu$
(a_3) $x' = 10\,\mu$
} $T = 1\,000°$K.
(b_1) $x' = 2\,\mu$
(b_2) $x' = 5\,\mu$
(b_3) $x' = 10\,\mu$
} $T = 1\,100°$K.

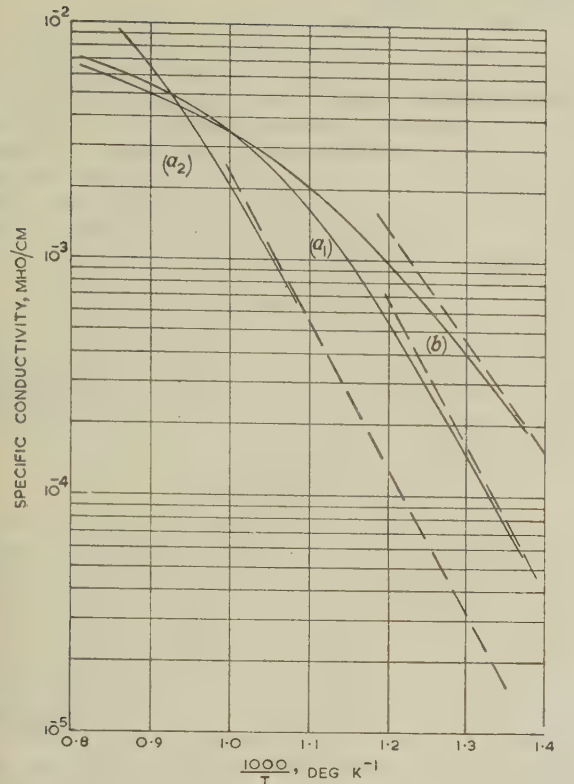

Fig. 8.—Specific conductivity of the pore of an oxide cathode.

Oxide temperature = $T°$ K; pore size = x' microns.
(a_1) $x' = 10\,\mu$ } $\phi = 1{\cdot}3$ eV.
(a_2) $x' = 2\,\mu$ }
(b) $x' = 10\,\mu$; $\phi = 1{\cdot}0$ eV.

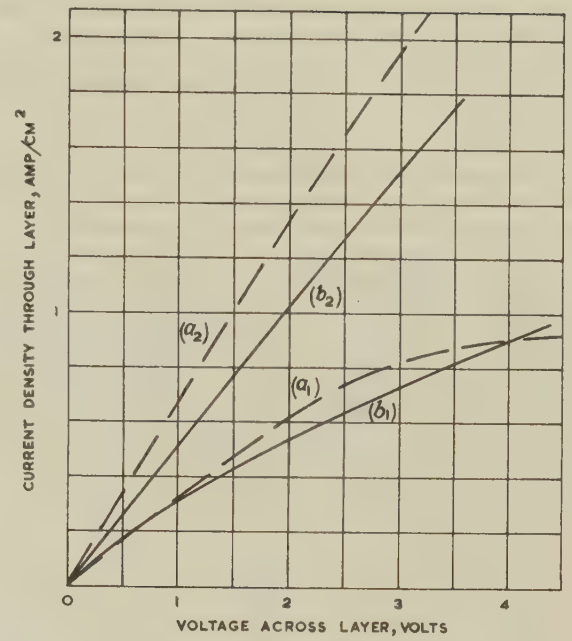

Fig. 9.—Theoretical current/voltage characteristics of oxide layer compared with experimental values.

Oxide temperature = $T°$ K; pore size $x' = 5\,\mu$; $\phi = 1{\cdot}3$ eV; thickness of layer = $100\,\mu$.
(a_1) $T = 1\,000°$ K } calculated.
(a_2) $T = 1\,100°$ K }
(b_1) $T = 1\,000°$ K } from the measurements of
(b_2) $T = 1\,100°$ K } Loosjes and Vink.

Secondly, although the curves embrace a modest range of pore size and work function, they all converge to a value of about 0·004 mho/cm at about 1 050° K, which is a typical working temperature for an oxide-coated cathode.

Comparisons between theoretical and measured values of conductivity must inevitably be treated with some reserve, on account of the difficulty of interpreting the words 'pore size'. Of the few experimenters who have attempted to assign a number to this quantity, Loosjes and Vink[11] quote 2–5 μ and Metson[8] 10 μ. With 5 μ and a work function of 1·3 eV, Fig. 9 shows a comparison between the resistive characteristics of Loosjes and Vink* and the calculated values now obtained. The agreement is considered to be very reasonable. Some curves of the logarithm of the specific conductivity against the reciprocal of the oxide temperature published by Loosjes and Vink, Hensley[13] and Metson[9] for 'well-activated' oxide matrices are plotted in Fig. 10 against the theoretical background. The curve due to Metson is typical of the many such curves which have been published in this temperature range, from the slopes of which values for the activation energy of the conduction have often been quoted in the region of 0·4–0·5 eV. In their paper, Loosjes and Vink have concluded that, on the pore conduction theory, the activation energy should be equal to the work function of the emitting surfaces. They considered that curves of the type obtained by Metson are not truly representative of pore conduction and must be corrected for the effects of a solid conduction process through the crystals of the oxide matrix. After making such a correction they produced the curve shown

* The parameters on Loosjes and Vink's curves are not precisely 1 000° and 1 100° K, but they show sufficient curves at other temperatures to permit the fairly accurate interpolation shown in Fig. 9.

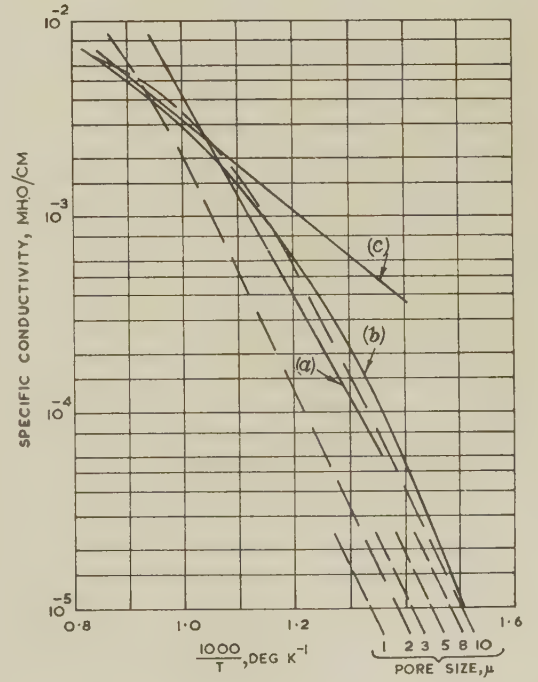

Fig. 10.—Comparison of theoretical and experimental values of specific conductivity.

Oxide temperature = $T°$ K; $\phi = 1{\cdot}3$ eV.
Theoretical curves as a function of pore size shown by broken lines.
Experimental curves (a) Loosjes and Vink.
(b) Hensley.
(c) Metson.

on Fig. 10. It is believed, however, that this correcting procedure is not entirely satisfactory; moreover, as shown by Hensley, when the parallel solid conduction process is eliminated by an ingenious experimental arrangement, the pore-conduction curve remains unaltered.

From the results of the present analysis it is readily seen that values of the apparent activation energy substantially less than the work function are by no means incompatible with the pore-conduction theory. The range of temperature over which pore-conductivity measurements can be made is normally quite limited, owing to activation effects at high temperatures (Loosjes and Vink consider the limit to be 1 100° K) and the proportionate increase in solid conductivity at low temperatures which imposes a limit at about 800° K. The curvature of the theoretical curves of Fig. 10 could therefore be easily lost in experimental error. It is interesting to observe that on the originals of both Metson's and Loosjes and Vink's curves experimental points are shown departing from the drawn lines in the way now predicted. Hensley's true pore-conduction curve shown in Fig. 10 bears a very satisfactory resemblance to the theoretical shape.

It is finally of interest to observe that the independence of specific conductivity on pore size and work function implies that any well-activated oxide coating of given area and thickness will tend to exhibit a constant resistance at customary operating temperatures. In particular, if the value mentioned (0·004 mho/cm) is applied to the oxide matrix used by Metson,[8] the calculated resistance of the matrix is 16·6 ohms, which is in very close agreement with his measured values of 14–15 ohms.

(5) SOME CONSIDERATIONS OF ACCURACY AND VALIDITY

As a solution to the explicit problem of the potential distribution and current transmission between parallel plane emitters, the analysis is believed to be accurate in so far as the mathematics is not compromised by doubtful assumptions. It is true that Meltzer[5] has recently sought to show that in Langmuir's diode theory the effect of the magnetic field produced by the flow of current is not negligible and ought to be taken into account. Langmuir's solution is, however, supported by both direct[4] and indirect[14] measurements. Since Meltzer's views have also been seriously challenged on theoretical grounds,[6] the question is still an open one. If, however, it should prove that the present theory is in error on this account, those results for which the current is either zero (thermo-electric effects) or vanishingly so (specific conductivities) will remain unaffected.

In the application of the results to practical thermionic systems the symmetrical diode fits the theoretical assumptions fairly closely, so that the calculated results should be accurate. When applied to the pore model, there are certainly several reasons for challenging the validity of the theory, not the least being that the pore of an oxide cathode is very far from resembling a cube. The theory also neglects the emission from those walls of the pores which lie parallel to the direction of electron flow. The effect of these side walls is considered by Hensley[15] in an approximate theory which suggests that neglect of the walls does result in some underestimation of the effects of space-charge. It is conceivable that an analysis could be obtained which would solve the potential distribution within a 'thermionic cube'. This notion has been developed by Paulisch,[16] who believes that the potential depression in the centre of the cube causes the electrons to traverse the cube along paths close to the walls of the pores.

(6) CONCLUSION

The theory of the system of parallel plane emitters, developed primarily as an analytical exercise, can be applied to practical thermionic systems. The analysis is believed to clarify the meaning of thermo-electric voltage and power as applied to systems of facing emitters. The analysis provides considerable support for the pore-conduction theory of oxide-coated cathodes, at the same time explaining some of the outstanding difficulties of the theory. In particular, while other writers have not overlooked the effect of space-charge in the pores, the present results indicate that it plays a more important part than has hitherto been realized. The analysis would provide a firm foundation for the development of any new thermionic systems or devices based on facing parallel plane emitters.

(7) ACKNOWLEDGMENTS

Acknowledgment is made to the Engineer-in-Chief of the Post Office for permission to make use of the information contained in the paper. The author also wishes to thank Miss V. S. Brook for preparing the digital-computer programme for the integrals of eqns. (30) and (32).

(8) REFERENCES

(1) Langmuir, I.: 'The Effect of Space-Charge and Initial Velocities on the Potential Distribution between Parallel Plane Electrodes', *Physical Review*, 1923, **21**, p. 419.

(2) Kleynen, P. H. J. A.: 'Extension of Langmuir's (ξ/η) Tables for a Plane Diode with a Maxwellian Distribution of the Electrons', *Philips Research Reports*, 1946, **1**, p. 81

(3) Van Der Ziel, A.: 'Extension and Application of Langmuir's Calculations on a Plane Diode with Maxwellian Velocity Distribution of the Electrons', *ibid.*, p. 97.

(4) Ferris, W. R.: 'Some Characteristics of Diodes with Oxide-Coated Cathodes', *RCA Review*, 1949, **10**, p. 134.

(5) Meltzer, B.: 'Magnetic Forces and Relativistic Speeds in Stationary Electron Beams', *Journal of Electronics and Control*, 1958, **4**, p. 350, and 1958, **5**, p. 348.

(6) Winwood, J. M.: 'Comment on Magnetic Forces and Relativistic Speeds in Stationary Electron Beams', *ibid.*, p. 161 and 1959, **6**, p. 258.

(7) Young, J. R.: 'Electrical Conductivity and Thermo-Electric Power of (BaSr)0 and Ba0', *Journal of Applied Physics*, 1952, **23**, p. 1129.

(8) Metson, G. H.: 'The Conductivity of Oxide Cathodes, Part 1.—Potential Distribution', *Proceedings I.E.E.*, Monograph No. 221 R, February, 1957 (**104** C, p. 316).

(9) Metson, G. H.: 'The Conductivity of Oxide Cathodes, Part 4.—Electron Transfer Mechanisms', *ibid.*, Monograph No. 269 R, December, 1957 (**105** C, p. 189).

(10) Metson, G. H., and Holmes, M. F.: 'The Conductivity of Oxide Cathodes, Part 9.—Thermo-Electric Power' (see page 83).

(11) Loosjes, R., and Vink, H. J.: 'The Conduction Mechanism in Oxide-Coated Cathodes', *Philips Research Reports*, 1949, **4**, p. 449.

(12) Herrmann, G., and Wagener, S.: 'The Oxide-Coated Cathode' (Chapman and Hall, 1951), Volume 2, p. 179.

(13) Hensley, E. B.: 'Conduction Mechanism in Oxide-Coated Cathodes', *Journal of Applied Physics*, 1956, **27**, p. 286.

(14) Liebmann, G.: 'The Calculation of Amplifier Valve Characteristics', *Journal I.E.E.*, 1946, **93**, Part III, p. 138.

(15) Hensley, E. B.: 'On the Electrical Properties of Porous Semiconductors', *Journal of Applied Physics*, 1952, **23**, p. 1122.

(16) Paulisch, A.: 'Über den Hochtemperatur—Leitungsmechanismus thermisch Elektronen emittierender Oxyde', *Zeitschrift für angewandte Physik*, 1957, **9**, p. 412.

(17) Lindsay, P. A., and Parker, F. W.: 'Potential Distribution between two Plane Emitting Electrodes', *Journal of Electronics and Control*, 1959, **7**, p. 289.

Table 1

VARIATION OF ξ WITH η AND T'/T FOR $J'/J = 1$

η	$T'/T = 1$	$T'/T = 0{\cdot}9$		$T'/T = 0{\cdot}8$		$T'/T = 0{\cdot}7$		$T'/T = 0{\cdot}6$	
	ξ_α ξ_β	ξ_α	ξ_β	ξ_α	ξ_β	ξ_α	ξ_β	ξ_α	ξ_β
0·0001	0·01414	0·01469	0·01469	0·01526	0·01528	0·01587	0·01589	0·01651	0·01654
0·0002	0·02000	0·02077	0·02078	0·02158	0·02161	0·02244	0·02248	0·02334	0·02340
0·0003	0·02449	0·02543	0·02545	0·02643	0·02647	0·02748	0·02754	0·02858	0·02866
0·0004	0·02828	0·02937	0·02939	0·03051	0·03056	0·03173	0·03180	0·03300	0·03310
0·0005	0·03162	0·03283	0·03286	0·03411	0·03417	0·03547	0·03556	0·03688	0·03702
0·0006	0·03464	0·03596	0·03600	0·03737	0·03744	0·03885	0·03896	0·04040	0·04056
0·0008	0·04000	0·04152	0·04157	0·04314	0·04323	0·04484	0·04500	0·04663	0·04685
0·0010	0·04472	0·04642	0·04648	0·04822	0·04834	0·05013	0·05032	0·05212	0·05239
0·0012	0·04898	0·05085	0·05091	0·05282	0·05296	0·05490	0·05513	0·05708	0·05740
0·0014	0·05291	0·05492	0·05500	0·05704	0·05721	0·05929	0·05956	0·06164	0·06202
0·0016	0·05656	0·05870	0·05879	0·06098	0·06117	0·06337	0·06368	0·06588	0·06631
0·0018	0·05999	0·06226	0·06236	0·06467	0·06488	0·06720	0·06755	0·06986	0·07035
0·0020	0·06324	0·06562	0·06574	0·06816	0·06840	0·07083	0·07121	0·07362	0·07417
0·0022	0·06632	0·06882	0·06895	0·07148	0·07174	0·07427	0·07470	0·07720	0·07780
0·0025	0·07070	0·07336	0·07350	0·07618	0·07648	0·07916	0·07964	0·08227	0·08295
0·0050	0·09996	0·1037	0·1040	0·1076	0·1082	0·1118	0·1128	0·1161	0·1175
0·0075	0·1224	0·1269	0·1273	0·1317	0·1326	0·1368	0·1382	0·1420	0·1441
0·0100	0·1413	0·1465	0·1471	0·1520	0·1532	0·1578	0·1597	0·1638	0·1665
0·015	0·1730	0·1793	0·1801	0·1859	0·1877	0·1929	0·1958	0·2002	0·2042
0·020	0·1997	0·2068	0·2080	0·2144	0·2168	0·2224	0·2262	0·2307	0·2361
0·025	0·2231	0·2311	0·2325	0·2395	0·2425	0·2483	0·2531	0·2575	0·2643
0·030	0·2443	0·2530	0·2547	0·2621	0·2657	0·2717	0·2774	0·2816	0·2898
0·035	0·2638	0·2731	0·2750	0·2828	0·2870	0·2931	0·2998	0·3038	0·3133
0·040	0·2819	0·2917	0·2940	0·3021	0·3069	0·3130	0·3206	0·3243	0·3351
0·045	0·2989	0·3092	0·3118	0·3201	0·3256	0·3316	0·3402	0·3435	0·3557
0·05	0·3149	0·3258	0·3286	0·3372	0·3432	0·3492	0·3588	0·3616	0·3752
0·06	0·3447	0·3564	0·3598	0·3688	0·3760	0·3817	0·3932	0·3952	0·4115
0·07	0·3720	0·3845	0·3885	0·3977	0·4061	0·4116	0·4250	0·4259	0·4449
0·08	0·3973	0·4106	0·4151	0·4246	0·4342	0·4392	0·4545	0·4544	0·4760
0·09	0·4211	0·4350	0·4401	0·4497	0·4605	0·4650	0·4822	0·4809	0·5053
0·10	0·4435	0·4581	0·4637	0·4734	0·4853	0·4894	0·5085	0·5060	0·5330
0·12	0·4850	0·5007	0·5074	0·5171	0·5315	0·5343	0·5572	0·5522	0·5846
0·14	0·5230	0·5397	0·5475	0·5571	0·5739	0·5754	0·6021	0·5943	0·6321
0·16	0·5582	0·5757	0·5847	0·5941	0·6132	0·6133	0·6438	0·6332	0·6763
0·18	0·5910	0·6094	0·6194	0·6286	0·6500	0·6487	0·6829	0·6694	0·7179
0·20	0·6220	0·6410	0·6522	0·6610	0·6848	0·6819	0·7198	0·7034	0·7572
0·22	0·6512	0·6710	0·6832	0·6917	0·7178	0·7132	0·7549	0·7355	0·7946
0·24	0·6791	0·6994	0·7128	0·7207	0·7492	0·7429	0·7884	0·7659	0·8303
0·26	0·7056	0·7265	0·7410	0·7485	0·7793	0·7713	0·8205	0·7948	0·8645
0·28	0·7310	0·7525	0·7680	0·7750	0·8081	0·7983	0·8513	0·8225	0·8975
0·30	0·7554	0·7774	0·7940	0·8004	0·8358	0·8243	0·8809	0·8490	0·9292
0·35	0·8125	0·8356	0·8549	0·8598	0·9010	0·8849	0·9508	0·9108	1·004
0·40	0·8649	0·8890	0·9111	0·9142	0·9612	0·9403	1·015	0·9673	1·074
0·45	0·9135	0·9385	0·9632	0·9646	1·017	0·9916	1·076	1·019	1·139
0·5	0·9589	0·9846	1·012	1·011	1·070	1·039	1·133	1·068	1·200
0·6	1·042	1·069	1·101	1·097	1·166	1·126	1·237	1·156	1·314
0·7	1·116	1·144	1·181	1·173	1·253	1·203	1·332	1·234	1·418
0·8	1·183	1·211	1·254	1·242	1·333	1·273	1·419	1·305	1·513
0·9	1·244	1·273	1·321	1·304	1·406	1·336	1·500	1·369	1·602
1·0	1·300	1·330	1·383	1·362	1·474	1·394	1·575	1·427	1·685
1·2	1·400	1·431	1·493	1·463	1·597	1·497	1·711	1·531	1·837
1·4	1·487	1·518	1·590	1·552	1·705	1·586	1·832	1·621	1·974
1·6	1·562	1·595	1·675	1·628	1·801	1·663	1·941	1·698	2·097
1·8	1·629	1·662	1·751	1·696	1·887	1·731	2·040	1·767	2·210
2·0	1·689	1·722	1·819	1·756	1·965	1·791	2·129	1·827	2·314
2·2	1·742	1·775	1·880	1·809	2·035	1·845	2·211	1·881	2·410
2·5	1·811	1·844	1·960	1·879	2·130	1·914	2·322	1·951	2·540
3·0	1·903	1·937	2·070	1·972	2·261	2·008	2·479	2·045	2·729
4·0	2·029	2·063	2·225	2·098	2·451	2·135	2·715	2·171	3·022
5·0	2·105	2·139	2·322	2·174	2·577	2·210	2·878	2·247	3·235
6·0	2·151	2·185	2·384	2·220	2·661	2·256	2·992	2·293	3·392
8·0	2·196	2·230	2·449	2·265	2·755	2·301	3·129	2·338	3·592
10·0	2·212	2·246	2·475	2·281	2·796	2·317	3·196	2·354	3·702
20·0	2·221	2·255	2·492	2·291	2·830	2·327	3·261	2·364	3·828
50·0	2·221	2·255	2·493	2·291	2·831	2·327	3·263	2·364	3·835

Table 2

VARIATION OF ξ WITH η AND J'/J WITH $T'/T = 1$

η	$J'/J = 0{\cdot}8$		$J'/J = 0{\cdot}4$		$J'/J = 0{\cdot}2$		$J'/J = 0{\cdot}1$	
	ξ_α	ξ_β	ξ_α	ξ_β	ξ_α	ξ_β	ξ_α	ξ_β
0·0001	0·01490	0·01491	0·01689	0·01692	0·01823	0·01828	0·01904	0·01910
0·0002	0·02108	0·02109	0·02388	0·02393	0·02577	0·02587	0·02691	0·02703
0·0003	0·02581	0·02583	0·02924	0·02932	0·03155	0·03169	0·03294	0·03312
0·0004	0·02980	0·02983	0·03375	0·03386	0·03642	0·03661	0·03802	0·03826
0·0005	0·03332	0·03335	0·03773	0·03786	0·04071	0·04094	0·04249	0·04279
0·0006	0·03649	0·03653	0·04132	0·04148	0·04458	0·04486	0·04653	0·04688
0·0008	0·04214	0·04219	0·04770	0·04792	0·05145	0·05182	0·05370	0·05417
0·0010	0·04711	0·04717	0·05331	0·05358	0·05750	0·05796	0·06001	0·06059
0·0012	0·05160	0·05167	0·05839	0·05871	0·06297	0·06352	0·06570	0·06641
0·0014	0·05573	0·05581	0·06305	0·06343	0·06799	0·06863	0·07094	0·07176
0·0016	0·05957	0·05967	0·06739	0·06782	0·07266	0·07339	0·07580	0·07674
0·0018	0·06318	0·06329	0·07146	0·07195	0·07704	0·07786	0·08037	0·08143
0·0020	0·06659	0·06672	0·07531	0·07585	0·08118	0·08210	0·08469	0·08586
0·0022	0·06984	0·06998	0·07897	0·07957	0·08512	0·08613	0·08879	0·09008
0·0025	0·07444	0·07460	0·08416	0·08484	0·09070	0·09185	0·09460	0·09607
0·0050	0·1052	0·1055	0·1188	0·1202	0·1279	0·1302	0·1333	0·1363
0·0075	0·1288	0·1293	0·1453	0·1473	0·1563	0·1598	0·1629	0·1673
0·0100	0·1486	0·1493	0·1676	0·1703	0·1802	0·1848	0·1877	0·1936
0·015	0·1819	0·1828	0·2048	0·2088	0·2200	0·2269	0·2290	0·2378
0·020	0·2099	0·2111	0·2360	0·2414	0·2534	0·2625	0·2636	0·2753
0·025	0·2344	0·2360	0·2634	0·2702	0·2826	0·2940	0·2939	0·3086
0·030	0·2566	0·2585	0·2881	0·2962	0·3089	0·3226	0·3211	0·3387
0·035	0·2770	0·2792	0·3107	0·3202	0·3330	0·3489	0·3461	0·3666
0·040	0·2959	0·2984	0·3317	0·3425	0·3553	0·3735	0·3691	0·3925
0·045	0·3137	0·3164	0·3513	0·3635	0·3761	0·3966	0·3907	0·4170
0·05	0·3304	0·3335	0·3699	0·3834	0·3958	0·4186	0·4110	0·4403
0·06	0·3615	0·3652	0·4042	0·4204	0·4322	0·4595	0·4485	0·4836
0·07	0·3900	0·3943	0·4356	0·4545	0·4654	0·4972	0·4828	0·5237
0·08	0·4164	0·4213	0·4646	0·4862	0·4961	0·5324	0·5144	0·5612
0·09	0·4411	0·4467	0·4918	0·5160	0·5247	0·5656	0·5439	0·5965
0·10	0·4645	0·4706	0·5173	0·5442	0·5517	0·5970	0·5717	0·6300
0·12	0·5076	0·5150	0·5645	0·5967	0·6013	0·6556	0·6227	0·6927
0·14	0·5471	0·5556	0·6075	0·6449	0·6465	0·7097	0·6691	0·7506
0·16	0·5836	0·5933	0·6472	0·6898	0·6881	0·7602	0·7118	0·8048
0·18	0·6177	0·6285	0·6841	0·7319	0·7268	0·8078	0·7515	0·8560
0·20	0·6497	0·6617	0·7188	0·7717	0·7630	0·8528	0·7886	0·9046
0·22	0·6800	0·6932	0·7515	0·8096	0·7972	0·8957	0·8235	0·9509
0·24	0·7088	0·7231	0·7825	0·8456	0·8295	0·9368	0·8565	0·9954
0·26	0·7362	0·7517	0·8120	0·8802	0·8602	0·9762	0·8879	1·038
0·28	0·7624	0·7790	0·8401	0·9134	0·8895	1·014	0·9179	1·079
0·30	0·7876	0·8053	0·8671	0·9454	0·9175	1·051	0·9465	1·119
0·35	0·8464	0·8669	0·9300	1·021	0·9828	1·137	1·013	1·214
0·40	0·9004	0·9236	0·9875	1·090	1·042	1·218	1·074	1·303
0·45	0·9503	0·9763	1·040	1·155	1·097	1·294	1·129	1·386
0·5	0·9969	1·025	1·090	1·216	1·148	1·365	1·181	1·465
0·6	1·082	1·115	1·179	1·329	1·240	1·498	1·274	1·613
0·7	1·157	1·196	1·258	1·430	1·321	1·619	1·357	1·749
0·8	1·226	1·269	1·330	1·523	1·394	1·731	1·430	1·876
0·9	1·288	1·336	1·394	1·609	1·460	1·834	1·497	1·995
1·0	1·345	1·397	1·454	1·688	1·521	1·931	1·558	2·107
1·2	1·447	1·507	1·559	1·831	1·627	2·108	1·666	2·313
1·4	1·534	1·602	1·649	1·957	1·719	2·266	1·758	2·500
1·6	1·611	1·686	1·727	2·068	1·798	2·408	1·838	2·671
1·8	1·679	1·760	1·796	2·167	1·868	2·536	1·908	2·827
2·0	1·738	1·826	1·857	2·256	1·929	2·651	1·969	2·971
2·2	1·792	1·884	1·911	2·335	1·983	2·756	2·024	3·103
2·5	1·861	1·961	1·981	2·440	2·054	2·896	2·095	3·281
3·0	1·954	2·064	2·075	2·582	2·148	3·088	2·189	3·532
4·0	2·081	2·205	2·202	2·779	2·276	3·358	2·317	3·896
5·0	2·157	2·289	2·278	2·898	2·352	3·524	2·393	4·125
6·0	2·202	2·341	2·324	2·970	2·398	3·626	2·439	4·267
8·0	2·247	2·390	2·368	3·040	2·442	3·725	2·483	4·407
10·0	2·263	2·409	2·385	3·066	2·458	3·762	2·500	4·459
20·0	2·273	2·419	2·394	3·081	2·468	3·783	2·509	4·489
50·0	2·273	2·419	2·394	3·081	2·468	3·783	2·509	4·489

(9) APPENDIX: DERIVATION OF THE ξ/η TABLES

The integrals of eqns. (30) and (32) have been programmed for a Mercury computer, using repeated Simpsonian quadrature. Series expansions have been obtained to express the integrals in the vicinity of the origin of η, where the integrands become infinite, a suitably accurate approximation being used to express the probability function. A desired set of Tables is readily obtained by punching the appropriate values of J'/J and T'/T on to a data tape. Tables now available include those for $J'/J=0$, $T'/T=0$; $J'/J=0{\cdot}1$, $T'/T=0{\cdot}6(0{\cdot}1)1{\cdot}0$; $J'/J=1{\cdot}0$, $T'/T=0{\cdot}6(0{\cdot}05)1{\cdot}0$; $J'/J=10$, $T'/T=0{\cdot}6(0{\cdot}1)1{\cdot}0$; $J'/J=20(10)40$, $T'/T=0{\cdot}9$ and $J'/J=0{\cdot}2(0{\cdot}2)0{\cdot}8$, $0{\cdot}9$, 20, 30, 40, $T'/T=1{\cdot}0$. Some of the most useful selected from this list, are given in abridged form as Tables 1 and 2.

Since the submission of the present paper, Lindsay and Parker[17] have also obtained eqns. (30) and (32), employing a somewhat different analysis. Their evaluation of the integrals is confined to the case of $T'/T=1$, for which they quote values in good agreement with those given in Table 2.

Finally, it should be noted that, by no rearrangement of eqns. (34)–(37) is it possible to obtain an explicit expression for J. Computation therefore proceeds by assigning an arbitrary value to x'/l in eqn. (37) and then finding, in turn, $J^{1/2}$, J, J_s/J, η_K, $\eta_{K'}$, ξ_K, $\xi_{K'}$, thus yielding a second value of x'/l from eqn. (36) for comparison with the arbitrarily chosen value. The procedure must then be repeated until equality is obtained. In practice, some preliminary test runs made to slide-rule accuracy, and without interpolation of the ξ/η Tables, will suggest two suitable values to assign to x'/l. A linear interpolation between these two values will then usually yield x'/l, and therefore J, correct to three significant figures.

621.372.823

The Institution of Electrical Engineers
Monograph No. 409 E
Oct. 1960

PROPAGATION ALONG UNBOUNDED AND BOUNDED DIELECTRIC RODS

Part 1. Propagation along an Unbounded Dielectric Rod

By P. J. B. CLARRICOATS, B.Sc.(Eng.), Ph.D., Graduate.

(*The paper was first received 11th March, and in revised form 22nd June,* 1960. *It was published as an* INSTITUTION MONOGRAPH *in October,* 1960.)

SUMMARY

The paper describes a method for evaluating the propagation coefficients of an unbounded lossless dielectric rod of infinite extent. The propagation coefficients are obtained as a function of the ratio of rod radius to free space wavelength, r_1/λ_0, for the three lowest modes of propagation possessing fields with θ dependence of the form $\varepsilon^{\pm j\theta}$. The method of solution enables the form of the complete mode spectrum to be identified. It is also established that the product of the rod permeability and permittivity, $\mu\epsilon$, primarily determines the propagation behaviour; the ratio μ/ϵ has only a secondary effect. An expression is obtained for the distribution of transmitted power between the rod and the surrounding space, and it is also demonstrated that the product $\mu\epsilon$ primarily determines this quantity. Correlation between power distribution and attenuation is demonstrated for a rod possessing small losses.

LIST OF SYMBOLS

(Numbers in parenthesis refer to the equations in which symbols first appear.)

$A = \bar{\beta}^2[1 - (K_1/K)^2]^2$ (7)

$a_n^i, b_n^i, a_n^e, b_n^e$ = Amplitudes of longitudinal components of electric and magnetic field respectively, inside and external to dielectric rod. (1), (2)

E_z = Longitudinal component of electric field. (1)

f = Function defined in eqn. (6).

$F(x) = xJ_1'(x)/J_1(x)$ (5)

H_z = Longitudinal component of magnetic field. (1)

$H_n^{(2)}(y)$ = Bessel function of the third kind. (2)

$J_n(x)$ = Bessel function of the first kind. (1)

j_m = mth root of $J_n(x)$.

$K_0(jy), K_1(jy)$ = Modified Bessel functions of the second kind. (12)

K, K_1 = Wavenumbers respectively inside and outside the dielectric rod. (1), (2)

$k_1 = jK_1$, modified wavenumber for region outside dielectric rod. (12)

$M(y) = y\dfrac{H_n^{(2)\prime}(y)}{H_n^{(2)}(y)}$

n = Azimuthal wavenumber. (5)

$N = (\bar{\mu}\bar{\epsilon})^{1/2}$

r, r_1 = Radial co-ordinate and radius of rod respectively.

T_1, T_2 = Integrals defined by eqn. (13).

u_m = mth root of $J_n'(x)$.

$V = K_1/K$ (7)

P_i, P_0 = Power transmitted respectively inside and outside dielectric rod.

$Z = (\bar{\mu}/\bar{\epsilon})^{1/2}$

z = Longitudinal co-ordinate.

β = Phase-change coefficient.

$\bar{\beta} = \lambda_0/\lambda$ = Normalized phase coefficient.

$\epsilon_0, \epsilon, \epsilon_1$ = Permittivity of free space, dielectric rod and surrounding medium respectively.

$\bar{\epsilon} = \epsilon/\epsilon_0$

κ = Off-diagonal component of ferrite permeability tensor.

θ = Angular co-ordinate.

$\lambda_0, \lambda, \lambda'$ = Wavelength in free space, unbounded rod structure, and surrounding medium respectively.

$\bar{\Lambda} = -j(\mu_0/\epsilon_0)^{1/2}b_n^i/a_n^i$ (12)

μ_0, μ, μ_1 = Permeability of free space, dielectric rod (or diagonal component of ferrite tensor permeability) and surrounding medium respectively.

$\bar{\mu} = \mu/\mu_0$

$[\mu_a], [\mu_b]$ = permeabilities associated with ferrite structure.

ω = Angular frequency.

(1) INTRODUCTION

In a recent paper[1] the present author described an accurate perturbation method for the evaluation of the propagation coefficients of a circular waveguide containing a longitudinally magnetized ferrite rod. The perturbation comprises a change in the permeability of a rod from the form

$$[\mu_a] = \begin{bmatrix} \mu - n\kappa & 0 & 0 \\ 0 & \mu - n\kappa & 0 \\ 0 & 0 & \mu_z \end{bmatrix} \text{ to } [\mu_b] = \begin{bmatrix} \mu & -j\kappa & 0 \\ j\kappa & \mu & 0 \\ 0 & 0 & \mu_z \end{bmatrix}$$

In order to obtain the phase-change coefficient after the perturbation has been made, it is first necessary to determine the propagation coefficient for a rod characterized by a permeability $[\mu_a]$. This propagation coefficient can be obtained quite rapidly if the propagation coefficient is already known for a rod with isotropic permeability $[\mu - n\kappa]$.* Furthermore, it can be shown that, with a slight reduction in accuracy but with far greater simplicity, the perturbation to permeability $[\mu_b]$ can be made directly from $[\mu - n\kappa]$. Also, in the general analysis of microwave ferrite devices employing the Faraday-rotation effect, it is often quite adequate to base approximate calculations on a rod with isotropic permeability $[\mu - n\kappa]$. The importance of determining the propagation coefficients of a circular waveguide containing a rod with isotropic permeability is therefore evident.

In the design of Faraday-rotation devices, the most important dimensional parameter is the diameter of the ferrite rod. Thus graphs showing propagation coefficient as a function of rod

Correspondence on Monographs is invited for consideration with a view to publication.

Dr. Clarricoats is in the Department of Light Electrical Engineering, Queen's University of Belfast. The paper is based on a part of a thesis approved for the degree of Doctor of Philosophy at London University.

* The reader is reminded that this is the permeability presented by a longitudinally magnetized ferrite to a circularly polarized wave having fields with a θ dependence of the form $\varepsilon^{-jn\theta}$. When $n = +1$ the wave is positive circularly polarized.

diameter are of most value. The effective permeability of the ferrite $[\mu - n\kappa]$ is another important parameter; this may be chosen as a second variable.

When the author first considered the problem of determining the propagation coefficients, it was apparent that very little information had been published on the behaviour of dielectric rods,* whether unbounded or bounded by a waveguide. It was therefore decided to approach the problem systematically and investigate the behaviour of unbounded dielectric rods before proceeding to the rod in circular waveguide. As many of the features of the two problems were found to be closely related, the detailed analysis of the unbounded rod was well justified. It is with this particular rod structure that the paper is concerned. The behaviour of a dielectric rod contained within a circular waveguide is considered in Part 2 (see page 177). In both papers discussion is restricted to modes with azimuthal dependence $\varepsilon^{\pm j\theta}$.

As no computer facilities were available to the author, a graphical method for obtaining the solution of the propagation equation was adopted; this is described in Section 2. Particular attention is paid to the behaviour of higher-order modes, since their properties do not appear to have been firmly established elsewhere. Section 3 is concerned with an evaluation of the distribution of transmitted power in an unbounded dielectric rod. As might be anticipated, there is close correlation between power distribution and the attenuation of a wave produced when the permeability and permittivity of the rod are complex.

(2) EVALUATION OF THE PROPAGATION COEFFICIENTS FOR LOSSLESS DIELECTRIC RODS

(2.1) Graphical Method of Solution

The characteristic equation for the propagation coefficients of waves guided by an infinitely long unbounded rod has been derived by several authors.[2, 3] The method is as follows: Maxwell's equations are solved yielding wave equations for the longitudinal components of electric and magnetic fields, inside and outside the rod. Solutions of these equations are chosen so that the fields are finite on the rod axis, zero at infinite radial distance and satisfy the boundary conditions at the rod surface, $r = r_1$. Then, if the permeability and permittivity for $r < r_1$ are μ and ϵ, and for $r > r_1$, μ_1 and ϵ_1,

$$\left.\begin{aligned} E_z &= a_n^i J_n(Kr)\varepsilon^{-jn\theta} \\ H_z &= b_n^i J_n(Kr)\varepsilon^{-jn\theta} \end{aligned}\right\} r < r_1 \quad . \quad . \quad . \quad . \quad (1)$$

$$\left.\begin{aligned} E_z &= a_n^e H_n^{(2)}(K_1 r)\varepsilon^{-jn\theta} \\ H_z &= b_n^e H_n^{(2)}(K_1 r)\varepsilon^{-jn\theta} \end{aligned}\right\} r > r_1 \quad . \quad . \quad . \quad (2)$$

where $K^2 = \omega^2\epsilon\mu - \beta^2$, $K_1^2 = \omega^2\epsilon_1\mu_1 - \beta^2$

and a factor $\varepsilon^{j(\omega t - \beta z)}$ has been omitted. $J_n(x)$ and $H_n^{(2)}(y)$† are Bessel functions of the first and third kind; $[H_n^{(2)}(y)$ is now abbreviated to $H_n(y)]$.

On equating tangential components of electric and magnetic fields on the rod surface, two expressions relating the constants a_n and b_n are obtained:

$$\frac{a_n^i}{b_n^i} = \frac{a_n^e}{b_n^e} = \frac{j\omega(Kr_1)^2(K_1r_1)^2}{n\beta[(K_1r_1)^2 - (Kr_1)^2]} \left[\frac{\mu}{(Kr_1)^2}\frac{Kr_1J_n'(Kr_1)}{J_n(Kr_1)} - \frac{\mu_1}{(K_1r_1)^2}\frac{K_1r_1H_n'(K_1r_1)}{H_n(K_1r_1)}\right] \quad (3)$$

$$\frac{b_n^i}{a_n^i} = \frac{b_n^e}{a_n^e} = \frac{j\omega(Kr_1)^2(K_1r_1)^2}{n\beta[(K_1r_1)^2 - (Kr_1)^2]} \left[\frac{\epsilon_1}{(K_1r_1)^2}\frac{K_1r_1H_n'(K_1r_1)}{H_n(K_1r_1)} - \frac{\epsilon}{(Kr_1)^2}\frac{Kr_1J_n'(Kr_1)}{J_n(Kr_1)}\right] \quad (4)$$

a_n^i/b_n^i may then be eliminated between eqns. (3) and (4) yielding the characteristic equation for the propagation coefficients; the functions $F(Kr_1)$ and $M(K_1r_1)$ are defined by eqn. (3):

$$\frac{n^2\beta^2}{\omega^2}\frac{[(K_1r_1)^2 - (Kr_1)^2]^2}{[(K_1r_1)^2(Kr_1)^2]^2} = \left[\frac{\mu F(Kr_1)}{(Kr_1)^2} - \frac{\mu_1 M(K_1r_1)}{(K_1r_1)^2}\right]\left[\frac{\epsilon F(Kr_1)}{(Kr_1)^2} - \frac{\epsilon_1 M(K_1r_1)}{(K_1r_1)^2}\right] \quad (5)$$

Eqn. (5) has been solved numerically when $\mu/\mu_0 = \bar{\mu} = 1$ and $\epsilon/\epsilon_0 = \bar{\epsilon} = 2{\cdot}5$, 4, 10 and 32,[4] but no information is evident when $\bar{\mu} \neq 1$. In order to determine the relative importance of $\bar{\mu}\bar{\epsilon}$ and $\bar{\mu}/\bar{\epsilon}$ respectively, a matter of some practical interest, eqn. (5) has been solved by the author for $\bar{\mu}/\bar{\epsilon}$, maintaining $\bar{\mu}\bar{\epsilon}$ constant and with $\bar{\mu}_1 = \bar{\epsilon}_1 = 1$ and $n = 1$. Thus $\bar{\mu}/\bar{\epsilon}$ has been obtained as an implicit function of r_1/λ_0 for various values of $\bar{\beta} = \lambda_0/\lambda$, where λ_0 is the free-space wavelength and λ the wavelength of the guided wave.

Eqn. (5) can be written

$$(\bar{\mu}/\bar{\epsilon}) + (\bar{\mu}/\bar{\epsilon})^{1/2}f + 1 = 0 \quad . \quad . \quad . \quad . \quad (6)$$

where

$$f = \left\{\frac{\bar{\beta}^2\left[1 - \left(\frac{K_1}{K}\right)^2\right]^2\left(\frac{K}{K_1}\right)^2}{(\bar{\mu}\bar{\epsilon})^{1/2}F(Kr_1)M(K_1r_1)} - \frac{(\bar{\mu}\bar{\epsilon})^{1/2}F(Kr_1)\left(\frac{K_1}{K}\right)^2}{M(K_1r_1)} - \frac{M(K_1r_1)\left(\frac{K}{K_1}\right)^2}{(\bar{\mu}\bar{\epsilon})^{1/2}F(Kr_1)}\right\} \quad (7)$$

For ease of understanding this expression, it is now rewritten as

$$f = \left(\frac{A}{NFMV^2} - \frac{NFV^2}{M} - \frac{M}{NFV^2}\right)$$

where

$$A = \bar{\beta}^2\left[1 - \left(\frac{K_1}{K}\right)^2\right]^2 = \left[1 - \left(\frac{K_1}{K}\right)^2\right]\left[1 - \bar{\mu}\bar{\epsilon}\left(\frac{K_1}{K}\right)^2\right]$$

$$N = (\bar{\mu}\bar{\epsilon})^{1/2}, \quad V = \left(\frac{K_1}{K}\right)$$

On rearranging eqn. (6),

$$f = -[(\bar{\mu}/\bar{\epsilon})^{1/2} + (\bar{\epsilon}/\bar{\mu})^{1/2}] \quad . \quad . \quad . \quad . \quad (8)$$

This indicates that two values of $\bar{\mu}/\bar{\epsilon}$ can be chosen for which $\bar{\beta}$ is the same. Fig. 1(*a*) shows f plotted as a function of $2r_1/\lambda_0$ using eqn. (7), for different values of $\bar{\beta}$ when $\bar{\mu}\bar{\epsilon} = 10$ and $n = 1$. Solutions of eqn. (5) are then obtained by mapping eqn. (8) on the same diagram. The variation of $\bar{\beta}$ with $2r_1/\lambda_0$ for a particular rod having $(\bar{\mu}/\bar{\epsilon})^{1/2} = Z$, is then obtained from the intercepts of the curves with the line $f = -(Z + 1/Z)$.

This method of solving the characteristic equation has the advantage that, once eqn. (7) is plotted for various values of $\bar{\beta}$, negligible labour is required in obtaining $\bar{\beta}$ as a function of $2r_1/\lambda_0$ for any $\bar{\mu}/\bar{\epsilon}$ ratio. Fig. 2 shows $\bar{\beta}$ as a function of $2r_1/\lambda_0$ for the rod with $\bar{\mu}\bar{\epsilon} = 10$, and with $\bar{\mu}/\bar{\epsilon} = 0{\cdot}017$, $0{\cdot}029$ and $0{\cdot}072$. These values correspond to $\bar{\mu} = 0{\cdot}41$, $0{\cdot}54$, $0{\cdot}85$ and $\bar{\epsilon} = 24{\cdot}4$, $18{\cdot}5$ and $11{\cdot}8$ respectively. Fig. 3 shows $\bar{\beta}$ as a

* The term *dielectric rod* is taken here to include rods with relative permeability different from unity.

† Note that $K_n(jK_1r)$, which is often quoted as the external radial function, differs from $H_n^{(2)}(K_1r)$ only by a constant factor.

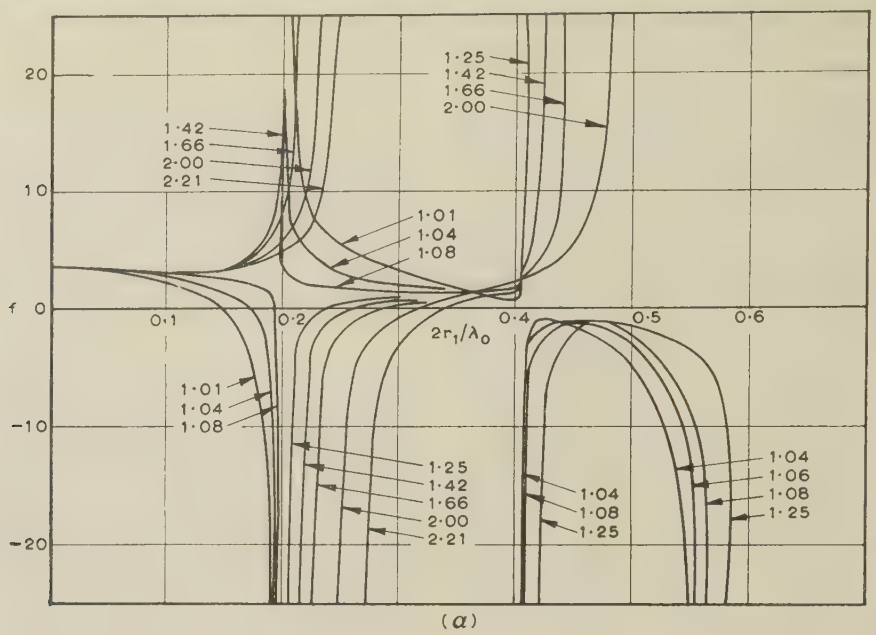

(*a*)

function of $2r_1/\lambda_0$ for rods with $\bar{\mu}/\bar{\epsilon} = 0{\cdot}029$ and with $\bar{\mu}\bar{\epsilon} = 2{\cdot}5$, 10 and 16. The above results illustrate clearly that the normalized phase coefficient $\bar{\beta}$ depends primarily on the product $\bar{\mu}\bar{\epsilon}$ and only slightly on the ratio $\bar{\mu}/\bar{\epsilon}$. The reason for this behaviour is explained when the principal features of Fig. 1(*a*) are discussed in Section 2.2. The above result can be alternatively stated as indicating that the actual values of $\bar{\mu}$ and $\bar{\epsilon}$ have only a slight influence on the phase-change coefficient, provided that the product $\bar{\mu}\bar{\epsilon}$ does not vary. The advantage offered by this knowledge is illustrated by the following example.

Unmagnetized Ferramic R1 ferrite has $\bar{\mu} = 0{\cdot}74$ and $\bar{\epsilon} = 13{\cdot}6$ (at frequencies around 9 Gc/s), so that $\bar{\mu}\bar{\epsilon} = 10{\cdot}06$; the propagation curve for an unbounded rod of this material should therefore correspond closely to that for a rod with $\bar{\mu} = 1$, $\bar{\epsilon} = 10$. This latter curve has been determined (Fig. 3).

(2.2) Interpretation of the Solutions

The Dominant Mode.—In Fig. 1(*a*) only values of $f < -2$ have physical significance, since eqn. (6) indicates that if $f > -2$, $(\bar{\mu}/\bar{\epsilon})^{1/2}$ becomes either complex or negative. Such solutions must be rejected since $(\bar{\mu}\bar{\epsilon})^{1/2}$ is assumed positive and real when solving eqn. (7); a complex or negative value for $(\bar{\mu}/\bar{\epsilon})^{1/2}$ would imply complex or negative values of $\bar{\mu}$ and $\bar{\epsilon}$. However, the region for which $f > -2$ is useful in the initial construction of the curves in the region $f < -2$. Eqn. (7) indicates that poles of f correspond to poles or zeros of the function F; these occur when $J_1(Kr_1) = 0$ and when $J_1'(Kr_1) = 0$, respectively, as shown in Figs. 1(*b*) and (*c*). The function M is monotonically increasing with r_1/λ_0, as in Fig. 1(*d*). It is readily shown, by considering the limiting form of eqn. (7), that when $r_1/\lambda_0 \to 0$, all f-curves originate with the value $f = [(\bar{\mu}\bar{\epsilon})^{1/2} + (1/\bar{\mu}\bar{\epsilon})^{1/2}]$. However, it can also be shown that as $\beta \to 1$ the condition for $f = 0$ corresponds to $r_1/\lambda_0 \to 0$. Thus for values of $\bar{\beta}$ close to unity the f-curves commence at $f = [(\bar{\mu}\bar{\epsilon})^{1/2} + (1/\bar{\mu}\bar{\epsilon})^{1/2}]$ and then decrease with almost infinite slope, as r_1/λ_0 increases from zero. This behaviour is consistent with the knowledge[5] that the lowest-order mode with $n = 1$ has no cut-off.

In closed-boundary structures (e.g. a waveguide with perfectly conducting walls), the term 'cut-off' has a well defined meaning, implying the condition that $\beta = 0$ for a particular mode. Furthermore, if this condition occurs when $\omega = \omega_c$ and the

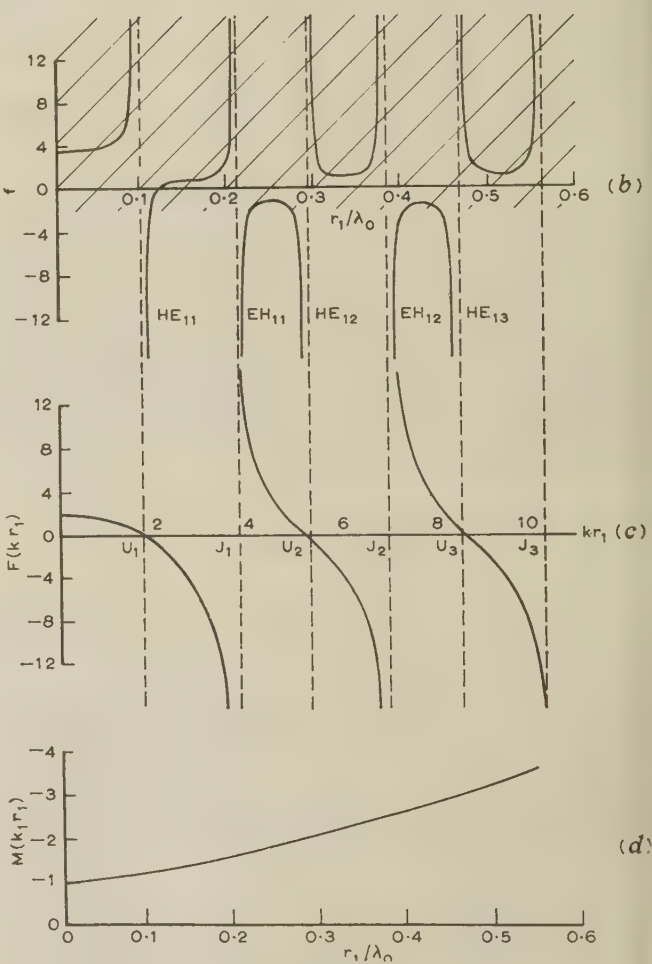

Fig. 1

(*a*) f as a function of $2r_1/\lambda_0$ for an unbounded dielectric rod with $(\bar{\mu}\bar{\epsilon})^{1/2} = 3{\cdot}162$.
Numbers refer to values of $\bar{\beta}$.
(*b*)–(*d*) $f = [A/NFMV^2 - (NFV^2/M) - (M/NFV^2)]$ and $M(k_1r_1)$ as a function of r_1/λ_0; and $F(Kr_1)$ as a function of Kr_1.
$\bar{\mu}\bar{\epsilon} = 10$ $\bar{\beta} = 1{\cdot}25$

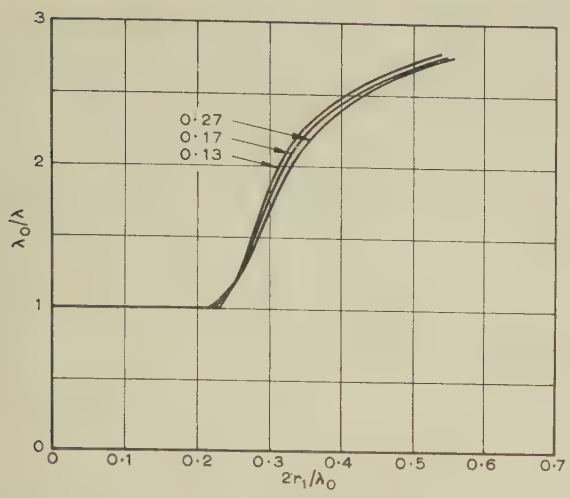

Fig. 2.—$\bar{\beta} = \lambda_0/\lambda$ as a function of $2r_1/\lambda_0$ for HE_{11} modes propagating along unbounded dielectric rods.
$(\mu\epsilon)^{1/2} = 3{\cdot}16$ $(\mu/\epsilon)^{1/2} = 0{\cdot}13$, $0{\cdot}17$ and $0{\cdot}27$

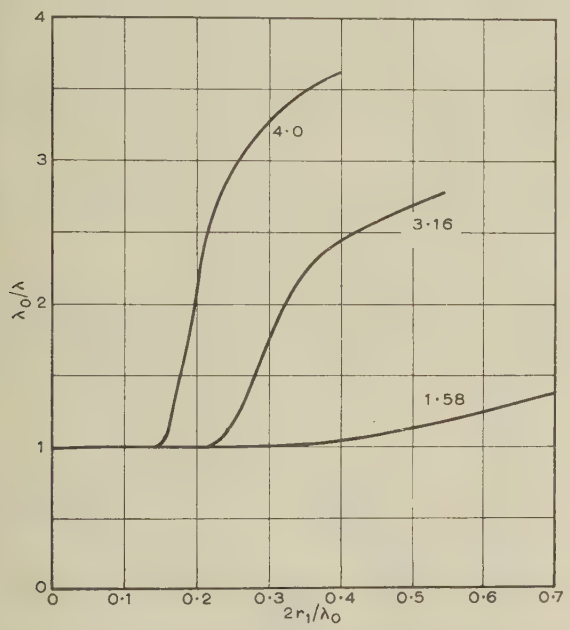

Fig. 3.—$\bar{\beta} = \lambda_0/\lambda$ as a function of $2r_1/\lambda_0$ for HE_{11} modes propagating along unbounded dielectric rods.
$(\mu/\epsilon)^{1/2} = 0{\cdot}17$ $(\mu\epsilon)^{1/2} = 1{\cdot}58$, $3{\cdot}16$ and $4{\cdot}0$

structure is lossless, then when $\omega < \omega_c$, $\gamma = \alpha$ and the mode is exponentially attenuated with a decay factor of the form $\varepsilon^{-\alpha z}$. However, with open-boundary structures (e.g. an unbounded dielectric rod), the condition $\beta = 0$ is never satisfied for any free mode.* In fact these free modes cease to exist when the frequency is such that $\beta^2 = \omega^2\epsilon_1\mu_1$; modes with $\gamma = \alpha$ cannot exist on a source-free open-boundary structure. When sources are present, it is necessary to employ a continuous spectrum of modes in addition to a finite (possibly zero) number of free modes, in order to represent the field.[6, 7]

Higher-Order Modes.—With reference to Fig. 1(*a*), as $\bar{\beta}$ increases, the value of r_1/λ_0 at which $f = 0$ increases until the value at which $F(Kr_1) = 0$ is passed; then the f-curves tend to $+\infty$ at the first zero of $F(Kr_1)$. They reappear at $-\infty$ for the same value of r_1/λ_0, then increase through the value of r_1/λ_0 at which $f = 0$. Beyond this they tend to infinity at the first pole of $F(Kr_1)$. It can be shown that f is finite when $\bar{\beta} = 1$ only when $F(Kr_1) = \infty$; these poles correspond to the 'cut-off' or genesis points of the higher-order modes of propagation.

Between the first zero of $J_1(Kr_1)$ and the second zero of $J_1'(Kr_1)$, designated by j_1 and u_2 respectively, or in general between j_m and u_{m+1}, $F(Kr_1) > 0$ and $f < 0$. Fig. 1(*b*) shows that the f-curves increase from $-\infty$ at j_m, pass through $f = -2$, and then reach a maximum value in the range $0 > f > -2$; they then pass through $f = -2$ again and decrease to $-\infty$ at u_{m+1}. Since in eqn. (7) the term $A/NFMV^2$ is always positive when $F > 0$ and the smallest negative value of $-[(NFV^2/M) + (M/NFV^2)]$ is -2, the maxima of the f-curves in the above region must always lie above the line $f = -2$. Furthermore as A is independent of r_1/λ_0, the term $A/NFMV^2$ decreases in magnitude rapidly with r_1/λ_0 compared with the term M/NFV^2. Thus for large r_1/λ_0, $f \simeq -[(NFV^2/M) + (M/NFV^2)]$; the nearer $\bar{\beta}$ approaches unity the larger r_1/λ_0 must be for this condition to be satisfied, since A/V^2 behaves like $N^2 - 1/1 - \bar{\beta}^2$ when $\bar{\beta} \to 1$. In the interval between j_m and u_{m+1}, two solutions of eqn. (5) exist for the same value of $\bar{\beta}$. Although the f-curve is continuous through the region $0 > f > -2$, the two branches in the region $f < -2$ correspond to two distinct modes of propagation. In Monograph No. 410 E it is shown that these modes are related to the E_{1m} and $H_1(_{m+1})$ modes of homogeneous waveguides. These higher-order modes on unbounded rods do not appear to have been previously studied,* although Kiely[8] quotes Horton as observing two branches of an HE_{12} mode (in his notation). In the present notation it appears that one of these branches is the EH_{11} mode (corresponding to the E_{11} mode of homogeneous waveguide) while the other is the HE_{12} mode (corresponding to the H_{12} waveguide mode). The use of HE to denote a hybrid mode of H-mode type, and vice versa, is conventional.

When $\bar{\beta} \to 1$, the maxima of the f-curves in the region $f < 0$ move nearer to j_m and the values at which $f = -2$ (after the maxima) also move towards j_m. In a manner analogous to that employed with the lowest-order HE_{11} mode,[9] it can be shown that when $\bar{\beta}$ is infinitesimally close to unity, the f-curves comprise a series of nearly vertical lines occurring in almost degenerate pairs at values j_m. The pairs are connected in the region $0 > f > -2$. Thus the higher-order mode pairs EH_{1m}, $HE_{1(m+1)}$ have the same values of r_1/λ_0, for cut-off, given by

$$Kr_1 = \frac{2r_1}{\lambda_0}\pi(\bar{\mu}\bar{\epsilon} - 1)^{1/2} = j_m \quad . \quad . \quad . \quad . \quad (9)$$

However, for EH modes it appears that f-curves are bunched near to the values $Kr_1 = j_m$ given by eqn. (9), while for HE modes the f-curves are bunched near $Kr_1 = u_m$. Fig. 4 shows β as a function of r_1/λ_0 for the first pair of higher-order modes when $\bar{\mu}\bar{\epsilon} = 10$ and $\bar{\mu}/\bar{\epsilon} = 0{\cdot}1$. It is now pertinent to consider the effect on the propagation behaviour of the parameters $\bar{\mu}\bar{\epsilon}$ and $\bar{\mu}/\bar{\epsilon}$. Changes in the product $\bar{\mu}\bar{\epsilon}$ shift the value of r_1/λ_0 at which the maximum slope of the $\bar{\beta}(r_1/\lambda_0)$ curve occurs, whereas changes in the ratio $\bar{\mu}/\bar{\epsilon}$ merely alter the magnitude of the maximum slope. The greatest magnitude occurs when $\bar{\mu}/\bar{\epsilon} = 0$ or ∞. For these values of $\bar{\mu}/\bar{\epsilon}$, $\bar{\beta}$ and r_1/λ_0 are related by the simple equations

$$\bar{\beta} = \left[\bar{\epsilon}\bar{\mu} - \left(\frac{\lambda_0}{2\pi r_1} u_m\right)^2\right]^{1/2} \quad . \quad . \quad . \quad . \quad (10)$$

* A free mode is one with exponential dependence of the form $\varepsilon^{-\gamma z}$ which can exist in the absence of any sources over a finite length of the structure.

* After the present work was completed, the attention of the author was drawn to a paper by M. Jouget[13] which contains a discussion of the behaviour of higher-order modes. Another more recent work[14] describes the behaviour of higher modes with $n > 1$ as well $n = 1$.

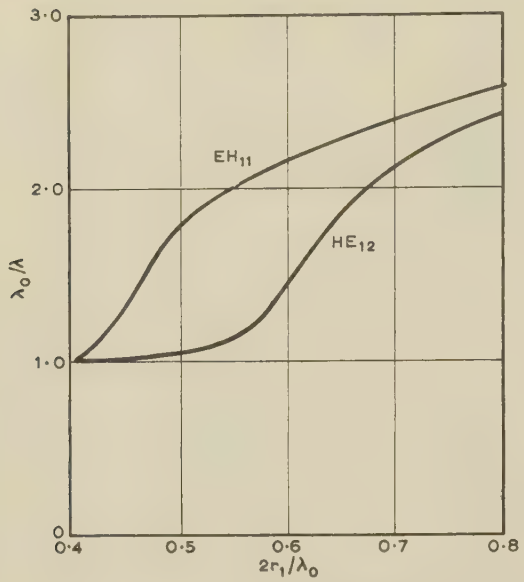

Fig. 4.—$\bar{\beta} = \lambda_0/\lambda$ as a function of $2r_1/\lambda_0$ for EH_{11} and HE_{12} modes propagating along an unbounded dielectric rod.
$\bar{\epsilon} = 10 \quad \bar{\mu} = 1{\cdot}0$

in the case of HE modes, and

$$\bar{\beta} = \left[\bar{\epsilon}\bar{\mu} - \left(\frac{\lambda_0}{2\pi r_1} j_m\right)^2\right]^{1/2} \quad . \quad . \quad . \quad . \quad (11)$$

in the case of EH modes. These equations are, incidentally, just those for a rod enclosed by a metallic wall. The smallest magnitude of the maximum slope occurs when $\bar{\mu}/\bar{\epsilon} = 1$. For this value of $\bar{\mu}/\bar{\epsilon}$ there is no simple expression relating $\bar{\beta}$ and r_1/λ_0.

Other External Media.—With regard to Fig. 1, there is of course no special significance in choosing the external medium to have $\bar{\mu}_1 = \bar{\epsilon}_1 = 1$. The f-curves can apply to any values of $\bar{\mu}_1$ and $\bar{\epsilon}_1$, provided that the ratio $\mu\epsilon/\mu_1\epsilon_1$ remains unchanged and λ_0 is replaced by $\lambda' = \lambda_0/(\bar{\mu}_1\bar{\epsilon}_1)^{1/2}$. Solutions are obtained by mapping $f = -[(\bar{\mu}\bar{\epsilon}_1/\bar{\mu}_1\bar{\epsilon})^{1/2} + (\bar{\mu}_1\bar{\epsilon}/\bar{\mu}\bar{\epsilon}_1)^{1/2}]$ on the same diagram. Since the ratio $\bar{\mu}/\bar{\epsilon}$ does not appreciably alter the form of the $\bar{\beta}(r_1/\lambda_0')$ graph, for qualitative purposes it is sufficient for the ratio $\bar{\mu}\bar{\epsilon}/\bar{\mu}_1\bar{\epsilon}_1$ to be correct. For example, a graph of $\bar{\beta}$ as a function of r_1/λ_0 for a rod with $\bar{\mu} = 1$, $\bar{\epsilon} = 4^4$ and $\bar{\mu}_1 = \bar{\epsilon}_1 = 1$ is qualitatively similar to that of λ'/λ_0 as a function of r_1/λ' for a rod with $\bar{\mu} = 0{\cdot}74$, $\bar{\epsilon} = 13{\cdot}6$, $\bar{\mu}_1 = 1$ and $\bar{\epsilon} = 2{\cdot}5$. These parameters correspond to an unmagnetized Ferramic R1 ferrite supported in a medium of polystyrene.

(3) EVALUATION OF THE DISTRIBUTION OF TRANSMITTED POWER BETWEEN ROD AND SURROUNDING MEDIUM

In a number of waveguide devices employing ferrites, e.g. the circularly-polarized-wave non-reciprocal attenuator,[10] the operation relies on a non-reciprocal distribution of transmitted power within a circular waveguide containing a magnetized ferrite rod. When the behaviour of this device was first analysed, the question arose whether the product $\bar{\mu}\bar{\epsilon}$ was the principal material factor determining the power transmitted through the rod. For this reason a study of the power distribution in unbounded rods was made. It was correctly assumed that the behaviour of unbounded rods would provide an insight into the behaviour of rods contained within a waveguide.

Although a number of curves showing the ratio of the power transmitted through the rod to the total power transmitted, P_i/P_0, as a function of r_1/λ_0 have been given by Gray,[4] the derivation of this ratio does not appear in any published work. As Gray's expression[11] contains an algebraic error, rendering the published results slightly inaccurate, the following expression used by the author is derived in the Appendix:

$$\frac{P_i}{P_0} = -\left(\frac{K_1}{K}\right)^4 \left[\frac{(\bar{\epsilon} + \bar{\mu}\bar{\Lambda}^2)T_1 + \bar{\Lambda}(\bar{\mu}\bar{\epsilon}/\bar{\beta} + \bar{\beta})}{(\bar{\epsilon}_1 + \bar{\mu}_1\bar{\Lambda}^2)T_2 + \bar{\Lambda}(\bar{\mu}_1\bar{\epsilon}_1/\bar{\beta} + \bar{\beta})}\right] \quad (12)$$

where

$$\bar{\Lambda} = -j(\mu_0/\epsilon_0)^{1/2}\frac{b_n^i}{a_n^i} \quad [\text{see eqn. (4)}]$$

$$T_1 = \tfrac{1}{2}(Kr_1)^2\frac{J_0^2(Kr_1)}{J_1^2(Kr_1)} - \left[1 - \frac{(Kr_1)^2}{2}\right]$$
$$= \tfrac{1}{2}F^2(Kr_1) + F(Kr_1) + \tfrac{1}{2}[(Kr_1)^2 - 1]$$

$$T_2 = \tfrac{1}{2}(k_1r_1)^2\frac{K_0^2(k_1r_1)}{K_1^2(k_1r_1)} - \left[1 + \frac{(kr_1)^2}{2}\right]$$
$$= \tfrac{1}{2}M^2(k_1r_1) + M(k_1r_1) - \tfrac{1}{2}[(k_1r_1)^2 + 1]$$

and $-jk_1r_1 = K_1r_1$.

The behaviour of P_i/P_0 when $\bar{\beta} \to (\bar{\mu}_1\bar{\epsilon}_1)^{1/2}$ can be predicted directly from eqn. (12). When $\bar{\beta} \to (\bar{\mu}_1\bar{\epsilon}_1)^{1/2}$, $K_1 \to 0$. For the HE_{11} mode, this corresponds to the condition $r_1/\lambda_0 \to 0$. When $r_1/\lambda_0 = 0$, the expression within square brackets is finite, whereas $K_1 = 0$. Then, since K is finite under this condition, $P_i/P_0 = 0$. Thus, as the rod radius tends to zero the transmitted power associated with the HE_{11} mode is confined to the region exterior to the rod.

For all other modes, as $\bar{\beta} \to (\bar{\mu}_1\bar{\epsilon}_1)^{1/2}$, $J_1(Kr_1) \to 0$. Then $K_1^4T_1$ remains finite and it can be readily shown that, in the limit,

$$\frac{P_i}{P_0} = \frac{1}{2}\left(\frac{\epsilon_1}{\epsilon} + \frac{\mu_1}{\mu}\right) \quad . \quad . \quad . \quad . \quad . \quad (13)$$

This result is independent of the mode in question. However, the value of r_1/λ_0 at which $\bar{\beta} \to (\bar{\mu}_1\bar{\epsilon}_1)^{1/2}$ does of course depend

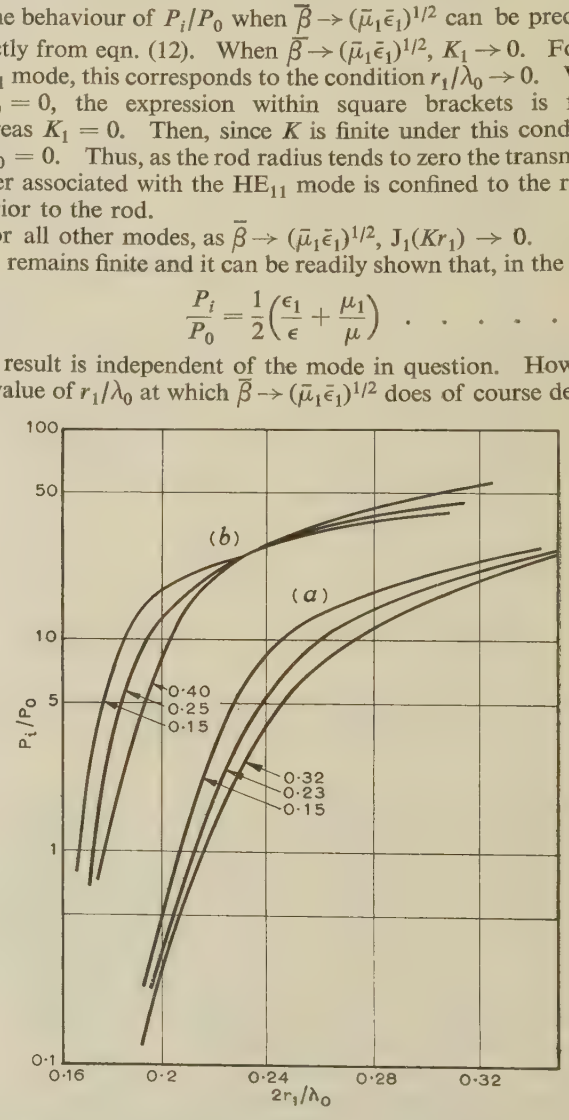

Fig. 5.—P_i/P_0 as a function of $2r_1/\lambda_0$ for an HE_{11} mode.
(*a*) $(\pi\epsilon)^{1/2} = 3{\cdot}16$
(*b*) $(\pi\epsilon)^{1/2} = 4{\cdot}0$
Parameter, $(\bar{\mu}/\bar{\epsilon})^{1/2}$

on the mode, as is evident from eqn. (9). The method of evaluating the ratio P_i/P_0 in general is now described.

With $\bar{\mu}\bar{\epsilon}$ constant, curves of $\bar{\mu}/\bar{\epsilon}$ as a function of r_1/λ_0 are drawn for different values of $\bar{\beta}$ using Fig. 1. From eqn. (12) P_i/P_0 is determined as a function of $\bar{\mu}/\bar{\epsilon}$ for different values of $\bar{\beta}$. Then with these two sets of curves P_i/P_0 can be plotted as a function of r_1/λ_0; results for different values of $\bar{\mu}/\bar{\epsilon}$ and with $\bar{\mu}\bar{\epsilon} = 16$ and 10 are given for the HE_{11} mode in Fig. 5. It is again evident that the parameter $\bar{\mu}\bar{\epsilon}$ largely determines the power distribution, compared with the parameter $\bar{\mu}/\bar{\epsilon}$.

For reference, Fig. 6(*a*) shows the ratio $P_i/(P_i + P_0)$, plotted as a function of r_1/λ_0 for rods with $\bar{\mu}\bar{\epsilon} = 16$, 10, 2·5 and $\bar{\mu}\bar{\epsilon} =$ 0·16, 0·025 ($\bar{\epsilon} = 10$, $\bar{\mu} = 1{\cdot}6$, 1·0 and 2·5). Fig. 6(*b*) shows β plotted for the same rod parameters. Fig. 7 shows attenuation and $P_i/(Pi + P_0)$ plotted as a function of $2r_1/\lambda_0$ for a polystyrene rod ($\bar{\mu} = 1$; $\bar{\epsilon}' = 2{\cdot}56$; $\bar{\epsilon}''/\bar{\epsilon}' = 0{\cdot}0005$) the former result being due to the author, the latter to Elsasser.[12] The correlation in the shape of the curves strongly suggests that power distribution and attenuation are closely related. In the particular case when $\beta \to (\bar{\mu}\bar{\epsilon}_1)^{1/2}$, at the genesis of a pair of higher-order modes, it is possible to obtain a simple relation which clearly shows that, under that condition, the attenuation coefficient α is directly proportional to the ratio $P_i/(Pi + P_0)$. An expression for the attenuation coefficient of a mode of the unbounded rod can be obtained directly from an expression for the attenuation of a mode of a rod in circular waveguide, derived in Part 2 of the paper.

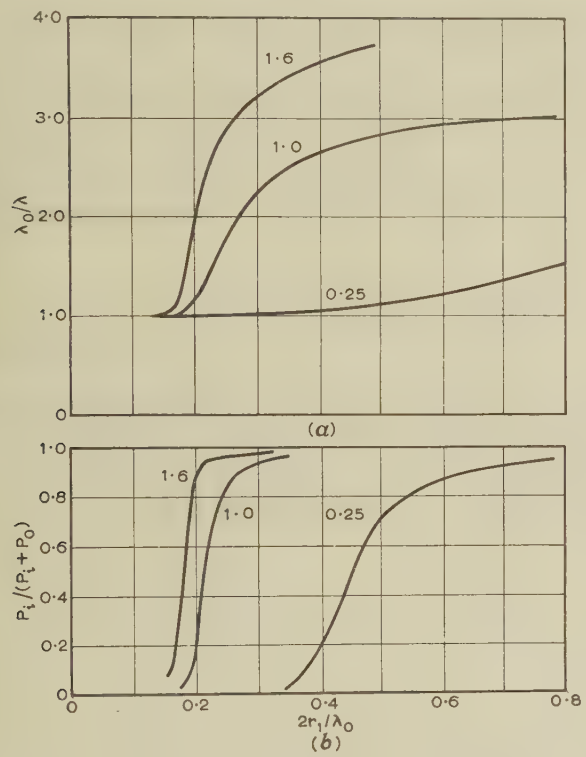

Fig. 6.—(*a*) $\beta = \lambda_0/\lambda$, and (*b*) $Pi/(Pi + P_0)$ as a function of $2r_1/\lambda_0$ for H_{11}-limit mode.
$\bar{\epsilon} = 10$ $\bar{\mu} = 1{\cdot}6$, 1·0 and 0·25

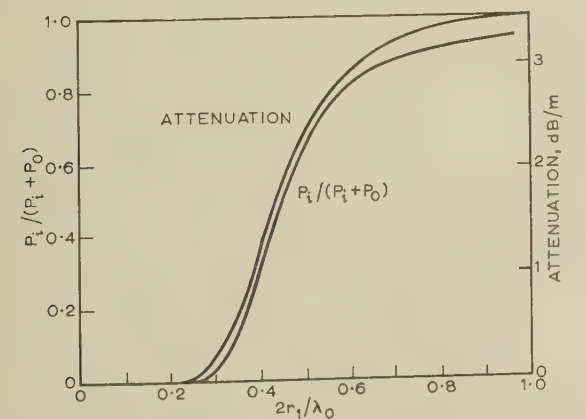

Fig. 7.—Attenuation and $P_i/(P_i + P_0)$ as a function of $2r_1/\lambda_0$ for an HE_{11} mode propagating along an unbounded polystyrene rod.

(4) CONCLUSIONS

In the paper, the mode spectrum of an unbounded dielectric rod of permeability μ and permittivity ϵ is established for modes with fields having a dependence on θ of the form $\varepsilon^{\pm j\theta}$. As previously recognized, the lowest-order hybrid mode, designated HE_{11}, can propagate when the frequency tends to zero. Also, as the ratio of rod radius to free-space wavelength, r_1/λ_0, increases, the phase-change coefficient increases and tends in the limit to the value corresponding to a plane wave propagating in an infinite medium of permeability μ and permittivity ϵ. A study of the higher-order modes shows that they are degenerate, in the sense that pairs of modes have the same genesis value of r_1/λ_0. However, there is a difference in the dependence on r_1/λ_0 of the phase-change coefficients of the modes. This difference can be understood when it is realized that the modes in a pair are associated with the E_{1m} and $H_{1(m+1)}$ modes of a rod in a waveguide. This matter is discussed further in Part 2 of the paper.

It is established that in general, the phase-change coefficients of the modes depend primarily upon r_1/λ_0 and $\bar{\mu}\bar{\epsilon}$, and only slightly upon the actual values of $\bar{\mu}$ and $\bar{\epsilon}$. The result is of practical significance in that it broadens the range of application of a given propagation curve.

The distribution of transmitted power between the rod and the surrounding space is investigated. For the HE_{11} mode, the ratio of the power transmitted within the rod to that outside tends to zero as r_1/λ_0 tends to zero. For any other mode, the ratio is finite for all values of r_1/λ_0 over which the mode can propagate. With r_1/λ_0 less than the genesis value for a particular pair of modes, the modes cease to exist. Again, the values of r_1/λ_0 and $\bar{\mu}\bar{\epsilon}$ primarily determine the power distribution, the actual values of $\bar{\mu}$ and $\bar{\epsilon}$ having a secondary effect. Correlation between the power transmitted within a rod with loss and the attenuation of a mode is illustrated.

(5) ACKNOWLEDGMENTS

The author would like to thank Dr. J. Brown, Dr. I. G. MacBean and Mr. M. Gumbrell for their helpful comments during the course of this work.

(6) REFERENCES

(1) CLARRICOATS, P. J. B.: 'A Perturbation Method for Circular Waveguides Containing Ferrites', *Proceedings I.E.E.*, Paper No. 2796 E, May, 1959 (**106** B, p. 335).
(2) STRATTON, J. A.: 'Electromagnetic Theory' (McGraw-Hill Book Co., 1941), p. 524.
(3) SCHELKUNOFF, S. A.: 'Electromagnetic Waves' (Van Nostrand Book Co., 1943), p. 425.
(4) GRAY, M.: Results given by Southworth, G. C.: 'Principles and Application of Waveguide Transmission' (Van Nostrand Book Co., 1950), p. 130.

(5) SCHELKUNOFF, S. A.: 'Electromagnetic Waves' (Van Nostrand Book Co., 1943), p. 428.
(6) ADLER, R. B.: 'Properties of Guided Waves on Inhomogeneous Cylindrical Structures', Massachusetts Institute of Technology Technical Report No. 102, 1949.
(7) BROWN, J.: 'The Types of Wave which may Exist near a Guiding Surface', *Proceedings I.E.E.*, Paper No. 1567 R, November, 1953 (**100**, Part III, p. 363).
(8) KIELY, D. G.: 'Dielectric Aerials', Methuen Monograph 1953, p. 26.
(9) CLARRICOATS, P. J. B.: 'Properties of Waveguides containing Ferrites with special reference to Waveguides of Circular Cross-Section', Thesis Presented for the Degree of Doctor of Philosophy at London University, 1958.
(10) CLARRICOATS, P. J. B.: 'Some Properties of Circular Waveguides Containing Ferrites'. *Proceedings I.E.E.*, Paper No. 2202 R, October, 1956 (**104** B Suppl. 6, p. 294).
(11) GRAY, M. C.: Private Communication to author.
(12) ELSASSER, W. M.: 'Attenuation in a Dielectric Circular Rod', *Journal of Applied Physics*, 1949, **20**, p. 1193.
(13) JOUGUET, M.: 'Problèmes de propagation cylindrique', *Cables et Transmission*, 1955, No. 1, p. 2.
(14) SCHLESINGER, S. P., DIAMENT, P., and VIGANTS, A.: 'On Higher-Order Hybrid Modes of Dielectric Cylinders' *Transactions of the Institute of Radio Engineers*, 1960, **MTT-8**, No. 2, p. 252.

(7) APPENDIX

Evaluation of the Power Ratio P_i/P_0 for Unbounded Rod

From Poynting's theorem it follows that

$$\frac{P_i}{P_0} = \frac{-\mathscr{R}\int_{S_1}(E_r H_\theta^* - E_\theta H_r^*)dS}{\mathscr{R}\int_{S_2}(E_r H_\theta^* - E_\theta H_r^*)dS}$$

where S_1 is the rod area and S_2 the area of the surrounding medium. The numerator expresses the integrated Poynting vector inside the rod; this is now evaluated for modes having $n=1$.

$$E_r H_\theta^* - E_\theta H_r^* = \frac{(a_1^i)^2}{K^3 r}\left\{(\omega\epsilon\beta + \Lambda^2\omega\mu\beta)\left[J_1'^2(Kr)(Kr) + \frac{J_1^2(Kr)}{(Kr)}\right] + (\Lambda\omega^2\mu E + \Lambda\beta^2)[2J_1(Kr)J_1'(Kr)]\right\} \quad (13)$$

whence

$$P_i = \frac{\pi(a_1^i)^2}{K^4}J_1^2(Kr_1)\{[\omega\epsilon\beta + \Lambda^2\omega\mu\beta]T_1 + \Lambda[\omega^2\mu\epsilon + \beta^2]\} \quad (14)$$

where T_1 is given in eqn. (12). Similarly, outside the rod,

$$E_r H_\theta^* - E_\theta H_r^* = \frac{(a_1^e)^2}{K_1^3 r}\left\{(\omega\epsilon_1\beta + \Lambda^2\omega\mu_1\beta)\left[H_1'^2(K_1 r)(K_1 r) + \frac{H_1^2(Kr)}{(K_1 r)}\right] + (\Lambda\omega^2\mu_1\epsilon_1 + \Lambda\beta^2)[2H_1(K_1 r)H_1'(K_1 r)]\right\} \quad (15)$$

whence

$$P_0 = \frac{-\pi(a_1^i)^2}{K_1^4}J_1^2(Kr_1)[(\omega\epsilon_1\beta + \Lambda^2\omega\mu_1\beta)T_2 + \Lambda(\omega^2\mu_1\epsilon_1 + \beta^2)] \quad (16)$$

where T_2 is as given in eqn. (12). On normalizing the expressions, the ratio P_i/P_0 given in eqn. (12) is obtained. The expression for P_0 used by Gray incorrectly contained the difference of the two terms in square brackets instead of their sum. Also, T_2 was incorrectly taken as $\frac{1}{2}M^2(k_1 r_1) + M(k_1 r_1) - (k_1^2 r_1^2 - 1)$.

621 372.853.1

The Institution of Electrical Engineers
Monograph No. 410 E
Oct. 1960

PROPAGATION ALONG UNBOUNDED AND BOUNDED DIELECTRIC RODS

Part 2. Propagation along a Dielectric Rod contained in a Circular Waveguide

By P. J. B. CLARRICOATS, B.Sc.(Eng.), Ph.D., Graduate.

(*The paper was first received 11th March, and in revised form 22nd June*, 1960. *It was published as an* INSTITUTION MONOGRAPH *in October*, 1960.)

SUMMARY

The paper describes both approximate and exact methods for evaluating the phase-change coefficients of a circular waveguide containing an axial dielectric rod. Close correlation is found between the phase-change coefficients of this waveguide structure and those of an unbounded rod over a wide range of rod radii. The correlation enables an unambiguous classification of the modes of an unbounded rod to be made. Exact and perturbation expressions are derived for total transmitted power, power distribution and attenuation in the dielectric-rod-waveguide structure. Correlation with the attenuation coefficients of an unbounded rod is again predicted. The application of the results of the paper to ferrite devices is briefly mentioned.

LIST OF SYMBOLS

(Figures in parenthesis refer to the equations in which symbols first appear.)

a, b, c, d = Constants defining amplitudes of electric and magnetic fields external to rod. (1)

a_n^l = Amplitude coefficient of longitudinal electric field within rod. (23)

$A = \bar{\beta}^2[1 - (K_1/K)^2]$ (16)

$C = J_1(K_1r_0)/Y_1(K_1r_0)$ (5)

$c = R(K_1r_1)/S(K_1r_1)$ (17)

$D(K_1r_1) = Y_1(K_1r_1)/J_1(K_1r_1)$ (5)

$E = J_1'(K_1r_0)/Y_1'(K_1r_0)$ (5)

E_z = Longitudinal component of electric field.

f = Function defined in equations (16) and (17).

$F(x) = xJ_1'(x)/J_1(x)$ (2)

F_M, F_D = Magnetic and dielectric attenuation factors defined by eqns. (31) and (32).

H_z = Longitudinal component of magnetic field.

$I_n(z)$ = Modified Bessel function of the first kind.

$J_n(x)$ = Bessel function of the first kind. (1)

j_m = mth root of $J_n(x)$.

K, K_1 = Wavenumbers within and external to dielectric rod. (1), (2)

$k_1 = jK_1$

$K_n(z)$ = Modified Bessel function of the second kind.

$L(y) = yY_1'(y)/Y_1(y)$ (4)

$M(y) = yH_1^{(2)}(y)/H_1^{(2)}(y)$ (I.5)

n = Azimuthal wavenumber. (1)

$N = (\bar{\mu}\bar{\epsilon})^{1/2}$ (16)

r, r_1, r_0 = Radial co-ordinate and radius of rod and waveguide respectively. (1)

$$R(K_1r_1) = (K_1r_1)\frac{J_n'(K_1r_1)Y_n'(K_1r_0) - J_n'(K_1r_0)Y_n'(K_1r_1)}{J_n(K_1r_1)Y_n'(K_1r_0) - J_n'(K_1r_0)Y_n(K_1r_1)}$$

$$S(K_1r_1) = (K_1r_1)\frac{J_n'(K_1r_1)Y_n(K_1r_0) - J_n(K_1r_0)Y_n'(K_1r_1)}{J_n(K_1r_1)Y_n(K_1r_0) - J_n(K_1r_0)Y_n(K_1r_1)}$$

T_1, T_2 = Evaluated integrals appearing in eqn. (12) of Monograph 409 E.

$T_1 = \frac{1}{2}F^2(Kr_1) + F(Kr_1) + \frac{1}{2}[(Kr_1)^2 - 1]$

$T_2 = \frac{1}{2}M^2(k_1r_1) + M(k_1r_1) - \frac{1}{2}[(k_1r_1)^2 + 1]$

T_3, T_4 = Evaluated integrals defined in eqn. (18).

T_5 = Evaluated integral defined in eqn. (25).

u_m = mth root of $J_n'(x)$.

$V = K_1/K$

P_i, P_0 = Power transmitted respectively inside and outside a dielectric rod. (18)

$Y_n(x)$ = Bessel function of the second kind.

z = Co-ordinate in direction of propagation.

α = Attenuation coefficient.

β = Phase-change coefficient.

$\bar{\beta} = \lambda_0/\lambda$ = Normalized phase-change coefficient.

$\epsilon_0, \epsilon, \epsilon_1$ = Permittivities of free space, rod and surrounding medium, respectively.

λ_0, λ = Wavelength in free space and guiding structure respectively.

κ = Off-diagonal component of ferrite tensor permeability.

$$\bar{\Lambda} = \frac{\bar{\epsilon}_1 S(K_1r_1)/(K_1r_1)^2 - \bar{\epsilon}F(Kr_1)/(Kr_1)^2}{n\bar{\beta}[1/(Kr_1)^2 - 1/(K_1r_1)^2]} \quad (18)$$

μ_0, μ, μ_1 = Permeabilities of free space, rod and surrounding medium, respectively.

$\bar{\mu} = \mu/\mu_0$

ω = Angular frequency.

(1) INTRODUCTION

In Part 1 of the paper,* relations between the behaviour of circular waveguides containing dielectric and ferrite rods were explained. It was stated that accurate values for the propagation coefficients in the ferrite case can be obtained under conditions of practical interest if the coefficients are known for a dielectric rod possessing particular values of permeability and permittivity. The propagation behaviour of unbounded dielectric rods was considered in that Part: the present Part is concerned with the behaviour of a dielectric rod bounded by a circular waveguide.

The determination of the phase-change coefficients for a lossless dielectric rod of radius r_1, contained in a perfectly conducting circular waveguide of radius r_0 ($r_1 \neq r_0$ in general),† is accomplished in two ways. First, special cases of the propagation equation for the bounded rod are considered which, together with propagation curves for unbounded rods, enable approximate propagation curves to be obtained. Secondly, the propagation equation is solved using a graphical method similar to that employed for unbounded rods. In general, the rapidity with which accurate values for the propagation

Correspondence on Monographs is invited for consideration with a view to publication.

Dr. Clarricoats is in the Department of Light Electrical Engineering, Queen's University of Belfast. The paper is based on a part of a thesis approved for the degree of Doctor of Philosophy at London University.

* Equations and references from Part 1 of this paper (page 170) are prefaced here by the symbol I; e.g. eqn. (I.1), Fig. I.6(*b*).

† For brevity referred to hereinafter as a 'bounded rod'.

coefficients can be obtained by the graphical method is increased by a knowledge of their approximate values obtained by the first method.

In Section 3, exact and perturbation expressions are developed for the power distribution and attenuation associated with a bounded rod. The exact expressions are most complicated and need be used only in the vicinity of cut-off, where the perturbation approach becomes invalid. Curves of normalized attenuation coefficient as a function of rod radius are given for the H_{11}-limit mode.

(2) EVALUATION OF THE PROPAGATION COEFFICIENTS FOR LOSSLESS DIELECTRIC RODS

(2.1) Derivation of the Characteristic Equation

The characteristic equation for the propagation coefficients of a waveguide containing an infinitely long lossless dielectric rod has been derived by several authors.[1, 2] Inside the rod the longitudinal components of electric and magnetic field are given by eqn. (I.1); outside the rod they are given by the following equations:

$$\left.\begin{aligned} E_z &= [aJ_n(K_1r) + bY_n(K_1r)]\varepsilon^{-jn\theta} \\ H_z &= [cJ_n(K_1r) + dY_n(K_1r)]\varepsilon^{-jn\theta} \end{aligned}\right\} r_1 > r > r_0 \qquad (1)$$

where $K_1^2 = \omega^2\epsilon_1\mu_1 - \beta^2$ and a factor $\varepsilon^{j(\omega t - \beta z)}$ is omitted. Application of the boundary conditions on the rod and waveguide surfaces yields the following characteristic equation, the functions being defined in the list of symbols:

$$\frac{n^2\beta^2}{\omega^2}\frac{[(K_1r_1)^2 - (Kr_1)^2]^2}{[(K_1r_1)^2(Kr_1)^2]^2} = \left[\frac{\mu F(Kr_1)}{(Kr_1)^2} - \frac{\mu_1 R(K_1r_1)}{(K_1r_1)^2}\right]\left[\frac{\epsilon F(Kr_1)}{(Kr_1)^2} - \frac{\epsilon_1 S(K_1r_1)}{(K_1r_1)^2}\right] \qquad (2)$$

For the case $n = 1$ and the lowest-order mode (H_{11}-limit),* Beam and Wachowski,[2] have obtained the normalized phase-change coefficient $\bar{\beta}$ as a function of r_0/λ_0 for different values of r_1/r_0 and with $\bar{\mu} = \mu/\mu_0 = 1$, $\bar{\epsilon} = \epsilon/\epsilon_0 = 2{\cdot}5$, while Suhl and Walker[1] give $\bar{\beta}$ as a function of r_1/r_0 for $\bar{\mu} = 1$, $\bar{\epsilon} = 10$ and $r_0/\lambda_0 = 0{\cdot}4$. After the present work was completed, Williams[3] gave $\bar{\beta}$ as a function of r_0/λ_0 with $r_1/r_0 = 0{\cdot}4$ and $\bar{\epsilon} = 10{\cdot}3$, $\bar{\mu} = 1{\cdot}5$ and $0{\cdot}46$. Neither the results of Beam and Wachowski nor those of Williams are sufficient to describe $\bar{\beta}$ as a function of r_1/r_0. More recently, Tompkins[4] and Waldron[5] have published computed results for certain ferrites and dielectrics. However, it is believed that the present study provides a more complete picture of the mode spectrum for dielectric rods.

It was first decided to obtain approximate curves of $\bar{\beta}$ as a function of r_1/r_0 for the H_{11}-limit mode, with $\bar{\epsilon} = 10$, $\bar{\mu} = 0{\cdot}25$, $1{\cdot}0$, $1{\cdot}6$, $\bar{\epsilon}_1 = \bar{\mu}_1 = 1$ and $r_0/\lambda_0 = 0{\cdot}4$, $0{\cdot}34$. Additional approximate curves have also been obtained for E_{11}-, H_{12}-, and E_{12}-limit modes with $\bar{\epsilon} = 10$, $\bar{\mu} = 1{\cdot}0$ and $r_0/\lambda_0 = 0{\cdot}4$. Subsequently, more accurate values of $\bar{\beta}$ have been obtained graphically in the above cases. The approximate curves are obtained by utilizing the following special cases of the characteristic equation.

(2.2) Special Cases of the Characteristic Equation

(2.2.1) Thin Dielectric Rod.

An expression for the propagation coefficient of the H_{11}-limit mode in a waveguide containing a thin dielectric rod can be obtained from eqn. (2) by expanding the functions $F(Kr_1)$, $R(K_1r_1)$ and $S(K_1r_1)$ in the range where r_1/λ_0 and r_1/r_0 are much less than unity. It may, however, be obtained directly from a general perturbation expression given in Appendix 7.1. In either case the result is as follows:

$$\bar{\beta} = \bar{\beta}_0 + \frac{u_1^2}{2J_1^2(u_1)(u_1^2 - 1)}\left(\frac{r_1}{r_0}\right)^2\left(\bar{\beta}_0\frac{\bar{\mu} - 1}{\bar{\mu} + 1} + \frac{1}{\bar{\beta}_0}\frac{\bar{\epsilon} - 1}{\bar{\epsilon} + 1}\right) \qquad (3)$$

where $\bar{\beta}_0$ is the phase-change coefficient in the empty waveguide and u_1 is the first root of $J_1'(x)$, the Bessel function of the first kind. The phase-change coefficient $\bar{\beta}$ can be obtained directly from eqn. (3) provided that the rod radius is such that $r_1/r_0 \ll 1$ and $r_1/\lambda_0 \ll 1$.

(2.2.2) Approximation to the Unbounded Dielectric Rod.

On comparing eqn. (I.5) and eqn. (2), it can be seen that their only difference lies in the replacement of the function $M(K_1r_1)$ in one case with the functions $R(K_1r_1)$ and $S(K_1r_1)$ in the other. It is now shown that under most conditions of practical interest when $n = 1$, $M(K_1r_1) \simeq R(K_1r_1) \simeq S(K_1r_1)$.

The expressions for $R(K_1r_1)$ and $S(K_1r_1)$ are now written as

$$R(K_1r_1) = \frac{F(K_1r_1) - ED(K_1r_1)L(K_1r_1)}{1 - ED(K_1r_1)} \qquad (4)$$

$$S(K_1r_1) = \frac{F(K_1r_1) - CD(K_1r_1)L(K_1r_1)}{1 - CD(K_1r_1)} \qquad (5)$$

where

$$F(K_1r_1) = K_1r_1\frac{J_1'(K_1r_1)}{J_1(K_1r_1)},\quad L(K_1r_1) = K_1r_1\frac{Y_1'(K_1r_1)}{Y_1(K_1r_1)},$$

$$D(K_1r_1) = \frac{Y_1(K_1r_1)}{J_1(K_1r_1)},$$

and $$C = \frac{J_1(K_1r_0)}{Y_1(K_1r_0)},\quad E = \frac{J_1'(K_1r_0)}{Y_1'(K_1r_0)}$$

assuming $n = 1$.

$Y_1(x)$ is a Bessel function of the second kind. When $\bar{\beta} > 1$, K_1 is imaginary; R and S retain their same form, only the functions F, L, D, C, and E are now given by

$$F(k_1r_1) = k_1r_1\frac{I_1'(k_1r_1)}{I_1(k_1r_1)},\quad L(k_1r_1) = k_1r_1\frac{K_1'(k_1r_1)}{K_1(k_1r_1)},$$

$$D(k_1r_1) = \frac{K_1(k_1r_1)}{I_1(k_1r_1)}$$

$$C = \frac{I_1(k_1r_0)}{K_1(k_1r_0)} \text{ and } E = \frac{I_1'(k_1r_0)}{K_1'(k_1r_0)}$$

where $k_1 = jK_1$. $I_1(z)$ and $K_1(z)$ are modified Bessel functions of the first and second kinds. Now when $\bar{\beta} > 1$, as is always the case for the unbounded rod $M(k_1r_1) = L(k_1r_1)$. It remains to show that under certain conditions $R(k_1r_1) \simeq S(k_1r_1) \simeq L(k_1r_1)$.

By considering the asymptotic expansions of $I_1(z)$, $I_1'(z)$, $K_1(z)$ and $K_1'(z)$ when z is large, it can be shown that

$$ED(k_1r_1) \simeq -\frac{k_1r_0 - \frac{1}{2}}{k_1r_0 + \frac{1}{2}}\varepsilon^{2k_1(r_0 - r_1)} \qquad (6)$$

and $$CD(k_1r_1) \simeq \varepsilon^{2k_1(r_0 - r_1)} \qquad (7)$$

provided that k_1r_1 is large. If $k_1r_1 > 3$, the validity of the approximate equations (6) and (7) is such that they give

* The H_{11}-limit mode is that mode in a waveguide containing a dielectric or ferrite rod which corresponds to the H_{11} mode in filled waveguides (and in the case of ferrite, zero magnetization). A similar nomenclature applies to other modes.

$ED(k_1r_1)$ and $CD(k_1r_1)$ to an accuracy better than 10%. However, even when $k_1r_1 < 3$, ED and CD behave approximately as ε^{2z}, when $z = k_1(r_0 - r_1)$. Since $F(k_1r_1)$ and $L(k_1r_1)$ are only linear in k_1r_1 when k_1r_1 is large, eqns. (4) and (5) show that $R(k_1r_1)$ and $S(k_1r_1)$ are approximately equal to $L(k_1r_1)$ over a considerable range of values of k_1r_1.

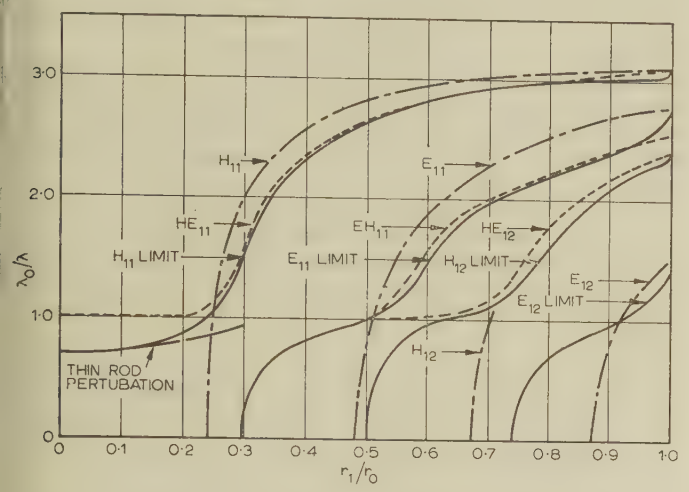

Fig. 1.—$\bar{\beta} = \lambda_0/\lambda$ as a function of r_1/r_0.
——— Sheathed dielectric rods.
– – – – – Unbounded dielectric rods.
——— Bounded dielectric rods.
$\bar{\epsilon} = 10 \quad \bar{\mu} = 1{\cdot}0 \quad 2r_0/\lambda_0 = 0{\cdot}8$

As an example, $R(k_1r_1)$, $S(k_1r_1)$ and $L(k_1r_1)$ have been calculated from the data in Fig. I.6(*b*) for the case $\bar{\mu} = 1$, $\bar{\epsilon} = 10$; $2r_0/\lambda_0$ was taken equal to 0·8. Over the range of r_1/r_0 between 0·28 and 0·72 the three functions agree to within 1%. Thus excellent agreement between unbounded and bounded propagation curves is to be expected over this range. Such agreement is in fact found, as illustrated in Fig. 1, where H_{11}-limit mode and HE_{11}-mode propagation curves are shown for the above rod parameters. The computed H_{11}-mode curve is taken from Reference 1, while the HE_{11}-mode curve comes from Fig. I.6(*b*). Similar agreement is to be expected for other rod and waveguide parameters, provided that k_1 and $(r_0 - r_1)$ are sufficient for $k_1(r_0 - r_1)$ to exceed about 2.

The larger the product $\bar{\mu}\bar{\epsilon}$, the larger will be the range of r_1/r_0 over which this condition is satisfied.

Since the literature contains unbounded propagation curves for rods with $\bar{\mu} = 1$, $\bar{\epsilon} = 2{\cdot}5$, 4·0, 5·0, 10, 13 and 32 (to which Part 1 of this paper adds $\bar{\mu} = 1$, $\bar{\epsilon} = 16$), it is evident that the above result is of considerable significance in the rapid determination of propagation curves for rods in waveguides. The additional knowledge from Part 1, that only the factor $\bar{\mu}\bar{\epsilon}$ is important with regard to the form of the propagation curves, renders the possible ranges of $\bar{\mu}$ and $\bar{\epsilon}$ far wider than the above seven values.

In the absence of unbounded-rod propagation curves for some specific material parameters, eqns. (I.10) and (I.11) for the limiting unbounded rod, cases $\bar{\mu}/\bar{\epsilon} = 0$ or $\bar{\mu}/\bar{\epsilon} = \infty$, enable propagation curves for bounded rods to be drawn very approximately over a part of the range of r_1/r_0. These equations incidentally correspond to those for a waveguide of radius r_1 filled with the dielectric, the so-called 'sheathed rod'. For comparison, $\bar{\beta}$ calculated from the above equations is shown in Fig. 1 as a function of r_1/r_0. Agreement is seen to be best as $r_1/r_0 \to 1$, a result which might be anticipated from power transmission considerations.

(2.2.3) **The Condition $\bar{\beta} = 1$, or More Generally $\beta = \omega(\epsilon_1\mu_1)^{1/2}$.**

Under the condition $\beta^2 = \omega^2(\epsilon_1\mu_1)$, eqn. (2) reduces to a more simple transcendental form. The most direct method of obtaining this equation is by consideration of the limiting values of $R(K_1r_1)$, $S(K_1r_1)$ and $[R(K_1r_1)S(K_1r_1)]$ as $K_1 \to 0$ (corresponding to the condition $\beta^2 = \omega^2\epsilon_1\mu_1$). Thus, by expanding these functions it may be shown that

$$R(K_1r_1) = \frac{\dfrac{r_1}{r_0} - \dfrac{r_0}{r_1}}{\dfrac{r_1}{r_0} + \dfrac{r_0}{r_1}} + O(K_1r_1)^2$$

$$S(K_1r_1) = \frac{\dfrac{r_1}{r_0} + \dfrac{r_0}{r_1}}{\dfrac{r_1}{r_0} - \dfrac{r_0}{r_1}} + O(K_1r_1)^2$$

and

$$[R(K_1r_1)S(K_1r_1)] = 1 + (K_1r_1)^2\left[\frac{2\log_\varepsilon\left(\dfrac{r_0}{r_1}\right)}{\left(\dfrac{r_1}{r_0}\right)^4 - 1} - \frac{1}{2}\right] + O(K_1r_1)^4$$

On inserting these expressions into the expanded form of eqn. (2) a quadratic for $F(Kr_1)$ is obtained, with solutions given by

$$F(Kr_1) = (Kr_1)^2\frac{\left[\left(\dfrac{\mu\epsilon_1}{\nu} + \mu_1\epsilon\nu\right) \pm \left\{\left(\dfrac{\mu\epsilon_1}{\nu} + \mu_1\epsilon\nu\right)^2 - 4\epsilon\mu(K_1r_1)^2\left[\dfrac{\epsilon_1\mu_1 + \epsilon\mu}{(Kr_1)^2} - \dfrac{2\mu_1\epsilon_1\log_\varepsilon\dfrac{r_0}{r_1}}{1-(r_1/r_0)^4} - \dfrac{\mu_1\epsilon_1}{2}\right]\right\}^{1/2}\right]}{2(K_1r_1)^2\mu\epsilon} \quad . \quad (8)$$

when $K_1 \to 0$, where $\nu = \dfrac{\dfrac{r_1}{r_0} - \dfrac{r_0}{r_1}}{\dfrac{r_1}{r_0} + \dfrac{r_0}{r_1}}$

Thus either $F(Kr_1) = \infty \quad . \quad . \quad . \quad . \quad . \quad (9)$

implying $J_1(Kr_1) = 0$ for E-modes,

or

$$F(Kr_1) = \frac{(\mu_1\epsilon_1 + \mu\epsilon) - \mu_1\epsilon_1(Kr_1)^2\left[\dfrac{2\log_\varepsilon\dfrac{r_0}{r_1}}{1-\left(\dfrac{r_1}{r_0}\right)^4} + \frac{1}{2}\right]}{\left(\dfrac{\mu\epsilon_1}{\nu} + \mu_1\epsilon\nu\right)} \text{ for H-modes} \quad . \quad . \quad . \quad . \quad (10)$$

Eqn. (10) can be solved numerically without difficulty, enabling the values of r_1/r_0 at which $\bar{\beta} = (\bar{\epsilon}_1\bar{\mu}_1)^{1/2}$ for H_{1m}-limit modes to be determined for given parameters. Calculations have been

made for H_{11}- and H_{12}-limit modes for the parameters of Fig. 1 in particular. For the H_{11}-limit mode, exact agreement is found between the value of r_1/r_0 predicted by eqn. (10) and that obtained from the propagation curve taken from Reference 1.

(2.2.4) **The Empty and Filled Waveguide ($r_1/r_0 = 0$ and $r_1/r_0 = 1$).**

The cases $r_1/r_0 = 0$ and $r_1/r_0 = 1$, although straightforward, nevertheless provide two useful points on the propagation curves. $\bar{\beta}$ is then obtained from the equation

$$\bar{\beta} = \left\{\bar{\mu}\bar{\epsilon} - \left[\frac{\lambda_0}{2\pi r_0}(Kr_0)\right]^2\right\}^{1/2} \quad . \quad . \quad . \quad (11)$$

where $Kr_0 = u_m$ for H-modes, $Kr_0 = j_m$ for E-modes, and $J_1'(u_m) = J_1(j_m) = 0$.

(2.2.5) **The Cut-off Condition, $\bar{\beta} = 0$.**

When $\bar{\beta} = 0$, eqn. (2) becomes

$$\left[\frac{\mu F(Kr_1)}{(Kr_1)^2} - \frac{\mu_1 R(K_1 r_1)}{(K_1 r_1)^2}\right]\left[\frac{\epsilon F(Kr_1)}{(Kr_1)^2} - \frac{\epsilon_1 S(K_1 r_1)}{(K_1 r_1)^2}\right] = 0 \quad (12)$$

The two sets of solutions given by

$$\epsilon_1 F(Kr_1) = \epsilon R(K_1 r_1) \quad . \quad . \quad . \quad . \quad . \quad (13)$$

and

$$\mu_1 F(Kr_1) = \mu S(K_1 r_1) \quad . \quad . \quad . \quad . \quad . \quad (14)$$

correspond to H- and E-mode cut-off conditions, respectively. This statement is proved by deriving eqns. (13) and (14) directly from Maxwell's equations, making E_z and H_z zero in turn. Only when $\bar{\beta} = 0$ is it possible to satisfy the boundary conditions at the rod surface without requiring both longitudinal E- and H-fields (except in the case of circularly symmetric modes, for which $n = 0$). Eqns. (13) and (14) have been solved graphically for rods with $\bar{\epsilon} = 10$, $\bar{\mu} = 1{\cdot}6$, $1{\cdot}0$ and $0{\cdot}25$ and with $2r_0/\lambda_0 = 0{\cdot}8$ and $0{\cdot}685$. Results of these calculations are given in Table 1.

Table 1

Mode	$2r_0/\lambda_0 = 0{\cdot}685$			$2r_0/\lambda_0 = 0{\cdot}8$		
	$\bar{\mu} = 0{\cdot}25$	$\bar{\mu} = 1{\cdot}0$	$\bar{\mu} = 1{\cdot}6$	$\bar{\mu} = 0{\cdot}25$	$\bar{\mu} = 1{\cdot}0$	$\bar{\mu} = 1{\cdot}6$
H_{11}	P	P	P	P	P	P
H_{12}	NP	0·440	0·325	NP	0·395	0·31
H_{13}	NP	NP	0·6	NP	NP	0·60
E_{11}	0·490	0·240	0·205	0·460	0·230	0·195
E_{12}	NP	0·585	0·465	NP	0·66	0·445
E_{13}	NP	NP	NP	NP	NP	0·78

Table 1 shows $2r_1/\lambda_0$ for cut-off as calculated from eqns. (13) and (14) respectively. P denotes propagating mode, NP denotes non-propagating mode, over the entire range $0 < r_1/r_0 < 1$, $\bar{\epsilon} = 10$ throughout.

(2.2.6) **The Slope of the Propagation Curves when $\bar{\beta} = 0$ and $r_1/r_0 = 1$.**

In Appendix 7.2 it is shown that, when $\bar{\beta} = 0$, $d\bar{\beta}/dr_1 = \infty$. When $r_1/r_0 = 1$, it can be shown, using eqn. (33) and assuming $\bar{\epsilon}_1 = \bar{\mu}_1 = 1$, that for the H_{11}-limit mode

$$\frac{d\bar{\beta}}{dr_1} = \frac{(\bar{\epsilon} - 1)\bar{\epsilon} + (\bar{\mu} - 1)[\bar{\beta}^2 + u_1^2(\bar{\epsilon}\bar{\mu} - \bar{\beta}^2)]}{\bar{\beta} r_0 (u_1^2 - 1)}$$

Similar expressions are obtainable for other modes of propagation.

(2.3) Graphical Evaluation of the Propagation Coefficients

(2.3.1) **Approximate Propagation Curves.**

A first step in the process of obtaining accurate propagation curves is to establish approximate curves by the methods of the previous Section. This procedure is not essential, but if it is adopted considerable labour can be avoided. The construction of the approximate curves of Fig. 1 is now briefly discussed following in sequence through the above methods.

With the parameters chosen, only the H_{11}-mode propagates in empty waveguide; thus the thin-rod approximation can be used only in this case. Since the H_{11}-limit curve has been computed,[1] the limits of the above approximation can be clearly seen.

The unbounded-rod approximation has already been mentioned with respect to the H_{11}-limit mode, while for E_{11}- and H_{12}-limit modes fairly close agreement can be expected for values of r_1/r_0 between $0{\cdot}58$ and $0{\cdot}85$, and $0{\cdot}75$ and $0{\cdot}8$, respectively. Within these ranges $R(K_1r_1)$, $S(K_1r_1)$ and $L(K_1r_1)$ agree to within 10%.

For E_{11}- and E_{12}-modes, the value of r_1/r_0 at which $\bar{\beta} = 1$ is readily obtained. At this point the propagation curves for the sheathed rod and dielectric rod intersect. For H_{11}- and H_{12}-modes the corresponding values of r_1/r_0 are found without difficulty if curves of the function $F(x)$ are available.

The empty and filled waveguide conditions establish two points for the H_{11}-mode, while the cut-off and filled-waveguide conditions establish two points for the E_{11}-, H_{12}- and E_{12}-modes. Also, the slope of the propagation curves is infinite for the above three modes when $\bar{\beta} = 0$.

With the aid of the unbounded propagation curves of Fig. I.6(*b*), approximate curves have been drawn in Fig. 2 for a waveguide containing rods with $\bar{\epsilon} = 10$, $\bar{\mu} = 1{\cdot}6$, $1{\cdot}0$ and $0{\cdot}25$.

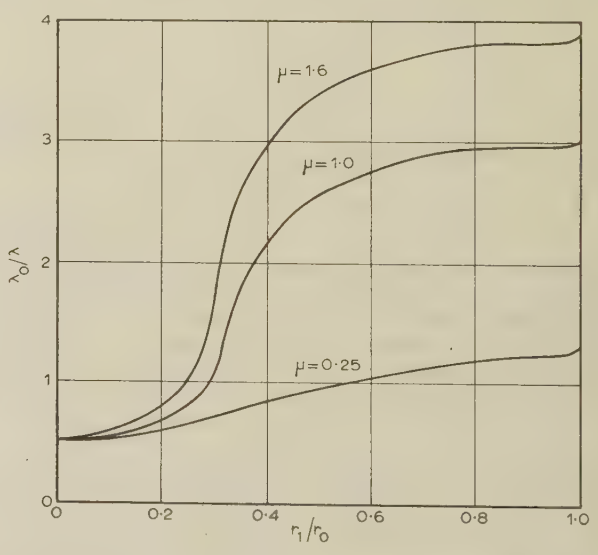

Fig. 2.—$\bar{\beta} = \lambda_0/\lambda$ as a function of r_1/r_0 for an H_{11}-limit mode.
$\bar{\epsilon} = 10$ $\bar{\mu} = 1{\cdot}6$, $1{\cdot}0$ and $0{\cdot}25$
$2r_0/\lambda_0 = 0{\cdot}685$

(2.3.2) **Exact Graphical Solutions.**

The method for obtaining exact graphical solutions follows from that described in Part 1. Eqn. (2) is put in a quadratic form for $(\bar{\mu}/\bar{\epsilon})^{1/2}$:

$$(\bar{\mu}/\bar{\epsilon}) + (\bar{\mu}/\bar{\epsilon})^{1/2} f + c = 0 \quad . \quad . \quad . \quad . \quad (15$$

where, adopting an abbreviated notation,

$$f = \frac{A}{NFSV^2} - \frac{R}{NFV^2} - \frac{NFV^2}{S} \quad . \quad . \quad . \quad (16)$$

Eqn. (15) when rearranged gives

$$f = -[(\bar{\mu}/\bar{\epsilon})^{1/2} + c(\bar{\epsilon}/\bar{\mu})^{1/2}] \quad . \quad . \quad . \quad (17)$$

where $c = R/S$

Solutions are again obtained by plotting f as a function of r_1/λ_0 (or conveniently, Kr_1) in the range $0 < r_1/\lambda_0 < r_0/\lambda_0$, for different values of $\bar{\beta}$; then eqn. (17) is mapped on the same diagram. The intersections between these curves give the values of r_1/λ_0 corresponding to $\bar{\beta}$ for the different modes. Fig. 3

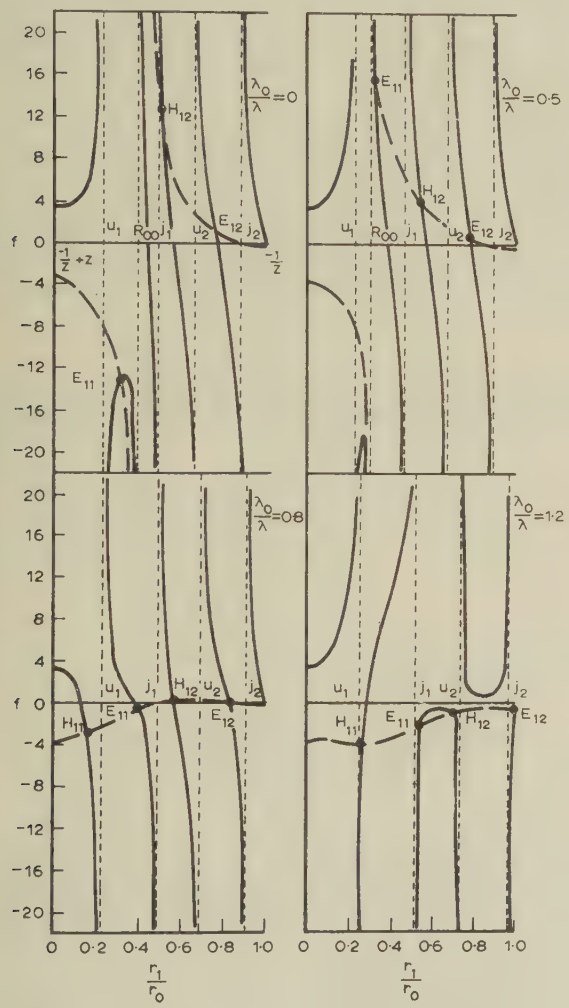

Fig. 3.—f as a function of r_1/r_0 for a dielectric rod.
— — f as given by eqn. (16).
—— f as given by eqn. (17).
$\bar{\epsilon} = 10 \quad \bar{\mu} = 1{\cdot}0 \quad 2r_0/\lambda_0 = 0{\cdot}8$

shows typical f-diagrams for the case $\bar{\mu} = 1$, $\bar{\epsilon} = 10$ and $\bar{\beta} = 0$, $0{\cdot}5$, $0{\cdot}8$ and $1{\cdot}2$.

The complication in the diagram compared with that for the unbounded rod arises from the behaviour of the functions $R(K_1r_1)$ and $S(K_1r_1)$ compared with $M(K_1r_1)$. Also, both sets of curves, given by eqns. (16) and (17), depend on $R(K_1r_1)$ and $S(K_1r_1)$, whereas in the unbounded case $M(K_1r_1)$ appeared in only one equation [eqn. (I.7)]. When $\bar{\beta} < 0{\cdot}681$, $R(K_1r_1)$ contains a singularity located at the value of K_1r_1 for which $ED(K_1r_1) = 1$. As $\bar{\beta}$ approaches $0{\cdot}681$, the corresponding r_1/r_0 value tends to zero. A study of the behaviour of the function $R(K_1r_1)$, when $r_1/\lambda_0 \to 0$ and $K_1r_0 \to u_1$, requires the evaluation of a number of expressions under limiting conditions and is consequently an involved process. Nevertheless, it is possible to establish an intersection between the two sets of curves at this point when $\bar{\beta} = 0{\cdot}681$, this solution corresponding to the H_{11}-mode of empty waveguide.

As $\bar{\beta}$ increases above unity, the f-diagram resembles more closely that for unbounded rods. However, since $R(K_1r_1)/S(K_1r_1) = 0$ when $r_1/r_0 = 1$, eqn. (17) gives $f = -(\bar{\mu}/\bar{\epsilon})^{1/2}$ compared with $-[(\bar{\mu}/\bar{\epsilon})^{1/2} + (\bar{\epsilon}/\bar{\mu})^{1/2}]$ for the unbounded rod case. This accounts for the differences observed in the propagation curves in the neighbourhood of $r_1/r_0 = 1$. Since, in general, $R(K_1r_1)/S(K_1r_1) = 1$, when $r_1/r_0 = 0$, eqns. (17) and (I.8) (quoted above) are then identical. Thus agreement between f-diagrams for the two cases is best for small values of r_1/r_0, provided that $\bar{\beta} > 1$. Values of $\bar{\beta}$ taken from Fig. 3 were incorporated in Fig. 1. In view of the known agreement with the unbounded-rod case for $\bar{\beta}$ exceeding about $1{\cdot}5$, it was considered unnecessary to evaluate more values of $\bar{\beta}$ than $0{\cdot}5$, $0{\cdot}8$ and $1{\cdot}2$. Since these confirmed the reliability of the approximate propagation curves, the basis for the mode nomenclature in the case of unbounded rods was considered to be justified.

(3) THE TRANSMITTED POWER DISTRIBUTION AND ATTENUATION COEFFICIENT

(3.1) Exact Expression for Power Distribution

An expression for the transmitted power distribution, P_i/P_0, in a waveguide containing a dielectric rod does not appear to have been given previously in the literature. Although the derivation is straightforward, the algebra involved is extremely tedious owing to the complicated nature of certain integrals, which involve functions such as $R(K_1r_1)$ and $S(K_1r_1)$. In Appendix 7.3 an outline of this derivation is given, and it is shown that

$$\frac{P_i}{P_0} = -\left(\frac{K_1}{K}\right)^4 \frac{(\bar{\epsilon} + \bar{\mu}\bar{\Lambda}^2)T_1 + \bar{\Lambda}\left(\frac{1}{\bar{\beta}}\bar{\mu}\bar{\epsilon} + \bar{\beta}\right)}{(\bar{\epsilon}_1 T_3 + \bar{\mu}_1\bar{\Lambda}^2 T_4) + \bar{\Lambda}\left(\frac{1}{\bar{\beta}}\bar{\mu}_1\bar{\epsilon}_1 + \bar{\beta}\right)} \quad . \quad (18)$$

$$T_3 = \left[\frac{\frac{2}{\pi}J_1(K_1r_0)Y_1(K_1r_0) + \frac{2}{\pi^2}}{\sigma^2(K_1r_1)} + \frac{J_1(K_1r_0)Y_1(K_1r_1)S(K_1r_1)}{\sigma(K_1r_1)} - \frac{K_1r_1J_1'(K_1r_1)Y_1(K_1r_0)}{\sigma(K_1r_1)} - \frac{1}{2}S^2(K_1r_1) - \frac{1}{2}(K_1^2r_1^2 - 1)\right]$$

$$T_4 = \left[\frac{\frac{2}{\pi}J_1'(K_1r_0)Y_1'(K_1r_0) + \frac{2}{\pi^2}\left(1 - \frac{1}{K_1^2r_0^2}\right)}{\rho^2(K_1r_1)} + \frac{J_1'(K_1r_0)Y_1(K_1r_1)R(K_1r_1)}{\rho(K_1r_1)} - \frac{K_1r_1J_1'(K_1r_1)Y_1'(K_1r_0)}{\rho(K_1r_1)} - \frac{1}{2}R^2(K_1r_1) - \frac{1}{2}(K_1^2r_1^2 - 1)\right]$$

$$\sigma(K_1r_1) = J_1(K_1r_1)Y_1(K_1r_0) - Y_1(K_1r_1)J_1(K_1r_0)$$

and $$\rho(K_1r_1) = J_1(K_1r_1)Y_1'(K_1r_0) - Y_1(K_1r_1)J_1'(K_1r_0)$$

Comparison can be made between eqns. (18) and (I.12), where P_i/P_0 is given for an unbounded rod, and all the other terms in the above equation are defined. The forms of the two equations are very similar, differing only in that the term $(\bar{\epsilon}_1 + \bar{\mu}_1\bar{\Lambda}^2)T_2$ in the denominator of eqn. (I.12) is replaced by $-(\bar{\epsilon}_1 T_3 + \bar{\mu}_1\bar{\Lambda}^2 T_4)$ in eqn. (18). On recollection of the close agreement between bounded and unbounded propagation curves when $R(k_1r_1) \simeq S(k_1r_1) \simeq M(k_1r_1)$, it might be expected that, in this range, $T_3 \simeq T_4 \simeq -T_2$. This is in fact so, as demonstrated in Appendix 7.4. Thus, within the range for which $\bar{\beta} > (\bar{\mu}_1\bar{\epsilon}_1)^{1/2}$ and r_1/r_0 is not too near unity, quite close agreement between the power distribution of bounded and unbounded rods may be expected. Since $P_i/P_0 \gg 1$ under these conditions and the ratio is almost independent of r_0/λ_0, an abrupt change in waveguide radius or even waveguide shape would not be expected to alter appreciably either $\bar{\beta}$ or P_i/P_0. A small reflection coefficient could therefore be expected at such a junction.

Support for the former statement has been provided by Tompkins.[4] He has found, under the above conditions, almost identical phase-change coefficients for circular and rectangular waveguides containing rods of the same diameter. The cut-off wavelengths of the empty waveguides were approximately the same. This observation suggests that a dielectric rod might provide a simple means for producing a broad-band impedance match between two joined waveguides of differing size or shape. It would, of course, be necessary to match the dielectric rod into each of the waveguides, but this could readily be accomplished by tapering the rod. The rod could be supported, for example, by means of polystyrene foam. Further work is in progress on this topic.

Since eqn. (18) is exact, it applies when $\bar{\beta} = 0$, i.e. at cut-off. For H-modes, $1/\bar{\Lambda} = 0$ and $\bar{\Lambda}\bar{\beta}$ is finite at cut-off, while for E-modes $\bar{\Lambda} = 0$ and $\bar{\Lambda}/\bar{\beta}$ is finite. Thus

$$\frac{P_i}{P_0} = -\left(\frac{K_1}{K}\right)^4 \frac{\bar{\mu}T_1 + 1/\bar{\Lambda}\bar{\beta}\bar{\mu}\bar{\epsilon}}{\bar{\mu}_1 T_4 + 1/\bar{\Lambda}\bar{\beta}\bar{\mu}_1\bar{\epsilon}_1} \text{ for H-modes when } \bar{\beta} = 0$$

$$\text{and} \quad \frac{1}{\bar{\Lambda}\bar{\beta}} = \frac{[1-(K_1/K)^2]}{\bar{\epsilon}F(Kr_1)(K_1/K)^2 - \bar{\epsilon}_1 S(K_1r_1)}, \left(\frac{K_1}{K}\right)^2 = \frac{\mu_1\epsilon_1}{\mu\epsilon} \qquad (19)$$

$$\frac{P_i}{P_0} = -(K_1/K)^4 \frac{\bar{\epsilon}T_1 + \bar{\Lambda}/\bar{\beta}\bar{\mu}\bar{\epsilon}}{\bar{\epsilon}_1 T_3 + \bar{\Lambda}/\bar{\beta}\bar{\mu}_1\bar{\epsilon}_1} \text{ for E-modes when } \bar{\beta} = 0$$

$$\text{and} \quad \bar{\Lambda}/\bar{\beta} = \frac{[1-(K_1/K)^2]}{\bar{\mu}F(Kr_1)(K_1/K)^2 - \bar{\mu}_1 R(K_1r_1)} \quad . \quad . \quad (20)$$

The above expressions enable the power distribution at cut-off to be readily determined. The limiting expressions for $1/\bar{\Lambda}\bar{\beta}$ and $\bar{\Lambda}/\bar{\beta}$ are required again when expressions are developed in Section 3.3.1 for the attenuation near cut-off.

When $\bar{\beta} = (\bar{\mu}_1\bar{\epsilon}_1)^{1/2}$, $K_1^2 = 0$ and eqn. (18) again reduces to a simple form in the case of E-modes:

$$\frac{P_i}{P_0} = -\frac{1}{2}(\bar{\epsilon}_1/\bar{\epsilon}\nu + \bar{\mu}_1\nu/\bar{\mu}), \nu < 0 \quad . \quad . \quad . \quad (21)$$

As $r_0 \to \infty$, $\nu \to -1$ and eqn. (21) reduces to the expression for an unbounded rod. Eqn. (21) has also been derived directly from a solution of Maxwell's equations with $K_1^2 = 0$. This analysis is simplified by the condition $H_z = E_z = 0$ when $r_0 > r > r_1$, for E-modes with $K_1^2 = 0$. With H-modes, however, eqn. (18) does not simplify and the alternative method is complicated by H_z and E_z remaining finite. Because of the similarity in power distribution between unbounded and bounded rods and the straightforward expressions which apply in the cases $\bar{\beta} = 0$ and $\bar{\beta} = (\bar{\mu}_1\bar{\epsilon}_1)^{1/2}$, the construction of approximat power distribution curves for bounded rods can readily b undertaken. However, since the attenuation of a mode i usually of more interest than the power distribution, onl curves of the former variable as a function of rod radius ar shown (Fig. 4). The evaluation of the attenuation coefficien will be considered in Section 3.3, where exact and perturbatio expressions for the total transmitted power, $P_i + P_0$, will b employed.

(3.2) Perturbation Expression for Total Transmitted Power

In view of the complicated form of eqn. (18), when $\bar{\beta}$ is such that approximations cannot be made it is convenient to have perturbation expression for the total transmitted power, $P_i + P_0$. Such an expression is required when the attenuation coefficient are determined.

Suhl and Walker[1] have obtained a perturbation expressio for the total transmitted power in a waveguide containing dielectric rod with $\bar{\mu} = 1$: a more general expression is no obtained for a rod with $\bar{\mu} \neq 1$.

Consider the effect of increasing the radius of a dielectric ro by an increment δr_1. Since the field components H_z, H_θ, E_z and E_θ, are continuous at the rod surface, they remain unchanged However, H_r and E_r are discontinuous and so change thei values when the boundary is displaced. If H_{ri} and E_{ri} are th fields just inside the rod and H_{ro} and E_{ro} the correspondin fields outside,

$$H_{ro} = \mu/\mu_1 H_{ri} \text{ and } E_{ro} = \epsilon/\epsilon_1 E_{ri}$$

On substitution in the general perturbation formula o Appendix 7.1, the following expression for the total transmitte power is obtained:

$$P_i + P_0 = \frac{2\pi\omega}{\frac{4}{r_1}d\beta/dr_1}\Big[(\epsilon-\epsilon_1)\Big(|E_z|^2 + |E_\theta|^2 + \frac{\epsilon}{\epsilon_1}|E_{ri}|^2\Big) + (\mu-\mu_1)\Big(|H_z|^2 + |H_\theta|^2 + \frac{\mu}{\mu_1}|H_{ri}|^2\Big)\Big] \quad . \quad . \quad . \quad . \quad (22)$$

whence on substitution for the fields,

$$P_i + P_0 = \frac{(a_n^i)^2 2\pi^3 \left(\frac{\epsilon_0}{\mu_0}\right)^{1/2}\left(\frac{r_1}{\lambda_0}\right)^2 J_n^2(Kr_1)}{(Kr_1)^4 \frac{1}{r}\frac{d\bar{\beta}}{dr_1}}$$

$$\Big[(\bar{\epsilon}-\bar{\epsilon}_1)\Big\{\Big(\frac{2\pi r_1}{\lambda_0}\Big)^2(\bar{\epsilon}\bar{\mu}-\bar{\beta}^2)^2 + [n\bar{\beta} + \bar{\mu}\bar{\Lambda}F(Kr_1)]^2 + \frac{\epsilon}{\epsilon_1}[n\bar{\mu}\bar{\Lambda} + \bar{\beta}F(Kr_1)]^2\Big\}$$

$$+ (\bar{\mu}-\bar{\mu}_1)\Big\{\bar{\Lambda}^2\Big(\frac{2\pi r_1}{\lambda_0}\Big)^2(\bar{\epsilon}\bar{\mu}-\bar{\beta}^2)^2 + [n\bar{\beta}\bar{\Lambda} + \bar{\epsilon}F(Kr_1)]^2 + \frac{\mu}{\mu_1}[n\bar{\epsilon} + \bar{\beta}\bar{\Lambda}F(Kr_1)]^2\Big\}\Big] \quad . \quad (23)$$

In order that eqn. (23) can be used to eliminate $P_i + P_0$ from particular problem, the slope of the propagation curve $d\bar{\beta}/dr_1$ must be known. Since this expression is the result of a perturbation it is clearly invalid near cut-off, where $d\bar{\beta}/dr_1 \to \infty$. However, it is particularly useful near $\bar{\beta} = 1$, where for H-modes the numerator and denominator of the exact expression tend to zero in such a way that accurate computation becomes impossible.

(3.3) Attenuation Coefficient for Waveguides Containing Dielectric Rods

(3.3.1) An Expression for the Attenuation Coefficient of Low-Loss Dielectric Rods.

From Poynting's theorem it can be shown that, provided the losses are small and β is not too near cut-off, the attenuation, α, per unit length along a structure is given by

$$\alpha = \frac{1}{2}\left[\frac{\omega\mu''\int_{S_1}|H|^2dS + \omega\epsilon''\int_{S_1}|E|^2dS}{(P_i + P_0)}\right] \quad . \quad . \quad (24)$$

It is assumed that only the rod possesses loss; hence the integrations in this equation extend just over the cross-section of the rod. On substitution for $|H|^2$ and $|E|^2$ and evaluation of the integrals, together with an expression for $P_i + P_0$ through Section 3.1, eqn. (24) becomes

$$\alpha = \frac{\bar{\mu}''\left[(\bar{\epsilon}^2 + \bar{\Lambda}^2\bar{\beta}^2)T_1 + 2\bar{\Lambda}\bar{\epsilon}\bar{\beta} + \left(\frac{\lambda_0}{2\pi}\right)^2\bar{\Lambda}^2K^4T_5\right] + \bar{\epsilon}''\left\{[\bar{\beta}^2 + (\bar{\Lambda}\bar{\mu})^2]T_1 + 2\bar{\Lambda}\bar{\mu}\bar{\beta} + \left(\frac{\lambda_0}{2\pi}\right)^2K^4T_5\right\}}{\left\{[(\bar{\epsilon} + \bar{\mu}\bar{\Lambda}^2)T_1 + \bar{\Lambda}(\bar{\mu}\bar{\epsilon}/\bar{\beta} + \bar{\beta})] + (K/K_1)^4[(\bar{\epsilon}_1T_3 + \bar{\mu}_1\bar{\Lambda}^2T_4 - \bar{\Lambda}(\bar{\mu}_1\bar{\epsilon}_1/\bar{\beta} + \bar{\beta})]\right\}} \quad . \quad . \quad (25)$$

Only T_5 has not previously been defined:

$$T_5 = \frac{1}{2}r_1^2\left\{\left[1 - \frac{1}{(Kr_1)^2}\right] + \frac{J'(Kr_1)^2}{J_1(Kr_1)^2}\right\}$$

Eqn. (25) is valid provided that the power lost per wavelength along the rod is small compared to the power flowing. For a 10% perturbation, the attenuation must not exceed 5 dB per wavelength.

Near cut-off, when $\bar{\beta} \to 0$, equation 25 simplifies considerably with neglect of terms of order $\bar{\beta}^2$.

For H_{1m}-limit modes,

$$\alpha = \frac{\bar{\mu}''\left(\frac{\lambda_0}{2\pi}\right)^2K^4T_5 + \bar{\epsilon}''\bar{\mu}^2T_1}{(\bar{\mu}T_1 + \bar{\mu}\bar{\epsilon}/\bar{\Lambda}\bar{\beta}) + (K/K_1)^4(\bar{\mu}_1T_4 - \bar{\mu}_1\bar{\epsilon}_1/\bar{\Lambda}\bar{\beta})}\left(\frac{\pi\lambda}{\lambda_0^2}\right) \quad (26)$$

For E_{1m}-limit modes,

$$\alpha = \frac{\bar{\mu}''\bar{\epsilon}^2T_1 + \bar{\epsilon}''(\lambda_0/2\pi)^2K^4T_5}{(\bar{\epsilon}_1T_1 + \bar{\Lambda}\bar{\mu}\bar{\epsilon}/\bar{\beta}) + (K/K_1)^4(\bar{\epsilon}_1T_3 - \bar{\Lambda}\bar{\mu}_1\bar{\epsilon}_1/\bar{\beta})}\left(\frac{\pi\lambda}{\lambda_0^2}\right) \quad (27)$$

The range of validity of the above equations is restricted, for three reasons. First, $\bar{\beta}$ must be sufficiently small that terms containing $\bar{\beta}^2$ can be neglected by comparison with those which do not contain $\bar{\beta}$. For an approximate result $\bar{\beta}$ should be less than, say, 0·3. Secondly, the losses must be sufficiently small that α/β is less than, say, 0·1. This implies that as $\bar{\beta}$ tends to zero the expressions are valid only for values of $\bar{\mu}''/\bar{\mu}'$ and $\bar{\epsilon}''/\bar{\epsilon}'$ of order $\bar{\beta}^2$ or less. Finally, in practice a further restriction prevents the use of the expressions in the limit of $\bar{\beta}$ vanishing; this is due to the finite conductivity of the waveguide walls. Even in the absence of losses within the guide, if the walls are not perfectly conducting α and β remain finite under the conditions which, in the ideal case, cause $\alpha = \beta = 0$.

Karbowiak[6] has determined exact expressions for the attenuation due to wall resistivity in an empty circular waveguide. While it is realized that these are not applicable to cut-off in a partially filled waveguide, it is to be expected that the order of attenuation could be the same. For an E_{11} mode which is just cut off in a perfectly conducting waveguide at 9 Gc/s, $\alpha = 0{\cdot}03$ dB/cm in a copper waveguide at the same frequency. By comparison, a calculation made using eqn. (27) gave $\alpha \simeq 0{\cdot}5$ dB/cm ($\simeq 5$ dB/wavelength) when $\bar{\beta} = 0{\cdot}3$ and $\bar{\epsilon} = 10$, $\bar{\mu} = 1{\cdot}6$, $\bar{\mu}'' = 0{\cdot}05$, and $2r_0/\lambda_0 = 0{\cdot}685$. Under these conditions the first two restrictions are just satisfied. The third appears to be well satisfied.

At $\bar{\beta} = (\bar{\mu}_1\bar{\epsilon}_1)^{1/2}$ for E-modes, eqn. (25) simplifies considerably; without loss of generality $\bar{\mu}_1$ and ϵ_1 are now put equal to unity; then, when $\bar{\beta} = 1$,

$$\alpha = \frac{\pi}{\lambda_0}\bar{\epsilon}\bar{\mu}\frac{(\tan\delta_m + \tan\delta_e)}{1 - 2\bar{\mu}\bar{\epsilon}\nu/(\bar{\mu} + \bar{\epsilon}\nu^2)} \quad . \quad . \quad . \quad (28)$$

where $\tan\delta_m = \mu''/\mu'$ and $\tan\delta_e = \epsilon''/\epsilon'$; ν is given in eqn. (8). With the aid of eqn. (21) the above equation can be rewritten as

$$\alpha = \frac{\bar{\epsilon}\bar{\mu}}{\bar{\beta}}\frac{P_i}{P_i + P_0}(\tan\delta_m + \tan\delta_e)$$

This equation is also valid for unbounded rods, and thus in this special case it is possible to show that attenuation and energy concentration are linearly related. This was anticipated in general for unbounded rods in Fig. I.7.

(3.3.2) The Attenuation Coefficient for Thin Dielectric Rods.

The attenuation coefficient of a waveguide containing a thin dielectric rod can be obtained directly from eqn. (33) of Appendix 7.1. On putting $\mu = \mu' - j\mu''$ and $\epsilon = \epsilon' - j\epsilon''$, the attenuation coefficient for the H_{11}-mode becomes

$$\alpha = \frac{u_1^2}{J_1^2(u_1)(u_1^2 - 1)}\frac{2\pi}{\lambda_0}\left(\frac{r_1}{r_0}\right)^2 \left[\bar{\beta}_0\frac{\bar{\mu}''}{(\bar{\mu}' + 1)^2 + \bar{\mu}''^2} + \frac{1}{\bar{\beta}_0}\frac{\bar{\epsilon}''}{(\bar{\epsilon}' + 1)^2 + \bar{\epsilon}''^2}\right] \quad (29)$$

where $\bar{\beta}_0$ is the phase-change coefficient in empty waveguide.

Later in this paper general results are given for the attenuation coefficient of an H_{11}-mode, and these are compared with those obtained from eqn. (29). This equation is valid even when losses are large, provided that r_1/r_0 is sufficiently small for the perturbation to be valid.

(3.3.3) The Attenuation Coefficient of a Filled Waveguide.

The attenuation coefficient of a waveguide filled with a loss dielectric is given exactly by

$$\alpha = \frac{\sqrt{2\pi}}{\lambda_0}\left(\left[\left(\frac{\lambda_0}{\lambda_c}\right)^2 + \bar{\epsilon}''\bar{\mu}'' - \bar{\epsilon}'\bar{\mu}'\right] + \left\{\left[\left(\frac{\lambda_0}{\lambda_c}\right)^2 + \bar{\epsilon}''\bar{\mu}'' - \bar{\epsilon}'\bar{\mu}'\right]^2 + (\bar{\epsilon}''\bar{\mu}' + \bar{\mu}''\bar{\epsilon}')^2\right\}^{1/2}\right)^{1/2} \quad . \quad . \quad . \quad . \quad (30)$$

(3.3.4) Perturbation Expression for Attenuation Coefficient.

If the perturbation expression for $P_i + P_0$ [eqn. (23)] is substituted into eqn. (24), the following expression for the attenuation coefficient is obtained:

$$\alpha = \bar{r}_1 \frac{d\bar{\beta}}{dr_1}\frac{2\pi}{\lambda_0}\frac{\bar{\mu}''\left[(\bar{\epsilon}+\bar{\Lambda}^2\bar{\beta}^2)T_1 + 2\bar{\Lambda}\bar{\epsilon}\bar{\beta} + \left(\frac{\lambda_0}{2\pi}\right)^2\bar{\Lambda}^2K^4T_5\right] + \bar{\epsilon}''\left\{[\bar{\beta}^2+(\bar{\Lambda}\bar{\mu})^2]T_1 + 2\bar{\Lambda}\bar{\mu}\bar{\beta} + \left(\frac{\lambda_0}{2\pi}\right)^2K^4T_5\right\}}{(\bar{\epsilon}-\bar{\epsilon}_1)\left\{\left(\frac{2\pi r_1}{\lambda_0}\right)^2(\bar{\epsilon}\bar{\mu}-\bar{\beta}^2)^2 + [\bar{\beta}+\bar{\mu}\bar{\Lambda}\mathrm{F}(Kr_1)]^2 + \frac{\epsilon}{\epsilon_1}[\bar{\beta}\mathrm{F}(Kr_1)+\bar{\mu}\bar{\Lambda}]^2\right\}} \quad (31)$$
$$+ (\bar{\mu}-\bar{\mu}_1)\left\{\bar{\Lambda}^2\left(\frac{2\pi r_1}{\lambda_0}\right)^2(\bar{\epsilon}\bar{\mu}-\bar{\beta}^2)^2 + [\bar{\beta}\bar{\Lambda}+\bar{\epsilon}\mathrm{F}(Kr_1)]^2 + \frac{\mu}{\mu_1}[\bar{\epsilon}+\bar{\beta}\bar{\Lambda}\mathrm{F}(Kr_1)]^2\right\}$$

This equation has been used to determine the attenuation coefficient of a waveguide containing a dielectric rod, the parameters being $\bar{\mu} = 1{\cdot}6$, $\bar{\epsilon} = 11{\cdot}4$ and $2r_0/\lambda_0 = 0{\cdot}685$. The corresponding waveguide diameter is 0·875 in at a frequency of 9·25 Gc/s; incidentally, the material parameters are those of a saturated nickel-zinc ferrite in a negatively circularly polarized field. The extent to which the field in a ferrite rod is in fact circularly polarized has been discussed elsewhere.[7] However, anticipating that the approximation is quite good, particularly for rods of small diameter, the following remarks have a wider implication than just for unmagnetized ferrite or dielectric rods.

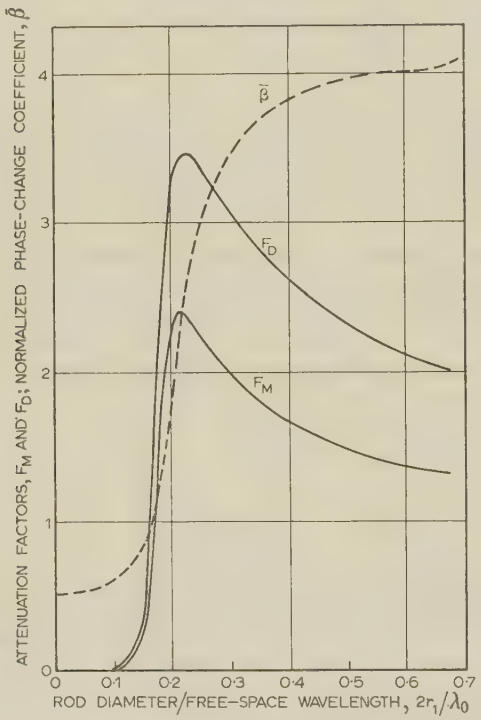

Fig. 4A.—Attenuation factors F_M and F_D and normalized phase-change coefficient, $\bar{\beta}$, as a function of $2r_1/\lambda_0$.
Scale for F_D multiplied by a factor of 10.

Fig. 4A shows the attenuation factors F_M and F_D for magnetic and dielectric loss respectively, in the above case, together with the phase-change coefficient $\bar{\beta}$, assuming zero loss; because of the choice of parameters the magnetic-loss term in eqn. (31) predominates. The actual attenuation coefficient, α, is given by

$$\alpha = \frac{2\pi}{\lambda_0}(\bar{\mu}''F_M + \epsilon''F_D)8{\cdot}686 \text{ decibels per unit length} \quad (32)$$

For comparison, curves of $\bar{\beta}$ and F_M obtained from the thin-rod formulae are shown in Fig. 4B. It can be seen that the range of values of r_1/r_0 for which the thin-rod perturbation is valid is much less for the attenuation coefficient than for the phase-change coefficient. This result follows from the neglect of the

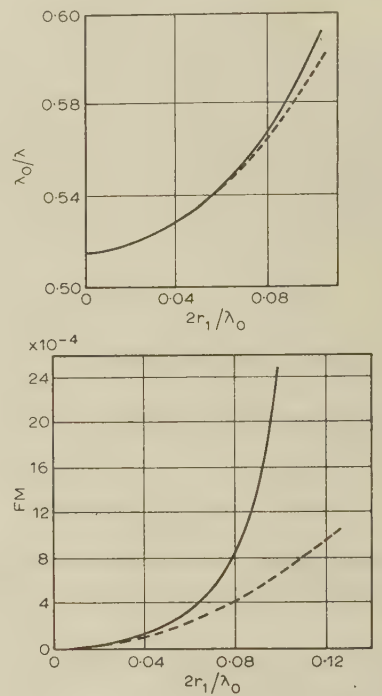

Fig. 4B.—$\bar{\beta}$ and attenuation factor F_M for H_{11}-limit mode as a function of $2r_1/\lambda_0$.
—— 'Exact' results.
---- Thin-rod perturbation results.
Parameters as in Fig. 4A.

guiding influence of the rod, when determining the internal r.
fields, which are substituted into the perturbation expressio
For small rod diameter this predominantly affects the attenuatio

(4) CONCLUSIONS

The mode spectrum of a circular waveguide containing dielectric rod has been established by means of approximat and exact graphical methods. Correlation between the propa gation coefficients and power distribution for unbounded an bounded rods is theoretically predicted. In the case of th phase-change coefficients, the correlation enables an unam biguous classification of the modes of an unbounded rod to b established. Exact and perturbation expressions for the tota transmitted power, power distribution and attenuation coeff cients are derived. Normalized attenuation coefficients ar calculated for the H_{11}-limit mode.

Although the numerical results provided here and in Part of the paper have resolved a number of general questio regarding the propagation behaviour of unbounded and bounde rods, it is felt that further computations would be well justifie As examples, the difference between the curves of attenuatio coefficient for unbounded and bounded rods warrants mor attention, as does the detailed behaviour of the phase-chang coefficients near $r_1/r_0 = 1$.

Finally, the application of the above results to problems involving ferrites is again worthy of mention. In an earlier paper[7] the author used the phase-change coefficient curve shown in Fig. 4A as the first stage in a perturbation calculation of the curve for a magnetically saturated ferrite rod. A comparison between this latter curve and one obtained from experimental results showed very satisfactory agreement. It was remarked in Part 1 that in the general analysis of Faraday-rotation devices it is often adequate to base approximate calculations on results obtained for rods with isotropic permeability [$\mu - n\kappa$]. Thus results such as those shown in Figs. 1, 2 and 4 can be applied in a study of ferrite devices. Approximate propagation curves derived using the method of Section 2 were given in Part 1 for a wide range of values of $\bar{\mu}\bar{\epsilon}$. These curves enable the variation in phase-change coefficient with permeability to be predicted. Since a change in the static field applied to a ferrite causes a change in the permeability, the corresponding change in phase-change coefficient can be approximately determined for a particular ferrite structure. These methods have been used by the author to explain successfully the experimentally observed behaviour of a circular waveguide containing nickel-zinc and magnesium-manganese ferrite rods.[1,9] In particular, a semi-quantitative explanation of the effects of multiple reflections and mode interference on the transmission coefficient have been provided.

The problem of determining the reflection from a ferrite rod of arbitrary diameter contained in a circular waveguide presents considerable theoretical difficulties. Although the analogous problem for a dielectric rod is quite complicated, it is more amenable to approximate methods of solution. The results of the present paper enable such methods to be explored.

(5) ACKNOWLEDGMENTS

The author would like to thank Dr. J. Brown, Dr. I. G. MacBean and Mr. M. Gumbrell for their helpful comments during the course of this work.

(6) REFERENCES

(1) SUHL, H., and WALKER, L. R.: 'Topics in Guided Wave Propagation through Gyromagnetic Media, Part III', *Bell System Technical Journal*, 1954, **33**, p. 1133.

(2) BEAM, R. E., and WACHOWSKI, H. M.: 'Shielded Dielectric Rod Waveguides', *Transactions of the American I.E.E.*, 1951, **70**, p. 874.

(3) WILLIAMS, R. R.: Discussion on Microwave Apparatus at the Convention on Ferrites, *Proceedings I.E.E.*, 1957, **104** B, Supp. 6, p. 395.

(4) TOMPKINS, J. E.: 'Energy Distribution and Field Configuration in Ferrites', Paper presented at Brussels Conference on Solid-State Physics in Electronics and Telecommunications, 1958 (to be published).

(5) WALDRON, R. A.: 'Electromagnetic Wave Propagation in Cylindrical Waveguides containing Gyromagnetic Media', *Journal of the British Institution of Radio Engineers*, 1958, **18**, pp. 597, 677 and 733.

(6) KARBOWIAK, A. E.: 'Waveguide Characteristics', *Electronic and Radio Engineer*, 1957, **34**, p. 379.

(7) CLARRICOATS, P. J. B.: 'A Perturbation Method for Circular Waveguides Containing Ferrites', *Proceedings I.E.E.*, Paper No. 2796 E, May, 1959 (**106** B, p. 335).

(8) CLARRICOATS, P. J. B.: 'The Gain of Travelling-Wave Ferromagnetic Amplifiers', *ibid.*, Monograph No. 334 E, May, 1959 (**106** C, p. 165).

(7) APPENDICES

(7.1) Perturbation Expression for the Change in Propagation Coefficient

Suhl and Walker[1] and the author[8] have shown that the change in the propagation coefficient, $\delta\gamma = \alpha + j\delta\beta$, caused by the introduction into a waveguide of a rod with permeability μ and permittivity ϵ is given by

$$\delta\gamma = \frac{j\omega}{2\int_{S_0} \boldsymbol{E}_{t\,nm} \times \boldsymbol{H}_{t\,nm}.d\boldsymbol{S}} \left\{ \int_{S_1} [(\mu - \mu_0)\boldsymbol{H}.\boldsymbol{H}^*_{nm} + (\epsilon - \epsilon_0)\boldsymbol{E}.\boldsymbol{E}^*_{nm}] dS \right\} \quad (33)$$

Where H and E are the perturbed fields and H_{nm} and E_{nm} the unperturbed fields. S_1 and S_0 are the cross-section surfaces of the rod and waveguide respectively.

(7.2) The Slope of the Propagation Curve at Cut-off

The characteristic equation for a waveguide containing a dielectric rod [eqn. (2)] can be written

$$\bar{\beta}^2 f_1^2 = f_2 f_3 \quad . \quad . \quad . \quad . \quad . \quad (34)$$

where

$$f_1 = [1/(Kr_1)^2 - 1/(K_1 r_1)^2],$$

$$f_2 = [\bar{\mu}F(Kr_1)/(Kr_1)^2 - \mu_1 R(K_1 r_1)/(K_1 r_1)^2]$$

and $f_3 = [\bar{\epsilon}F(Kr_1)/(Kr_1)^2 - \bar{\epsilon}_1 S(K_1 r_1)/(K_1 r_1)^2]$. On differentiating the above equation with respect to r_1 (maintaining λ_0 and r_0 constant),

$$\frac{d\bar{\beta}}{dr_1}(2f_1^4\bar{\beta}) = f_1^2\left(f_2\frac{d}{dr_1}f_3 + f_3\frac{d}{dr_1}f_2\right) - f_2 f_3\frac{df_1^2}{dr_1} \quad . \quad (35)$$

On expanding the differential terms in this equation,

$$\frac{d\bar{\beta}}{dr_1}\left(2f_1^4\bar{\beta} - f_1^2 f_2\frac{\partial f_3}{\partial\bar{\beta}} - f_1^2 f_3\frac{\partial f_2}{\partial\bar{\beta}} + f_2 f_3\frac{\partial f_1^2}{\partial\bar{\beta}}\right) = f_1^2\left(f_2\frac{\partial f_3}{\partial r_1} + f_3\frac{\partial f_2}{\partial r_1}\right) - f_2 f_3\frac{\partial f_1^2}{\partial r_1}$$

When $\bar{\beta} = 0$ it is simply demonstrated that $d\bar{\beta}/dr_1 = \infty$. Since either f_2 or f_3 is then zero, it is merely necessary to show, respectively, that either $\partial f_2/\partial\bar{\beta}$ or $\partial f_3/\partial\bar{\beta} = 0$ while either $\partial f_2/\partial r_1$ or $\partial f_3/\partial r_1$ remains finite. These conditions are readily proved.

(7.3) Transmitted Power Ratio P_i/P_0 for Dielectric Rod in Waveguide

The expression for P_i is the same as that given in Part 1, Appendix 7 only where β and Λ are determined from eqn. (2) and the equation

$$\bar{\Lambda}^2 = \frac{\left[\bar{\epsilon}_1\frac{S(K_1 r_1)}{(K_1 r_1)^2} - \bar{\epsilon}\frac{F(Kr_1)}{(Kr_1)^2}\right]}{\left[\bar{\mu}_1\frac{R(K_1 r_1)}{(K_1 r_1)^2} - \bar{\mu}\frac{F(Kr_1)}{(Kr_1)^2}\right]} \quad . \quad . \quad . \quad (36)$$

P_0 is then obtained from the field components:

$$E_r = -ja_1^i\frac{J_1(Kr_1)}{K_1^2}\left[\beta K_1\frac{D'(K_1 r)}{\sigma(K_1 r)} + \frac{\omega\mu_1\Lambda}{r}\frac{E(K_1 r)}{\rho(K_1 r)}\right]\varepsilon^{-j\theta} \quad (37)$$

$$E_\theta = -a_1^i\frac{J_1(Kr_1)}{K_1^2}\left[\frac{\beta}{r}\frac{D(K_1 r)}{\sigma(K_1 r)} + K_1\omega\mu_1\Lambda\frac{E'(K_1 r)}{\rho(K_1 r)}\right]\varepsilon^{-j\theta} \quad (38)$$

$$H_r = -ja_1^i \frac{J_1(Kr_1)}{K_1^2}\left[K_1\omega E_1 \frac{D'(K_1r_1)}{\sigma(K_1r_1)} + \frac{\Lambda\beta}{r}\frac{E(K_1r_1)}{\rho(K_1r_1)}\right]\varepsilon^{-j\theta} \quad (39)$$

$$H_\theta = a_1^i \frac{J_1(Kr_1)}{K_1^2}\left[\frac{\omega\epsilon_1}{r}\frac{D(K_1r_1)}{\sigma(K_1r_1)} + \beta\Lambda K_1 \frac{E'(K_1r_1)}{\rho(K_1r_1)}\right]\varepsilon^{-j\theta} \quad (40)$$

where $D(K_1r) = J_1(K_1r)Y_1(K_1r_0) - Y_1(K_1r)J_1(K_1r_0)$. (41)

$$E(K_1r) = J_1(K_1r)Y_1'(K_1r_0) - Y_1(K_1r)J_1'(K_1r_0) \quad . \quad (42)$$

On evaluation of the integral $\int_S (E_rH_\theta^* - E_\theta H_r^*)$ for the region outside the rod, P_0 is given by

$$P_0 = \pi(a_1^i)^2 \frac{J_1^2(Kr_1)}{K_1^4}[(\omega\epsilon_1\beta T_3 + \Lambda^2\omega\mu_1\beta T_4) + \Lambda(\omega^2\mu_1\epsilon_1 + \beta^2)] \quad (43)$$

where T_3 and T_4 are given in eqn. (18), in which the final expression for P_i/P_0 is stated.

(7.4) Behaviour of the Functions T_3 and T_4 when $\bar{\beta} > 1$ and $r_1/r_0 \neq 1$

When $\bar{\beta} > 1$, $K_1 = -jk_1$, where k_1 is real, and T_3 is given by

$$T_3 = \frac{-I_1(k_1r_0)K_1(k_1r_0) + \frac{1}{2}}{\bar{\sigma}^2(k_1r_1)} + \frac{K_1(k_1r_1)I_1(k_1r_0)S(k_1r_1)}{\bar{\sigma}(k_1r_1)} + \frac{k_1r_1K_1(k_1r_0)I_1'(k_1r_1)}{\bar{\sigma}(k_1r_1)} - \tfrac{1}{2}S^2(k_1r_1) + (k_1^2r_1^2 + 1) \quad . \quad (44)$$

where $\bar{\sigma}(k_1r_1) = [I_1(k_1r_1)K_1(k_1r_0) - K_1(k_1r_1)I_1(k_1r_0)]$

and $S(k_1r_1)$ is defined in eqn. (5). Since, when z is large,

$$I_1(z) \simeq \frac{\varepsilon^z}{(2\pi z)^{1/2}} \text{ and } K_1(z) \simeq \left(\frac{\pi}{2z}\right)^{1/2}\varepsilon^{-z}$$

the first and third terms in T_3 may be neglected, provided tha $k_1(r_0 - r_1)$ is large. Also, the second term reduces to $-S(k_1r_1$ Thus T_3 becomes

$$-[\tfrac{1}{2}S^2(k_1r_1) + S(k_1r_1) - \tfrac{1}{2}(k_1^2r_1^2 + 1)]$$

However, in Section 2.2.2 it was shown that, when $k_1(r_0r_1)$ i large, $S(k_1r_1) \simeq M(k_1r_1)$, whereby T_3 reduces to $-T_2$ as give in eqn. (12). (See also the List of Symbols.)
Similarly,

$$T_4 = -\frac{K_1'(k_1r_0)I_1'(k_1r_0) + \frac{1}{2}[(1 + 1/(k_1r_0)^2]}{\bar{\rho}^2(k_1r_1)} + \frac{K_1(k_1r_1)I_1'(k_1r_0)R(k_1r_1)}{\bar{\rho}(k_1r_1)} - \frac{k_1r_1I_1(k_1r_1)K_1'(k_1r_0)}{\bar{\rho}(k_1r_1)} - \tfrac{1}{2}R^2(k_1r_1) + \tfrac{1}{2}(k_1^2r_1^2 + 1) \quad (45)$$

where $\bar{\rho}(k_1r_1) = [K_1'(k_1r_0)I_1(k_1r_1) - I_1'(k_1r_0)K_1(k_1r_1)]$

This reduces in a similar manner as above to

$$-[\tfrac{1}{2}R^2(k_1r_1) + R(k_1r_1) - \tfrac{1}{2}(k_1^2r_1^2 + 1)]$$

Since $R(k_1r_1) \simeq M(k_1r_1)$ when $k_1(r_0 - r_1)$ is large, T_4 is als approximately equal to $-T_2$.

621.372.821:621.396.677

The Institution of Electrical Engineers
Monograph No. 411 E
Oct. 1960

THE LAUNCHING OF SURFACE WAVES BY A MAGNETIC LINE SOURCE

By Prof. C. M. ANGULO and Prof. W. S. C. CHANG.

(*The paper was first received* 10*th March, and in revised form* 30*th December*, 1958. *It was published as an* INSTITUTION MONOGRAPH *in October*, 1960.)

SUMMARY

The paper deals with the idealized problem of the excitation of surface waves along two infinite, identical, separate and parallel dielectric slabs by a magnetic line source (slot). The problem is reduced to a superposition of simpler ones, namely two parallel slabs with symmetrical excitation and two parallel slabs with antisymmetrical excitation.

The simplified problems are solved by the modal-analysis approach, and the synthesis of the modal components is carried out to obtain the far fields excited by the magnetic line.

Radiation pattern, total power of the surface waves, total radiation loss and the efficiency of launching the surface wave are derived and computed numerically for various thicknesses of the slabs, various air-gaps between the slabs and different positions of the magnetic line source. The theoretical results indicate that, for each thickness of the slabs, high efficiency is obtained with an optimum location of the source and an optimum air-gap. Moreover, the thicker the slabs, the higher is the maximum efficiency. The thickness of the slabs and the air-gap are ultimately limited by the requirement that only one surface wave should exist for the structure.

LIST OF SYMBOLS

α = Normalized thickness of slabs $= 2K_0d$.
β = Normalized separation (air-gap) between slabs $= 2K_0g$.
Γ = $+1$ for antisymmetrical excitation or -1 for symmetrical excitation.
$\delta(y)$ = Dirac delta function (or unit impulse function).
$\epsilon(y)$ = Relative permittivity.
ϵ_0 = Permittivity of vacuum $= 10^{-9}/36\pi$.
$\phi_{n(y)}$ = Eigen-function corresponding to the nth surface wave (discrete mode).
$\phi_{(\eta, y)}$ = Eigen-function corresponding to one of the continuous modes.
ϕ = Polar angle (Fig. 1).
ζ = Characteristic propagation coefficient of the transmission line in the z-direction.
η = Wave number of the continuous mode in the y-direction in air.
η' = Wave number of the continuous mode in the y-direction in the dielectric.
η_n = Wave number of the discrete mode in the y-direction in air.
η_n' = Wave number of the discrete mode in the y-direction in the dielectric.
μ_0 = Permeability of vacuum $= 4\pi \times 10^{-7}$.
σ = Launching efficiency of the surface wave.
d = Thickness of dielectric slabs.
$2g$ = Separation distance between two parallel slabs.
$H_{x(rad)}$ = Component in the x-direction of the radiated magnetic field (i.e. the surface wave excluded).
$I_{n(z)}$ = Amplitude of the modal current for the nth surface wave [eqn. (16)].
$I_{(\eta, z)}$ = Amplitude of the modal current for one mode of the continuous part of the spectrum [eqn. (1*b*)].
K_0 = Propagation wave number of a plane wave of angular frequency ω in free space in the direction of propagation $= \omega\sqrt{(\mu_0\epsilon_0)}$.
N_r = Normalization constant of nth surface wave [eqn. (4*d*)].
R = Radial co-ordinate (Fig. 1).
γ_n = Normalized wave number in y-direction, inside the dielectric, of the nth surface wave $= \eta_n'/K_0$.
P_n = Total power contained in the nth surface wave [eqn. (16)].
S_{rad} = Radiated power per unit angle [eqn. (13*a*)].
s_n = Normalized modulus of the wave number in y-direction in air for the nth surface wave $= -jn_n/K_0$.
$u(y)$ = Unit step function, zero for negative argument and 1 for positive argument.
$V_n(z)$ = Amplitude of the modal voltage for the nth surface wave [eqn. (1*a*)].
$V_{(\eta, z)}$ = Amplitude of the modal voltage for one mode of the continuous part of the spectrum [eqn. (1*a*)].
x, y, z = Cartesian co-ordinates.
y' = Distance from the magnetic line source to the outer surface of the slab (Figs. 1 and 2).
$Y = 1/Z$ = Characteristic admittance of the transmission line.

(1) INTRODUCTION

We will assume that the reader is familiar with surface waves. There has been a large number of papers written on the subject and reference should be made to Zucker's paper[1] for a complete bibliography. The recent development of high-speed aircraft has been the main reason for the interest in surface-wave antennae and the problem of excitation of the surface wave is of practical interest.

The excitation of a single slab by a magnetic line source has been previously carried out by the authors[2] and compared with Cullen's[3] results. The results obtained agree qualitatively with those of Cullen, but owing to the approximations in his paper, the agreement is quantitative for very thin dielectric slabs only. It was found that, for a thin dielectric slab, there is a position of the source outside the slab which yields maximum excitation efficiency of the surface wave. Recently, Friedmann and Williams[4] have considered the excitation of earthed layers of dielectric by a magnetic line source above the dielectrics. They carry out the analysis by the Wiener–Hopf method and their results also agree with those previously reported by Cullen.

In this paper we discuss the excitation of surface waves in a structure made of two dielectric slabs with an air-gap by means of a magnetic line source inside or outside the dielectrics (Fig. 1). This is the idealized problem of the excitation by a slot. It is also the 2-dimensional Green's function for such a structure, and therefore the results can be used in the analysis of other types of 2-dimensional excitation such as excitation by a parallel-plate waveguide.

Correspondence on Monographs is invited for consideration with a view to publication.
Prof. Angulo is, and Prof. Chang was formerly, at Brown University, Rhode Island. Prof. Chang is now Professor of Electrical Engineering, Ohio State University.

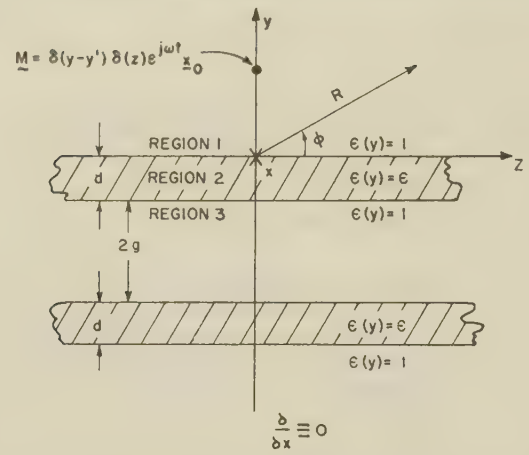

Fig. 1.—Two infinite dielectric slabs excited by a magnetic line source.

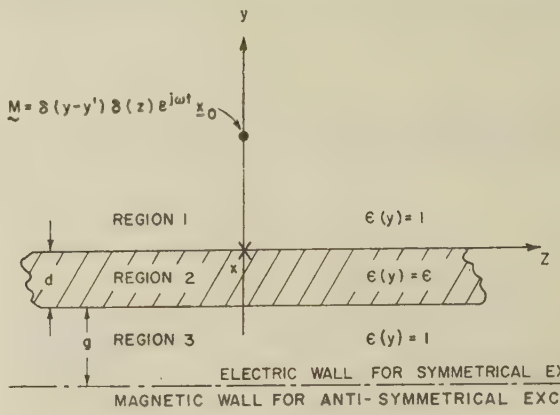

Fig. 2.—The half-structure.

The excitation of a single dielectric slab[2] is a special case where the two slabs lie next to each other.

It is evident from Fig. 1 that in our problem $H_y = H_z = E_x = 0$. Furthermore, the linearity of Maxwell's equations and the symmetry of the two slabs suggest that the excitation by a single magnetic line source may be considered as a superposition of the two following types of excitation:

(*a*) Symmetrical excitation by two identical magnetic lines. In this case H_x is symmetrical with respect to the plane $y = -(g + d)$, and $E_z = 0$ at $y = -(g + d)$. Hence the fields will not be disturbed by the insertion of an electric wall at $y = -(g + d)$. The reflection coefficient at $y = -(g + d)$ looking toward $y = -\infty$ is $\Gamma = -1$.

(*b*) Antisymmetrical excitation by two magnetic lines 180° out of phase. In this case H_x is antisymmetrical with respect to the plane $y = -(g + d)$ and the fields will not be disturbed by the insertion of a magnetic wall at $y = -(g + d)$. The reflection coefficient at $y = -(g + d)$ looking toward $y = -\infty$ is $\Gamma = +1$.

In either type of excitation the fields for $y < -(g + d)$ can be deduced immediately from the fields for $y > -(g + d)$. Therefore only half-space structures with an electric or magnetic wall placed at $y = -(g + d)$ will be considered. All derivations will be carried out simultaneously for the symmetrical ($\Gamma = -1$) and antisymmetrical excitation ($\Gamma = +1$). The total fields excited by a single magnetic line source are obtained by superposition. It should be noted here that the case of symmetrical excitation is of particular interest by itself since it is the problem of a magnetic line source exciting a slab suspended above a conductor.

(2) REPRESENTATION OF THE FIELDS TAKING *Oz* AS THE DIRECTION OF PROPAGATION

The problem of an infinite dielectric slab suspended above an electric or magnetic wall (the half-space structure) can naturally be regarded as a parallel-plate waveguide of infinite cross-section (Fig. 2). It can be analyzed either as a parallel-plate waveguide partially filled with dielectric, which has *Oz* as its direction of propagation, or as three homogeneous parallel-plate waveguides in cascade with *Oy* as their direction of propagation. In either case, Maxwell's equations are reduced to a differential equation with the appropriate boundary conditions characteristic of the cross-section and a transmission line with sources for the modal amplitudes. The fields are given by the synthesis of all their modal components.

The first approach (regarding *Oz* as the direction of propagation) has the advantage that the surface waves appear explicitly from the beginning as the discrete part of the characteristic mode spectrum. The orthogonality properties of the surface waves and the radiated waves (the continuous part of the spectrum) further enables us to compute the total surface-wave power and radiation loss separately. This is the approach that we will follow throughout this part of the paper.

We consider, therefore, the half-space structure as a parallel-plate waveguide of infinite cross-section (z = constant) with an electric wall removed to $y = +\infty$ and an electric or magnetic wall at $y = -(g + d)$. The guide is partially filled with dielectric slab from $y = -d$ to $y = 0$.

The fields transverse to the z-axis can be represented as a superposition of all the characteristic modes of the parallel-plate open waveguide:

$$-E_y(y, z) = \sum_1^N V_n(z)\frac{\phi_n(y)}{\epsilon(y)} + \int_{-\infty}^{+\infty} V(\eta, z)\frac{\phi(\eta, y)}{\epsilon(y)}d\eta \quad . \quad (1a)$$

$$H_x(y, z) = \sum_1^N I_n(z)\phi_n(y) + \int_{-\infty}^{+\infty} I(\eta, z)\phi(\eta, y)d\eta \quad . \quad (1b)$$

where $\phi_n(y)$ are modes of the discrete mode spectrum (surface waves) and $\phi(\eta, y)$ are modes of the continuous part of the mode spectrum. The propagation of E_y and H_x can be regarded as the sum of all these modes propagating in the z-direction along their individual transmission lines with characteristic impedance Z formed by the open parallel-plate waveguide.

This representation is discussed in some detail in References 4 and 5 and we will not elaborate here on the interpretation of eqns. (1).

Maxwell's equations are satisfied if the modal amplitudes V and I of each of the discrete and continuous modes satisfy the inhomogeneous transmission-line equations

$$\frac{dV}{dz} + jZ\zeta I = -\delta(z)\phi(y') \quad . \quad . \quad . \quad . \quad (2a)$$

and

$$\frac{dI}{dz} + jY\zeta V = 0 \quad . \quad . \quad . \quad . \quad . \quad (2b)$$

with the boundary condition that there is no incoming wave from $z = \pm\infty$. On the other hand, each characteristic mode must also satisfy the characteristic equation

$$\left[\frac{d}{dy}\frac{1}{\epsilon(y)}\frac{d}{dy} + \frac{\eta(y)}{\epsilon(y)}\right]\phi(y) = 0 \quad . \quad . \quad . \quad (2c)$$

with the boundary conditions that

$$(1 - \Gamma)\frac{d\phi}{dy} + (1 + \Gamma)\phi = 0 \quad \text{at} \quad y = -(d + g) \quad . \quad (2d)$$

ϕ and $\frac{1}{\epsilon(y)}\frac{d\phi}{dy}$ are continuous at $y = 0$ and $y = -d$. (2e)

In addition, the proper modes or discrete part of the mode spectrum will also satisfy the following boundary conditions plus the radiation condition:

$$\frac{d\phi}{dy} = \phi = 0 \text{ at } y = \infty \quad . \quad . \quad . \quad . \quad (2f)$$

In eqns. (2), ζ obviously has the meaning of the propagation coefficient of the individual transmission lines in the z-direction, Y and Z are the characteristic admittance and impedance of the transmission line associated with the mode ϕ, and ϵ is the relative permittivity:

$$\epsilon(y) = \begin{cases} \epsilon & \text{for } 0 > y > -d \\ 1 & \text{for } y > 0 \text{ or } -d > y > -(g+d) \end{cases} \quad . \quad (3a)$$

$\eta(y)$, Z, Y, and ζ are related to each other by the following equations:

For any mode of the discrete mode spectrum.	For any mode of the continuous mode spectrum.
$V = V_n(z)$	$V = V(\eta, z)$ . . . . (3b)
$I = I_n(z)$	$I = I(\eta, z)$ . . . . (3c)
$\zeta = \zeta_n = \sqrt{[K_0^2\epsilon(y) - \eta_n^2(y)]}$	$\zeta = \sqrt{[K_0^2\epsilon(y) - \eta^2(y)]}$. (3d)
$\eta_n(y) = \begin{cases} \eta_n' & 0 > y > -d \\ \eta_n & y > 0, \\ & -d > y > -(g+d) \end{cases}$	$(y) = \begin{cases} \eta' & 0 > y > -d \\ \eta & y > 0, \\ & -d > y > -(g+d) \end{cases}$ . . . . (3e)
$Y = \frac{1}{Z} = \frac{K_0 Y_0}{\zeta_n}$	$Y = \frac{1}{Z} = \frac{K_0 Y_0}{\zeta}$ . . . (3f)
$\phi(y') = \phi_n(y')$	$\phi(y') = \phi(\eta, y')$ . . (3g)

$Y_0 = \sqrt{(\epsilon_0/\mu_0)}$ is the intrinsic admittance of free space and $K_0 = \omega\sqrt{(\epsilon_0\mu_0)}$ is the free-space wave-number. Therefore η_n' and η' are the wave numbers of the mode ϕ in the y-direction in the dielectric, while η_n and η are the wave numbers of the mode ϕ in the y-direction in air. η_n, η_n', ζ_n, η, η' and ζ are the characteristic values (or eigen-values) determined by eqns. (2c), (2d), (2e) and (2f).

The orthogonality and normalization properties of the mode spectrum are specified by the completeness relation

$$\epsilon(y')\delta(y - y') = \sum_1^N \phi_n(y)\phi_n(y') + \int_{-\infty}^{+\infty} \phi(\eta, y)\phi(\eta, y')d\eta \quad . \quad (3h)$$

The solution of the characteristic mode equation (2c) is carried out by the characteristic Green's function method. The reader is referred to Marcuvitz[6] for a discussion of the method and to Angulo and Chang[7] for details of the application to the present problem; only the results are given here.

The modes of the discrete spectrum (the surface waves) are given by

$$\phi_n(y) = \phi_n^{(1)}(y) = \frac{\varepsilon^{-s_n K_0 y}}{N_n} \quad . \quad . \quad . \quad . \quad (4a)$$

for region 1 in Fig. 2;

$$\phi_n(y) = \phi_n^{(2)}(y) = \frac{\cos\gamma_n K_0 y - \frac{\epsilon s_n}{\gamma_n}\sin\gamma_n K_0 y}{N_n} \quad . \quad (4b)$$

for region 2; and

$$\phi_n(y) = \phi_n^{(3)}(y) = \frac{\frac{1-\Gamma\varepsilon^{-\beta s_n}}{1+\Gamma\varepsilon^{-\beta s_n}}\cosh[K_0 s_n(y+d)] + \sinh[K_0 s_n(y+d)]}{\left(\frac{1-\Gamma\varepsilon^{-\beta s_n}}{1+\Gamma\varepsilon^{-\beta s_n}} + \frac{\epsilon^{s_n}}{\gamma_n}\tan\frac{\alpha\gamma_n}{2}\right)N_n\cos\frac{\alpha\gamma_n}{2}} \quad . \quad . \quad . \quad . \quad (4c)$$

for region 3.

In the above expressions, $\alpha = 2K_0 d$ is the normalized thickness of the slabs, $\beta = 2K_0 g$ is the normalized separation distance between the slabs, $\gamma_n = \eta_n'/K_0$ is the propagation wave-number in the y-direction inside the dielectric for mode η, normalized with respect to the free-space wave-number of the excitation, $s_n = -j\eta_n/K_0$ is the normalized modulus of the wave-number of mode η in the y-direction in air, and N_n is a normalization constant.

$$N_n^2 = \frac{1}{2K_0}\left[\frac{\frac{\epsilon-1}{\epsilon\gamma_n s_n^2}\tan\left(\frac{\alpha\gamma_n}{2}\right)\left(\frac{1-\Gamma\varepsilon^{-\beta s_n}}{1+\Gamma\varepsilon^{-\beta s_n}} + \frac{\epsilon^2 s_n^2}{\gamma_n^2}\right)}{\frac{1-\Gamma\varepsilon^{-\beta s_n}}{1+\Gamma\varepsilon^{-\beta s_n}} + \frac{\epsilon s_n}{\gamma_n}\tan\frac{\alpha\gamma_n}{2}} + \frac{\frac{\alpha}{2\epsilon}\sec^2\left(\frac{\alpha\gamma_n}{2}\right)\left(\frac{1-\Gamma\varepsilon^{-\beta s_n}}{1+\Gamma\varepsilon^{-\beta s_n}} - \frac{\epsilon^2 s_n^2}{\gamma_n^2}\right) - \frac{2\beta\Gamma\varepsilon^{-\beta s_n}}{(1+\Gamma\varepsilon^{-\beta s_n})^2}\left(\frac{\gamma_n}{\epsilon s_n}\tan\frac{\alpha\gamma_n}{2} - 1\right)}{\frac{1-\Gamma\varepsilon^{-\beta s_n}}{1+\Gamma\varepsilon^{-\beta s_n}} + \frac{\epsilon s_n}{\gamma_n}\tan\frac{\alpha\gamma_n}{2}}\right] \quad . \quad . \quad . \quad (4d)$$

In eqns. (4) we have chosen to designate by $\phi_n^{(1)}(y)$, $\phi_n^{(2)}(y)$, $\phi_n^{(3)}(y)$ the analytical expressions of $\phi_n(y)$ for the respective regions of the space. This notation will simplify the results given below.

The values of γ_n and s_n are the solutions of the resonance in the y-direction and they are obtained from

$$1 + \frac{1-\Gamma\varepsilon^{-\beta s_n}}{1+\Gamma\varepsilon^{-\beta s_n}} = \left(\frac{\gamma_n}{\epsilon s_n}\frac{1-\Gamma\varepsilon^{-\beta s_n}}{1+\Gamma\varepsilon^{-\beta s_n}} - \frac{\epsilon s_n}{\gamma_n}\right)\tan\frac{\alpha\gamma_n}{2} \quad . \quad (5a)$$

$$\gamma_n^2 + s_n^2 = \epsilon - 1 \quad . \quad . \quad . \quad . \quad . \quad (5b)$$

The value of the normalization constant is derived in Reference 7, p. 17.

For $0 < \alpha < 2\pi/\sqrt{(\epsilon-1)}$ there is one and only one symmetrical mode in the discrete part of the mode spectrum ($\Gamma = -1$). This mode always exists, no matter how small is the product of the angular frequency, ω, and the thickness of the slab, d. This is the lowest mode. For $\Gamma = +1$ the antisymmetrical discrete part of the mode spectrum exists only for $\alpha > \frac{2}{\sqrt{(\epsilon-1)}}\arctan\frac{2\epsilon}{\beta\sqrt{(\epsilon-1)}}$. There is one and only one antisymmetrical mode if

$$\frac{2}{\sqrt{(\epsilon-1)}}\arctan\frac{2\epsilon}{\beta\sqrt{(\epsilon-1)}} < \alpha < \frac{2}{\sqrt{(\epsilon-1)}}\left[\arctan\frac{2\epsilon}{\beta\sqrt{(\epsilon-1)}} + \pi\right]$$

In most practical cases the frequency and the dimensions of the structure will be chosen in such a way that only one symmetrical and antisymmetrical surface wave can exist. This is our assumption throughout the paper, and numerical computations have been carried out only for the lowest symmetrical and antisymmetrical surface waves for $\epsilon = 2{\cdot}49$. Fig. 3(a) shows the normalized wave-numbers for the lowest symmetrical surface wave ($\Gamma = -1$), and Fig. 3(b) shows the normalized wave-numbers for the lowest antisymmetrical surface wave. We

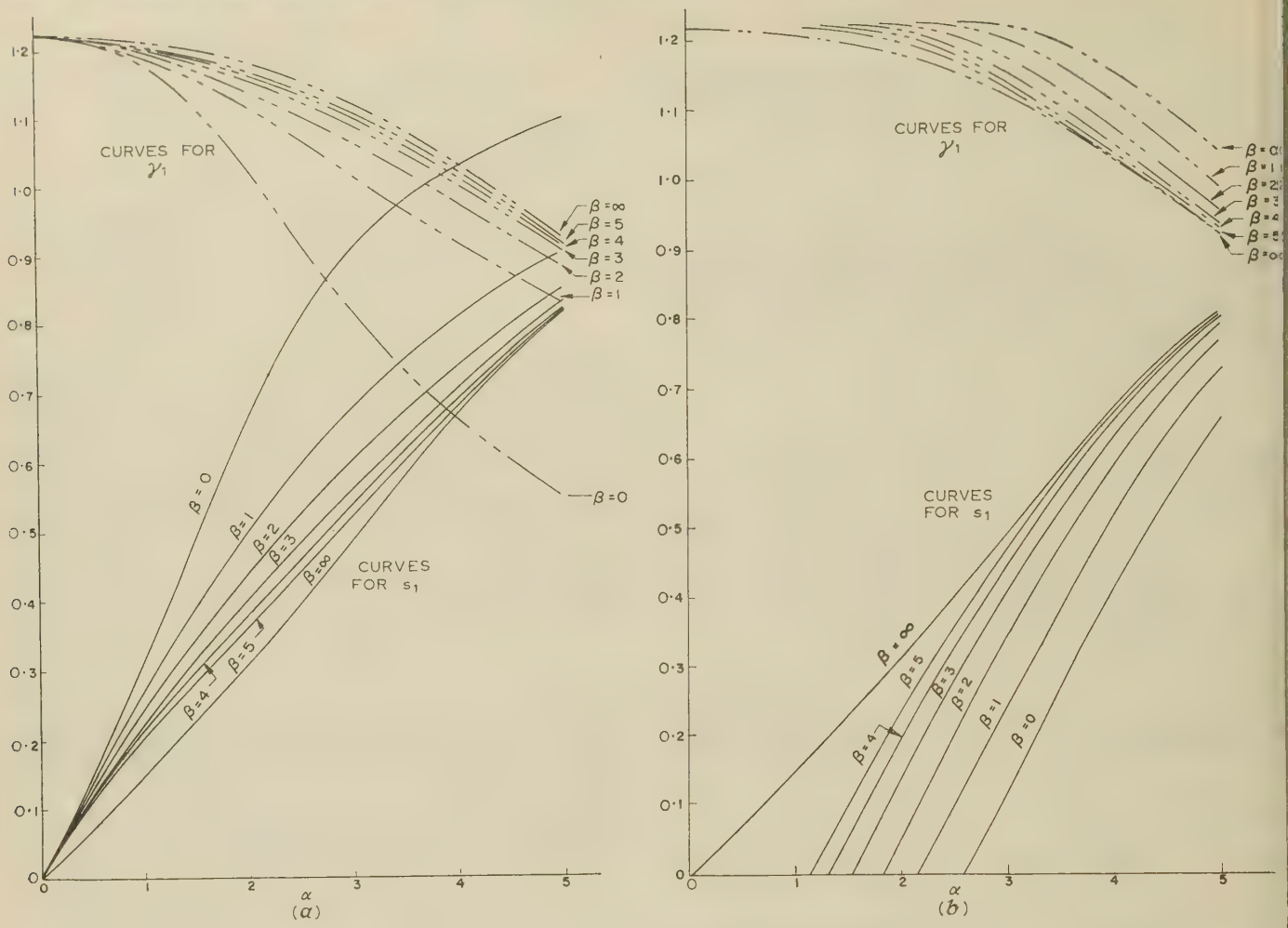

Fig. 3.—Variation of γ_1 and s_1 with α, for $\epsilon = 2{\cdot}49$.

(*a*) Symmetrical surface wave ($\Gamma = -1$).
(*b*) Antisymmetrical surface wave ($\Gamma = +1$).

notice in Fig. 3(*a*) that, as the slab is moved away from the electric wall, s_1 decreases, i.e. the surface wave has more and more power contained in the air outside the slab. On the contrary, the wave numbers for the antisymmetrical surface wave show that, as the slab is moved away from the magnetic wall, s_1 increases and the antisymmetrical surface wave would have a larger proportion of the power concentrated in the slab. In the limit, as $\beta \to \infty$, the symmetrical and antisymmetrical wave-numbers coincide with each other. They are the wave numbers of a single isolated slab of thickness α. For any finite air-gap ($g \neq \infty$) the antisymmetrical surface wave would have a value of s_1 smaller (larger phase velocity) than that of a single isolated slab, while the symmetrical surface wave would have a value of s_1 larger (smaller phase velocity) than that of the isolated slab. This also means that the symmetrical waves are bound more closely to the slabs.

It is clear from Fig. 3(*a*) that we have two ways of modulating the phase velocity along an earthed dielectric slab; one is by varying the thickness of the slab, and the other, by separating the slab from the earth.

The expressions for the continuous part of the mode spectrum are as follows:

$$\phi(\eta, y) = \phi^{(1)}(\eta, y) = \frac{\cos \eta y - jA \sin \eta y}{[\pi(1 + A)]^{1/2}} \quad . \quad . \quad (6a)$$

for $y > 0$

$$\phi(\eta, y) = \phi^{(2)}(\eta, y) = \frac{\cos \eta' y - j\frac{\epsilon\eta}{\eta'} A \sin \eta' y}{[\pi(1 + A)]^{1/2}} \quad . \quad (6b)$$

for $0 > y > -d$

and $\phi(\eta, y) = \phi^{(3)}(\eta, y) =$

$$\frac{\frac{1 - \Gamma\varepsilon^{2j\eta g}}{1 + \Gamma\varepsilon^{2j\eta g}} \cos \eta(y + d) - j \sin \eta(y + d)}{\left(\frac{1 - \Gamma\varepsilon^{2j\eta g}}{1 + \Gamma\varepsilon^{2j\eta g}} - j\epsilon\frac{\eta}{\eta'} \tan \eta' d\right) \cos \eta' d[\pi(1 + A)]^{1/2}} \quad . \quad (6c)$$

for $-d > y > -(g + d)$

where

$$A = \frac{1 - j\frac{\eta'}{\epsilon\eta} \frac{1 - \Gamma\varepsilon^{2j\eta g}}{1 + \Gamma\varepsilon^{2j\eta g}} \tan \eta' d}{\frac{1 - \Gamma\varepsilon^{2j\eta g}}{1 + \Gamma\varepsilon^{2j\eta g}} - j\epsilon\frac{\eta}{\eta'} \tan \eta' d} \quad . \quad . \quad . \quad (6d)$$

and

$$\eta' = [K_0^2(\epsilon - 1) + \eta^2]^{1/2} \quad . \quad . \quad . \quad . \quad (6e)$$

In eqns. (6) we call $\phi^{(1)}(\eta, y)$, $\theta^{(2)}(\eta, y)$ and $\phi^{(3)}(\eta, y)$ th analytical expressions that $\phi(\eta, y)$ takes in the different regio of space.

The solution of the transmission-line equations (3) is quite obvious:

$$\left.\begin{aligned} V &= \mp \frac{\phi(y')}{2} \exp(-j\zeta|z|) \\ I &= -Y\frac{\phi(y')}{2} \exp(-j\zeta|z|) \end{aligned}\right\} \quad . \quad . \quad . \quad . \quad (7)$$

or $z \gtrless 0$.

The fields can be obtained immediately in integral form by the proper substitutions. Since the structure considered is obviously symmetrical with respect to the plane $z = 0$, we will only give the fields for $z > 0$. They are

$$E_y(y, z) = \sum_{n=1}^{N} \frac{\phi_n(y')\phi_n(y)}{2\epsilon(y)} \exp(-j\zeta_n z) + \int_{-\infty}^{+\infty} \frac{\phi(\eta, y')\phi(\eta, y)}{2\epsilon(y)} \exp[-j\sqrt{(K_0^2 - \eta^2)}z]d\eta \quad . \quad (8a)$$

$$H_x(y, z) = -\sum_{n=1}^{N} \frac{Y_n\phi_n(y')\phi_n(y)}{2} \exp(-j\zeta_n z) - \int_{-\infty}^{+\infty} Y(\eta)\frac{\phi(\eta, y')\phi(\eta, y)}{2} \exp[-j\sqrt{(K_0^2 - \eta^2)}z]d\eta \quad . \quad (8b)$$

We will evaluate these expressions in Section 3.

The alternative approach, which considers the half-space structure as three homogeneous parallel-plate waveguides of infinite cross-section (y = constant) having walls at $z = \pm\infty$ connected in cascade, is carried out in Reference 7. This method yields asymptotic expressions for E_y and H_x identical with those given by eqns. (8).

(3) THE FAR ZONE FIELDS

The fields are obtained by substituting eqns. (4) and (6) into eqns. (8). We do not have to integrate eqns. (8*a*) and (8*b*) separately since the knowledge of H_x yields the electric field components. Therefore we will discuss only the synthesis of the magnetic field.

Let us first calculate the magnetic field at a point above the slab. In that case the analytical expressions for $\phi_n(y)$ and $\phi(\eta, y)$ in eqn. (8*b*) are the functions $\phi_n^{(1)}(y)$ and $\phi^{(1)}(\eta, y)$ given in eqns. (4*a*) and (6*a*) respectively. The admittances are defined in eqn. (3*f*). Eqn. (8*b*) becomes

$$H_x(y, z) = -\frac{Y_0}{2}\sum_{n=1}^{N} \frac{\phi_n^{(1)}(y)\phi_n(y')}{\sqrt{(1 + s_n^2)}} \exp[-j|z|K_0\sqrt{(1 + s_n^2)}] - \frac{Y_0}{2}\int_{-\infty}^{+\infty} \frac{K_0}{\sqrt{(K_0^2 - \eta^2)}}\phi^{(1)}(\eta, y)\phi(\eta, y') \exp[-j|z|\sqrt{(K_0^2 - \eta^2)}] \quad . \quad (9)$$

for $y > 0$.

The analytical expressions for $\phi(\eta, y')$ and $\phi_n(y')$ will depend on the position of the source. We must write $\phi^{(1)}(\eta, y')$ and $\phi_n^{(1)}(y')$ if $y' > 0$; $\phi^{(2)}(\eta, y')$ and $\phi_n^{(2)}(y')$ if $0 > y' > -d$ and $\phi^{(3)}(\eta, y')$ and $\phi_n^{(3)}(y')$ if $-d > y' > -(g + d)$. Therefore we must perform three different integrations in the η-plane.

All three integrals have branch points at $\eta = \pm K_0$ and poles at the positive imaginary axis of the η-plane corresponding to the surface waves. The path of integration is chosen around the branch points in such a way that $\mathcal{I}\sqrt{(K_0^2 - \eta^2)} < 0$ to suit the physical conditions. The poles, branch cuts and paths of integration are indicated in Fig. 4.

The integrals of eqn. (9) are obtained by the method of steepest descents after a customary change of variables from ζ and η to

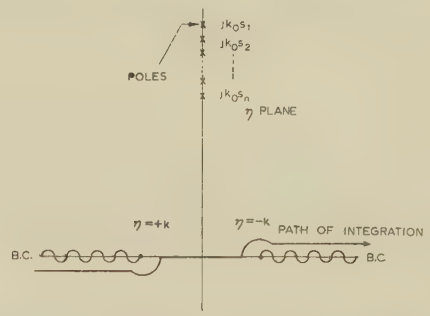

Fig. 4.—Path of integration for synthesis of the fields.

K and θ, together with a change from Cartesian co-ordinates to the polar co-ordinates shown in Fig. 1, as follows:

$$\left.\begin{aligned} \zeta &= K_0\cos\theta \quad y = R\sin\phi \\ \eta &= K_0\sin\theta \quad z = R\cos\phi \end{aligned}\right\} \quad . \quad . \quad . \quad (10)$$

The algebraic manipulations are omitted here. The final first approximation for the far field (first term of the asymptotic series) is

$$H_x = -\frac{Y_0}{2}\sum_{n=1}^{N} \frac{\phi_n^{(1)}(y)\phi_n^{(1)}(y')}{\sqrt{(1 + s_n^2)}} \exp[-jK_0|z|\sqrt{(1 + s_n^2)}] \, u\left[\frac{s_n}{1 + \sqrt{(1 + s_n^2)}} - \tan\frac{\phi}{2}\right] - \frac{\omega\epsilon_0(1 - j)}{2\sqrt{(\pi K_0 R)}} \exp(-jK_0R)\left[j\frac{\exp(-jK_0y'\sin\phi)}{F(\phi)} - \sin(K_0y'\sin\phi)\right] \quad . \quad . \quad . \quad . \quad (11a)$$

for $y > 0$, $y' > 0$.

$$H_x = -\frac{Y_0}{2}\sum_{n=1}^{N} \frac{\phi_n^{(1)}(y)\phi_n^{(2)}(y')}{\sqrt{(1 + s_n^2)}} \exp[-jK_0|z|\sqrt{(1 + s_n^2)}] \, u\left[\frac{s_n}{1 + \sqrt{(1 + s_n^2)}} - \tan\frac{\phi}{2}\right] - \frac{\omega\epsilon_0(1 - j)}{2\sqrt{(\pi K_0 R)}} \exp(-jK_0R) \left[\frac{1 + j\frac{\sqrt{(\epsilon - \cos^2\phi)}}{\epsilon\sin\phi}\cot[K_0y'\sqrt{(\epsilon - \cos^2\phi)}]}{F(\phi)} - 1\right] \frac{\epsilon\sin\phi}{\sqrt{(\epsilon - \cos^2\phi)}}\sin[K_0y'\sqrt{(\epsilon - \cos^2\phi)}] \quad . \quad . \quad . \quad (11b)$$

for $y > 0 \quad 0 > y' > -d$

and

$$H_x = -\frac{Y_0}{2}\sum_{n=1}^{N} \frac{\phi_n^{(1)}(y)\phi_n^{(3)}(y')}{\sqrt{(1 + s_n^2)}} \exp[-jK_0|z|\sqrt{(1 + s_n^2)}]u\left[\frac{s_n}{1 + \sqrt{(1 + s_n^2)}} - \tan\frac{\phi}{2}\right] - \frac{\dfrac{1 - \Gamma\exp(j\beta\sin\phi)}{1 + \Gamma\exp(-j\beta\sin\phi)} + j\tan[K_0(y' + d)\sin\phi]}{\dfrac{1 - \Gamma\exp(-j\beta\sin\phi)}{1 + \Gamma\exp(-j\beta\sin\phi)} + j\dfrac{\epsilon\sin\phi}{\sqrt{(\epsilon - \cos^2\phi)}}\tan\left[\dfrac{\alpha}{2}\sqrt{(\epsilon - \cos^2\phi)}\right]} \times \frac{\cos[K_0(y' + d)\sin\phi]}{\cos\left[\dfrac{\alpha}{2}\sqrt{(\epsilon - \cos^2\phi)}\right]} \times \frac{\omega\epsilon_0(1 + j)\exp(-jK_0R)}{2F(\phi)\sqrt{(\pi KR)}} \quad . \quad (11c)$$

for $y > 0$, $-d > y' > -(g + d)$.

We have retained Cartesian co-ordinates for the contribution of the surface waves for convenience.

In eqns. (11),

$$F(\phi) = 1 + \frac{1 + j\dfrac{1-\Gamma\exp(-j\beta\sin\phi)}{1+\Gamma\exp(-j\beta\sin\phi)}\dfrac{\sqrt{(\epsilon-\cos^2\phi)}}{\epsilon\sin\phi}\tan\left[\dfrac{\alpha}{2}\sqrt{(\epsilon-\cos^2\phi)}\right]}{\dfrac{1-\Gamma\exp(-j\beta\sin\phi)}{1+\Gamma\exp(-j\beta\sin\phi)} + j\dfrac{\epsilon\sin\phi}{\sqrt{(\epsilon-\cos^2\phi)}}\tan\left[\dfrac{\alpha}{2}\sqrt{(\epsilon-\cos^2\phi)}\right]} \quad . \quad . \quad . \quad . \quad (11d)$$

Now we will evaluate the field at a point which is not above the dielectric slab, i.e. $0 > y > -(g+d)$.

In each case, H_x is distinctly made up of two parts, H_x (surface wave) and H_x (radiated waves). The radiated contribution for $0 > y > -(g+d)$ has zero first-order effect for $K_0R \gg 1$. Therefore only the surface-wave contribution is computed. The results are as follows:

$$H_x(y,z) = -\frac{Y_0}{2}\sum_1^N \frac{\phi_n(y')\phi_n^{(2)}(y)}{\sqrt{(1+s_n^2)}}\exp\left[-jK_0|z|\sqrt{(1+s_n^2)}\right]$$
(surface waves) . . . . . (11e)

for $0 > y > -d$

$$H_x(y,z) = -\frac{Y_0}{2}\sum_1^N \frac{\phi_n(y')\phi_n^{(3)}(y)}{\sqrt{(1+s_n^2)}}\exp\left[-jK_0|z|\sqrt{(1+s_n^2)}\right]$$
(surface waves) . . . . . (11f)

for $-d > y > -(g+d)$

The analytical expressions for $\phi_n(y')$ in eqns. (11e) and (11f) depend on the position of the source. This was explained in the paragraph following eqn. (9).

It should be noted here that the unit step function which appears in eqns. (11a), (11b) and (11c) is, of course, inconsistent with the continuity of the fields. It is present because we are using only a first-order approximation to H_x. The approximation is, however, good enough except at $\phi/2 = \arctan s_n/[1+\sqrt{(1+s_n^2)}]$.

The electric fields can be obtained by differentiation of the magnetic field:

$$\left.\begin{aligned} E_y &= \frac{1}{j\omega_0}\frac{H_x}{z} \\ E_z &= \frac{j}{\omega_0}\frac{H_x}{y} \end{aligned}\right\} \quad . \quad . \quad . \quad . \quad . \quad . \quad (12)$$

(4) THE RADIATION PATTERN

The term 'radiation pattern' is used here to denote the pattern of the radiation loss or radiated wave. This pattern and the total radiation loss are found by means of H_x (radiated) alone, where H_x (radiated) is the total H_x minus the surface-wave contribution. The validity of such a formulation is assumed owing to two properties of H_x:

(a) There is no coupling of power between the surface wave and the radiated wave, due to the orthogonality of modes established in Section 2.

(b) For large values of R, H_x (radiated) has a negligible first order effect at $\phi \simeq 0$, while H_x (surface waves) has negligible effect for $K_0R\phi \gg 0$.

Since our problem is perfectly symmetrical with respect to the plane $z = 0$, only the radiation patterns for $z > 0$ are written and computed explicitly.

We shall first proceed to find radiation patterns for symmetrical and antisymmetrical excitations, and afterwards the radiation pattern of the single source excitation for the complete structure.

By an obvious application of Poynting's theorem to the fields given in eqns. (11), we obtain the following expressions for the average power radiated per unit angle for symmetrical ($\Gamma = -1$) and antisymmetrical ($\Gamma = +1$) excitations:

$$\bar{S}_{rad} = \frac{K_0R}{2\omega\epsilon_0}|H_{x(rad)}|^2 \quad . \quad . \quad . \quad . \quad (13a)$$

The notation will be more compact if we make use of the following functions:

$$f(\phi) = \frac{\Gamma - \cos(\beta\sin\phi)}{\sin(\beta\sin\phi)} \quad . \quad . \quad . \quad . \quad (13b)$$

$$\Psi(\phi) = f(\phi)\cos\left[\frac{\alpha}{2}\sqrt{(\epsilon-\cos^2\phi)}\right] + \frac{\epsilon\sin\phi}{\sqrt{(\epsilon-\cos^2\phi)}}\sin\left[\frac{\alpha}{2}\sqrt{(\epsilon-\cos^2\phi)}\right] \quad . \quad (13c)$$

The average power radiated per unit angle for a position of the source above the dielectric slab is

$$\bar{S}_{rad} = \frac{\omega\epsilon_0}{4\pi}\left\{1 + \frac{\cos\left[\dfrac{\alpha}{2}\sqrt{(\epsilon-\cos^2\phi)}\right] - \dfrac{\sqrt{(\epsilon-\cos^2\phi)}}{\epsilon\sin\phi}f(\phi)\sin\left[\dfrac{\alpha}{2}\sqrt{(\epsilon-\cos^2\phi)}\right]}{\Psi(\phi)}\tan\left[K_0y'\sin\phi\right]\right\}^2 \frac{\cos^2\left[Ky'\sin\phi\right]}{|F(\phi)|^2} \quad . \quad (13d)$$

The function $F(\phi)$ is given in eqn. (11d).

If the source is inside the dielectric,

$$\bar{S}_{rad} = \frac{\omega\epsilon_0}{4\pi}\left\{\frac{\sin\left[\left(K_0y' + \dfrac{\alpha}{2}\right)\sqrt{(\epsilon-\cos^2\phi)}\right]\dfrac{\epsilon\sin\phi}{\sqrt{(\epsilon-\cos^2\phi)}} + \cos\left[\left(K_0y' + \dfrac{\alpha}{2}\right)\sqrt{(\epsilon-\cos^2\phi)}\right]f(\phi)}{|F(\phi)|\Psi(\phi)}\right\}^2 \quad . \quad . \quad (13e)$$

And finally, if the source is in between the dielectric slab and the plane of symmetry,

$$\bar{S}_{rad} = \frac{\omega\epsilon_0}{4\pi}\left\{\frac{\sin\left[\left(K_0y' + \dfrac{\alpha}{2}\right)\sin\phi\right] + f(\phi)\cos\left[\left(K_0y' + \dfrac{\alpha}{2}\right)\sin\phi\right]}{|F(\phi)|\Psi(\phi)}\right\}^2 \quad . \quad . \quad . \quad (13f)$$

Many radiation patterns have been computed, but we show here only some typical ones. Fig. 5(a) is a plot of the radiation patterns for symmetrical excitation for $\alpha = 3$, $\beta = 3$ and several positions of the source. Fig. 5(b) shows some radiation patterns for $\alpha = 3$, $\beta = 3$ and antisymmetrical excitation.

As we would expect, the radiation patterns are just deviations of those obtained from two parallel line sources in free space and we will not go into a detailed discussion, which can

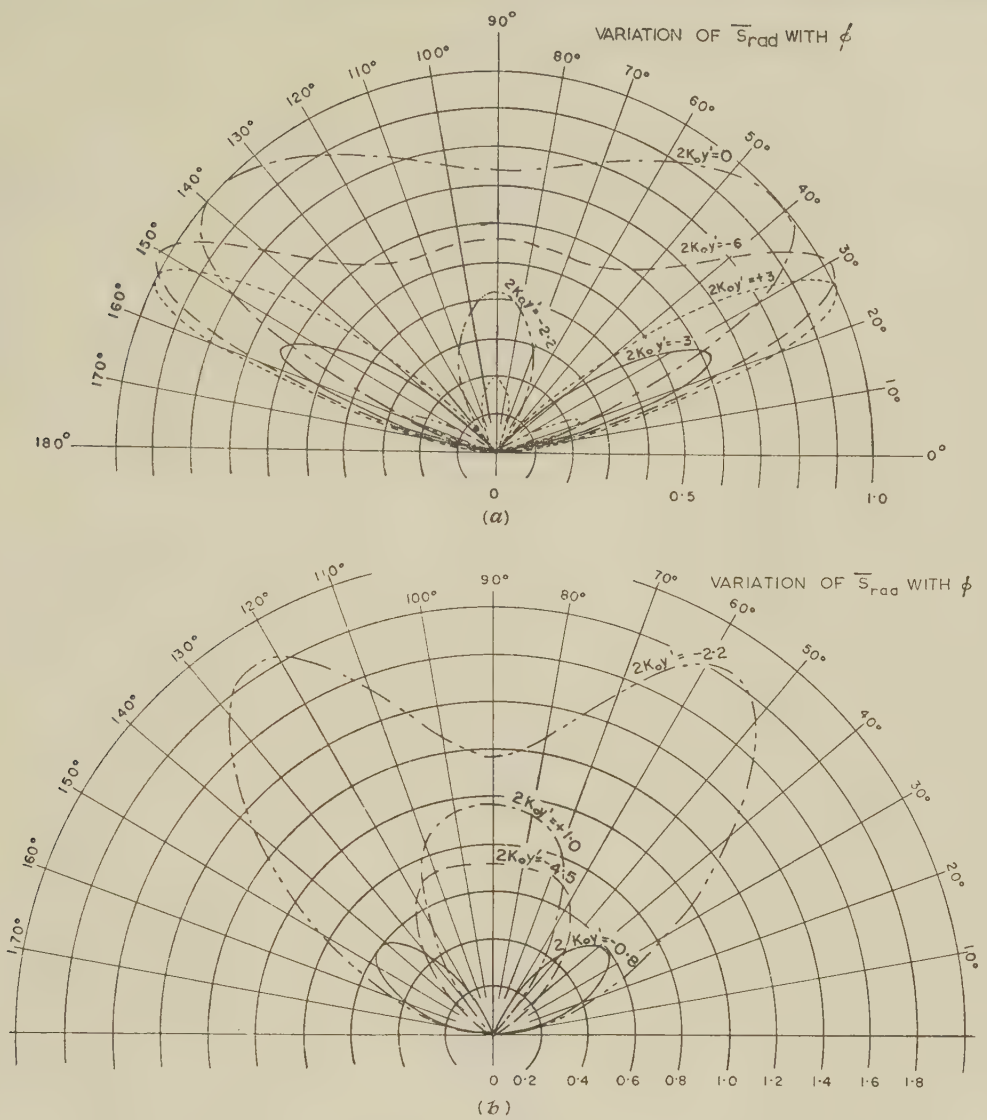

Fig. 5.—Radiation pattern for several heights of source for $\alpha = 3$ and $\beta = 3$.

(*a*) Symmetrical excitation ($\Gamma = -1$).
(*b*) Antisymmetrical excitation ($\Gamma = +1$).

found elsewhere.[7] We will simply state that the area enclosed by the loops (radiation loss) will pass alternately through maximum and minimum as the source is raised above the plane of symmetry, and the efficiency of excitation can be controlled in this way.

We can obtain by superposition of the fields the radiation pattern of the complete structure shown in Fig. 1 excited by a single line source. The magnetic field is given by

$$2H_{x(rad)} = \underset{\Gamma=-1}{[H_{x(rad)}]} \pm \underset{\Gamma=+1}{[H_{x(rad)}]} \quad . \quad . \quad . \quad (14)$$

for $\phi \gtrless 0$.

(5) THE TOTAL RADIATION LOSS AND THE POWER CARRIED IN THE SURFACE WAVES

Evidently the total radiation loss is

$$2\int_0^{\pi/2} \bar{S}_{rad} d\phi \quad . \quad . \quad . \quad . \quad . \quad . \quad (15a)$$

for the half-space structures and

$$\int_0^{\pi/2} \underset{(\Gamma=+1)}{\bar{S}_{rad}} d\phi + \int_0^{\pi/2} \underset{(\Gamma=-1)}{\bar{S}_{rad}} d\phi \quad . \quad . \quad . \quad . \quad (15b)$$

for the complete structure with single source excitation. The integrals have been calculated numerically for different values of the parameters.[7] Fig. 6(*a*) gives the power radiated versus the position of the source for three values of the thickness of the slab ($\alpha = 1$, 3, and 5) and three separations for the slabs ($\beta = 1$, 3, and 5) for symmetrical excitation. Fig. 6(*b*) gives similar results for antisymmetrical excitation, and Fig. 6(*c*) for the complete structure excited by a single source.

The shaded area represents the position of the dielectric slab. The curves can be used for any frequency, since all the dimensions are normalized with respect to wavelength. These curves exhibit the familiar oscillating patterns caused by changes in the phase between the radiation from the line source and radiation from the induced sources.

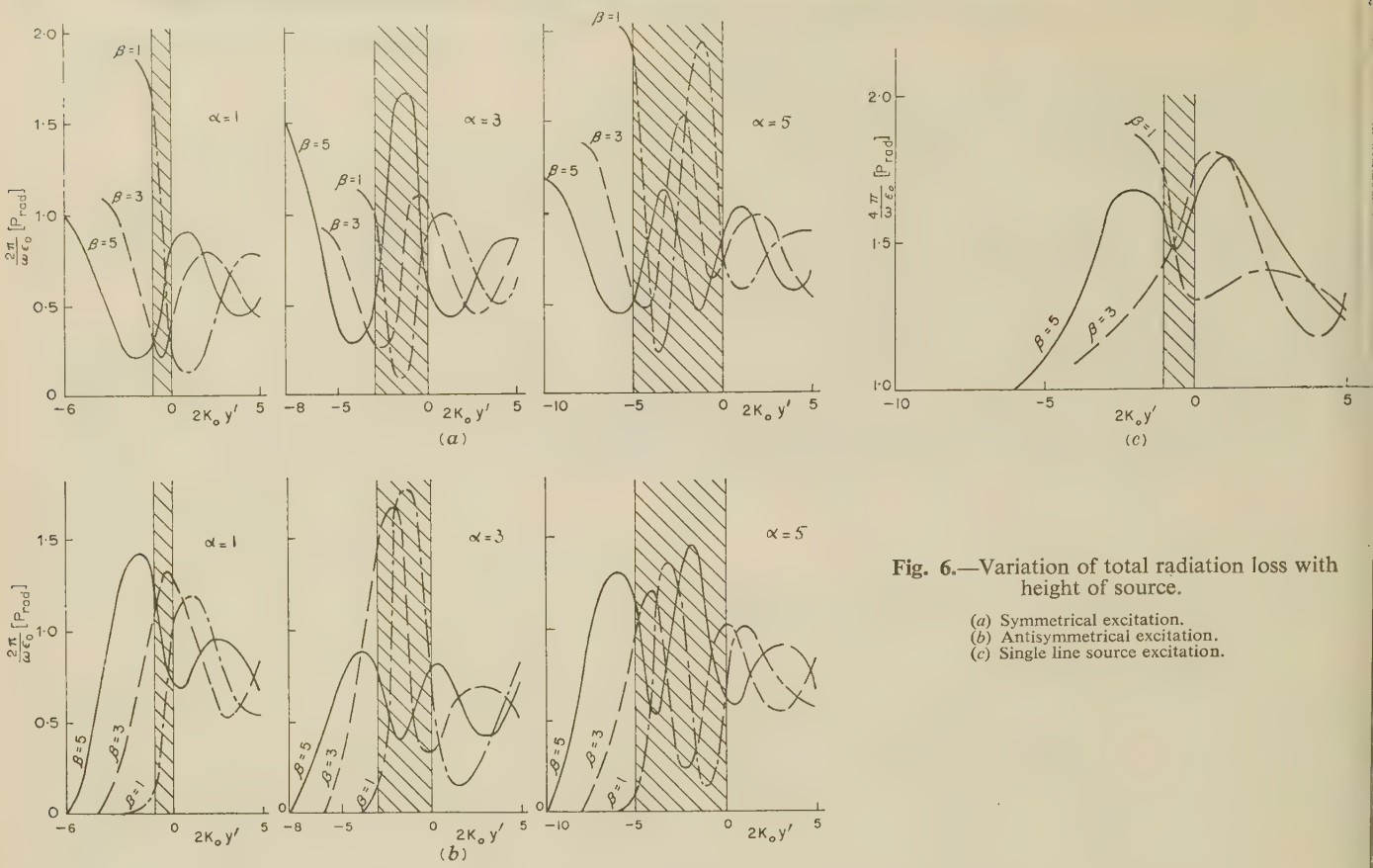

Fig. 6.—Variation of total radiation loss with height of source.

(*a*) Symmetrical excitation.
(*b*) Antisymmetrical excitation.
(*c*) Single line source excitation.

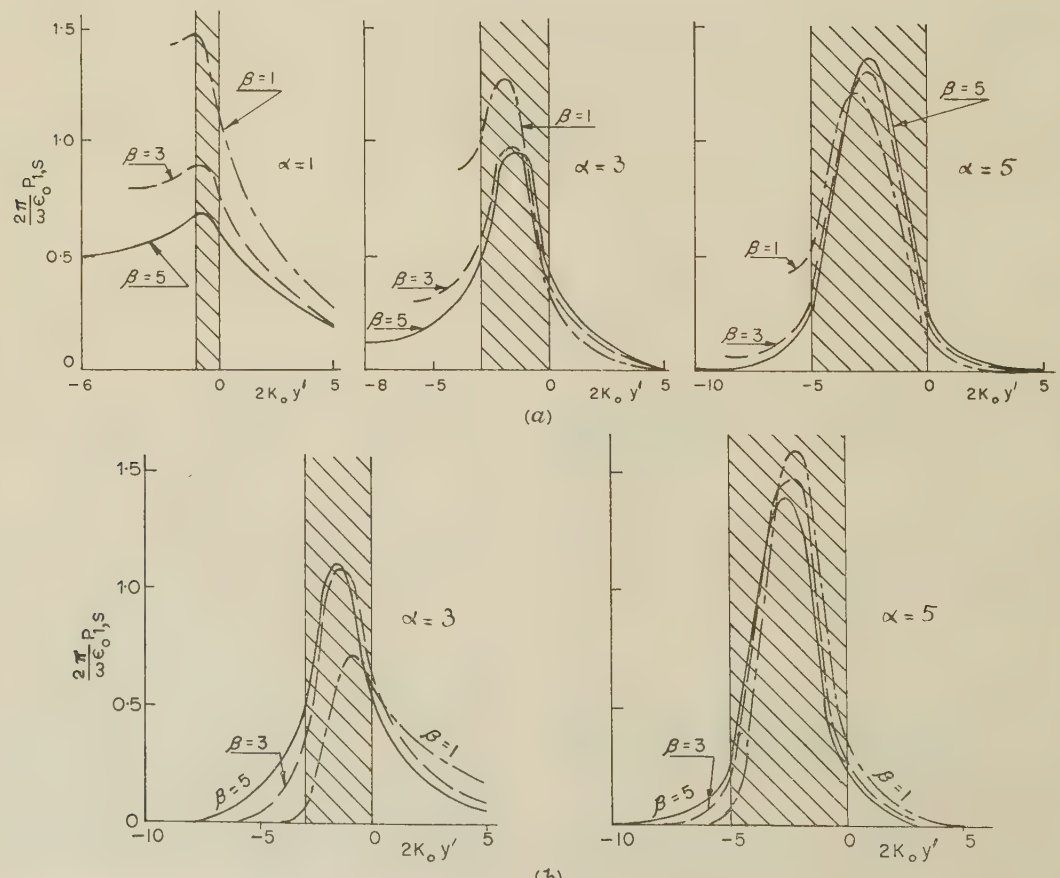

Fig. 7.—Variation in power carried with height of source.

(*a*) By the lowest symmetrical surface wave. (*b*) By the lowest antisymmetrical surface wave.

By simple considerations we obtain for the power contained in the nth surface wave for the half structure:

$$P_n = \frac{Y_0}{4\sqrt{(1+s_n^2)}}\phi_n^2(y') \quad . \quad . \quad . \quad . \quad (16)$$

The analytical expression for $\phi_n(y')$ will be $\phi_n^{(1)}(y')$, $\phi_n^{(2)}(y')$ or $\phi_n^{(3)}(y')$ depending on the position of the source, i.e. on the value of y'.

surface wave versus $2K_0y'$ for $\alpha = 1, 3, 5$ and $\beta = 1, 3, 5$. Fig. 8(*b*) gives similar curves for antisymmetrical excitation. Finally, Fig. 8(*c*) presents the efficiency curves for the lowest surface wave excited in the complete structure by a single line source for $\alpha = 1$. The shaded area indicates the position of one dielectric slab.

The curves given only illustrate the results. Many more curves have been plotted[7] to consider the effect of changes in α.

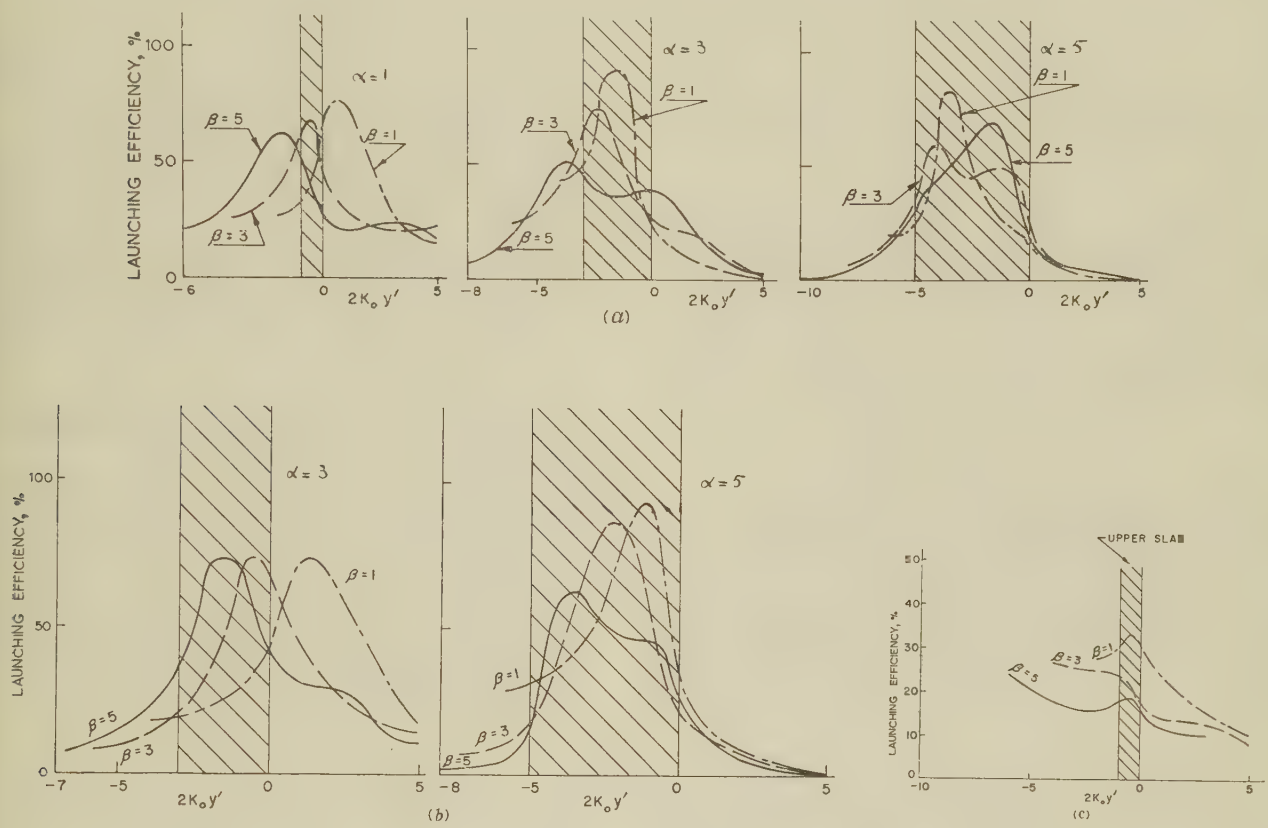

Fig. 8.—Variation in efficiency of excitation with height of source.

(*a*) Symmetrical excitation.
(*b*) Antisymmetrical excitation.
(*c*) Complete structure excited by a single line source.

The total power carried by all surface waves is the sum of the individual powers.

The only powers computed have been those for the lowest symmetrical and antisymmetrical surface wave[7] for such values of α and β that only one surface wave exists. Figs. 7(*a*) and (*b*) illustrate the variation of the power in the surface wave with respect to the position of the source. For a given value of β a maximum surface-wave power is always obtained by placing the source approximately in the middle of the slab. In addition, we may adjust β and obtain an even higher surface-wave power.

(6) THE LAUNCHING EFFICIENCY

We use Cullen's definition[3] of launching efficiency:

$$\sigma = \frac{\text{Power carried by the desired surface wave}}{\text{Sum of the powers carried by surface waves plus radiated power}} \quad . \quad (17)$$

Fig. 8(*a*) gives efficiency curves for the lowest symmetrical

A very high efficiency of 93% is obtained for $\alpha = 3$, $\beta = 1$, $2K_0y' = -1{\cdot}5$ and $\Gamma = -1$.

(7) CONCLUSIONS

Examination of the curves for the total radiated power shows that an increase of β (air-gap distance) for a given value of α (thickness) shifts towards the plane of symmetry the value of $2K_0y'$ for which the first radiation minimum occurs.

For $\alpha = 3$, $\beta = 1$ and $\Gamma = -1$, the absolute minimum of radiation and the maximum power put into the surface wave are obtained simultaneously when the source is approximately at the centre of the slab ($2K_0y' = -1{\cdot}5$). This minimum is the smallest among those calculated for different values of α and β and the maximum is the highest maximum. We conclude that the efficiency obtained in this case (93%) is about the maximum obtainable from the structure under consideration when excited by a magnetic line source.

Similar properties are exhibited by the efficiencies of antisymmetrical excitation. The only difference is that for

$$\alpha < \frac{2}{\sqrt{(\epsilon - 1)}} \arctan\left[\frac{2\epsilon}{\beta\sqrt{(t-1)}}\right]$$

the structure does not have an antisymmetrical surface wave as a mode and therefore the excitation efficiency is zero.

The curves for the radiation loss also indicate that, for each value of α, there is a value of β which gives the minimum radiation loss when the source is placed at the centre of the slab. In this case, a high efficiency is achieved for both symmetrical and antisymmetrical excitation. This may not be the maximum efficiency obtainable.

From the investigation carried out, we can formulate some general rules to be followed if a high launching efficiency is desired:

(*a*) For a given value of α and either a symmetrical (slab above ground) or antisymmetrical excitation, we can be sure of a reasonably high efficiency (above 70%) by placing the source in the middle of the slab, provided that β is adjusted to obtain a minimum radiation loss. The approximate required value of β can be estimated from the plots in Figs. 6–8.

(*b*) An increase of the thickness of the slab will allow a higher efficiency of excitation provided that the thickness of the slab is not made so large that the structure can propagate more than one surface wave, i.e. we must keep

$$\alpha < 2\pi/\sqrt{(\epsilon - 1)} \qquad (\Gamma = -1)$$

and

$$\alpha < \frac{2}{\sqrt{(\epsilon - 1)}}\left[\arctan\frac{2\epsilon}{\beta\sqrt{(\epsilon - 1)}} + \pi\right] \quad (\Gamma = +1)$$

(*c*) It is not desirable to have two slabs in free space excited by a single source; a symmetrical or antisymmetrical excitation of the surface wave is more efficient.

(*d*) H_x (surface wave) has a real dependence on y', but H_x (radiated) has a complex dependence on y'. Therefore the excitation of the structure by more than one coherent parallel line source at the plane $z = 0$ near the middle of the slab may increase the launching efficiency. This is due to the fact that the H_x radiated by the different lines interfere, while the surface-wave intensities add in phase.

(8) ACKNOWLEDGMENT

The research described in the paper was sponsored by the Cambridge Air Force Research Center under contract AF 19(604)–1391 with Brown University.

(9) REFERENCES

(1) ZUCKER: F. J.: 'The Guiding and Radiation of Surface Waves', Proceedings of the Symposium on Modern Advances in Microwave Techniques, Polytechnic Institute of Brooklyn, November, 1954, p. 403.

(2) ANGULO, C. M., and CHANG, W. S. C.: 'On the Excitation of Surface Waves in Dielectric Slabs', Part I, Report No. AF–1391/2 of the Division of Engineering, Brown University under Contract AF 19(604)–1391 with the Air Force Cambridge Research Center, June, 1956.

(3) CULLEN, A. L.: 'The Excitation of Plane Surface Waves', *Proceedings I.E.E.*, Monograph No. 93 R, February, 1954 (**101,** Part IV, p. 225).

(4) FRIEDMANN, B., and WILLIAMS, W. E.: 'Excitation of Surface Waves', Research Report No. EM–99 of the Division of Electromagnetic Research, Institute of Mathematical Sciences, New York University under Contract AF 19 (604)–1717 with the Air Force Cambridge Research Center, October, 1956.

(5) ANGULO, C. M.: 'Diffraction of Surface Waves by a Semi-Infinite Dielectric Slab', *Transactions of the Institute of Radio Engineers*, 1957, **AP–5**, p. 100.

(6) MARCUVITZ, N.: 'Field Representations in Spherically Stratified Regions', Symposium of the Theory of Electromagnetic Waves, Interscience Publishers, Inc. (1951) p. 263.

(7) ANGULO, C. M., and CHANG, W. S. C.: 'Excitation of Surface Waves in Dielectric Slabs', Part II, Report No. 1391/3 of the Division of Engineering, Brown University, under Contract AF 19(604)–1391 with the Air Force Cambridge Research Center, September, 1956.

621.376.33:621.396.96

The Institution of Electrical Engineers
Monograph No. 412 E
Oct. 1960

THE OUTPUT SPECTRAL DENSITY OF A DETECTOR OPERATING ON A F.M. C.W. RADAR SIGNAL IN THE PRESENCE OF BAND-LIMITED WHITE NOISE

By J. LAIT, M.A., and A. J. HYMANS, M.Sc., A.Inst.P., Associate Member.

(*The paper was first received* 11*th March, and in revised form* 25*th June*, 1960. *It was published as an* INSTITUTION MONOGRAPH *in October*, 1960.)

SUMMARY

A method of analysis suggested by Lawson and Uhlenbeck is used to examine the interaction between reference signal, echo and noise in the detector stage of a frequency-modulated c.w. radar receiver.

The paper gives a method of approximation which may be used in most practical cases and states the restrictions on system parameters for which the approximations are valid.

Expressions for spectral density are derived separately for both quadratic and linear detectors, and the question of optimum pre-detector bandwidth is examined. Finally, the authors consider how signal/noise ratio will be affected by choice of bandwidth in stages which follow the detector.

LIST OF SYMBOLS

A_0 = Coefficient of d.c. term in Fourier-series expansion of beat note, volts.
a_k, b_k = Random coefficient in Fourier-series representation of noise, volts.
C_{m1}, C_{m2}, C_{m3}, C_{m4} = Coefficient of mth harmonic in Fourier-series representation of beat note, volts.
F_1, F_2, F_3, F_4 = Amplitudes of terms in Fourier transform of beat note, volts.
f = Frequency, c/s.
f_0 = Undeviated carrier frequency, c/s.
f_1 = Total sweep-frequency excursion, c/s.
f_2 = Pre-detector bandwidth, c/s.
f_3 = Post-detector bandwidth, c/s.
f_s = Beat-note fundamental frequency ($=1/T_s$), c/s.
$G(f) = \Sigma G_i$ = Power spectral density, volts^2-sec.
k = Boltzmann's constant $= 1{\cdot}37 \times 10^{-23}$ joules/deg K.
m = Order of beat-note harmonic.
N = Noise factor.
n = Serial number of sweep interval.
p = Order of term in series expansion of auto-correlation function.
P_e = Echo power per unit frequency excursion, watt-sec.
P_g = Reference signal power per unit frequency excursion, watt-sec.
P_n = Noise power per unit pre-detector bandwidth, watt-sec.
P_p = Pre-detector noise power, watts.
$R(\tau) = \overline{r(t)r(t+\tau)}$ = Auto-correlation function.
$r_L(t)$ = Output of linear detector
$r_Q(t)$ = Output of quadratic detector
} These may be currents or voltages (see Section 2.2).
$S(t)$ = Signal waveform, volts.
T_e = Delay time of echo, sec.
T_s = Sweep duration time, sec.
T = Temperature of system, deg K.
t = Time variable, sec.
t_1, t_2 = Instants separated by correlation interval τ, sec.
t_n = Time variable measured from mid-point of nth sweep interval, sec.
t_{n1}, t_{n2} = Instants of time during the nth sweep separated by correlation interval τ, sec.
V_e = Amplitude of echo, volts.
V_g = Amplitude of reference signal, volts.
$X_n(t)$, $Y_n(t)$, $X_s(t)$, $Y_s(t)$ = Orthogonal components of noise and signal voltage at carrier frequency, volts.
$X(t)$, $Y(t)$ = General orthogonal components of an a.c. signal, volts.
2α = Angular-frequency sweep rate, rad/s^2.
$\gamma = T_e/T_s$ = Range factor.
δ = Error limit.
ϕ_e = Instantaneous phase of echo, rad.
ϕ_g = Instantaneous phase of reference signal, rad.
ρ = Normalized auto-correlation function of noise.
τ = Correlation time intervals, sec.
τ_p = Excess of correlation time interval over nearest lower integral multiple of T_s, sec.
ω_0 = Undeviated angular carrier frequency, rad/s.

(1) INTRODUCTION

In certain types of f.m. radar[1, 2, 3, 4, 5] a portion of the transmitted signal is picked up by the receiver and made to beat with the echo signal in a detector or demodulator. In some applications, this may be achieved by means of a direct connection between transmitter and receiver; in others it is provided automatically by using the same aerial both for transmission and for reception, or by spill-over from the transmitting aerial to the receiving aerial when independent aerials are used. The interaction between this reference signal and the echo signal (which is similar to it in form but is delayed by a time $T_e = \gamma T_s$) produces a video-frequency beat note containing the range/amplitude information.[3]

The receiver will normally have a directive aerial and some frequency-selective circuits before the detector, if only to limit interference from unwanted signals. There may or may not be amplification, depending on whether

(*a*) Amplifiers are available at the operating frequency of the radar.
(*b*) The reference signal and signals such as those from short-range objects are not so strong as to cause saturation (and hence non-linearity) at any stage prior to the detector.

Thus, there will be present at the detector output

(i) The desired beat-note.
(ii) The normally detected noise.
(iii) A random signal produced by interaction between the frequency-modulated wave and the noise.

This situation should be compared with that in the conventional superhet receiver, where the (strong) output from a local oscillator is heterodyned with the signal to produce a beat at

Correspondence on Monographs is invited for consideration with a view to publication.
Mr. Lait and Mr. Hymans are at the Royal Military College of Science.

intermediate frequency. The local-oscillator output also interacts with the noise in the r.f. pass band to produce noise at intermediate frequency (in addition to any convertor noise present). In the f.m. radar, the reference signal takes the place of the local-oscillator output but is itself frequency-modulated, and hence the interaction with the noise produces a complex beat-note spectrum.

The purpose of the paper is to analyse this situation with the aid of some simplifying assumptions.

(2) BASIC ASSUMPTIONS AND METHOD

(2.1) Assumptions

In such a system the detector accepts the sum of three waveforms, namely

(*a*) Reference signal.
(*b*) Wanted echo.
(*c*) Noise.

A complete treatment would take all three waveforms simultaneously and produce the video-frequency beat notes by a single procedure. The analysis is possible in the case of a quadratic detector, but is exceedingly complex and the physical significance of the results is not immediately apparent. For the linear detector the analysis is more difficult still.

It is assumed that the reference signal is much stronger than either the echo or the noise, and that one may separate the analysis into two independent portions, dealing with the interactions between (*a*) and (*b*), and between (*a*) and (*c*) only. These two results can then be combined to give the complete output. The contribution from the interaction between (*b*) and (*c*) is regarded as so small as to be insignificant. If required, it can be obtained by suitable modification of the results of the interaction between (*a*) and (*c*). The normal detected outputs due to (*a*), (*b*) and (*c*) will, of course, be present, but these are included automatically in the expressions which arise.

(2.2) Method

The model of a detector used here is that described by Lawson and Uhlenbeck (Reference 6, p. 152). It is assumed that there exists a channel of finite bandwidth f_2, centred at a frequency f_0, which is used to transmit, filter, and perhaps amplify the signals and the noise. The output of the channel is detected by a device which effectively 'demodulates' the carrier waves. Thus all signals can be written in the form

$$\mathrm{X}(t)\cos 2\pi f_0 t + \mathrm{Y}(t)\sin 2\pi f_0 t$$

where $\mathrm{X}(t)$ and $\mathrm{Y}(t)$ are functions of time which vary slowly compared with f_0. Two forms of output are possible:

$$r_L(t) = \sqrt{(\mathrm{X}^2 + \mathrm{Y}^2)} \text{ (for the linear detector)} \quad . \quad . \quad (1)$$

$$r_Q(t) = \mathrm{X}^2 + \mathrm{Y}^2 \text{ (for the quadratic detector)} \quad . \quad (2)$$

The output of any detector is, dimensionally, either a voltage or a current. In eqns. (1) and (2), $r_L(t)$ and $r_Q(t)$ appear to be dimensionally different, and this difference will persist throughout the treatment. Strictly, constants of proportionality with appropriate dimensions should be included in each case. These constants would also allow for any conversion loss in the detector. They will, however, be omitted throughout this treatment to permit the ready use of expressions developed by Lawson and Uhlenbeck.[6]

(3) MATHEMATICAL FORMULATION

The signal used in this type of radar is frequency-modulated in a sawtooth fashion and may be described[3] by a function $V\sin\phi$ where

$$\left.\begin{aligned} \phi &= n\omega_0 T_s + \omega_0 t_n + \alpha t_n^2 \\ \text{and} \qquad t_n &= t - nT_s;\ -\tfrac{1}{2}T_s \leqslant t_n \leqslant \tfrac{1}{2}T_s \end{aligned}\right\} \quad . \quad . \quad . \quad (3)$$

The sweep rate 2α and duration time T_s are related to the total frequency excursion f_1 cycles per second by the identity $\alpha T_s = \pi f_1$.

The reference signal and echo will be designated by suffices as V_g, V_e, ϕ_g, ϕ_e. There is no loss of generality if ϕ_g is taken as above and

$$\phi_e(t) = \phi_g(t - \gamma T_s)$$

where γT_s is the echo delay (in practice, $0 \leqslant \gamma \leqslant 1$).

Thus the reference signal may be written in the form

$$\mathrm{S}(t) = \mathrm{X}_s(t)\cos\omega_0 t + \mathrm{Y}_s(t)\sin\omega_0 t$$

where

$$\left.\begin{aligned} \mathrm{X}_s(t) &= V_g \sin \alpha t_n^2 \\ \mathrm{Y}_s(t) &= V_g \cos \alpha t_n^2 \end{aligned}\right\} \quad . \quad . \quad . \quad . \quad . \quad (4)$$

The echo takes a similar form with the appropriate delay and with amplitude V_e instead of V_g.

The noise voltage is formulated as in Reference 6, and may therefore be written

$$\left.\begin{aligned} \mathrm{X}_n(t) &= \sum_k (a_k \cos\omega_0 t + b_k \sin\omega_0 t) \\ \mathrm{Y}_n(t) &= \sum_k (-a_k \sin\omega_0 t + b_k \cos\omega_0 t) \end{aligned}\right\} \quad . \quad . \quad (5)$$

with a_k and b_k distributed in a Gaussian manner.

Following their procedure,[6] the auto-correlation coefficient of the output is first calculated, obtaining

$$\mathrm{R}(\tau) = \overline{r(t)r(t+\tau)} \quad . \quad . \quad . \quad . \quad . \quad (6)$$

where the bar denotes a time average. As outlined by Woodward,[7] the spectral density is then obtained by taking the Fourier transform of the auto-correlation function $\mathrm{R}(\tau)$.

Thus

$$\mathrm{G}(f) = \int_{-\infty}^{\infty} \mathrm{R}(\tau)\varepsilon^{-j2\pi f\tau} d\tau \quad . \quad . \quad . \quad . \quad (7)$$

Using the assumption set out in Section 2, the calculation is performed in two parts. We obtain

(*a*) $\mathrm{R}(\tau)$ and hence $\mathrm{G}(f)$ for the interaction between noise and reference signal.
(*b*) $\mathrm{G}(f)$ directly for the product of echo and reference signal.

The required result is taken as the linear superposition of the two. Magnitude considerations enable the interaction between echo and noise to be ignored, and the individually detected outputs for noise, reference signal and echo appear in the appropriate parts of the computation.

(4) CALCULATION OF R(τ) FOR NOISE AND REFERENCE SIGNAL

(4.1) Case of the Quadratic Detector

If the suffices 1 and 2 refer to instants of time t_1, t_2 such that $t_2 - t_1 = \tau$, it has been shown[6] that, for the quadratic detector

$$\mathrm{R}_Q(\tau) = \overline{r_Q(t_1)r_Q(t_2)}$$

$$= \lim_{\theta\to\infty} \frac{1}{\theta}\int_{-\frac{1}{2}\theta}^{\frac{1}{2}\theta} [(\mathrm{X}_{s1}^2 + \mathrm{Y}_{s1}^2 + 2P_p)(\mathrm{X}_{s2}^2 + \mathrm{Y}_{s2}^2 + 2P_p) + 4P_p\rho(\mathrm{X}_{s1}\mathrm{X}_{s2} + \mathrm{Y}_{s1}\mathrm{Y}_{s2}) + 4P_p{}^2\rho^2]$$

$$. \quad . \quad . \quad . \quad (8)$$

where

$$P_p = kTf_2N, \text{ and } \rho = \frac{\sin\pi f_2\tau}{\pi f_2\tau}$$

is the normalized auto-correlation function of the noise alone.

In calculating $R(\tau)$ account is taken of the reference signal but not of the echo; hence, using eqns. (4),

$$\left.\begin{aligned} X_{s1}^2 + Y_{s1}^2 = X_{s2}^2 + Y_{s2}^2 = V_g^2 \\ \text{and} \quad X_{s1}X_{s2} + Y_{s1}Y_{s2} = V_g^2 \cos[\alpha(t_{n2}^2 - t_{n1}^2)] \end{aligned}\right\} \quad . \quad . \quad (9)$$

The expression to be averaged is thus

$$(V_g^2 + 2P_p)^2 + 4V_g^2P_p \frac{\sin \pi f_2\tau}{\pi f_2\tau} \cos[\alpha(t_{n2}^2 - t_{n1}^2)] + 4P^2\left(\frac{\sin \pi f_2\tau}{\pi f_2\tau}\right)^2 \quad . \quad (10)$$

Only the middle term contains the time t_1, and as $\alpha(t_{n2}^2 - t_{n1}^2)$ is an exactly repetitive function of t_1, the complete time average may be obtained by averaging over a single sweep-repetition cycle.

Let $pT_s \leqslant \tau \leqslant (p+1)T_s$ and write τ_p for $\tau - pT_s$; this substitution is comparable with that used when expressing the phase ϕ in Section 3.

$$\left.\begin{aligned} &\text{For} && -\tfrac{1}{2}T_s \leqslant t_{n1} \leqslant \tfrac{1}{2}T_s - \tau_p, \quad t_{n2} = t_{n1} + \tau_p \\ &\text{so that} && \alpha(t_{n2}^2 - t_{n1}^2) = \alpha\tau_p(2t_{n1} + \tau_p) \\ &\text{while for} && \tfrac{1}{2}T_s - \tau_p \leqslant t_{n1} \leqslant \tfrac{1}{2}T_s, \quad t_{n2} = t_{n1} + \tau_p - T_s \\ &\text{so that} && \alpha(t_{n2}^2 - t_{n1}^2) = \alpha(\tau_p - T_s)(2t_{n1} + \tau_p - T_s) \end{aligned}\right\} \quad . \quad (11)$$

The required time average of $\cos[\alpha(t_{n2}^2 - t_{n1}^2)]$ is

$$\frac{1}{T_s}\left\{\int_{-\frac{1}{2}T_s}^{\frac{1}{2}T_s - \tau_p} \cos[\alpha\tau_p(2t_{n1} + \tau_p)]dt_{n1} + \int_{\frac{1}{2}T_s - \tau_p}^{\frac{1}{2}T_s} \cos[\alpha(\tau_p - T_s)(2t_{n1} + \tau_p - T_s)]dt_{n1}\right\}$$

and this reduces to

$$\frac{\sin \alpha\tau_p(T_s - \tau_p)}{\alpha\tau_p(T_s - \tau_p)} \quad . \quad . \quad . \quad . \quad . \quad . \quad (12)$$

Hence

$$R_Q(\tau) = (V_g^2 + 2P_p)^2 + 4V_g^2P_p \frac{\sin \pi f_2\tau}{\pi f_2\tau} \frac{\sin \alpha\tau_p(T_s - \tau_p)}{\alpha\tau_p(T_s - \tau_p)} + 4P_p^2\left(\frac{\sin \pi f_2\tau}{\pi f_2\tau}\right)^2 \quad . \quad (13)$$

(4.2) Case of the Linear Detector

Lawson and Uhlenbeck[6] show that the linear detector must be treated as an approximation to one or other of two limiting cases having either very small or very large signal/noise ratio.

(*a*) Substitution in their expressions shows that, for a very small signal/noise ratio, the function to be averaged is given by

$$r_L(t_1)r_L(t_2) \simeq \frac{\pi}{32P_p}\left\{(V_g^2 + 4P_p)^2 + 4V_g^2P_p\rho \cos[\alpha(t_{n2}^2 - t_{n1}^2)] + 4P_p^2\rho^2\right\}$$

whence, as above

$$R_L(\tau) \simeq \frac{\pi}{32P_p}\left[(V_g^2 + 4P_p)^2 + 4V_g^2P_p \frac{\sin \pi f_2\tau}{\pi f_2\tau} \frac{\sin \alpha\tau_p(T_s - \tau_p)}{\alpha\tau_p(T_s - \tau_p)} + 4P_p^2\left(\frac{\sin \pi f_2\tau}{\pi f_2\tau}\right)^2\right] \quad . \quad (14)$$

(*b*) For very large signal/noise ratio we find on substitution that

$$r_L(t_1)r_L(t_2) \simeq V_g^2 + P_p\rho \cos[\alpha(t_{n2}^2 - t_{n1}^2] + \frac{P_p^2\rho^2}{2V_g^2} \cos^2[\alpha(t_{n2}^2 - t_{n1}^2)]$$

Integrating over T_s as in eqn. (12), the time average of $\cos^2[\alpha(t_{n2}^2 - t_{n1}^2)]$ is seen to be

$$\frac{1}{2}\left[1 + \frac{\sin 2\alpha\tau_p(T_s - \tau_p)}{2\alpha\tau_p(T_s - \tau_p)}\right] \quad . \quad . \quad . \quad (15)$$

which leads to the alternative form

$$R_L(\tau) \simeq V_g^2 + P_p \frac{\sin \pi f_2\tau}{\pi f_2\tau} \frac{\sin \alpha\tau_p(T_s - \tau_p)}{\alpha\tau_p(T_s - \tau_p)} + \frac{P_p^2}{4V_g^2}\left(\frac{\sin \pi f_2\tau}{\pi f_2\tau}\right)^2\left[1 + \frac{\sin 2\alpha\tau_p(T_s - \tau_p)}{2\alpha\tau_p(T_s - \tau_p)}\right] \quad . \quad (16)$$

(5) SPECTRAL DENSITY FOR NOISE AND REFERENCE SIGNAL

(5.1) Method of Approximation for the Case of a F.M.C.W. Receiver

To obtain the spectral density, one must in general take the Fourier transforms of the auto-correlation functions $R_Q(\tau)$ and $R_L(\tau)$. Thus

$$G(f) = \int_{-\infty}^{\infty} R(\tau)\varepsilon^{-j2\pi f\tau}d\tau, \text{ as in eqn. (7)}$$

The resulting expressions contain terms involving both positive and negative 'frequencies'. As they are even in amplitude and odd in phase, appropriate terms may be paired to give a real spectrum which extends throughout the positive frequency domain. When $R(\tau)$ is itself an even function, the manipulation can be simplified by changing from the exponential form of eqn. (7) to the cosine form employed by Lawson and Uhlenbeck,[6] namely,

$$G(f) = 4\int_0^{\infty} R(\tau) \cos 2\pi f\tau d\tau \quad . \quad . \quad . \quad . \quad (17)$$

Neither integration can be performed explicitly in this case. The difficulty arises from the presence in eqns. (13), (14) and (16) of terms containing factors

$$\frac{\sin \alpha\tau_p(T_s - \tau_p)}{\alpha\tau_p(T_s - \tau_p)} \quad \text{and} \quad \frac{\sin 2\alpha\tau_p(T_s - \tau_p)}{2\alpha\tau_p(T_s - \tau_p)}$$

These are oscillatory functions contained within repetitive envelopes. The functions are symmetrical about $\tau_p = \frac{1}{2}T_s$, where the envelopes have minima $4/\alpha T_s^2$ and $2/\alpha T_s^2$, respectively, and both envelopes have maxima of unit magnitude at $\tau_p = 0$. (Hence, by symmetry, they approach similar unity maxima as $\tau_p \to T_s$.)

When τ_p is small, we may write

$$\alpha\tau_p(T_s - \tau_p) = \alpha T_s\tau_p - \alpha\tau_p^2 \simeq \alpha T_s\tau_p$$

and when $\tau_p \to T_s$, making $T_s - \tau_p$ small, the alternative form may be used:

$$\alpha\tau_p(T_s - \tau_p) = \alpha T_s(T_s - \tau_p) - \alpha(T_s - \tau_p)^2 \simeq \alpha T_s(T_s - \tau_p)$$

It is thus possible, by using the latter approximation for the range $(p - \frac{1}{2})T_s \leqslant \tau_p \leqslant pT_s$ and the former for the range $pT_s \leqslant \tau \leqslant (p + \frac{1}{2})T_s$, to write

$$\frac{\sin \alpha\tau_p(T_s - \tau_p)}{\alpha\tau_p(T_s - \tau_p)} \text{ as } \sum_p \frac{\sin \alpha T_s(\tau - pT_s)}{\alpha T_s(\tau - pT_s)}$$

and to write

$$\frac{\sin 2\alpha\tau_p(T_s - \tau_p)}{2\alpha\tau_p(T_s - \tau_p)} \text{ as } \sum_p \frac{\sin 2\alpha T_s(\tau - pT_s)}{2\alpha T_s(\tau - pT_s)}$$

The first of these functions falls in magnitude to a small predetermined value δ (which might be fixed for assessment purposes at, say, 0·01) when τ_p or $T_s - \tau_p$, as appropriate, reaches the value $1/\alpha T_s\delta$; for the second function the corresponding value of τ_p or $T_s - \tau_p$ is $1/2\alpha T_s\delta$. For the approximations to be valid, the requirement is, therefore, that $1/\alpha T_s\delta \ll T_s$, i.e. that $\pi f_1 T_s \gg 1/\delta$.

In the interests of symmetry, a change of notation will be made at the same time. Assuming unit input impedance, the power contained in the reference signal is $\frac{1}{2}V_g^2$ and the echo power is $\frac{1}{2}V_e^2$. We shall therefore write

$$\left.\begin{aligned} P_g &= \tfrac{1}{2}V_g^2/f_1 \text{ (Reference signal power per unit frequency excursion)} \\ \text{and (later)} \\ P_e &= \tfrac{1}{2}V_e^2/f_1 \text{ (Echo power per unit frequency excursion)} \end{aligned}\right\} . \quad (18)$$

Likewise

$$P_n = P_p/f_2 \text{ (Noise power per unit pre-detector bandwidth)} \quad . \quad . \quad . \quad . \quad (19)$$

The auto-correlation functions thus take the following form, to a close approximation:

$$R_Q(\tau) = 4(f_1P_g + f_2P_n)^2 + \frac{8P_gP_n}{\pi^2}\sum_{-\infty}^{\infty}\frac{\sin\pi f_1(\tau - pT_s)}{\tau - pT_s}\frac{\sin\pi f_2\tau}{\tau} + \frac{4P_n^2}{\pi^2}\left(\frac{\sin\pi f_2\tau}{\tau}\right)^2 \quad . \quad (20)$$

$$R_L(\tau) = \frac{\pi}{8f_2P_n}(f_1P_g + 2f_2P_n)^2 + \frac{P_g}{4\pi f_2}\sum_{-\infty}^{\infty}\frac{\sin\pi f_1(\tau - pT_s)}{\tau - pT_s}\frac{\sin\pi f_2\tau}{\tau} + \frac{P_n}{8\pi f_2}\left(\frac{\sin\pi f_2\tau}{\tau}\right)^2 \quad . \quad . \quad . \quad . \quad (21)$$

in the case of small signal/noise ratio, and

$$R_L(\tau) = 2f_1P_g + \frac{P_n}{\pi^2 f_1}\sum_{-\infty}^{\infty}\frac{\sin\pi f_1(\tau - pT_s)}{\tau - pT_s}\frac{\sin\pi f_2\tau}{\tau} + \frac{P_n^2}{8\pi^2 f_1P_g}\left(\frac{\sin\pi f_2\tau}{\tau}\right)^2 + \frac{P_n^2}{16\pi^3 f_1^2P_g}\sum_{-\infty}^{\infty}\frac{\sin 2\pi f_1(\tau - pT_s)}{\tau - pT_s}\left(\frac{\sin\pi f_2\tau}{\tau}\right)^2 \quad . \quad (22)$$

when the signal/noise ratio is large.

(5.2) Calculation of G(f)

It remains to calculate G(f) from the expressions for R(τ). The Fourier transform of A is $A\delta(f)$ and that of $(\sin c\tau/\tau)^2$ is available from the standard tables.[8, 9] In addition, one requires transforms for the functions

$$\frac{\sin a(\tau - b)}{\tau - b}\frac{\sin c\tau}{\tau}$$

and

$$\frac{\sin a(\tau - b)}{\tau - b}\left(\frac{\sin c\tau}{\tau}\right)^2$$

These transforms are derived in Section 12.

Table 1 gives R(τ) and G(f) with appropriate frequency limits for the case of the quadratic detector. Table 2 gives similar information for the linear detector when the signal/noise ratio is small and Table 3 deals with large signal/noise ratios.

Several terms give rise to expansions for G(f), and these may be approximated by taking only the $p = 0$ term, listed in column 4. The fifth column in each Table deals with the error introduced by neglecting the rest of the series. The sum of the remaining terms is, in each case, a repetitive function and its limits of variation are stated here. These limits are, indeed, small; to take typical cases, the possible errors in G_{2B} (Table 1) and in G_{5B} (Table 2) are only $\pm 1/2f_1T_s$ times the corresponding $p = 0$ terms. Remembering that, in Section 5, a necessary condition was found to be $\pi f_1T_s \gg 1/\delta$ where δ was very small, the errors in question will be seen to be very much less than $\frac{1}{2}\pi\delta$ of the corresponding $p = 0$ terms, which can therefore be used alone with confidence.

The situation regarding terms such as G_{2C} and G_{5C}, which decline with frequency, is not quite so straightforward; further examination shows that not only are the errors repetitive and within the limits stated, but, in addition, they reach zero at precisely the same frequencies as the $p = 0$ terms to which they refer.

(6) SPECTRAL DENSITY FOR ECHO AND REFERENCE SIGNAL

Consider now the output from a detector which handles reference signal and echo, but no noise.

$$\left.\begin{aligned} \text{Here} \quad X_s(t) &= V_g\sin(\phi_g - \omega_0t) + V_e\sin(\phi_e - \omega_0t) \\ \text{and} \quad Y_s(t) &= V_g\cos(\phi_g - \omega_0t) + V_e\cos(\phi_e - \omega_0t) \end{aligned}\right\} . \quad (23)$$

By definition, the detector output will have one of two forms:

$$\left.\begin{aligned} r_Q(t) &= X_s^2 + Y_s^2 \text{ (for a quadratic detector)} \\ \text{or} \quad r_L(t) &= \sqrt{(X_s^2 + Y_s^2)} \text{ (for a linear detector)} \end{aligned}\right\} . \quad (24)$$

$$\text{Now} \quad X_s^2 + Y_s^2 = V_g^2 + V_e^2 + 2V_gV_e\cos(\phi_g - \phi_e) = 2f_1[P_g + P_e + 2\sqrt{(P_gP_e)}\cos(\phi_g - \phi_e)]$$

so that, immediately,

$$r_Q(t) = 2f_1[P_g + P_e + 2\sqrt{(P_gP_e)}\cos(\phi_g - \phi_e)] \quad . \quad (25)$$

In practice, $P_g \gg P_e$ save at the very shortest ranges and $\sqrt{(X_s^2 + Y_s^2)}$ may therefore be expanded binomially to give

$$r_L(t) = \sqrt{(2f_1P_g)}\left[1 + \frac{P_e + 2\sqrt{(P_gP_e)}\cos(\phi_g - \phi_e)}{P_g}\right]^{1/2}$$

$$\simeq \sqrt{\frac{f_1}{2P_g}}[2P_g + P_e + 2\sqrt{(P_gP_e)}\cos(\phi_g - \phi_e)] \quad . \quad (26)$$

One could proceed, as in Section 5, to calculate first the auto-correlation function and then the spectral density, but this method is long and tedious. The Fourier transform of the function $\cos(\phi_g - \phi_e)$ has already been stated,[3] and it is quicker to derive the spectral density from this. The required Fourier transform was, in fact, shown to be

$$\frac{1}{T_s}\sum_{m=-\infty}^{\infty}\delta(f - mf_s)[F_1(f) + F_2(f) + F_3(f) + F_4(f)]$$

In Reference 3 the symbol τ was used for the time delay $2R/c$ of an echo from range R; in the present paper τ is reserved for the calculation of auto-correlation functions and expresses the echo time delay as γT_s, so that γ is a dimensionless constant less than unity in the practical case.

Originating term in $R_Q(\tau)$	Corresponding term in $G_Q(f)$	Appropriate frequency band	Value of $p = 0$ term	Maximum error if rest of series is omitted
$R_1 = 4(f_1P_g + f_2P_n)^2$	$G_1 = 4(f_1P_g + f_2P_n)^2$	D.C. component	—	—
$R_2 = \frac{8P_gP_n}{\pi^2} \sum_{-\infty}^{\infty} \frac{\sin \pi f_1(\tau - pT_s)}{\tau - pT_s} \frac{\sin \pi f_2\tau}{\tau}$	$G_{2A} = 8P_gP_n \sum_0^{\infty} \frac{1}{p\pi T_s}[\sin p\pi T_s(f_2 - 2f) + \sin p\pi T_s(f_2 + 2f)]$	$0 \leqslant 2f \leqslant f_1 - f_2, f_2 \leqslant f_1$	$16P_gP_nf_2$	$\pm 8P_gP_n/T_s$
	$G_{2B} = 16P_gP_n \sum_0^{\infty} \frac{1}{p\pi T_s} \sin p\pi T_s f_1$	$0 \leqslant 2f \leqslant f_2 - f_1, f_1 \leqslant f_2$	$16P_gP_nf_1$	$\pm 8P_gP_n/T_s$
	$G_{2C} = 8P_gP_n \sum_0^{\infty} \frac{1}{p\pi T_s}[\sin p\pi T_s(f_2 - 2f) + \sin p\pi T_s f_1]$	$\lvert f_2 - f_1\rvert \leqslant 2f \leqslant f_2 + f_1$	$8P_gP_n(f_2 + f_1 - 2f)$	$\pm 8P_gP_n/T_s$
	$G_{2D} = 0$	$f_2 + f_1 \leqslant 2f$	—	—
$R_3 = \frac{4P_n^2}{\pi^2}\left(\frac{\sin \pi f_2\tau}{\tau}\right)^2$	$G_{3A} = 8P_n^2(f_2 - f)$	$0 \leqslant f \leqslant f_2$	—	—
	$G_{3B} = 0$	$f_2 \leqslant f$	—	—

Table 2.—Linear Case—Small Signal/Noise Ratio

Originating term in $R_L(\tau)$	Corresponding term in $G_L(f)$	Appropriate frequency band	Value of $p = 0$ term	Maximum error if rest of series is omitted
$R_4 = \frac{\pi}{8f_2P_n}(f_1P_g + 2f_2P_n)^2$	$G_4 = \frac{\pi}{8f_2P_n}(f_1P_g + 2f_2P_n)^2$	D.C. component	—	—
$R_5 = \frac{P_g}{4\pi f_2} \sum_{-\infty}^{\infty} \frac{\sin \pi f_1(\tau - pT_s)}{\tau - pT_s} \frac{\sin \pi f_2\tau}{\tau}$	$G_{5A} = \frac{\pi P_g}{4f_2} \sum_0^{\infty} \frac{1}{p\pi T_s}[\sin p\pi T_s(f_2 - 2f) + \sin p\pi T_s(f_2 + 2f)]$	$0 \leqslant 2f \leqslant f_1 - f_2, f_2 \leqslant f_1$	$\frac{1}{2}\pi P_g$	$\pm\frac{1}{4}\pi \frac{P_g}{f_2T_s}$
	$G_{5B} = \frac{\pi P_g}{2f_2} \sum_0^{\infty} \frac{1}{p\pi T_s} \sin p\pi T_s f_1$	$0 \leqslant 2f \leqslant f_2 - f_1, f_1 \leqslant f_2$	$\frac{1}{2}\pi \frac{f_1P_g}{f_2}$	$\pm\frac{1}{4}\pi \frac{P_g}{f_2T_s}$
	$G_{5C} = \frac{\pi P_g}{4f_2} \sum_0^{\infty} \frac{1}{p\pi T_s}[\sin p\pi T_s(f_2 - 2f) + \sin p\pi T_s f_1]$	$\lvert f_2 - f_1\rvert \leqslant 2f \leqslant f_2 + f_1$	$\frac{1}{4}\pi \frac{P_g}{f_2}(f_2 + f_1 - 2f)$	$\pm\frac{1}{4}\pi \frac{P_g}{f_2T_s}$
	$G_{5D} = 0$	$f_2 + f_1 \leqslant 2f$	—	—
$R_6 = \frac{P_n}{8\pi f_2}\left(\frac{\sin \pi f_2\tau}{\tau}\right)^2$	$G_{6A} = \frac{\pi P_n}{4f_2}(f_2 - f)$	$0 \leqslant f \leqslant f_2$	—	—
	$G_{6B} = 0$	$f_2 \leqslant f$	—	—

Table 3.—Linear Case—Large-Signal/Noise Ratio

Originating term in $R_L(\tau)$	Corresponding term in $G_L(f)$	Appropriate frequency band	Value of $p = 0$ term	Maximum error if rest of series is omitted
$R_7 = 2f_1P_g$	$G_7 = 2f_1P_g$	D.C. component	—	—
$R_8 = \frac{P_n}{\pi^2 f_1} \sum_{-\infty}^{\infty} \frac{\sin \pi f_1(\tau - pT_s)}{\tau - pT_s} \frac{\sin \pi f_2 \tau}{\tau}$	$G_{8A} = \frac{P_n}{f_1} \sum_0^{\infty} \frac{1}{p\pi T_s} [\sin p\pi T_s(f_2 - 2f) + \sin p\pi T_s(f_2 + 2f)]$	$0 \leqslant 2f \leqslant f_1 - f_2, f_2 \leqslant f_1$	$\frac{2f_2P_n}{f_1}$	$\pm \frac{P_n}{f_1T_s}$
	$G_{8B} = \frac{2P_n}{f_1} \sum_0^{\infty} \frac{1}{p\pi T_s} \sin p\pi T_s f_1$	$0 \leqslant 2f \leqslant f_2 - f_1, f_1 \leqslant f_2$	$2P_n$	$\pm \frac{P_n}{f_1T_s}$
	$G_{8C} = \frac{P_n}{f_1} \sum_0^{\infty} \frac{1}{p\pi T_s} [\sin p\pi T_s(f_2 - 2f) + \sin p\pi T_s f_1]$	$\lvert f_2 - f_1 \rvert \leqslant 2f \leqslant f_2 + f_1$	$\frac{P_n}{f_1}(f_2 + f_1 - 2f)$	$\pm \frac{P_n}{f_1T_s}$
	$G_{8D} = 0$	$f_2 + f_1 \leqslant 2f$	—	—
$R_g = \frac{P_n^2}{8\pi^2 f_1 P_g} \left(\frac{\sin \pi f_2 \tau}{\tau}\right)^2$	$G_{9A} = \frac{P_n^2}{4f_1P_g}(f_2 - f)$	$0 \leqslant f \leqslant f_2$	—	—
	$G_{B9} = 0$	$f_2 \leqslant f$	—	—
$R_{10} = \frac{P_n^2}{16\pi^3 f_1^2 P_g} \times \sum_{-\infty}^{\infty} \frac{\sin 2\pi f_1(\tau - pT_s)}{\tau - pT_s} \left(\frac{\sin \pi f_2 \tau}{\tau}\right)^2$	$G_{10A} = \frac{P_n^2}{32f_1^2P_g} \sum_0^{\infty} \left(\frac{1}{p\pi T_s}\right)^2 [2\cos 2p\pi T_s f - \cos 2p\pi T_s(f_2 - f) - \cos 2p\pi T_s(f_2 + f)]$	$0 \leqslant f \leqslant f_1 - f_2, f_2 \leqslant f_1$	$\frac{f_2^2P_n^2}{8f_1^2P_g}$	$\pm \frac{P_n^2}{64f_1^2P_gT_s^2}$
	$G_{10B} = \frac{P_n^2}{16f_1^2P_g} \sum_0^{\infty} \left(\frac{1}{p\pi T_s}\right)^2 [\cos 2p\pi T_s f - \cos 2p\pi T_s f_1] + \frac{P_n^2}{8f_1^2P_g}(f_2 - f_1) \sum_0^{\infty} \frac{1}{p\pi T_s} \sin 2p\pi T_s f_1$	$\left.\begin{matrix} 0 \leqslant f \leqslant f_2 - f_1 \\ f_1 \leqslant f_2 \leqslant 2f_1 \end{matrix}\right\}$ and $0 \leqslant f \leqslant f_1, 2f_1 \leqslant f_2$	$\frac{P_n^2}{8f_1^2P_g}(2f_2f_1 - f_1^2 - f^2)$	$\pm \frac{P_n^2}{64f_1^2P_gT_s^2}[1 + 4(f_2 - f_1)T_s]$
	$G_{10C} = \frac{P_n^2}{32f_1^2P_g} \sum_0^{\infty} \left(\frac{1}{p\pi T_s}\right)^2 [2\cos 2p\pi T_s f - \cos 2p\pi T_s f_1 - \cos 2p\pi T_s(f_2 - f)] + \frac{P_n^2}{16f_1^2P_g}(f_2 - f_1 + f) \sum_0^{\infty} \frac{1}{p\pi T_s} \sin 2p\pi T_s f_1$	$\left.\begin{matrix} \lvert f_2 - f_1 \rvert \leqslant f \leqslant f_1 \\ 0 \leqslant f_2 \leqslant 2f_1 \end{matrix}\right\}$	$\frac{P_n^2}{16f_1^2P_g}[2f_2^2 - (f_2 - f_1 + f)^2]$	$\pm \frac{P_n^2}{64f_1^2P_gT_s^2}[1 + 2(f_2 - f_1 + f)T_s]$
	$G_{10D} = \frac{P_n^2}{8f_1^2P_g}(f_2 - f) \sum_0^{\infty} \frac{1}{p\pi T_s} \sin 2p\pi T_s f_1$	$f_1 \leqslant f \leqslant f_2 - f_1, 2f_1 \leqslant f_2$	$\frac{P_n^2}{4f_1P_g}(f_2 - f)$	$\pm \frac{P_n^2}{16f_1^2P_gT_s}(f_2 - f)$
	$G_{10E} = \frac{P_n^2}{32f_1^2P_g} \sum_0^{\infty} \left(\frac{1}{p\pi T_s}\right)^2 [\cos 2p\pi T_s f_1 - \cos 2p\pi T_s(f_2 - f)] + \frac{P_n^2}{16f_1^2P_g}(f_2 + f_1 - f) \sum_0^{\infty} \frac{1}{p\pi T_s} \sin 2p\pi T_s f_1$	$\left.\begin{matrix} f_1 \leqslant f \leqslant f_2 + f_1 \\ 0 \leqslant f_2 \leqslant 2f_1 \end{matrix}\right\}$ and $\left.\begin{matrix} f_2 - f_1 \leqslant f \leqslant f_2 + f_1 \\ 2f_1 \leqslant f_2 \end{matrix}\right\}$	$\frac{P_n^2}{16f_1^2P_g}(f_2 + f_1 - f)^2$	$\pm \frac{P_n^2}{128f_1^2P_gT_s^2}[1 + 4(f_2 + f_1 - f)T_s]$
	$G_{10F} = 0$	$f_1 + f_2 \leqslant f$	—	—

The functions $F_n(f)$ then take the form

$$\left.\begin{aligned}
F_1(f) &= \frac{\gamma T_s}{2}\exp -j\pi T_s[2\gamma f_0-(1-\gamma)f]\,\frac{\sin\pi\gamma T_s\left[f-\frac{\alpha}{\pi}(1-\gamma)T_s\right]}{\pi\gamma T_s\left[f-\frac{\alpha}{\pi}(1-\gamma)T_s\right]}\\
F_2(f) &= \frac{\gamma T_s}{2}\exp +j\pi T_s[2\gamma f_0+(1-\gamma)f]\,\frac{\sin\pi\gamma T_s\left[f+\frac{\alpha}{\pi}(1-\gamma)T_s\right]}{\pi\gamma T_s\left[f+\frac{\alpha}{\pi}(1-\gamma)T_s\right]}\\
F_3(f) &= \frac{(1-\gamma)T_s}{2}\exp +j\pi T_s(2\gamma f_0-\gamma f)\,\frac{\sin\pi(1-\gamma)T_s\left(f-\frac{\alpha}{\pi}\gamma T_s\right)}{\pi(1-\gamma)T_s\left(f-\frac{\alpha}{\pi}\gamma T_s\right)}\\
F_4(f) &= \frac{(1-\gamma)T_s}{2}\exp -j\pi T_s(2\gamma f_0+\gamma f)\,\frac{\sin\pi(1-\gamma)T_s\left(f+\frac{\alpha}{\pi}\gamma T_s\right)}{\pi(1-\gamma)T_s\left(f+\frac{\alpha}{\pi}\gamma T_s\right)}
\end{aligned}\right\}\quad(27)$$

When positive- and negative-frequency components are appropriately combined, remembering that $f=m/T_s$, $\cos(\phi_g-\phi_e)$ appears as a Fourier series

$$\begin{aligned}
&\tfrac{1}{2}A_0+\sum_{m=1}^{\infty}\{C_{m1}\cos[2\pi\gamma T_s f_0-(1-\gamma)m\pi-2m\pi f_s t]\\
&\quad+C_{m2}\cos[2\pi\gamma T_s f_0+(1-\gamma)m\pi+2m\pi f_s t]\\
&\quad+C_{m3}\cos(2\pi\gamma T_s f_0-\gamma m\pi+2m\pi f_s t)\\
&\quad+C_{m4}\cos(2\pi\gamma T_s f_0+\gamma m\pi-2m\pi f_s t)\}\quad\ldots\quad(28)
\end{aligned}$$

where

$$\begin{aligned}
C_{m1}&=\frac{\sin\gamma[m\pi-\alpha(1-\gamma)T_s^2]}{m\pi-\alpha(1-\gamma)T_s^2},\\
C_{m2}&=\frac{\sin\gamma[m\pi+\alpha(1-\gamma)T_s^2]}{m\pi+\alpha(1-\gamma)T_s^2},\\
C_{m3}&=\frac{\sin(1-\gamma)(m\pi-\alpha\gamma T_s^2)}{m\pi-\alpha\gamma T_s^2},\\
C_{m4}&=\frac{\sin(1-\gamma)(m\pi+\alpha\gamma T_s^2)}{m\pi+\alpha\gamma T_s^2}\quad\ldots\quad(29)
\end{aligned}$$

and

$$\begin{aligned}
A_0&=(C_{01}+C_{02}+C_{03}+C_{04})\cos 2\pi\gamma T_s f_0\\
&=2\,\frac{\sin\alpha\gamma(1-\gamma)T_s^2}{\alpha\gamma(1-\gamma)T_s^2}\cos 2\pi\gamma T_s f_0\quad\ldots\quad(30)
\end{aligned}$$

Proceeding to the spectral densities and substituting for V_g^2 and V_e^2, the detector outputs are thus seen to have the following distributions:

In the quadratic case

$$\left.\begin{aligned}
&\text{Power in d.c. component}=4f_1^2[P_g+A_0\sqrt{(P_gP_e)}+P_e]^2\\
&\text{Power in } m\text{th harmonic}\quad=8f_1^2P_gP_eC_m^2
\end{aligned}\right\}(31)$$

In the linear case

$$\left.\begin{aligned}
&\text{Power in d.c. component}=\frac{f_1}{2P_g}[2P_g+A_0\sqrt{(P_gP_e)}+P_e]^2\\
&\text{Power in } m\text{th harmonic}\quad=f_1P_eC_m^2
\end{aligned}\right\}(32)$$

In expressions (31) and (32), C_m is the magnitude of the composite mth harmonic term which appears within the bracket of expression (28). In Fig. 1, the amplitudes C_{m1} to C_{m4} of the

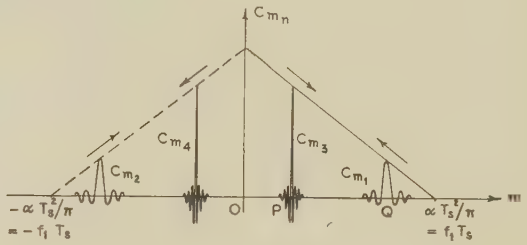

Fig. 1.—Plot of C_{m_n} against m for $\gamma=0{\cdot}25$.

individual terms are plotted against m for $\gamma=0{\cdot}25$. Observation of a target at the corresponding range involves study of the region around the point P at the centre of the C_{m3} envelope; when γ exceeds $0{\cdot}5$, the C_{m1} spike will be the larger, and, if preferred, attention may then be diverted to the region around Q. If no significant overlapping of the individual envelopes arises (as in the example shown) C_m is, to a close approximation, equal to C_{m3} for observation around P, or to C_{m1} for observation around Q.

As γ increases, the envelopes move in the directions of the arrows (near their tips). At very short range indeed, there is overlapping between C_{m3} and C_{m4} and both contribute significantly to C_m; at mid-range, C_{m1} and C_{m3} overlap; and as γ approaches unity there begins to be overlapping near zero frequency between C_{m1} and C_{m2}.

If such overlapping occurs, it becomes evident as a rapid beating of the echo for comparatively small variations in γ or for slight drifting of the carrier frequency f_0, since typical signal components with amplitudes C_{m1} and C_{m3} (to take one possible example) have a phase difference $(4\gamma f_0T_s-m)\pi$.

(7) CHOICE OF PRE-DETECTOR BANDWIDTH f_2

To estimate signal/noise ratio in the post-detector stages of an f.m. radar receiver, both the pre-detector bandwidth f_2 and the post-detector bandwidth f_3 must be known.

Considerations of noise power notwithstanding, f_2 must be adequate to convey both reference signal and echo to the detector without under distortion. Each is a frequency-modulated oscillation of the general form $V\sin(n\omega_0T_s+\omega_0t_n+\alpha t_n^2)$ whose spectrum is a line group with separation $1/T_s$ centred upon the carrier frequency f_0 as shown in Fig. 2, which shows the width of the envelope to be f_1 at the 6 dB points and $f_1+3{\cdot}15\sqrt{(f_1/T_s)}$ at the 20 dB points. For practical values of the parameters, $\sqrt{(f_1/T_s)}\ll f_1$; thus the minimum safe value for f_2 can be taken to be somewhat greater than f_1. We shall now examine the effects on signal/noise ratio of increasing f_2 beyond this value.

In Fig. 3 'unwanted power' (i.e. power due to normal rectification of reference signal or noise, or due to interaction between them) is plotted against frequency. As in Fig. 1, the horizontal scale is equivalent to a scale of target range; echo positions could be readily superimposed and signal/noise ratios derived.

The results shown in Fig. 3(*a*) for the case of the quadratic

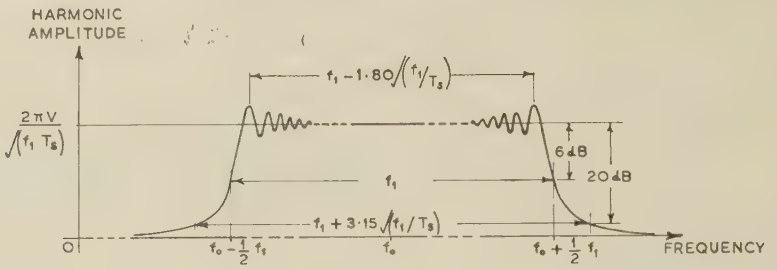

Fig. 2.—Envelope of line spectrum of reference signal or echo.

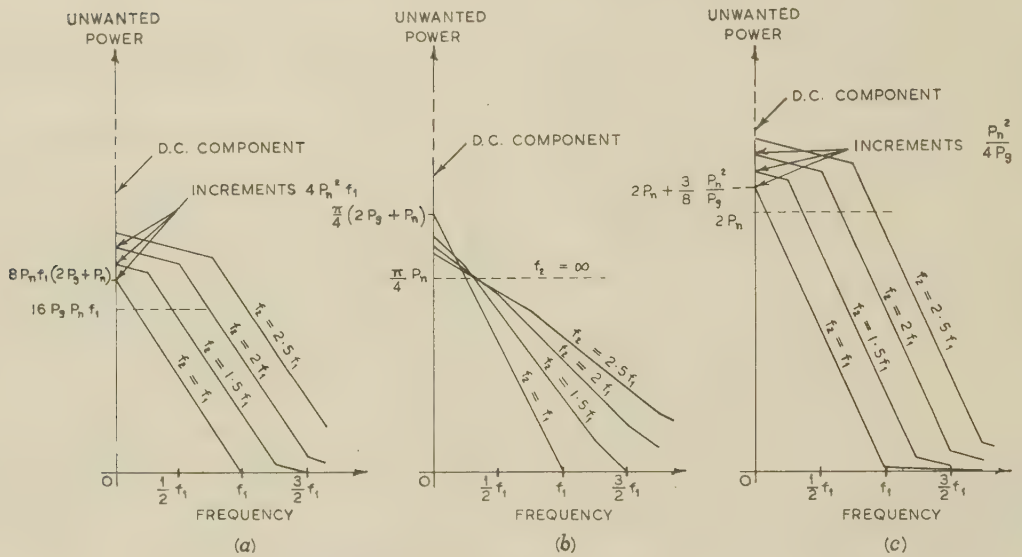

Fig. 3.—'Unwanted power' plotted against frequency for various values of pre-detector bandwidth f_2.
(*a*) Quadratic detector.
(*b*) Linear detector. Small signal/noise ratio.
(*c*) Linear detector. Large signal/noise ratio.

detector, and in Fig. 3(*c*) for the linear detector with large signal/noise ratio, are exactly those one would expect. At all frequencies, an increase in pre-detector bandwidth leads to an increase in unwanted power. For small signal/noise ratios, however, the situation is different. Integration over all frequencies shows the total unwanted power to be

$$\frac{\pi}{8f_2P_n}(f_1^2P_g^2 + 6f_1f_2P_gP_n + 5f_2^2P_n^2)$$

This increases with f_2 provided that

$$f_2 \geqslant \frac{f_1P_g}{\sqrt{5}P_n}$$

and this will be satisfied for all values of f_2 which are acceptable on distortion grounds. But although the total unwanted power increases with f_2, it is also redistributed; some goes into the d.c. component and some migrates towards the high-frequency end of the spectrum. Thus, for very small targets at relatively short range, an increase in f_2 beyond the minimum could produce a decrease in unwanted power at the low frequencies on which observation is concentrated. This distinction between the large and small signal/noise ratio cases is somewhat analogous to 'capture effect' in the field of f.m. communications.

A significant difference may also be noted between the results shown, for example, in Fig. 3(*a*) and the corresponding frequency distribution for a.m.c.w. or unmodulated c.w. cases.* For each of the latter types of signal, that part of the spectrum which arises from intermodulation between the noise and the c.w. oscillation consists of one or more constant-amplitude 'blocks', whereas there are no comparable amplitude steps in the frequency-modulation case. Instead, there is a continuous decrease with rising frequency.

(8) EFFECT OF POST-DETECTOR BANDWIDTH f_3

The bandwidth f_3 of the post-detector circuits will affect both wanted power (due to interaction of echo and reference signal) and unwanted power. In Reference 3, the authors examined the possibility of using a coherent system with phase-sensitive detection and a bandwidth sufficiently narrow to isolate a single spectral line. This would give extreme sensitivity at the price of a very low information rate. Other applications might well demand a non-coherent detector feeding a bank of narrow-band filters, with mid-frequencies increasing progressively, to distribute echoes automatically into their correct range channels. Such an arrangement could provide continuous data output in readily usable form at the expense of some sacrifice in range resolution and target discrimination. These systems would call for post-detector bandwidths ranging from f_s to, perhaps, $10f_s$.

* See, for example, Reference 6, pp. 157–160.

and we shall discuss the implication of variations within this range.

One might say intuitively that the narrowest practicable value of f_3 will give rise to the best signal/noise ratio, and this verdict is borne out by the analysis. Fig. 3 shows the spectral density of the unwanted power for a variety of conditions and parameters, and, in all cases, the power spectra are continuous. The unwanted power is computed by integrating $G(f)$ throughout the post-detector pass band, and for values of f_3 such as are considered here, this integral is, to a very fair approximation, the product of f_3 and $G(f)$. Thus the unwanted power is seen to increase in a sensibly linear way with f_3.

The echo power from an ideal stationary target is contained in a spectrum of discrete lines, being bounded by an envelope of form $(\sin u)/u$ as described in Section 6. Not only is the height of the spectrum envelope dependent on the range factor γ for a given echo, but so is the width of the envelope between zeros, and hence the relative amplitudes of the several lines passed by post-detector stages having a bandwidth greater than f_s. The growth of signal power with bandwidth will thus vary with target range. Summation of the power contributions from neighbouring lines leads to the data presented in Fig. 4, which shows (for an ideal target) the ratio of the power available from post-detector stages having a given bandwidth $f_3 > f_s$ to that available when the bandwidth is just f_s.

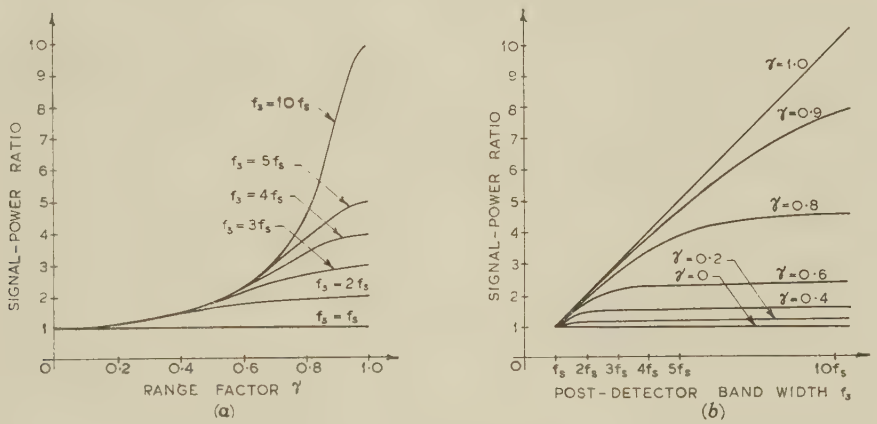

Fig. 4.—Graphs showing the ratio of signal power for given post-detector bandwidths f_3 to signal power when the post-detector bandwidth is f_s.

The data have been plotted against γ in Fig. 4(*a*) and against f_3 in Fig. 4(*b*), and the following facts emerge:

(*a*) For short- and medium-range targets ($\gamma \leqslant 0{\cdot}6$), no useful increase in signal power can be obtained by increasing f_3 beyond $3f_s$ or $4f_s$.

(*b*) For long-range targets ($\gamma \geqslant 0{\cdot}8$), the signal power can be usefully increased by using bandwidths as great as $10f_s$ if considerations of resolution permit.

(*c*) Only for $\gamma = 1{\cdot}0$ does signal power increase linearly with post-detector bandwidth. As unwanted power is proportional to f_3 at all ranges, it follows that no improvement in signal/noise ratio can be hoped for from any widening of the post-detector pass band.

At first sight, the replacement of a continuous-band filter by a 'comb' filter having several very narrow pass bands of widths f_s/β, each centred upon a spectral line, might enable the signal/noise ratio to be improved by a factor β. In practice, however, such a filter could only cope adequately with stationary targets. For moving targets, the lines will experience a Doppler shift; where there is turbulence in the signal path leading to random fluctuations of propagation coefficient, the lines will be broadened and may even form a continuous spectrum. This broadening will also occur when fading superimposes an amplitude modulation on the frequency modulation of the received oscillation.

(9) CONCLUSION

The method developed in the foregoing Section leads to expressions for 'wanted' and 'unwanted' power at the output terminals of the linear or quadratic detector of a f.m. radar receiver. The expressions are in such a form that signal/noise ratio may be readily computed from them. The approximations on which the method depends are shown to be valid if the product of pre-detector bandwidth and sweep duration is of the order of 100, and this condition is one which will be satisfied in the majority of practical applications.

The most powerful signal to be considered will almost always be the reference signal; this must in any case be present at a high enough power level for heterodyning purposes. Under these conditions, no improvement in signal/noise ratio will accrue from the use of a pre-detector bandwidth any wider than that which is necessary to convey signals to the detector without undue distortion.

If maximum sensitivity is sought, the bandwidth of the post-detector filters or amplifiers should be kept as small as possible, though difficulty may then arise in dealing with moving targets. The need for improved information rate or for a readily processed data output may, however, demand a somewhat wider post-detector bandwidth. Such a compromise would not seriously affect signal power at long range, as the greatest deterioration would be experienced at short ranges when power can be most readily spared.

(10) ACKNOWLEDGMENT

The authors gratefully acknowledge the facilities made available to them at the Royal Military College of Science. They wish to thank the Dean for permission to publish the paper.

(11) REFERENCES

(1) KEEP, D. N.: 'Frequency Modulation Radar for use in the Mercantile Marine', *Proceedings I.E.E.*, Paper No. 1940 R, November, 1955 (**103** B, p. 523).

(2) GNANALINGAM, S.: 'An Apparatus for the Detection of Weak Ionospheric Echoes', *ibid.*, Paper No. 1670, July, 1954 (**101**, Part III, p. 243).

(3) HYMANS, A. J., and LAIT, J.: 'Analysis of a Frequency-Modulated Continuous-Wave Ranging System', *ibid.*, Paper No. 3264 E, July, 1960 (**107** B, p. 365).
(4) KAY, L.: 'A Comparison between Pulse and Frequency Modulation Echo Ranging Systems', *Journal of the British Institution of Radio Engineers*, 1959, **19**, p. 105.
(5) TUCKER, D. G.: 'Underwater Echo Ranging', *ibid.*, 1956, **16**, p. 243.
(6) LAWSON, J. L., and UHLENBECK, G. E.: 'Threshold Signals', M.I.T. Radiation Laboratory Series, Vol. 24 (McGraw-Hill, 1950), p. 151.
(7) WOODWARD, P. M.: 'Probability and Information Theory, with Application to Radar' (Pergamon Press, 1953), p. 27.
(8) THE BATEMAN MANUSCRIPT PROJECT: 'Tables of Integral Transforms', Vol. I, California Institute of Technology (McGraw-Hill, 1954).
(9) OBERHETTINGER, F.: 'Tabellen zur Fourier Transformation' (Springer-Verlag, 1957).

(12) APPENDIX

BY J. LAIT

(12.1) Fourier Transforms needed in the Derivation of G(f)

In Section 5.2, it becomes necessary to use certain Fourier transforms which do not appear in the standard tables.[8, 9]

(12.1.1) Fourier Transform of $\frac{\sin a(\tau-b)}{\tau-b}\frac{\sin c\tau}{\tau}$.

The Tables quote the transform of $\frac{\sin a\tau}{\tau}$, whence that for $\frac{\sin a(\tau-b)}{\tau-b}$ follows as $\int_{-\infty}^{\infty}\frac{\sin a(\tau-b)}{\tau-b}\varepsilon^{-j2\pi f\tau}d\tau$

$$=\varepsilon^{-j2\pi fb}\int_{-\infty}^{\infty}\frac{\sin a\tau}{\tau}\varepsilon^{-j2\pi f\tau}d\tau$$

The relationship $\int_{-\infty}^{\infty}\frac{\sin a(\tau-b)}{\tau-b}\frac{\sin c\tau}{\tau}\varepsilon^{-j2\pi f\tau}d\tau$

$=\frac{1}{2}\int_0^c\int_0^{\infty}\frac{\sin a(\tau-b)}{\tau-b}[\varepsilon^{-j(2\pi f-q)\tau}+\varepsilon^{-j(2\pi f+q)\tau}]d\tau dq$ enables the transform of $\frac{\sin a(\tau-b)}{\tau-b}\frac{\sin c\tau}{\tau}$ to be obtained. It takes the form given in Table 4.

(12.1.2) Fourier Transform of $\frac{\sin a(\tau-b)}{\tau-b}\left(\frac{\sin c\tau}{\tau}\right)^2$.

The transform of $\frac{\sin a(\tau-b)}{\tau-b}\left(\frac{\sin c\tau}{\tau}\right)^2$ may now be obtained by further integration.

$$\int_{-\infty}^{\infty}\frac{\sin a(\tau-b)}{\tau-b}\left(\frac{\sin c\tau}{\tau}\right)^2\varepsilon^{-j2\pi f\tau}d\tau$$

$$=\frac{1}{2}\int_0^{2c}\int_{-\infty}^{\infty}\frac{\sin a(\tau-b)}{\tau-b}\frac{\sin q\tau}{\tau}\varepsilon^{-j2\pi f\tau}d\tau dq$$

The resulting forms are given in Table 5.

(12.1.3) Extraction of Expressions for G(f).

As Woodward[7] points out, the Fourier transform suggests a frequency spectrum containing both positive- and negative-frequency components. For a real time function, these combine so that their real parts reinforce and their imaginary parts cancel.

Table 4

Range for $2\pi f$	Fourier transform
$2\pi f \leqslant -a-c$	0
$-a-c \leqslant 2\pi f \leqslant -a+c$ when $a \geqslant c$ $-a-c \leqslant 2\pi f \leqslant -c+a$ when $c \geqslant a$	$\frac{\pi}{2jb}(\varepsilon^{jab}-\varepsilon^{-j(2\pi f+c)b})$
$-a+c \leqslant 2\pi f \leqslant a-c$ when $a \geqslant c$	$\frac{\pi}{2jb}(\varepsilon^{-j(2\pi f-c)b}-\varepsilon^{-j(2\pi f+c)b})$
$-c+a \leqslant 2\pi f \leqslant c-a$ when $c \geqslant a$	$\frac{\pi}{2jb}(\varepsilon^{jab}-\varepsilon^{-jab})$
$a-c \leqslant 2\pi f \leqslant a+c$ when $a \geqslant c$ $c-a \leqslant 2\pi f \leqslant a+c$ when $c \leqslant a$	$\frac{\pi}{2jb}(\varepsilon^{-j(2\pi f-c)b}-\varepsilon^{-jab})$
$a+c \geqslant 2\pi f$	0

For example, the contributions from the two transforms marked* in Table 5 combine in the following manner:

The lower of the two expressions gives a positive-frequency contribution

$$\frac{\pi}{4b^2}(2\varepsilon^{-j2\pi fb}-\varepsilon^{-jab}-\varepsilon^{-j2b(\pi f-c)})-\frac{\pi}{4jb}(2c-a+2\pi f)\varepsilon^{-jab}$$

and the upper expression gives a negative-frequency contribution

$$\frac{\pi}{4b^2}(2\varepsilon^{j2\pi fb}-\varepsilon^{jab}-\varepsilon^{-j2b(-\pi f+c)})+\frac{\pi}{4jb}(2c-a+2\pi f)\varepsilon^{jab}$$

These exponential terms combine to produce

$$\frac{\pi}{2b^2}[2\cos 2\pi fb-\cos ab-\cos 2b(\pi f-c)]$$

$$-\frac{\pi}{2b}(2c-a+2\pi f)\sin ab,$$

and with the relevant substitutions ($a=2\pi f_1$, $b=pT_s$, $c=\pi f_2$) this leads directly to the form stated for $G_{10c}(f)$ in Table 3.

It remains merely to sum certain series over the range $p=0$ to $p=+\infty$. In each series, the $p=0$ term has been stated separately, the rest of the series being treated as a correction.

We require $\sum_1^{\infty}\frac{\sin p\theta}{p}$ and $\sum_1^{\infty}\frac{\cos p\theta}{p^2}$ for various values of θ.

If $0\leqslant\theta\leqslant 2\pi$, $\sum_1^{\infty}\frac{\sin p\theta}{p}=\frac{1}{2}(\pi-\theta)$. If $2N\pi\leqslant\theta\leqslant 2(N+1)\pi$ we may write $\theta_N=\theta-2N\pi$

whence $\sum_1^{\infty}\frac{\sin p\theta}{p}=\sum_1^{\infty}\frac{\sin p\theta_N}{p}=\frac{1}{2}(\pi-\theta_N)$

which must always lie between $\pm\frac{1}{2}\pi$.

In the same way $\sum_1^{\infty}\frac{\cos p\theta}{p^2}=\frac{1}{4}(\pi-\theta_N)^2-\frac{1}{12}\pi^2$ which must always lie between $-\frac{1}{12}\pi^2$ and $+\frac{1}{6}\pi^2$.

Thus the tolerances stated in the final columns of Tables 1–3 of Section 5.2 may be readily computed.

Table 5

Range for $2\pi f$	Fourier transform
$2\pi f \leqslant -2c - a$	0
$-2c - a \leqslant 2\pi f \leqslant -a$ when $0 \leqslant c \leqslant a$ $-2c - a \leqslant 2\pi f \leqslant -2c + a$ when $a \leqslant c$	$\frac{\pi}{4b^2}(\varepsilon^{jab} - \varepsilon^{-j2b(\pi f+c)}) + \frac{\pi}{4jb}(2c + a + 2\pi f)\varepsilon^{jab}$
$-2c + a \leqslant 2\pi f \leqslant -a$ when $a \leqslant c$	$\frac{\pi}{4b^2}(\varepsilon^{jab} - \varepsilon^{-jab}) + \frac{\pi}{4jb}(2c + a + 2\pi f)\varepsilon^{jab} - \frac{\pi}{4jb}(2c - a + 2\pi f)\varepsilon^{-jab}$
$-a \leqslant 2\pi f \leqslant -a + 2c$ when $0 \leqslant 2c \leqslant a$ $-a \leqslant 2\pi f \leqslant -2c + a$ when $a \leqslant 2c \leqslant 2a$	$\frac{\pi}{4b^2}(2\varepsilon^{-j2\pi fb} - \varepsilon^{jab} - \varepsilon^{-j2b(\pi f+c)}) + \frac{\pi}{4jb}(2c - a - 2\pi f)\varepsilon^{jab}$ *
$-a + 2c \leqslant 2\pi f \leqslant a - 2c$ when $0 \leqslant 2c \leqslant a$	$\frac{\pi}{4b^2}(2\varepsilon^{-j2\pi fb} - \varepsilon^{-j2b(\pi f-c)} - \varepsilon^{-j2b(\pi f+c)})$
$-a \leqslant 2\pi f \leqslant a$ when $a \leqslant c$ $-2c + a \leqslant 2\pi f \leqslant 2c - a$ when $a \leqslant 2c \leqslant 2a$	$\frac{\pi}{4b^2}(2\varepsilon^{-j2\pi fb} - \varepsilon^{jab} - \varepsilon^{-jab}) + \frac{\pi}{4jb}(2c - a - 2\pi f)\varepsilon^{jab} - \frac{\pi}{4jb}(2c - a + 2\pi f)\varepsilon^{-jab}$
$a - 2c \leqslant 2\pi f \leqslant a$ when $0 \leqslant 2c \leqslant a$ $2c - a \leqslant 2\pi f \leqslant a$ when $a \leqslant 2c \leqslant 2a$	$\frac{\pi}{4b^2}(2\varepsilon^{-j2\pi fb} - \varepsilon^{-jab} - \varepsilon^{-j2b(\pi f-c)}) - \frac{\pi}{4jb}(2c - a + 2\pi f)\varepsilon^{-jab}$ *
$a \leqslant 2\pi f \leqslant 2c - a$ when $a \leqslant c$	$\frac{\pi}{4b^2}(\varepsilon^{-jab} - \varepsilon^{jab}) + \frac{\pi}{4jb}(2c - a - 2\pi f)\varepsilon^{jab} - \frac{\pi}{4jb}(2c + a - 2\pi f)\varepsilon^{-jab}$
$a \leqslant 2\pi f \leqslant 2c + a$ when $0 \leqslant c \leqslant a$	$\frac{\pi}{4b^2}(\varepsilon^{-jab} - \varepsilon^{-j^2b(\pi f-c)}) - \frac{\pi}{4jb}(2c + a - 2\pi f)\varepsilon^{-jab}$
$2c + a \leqslant 2\pi f$	0

*See Section 12.1.3.

621.313.361

The Institution of Electrical Engineers
Monograph No. 413 U
Nov. 1960

QUANTITATIVE TREATMENT OF THREE-PHASE BRUSH-SHIFTING SERIES COMMUTATOR MOTOR

By O. E. MAINER, M.Sc.(Tech.), Associate Member.

(*The paper was first received 24th February, and in revised form 2nd August*, 1960. *It was published as an* INSTITUTION MONOGRAPH *in November*, 1960.)

SUMMARY

Previous quantitative treatments appear to have ignored the loss component of motor current. In this paper an approximate equivalent circuit, which makes allowance for this component, is developed from first principles. A method is devised for correcting the errors introduced by the approximate treatment so as to obtain an accurate solution. The average percentage errors in motor current, power factor and input obtained by both approximate and accurate treatments are given for a wide range of operating conditions.

LIST OF SYMBOLS

I = Total motor current.
I_L = Transformer magnetizing current.
I_{n1}, I_{n2} = M.M.F. components of stator and rotor currents.
I_p, I_{p2} = Loss components of stator and rotor currents.
$k = N_{2m}/N_{1m}$ = Effective rotor/stator turns ratio.
$k_1 = N_1/N_2$ = Transformer primary/secondary turns ratio.
L_1, L_2 = Stator and rotor inductances.
M = Mutual stator/rotor inductance.
P_{si}, P_{ri}, P_p = Stator iron, rotor iron and brush parasitic current losses.
R_{1e}, R_{2e} = Effective stator and rotor resistances.
R_t = Transformer short-circuit resistance.
R_{t1}, R_{t2} = Transformer primary and secondary effective resistances.
V_s = Supply voltage per phase.
V, V_1, V_2 = Total, stator and rotor internal e.m.f.'s per phase.
X_L = Transformer magnetizing reactance.
X_{m1} = Stator magnetizing reactance.
X_1, X_2 = Stator and rotor leakage reactances.
X_t = Transformer short-circuit reactance.
X_{t1}, X_{t2} = Transformer primary and secondary leakage reactances.
Z_1, Z_2 = Stator and rotor leakage impedances.
Z_M = Total impedance of ideal motor.
α = Brush shift, in a direction against that of rotation, from the high-impedance neutral position.
θ, β = Angles between vectors.

(1) INTRODUCTION

The 3-phase series commutator motor was invented by Görges[1] in 1891 and initially developed in Germany. During the first 15 years of the present century a number of theoretical papers, nearly all of a qualitative nature, appeared in the German technical Press. However, interest in this motor seems to have waned until fairly recently, possibly because 3-phase motors with shunt characteristics have wider fields of application. Probably the most thorough theoretical investigation into the properties of this motor was that of Dreyfus and Hillebrand.[2] A more recent contribution to the theory is that of Stix.[3] An equivalent circuit for the simple motor was developed by Kostenko.[4] More recently Adkins and Gibbs[5] have shown that the equivalent circuit of a stator-fed shunt commutator motor may be modified to suit the series motor. Quantitative treatments have been contributed by Dreyfus and Hillebrand,[2] Kostenko[6] and Kleist.[7] In all of these the loss component of motor current is neglected. A recent paper dealing with the characteristics of the motor has been published by Hibbert.[8]

Since the theory of this motor has not been widely publicized in the British technical Press, it has been developed from first principles in the present paper.

(2) M.M.F. COMPONENT OF CURRENT, I_n

In its simplest form the motor comprises a 3-phase stator winding having three terminals connected to brushes occupying positions separated by 120° (electrical) on the commutator of a wound rotor. The mesh formed by the rotor winding may be replaced by an equivalent star winding, as shown in Fig. 1.

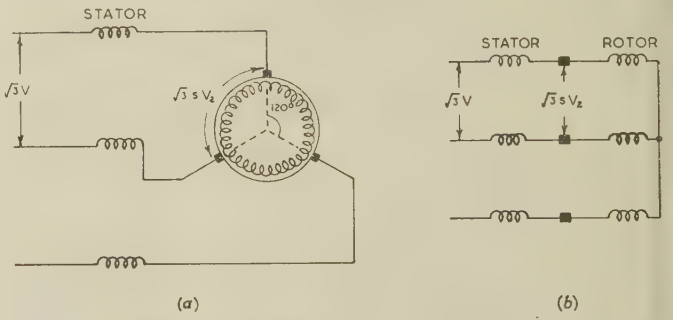

Fig. 1.—(*a*) Simple motor connections.
(*b*) Equivalent rotor star winding.

The normal practice with transformers, induction motors and other machines in which the secondary current is set up by an induced e.m.f. is to divide the primary current into two components: one component neutralizes the m.m.f. of the secondary current; the other is often loosely referred to as the magnetizing component. It is not a true magnetizing current, because, in addition to providing flux, it also provides for the iron losses. In the treatment used here it has also been found convenient to divide the current into two components. One of these supplies the iron losses and brush parasitic-current losses, and has its m.m.f. neutralized by iron-loss currents and brush parasitic currents. The other and major component of the current in both windings is free to produce flux and in this sense is a magnetizing current, although, by reference to the internal e.m.f., it is vectorally divisible into active and reactive currents. In most literature on this motor the reactive component is referred to as the magnetizing component. In the present paper

Correspondence on Monographs is invited for consideration with a view to publication.
Mr. Mainer is Principal Lecturer in Electrical Engineering, Royal Military College of Science.

here is no subdivision of this major component of current: it is denoted by I_n and will be referred to as the m.m.f. component.

(3) LOSS COMPONENT OF CURRENT, I_p

The voltages induced in the stator iron, the rotor iron and the coils short-circuited by the brushes set up iron-loss currents and brush parasitic currents. Because the brush contact resistance is large compared with the reactance of a short-circuited coil, the brush parasitic currents can without appreciable error be treated as pure loss currents. The magnetizing effect of all these loss currents is neutralized by a corresponding flow of active or loss current through the stator and rotor windings, which combine to act as one stationary winding in which a loss current, I_p, sets up the required neutralizing m.m.f.

So far as the induced rotor losses are concerned, the motor behaves in the same way as an induction motor. The gap power in respect of these losses is P_g, which is divisible into two parts, $(1 - s)P_g$ doing mechanical work and sP_g representing the power dissipated in the rotor. If the brush parasitic loss is P_p and the rotor iron loss is P_{ri} it follows that $sP_g = P_p + P_{ri}$, so that $P_g = (P_p + P_{ri})/s$. Adding the stator iron loss, P_{si}, the total input in respect of induced loss currents is $P_{si} + (P_p + P_{ri})/s$, so that the primary loss current I_p flowing through the stator and rotor winding is

$$I_p = -\frac{\frac{1}{3}\left(P_{si} + \frac{P_p + P_{ri}}{s}\right)}{V} \quad . \quad . \quad . \quad (1)$$

If a 1 : 1 transformer is placed between the stator and the rotor, quite clearly it cannot effect the flow of current I_p in the stator and rotor windings. However, if the stator/rotor transformer has a primary/secondary turns ratio of k_1, the loss component of current on the secondary side is

$$I_{p2} = k_1 I_p \quad . \quad . \quad . \quad . \quad . \quad . \quad . \quad (2)$$

Although I_p and I_{p2} are termed loss components, it will be realized that the portion given by $(P_p + P_{ri})/3sV$ represents gap power, of which only the part $(P_p + P_{ri})/3V$ is wasted in rotor losses.

(4) E.M.F. EQUATION

With the simple arrangement shown in Fig. 1 both windings carry the same current, so that, with the brushes placed in the neutral position, the e.m.f. in a stator phase is given by

$$-V_1 = jI_n\omega L_1 + jI_n\omega M$$

Here ωL_1 is the stator magnetizing reactance and may be denoted by X_{m1}. Moreover, if the ratio of the effective turns per phase in the equivalent rotor star winding to the effective turns per stator phase is denoted by k, the mutual inductance is $M = kL_1$, so that

$$-V_1 = jI_nX_{m1}(1 + k)$$

If now the rotor brushes are rocked out of the neutral position and against the rotating fields through angle α, the contribution of the rotor m.m.f. to the stator e.m.f. is retarded by angle α and becomes $jI_n\omega M\varepsilon^{-j\alpha}$, so that

$$-V_1 = jI_nX_{m1}(1 + k\varepsilon^{-j\alpha})$$

Similar considerations show that the standstill e.m.f. in a phase of the equivalent star rotor winding is

$$-V_2 = jI_n\omega L_2 + jI_n\omega M\varepsilon^{j\alpha}$$
$$= jI_nX_{m1}(k^2 + k\varepsilon^{j\alpha})$$

At a speed giving a fractional slip s, the rotor e.m.f. becomes

$$-sV_2 = jI_nX_{m1}(sk^2 + sk\varepsilon^{j\alpha})$$

and the total e.m.f. in both phase windings is

$$-V = jI_nX_{m1}(1 + k\varepsilon^{-j\alpha} + sk^2 + sk\varepsilon^{-j\alpha}) \quad . \quad (3)$$

(5) EQUIVALENT CIRCUIT OF SIMPLE SERIES MOTOR

The m.m.f. component I_n and loss component I_p combine to give the motor current I which flows through the leakage impedances of the stator and rotor windings, corresponding to the equivalent circuit shown in Fig. 2.

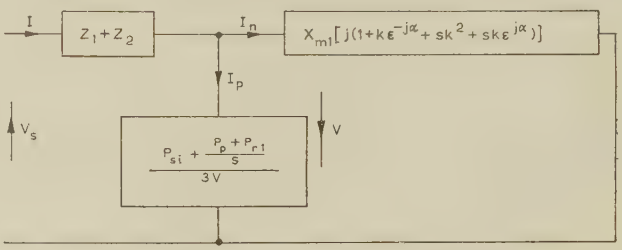

Fig. 2.—Equivalent circuit for simple series motor.

(6) MOTOR WITH STATOR/ROTOR TRANSFORMER

It is desirable to prevent the voltage induced in an armature coil from appreciably exceeding 2 volts, so as to limit the parasitic-current loss and ensure satisfactory commutation. To avoid the cost of a commutator with an excessively large number of segments, it is normal practice to employ some voltage step-down device for reducing the voltage applied to the commutator. In the series brush-shifting commutator motor a step-down transformer is placed between stator and rotor, thereby reducing the transformer rating to that of the rotor. It is normal to employ a gapped transformer with a magnetizing reactance adjusted to be about equal to that of the rotor reactance referred to the primary of the transformer, since this lowers the no-load speed limit to a safe value. The presence of this transformer produces a marked change in the speed/torque characteristic. Theoretically, a motor without transformer or with a step-down transformer between the supply and the stator is unstable at low speeds, although in practice it seems doubtful whether instability would exist in modern motors. At low speeds the rotor voltage would increase to such a high value that the auxiliary torques due to rotor iron losses and to parasitic currents induced in the coils short-circuited by the brushes would be likely to more than compensate for the reduction in the torque due to series motor action. However, excessive parasitic currents would burn both brushes and commutator. On the other hand, the presence of a stator/rotor transformer enables the motor to develop appreciable low-speed torques without generating injurious parasitic brush currents.

(6.1) Motor and Transformer Without Leakage Impedance or Losses

In order to establish the theory of the motor with stator/rotor transformer, it is convenient to neglect the losses and assume that neither motor nor transformer has either leakage reactance or resistance, giving the equivalent circuit shown in Fig. 3.

A comparison with Section 5 shows that the e.m.f.'s in the stator and rotor are given by

$$-V_1 = jI_{n1}X_{m1} + jI_{n2}kX_{m1}\varepsilon^{-j\alpha} \quad . \quad . \quad . \quad (4)$$

$$-sV_2 = jI_{n2}sk^2X_{m1} + jI_{n1}skX_{m1}\varepsilon^{j\alpha} \quad . \quad . \quad . \quad (5)$$

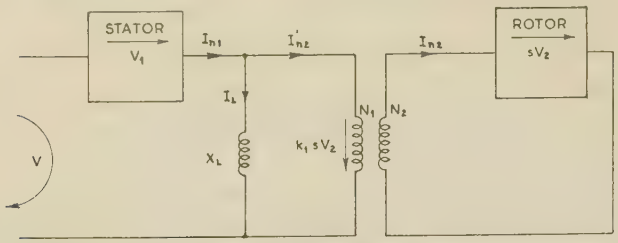

Fig. 3.—Equivalent circuit of ideal motor and transformer.

With a magnetizing reactance of X_L, a transformer magnetizing current of I_L and a transformer ratio of k_1,

$$I_L = I_{n1} - I'_{n2} = I_{n1} - \frac{I_{n2}}{k_1}$$

But

$$I_L = -\frac{k_1 s V_2}{jX_L}$$

and substituting the value of sV_2 given by eqn. (5) gives

$$I_L = I_{n2} s k_1 k^2 \frac{X_{m1}}{X_L} + I_{n1} s k_1 k \frac{X_{m1}}{X_L} \varepsilon^{j\alpha}$$

Combining these two equations in I_L gives

$$I_{n2} = k_1 I_{n1} \frac{X_L - s k_1 k X_{m1} \varepsilon^{j\alpha}}{X_L + s k_1^2 k^2 X_{m1}} \quad . \ . \ . \quad (6)$$

The total internal e.m.f. on the primary side is $V = V_1 + sk_1 V_2$ and substituting the value of I_{n2} obtained from eqn. (6) in eqns. (4) and (5) gives

$$-V = \frac{I_{n1} X_L X_{m1}}{X_L + s k_1^2 k^2 X_{m1}} [j(1 + k_1 k \varepsilon^{-j\alpha} + s k_1^2 k^2 + s k_1 k \varepsilon^{j\alpha})] \quad (7)$$

The motor impedance is therefore

$$Z_M = \frac{X_L X_{m1}}{X_L + s k_1^2 k^2 X_{m1}} [\qquad] \quad . \ . \ . \quad (8)$$

If the transformer magnetizing reactance is so large as to make I_L negligible, the motor impedance is

$$Z_M = X_{m1} [\qquad]$$

Thus the effect of the magnetizing reactance of the transformer is to alter the magnitude of the motor impedance in the ratio $X_L/(X_L + sk_1^2 k^2 X_{m1})$ without changing the power factor.

It is apparent from eqn. (8) that the motor impedance becomes infinitely large at the supersynchronous speed corresponding to

$$s = -\frac{X_L}{k_1^2 k^2 X_{m1}}$$

Now $k^2 X_{m1}$ is the rotor magnetizing reactance and $k_1^2 k^2 X_{m1}$ is that reactance referred to the primary side. If $X_L = sk_1^2 k^2 X_{m1}$, zero current occurs at $s = -1$ and zero torque is developed by series-motor action at twice synchronous speed. The no-load speed is therefore limited to some lower value depending on the rotational losses, and the motor cannot attain dangerously high speeds.

(6.2) Approximate Equivalent Circuit

The equivalent circuit of the ideal motor and transformer shown in Fig. 3 may be more simply represented by connecting the impedance Z_M of eqn. (8) across the voltage V. If a parallel branch is now added to carry the current I_p evaluated from eqn. (1), and the leakage impedance $Z_{12} = Z_1 + Z'_2 = Z_1 + k_1 Z_2$

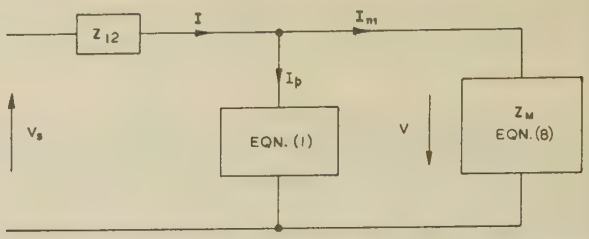

Fig. 4.—Approximate equivalent circuit for motor with stator/rotor transformer.

is inserted, the approximate equivalent circuit shown in Fig. 4 is obtained.

In this circuit no allowance has been made for the transformer iron loss, P_t, which gives rise to a loss current in the transformer primary given by

$$I_{pt} \simeq \frac{P_t}{3k_1 s V_2}$$

where $k_1 sV_2$ is the primary e.m.f. in the transformer obtained by neglecting the leakage-impedance voltage drop on the secondary side.

This current is not reflected into the secondary side and is in phase opposition to the internal primary e.m.f. of the transformer and therefore not in phase with I_p. Like the transformer magnetizing component I_L, the current I_{pt} produces an m.m.f. in the stator winding. However, with the gapped transformers normally employed, this current is extremely small compared with I_L and can be safely neglected without introducing any significant error.

Apart from the iron-loss component of the transformer, which has no significant effect, there are two errors in the circuit shown in Fig. 4. First, the primary current contains the component I_L, but there is no secondary component corresponding to I_L, so that the volt drop IZ'_2 is too large by the amount $I_L Z'_2$. Secondly, the assumption is made that

$$I_L = -\frac{k_1 s V_2}{jX_L}$$

whereas the voltage behind I_L opposes the transformer primary e.m.f. and is given by $V_{t1} = k_1(-sV_2 + I_2 Z_2)$. Consequently I_L as evaluated by this equivalent circuit is too small.

So far as the relationship between mains voltage and current is concerned, these errors are partly self-compensating. By under estimating I_L this approximate method should give slightly optimistic values for the power factor.

(6.3) Evaluation of Approximate Equivalent Circuit

Many of the motor parameters are non-linear, so that a solution of the equivalent circuit shown in Fig. 4 is possible only by the method of successive approximations. For a given supply voltage V_s, brush angle α and slip s, it is necessary to guess the internal e.m.f., V. The vector relationship of the internal e.m.f.'s is shown in Fig. 5, from which it can be seen that

$$V_1 = \frac{V}{\sqrt{[1 + 2sk_1 k \cos\alpha + (sk_1 k)^2]}} \quad . \ . \ . \quad (9)$$

With V_1 determined the value of X_{m1} is obtained from the stator magnetization curve.

Referring to eqn. (8), it is convenient to write the term in the square brackets in the form $a + jb$, where

$$a = k_1 k(1 - s) \sin\alpha$$

$$b = 1 + s k_1^2 k^2 + k_1 k(1 + s) \cos\alpha$$

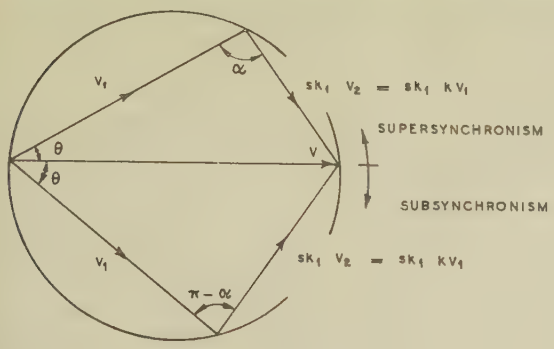

Fig. 5.—E.M.F. locus.

Then the modulus of $\boldsymbol{Z}_M$ is

$$\frac{X_L X_{m1}}{X_L + sk_1^2 k^2 X_{m1}} \sqrt{(a^2 + b^2)}$$

and its argument is arc tan b/a.

The primary m.m.f. current is then given by

$$\boldsymbol{I}_{n1} = -V \frac{X_L + sk_1^2 k^2 X_{m1}}{X_L X_{m1} \sqrt{(a^2 + b^2)}} \angle - \text{arc tan} \frac{b}{a} \quad . \quad (10)$$

Since both s and V_1 are now known, the losses P_{si} and P_{ri} may be determined. Strictly speaking it is also necessary to know the rotor current, $I_2 = I_{n2} + I_{p2}$, given by eqns. (6) and (2) in order to determine the parasitic-current loss, P_p, from a family of curves relating this loss to sV_1 for different values of I_2. However, the work involved in this refinement is hardly justified and P_p may be estimated by assuming $I_2 = k_1 I_{n1}$. With the various losses determined the loss component I_p is obtained from eqn. (1), and

$$\boldsymbol{I} = \boldsymbol{I}_{n1} + \boldsymbol{I}_p$$

The effective rotor resistance, R_{2e}, includes the brush contact resistance and so varies with the rotor current I_2. In the approximate treatment R_{2e} may be taken to correspond to a rotor current $k_1 I$. The leakage impedance is then given by

$$\boldsymbol{Z}_{12} = (R_{1e} + R_t + k_1^2 R_{2e}) + j(X_1 + X_t + k_1^2 s X_2)$$

Then the impedance drop is $I\boldsymbol{Z}_{12}$ and the phase terminal voltage is

$$\boldsymbol{V}_s = -\boldsymbol{V} + I\boldsymbol{Z}_{12}$$

It is unlikely that this voltage will agree exactly with the required terminal voltage, so that it is now necessary to make an amended guess at the internal e.m.f., V, and repeat the calculations. This second approximation is usually accurate enough for practical purposes.

(7) EVALUATION BY ACCURATE METHOD

The approximate method is based on values of $\boldsymbol{I}_{n1}$ and $\boldsymbol{I}_{n2}$ which will combine to provide the assumed internal e.m.f. V when $\boldsymbol{I}_L = -k_1 s \boldsymbol{V}_2 / jX_2$.

In fact,

$$\boldsymbol{I}_L = \frac{\boldsymbol{V}_{t1}}{jX_L}$$

where $$\boldsymbol{V}_{t1} = k_1(-s\boldsymbol{V}_2 + \boldsymbol{I}_2 \boldsymbol{Z}_2)$$

so that the stator winding of the motor is magnetized by an additional current

$$\Delta \boldsymbol{I}_L = \frac{k_1 \boldsymbol{I}_2 \boldsymbol{Z}_2}{jX_L} \quad . \quad . \quad . \quad . \quad . \quad . \quad . \quad . \quad . \quad (11)$$

where $$\boldsymbol{Z}_2 = (R_{t2} + R_{2e}) + j(X_{t2} + sX_2)$$

It is therefore necessary to make a correction to the m.m.f. currents $\boldsymbol{I}_{n2}$ and $\boldsymbol{I}_{n1}$ as determined by eqns. (6) and (10).

The space-vector diagram for the m.m.f.'s of a motor having a transformer with zero magnetizing current is shown in Fig. 6:

$$\begin{aligned} F_1 &= k_2 I_{n1} N_{1m} \\ F_2 &= k_2 I_{n2} N_{2m} \\ &= k_2 k_1 I_{n1} k N_{1m} \\ &= k_1 k F_1 \end{aligned}$$

From which

$$F = F_1 \sqrt{[1 + 2k_1 k \cos \alpha + (k_1 k)^2]}$$

and $$\tan \beta = \frac{k_1 k \sin \alpha}{1 + k_1 k \cos \alpha} \quad . \quad . \quad . \quad . \quad (12)$$

When the transformer magnetizing current is not negligible the rotor current is $\boldsymbol{I}_{n2} = k_1(\boldsymbol{I}_{n1} - \boldsymbol{I}_L)$ and the m.m.f.'s set up by $\boldsymbol{I}_{n2}$ in the rotor and by $\boldsymbol{I}_{n1} - \boldsymbol{I}_L$ in the stator have the relationship in Fig. 6. With this fact in mind it follows from the

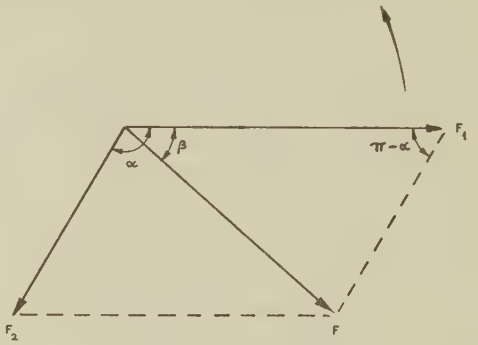

Fig. 6.—M.M.F. diagram.

$F_1 = k_2 I_{n1} N_{1m}$
$F_2 = k_2 I_{n2} N_{2m}$
N_{1m}, N_{2m} = Stator and rotor effective turns.
k_2 = Constant of rotating field.

equation relating F and F_1 that an additional current $\Delta \boldsymbol{I}_L$ flowing in the stator winding only will have the same m.m.f. as currents $\boldsymbol{I}_e$ in the stator and $k_1 \boldsymbol{I}_e$ in the rotor, provided that

$$\boldsymbol{I}_e = \frac{\Delta \boldsymbol{I}_L}{\sqrt{[1 + 2k_1 k \cos \alpha + (k_1 k)^2]}} \varepsilon^{j\beta} \quad . \quad . \quad (13)$$

Thus, in order to preserve the internal e.m.f. unchanged, the stator m.m.f. current $\boldsymbol{I}_{n1}$ and rotor m.m.f. current $\boldsymbol{I}_{n2}$, determined by the approximate method on the assumption that $\boldsymbol{I}_L = -k_1 s \boldsymbol{V}_2 / jX_L$ must be corrected to

$$\begin{aligned} \boldsymbol{I}_{n1}^{\mathrm{I}} &= \boldsymbol{I}_{n1} + \Delta \boldsymbol{I}_L - \boldsymbol{I}_e \\ \boldsymbol{I}_{n2}^{\mathrm{I}} &= \boldsymbol{I}_{n2} - k_1 \boldsymbol{I}_e \end{aligned}$$

However, the current $\Delta \boldsymbol{I}_L$ was determined for a rotor current $\boldsymbol{I}_2 = \boldsymbol{I}_{n2} + \boldsymbol{I}_{p2}$ and it is now necessary to use the corrected value $\boldsymbol{I}_2^{\mathrm{I}} = \boldsymbol{I}_{n2}^{\mathrm{I}} + \boldsymbol{I}_{p2}$ to determine corrected values $\Delta \boldsymbol{I}_L^{\mathrm{I}}$ and $\boldsymbol{I}_e^{\mathrm{I}}$. These, in turn, are used to obtain second corrected values

$$\begin{aligned} \boldsymbol{I}_{n1}^{\mathrm{II}} &= \boldsymbol{I}_{n1} + \Delta \boldsymbol{I}_L^{\mathrm{I}} - \boldsymbol{I}_e^{\mathrm{I}} \\ \boldsymbol{I}_{n2}^{\mathrm{II}} &= \boldsymbol{I}_{n2} - k_1 \boldsymbol{I}_e^{\mathrm{I}} \end{aligned}$$

It has been found that further approximations are not justified, so that

$$\boldsymbol{I} = \boldsymbol{I}_{n1}^{\mathrm{II}} + \boldsymbol{I}_p$$

and $$\boldsymbol{I}_2 = \boldsymbol{I}_{n2}^{\mathrm{II}} + \boldsymbol{I}_{p2}$$

Table 1

PERCENTAGE ERRORS

Brush angle α	Speeds	Current		Power factor		Power	
		Approximate	Accurate	Approximate	Accurate	Approximate	Accurate
deg	r.p.m.						
165	2000 1750	+17·6 +17·5	−10 −3·9	+2·1 0	+1·1 +0·5	+19·7 +17·5	−7·9 −3·4
	1500 1250	+13·7 +16·4	−2·4 +0·9	+0·4 −0·4	0 −0·5	+14·1 +16	−2·4 +0·4
150	2000 1750	+10·7 +14·2	−3·9 +2·6	+4·3 +2·2	+1·9 +0·8	+15 +16·4	−2 +3·4
	1500 1250	+11·1 + 7·8	+3·4 +1·9	+1·6 −1	+0·6 −1·3	+12·7 +6·8	+4 +0·6
135	1750 1500	+ 9·7 +12·5	+0·7 +3·2	+3·4 +0·2	+1·4 −1·4	+13·1 +12·7	+2·1 +1·8
	1250 1000	+11·8 + 1·7	+3·5 −0·7	−1 −1·2	−3·3 −2·1	+10·8 +0·5	+0·2 −2·8
120	1750 1500	+ 2·5 + 8·9	−2·9 +2·9	+3 +0·1	−0·7 −1·1	+ 5·5 +9	−3·6 +1·8
	1250 1000	+ 6·9 + 2·9	+3·3 +1·7	−1·5 −2·5	−0·8 −3·1	+ 5·4 +0·4	+2·5 −1·4
	750 500	− 1·6 − 1	+0·3 +1·9	−5·4 −5·8	−5·7 −7·2	− 7 −6·8	−5·4 −5·3
90	1750 1500	+ 3·6 + 8·5	+2·2 +4·9	+5·1 +6·8	+1·7 +3·7	+ 8·7 +15·3	+3·9 +8·6
	1250 1000	+ 6·1 − 1·9	+4·7 +1·7	+1·5 +5·1	−1·4 +2·2	+ 7·6 + 3·2	+3·3 +3·9
	750 500	0 − 0·5	+1·5 +2	+1·1 −4·5	−3·7 −5·4	+ 1·1 −5	−2·2 −3·4
	250	− 2·1	0	−10·6	−13·7	− 12·7	−13·7
All angles and speeds		+ 8·3	+2·04	+0·29	−1·24	+8·55	−0·72
All angles	1250	+ 9·8	+2·9	−0·48	−1·46	+9·3	+1·44
	1500	+13·2	+2·6	+1·82	+0·36	+15·0	+2·96
	1750	+ 9·5	−0·26	+2·74	+0·74	+13·2	+0·48

The leakage-impedance drop between terminals is then

$$IZ_1 + k_1 I_2 Z_2$$

where $$Z_1 = (R_{t1} + R_{1e}) + j(X_{t1} + X_1)$$

$$Z_2 = (R_{t2} + R_{2e}) + j(X_{t2} + X_2)$$

and the phase terminal voltage is

$$V_s = -V + (I_1 Z_1 + k_1 I_2 Z_2)$$

(8) CHECKING CALCULATIONS

It is essential to have some means of checking the accuracy of the currents determined from eqns. (6) and (10). From Fig. 5 it is apparent that V_1 lags or leads V by θ, so that $V_1 = V_1 \angle \pm\theta$, where the angle θ is readily determined. The stator magnetizing current which will produce this e.m.f. is $I_{m1} = -V_1/jX_{m1}$, i.e.

$$I_{m1} = -\frac{V_1}{X_{m1}} \angle \pm\theta - 90° \quad . \quad . \quad . \quad (14)$$

Now I_{n1} in the stator winding and I_{n2} in the rotor winding must combine to produce the same m.m.f. as I_{m1} in the stator only. But I_{n2} in the rotor gives the same m.m.f. as $kI_{n2} \angle -\alpha$ in the stator. It follows that

$$I_{n1} + kI_{n2} \angle -\alpha = I_{m1} \quad . \quad . \quad . \quad . \quad (15)$$

Then the values of I_{m1}, I_{n1} and I_{n2} given by eqns. (6), (10) and (14) should satisfy eqn. (15). Similarly, the corrected values I_{n1}^{II} and I_{n2}^{II}, when substituted for I_{n1} and I_{n2}, should satisfy eqn. (15).

(9) COMPARISON OF MEASURED AND CALCULATED DATA

Tests for determining the motor parameters are outlined in Section 12. The motor current, power factor and input were calculated by both the approximate and the accurate method for a wide range of brush angles and speeds. The motor was loaded and corresponding test values were obtained. For this purpose first-grade instruments were used, the accuracy of which

Table 2

PERCENTAGE LOSS CURRENT BY ACCURATE METHOD

Brush angle α	Speed	Calculated $100I_p/I$
	r.p.m.	%
165	1250	10·7
	1500	3·1
	1750	−2·3
	2000	0
150	1250	11·9
	1500	5·3
	1750	0·9
	2000	0
135	1000	12·6
	1250	11·4
	1500	7·4
	1750	1·8
120	500	21·2
	750	18·4
	1000	17
	1250	14·3
	1500	9·1
	1750	4·2
90	250	19·2
	500	19·4
	750	17·8
	1000	16·9
	1250	16·3
	1500	11·5
	1750	5·7

was well within the permitted margin of errors for such instruments. The errors in the calculated values, based on the assumption that the measured values are correct, are shown in Table 1.

For reasons connected with the brushes it is very doubtful whether exact agreement between measured and calculated results ought to be obtained. Thus the arc subtended by a brush on the commutator amounted to 10° (electrical), so that there would appear to be ample room for a variation of perhaps 2° in the effective brush position, depending on the variation of current distribution across the brush with load. Another uncertain factor is the brush contact resistance, which to some extent depends on previous load conditions.

Summing up, it is fair to say that the errors obtained by the accurate method are quite as small as could be hoped for and that the method gives reliable results.

Table 2 gives the loss current as a percentage of the total current calculated by the accurate method. In general, it is clear that the loss component is too large to be neglected, except possibly at large brush angles and supersynchronous speeds, where there is a tendency for the negative gap powers due to parasitic brush current and rotor iron losses to neutralize the power drawn from the supply in respect of stator iron losses.

(10) ACKNOWLEDGMENT

The author wishes to thank the authorities of the Royal Military College of Science for the facilities made available and for permission to publish the paper.

(11) REFERENCES

(1) GÖRGES, H.: 'Mitteilungen über neuere Untersuchungen an Wechelstrommotoren', *Elektrotechnische Zeitschrift*, 1891, **12**, p. 699.

(2) DREYFUS, L., and HILLEBRAND, H.: 'Das Kreisdiagramm des Drehstromkollektor—Serienmotors', *Elektrotechnik und Maschinenbau*, 1912, **30**, pp. 389, 458 and 478.

(3) STIX, R.: 'Beitrag zur Ermittelung des Vektordiagrammes beim Drehstromreihenschlussmotor', *ibid.*, 1933, **51**, p. 673.

(4) KOSTENKO, M. P.: 'Die mehrphasigen Kollektor- und Induktionsmachinen als Sonderfall des allgemeinen Transformators', *Archiv für Elektrotechnik*, 1930, **23**, p. 413.

(5) ADKINS, B., and GIBBS, W. J.: 'Polyphase Commutator Machines' (University Press, Cambridge, 1951).

(6) KOSTENKO, M., and SAWALISCHIN, D.: 'Experimentelle and theoretische Kreisdiagramme der mehrphasigen Kollektormaschinen nach der Methode des allgemeinen Transformators', *Elektrotechnik und Maschinenbau*, 1931, **49**, p. 101.

(7) KLEIST, F.: 'Zur quantitativen Berechnung von Drehstrommotoren mit kollektoren Serienschaltung', *Elektrotechnische Zeitschrift*, 1914, **35**, p. 1005.

(8) HIBBERT, J. W.: 'Some Notes on the Characteristics of the Polyphase Series Motor', *BEAMA Journal*, 1951, **58**, p. 346.

(9) MAINER, O. E.: 'Measurement of Effective Stator and Rotor Resistances of Stator-Fed Polyphase Commutator Motors', *Bulletin of Electrical Engineering Education*, December, 1959, p. 21.

(10) MAINER, O. E., and EDWARDS, J. R.: 'Induction Motor Losses', *Electrical Review*, 1960, **166**, p. 103.

(11) MAINER, O. E.: 'Brush Contact Losses due to Load and Parasitic Currents in Polyphase Commutator Motors', *Proceedings I.E.E.*, Monograph No. 375 U, April, 1960 (**107** C, p. 283).

(12) SCHWARZ, B.: 'The Stator-Fed A.C. Commutator Motor with Induction-Regulator Control', *Proceedings I.E.E.*, Paper No. 849 U, October, 1949 (**96**, Part II, p. 755).

(13) CULLWICK, E. G.: 'The Theory of Some A.C. Commutator Motors with Series Characteristics; Part III.—The 3-Phase Series Motor', *Canadian Journal of Research*, Section A, 1942, **20**, p. 97.

(14) TAYLOR, E. O.: 'The Performance and Design of A.C. Commutator Motors' (Pitman, 1958).

(12) APPENDICES

(12.1) Details of Motor Tested

The experimental work was carried out on a small motor rated at 3·5 h.p. at 1 800 r.p.m. The stator had been specially wound for low-voltage operation (55 volts between lines) for use without stator/rotor transformer. In order to test the motor under the conditions normal in practice a 1 : 1 gapped transformer was inserted between stator and rotor, so that $k_1 = 1$.

The effective rotor/stator turns ratio was calculated and checked by the voltmeter method, giving $k = 1{\cdot}02$.

(12.2) Leakage Impedances

A short-circuit test was carried out on the rotor side. The theory of this method of testing has been described by Mainer.[9] With the connections shown in Fig. 7 the terminal impedance is given by

$$Z_T = R_{2e} + sk^2(R_{1e} + R_t) + js[X_2 + k^2(X_1 + X_t)]$$

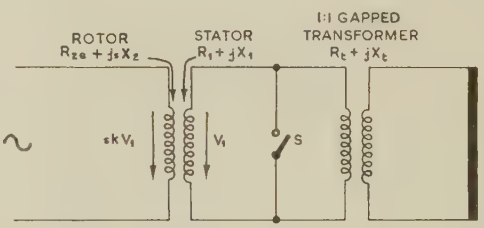

Fig. 7.—Equivalent phase circuit during short-circuit test.

Tests were carried out at full-load current and synchronous speed with

(*a*) Forward field ($s = 0$).
(*b*) Reverse field ($s = 2$) with switch S closed.
(*c*) Reverse field ($s = 2$) with switch S open.

From these tests the following parameters were evaluated:

$R_{1e} + R_t = 0{\cdot}08$ ohm
$R_t = 0{\cdot}05$ ohm
$R_{t1} = R_{t2} = 0{\cdot}025$ ohm (assuming that $R_{t1} = R_{t2} = \frac{1}{2}R_t$)
$X_t = 0{\cdot}004$ ohm
$X_{t1} = X_{t2} = \frac{1}{2}X_t = 0{\cdot}002$ ohm (assumption)
$X_2 + k^2X_1 = 0{\cdot}084$ ohm
$X_2 = k^2X_1 = 0{\cdot}042$ ohm (assumption)
$X_1 = 0{\cdot}040\,5$ ohm

Since the effective rotor resistance R_{2e} is largely determined by the brush contact resistance, the test at $s = 0$ was repeated for different currents and the graph shown in Fig. 8 was plotted.

(12.3) Stator and Transformer Magnetization Curves

By far the most important parameter is the stator magnetizing reactance, which is given by $X_{m1} = V_1/I_{m1}$, where V_1 is the stator phase e.m.f. and I_{m1} is the magnetizing current when only

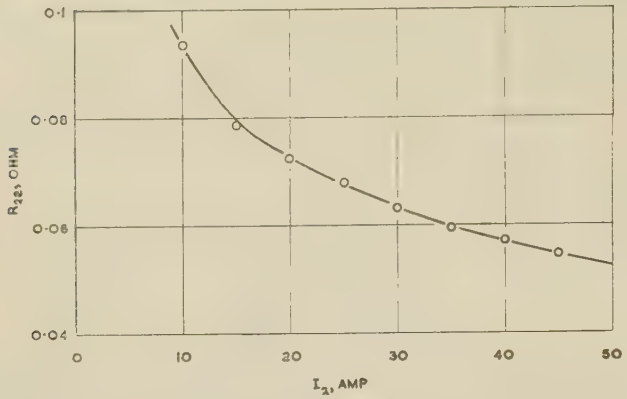

Fig. 8.—Relationship between effective rotor resistance and rotor current.

the stator is excited. Because of the very low lagging power factor the stator phase e.m.f. was taken as $V_1 = V_s - I_{m1}X_1$. Strictly speaking, the line current contains a power component in respect of iron losses. This could be eliminated by driving the rotor with raised brushes at such a high synchronous speed that the negative gap power in respect of rotor iron losses equalled the stator iron loss. Since the power component in the motor tested was small, the rotor was driven round at just over synchronous speed and the measured current was assumed to equal the true magnetizing current. The magnetization

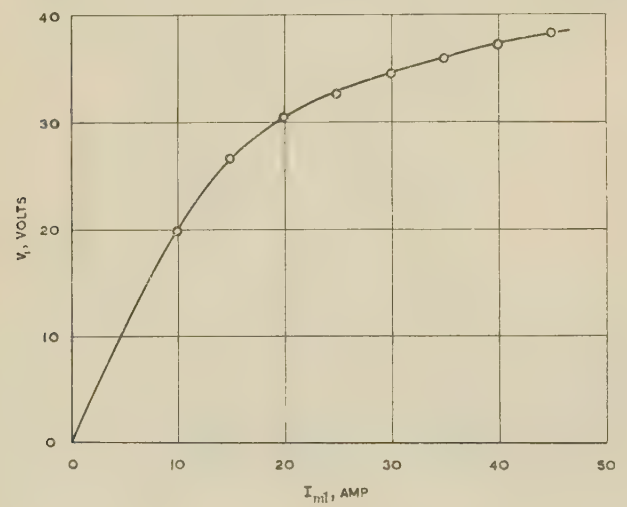

Fig. 9.—Stator magnetization curve.

curve of the stator is shown in Fig. 9; that of the transformer was found to be a straight line giving $X_L = 1{\cdot}32$ ohms.

(12.4) Iron Losses

The stator iron losses were measured and plotted on the base of stator phase e.m.f. V_1 as shown in Fig. 10. The rotor I^2R losses were measured for various values of V_1 at standstill and half synchronous speed. With the method devised by Mainer and Edwards[10] it was found that the rotor iron losses = (standstill loss) $\times |s|^{1{\cdot}313}$. Furthermore, it was found that the rotor standstill loss varied roughly as V_1^2. This enabled the rotor iron loss to be expressed by the empirical equation

$$P_{ri} = 0{\cdot}132V_1^2|s|^{1{\cdot}313} \quad . \quad . \quad . \quad . \quad (16)$$

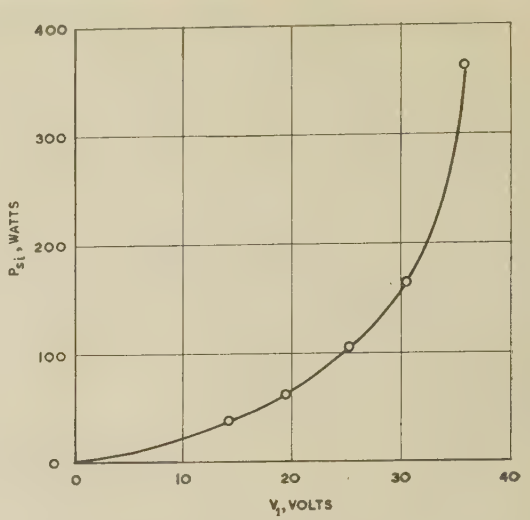

Fig. 10.—Stator iron loss.

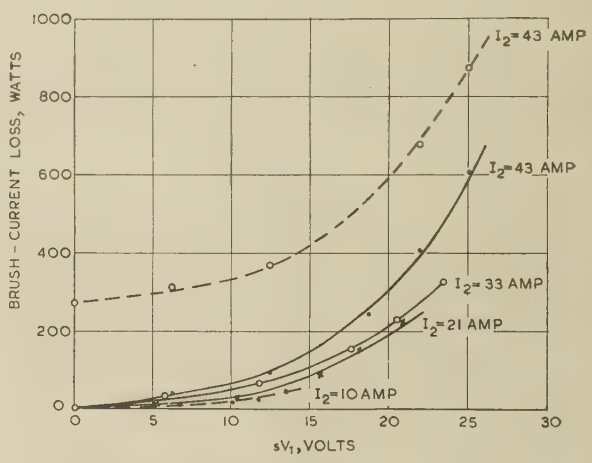

Fig. 11.—Brush parasitic-current loss.

---- Total rotor ohmic loss.
—— Parasitic-current loss P_p.

(12.5) Brush Parasitic-Current Loss

The total rotor ohmic losses were determined by the method described by Mainer.[11] The curve for full-load current is shown by the broken line in Fig. 11; for convenience, the curve was plotted on a base of sV_1 rather than coil e.m.f., to which sV_1 is proportional.

At synchronous speed $sV_1 = 0$, so that there is only a load current loss. The full-line curve in Fig. 11 was obtained by deducting the loss at synchronous speed from the broken-line curve and has been assumed to represent the brush parasitic current loss, P_p. This method gives the correct total ohmic losses but underestimates the parasitic-current loss. However it assumes the same value for load-current loss as that corresponding to the effective rotor resistance R_{2e} as measured by the short-circuit test described in Section 12.2.

It is necessary to evaluate the relationship between P_p and sV_1 for a number of load currents, so as to obtain a family of curves from which the brush parasitic-current loss may be estimated for any values of sV_1 and I_2. These curves are shown by the full lines in Fig. 11.

621.372.6.011.1

The Institution of Electrical Engineers
Monograph No. 414 E
Nov. 1960

THE ALGEBRA AND TOPOLOGY OF ELECTRICAL NETWORKS

By P. R. BRYANT, M.A., M.Sc., Ph.D.

(*The paper was first received 9th November*, 1959, *and in revised form 29th July*, 1960. *It was published as an* INSTITUTION MONOGRAPH *in November*, 1960.)

SUMMARY

The paper gathers together the various results and methods used in an elementary algebraic and topological study of electrical networks. Considerations are restricted to networks containing a finite number of lumped resistors, capacitors and self- and mutual inductors. The result is a connected logical presentation leading, by use of the concepts of incidence, loop and cut-set matrices, to the corresponding nodal, loop and cut-set analysis methods.

LIST OF PRINCIPAL SYMBOLS

$\boldsymbol{A}_a$ = Incidence matrix.
$\boldsymbol{A}$ = Reduced incidence matrix (r.i.m.).
$\boldsymbol{A}'$ = Transpose of $\boldsymbol{A}$.
$\boldsymbol{B}_a$ = 'All-loop' matrix.
$\boldsymbol{B}_f$ = Fundamental loop matrix.
$\boldsymbol{B}$ = Loop matrix.
b = Number of branches in a network $\mathcal{N}$.
b_c = Number of capacitors in $\mathcal{N}$.
b_l = Number of inductors in $\mathcal{N}$.
b_r = Number of resistors in $\mathcal{N}$.
$\boldsymbol{C}_a$ = 'All-cut-set' matrix.
$\boldsymbol{C}_f$ = Fundamental cut-set matrix.
$\boldsymbol{C}$ = Cut-set matrix. In Sections 5 and 7, the diagonal branch-capacitance matrix of order $b_c \times b_c$.
e_k = kth-branch voltage source.
$\boldsymbol{e}$ = Branch voltage-source vector.
$\boldsymbol{E}$ = Loop voltage-source vector. In Section 8, columns of $\boldsymbol{C}_f$ corresponding to the branches of a tree.
$\boldsymbol{F}$ = Columns of $\boldsymbol{B}_f$ corresponding to a set of chords.
$\boldsymbol{G} = \boldsymbol{R}^{-1}$.
i_k = kth-branch current.
$\boldsymbol{i}$ = Branch current vector.
$\boldsymbol{I}$ = Loop current vector.
j_k = kth-branch current source.
$\boldsymbol{j}$ = Branch current-source vector.
$\boldsymbol{J} = \boldsymbol{A}\boldsymbol{j}$ = Nodal current-source vector.
$\boldsymbol{J}^c = \boldsymbol{C}\boldsymbol{j}$ = Cut-set current-source vector.
$\boldsymbol{K}$ = Columns of $\boldsymbol{A}$ corresponding to a tree.
$\boldsymbol{L}$ = Branch self- and mutual inductance matrix of order $b_l \times b_l$.
m = Number of independent loops in $\mathcal{N}$.
n = Number of nodes in $\mathcal{N}$.
$\mathcal{N}$ = Typical *RLC* or *RLCM* network.
p = Laplace transform (or complex frequency) variable.
$\boldsymbol{P}(p)$ = Nodal admittance matrix.
$\boldsymbol{P}^c(p)$ = Cut-set admittance matrix.
$\boldsymbol{Q}(p)$ = Loop impedance matrix.
$\boldsymbol{R}$ = Diagonal branch resistance matrix of order $b_r \times b_r$.
s = Connectivity, or number of separate disconnected parts of $\mathcal{N}$.
$\boldsymbol{S} = \boldsymbol{C}^{-1}$.
t = Time.
v_k = kth-branch voltage.
$\boldsymbol{v}$ = Branch voltage vector.
$\boldsymbol{V}$ = Nodal voltage vector.
$\boldsymbol{V}^c$ = Cut-set voltage vector.
$\boldsymbol{X}$ = Columns of $\boldsymbol{A}$ corresponding to a set of chords.
$\boldsymbol{Y}(p) = \boldsymbol{Z}^{-1}$ = Branch admittance matrix of order $b \times b$.
$\boldsymbol{Z}(p) = \boldsymbol{Y}^{-1}$ = Branch impedance matrix of order $b \times b$.
$\boldsymbol{\Gamma} = \boldsymbol{L}^{-1}$.
$\mathbf{1}_m$ = Unit matrix of order $m \times m$.
$+$ = Direct addition of square matrices.

(1) INTRODUCTION

The use of algebraic topology and matrix algebra in the study of electrical network theory has been written about by many authors and is now well established. Unfortunately, these various writings are scattered both in time and place. The purpose of the paper is to gather together various results and to present them in a connected logical way. Apart from the presentation, very little in the paper is new.

Algebraic topology and matrix algebra together provide an extremely useful mathematical language for network theory, and their concepts and results enable this theory to be developed rigorously. Topology can be applied to electrical network theory at two different levels. The more sophisticated level, which we do not consider, makes use of the theories of homology and cohomology of 1- and 2-dimensional linear complexes.[22, 32, 39, 40] The more elementary topology which we use is historically the early beginnings of algebraic topology.[48] Matrix algebra plays a very important part in the development given here.

No mention is made in the paper of the concept of duality. This omission arises from the inability to do justice in a short space to this most important concept, rather than from any lack of appreciation of its significance. References 22 and 32 give interesting accounts of the algebraic and topological approach to duality.

(2) ELECTRICAL NETWORKS

The electrical networks considered are made up entirely of a finite number of lumped resistors, capacitors, self-inductors and mutual inductors. It is hoped to include ideal transformers in a later paper. An extension of topological methods to networks containing more general electrical elements has been made by Percival[34, 35] and Coates.[12]

Our networks are assumed to be driven by ideal current and voltage sources; the philosophy of assuming ideal sources is fully discussed by Guillemin,[20] and we shall not mention it further.

We consider first networks which contain no mutual inductance. Such networks are made up entirely of resistors, self-inductors and capacitors, and are called *RLC* networks. It is

Correspondence on Monographs is invited for consideration with a view to publication.
This is an 'integrating' paper. Members are invited to submit papers in this category, giving the full perspective of the developments leading to the present practice in a particular part of one of the branches of electrical science.
Dr. Bryant is at the Research Laboratories of The General Electric Company, Limited, Wembley, England.
The paper is based on an introductory chapter to a dissertation submitted for the degree of Doctor of Philosophy at Cambridge University.

assumed, until Section 7, that all networks considered are *RLC* networks.

As the elements are lumped, it does not matter about their absolute spatial positions; only the way in which they are connected together is of significance. Because of this we prefer not to talk of the network 'geometry', which conjures up ideas of dimensions and absolute positions, but rather of the network 'topology'. Thus we are concerned only with the interconnections of the elements at their junction points, and algebraic topology provides a method of specifying and studying this.

Denote a typical *RLC* network by $\mathcal{N}$; each element of $\mathcal{N}$ is called a 'branch'; thus a branch is a resistor, a self-inductor or a capacitor. This definition of a branch is by no means the only one possible; several writers find it more convenient to consider a series or parallel arrangement of resistors, inductors and capacitors as forming a branch. We have found the present definition to be of most use. We shall assume that all resistances, inductances and capacitances are positive and non-zero. The junctions of the branches are called 'nodes' of $\mathcal{N}$; it is assumed that $\mathcal{N}$ contains n nodes and b branches, made up of b_l self-inductors, b_r resistors and b_c capacitors, where $b_l + b_c + b_r = b$. The nodes are labelled 1, 2, . . . n, and the branches 1, 2, . . . b.

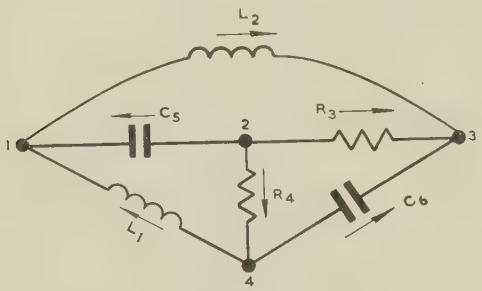

Fig. 1.—A typical *RLC* network $\mathcal{N}$.

Fig. 1 shows a typical connected *RLC* network, $\mathcal{N}$, containing 6 branches and 4 nodes. Thus, for Fig. 1,

$$b = 6 \ (b_c = b_l = b_r = 2)$$
$$n = 4$$

The nodes have been arbitrarily numbered from 1 to 4, and the branches from 1 to 6.

It is stipulated that $\mathcal{N}$ is driven only by ideal voltage sources connected into branches and ideal current sources connected across branches. For example, the kth branch of $\mathcal{N}$ is assumed to have voltage source $e_k(t)$ in series and current source $j_k(t)$ in parallel, as shown in Fig. 2. This stipulation is justified by

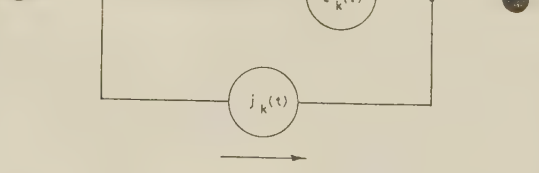

Fig. 2.—The kth active branch.

Guillemin[20] (Chapter 2, Section 7) on the grounds that the network configuration must not be modified by these sources. We shall be general and assume that every branch of $\mathcal{N}$ has two ideal sources so connected. The combination of the 'passive branch' and the two ideal sources is called an 'active branch'.

(3) INCIDENCE AND THE INCIDENCE MATRIX

Disregarding the electrical properties of the *RLC* network, $\mathcal{N}$, and considering only the nodes and their interconnecting branches—which may for this purpose be thought of as lines—we obtain what topologists call a 'one-dimensional linear complex' or a 'linear graph'.[48] The topological properties of $\mathcal{N}$ are precisely those of this graph of $\mathcal{N}$.

Going back for a moment to the electrical case, it is obvious that we shall need to introduce an orientation of the branches, e.g. for defining potential difference. We shall assume that each branch of $\mathcal{N}$ has an arbitrary orientation applied to it by means of an arrowhead, as shown in Fig. 1.

For the moment it will be assumed that $\mathcal{N}$ does not contain any 'degenerate branch loops', i.e. branches which are closed upon themselves. With this limitation it is obvious that each branch has associated with it precisely two nodes, called the 'vertices' of the branch. These two nodes and the branch are said to be 'incident'. The incidence of the nodes and branches of $\mathcal{N}$ may be described algebraically by means of an $n \times b$ matrix, denoted[29,36] by A_a, whose rows correspond to the nodes of $\mathcal{N}$ and whose columns correspond to the branches. Its elements A_{jk} are defined as follows:

$A_{jk} = +1$, if branch k is incident with node j and oriented away from it.
$A_{jk} = -1$, if branch k is incident with node j and oriented towards it.
$A_{jk} = 0$, if branch k is not incident with node j.

A_a is called the 'incidence matrix'* of the network. It corresponds to the matrix Π used by Ingram and Cramlett,[21] and to the negative of the matrices M used by Cauer[7] and E_1 used by Veblen.[48] Veblen points out that the use of this matrix dates back to Kirchhoff's famous article,[23] which he says 'is doubtless the first important contribution to the theory of linear graphs'.

For the network of Fig. 1, we have

$$A_a = \begin{bmatrix} -1 & +1 & 0 & 0 & -1 & 0 \\ 0 & 0 & +1 & +1 & +1 & 0 \\ 0 & -1 & -1 & 0 & 0 & -1 \\ +1 & 0 & 0 & -1 & 0 & +1 \end{bmatrix}$$

A_a not only gives all the information about the incidence of branches and nodes but also indicates the branch orientations. Obviously each column of A_a, corresponding to a branch of $\mathcal{N}$, contains exactly two non-zero elements, namely $+1$ and -1. Hence, if we add together all the rows we get a row of zeros, i.e. the rows of A_a are not linearly independent. The number of linearly independent rows (or columns) of a matrix is called its rank.[1,18] The rank of A_a, which depends on the number of nodes in $\mathcal{N}$, also depends upon what is called the 'connectivity' of $\mathcal{N}$ which is now defined. First, $\mathcal{N}$ is said to be 'connected' if there exists a path of network branches between any two nodes of $\mathcal{N}$. If $\mathcal{N}$ is not connected then it must consist of a finite number, say s, of separate parts. This number s is called the connectivity of $\mathcal{N}$. The network of Fig. 1 is connected and so has $s = 1$.

We now have the following results:

(*a*) The rank of A_a is $n - s$.

This result is proved by Veblen,[48] and for the case $s = 1$ by Reed and Seshu.[36]

(*b*) A necessary and sufficient condition for an $n \times b$ matrix to be the incidence matrix of an *RLC* network (not necessarily connected) is that each column of the matrix contains precisely

* A_a is sometimes called the vertex matrix.[36]

one $+1$ and one -1, all other elements in the column being zero. If such a matrix is of rank r, the associated network has $n - r$ separate parts.

Necessity is obvious. Sufficiency follows by construction. The last part of the result follows by applying (a) to the network so constructed.

We shall now assume until Section 7 that $\mathcal{N}$ is connected, i.e. that $s = 1$. The modifications necessary to extend what follows to the case $s > 1$ are in most cases fairly obvious, and no mention will be made of them until Section 7.

In the case of a connected network, A_a contains a certain redundancy. Thus suppose we form from the $n \times b$ matrix A_a an $(n-1) \times b$ matrix, by deleting the row corresponding to node n. Denote[29, 36] this new matrix by A; it is called the reduced incidence matrix (r.i.m.) of $\mathcal{N}$.

The reduced incidence matrix A of the network in Fig. 1 is obtained from A_a by deleting the fourth row, and is given by

$$A = \begin{bmatrix} -1 & +1 & 0 & 0 & -1 & 0 \\ 0 & 0 & +1 & +1 & +1 & 0 \\ 0 & -1 & -1 & 0 & 0 & -1 \end{bmatrix}$$

Some of the columns of A will not now contain both a $+1$ and a -1. Any such column must obviously correspond to a branch incident with node n; the sign of the single non-zero element in that column will indicate the orientation of that branch. Thus, provided that we know $\mathcal{N}$ is connected, the matrix A gives as much information about $\mathcal{N}$ as A_a. The significance of the suffix a in A_a may now be explained: it is meant to show that *all* the nodes of $\mathcal{N}$ are considered in its definition.[29] The node numbered n, corresponding to the row of A_a deleted, is called the reference node of $\mathcal{N}$. It is usual to decide which of the nodes is to be the reference node before numbering them.

(c) The rank of the r.i.m., A, of a connected network containing n nodes is $(n-1)$.

This is proved by Reed and Seshu.[36]

(d) Necessary and sufficient conditions for a matrix M of order $\alpha \times \beta$ to be the r.i.m. of a connected RLC network are:

(i) Elements of M are $+1$, -1, or 0.

(ii) Each column of M contains at most one $+1$ and one -1 and at least one non-zero element.

(iii) The rank of M is α.

Necessity follows from the definition of an r.i.m., and from (c). For sufficiency we note that we may complete those columns of M containing only a single non-zero element by adding an extra row to M so that it satisfies the conditions of (b) for a non-reduced incidence matrix of a connected network.

As mentioned at the beginning of the Section, it has so far been assumed that $\mathcal{N}$ does not contain any degenerate branch loops. Such degenerate branches are usually not admitted in the classical study of the theory of linear graphs,[48] but it is often found convenient to allow them in the study of electrical networks. Their presence immediately complicates the concept of the incidence matrix; thus, since the branch starts and finishes on the same node, then from our original ideas, the column of A_a corresponding to this branch requires both a $+1$ and a -1 as the element corresponding to the node on which the branch is looped. Mathematically we wish to treat this element of the matrix as zero, but if we just put a zero as the corresponding element of A_a, we obtain a column of zeros corresponding to the branch and lose the information telling us on which node the branch is looped. We thus adopt the symbolic convention of using a zero with a bar across it, $\bar{0}$, to indicate this node. This zero, $\bar{0}$, obeys all the normal arithmetical rules of zero. Notice that when we obtain the reduced incidence matrix, A, a branch looped on the reference node will now be indicated by a column of plain zeros, the barred zero having been lost in the elimination of the 'reference row'.

Some of the properties (a)–(d) of the matrices A_a and A now need to be slightly modified to allow the existence of these degenerate loops. Result (a) remains as before, the rank of A_a being unaffected by these branches. Property (b) requires modification; thus:

(b') A necessary and sufficient condition for an $n \times b$ matrix to be the incidence matrix of an RLC network, not necessarily connected but including, possibly, degenerate branch loops, is that each column of the matrix falls into just one of the following categories:

(i) Contains precisely one $+1$ and one -1, all other elements in the column being plain zeros.

(ii) Contains just one $\bar{0}$, all other elements being plain zeros.

If such a matrix is of rank r, the associated network has $n - r$ separate parts.

The property (c) concerning the rank of the reduced incidence matrix A remains unchanged, but property (d) requires modification:

(d') Necessary and sufficient conditions for a matrix M of order $\alpha \times \beta$ to be the r.i.m. of a connected RLC network, possibly containing degenerate branch loops, are:

(i) Elements of M are $+1$, -1, $\bar{0}$ or 0.

(ii) Each column of M falls into just one of the following categories:

Contains precisely one $+1$ and one -1, other elements being plain zeros.

Contains just one $+1$, other elements being plain zeros.

Contains just one -1, other elements being plain zeros.

Contains just one $\bar{0}$, ther elements being plain zeros.

All elements are plain zeros.

(iii) The rank of M is α.

Having pointed out the possibility of the existence of these degenerate branch loops, and also indicated a method of including them in a matrix analysis of the network, we assume for the rest of the paper that no degenerate branch loops exist in the networks being considered. The only modification required in what follows, in order that the results may include these loops, is in the definition in the next Section of the term 'loop' itself. If this definition is slightly modified so that the degenerate loops are admitted as loops, then all the results and methods obtained in the paper will carry over.

(4) LOOPS AND THE LOOP MATRIX

It is well known to electrical engineers that closed paths within a network provide a very useful concept. Such a closed path is called a 'loop' of $\mathcal{N}$; the terms 'circuit',[36] '1-circuit',[48] 'cycle'[39,40] and '1-cycle'[32] are used by some writers. Following Guillemin we reserve the term 'mesh' for those loops which form the 'windows' of a planar network. The precise definition of a loop must be made with care; the following formal definition is fairly rigorous but is probably not very intuitive. It is difficult to make it more intuitive without losing rigour.

Definition 1.[48]—A loop of a network $\mathcal{N}$ is a connected subnetwork of $\mathcal{N}$ (i.e. a network contained in $\mathcal{N}$) having precisely two branches incident with each node.

In general $\mathcal{N}$ will contain many loops, which may be arbitrarily numbered and oriented. All the loops of the network of Fig. 1 are shown in Fig. 3.

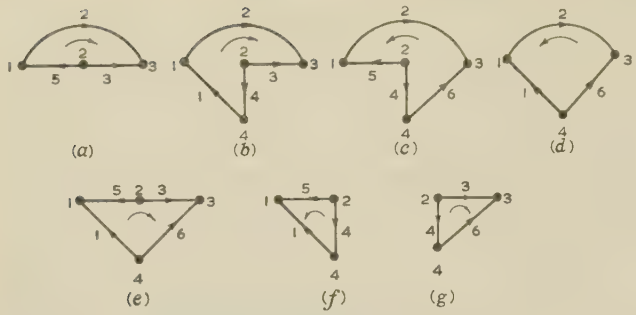

Fig. 3.—The seven loops of $\mathcal{N}$.

If a particular loop contains a particular branch, that loop and branch are said to be 'incident'. Thus any loop may be defined in terms of its incidence with the branches of $\mathcal{N}$. This incidence may be described algebraically by a matrix, denoted[36] by $\boldsymbol{B}_a$, containing b columns, one for each branch of $\mathcal{N}$, and a finite number of rows, one for each possible loop of $\mathcal{N}$. Its elements B_{jk} are $+1$, -1 or 0, as follows:

$B_{jk} = +1$, if branch k is incident with loop j and their orientations coincide there.

$B_{jk} = -1$, if branch k is incident with loop j and their orientations are opposed there.

$B_{jk} = 0$, if branch k and loop j are not incident.

The matrix $\boldsymbol{B}_a$ for the arbitrary numbering and orientation of the loops shown in Fig. 3, is

$$\boldsymbol{B}_a = \begin{bmatrix} 0 & 1 & -1 & 0 & 1 & 0 \\ 1 & 1 & -1 & -1 & 0 & 0 \\ 0 & -1 & 0 & 1 & -1 & 1 \\ -1 & -1 & 0 & 0 & 0 & 1 \\ 1 & 0 & 1 & 0 & -1 & -1 \\ -1 & 0 & 0 & -1 & 1 & 0 \\ 0 & 0 & 1 & -1 & 0 & -1 \end{bmatrix}$$

There exists an important relation between the matrices $\boldsymbol{A}_a$ and $\boldsymbol{B}_a$. If we denote the transpose of a matrix, $\boldsymbol{B}_a$, i.e. the matrix with its rows and columns interchanged,[1] by $\boldsymbol{B}'_a$, this relation becomes

$$(e) \qquad \boldsymbol{A}_a\boldsymbol{B}'_a = \boldsymbol{0} \quad \boldsymbol{B}_a\boldsymbol{A}'_a = \boldsymbol{0}$$

This important result, which, as we shall show, provides the mathematical justification of nodal and loop analysis of networks, is proved by Reed and Seshu;[36] it also follows from Veblen[48] (Chapter 1, Section 42) and Cauer[7] [eqn. (5*a*), Chapter 2].

The concept of a 'tree' is now defined; this important concept was first used by Kirchhoff[23] in 1847.

Definition 2.—A tree of a connected network $\mathcal{N}$ is a connected subnetwork containing all the nodes of $\mathcal{N}$ but containing no loops.

Note that this definition differs from that given by Veblen[48] (Chapter 1, Section 26); the term 'complete tree' is used by Cauer.[7]

(*f*) Every tree of $\mathcal{N}$ has $n - 1$ branches.

This is proved by Veblen[48] (Chapter 1, Section 26) and by Ingram[21] (theorem 3).

In general $\mathcal{N}$ will contain several trees; it may be shown[46] that the total number of trees of $\mathcal{N}$ is given by the determinant $\det(\boldsymbol{A}\boldsymbol{A}')$, where $\boldsymbol{A}'$ denotes the transpose[1] of the matrix $\boldsymbol{A}$.

From this result, we see that the network of Fig. 1 contains sixteen trees. These are shown in Fig. 4.

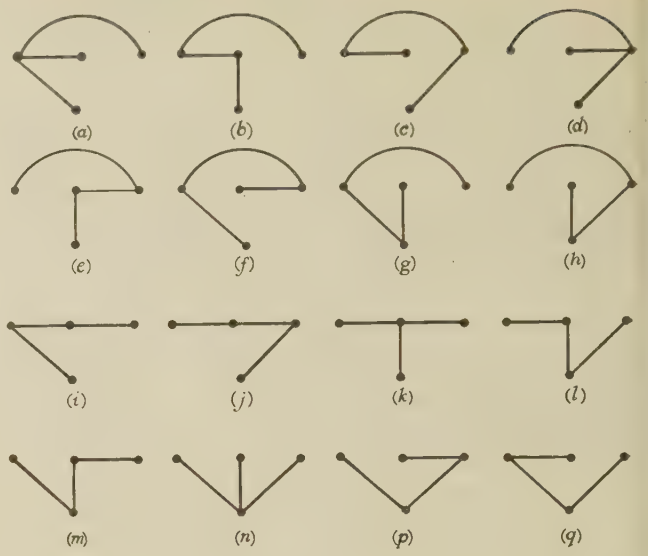

Fig. 4.—The sixteen trees of $\mathcal{N}$.

Each tree of $\mathcal{N}$ will divide the b branches into two sets: the $n - 1$ branches contained in the tree, and the $b - n + 1$ branches not contained in the tree. These latter $b - n + 1$ branches are called 'chords'[21, 36] (or 'links'[8, 20]) of the tree, and are said to form a 'co-tree'[22] of $\mathcal{N}$ (see Fig. 5). It is of interest

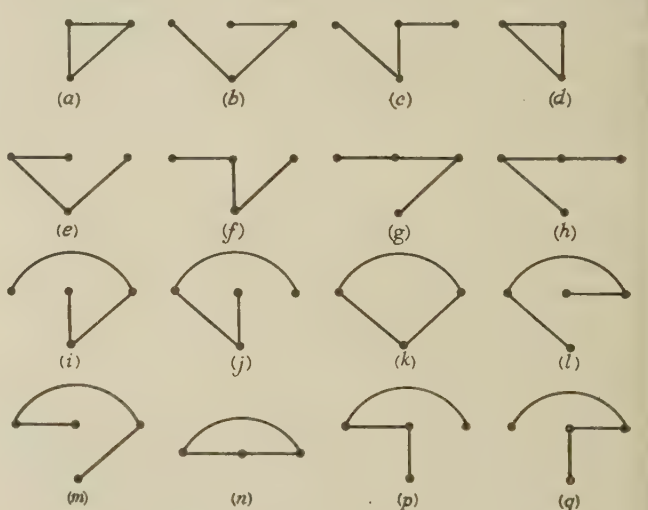

Fig. 5.—The sixteen co-trees of $\mathcal{N}$.

to note that a co-tree may be defined in its own right as a minimal set of branches, such that, if all the other branches of $\mathcal{N}$ are contracted,* the resulting network contains only one node.† This definition is the dual of definition 2 for a tree. We do not make any use of this alternative definition here.

Whitney[52] has shown an interesting relation between the loops and trees of $\mathcal{N}$, namely that a loop is a minimal set of branches containing at least one chord of every tree. Trees have another important application to the study of the loops of $\mathcal{N}$. Thus, consider any tree. Since it is connected, there exists a path of tree branches, called a 'tree path', between any

* By the 'contraction' of a branch we mean the process of shrinking the branch to nothing, and identifying together as a single node the original two terminating nodes of the branch: the term was suggested to the author by Mr. S. Deards, of the College of Aeronautics, Cranfield.

† A more precise statement would be that the resulting network contains no 'cut-sets' (see Section 8).

wo nodes. Since a tree contains no loops, this tree path must e unique for any pair of nodes. Now consider the tree together vith one of its chords. Between the two nodes terminating the hord there is, by the above discussion, a unique tree path. The chord together with this tree path must obviously define a oop of $\mathcal{N}$. Similarly each of the $b - n + 1$ chords of the ree defines a loop of $\mathcal{N}$. These $b - n + 1$ loops are called a et of 'fundamental' loops of $\mathcal{N}$: their orientations are defined o coincide with those of the chords. Thus, the tree of Fig. 4(*l*) lefines the set of three fundamental loops shown in Fig. 6(*a*).

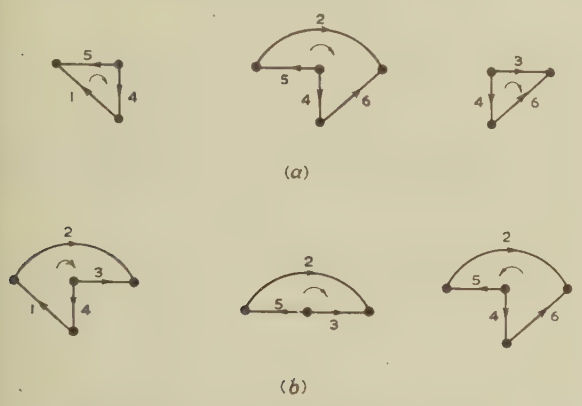

Fig. 6.—(*a*) A set of fundamental loops of $\mathcal{N}$.
(*b*) A set of independent non-fundamental loops of $\mathcal{N}$.

A set of fundamental loops of a network defines a submatrix of order $(b - n + 1) \times b$ of $\boldsymbol{B}_a$, called a 'fundamental loop matrix' of $\mathcal{N}$, and denoted by $\boldsymbol{B}_f$. Thus the set of fundamental loops of Fig. 6(*a*) defines the matrix $\boldsymbol{B}_f$ given by

$$\boldsymbol{B}_f = \begin{bmatrix} 1 & 0 & 0 & 1 & -1 & 0 \\ 0 & 1 & 0 & -1 & 1 & -1 \\ 0 & 0 & 1 & -1 & 0 & -1 \end{bmatrix}$$

By the definition, each chord of the tree is incident with precisely one of the fundamental loops, and so the corresponding $b - n + 1$ columns of $\boldsymbol{B}_f$ form, with a suitable numbering, a unit matrix of order $b - n + 1$. Hence $\boldsymbol{B}_f$ is of rank $(b - n + 1)$ (see Reference 36, theorem 9). From this result and using (*a*) and (*e*) it follows that $\boldsymbol{B}_a$ is also of rank $b - n + 1$ (Reference 36, theorem 10). This result means that $\boldsymbol{B}_a$ contains only $b - n + 1$ linearly independent rows. As each row defines a loop of $\mathcal{N}$ we see that $\mathcal{N}$ contains only $b - n + 1$ independent loops. The systems of fundamental loops are examples of such independent systems: there exist other systems, however, besides these [see Fig. 6(*b*)]. Thus the rows of any $(b - n + 1) \times b$ submatrix of $\boldsymbol{B}_a$ of rank $b - n + 1$ will define such an independent system. Such a submatrix is denoted by $\boldsymbol{B}$,[29, 36] and called a 'loop-matrix' of $\mathcal{N}$. The matrix $\boldsymbol{B}$ corresponds to the matrix Γ used by Ingram and Cramlett and by Cauer. A set of three independent loops of the network of Fig. 1, which is not a fundamental set, is shown in Fig. 6(*b*). The corresponding loop matrix $\boldsymbol{B}$ is

$$\boldsymbol{B} = \begin{bmatrix} 1 & 1 & -1 & 1 & 0 & 0 \\ 0 & 1 & -1 & 0 & 1 & 0 \\ 0 & -1 & 0 & 1 & -1 & 1 \end{bmatrix}$$

The number $b - n + 1$ is denoted by m, and is called the 'nullity'[21] or 'cyclomatic number'[48] of $\mathcal{N}$. We shall assume that a system of m independent loops of $\mathcal{N}$ has been chosen and denote the corresponding loop matrix by $\boldsymbol{B}$. Since $\boldsymbol{A}$ is a submatrix of $\boldsymbol{A}_a$, and $\boldsymbol{B}$ is a submatrix of $\boldsymbol{B}_a$, then (*e*) gives us immediately that $\boldsymbol{B}\boldsymbol{A}' = \boldsymbol{0}$. We give now some further properties of these matrices $\boldsymbol{A}$ and $\boldsymbol{B}$.

(*g*) Any $(n - 1)$-minor of $\boldsymbol{A}$ is non-singular if and only if the $n - 1$ columns of the minor correspond to the branches of some tree of $\mathcal{N}$.

(*h*) Any m-minor of $\boldsymbol{B}$ is non-singular if and only if the m columns of the minor correspond to the branches of some co-tree of $\mathcal{N}$.

(*g*) and (*h*) are proved by Reed and Seshu[36] (theorems 12 and 14).

A class of matrices, that has been investigated by Cederbaum[8, 10, 11] and shown to have important applications to network theory, is the class of 'unimodular' or 'E-matrices'; these are defined to be matrices having all their subdeterminants, including the elements themselves, of value $+1$, -1 or 0. We have the following result:

(*i*) $\boldsymbol{A}$ and $\boldsymbol{B}_f$ are E-matrices.

This is proved for $\boldsymbol{A}$ by Veblen and Franklin;[49] Seshu[42] gives the same proof; for $\boldsymbol{B}_f$ it is proved by Cederbaum.[11]

A general loop matrix is not necessarily an E-matrix, but we do have the following result:

(*j*) All non-zero m-minors of $\boldsymbol{B}$ have the value $+k$ or $-k$, where k is some integer.

This result follows from the next, which is proved by Reed and Seshu[36] as part of their theorem 14.

(*k*) $\boldsymbol{B}$ and $\boldsymbol{B}_f$ are related by $\boldsymbol{B} = \boldsymbol{T}\boldsymbol{B}_f$, where $\boldsymbol{T}$ is a non-singular square matrix having elements $+1$, -1 and 0.

Notice that, since the m columns of $\boldsymbol{B}_f$ which correspond to the co-tree defining the fundamental loops form a unit matrix, then $\boldsymbol{T}$ must be identical with the $m \times m$ submatrix of $\boldsymbol{B}$ formed from the corresponding m columns.

Those systems of loops having the value $k = 1$ in result (*j*) are called by Cederbaum[9] 'simple' systems. We refer again to simple systems in Section 6.1.

The result (*j*) has been somewhat extended by Okada,[31] who shows that for certain types of loops the integer k is of the form 2^i. He shows that this will be so if the m independent loops together with m surfaces, obtained by assuming each loop to be the boundary of a surface, form what topologists call a non-orientable manifold. Not all independent systems have this property: a counter example is given by Cederbaum[9] in which k has the value 3. Mayeda and Seshu[29] imply that Okada's result is true for all loop matrices $\boldsymbol{B}$; we hope that we have clarified the situation.

The connection between $\boldsymbol{B}_f$ and $\boldsymbol{A}$ is given by the following:

(*l*) If, for a given tree of $\mathcal{N}$, the branches and fundamental loops are so numbered and oriented that $\boldsymbol{B}_f$ and $\boldsymbol{A}$ are of the form:

$$\boldsymbol{B}_f = [\boldsymbol{1}_m, \boldsymbol{F}]$$
$$\boldsymbol{A} = [\boldsymbol{X}, \boldsymbol{K}]$$

then

$$\boldsymbol{F}' = -\boldsymbol{K}^{-1}\boldsymbol{X}$$

The proof follows directly from the relation $\boldsymbol{A}\boldsymbol{B}_f' = \boldsymbol{0}$. As Cederbaum[11] points out, (*l*) provides a necessary and sufficient condition for a matrix to be a fundamental loop matrix of a connected network:

(*m*) A necessary and sufficient condition for an $m \times b$ matrix $\boldsymbol{B}_f$ to be a fundamental loop matrix of a connected network is

that, possibly after a permutation of its columns, B_f may be presented in the form

$$B_f = [1_m, F]$$
$$= [1_m, -(K^{-1}X)']$$

where K and $[X, K]$ are respectively the r.i.m.'s of a tree and of a connected network. This tree and connected network then realize B_f.

The 'arbitrary' numbering of the branches given in Fig. 1 was in fact chosen so that branches 1, 2 and 3 are chords to the tree of Fig. 4(*l*), while branches 4, 5 and 6 are the tree branches. Hence A is already in the form

$$A = (X, K)$$

giving

$$X = \begin{bmatrix} -1 & 1 & 0 \\ 0 & 0 & 1 \\ 0 & -1 & -1 \end{bmatrix}$$

$$K = \begin{bmatrix} 0 & -1 & 0 \\ 1 & 1 & 0 \\ 0 & 0 & -1 \end{bmatrix}$$

Hence

$$K^{-1} = \begin{bmatrix} +1 & +1 & 0 \\ -1 & 0 & 0 \\ 0 & 0 & -1 \end{bmatrix}$$

giving

$$K^{-1}X = \begin{bmatrix} -1 & +1 & +1 \\ +1 & -1 & 0 \\ 0 & +1 & +1 \end{bmatrix}$$

The truth of result (*l*) is illustrated when this product, $K^{-1}X$, is compared with $-F'$, where F is the last three columns of B_f.

An interesting interpretation of the matrix K^{-1} is given by Branin[53] in terms of what he calls the 'node-to-datum path-matrix' of the tree defining K. His paper contains many other interesting results.

A process for realizing a matrix B_f is given by Gould.[19] The following result is proved by Reed and Seshu[36] (theorem 15):

(*n*) If M is any matrix of order $m \times b$ and rank m, having $M_{ij} = \pm 1$ or 0 and satisfying $AM' = 0$, then each row of M represents a loop of $\mathcal{N}$ or a disjoint union of such loops.

(5) ELECTRICAL CONSIDERATIONS OF *RLC* NETWORKS

As before, we assume a connected network, $\mathcal{N}$, and each branch of $\mathcal{N}$ is assumed to have an ideal voltage source in series and an ideal current source in parallel, as shown in Fig. 2. The values of these ideal sources, as functions of time t, are assumed known. The unknowns in the network are taken to be the passive branch currents and potential differences which exist as a result of the sources. Each passive branch, e.g. the kth, will be assumed to have a current $i_k(t)$ flowing in the direction of orientation, and a potential difference $v_k(t)$ such that the orientation arrow points towards the lower potential. The relative orientations of $i_k(t)$, $v_k(t)$, $e_k(t)$ and $j_k(t)$ are shown in Fig. 7, where the arrows indicating potentials are supposed to point towards the higher potential.

It is convenient to deal straight away in Laplace transforms of these time-varying parameters. We shall assume that we are interested only in the steady-state solution, and so initial conditions of the variables may be neglected. In this way the transform variable, which we denote by p, corresponds to the well-known electrical-engineering complex-frequency variable.

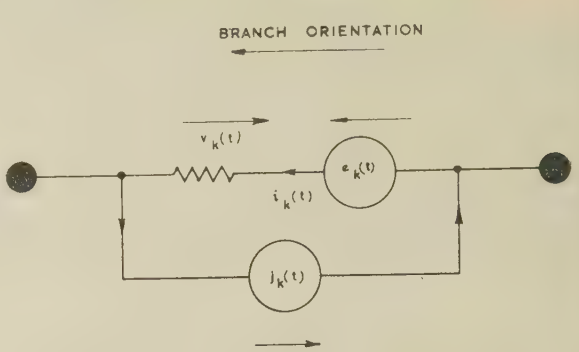

Fig. 7.—Relative orientations of the parameters of an active branch.

As there is no danger of confusion, the transforms of the various time functions $v_k(t)$, $e_k(t)$, etc., are denoted by $v_k(p)$, $e_k(p)$, etc. The variable p will not be explicitly included in much of the following.

The branch currents and potentials have to obey certain well-known laws; these are the generalized Ohm's law and the two Kirchhoff laws. Now Kirchhoff's voltage law as originally stated[23] included also Ohm's law. We find it convenient to separate them out; in this way Kirchhoff's voltage law equates to zero the net voltage drop around any loop of $\mathcal{N}$. The matrix B_f specifies all the loops of $\mathcal{N}$ in terms of their incidence with the branches. The potential drop across, say, the kth oriented active branch is $v_k - e_k$. The b branch variables, v_k, may be arranged in the form of a $b \times 1$ column vector, which we denote by $\boldsymbol{v}(p)$; similarly the $b \times 1$ column vector $\boldsymbol{e}(p)$ is defined. When this is done Kirchhoff's voltage law applied to every loop of $\mathcal{N}$ becomes the matrix equation

$$B_a(\boldsymbol{v} - \boldsymbol{e}) = \mathbf{0} \quad . \quad . \quad . \quad . \quad . \quad . \quad (1)$$

As B_a is of rank m, eqns. (1) are not in general independent. If we choose m independent loops, denoting the corresponding loop matrix by B, eqns. (1) may be reduced to the set of m independent equations:[29, 37]

$$B(\boldsymbol{v} - \boldsymbol{e}) = 0 \quad . \quad . \quad . \quad . \quad . \quad . \quad . \quad (2)$$

Kirchhoff's current law equates to zero the net current leaving any node of $\mathcal{N}$. The matrix A_a specifies all the nodes of $\mathcal{N}$ in terms of their incidence with the branches. Denoting the $b \times 1$ current and current-source vectors by $\boldsymbol{i}(p)$ and $\boldsymbol{j}(p)$ respectively, the Kirchhoff current law applied to every node becomes the matrix equation

$$A_a(\boldsymbol{i} - \boldsymbol{j}) = 0 \quad . \quad . \quad . \quad . \quad . \quad . \quad . \quad (3)$$

A_a is of rank $n - 1$, and so the n equations (3) are not independent. Using the r.i.m., A, eqns. (3) may be reduced to the set of $n - 1$ independent equations[29, 37]

$$A(\boldsymbol{i} - \boldsymbol{j}) = \mathbf{0} \quad . \quad . \quad . \quad . \quad . \quad . \quad . \quad (4)$$

The two Kirchhoff laws, eqns. (2) and (4), are constraints imposed upon $\boldsymbol{v}$ and $\boldsymbol{i}$ solely by the topology of $\mathcal{N}$. The actual type of electrical elements used to make up $\mathcal{N}$ has not had to be considered. By assuming that the branches are in fact resistors, inductors and capacitors we may obtain further equations relating $\boldsymbol{v}$ and $\boldsymbol{i}$. These equations are given by a generalized Ohm's law applied to each branch. Expressed in terms of the transformed variables $\boldsymbol{v}(p)$ and $\boldsymbol{i}(p)$, this law becomes:

For a resistive kth branch,

$$v_k(p) = r_k i_k(p) \ (r_k > 0) \quad . \quad . \quad . \quad . \quad (5)$$

For a self-inductive branch,

$$v_k(p) = l_k p i_k(p) \ (l_k > 0) \quad . \ . \ . \ . \quad (6)$$

For a capacitive branch,

$$i_k(p) = c_k p v_k(p) \ (c_k > 0) \quad . \ . \ . \ . \ . \quad (7)$$

For each of the b branches of $\mathcal{N}$ one of the relations (5), (6) or (7) will hold, giving a total of b Ohm's law equations. These may be written in the matrix form

$$\boldsymbol{v}(p) = \boldsymbol{Z}(p)\boldsymbol{i}(p) \quad . \ . \ . \ . \ . \ . \quad (8)$$

where $\boldsymbol{Z}(p)$ is a diagonal $b \times b$ matrix called the branch-impedance matrix. Its diagonal elements are defined by

$Z_{kk} = r_k$, if the kth branch is resistive and of value r_k ohms.
$= pl_k$, if the kth branch is self-inductive and of value l_k henries.
$= 1/pc_k$, if the kth branch is capacitive and of value c_k farads.

The branch-impedance matrix for the network of Fig. 1 is

$$\boldsymbol{Z}(p) = \begin{bmatrix} L_1 p & . & . & . & . & . \\ . & L_2 p & . & . & . & . \\ . & . & R_3 & . & . & . \\ . & . & . & R_4 & . & . \\ . & . & . & . & \dfrac{1}{C_5 p} & . \\ . & . & . & . & . & \dfrac{1}{C_6 p} \end{bmatrix}$$

Because of the stipulation of non-zero resistances, inductances and capacitances, the matrix $\boldsymbol{Z}$ is non-singular, and so eqn. (8) may be inverted to give

$$\boldsymbol{i}(p) = \boldsymbol{Y}(p)\boldsymbol{v}(p) \quad . \ . \ . \ . \ . \ . \quad (9)$$

where $\boldsymbol{Y}(p) = \boldsymbol{Z}^{-1}(p)$. Obviously, for $p > 0$, both $\boldsymbol{Z}$ and $\boldsymbol{Y}$ are positive definite.[1]

The numbering of the branches has so far been assumed to be arbitrary. For various problems it is sometimes convenient to assume some particular ordering. Thus, at this stage we may assume that the numbering has been according to the type of element, say inductors followed by resistors followed by capacitors. In this way $\boldsymbol{Z}$ and $\boldsymbol{Y}$ may be expressed as the direct sum* of three matrices:

$$\left.\begin{aligned} \boldsymbol{Z}(p) &= p\boldsymbol{L} \dotplus \boldsymbol{R} \dotplus \frac{1}{p}\boldsymbol{S} \\ \boldsymbol{Y}(p) &= \frac{1}{p}\boldsymbol{\Gamma} \dotplus \boldsymbol{G} \dotplus p\boldsymbol{C} \end{aligned}\right\} \quad . \ . \ . \quad (10)$$

where $\boldsymbol{L}$ is a non-singular diagonal square matrix of order $b_l \times b_l$ and $\boldsymbol{\Gamma} \equiv \boldsymbol{L}^{-1}$; $\boldsymbol{R}$ is a non-singular diagonal square matrix of order $b_r \times b_r$ and $\boldsymbol{G} \equiv \boldsymbol{R}^{-1}$; $\boldsymbol{C}$ is a non-singular diagonal square matrix of order $b_c \times b_c$ and $\boldsymbol{S} \equiv \boldsymbol{C}^{-1}$.

For the network of Fig. 1, $\boldsymbol{Z}(p)$ may be expressed in the form

$$\boldsymbol{Z}(p) = \begin{bmatrix} L_1 p & . \\ . & L_2 p \end{bmatrix} \dotplus \begin{bmatrix} R_3 & . \\ . & R_4 \end{bmatrix} \dotplus \begin{bmatrix} \dfrac{1}{C_5 p} & . \\ . & \dfrac{1}{C_6 p} \end{bmatrix}$$

* The direct sum, $\boldsymbol{A} \dotplus \boldsymbol{B}$, of two square matrices $\boldsymbol{A}$ and $\boldsymbol{B}$ is the matrix $\begin{bmatrix} \boldsymbol{A} & \boldsymbol{0} \\ \boldsymbol{0} & \boldsymbol{B} \end{bmatrix}$.

The two Kirchhoff laws (2) and (4) together with Ohm's law (8) provide a total of $m + (n-1) + b$, i.e. $2b$, independent algebraic equations for the $2b$ unknowns i_k and $v_k (k = 1, 2, \ldots b)$. We may thus obtain a network solution from these equations.

(6) OTHER ANALYSIS METHODS

Eqns. (2), (4) and (8) are called the network branch equations. Two other methods of analysis are available, both well known to electrical engineers. The first involves the use of 'loop currents', and is called the loop method, while the second involves the use of 'nodal potentials' and is called the nodal method. Although each method can be used when both current and voltage sources are present, the solutions obtained in each case are very much simpler if for loop analysis it is assumed that no current sources are present, while for nodal analysis it is assumed that no voltage sources are present. Hence, to illustrate the methods, we shall assume at first that for loop analysis $\boldsymbol{j}(p) \equiv \boldsymbol{0}$, while for nodal analysis $\boldsymbol{e}(p) \equiv \boldsymbol{0}$. It should be noticed that each method depends on one of the relations $\boldsymbol{AB}' = \boldsymbol{0}$ or $\boldsymbol{BA}' = \boldsymbol{0}$ of (e).

(6.1) Loop Method[7, 20, 44]

We assume that $\boldsymbol{j} \equiv \boldsymbol{0}$. Eqns. (2), (4) and (8) become

$$\left.\begin{aligned} \boldsymbol{Bv} &= \boldsymbol{Be} \\ \boldsymbol{Ai} &= \boldsymbol{0} \\ \boldsymbol{v} &= \boldsymbol{Zi} \end{aligned}\right\} \quad . \ . \ . \ . \ . \ . \ . \quad (11)$$

First consider $\boldsymbol{Be}$; this represents a column vector of m rows. Each element, corresponding to one of the m independent loops chosen in $\mathcal{N}$, is the algebraic sum of the voltage sources contained in that loop. Thus, if we put

$$\boldsymbol{Be}(p) \ \boldsymbol{E}(p) = \quad . \ . \ . \ . \ . \ . \quad (12)$$

then $\boldsymbol{E}(p)$ is an $m \times 1$ column vector representing the loop voltage sources. Next consider $\boldsymbol{Ai} = \boldsymbol{0}$. We have $\boldsymbol{AB}' = \boldsymbol{0}$, where $\boldsymbol{A}$ is of order $(n-1) \times b$ and rank $n-1$, while $\boldsymbol{B}'$ is of order $b \times m$ and rank $m = b - n + 1$. Hence, from the theory of homogeneous equations,[1, 18] the m columns of $\boldsymbol{B}'$ form a basis for the solutions of the equation $\boldsymbol{Ai} = \boldsymbol{0}$, i.e. any solution of this equation must be of the form

$$\boldsymbol{i}(p) = \boldsymbol{B}'\boldsymbol{I}(p) \quad . \ . \ . \ . \ . \ . \quad (13)$$

for some $m \times 1$ column vector $\boldsymbol{I}(p)$. A physical interpretation of eqn. (13) shows that the elements of $\boldsymbol{I}$ form a set of independent loop or circulating currents, the use of which is well known to electrical engineers;[2, 20] a rigorous discussion of them is given by Ingram and Cramlett.[21] Eqn. (13) expresses the branch currents in terms of the loop currents.

Using eqns. (12) and (13), eqns. (11) may be transformed as follows:

$$\begin{aligned} \boldsymbol{E} &= \boldsymbol{Be} && \text{from eqn. (12)} \\ &= \boldsymbol{Bv} && \text{from eqn. (11)} \\ &= \boldsymbol{BZi} && \text{from eqn. (11)} \\ &= \boldsymbol{BZB}'\boldsymbol{I} && \text{from eqn. (13)} \\ &= \boldsymbol{Q}(p)\boldsymbol{I}(p) && \text{(say)} \quad . \ . \ . \ . \ . \ . \quad (14) \end{aligned}$$

where we have denoted the $m \times m$ matrix $[\boldsymbol{BZ}(p)\boldsymbol{B}']$ by $\boldsymbol{Q}(p)$. From this definition, remembering that $\boldsymbol{Z}$ is diagonal, the (i, j)th element of $\boldsymbol{Q}$ is given by

$$Q_{ij} = \sum_{k=1}^{b} B_{ik} Z_{kk} B_{jk} \ (i, j = 1, 2, \ldots m) \quad . \ . \quad (15)$$

Hence if $i \neq j$, Q_{ij} is made up of those branch impedances

common to both loops i and j, including a branch impedance positively if the two loops agree in orientation on the branch, while including it negatively if they disagree in orientation. If $i = j$,

$$Q_{ii} = \sum_{k=1}^{b} (B_{ik})^2 Z_{kk} \quad (i = 1, 2, \ldots m)$$

from which it is seen that Q_{ii} is made up of the positive sums of all the branch impedances contained in loop i. Thus we see that $\boldsymbol{Q}(p)$ is the well-known loop-impedance matrix, and that eqn. (14) is the set of loop equations.[2, 20]

The loop-impedance matrix for the set of loops of Fig. 6(*a*) is

$$\boldsymbol{Q}(p) = \begin{bmatrix} \left(L_1 p + R_4 + \frac{1}{C_5 p}\right) & \left(-R_4 - \frac{1}{C_5 p}\right) & -R_4 \\ \left(-R_4 - \frac{1}{C_5 p}\right) & \left(L_2 p + R_4 + \frac{1}{C_5 p} + \frac{1}{C_6 p}\right) & R_4 + \frac{1}{C_6 p} \\ -R_4 & R_4 + \frac{1}{C_6 p} & \left(R_3 + R_4 + \frac{1}{C_6 p}\right) \end{bmatrix}$$

To solve the loop equations (14) for $\boldsymbol{I}$, it is necessary to show that $\boldsymbol{Q}$ is non-singular, i.e. that det $\boldsymbol{Q}(p)$ is not identically zero in p. This follows from the fact that $\boldsymbol{Z}(p)$ is positive definite for $p > 0$, and that $\boldsymbol{B}$ is of rank m. An explicit expression may be given for det $\boldsymbol{Q}$ in the *RLC* case. This expression, which is now often called 'Kirchhoff's rule',* has its origins in a paper by Kirchhoff[23] written in 1847; it is

$$\det \boldsymbol{Q} = k^2 \sum_{\text{all co-trees of } \mathcal{N}} [\text{co-tree impedance product}] \quad . \quad (16)$$

where k is an integer, and a 'co-tree impedance product' is the product of the m branch impedances forming a co-tree of $\mathcal{N}$. Kirchhoff's rule has been discussed by many writers, e.g. References 7, 13, 16, 17, 25, 29, 31, 32, 33, 38, 45 and 50. Some of these references give proofs of eqn. (16), which follows directly from the definition of $\boldsymbol{Q}(p)$ as $\boldsymbol{BZ}(p)\boldsymbol{B}'$, by use of the Binet–Cauchy theorem[1] and results (*h*) and (*j*) above. The integer k in eqn. (16) arises from the result (*j*) concerning the m-minors of $\boldsymbol{B}$. In the particular cases of systems of loops of $\mathcal{N}$ giving k the value of unity, we obtain what Cederbaum[9] calls the 'basic' value of det $\boldsymbol{Q}$; the corresponding systems of loops he calls 'simple'. Important simple systems are the fundamental systems and also the 'meshes'† for a planar network.

of $\boldsymbol{Q}(p)$ is given as the sum of all the products shown in Table 1. This gives

$$\begin{aligned} \det \boldsymbol{Q}(p) = {} & \frac{R_3 R_4}{C_6 p} + \frac{L_1 R_3}{C_6} + L_1 R_3 R_4 p + \frac{L_1 R_4}{C_5} + \frac{L_1}{C_5 C_6 p} \\ & + \frac{R_4}{C_5 C_6 p^2} + \frac{R_3}{C_5 C_6 p^2} + \frac{L_1 R_3}{C_5} + \frac{L_2 R_4}{C_6} + L_1 L_2 R_4 p^2 \\ & + \frac{L_1 L_2 p}{C_6} + L_1 L_2 R_3 p^2 + \frac{L_2}{C_5 C_6 p} + \frac{L_2 R_3}{C_5} \\ & + \frac{L_2 R_4}{C_5} + L_2 R_3 R_4 p \end{aligned}$$

Collecting terms together, we obtain

$$\begin{aligned} \det \boldsymbol{Q}(p) = {} & \frac{1}{C_5 C_6 p^2}\{[L_1 L_2 C_5 C_6 (R_3 + R_4)] p^4 + [L_1 L_2 C_5 \\ & + L_1 L_2 R_3 R_4 C_5 C_6] p^3 + [(L_1 + L_2)(R_3 + R_4) C_6 \\ & + (L_1 R_3 + L_2 R_4) C_5] p^2 + [R_3 R_4 C_5 \\ & + (L_1 + L_2)] p + R_3 + R_4\} \end{aligned}$$

Since $\boldsymbol{Q}$ is non-singular, eqn. (14) may be inverted to give

$$\boldsymbol{I} = \boldsymbol{Q}^{-1}\boldsymbol{E} \quad . \quad . \quad . \quad . \quad . \quad . \quad . \quad (17)$$

From eqns. (12), (13) and (17),

$$\boldsymbol{i} = \boldsymbol{B}'\boldsymbol{Q}^{-1}\boldsymbol{B}\boldsymbol{e}$$

i.e.

$$\boldsymbol{i} = \boldsymbol{B}'(\boldsymbol{B}\boldsymbol{Z}\boldsymbol{B}')^{-1}\boldsymbol{B}\boldsymbol{e} \quad . \quad . \quad . \quad . \quad . \quad . \quad (18)$$

This last equation giving $\boldsymbol{i}$ in terms of $\boldsymbol{e}$ is that given by Kron[24, 25] and Synge;[44] from it, $\boldsymbol{v}$ is easily obtained using eqn. (8). It is of interest to note that, in this solution for $\boldsymbol{i}$ and $\boldsymbol{v}$, the branch voltage sources, $\boldsymbol{e}$, are included only as the product $\boldsymbol{Be}$, i.e. $\boldsymbol{E}$. This means that the actual branch distribution of the voltage sources is not important; only their loop distribution, $\boldsymbol{E}$, matters.

Table 1

THE CO-TREE IMPEDANCE PRODUCTS OF $\mathcal{N}$

Part of Fig. 5:	(*a*)	(*b*)	(*c*)	(*d*)	(*e*)	(*f*)	(*g*)	(*h*)
Co-tree impedance product	$\frac{R_3 R_4}{C_6 p}$	$\frac{L_1 R_3}{C_6}$	$L_1 R_3 R_4 p$	$\frac{L_1 R_4}{C_5}$	$\frac{L_1}{C_5 C_6 p}$	$\frac{R_4}{C_5 C_6 p^2}$	$\frac{R_3}{C_5 C_6 p^2}$	$\frac{L_1 R_3}{C_5}$
Part of Fig. 5:	(*i*)	(*j*)	(*k*)	(*l*)	(*m*)	(*n*)	(*p*)	(*q*)
Co-tree impedance product	$\frac{L_2 R_4}{C_6}$	$L_1 L_2 R_4 p^2$	$\frac{L_1 L_2 p}{C_6}$	$L_1 L_2 R_3 p^2$	$\frac{L_2}{C_5 C_6 p}$	$\frac{L_2 R_3}{C_5}$	$\frac{L_2 R_4}{C_5}$	$L_2 R_3 R_4 p$

The 16 co-tree impedance products of Fig. 1 are shown in Table 1. Since the system of loops defining $\boldsymbol{Q}(p)$ is fundamental, and hence simple, we obtain from eqn. (16) that the determinant

There is also a choice in the actual system of independent loops used, giving further possible distributions. For example, suppose a system of fundamental loops is chosen; then the network response will be unchanged if, instead of having the branch voltage sources $e_1, e_2, \ldots e_b$, only m voltage sources are used, one in each chord and having the values $E_1, E_2, \ldots E_m$, where

* Strictly, Kirchhoff's rule provides a method of solving for the branch currents in terms of the branch voltage sources. The essence of this rule, however, is contained in eqn. (16).

† As we have already remarked, we use the term 'mesh' to refer to those loops which form the 'windows' of a planar network.

$= \boldsymbol{B}_f \boldsymbol{e}$. Further, any other fundamental system may be used, with a corresponding change in $\boldsymbol{B}_f$ and $\boldsymbol{E}$. It is important to remember that by the term 'network response' we mean the *passive-branch* currents and potentials.

(6.2) Nodal Method[20, 41]

We assume now that $\boldsymbol{e} \equiv \boldsymbol{0}$ and $\boldsymbol{j} \neq \boldsymbol{0}$. Instead of eqn. (8) we use instead its inverse eqn. (9), together with eqns (2) and (4). Thus

$$\left.\begin{aligned} \boldsymbol{Bv} &= \boldsymbol{0} \\ \boldsymbol{Ai} &= \boldsymbol{Aj} \\ \boldsymbol{i} &= \boldsymbol{Yv} \end{aligned}\right\} \quad . \quad . \quad . \quad . \quad . \quad . \quad . \quad (19)$$

First consider $\boldsymbol{Aj}$; this represents a column vector of $n-1$ rows; each element corresponds to one of the nodes 1, 2, . . . $(n-1)$ of $\mathcal{N}$ and is the algebraic sum of the branch sources entering that node. Thus, if we put

$$\boldsymbol{Aj}(p) \equiv \boldsymbol{J}(p) \quad . \quad . \quad . \quad . \quad . \quad . \quad (20)$$

then $\boldsymbol{J}$ is an $(n-1) \times 1$ column vector representing the nodal current sources. Next consider $\boldsymbol{Bv} = \boldsymbol{0}$. We have $\boldsymbol{BA}' = \boldsymbol{0}$, where $\boldsymbol{B}$ is of order $m \times b$ and rank m, while $\boldsymbol{A}'$ is of order $b \times (n-1)$ and rank $n-1 = b-m$. Hence we have, from the theory of homogeneous equations,[1, 18] that the $n-1$ columns of $\boldsymbol{A}'$ form a basis for the solutions of the equations $\boldsymbol{Bv} = \boldsymbol{0}$, i.e. any solution of this equation must be of the form

$$\boldsymbol{v}(p) = \boldsymbol{A}'\boldsymbol{V}(p) \quad . \quad . \quad . \quad . \quad . \quad (21)$$

for some $(n-1) \times 1$ column vector $\boldsymbol{V}(p)$. A physical interpretation of eqn. (21) shows that the $n-1$ elements of the vector $\boldsymbol{V}$ are the potentials of nodes 1, 2, . . . $(n-1)$ relative to that of node n; the use of these nodal potentials is well known to electrical engineers.[2] Eqn. (21) expresses the branch potential differences in terms of the nodal potentials.

Using eqns. (20) and (21), eqn. (19) may be transformed as follows:

$$\begin{aligned} \boldsymbol{J} &= \boldsymbol{Aj} && \text{from eqn. (20)} \\ &= \boldsymbol{Ai} && \text{from eqn. (19)} \\ &= \boldsymbol{AYv} && \text{from eqn. (19)} \\ &= \boldsymbol{AYA}'\boldsymbol{V} && \text{from eqn. (21)} \\ &= \boldsymbol{P}(p)\boldsymbol{V}(p) && \text{(say)} \quad . \quad . \quad . \quad . \quad . \quad . \quad (22) \end{aligned}$$

where we have denoted the $(n-1) \times (n-1)$ matrix $[\boldsymbol{AY}(p)\boldsymbol{A}']$ by $\boldsymbol{P}(p)$. From this definition, remembering that $\boldsymbol{Y}$ is diagonal, the (i, j)th element of $\boldsymbol{P}$ is given by

$$P_{ij} = \sum_{k=1}^{b} A_{ik} Y_{kk} A_{jk} \quad [i, j = 1, 2, \ldots (n-1)] \quad . \quad (23)$$

Hence if $i \neq j$, P_{ij} is the negative sum of the branch admittances incident with both nodes i and j. If $i = j$,

$$P_{ii} = \sum_{k=1}^{b} (A_{ik})^2 Y_{kk} \quad [i = 1, 2, \ldots (n-1)]$$

from which it is seen that P_{ii} is the sum of all the branch admittances incident at node i. Thus we see that $\boldsymbol{P}(p)$ is the well-known nodal admittance matrix of $\mathcal{N}$ with respect to node n, and that eqn. (22) is the set of nodal equations.[2, 20]

The non-singularity of $\boldsymbol{P}$ follows from considerations similar to those for $\boldsymbol{Q}$. An explicit expression for $\det \boldsymbol{P}$ may be obtained for *RLC* networks, this expression often being known as the 'dual Kirchhoff rule', or 'Maxwell's rule'.[28]* It has been written about by many authors, e.g. References 4, 13, 14, 17, 25, 26, 29, 31, 32, 33, 38, 42 and 50. The expression is as follows:

$$\det \boldsymbol{P} = \sum_{\text{all trees of } \mathcal{N}} [\text{tree admittance product}] \quad . \quad . \quad (24)$$

where a 'tree admittance product' is the product of the $n-1$ branch admittances forming a tree of $\mathcal{N}$. Notice that there is no constant multiplier of the form k^2, as there was in eqn. (16) for $\det \boldsymbol{Q}$; this is because $\boldsymbol{A}$ is an E-matrix [see (*i*)].

Eqn. (22) may now be inverted to give

$$\boldsymbol{V} = \boldsymbol{P}^{-1}\boldsymbol{J} \quad . \quad . \quad . \quad . \quad . \quad . \quad (25)$$

From eqns. (20), (21) and (25),

$$\boldsymbol{v} = \boldsymbol{A}'\boldsymbol{P}^{-1}\boldsymbol{Aj}$$

i.e.

$$\boldsymbol{v} = \boldsymbol{A}'(\boldsymbol{AYA}')^{-1}\boldsymbol{Aj} \quad . \quad . \quad . \quad . \quad . \quad (26)$$

This last equation, giving $\boldsymbol{v}$ in terms of $\boldsymbol{j}$, is that given by Saltzer[41] and is a particular case of Kron's node-pair equations.[24, 27] Using eqn. (9), $\boldsymbol{i}$ is easily obtained from $\boldsymbol{v}$. It is of interest to note that, in this solution for $\boldsymbol{v}$ and $\boldsymbol{i}$, the branch current sources $\boldsymbol{j}$ are included only as the product $\boldsymbol{Aj}$, i.e. $\boldsymbol{J}$. This means that the actual branch distribution of the current sources is not important; only the nodal distribution $\boldsymbol{J}$ matters. Thus the network response will be unchanged if, instead of having the branch current sources $j_1, j_2, \ldots j_b$, only $n-1$ current sources are used, one across each of the node-pairs $(n1)$, $(n2)$, . . . $[n(n-1)]$, of values $J_1, J_2, \ldots J_{n-1}$, where $\boldsymbol{J} = \boldsymbol{Aj}$. As in the loop case, the precise meaning of the term 'network response' must be clearly understood to be the *passive-branch* currents and potentials.

(6.3) Mixed Method

If both $\boldsymbol{j} \not\equiv \boldsymbol{0}$ and $\boldsymbol{e} \not\equiv \boldsymbol{0}$, then to analyse the network by either a loop or nodal method requires some slight modification from the above. Thus, instead of, in the loop case, $\boldsymbol{i}$ being expressible in terms of loop currents $\boldsymbol{I}$, it is the difference $\boldsymbol{i} - \boldsymbol{j}$ which is equal to the product $\boldsymbol{B}'\boldsymbol{I}$. Loop analysis now involves the following steps:

(i) Since $\boldsymbol{A}(\boldsymbol{i} - \boldsymbol{j}) = 0$, then $(\boldsymbol{i} - \boldsymbol{j}) = \boldsymbol{B}'\boldsymbol{I}$, thus defining the 'loop-currents' $\boldsymbol{I}$.

(ii) Defining $\boldsymbol{E} = \boldsymbol{Be} = \boldsymbol{Bv}$ as before, then $\boldsymbol{v} = \boldsymbol{Zi}$ gives

$$\boldsymbol{E} = \boldsymbol{BZB}'\boldsymbol{I} + \boldsymbol{BZj}$$

i.e.

$$\boldsymbol{I} = \boldsymbol{Q}^{-1}(\boldsymbol{E} - \boldsymbol{BZj})$$

(iii) Using (i), gives

$$(\boldsymbol{i} - \boldsymbol{j}) = \boldsymbol{B}'\boldsymbol{Q}^{-1}\boldsymbol{B}(\boldsymbol{e} - \boldsymbol{Zj}) \quad . \quad . \quad . \quad (27)$$

giving $\boldsymbol{i}$ and hence also $\boldsymbol{v}$.

A more elegant method of solution, however, makes use of the linearity of the network and applies the principle of superposition to the solutions already obtained in Sections 6.1 and 6.2. By this method we obtain immediately from eqns. (18) and (26)

$$\left.\begin{aligned} \boldsymbol{i} &= \boldsymbol{B}'\boldsymbol{Q}^{-1}\boldsymbol{Be} + \boldsymbol{YA}'\boldsymbol{P}^{-1}\boldsymbol{Aj} \\ \text{and} \quad \boldsymbol{v} &= \boldsymbol{ZB}'\boldsymbol{Q}^{-1}\boldsymbol{Be} + \boldsymbol{A}'\boldsymbol{P}^{-1}\boldsymbol{Aj} \end{aligned}\right\} \quad . \quad . \quad (28)$$

This solution can be put into the form of eqn. (27) by using the following relations, which may be proved by matrix manipulation:

$$\boldsymbol{YA}'\boldsymbol{P}^{-1}\boldsymbol{A} + \boldsymbol{B}'\boldsymbol{Q}^{-1}\boldsymbol{BZ} = \boldsymbol{1}_b \quad . \quad . \quad . \quad . \quad (29)$$

and

$$\boldsymbol{ZB}'\boldsymbol{Q}^{-1}\boldsymbol{B} + \boldsymbol{A}'\boldsymbol{P}^{-1}\boldsymbol{AY} = \boldsymbol{1}_b \quad . \quad . \quad . \quad (30)$$

* As with Kirchhoff's rule, this dual, first given by Maxwell, is strictly a method of solving for the branch voltages in terms of the branch current sources. The essence of the rule, however, is contained in eqn. (24).

Applying these to eqn. (28), we obtain

$$(i - j) = B'Q^{-1}B(e - Zj) \quad . \quad . \quad . \quad . \quad (31)$$

and

$$(v - e) = A'P^{-1}A(j - Ye) \quad . \quad . \quad . \quad . \quad (32)$$

The form of this solution has an interesting interpretation. Thus the left-hand side of eqn. (31), i.e. $i - j$, represents the active-branch currents, as shown in Fig. 8. An interpretation of the

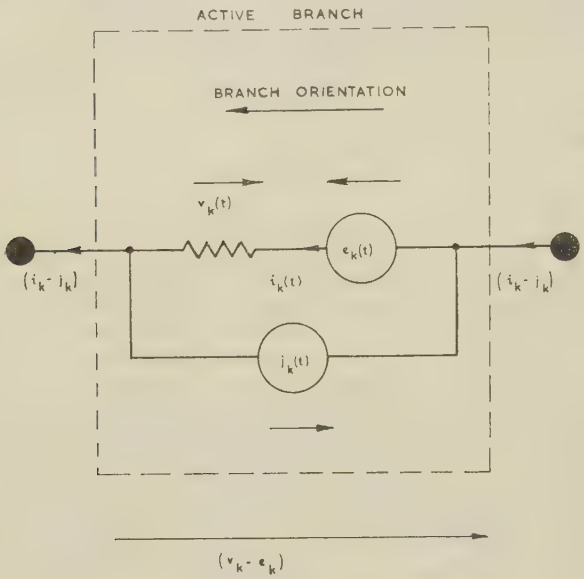

Fig. 8.—Active branch currents and potentials.

right-hand side of eqn. (31) shows that if each branch current source, j_k, in parallel with the branch is replaced by a voltage source in series with the branch and of value $-Z_{kk}j_k$, then the active-branch currents $i - j$ will remain unchanged. It is important to realize, however, that in general the passive-branch currents and so also the passive-branch potentials will change. A similar argument may be applied to eqn. (32), replacing the branch voltage sources in series by branch current sources in parallel and leaving unchanged the active-branch potentials $v - e$. Again, however, the passive-branch potentials and currents will change.

(6.4) Possibility of Other Methods

The basis of the loop and nodal methods of analysis is the existence of the loop and nodal matrices B and A having the properties:

(i) They are of orders $m \times b$ and $(n - 1) \times b$, respectively, where $m + n - 1 = b$.

(ii) They are of ranks m and $n - 1$, respectively.

(iii) They satisfy the relation $BA' = 0$, and so also $AB' = 0$.

(iv) They are such that the Kirchhoff laws may be expressed in the forms

$$B(v - e) = 0$$

$$A(i - j) = 0$$

Any two matrices possessing all the properties (i)–(iv) may obviously be used to carry out two corresponding methods of analysis. This is in fact done in Section 8, using the 'cut-set' matrix, C, and the loop matrix, B, as our pair of matrices. It is important to notice that, if any two matrices, say M and N, have the properties (i)–(iv), they must be related to B and A by the relations

$$M = T_1B \quad . \quad . \quad . \quad . \quad . \quad . \quad (33)$$

$$N = T_2A \quad . \quad . \quad . \quad . \quad . \quad . \quad (34)$$

where T_1 and T_2 are two non-singular matrices of orders $m \times$ and $(n - 1) \times (n - 1)$, respectively. These relations are als sufficient, as is obvious. To prove necessity we proceed a follows:

Since $MN' = 0$, then for any $(n - 1) \times 1$ vector V_1, th vector x given by $x = N'V_1$, will satisfy $Mx = 0$, and so satisf Kirchhoff's voltage law by condition (iv). Hence there is a $(n - 1) \times 1$ vector V_2 such that $x = A'V_2$ for this V_1, i.e.

$$N'V_1 = A'V_2 \quad . \quad . \quad . \quad . \quad . \quad . \quad (35$$

This is true for any V_1; choose a set of $n - 1$ linearly indep pendent vectors $(V_1)_1(V_1)_2 \ldots (V_1)_{n-1}$ and denote by W_1 th non-singular $(n - 1) \times (n - 1)$ matrix formed from thes vectors. Denote the $(n - 1) \times (n - 1)$ matrix of the corre sponding vectors V_2 by W_2. Then

$$N = T_2A \quad . \quad . \quad . \quad . \quad . \quad . \quad (36$$

where $T_2 = (W_2W_1^{-1})'$. T_2 is non-singular since N and A a both of rank $n - 1$. Similarly for M and B.

(7) MUTUAL INDUCTANCE

An *RLC* network containing mutual inductance is called a *RLCM* network, and is denoted by $\mathcal{N}$ as before. The ter 'mutual inductance' is not meant to include the case of the ide transformer. Mutual inductance is defined as follows. Co sider a set of b_l self-inductors of values $l_{11}, l_{22}, \ldots l_{b_lb_l}$. The we say that mutual-inductive coupling exists between them the following equations hold:

$$\left.\begin{aligned} v_1(p) &= l_{11}pi_1(p) + l_{12}pi_2(p) + \ldots + l_{1b_l}pi_{b_l}(p) \\ v_2(p) &= l_{21}pi_1(p) + l_{22}pi_2(p) + \ldots + l_{2b_l}pi_{b_l}(p) \\ &\cdot \\ &\cdot \\ &\cdot \\ v_{b_l}(p) &= l_{b_l1}pi_1(p) + l_{b_l2}pi_2(p) + \ldots + l_{b_lb_l}pi_{b_l}(p) \end{aligned}\right\} \quad . \quad (37$$

together with the restriction

$$[l_{jk}] \text{ is a positive semi-definite matrix}^1 \quad . \quad . \quad (38$$

The restriction (38) is usually looked upon as a stipulation t ensure the passivity of the network.[7, 20] It may also b considered in a rather different way. Thus we have so far mad no mention of the physical realization of mutual inductanc As is well known, however, realization is obtained by having coils with magnetic coupling between them. Hence condi tion (38) should follow from a consideration of the magnet flux linkage of the coils. This is shown for the case of tw coils by Guillemin,[20] and by Duffin[15] for the general case. Th sufficiency of the restriction (38) has been shown by Cauer[7] an Duffin.[15]

Let us now consider the semi-definiteness of $[l_{jk}]$. If $[l_{jk}]$ not positive definite, it contains some principal submatri which is singular. If any inductors are so coupled that the matrix is singular, while no principal submatrix, correspondin to some subset of the inductors, is singular, then the set o inductors is called 'tightly coupled'. If $\mathcal{N}$ contains no tight coupled inductors, the matrix $[l_{jk}]$ will be non-singular and s positive definite. We shall assume that this is the case unles the contrary is specified.

Consider now a general *RLCM* network, $\mathcal{N}$, containing m tight coupling. The generalized Ohm's law equations for th resistive and capacitive branches are still eqns. (5) and (7 namely

$$v_k(p) = r_ki_k(p)$$

and

$$i_k(p) = c_kpv_k(p)$$

The inductive branches now obey eqns. (37), together with the restriction (38). Thus, if we express the branch-impedance matrix $Z(p)$ as a direct sum as in eqn. (10), namely

$$Z(p) = pL \dot{+} R \dot{+} \frac{1}{p}S \quad . \quad . \quad . \quad . \quad . \quad (39)$$

the matrix L is no longer diagonal but is the matrix $[l_{jk}]$ of eqn. (37). Matrices R and C are, of course, still diagonal. Because we are assuming no tight coupling, Z is non-singular and so may be inverted to give

$$Y(p) = \frac{1}{p}\Gamma \dot{+} G \dot{+} pC \quad . \quad . \quad . \quad . \quad (40)$$

where $\Gamma \equiv L^{-1}$, $G \equiv R^{-1}$ and $S \equiv C^{-1}$. Now, Γ is no longer diagonal, though G and C are. The matrices L, Γ, R, G, S and C are all positive definite, and hence so also are $Z(p)$ and $Y(p)$ for $p > 0$.

The graph of an *RLCM* network, which is obtained by ignoring the mutual coupling, may be studied topologically as in the *RLC* case. Now, however, the network will probably not be connected, and so slight modifications must be made to allow for this. We shall assume that $\mathcal{N}$ consists of s separate parts. The incidence matrix A_a may be defined as in Section 3, and by result (*a*) of that Section, A_a will be of rank $n - s$. A reduced incidence matrix A of order $(n - s) \times b$ is obtained from A_a by deleting s rows, one corresponding to a node in each separate part. These s nodes form a set of s 'reference nodes', one in each part of $\mathcal{N}$; we shall assume that they have been numbered as the last s nodes, i.e. from $n - s + 1$ to n inclusive. By considering separately each part of A_a and A corresponding to each part of $\mathcal{N}$, it is easy to see that A is of rank $n - s$. Oriented loops in $\mathcal{N}$ may be defined exactly as in the connected case, and a corresponding matrix B_a defined. The concept of a tree, however, needs some discussion. If $\mathcal{N}$ is not connected it will not contain any trees: however, the separate parts of $\mathcal{N}$ will each contain trees and we consider a subnetwork of $\mathcal{N}$ made up of s trees, one from each separate part. This subnetwork is made up of s separate parts, it contains all the nodes of $\mathcal{N}$, but contains no loops. Such a subnetwork of $\mathcal{N}$ we call a 'forest' of $\mathcal{N}$.[5, 6, 46] Obviously, any forest of $\mathcal{N}$ contains $n - s$ branches. Given any forest, the $b - n + s$ branches of $\mathcal{N}$ not contained in it are called 'chords' of the forest, and are said to form a 'co-forest' of $\mathcal{N}$. By considering each separate part of $\mathcal{N}$ it is seen that a system of $b - n + s$ 'fundamental loops' is defined by these chords, having matrix B_f, say, of order $(b - n + s) \times b$; the rank of B_f will be $b - n + s$, since it will contain a unit matrix of that order. Thus we see, by arguments similar to those of Section 4, that B_a is of rank $b - n + s$, so that $\mathcal{N}$ contains this number of independent loops. We again use m to denote the number $b - n + s$, which is again called the nullity or cyclomatic number of $\mathcal{N}$. Any set of m independent rows of B_a will define a submatrix of B_a of rank m, called a loop matrix of $\mathcal{N}$ and denoted by B; the corresponding loops of $\mathcal{N}$ form an independent set.

The electrical considerations of our *RLCM* network are similar to those of Sections 5 and 6 for *RLC* networks. Ohm's law has already been considered, and the two Kirchhoff laws may again be written in the form

$$B(v - e) = 0 \quad . \quad . \quad . \quad . \quad . \quad (41)$$

$$A(i - j) = 0 \quad . \quad . \quad . \quad . \quad . \quad (42)$$

We again obtain a total of $2b$ equations for the $2b$ unknowns v_k and i_k, and so a solution may be found. The algebraic processes of the nodal and loop methods of analysis still apply, but the physical interpretation of the nodal voltage vector V and the nodal current source vector J must be made with a little care. We obtain, as before, a loop impedance matrix Q and a nodal admittance matrix P, given by

$$Q = BZB' \quad . \quad . \quad . \quad . \quad . \quad . \quad (43)$$

$$P = AYA' \quad . \quad . \quad . \quad . \quad . \quad . \quad (44)$$

Because Z and Y are no longer diagonal, the elements of Q and P are not quite so simply stated in words as in Section 6. Assuming that there is no tight coupling, both matrices are non-singular, although the explicit forms for det Q and det P given by the Kirchhoff rule and its dual no longer hold. An interesting relation between det Q and det P has been given by Cederbaum;[9] this is a generalization of a result by Tsang[47] for *RLC* networks, and is as follows:

$$\det Q = k^2 (\det Z)(\det P) \quad . \quad . \quad . \quad . \quad (45)$$

This relation also follows from the work of Bott and Duffin,[3] who give a very interesting algebraical interpretation of the currents and potentials in electrical networks.

The results and discussions of Sections 6.3 and 6.4, concerning the mixed method of solution and the possibility of other methods, extend to *RLCM* networks.

We end this Section by giving a slightly different approach which may be used when dealing with non-connected networks; this approach is sometimes simpler than the one used above. The method is to make $\mathcal{N}$ connected by identifying all the s reference nodes as one single reference node. This new network will then be connected and will contain $n - s + 1$ nodes. The reduced incidence matrix, A, of this new network will be identical with that of the original non-connected network. The distribution of branch currents and potentials in the modified network will be the same as the original distribution, and so the two networks are electrically equivalent. The modified network is, in fact, a 'separable' network,[36] which is defined to be a network containing at least one subnetwork which has only one node in common with its complement.

(8) CUT-SETS

The concept of a 'cut-set' of a network was first introduced by Whitney.[51] A study of their properties and applications to network theory has also been made by Guillemin,[20] Seshu and Reed[43] and Cederbaum,[8, 9, 11] from which sources much of the following treatment derives.

(8.1) Cut-Sets and Cut-Set Matrices

Definition 3.—A cut-set of a network is a set of network branches whose removal increases the connectivity of the network by one, provided that no proper subset of the set has this property (see Fig. 9).

In this Section we shall consider only connected networks.

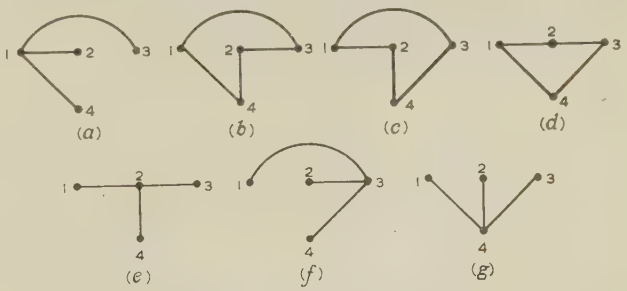

Fig. 9.—The seven cut-sets of $\mathcal{N}$.

Non-connected networks may be considered as connected by the method discussed in Section 7, or the results may be extended to include the non-connected case without much difficulty.

Since the removal of a cut-set divides $\mathcal{N}$ into two separate pieces, $\mathcal{N}_1$ and $\mathcal{N}_2$, say, each branch of the cut-set has one vertex (i.e. terminating node) in $\mathcal{N}_1$ and the other vertex in $\mathcal{N}_2$ (see Fig. 10). We may thus define an orientation of the cut-set by an ordering of $\mathcal{N}_1$ and $\mathcal{N}_2$ as either $(\mathcal{N}_1\mathcal{N}_2)$ or $(\mathcal{N}_2\mathcal{N}_1)$. If the cut-set is oriented as $(\mathcal{N}_1\mathcal{N}_2)$, an oriented branch of the cut-set is said to have the same orientation as the cut-set if it is oriented away from its vertex in $\mathcal{N}_1$ and towards its vertex in $\mathcal{N}_2$.

Fig. 9 shows all the cut-sets of the network of Fig. 1. These are shown dividing $\mathcal{N}$ into two parts $\mathcal{N}_1$ and $\mathcal{N}_2$ in Fig. 10, where an arbitrary orientation of each cut-set is also indicated.

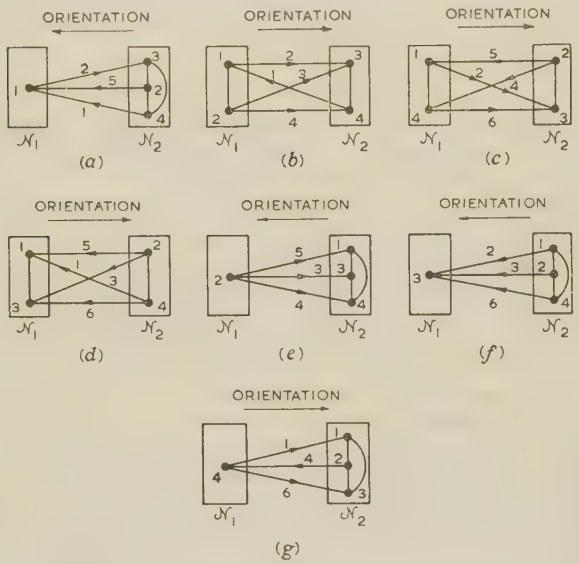

Fig. 10.—An orientation of the seven cut-sets of $\mathcal{N}$.

Notice that the two networks $\mathcal{N}_1$ and $\mathcal{N}_2$ must each be connected when $\mathcal{N}$ is connected, for otherwise removal of the cut-set will divide $\mathcal{N}$ into more than two separate subnetworks, contrary to the definition of a cut-set. Hence contraction of those network branches not contained in the cut-set leaves the cut-set as a parallel arrangement of branches between two nodes.

In general, $\mathcal{N}$ will contain many cut-sets, which may be arbitrarily numbered and oriented. Incidence between network branches and cut-sets may be described algebraically by a matrix $\boldsymbol{C}_a$, containing b columns, one for each branch of $\mathcal{N}$, and a finite number of rows, one for each cut-set of $\mathcal{N}$. The elements C_{jk} of $\boldsymbol{C}_a$ are $+1$, -1 or 0 as follows:

$C_{jk} = +1$, if branch k is incident with cut-set j and has the same orientation.

$C_{jk} = -1$, if branch k is incident with cut-set j and has the opposite orientation.

$C_{jk} = 0$ if branch k and cut-set j are not incident.

The matrix $\boldsymbol{C}_a$ for the cut-sets of Fig. 10 is

$$\boldsymbol{C}_a = \begin{bmatrix} 1 & -1 & 0 & 0 & 1 & 0 \\ -1 & 1 & 1 & 1 & 0 & 0 \\ 0 & 1 & 0 & -1 & -1 & 1 \\ -1 & 0 & -1 & 0 & -1 & -1 \\ 0 & 0 & -1 & -1 & -1 & 0 \\ 0 & 1 & 1 & 0 & 0 & 1 \\ 1 & 0 & 0 & -1 & 0 & 1 \end{bmatrix}$$

Seshu and Reed[43] have shown that $\boldsymbol{C}_a$ satisfies the relation $\boldsymbol{B}\boldsymbol{C}_a' = \boldsymbol{0}$, and so also $\boldsymbol{C}_a\boldsymbol{B}' = \boldsymbol{0}$. They have also shown an intimate relation between cut-sets and trees, namely that a cut-set is a minimal set of branches containing at least one branch of every tree of $\mathcal{N}$. As with loops, trees provide the basis of defining a 'fundamental' system of independent cut-sets as follows:

Consider any tree of $\mathcal{N}$; each branch of this tree is a cut-set *of the tree* and so divides its nodes, i.e. the nodes of $\mathcal{N}$, into two sets. Thus each tree branch, together with certain of the tree chords, will define a cut-set of $\mathcal{N}$. It may be shown[43] that those chords which combine with any one tree branch to form this cut-set are the chords whose fundamental loops contain the tree branch. We thus obtain a system of $n-1$ cut-sets of $\mathcal{N}$, one from each tree branch. Such a system is called a 'fundamental system', and has the following properties. Because each cut-set of the fundamental system contains precisely one branch of the tree, the corresponding submatrix of order $(n-1) \times b$ of $\boldsymbol{C}_a$ will, with suitable ordering and orientation of the cut-sets, contain a unit matrix of order $n-1$. This, together with the relation $\boldsymbol{B}\boldsymbol{C}_a' = \boldsymbol{0}$, gives:[43]

(*o*) $\boldsymbol{C}_a$ is of rank $n-1$ for a connected network.

Any submatrix of $\boldsymbol{C}_a$, of order $(n-1) \times b$ and defining a fundamental system, is denoted by $\boldsymbol{C}_f$; we see from the above discussion that the rows of $\boldsymbol{C}_f$ form a basis for the rows of $\boldsymbol{C}_a$. However, any $(n-1) \times b$ submatrix of $\boldsymbol{C}_a$ which is of rank $n-1$ will also have this property, and so will define a system of $n-1$ independent cut-sets. Such a matrix is called a 'cut-set matrix' of $\mathcal{N}$ and is denoted by $\boldsymbol{C}$. Because the rows of $\boldsymbol{C}$ and $\boldsymbol{C}_f$ form bases for the rows of $\boldsymbol{C}_a$, there exists a non-singular matrix $\boldsymbol{T}$ such that

$$\boldsymbol{C} = \boldsymbol{T}\boldsymbol{C}_f \quad . \quad . \quad . \quad . \quad . \quad . \quad . \quad (46)$$

But $\boldsymbol{C}_f$ contains a unit matrix, and the elements of $\boldsymbol{C}$ are ± 1 or 0; hence the elements of $\boldsymbol{T}$ are also ± 1 or 0.

Suppose the numbering and orientations of the cut-sets are such that, for a particular fundamental system, $\boldsymbol{C}_f$ is of the form

$$\boldsymbol{C}_f = (\boldsymbol{E}, \boldsymbol{1}_{n-1}) \quad . \quad . \quad . \quad . \quad . \quad . \quad (47)$$

while the loops have been so numbered and oriented that the corresponding matrix $\boldsymbol{B}_f$ is of the form

$$\boldsymbol{B}_f = (\boldsymbol{1}_m, \boldsymbol{F}) \quad . \quad . \quad . \quad . \quad . \quad . \quad . \quad (48)$$

Let the corresponding form of $\boldsymbol{A}$ be

$$\boldsymbol{A} = (\boldsymbol{X}, \boldsymbol{K}) \quad . \quad . \quad . \quad . \quad . \quad . \quad . \quad (49)$$

where, from eqn. (47), $\boldsymbol{K}$ is the r.i.m. of a tree, and so is non-singular by (*g*). From the relations

$$\boldsymbol{B}_f\boldsymbol{A}' = \boldsymbol{B}_f\boldsymbol{C}_f' = \boldsymbol{0} \quad . \quad . \quad . \quad . \quad . \quad (50)$$

(*p*)
$$\boldsymbol{E} = -\boldsymbol{F}' = \boldsymbol{K}^{-1}\boldsymbol{X} \quad . \quad . \quad . \quad . \quad . \quad (51)$$

and
$$\boldsymbol{C}_f = \boldsymbol{K}^{-1}\boldsymbol{A} \quad . \quad . \quad . \quad . \quad . \quad . \quad (52)$$

The fundamental system of cut-sets corresponding to the tree of Fig. 4(*l*) are those numbered (*a*), (*b*) and (*f*) in Figs. 9 and 10. The corresponding matrix $\boldsymbol{C}_f$ is given by

$$\boldsymbol{C}_f = \begin{bmatrix} -1 & 1 & 1 & 1 & 0 & 0 \\ 1 & -1 & 0 & 0 & 1 & 0 \\ 0 & 1 & 1 & 0 & 0 & 1 \end{bmatrix} \quad . \quad . \quad (53)$$

This is of the form

$$\boldsymbol{C}_f = [\boldsymbol{E}, \boldsymbol{1}_3]$$

where

$$E = \begin{bmatrix} -1 & 1 & 1 \\ 1 & -1 & 0 \\ 0 & 1 & 1 \end{bmatrix}$$

The matrix E should be compared with the product $K^{-1}X$ given in Section 4; their equality illustrates the result (p).

From eqns. (46) and (52), and using (g), we obtain:

(q) An $(n-1)$ — minor of C (or C_f) is non-singular if and only if the columns of the minor correspond to branches of a tree of $\mathcal{N}$.

Further, because the elements of K^{-1} and T in eqns. (52) and (46) are ± 1 or 0,

(r) The value of all non-zero $(n-1)$ — minors of C is $+k$ or $-k$, for some integer k.

Cederbaum[8, 11] has shown the following result:

(s) C_f is an E-matrix.

A method of realizing a fundamental cut-set matrix C_f has been developed by Gould.[19] Seshu and Reed[43] have obtained the following result:

(t) If M is any matrix of order $(n-1) \times b$ and of rank $n-1$, having $M_{jk} = \pm 1$ or 0, and satisfying

$$BM' = 0$$

for some loop matrix B of $\mathcal{N}$, then each row of M represents either a cut-set of $\mathcal{N}$ or a disjoint union of such cut-sets.

(8.2) Electrical Applications of Cut-Sets

The basis of the application of cut-sets to network analysis lies in the considerations of Section 6.4. Thus, from eqns. (46) and (52),

$$C = TK^{-1}A \quad . \quad . \quad . \quad . \quad . \quad . \quad (54)$$

and so C and B satisfy the necessary and sufficient conditions of Section 6.4 to possess properties (i)–(iv) of that Section. Hence, a cut-set analysis of $\mathcal{N}$ may be carried through, analogous to nodal analysis. We assume at first that $e \equiv 0$, and define the $(n-1) \times 1$ column vector

$$J^c(p) = Cj(p)$$

calling it the cut-set current-source vector. We may also define the $(n-1) \times 1$ column vector $V^c(p)$ satisfying

$$v(p) = C'V^c(p) \quad . \quad . \quad . \quad . \quad . \quad (55)$$

V^c is the cut-set potential vector. Carrying through a process similar to that of nodal analysis we obtain

$$J^c = CYC'V^c \quad . \quad . \quad . \quad . \quad . \quad . \quad (56)$$

We denote the matrix $CY(p)C'$ by $P^c(p)$, and call it the 'cut-set admittance matrix'.

The cut-set admittance matrix for the system of fundamental cut-sets defined by eqn. (53) is

$$P^c(p) = \begin{bmatrix} \left(\frac{1}{L_1p} + \frac{1}{L_2p} + \frac{1}{R_3} + \frac{1}{R_4}\right) & -\frac{1}{L_1p} - \frac{1}{L_2p} & \frac{1}{L_2p} + \frac{1}{R_3} \\ -\frac{1}{L_1p} - \frac{1}{L_2p} & \left(\frac{1}{L_1p} + \frac{1}{L_2p} + C_5p\right) & -\frac{1}{L_2p} \\ \frac{1}{L_2p} + \frac{1}{R_3} & -\frac{1}{L_2p} & \left(\frac{1}{L_2p} + \frac{1}{R_3} + C_6p\right) \end{bmatrix}$$

Notice that, from eqn. (54),

$$\det P^c = (\det T)^2 (\det K^{-1})^2 (\det P)$$
$$= k^2 \det P \quad . \quad . \quad . \quad . \quad . \quad . \quad . \quad (57)$$

where P is the nodal admittance matrix and k is an integer; [cf. result (r)]. The particular cases of systems of cut-sets giving $k = \pm 1$ in eqn. (57) give what Cederbaum[8, 9] calls the 'basic' value of $\det P^c$; the corresponding systems of cut-sets he calls 'simple'. Fundamental systems are particular cases of simple systems. From eqn. (57), since P is non-singular, so also is P^c. Hence, from eqns. (55) and (56),

$$v = C'(P^c)^{-1}Cj \quad . \quad . \quad . \quad . \quad . \quad (58)$$

and so

$$i = YC'(P^c)^{-1}Cj \quad . \quad . \quad . \quad . \quad . \quad (59)$$

If voltage sources are assumed to be present, arguments similar to those used in Section 6.3 show that a mixed method will give

$$i = B'Q^{-1}Be + YC'(P^c)^{-1}Cj \quad . \quad . \quad . \quad (60)$$

and

$$v = ZB'Q^{-1}Be + C'(P^c)^{-1}Cj \quad . \quad . \quad . \quad (61)$$

which are the equations equivalent to eqn. (28).

(9) CONCLUSION

A rigorous development of three methods of network analysis has been obtained. These are nodal analysis, loop analysis and cut-set analysis. In a later paper it is hoped to present two further methods of analysis which are believed to be more basic than those given here. One of these methods is well known, being the node-pair method, while the other is new, involving the dual concept of a node-pair, which we have called a 'split-node'. The results and methods used in this paper will serve as a basis for the development of the new paper.

The node-pair and split-node methods of analysis become important when the behaviour of multi terminal-pair networks is investigated.

(10) ACKNOWLEDGMENTS

The paper was made possible by the award to the author of a scholarship by The General Electric Company Ltd. which he gratefully acknowledges. He is also indebted to Dr. K. F. Sander of the Department of Engineering, University of Cambridge, and to Dr. A. Talbot of the Imperial College of Science and Technology, University of London, for valuable discussions.

(11) REFERENCES

(1) AITKEN, A. C.: 'Determinants and Matrices' (Oliver and Boyd, 2nd edition, 1942).

(2) BODE, H. W.: 'Network Analysis and Feedback Amplifier Design' (Van Nostrand, 1945).

(3) BOTT, R., and DUFFIN, R. J.: 'On the Algebra of Networks', *Transactions of the American Mathematical Society*, 1953, **74**, p. 99.

(4) Brooks, R. L., Smith, C. A. B., Stone, A. H., and Tutte, W. T.: 'Dissection of Rectangles into Squares', *Duke Mathematical Journal*, 1940, **7**, p. 312.

(5) Bryant, P. R.: 'A Topological Investigation of Network Determinants', *Proceedings I.E.E.*, Monograph No. 312 R, September, 1958 (**106** C, p. 16).

(6) Bryant, P. R.: 'The Order of Complexity of Electrical Networks', *ibid.*, Monograph No. 335 E, June, 1959 (**106** C, p. 174).

(7) Cauer, W.: 'Synthesis of Linear Communication Networks' (McGraw-Hill, 1958).

(8) Cederbaum, I.: 'Some Fundamental Properties of Multi-Port Networks', Ph.D. Thesis, University of London, 1956.

(9) Cederbaum, I.: 'Invariance and Mutual Relations of Electrical Network Determinants', *Journal of Mathematics and Physics*, 1956, **34**, p. 236.

(10) Cederbaum, I.: 'Matrices All of Whose Elements and Sub-Determinants are 1, −1 or 0', *ibid.*, 1958, **36**, p. 351.

(11) Cederbaum, I.: 'Conditions for the Impedance and Admittance Matrices of *n*-Ports without Ideal Transformers', *Proceedings I.E.E.*, Monograph No. 276 R, January, 1958 (**105** C, p. 245).

(12) Coates, C. L.: 'General Topological Formulas for Linear Network Functions', *Transactions of the Institute of Radio Engineers*, 1958, **CT–5**, p. 42.

(13) Deards, S. R.: 'Dual of Kirchhoff's Branch-Current Rule', *Wireless Engineer*, 1956, **33**, p. 251.

(14) Duffin, R. J.: 'Non-Linear Networks IIB', *Bulletin of the American Mathematical Society*, 1948, **54**, p. 119.

(15) Duffin, R. J.: 'Non-Linear Networks IV', *Proceedings of the American Mathematical Society*, 1950, **1**, p. 233.

(16) Feussner, W.: 'Über Stromverzweigung in Netzförmigen Leitern', *Annalen der Physik*, 1902, **9**, p. 1304.

(17) Franklin, P.: 'The Electric Currents in a Network', *Journal of Mathematics and Physics*, 1925, **4**, p. 97.

(18) Frazer, R. A., Duncan, W. J., and Collar, A. R.: 'Elementary Matrices' (Cambridge University Press, 1938).

(19) Gould, R.: 'Graphs and Vector Spaces', *Journal of Mathematics and Physics*, 1958, **37**, p. 193.

(20) Guillemin, E. A.: 'Introductory Circuit Theory' (Wiley, 1953).

(21) Ingram, W. H., and Cramlet, C. M.: 'On the Foundations of Electrical Network Theory', *Journal of Mathematics and Physics*, 1944, **23**, p. 134.

(22) Iri, M.: 'Network Theory Based on Topology', Research Association of Applied Geometry (Japan), Research Note (Second series) No. 10, June, 1956. [Also of interest in this series are Research Notes 17 (November, 1956), 26 (May, 1957) and 32 (August, 1957).]

(23) Kirchhoff, G.: 'Über die Auflösung der Gliechungen auf Welche man bei der Untersuchung der Linearen Verteilung Galvanischer Ströme geführt Wird', *Annalen der Physik und Chemie*, 1847, **72**, p. 497.

(24) Kron, G.: 'Tensor Analysis of Networks' (Wiley, 1939).

(25) Ku, Y. H.: 'Résumé of Maxwell's and Kirchhoff's Rules for Network Analysis', *Journal of the Franklin Institute*, 1952, **253**, p. 211.

(26) Lantieri, J.: 'Methode de determination des arbres d'un reseau', *Annales de Télécommunication*, 1950, **5**, p. 204.

(27) Le Corbeiller, P.: 'Matrix Analysis of Electrical Networks' (Wiley, 1950). (This book interprets much of the work of Kron in Reference 24.)

(28) Maxwell, J. C.: 'Electricity and Magnetism' (Oxford University Press, 3rd Edition, 1892), Vol. 1, Part II, p. 409.

(29) Mayeda, W., and Seshu, S.: 'Topological Formulas fo Network Functions', University of Illinois Engineerin Experiment Station Bulletin No. 446, November, 195 **55**, No. 23.

(30) Ohm, G. S.: 'The Galvanic Circuit Investigated Mathe matically' (Original German edition: Berlin, 1827 Translation by W. Francis (Van Nostrand, 2nd editio 1905).

(31) Okada, S.: 'On Node and Mesh Determinants', *Proceedin of the Institute of Radio Engineers*, 1955, **43**, p. 1527.

(32) Okada, S.: 'Algebraic and Topological Foundations Network Synthesis', Proceedings of the Symposium o Modern Network Synthesis II, Polytechnic Institute Brooklyn, 1955, p. 283.

(33) Percival, W. S.: 'The Solution of Passive Electrical Ne works by means of Mathematical Trees', *Proceedin I.E.E.*, Paper No. 1492 R, May, 1953 (**100**, Part II p. 143).

(34) Percival, W. S.: 'Improved Matrix and Determina Methods for Solving Networks', *ibid.*, Monogra No. 96 R, April, 1954 (**101**, Part IV, p. 258).

(35) Percival, W. S.: 'The Graphs of Active Networks', *ibi* Monograph 129 R, April, 1955 (**102** C, p. 270).

(36) Reed, M., and Seshu, S.: 'On Topology and Netwo Theory', Proceedings of the Symposium on Circu Analysis, University of Illinois, 1955.

(37) Reed, M., and Seshu, S.: 'The Role of the Tree in Electri Network Theory', *Proceedings of the National Electroni Conference*, 1956, **12**, p. 522.

(38) Reza, F. M.: 'Some Topological Considerations in Netwo Theory', *Transactions of the Institute of Radio Engineer* 1958, **CT–5**, p. 30.

(39) Roth, J. P.: 'An Application of Algebraic Topology Numerical Analysis: on the Existence of a Solution the Network Problem', *Proceedings of the Nation Academy of Sciences*, 1955, **41**, pp. 518 and 599.

(40) Roth, J. P.: 'An Application of Algebraic Topolog Kron's Method of Tearing', *Quarterly of Applied Math matics*, 1959, **17**, p. 1.

(41) Saltzer, C.: 'The Second Fundamental Theorem Electrical Networks', *ibid.*, 1953, **11**, p. 119.

(42) Seshu, S.: 'Topological Considerations in the Design Driving Point Functions', *Transactions of the Institute Radio Engineers*, 1955, **CT–2**, p. 356.

(43) Seshu, S., and Reed, M.: 'On the Cut-Sets of an Electric Network', presented at the Symposium on Circuit Theor E. Lansing, Michigan, December, 1956.

(44) Synge, J. C.: 'The Fundamental Theorem of Electric Networks', *Quarterly of Applied Mathematics*, 1951, p. 113.

(45) Talbot, A.: 'Some Fundamental Properties of Networ without Mutual Inductance', *Proceedings I.E.E.*, Mon graph No. 118 R, January, 1955 (**102** C, p. 168).

(46) Trent, H. M.: 'A Note on the Enumeration and Listing all possible Trees in a Connected Linear Graph', *Pr ceedings of the National Academy of Sciences*, 1954, **40** p. 1004.

(47) Tsang, N. F.: 'On Electrical Network Determinant *Journal of Mathematics and Physics*, 1954, **33**, p. 185.

(48) Veblen, O.: 'Analysis Situs' (American Mathemati Society Colloquium Publications, Second Edition, 193 Vol. 5, Part II.

(49) Veblen, O., and Franklin, P.: 'On Matrices wh Elements are Integers', *Annals of Mathematics*, 19 **23**, p. 1. (This is also contained as Appendix II Reference 48.)

(50) WEINBERG, L.: 'Kirchhoff's Third and Fourth Laws', *Transactions of the Institute of Radio Engineers*, 1958, **CT–5**, p. 8.

(51) WHITNEY, H.: 'Planar Graphs', *Fundamenta Mathematicae*, 1933, **21**, p. 73.

(52) WHITNEY, H.: 'On the Abstract Properties of Linear Dependence', *American Journal of Mathematics*, 1935, **57**, p. 509.

(53) BRANIN, F. H.: 'The Relations between Kron's Method and the Classical Methods of Network Analysis', *Institute of Radio Engineers Wescon Convention Record*, 1959, Part 2, p. 3.

621.315.1.015.532 : 621.387

The Institution of Electrical Engineer
Monograph No. 415
Nov. 196

THE SURGE CORONA DISCHARGE

By R. DAVIS, M.Sc., Member, and R. W. E. COOK.

With an Appendix by W. G. STANDRING, M.A.

(*The paper was first received 5th May, and in revised form 5th August*, 1960. *It was published as an* INSTITUTION MONOGRAPH *in November*, 1960.)

SUMMARY

Exploratory experiments are described followed by an account of a more systematic study of the corona discharge with concentric-cylinder electrodes. From experimental records which relate the charge flow in an external circuit to the applied voltage, the corona current and energy loss were derived. An attempt is made to interpret the observations in terms of modern views on the mechanism of electrical breakdown in gases. The attenuation by corona of surges on transmission lines is examined in an Appendix.

LIST OF PRINCIPAL SYMBOLS

A and a = Radii of outer and inner conductors of concentric-cylinder electrode system, cm.
W = Energy dissipated by the corona discharge, joules $\times 10^{-4}$.
V_p = Peak applied voltage, kV.
V_i = Inception voltage, kV.
q = Charge flow in external circuit, C/cm $\times 10^{-10}$.
q_c = Charge flow due to corona, C/cm $\times 10^{-10}$.
$(q_c)_1$ = Charge flow due to corona at end of high-current epoch, C/cm $\times 10^{-10}$.
$(q_c)_2$ = Charge flow due to corona at end of voltage excursion, C/cm $\times 10^{-10}$.
q_s = Net space charge, C/cm $\times 10^{-10}$.
T = Duration of high-current epoch, microsec.
E = Electric field, kV/cm.
α = Primary ionization coefficient, cm^{-1}.
γ = Secondary ionization coefficient, cm^{-1}.

(1) INTRODUCTION

In non-uniform fields in gases discharge may occur at a voltage below that required for a complete breakdown between the electrodes; this phenomenon is called corona. If the non-uniform field results from the use of electrodes of different shapes or dimensions, e.g. point-plane or concentric cylinders, any visible discharge is located mainly in the high-field region. The corona is defined as positive or negative according to whether the electrode associated with the high field is the positive or negative one. The corona produces a current in the external circuit of the electrode system, and this current or its integral, i.e. the charge flow up to any instant, can be measured; the existence of a corona current implies that energy is being abstracted from the voltage source, and this can also be determined. The process of corona formation involves the creation and separation of charged particles—electrons and positive ions—in the electric field and these charges may modify the field; no experimental technique for measuring field distribution in the presence of a corona discharge has yet been successfully applied. A study of the light emitted during the corona is essential to a complete understanding of the mechanism, and experimental techniques are available which should make this study practicable, but no systematic data are yet available.

The corona discharge is of considerable technical interes It is a source of power loss when energy is transmitted at hig voltages by overhead lines, and it can exercise a beneficial effe in attenuating the over-voltages produced on an overhead li during thunderstorms. A study of the corona discharge ma therefore, in addition to providing information on the mechanis of breakdown in gases, have useful practical applications.

In the paper are described the results so far obtained in a investigation which began as a study of the effect of corona c surges on transmission lines but which soon indicated that th phenomenon appeared to be so complicated that it seeme desirable to study first the nature of corona with simple electro arrangements in the laboratory. The results of this study a given, and a qualitative application of laboratory observatio to the attenuation of impulse voltages on transmission lines given in Appendix 7.

(2) EXPLORATORY EXPERIMENTS

The experiments described in this Section were of an explor tory character intended to assist in planning a more systemat investigation.

(2.1) Effect on Transmission-Line Characteristics

On a loss-free transmission line surges travel without attenu tion and with a velocity $(LC)^{-1/2}$, where L and C are the indu tance and capacitance per unit length; the ratio of the volta to the current, defined as the surge impedance, is $L^{1/2}C^{-1}$ Energy losses are introduced by resistance in the conductor a in the earth path and by leakage, and if the voltage is above th corona inception value by corona; these losses produce volta attenuation and waveshape changes. Several attempts[1] ha been made to explain the results of field measurements; e.g. t corona discharge has been assumed to constitute an extensio of the conductor made up of an infinite number of concentr sheaths corresponding to infinitesimal increments of voltag These sheaths increase the capacitance of the conductor, b since they carry no appreciable longitudinal current they do n affect the inductance of the line. The increase in capacitan varies for each sheath and is greatest for the outermost. As result the velocity of propagation of the outer sheaths is le than that of the inner ones so that the wavefront is distorted its travel.

One consequence of this hypothesis is that if a surge is appli to a transmission line the voltage/current ratio should decrea as the voltage increases. To test this, surge voltages we applied to an experimental transmission line comprising a co ductor 2 cm in diameter suspended 18 m above ground a about 550 m in length, via a resistance of 500 ohms. The inp voltage to the line and the current at the earthed end of t generator were measured 1·5 microsec after the start of the wa when violent oscillations had subsided and the wave reflect from the far end had not reached the near end of the line.

With surges of positive polarity the voltage/current ra decreased from 570 at 100 kV peak by 20% at 700 kV; w

Correspondence on Monographs is invited for consideration with a view to publication.
The paper is an official communication from the National Physical Laboratory.

egative polarity the corresponding figure was 5%, and this as comparable with the repeatability of the observations.

A change in the ratio of 20% would, if attributed to a change nly in the capacitance per unit length of the line, require an ncrease in the capacitance of the line of nearly 50%, correspondng to fifteenfold increase in conductor size.

(2.2) Effect on the Output Wave of a Surge Generator

Tests were made to check whether any significant modification ccurred to the shape of the wave applied to a test object from surge generator if corona was produced on the conductor onnecting them. Unidirectional surges of 1 microsec front ere applied to a conductor 20 m long and 0·1 cm diameter uspended in the laboratory. Oscillograms of the applied oltage showed that the upper part of the wave was progresively flattened as the voltage was increased, the effect being reater for positive than negative polarity. This effect was ttributed to corona current, which presumably produced a oltage drop in the damping resistance of the circuit of significant agnitude relative to that produced by the charging current to he load capacitance. It was inferred, as later experiments howed, that substantial corona currents could be produced vithin 1 microsec of the instant of application of the voltage.

The experiment illustrates the need for low damping resistance nd large load capacitance in the test circuit especially for the erivation of time-lag curves of insulators and spark-gaps at igh over-voltages.

(2.3) Point-Sphere Electrodes

The corona discharge for a point-sphere electrode system in ir was investigated. The sphere of 75 cm diameter was the igh-voltage electrode. To minimize the inter-electrode capaciance the point was shielded by an earthed hemispherical conuctor of 5 cm diameter, through a hole in the pole of which he point projected about 2 mm. The current in the external ircuit was derived from the voltage developed across a nonnductive resistance located between the point and earth; for neasurements of charge flow in the external circuit a capacitor vas substituted for the resistor. The current measured by this rrangement is the sum of the capacitive current $C(dv/dt)$ (v is he instantaneous applied voltage) and the corona current. If orona current is established on the wavefront when the rate of hange of voltage is high the corona current could be masked by he capacitive current; with this electrode arrangement, however, he contribution of the capacitive current to the total was egligible.

Tests were made with aperiodic surge voltages (waveshape nainly 1/115) of different amplitudes and gaps between the lectrodes.

The positive corona current was very steep fronted (approxinately 10^{-2} microsec duration), decreasing to a very low value n about 0·5 microsec. The corresponding negative corona urrent was similar in shape, the measurable portion of the urrent was appreciably shorter in duration and generally the mplitude was less. The interval between the instant of applicaion of the voltage and the beginning of the corona current was ariable but tended to decrease as the voltage amplitude was ncreased, so that at the lower amplitudes the current flow tarted on the wave back and at higher amplitudes on the ront.

The charge/time curve for the positive corona showed that pproximately 95% of the total charge flow took place within a raction of a microsecond, the remaining 5% being contributed uring the succeeding 30 microsec, indicating that the corona urrent consists of an initial pulse of relatively high amplitude nd short duration followed by a low-amplitude current of much longer duration. The charge/time curves for the negative corona also indicated that there was a short-duration high-current epoch followed by a long-duration low-current one. Only about 20% of the total negative charge flow was associated with the initial current pulse, the remainder being supplied during the following 30 microsec. The total charge flow for the positive corona discharge was approximately twice that for the negative for the same conditions of electrode spacing and applied voltage.

(3) CONCENTRIC-CYLINDER ELECTRODES

For the systematic study of the corona discharge concentric-cylinder electrodes were selected. They have the advantages that the applied field can readily be calculated and the field geometry approximates to that of a transmission line.

(3.1) Experimental

Two electrode arrangements were used. Particulars of these are as follows:

	Arrangement A	Arrangement B
Radius A of outer electrode, cm ..	$8{\cdot}25$	$2{\cdot}92$
Radius a of inner electrode, cm ..	$2{\cdot}8 \times 10^{-2}$	$8{\cdot}2 \times 10^{-3}$
Active length of electrodes, cm ..	90	15
$\log_e A/a$	$5{\cdot}7$	$5{\cdot}9$
Inter-electrode capacitance, pF/cm ..	$9{\cdot}75 \times 10^{-2}$	$9{\cdot}45 \times 10^{-2}$

The outer electrode of arrangement A was fitted with guard rings and completely shielded from external fields by a third cylinder connected to the guard rings and earthed. The outer cylinder of arrangement B was fitted with guard rings; the complete electrode system was assembled in a closed glass cylinder provided with facilities for filling with clean dry gases to different pressures.

The outer electrode was connected to earth via a measuring capacitor and surge voltages were applied between the inner electrode and earth; the voltage waveshape was aperiodic with front times varying between 1·6 and 10 microsec, and times to half value on the wave back of about 50 microsec. The voltage developed across the measuring capacitor, which was proportional to the charge flow in the circuit external to the electrode system, was applied to one pair of plates of an oscillograph, and a fraction of the test voltage was applied to a second pair of plates at right angles to the first. The oscillograph thus produced a record of the relation between the voltage on the electrodes at any instant and the charge flow in the circuit up to that instant. Oscillograms of the time variation of the voltage were also obtained, so that from the two curves the relation between charge and time could be derived, and subsequently the corona current. Direct recording of surge corona current was not practicable with concentric-cylinder electrodes because of the large inter-electrode capacitance.

If q is the charge flow at any voltage v, the energy absorbed by the corona is

$$\int_0^q v\,dq - \tfrac{1}{2}cv^2$$

where c is the inter-electrode capacitance per centimetre length of electrode. The value can be derived by mechanical integration of the q/v curve. For the complete excursion of voltage the total energy absorbed is given by the area enclosed by the q/v curve and the q-axis. The energy as a function of time can also be derived, and hence the power absorbed at any instant.

(3.1.1) Experimental Results.

Oscillograms were redrawn, giving the charge flow per centimetre length of electrode as a function of the applied voltage; examples of these are reproduced in Figs. 1–3. In the absence

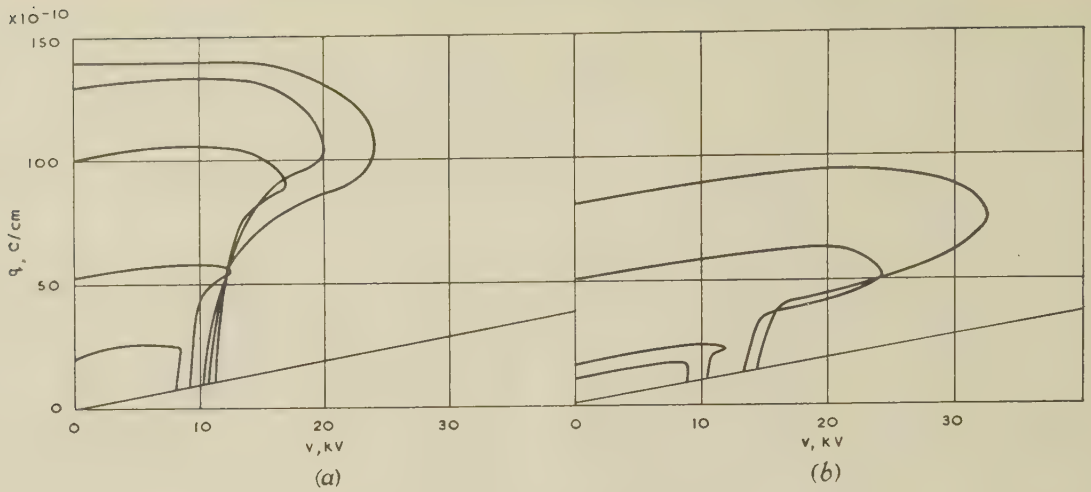

Fig. 1.—q/v curves. Arrangement A.
(*a*) Positive corona. Waveshape; 3·6/60 microsec.
(*b*) Negative corona. Waveshape; 2·4/60 microsec.

of a corona discharge the q/v relation is a straight line represented by the equation

$$q = cv$$

In the presence of a discharge the curve leaves the straight line at a voltage V_i defined as the corona inception voltage, the additional charge flow in the circuit, q_c, being that due to the discharge; beyond the inception voltage q increased rapidly with voltage for a small increment of voltage, and then less rapidly; q usually continued to increase to some point on the wave back and then decreased for the remainder of the voltage excursion. Analysis of the q/v curves in conjunction with the corresponding v/t curves indicates that the corona current had an initial high-current short-duration epoch followed by a long-duration low-current epoch similar to that observed with a sphere-point electrode system. The end of the high-current epoch and therefore its duration was not always clearly defined. With arrangement A the current in the low-current epoch decreased continuously to zero (corresponding to the point on the q/v curve where the tangent is parallel to the line $q = cv$) and then reversed sign; with arrangement B no current reversal occurred. Typical current/time curves are illustrated in Fig. 4. By analysing q/v curves electrical characteristics of the corona discharge were determined; some of the characteristics are given in Tables 1–5.

(3.2) Discussion

(3.2.1) Mechanism of Electrical Breakdown in Gases.[2]

Most breakdown processes in gases are initiated by an electron avalanche, which is the term applied to the process of electron multiplication in an electric field. If α_x represents the number

Table 1

ARRANGEMENT A; POSITIVE CORONA; WAVESHAPE 3·6/60 MICROSEC. ELECTRICAL CHARACTERISTICS

V_p	V_i	T	W	$(q_c)_1$	$(q_c)_2$
kV	kV	microsec	joules/cm × 10^{-4}	C/cm × 10^{-10}	C/cm × 10^{-10}
50	20	0·25	2·14	35·6	55·5
40	20·5	0·25	1·44	31·4	47·5
30	19·5	0·25	0·95	28·0	37·3
20	17·8	0·40	0·49	24·0	23·0

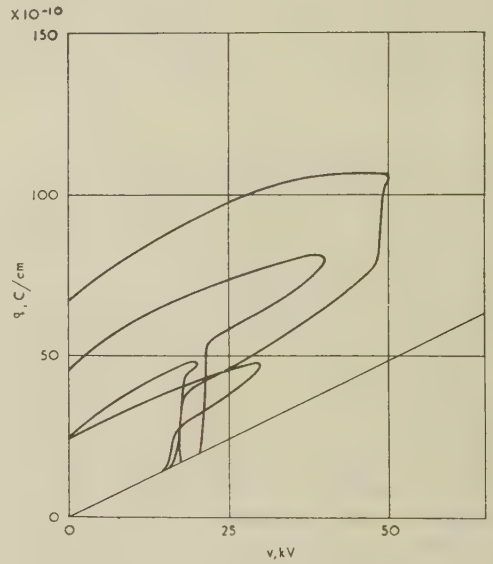

Fig. 2.—q/v curves. Arrangement A.
Positive polarity. Waveshape; 10/40 microsec.

Table 2

ARRANGEMENT A; POSITIVE CORONA; WAVESHAPE 10/40 MICROSEC. ELECTRICAL CHARACTERISTICS

V_p	V_i	T	W	$(q_c)_1$	$(q_c)_2$
kV	kV	microsec	joules/cm × 10^{-4}	C/cm × 10^{-10}	C/cm × 10^{-10}
50	20	0·25	1·3	31·6	53·5
50	16	(1)0·5 (2)2·5	2·07	(1)19·2 (2)26·0	64·0
40	20	0·20	0·97	32·0	44·4
40	16·4	0·30	0·81	21·6	40·7
30	18·6	0·20	0·68	26·6	33·5
30	15·3	0·40	0·42	9·7	23·2
20	14·8	0·50	0·22	8·0	14·0
20	16·8	0·70	0·47	20·0	23·2

The figures 1 and 2 in the second row refer to the first and second high-curr epochs.

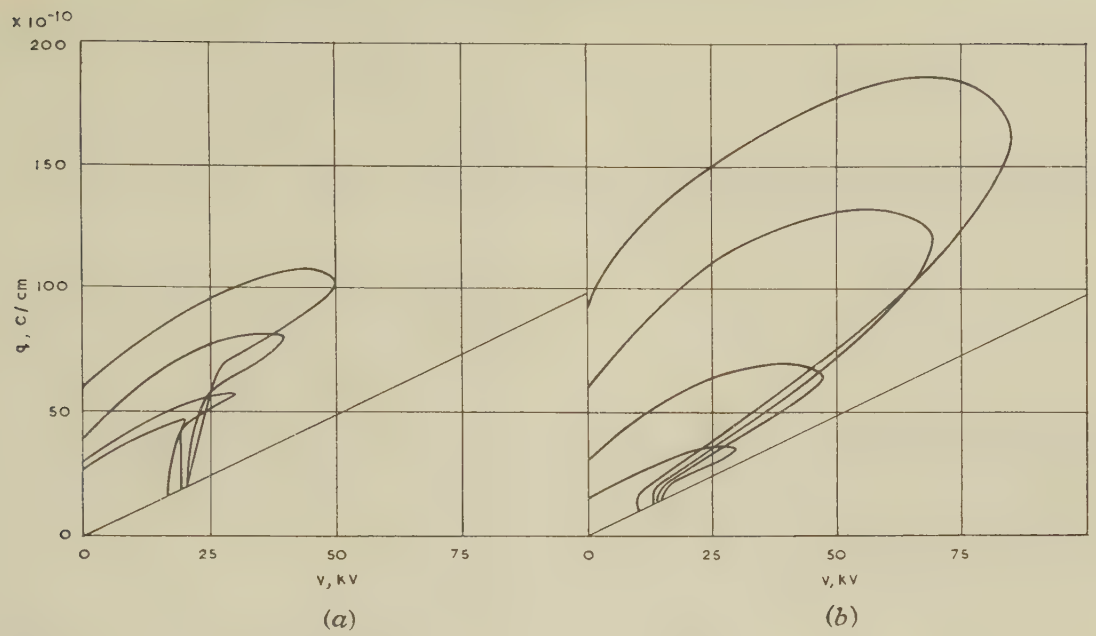

Fig. 3.—q/v curves. Arrangement B.

Waveshape 1·6/60 microsec.
(*a*) Positive corona.
(*b*) Negative corona.

Table 3

ARRANGEMENT A; NEGATIVE CORONA; WAVESHAPE 2·4/60 MICROSEC. ELECTRICAL CHARACTERISTICS

V_p	V_i	T	W	$(q_c)_1$	$(q_c)_2$
kV	kV	microsec	joules/cm × 10^{-4}	C/cm × 10^{-10}	C/cm × 10^{-10}
85	11·9	0·10	7·9	9·3	93·0
69	11·0	0·10	4·3	11·5	55·0
55·5	12·2	0·10	2·1	5·6	25·0
47	14·1	0·10	1·4	6·2	22·6
40	12·0	0·10	0·85	2·3	18·5
30	13·8	0·15	0·37	5·8	8·7

Table 4

ARRANGEMENT B; POSITIVE CORONA; WAVESHAPE 1·6/60 MICROSEC. ELECTRICAL CHARACTERISTICS

V_p	V_i	T	W	$(q_c)_1$	$(q_c)_2$
kV	kV	microsec	joules/cm × 10^{-4}	C/cm × 10^{-10}	C/cm × 10^{-10}
24·1	10·8	1·15	3·40	114	200
24·1	9·1	0·60	1·93	59·5	116
24·1	11·7	0·50	4·00	127	245
20·1	10·6	0·35	1·84	73·2	132
20·1	9·8	0·25	1·47	53·0	110
16·8	10·3	0·50	1·04	61·0	94·0
16·8	9·3	0·35	0·94	49·0	83·5
16·8	10·5	0·35	1·27	63·5	104
12·3	8·4	0·25	0·33	23·6	37·4
12·3	9·1	0·30	0·44	30·4	45·0
8·5	7·8	0·10	0·15	12·5	18·6

Table 5

ARRANGEMENT B; NEGATIVE CORONA; WAVESHAPE 1·6/60 MICROSEC. ELECTRICAL CHARACTERISTICS

V_p	V_i	T	W	$(q_c)_1$	$(q_c)_2$
kV	kV	microsec	joules/cm × 10^{-4}	C/cm × 10^{-10}	C/cm × 10^{-10}
32·5	13·1	0·05	1·78	10·9	72·5
28·2	7·3	0·05	1·12	5·0	56·0
24·4	15·1	0·10	1·10	22·1	63·0
24·4	7·0	0·05	0·95	5·7	56·8
16·4	12·9	0·05	0·36	12·5	28·4
12·0	11·7	0·15	0·18		15·4
9·4	9·1	0·05	0·10		10·5

of ionizing collisions per centimetre length at a position x, then for each electron at x_1 there are $\exp\left(\int_{x_1}^{x_2}\alpha_x dx\right)$ electrons at x_2. The symbol α_x represents the first Townsend ionizing coefficient and it is a function of the field; in a uniform field α_x is a constant α, say, and the integral term is replaced by $\alpha(x_2 - x_1)$. As many positive ions as electrons are created in the avalanche, the number dn in a short path length dx being given by the equation

$$dn = \alpha_x \exp\left(\int_{x_1}^{x}\alpha_x dx\right)dx \quad . \quad . \quad . \quad . \quad (1)$$

Breakdown requires, in addition to the initial avalanche, secondary ionizing processes which lead to secondary avalanches; processes which have been identified include the release of electrons from the cathode by positive ions and by the photoelectric effect, and ionization in the gas by photons or positive ions.

In the Townsend theory of breakdown, for each electron created in the primary avalanche, γ secondary electrons avail-

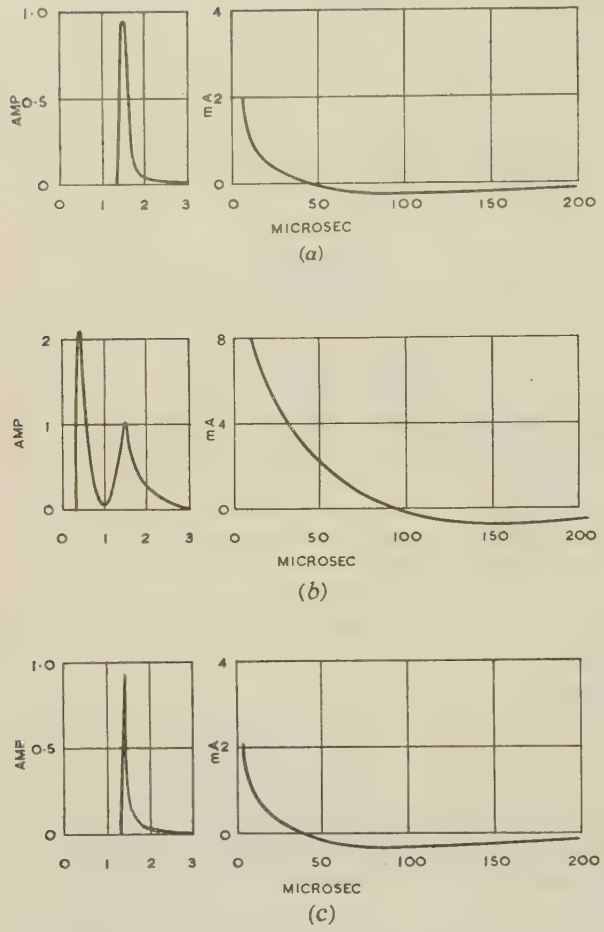

Fig. 4.—Typical corona currents. Arrangement A.
(*a*) Positive corona. 19 kV.
(*b*) Positive corona. 56 kV.
(*c*) Negative corona. 56 kV.

able for initiating secondary avalanches are produced; since $\alpha\,(\varepsilon^{\alpha d} - 1)$ electrons are created in the primary avalanche the number of secondary avalanches is $\gamma(\varepsilon^{\alpha d} - 1)$, and the condition for breakdown is

$$\gamma(\varepsilon^{\alpha d} - 1) = 1 \quad . \quad . \quad . \quad . \quad . \quad . \quad (2)$$

The streamer theory of breakdown has been proposed as an alternative. In this the initial process is again the electron avalanche which grows until it produces an increase in field at the head due to the positive space charge; secondary avalanches originating in electrons created by photo-ionization in the gas are directed into the positive space-charge region. In this way the region of high positive space charge is rapidly extended towards the electrodes and is also permeated with electrons or negative ions. This channel of positive and negative ions constitutes the so-called streamer, and when its growth is extended to the two electrodes the gas path is effectively short-circuited and breakdown is effected.

Both Townsend and streamer theories have been given quantitative significance, permitting the prediction with good accuracy of the breakdown voltages in uniform fields. Thus, for the former, α and γ can be determined experimentally, and if the values which satisfy eqn. (2) are associated with a field E the breakdown voltage is Ed, where d is the electrode separation. In one form of the streamer theory* it is postulated that a streamer will form when the avalanche has grown to such a si that the positive space charge at the head produces a field so fraction of that applied; in another* it is postulated that streamer will form provided that $\int \alpha dx$ has a value of 18 to 2 The quantitative application of streamer theory is essentia empirical; the good agreement between calculated and measure breakdown in uniform fields obtained with the three quantitati treatments has been attributed to the fact that a common a dominating feature of all calculations is the size of the prima avalanche.

* Associated with the name of Dr. J. M. Meek.

(3.2.2) **Qualitative Discussion of the Corona Discharge Mechanism.**

The process is initiated by one or more electron avalanche directed outwards from the inner conductor for negative a inwards for positive corona. For a direct voltage applied to t electrode system the source of the primary electrons is usua attributed to the ionizing action of cosmic rays; with impu voltages of 1 or 2 microsec front duration, experiment shows th an electron is always available in a suitable position for t extremely short time of a fraction of a microsecond corresp ing to the observed variability in inception voltage, which wo imply, if cosmic rays were the source, an activity correspond to several per microsecond. This activity is unlikely and so other source is needed. This, it is suggested, is provided by t action of the field on the positive or negative ions which a present in the atmosphere in numbers of 500–1 000 per cu centimetre. Two possible mechanisms are the emission electrons from the cathode by positive-ion impact, and t stripping of electrons from negative ions in the applied fie The yield of electrons from positive-ion bombardment of t cathode is small at low energies[3] and is therefore a more lik source with negative corona where the cathode is in the high-fie region than with positive corona. The stripping process occu according to Loeb,[4] at values of E/p of 90 (where E is in vo per centimetre and p is in mm Hg), corresponding to a fi of 68·5 kV/cm at atmospheric pressure.

(3.2.2.1) *Negative Corona.*

The first avalanche will start near the cathode, which is t inner electrode, and move outwards, the number of electrons the head continuing to increase until the field is too small f further ionization. In the low-field region near the anode t electrons will be slowed down, and many will become attach to atoms to form negative ions, and so reduce still more t velocity of the negatively charged particles. In the avalanc path relatively immobile positive ions will be left with a densi distribution starting at zero, increasing to a maximum, a falling to zero at the point where avalanche multiplication h ceased. This positive space charge will tend to increase t field on the cathode and decrease it on the anode side. Seconda avalanches, originating in electrons derived from positive-i bombardment of the cathode or other means, will feed into t positive space charge and extend the high-density positiv space-charge region towards the cathode. The charge sepa tion associated with these processes produces the initial cha flow q_c in the external circuit. Meanwhile the charge on t cathode is increased by the charge flow in the external circ and decreased by the entry of positive ions, the net effect bei a decrease to such a value that the field becomes too low f further ionization by collision. This terminates the high-curre epoch of the corona discharge. If no negative carriers ha entered the anode the net negative space charge in the dielect will equal the positive space charge which has entered t cathode.

When electrons enter a low-field region they will beco

* Associated with the name of H. Raether.

ttached to atoms to form negative ions and be slowed down. Vhen avalanche activity has ceased negative ions will be dis- ibuted along the avalanche channel together with positive ns which will not have moved far from the position at which ey were created. The ratio of negative to positive ions will crease outwards from the inner electrode. Since the high- rrent epoch lasts for only 0·1 microsec, similar primary and condary avalanches will have developed almost simultaneously long the length of the cathode.

When avalanche activity has ceased charge separation will ntinue and produce a small corona charge flow in the external rcuit. As the applied voltage increases, the field at the cathode creases, and more positive charge can enter and so increase the et negative space charge in the gas; this increase will continue ntil at least the maximum value of q is reached. Subsequently, s q decreases, the field at the inner electrode will tend to reverse nd further entry of positive ions into the cathode will be hibited. At a later stage in the cycle, reversal of corona harge flow can occur corresponding to a reversal of the corona urrent. This phenomenon is discussed further in Section 3.2.3.

3.2.2.2) *Positive Corona.*

The primary avalanche moves to the anode, which is now he inner electrode, and grows continuously provided that the eld is not modified by space charge. The positive space-charge ensity, which is zero at the point where electron multiplication egins, increases continuously to the anode. Secondary ava- nches, which probably originate by photo-ionization in the as, the photons being created during the primary avalanche, nen feed into the positive space-charge region. Electrons enter he anode and reduce the field there at the same time as the ositive space charge extends outwards to a region where the eld is too low for electron multiplication. The high-current poch can be regarded as terminated when the entry of electrons nto the anode is temporarily interrupted because the field at he surface has fallen to zero. For the low-current epoch the orona current as with the negative corona is due to the separa- ion of positive and negative ions.

With the positive corona a second high-current epoch was ccasionally observed as illustrated by the q/v curve for an applied oltage of 50 kV in Fig. 2 and by Fig. 4(*b*), indicating that during he increase in voltage after the end of the initial avalanche the eld near the inner electrode can increase sufficiently to permit a enewal of avalanche activity.

3.2.3) **Space-Charge Considerations.**

If v is the instantaneous voltage, q_w the charge per centimetre n the inner electrode, and $q(r)$ the net space charge per centi- netre radial distance at radius r per centimetre length, then, n appropriate units,

$$2\left[q_w \log_\varepsilon \frac{A}{a} + \int_a^A \frac{\int_a^r q(r)dr}{r} dr\right] = v \quad . \quad . \quad . \quad (3)$$

he charge q_w, assuming that no charge particles have entered he outer electrode, is the difference between the charge flow in he external circuit and the charge on the particles which have ntered the inner electrode, i.e. the net space charge. Hence

$$q_w = \frac{v}{2\log_\varepsilon \frac{A}{a}} + q_c - \int_a^A q(r)dr \quad . \quad . \quad . \quad (4)$$

here q_c is the charge flow due to corona per centimetre length.

Thus
$$q_c = \int_a^A q(r)dr - \frac{1}{\log_\varepsilon \frac{A}{a}}\left[\int_a^A \frac{\int_a^r q(r)dr}{r} dr\right] \quad . \quad . \quad (5)$$

The experiments provide no information about the form of $q(r)$. On the simplest assumption that the net space charge q_s is located in a sheath concentric with the electrodes at radius r, eqn. (5) takes the form

$$q_c = q_s - q_s \frac{\log_\varepsilon \frac{A}{r}}{\log_\varepsilon \frac{A}{a}} = q_s \frac{\log_\varepsilon \frac{r}{a}}{\log_\varepsilon \frac{A}{a}} \quad . \quad . \quad . \quad (6)$$

The qualitative discussion of the corona discharge shows that this assumption is quite untenable. Its only justification is that it permits a crude quantitative discussion of the experimental data which would be otherwise impossible, and when for any good reasons a value can be assigned to q_s it enables through eqn. (6) a mean position for the net space charge to be determined which is not likely to be seriously in error.

The field, E_a, at the inner electrode, whatever the space-charge distribution, is

$$E_a = \frac{2}{a}(q - q_s)$$

$$= \frac{0{\cdot}18}{a}(q - q_s) \quad . \quad . \quad . \quad . \quad . \quad . \quad (7)$$

The field, E_r, controlling the movement of the space-charge sheath, which is the mean of the field at each side, is given by the equation

$$E_r = \frac{2}{r}(q - q_s/2) \quad . \quad . \quad . \quad . \quad . \quad (8)$$

$$= \frac{2}{r}\left[\frac{v}{2\log_\varepsilon A/a} + q_c \frac{\log_\varepsilon \frac{r}{\sqrt{(Aa)}}}{\log_\varepsilon r/a}\right] \quad . \quad . \quad . \quad (9)$$

If the corona current changes sign, then, at the instant of reversal, from eqn. (8),

$$q_s = 2q \quad . \quad . \quad . \quad . \quad . \quad . \quad . \quad (10)$$

If during the voltage excursion the space-charge sheath reaches a position such that $r = \sqrt{(Aa)}$, eqn. (9) shows that current reversal cannot occur.

After the voltage had fallen to zero no measurable charge flow in the circuit was observed. If r is the position of the net charge q_s, a fraction $-\beta q_s$ will be induced on the inner and $-(1-\beta)q_s$ on the outer electrode, where

$$\beta = \frac{\frac{1}{\log_\varepsilon r/a}}{\frac{1}{\log_\varepsilon r/a} + \frac{1}{\log_\varepsilon A/r}} = \frac{\log_\varepsilon A/r}{\log_\varepsilon A/a}$$

$$1 - \beta = \frac{\log_\varepsilon r/a}{\log_\varepsilon A/a}$$

If the fraction β enters the inner electrode and the fraction $(1-\beta)$ enters the outer electrode the charge flow in the external circuit is

$$-\beta q_s \frac{\log_\varepsilon r/a}{\log_\varepsilon A/a} + (1-\beta) q_s \frac{\log_\varepsilon A/r}{\log_\varepsilon A/a}$$

$$= \frac{q_s}{\log_\varepsilon \frac{A}{a}} \left(\frac{-\log_\varepsilon \frac{A}{r} \log \frac{r}{a} + \log_\varepsilon \frac{A}{r} \log_\varepsilon \frac{r}{a}}{\log_\varepsilon \frac{A}{a}} \right) = 0$$

A more sophisticated examination suggests that, depending on the value of r, there may be an increase or decrease of charge flow, but, as stated, the effect was not detected experimentally.

Once the excess charge has been removed the remaining charged particles will combine under their mutual fields.

(3.2.4) Examination of Experimental Data.

(3.2.4.1) *Inception Voltage and Primary Avalanches.*

In Table 6 are given the minimum inception voltages, $V_{i\,min}$, abstracted from Tables 1–5 and the corresponding values of $\int_a^A \alpha_r dr$, where α has been assumed to be a function of the applied field unmodified by space charge. Included in the Table are the values of v corresponding to $\int_a^A \alpha_r dr = 20$, which is the Raether criterion for streamer formation.

Table 6

RELATION BETWEEN INCEPTION VOLTAGE AND $\int_a^A \alpha_r dr$

Test condition and Table number	1	2	3	4	5
Electrode arrangement	A	A	A	B	B
Corona polarity ..	+	+	−	+	−
$V_{i\,min}$, kV	17·8	14·8	11·0	7·8	7·0
$\int_a^A \alpha_r dr$ corresponding to $V_{i\,min}$	16·5	10·5	4·0	13	10
Value of V_i corresponding to $\int_a^A \alpha_r dr = 20$	19·0	19·0	19·0	9·7	9·7

Table 6 shows that the corona discharge can be initiated when the amplification of the primary avalanche is as low as ε^4. If the condition for corona discharge inception were governed by Raether's criterion the inception voltage would be as given in the last row of the Table, and would be independent of polarity for a given electrode geometry but dependent on the geometry. The actual inception voltage depended on the geometry, the mean value for arrangement A being greater than for arrangement B, which would be expected if inception voltage were related to the amplification factor of the primary avalanche.

(3.2.4.2) *High-Current Epoch.*

(*a*) *Negative Corona.*

Initially the maximum charge generation and separation take place between one and two cathode radii from the cathode surface. The resulting positive space charge increases the field between it and the cathode, and this region is rapidly ionized; positive charge enters the cathode reducing the field there, avalanche creation ceases, and the high-current epoch can be considered as terminated when the field at the cathode has fallen to zero. Thus the high-current epoch is of short duration—actually of the order of 0·1 microsec—with the ionization restricted to a narrow region round the cathode.

If q and q_c are the total charge flow and the charge flow due to corona at the end of the high-current epoch, the net space charge q_s and its mean position r are, from eqns. (7) and (5),

$$q = q_s$$

$$q_c = q_s \log_\varepsilon r/a / \log_\varepsilon A/a$$

Values of q_s and r derived from Figs. 1(*b*) and 3(*b*) are given in Table 7.

Table 7

MEAN POSITION r AND MAGNITUDE OF NET SPACE CHARGE q_s AT END OF NEGATIVE HIGH-CURRENT EPOCH

Electrode arrangement	A				B			
Fig. No.	1(*b*)				3(*b*)			
V_p, kV	30	47	69	85	9·0	12	26·4	32·5
V_i, kV ..	15	14	13	10	9·0	10·6	13·4	14·4
q_s, C/cm × 10^{-10}	21·0	21·0	20·0	20·0	14·8	19·5	33·5	40
r/a	3·9	5·1	5·6	10	13·8	17·6	31·0	36·3
r, cm	0·11	0·14	0·16	0·28	0·11	0·14	0·25	0·36

The values of q_s are practically constant and independent of the inception voltage for arrangement A; with arrangement B they increase with inception voltage. For both arrangements the mean value of r increases with the peak voltage and therefore with the rate of change of voltage during avalanche activity.

(*b*) *Positive Corona.*

Maximum charge generation and separation are initially at the anode. The resulting positive space charge is gradually extended outwards by later avalanches until the field is too low for ionization. Meanwhile electrons continue to enter the anode until the field there is reduced to zero and the high-current epoch is terminated; the duration is three to four times that of the negative corona.

Table 8 gives the value and mean position of the net positive space charge at the end of the high-current epoch. Both q_s and r at the end of the high-current epoch are much greater than the corresponding values for negative corona; they increase with increasing inception voltage.

The field at r is $0{\cdot}18q/r$ kilovolts per centimetre, which is equal to $0{\cdot}18q_s/r$ kilovolts per centimetre at the instant considered. For all the values of q_s and r given in Table 8 the fields are less than 20 kV/cm. The existence of positive ions at r can, because of mobility considerations, only be attributed to avalanche activity, so that fields considerably higher than 20 kV/cm must have existed. This suggests that, as the positive space charge extended outwards from the anode, there was associated with it a high field at the tip which extended the region towards the cathode where avalanche activity was possible. This suggests, further, that the discharge consists of a number of narrow discrete channels or streamers extending well out towards the cathode in contrast with the narrow zone of ionization around the inner electrode atrributed to the negative corona. These suggestions are supported by the electrical discharge between coaxial electrodes reported by Looms.[5]

The q/v curve in Fig. 2 for a peak voltage of 50 kV shows a second high-current epoch on the wavefront at $q = 79$. This suggests that the field at the anode has increased from zero at the end of the first high-current epoch to a value sufficient to permit a renewal of avalanche activity. In the expression for the field at the inner electrode, i.e. eqn. (7), q_s is unknown at this

Table 8

MEAN POSITION, r, AND MAGNITUDE OF NET SPACE CHARGE q_s AT END OF POSITIVE HIGH-CURRENT EPOCH

Electrode arrangement	A								B				
Fig. No.	1(*a*)				2				3(*a*)				
V_p, kV	20	30	40	50	20	30	40	50	8·5	12·3	16·8	20	24
V_i (peak)	19	16·5	20	20	17	15	20	16	8·0	9·0	10·6	11·3	10·2
q_s, C/cm × 10^{-10} ..	45	45	57	69	44	28	54	38·5	24	48	74	90	68
r/a	27	24	28	32	31	9	31	21	50	105	135	135	119
r, cm	0·75	0·68	0·78	0·89	0·86	0·26	0·86	0·58	0·41	0·87	1·02	1·02	0·98

eginning of the second high-current epoch. However, if r is ssumed to be as given in Table 8, then, from eqn. (5),

$$q_s = q_c \frac{\log_\varepsilon A/a}{\log_\varepsilon r/a} = \frac{32 \times 5{\cdot}7}{3{\cdot}05} = 60$$

hence $$E_a = \frac{0{\cdot}18(q - q_s)}{a} = \frac{0{\cdot}18(79 - 60)}{2{\cdot}8 \times 10^{-2}} = 122\,\text{kV/cm}$$

which is a value sufficient to permit avalanche activity.

The field E_a at the peak voltage corresponding to the other $/v$ curves of Fig. 2 and those of Fig. 1(*a*) calculated on the same ssumption was approximately zero at the lowest voltage ampli- ude, it increased with the amplitude and had a maximum value f 97 kV/cm for the 50 kV curve of Fig. 1(*a*).

The maximum rate of change of current in the high-current poch, for both the positive and negative corona, is many orders igher than in the low-current epoch. To this high-current poch the radio interference associated with a corona discharge an be attributed.

c) *Low-Current Epoch.*

The low-current epoch begins at an instant not clearly defined vhen avalanche activity has ceased, and ends when the voltage as fallen to zero; current reversal may occur. Exceptionally he low-current epoch may be interrupted by a second period of avalanche activity. The charge flow due to corona, q_c, in the low-current epoch is attributed to the movement of positive and negative ions and not of electrons. The total charge flow q increases continuously to a maximum which is usually at some point on the wave back, and then decreases. During the increase the field at the inner electrode will tend to increase, and charge of the appropriate sign will enter, thus increasing q_s; this process will continue until at least the maximum value of q is reached. Subsequently the field at the inner electrode will either get smaller or possibly reverse, and the entry of charge into that electrode will be inhibited. Thereafter q_s remains constant since any charge which may have entered the outer electrode can be considered as located infinitely close to it, where it influences r only.

It is assumed that, at the instant q_{max} is reached, the field at the inner electrode is zero, from which

$$(q_s)_{max} = q_{max}$$

and the mean position r of the space charge can be derived from eqn. (6) by the use of the appropriate value of q_c and the value of q_{max} derived from Figs. 1–3. The results of this calculation are given in Table 9. Tables 7–9 show that at q_{max}, r/a although generally greater can be less than its value at the end of the high-current epoch. In the period separating these two events q_s increases because of the entry of charged particles into the inner electrode, with the consequence that the net space-

Table 9

MEAN POSITION r AND MAGNITUDE OF NET SPACE CHARGE $(q_s)_{max}$

V_p, kV	20	30	40	50		Electrode arrangement A positive corona, Fig. 1(*a*)
$(q_s)_{max}$, C/cm × 10^{-10}	47	58	82	108		
r/a	28	17·7	28·1	31·6		
r, cm	0·78	0·50	0·79	0·89		
V_p	20	30	40	50		Electrode arrangement A positive corona, Fig. 2
$(q_s)_{max}$, C/cm × 10^{-10}	48	48	81	107		
r/a	32·4	9·4	20·8	24·5		
r, cm	0·91	0·26	0·58	0·69		
V_p, kV	30	47	69	85		Electrode arrangement A negative corona, Fig. 1(*b*)
$(q_s)_{max}$, C/cm × 10^{-10}	36	70	133	186		
r/a	4·2	12·9	29·5	38		
r, cm	0·12	0·36	0·83	1·06		
V_p, kV	8·5	12·3	16·8	20	24	Electrode arrangement B positive corona, Fig. 3(*a*)
$(q_s)_{max}$, C/cm × 10^{-10}	26	58	105	134	140	
r/a	122	160	219	229	249	
r, cm	1·0	1·32	1·79	1·88	2·04	
V_p, kV	9·0	12·0	26·4	32·5		Electrode arrangement B negative corona, Fig. 3(*b*)
$(q_s)_{max}$, C/cm × 10^{-10}	16	23	53	94		
r/a	33	34·5	150	107·5		
r, cm	0·27	0·28	1·23	0·98		

charge density near the inner electrode is increased and the mean position r is reduced; the effect of the field is to increase the value of r. Either of these opposing effects can predominate.

Beyond q_{max} the net space charge q_s remains constant and the mean position depends solely on the field. If, subsequently, the variation of r were controlled by the field E_r given by eqn. (8), then, at zero corona current corresponding to the point where the tangent to the q/v curve is parallel to the line $q = cv$, the field is zero and

$$q = 0{\cdot}5q_s = 0{\cdot}5q_{max}$$

The q/v curves for electrode arrangement A (Figs. 1 and 2) indicate a current zero for which, on the average,

$$q = 0{\cdot}85q_{max}$$

the numerical factor varying between 0·61 and 0·96. This result provides reasonable support for the assumption made in Section 3.2.3 that the mean position r of the net space charge q_s can be defined by eqn. (6).

If the equation of the field E_r is expressed in the form

$$E_r = \frac{0{\cdot}18}{r}(q - \rho q_{max}) \text{ kilovolts per centimetre}$$

where ρ is a constant, a value for ρ can be derived from the experimental data by assuming that

$$\frac{dr}{dt} = ME_r$$

where M is a constant of the nature of a mobility. The value of dr/dt can be derived from a curve relating r and t, where r is derived from eqn. (6) with q_{max} in place of q_s, and t is derived from a v/t curve.

This procedure was carried out for the q/v curve for 85 kV of Fig. 1(*b*) and the q/v curve for 24 kV of Fig. 3(*b*). The value assigned to M was 2000 cm^2/kVs, corresponding approximately to the mobility of positive and negative ions. The values derived for ρ were as follows:

q/v curve 85 kV for $r = 1{\cdot}1$ cm; $\rho = 0{\cdot}67$
q/v curve 24 kV for $r = 1{\cdot}7$ cm; $\rho = 0{\cdot}68$
q/v curve 24 kV for $r = 2{\cdot}7$ cm; $\rho = 0{\cdot}71$

These values of ρ were in reasonable agreement with the theoretical value of 0·5 and the other experimental value of 0·85.

The values of r/a at q_{max} were generally appreciably higher for electrode arrangement B than for A, and this suggests, from consideration of eqn. (9), that current reversal is more likely with arrangement A than B.

Energy Dissipation in the Corona Discharge.

The energy, W, dissipated in the corona discharge depends on the inception voltage and the peak value of the applied voltage. Insufficient data are available to provide a functional relation between W and V_i for constant V_p, or between W and V_p for constant V_i. The data in Tables 2 and 4 indicate generally that, for a given value of V_p, the energy increases with increasing inception voltage. The relation between the average value of W and V_p could be represented approximately by an equation of the form

$$E = \text{constant} \times (V_p)^n$$

where n for the two arrangements and the two polarities is as follows:

Arrangement A, positive corona	$n = 1{\cdot}8$
Arrangement A, negative corona	$n = 2{\cdot}8$
Arrangement B, positive corona	$n = 3{\cdot}0$
Arrangement B, negative corona	$n = 2{\cdot}4$

(4) CONCLUSION

The interpretation of the experimental data provides a reasonably consistent picture of the processes in the gas during the corona discharge; they are summarized below.

At a certain applied voltage, defined as the inception voltage, electrons are created which, through ionization by collision in the applied field, produce a primary avalanche. The electrons may be produced by the impact of positive ions with the cathode or by the stripping of electrons from negative ions in the applied field. On the average the applied field at the inception voltage is such that $\int_a^A \alpha_r dr$ is about 20, although a value as low as 4 has been observed.

The primary avalanche is followed by secondary avalanches until the field everywhere in the dielectric has been so modified by space charge that further collisional ionization is stopped. The charge separation which occurs during the period of avalanche activity and which is attributed to the movement of electrons and to a lesser extent of positive ions provides the high-current epoch of the corona discharge, which lasts about 0·1 microsec with the negative and 0·3 microsec with the positive corona.

In the negative discharge the positive ions resulting from the earlier avalanches are located one or two radii from the inner electrode and enhance the field between the inner electrode and this position; this region is rapidly ionized by subsequent avalanches. The region of ionization is thus restricted to a narrow band round the inner electrode. Positive ions enter the cathode and reduce the field there until the ionizing process is stopped. The high-current epoch can be expected to be completed in a very short time.

In the positive corona discharge, the positive ions created during the earlier avalanches are located at the inner electrode and as further avalanches travel inwards, the positive ions extend outwards until the field becomes too small for avalanche production. Analysis shows that the applied field at the mean position of the net positive space charge at the end of the high-current epoch is too low for avalanche production. This suggests that as the positive space charge extends outwards it produces a high-field region at the tip which permits ionization so far from the inner electrode. Such a high-field region would be produced if the positive ions extended radially outwards in narrow discrete channels. It is reasonable to assume that the avalanche process, extending as it does so much further towards the outer electrode, will require a longer time for completion than the avalanche process associated with the negative corona. The form of the ionized region and presumably the light associated with it will be very different for the two polarities.

The low-current which follows the high-current epoch is attributed solely to the separation of positive and negative ions. Exceptionally, with one particular geometry, positive polarity and the highest applied voltage, the low-current epoch was interrupted by a second high-current epoch, associated with a renewal of avalanche activity. Apart from this one exception all charge creation occurs over a very short interval at the beginning of the corona discharge. Reversal of the current in the low-current epoch can occur, depending on the electrode geometry.

(5) ACKNOWLEDGMENTS

The work described was carried out at the National Physical Laboratory as part of the research programme of the Laboratory and also in part on behalf of the British Electrical and Allied Industries Research Association. The paper is published by permission of the Directors of both these establishments.

(6) REFERENCES

1) Surge Phenomena (British Electrical and Allied Industries Research Association, 1941), p. 134.
2) Llewellyn Jones, F.: 'Ionization and Breakdown in Gases' (Methuen and Co. Ltd., 1957). This gives a modern survey and a bibliography of recent books and references.
3) Massey, H. S. W., and Burhop, E. H. S.: 'Electronic and Ionic Impact Phenomena' (Clarendon Press, 1952), Chap. IX.
4) Loeb, L. B.: 'Fundamental Processes of Electrical Discharge in Gases' (Wiley, 1939).
5) Looms, J. S. T.: 'Electrical Discharges between Coaxial Electrodes', *Nature*, 1958, **181**, p. 696.

(7) APPENDIX

Attenuation by Corona of Surges on Transmission Lines

By W. G. Standring

Suppose a wave of voltage δV and current δI is travelling along a transmission line of inductance L and capacitance C per unit length, and that the charge flow in the conductor on account of corona is δQ per unit length. In a length of line δx of inductance $L\delta x$ across which the voltage is δV the current is changing at a rate $\delta I/\delta t$, δt being the time in which the wave moves a distance δx, so that

$$L\delta x\delta I/\delta t = \delta V$$

The current δI flowing for a time δt charges up a capacitance $C\delta x$ to a voltage δV and supplies a corona charge flow $\delta Q\delta x$, so that

$$(C\delta V + \delta Q)\delta x = \delta I\delta t$$

Thus $$\delta(V/L)\delta I = \delta x/\delta t = \delta I/(C\delta V + \delta Q)$$

whence $$\delta x/\delta t = [L(C + \delta Q/\delta V)]^{-1/2}$$

Below the corona voltage the velocity of a travelling wave is $(LC)^{-1/2}$. Above the corona voltage the velocity of a voltage increment δV accompanied by a corona charge flow δQ is $(LC)^{-1/2}(1 + \delta Q/C\delta V)^{-1/2}$. Thus the effect of corona on any wavefront can be predicted if sufficient information is available about the charge flow due to corona. Unfortunately the experimental work described in the paper shows that the inception of corona, and the charge flow which occurs on an increment of voltage, are not simply functions of voltage but of the previous rate of change of voltage. A general treatment is not possible without simplifying assumptions.

In general, the total charge flow due to corona nearly all occurs on the wavefront and increases with the voltage. On the assumptions that the inception voltage is constant and that above this voltage $\delta Q/\delta V$ is constant on the wavefront and zero on the wave back, the travelling wave can be regarded as the sum of a wave V_1 travelling with the velocity $(LC)^{-1/2}$ and a wave V_2 having a front velocity of $(LC)^{-1/2}(1 + Q/V_2C)^{-1/2}$ and a back velocity of $(LC)^{-1/2}$.

If $\delta Q/\delta V$ is not constant the wavefront of V_2 alters in shape as it travels along. Where $\delta Q/\delta V$ increases with voltage the wavefront lengthens. Where $\delta Q/\delta V$ decreases with increase of voltage the wavefront steepens, subject to the limitation that the rate of rise cannot be faster than instantaneous.

Perhaps the most important effect of corona on travelling waves is the reduction of amplitude of very high voltages of very short duration such as are produced by high over-voltages on line insulators. Suppose the voltage on a line at a point A exceeds the value V for a time T_0. At a time t later the point V on the wavefront moving with a velocity $L^{-1/2}C^{-1/2}(1 + \delta Q/C\delta V)^{-1/2}$ has reached a point B distant $L^{-1/2}C^{-1/2}(1 + \delta Q/C\delta V)^{-1/2}t$ from A. The point V on the wave back moving with the velocity $L^{-1/2}C^{-1/2}$ has reached a point D distant $L^{-1/2}C^{-1/2}(t - T_0)$ from A. The voltage above V is therefore wiped out when B and D coincide in a time $T_0K/(K - 1)$ and in a distance $T_0L^{-1/2}C^{-1/2}/(K - 1)$ where $K = (1 + \delta Q/C\delta V)^{-1/2}$. Precise calculations cannot be made in practice because, as already stated, $\delta Q/\delta V$ is not simply a function of voltage, but measurements on a short length of line of the total charge flow as a function of the peak value of short test waves should provide sufficient data for useful approximate calculations.

621.313.1.017.7

The Institution of Electrical Engineer
Monograph No. 416 U
Nov. 196

TEMPERATURE RISES IN ELECTRICAL MACHINES WITH SUSTAINED VARIATIONS IN LOAD AND SPEED

By B. J. PRIGMORE, M.A., M.Sc.(Eng.), Associate Member.

(*The paper was first received 6th May, and in revised form 9th August*, 1960. *It was published as an* INSTITUTION MONOGRAPH *in November*, 1960.)

SUMMARY

A method is presented for obtaining the temperature-rise/time curve for a given machine for an arbitrary sequence of operating currents and speeds; the method is demonstrated to give results for such a run correct to about $\pm 2°$ C in 60–70° C.

The method is to suppose that the equivalent thermal network of the machine is linear, its temperature/time curve thus being the sum of the temperature/time transient responses for a series of short times, δt, successive transients corresponding to the average operating conditions during successive intervals; and then to modify this curve to that for the actual non-linear machine by adding a correction curve which is itself composed of two series of transient responses: one of these allows for the effects of non-linearity due to temperature rise, and is based upon the succession of average temperatures, given from the first curve, during the intervals δt; the other allows for the effects of changes in dissipation coefficients due to changes in speed.

The test-bed procedure for obtaining the temperature/time transients for the linear machine, and the corrections for non-linearity, is specified. It is recommended that this procedure, lasting about 36 hours, should be applied to samples of appropriate types of machine.

LIST OF SYMBOLS

Note.—The units are not always necessary: they are given here to correspond with those used when the theory is applied numerically.

α_s = Temperature coefficient of increase of resistance based on θ_s.
C_n = Temperature correction, nth ordinate, deg C/amp^2 per degree difference from standard temperature.
δc = Small change in dissipation coefficient, i.e. in rate of heat dissipation per unit temperature rise.
δt = Small time interval, min.
D_n = Dissipation correction, nth ordinate, deg C per degree of temperature rise.
f = Fractional deficit of exponential rise from its tangent through the origin.
I = Current, amp.
I_m = Maximum service (or accelerating) current, amp.
k = Various temporary constants of proportionality.
R_a = Conductor resistance at temperature θ_a, ohms.
R_s = Conductor resistance at temperature θ_s, ohms.
τ = Time-constant of exponential, min.
θ_{an} = Average temperature rise during nth time interval, deg C.
θ_{cn} = Temperature-correction transient, nth ordinate, to allow for non-linearity due to temperature, deg C.
θ_{dn} = Temperature correction, nth ordinate, to allow for non-linearity due to changes in dissipation coefficient, deg C.
θ_m = Temperature rise during first interval of zero-speed test in which $I = I_m$, deg C.
θ_s = Standard temperature; 85° C, or 65° C rise.
θ_t = Actual temperature rise after time δt, deg C.
θ_x = Temperature rise after time δt, assuming straight-line heating, deg C.
β = Proportion of copper loss, P, which is eddy loss.
P = Copper loss at standard temperature, θ_s, watts.
θ_e = Ultimate temperature rise of non-linear machine, deg C.
θ_l = Ultimate temperature rise of linear machine, deg C.
θ_n = Ultimate temperature rise of non-linear machine if β is assumed to be zero, deg C.

(1) INTRODUCTION

In selecting and using electrical machines such as traction motors for operations involving varying loads and speeds, it is required to estimate the temperatures, especially the maximum temperatures, which may arise from specified operations. During design such predictions require estimates of the heat input and its distribution, and of thermal conductances and capacitances. However, when a sample machine is available for tests it is possible to attempt to relate the temperature rises in service to those found on the test bed, so avoiding the need to evaluate the various parameters. This gives fairly direct means of assessing the severity of duty which could safely be undertaken by an existing motor. In traction, for instance, it gives a means of assessing the effect of adding extra vehicles to a train, of stopping more frequently, or of using weak-field operation to a greater extent; or for determining the load which a locomotive could take over a route other than that for which it had originally been designed.

Such methods have been shown by Tustin and Bates[1,2] to be straightforward when the durations of individual runs are short compared with the thermal time-constants of the machine; it then suffices to estimate the mean equilibrium temperature, with if required, a simple approximate addition to give the peak temperature.

The paper discusses how the varying service temperatures may be related to test-bed temperatures when the durations of individual runs are appreciable compared with the thermal time-constants of the machine. This applies to a main-line locomotive on a route with varying grades, where the maximum temperature rise usually occurs after the locomotive has surmounted the most severe grade, but also depends on the temperature rises of the parts at the commencement of the climb: it also applies to some city and suburban services, where a train may average 40 starts an hour for 30 min in each 90 min and about 25 during the remaining hour. When the thermal time-constants play such a decisive part, estimates of the mean equilibrium temperature would give little help.

The problem is awkward because the dissipation coefficients (or thermal conductance from the various parts) of the motor vary with speed, while the I^2R losses vary with the temperatures of the resistive elements (mainly the windings). If these two features were absent there would remain a linear system in which the heat inputs to the components depended only on the operating conditions (speed, current and flux). The temperature

Correspondence on Monographs is invited for consideration with a view to publication.

Mr. Prigmore is a Lecturer in Electrical Engineering, Imperial College of Science and Technology, University of London.

contributions in each short period, δt, of operation at specified conditions could then be added or superposed.

(2) BASIS OF PROPOSED METHOD

The proposal explored in the paper is to estimate the temperature rise in two stages. First, the temperature-rise/time relation is calculated on the basis of constant thermal conductances and constant electrical resistances (the R factors of the I^2R losses). A hypothetical machine for which these constancies apply will be called a 'linear machine'. Secondly, corrections are made for the variations in the thermal conductances and electrical resistances.

An increased thermal conductance, due to increase in speed, results in extra dissipation of heat; an increased resistance, due to increase in temperature, results in extra I^2R loss; the I^2R loss depends also on the momentary current, and both depend upon the momentary temperature rise. Exact calculation of the additional temperature rises (or falls) due to these factors, as a function of time, would be very laborious. It is shown that these additional rises are usually small, and that a sufficiently good approximation for this correction may be made fairly simply.

A scheme of calculations for the above necessitates the specification of suitable tests, and of procedures for deriving data from them in a form suitable for the calculations. This is discussed and demonstrated in the rest of the paper.

(3) TEMPERATURE VARIATIONS IN THE LINEAR MACHINE

The operating condition of a machine in service changes either continuously or in steps. To estimate the changes of temperature rise with time, the time of operation must be divided into short intervals, δt, during each of which the operating condition may be regarded as constant. If the motor were to be switched on only for the interval δt the temperature-rise/time curve during and after the interval would have the almost linear rise and roughly exponential fall of the curves at the bottom of Fig. 1.

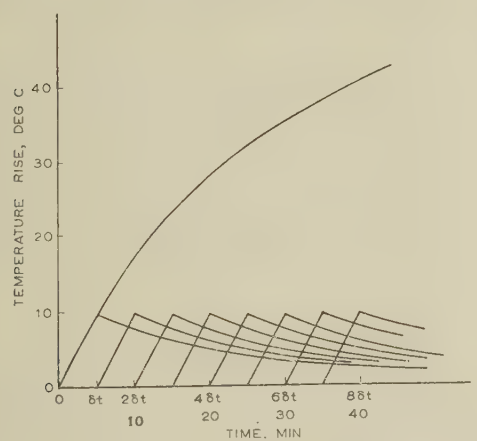

Fig. 1.—Standard heating transients for 92 amp 590 r.p.m. motor.

With a linear machine (Section 2), superposition of the above curves, one for each time interval, would give the overall temperature/time curve, as in Fig. 1. More formally, the temperature-rise/time relation for any given part of the linear machine is the sum of the succession of its temperature/time transients which correspond to the operating conditions during successive intervals δt.

To use this method in a general calculation for a linear machine, a set of temperature/time transients is required which covers the range of operating conditions likely to be met in service. For a series motor these comprise transients for various currents at normal voltage (as in Fig. 2, where larger rises are due to the greater I^2R losses arising from higher currents), and

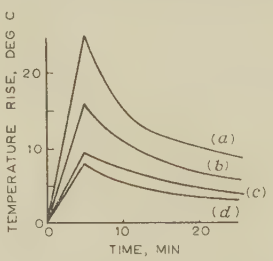

Fig. 2.—Normal-voltage (230 volts) heating transients.
(*a*) 150 amp.
(*b*) 120 amp.
(*c*) 92 amp.
(*d*) 75 amp.
δt = 5 min.

for various speeds at the maximum accelerating current (as in Fig. 3, where larger rises are due to the greater iron losses arising from higher speeds). Such data could alternatively be presented as curves giving the temperature rises at times δt, $2\delta t$, $3\delta t$, etc., on a base of current or speed.

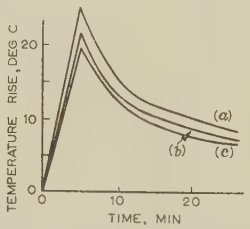

Fig. 3.—Maximum-current (150 amp) heating transients.
(*a*) 500 r.p.m.
(*b*) 200 r.p.m.
(*c*) 0 r.p.m.
δt = 5 min.

These transients must be derived from tests made on the real, non-linear, machine, and corrections must be found for the effects of non-linearity if the temperature/time curve for a real machine is to be predicted. This is discussed below.

(4) TEMPERATURE DIFFERENCES DUE TO NON-LINEARITY

Let a real machine be the same as its linear counterpart when it has a standard temperature (and hence equal winding resistances) and a standard speed (and hence equal dissipation coefficients).

Let the linear machine be subjected to a sequence of operating conditions and its temperature-rise/time relation be recorded. To make this machine identical with the real one, two different, varying losses must be added (algebraically) to those of the linear machine: the first is an additional I^2R loss arising from any increase of winding resistance with temperature; the second is an additional rate of heat input to all those parts for which the dissipation coefficients vary with speed. (This power corresponds to the reduction in power dissipation caused by any reduction in dissipation coefficients, usually arising from a reduction in speed.)

(4.1) Difference due to Variation of Winding Resistance with Temperature

The additional I^2R loss in the winding is $I^2R\alpha(\theta_s - \theta_a)$, where α is the fractional increase of resistance per degree temperature rise referred to the standard temperature θ_s, R is the winding resistance at temperature θ_s, and θ_a is the actual temperature. The additional energy input during the short time δt is thus $I^2R\alpha(\theta_s - \theta_a)\delta t$ (where θ_a is now the average actual temperature during δt), and will give rise to an additional temperature rise θ_c, where, k being a constant,

$$\theta_c = kI^2R\alpha(\theta_s - \theta_a)\delta t \quad . \quad . \quad . \quad . \quad (1)$$

For a fixed time δt and a given winding, since k, R, α and δt are all constant, their product may be called C, giving

$$\theta_c = CI^2(\theta_s - \theta_a) \quad . \quad . \quad . \quad . \quad . \quad (2)$$

If current I and temperature θ_a apply for a time δt only, their effect on the motor temperature will thus itself be a temperature/time transient consisting of a rise during time δt followed by cooling. The extra temperature rise, as a function of time, due to changes in temperature for the whole sequence of operating conditions may thus itself be obtained by summation of the temperature-correction/time transients corresponding to the operating currents and temperatures during the succession of intervals δt.

Another temperature-dependent loss in armature windings is eddy loss, which is inversely proportional to the resistance of the armature winding. This is discussed in Section 12, in which it is shown that, if the proportion of eddy loss is small, corrections based on eqn. (2) will be a little large, but in error by less than 1° C in the important temperature range.

(4.2) Difference due to Variation of Dissipation Coefficients with Speed

The additional rate of heat input to each of those parts for which dissipation coefficients vary with speed will be $-\delta c\theta_a$, where δc is the increase in thermal conductance from the part and θ_a its actual temperature rise. The negative sign arises because an increase of conductance, due to an increase in speed, increases the rate of removal of heat, the actual rate also being proportional to the temperature rise θ_a.

Thus for a given θ_a, if the speed is greater or less than the standard speed for a short time δt, there will be an extra temperature fall or rise compared with that due to dissipation at standard speed over the same interval.

This extra temperature rise will be $D\theta_a$, where D is a constant (positive or negative) for any one speed, and is a function of the departure (negative or positive respectively) of the speed from standard. If a certain speed difference persists for time δt only (after which the speed reverts to standard), its effect on the temperature of the machine will be given by a temperature/time transient consisting of a rise or fall of θ_d $(=D\theta_a)$ during time δt, followed by cooling or heating respectively.

The extra temperature rise, as a function of time, due to the succession of departures of speed from the standard may thus be obtained by summation of the temperature-correction/time transients corresponding to the sequence of speeds and temperature rises appropriate to the succession of intervals δt.

(5) TEST PROCEDURE

If the constants C and D of Section 4 can be found from tests on the test bed, then from any temperature/time curve so obtained the corresponding curve for the linear machine can be derived, and conversely. An approximation in the procedure arises here. The corrections depend on θ_a, the average temperature during an interval δt. The first prediction will give the uncorrected temperature/time curve for the linear machine; corrections are first based on rough values of θ_a from this uncorrected curve. Strictly, the corrections should be reassessed on the basis of the new values of θ_a obtained by applying the first corrections to the uncorrected curve. This iteration will rarely be necessary, since its omission rarely gives rise to more than 1% error in the final prediction. Moreover, corrections are often of opposite sign, so that the total correction may be small and its reassessment unnecessary.

A strictly algebraic approach to the above is impossible, since the total correction is often more dependent on what has gone before than on conditions through any given interval.

A test procedure, comprising four groups of tests, to give D (associated with dissipation-dependent non-linearity) and C (associated with temperature-dependent non-linearity), as well as the temperature/time transients for different operating conditions, is outlined below. For these tests a machine with embedded temperature detectors is required if armature-winding temperatures are to be studied. Sections 10.1 and 10.2 of Reference 1 describe such equipment and a spiral-belt substitute for brushes.

(5.1) Effect of Speed Differences

To obtain D, cooling curves which differ only because of differences in speed must be obtained; each cooling test must thus be started from the same temperature rise and with the same temperature distribution between the parts. The first tests are thus made by heating the machine to the equilibrium temperature at the r.m.s. current and average service speed, this temperature and speed being taken as standard. (This will result in corrections often being small and averaging roughly zero; the effects of approximations will thus be minimized. From the heating curve can also be derived a heating transient.

Tests 1, to give the heating transients due to changes in dissipation, are thus:

(1*a*) Heat to given conditions at standard speed; cool at standard speed.

(1*b*) Heat exactly as in Test (1*a*); cool at a series of different speeds.

(5.2) Effect of Temperature Differences

To obtain C, a heating curve is required which is due only to the winding I^2R loss. This curve must thus be obtained from a test at zero speed (no iron loss), and for convenience should be at the maximum service current I_m. The second test, to give the heating transient due to changes in temperature, is thus:

(2) Heat to approximately standard temperature with the maximum service current at zero speed; cool at standard speed.

(5.3) Basic Heating Transients

The third tests, to give the heating transients due to various currents at the speeds corresponding to normal voltage are:

(3*a*) Heat to approximately standard temperature at the continuous rating current and corresponding speed at normal voltage; cool at standard speed.

(3*b*) Heat to approximately standard temperature at several higher currents up to the maximum service current I_m at the corresponding speeds at normal voltage; cool at standard speed.

(3*c*) Heat to equilibrium temperature at a few currents below the continuous rating current at the corresponding speeds at normal voltage; cool at standard speed.

The fourth tests, to give the heating transients due to the maximum service current I_m at various speeds are:

(4*a*) Heat to approximately standard temperature at the maximum service current I_m at a few speeds between zero and that corresponding to normal voltage; cool at standard speed.

(6) TEST ANALYSIS

To derive the sets of temperature transients for the linear machine the procedure is as follows. First, find heating transients due to changes in dissipation from the groups of cooling curves of Tests 1, and apply these by successive summation, as temperature/time corrections, to the results of Tests 2–4, to give the heating curves of the linear machine. Finally, analyse these heating curves into their heating transients, which may be called the standard heating transients. Data thus become available for the prediction of actual temperature/time curves.

(6.1) Choice of Time Interval, δt

To reduce the task of summing transients over a long run it is preferable that δt should be as long as possible. But so that the average operating conditions during δt might reasonably account for the integrated effects of the varying conditions possibly occurring, δt should be short compared with the thermal time-constant of the motor.

For very short times the temperature rise of a part from cold is proportional to the total energy loss, whatever its time distribution, in that part. With the first two terms of the series for ε^x it is found that an exponential heating curve of time-constant τ departs by a small fraction, f, from its tangent through the origin when $\delta t/\tau = 2f$. This means that fraction $1 - f$ of the temperature rise is dependent on the losses, and fraction f may be affected by speed variation to the small extent that average cooling is not necessarily equal to cooling at average speed. In addition, when δt is short, the mean temperature θ_a during δt is closely the mean of those at the beginning and end of the interval.

For the author's tests, $\delta t/\tau$ was about 10% and f thus about 5%, so that θ_a for each interval was in error by no more than 2½% of the increment during each interval. Since conditions were constant during each interval, no errors arose from averaging either losses or speeds; longer intervals could thus have been used, but they would have rendered the demonstration artificial.

(6.2) Cooling Corrections

To find the dissipation 'heating' transient which accounts for the difference between a zero-speed (say) cooling curve and that at standard speed, the pair of cooling curves from Tests 1, as shown in Fig. 4, is used. The heating transient is defined by its

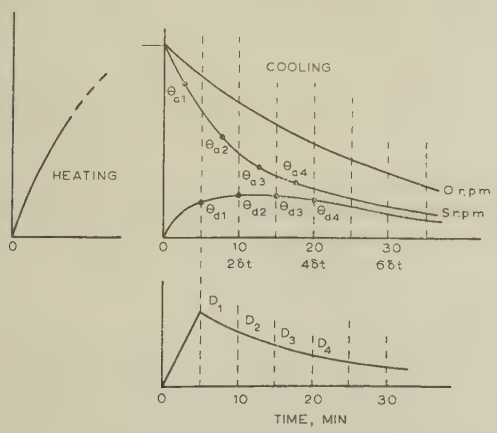

Fig. 4.—To find the dissipation heating transients.

ordinates D_1, D_2, D_3, . . ., D_n at intervals δt, $2\delta t$, $3\delta t$, . . ., $n\delta t$ from the start, and the correction curve by its corresponding ordinates θ_{d1}, θ_{d2}, . . ., θ_{dn}. The mean actual temperatures on the standard curve during these intervals are θ_{a1}, θ_{a2}, . . ., θ_{an}.

Then

$$\left.\begin{aligned}\theta_{d1} &= \theta_{a1}D_1\\ \theta_{d2} &= \theta_{a1}D_2 + \theta_{a2}D_1\\ \theta_{d3} &= \theta_{a1}D_3 + \theta_{a2}D_2 + \theta_{a3}D_1\end{aligned}\right\} \quad . \quad . \quad . \quad (3)$$

From Fig. 4 and eqns. (3), it being remembered that θ_{an} and θ_{dn} are known and D_n is to be found, it will be seen that

$$D_1 = \theta_{d1}/\theta_{a1} \quad . \quad . \quad . \quad . \quad . \quad . \quad . \quad . \quad . \quad (4)$$

$$D_2 = (\theta_{d2} - \theta_{a2}D_1)/\theta_{a1} \quad . \quad . \quad . \quad . \quad . \quad . \quad (5)$$

$$D_3 = (\theta_{d3} - \theta_{a2}D_2 - \theta_{a3}D_1)/\theta_{a1} \quad . \quad . \quad . \quad (6)$$

etc., each value of D_n depending upon knowledge of D_{n-1}.

By procedures such as the above a set of heating transients (per unit temperature rise) which account for changes of dissipation coefficient due to changes in speed will be obtained.

(6.3) Temperature Correction: I^2R Loss

To find the temperature heating transient which accounts for the difference between I^2R heating at standard temperature and at any other temperature, the result of Test 2 (of heating at I_m and zero speed, with cooling at standard speed) is used, as shown in Fig. 5. The temperature rise, θ_m, during the first

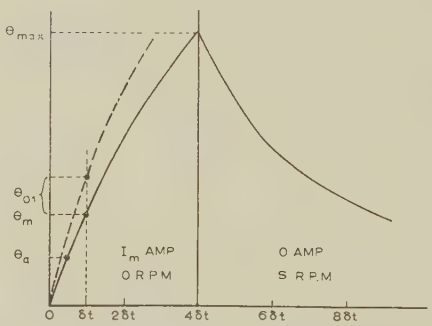

Fig. 5.—To find the temperature heating transient.
590 r.p.m. is standard speed.

interval, at a mean temperature of θ_a (approximately $\frac{1}{2}\theta_m$), is proportional to I_m^2 since there are no other losses, and to R_a, the winding resistance at the mean temperature θ_a.

With k as a constant of proportionality,

$$\theta_m = kR_aI_m^2 \quad . \quad . \quad . \quad . \quad . \quad . \quad . \quad (7)$$

whence

$$kR_a = \theta_m/I_m^2 \quad . \quad . \quad . \quad . \quad . \quad . \quad . \quad (8)$$

But

$$R_a = R_s[1 - \alpha_s(\theta_s - \theta_a)] \quad . \quad . \quad . \quad (9)$$

where θ_s is the standard temperature and α_s the corresponding temperature coefficient of resistance [α_s is $1/(234{\cdot}5 + \theta_s)$ for copper, θ_s being in degrees Celsius].

If θ_{C1} is the correction to be added to make the temperature rise what it would be if the mean temperature were the standard temperature,

$$\theta_m + \theta_{C1} = kR_sI_m^2 \quad . \quad . \quad . \quad . \quad . \quad (10)$$

whence, subtracting eqn. (7) from eqn. (10),

$$\theta_{C1} = kI_m^2(R_s - R_a) \quad . \quad . \quad . \quad . \quad (11)$$

But, from eqn. (9),

$$R_s - R_a = R_a\frac{\alpha_s(\theta_s - \theta_a)}{1 - \alpha_s(\theta_s - \theta_a)} \quad . \quad . \quad . \quad (12)$$

Substituting eqns. (12) and (8) in eqn. (11) gives

$$\theta_{C1} = \theta_1 \frac{\alpha_s(\theta_s - \theta_a)}{1 - \alpha_s(\theta_s - \theta_a)} \quad . \quad . \quad . \quad . \quad (13)$$

whence, from eqn. (2),

$$C_1 = \theta_1 / I_m^2(\theta_s - \theta_a) = \frac{\theta_1}{I_m^2} \frac{\alpha_s}{1 - \alpha_s(\theta_s - \theta_a)} \quad . \quad (14)$$

which was to be found.

Since the correction transient is regarded as arising from resistance loss only, its cooling part is the same shape as that due to resistance loss only.

(7) REVIEW OF TESTS AND RESULTS

(7.1) The Machine, and Temperature Measurements

The machine used to verify the above proposals was a 230-volt 25 h.p. d.c. series steelworks mill motor with forced ventilation; its continuous rating was 92 amp at 590 r.p.m. The machine and thermometer arrangements were as used earlier by Tustin and Bates.[1,2] This had the advantage that the machine was of known characteristics and was well equipped for temperature measurements; the sole disadvantage was that the forced ventilation reduced the range of change of dissipation coefficients with speed. Thus, although the equivalent conductance from the armature winding to the ambient air varied by about ±30% from that at the mean speed[1] over the speed range used in the present tests, a severe test of the validity of the dissipation (speed) correction was not possible.

The resistance thermometer used for these tests was inserted between the top and bottom coil sides in an armature slot, to give the slot-centre copper temperature. With a potentiometer method of measuring the thermometer resistance, temperature rises with less than ½° C error could be obtained when all was well. Unfortunately, oil seepage on to the spiral belts which tapped the voltages from the pulley 'slip-rings' on the armature shaft increased the error of a number of readings, and the tails of many of the cooling curves were less accurate than had been hoped. In addition, the varying sunlight through the glass-roofed laboratory gave short-time fluctuations of ±2° C to the ambient temperature.

(7.2) Basic Results

An outline series of tests was made as in Section 5, except that the normal-voltage continuous-rating speed (590 r.p.m.) and temperature (85° C, or 65° C rise) were taken as standard. To allow for the appreciable fluctuation of ambient air temperature, the effective ambient temperature was obtained by smoothing the ambient-air-temperature curve with a time-constant of about 50 min—roughly equal to that of the motor viewed as a single body.

The temperature-rise/time curves obtained were treated as outlined in Section 6, to give the standard heating transients of Figs. 2 and 3, the temperature heating transient of Fig. 6 and

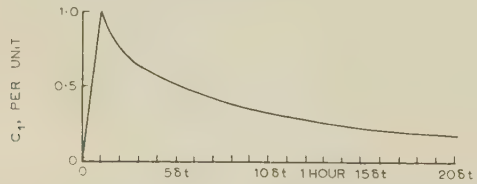

Fig. 6.—The basic temperature correction heating transient.
C_1 is of magnitude $2{\cdot}53 \times 10^{-6} I^2$ for a current of I amperes.

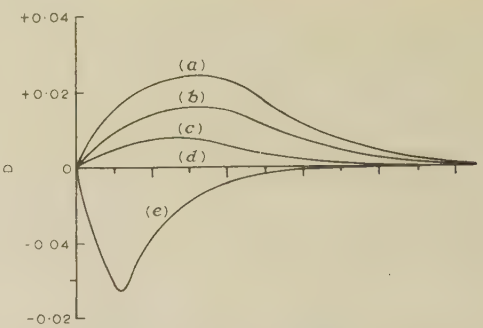

Fig. 7.—The dissipation correction heating transients for an arbitrary run containing extreme conditions.
(*a*) 0 r.p.m.
(*b*) 200 r.p.m.
(*c*) 400 r.p.m.
(*d*) 590 r.p.m. (standard).
(*e*) 1 200 r.p.m.

the dissipation heating transients of Fig. 7. Since the derived curves were generally based upon the relatively small differences between two test curves, they were often ill-defined. The best curves to fit the derived points were chosen by making positive and negative errors roughly equal; to do this, a short-time departure of ±2° C had to be accepted, but in general the errors were less than this.

(7.3) Prediction of Temperature/Time Curves for Arbitrary Run

Fig. 8 shows the test points for an arbitrary run performed for comparison with a predicted curve; it consisted of a sequence

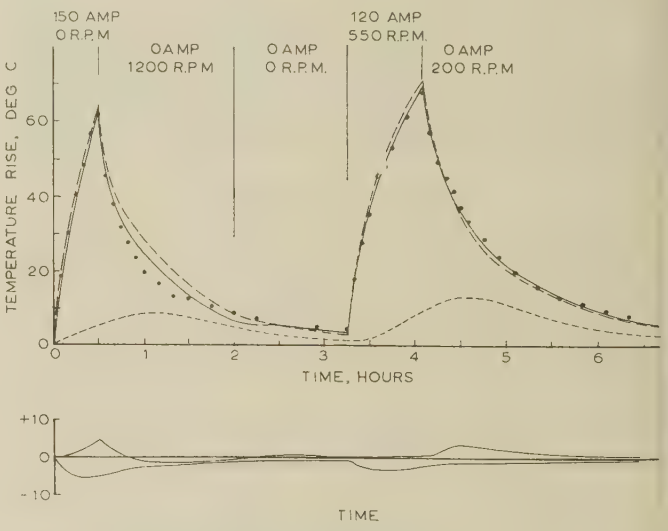

Fig. 8.—Comparison of prediction and test for arbitrary run.
— — — Uncorrected prediction of temperature rise.
——— Corrected prediction of temperature rise.
····· Test points.
– – – – – Frame temperature rise.
In the lower Figure the upper curve gives the dissipation correction and the lower curve the temperature correction.

of five extreme conditions, each sustained for from half to twice or more the overall thermal time-constant of the motor (about 50 min). The final cooling was chosen to be at 200 r.p.m. because earlier work[1] had shown an anomaly in the equivalent thermal conductance from the armature winding at this speed: this anomaly did not obtrude in the present study. Fig. 8 shows the temperature/time prediction for the linear machine, the corrected prediction for the actual machine and the test points; the lower graph shows the individual corrections.

In general, the predicted and test temperature rises agree to within 2° C (and often less) even when rates of change are large; and the total correction almost always has the sign and magnitude to improve the prediction.

The least successful prediction occurs during maximum-speed cooling after zero-speed high-current heating—a succession of extremes unlikely in practice. Here (from $\frac{3}{4}$ to 2 hours or more) the test curve had greater curvature than the predicted curve, but (except at low temperature rises) the correction had the correct sign; and at high temperature rises and with large rates of change, errors were still under about 2° C. The greater curvature occurs, however, when the inactive parts of the machine are relatively cool (frame temperature rise about 10° C), and this would cause accelerated cooling of the active parts. During the second part of the test, when the inactive parts had become warm (frame temperature rise about 15° C) and conditions were less extreme, prediction was generally within ±2° C and often closer to the test results.

Comparison of the first and second heating-cooling sequences shows that the prediction of peak temperatures was a little high (+0·7° C and +2·5° C), and that of temperature rises in the range 40–60° C was within ±2° C of test results; but the preceding paragraph shows that prediction of the lower rises seems influenced by the temperature rise of the inactive parts, being less in error when these are warm. It is thus concluded that the prediction of peak temperatures is little affected by the temperature of the inactive parts, but that the prediction of lower temperatures is so affected. To reduce errors due to this, lower-current tests (more liable to these errors) should be performed when the inactive parts are warm.

(7.4) Examination of Results

(7.4.1) Basic Heating Transients.

The normal voltage transients of Fig. 2 show the somewhat sharper knee that is expected for cooling from higher-current operation, owing to the increasing predominance of I^2R losses and the shorter thermal time-constant of the copper; the maximum-current transients of Fig. 3 show the expected increase in rate of increase of temperature rise due to the increase in iron losses at higher speeds.

(7.4.2) Assumption of Linearity: Temperature Correction.

Section 4.1 shows how to allow for the non-linearity due to temperature changes. Applying the correction of Section 4.1 to test (1*a*) gives the heating curve for the linear machine with constant losses equal to those at standard temperature. The cooling curve of this test should be the inverse of the heating curve of the linear machine: if the temperature correction is exact, the two curves should coincide. Fig. 9 shows the inverted cooling curve plotted with the corrected (constant-loss) heating curve. The correction is seen to be high for much of the temperature range. Since eddy-current losses vary inversely as resistance and are ignored in this correction, the high tendency is acceptable.

At longer times the cooling curve is high, giving rise to the lowness of the inverted cooling curve compared with the constant-loss heating curve. This is because the warm inactive parts (towards the end of the test) delay the final cooling when temperature rises are low, but have very little effect on the heating when temperature differences are appreciable.

(7.4.3) Dissipation Correction Heating Transients.

Fig. 7 shows that, in general, these are not sharp rises over the first interval δt followed by falls commencing promptly at time δt. This is because the change in dissipation coefficient is

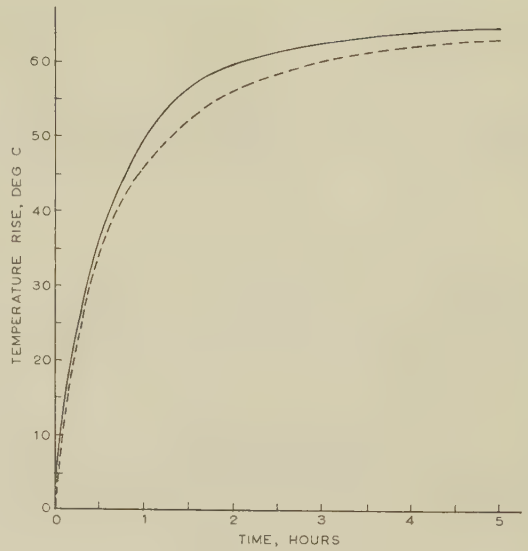

Fig. 9.—Comparison of inverted cooling curve from standard conditions with linearized (constant-loss) heating curve to standard conditions.

----- Inverted cooling curve.
——— Constant-loss heating curve.

felt first at the armature surface and its effects take some little time to be felt at the slot centre. This is supported by the much sharper cooling/heating transition at 1 200 r.p.m., where the much increased dissipation coefficient would give a very much shortened thermal time-constant, and hence sharper response to conditions at the surface for the slot centre copper.

(8) SUGGESTED APPLICATIONS

(8.1) To Obtain Peak Temperatures

To apply the method to obtain a whole temperature/time curve for a long run is tedious: to use the method to obtain peak temperatures it suffices to obtain a temperature/time curve for about two hours preceding the peak and to start this curve from a rough estimate of the temperature rise, θ_0, at that time. Since, even from a cold start, 80% or more of the peak temperature rise of a continuous run would be reached after two hours, the error after a hot start from θ_0 will be only 20% of the error in the estimate of θ_0. Similarly, since corrections are a small fraction of the total, they may be ignored up to two hours before the peak.

(8.2) Computation: Computers

For practical application the heating transients are required as Tables of ordinates at intervals δt. For currents or speeds not explicit within the Tables, interpolation will be necessary. It is thus felt that the method, with its tedious but simple calculations, is especially applicable to digital-computer procedures if many runs or many motors are to be studied.

Nevertheless, with a 5 min basic interval and the need only to compute for the two hours preceding a temperature peak, the sequence of 24 computations is not excessive and could easily be performed by suitably trained junior staff.

(8.3) Short-Time Variations

For accurate estimation of the effects of variation of conditions within a basic time interval (as for a suburban train, which would have more than one duty cycle within the 5 min suggested), a sequence of composite heating transients must be

compiled. If during an interval δt there are n equal short intervals during which the current and speed may reasonably be averaged, the composite heating transient for the linear machine will be $1/n$ of the sum of the n appropriate transients, the composite dissipation transient $1/n$ of the sum of its n appropriate transients; the temperature heating transients can still be based on the predicted mean temperature and the r.m.s. current for the whole interval δt.

(9) REVIEW AND RECOMMENDATIONS

The paper has surveyed and demonstrated a method of predicting temperature/rise time curves for a given part of a machine operating with sustained variations in load and speed: the part chosen for demonstration was the winding in the centre of a slot. It seems that, given sufficiently precise data from which to derive the heating transients, errors of less than $\pm 2°$ C should be possible. The method should be of special value for application to self-ventilated motors; but was verified on a force-ventilated motor, for which, however, the dissipation was a function of speed.

It is recommended that the characteristic heating transients of a sample of a line of motors might be verified: this will necessitate equipping a representative motor with embedded temperature detectors, to permit testing.

By performing high-current tests first (for their results are least affected by the temperatures of the inactive parts) and the low-current tests later (when the inactive parts are warm) one continuous sequence of tests should suffice. It should suffice, even at lower currents, to perform heating tests for 2–3 hours, since exponential extrapolation of the curves will then lead to little error.

The test-bed time needed for the method is thus 36–48 hours; and for a line of motors of which several hundred may be produced, this should be time well spent. Moreover, when a number of lines have been sample-tested in this way, general similarities between the results will become apparent. It will thus ultimately be necessary to test a motor only under standard and extreme conditions to obtain outline characteristics within which the form of interpolation will have become known. By then, a total test-bed occupation, for thermal tests, of about 24 hours should suffice.

(10) ACKNOWLEDGMENTS

The author is grateful to Professor A. Tustin for the interest, encouragement and advice given throughout the performance of this work; to the British Iron and Steel Research Association, and Dr. L. N. Bramley of its Plant Engineering Division, for making available the motors and laboratory facilities used in performing the tests; and to Messrs. J. Griglazewski, B.Sc., and B. Martin, for assistance in the experimental work.

(11) REFERENCES

(1) BATES, J. J., and TUSTIN, A.: 'Temperature Rises in Electrical Machines as Related to the Properties of Thermal Networks', *Proceedings I.E.E.*, Paper No. 2026 U, April, 1956 (**103** A, p. 471).

(2) TUSTIN, A., and BATES, J. J.: 'Temperature Rises in Electrical Machines on Variable Load and with Variable Speed', *ibid.*, Paper No. 2031 U, April, 1956 (**103** A, p. 483).

(12) APPENDIX

Let a linear motor have a constant I^2R loss, P. Its ultimate temperature rise, θ_l, due to this will be

$$\theta_l = kP \quad . \quad . \quad . \quad . \quad . \quad . \quad . \quad (15)$$

where k is the appropriate constant of proportionality.

Let a non-linear motor with constant current have an I^2R loss P at the standard temperature θ_s and a corresponding temperature coefficient of resistance α. Its loss at temperature θ_l will thus be $P[1 + \alpha(\theta_l - \theta_s)]$, whence the ultimate temperature rise, θ_n, will be approximately (since θ_n is not a lot different from θ_l)

$$\begin{aligned}\theta_n &= kP[1 + \alpha(\theta_l - \theta_s)] \\ &= \theta_l[1 + \alpha(\theta_l - \theta_s)] \quad . \quad . \quad . \quad . \quad (16)\end{aligned}$$

Let the non-linear motor, now with constant current, field flux and speed, have a copper loss P at the standard temperature θ_s, of which loss proportion β is eddy-current loss, which varies inversely as conductor resistance; the rest, $(1 - \beta)$, is I^2R loss varying as resistance. Its loss at temperature θ_l will thus be

$$P(1 - \beta)[1 + \alpha(\theta_l - \theta_s)]$$

for the I^2R loss, plus

$$P\beta/[1 + \alpha(\theta_l - \theta_s)]$$

for the eddy-current loss. With the same approximation as above, the new temperature rise, θ_e, is given by

$$\theta_e = kP\left\{(1 - \beta)[1 + \alpha(\theta_l - \theta_s)] + \frac{\beta}{1 + \alpha(\theta_l - \theta_s)}\right\}$$

Putting θ_l for kP, and

$$\beta[1 - \alpha(\theta_l - \theta_s)] \text{ for } \beta/[1 + \alpha(\theta_l - \theta_s)],$$

and simplifying, gives

$$\theta_e = \theta_l[1 + \alpha(1 - 2\beta)(\theta_l - \theta_s)] \quad . \quad . \quad . \quad (17)$$

Eqn. (16) gives the correction applied in this paper in which the copper loss is assumed to be all I^2R, and eqn. (17) gives the accurate correction. The error in the correction is thus eqn. (16) minus eqn. (17), or $2\alpha\beta\theta_l(\theta_l - \theta_s)$; the correction applied is thus a little large.

In the motor tested, for continuous-rating current and speed, θ was a 65° C rise with 20° C ambient temperature; θ_s was also a 65° C rise; the corresponding temperature coefficient of resistance is 1/319·5. β was estimated to be about 0·1.

For temperatures near θ_s the correction itself is small; for temperatures in excess of θ_s say an 80° C rise—even assuming that the whole temperature rise is due to copper loss, insertion of these figures gives the error to be $2 \times 0{\cdot}1 \times 80(80 - 65)/319{\cdot}5$, or about 0·8° C, which is an error on the right side, and since temperature could not be reliably measured to much closer than $\pm 2°$ C, not a significant error.

621.396.969.1.088

The Institution of Electrical Engineers
Monograph No. 417 E
Nov. 1960

THE INDETERMINACIES OF MEASUREMENTS USING PULSES OF COHERENT ELECTROMAGNETIC ENERGY

By R. MADDEN, B.S.

(*The paper was first received* 11*th April, and in revised form* 17*th August*, 1960. *It was published as an* INSTITUTION MONOGRAPH *in November*, 1960.)

SUMMARY

The measurements, on a single pulse function of electromagnetic radiation, of the position of a scatterer with polar co-ordinates R, ϕ are interdeterminate in themselves. The positional indeterminacies are related by $\Delta R \Delta\phi \simeq \frac{1}{2}\lambda_t$, where λ_t is the wavelength of the source. The relation between the indeterminacies of range R and radial velocity V_r is found to be $\Delta R \Delta V_r \simeq \frac{1}{4}\lambda_t c$. It is shown that vector position and vector velocity are not measurable simultaneously, and it is suggested that the 3-dimensional measurement problem is basically limited to non-simultaneous measurements which have restrictions in the presence of multiple scatterers. Similarity is noted to the quantum-mechanical problem.

(1) INTRODUCTION

During the past two decades the use of pulses of radio waves for the measurement of the position of objects has become commonplace. More recently, the demands placed upon radar for the measurement of velocity and acceleration of objects has caused a growing realization that further perfection of equipments and further development of measuring techniques may not yield an increase in the quality of measurements because of the limitations inherent in the pulses themselves. In the paper, consideration will be given to the limitations which stem from well-established physical principles which, in more recent times, appear to have received less attention than they deserve.

It will be seen that the measurement of position and velocity by the use of the methods of radar is similar to the measurement problem which is treated in detail in quantum mechanics. In that subject it is found that, in the microscopic world, the measurement of the position and momentum of a particle, along a single axis, cannot be found to an arbitrary degree of accuracy, but that the product of the indeterminacies of these quantities has an irreducible minimum. In the macroscopic world, measurements are similarly limited when made by pulses of electromagnetic energy, even though it can be verified by independent measurement that the pulses used do not appreciably affect the quantities being measured—the usual explanation set forth for the origin of the indeterminacies in the microscopic world.* This view is often received with surprise in spite of the fact that the Heisenberg uncertainty principle can be obtained directly from the use of de Broglie's relations of energy and wavelength, together with Rayleigh's criterion relating the spread of the wave number to the length of the wave packet in space.

The development of radar affords an excellent opportunity to consider the limitation imposed on measurements using pulses of radiation. As will be shown, the limits which are imposed are by no means negligible from the viewpoint of the quality of measurements which may be desired. In addition, the limitations which are derived for the macroscopic world may be applicable to the microscopic world, for the ratio of the lengths of the objects of interest to the wavelengths of the radiation employed is not appreciably different in the two cases.

* The photons used in the microscopic measurements are subject to the limitations set forth in Section 3. Because of this, it is unprovable and quite unessential that a view be taken that the act of measurement affects the quantities being measured.

Mr. Madden is with the Radio Corporation of America, Burlington, Mass.

(2) THE GENERAL PROBLEM

The problem of the measurements of position and momentum generally treated in quantum mechanics is restricted to a single space co-ordinate.[5, 6] But position and momentum are vector quantities and the extension of measurements to the three dimensions is not an obvious one. The problem to be treated here is 3-dimensional, and it will be assumed that the desired quantities are vector position and vector velocity. It is also assumed that measurements must be made on an arbitrary number of objects distributed in any manner in a volume of space which is not necessarily bounded (i.e. one of the measurements to be made is the number of objects to be measured). It is further assumed that the measuring equipment is noiseless and that space is non-dispersive.

Measurements performed by radar have an attractive degree of simplicity and can be described quite completely in terms of clock readings, antenna directivity and receiver bandwidth. The universal practice of using equally spaced repetitive pulses, however, has obscured the basic limitations of a single pulse measurement. Here, attention will be brought to bear on the basic limitations of a single pulse measurement in a noiseless environment. The implications of multiple measurements and the limitations of such techniques, briefly mentioned in Section 6, will be considered in a separate monograph, in detail, at a later time; it is only suggested here that such techniques do not eliminate the basic limitations discussed in this paper, but rather couch these limitations in more obscure forms.

(2.1) Minimum Required Equipment

For the purposes of explanation, a perfect radar is now envisaged which will operate in an idealized fashion. This radar consists of an omnidirectional transmitting antenna which will emit a single pulse of wavelength λ_t and duration τ at time $t = t_0$. The pulse propagates outward through space and is confined to a shell of thickness $c\tau$ expanding at the speed of light, c. Some portion of the energy contained in the expanding shell is scattered or reflected back to the receiver system, which is located next to the transmitter. The energy which is returned to the receiver is gathered by a directional antenna, here assumed to be a paraboloid, of diameter $2a$. It is supposed that the image plane of the antenna can be examined for the reflected pulse without turning the antenna. This examination might be carried out by having an array of isolated dipoles or horns, each of which is connected to a bank of staggered filters, each having a known tuned frequency and bandwidth. The output of every filter then activates circuits which operate a clock. The receiver system is shown schematically in Fig. 1. These changes in the methods of current radar practice do not in any way alter the measurements obtained by radar, but focus attention on the more basic problems.

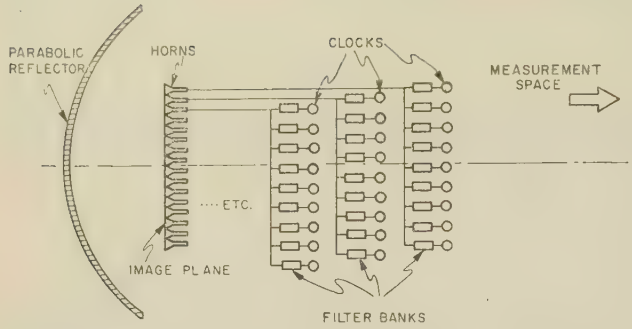

Fig. 1.—The receiver system.

The operation of the system is as follows:

(*a*) A spherical shell of radiation is propagated throughout space. At the instant of transmission, all clocks begin to record time.

(*b*) Objects at various positions in space reflect a portion of the energy to the receiving site.

(*c*) The receiving antenna focuses the energy on to a particular elemental horn located on the image plane.

(*d*) The horn which receives the energy is connected to a frequency-determining bank of filters for the measurement of the Doppler effect.

(*e*) The time at which the energy focused on the horn passes through the filter and is detected is determined by activating circuits which stop a clock.

(*f*) For each and every pulse that is returned, the time is recorded; simultaneously the filter is noted and the horn element is noted.

The foregoing discussion may seem somewhat prolix, but it is important to recognize that the concern here is associated with the nature of radiation, and that all measuring apparatus must be recognized for its essential role.

(2.2) Measured and Desired Quantities

The following relations provide the desired quantities from the measured quantities:

$$H_{\theta,\psi} \rightarrow \theta, \psi \quad . \quad . \quad . \quad . \quad . \quad . \quad . \quad (1)$$

$$V_r = \frac{f_r - f_t}{f_r + f_t} c \quad . \quad . \quad . \quad . \quad . \quad . \quad (2)^*$$

$$R = \tfrac{1}{2} t_t c \quad . \quad . \quad . \quad . \quad . \quad . \quad . \quad . \quad (3)$$

where $H_{\theta,\psi}$ = A horn element in the image plane.
θ = Angular position of the horn in the image plane in the x-direction.
ψ = Angular position of the horn in the image plane in the y-direction.
V_r = Radial velocity, positive when towards the receiver at the time of reflection.
f_t = Transmitted frequency.
f_r = Received frequency.
R = Distance between receiver and reflector at the time of reflection.
t_t = Transit time of the pulse.
c = Speed of light.

Before proceeding to a detailed discussion of the interdependence of these relations, it is important to observe that the measuring experiment described cannot perform all the desired measurements. The vector velocity could be obtained from a measurement of angular rates, in combination with range, R, but it will be shown later that the angular rates cannot be measured simultaneously with the quantities R, V_r, θ and ψ. In fact, there appear to be no simple measurements which can be performed simultaneously that will yield vector velocity.

* Eqn. (2) is exact for the electromagnetic case: it is identical to the Doppler shift in the two-way acoustical case.

(3) THE ORIGIN OF THE INDETERMINACIES

The fundamental indeterminacies to be derived arise from the fact that the time and frequency which can be associated with the energy within a pulse of electromagnetic radiation are not independent.[1] Thus, the time t which can be associated with the existence of frequency f is not exact, but only possible to the degree

$$\Delta t \Delta f \simeq 1 \quad . \quad . \quad . \quad . \quad . \quad . \quad . \quad (4)$$

where Δt and Δf are the indeterminacies of t and f respectively.

A further consequence is that the formation of an image in an optical system is a function of time, since the frequency distribution of a wave packet intercepted by an image-forming device is a function of time. The resolution of an optical system whose aperture is $2a$ and central disc radius approximately $\Delta\phi$, when using incident energy of wavelength λ, is given by

$$\Delta\phi \simeq \frac{\lambda}{2a} \quad . \quad . \quad . \quad . \quad . \quad . \quad . \quad . \quad (5)$$

But this relation describes a steady-state phenomenon and reveals nothing about the formation of the image. Although this point is of little consequence in the general study of optics, it has serious implications in the measurement problem under discussion here, since the time of arrival of the pulse of energy represents one of the important measurements being made.[10]

The Fourier integral provides considerable insight into the indeterminacy, eqn. (4), and the resolving power, eqn. (5), mentioned above. This integral relates both the frequency distribution of energy to its distribution in time and the angular distribution of energy from an extended source to its current distribution along its extent.

That is, an integral of the form

$$G(f, \tau) = \int_{-\tau/2}^{+\tau/2} F(t) \exp(j2\pi ft) dt \quad . \quad . \quad . \quad . \quad . \quad (6)$$

$$F(t) = A_1 \sin 2\pi ft \text{ when } -\frac{\tau}{2} < t < +\frac{\tau}{2}$$

$$F(t) = 0 \text{ elsewhere}$$

describes the distribution as a function of frequency for an equal-amplitude rectangular-modulated pulse of duration τ, and an integral of the form

$$G(\phi, a) = \int_{-a}^{+a} F(x) \exp\left(jx \frac{2\pi}{\lambda_t} \sin\phi\right) dx \quad . \quad . \quad . \quad (7)$$

$$F(x) = A_2 \sin \frac{2\pi}{\lambda_t} x \text{ when } -a < x < +a$$

$$F(x) = 0 \text{ elsewhere}$$

describes the energy distribution as a function of angle (for small values of ϕ) for a rectilinear distribution of current of constant amplitude of length $2a$.[9]

The usual interpretation placed on eqn. (4) is that the first minimum of the intensity/frequency pattern given by the square of eqn. (6) falls at a frequency different from the central frequency by an amount equal to the reciprocal of the length of the pulse examined. While this represents a view of the problem which would suggest that the difficulty arises because the energy per unit bandwidth need only be compared to find the precise frequency being examined, Reference 3 points out that a better view of the problem is obtained when it is recognized that events are equally well described by their frequency/amplitude relations or their amplitude/time relations, and that eqn. (4) is really an identity because it is desired to describe events in

terms of both quantities, variation of amplitude with time and frequency. This places the difficulty squarely on the way we have chosen to make the measurements, not on the design of a better filter bank, namely a filter bank which attempts to measure the energy of a wave train independently of the amount that the central frequency of the wave train may be removed from the central frequency of the tuned filter.

A similar view may also be taken of the relation between eqns. (5) and (7). Namely, the first minimum of the intensity/angle pattern falls at an angle different from the axial angle by an amount equal to the reciprocal of the length of the aperture used. What is of concern here, however, is the formation of the image with time, and it is suggested that the only substitution which has meaning in eqn. (7) is $x = ct$. Geometric analysis depicting a wavefront incident on an aperture would indicate that the image forms at a rate which is a function of the direction of the wave train relative to the centre-line of the paraboloid. This would indicate that the delay in the image formation is a quantity capable of calibration. Such arguments rest on the assumption that it is phase velocity as a result of geometric velocities which rules the formation of images, and that the transient behaviour is therefore a function of the relative aperture (the ratio of the focal length to the diameter). At the foundation of such analysis is the assumption that the spacing between equi-phase planes composing the leading edge of the wave packet is as well defined as subsequent spacing. Because this is not so [eqn. (4)], the signal velocity c must be substituted into expression (7) irrespective of the direction of the incident wave packet. This, of course, is true in the region where the distortion of the image on the image plane is negligible, and this is the only region of interest. A plot of these equations is given in Fig. 2. It depicts the intensity incident on the image

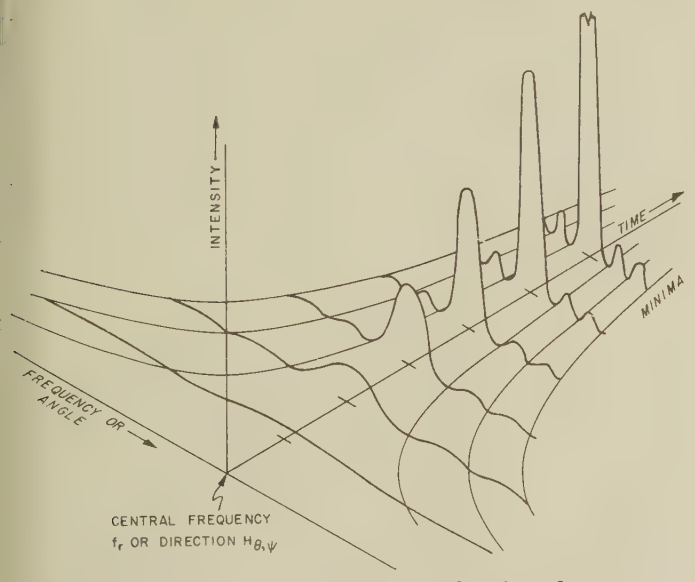

Fig. 2.—Intensity growth as a function of angle or frequency.

plane as a function of time, or the intensity incident on the filter bank as a function of time.

The two equations (6) and (7) have been considered together to demonstrate that eqns. (4) and (5) have similar origins. It is sufficient for the purposes of this discussion to deal with the latter two. The interpretation of eqn. (4) is that, in order to specify the time of arrival of a pulse to the degree Δt, it is essential to provide a filter bandwidth of Δf. But Δt is related to the accuracy with which range can be measured through eqn. (3), and Δf is related to the accuracy with which velocity can be measured through eqn. (2). Hence, differentiating eqn. (3) partially with respect to t_t, differentiating eqn. (2) partially with respect to f_r, and substituting the result in eqn. (4), the desired result is obtained:

$$\Delta R \Delta V_r \simeq \tfrac{1}{4}\lambda_t c \ (V_r \ll c) \quad . \quad . \quad . \quad . \quad . \quad (8)$$

The interpretation of eqn. (5) is that, in order to establish the steady-state diffraction pattern of a conductive reflector, the length of the pulse must be at least as long as the aperture ($\tau > 2a/c$). But this pulse length is approximately the degree to which range is known [through the partial differentiation of eqn. (3)]. Hence

$$\Delta\phi \Delta R \simeq \tfrac{1}{2}\lambda_t \ (V_r \ll c) \quad . \quad . \quad . \quad . \quad . \quad (9)$$

The restriction $V_r \ll c$ is placed on this problem so that the returned wavelength will not be sensibly different from the transmitted wavelength which would make the angular resolution a function of velocity also. This restriction is quite applicable to the measurement problems encountered in radar.

(4) CONCLUSIONS

The accuracy of simultaneous measurements of position and velocity performed by radar is limited. The limitation of the position accuracy itself is a function of the wavelength of the radiation employed. Eqn. (9) may be interpreted to mean that the best measurements which may be made of angle and range are reciprocally related. The larger antenna requires a longer pulse, which, in turn, means less definition in range. Of course, if the pulse function, $c\tau$, is much greater than the diameter of the antenna, the image formed is not improved beyond that obtained with the extent of the pulse, equal to the diameter, which enters the antenna. Another important interpretation may be made regarding the bandwidth to be associated with highly directive antennae. In eqn. (7) it was assumed that the pulse was a constant-frequency sinusoid, i.e. a coherent wavetrain; any deviation from this coherence will cause smearing on the image plane of the antenna. Manifestation of this principle should also be evident in optical instruments,[2, 3] for, if the length of coherence of an optical wavetrain is not approximately equal to the aperture of the optical instrument, the interference pattern will become fuzzy and further increase of the stops will not improve the resolving power. These considerations also may limit the information obtainable with large antennae used in radio astronomy.

The measurement of velocity can only be performed simultaneously along the line of sight. Measurements of radial velocity and range are reciprocally related by $\Delta R \Delta V_r \simeq \frac{1}{4}\lambda_t c$. Hence, as eqns. (8) and (9) show, the necessary requirement for reducing indeterminacies is a reduction in the wavelength of the radiation employed. This is hardly a surprising conclusion, and any other result would be difficult to imagine.

As was pointed out earlier, the tangential component of velocity can be computed from a knowledge of range, R, and angular rates, $\dot{\phi}$ and $\dot{\psi}$. But the measurement of the angular rates requires that the image of the object on the image plane should move from one horn to an adjacent horn. Such motion cannot take place in a time less than τ or else the radial velocity V_r will not be measured simultaneously to the degree ΔV_r corresponding to the chosen bandwidth $1/\tau$. Conversely, such motion cannot be less than that required to move to the next horn; otherwise no motion is recorded. This difficulty compares exactly with the difficulties encountered in measuring a changing frequency since the signal must pass from one filter to the next. Hence it is concluded that there is a remarkable similarity between the measurement of angular velocity and radial acceleration, and

in no case can these measurements be made simultaneously since the signal must pass from one horn to another or from one filter to another.

Inherent in the measuring equipment is a sort of quantization of the image plane (horn size), the velocity continuum (filter width) and range continuum (pulse length). However, control of the quantization is in the hands of the observer. The horn size may be made as small as desired if the antenna is made large; the filter size and the range resolution, for simultaneous measurement, are determined by the pulse length and are not separately adjustable. However, wavelength is adjustable and is restricted only by practical considerations.

Both of the fundamental limits imposed by eqns. (8) and (9) have caused the abandonment of any attempts to measure the quantities R, V_r, and θ and ψ simultaneously. Many techniques have been evolved to remove these limits by successive measurements.[4, 7, 8] For example, average velocity has often been obtained by the differentiation of successive position measurements. Often this technique requires a relative-phase measurement between successive received pulses and a local oscillator. Such methods yield velocity ambiguities and range ambiguities (velocities and ranges which cannot be distinguished from one another). A manifestation of the fundamental limits expressed by eqn. (8) is that the product of these ambiguities is also the product of the indeterminacies, although the interpretation is less obvious. Another example of a non-simultaneity is the rotating antenna lobe (central beam) which is often used to obtain greater angular accuracy measurement on a single-point scatterer. Obviously, considerable difficulty is encountered when several scatterers located in less than the antenna beamwidth are found within the same approximate range.

A more fundamental question arises when it is recognized that simultaneity is a property which can only be achieved by a single measuring site which a radar represents. This is particularly applicable to the quantum-mechanical measurement and indeterminacies which involve small particles. The question to be answered is whether the 3-dimensional problem can ever be solved when multiple objects must be measured without the use of multiple-site measuring equipment and therefore non-simultaneous measurements.

(5) REFERENCES

(1) GABOR, D.: 'Theory of Communication', *Journal I.E.E.*, 1946, **93**, Part III, p. 429.

(2) CHU, L. J.: 'The Physical Limitations of Omni-Directional Antennas', *Journal of Applied Physics*, 1948, **19**, p. 1163.

(3) DI FRANCIA, G. TORALDO: 'Super-Gain Antennas and Optical Resolving Power', *Nuovo Cimento*, 1952, **9**, Suppl. No. 3, p. 426.

(4) SIEBERT, W. M.: 'A Radar Detection Philosophy', Transactions of the 1956 Symposium on Information Theory of the Institute of Radio Engineers, 1956, **IT-2**, No. 3, p. 204.

(5) BOHM, D.: 'Quantum Theory' (Prentice Hall, 1951), p. 105.

(6) BRILLOUIN, L.: 'Science and Information Theory' (Academic Press, 1956).

(7) WOODWARD, P. M.: 'Probability and Information Theory, with Application to Radar' (McGraw-Hill, 1955).

(8) HANSEN, W. W.: 'Radar Systems Engineering' Radiation Laboratory Series (McGraw-Hill, 1947), Chap. 5, C-W Radar Systems.

(9) SCHELKUNOFF, S. A.: 'Electromagnetic Waves' (Van Nostrand, 1943), Chap. 17.

(10) SOMMERFELD, A.: 'Optics' (Academic Press, 1954), p. 114.

(6) APPENDIX

A Brief Discussion of Non-Simultaneous Measurements

The conclusion that 3-dimensional space (R, ϕ, ψ) or that 2-dimensional phase space (R, V_r), when surveyed by radar in the absence of noise, can be divided into cells within which no further detail is discernible has never been generally accepted. Eqns. (8) and (9) show that a precise measurement of a single quantity can be obtained only at the expense of knowledge of its conjugate quantity, quite analogous to the indeterminacies encountered in quantum mechanics. These relations are the results of the consideration of a single pulse function of an electromagnetic wave and the minimum equipment which would be required to measure the time of arrival, direction of arrival and frequency content of an ideal reflection of that pulse. Since limitations exist when a single measurement is made, it is appropriate to investigate the benefits which might result from multiple measurements or, more generally, modulation of the carrier wave. Such multiple measurements are non-simultaneous. It is the purpose of this appendix to point out the nature of the problem and to elaborate briefly on several of its facets.

A complete theory of non-simultaneous measurements must deal with a wide variety of radar systems. However, for the fundamental purposes of interest here, it appears that all radar systems belong to one of two large classes:

(*a*) Radar systems which use multiple measurements of position where no attempt is made to measure frequency shift due to motion of scatterers and the receiver bandwidth is sufficiently large to accommodate motion of the scatterers of interest.

(*b*) Radar systems which employ multiple measurements of position, but which are capable of distinguishing a frequency shift of the returned signal by the measurement of the relative phase between the returned signal and the transmitted signal, or by the use of narrow-band tuned filters.

It was recognized long ago that the effect of using multiple equally spaced pulses could cause confusion when scatterers at ranges greater than one-half the range traversed by a pulse during the interpulse period returned energy to the receiver. Generally, the inter-pulse period was made sufficiently long so that the natural attenuation of the pulse due to the large range traversed could produce, at best, only weak returns. This range separation which would produce a return at the same relative time with respect to the transmitted pulse is called the ambiguous range, R_{amb}, and is given by

$$R_{amb} = \tfrac{1}{2}cT_{ip} \quad . \quad . \quad . \quad . \quad . \quad (10)$$

where T_{ip} is the inter-pulse period.

In addition, radars which attempt to distinguish a frequency shift due to the Doppler effect for either the recognition of moving targets or the measurement of azimuth in certain 'side-looking' radars, have encountered a velocity ambiguity as well. The velocity ambiguity arises from the fact that the transmission of a regularly interrupted wavetrain generates equally spaced harmonics, and if scatterers have range rate separations which produce the same relative frequency shift of the harmonics as of the carrier frequency, the motion cannot be unambiguously measured. The velocity ambiguity, V_{amb}, is given by

$$V_{amb} = \frac{1}{2}\frac{\lambda_t}{T_{ip}} \quad . \quad . \quad . \quad . \quad . \quad (11)$$

where λ_t is the carrier wavelength. The product of the ambiguities is independent of the modulation and equal to the indeterminacies:

$$R_{amb}V_{amb} = \tfrac{1}{4}\lambda_t c \quad . \quad . \quad . \quad . \quad . \quad (12)$$

Thus, if the ambiguities are not tolerable as, for example, in a moving target indicator wherein the inter-pulse period is selected

on the basis of the maximum range which must be surveyed and he velocity ambiguities are accepted as a matter of course, all hat can be done to remedy the situation is to change the carrier wavelength, λ_t, or to prevent illumination of scatterers whose anges or range rates might be ambiguously interpreted.

Thus, the consequences of non-simultaneous measurements are ambiguities rather than indeterminacies, the product of the ambiguities being equal to the product of the indeterminacies. However, the measurement of range and range rate in particular physical situations can be accomplished if certain restrictions are observed (e.g. only scatterers having a maximum relative velocity are illuminated, as in a side-looking radar). The degree to which the conjugate quantities R and V_r can be measured, in a restricted cell in phase space, is such that the product of the indeterminacies of these quantities is less than that given in eqn. (8), but in no case does this product become zero. The development of this fact is complex and lengthy and will be undertaken in a separate monograph.

621.313.011.2:681.142

The Institution of Electrical Engineer
Monograph No. 418
Nov. 196

NUMERICAL EVALUATION OF INDUCTANCE AND A.C. RESISTANCE

With Particular Reference to Electrical Machines

By R. S. MAMAK, B.Sc., Graduate, and E. R. LAITHWAITE, M.Sc., Ph.D., Associate Member.

(*The paper was first received 9th May, and in revised form 12th August*, 1960. *It was published as an* INSTITUTION MONOGRAPH *in November*, 1960)

SUMMARY

The electric and magnetic circuits of electrical machines are generally so complex that the exact evaluation of such quantities as leakage reactance and a.c. resistance is virtually impossible. With the advent of digital computers it has become feasible to develop numerical methods of predetermining the flux pattern in such cases. In the paper the finite-difference equations for electromagnetic systems are obtained, and the inductance is calculated by integrating the magnetic vector potential over conducting surfaces. The same finite-difference equations are applied to the calculation of a.c. resistance of conductors in slots. The use of the method is illustrated by examples of standard transformers, a tap-changing transformer, calculation of the leakage reactance of the field winding of a salient-pole-alternator and the screening of d.c. poles in a new type of oscillating synchronous linear machine.

LIST OF PRINCIPAL SYMBOLS

A = Magnetic vector potential, c.g.s. units.
A, A_z = Components of A in the z-direction.
$\bar{A}$ = Average value of A.
a = Mesh length.
B = Flux density, gauss.
E = Electric force, c.g.s. units.
E, E_z = Components of E in the z-direction.
H = Magnetizing force, c.g.s. units.
I = Current, c.g.s. units.
j = Current density, c.g.s. units.
j, j_1, j_2, j_z = Components of j in the z-direction.
L = Inductance, henrys.
R_{ac} = A.C. resistance, ohms.
R_{dc} = D.C. resistance, ohms.
S, S_1, S_2 = Surface area, cm^2.
v = Volume, cm^3.
α = Iterative factor.
μ, μ_1, μ_2 = Permeabilities.
ϕ = Magnetic scalar potential.
ρ = Resistivity, ohm-cm.
σ = Conductivity, mho-cm.
ω = Angular frequency.

(1) INTRODUCTION

Calculations of inductance in elementary textbooks are generally limited to simple cases of circular coils and closed magnetic circuits, and such assumptions are made as are needed to make the calculation possible by purely analytical methods. In electrical machines the electric and magnetic circuits are generally so complex that exact evaluation of such quantities as leakage inductance and a.c. resistance is virtually impossible. In particular, in induction machines the problem may be stated in the following way: until the flux pattern is known, the induced e.m.f. and secondary current are not known; yet until th secondary current is known, the flux pattern is unknown However, in some machines, such as the transformer, th current distribution is known to a first approximation, whic makes the problem somewhat easier.

Methods of plotting flux distribution with a view to calculatin inductance include the fitting of a pattern of curvilinear square by free-hand drawing, electrolytic tanks, resistance network differential analysers, membranes, etc. With the advent c digital computers it has become possible to develop methods c predetermining the flux pattern quite accurately and quickl without having to resort to analogues. Two papers[1, 2] hav already been published reporting the application of numerica techniques to flux plotting; both converted the electromagneti problem into a magnetostatic one by approximation.

No such approximation is made in the present paper: instead use is made of the concept of vector potential. The relevan finite-difference equations for a 2-dimensional problem may b obtained. Both the flux plot and the inductance of a windin can then be immediately calculated from these equations. Th same finite-difference equations may be applied to calculate th a.c. resistance of conductors in slots.

(2) THE USE OF VECTOR POTENTIALS

The equations of electromagnetism were first formulated b Clerk Maxwell and form the basis of the analysis of electro magnetic systems. If the displacement current is negligibl compared with the conduction current, his formulation o Ampère's law is

$$\nabla \times H = 4\pi j$$

In current-free regions this reduces to $\nabla \times H = 0$, which, a is shown in any standard textbook on vector analysis, allow the introduction of an arbitrary potential function such that H is the gradient of this scalar potential, i.e.

$$\nabla \times H = \nabla \times (\nabla\phi) = 0 \quad . \quad . \quad . \quad . \quad (1$$

and since $\nabla \cdot H = 0$ in linear regions, it follows that

$$\nabla^2\phi = 0$$

Eqn. (1) is the well-known Laplace equation. Carter, in classic series of papers[3, 4] showed how certain electromagneti problems could be tackled by an approximation such that th 2-dimensional form of eqn. (1) described their behaviour although his technique applies only to current-free regions However, the concept of a vector potential can be used eve when curl H is not zero. If $H = (\nabla \times A)/\mu$,

$$\nabla \times H = \frac{1}{\mu}\nabla \times \nabla \times A$$

$$= \frac{1}{\mu}[\nabla(\nabla \cdot A) - \nabla^2 A]$$

Correspondence on Monographs is invited for consideration with a view to publication.

Mr. Mamak is now in the Electrical Engineering Department, University of Leeds. Mr. Mamak was formerly, and Dr. Laithwaite is, in the Electrical Engineering Laboratories, University of Manchester.

If the vector-potential function is also stipulated to have zero ivergence, it is seen that

$$\nabla^2 A = 4\pi j\mu \quad . \quad . \quad . \quad . \quad . \quad . \quad (2)$$

n regions containing current, while

$$\nabla^2 A = 0 \quad . \quad . \quad . \quad . \quad . \quad . \quad . \quad (3)$$

n current-free regions.

It is thus seen that the Laplace and Poisson equations still lescribe the electromagnetic system. To overcome the necessity of stipulating potential surfaces when calculating transformer eactances, Rogowski[5] obtained analytical solutions of eqns. (2) nd (3) and matched the solutions at the boundaries between he two regions. Roth[6] extended Rogowski's technique by sing double Fourier series.

Since the known analytical methods of solving eqn. (1) rapidly ecome extremely complicated, and the known solutions of qns. (2) and (3) allow only certain simple boundary conditions, lectrical engineers have used flux-plotting techniques[7, 8] exten- ively, although mention should be made of the application of onformal mapping to simplify the boundary conditions, ollowed by the analytical solutions of the differential equa- ions.[9, 10] This technique is obviously useful only if the dif- erential equations are not rendered more complex as a result of the mapping. Flux plotting requires a certain aptitude which ot everybody possesses, and consequently flux plotting by nalogy[11, 12] is often used.

In the papers on the applications of numerical techniques[1, 2] the problem has been stated in terms of the Laplace equation. This necessitates the approximation of a magnetostatic potential, and in order to obtain the flux lines a free-hand drawing of orthogonal curves is required.

As has been shown, eqns. (2) and (3) may be formulated in terms of a vector potential such that $\nabla^2 A = 0$ in current-free regions and $4\pi j\mu$ in current-carrying regions. From this point onwards, the problem will be considered in two dimensions only.

In the 2-dimensional case, eqns. (2) and (3) reduce to

$$\frac{\partial^2 A_z}{\partial x^2} + \frac{\partial^2 A_z}{\partial y^2} = 4\pi j_z$$

Since all the current-carrying conductors are considered to have $\mu = 1$, and

$$\frac{\partial^2 A_z}{\partial x^2} + \frac{\partial^2 A_z}{\partial y^2} = 0$$

To obtain a numerical solution, the above two continuous equations must be replaced by a mesh such that the relevant equation is correctly obeyed at the nodal points of the mesh.

The 'finite difference' approximation to $\frac{\partial^2 A}{\partial x^2} + \frac{\partial^2 A}{\partial y^2}$ is:[1, 2]

$$-\frac{1}{a^2}[4A_0 - (A_1 + A_2 + A_3 + A_4)]$$

Thus to formulate the electromagnetic problem in terms of finite-difference equations, the following equations must be solved:

$$\frac{1}{a^2}[4A_0 - (A_1 + A_2 + A_3 + A_4)] = 0$$

in the current-free region.

$$\frac{1}{a^2}[4A_0 - (A_1 + A_2 + A_3 + A_4)] = -4\pi j$$

in the current-carrying regions.

At the boundary between the two regions the conditions to be obeyed are

(*a*) Continuity of the tangential components of H.
(*b*) Continuity of the normal components of B.

The finite-difference equation which satisfies these conditions is developed in Section 9.1, yielding

$$\frac{1}{a^2}[4A_0 - (A_1 + A_2 + A_3 + A_4)] = -2\pi j$$

Similarly it can also be shown that at the corner points between the two regions the finite-difference equation to be obeyed is

$$\frac{1}{a^2}[4A_0 - (A_1 + A_2 + A_3 + A_4)] = -\pi j$$

At boundaries between two regions of different permeability, μ_1 and μ_2, it has already been shown[13] that the finite-difference equation to be used, referring to Fig. 1, is

$$\frac{1}{a^2}\left[4A_0 - \left(\frac{2\mu_2}{\mu_1 + \mu_2}A_3 + A_1 + \frac{2\mu_1}{\mu_1 + \mu_2}A_4 + A_2\right)\right] = 0 \quad (4)$$

For engineering purposes the permeability of iron (μ_1) is usually assumed to be infinite, i.e. the finite-difference equation

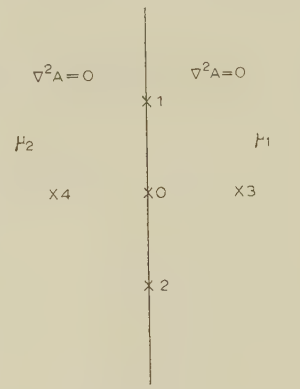

Fig. 1.—Definition of mesh points for determining the finite difference equation at a boundary between regions of different permeability.

to be solved at an iron boundary is given by putting $\mu_1 = \infty$ and $\mu_2 = 1$ in eqn. (4) to give

$$\frac{1}{a^2}[4A_0 - (2A_4 + A_1 + A_2)] = 0$$

The 'finite difference' equations for the complete electromagnetic region have now been formulated, there being as many equations as the number of nodal points selected, and these can be collected in the form of matrices such that $R\Phi = S$. It is required to write $\Phi = R^{-1}S$, and this requires the inversion of the matrix R. Since the matrix is a very special one in that it contains a large number of zeros, it is wasteful to invert it to obtain the required values at the nodal points.

If the equations are to be solved manually the quickest way is to use Southwell's relaxation technique.[1, 2] However, if a computing machine is available, programming difficulties make iterative techniques preferable, and the basic finite-difference equation used to accelerate convergence was

$${}_2A_0 = A_0 - \alpha[A_0 - \tfrac{1}{4}(A_1 + A_2 + A_3 + A_4)]$$

where ${}_2A_0$ is the new value of A_0 and A_0–A_4 are the existing

values.* To determine ${}_2A_0$ consequently involves a knowledge of α.

The determination of α entails the knowledge of the principal eigenvalue. This can conveniently be calculated for regular shapes by simple formulae, but, unfortunately, the boundaries in electrical-machine problems are seldom simple. This introduces difficulties, and experience suggests that the best way of determining α is to obtain an approximate value using Frankel's formula

$$\alpha = 2 - \sqrt{2\pi}\left(\frac{1}{p^2} + \frac{1}{q^2}\right)^{1/2}$$

where p and q are the number of rows and columns of a rectangular mesh which circumscribes the shape of the area under consideration. This is discussed fully in Reference 14. If one is starting from initial values, the value obtained from Frankel's formula may be further refined by studying the growth of the values of some arbitrary points.

Convergence to the required accuracy having been obtained, the value of A at all the nodal points is known. As shown in Section 9.2, the flux plot is obtained by drawing lines joining points for which A is constant.

The accuracy of the numerical solution is governed by the same considerations as that of the earlier techniques and will not therefore be discussed here.

(3) CALCULATION OF INDUCTANCE

The inductance of a system is defined by

$$\text{Magnetic energy} = \tfrac{1}{2}LI^2 10^9 = \frac{1}{8\pi}\iiint \boldsymbol{BH}dV \text{ c.g.s. units}$$

But, $$\boldsymbol{BH} = \frac{\boldsymbol{B} \,.\, \nabla \times \boldsymbol{A}}{\mu}$$

$$= \frac{1}{\mu}[\boldsymbol{A} \,.\, \nabla \times \boldsymbol{B} + \text{Div}\,(\boldsymbol{A} \times \boldsymbol{B})]$$

$$= \boldsymbol{A} \,.\, 4\pi\boldsymbol{j} + \frac{1}{\mu}\,\text{Div}\,(\boldsymbol{A} \times \boldsymbol{B})$$

Hence[16]

$$\iiint \boldsymbol{BH}dV = \iiint 4\pi\boldsymbol{j} \,.\, \boldsymbol{A}dV + \iiint \frac{\text{Div}\,(\boldsymbol{A} \times \boldsymbol{B})}{\mu}dV$$

$$= \iiint 4\pi\boldsymbol{j} \,.\, \boldsymbol{A}dV\dagger$$

Consequently, for a 2-dimensional system in air,

$$\text{inductance/unit length} = \frac{1}{I^2}\iint_S \boldsymbol{j} \,.\, \boldsymbol{A}dS \text{ c.g.s. units} \qquad (5)$$

It is thus seen that it is necessary to evaluate the surface integral of the scalar product of the vector potential and current density in order to calculate the inductance. In the particular case where the current density is assumed to be uniform it is seen that, to evaluate the inductance of the system, it is necessary to evaluate only the integral of the vector potential over the current-carrying surfaces.

In the previous Section it was shown how the values of A at the nodal points of a mesh may be determined. To obtain the inductance it is necessary to substitute the values of A over the current-carrying regions into an appropriate numerical integration formula.

The evaluation of integrals by numerical means is a standard technique. The accuracy of the integration depends on the number of sections into which the region has been divided and the number of derivatives taken into account. For the accuracy of the finite-difference equations the Simpson double-surface integral formulae was sufficiently accurate. Simpson's formula, which may be found in any standard textbook on numerical analysis, states that (referring to Fig. 2)

$$\iint A ds = \frac{a^2}{9}[16A_0 + 4(A_1 + A_2 + A_3 + A_4) + (A_5 + A_6 + A_7 + A_8)]$$

The following examples of the use of the foregoing technique are chosen to compare it with other known methods and to illustrate its application to electromagnetic systems, analysis of which has been found impossible by analytical means alone.

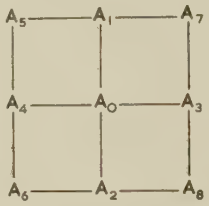

Fig. 2.—Definition of mesh points for the calculation of the surface integral.

(3.1) Calculation of the Leakage Reactance of Transformers

The calculation of the leakage reactance of transformers is usually performed by first approximating the problem to a 2-dimensional one. Rogowski first solved the 2-dimensional problem by obtaining analytical solutions for the 2-dimensional forms of eqns. (2) and (3) and matching the two solutions at the boundary. Roth extended Rogowski's analysis by using a double-Fourier-series solution. Unfortunately Roth's series converged very slowly, and several attempts have been made to reduce the labour involved; Billig[18] gives useful formulae which may be used within certain limits. The method outlined will also be applied to a case which does not fall within these limits.

Since no flux line is known, the value of A at any point is unknown; in consequence, a value at one point is stipulated and those at all the other points are iterated relative to this selected point. Experience suggests that, to obtain most rapid convergence after iterating all the points, the residue accumulated at the selected point should be wiped out and the cycle repeated until the required accuracy is obtained. It will be noted that the values of A finally obtained contain an arbitrary reference. This obviously makes no difference to the flux plot, in which only differences of A are required. Section 9.3 shows that this arbitrary reference also makes no difference to the calculated inductance.

The final flux plot obtained is shown in Fig. 3, and the calculated leakage inductances per centimetre perpendicular to the plane of the Figure are

Kapp approximate formula	658×10^{-8} henry
Rogowski approximate formula ..	595×10^{-8} henry
Numerical technique suggested ..	585×10^{-8} henry

The leakage reactance of a general tap-changing transformer was also calculated, for which the flux plot is shown in Fig. 4.

Eqn. (5) shows that the leakage inductance per unit length is obtained from $(1/I^2)\iint j \,.\, Ads$. When the relationship between currents is known, this may be further simplified: for example

* If $\alpha = 1$, it will be noted that this equation reduces to the relaxation finite-difference equation.

† A physical interpretation of this mathematical manipulation is given in Reference 17.

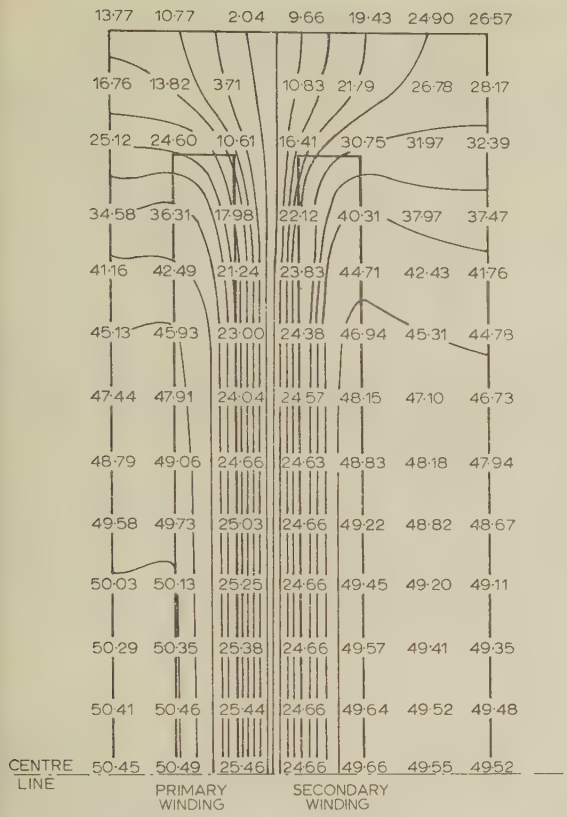

Fig. 3.—Flux plot for a standard transformer window.

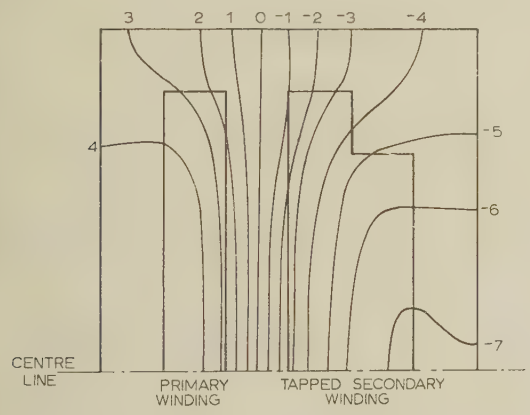

Fig. 4.—Flux plot for tap-changing transformer.

n a 2-coil transformer the relationship, ignoring magnetizing current, is $I_1N_1 = -I_2N_2$, whence

$$j_1 = \frac{N_1I_1}{S_1},\quad j_2 = \frac{N_2I_2}{S_2} \text{ and}$$

$$\frac{L}{\text{Unit length}} = \frac{1}{I_1^2}\left(\frac{N_1I_1}{S_1}\iint_{S_1} A_1 ds_1 + \frac{N_2I_2}{S_2}\iint_{S_2} A_2 ds_2\right) \times 10^{-9}$$

$$= \left(\frac{N_1}{I_1}\bar{A}_1 + \frac{N_2I_2}{I_1^2}\bar{A}_2\right) \times 10^{-9}$$

$$= \frac{N_1}{I_1}(\bar{A}_1 - \bar{A}_2) \times 10^{-9}$$

In this case the flux plot was drawn for $N_1I_1 = 36$, so that the inductance per unit length is given by $(N_1^2/36)(3{\cdot}74 + 4{\cdot}91) \times 10^{-9}$ henry/cm.

(3.2) Calculation of the Leakage Inductance of the Field Winding of a Salient-Pole Machine

In an analysis of the starting performance of synchronous machines the effect of any inaccuracy in the calculation of leakage reactance is considerably magnified in calculating the torque. The known approximations to the problem were found to be insufficiently accurate.[19] Talaat,[20] after considering the transient and subtransient reactances of synchronous machines, arrived at the same conclusion.

The two well-known analytical expressions for the calculations of the leakage reactance were developed by Carter, whose analysis was then extended by Terry and Keller.[21] Both of these are based on the assumption that, away from the corner, 'the flux goes straight across from pole to pole'.[21] This allows the stipulation of magnetostatic potentials. In fact, as the flux plot in Fig. 5 shows, this is never correct. The inductance of the

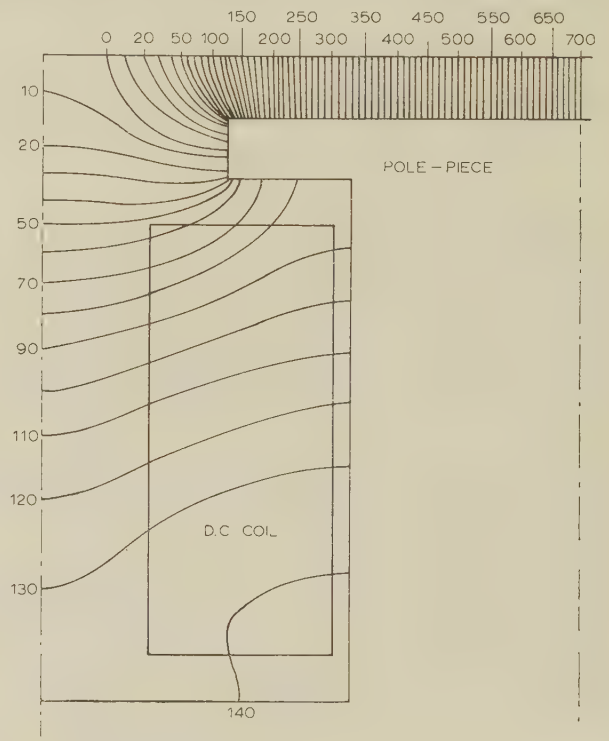

Fig. 5.—Flux plot for salient-pole alternator.

coil may be immediately calculated from the flux plot and is found to be $(N_3^2/84)(1\,634) \times 10^{-9}$ henry/cm length. The mutual inductance between the coil and the armature is $(N_3N_4/84) \times (1\,416) \times 10^{-9}$ henry/cm, where N_3 is the number of turns on the exciting winding and N_4 is the equivalent full-pitch turns per phase of the armature.

(4) CALCULATION OF THE A.C. RESISTANCE OF CONDUCTORS IN SLOTS

The problem of calculating the a.c. resistance was first formulated by Field and solved for the one-dimensional case. The limitations of Field's analysis have already been discussed.[23]

Analogue methods have been used to overcome the analytical difficulties in a recent paper by Roberts,[22] the analogue consisting of an *RC* network. As stated earlier,[23] this is not essential,

and it will now be shown how the a.c. resistance may be calculated (using the developed finite-difference equations).

Maxwell's equations, neglecting displacement current, are:

$$\nabla \times E = \frac{-\partial B}{\partial t}$$

$$\nabla \times H = 4\pi j$$

$$j = \sigma E$$

i.e. $$\frac{1}{\mu}\left(\nabla \times \frac{\partial B}{\partial t}\right) = 4\pi \frac{\partial j}{\partial t} = 4\pi\sigma \frac{\partial E}{\partial t}$$

i.e. $$\nabla \times \nabla \times E = \frac{-\mu 4\pi\sigma \partial E}{\partial t}$$

i.e. $$\nabla^2 E = \frac{-\mu 4\pi\sigma \partial E}{\partial t}$$

If all time variations are assumed to be of the form $\varepsilon^{j\omega t}$, the equation which describes the system is

$$\nabla^2 E = -j\omega\mu 4\pi\sigma E$$

If the problem is approximated to a 2-dimensional one,

$$\nabla^2 E_z = -j\omega\mu 4\pi\sigma E_z$$

In air, $\sigma = 0$, i.e. $\nabla^2 E_z = 0$.

The finite-difference equation for $\nabla^2 E_z$ is known. At the boundary between the conducting region and the non-conducting regions, both the tangential components of H and the normal components of flux density must be continuous. Since all time variations are of the form $\varepsilon^{j\omega t}$ and $\nabla \times E = -\partial B/\partial t$, these conditions are analogous to those required for the vector potential. Consequently, the finite-difference equations at the boundary between the conducting and non-conducting regions are known.

Taking the analogy a stage further, it follows that a line along which the value of E is constant is the same as a line of force, and at an iron boundary the line of force enters normally, i.e. $\partial E/\partial n = 0$, giving $E_1 - E_2 = 0$.

Thus, for a 2-dimensional system the continuous region may be replaced by a mesh where the relevant equations at each nodal point are known.

The matrix thus obtained differs from that obtained for the calculation of inductance inasmuch as it is complex, the basic finite-difference pattern now being

$$(4 + j\omega\mu 4\pi\sigma)E - (E_1 + E_2 + E_3 + E_4) = 0 \quad . \quad (6)$$

It should also be noted that the mutual interaction between the various points is reciprocal, and consequently an equivalent circuit may be set up.

When the equations for all the nodal points have been derived from the general equation (6), they may be collected in the form of matrices P, θ and Q such that

$$P\theta = Q \quad . \quad . \quad . \quad . \quad . \quad . \quad . \quad (7)$$

where P, θ and Q are all complex.

A well-known method of inverting complex matrices consists of first converting them into real matrices of double the order. This is accomplished by the following method:

Since P is a complex matrix, it may be divided into two real matrices, C and D, such that $P = C + jD$. θ and Q can be similarly treated, so that

$$\theta = \gamma - j\lambda$$

and $Q = G + jK$, say.

Substitution into eqn. (7) gives

$$(C + jD)(\gamma + j\lambda) = G + jK$$

This equation may be separated into its real and imaginary parts, so that

$$C\gamma - D\lambda = G$$

and

$$D\gamma + C\lambda = K$$

which may be written

$$\begin{bmatrix} C & -D \\ D & C \end{bmatrix}\begin{bmatrix} \gamma \\ \lambda \end{bmatrix} = \begin{bmatrix} G \\ K \end{bmatrix}$$

which results in the first matrix being of twice the order of but completely real. The inversion of this matrix is now possible and consequently γ and λ may be determined. From these values, θ may be derived.

In general, for calculation purposes, the boundary condition will be the knowledge of a line of H, i.e. a line along which E is constant, so that the value of E at the boundary will be stipulated and may be taken as real, i.e. $K = 0$.

The value of E at the nodal points having been determined, the ratio of a.c. to d.c. resistance may be determined by the fact that

$$\text{Actual loss per unit length} = \iint \left[\frac{E dS}{\rho}\right]^2 \frac{\rho}{dS}$$

$$= \iint \frac{E^2}{\rho} dxdy$$

$$\text{Total current} = \iint \frac{E}{\rho} dxdy$$

$$\text{D.C. loss} = \left[\iint \frac{E}{\rho} dxdy\right]^2 \frac{\rho}{S}$$

whence $$\frac{R_{ac}}{R_{dc}} = \frac{\iint E^2 dxdy}{\frac{1}{S}\left[\iint E dxdy\right]^2}$$

To determine the a.c. resistance it is required to evaluate the surface integral of E. To do this, the values of E at the relevant nodal points of the mesh are substituted in the integral formula given in Section 3.

The following example compares the values obtained using this method and the one due to Roberts, who chose a one-dimensional problem as example.

The basic finite-difference equation for the one-dimensional case is $2E_0 + j\omega\mu 4\pi\sigma E_0 - (E_1 + E_3) = 0$. Inverting the matrix for the problem chosen by Roberts and using the same mesh length gives $R_{ac}/R_{dc} = 1{\cdot}82$; Roberts's analogy gives a value of $1{\cdot}78$, while Field's analytical solution gives $1{\cdot}90$.

(5) EVALUATION OF THE SCREENING EFFECT OF COPPER IN A LINEAR ALTERNATOR

A new type of synchronous machine, described in a separate paper,[24] operates on linear rather than rotational motion and has the basic layout shown in Fig. 6. A reciprocating conducting loop slides along the centre limb, and the energizing coils on the pole-pieces set up flux around magnetic circuits, as shown. The oscillating loop moves through this flux, experiencing an alternating induced e.m.f., the alternating flux path being as shown. The machine is essentially a synchronous device and the transformer in series, with the oscillating loop as common member. So far as the transformer action is concerned, the

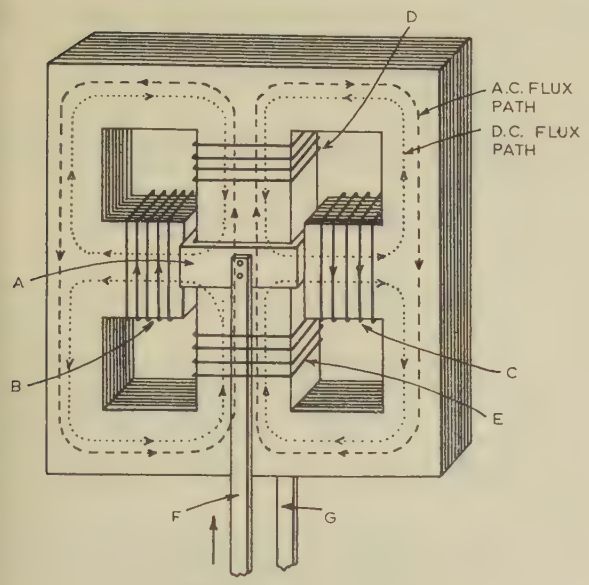

Fig. 6.—Basic layout of linear alternator.

A. Oscillating conducting windings.
B, C. D.C. exciting windings.
D, E. A.C. coils.
F, G. Mechanical driving strips.

resence of the d.c. poles produces excessive leakage flux and ıe regulation of the linear alternator is rather high. It was ecided to introduce a conducting sheet between the oscillating ıember and the pole-faces in order to reduce the leakage flux. 'he problem is to design the screening for minimum leakage ıductance. It is virtually impossible to solve the problem nalytically. To enable predictions of the performance to be ıade, the numerical technique was applied with the following ssumptions:

(*a*) The problem is treated as a 2-dimensional one.
(*b*) There is perfect coupling between the oscillating loop and the conducting sheet and between the loop and the main windings.
(*c*) The current is distributed uniformly over the coil cross-section.

One of the flux patterns obtained using the vector-potential quation is shown in Fig. 7, and other plots are given in

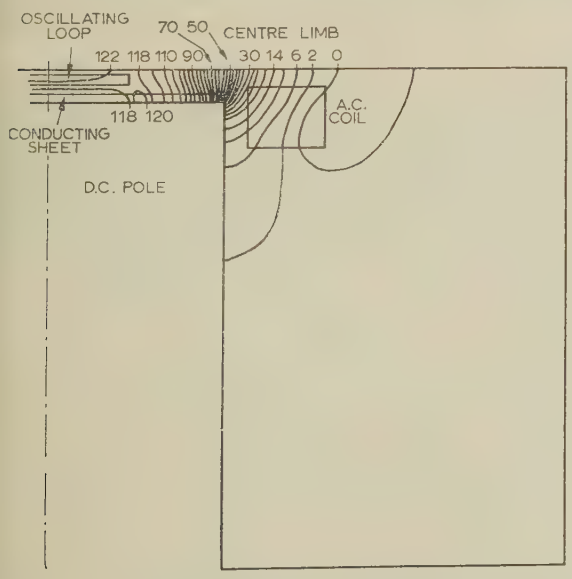

Fig. 7.—Flux plot for linear alternator with copper shield.

Reference 24. The inductance was found to be 14·5 ohms without the copper sheet and 7·34 ohms with it. Experimental results showed a reduction of 5·78 ohms.

(6) CONCLUSIONS

The technique developed in the paper is believed to be an extension and improvement of the earlier methods of application of numerical techniques to electromagnetic problems. It has also made possible the analysis of certain electromagnetic systems which would otherwise have been impossible. For simple boundary problems, such as the transformer-reactance calculation examples, a Mercury computer using Autocode instructions took 3–5 min of computing time. Problems with more complicated boundaries, such as those concerned with the linear alternator, took 10–15 min. With the continual advance in both computer speeds and the development of mathematical techniques, these times will undoubtedly be considerably reduced. In any case, the times quoted above refer to solutions *ab initio*, where no judicious guess was made which might have reduced the computing time.

(7) ACKNOWLEDGMENTS

The authors are grateful to Messrs. Brooker and Evans of the computing Machine Laboratory at Manchester University for advice on numerical aspects of the problem.

(8) REFERENCES

(1) Motz and Worthy: 'Calculation of Magnetic Field by Southwell's Relaxation Method', *Journal I.E.E.*, 1945, **92**, Part II, p. 522.
(2) Grad, E. M.: 'Solution of Electrical Engineering Problems by Southwell's Relaxation Method', *Transactions of the American I.E.E.*, 1952, **71**, Part I, p. 205.
(3) Carter, F. W.: 'Air-Gap Induction', *Electrical World and Engineer*, 1901, **28**, p. 884.
(4) Carter, F. W.: 'The Magnetic Field of the Dynamo-Electric Machine', *Journal I.E.E.*, 1926, **64**, p. 1117.
(5) Rogowski, W.: 'Über das Strendfeld mad den Streuinduktionskoeffizienten eines Transformators mit Schiebenwicklung und geteilten Endspulen', *V.D.I. Zeitschrift*, 1909, **71**, p. 1.
(6) Roth, E.: 'Introduction a l'étude analytique de l'échauffement des machines électriques', *Bulletin de la Société Française des Electriciens*, 1927, **7**, p. 840.
(7) Wieseman, R. W.: 'Graphical Determination of Magnetic Fields—Practical Applications', *Transactions of the American I.E.E.*, 1927, **46**, p. 141.
(8) Moore, A. D.: 'Fundamentals of Electrical Design' (McGraw-Hill, 1927).
(9) Higgins, T. J.: 'The Inductance of Tubular Conductors of Eccentric Annular Cross-Section', *Journal of Mathematics and Physics*, 1942, **21**, p. 159.
(10) Poritzky, H.: 'Some Industrial Application of Conformal Mapping', *National Bureau of Standards Applied Mathematical Series*, 1952, **18**, p. 15.
(11) Hartill, E. R.: 'The Electrolytic Tank and its application to Engineering Design', *Metropolitan–Vickers Gazette*, 1952, **24**, p. 147.
(12) Liebmann, G.: 'Electrical Analogues', *British Journal of Applied Physics*, 1953, **4**, p. 193.
(13) Allen, D. N. De G.: 'Relaxation Methods' (McGraw-Hill, 1954).
(14) Young, D. M.: 'Ordvac Solutions of the Dirichlet Problem', *Journal of the Association for Computing Machinery*, 1955, **2**, p. 137.

(15) EVANS, D. J.: 'Solution of Elliptic Difference Equations by Stationary Iterative Processes', International Conference on Information Processing, Paris, 1959 (to be published).
(16) ABRAHAM, M., and BECKER, R.: 'Classical Electricity and Magnetism' (Blackie, 1932).
(17) ROGERS, W. E.: 'An Introduction to Electrical Fields: A Vector Analysis Approach' (McGraw-Hill, 1954).
(18) BILLIG, E.: 'The Calculation of the Magnetic Field of Rectangular Conductors in a closed slot and its application to the Reactance of Transformer Windings', E.R.A. Report Ref. Q/T106.
(19) MAMAK, R. S.: 'An Analysis of Synchronous Motors', Brush Electrical Research Report, No. E2, 1956.
(20) TALAAT, M. E.: 'A New Approach to the Calculation of Synchronous-Machine Reactances', Part I, *Transactions of the American I.E.E.*, 1955, **74**, Part III, p. 176.
(21) TERRY, I. A., and KELLER, E. G.: 'Field Pole Leakage Flux in Salient-Pole Dynamo-Electric Machines', *Journal I.E.E.*, 1938, **83**, p. 845.
(22) ROBERTS, J.: 'Analogue Treatment of Eddy-Current Problems involving 2-Dimensional Fields', *Proceedings I.E.E.*, Monograph No. 341 M, July, 1959 (**107** C, p. 11).
(23) MAMAK, R. S.: Discussion on Reference 22, *ibid.*, 1960, **107** C, p. 18.
(24) LAITHWAITE, E. R., and MAMAK, R. S.: 'An Oscillating Synchronous Linear Machine', *ibid.*, Paper No. 3351 U, November, 1960 (**108** A).

(9) APPENDICES

(9.1) Finite-Difference Equation at a Boundary

Referring to Fig. 8, it is assumed that ϕ_3 and ψ_4 exist, so that

$$4\phi_0 - (\phi_1 + \phi_2 + \phi_3 + \phi_4) = 0 \quad . \quad . \quad . \quad (8)$$

$$4\psi_0 - (\psi_1 + \psi_2 + \psi_3 + \psi_4) = -4\pi ja^2 \quad . \quad (9)$$

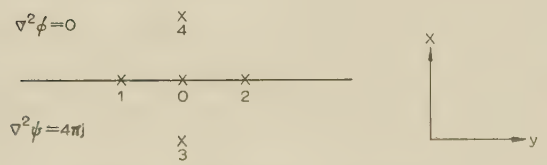

Fig. 8.—Mesh points on a boundary.

The boundary conditions are

$$\left.\begin{aligned} B_x &= B_x' \\ H_y &= H_y' \end{aligned}\right\} \quad . \quad . \quad . \quad . \quad . \quad . \quad . \quad (10)$$

From eqn. (10), using the condition that $H_y = \partial A/\partial x$, we have

$$\psi_4 - \psi_3 = \phi_4 - \phi_3$$

i.e.

$$\psi_4 + \phi_3 = \psi_3 + \phi_4$$

Moreover, $B_x = B_x'$ means that $\phi_0 = \psi_0$, $\psi_1 = \phi_1$, etc.

Combining eqns. (8) and (9) and using the boundary condition gives

$$\psi_0 - (\psi_1 + \psi_2 + \psi_3 + \phi_4) = -2\pi ja^2$$

(9.2) Lines for which the Value of A is Constant

$$\frac{1}{\mu}(\nabla \times \boldsymbol{A}) = \boldsymbol{H} \text{ and } \frac{\partial A}{\partial y} = \mu H_x, \frac{\partial A}{\partial x} = -\mu H_y$$

$$dA = \frac{\partial A}{\partial x}dx + \frac{\partial A}{\partial y}dy \quad . \quad . \quad . \quad . \quad . \quad . \quad (11$$

Along a line joining points for which A is constant eqn. (11 reduces to

$$0 = H_x dx - H_y dy$$

or $dx/dy = H_y/H_x$, i.e. the line of constant A traces a line of H

(9.3) Proof that the Addition of a Constant to the Value of A makes no Difference to the Calculated Inductance

If the value of A differs from the value used by K an amoun so that $A = K + A'$,

$$j_1 \iint_{S_1} A dxdy = j_1 KS_1 + j_1 \iint A' dxdy$$

$$j_2 \iint_{S_2} A dxdy = j_2 KS_2 + j_2 \iint A' dxdy$$

But $j_1 S_1$ is the total primary current and $j_2 S_2$ the total secondar current; therefore

$$j_1 S_1 = -j_2 S_2$$

Thus, when adding contributions from S_1 and S_2,

$$j_1 S_1 K + j_2 S_2 K = 0$$

From the above it will seem that, so long as there is no ne current in the region for which the inductance has been calculate the arbitrary constant makes no difference, provided that th integral of vector potential for all the current-carrying surface is calculated.

For a transformer it is necessary to ignore only the magnetizin current. For Fig. 5 the calculation should actually be performe for the region shown, together with the anti-symmetrical half t the right of the diagram. Under these circumstances it would b preferable to take the centre-line as zero, since correspondin lines on either side of the centre would have the same value bu be of different sign. Clearly it is therefore necessary to sho only one half of the plot. In Fig. 7, symmetry exists about th centre-line.

1—526

The Institution of Electrical Engineers
Monograph No. 419 M
Nov. 1960

FREQUENCY SPECTRUM DISTORTION OF RANDOM SIGNALS IN NON-LINEAR FEEDBACK SYSTEMS

By Professor J. C. WEST, Ph.D., D.Sc., Associate Member, J. L. DOUCE, Ph.D., M.Sc., and B. G. LEARY, B.E.

(*The paper was first received* 21*st April, and in revised form* 2*nd September*, 1960. *It was published as an* INSTITUTION MONOGRAPH *in November*, 1960.)

SUMMARY

The paper considers the distortion introduced by torque saturation a servo mechanism when responding to a randomly varying input gnal, with emphasis on the spectral distribution of this distortion. It shown that low-frequency errors are produced by the application an input signal whose spectrum extends beyond the pass band of e system.

An approximate expression is derived which enables the magnitude the low-frequency errors to be evaluated in a simple manner. xperimental results are presented for a particular system.

(1) INTRODUCTION

Existing methods of analysing the behaviour of a feedback ntrol system subjected to a random input when some non-ear element is present use a linearizing technique.[1–5] They volve the replacement of the non-linearity by a linear element ith an equivalent gain determined by the magnitude of the gnal and the non-linear characteristic. One of the conse-uences of this linearization process is the neglect of the dis-rtion component which is ignored in this form of analysis. ny attempt to take into account the effects of distortion in a ntrol system requires a solution to the problem of determining e frequency spectrum produced in a non-linear element when e spectrum of the input signal to this element is given. This roblem, which is also of considerable interest in the fields of mmunication[6] and information theory, has as yet no general lution, although results have been obtained for particular ses,[2, 3, 7] e.g. simple characteristics such as square law, half-ave rectification and saturation subjected to particular types f input signal.

The distortion produced by a non-linearity

$$x_o = f(x_i) \quad . \quad . \quad . \quad . \quad . \quad . \quad (1)$$

hen the input signal x_i is sinusoidal, consists of a series of armonics. Generally these harmonics are of little consequence control systems because of the high-frequency filtering of the stem itself. If the input signal consisted of the sum of two nusoidal signals of differing frequencies, then sum and dif-rence frequency terms would appear in the output x_o. The ifference frequency term might be of very low frequency to hich a control system would readily respond, producing a low-equency error. If one now considers the input x_i to be a ndomly varying signal with a frequency spectrum continuous ver a wide band, there is seen to be an infinite number of ossible 'difference'-type combinations which might occur, pro-ucing an output spectrum the low-frequency end of which xtends down to zero frequency. This has an important effect n control-system performance. It is normally recognized that e error of a control system should become vanishingly small as the frequency decreases towards zero. Low-frequency error is a much greater defect of system 'goodness' than errors at high frequencies. The result of distortion will be shown to be the production of low-frequency errors of uniform power per unit bandwidth extending down to zero frequency.

(2) DISTORTION POWER AND EQUIVALENT GAIN

The power σ_i^2 of a random signal $x_i(t)$ which is assumed to exist for a long period of time, during which its statistical properties remain stationary, can be determined from the amplitude probability density function $p(x_i)$:

$$\sigma_i^2 = \int_{-\infty}^{\infty} x_i^2 p(x_i) dx_i \quad . \quad . \quad . \quad . \quad . \quad (2)$$

The output power σ_o^2 of the signal from a non-linear element characterized as in eqn. (1) is also of the same form:

$$\sigma_o^2 = \int_{-\infty}^{\infty} f^2(x_i) p(x_i) dx_i \quad . \quad . \quad . \quad . \quad . \quad (3)$$

The output signal $x_o(t)$ can be considered to be composed of the sum of two components: a signal proportional to the input signal, say $Kx_i(t)$, and a distortion signal, $D(t)$; i.e.

$$x_o(t) = Kx_i(t) + D(t) \quad . \quad . \quad . \quad . \quad . \quad (4)$$

This definition is true for all values of K. In order that these two components can be regarded as true signal and distortion, it is necessary to ensure that an appropriate value of K is taken, for which the cross-correlation between input signal and distortion is zero.

Since the non-linearity is independent of time, eqn. (4) may also be written as

$$x_o(t+\tau) = Kx_i(t+\tau) + D(t+\tau) \quad . \quad . \quad . \quad (5)$$

for all values of K.

The auto-correlation of the output signal, $g_o(\tau)$, using eqns. (4) and (5) is

$$\begin{aligned} g_o(\tau) = \overline{x_o(t)x_o(t+\tau)} &= \overline{[Kx_i(t) + D(t)][Kx_i][(t+\tau) + D(t+\tau)]} \\ &= \overline{K^2 x_i(t)x_i(t+\tau)} + \overline{D(t)D(t+\tau)} \\ &\quad + \overline{Kx_i(t)D(t+\tau)} + \overline{Kx_i(t+\tau)D(t)} \end{aligned}$$

the bar denoting an average over an infinite period of time. The first term is K^2 times the auto-correlation of the input signal $g_i(\tau)$, the second term is the auto-correlation of the distortion, say $g_D(\tau)$. The last two terms have the same average value and each represents the cross-correlation between the signal component $Kx_i(t)$ of eqn. (4) and the distortion $D(t)$, say $g_{SD}(\tau)$. Thus the equation can be written

$$g_o(\tau) = K^2 g_i(\tau) + g_D(\tau) + 2g_{SD}(\tau)$$

and is still true for all values of K.

Correspondence on Monographs is invited for consideration with a view to ublication.

Prof. West is Professor of Electrical Engineering, and Dr. Douce and Mr. Leary e in the Department of Electrical Engineering, Queen's University, Belfast.

If the cross-correlation, $g_{SD}(\tau)$, is zero, then

$$g_o(\tau) = K^2 g_i(\tau) + g_D(\tau)$$

and, in particular, for $\tau = 0$,

$$\sigma_o^2 = K^2\sigma_i^2 + \sigma_D^2 \quad . \quad . \quad . \quad . \quad . \quad (6)$$

Now the power of the distortion signal σ_D^2 is

$$\sigma_D^2 = \int_{-\infty}^{\infty} [f(x_i) - Kx_i]^2 p(x_i) dx_i$$

since $D(t) = f(x_i) - Kx_i$ from eqns. (1) and (4). By expanding and substituting eqns. (2) and (3),

$$\sigma_D^2 = \sigma_o^2 + K^2\sigma_i^2 - 2K\int_{-\infty}^{\infty} x_i f(x_i) p(x_i) dx_i \quad . \quad . \quad (7)$$

Elimination of σ_o and σ_D between eqns. (6) and (7) results in the appropriate value of K to ensure the non-correlation of the distortion component:

$$K = \frac{1}{\sigma_i^2}\int_{-\infty}^{\infty} x_i f(x_i) p(x_i) dx_i \quad . \quad . \quad . \quad . \quad (8)$$

This factor, K, is identical with that of the equivalent gain technique[1, 2, 5] obtained by finding that value of K which makes σ_D^2 a minimum.

For a simple type of non-linearity representing saturation, defined by

$$x_o = x_i \text{ when } |x_i| < h$$
$$x_o = -h \text{ when } x_i < -h$$
$$x_o = +h \text{ when } x_i > h$$

and for a Gaussian probability density function

$$p(x_i) = \frac{1}{\sigma_i\sqrt{(2\pi)}} \exp(-x_i^2/2\sigma_i^2)$$

the gain factor K from eqn. (8) is

$$K = \frac{2}{\sqrt{\pi}}\int_0^{h/\sigma_i\sqrt{2}} \exp(-z^2) dz = \operatorname{erf}\frac{h}{\sigma_i\sqrt{2}} \quad . \quad . \quad (9)$$

z being an arbitrary variable of integration.

(3) FREQUENCY SPECTRUM ANALYSIS

A relationship is known[2, 3] between the auto-correlation functions of the input and output signals of the non-linear element based on the assumption of Gaussian amplitude probability density of the input. Since the auto-correlation function of a signal and its power spectrum are Fourier transform pairs, it is possible by transformation to obtain a spectral relationship, i.e. to obtain the output spectrum of the signal x_o in terms of the input signal spectrum.

The auto-correlation function $g(\tau)$ of a signal is related to the power spectrum of the signal $G(\omega)$ by the Fourier transforms

$$g(\tau) = \frac{1}{2\pi}\int_{-\infty}^{\infty} G(\omega)\varepsilon^{j\omega\tau} d\omega \quad . \quad . \quad . \quad . \quad (10)$$

and

$$G(\omega) = \int_{-\infty}^{\infty} g(\tau)\varepsilon^{-j\omega\tau} d\tau. \quad . \quad . \quad . \quad . \quad (11)$$

It is convenient to use the normalized auto-correlation function $g_n(\tau)$ defined by $g_n(\tau) = g(\tau)/g(0)$. This ensures unit amplitude at zero τ.

If $g_o(\tau)$ is the auto-correlation function of the output signal $x_o(t)$ from the non-linear element, and if $g_{ni}(\tau)$ is the normalized auto-correlation function of the input signal $x_i(t)$ to the non-linearity, then the desired relation is the power series

$$g_o(\tau) = a_1^2 g_{ni}(\tau) + a_2^2 g_{ni}^2(\tau) + \ldots + a_r^2 g_{ni}^r(\tau) + \ldots \quad (12)$$

The relationship is true only for Gaussian probability distribution of x_i.

The coefficients $a_1 \ldots a_r$ depend on the non-linear characteristic $f(x_i)$ and on the input signal power σ_i^2:

$$a_r = \frac{2}{\sigma_i\sqrt{2\pi}}\int_0^{\infty} f(x_i) \mathrm{H}_r\left(\frac{x_i}{\sigma_i}\right) \exp(-x_i^2/2\sigma_i^2) dx_i$$

where H_r is the rth Hermitian polynomial, the first three of which are:

$$\mathrm{H}_1\left(\frac{x_i}{\sigma_i}\right) = \frac{x_i}{\sigma_i}$$

$$\mathrm{H}_2\left(\frac{x_i}{\sigma_i}\right) = \frac{1}{\sqrt{2}}\left[\left(\frac{x_i}{\sigma_i}\right)^2 - 1\right]$$

$$\mathrm{H}_3\left(\frac{x_i}{\sigma_i}\right) = \frac{1}{\sqrt{6}}\left[\left(\frac{x_i}{\sigma_i}\right)^3 - 3\frac{x_i}{\sigma_i}\right]$$

When the non-linear characteristic is an odd function of x_i, as is the case for saturation, all even terms of the coefficient $a_1 \ldots a_r$ are zero. In addition, for the saturation case, it is found that the higher terms successively tend to zero. It has proved sufficient to take the approximate solution

$$g_o(\tau) = a_1^2 g_{ni}(\tau) + a_3^2 g_{ni}^3(\tau) \quad . \quad . \quad . \quad . \quad (13)$$

For the saturation characteristic previously defined, the first coefficients are

$$a_1 = \frac{2\sigma_i}{\sqrt{\pi}}\int_0^{h/\sigma_i\sqrt{2}} \exp(-z^2) dz$$

$$= \sigma_i \operatorname{erf}\frac{h}{\sigma_i\sqrt{2}} \quad . \quad . \quad . \quad . \quad . \quad . \quad . \quad . \quad . \quad (14)$$

$$a_3 = \frac{h}{\sqrt{(3\pi)}} \exp(-h^2/2\sigma_i^2) \quad . \quad . \quad . \quad . \quad . \quad . \quad (15)$$

$$a_5 = \frac{\sigma_i}{\sqrt{(60\pi)}}\left(3\frac{h}{\sigma_i} - \frac{h^3}{\sigma_i^3}\right) \exp(-h^2/2\sigma_i^2)$$

Fig. 1 shows these coefficients as functions of the amplitude ratio σ_i/h.

For large input powers, i.e. $\sigma_i^2 > 4h^2$, the expression for the output auto-correlation function becomes[2]

$$g_o(\tau) = \frac{2h^2}{\pi} \arcsin g_{ni}(\tau)$$

$$= \frac{2h^2}{\pi}\left[g_{ni}(\tau) + \frac{1}{6}g_{ni}^3(\tau) + \frac{3}{40}g_{ni}^5(\tau) + \ldots\right] \quad (16)$$

It is important to notice that a_1 is simply related to the equivalent gain K [see eqns. (9) and (14)] by $K\sigma_i = a_1$, and hence the first term of eqn. (13) represents the proportional signal $Kx_i(t)$ and the remaining terms the distortion signal $D(t)$.

(3.1) Low-Frequency Spectrum

Consider the non-linearity subjected to a random signal obtained by passing white noise through a single-stage low-pass RC filter so that

$$G_i(\omega) = \frac{G}{1 + (\omega/\omega_o)^2} \quad . \quad . \quad . \quad . \quad (17)$$

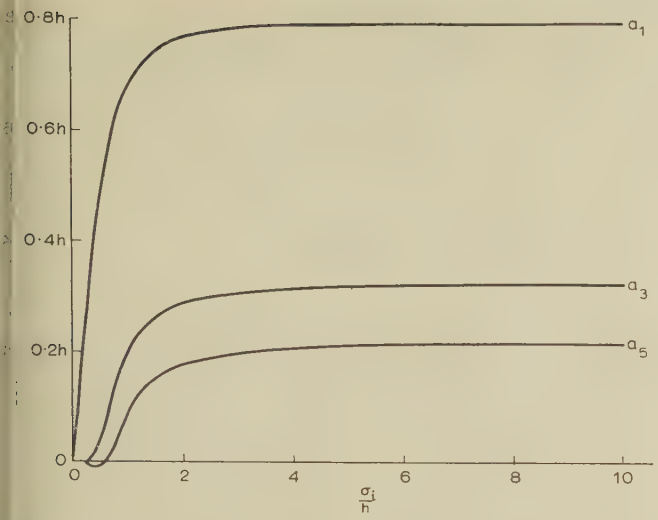

Fig. 1.—Series coefficient magnitudes, saturation-type non-linearity.

This power spectrum is uniform at low frequencies, falling at 6 dB/octave at high frequencies, with a 'break' frequency (−3 dB) at $\omega = \omega_o$. This is a convenient form for its engineering application,[8] and gives an auto-correlation function which is very suitable for substitution in the power series of eqn. (12). From eqn. (10)

$$g_i(\tau) = \frac{G\omega_o}{2} \exp(-\omega_o|\tau|) \quad . \quad . \quad . \quad . \quad (18)$$

and the normalized auto-correlation function is

$$g_{ni}(\tau) = \exp(-\omega_o|\tau|)$$

Substituting in eqn. (12), the output auto-correlation function is

$$g_o(\tau) = a_1^2 \exp(-\omega_o|\tau|) + a_3^2 \exp(-3\omega_o|\tau|) + \ldots \quad (19)$$

The output power spectrum is the Fourier transform of this expression, and performing this operation term by term,

$$G_o(\omega) = \frac{2a_1^2}{\omega_o} \frac{1}{1 + \left(\frac{\omega}{\omega_o}\right)^2} + \frac{2a_3^2}{3\omega_o} \frac{1}{1 + \left(\frac{\omega}{3\omega_o}\right)^2} + \ldots$$

Thus the output spectrum is the sum of spectra, each being of the same shape as the input spectrum, but having cut-off frequencies ω_o, $3\omega_o$, $5\omega_o$, etc. At low frequencies, $\omega \ll \omega_0$, the magnitude of the output spectrum becomes

$$\underset{\omega \to 0}{G_o(\omega)} = \frac{2a_1^2}{\omega_o} + \frac{2a_3^2}{3\omega_o} + \ldots + \text{(negligible terms)}$$

The first term represents the component of the output correlated with the input, and the remainder are due to distortion. It follows that the signal/noise ratio at low frequencies is $3a_1^2/a_3^2$.

For large signals applied to the saturating non-linearity ($\sigma_i \gg h$), eqn. (16) may be used to evaluate a_1^2/a_3^2, giving the low-frequency signal/noise ratio equal to 18/1.

Thus, this form of input spectral density produces a distortion signal with a wide power spectrum, which is uniform at low frequencies.

(3.2) Limited Bandwidth Input

The low-frequency distortion becomes of greater significance when the input signal contains little power at the lower frequencies. Consider an input power spectrum of the form

$$G_i(\omega) = G\left[\frac{1}{1 + \left(\frac{\omega}{n\omega_o}\right)^2} - \frac{1}{1 + \left(\frac{\omega}{\omega_o}\right)^2}\right] \quad . \quad (20)$$

where $n > 1$.

This power spectrum is the difference between two spectra of the form previously discussed, each of constant power per unit bandwidth at low frequencies, one falling at 6 dB/octave from a frequency ω_o, and the other falling at the same rate from a frequency $n\omega_o$. At low frequencies, such that $\omega \ll \omega_o$, the power spectrum becomes

$$\underset{\omega \to 0}{G_i(\omega)} = G\frac{n^2 - 1}{n^2}\left(\frac{\omega}{\omega_o}\right)^2$$

The construction of the input power spectrum is illustrated in Fig. 2.

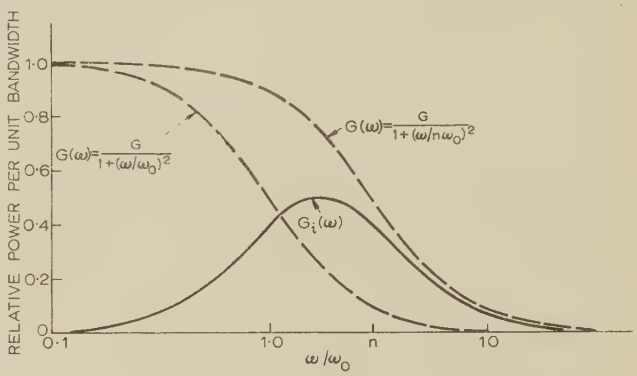

Fig. 2.—Construction for power spectrum, limited bandwidth input.

$$G_i(\omega) = G\left[\frac{1}{1 + \left(\frac{\omega}{n\omega_o}\right)^2} - \frac{1}{1 + \left(\frac{\omega}{\omega_o}\right)^2}\right]$$

A useful property of the spectrum considered is the simple form of the corresponding auto-correlation function, permitting the power series expansion, eqn. (13), to be used to determine the output spectrum.

To obtain the input auto-correlation function, the Fourier transform, eqn. (10), may be applied term by term to eqn. (20). Using the result of the previous Section, eqns. (17) and (18), the input auto-correlation is found to be

$$g_i(\tau) = \frac{Gn\omega_o}{2} \exp(-n\omega_o|\tau|) - \frac{G\omega_o}{2} \exp(-\omega_o|\tau|)$$

so that

$$g_{ni}(\tau) = \frac{1}{n-1}[n \exp(-n\omega_o|\tau|) - \exp(-\omega_o|\tau|)]$$

The auto-correlation function of the output signal is obtained as a power series of $g_{ni}(\tau)$, by eqn. (13), giving

$$g_o(\tau) = \frac{a_1^2}{n-1}[n \exp(-n\omega_o|\tau|) - \exp(-\omega_o|\tau|)]$$

$$+ \frac{a_3^2}{(n-1)^3}\{n^3 \exp(-3n\omega_o|\tau|) - 3n^2 \exp[-(2n+1)\omega_o|\tau|]$$

$$+ 3n \exp[-(n+2)\omega_o|\tau|] - \exp(-3\omega_o|\tau|)\} + \ldots \quad (21)$$

The coefficient a_1^2 determines the amplitude of the output which is correlated with the input and is of the same spectral shape.

The output spectrum is obtained by the inverse transformation of eqn. (21). Each term is of the form $A \exp(-B\omega_o|\tau|)$, and by eqns. (17) and (18) this transforms to

$$G(\omega) = \frac{2A}{B\omega_o} \frac{1}{1 + \left(\frac{\omega}{B\omega_o}\right)^2}$$

Hence the output spectrum is the sum of many spectra, each of uniform power per unit bandwidth at low frequency, and each falling at high frequencies at the rate of 6 dB/octave.

The output spectrum, neglecting the coefficients a_5^2 and above, is given by

$$G_o(\omega) = \frac{2a_1^2}{\omega_o(n-1)}\left[\frac{1}{1+\left(\frac{\omega}{n\omega_o}\right)^2} - \frac{1}{1+\left(\frac{\omega}{\omega_o}\right)^2}\right] + \frac{2a_3^2}{\omega_o(n-1)^3}\left\{\frac{\frac{1}{3}n^2}{1+\left(\frac{\omega}{3n\omega_o}\right)^2} - \frac{3n^2}{2n+1}\frac{1}{1+\left[\frac{\omega}{(2n+1)\omega_o}\right]^2} + \frac{3n}{n+2}\frac{1}{1+\left[\frac{\omega}{(n+2)\omega_o}\right]^2} - \frac{1}{3}\frac{1}{1+\left(\frac{\omega}{3\omega_o}\right)^2}\right\} \quad . \quad (22)$$

At low frequencies, $\omega \ll \omega_o$, such that both the input signal and the correlated component of the output are negligible, the distortion term represents a signal of constant power per unit bandwidth. In eqn. (22), if $\omega \to 0$, the power per unit bandwidth is given by

$$\underset{\omega\to 0}{G_o(\omega)} = \frac{2a_3^2}{\omega_o(n-1)^3}\left(\frac{n^2}{3} - \frac{3n^2}{2n+1} + \frac{3n}{n+2} - \frac{1}{3}\right) = \frac{4a_3^2}{3\omega_o}\left[\frac{(n+1)}{(n+2)(2n+1)}\right] \quad . \quad . \quad . \quad . \quad . \quad (23)$$

This feature has formed the theoretical basis for the construction of a low-frequency noise generator.[9]

The maximum power of the correlated component of the output occurs about the frequency $\omega = \sqrt{n}\omega_o$, and, from eqn. (21), this power is found to be

$$G(\omega)_{max} = \frac{2a_1^2}{\omega_o(n-1)}\left(\frac{1}{1+\frac{1}{n}} - \frac{1}{1+n}\right) = \frac{2a_1^2}{\omega_o(n+1)} \quad (24)$$

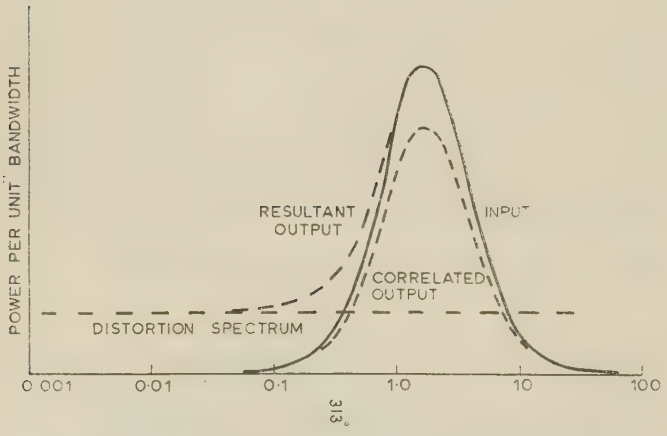

Fig. 3.—Input and output spectra, saturation type non-linearity.
$\sigma^2 > 4h$; amplitudes not to scale.

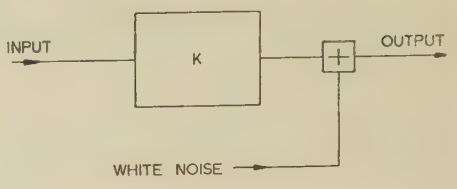

Fig. 4.—Low-frequency equivalent circuit, random input to non-linearity.

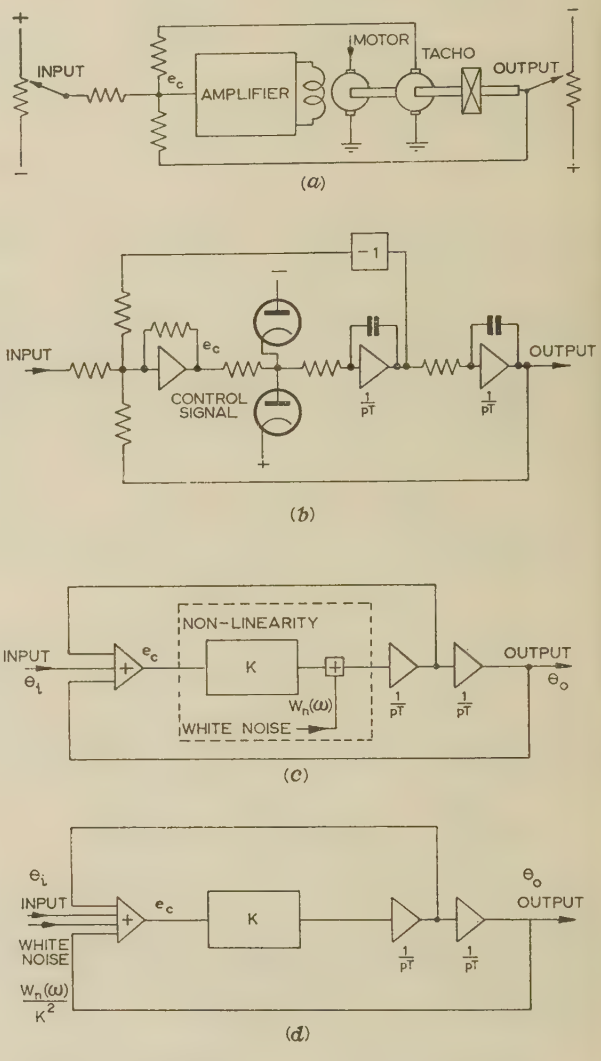

Fig. 5.—Analysis of a particular system.
(*a*) The mechanical system.
(*b*) Electronic analogue.
(*c*) Block diagram.
(*d*) Block diagram for analysis.

Hence the ratio

$$\frac{\text{Low-frequency output distortion power per unit bandwidth}}{\text{Maximum power per unit bandwidth of the correlated output signal}}$$

is equal to $2a_3^2(n+1)^2/[3a_1^2(n+1)(2n+1)]$.

This ratio varies by less than 10% for $1 \leqslant n \leqslant \infty$, and hence may be considered independent of the frequency range of the input signal.

When a large signal is applied to a limiter, $\sigma_i^2 > 4h^2$, eqn. (16) ows that a_3^2/a_1^2 tends to 1/6, and the above ratio becomes proximately equal to 1/18 for all values of n.

Relevant spectra are shown in Fig. 3 for the particular case a large signal applied to a saturating non-linearity ($\sigma_i^2 > 4h^2$), th $n = 3$, so that the input power spectrum is

$$G_i(\omega) = G\left[\frac{1}{1+\left(\frac{\omega}{3\omega_o}\right)^2} - \frac{1}{1+\left(\frac{\omega}{\omega_o}\right)^2}\right]$$

The distortion component of the output has been shown ıcorrelated with the input signal, and hence the total power any frequency range is the sum of the powers of correlated ıd distortion signals. The relative amplitude is proportional root power per unit bandwidth, and represents a convenient ·actical and theoretical unit.

Fig. 3 shows that the distortion component possesses a uniform ıectrum over a wide range of frequencies. When interest is ·imarily in the low-frequency response of a system, the non-ıearity subjected to the type of input considered may be presented by an equivalent gain, K, and a white-noise generator, ; in Fig. 4.

For the saturating non-linearity subjected to the type of input ıectrum considered, the distortion power per unit bandwidth ıay be assumed to be independent of both input bandwidth ı and ω_o) and input power, provided that appreciable limiting ccurs ($\sigma_i^2 > 4h^2$). The ratio

$$\frac{\text{Low-frequency distortion amplitude per unit bandwidth}}{\text{Maximum amplitude per unit bandwidth of the correlated output signal}}$$

ıay be taken as $1/\sqrt{18} = 1/4{\cdot}5$.

(4) CLOSED-LOOP RESPONSE OF A PARTICULAR SYSTEM

Consider the system shown in Fig. 5(*a*), where the non-linearity arises owing to torque limitation in the servo motor. The input is a random signal whose spectral distribution is of the form

$$G_{\theta i}(\omega) = \frac{G_i}{1+(\omega/\omega_i)^2}$$

The analogue of this system is shown in Fig. 5(*b*). To analyse the closed-loop response, the non-linear element is replaced by a linear equivalent gain, K, and a distortion generator. The operating value of K is determined using Booton's method,[1] distortion being neglected at this stage of the analysis, since the distortion power is small and K depends solely on the power of the signal applied to the non-linearity.

The system has now been reduced to a linear network, enabling the control-signal spectrum to be evaluated (Fig. 6). At high frequencies the power per unit bandwidth falls as the input power, since $e_c \simeq \theta_i$, $\underset{\omega\to\infty}{\to} 0$, and at low frequencies the error and control signals become vanishingly small as the loop gain increases. Hence, to estimate the distortion, the control signal may be approximated to that in eqn. (20), so that the distortion is of uniform power at low frequencies and this power, $W_n(\omega)$, is known in terms of the maximum power per unit bandwidth of the correlated signal at the output of the non-linearity [Fig. 5(*c*)].

The response to this distortion produces an output signal uncorrelated with the input θ_i, increasing the error of the system. The total error power about any frequency is the sum of the powers of the error due to imperfect following of the linear system and the power of the output due to distortion.

The distortion signal can be represented as a signal of power

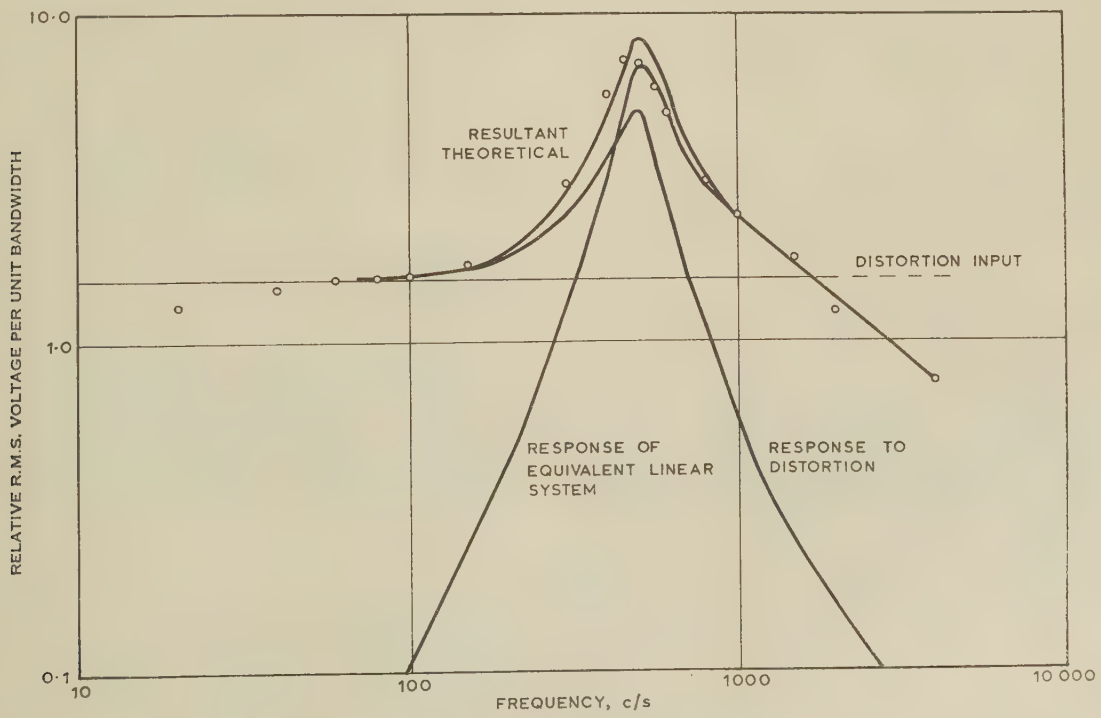

Fig. 6.—Control signal spectra.

—— Analytical results.
○ Experimental results.

$\frac{1}{K^2} W_n(\omega)$ applied before the element of gain K, where the ratio

$$\frac{\text{Low-frequency distortion power per unit bandwidth}}{\text{Peak power per unit bandwidth of control signal } e_c}$$

has the same value as for the signals at the output of the non-linearity.

Hence, as shown in Fig. 5(*d*), the distortion can be regarded as an additional input to the system and the power per unit bandwidth is known in terms of the peak power per unit bandwidth of the control signal. Fig. 6 shows this equivalent input signal and the response of the system to this distortion signal. The resultant control signal power is the sum of the individual powers, so that the r.m.s. signal in a given bandwidth is the square root of the sum of the individual powers. Thus, the effect of distortion is important at low frequencies and becomes insignificant where large errors are predicted from the linearization technique. Experimental values for the particular input considered are also presented in Fig. 6, showing good agreement with the theoretical results.

The distortion also has an appreciable effect on the closed-loop gain, $|\theta_o/\theta_i|$, at low frequencies. Saturation produces an additional error of magnitude 1/4·5 times the peak value of the control signal. In the example considered, the peak magnification $|e_c/\theta_i| \simeq 3$, and thus the ratio (distortion input magnitude)/(signal input magnitude) is equal to 1/1·5 at low frequencies. Thus $\left|\frac{\theta_o}{\theta_i}\right|_{\omega \to 0} = \frac{\sqrt{\left(1 + \frac{1}{1 \cdot 5^2}\right)}}{1} = 1 \cdot 2$. Fig. 7 shows the closed-loop gain $|\theta_o/\theta_i|$ for the system considered.

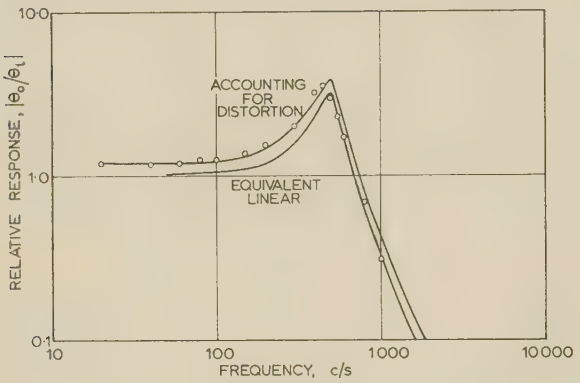

Fig. 7.—Closed loop response of system.
—— Analytical results.
○ Experimental results.

This effect will occur in any saturating feedback system, but the accuracy of measurement required is often difficult to achieve in practice in view of the low frequencies involved. For this reason it is considered more convenient to consider error or control signal spectra when assessing performance.

(5) CONCLUSIONS

It has been shown how the distortion produced in a non-linear system can seriously impair the response of the system to a random input signal. In particular, the distortion can contain very-low-frequency components, giving appreciable errors where excellent performance is expected.

The distortion may be considered as an additional disturbance to the system, and the magnitude of this signal, and its frequency distribution, may be evaluated. For an approximate evaluation a simple spectrum is considered, producing a distortion signal having constant power per unit bandwidth over a wide frequency range.

Since all mechanical servo systems will saturate for sufficiently large input signals, the use of the servo as a low-pass filter requires caution to prevent high-frequency signals generating spurious low-frequency terms. An ideal solution may be the use of a low-pass filter preceding the servo, with the cut-off frequency dependent on input magnitude. Further research is being pursued into the design of such optimum filters, taking into account inevitable physical limitations on the basic elements of the control system.

(6) REFERENCES

(1) Booton, R. C.: 'Non-Linear Control Systems with Statistical Inputs', Dynamic Analysis and Control Laboratory Report No. 61, Massachusetts Institute of Technology, March, 1952.

(2) Barrett, J. F., and Coales, J. F.: 'An Introduction to the Analysis of Non-Linear Control Systems with Random Inputs', *Proceedings I.E.E.*, Monograph No. 154 M, November, 1955 (**103** C, p. 190).

(3) Laning, J. H., and Battin, R. H.: 'Random Processes in Automatic Control' (McGraw-Hill, 1956).

(4) Nikiforuk, P. N., and West, J. C.: 'The Describing-Function Analysis of a Non-linear servo Mechanism Subjected to Stochastic Signals and Noise', *Proceedings I.E.E.*, Monograph No. 207 M, November, 1956 (**104** C, p. 193).

(5) West, J. C.: 'The Describing Function Technique', *Transactions of the Society of Instrument Technology*, 1959, **11**, p. 1.

(6) Rice, S. O.: 'Mathematical Analysis of Random Noise', *Bell System Technical Journal*, 1944, **23**, p. 282, and 1945, **24**, p. 46.

(7) Johnson, E. C.: 'Sinusoidal Analysis of Feedback Control Systems Containing Non-Linear Elements', *Transactions of the American I.E.E.*, 1952, **71**, p. 169.

(8) Newton, G. C., Gould, L. A., and Kaiser, J. L.: 'Analytical Design of Linear Feedback Controls' (Wiley, 1957).

(9) Douce, J. L., and Shackleton, J. M.: 'L.F. Random Signal Generator', *Electronic and Radio Engineer*, 1958, **35**, p. 295.

l—526

The Institution of Electrical Engineers
Monograph No. 420 M
Dec. 1960

TABILITY OF A FEEDBACK SYSTEM CONTAINING A LIMITED-FIELD-OF-VIEW ERROR DETECTOR

By D. P. ATHERTON, B.Eng., Student.

(*The paper was first received* 3*rd June, and in revised form* 9*th September*, 1960. *It was published as an* INSTITUTION MONOGRAPH *in December*, 1960.)

SUMMARY

A class of non-linear error-detector characteristics is considered here, for large magnitudes of error, the error signal decreases with increased error. Sinusoidal and random-input analysis of a closed-loop system containing such a non-linearity is shown to necessitate the calculation of a family of describing-function curves to cover operation with a d.c. input signal to the non-linear error detector. The peculiarities of such a non-linear system are discussed, and a simple method using a non-linear circuit to correct the adverse behaviour is described.

(1) INTRODUCTION

Practical control systems invariably contain a power transducer which behaves non-linearly for large error signals. In particular cases, a non-linearity may be inserted intentionally in order to improve the system response to particular inputs[1] or to limit the peak magnitude of some system parameter, such as velocity or acceleration.

The type of system to be considered contains an error detector which behaves linearly for small error signals, but for larger errors gives an output signal which reduces in magnitude, eventually becoming zero. An example of this characteristic is in automatic-follow radar systems, being the form of the non-linear relationship between error signal and angular misalignment.

The following non-linear characteristic, shown in Fig. 1(*a*), will be considered to illustrate the various analyses:

$$\left.\begin{aligned} e_o &= e_i \text{ for } |e_i| < h \\ e_o &= 0 \text{ for } |e_i| > h \end{aligned}\right\} \quad \ldots\ldots (1)$$

It is referred to as a *limited-field-of-view*, or l.f.v., non-linearity.

In a system containing this non-linearity, control may be lost if the error becomes larger than h. When this occurs the output quantity can, in general, drift to its extreme value, and future correct operation is unlikely. Loss of control can thus be caused by large transient or continuous (sinusoidal or random) signals.

The usual method of sinusoidal analysis applied to a feedback system containing an l.f.v. non-linearity proves to be inadequate since, under overload conditions, a d.c. signal can be shown to appear at the input to the non-linearity. A more detailed description of the non-linearity is, in fact, required, to show the relationship between the fundamental a.c. and the d.c. output from the non-linearity in response to an input signal consisting of both sinusoidal and d.c. components.

To overcome the possible loss of control when a system contains the specified type of non-linearity, it is apparent that some form of memory circuit is required whereby a constant signal of the correct sign will be stored if the error signal from the non-linear detector disappears. A suitable arrangement employing a hysteretic circuit is shown in Fig. 7.

Correspondence on Monographs is invited for consideration with a view to publication.

Mr. Atherton is in the Electrical Engineering Laboratories, University of Manchester.

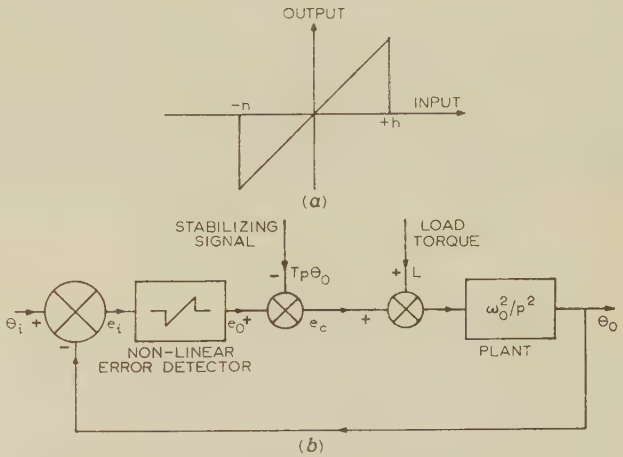

Fig. 1.—Second-order system containing an l.f.v. non-linearity.
(*a*) L.F.V. characteristic.
(*b*) Basic system.

(2) BASIC SYSTEM

The system shown in Fig. 1(*b*), including the l.f.v. non-linearity, will be taken to illustrate the various effects with transient, sinusoidal or random inputs. For this feedback loop the error-to-output transfer function has the value

$$\frac{\theta_o}{e_o} = \frac{1}{p^2/\omega_o^2 + Tp} \quad \ldots\ldots (2)$$

In a practical system the true error signal, e_i, is, of course, not available and hence any additional elements must operate on the modified error signal, e_o, as shown in Fig. 7(*a*).

(2.1) Step Response

The response of the uncompensated system, initially at rest, to a step input of height H, will obviously be zero if $|H| > h$, since the control signal e_i is then zero. With $|H| < h$ the response is linear. If an initial velocity exists at the instant of applying the step, the linear regime is entered at a finite velocity, and the subsequent response can either remain linear or pass completely through the linear regime without gaining control. Typical phase-plane trajectories for the system are shown in Fig. 2 for the case of critical velocity-feedback damping ($T\omega_o = 2$). When the error signal is greater than h, the control signal consists only of the damping component, $Tp\theta_0$, and the equation of motion is

$$\left(\frac{p^2}{\omega_o^2} + \frac{2p}{\omega_o}\right)\theta_o = 0 \quad \ldots\ldots (3)$$

the solution of which is

$$\frac{d\theta_o}{dt} = \dot{\theta}_o = 0 \text{ or } \frac{d\dot{\theta}_o}{d\theta_o} = -2\omega_o \quad \ldots\ldots (4)$$

Thus, outside the linear regime the phase-plane trajectory is a straight line of slope -2, terminating when zero velocity is reached. The solution of eqn. (4) for the initial conditions $\theta_o = H$, $\dot{\theta}_o = v$ is

$$\theta_o = \frac{v\omega_o}{2} + \left(\omega_o^2 H - \frac{v\omega_o}{2}\right)\varepsilon^{-2\omega_o t} \quad . \quad . \quad (5)$$

indicating that the output position varies exponentially with time.

The linear regime will be entered provided that the velocity in the non-linear region is greater than $2\omega_o(|e_i| - h)$, the lowest value being trajectory (*a*), Fig. 2. If, however, the linear regime is entered at a velocity[2] greater than $4{\cdot}6h\omega_o$, a trajectory such as (*c*) results. Therefore with velocities (outside the linear regime) greater than $2\omega_o(|e_i| - h) + 4{\cdot}6h\omega_o$, control is lost; the trajectory emerges from the other side of the linear regime to reach zero velocity with $e_i > h$. Thus trajectory (*b*), for which the linear regime is entered at the velocity $4{\cdot}6h\omega_o$, marks the highest velocity, and trajectory (*a*) the lowest velocity, between which control will be regained. This region is shown

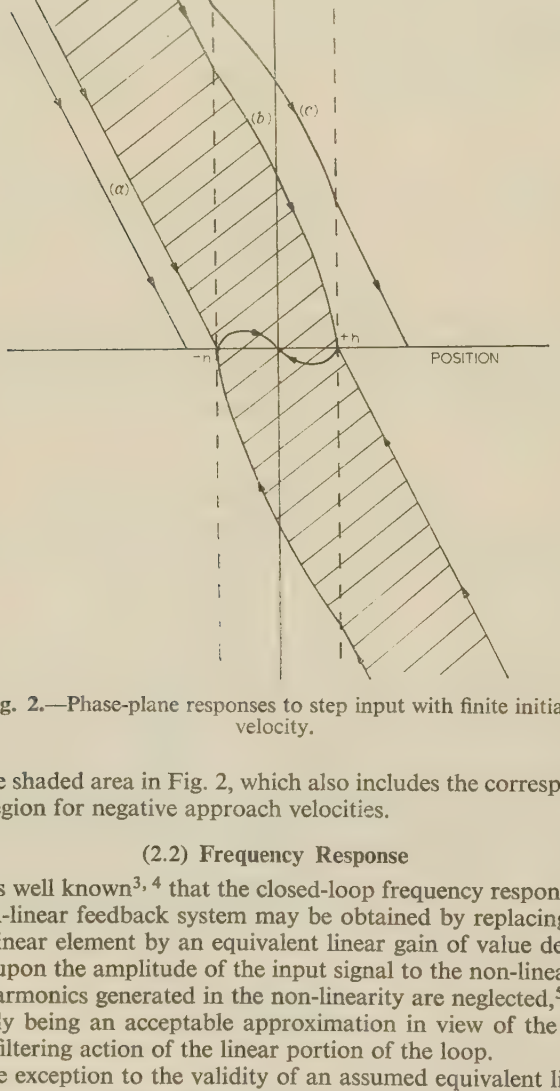

Fig. 2.—Phase-plane responses to step input with finite initial velocity.

by the shaded area in Fig. 2, which also includes the corresponding region for negative approach velocities.

(2.2) Frequency Response

It is well known[3, 4] that the closed-loop frequency response of a non-linear feedback system may be obtained by replacing the non-linear element by an equivalent linear gain of value dependent upon the amplitude of the input signal to the non-linearity. All harmonics generated in the non-linearity are neglected,[5] this usually being an acceptable approximation in view of the low-pass filtering action of the linear portion of the loop.

One exception to the validity of an assumed equivalent linear gain is when sub-harmonic oscillations[6] can take place. A second exception will be shown to occur with non-linearities of the l.f.v. type, when it becomes necessary to consider the d.c conditions through the non-linearity, since it is possible for the gain to a d.c. signal, in the presence of a sinusoidal signal, to reverse sign, thereby giving rise to a form of d.c. instability.

In general, to study the stability of a non-linear system under forced conditions of sinusoidal input, it is necessary to consider not only the actual equivalent linear gain of the non-linearity to a sinusoidal signal, but also the gain to a small d.c. signal in the presence of the sinusoidal signal. When, for example, the magnitude of the sinusoidal input to the system of Fig. 1(*b*) is such that linear operation takes place, the gain through the non-linear element is positive and equal to unity for the small d.c. signal, and through the linear elements, i.e. from e_o to e_i Fig. 1(*b*), the gain to the small d.c. signal is negative. The overall sign of d.c. feedback is thus negative and the system possesses d.c. stability. If, when non-linear operation takes place, the gain through the non-linear element becomes negative for the small d.c. signal, the overall feedback is positive and d.c. instability results. The gain of the non-linear element to the small d.c. signal in the presence of another signal is referred to as the d.c. incremental gain.[7] Under symmetrical operation with no superimposed d.c. input the d.c. incremental gain of, for example, the non-linear elements of saturation and dead space is positive in the presence of all magnitudes of sinusoidal input. This is not the case for the l.f.v. type of non-linearity where, under symmetrical operation, the d.c. incremental gain can become negative. Thus, to understand the performance of a closed-loop system containing the l.f.v. non-linearity it becomes necessary to evaluate the response of the non-linearity to an a.c. signal in the presence of a superimposed d.c. signal, i.e. under non-symmetrical operation. The slope of the d.c.-output/d.c.-input curves, taken for various fixed a.c. inputs, gives the incremental d.c. gain. To include the case of non-symmetrical operation, a wide range of d.c. inputs needs to be considered.

Evaluation of the fundamental and d.c. content of the output is obtained by Fourier analysis, but involves a considerable amount of calculation. Results were, in fact, obtained using a digital computer, the input waveform being represented by spot values at angular intervals of 2°. These data are plotted in Figs. 3(*a*) and (*b*), all magnitudes having been normalized with respect to the limits $\pm h$ of linear operation. It will be observed that, for input sinusoidal magnitudes greater than unity, the slope of the d.c.-input/d.c.-output curve at the origin is negative.

Similar results are obtained where the output from the error detector is proportional to the sine of the true error, as in the case of magslips used for position measurement. A theoretical analysis of the response of this non-linear characteristic to a sinusoidal plus d.c. input is possible and is given in the Appendix.

In the feedback loop of Fig. 1(*b*) the net d.c. component in the sum of the control signal and the (normalized) load force L, must be approximately zero, since the d.c. gain through the assumed plant transfer function of ω_{ol}^2/p^2 is high. Thus, in the absence of any d.c. load torque, the d.c. output from the non-linearity must be zero. Applying this requirement, and also the condition that the d.c. incremental gain must remain positive, it is seen from the curves of Fig. 3(*a*) that, with no d.c. input to the non-linearity, a sinusoidal error signal of peak value greater than unity results in d.c. instability. Points X_1, X_2, etc., represent stable operating conditions and indicate that the magnitude of steady error signal varies with the a.c. input to the non-linearity. From Fig. 3(*b*), points Y_1, Y_2, etc. corresponding to the operating conditions at X_1, X_2, etc., can be obtained, and hence values of the fundamental output signal e_o. Curve (*a*) in Fig. 4 shows the variation of fundamental output, e_o, which satisfies the conditions of positive d.c. incre

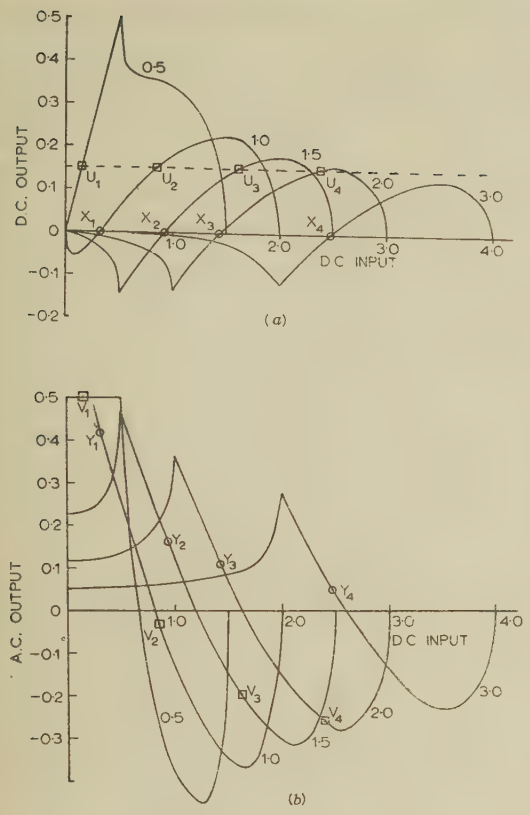

Fig. 3.—Response of the l.f.v. non-linearity for various magnitudes of a.c. input.

(*a*) D.C.-input/d.c.-output characteristics.
(*b*) D.C.-input/a.c.-output characteristics.

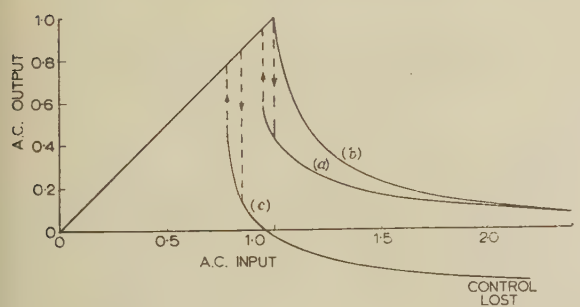

Fig. 4.—Curves showing the variation of fundamental a.c. output from the l.f.v. with the magnitude of a.c. input.

(*a*) For positive d.c. incremental gain and zero d.c. output.
(*b*) For zero d.c. input to the non-linearity.
(*c*) For positive d.c. incremental gain and a d.c. output of 0·15.

ıental gain as a function of the sinusoidal input amplitude. he same relationship determined on the erroneous assumption ıat d.c. conditions can be ignored is shown in curve (*b*). A mall hysteretic effect is seen to be included in curve (*a*). This ffect is due to the different entry into change-over from linear o non-linear operation, or vice versa, when the input amplitude increased, or decreased, and it will occur also in the case ext to be considered, when a finite load force, L, has to be vercome.

Fig. 5 shows the closed-loop frequency response for two agnitudes of input θ_i, normalized with respect to h, the limit f linear operation of the non-linearity. This response is btained[4] by combination of curve (*a*) in Fig. 4 with loci for

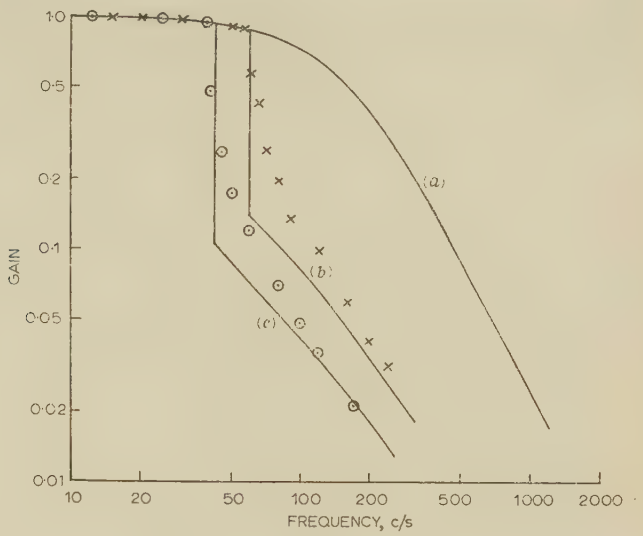

Fig. 5.—Closed-loop frequency response.

(*a*) Linear system.
(*b*) $\theta_i = 1 \cdot 5$.
(*c*) $\theta_i = 2 \cdot 0$.

the response of the linear elements of the system with $T\omega_o = 2$ and $\omega_o = 1\,000$ rad/sec. Experimental points obtained using a simulator are seen to be in close agreement. The simulated l.f.v. non-linearity had a slope of -10 (not infinite) outside the linear regime, which, together with the imperfect 'break points', partly accounts for the divergence of experimental and theoretical results in the region of the d.c. jump, although it is to be expected that harmonics, ignored in the analysis, will also contribute to the slight differences observed.

When a constant load disturbance, $-L$, exists, the non-linearity has to provide a d.c. output of magnitude $+L$, since the sum of these two signals must, in the system of Fig. 1(*b*), be zero. The particular case of $L = 0 \cdot 15$ is considered as an example: the d.c. operating points for various magnitudes of sinusoidal input are then U_1, U_2, U_3 and U_4 [Fig. 3(*a*)]. The corresponding points V_1, V_2, V_3 and V_4 showing the a.c. output are indicated on Fig. 3(*b*). The non-linearity is now described by curve (*c*) in Fig. 4, which would be used to calculate the closed-loop frequency response. As seen from Fig. 3(*a*) the d.c. output of 0·15 from the non-linearity can only be obtained provided that the a.c. input is less than about 2·2: the system loses control if the a.c. input exceeds this value.

The procedure for obtaining the above operating conditions, for the case when constant load torque exists, would, in fact, have to be carried out in all similar cases, irrespective of the type of non-linearity; i.e. a series of curves for the particular non-linearity would be required to calculate the resulting non-symmetrical operation.

(2.3) Response to Random Signals

Figs. 6(*a*) and (*b*) show how the d.c. output and the equivalent gain for the l.f.v. non-linearity vary with d.c. input for various powers of Gaussian random input signal; the curves were obtained using cursors.[7] For all input powers, the d.c. incremental gain is positive at the origin, and thus, in all cases, symmetrical operation about the non-linearity takes place when L is zero. For large random input signals the maximum d.c. output which can be obtained from the non-linearity becomes very small, and thus only a small disturbance, L, which may be caused by d.c. drift in the error amplifier or by low-frequency distortion products,[8] can cause instability. It is of interest to

note that the curves of Figs. 6(*a*) and (*b*) are simply related since the equivalent gain is equal to the d.c. incremental gain[7] (slope of d.c. output/input curve) with a Gaussian random input.

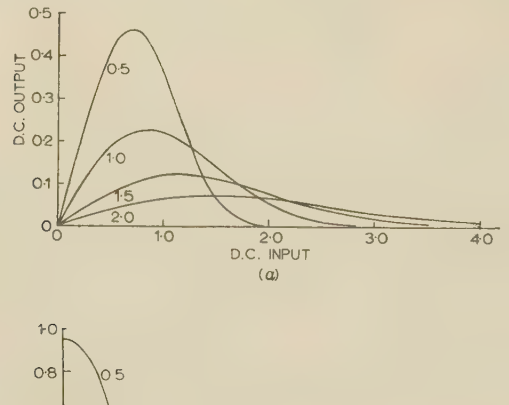

Fig. 6.—Response of the l.f.v. non-linearity for various magnitudes of random signal input.
(*a*) D.C.-input/d.c.-output characteristics.
(*b*) D.C.-output/equivalent-gain characteristics.

(3) COMPENSATION OF THE L.F.V. NON-LINEARITY BY INCLUSION OF A MEMORY CIRCUIT

The adverse behaviour of a system containing an l.f.v. non-linearity occurs mainly because there is no indication of error when the error magnitude is greater than $\pm h$. Ideally, therefore, a memory circuit is required to correct this characteristic so that a positive signal is stored for large positive errors, and a negative signal is stored for large negative errors. A simple form of correcting circuit is the hysteretic memory circuit of Fig. 7(*b*), with 'dead zone' $\pm h_m$, inserted immediately after the l.f.v. non-linearity. For purposes of analysis it is desirable to treat the series combination of the l.f.v. and memory circuit as one overall non-linear element; the theoretical input/output characteristic is shown in Fig. 7(*c*) for the range $0{\cdot}5 < h_m/h < 1{\cdot}0$. Owing to the simplicity of the memory circuit, the overall characteristic does not behave ideally, but if the components of the memory circuit are suitably chosen, a good approximation can be obtained over the desired frequency range of operation. (At high frequencies the capacitor C is unable to charge up completely and at low frequencies it loses its charge through the resistor R.) R is included so that the output returns to zero when the input is decreased below the level h_m.

To eliminate the dead zone and reduce the phase shift obtained using the series combination of the l.f.v. and memory circuit, a signal direct from the l.f.v. non-linearity output is added to ρ times the signal from the memory circuit, as shown in Fig. 7(*a*). This produces an overall non-linear characteristic of the form shown in Fig. 7(*d*). The parameters ρ and h_m can be varied to suit a particular design. Factors affecting the choice of the values of ρ and h_m may be summarized as follows:

(*a*) The normalized range of linear operation is reduced to h_m/h and therefore h_m/h should be large.
(*b*) A signal $\rho(h - h_m) = \rho h(1 - h_m/h)$ is obtained for large errors and therefore h_m/h should be small and ρ should be large.
(*c*) The phase shift introduced (with large sinusoidal signal) b

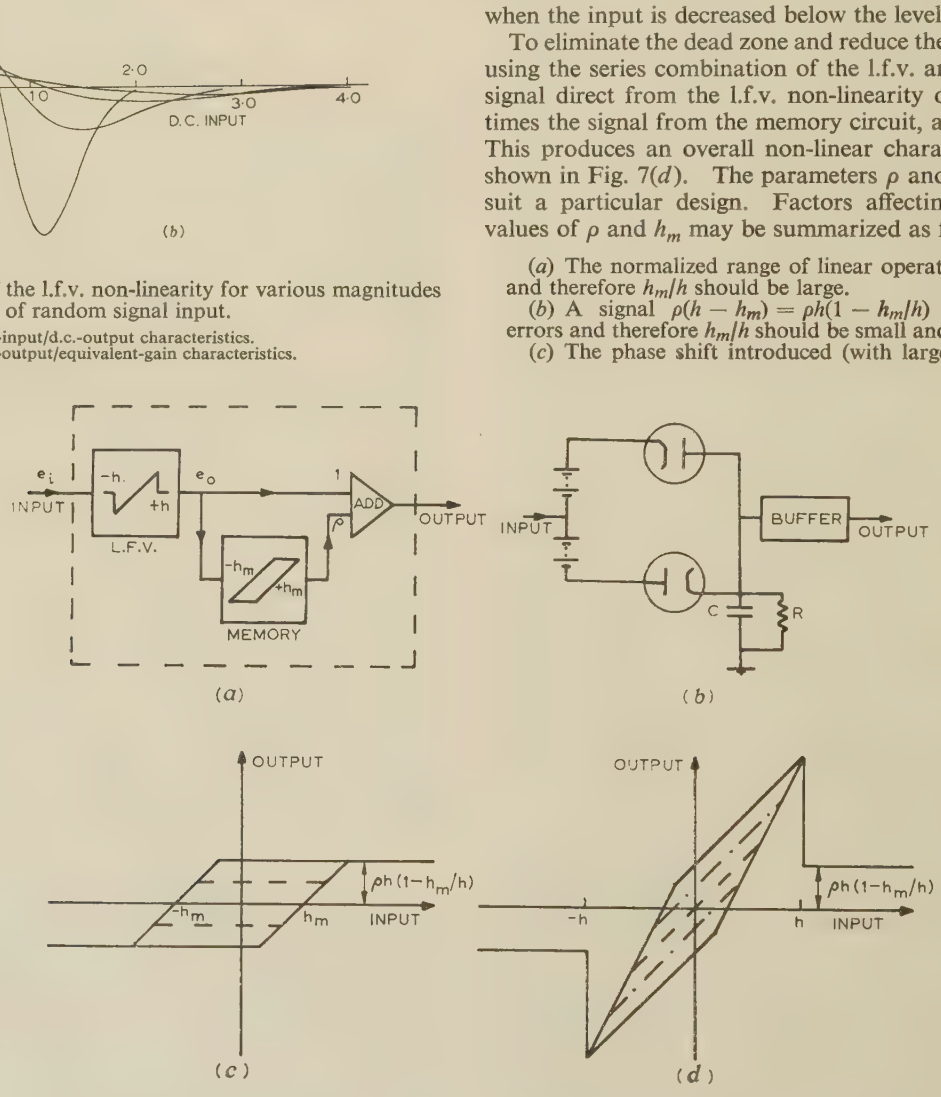

Fig. 7.—Compensating circuit to prevent loss of control.
(*a*) Composition of overall non-linearity.
(*b*) Hysteretic memory circuit.
(*c*) Characteristic of l.f.v. and memory circuit in series.
(*d*) Overall non-linear characteristic.

the memory circuit is increased if h_m or ρ is increased and therefore h_m/h and ρ should be small.

From a consideration of the above factors, values of $h_m/h = 6$ and $\rho = 1{\cdot}0$ have been taken, representing a compromise between the conflicting requirements. The overall non-linearity then behaves as indicated in Fig. 7(*d*).

(4) PERFORMANCE OF THE MODIFIED SYSTEM

(4.1) Step Response

For errors greater than $|h|$ [region (i) Fig. 8(*a*) and (*b*)] the control signal has a limited value $h - h_m$; over this region the

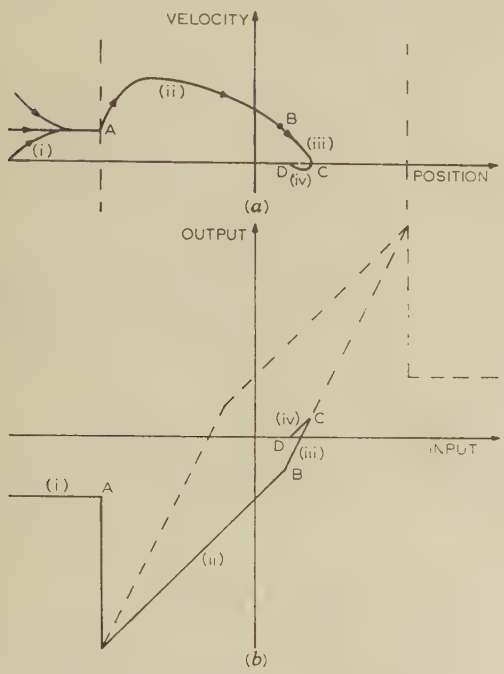

Fig. 8.—Step response of modified system.
(*a*) Phase plane.
(*b*) Overall non-linearity output.

output can reach a maximum velocity of $(h - h_m)\omega_o/2$ with the system critically damped, i.e. $T\omega_o = 2$. When the error falls below $|h|$ the response follows the trajectory (ii), (iii), (iv), Fig. 8(*a*), the corresponding output from the non-linearity being as shown in Fig. 8(*b*). A small residual error can result, with maximum possible value $0{\cdot}3h$ (for $h_m/h = 0{\cdot}6$). This can be overcome by the use of a coarse/fine system, whereby the memory circuit is made inoperative for errors below, say, $0{\cdot}5h$; or by the inclusion of an a.c. coupling in the memory circuit of Fig. 7(*b*), thereby converting it to a transient memory.

(4.2) Frequency Response

Fig. 9 shows the d.c. input/output characteristic of the overall non-linearity for various magnitudes of sinusoidal input, from which it can be seen that the incremental d.c. gain is positive at the origin, except for sinusoidal inputs of approximately unity. Thus the modified system, i.e. the overall non-linearity replacing the l.f.v. non-linearity in Fig. 1(*b*), will have no d.c. error for large input signals, and usual techniques (neglecting the requirement of positive d.c. incremental gain) can be used in the analysis.

The phase lag introduced by the circuit is shown in the describing-function locus (Fig. 10) for the overall non-linearity. The open-loop frequency response locus for $T\omega_o = 1$ of the

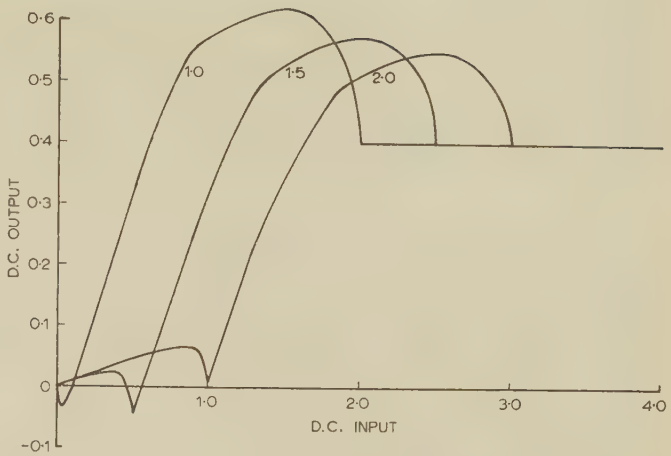

Fig. 9.—D.C.-input/d.c.-output characteristics of overall non-linearity for various magnitudes of a.c. input.

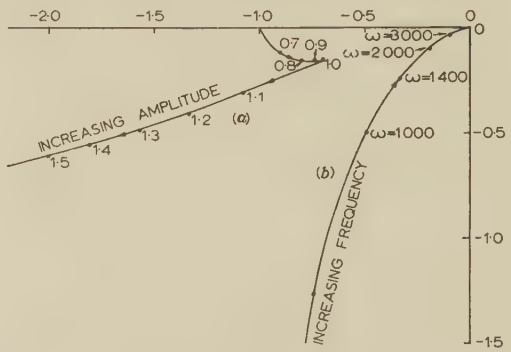

Fig. 10.—Polar response loci for the compensated system.
(*a*) Describing function for overall non-linearity.
(*b*) Open-loop frequency response of linear elements ($T\omega_o = 1$, $\omega_o = 1000$).

basic system in Fig. 1(*b*) is also shown in Fig. 10, and it is seen that the system should now be stable for all values of input signal. Stability under these conditions is verified by simulation; reduction of the damping produces oscillations within $\pm 10\%$ of the conditions predicted using the describing-function technique.

(4.3) Response to Random Signals

Experimental results show that the d.c. incremental gain of the overall non-linearity is positive for no d.c. input in the presence of a random signal of any magnitude. The performance of the modified system subjected to random inputs is satisfactory and there is no tendency towards loss of control with large inputs, as was the case with the original system. Theoretical analysis of double-valued non-linearities subjected to random inputs is somewhat difficult: experimental observations suggest that an equivalent-gain approach does not provide an accurate description. Experimental minimization of the mean square error, in a selected narrow bandwidth of the input spectrum between the output from a hysteretic non-linearity and a variable-gain element, shows that the equivalent gain varies appreciably with the bandwidth selected, being higher and with smaller phase lags for the lower-frequency components of the input spectrum.

(5) CONCLUSIONS

Analysis of the stability of an l.f.v.-type system is found to require a '2-dimensional' approach, d.c. incremental gain being

required as well as a.c. gain. The intolerable behaviour in regard to loss of control in the basic l.f.v. system is shown to be alleviated by the inclusion of a simple hysteretic memory circuit. Better compensation could undoubtedly be obtained by a superior form of memory circuit should the added complication justify the improvement obtained.

(6) ACKNOWLEDGMENTS

The work described was carried out in the Electrical Engineering Laboratories of the University of Manchester. The author is indebted to his former colleagues, Professor J. C. West and Dr. J. L. Douce, and to Dr. M. J. Somerville, for much advice; also to Mr. P. H. Hammond who initiated the problem.

(7) REFERENCES

(1) West, J. C., Douce, J. L., and Naylor, R.: 'The Effects of the Addition of some Non-Linear Elements on the Transient Performance of a Simple R.P.C. System Possessing Torque Limitation', *Proceedings I.E.E.*, Paper No. 1549 M, August, 1953 (**101**, Part II, p. 156).

(2) West, J. C.: 'Textbook of Servomechanisms' (English Universities Press, 1953), p. 210.

(3) West, J. C., and Douce, J. L.: 'The Frequency Response of a Certain Class of Non-Linear Feedback Systems', *British Journal of Applied Physics*, 1954, **5**, p. 204.

(4) West, J. C., and Nikiforuk, P. N.: 'The Behaviour of a Remote-Position-Control Servo Mechanism with Hard-Spring Non-Linear Characteristics', *Proceedings I.E.E.*, 1954 (**101**, Part II, p. 481).

(5) Johnson, E. C.: 'Sinusoidal Analysis of Feedback Control Systems Containing Non-Linear Elements', *Transactions of the American I.E.E.*, 1952, **71**, p. 169.

(6) West, J. C., and Douce, J. L.: 'The Mechanism of Sub-Harmonic Generation in a Feedback System', *Proceedings I.E.E.*, Paper No. 1693 M, July, 1954 (**102** B, p. 569).

(7) Somerville, M. J., and Atherton, D. P.: 'Multi-Gain Representation for a Single-Valued Non-Linearity with Several Inputs, and the Evaluation of their Equivalent Gains by a Cursor Method', *ibid.*, Monograph No. 309 M, July, 1958 (**105** C, p. 537).

(8) West, J. C., Douce, J. L., and Leary, B. G.: 'Frequency Spectrum Distortion of Random Signals in Non-Linear Feedback Systems' (see page 259).

(8) APPENDIX

Sinusoidal Error Detector Characteristic

The equation of an error detector, using magslips, is

$$e_o = A \sin e_i$$

For an input consisting of a sinusoidal signal of peak value a and a d.c. signal, b,

$$e_i = a \sin \theta + b$$

and hence

$$\begin{aligned} e_o &= A \sin (a \sin \theta + b) \\ &= A [\sin (a \sin \theta) \cos b + \cos (a \sin \theta) \sin b] \end{aligned}$$

Thus, the fundamental component of the output is

$$\frac{A}{\pi}\int_0^{2\pi}\{\cos b [\sin (a \sin \theta) \sin \theta] + \sin b [\cos (a \sin \theta) \sin \theta]\} d\theta$$

$$= \frac{A}{\pi}[\cos b 2\pi J_1(a) + 0] = 2AJ_1(a) \cos b$$

where J_1 is the first-order Bessel function.

The d.c. output is

$$\frac{A}{2\pi}[\cos b \sin (a \sin \theta) + \sin b \cos (a \sin \theta)] d\theta$$

$$= \frac{A}{2\pi}[0 + \sin b 2\pi J_0(a)] = AJ_0(a) \sin b$$

where $J_0(a)$ is the zero-order Bessel function.

Thus, d.c.-input/d.c.-output curves for various a.c. inputs, a, are sine curves with amplitude $J_0(a)$. The d.c. incremental gain for zero d.c. input is $AJ_0(a)$ and this becomes negative when $a > 2{\cdot}405$. Therefore, if the non-linearity is in a closed-loop system, a d.c. jump from symmetrical operation to non-symmetrical operation with a d.c. input of π takes place when the peak a.c. input exceeds $2{\cdot}405$.

1.316.925 : 621.315.1

The Institution of Electrical Engineers
Monograph No. 421 S
Dec. 1960

LIMITATIONS OF DISTANCE-TYPE PROTECTIVE EQUIPMENT WHEN APPLIED TO LONG EXTREMELY-HIGH-VOLTAGE POWER LINES

By A. WRIGHT, M.Sc., Associate Member.

The paper was first received 19*th November*, 1959, *in revised form* 12*th April, and in final form* 21*st September*, 1960. *It was published as an* INSTITUTION MONOGRAPH *in December*, 1960.)

SUMMARY

On power lines the currents which flow solely in the phase conductors travel near the velocity of light whereas those which return through the ground and overhead earth wires travel more slowly, the speed depending on the line spacings, conductor sizes and nature of the ground. The full steady-state equations for a 3-phase line are developed and a particular line is examined to show the magnitude of this effect. The effect of transposing a line is also indicated.

The steady-state performance of basic distance protection fitted with compensating equipment to allow for the effects of the currents in the ground phases during earth faults is studied, using the line equations. It is shown that large errors of measurement occur under earth-fault conditions on long lines fed from small sources. The performance for faults which do not involve earth is satisfactory.

It is shown that non-transposition of a line makes the apparent impedance of a fault on a line depend on the source impedance. This causes further errors in the assessment of the positions of faults of all types.

The high transient time-constants on long lines increase the chance of maloperation during the transient period.

It is concluded that distance protection may not be satisfactory on very long lines and that a study must be made of the complete power system before a decision can be made about its suitability for any particular application.

LIST OF SYMBOLS

ρ = Resistivity of ground.
γ_1 = Positive- and negative-sequence propagation coefficient.
γ_0 = Zero-sequence propagation coefficient.
f = System frequency, c/s.
V_{ga} = Generated e.m.f. in phase A.
y_{bc}, etc. = Admittance between phases B and C, etc.
Z_{cb}, etc. = Voltage drop per metre along phase C due to unit current flowing in phase B, etc.
Z_{app} = Apparent impedance seen by a measuring element.
Z_{01} = Positive- and negative-sequence characteristic impedance.
Z_{00} = Zero-sequence characteristic impedance.
Z_{s1}, Z_{s2}, Z_{s0} = Sequence impedances of the source.

Suffixes used in association with the current and voltage symbols:

a, b, c and d = Quantities associated with phases A, B, C and the neutral or earth.
s = Sending-end quantities.
x = Fault-position quantities.
1 = Positive-sequence quantities.
2 = Negative-sequence quantities.
0 = Zero-sequence quantities.

(1) INTRODUCTION

Although Merz–Price-type protective equipments operate satisfactorily on relatively short lines, they are unsuitable for lines in excess of about 100 miles because of difficulties introduced by the line-capacitance currents and the transit time for the comparison signals to be interchanged between the line ends. The second factor does not affect distance-type protective schemes, as in these the positions of faults are determined by measuring elements to which the appropriate voltages and currents are applied. In addition, it is generally considered that allowance can be made for the effects of the line-capacitance currents when setting the measuring elements, and, as a result, distance protection is now regarded as the most suitable equipment for protecting long lines.

Very long extremely-high-voltage lines will seldom, if ever, be used in radial systems, and therefore, because of the system interconnection, when a fault occurs on such a line there will normally be fault current fed to it from both ends of the line. One of the ends may, however, at times be supplied only from a fairly remote generating station through a circuit of appreciable impedance, in which event the current fed into a line fault from that end may be very small. This result can, for convenience, be simulated by assuming an equivalent source of the appropriate apparent power at the end of the line. In under-developed countries where the amount of interconnection is small and where, in addition, the sources may tend to be small at certain times of the year, it is possible that the apparent power of the equivalent source may fall to very low values.

If distance-type protective equipment is applied to such lines it should operate correctly, even under the above conditions, and it should thus be capable of assessing fault positions correctly at very low fault currents. This has been recognized, and in recent years a number of types of distance-measuring element have been produced, all of which operate at an almost constant ratio of voltage to current input over a wide range of current and voltage, a typical characteristic being shown in Fig. 1. Some of these elements can operate satisfactorily down to 2–3% of normal voltage, and they are thus very suitable for systems where high source impedances may be encountered.

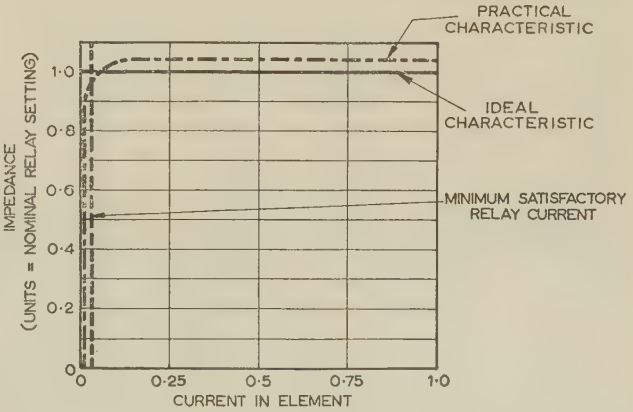

Fig. 1.—Characteristic of a typical modern impedance-measuring element.

Correspondence on Monographs is invited for consideration with a view to publication.
Mr. Wright is in the Electrical Engineering Department, University of Nottingham.

Tests have been made in laboratories on the various types of measuring elements and on complete protective schemes applied to mimic lines. Large-scale testing of schemes applied to actual lines has not been carried out, however, as lines cannot be obtained for test purposes for long periods.

The mimic lines used in protective-equipment laboratories are usually designed primarily for simulating short- and medium-length lines, and, as a result, they have the following limitations:

(*a*) No allowance is made for the distributed nature of line impedance.
(*b*) No allowance is made for the effects of asymmetric conductor configurations.
(*c*) The differences in behaviour between the zero-sequence and the positive- and negative-sequence quantities tend to be ignored.

Because of the above limitations it was felt by the author that, if protective schemes intended for use on very long lines were tested in conjunction with such mimic lines, there might be errors of a magnitude which could not be neglected when the schemes were operated on the actual lines. In the following Sections, therefore, the behaviour of long lines is examined analytically and then the errors in the performance of distance protection are investigated. As it is difficult to assess the importance of such errors from the general equations, a particular line is studied and the magnitudes of the possible effects are indicated.

(2) BEHAVIOUR OF LONG LINES

In the early days of overhead-line transmission the phase conductors were usually transposed. The benefits obtained from this practice are small, but the cost of making transpositions on extremely-high-voltage lines is quite considerable, and therefore, while some supply authorities continue to transpose their lines, others now leave them untransposed. The behaviour of both these types of lines is considered below.

(2.1) Performance of Asymmetrically-Spaced Untransposed Lines

When a fault involving earth occurs on a multi-phase line, some of the residual current returns through the earth itself while the remainder returns through the overhead earth wire or wires. It is well known that current waves associated with a conductor and the earth travel at a velocity considerably less than that of light. Allowance is made for this when a line is studied analytically by using an image conductor in the ground to determine the line-to-earth capacitance and a return conductor at a considerable depth in the ground to determine the inductance. Residual-current waves returning in the earth wires of a line would travel near the velocity of light if the effect of the presence of the earth itself could be nullified. In practice, therefore, residual-current waves, which must travel at the same velocity in both earth wires and ground since they are bonded together at frequent intervals, will travel at a velocity between that which would obtain in a line without earth wires and that of light. The actual velocity of propagation of the residual current in a line is dependent on various factors including the line spacings, the conductor radii, the earth-wire material and the nature of the ground over which the line passes.

The currents which circulate only in the phase conductors are not appreciably affected by the presence of the ground and thus they travel at nearly the velocity of light. The actual velocity is slightly below the ideal one because of the losses in the line and the effect of the internal inductance of the conductors. The latter factor causes the velocity to depend on the line configuration, and, as a result, there is not just one propagation velocity for all currents traversing paths in the phase conductors when the line is asymmetrically spaced.

In Appendix 7.1 the steady-state current equations for an asymmetrically spaced line are derived, and it can be seen from these that the above results are obtained, there being three propagation coefficients—one for the residual current and the two others for the currents circulating in the phases. Because of the large number of terms in the equations their significance cannot readily be appreciated, and therefore the appropriate numerical values for the assumed 500 kV line shown in Fig. 2 were inserted

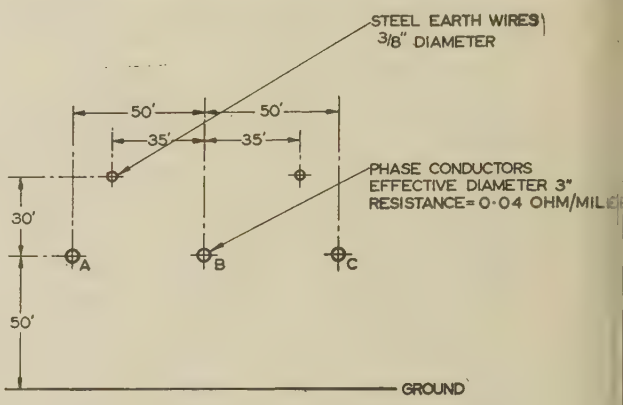

Fig. 2.—Assumed 500 kV line configuration.

the results obtained being given in eqns. (18)–(20). The effects of the ground, losses, etc., on the propagation coefficients can be seen from these equations. It will be noted that the two inter-phase propagation coefficients are both near the ideal value of $1 \cdot 69 \times 10^{-3} \underline{|90°}$. The propagation coefficient for the residual current is considerably above the ideal value, being $2 \cdot 62 \times 10^{-3} \underline{|89° 23'}$, which corresponds to a velocity about two-thirds that of light.

As stated in Appendix 7.2, the above results were obtained by assuming that the ground can be replaced by an equivalent conductor at a depth of 3 000 ft below the surface when considering inductive effects. While the assumption of a different effective depth would naturally have affected the results, the differences would not have been great, since the various impedances are dependent on the logarithms of the spacings.

(2.2) Performance of Ideally Transposed Lines

When a line is transposed the number of transpositions is usually small, but these nevertheless tend to make the performance approach that of an ideally transposed line. On such a line the phases behave identically, and, as a result, there are only two propagation coefficients, one for those currents which circulate solely in the phase conductors (positive- and negative-sequence currents) and the other for the residual or zero-sequence currents. This is shown in eqns. (30) and (31). It can also be seen that the zero-sequence characteristic impedance of a line is different from that for the positive and negative sequences.

The propagation coefficients and characteristic impedances for an ideally transposed line of the configuration shown in Fig. were determined by substituting the appropriate values in the equations of Appendix 7.3, the results being:

Positive- and negative-sequence propagation coefficient (γ_1)
$= 1 \cdot 719 \times 10^{-3} \underline{|88° 15}$

Zero-sequence propagation coefficient (γ_0)
$= 2 \cdot 620 \times 10^{-3} \underline{|89° 23}$

Positive- and negative-sequence characteristic impedance (Z_{01})
$$= 365\angle -1°\,49'$$
Zero-sequence characteristic impedance (Z_{00})
$$= 690\angle -38'$$

It can be seen, by comparing these results with those obtained the previous Section, that transposing a line does not greatly fect the propagation coefficients.

(3) PERFORMANCE OF DISTANCE PROTECTION

There are many arrangements of distance-type protective hemes, all of which, as stated earlier, have means whereby the sitions of faults are assessed by applying the appropriate ltages and currents to measuring elements. The schemes ust operate correctly for 3-phase, inter-phase and phase-to-rth faults. The ways in which this is attempted will be amined in the following Sections.

It will be assumed initially that a scheme is to be applied to an eally transposed line and that all the faults which occur are mplete short-circuits. The second assumption ensures that, the fault position, there is no voltage between the faulty phases r faults not involving earth, and that there is no voltage tween the faulty phases and earth during earth faults. Both sumptions tend to make the operating conditions of the pro-ction easier, and, as a result, the performance and accuracy obtained will represent the best which can be achieved. A rther assumption which will be made is that the main voltage id current transformers have transformation ratios of unity, that the number of symbols in the various equations is kept a minimum. In practice, a constant factor would have to be troduced to allow for these transformations.

(3.1) Single-Phase-to-Earth Faults

At the fault position, assumed to be a distance x along phase , the voltage to earth is zero and therefore substitution in n. (31) gives

$$V_{xa} - V_{xd} = (V_{sa1} + V_{sa2})\cosh\gamma_1 x + V_{s0}\cosh\gamma_0 x - (I_{sa1} + I_{sa2})Z_{01}\sinh\gamma_1 x - I_{s0}Z_{00}\sinh\gamma_0 x = 0 \quad (1)$$

It is not possible, because of the complexity of the above uation, to express the distance x to the fault as a simple nction of the various line voltages and currents. On very ort lines, however, the following simplifying assumptions can e made:

$$\cosh\gamma_1 x = \cosh\gamma_0 x = 1$$
$$\sinh\gamma_1 x = \gamma_1 x \text{ and } \sinh\gamma_0 x = \gamma_0 x$$

Substitution of these approximations in eqn. (1) gives

$$V_{sa} - V_{sd} = [I_{sa}Z_{01}\gamma_1 + I_{s0}(Z_{00}\gamma_0 - Z_{01}\gamma_1)]x$$

herefore
$$x = \frac{V_{sa} - V_{sd}}{I_{sa}Z_{01}\gamma_1 + I_{s0}(Z_{00}\gamma_0 - Z_{01}\gamma_1)} \quad . \quad . \quad . \quad (2)$$

Substitution of $I_{s0} = \frac{1}{3}(I_{sa} + I_{sb} + I_{sc})$ in this equation gives

$$x = \frac{3(V_{sa} - V_{sd})}{I_{sa}(Z_{00}\gamma_0 + 2Z_{01}\gamma_1) + (I_{sb} + I_{sc})(Z_{00}\gamma_0 - Z_{01}\gamma_1)}$$

e.
$$x = \frac{V_{sa} - V_{sd}}{Z_s I_{sa} + Z_m(I_{sb} + I_{sc})} \quad . \quad . \quad . \quad . \quad (3)$$

where

$$Z_s = \tfrac{1}{3}(Z_{00}\gamma_0 + 2Z_{01}\gamma_1) \text{ and } Z_m = \tfrac{1}{3}(Z_{00}\gamma_0 - Z_{01}\gamma_1)$$

To obtain correct discrimination, the phase A earth-fault relay must determine, from the information given to it, whether faults are within a given distance of the sending end of the line, i.e. whether x is below a particular value.

Although there are a number of types of measuring elements available, they all work on the basic principle that the movement is restrained by one quantity and is operated by another. Ideally, neglecting such factors as the friction of the measuring element, etc., operation will occur whenever the operating signal exceeds the restraining signal. Using such an ideal element, restrained by a signal proportional to the phase-A′-to-neutral voltage at the sending end of the line and operated by a signal proportional to $Z_s I_{sa} + Z_m(I_{sb} + I_{sc})$, it can be seen from eqn. (3) that operation will always occur for faults within a given distance along the line. The operation is correct whatever currents are flowing in the sound phases (B and C). Because of this, the well-known principle of feeding the earth-fault elements with an operating signal made up of proportions of all three phase currents is called 'sound-phase compensation'.

It is evident from eqn. (2) that correct operation can also be obtained for earth faults on phase A of a short line by feeding the A-phase measuring element with an operating signal made up of proportions of the zero-sequence and A-phase currents at the sending end of the line. This commonly-used arrangement, which is known as 'residual compensation', gives precisely the same results as sound-phase compensation.

Distance protection provided with one or other of the above types of compensation is applied at present on all lengths of lines, and clearly there must be measuring errors on the longer lines since both types of compensation are based on assumptions which are only valid on short lines.

In Appendix 7.4, the ratio of the phase-A-to-neutral voltage to $Z_s I_{sa} + Z_m(I_{sb} + I_{sc})$ is determined without making any simplifying assumptions. The expression for this ratio [eqn. (43)], which can be regarded as the apparent impedance seen by the A-phase earth-fault element, is very complex. It can, however, be seen that it is no longer directly proportional to the distance between the fault and the sending end of the line. It is affected by the currents in the sound phases, and also by the zero-sequence impedance of the source. The effects of these factors cannot be judged from the general equations, and therefore various particular examples are considered below to determine the magnitudes of the possible errors.

For an earth fault on phase A when there is zero current flowing in the two sound phases at the fault position, eqn. (43) becomes

$$Z_{app} = \frac{M + 2N}{P + 2Q}$$

If the values for a 500 kV loss-free line of the configuration considered earlier are inserted in this equation, and it is assumed that the source impedance is purely inductive, the apparent impedance is given by

$$Z_{app} = j\frac{1}{\gamma_1}\,\frac{690\sin\gamma_0 x\cos\gamma_1 x + 730\sin\gamma_1 x\cos\gamma_0 x + X_{s0}(\cos\gamma_1 x\cos\gamma_0 x - 1 - 1{\cdot}06\sin\gamma_1 x\sin\gamma_0 x)}{690(1{\cdot}51 - \sin\gamma_1 x\sin\gamma_0 x + 1{\cdot}06\cos\gamma_1 x\cos\gamma_0 x) - X_{s0}(\sin\gamma_1 x\cos\gamma_0 x + 1{\cdot}06\cos\gamma_1 x\sin\gamma_0 x)}$$

The variation of this apparent impedance with change in the zero-sequence source reactance for faults at various distances along the line is shown in Fig. 3. It can be seen that the variation for an earth fault 200 miles along the line is only about 12% for a range of zero-sequence source reactances between 0 and 500 ohms, i.e. for sources from infinity down to 100 MVA at 500 kV assuming a zero-sequence reactance of 20%. For faults

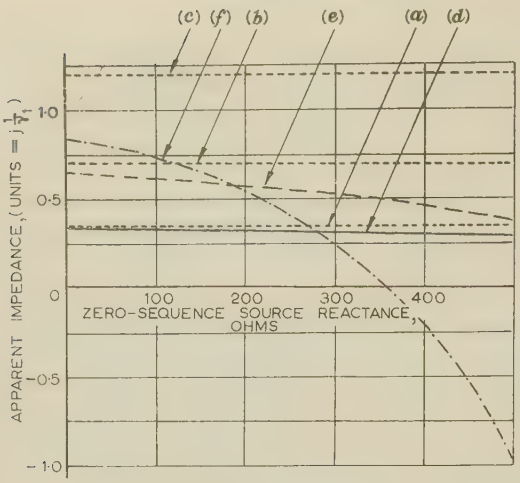

Fig. 3.—Variation of the apparent impedance seen by a relay for 3-phase and single-phase earth faults at various distances from the sending end of a line.

(*a*) 3-Phase fault 200 miles along line.
(*b*) 3-Phase fault 350 miles along line.
(*c*) 3-Phase fault 500 miles along line.
(*d*) Earth fault 200 miles along line.
(*e*) Earth fault 350 miles along line.
(*f*) Earth fault 500 miles along line.

500 miles along the line, the apparent impedance varies greatly and it can even appear capacitive for the higher source impedances.

On a practical line, because of the losses, the impedance seen by the measuring elements will not fall to zero, nor will it suddenly change from purely inductive to purely capacitive. Large changes will nevertheless occur on long lines with relatively low losses.

The effect of current flow in the sound phases of the above loss-free line was determined from eqn. (43), the results obtained being shown in Fig. 4. These loci for various sound-phase current conditions again show that the variations are not great for faults 200 miles along the line but that they can be very great for faults 500 miles along it. They also show that the greater the size of the source, the smaller is the variation.

It will be noted in the above that sources down to 100 MVA have been considered. While a long extremely-high-voltage line could never be energized solely from such a source, it is quite possible, as stated earlier, that a line could be connected to a large source at one end and appear to be connected, owing to the system interconnection, to a source as small as 100 MVA at the other.

It is evident from Figs. 3 and 4 that correct operation can never be achieved for earth faults on very long lines which may at times be fed from a small effective source, as it is possible for faults which are actually towards the remote end of the line to appear nearer than faults which are close to the sending end. The normal discriminating basis is thus not applicable and the ability of modern measuring elements to operate with small sources and low fault currents is valueless in such applications. It is also clear that there is a considerable risk of the earth-fault elements causing the line to be tripped incorrectly for faults beyond its remote end, as such faults may present a very low impedance to the measuring elements and thus appear to be on the line.

(3.2) Phase-to-Phase Faults

For a fault between phases A and B, the voltage between these phases at the fault position is zero, and therefore

$$V_{xa} - V_{xd} = V_{xb} - V_{xd}$$

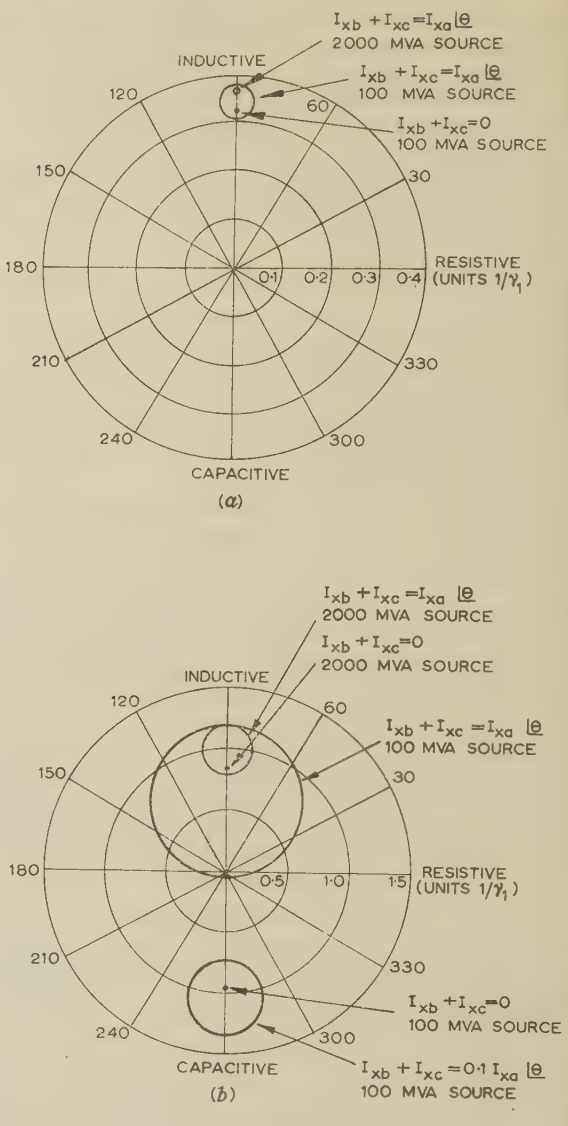

Fig. 4.—Loci of the apparent impedances seen by a relay during an earth fault.

Zero-sequence source reactance = 20%
(*a*) Fault 200 miles along line. (*b*) Fault 500 miles along line.

For such a fault, there are no zero-sequence quantities present and thus it can be seen from eqn. (31) that

$$(V_{sa1} + V_{sa2}) \cosh \gamma_1 x - (I_{sa1} + I_{sa2}) Z_{01} \sinh \gamma_1 x$$
$$= (V_{sb1} + V_{sb2}) \cosh \gamma_1 x - (I_{sb1} + I_{sb2}) Z_{01} \sinh \gamma_1 x$$

Therefore
$$\frac{V_{sa} - V_{sb}}{I_{sa} - I_{sb}} = Z_{01} \tanh \gamma_1 x$$

In this instance, if the AB phase-fault relay is fed with a restraining signal proportional to the difference of the sending-end voltages of the A and B phases and an operating signal proportional to the difference of the sending-end currents in phases A and B, operation will always occur when $\tanh \gamma_1 x$ falls below a fixed value. The protection will thus perform correctly and will operate only for faults up to a fixed distance along the line. Operation is not dependent in any way on the current in the sound phase, or on the source impedances, and is satisfactory for all lengths of lines.

(3.3) Three-Phase Faults

For a 3-phase fault, the voltages between phases and to earth at the fault position are all zero, and thus

$$V_{xa} - V_{xd} = V_{xb} - V_{xd} = V_{xc} - V_{xd} = 0$$

In addition, there are no zero-sequence quantities present. On this basis the equations in the preceding Section are still applicable and therefore the AB phase-fault measuring element will operate as though there were a 2-phase fault between phases A and B. It will, as before, operate correctly for all lengths of line.

It is clear that the two other phase-fault measuring elements (CA and BC) will receive similar signals and thus they also will operate and clear the fault correctly.

The phase-A earth-fault measuring element receives signals proportional to $V_{sa} - V_{sd}$ and $I_{sa} + (I_{sb} + I_{sc})Z_m/Z_s$. As all the conditions laid down in Appendix 7·4 also apply during 3-phase faults, the apparent impedance seen by the element is still given by the same formulae.

Substitution from eqns. (41) and (42) with the zero-sequence terms omitted gives

$$Z_{app} = \frac{1}{\gamma_1} \tanh \gamma_1 x$$

This, again, is not dependent on the source conditions, and correct operation of the earth-fault elements is thus obtained under 3-phase fault conditions for all lengths of line.

(3.4) Compensation Equipment

It has been shown in Section 3.1 that compensation equipment must be used in conjunction with the earth-fault measuring elements, as otherwise the operation is dependent on the sound-phase currents, even on short lines.

When using sound-phase-compensation equipment, three output currents are required, one for feeding to each of the earth-fault measuring elements. Each of these output currents should contain a proportion of the current in one of the phases and smaller proportions of the currents in the other two phases. These proportions should, as shown earlier, be in the ratio Z_s/Z_m. In practice, Z_s and Z_m have almost the same phase angle, and therefore, to keep the equipment as simple as possible, the phase difference is ignored and a transformer with three primary windings and one secondary winding per phase, connected as shown in Fig. 5, is used. By making the primary turns in the

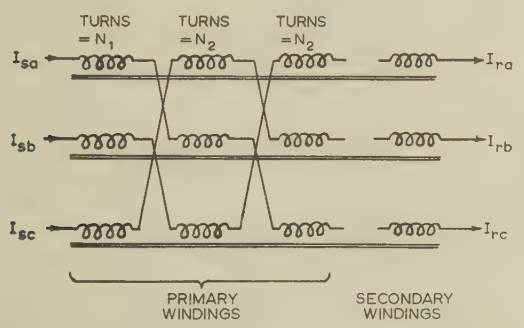

Fig. 5.—Sound-phase-compensation transformer.
$N_1/N_2 = |Z_s/Z_m|$

ratio of the magnitudes of Z_s and Z_m, as shown, the desired outputs can be obtained within reasonable limits. There is, nevertheless, a small error present in such compensating equipment, although it is undoubtedly small compared with the error examined in Section 3.1.

When residual compensation is used, each earth-fault element is fed with suitable proportions of a phase current and the zero-sequence current. To obtain accurate performance, one of these currents should be phase-shifted to allow for the phase difference between the terms in the denominator of eqn. (2). In practice, however, the residual compensation equipment is usually arranged as shown in Fig. 6, the phase correction being omitted for simplicity. Thus, such equipment also causes a small error to be introduced.

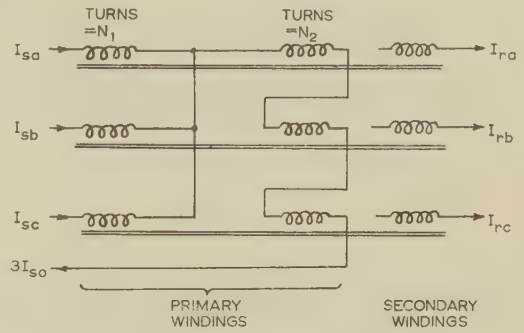

Fig. 6.—Residual-compensation equipment.
$\frac{N_1}{N_2} = \left|\frac{3Z_{01}Y_1}{Z_{00}Y_0 - Z_{01}Y_1}\right|$

(3.5) Behaviour of Distance Protection on Untransposed Lines

In the preceding Sections the behaviour of distance protection applied to ideally transposed lines has been examined. As, however, some lines are untransposed, the extra effects due to this factor will now be examined.

By using eqns. (15)–(17) and the corresponding voltage equations, the various voltages and currents at the sending end of a line can be determined for any fault and source conditions. As the equations tend to be quite complex, their significance cannot readily be appreciated. To illustrate the effect of the line asymmetry clearly, the ratios of the sending-end phase-to-neutral voltages to their corresponding phase currents were determined for a 3-phase fault on the line shown in Fig. 2, for various source conditions. It was shown that the ratios were not affected by the presence of positive-sequence source impedance and that the effect of negative-sequence source impedance was very slight. An appreciable change in the ratios is produced, however, as the zero-sequence source impedance is varied.

The variation in the ratios with zero-sequence source impedance is shown in Fig. 7, assuming a 3-phase fault 500 miles along the line. It can be shown that the addition of earth-fault compensation of the types described earlier does not eliminate these variations caused by the line asymmetry, effects similar to those shown in Fig. 7 still being obtained.

These variations introduce an error into the assessment of fault position since faults in a given position have apparent impedances which are dependent on the source impedance. This error is, however, relatively small, being only about 7% for sources ranging between zero and infinite impedance.

Although the above work shows only the behaviour during 3-phase faults, similar effects occur for other types of fault. Again the errors are small, and thus it is clear that the lack of transposition does not seriously affect the performance of distance-type protection.

(3.6) Transient Behaviour of Distance Protection

The earlier work has all been based on steady-state conditions. As it is vital that maloperation should not occur under any conditions, the transient behaviour must also be considered.

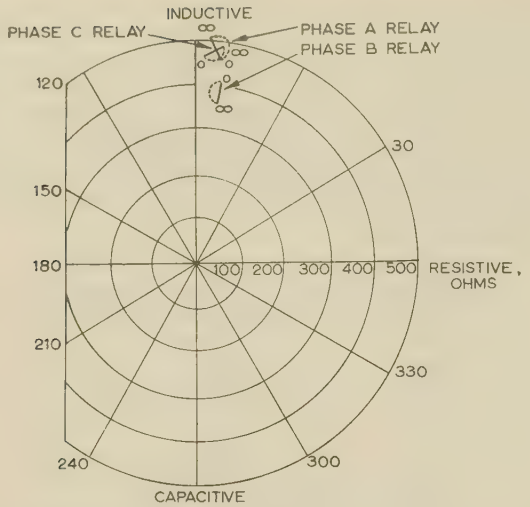

Fig. 7.—Variation of the impedances seen by relays with zero-sequence source impedance for a 3-phase fault 500 miles along a line.

At positions marked ○ the source impedance is zero.
At positions marked ∞ the source impedance is infinite.
Dotted loci are for resistive sources.
Full loci are for inductive sources.

The losses per unit length of normal 132 kV lines are appreciable, and therefore transient travelling waves are damped fairly rapidly. In addition, the frequency of the travelling waves tends to be high because of the large number of reflections which occur when lines are relatively short. This causes an increase in the effective source and line resistances which further increases the damping of the transients.

The steady-state resistance of long lines suitable for operating at 500 kV will usually be low, and this, combined with the low frequency of the travelling waves, will cause the line transients to persist for considerable periods.

It is inevitable that there will be distance-measuring errors during the transient period, but as these are dependent on the designs of the individual relays, they cannot be examined in a general manner. It is clear, however, that the chances of maloperation will be greater on long extremely-high-voltage lines than they are on shorter lower-voltage lines, where the transients normally become insignificant within the operating time of the relays.

(4) CONCLUSIONS

On 3-phase lines of any configuration, the residual currents tend to travel more slowly than those which circulate only in the phase conductors. This is because of the presence of the ground. A further factor, which is important when considering distance protection, is that such lines have a number of characteristic impedances which are dependent on the paths of the currents flowing. If a line were ideally transposed it would have one common value of propagation coefficient for positive- and negative-sequence quantities and another, higher, value for the zero-sequence quantities. It would also have one common value of characteristic impedance for the positive- and negative-sequence quantities and a higher value for the zero-sequence quantities.

Distance protection operates by assessing the impedance between the sending end of a line and any fault on the system, and it is thus clear that it should allow for these differences in the behaviour of the sequence quantities. It is shown in Section 3.1, however, that the measuring elements cannot be fed with quantities which make the correct allowance for these factors during earth faults on very long lines, although it is possible, by using the well-known sound-phase or residual types of compensation, to obtain satisfactory results on short lines. At present these compensation equipments, which are based on assumptions which are only valid on short lines, are used on all lengths of line, and, as a result, very large measuring errors can occur during earth faults on very long lines if the size of the source varies over a considerable range. It is possible for these errors to be so great that remote faults appear to be nearer than faults near the sending end of the line. A serious consequence of this is that the protection could disconnect the line wrongly for earth faults beyond its remote end.

For inter-phase faults clear of earth and for 3-phase faults, there are no zero-sequence quantities present and therefore the above differences between the sequences do not cause measuring errors. Distance protection will operate satisfactorily for these types of fault on all lengths of ideally transposed line.

Lack of transposition of a line causes the apparent impedance of inter-phase and 3-phase faults to be dependent on the source impedance; although satisfactory operation is obtained for such faults on transposed lines, there are errors introduced into the distance measurement if a line is untransposed. These errors are not very serious, as they are unlikely to exceed about 7% of the average impedance to the fault. Similar effects occur during earth faults and these will add to the errors produced by the incorrect compensation.

The long transient time-constants which are likely on long extremely-high-voltage lines make distance-type protective schemes more prone to maloperation, particularly if very-high speed relays are incorporated.

It is evident from the above that the present distance-type protective schemes are quite satisfactory for application to short lines but that they may assess fault positions quite incorrectly when they are applied to long lines, and therefore a complete study of the power system must be made before they can be reliably used on such lines.

(5) ACKNOWLEDGMENTS

The author wishes to thank the University of Nottingham for facilities made available during the preparation of the paper. He also wishes to thank Mr. E. B. Davison for his assistance and helpful criticism.

(6) REFERENCES

(1) ADAMSON, C., and WEDEPOHL, L. M.: 'Power System Protection, with particular reference to the Application of Junction Transistors to Distance Relays', *Proceedings I.E.E.*, Paper No. 2085 S, August, 1956 (**103** A, p. 379).

(2) ADAMSON, C., and WEDEPOHL, L. M.: 'A Dual-Comparator Mho-Type Distance Relay utilizing Transistors', *ibid.*, Paper No. 2177 S, September, 1956 (**103** A, p. 509).

(3) LEYBURN, H., and LACKEY, C. H. W.: 'The Protection of Electrical Power Systems: A Critical Review of Present-Day Practice and Recent Progress', *ibid.*, Paper No. 1135 S, April, 1951 (**99**, Part II, p. 47).

(4) LACKEY, C. H.: 'A Review of British Practice in the Protection of Electrical Power Systems', *Transactions of the South African I.E.E.*, 1949, **40**, p. 215.

(5) CARSON, J. R.: 'Wave Propagation in Overhead Wires with Ground Return', *Bell System Technical Journal*, 1926, **5**, p. 539.

(6) ELLIS, N. S.: 'Distance Protection of Feeders', *Reyrolle Review*, 1957, No. 168, p. 16 and No. 169, p. 6.

(7) ELLIS, N. S., and HAMILTON, F. L.: 'Performance of Distance Relays', *ibid.*, 1956, No. 166, p. 14.

BAGALA, E.: 'Behaviour of Distance Protections during Heavy Loads. A Study by Means of Circle Diagrams', C.I.G.R.É., Paris, 1954, Paper No. 313.

(7) APPENDICES

(7.1) General Steady-State Equations for a Long Asymmetrically-Spaced Untransposed Line

As the earth wires of an overhead line are effectively connected ground at each tower, the potentials along them must be the me as that along the ground, and they and the ground can thus replaced by an equivalent conductor having the correct pacitances and self and mutual inductances with the phase nductors.

At very high voltages it is unlikely that two lines will be run n the same towers and it is not necessary to allow for the terference of a second line in this analysis.

The general steady-state voltage and current equations for a wire line are therefore adequate for considering the performance of major overhead lines, and they are developed below.

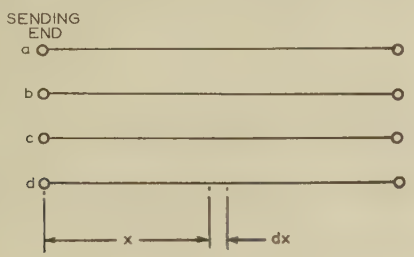

Fig. 8.—Four-wire line.

For the line shown in Fig. 8,

$$\frac{dI_{xa}}{dx} = -y_{ab}(V_{xa} - V_{xb}) - y_{ac}(V_{xa} - V_{xc}) - y_{ad}(V_{xa} - V_{xd}) \quad (4)$$

$$\frac{dI_{xb}}{dx} = -y_{ba}(V_{xb} - V_{xa}) - y_{bc}(V_{xb} - V_{xc}) - y_{bd}(V_{xb} - V_{xd}) \quad (5)$$

$$\frac{dI_{xc}}{dx} = -y_{ca}(V_{xc} - V_{xa}) - y_{cb}(V_{xc} - V_{xb}) - y_{cd}(V_{xc} - V_{xd}) \quad (6)$$

$$\frac{dI_{xd}}{dx} = -y_{da}(V_{xd} - V_{xa}) - y_{db}(V_{xd} - V_{xb}) - y_{dc}(V_{xd} - V_{xc}) \quad (7)$$

It is clear that $y_{bc} = y_{cb}$, etc., and when these substitutions e made in the above equations it can be seen that

$$\frac{dI_{xd}}{dx} = -\left(\frac{dI_{xa}}{dx} + \frac{dI_{xb}}{dx} + \frac{dI_{xc}}{dx}\right)$$

The voltage gradient is given by

$$\frac{dV_{xa}}{dx} = -I_{xa}Z_{aa} - I_{xb}Z_{ab} - I_{xc}Z_{ac} - I_{xd}Z_{ad}$$

or a 4-wire line, $I_{xd} = -(I_{xa} + I_{xb} + I_{xc})$

Therefore

$$\frac{dV_{xa}}{dx} = -I_{xa}(Z_{aa} - Z_{ad}) - I_{xb}(Z_{ab} - Z_{ad}) - I_{xc}(Z_{ac} - Z_{ad}) \quad (8)$$

Similarly,

$$\frac{dV_{xb}}{dx} = -I_{xa}(Z_{ba} - Z_{bd}) - I_{xb}(Z_{bb} - Z_{bd}) - I_{xc}(Z_{bc} - Z_{bd}) \quad (9)$$

$$\frac{dV_{xc}}{dx} = -I_{xa}(Z_{ca} - Z_{cd}) - I_{xb}(Z_{cb} - Z_{cd}) - I_{xc}(Z_{cc} - Z_{cd}) \quad (10)$$

$$\frac{dV_{xd}}{dx} = -I_{xa}(Z_{da} - Z_{dd}) - I_{xb}(Z_{db} - Z_{dd}) - I_{xc}(Z_{dc} - Z_{dd}) \quad (11)$$

Differentiating eqns. (4)–(6) the following results are obtained:

$$\frac{d^2I_{xa}}{dx^2} = m_1I_{xa} + m_2I_{xb} + m_3I_{xc} \quad (12)$$

$$\frac{d^2I_{xb}}{dx^2} = n_1I_{xa} + n_2I_{xb} + n_3I_{xc} \quad (13)$$

$$\frac{d^2I_{xc}}{dx^2} = p_1I_{xa} + p_2I_{xb} + p_3I_{xc} \quad (14)$$

where

$$\begin{aligned}
m_1 &= a_1 + b_1 + c_1 \\
m_2 &= a_2 + b_2 + c_2 \\
m_3 &= a_3 + b_3 + c_3 \\
n_1 &= -a_1 + d_1 + f_1 \\
n_2 &= -a_2 + d_2 + f_2 \\
n_3 &= -a_3 + d_3 + f_3 \\
p_1 &= -b_1 - d_1 + g_1 \\
p_2 &= -b_2 - d_2 + g_2 \\
p_3 &= -b_3 - d_3 + g_3
\end{aligned}$$

and

$$\begin{aligned}
a_1 &= y_{ab}(Z_{aa} - Z_{ad} - Z_{ba} + Z_{bd}) \\
a_2 &= y_{ab}(Z_{ab} - Z_{ad} - Z_{bb} + Z_{bd}) \\
a_3 &= y_{ab}(Z_{ac} - Z_{ad} - Z_{bc} + Z_{bd}) \\
b_1 &= y_{ac}(Z_{aa} - Z_{ad} - Z_{ca} + Z_{cd}) \\
b_2 &= y_{ac}(Z_{ab} - Z_{ad} - Z_{cb} + Z_{cd}) \\
b_3 &= y_{ac}(Z_{ac} - Z_{ad} - Z_{cc} + Z_{cd}) \\
c_1 &= y_{ad}(Z_{aa} - Z_{ad} - Z_{da} + Z_{dd}) \\
c_2 &= y_{ad}(Z_{ab} - Z_{ad} - Z_{db} + Z_{dd}) \\
c_3 &= y_{ad}(Z_{ac} - Z_{ad} - Z_{dc} + Z_{dd}) \\
d_1 &= y_{bc}(Z_{ba} - Z_{bd} - Z_{ca} + Z_{cd}) \\
d_2 &= y_{bc}(Z_{bb} - Z_{bd} - Z_{cb} + Z_{cd}) \\
d_3 &= y_{bc}(Z_{bc} - Z_{bd} - Z_{cc} + Z_{cd}) \\
f_1 &= y_{bd}(Z_{ba} - Z_{bd} - Z_{da} + Z_{dd}) \\
f_2 &= y_{bd}(Z_{bb} - Z_{bd} - Z_{db} + Z_{dd}) \\
f_3 &= y_{bd}(Z_{bc} - Z_{bd} - Z_{dc} + Z_{dd}) \\
g_1 &= y_{cd}(Z_{ca} - Z_{cd} - Z_{da} + Z_{dd}) \\
g_2 &= y_{cd}(Z_{cb} - Z_{cd} - Z_{db} + Z_{dd}) \\
g_3 &= y_{cd}(Z_{cc} - Z_{cd} - Z_{dc} + Z_{dd})
\end{aligned}$$

The solutions of eqns. (12)–(14) are

$$I_{xa} = A\cosh\sqrt{(s)}x + B\sinh\sqrt{(s)}x + k_1C\cosh\sqrt{(r)}x + k_1D\sinh\sqrt{(r)}x + k_2E\cosh\sqrt{(q)}x + k_2F\sinh\sqrt{(q)}x \quad (15)$$

$$I_{xb} = C\cosh\sqrt{(r)}x + D\sinh\sqrt{(r)}x + k_3A\cosh\sqrt{(s)}x + k_3B\sinh\sqrt{(s)}x + k_4E\cosh\sqrt{(q)}x + k_4F\sinh\sqrt{(q)}x \quad (16)$$

$$I_{xc} = E\cosh\sqrt{(q)}x + F\sinh\sqrt{(q)}x + k_5A\cosh\sqrt{(s)}x + k_5B\sinh\sqrt{(s)}x + k_6C\cosh\sqrt{(r)}x + k_6D\sinh\sqrt{(r)}x \quad (17)$$

The coefficients A to F are dependent on the line operating conditions. The other terms (k_1, k_2, etc., and q, r and s) are dependent on the constants of the line and are determined from the following equations:

$$\begin{aligned} m_1 + m_2k_3 + m_3k_5 &= s \\ m_1k_1 + m_2 + m_3k_6 &= k_1r \\ m_1k_2 + m_2k_4 + m_3 &= k_2q \\ n_1 + n_2k_3 + n_3k_5 &= k_3s \\ n_1k_1 + n_2 + n_3k_6 &= r \\ n_1k_2 + n_2k_4 + n_3 &= k_4q \\ p_1 + p_2k_3 + p_3k_5 &= k_5s \\ p_1k_1 + p_2 + p_3k_6 &= k_6r \\ p_1k_2 + p_2k_4 + p_3 &= q \end{aligned}$$

By differentiating eqns. (8)–(11) the corresponding set of voltage equations can be produced.

(7.2) Steady-State Current Equations for the Line shown in Fig. 2

The shunt admittances y_{bd}, etc., can be found in the conventional manner by assuming images of all the conductors to exist in the ground.

When determining the series impedances the earth can be replaced by an equivalent conductor at a depth, D_e, below the ground of $2160\rho/f$ feet. This depth may vary, for a 50 c/s system, between 350 and 10000 ft, depending on the nature of the ground. A reasonable average value, and the one used in obtaining the following results, is 3000 ft.

The voltage gradient along the earth is normally taken to be zero, and, as stated earlier, this must also be the gradient along the earth wires. If a current flows along a phase conductor and returns via an earth path it must split between the earth wires and ground in a ratio which ensures zero voltage gradient along the earth wires. Proceeding on this basis, the voltage drops along the phase conductors for currents traversing the various possible paths can be determined, and thus the series impedances can also be obtained.

Determination of the series impedances and shunt admittances for the line shown in Fig. 2 and substitution of the values in the equations given in Appendix 7.1 enables the following results to be obtained:

$$\begin{aligned} I_{xa} = {} & A\cosh\frac{1\cdot743}{10^3}\underline{|88°\ 18'}\,x + B\sinh 1\cdot743\times10^{-3}\underline{|88°\ 18'}\,x \\ & + 0\cdot514C_1\underline{|180°\ 7'}\cosh 1\cdot700\times10^{-3}\underline{|88°\ 3'}\,x \\ & + 0\cdot514D_1\underline{|180°\ 7'}\sinh 1\cdot700\times10^{-3}\underline{|88°\ 3'}\,x \\ & + 1\cdot032C_2\underline{|-10'}\cosh 2\cdot620\times10^{-3}\underline{|89°\ 23'}\,x \\ & + 1\cdot032D_2\underline{|-10'}\sinh 2\cdot620\times10^{-3}\underline{|89°\ 23'}\,x \quad (18) \end{aligned}$$

$$\begin{aligned} I_{xb} = {} & C_1\cosh 1\cdot700\times10^{-3}\underline{|88°\ 3'}\,x \\ & + D_1\sinh 1\cdot700\times10^{-3}\underline{|88°\ 3'}\,x \\ & + C_2\cosh 2\cdot620\times10^{-3}\underline{|89°\ 23'}\,x \\ & + D_2\sinh 2\cdot620\times10^{-3}\underline{|89°\ 23'}\,x \quad (19) \end{aligned}$$

$$\begin{aligned} I_{xc} = {} & -A\cosh 1\cdot743\times10^{-3}\underline{|88°\ 18'}\,x \\ & - B\sinh 1\cdot743\times10^{-3}\underline{|88°\ 18'}\,x \\ & + 0\cdot514C_1\underline{|180°\ 7'}\cosh 1\cdot700\times10^{-3}\underline{|88°\ 3'}\,x \\ & + 0\cdot514D_1\underline{|180°\ 7'}\sinh 1\cdot700\times10^{-3}\underline{|88°\ 3'}\,x \\ & + 1\cdot032C_2\underline{|-10'}\cosh 2\cdot620\times10^{-3}\underline{|89°\ 23'}\,x \\ & + 1\cdot032D_2\underline{|-10'}\sinh 2\cdot620\times10^{-3}\underline{|89°\ 23'}\,x \quad (20) \end{aligned}$$

The values of the coefficients A to D are determined from the system operating conditions in a manner similar to that used when dealing with a single-phase line:

$$\begin{aligned} I_{sa} &= A + 0\cdot514\underline{|180°\ 7'}\,C_1 + 1\cdot032\underline{|-10'}\,C_2 \\ I_{sb} &= C_1 + C_2 \\ I_{sc} &= -A + 0\cdot514\underline{|180°\ 7'}\,C_1 + 1\cdot032\underline{|-10'}\,C_2 \end{aligned}$$

The current gradient at the sending end of a phase can be related to the sending-end voltages as follows:

$$\begin{aligned} \frac{dI_{sa}}{dx} &= 1\cdot743\times10^{-3}\underline{|88°\ 18'}\,B + 0\cdot874\times10^{-3}\underline{|268°\ 10'}\,D_1 \\ &\quad + 2\cdot7\times10^{-3}\underline{|89°\ 13'}\,E \\ &= -y_{ab}(V_{sa}-V_{sb}) - y_{ac}(V_{sa}-V_{sc}) - y_{ad}(V_{sa}-V_{sd}) \end{aligned}$$

There are similar equations for the two other phases and thus the constants B, D_1 and D_2 can be found.

(7.3) Steady-State Equations for a Long Ideally Transposed Three-Phase Line

On an ideally transposed line, the phases behave identically and thus

$$\begin{aligned} & y_{ab} = y_{ac} = y_{bc};\quad y_{ad} = y_{bd} = y_{cd};\quad Z_{aa} = Z_{bb} = Z_{cc} \\ & Z_{ab} = Z_{ac} = Z_{ba} = Z_{bc} = Z_{ca} = Z_{cb} \\ & Z_{aa} = Z_{bd} = Z_{cd};\quad Z_{da} = Z_{db} = Z_{dc} \end{aligned}$$

Making these substitutions in eqns. (4)–(11) and differentiating,

$$\frac{d^2I_{xa}}{dx^2} = m_4I_{xa} + m_5(I_{xb} + I_{xc}) \quad . \ . \ . \quad (21)$$

$$\frac{d^2I_{xb}}{dx^2} = m_4I_{xb} + m_5(I_{xa} + I_{xc}) \quad . \ . \ . \quad (22)$$

$$\frac{d^2I_{xc}}{dx^2} = m_4I_{xc} + m_5(I_{xa} + I_{xb}) \quad . \ . \ . \quad (23)$$

where

$$m_4 = 2y_{ab}(Z_{aa} - Z_{ab}) + y_{ad}(Z_{aa} - Z_{ad} - Z_{da} + Z_{dd})$$

and $$m_5 = y_{ab}(Z_{ab} - Z_{bb}) + y_{ad}(Z_{ab} - Z_{ad} - Z_{da} + Z_{dd})$$

The solutions of eqns. (21)–(23) are of the form

$$\begin{aligned} I_{xa} = {} & (A - \tfrac{1}{2}B - \tfrac{1}{2}C)\cosh\sqrt{(m_4 - m_5)}x \\ & + (D - \tfrac{1}{2}E - \tfrac{1}{2}F)\sinh\sqrt{(m_4 - m_5)}x \\ & + G\cosh\sqrt{(m_4 + 2m_5)}x + H\sinh\sqrt{(m_4 + 2m_5)}x \quad (24) \end{aligned}$$

$$\begin{aligned} I_{xb} = {} & (B - \tfrac{1}{2}A - \tfrac{1}{2}C)\cosh\sqrt{(m_4 - m_5)}x \\ & + (E - \tfrac{1}{2}D - \tfrac{1}{2}F)\sinh\sqrt{(m_4 - m_5)}x \\ & + G\cosh\sqrt{(m_4 + 2m_5)}x + H\sinh\sqrt{(m_4 + 2m_5)}x \quad (25) \end{aligned}$$

$$\begin{aligned} I_{xc} = {} & (C - \tfrac{1}{2}A - \tfrac{1}{2}B)\cosh\sqrt{(m_4 - m_5)}x \\ & + (F - \tfrac{1}{2}D - \tfrac{1}{2}E)\sinh\sqrt{(m_4 - m_5)}x \\ & + G\cosh\sqrt{(m_4 + 2m_5)}x + H\sinh\sqrt{(m_4 + 2m_5)}x \quad (26) \end{aligned}$$

Considering conditions at the sending end of the line, i.e. en $x = 0$,

$$I_{sa} = A - \tfrac{1}{2}B - \tfrac{1}{2}C + G \quad I_{sb} = B - \tfrac{1}{2}A - \tfrac{1}{2}C + G$$
$$I_{sc} = C - \tfrac{1}{2}A - \tfrac{1}{2}B + G$$

Adding these equations,

$$3G = I_{sa} + I_{sb} + I_{sc} = 3I_{s0}$$
$$G = I_{s0}$$

ice
$$A - \tfrac{1}{2}B - \tfrac{1}{2}C + I_{s0} = I_{sa}$$
$$A - \tfrac{1}{2}B - \tfrac{1}{2}C = I_{sa1} + I_{sa2}$$

nilarly
$$B - \tfrac{1}{2}A - \tfrac{1}{2}C = I_{sb1} + I_{sb2}$$

d
$$C - \tfrac{1}{2}A - \tfrac{1}{2}B = I_{sc1} + I_{sc2}$$

$\frac{ca}{c}$ at $x = 0 = \sqrt{(m_4 - m_5)}(D - \tfrac{1}{2}E - \tfrac{1}{2}F) + \sqrt{(m_4 + 2m_5)}H$

$$= -y_{ab}(V_{sa} - V_{sb}) - y_{ab}(V_{sa} - V_{sc}) - y_{ad}(V_{sa} - V_{sd}) \quad (27)$$

nilarly

$$\sqrt{(m_4 - m_5)}(E - \tfrac{1}{2}D - \tfrac{1}{2}F) + \sqrt{(m_4 + 2m_5)}H$$
$$= -y_{ab}(V_{sb} - V_{sa}) - y_{ab}(V_{sb} - V_{sc}) - y_{ad}(V_{sb} - V_{sd}) \quad (28)$$

d

$$\sqrt{(m_4 - m_5)}(F - \tfrac{1}{2}D - \tfrac{1}{2}E) + \sqrt{(m_4 + 2m_5)}H$$
$$= -y_{ab}(V_{sc} - V_{sa}) - y_{ab}(V_{sc} - V_{sb}) - y_{ad}(V_{sc} - V_{sd}) \quad (29)$$

lving eqns. (27)–(29),

$$H = -\frac{V_{s0}}{Z_{00}}$$

$$D - \tfrac{1}{2}E - \tfrac{1}{2}F = -\frac{V_{sa1} + V_{sa2}}{Z_{01}}$$

$$E - \tfrac{1}{2}D - \tfrac{1}{2}F = -\frac{V_{sb1} + V_{sb2}}{Z_{01}}$$

$$F - \tfrac{1}{2}D - \tfrac{1}{2}E = -\frac{V_{sc1} + V_{sc2}}{Z_{01}}$$

here $Z_{00} = \dfrac{\sqrt{(m_4 + 2m_5)}}{y_{ad}}$ and $Z_{01} = \dfrac{\sqrt{(m_4 - m_5)}}{3y_{ab} + y_{ad}}$

he current equations for the line are thus of the form

$$_a = (I_{sa1} + I_{sa2}) \cosh \sqrt{(m_4 - m_5)}x - \frac{V_{sa1} + V_{sa2}}{Z_{01}} \sinh \sqrt{(m_4 - m_5)}x$$
$$+ I_{s0} \cosh \sqrt{(m_4 + 2m_5)}x - \frac{V_{s0}}{Z_{00}} \sinh \sqrt{(m_4 + 2m_5)}x \quad (30)$$

he corresponding voltage equations can be shown to be of ıe form

$$_{xa} - V_{xd} = (V_{sa1} + V_{sa2}) \cosh \sqrt{(m_4 - m_5)}x - (I_{sa1} + I_{sa2})Z_{01} \sinh \sqrt{(m_4 - m_5)}x$$
$$+ V_{s0} \cosh \sqrt{(m_4 + 2m_5)}x - I_{s0}Z_{00} \sinh \sqrt{(m_4 + 2m_5)}x \quad . \quad (31)$$

n the above equations, $\sqrt{(m_4 - m_5)}$, which is the propagation oefficient for positive- and negative-sequence quantities, can for implicity be replaced by γ_1; and $\sqrt{(m_4 + 2m_5)}$, which is the ero-sequence propagation coefficient, can be replaced by γ_0.

(7.4) Behaviour of Phase-to-Earth Fault Relays Operated from Normal Sound-Phase-Compensation Equipment

As shown in eqn. (3) the A-phase earth-fault relay is fed with an operating signal proportional to $I_{sa} + (I_{sb} + I_{sc})Z_m/Z_s$ and a restraining signal proportional to $V_{sa} - V_{sd}$. The ratio of these quantities can be considered as the apparent impedance Z_{app} seen by the relay; i.e.

$$Z_{app} = \frac{V_{sa} - V_{sd}}{I_{sa} + \dfrac{Z_m}{Z_s}(I_{sb} + I_{sc})}$$

On an ideally transposed line the sequence components do not interact with one another and they can thus be considered separately. Eqn. (30) can be separated into components so that

$$I_{x0} = I_{s0} \cosh \gamma_0 x - \frac{V_{s0}}{Z_{00}} \sinh \gamma_0 x \quad . \quad . \quad . \quad (32)$$

The source at the sending end of the line will only generate positive-sequence voltage, so that the zero-sequence voltage input to the line is merely the zero-sequence voltage drop in the source impedance, Z_{s0}, i.e. $V_{s0} = -I_{s0}Z_{s0}$.

Substituting for V_{s0} in eqn. (32),

$$I_{s0} = \frac{Z_{00}I_{x0}}{Z_{00} \cosh \gamma_0 x + Z_{s0} \sinh \gamma_0 x} \quad . \quad . \quad (33)$$

Similarly the negative-sequence current referred to the A phase is given by

$$I_{sa2} = \frac{Z_{01}I_{xa2}}{Z_{01} \cosh \gamma_1 x + Z_{s2} \sinh \gamma_1 x} \quad . \quad . \quad (34)$$

The positive-sequence current at a point a distance x from the sending end of the line is

$$I_{xa1} = I_{sa1} \cosh \gamma 1x - \frac{V_{sa1}}{Z_{01}} \sinh \gamma_1 x \quad . \quad . \quad (35)$$

The positive-sequence input voltage to the line is given by

$$V_{sa1} = V_{ga} - I_{sa1}Z_{s1}$$

Substituting for V_{sa1} in eqn. (35),

$$I_{sa1} = \frac{Z_{01}I_{xa1} + V_{ga} \sinh \gamma_1 x}{Z_{01} \cosh \gamma_1 x + Z_{s1} \sinh \gamma_1 x} \quad . \quad . \quad . \quad (36)$$

From eqn. (31) the zero-sequence components can be isolated to give

$$V_{x0} = V_{s0} \cosh \gamma_0 x - I_{s0}Z_{00} \sinh \gamma_0 x$$

Substituting for V_{s0},

$$V_{x0} = -I_{s0}(Z_{s0} \cosh \gamma_0 x + Z_{00} \sinh \gamma_0 x) \quad . \quad (37)$$

Similarly

$$V_{xa2} = -I_{sa2}(Z_{s2} \cosh \gamma_1 x + Z_{01} \sinh \gamma_1 x) \quad . \quad . \quad (38)$$

and

$$V_{xa1} = V_{ga} \cosh \gamma_1 x - I_{sa1}(Z_{s1} \cosh \gamma_1 x + Z_{01} \sinh \gamma_1 x) \quad (39)$$

When a fault occurs to earth at a distance x from the sending end of the line on the A phase,

$$V_{xa1} + V_{xa2} + V_{x0} = 0$$

Substitution in this equation for V_{xa1}, V_{xa2} and V_{x0} from eqns. (37)–(39) enables the generated voltage, V_{ga}, to be

expressed as a function of the sequence currents at the fault position; i.e.

$$V_{ga} = I_{xa1}(Z_{s1}\cosh\gamma_1 x + Z_{01}\sinh\gamma_1 x) + I_{xa2}\left[\frac{(Z_{s2}\cosh\gamma_1 x + Z_{01}\sinh\gamma_1 x)(Z_{s1}\sinh\gamma_1 x + Z_{01}\cosh\gamma_1 x)}{Z_{s2}\sinh\gamma_1 x + Z_{01}\cosh\gamma_1 x}\right]$$
$$+ \frac{Z_{00}}{Z_{01}} I_{x0}\left[\frac{(Z_{s0}\cosh\gamma_0 x + Z_{00}\sinh\gamma_0 x)(Z_{s1}\sinh\gamma_1 x + Z_{01}\cosh\gamma_1 x)}{Z_{s0}\sinh\gamma_0 x + Z_{00}\cosh\gamma_0 x}\right] \quad (40)$$

Now

$$V_{sa} - V_{sd} = V_{sa1} + V_{sa2} + V_{s0}$$
$$= V_{ga} - I_{sa1}Z_{s1} - I_{sa2}Z_{s2} - I_{s0}Z_{s0}$$

Substitution in this equation for V_{ga}, I_{sa1}, I_{sa2} and I_{s0} from the earlier equations gives

$$V_{sa} - V_{sd} = Z_{01}\sinh\gamma_1 x(I_{xa1} + I_{xa2})$$
$$+ \frac{Z_{00}\sinh\gamma_0 x\cosh\gamma_1 x + Z_{s0}(\cosh\gamma_1 x\cosh\gamma_0 x - 1)}{Z_{00}\cosh\gamma_0 x + Z_{s0}\sinh\gamma_0 x} Z_{00} I_{x0}$$
$$\ldots \quad (41)$$

The relay operating signal, as shown earlier, is proportional to $I_{sa} + Z_m/Z_s(I_{sb} + I_{sc})$, which, by substituting for Z_m and Z_s, gives, as shown in Section 3.1,

$$I_{sa} + \frac{Z_m}{Z_s}(I_{sb} + I_{sc}) = I_{sa}Z_{01}\gamma_1 + I_{s0}(Z_{00}\gamma_0 - Z_{01}\gamma_1)$$
$$= (I_{sa1} + I_{sa2})Z_{01}\gamma_1 + I_{s0}Z_{00}\gamma_0$$

By substituting for I_{sa1}, I_{sa2} and I_{s0} from eqns. (33), (34) and (36) we get

$$I_{sa} + \frac{Z_m}{Z_s}(I_{sb} + I_{sc}) = Z_{01}\gamma_1\cosh\gamma_1 x(I_{xa1} + I_{xa2}) + \frac{Z_{00}(\gamma_0 + \gamma_1\sinh\gamma_1 x\sinh\gamma_0 x) + Z_{so}\gamma_1\sinh\gamma_1 x\cosh\gamma_0 x}{Z_{00}\cosh\gamma_0 x + Z_{s0}\sinh\gamma_0 x} Z_{00} I_{x0} \quad (42)$$

By substituting from eqns. (41) and (42) it can be shown that the apparent impedance seen by the relay is

$$Z_{app} = \frac{V_{sa} - V_{sd}}{I_{sa} + \frac{Z_m}{Z_s}(I_{sb} + I_{sc})} = Z\left[\frac{1 + k_1\left(\frac{I_{xb} + I_{xc}}{I_{xa}}\right)}{1 + k_2\left(\frac{I_{xb} + I_{xc}}{I_{xa}}\right)}\right] \quad (43)$$

where $Z = \frac{M + 2N}{P + 2Q}$; $k_1 = \frac{M - N}{M + 2N}$; $k_2 = \frac{P - Q}{P + 2Q}$

the values of M, N, P and Q being given by the following equations:

$$M = Z_{00}[(Z_{00}\sinh\gamma_0 x\cosh\gamma_1 x + Z_{s0}(\cosh\gamma_1 x\cosh\gamma_0 x - 1)]$$
$$N = Z_{01}\sinh\gamma_1 x(Z_{00}\cosh\gamma_0 x + Z_{s0}\sinh\gamma_0 x)$$
$$P = Z_{00}[Z_{00}(\gamma_0 + \gamma_1\sinh\gamma_1 x\sinh\gamma_0 x) + Z_{s0}\gamma_1\sinh\gamma_1 x\cosh\gamma_0 x)]$$
$$Q = Z_{01}\gamma_1\cosh\gamma_1 x(Z_{00}\cosh\gamma_0 x + Z_{s0}\sinh\gamma_0 x)$$

PROCEEDINGS OF THE INSTITUTION OF ELECTRICAL ENGINEERS

PART C—MONOGRAPHS, MARCH 1961

CONTENTS

Bibliographical References.—It is requested that bibliographical reference to an Institution paper should always include the serial number of the paper and the month and year of publication, which will be found at the top right-hand corner of the first page of the paper. This information should precede the reference to the Volume and Part.

Example.—SMITH, J.: 'Reflections from the Ionosphere', *Proceedings I.E.E.*, Paper No. 5001 E, December, 1960 (107 B, p. 1234).

Published by The Institution, Savoy Place, London, W.C.2. *Telephone:* COVent Garden 1871. *Telegrams:* 'Voltampere, Phone, London.'
Printed by Unwin Brothers Limited, Woking and London.